Number 1 Volume 24 1960

PI

BULLETIN

of the

ACADEMY OF SCIENCES OF THE USSR

— PHYSICAL SERIES —

(Izvestiya Akademii Nauk SSSR)
(Seriya fizicheskaya)

Reproduction rights reserved
by
Columbia Technical Translations
5 Vermont Avenue
White Plains, New York

Single Issues
$20

Annual Subscription
$215

Lithoprinted in U.S.A.
EDWARDS BROTHERS, INC.
Ann Arbor, Michigan

TRANSACTIONS

# of the

SECOND ALL-UNION CONFERENCE ON THE PHYSICS OF DIELECTRICS

(Moscow, 20-27 November 1958)

To be continued in Vol.24, No.2

Digitized by the Internet Archive
in 2024

https://archive.org/details/russian-academy-of-sciences-physics-bulletin_1960_24

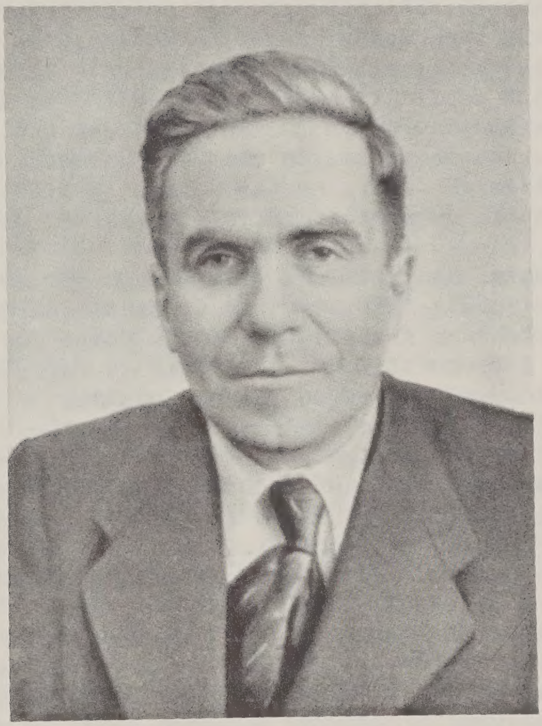

Georgii Ivanovich Skanavi
(1910-1959)

GEORGII IVANOVICH SKANAVI
1910-1959

Dr. Georgii Ivanovich Skanavi, eminent Soviet scientist and outstanding specialist in the field of physics of dielectrics, died suddenly on the 11th of November, 1959.

Georgii Ivanovich graduated in 1931 from the Leningrad polytechnical Institute and went to work at the "Elektrosila" (Electric Power) Plant. Working in the plant laboratory, he soon won recognition not only as a capable engineer and good organizer, but also as a talented investigator. Within four years he had more than ten scientific publications to his credit. In 1935 Georgii Ivanovich transferred to scientific work at the Scientific Research Institute of the Radio Industry, and then in 1940 went over to the "P.N.Lebedev" Physical Institute of the USSR Academy of Sciences, where he was active to within a few days of his death. He was awarded the degree of doctor of physical-mathematical sciences in 1946.

During the war years, Georgii Ivanovich worked on the development of new ceramic capacitor materials. This work was continued during the post-war years. In 1952 Georgii Ivanovich was awarded the Stalin Prize for his research on ceramic materials and the introduction of the developed materials to industry.

The activity of Georgii Ivanovich was not bounded by laboratory walls. Over a number of years he supervised the industrial laboratory in a Moscow plant, served as a consultant to the dielectrics industry, lectured and presented reports, organized conferences and participated in international conferences.

Since 1958, Georgii Ivanovich headed the Laboratory of the Physics of Dielectrics at the "P.N.Lebedev" Physical Institute. Under his guidance, within six years, the new laboratory became the outstanding research center in its field in the USSR.

Georgii Ivanovich was ever attentive to the education of new scientific workers. There are many whom he taught to love science, to be conscientious researchers and scrupulous investigators. His students work not only in his laboratory but in many other scientific research institutes.

The development of the physics of dielectrics in the Soviet Union is indissolubly linked with the name of Georgii Ivanovich Skanavi. He is the author of more than 70 scientific reports and four monographs. His two volume "Physics of Dielectrics" is a unique contribution to world scientific literature and serves as a guide and reference for physicists and engineers specializing in this field. The last researches of Georgii Ivanovich, devoted to the development of a new type of dielectric (strontium-bismuth titanate), have been highly evaluated by Soviet and foreign scientists.

Georgii Ivanovich also carried on extensive pedagogical work; he occupied the chair of general physics in the Physics Department of Moscow State University.

A member of the Communist Party of the Soviet Union since 1944, Georgii Ivanovich always participated actively in community and political life. At the time of his death he was secretary of the Party Committee at the "P.N.Lebedev" Physical Institute.

Georgii Ivanovich Skanavi was a gifted person distinguished by the breadth of his interests in the fields of science and culture. Being a demanding and at the same time responsive leader, who attentively followed the scientific growth of his colleagues, he imbued them with his bubbling energy and buoyant enthusiasm. Death carried him off in the full flower of his creative development, full of plans for the future. All who had the privilege to work with Georgii Ivanovich will long remember him as an outstanding scientist and devoted comrade.

DIELECTRIC RELAXATION IN LIQUID ALCOHOLS, ALKYL HALIDES AND SOLUTIONS*

Robert H.Cole

I. Introduction

The explanation and understanding of the constitution of liquids presents a difficult problem which can be approached by study of many kinds of properties, of which their response to applied external electric fields is only one. The dielectric behavior is particularly interesting and revealing in the case of liquids or solutions containing polar molecules. Like other macroscopic properties, the observed dielectric behavior is a statistical average result of many macroscopic processes, and so can give only a limited amount of information about them. At the same time, however, dielectric measurements can give information about both equilibrium response and the way in which equilibrium is reached after a change in the external forces acting on the system. Dielectric constant and loss measurements are particularly valuable for the latter problem, because when they are applicable they can be made over a much wider range of times than has so far been possible for any other kind of relaxation effect.

Liquids composed of small and comparatively simple molecules characteristically show relaxation effects at microwave frequencies when they are at room temperature. Although techniques for this region have become available in recent years and are rapidly being developed, the experimental evidence is still very limited and incomplete. An alternative approach is possible in some cases by taking advantage of the fact that the rate of response becomes very much slower at low temperatures, just as in other relaxation processes and problems in chemical kinetics. At sufficiently low temperatures, relaxation effects appear at radio or audio frequencies where they can be measured much more easily and with great accuracy over wide ranges of times of response.

In recent years, my associates and I have used this approach to study two interesting and representative types of polar molecules as liquids and in solutions: alkyl halides and aliphatic alcohols. This paper is an attempt to summarize some of the findings and possible interpretations in terms of molecular structure and interactions, together with some discussion of the unsolved problems and further investigations which are needed.

II. Alcohols

Measurements have been made on seven aliphatic alcohols[1] at frequencies from a few cycles to 10^6 cycles/sec and in some cases to 250 megacycles/sec over the temperature ranges in which dispersion effects could be observed, these temperatures normally being in the range -140°C to -50°C. The experimental methods employed a transformer ratio arm bridge for frequencies below 1 megacycle/sec[2] and a modified Schering bridge with special coaxial cell for frequencies to 250 megacycles/sec[3].

These alcohols have equilibrium dielectric constants which are considerably larger and increase more rapidly at low temperatures than expected for normal polar liquids, as shown, for example, by their deviations from Onsager's theory[4]. The large values have been attributed to the fact that the polar molecules are associated into linear hydrogen bonded chains with enhanced dipole moments by correlation of neighbors[5], and the temperature effects can be explained by assuming a statistical distribution of chain lengths which increase at low temperatures[1d].

---

*We are grateful to Prof.Cole for supplying a copy of his paper and for permission to reproduce it. Translation editor.

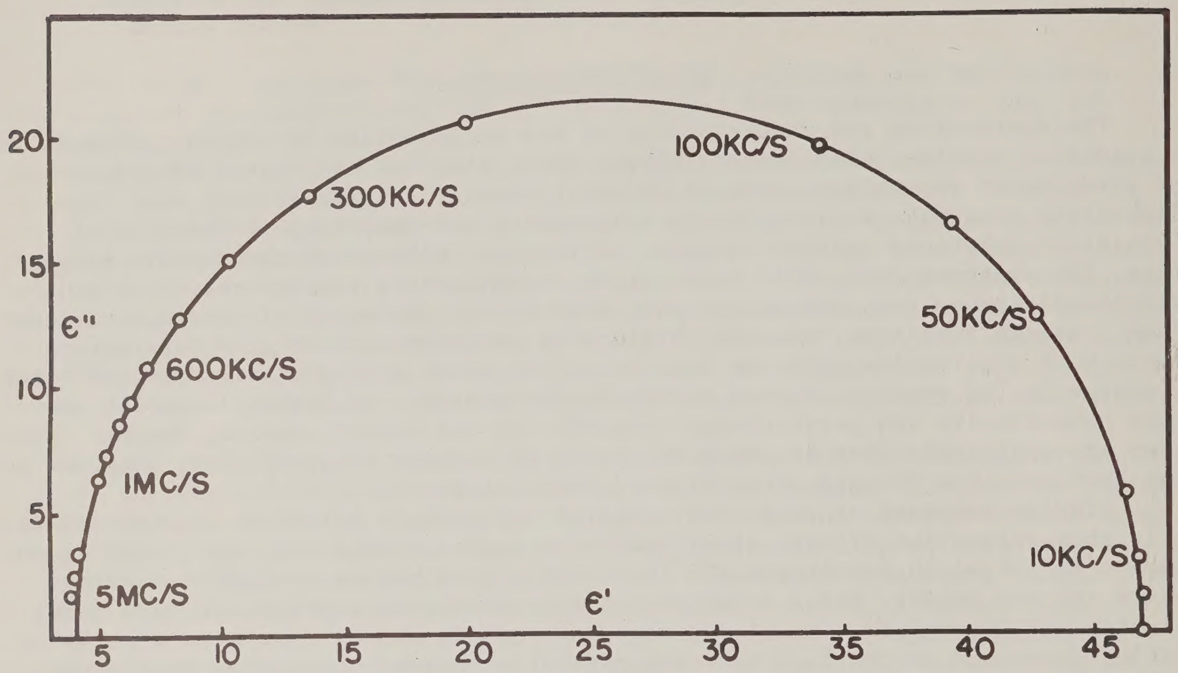

Fig.1. Complex dielectric constant of 2-propanol at -95°C.

At sufficiently high frequencies, the dipole contributions must decrease and ultimately vanish, leaving only the induced polarization and dielectric constants of order 2 to 3, compared with static values of 10 to 100. Most of the decrease is found to occur in a simple process described by the Debye equation

$$\varepsilon^* = \varepsilon' - i\varepsilon'' = \varepsilon_1 + \frac{\varepsilon_0 - \varepsilon_1}{1 + i\omega\tau_1}, \tag{1}$$

where ε^* is the complex dielectric constant, ε_0 and ε_1 are the limiting low and high frequency values, ω is radian frequency, and τ_1 is the relaxation time for the dispersion. This simple behavior is found for all the alcohols studied and at all temperatures; such behavior is rare in other liquids and hence strongly suggests a quite specific mechanism of molecular reorientation. An example of the measurements is shown in the complex plane plot of ε'' vs ε' in Fig.1, the locus of points being a semicircle as required if Eq.(1) is to be valid[6].

In other respects, however, the dispersion is different from the simplest behavior one could expect. First, the relaxation time τ_1 does not vary with absolute temperature T according to the simple rate law

$$\ln \tau_1 = A + \frac{\Delta H}{RT}, \tag{2}$$

the plot of $\ln \tau_1$ against 1/T being strongly curved with larger slopes at low temperatures, as shown for one example in Fig.2.

The second remarkable feature of the principal dispersion in alcohols is the fact that the high frequency limit ε_1 is substantially larger than any reasonable value ε_∞ for electronic and atomic polarizations only. Thus for 1-propanol at -140°C, $\varepsilon_1 = 5.40$, whereas ε_∞ can hardly be much larger than 2.2, and similar behavior is found for other alcohols.

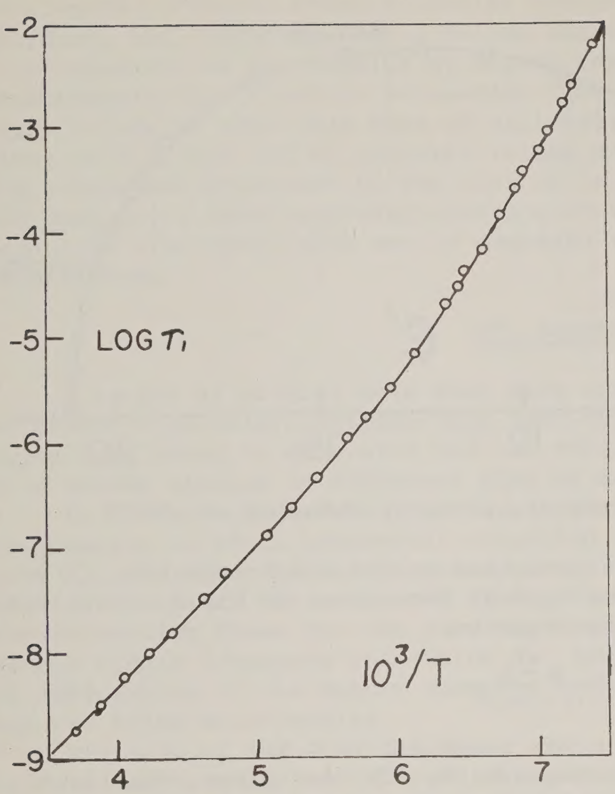

Fig.2. Relaxation Times of 1-butanol plotted against reciprocal temperature.

For several alcohols, measurements by Davidson and others at much higher frequencies than those of the primary dispersion clearly show a second region of dispersion at low temperatures[7,1d]. Moreover, there is more limited but definite evidence from these data for a third dispersion region at still higher frequencies. Both of these further dispersions are strongly temperature dependent with rate laws similar to that for the primary dispersion.

Brot[8] has also found evidence of further dispersions in higher alcohols at higher temperatures and frequencies than in our investigations. As best can be judged by comparing data for different alcohols and temperatures, the two sets of results are consistent and are observations of the same kind of effect under different conditions.

We have interpreted these effects in terms of changes in arrangements of hydrogen bonded chains

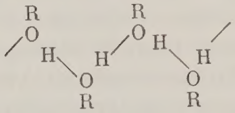

The primary dispersion is most reasonably interpreted as reorientation of the OH dipole by breaking the hydrogen bond with one neighbor and forming it with a new neighbor.

The second higher frequency dispersion appears to be associated with chains also, rather than single molecules or molecules at the ends of chains, the evidence being that its magnitude becomes larger at low temperatures. A possible explanation is that partial orientation of the O-R group can occur by a shift from one to the other of the two oxygen lone pair electron distributions available for hydrogen bonding.

Brot[8] has suggested that the third dispersion at still higher frequencies arises from unbonded molecules or molecules at ends of chains. In recent unpublished work, D.J.Denney has found that dilution of 1-propanol with the non-polar solvent 2-methyl pentane greatly decreases the relative amplitude of the low frequency dispersion. This suggests that one or both of the high frequency dispersions is associated with the increased proportions of single molecules to be expected in dilute solutions, but the evidence is not yet complete enough to make more definite statements.

III. Alkyl Halides

Liquid alkyl halides such as iso-butyl and iso-amyl chlorides and bromides can also be cooled to low enough temperatures (-160 to -100°C) that the dispersion processes occur at frequencies in the range 10 to 10^6 cycles/sec. Under

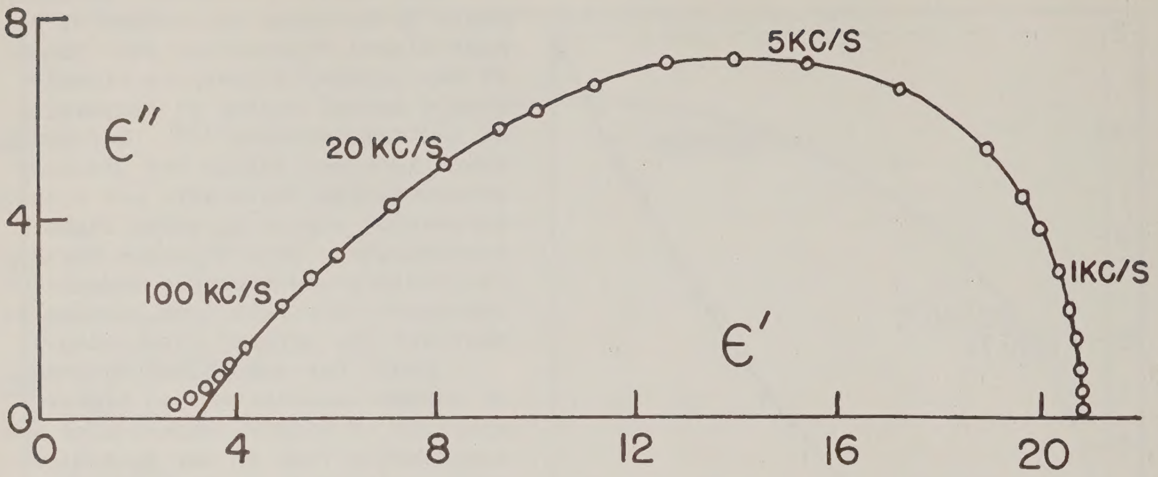

Fig.3. Complex dielectric constant of iso-butyl chloride at -167°C.

these conditions, the relaxation is not described by the simple equation (1), the complex plane locus of ε^* having the typical form shown in Fig.3. This frequency dependence can be described by the equation

$$\varepsilon^* = \varepsilon_1 + \frac{\varepsilon_0 - \varepsilon_1}{(1 + i\omega\tau_1)^\beta} \qquad (3)$$

by choosing values of the parameter β in the range 0.5 to 0.6.

Relaxation effects of the form expressed by Eq.(3) were first established by Davidson & Cole[1c] for glycerol and glycols at relatively low temperatures. These molecules contain two or more OH groups, and it was originally thought that the more complex behavior was related to the great number of ways in which the molecules could be hydrogen bonded to their neighbors. The alkyl halides, however, behave as normal polar liquids, with no reasonable possibility of hydrogen bonding, so other explanations of the relaxation behavior expressed by Eq. (3) are necessary for these liquids, and quite probably for other liquids such as glycols in which show such behavior. About the only common feature in the examples known is the fact that the temperatures are very low, being near or below the freezing points, suggesting that the explanation should be sought in terms of structural effects in interactions of molecules with their neighbors.

The temperature dependence of the relaxation times τ_1 for the alkyl halides is very similar to that found for the alcohols, the slope of the plot of log τ_1 against 1/T increasing rapidly at temperatures below room temperature. This kind of effect is, moreover, not confined to dielectric relaxation, as similar temperature dependences are found for other transport processes at low temperatures. Examples are the viscosities of a variety of liquids[10], mobilities of ions in alcohols and other solvents[11], and the viscoelastic relaxation times of polymer solutions[12]. The great variety of transport processes and of chemical constitution suggests that the only common feature is the low temperature.

The temperature dependence of τ_1 is approximately described by an equation of the form

$$\ln \tau_1 = A + \frac{B}{T - T_\infty}, \qquad (4)$$

where the constant T_∞ is 10 to 15° below the glass transition temperature for the liquid. Ferry[12] found a similar equation for viscoelastic relaxation of polymers, and suggested that a volume dependent activation energy which decreased with expansion of the liquids at higher temperatures could explain the effects. Measurements of dielectric relaxation times in alcohols have been made at constant volume to test this kind of explanation[13]. It was found that the variations of $\ln\tau_1$ with 1/T at constant volume did not satisfy Eq.(2), there still being pronounced curvature of the plot of $\ln\tau_1$ against 1/T. The results indicate the need for a more searching analysis of the mechanisms by which directed mechanical or electrical work can be degraded to thermal energy in liquids at low temperatures.

IV. Solutions

A number of studies have been made recently in our laboratory of solutions of alcohols and alkyl halides with each other and with non-polar solvents, the objectives being to determine how the relaxation effects are changed by addition of a second similar or different kind of molecule.

In mixtures of methanol and 1-propanol[1a], the principal dispersion at low frequencies is still accurately described by Eq.(1) with a simple relaxation time τ_1. In other words, there is no way to recognize, from the data on the principal dispersion, the existence of two kinds of alcohol molecules, even though the relaxation times for the pure liquids differ by a factor 50 or more. The second higher frequency dispersion is, however, clearly spread over a wider range of frequencies in the manner expected for a sum of overlapping contributions from the two kinds of molecules.

Mixtures of two alkyl halides, also studied by D.J.Denney[14], give relaxation effects very similar to those of the pure liquids. The complex plane plots have exactly the same appearance as in Fig.3, the only difference being that the frequency range is between the two widely different ranges for the pure liquids.

When an alcohol and an alkyl halide are mixed, for example 1-propanol and iso-amyl bromide, two distinct dispersion regions are found. The one at lower frequencies has the Debye form (Eq.(1)), while the one at higher frequencies has the form expressed by Eq.(3) and shown in Fig.3. The frequency ranges are similar to those for the pure alcohol and alkyl halide, and the observations are entirely consistent with assuming that the two kinds of molecules contribute quite independently to their respective relaxation processes.

Solutions in non-polar solvents have also been studied, a solvent such as 2-methyl pentane being used to avoid difficulties with freezing. The results for 1-propanol solutions have been mentioned above. Solutions of iso-amyl bromide were investigated to determine the effect of dilution with the non-polar solvent on the broad frequency range of dispersion for the pure polar liquid. Dilution to 0.08 mole fraction of iso-amyl bromide shifted the dispersion to very much higher frequencies by factors from 10^4 to 10^6, but the shape of the dispersion and absorption curves changed only slightly. Thus the rates of reorientation of the polar molecules increase enormously with decreased dipole interaction, but the nature of the interactions giving rise to the broader frequency range of relaxation effects is not significantly affected.

V. Conclusions

The present work has shown dielectric relaxation effects at low temperatures which appear to be quite general in nature, rather than specific to the particular kinds of polar molecules studied. The characteristic temperature dependence of relaxation times is found in a variety of other systems at low temperatures and particularly as the glass transformation and glassy state are approached.

The broad asymmetrical relaxation in alkyl halides giving rise to the skewed arc locus of Fig.(3) seems also to be found in a number of liquids, and one can suspect that similar behavior will be found in other liquids at sufficiently low temperatures. The alcohols show no such behavior, but the simple Debye relaxation at even the lowest temperatures is most probable because it is governed by highly specific hydrogen bonding mechanisms. The reasons for the behavior are not yet understood, but the results of the solution measurements indicate that dipole-dipole interaction is not a major factor.

The results described here relate primarily to liquids well below room temperature. Some of their features, such as the existence of several dispersions in alcohols, appear to remain at room temperature, while others change considerably at higher temperatures. One example of the latter is the temperature dependence of relaxation times, another is the fact that microwave measurements for alkyl halides at room temperature[15] show dispersion much more like simple Debye behavior.

The available data for polar liquids at and not far below room temperature are as yet too incomplete to define the dielectric behavior adequately, and more measurements at intermediate temperatures over wide ranges of frequency are needed. Other studies needed are of solutions in non-polar solvents over wider ranges of temperature, frequency, and concentration.

Chemistry Department,
Brown University,
Providence, R.I.

References

1.a. Methanol, D.J.Denney and R.H.Cole, J.Chem.Phys., 23, 1767 (1955);
b. Ethanol and 2-Propanol, F.X.Hassion and R.H.Cole, J.Chem.Phys, 23, 1756 (1955);
c. 1-Propanol, D.W.Davidson and R.H.Cole, J.Chem.Phys., 19, 1484 (1951);
d. Butyl Alcohols, W.Dannhauser and R.H.Cole, 23, 1762 (1955).
2. R.H.Cole and P.M.Gross, Jr., Rev.Sci.Inst., 20, 252 (1949).
3. S.E.Lovell & R.H.Cole, to appear in Rev.Sci.Inst.
4. L.Onsager, J.Am.Chem.Soc., 58, 1486 (1936).
5. G.Oster and J.G.Kirkwood, J.Chem.Phys., 11, 175 (1943).
6. K.S.Cole and R.H.Cole, J.Chem.Phys, 9, 341 (1941).
7. R.H.Cole and D.W.Davidson, J.Chem.Phys., 20, 1389 (1952).
8. C.Brot, Thesis, Paris (1956). See also Mayat, Brot and Reinisch, Kolloid Zeits., 134, 101 (1953).
9. F.X.Hassion and R.H.Cole, Nature, 172, 212 (1953).
10. G.Taummann and W.Hesse, Z.Anorg.Allgem Chem., 156, 245 (1926).
11. Kobeho, Kuvshinski and Shishkin, J.Tech.Phys., USSR, 5, 413 (1938).
12. Williams, Landel and Ferry, J.Am.Chem.Soc., 77, 3701 (1955).
13. Gilchrist, Earley and Cole, J.Chem.Phys., 26, 196 (1957).
14. D.J.Denney, J.Chem.Phys, 27, 259 (1957).
15. Hennelley, Heston and Smyth, J.Am.Chem.Soc., 70, 4093 (1948).

ON THE DIELECTRIC DISPERSION OF SOME ALIPHATIC ALCOHOLS*

- M.Magat & C.Brot

1. Introduction

In 1944, Bauer[1], in developing a theory of dielectric dispersion in solids and liquids, called attention to the appreciable difference between the critical frequencies of water and ice at the melting point: whereas the critical wavelength λ_c is $4 \cdot 10^6$ cm in ice, it is only 3 cm in water at the same temperature. This disparity is all the more incomprehensible in view of the fact that according to the available data (x-rays, Raman and infrared spectra) the structure of water in the vicinity of a molecule differs little from that of ice. Bauer concluded that the mechanisms responsible for the dispersion must be different and that this difference is connected with the existence of long-range order in ice and its absence in water.

Here is the explanation proposed by Bauer, which, as we shall see, appears to be valid at least for liquids in which hydrogen bonds are important:

The position and orientation of the molecules in a crystal are fixed in a more or less permanent manner by the lattice. Reorientation of a molecule must occur in the field of its neighbors and it is possible to calculate with good approximation the height of the potential barrier (activation energy for dispersion) by means of an electrostatic hydrogen bond model[1,2].

In contrast, a characteristic feature of liquids is the limited lifetime of the microcrystalline structures surrounding a given molecule, microcrystalline structures that form and break up within a relatively short time. If the lifetime of these structures is shorter than the period of rotation in the crystal, the molecule becomes "free" before it can turn in the crystal field. If the period of rotation of a "free" molecule is very short compared to the lifetime of the crystalline complex, and we shall see that this is indeed the case, obviously the lifetime of the crystalline complexes will determine the orientation (or relaxation) time of a molecule. In other words, whereas in crystals the dispersion frequency will be determined by the molecular reorientation time in associated liquids the relaxation time will be determined by the lifetime of the microcrystalline complexes.

Bauer[1] further noted that the libratory movement (rotary oscillation) can also contribute to the polarization as long as the frequency of the external field is lower than the libration frequency, which for most liquids associated by hydrogen bonds lies in the far infrared and is temperature independent. The theory of this libration dispersion, which was termed resonance dispersion by Frölich[3], was developed in greater detail by this author some years later.

It was found that in liquids with a not excessively high molecular weight the polarization associated with libration is the factor responsible for the greater part of the disparity observed between ϵ' for very short wavelengths and n_D^2.

Back in 1945, Girard & Abadie[4] published a study of the dielectric dispersion of some alcohols, including octanol and decanol, in a wide range of frequencies - from 50 cps to 10 000 Mc - and noted that these substances are characterized by not one but two dispersion regions. At about the same time measurements (not published), carried out by one of us (M.M.) in the laboratory of Prof. Smyth, on the temperature dependence of the dielectric constant of octanol at 10 cm showed that the dispersion of this substance also had a complex character.

---

*Translated from the French. We take this opportunity to thank MM. Magat and Brot for providing a copy of the original and for permission to publish this translation. Translation Editor.

These experimental results and the theoretical considerations set forth above, led Bauer, Magat and a number of other investigators (Refs.5-10) to undertake a systematic experimental study of the dispersion of alcohols from C_4 to C_{12} in a wide range of frequencies (50 cps to 25 000 Mc) and temperatures (-50 to +50°C). These results together with the results of Lebrun[11] and Cole and his co-workers[12-15] have been analyzed and interpreted in the doctorate thesis of one of us (C.B.). A more detailed description of the results and calculations that we shall mention below will be found in this publication[10].

2. Experimental Results

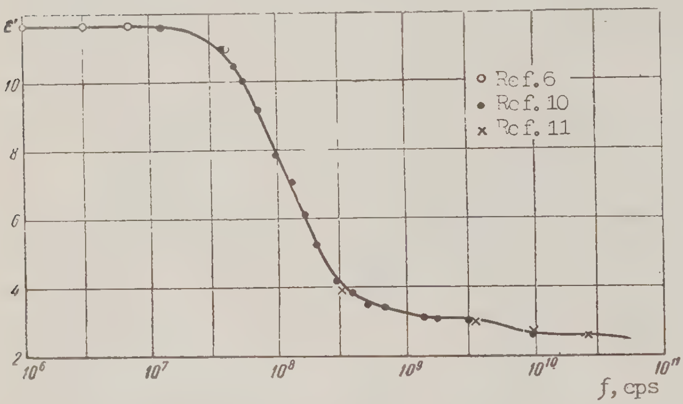

Fig.1. Frequency dependence of ϵ' for 1-n-heptanol at 20°.

It follows from all the cited investigations as well as from earlier studies that all the alcohols up to C_{12} have in the liquid state not two but three relaxation regions, the precise positions of which depend on the temperature and the length of the carbon chain; we shall distinguish these regions as the meter, decimeter and centimeter wavelength regions.

By way of illustration in Fig.1 we give the frequency dependence of the real part of the dielectric constant for heptanol; in Fig.2 the variation of ϵ' with ϵ''/λ for the same alcohol, as given by Cole[19]. There are evident in Fig.2 three straight line sections corresponding to the three distinctive dispersion regions. It will be evident that at the end of the third dispersion region the dielectric constant ($\epsilon_{\infty 3}$) for heptanol is still 2.28, whereas $n_D^2 = 2.02$, which indicates the existence of other dispersion regions. It may be noted that $\epsilon_{\infty 3}$ varies with the temperature only because of variation in density, this variation obeying the Lorentz-Lorentz relation

$$\frac{\epsilon_{\infty 3} - 1}{\epsilon_{\infty 3} + 2}\cdot\frac{M}{d} = C^{te}$$

From this we conclude that the difference $\epsilon_{\infty 3} - n_D^2$ must be due to libration and atomic polarization. Some absorption in the far infrared (50-150 μ) was actually observed by Sack & Errera[16]. No interpretation of this effect was proposed by the authors, but by analogy with the infrared dispersion of water observed by Rubens & Ladenburg[17] and by Cartwright[18] and which is situated at frequencies corresponding to the Raman bands associated with intermolecular librations and vibrations, we can conclude that in the case of alcohols we are dealing with the same mechanism.

The critical frequencies of the three regions of dispersion increase with temperature. Moreover, increase in temperature results in a reduction of the "width" ($\epsilon_{01} - \epsilon_{\infty 1}$) of the meter wavelength region and in an increase of the "width" of the centimeter region.

Upon freezing, the three dispersion regions are replaced by a single dispersion region located at a lower frequency range. Thus for liquid heptanol λ_{cl} = 60 cm, in liquid heptanol λ_{cl} = 3000 m. On the other hand, $\epsilon_{\infty solid} \approx$

Table 1

Substance	E_1 Kcal	S_1	Substance	E_1 Kcal	S_1
C_3H_7OH	5,3	+2,1	$C_7H_{15}OH$	8,5	+10,9
n-C_4H_9OH	7,8	+11,0	*n*-$C_8H_{17}OH$	8,9	+11,9
iso-C_4H_9OH	6,8	+6,5	*n*-$C_8H_{17}OH$ (*d*)	8,6	+10,9
n-$C_5H_{11}OH$	8,8	+13,3	2-$C_8H_{17}OH$	12,2	+23,2
iso-$C_5H_{11}OH$	8,9	+13,6	$C_9H_{19}OH$	9,9	+15,0
$C_6H_{13}OH$	8,3	+10,9			

Table 2

R	E_3		S_3	
	R — Br	R—OH	R — Br	R—OH
C_6H_{13}	2,29	1,9	—1,6	+2,4
C_7H_{15}	2,36	2,3	—1,8	+1,6
C_8H_{17}	2,29	2,3	—2,4	+2,3
C_9H_{19}	2,34	2,5	—2,7	+3,2

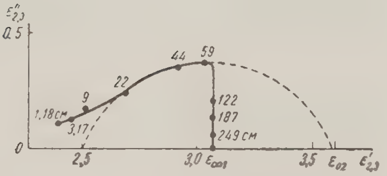

Fig.3. Cole-Cole diagram for nonanol at 0°C. $\epsilon^*_{2,3} = \epsilon^*_{exp} - \epsilon^*_1$.

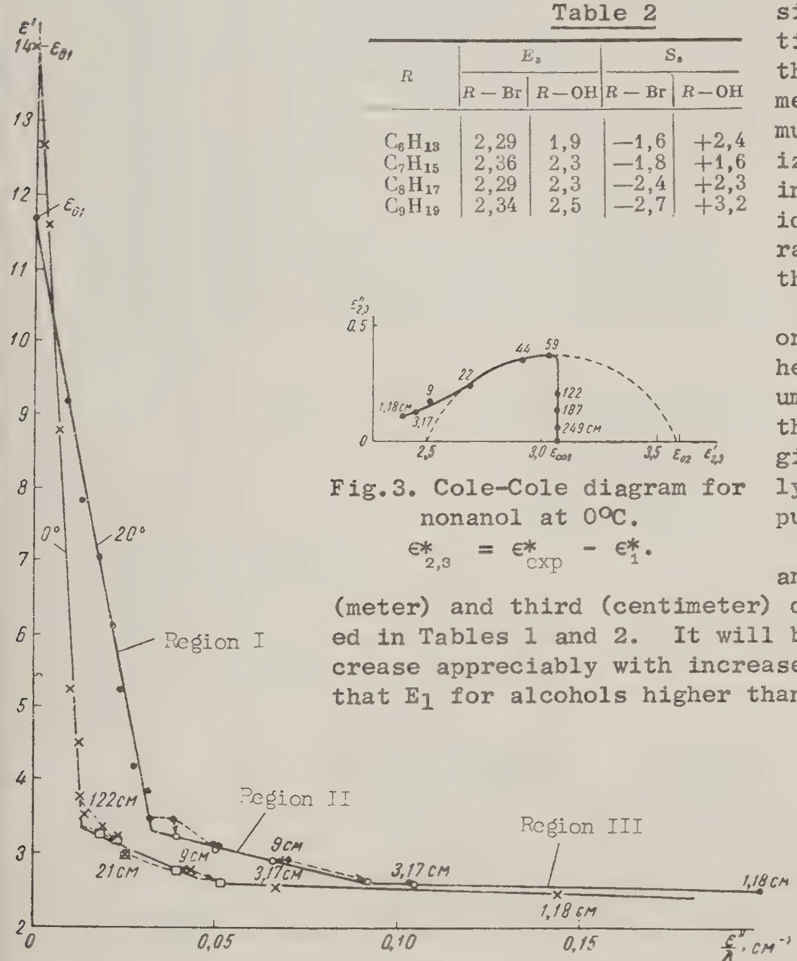

Fig.2. Variation of ϵ' with ϵ''/λ for 1-n-heptanol according to Cole.

$\approx \epsilon_{\infty 3}$liquid, which is consistent with the above mentioned hypothesis regarding the nature of the submillimeter dispersion domain inasmuch as the libration polarization is no doubt the same in the solid and in the liquid state because the short range order is the same in the two states.

On the other hand, if one dilutes the heptanol in heptane (1% alcohol by volume)^{10} there remains only the centimeter dispersion region, located at approximately the same frequency as in pure heptanol.

The activation energies and entropies for the first (meter) and third (centimeter) dispersion regions are listed in Tables 1 and 2. It will be seen that E_1 and S_1 increase appreciably with increase of the chain length and that E_1 for alcohols higher than propanol is greater than the hydrogen bond energy.

In contrast, E_3 and S_3 increase but little with increase in chain length. E_3 is close to the value for the corresponding bromide hydrocarbons. The indicated values for S_3 are only approximate in view of the appreciable uncertainty in the experimental results and the small magnitude of this parameter; however, the sign is opposite to that of the activation entropy of the corresponding bromide compounds. Moreover, E_3 is not very different from the viscosity activation energy of the neighboring hydrocarbons. The second dispersion region (the decimeter wavelength region for alcohols with a medium chain length at ambient temperature) differs appreciably from the two other regions: thus whereas the meter and centimeter regions are characterized by the "classic" diagrams of Cole & Cole, the diagram for the second region has an entirely different appearance as may be seen in Fig.3. We shall return to this point below.

First, however, we want to propose an interpretation for the metric and centimetric dispersion domains and indicate the deductions we can draw therefrom.

3. Liquid Alcohol Model

On the basis of spectroscopic, x-ray diffraction and similar data one must admit that liquid alcohols are composed of "free" molecules or monomers and of molecules bound in associated structures. These complexes represent chain polymers linked by hydrogen bonds (see Fig.4). These chains of finite length differ from conventional polymer chains by the fact that their lifetime is relatively short. They break up and reform at a certain rate which we shall calculate below. But as long as a chain exists it possesses a certain rigidity and rotation about the hydrogen bonds is not free; the configuration of a chain can be calculated, for example, by means of the equations deduced by Sardon and Benoit for polymers with chemical bonds. On the other hand, for each temperature and degree of dilution there will be a corresponding "polymerication equilibrium" which will determine the mean length of the chains (degree of polymerization DP).

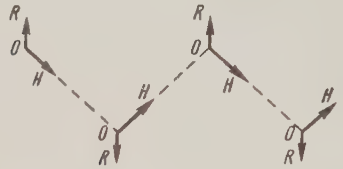

Fig.4

Simple calculations[19] show that if α is the fraction of molecules in the monomer state the dissociation equilibrium constant is

$$K = \frac{\alpha C}{1 - \sqrt{\alpha}}$$

(here C is the concentration in mole/liter), and the total number of polymers of all orders (including monomers) per liter will be $C\sqrt{\alpha}$. Only "free" molecules and the molecules situated at the end of a chain will be able to reorient rapidly, while the reorientation of the dipoles located in the middle of the chain will involve reorientation of whole segments and consequently will be a relatively slow process.

4. Interpretation of the Centimeter Dispersion Region

The behavior of this region as a result of freezing, the high frequencies at which it is located, and the variation in its location with temperature and dilution, all indicate that it corresponds to the relaxation of molecules capable of reorienting rapidly, i.e., free molecules and molecules located at the ends of chains with an unlinked OH dipole. The number of these molecules can be calculated by means of the Frölich equation

$$g\mu^2_{\mathrm{OH}} = \frac{9kT}{4\pi N}\cdot\frac{M}{d}\cdot\frac{(2\varepsilon_{03} - \varepsilon_{\infty 3})(2\varepsilon_{03} + \varepsilon_{\infty 3})}{9\varepsilon_{03}}\left(\frac{3}{\varepsilon_{\infty 3} + 2}\right)^2,$$

where μ_{OH} is the permanent dipole moment (for orientation in vacuum $\mu_{OH} = 1.5$ D), k is Boltzmann's constant, T is the absolute temperature, M is the molecular weight, d is the density, and g is the Kirkwood correlation parameter, which is equal to unity for molecules capable of free orientation. We introduce the parameter $p = N/Na$ (N is Avogadro's number) to indicate the fraction of freely reorienting molecules. This parameter can be calculated by means of the above formula. Inasmuch as there is one freely orienting molecule per polymer chain

Table 3

Substance	T, °C	α	$\overline{DP} = 1/\sqrt{\alpha}$	K	g_{theo}	g_{exp}
$C_6H_{13}OH$	35	0,052	4,4	0,536	2,42	2,58
	0	0,017	7,7	0,161	2,91	2,92
	—50	0,0017	24,0	0,0155	3,50	3,2
$C_7H_{15}OH$	50	0,067	3,9	0,625	2,34	2,39
	20	0,0306	5,7	0,263	2,72	2,80
	0	0,0152	8,1	0,125	2,95	3,0
	—15	0,0086	10,8	0,069	3,13	3,13
	—35	0,0034	17	0,027	3,37	3,30
$C_8H_{17}OH$	50	0,071	3,75	0,596	2,31	2,39
	20	0,0312	5,65	0,24	2,72	2,77
	0	0,016	7,9	0,118	2,93	2,99
	—15	0,0088	10,6	0,0566	3,12	3,10
$C_9H_{19}OH$	50	0,071	3,75	0,54	2,31	—
	20	0,0318	5,6	0,221	2,66	2,70
	0	0,016	7,9	0,107	2,93	2,98
$C_{10}H_{21}OH$	25	0,044	4,8	0,293	2,44	2,46

(we recall that a monomer is regarded as a polymer of order $n = 1$), the number of such freely orienting molecules will be equal to the total number of polymers; consequently, at a given concentration C the number will be equal to $C\sqrt{\alpha}$ from which it follows that $p = \sqrt{\alpha}$. Then by definition the mean degree of polymerization $\overline{DP} = 1/\sqrt{\alpha} = 1/p$.

Table 3 lists the values of α, $\overline{DP}$ and K derived from dielectric measurements carried out in our laboratory. The values of K for 200°C are in good agreement with the values of the equilibrium constant calculated by Mecke & Kreutzer[20] for ethanol, propanol and butanol on the basis of the infrared spectra of these alcohols in CCl_4 (0.30 to 0.34). The value calculated by Goggeshall & Saier[21] (also on the basis of infrared data) for octanol is K = 0.35 mole/liter, which is slightly higher than our value.

On the basis of the plot of log K as a function of 1/T we can calculate the energy of dissociation of the hydrogen bonds in alcohols. The value found in this manner, namely, 5.8 kcal/mole is in good agreement with the value of 6 kcal given by Pauling[22] and Ketelaar[23] as well as the value of 6.0 kcal derived by Weltner & Pitzer[24] on the basis of the specific heat of metanol in the vapor state, and is not far from the value of 5.4 ± 0.5 kcal deduced by Hoffman[25] from the intensity of the infrared absorption of butanol.

This agreement substantiates our hypotheses.

It will be evident from Table 3 that the association polymer chains are short (5 to 8 links at 20°); consequently, a priori calculations of the factor g based on the assumption that the chains are infinitely long cannot and, as a matter of fact, does not lead to true values of this factor.

5. Interpretation of the Meter Dispersion Region
Kinetics of association

We assume, following the hypothesis of Bauer[1], that the relaxation time τ_1 corresponding to the first dispersion domain (the meter region for medium alcohols) depends on the lifetime of the complexes. In this case $1/\tau_1$ is equal to the rate k_d of dissociation of the complexes.

For propanol the value of k_d derived in this manner is in agreement with that found by Maier[27] on the basis of ultrasonic dispersion.

Thus we now know, on the one hand, the equilibrium dissociation constant K and, on the other hand, the rate of dissociation of the complexes. Consequently, we can readily calculate the association rate constant k_a by means of the obvious relation: $K = k_d/k_a$.

The association constant k_a is only weakly dependent on the length of the carbon chains. At 20°C this constant is of the order of $2 \cdot 10^9$ liter mole^{-1} sec^{-1}. The corresponding activation energies - 2.24 kcal/mole for heptanol, for example - are low and of the order of magnitude of the viscosity activation energy; this is not surprising since one expects the process of association, not having its own activation energy, to depend only on the viscosity of the medium (consisting of the neighboring hydrocarbon chains).

Arrhenius' constant is of the order of $5 \cdot 10^{-11}$; consequently, the steric factor is small. Knowing k_a and the concentration of freely orientable molecules, we can calculate the lifetime of molecules of this type. For our theory to be free of internal contradictions it is necessary that the lifetime calculated in this manner be greater than the molecular relaxation time. It can easily be shown that this is the case: for heptanol at 20°, for example, we find that the lifetime of a free molecule is of the order $3.2 \cdot 10^{-10}$ sec, while its relaxation time is about $4 \cdot 10^{-12}$ sec. Similar relations obtain for all the alcohols investigated.

6. Static Dielectric Constant

Knowing the length and "rigidity" of the associated polymer chains, we can calculate the correlation factor g for alcohols to a closer approximation than was done by earlier authors[26] who assumed that the chain length is infinite and temperature independent and that there obtains free rotation about the H bonds; they obtained $g = 2.40$, which is the value originally obtained by Cole & Dannhauser[14]. These last authors subsequently took into account the finite length of the polymer chains, which led them to values of g which, although too low in absolute magnitude, decrease with increasing temperature, as is the experimental case.

In our case, since we knew the average chain length, we could calculate the mean quadratic electric moment of the chains also taking into account their relative "rigidity". To this end, we introduced, following Sadron[28] and Benoit[29,30] a parameter η which takes into account the fact that the trans position is favored in the polymers in question, probably because of a steric effect. We found that a single value of η is sufficient for all the alcohols and all the temperatures involved to bring into satisfactory agreement the calculated values of g with the experimental values. This will be evident from the last two columns of Table 3.

7. Tentative Interpretation of the Intermediate Decimeter Dispersion Region

We indicated above that this dispersion region does not have the classical shape. It must be noted also that when one attempts to analyze the experimental data pertaining to this region, one finds that the accuracy attained is low due precisely to the fact that this region is intermediate between the two other regions and to the fact that the contributions of ϵ' and ϵ'' must be obtained by subtraction. Fig.3 shows the Cole-Cole diagram for $\epsilon'' = f(\epsilon')$ obtained by subtracting from the experimental values the values of $\epsilon'_1 - \epsilon_{\infty 1}$ and ϵ''_1 for the first region, these having been determined on the basis of measurements at a lower frequency. One thus obtains the joint contributions of the second and third regions, contributions which we have designated $\epsilon'_{2,3}$ and $\epsilon''_{2,3}$. There will be seen in Fig.3 on the low frequency side of the region under consideration an abrupt drop of the point representative of ϵ^*, although it would seem that in extrapolating towards low frequencies the curves should tend to a value ϵ_{02} which is larger than $\epsilon_{\infty 1}$; this is a rather surprising effect.

In 1956 one of us[31] proposed an interpretation of anomalies of this type. Although as we have indicated the relative errors in analysis of regions of this type are very appreciable, we have assumed that the effect is real and that it is not due to experimental errors exceeding the estimated uncertainty. Incidentally, we note that recently other authors report having observed dispersions for which the high frequency limit of one region is lower than the low frequency limit of the next region: thus Wemelle[32] observed such overlapping for ethyl-2-hexanol and Moriamez[33] observed it for 1,3-butane-diol (for this substance at 20°C, $\epsilon_{\infty 1} = 9.2 \pm 0.2$, while $\epsilon_{02} = 10.2 \pm 0.2$).

The interpretation we propose is the following: it is usually assumed, at least implicitly, that the contributions from different dispersion regions are linearly additive, which is equivalent to assuming that the relaxation processes responsible for each of these regions occur in parallel and independently of each other. We, on the contrary, assume that the relaxation processes occur not in parallel but in series, that is to say, that the development of one process conditions and determines the development of the next, etc.

We shall attempt to show in simplified form how such processes in series can lead to the anomaly mentioned above.

Assume that n_0 electric dipoles are initially in a state I and that they can go over after a certain mean time τ_I into state II, this transition constitutes the first relaxation process. Suppose further that the orientations of the dipoles are blocked in state I, but that after they have gone over into state II they can reorient with an orientation time τ_l; this constitutes the second relaxation process, the development of which obviously depends on the course of the first process.

Assume that we have applied an electric field to the system and that we cut off the field at the instant $t = 0$; if p_0 is the contribution to the macroscopic polarization made by one of the dipoles, the total polarization at the instant $t = 0$ will be $p_0 n_0$.

At the instant t, there will be $n_0 e^{-t/\tau_I}$ dipoles remaining in position I, and their contribution to the polarization will be $p_0 n_0 e^{-t/\tau_I}$. On the other hand, there will be $n_0(1 - e^{-t/\tau_I})$ dipoles in position II; each of them, if it has gone over from I to II at a certain instant $u\,(0 < u < t)$ contributes to the polarization to the extent of $p_0 e^{-\frac{t-u}{\tau_l}}$. Then the total polarization at the instant t is

$$P = p_0 n_0 e^{-t/\tau_I} + \int_0^t p_0 e^{-\frac{t-u}{\tau_l}} \frac{d}{du} n_0 (1 - e^{-\frac{u}{\tau_I}})\, du = \frac{p_0 n_0}{\tau_I - \tau_l} (\tau_I e^{-t/\tau_I} - \tau_l e^{-t/\tau_l}).$$

Thus we have obtained two decreasing exponential functions, one of which has a negative coefficient. If we now go over to a sinusoidal field and formally carry out the classical calculations, we again encounter this negative coefficient in the form of a "negative" dispersion region $-\frac{B}{1 - i\omega\tau_l}$ which will be located between the usual regions (a more complete calculation shows that in this subtraction of the "negative" regions, ϵ'' remains positive, and ϵ' decreases with increasing frequency, as in the classical case). It can readily be seen that the coefficient in the expression above must be equal exactly to the difference $\epsilon_{02} - \epsilon_{\infty 1}$.

In the case of alcohols we believe that position I is that wherein the dipoles in the central portion of the polymers have their reorientation virtually blocked, while position II is the position of these same dipoles when they are located close to the end of a chain, and the transition I→II involves the rupture of a neighboring hydrogen bond. In state II these dipoles can reorient with a time τ_l by "viscous" rotation of the segment of the chain in which they are held.

Thus we see that the structure of the decimetric dispersion is complex; it includes a contribution from dipoles going over into the orientable state characterized by τ_l and also from dipoles that are already close to chain ends and reorient with a close time. It is probable that the reorientation of the OR dipoles linked in the hydrocarbon chains also makes some contribution to the dispersion.

Université de Paris
Paris 5^e, France

References

1. E.Bauer, Cahiers phys., 1, Nos.20 & 21 (1944).
2. M.Magat, Compt.rend., 196, 1981 (1933).
3. H.Fröhlich, Theory of Dielectrics, Oxford, 1949.
4. P.Girard & P.Abadie, Bull.Soc.Chim. de France, 12, 207 (1945); Trans. Faraday Soc.A, 42, 40 (1946).
5. R.Dalbert & M.Magat, Surdut, Colloque CNRS XVII, 1948.
6. C.Oppenheim, J.Chim.Phys., 48, 377 (1951).
7. R.Dalbert, J.Chim.Phys., 50, 329 (1953).
8. L.Reinisch, J.Chim.Phys., 51, 113 (1954).
9. M.Bruma, Thèse Ingénieur Docteur. Paris, 1952.
10. C.Brot, Ann.phys. (Fr) (1955); Ibid., 13, 714 (1957).
11. A.Lebrun, Ann.phys. (Fr.), 10, 16 (1955).
12. R.H.Cole & D.W.Davidson, J.Chem.Phys., 20, 1389 (1952).
13. R.H.Cole & F.X.Hassion, Nature, 172, 213 (1953).
14. R.H.Cole & W.Dannhauser, J.Chem.Phys, 23, 1762 (1955).
15. R.H.Cole, J.Chem.Phys., 23, 493 (1955).
16. J.Errera, Phys. 5, 304 (1924).
17. H.Rubens & R.Ladenburg, Verhandl. Verh. Deutsche Phys. Ges., 11, 25 (1909).
18. C.H.Cartwright, Nature, 135, 872 (1935); 136, 181 (1935); Phys.Rev., 49, 490 (1936).
19. Mecke & Kempter, Z.Phys., 46, 229 (1940).
20. Mecke & Kreutzer, Z.phys.Chem.B 49, 309 (1941).
21. N.D.Goggeshall & J.Saier, Amer.Chem.Soc., 75, 5414 (1951).
22. Pauling, The Nature of Chemical Bond. New York, 1945.
23. J.A.Ketelaar, Chemical Constitution. Amsterdam, 1953.
24. K.Weltner & K.S.Pitzer, J.Amer.Chem.Soc., 73, 2606 (1951).
25. Hoffman, Z.phys.Chem., 53, 179 (1943).
26. J.G.Kirkwood & G.Oster, J.Chem.Phys., 11, 175 (1943).
27. W.Maier, Symposium on Hydrogen Bonding. Ljubljana, 1957. (Pergamon, London).
28. Ch.Sadron, J.Chim.Phys., 43, 145 (1946).
29. H.Benoit, J.Chim.Phys., 44, 18 (1947).
30. H.Benoit, J.Polym.Sc., 3, 376 (1948).
31. C.Brot, J.Chim.Phys., 53, 541 (1936).
32. R.Wemelle, Compt.rend., 244, 775 (1957).
33. C.Moriamez, Colloque Ampère 1958, to be published in Archives des Sciences, Geneva.

DIELECTRIC CONSTANT OF DIELECTRIC LIQUIDS IN STRONG ELECTRIC FIELDS*

- A.Piekara

When a strong electric field is applied to a gas or liquid comprised of polar molecules there is observed a dielectric saturation effect evinced by a change of the dielectric constant ϵ. This effect, which was predicted and calculated by Debye first for gases[1] and then for liquids[2], was observed for the first time by Herveg[3] in ethyl ether. A chronological listing of subsequent researches is given in the table below. (The dashes in the table indicate that the measurements were impossible because of high electric conductivity.)

Ref.	Authors	Procedure	Ethyl ether	Nitro-benzene	Water & alcohols
3	J.Herveg (1920)	beats (audio)	$\Delta\epsilon < 0$	---	---
4	J.Kautzsch (1928)	beats (audio)	$\Delta\epsilon < 0$	---	---
5	J.Malsch (1928)	spark		$\Delta\epsilon < 0$	$\Delta\epsilon < 0$
6	H.Gundermann (1930)	spark	$\Delta\epsilon < 0$		$\Delta\epsilon < 0$
7	A.Piekara (1936) & B.Piekara	resonance	$\Delta\epsilon < 0$	$\Delta\epsilon > 0$	---
8	A.Piekara (1939) & Lempicki	beats (oscil.)	$\Delta\epsilon < 0$	$\Delta\epsilon > 0$	---
9	A.Piekara (1956) & A.Chelkowski	beats (oscil.)	$\Delta 2 < 0$	$\Delta\epsilon > 0$	---

It will be evident from the table that the decrease of the dielectric constant of nitrobenzene reported by Malsch[5] was not substantiated: in 1936 we[7] established that in highly purified benzene $\Delta\epsilon$ is positive, i.e., the dielectric constant of pure nitrobenzene increases in an external electric field. At the same time we found that, owing to electric conduction, the temperature of insufficiently purified nitrobenzene increases, which leads to a decrease of the dielectric constant; this phenomenon, however, has nothing to do with the effect of dielectric saturation. Subsequently, the effect of positive dielectric saturation ($\Delta\epsilon > 0$) was observed in purified nitrobenzene and a number of other liquids by Chelkowski.[10]

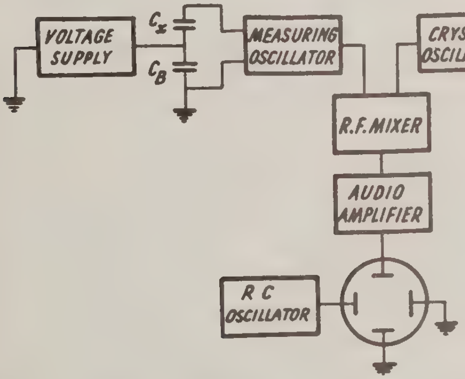

Fig.1. Block diagram of the experimental arrangement for measurement of $\Delta\epsilon = \epsilon - \epsilon_0$ (ϵ_0 is the normal dielectric constant of the investigated liquid filling the capacitor C_x; ϵ is the dielectric constant of the same liquid under the influence of the applied external field).

The arrangement used in our experiments is diagramed in Fig.1. The two oscillators, one of which is the measuring oscillator with variable frequency, and the other the reference oscillator stabilized at ~1 Mc by a quartz crystal, give audio frequency beats which after detection and amplification are applied to one pair of the deflecting plates of a cathode-ray oscillograph. A voltage of the same frequency from an RC oscillator is applied to the other pair of plates. Thus there appears a stationary ellipse on the oscillograph screen. The capacitor C_x containing the test liquid forms a part of the measuring oscillator circuit. Upon application of the voltage from an external source, there occurs a change in frequency, which is then compensated by a special calibrated low capacitance capacitor.

---

*Translated from the amplified French version. We take this opportunity to thank Dr. Piekara for supplying the French reprint and for permission to print the translation. Translation editor.

One of the special capacitors used in our measurements is shown in Fig.2. This capacitor is made of stainless steel; the internal plate is located inside the hollow cylinder. The capacitor is mechanically strong and its design allows of introduction of the test liquid by vacuum distillation.

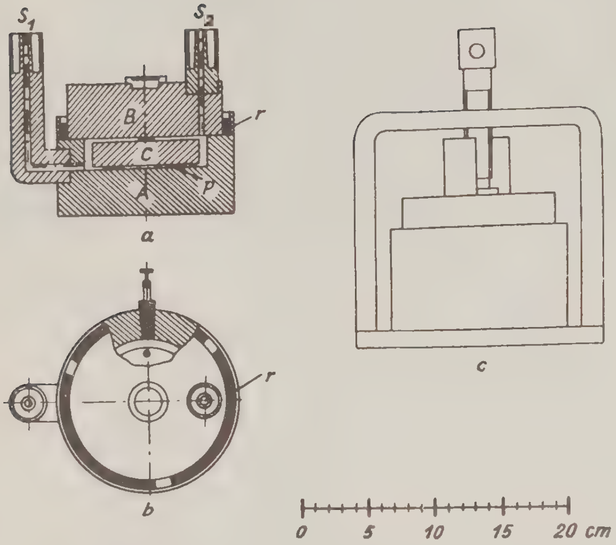

Fig.2. One type of liquid capacitor.

Of particular interest from the standpoint of the mechanism of the dielectric saturation effect in the liquid is the variation of $\Delta\epsilon$ in solutions of polar liquids in nonpolar solvents for which $\Delta\epsilon = 0$. According to our experiments, there exist three different types of dielectric saturation effect (Fig.3):

1. Negative effect ($\Delta\epsilon < 0$). This effect occurs in pure liquids and in solutions of any concentration; it was observed, for example, in ether, ethyl bromide, o-nitroanisole and other liquids.

2. Positive effect with inversion. In this case $\Delta\epsilon > 0$ in the pure liquid but changes sign below a certain concentration in solutions; this is the case, for example, for nitrobenzene as well as ortho- and meta-nitrotoluene.

3. Positive effect without inversion. In this case $\Delta\epsilon > 0$ both in the pure liquid and in solutions of any concentration in a nonpolar solvent. The positive effect without inversion was observed, for example, in 1,2-dichloroethane and 1,2-dibromoethane.

An explanation of the molecular mechanism responsible for the positive effect with inversion was proposed by the writer[11,12] in 1937. The interpretation is based on the assumption that the nearest neighbor molecule plays an important role in the molecular interaction of a given molecule with the medium. In a liquid such as nitrobenzene, the molecules of which are strongly polar, there form temporary molecular pairs. Their coupling energy W is a minimum for the antiparallel arrangement of the molecular dipoles. The effect of an external electric field is to reduce on the average the angle between the dipoles, which leads to an increase of the effective moment of the pair and hence to an increase of the dielectric constant of the liquid. If this increase exceeds the decrease of the dielectric constant due to orientation there will be observed a positive saturation effect.

This hypothesis leads to the following formula for the mean value of the static component of the dielectric moment of the molecule in the direction of the field vector:

$$< m_E > = \frac{\mu^2 F}{3kT} R_p - \frac{\mu^4 F^3}{45k^3 T^3} R_s, \tag{1}$$

where F is the strength of the internal field. Here the "correlation factors" of the polarization (R_p) and the saturation (R_s) are described by the following relations:

$$R_p = 1 - L, \tag{2}$$

and

$$R_s = 6\frac{L}{y} - (1 - L)(1 + 5L), \tag{3}$$

where $L = L(y)$ is the Langevin function of the variable

$$y = \frac{W}{kT}, \tag{4}$$

the coupling energy expressed in dimensionless units.

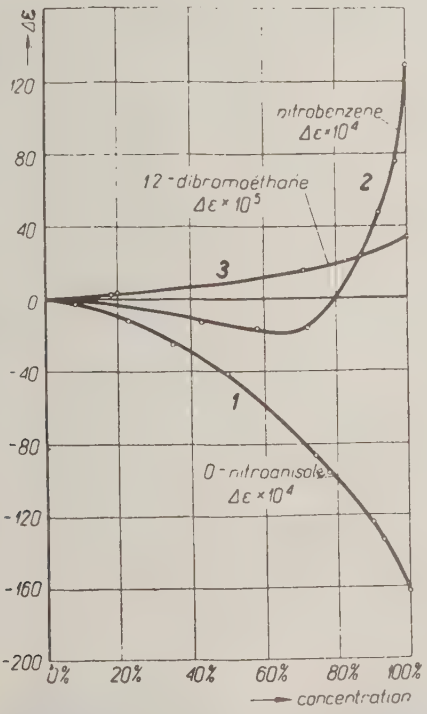

Fig.3. Three types of saturation effect observed in solutions of polar liquids in nonpolar solvents: 1) negative effect (ether, o-nitroanisole, etc.), 2) positive effect with inversion (nitrobenzene, ortho- and meta-nitrotoluene), 3) positive effect without inversion (1,2-dichloroethane, 1,2-dibromoethane, etc.). External electric field E = 60 kv/cm.

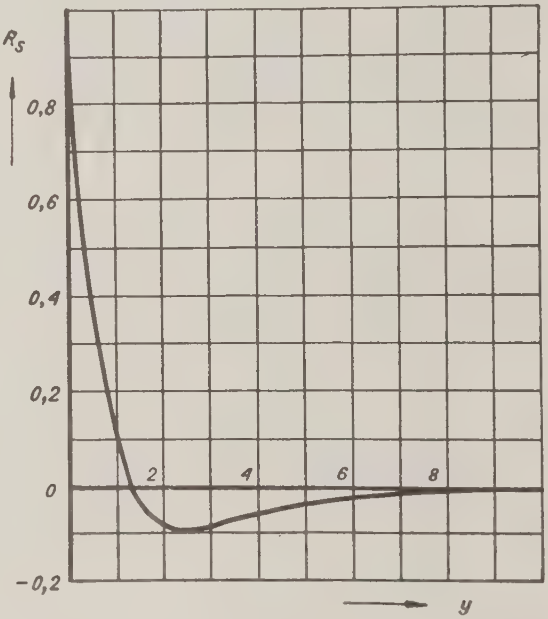

Fig.4. Variation of the saturation correlation factor R_s as a function of the dipole coupling energy y.

The variation of R_s as a function of the coupling energy y is shown in Fig.4. It will be seen that the saturation correlation factor changes sign at $y = 1.33$. This explains the existence of the positive effect with inversion, for y increases with the concentration. Comparison of the theoretical and experimental results gives very good agreement not only as regards the saturation effect but also as regards polarization effects associated with molecular orientation such as electric and magnetic birefringence[13,14].

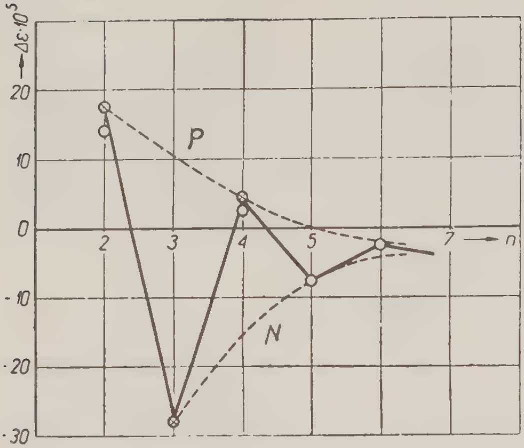

Fig.5. Variation of $\Delta\epsilon$ in 1,n-dichloroalkanes (⊗) and 1,n-dibromoalkanes (○) as a function of the number n of carbon atoms in the chain; measurements of Chelkowski[15]. External field E = 35 kv/cm.

The fact that the sign of the positive dielectric saturation effect without inversion does not depend on the concentration, i.e., is independent of the distance between the polar molecules in solution, indicates that we have here an intramolecular phenomenon. Thus, in 1,2-dichloroethane $H_2\underset{Cl}{C}—\overset{Cl}{C}H_2$; there are two polar groups that can rotate about the C-C bond. This is, however, a case of hindered rotation because the trans configuration (antiparallel dipoles) corresponds to a minimum of the potential energy. Thus this situation resembles that obtaining for pairs of molecules in nitrobenzene with the difference that in this case the coupled dipoles are part of the same molecule; as a result, any increase in dilution cannot substantially influence the coupling energy of the Cl-Cl moments and thus change the sign of $\Delta\epsilon$.

In the series of 1,n-dihalogen derivatives of alkanes the separation between the moments of the C-Cl (or C-Br) bonds increases with the number of carbon atoms in the chain. With a view to determining whether increase of the distance between the C-Cl bonds (which is equivalent to reduction of the coupling energy of their moments) induces a change in the sign of the saturation effect to make it negative, Chelkowski[15], working in our institute, measured the effect in a series of 1,n-halogen derivatives of ethane, propane, butane, etc. Fig.5 shows the results obtained, i.e., the variation of $\Delta\epsilon$ as a function of the number n of carbon atoms in the molecule.

It will be seen that the plot for $\Delta\epsilon$ is a zigzag. What is particularly characteristic is the change in the sign of $\Delta\epsilon$ which becomes negative in going from $n = 2$ to $n = 3$ and then again positive for $n = 4$. This must be attributed to the geometry of the C-C bonds which form an angle of about 110°. Consequently, in a molecule with two carbon atoms the moments of the C-C bonds can rotate with respect to one another, describing two very obtuse cones with a common axis

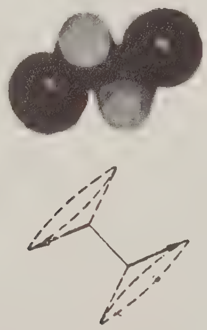

Fig.6. 1,2-dichloroethane molecule with antiparallel configuration of the electric moments of the C-Cl bonds.

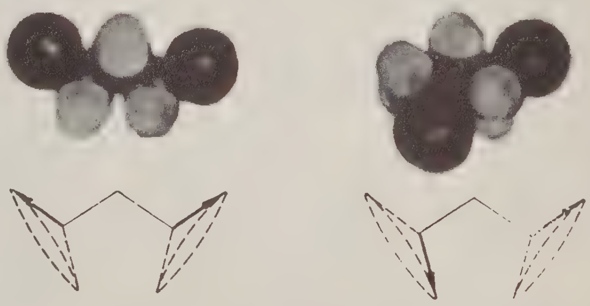

Fig.7. 1,3-dichloropropane molecule in two configurations with the electric moments of the C-Cl bonds almost perpendicular.

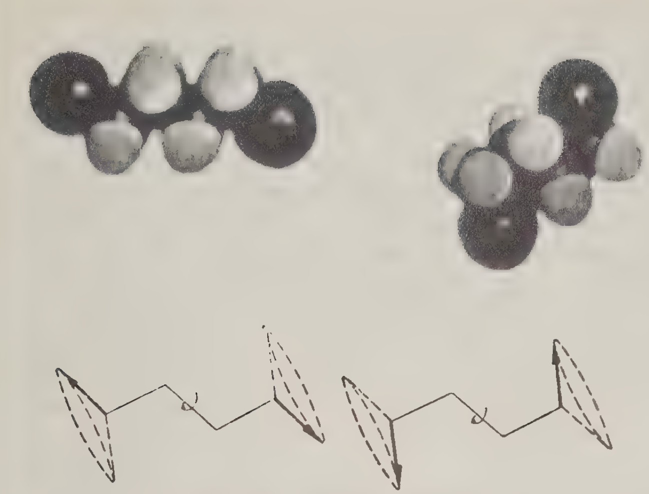

Fig.8. 1,4-dichlorobutane molecule in two configurations with the C-Cl moments antiparallel.

(Fig.6). Their preferred orientation is the antiparallel configuration; when the coupling energy is sufficiently high this leads to a change in the sign of R_s (Fig.4) and hence a positive saturation effect. The situation is different in a molecule with three carbon atoms (Fig. 7); here the axes of the two cones form an angle of 110°, i.e., are almost perpendicular. Consequently, there is only weak coupling between the moments of the C-Cl bonds and the configuration at which they are almost antiparallel is realized with a far lower probability than in the preceding case. Hence we observe a negative saturation effect. In the molecule with four carbon atoms we have a situation similar to that for n = 2 but with some admixture of configurations possible in the n = 3 case. Owing to the greater distance between the C-Cl bonds (Fig.8), the antiparallel coupling is much weaker; hence the positive saturation effect is far less pronounced. In going to still longer chains the coupling between the moments of the C-Cl bonds is further weakened with increase in the number of carbon atoms in the chain and the mutual orientation of the C-Cl bonds can no longer influence the sign of the saturation effect, which owing to the low value of the coupling energy remains negative. Hence the two curves P and N in Fig.5, corresponding to odd and even numbers of carbon atoms, converge below the n axis.

The zigzag behavior of the saturation effect as a function of the number n is substantiated by a comparison of the experimental values of the dipole moments (μ_{exp}) of 1,n-dihalogen derivatives of alkanes with the theoretical values of these moments (μ_{calc}), calculated on the assumption of free rotation of the C-Br bonds (Smyth[16]). The difference $\mu_{calc}-\mu_{exp}$ may be taken as a measure of the coupling between the moments of the two C-Br bonds:

	μ_{exp}	μ_{calc}	$\mu_{calc}-\mu_{exp}$
1,2-dibromoethane	~0.9	1.99	1.1
1,3-dibromopropane	2.03	2.36	0.3
1,4-dibromobutane	2.00	2.67	0.7
1,5-dibromopentane	2.27	2.68	0.4
1,6-dibromohexane	2.40	2.68	0.3

It will be noted that for n = 3 the coupling between the moments of the C-Br bonds is as weak as for large values of n, while for the two first even values of n this coupling is exceptionally great; this is in qualitative accord with the variation of $\Delta\epsilon$ as a function of n (Fig. 5).

That the decisive role in the positive saturation effect without inversion (curve 3 in Fig.3) is played by this hindered rotation about the C-C bond was shown by Chelkowski[15] in studying the behavior of $\Delta\epsilon$ in 1,2-dichloroethylene, in which the two C-Cl groups are linked by a double bond: 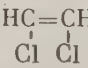 $\underset{Cl}{HC}=\underset{Cl}{CH}$; he found that in this case the saturation effect is normal, i.e., negative. This view was confirmed by subsequent cryogenic measurements[17]. It was found that the interaction of the C-Br dipoles belonging to different molecules does not play a decisive role, for in monobromoethane, C_2H_5Br, the effect is also negative: $\Delta\epsilon = -11\cdot10^{-5}$ for E = 35 kv/cm.

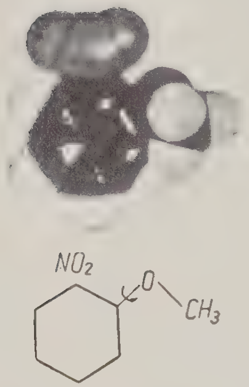

Fig.9. O-nitroanisole molecule; the radical $\diagup^{O}\diagdown CH_3$ hinders the coupling between the benzene rings of two neighboring molecules.

More or less free rotation of the radicals in the molecule does not favor coupling between molecules in liquids. This becomes clear when we consider the case of ether which exhibits a dielectric polarization, the variation of which as a function of the concentration (for example, in solutions in benzene) is not indicative of the existence of coupling between the molecules; accordingly in this case $\Delta\epsilon$ is negative. An even stronger argument in support of this view is furnished by comparison of the effect of dielectric saturation in nitrobenzene and in o-nitroanisole. The o-nitroanisole molecule differs from that of nitrobenzene in that it comprises a $\diagup^{O}\diagdown CH_3$ radical (Fig.9) which owing to steric hindrance can only rotate about the C-O bond. In view of the presence of this radical, the formation of temporary pairs by the planar molecules of o-nitroanisole is hampered (as compared with the case of nitrobenzene). This explains why the saturation effect, which is essentially positive in nitrobenzene, is negative in o-nitroanisole (Fig.3). The polar $\diagup^{O}\diagdown CH_3$ group by itself cannot produce a positive effect because its $O-CH_3$ moment, owing to the steric effect, forms an angle differing little from 90° with the moment of the neighboring $C-NO_2$ group.

There are at present several ways of theoretical treatment of dielectric saturation in liquids. Some of these theories, however, do not lead to a negative saturation effect (Debye[2], Frenkel[18] & Anselm[19]). The most general theory was developed by Buckingham[20] and Kielich and the writer[21] taking into account the deformation of the molecules in the external electric field. We have applied the same formalism to molecules with hindered internal rotation and have shown that this makes possible a quantitative explanation of the phenomenon.[22]

Institute of Physics,
Polish Academy of Sciences
Poznan, Polish People's Republic

References

1. P.Debye, Marx Handbuch der Radiologie, 6, 633 (1925).
2. P.Debye, Phys.Z., 36, 193 (1935).
3. J.Herveg, Z.Phys., 3, 36 (1920).
4. F.Kautzsch, Phys.Z., 29, 105 (1928).
5. J.Malsch, Phys.Z., 29, 770 (1928).
6. H.Gundermann, Ann.Phys., 6, 545 (1930).
7. A.Piekara & B.Piekara, Compt.rend., 205, 852 (1936).
8. A.Piekara & A.Lempicki (Not published; work interrupted by the war in 1939).
9. A.Piekara & A.Chelkowski, J.Chem.Phys., 25, 794 (1956).
10. A.Chelkowski, J.Chem.Phys., 28, 1249 (1958).
11. A.Piekara, Compt.rend., 204, 1106 (1937).
12. A.Piekara, Proc.Roy.Soc., A., 172, 360 (1939).
13. A.Piekara, Nature, 159, 337 (1947).

14. A.Piekara, Acta phys. polon., 10, 37, 107 (1950).

15. A.Chelkowski, Acta phys. polon. (1959).

16. Ch.P.Smyth, Dielectric Behavior and Structure. - N.Y., 1955.

17. A.Piekara, A.Chelkowski & S.Kielich, Z.phys.Chemie, (DDR), 206, 375 (1957).

18. Ya.I.Frenkel', Kineticheskaya teoriya zhidkostei, M.-L., 1945. (Trans. Kinetic theory of liquids, Oxford, 1946.)

19. A.Ya.Ansel'm, Zhur.eksp.i teor.fiz., 14, 364 (1944).

20. A.D.Buckingham, J.Chem.Phys., 25, 428 (1956).

21. A.Piekara & S.Kielich, Acta Phys.Polon., 17, 209 (1958). (Trans.J. Chem.Phys., 29, 1297 (1958).)

22. A.Piekara & S.Kielich, Compte rendu du 8^e Colloque Ampére, Londres, 1959, Archives des Sciences, 12, fasc.spec, 59 (1959).

DIELECTRIC RELAXATION AND MOLECULAR SIZE AND SHAPE*

- Charles P.Smyth

Many measurements of the dielectric constant and loss at microwave frequencies have been made and used to calculate dielectric and molecular relaxation times in liquids.[1-3] The present paper summarizes recent work in the writer's laboratory on the relations between dielectric relaxation, structure and intermolecular forces.

If the dielectric is a dilute solution of polar molecules in a non-polar solvent, the measured macroscopic relaxation time may be regarded as the molecular relaxation time. If, however, each polar molecule is immediately surrounded by other polar molecules, the change in local internal field caused by the turning of one molecule requires the neighboring molecules to assume new orientations, with consequent longer relaxation time for the dielectric as a whole, i.e., the macroscopic relaxation time. No generally satisfactory relationship between the two relaxation times has as yet been obtained, but an approximate relationship derived independently by O'Dwyer and Sack[4] in Australia and by Powles[5] in Princeton requires the ratio of the macroscopic to the molecular relaxation time to lie between 1 and 1.5. Experiment has shown[6] that the ratio lies within this range for a large number of molecules, while an extension of the range to 0.9-2.0 would include most of the molecules which have been examined. For approximate consideration of the magnitudes of the relaxation times, the difference between the macroscopic and the molecular values can evidently be neglected in most cases, but, in detailed consideration of structural effects, account should be taken as far as possible of the difference.

Five homologous series of compounds with more or less flexible molecules have been investigated. Interpretation of the results for alcohols[7] is complicated by the existence of a relaxation process apparently associated with hydrogen bonding, which tends to obscure somewhat the high-frequency loss region arising from the rotational orientation of the molecules. For alkyl bromides,[8] aliphatic esters,[8] ethers,[9] and ketones[9,10] the relaxation times have been found to increase with increasing chain length, though at different rates in different series. The fact that the relaxation time may increase more slowly than would be expected from the increase in viscosity may arise, in part, from increase in dipole orientation by twisting around the C-C bonds of the chain. The increase with increase in solvent viscosity is somewhat irregular, as shown, for example, by higher relaxation times in benzene than in cyclohexane solution, although the viscosity of cyclohexane is 50% higher than that of benzene.[8]

Measurements on rigid molecules avoid the complication introduced by the possibility of dipole orientation by intramolecular rotation. Viscosities and dielectric relaxation times calculated[11] from measured dielectric constants and losses for liquids consisting of such molecules are assembled in Table 1. Although the macroscopic relaxation times, τ_M, are adequate for most discussions, the values of the molecular relaxation time, τ_μ, calculated by the method of Powles[5], however approximate, give a somewhat better basis for a discussion of molecular behavior. The molecules of pyridine and s-trioxane are very similar to each other in size and shape, as are those of 2,4,6-trimethylpyridine, and three of the four liquids have almost identical viscosities[12]. The molecular relaxation time of 2,4,6-trimethylpyridine is almost 6 times that of pyridine at 20° and 5 times longer at 60°, because of the larger size of its molecule and also because of the close packing of the triangular slabs formed by the molecules.

---

*We thank Prof.Smyth for permission to print this paper and for supplying a copy. Translation editor.

Table 1

Viscosities (centipoises) and relaxation times (10^{-11} sec) at 20°C.

Substance	η	τ_M	τ_μ	Substance	η	τ_M	τ_μ
Benzene	0.65	....	....	Pyridine	0.95	0.74	0.53
CH_3	0.59	0.63	0.62	4-CH_3	0.94	1.33	0.97
1,2-$(CH_3)_2$	0.81	1.0	1.0	2,6-$(CH_3)_2$	0.87	2.32	1.79
C_2H_5	0.68	1.27	1.24				
$(CH_3)_2CH$	0.79	1.80	1.76	2,4,6-$(CH_3)_3$	0.98	4.03	3.08
				Naphthalene	....	....	....
F	0.58	0.60	0.49	1-CH_3	3.10	5.57	5.33
Cl	0.80	1.11	0.90	1-Cl	3.33	5.84	4.75
Br	1.16	1.80	1.50	1-Br	4.98	9.34	7.68
I	1.62	2.76	2.39	Quinoline	3.95	4.45	3.30
CN	1.32	4.67	3.33				
NO_2	2.01	5.25	3.56	Isoquinoline	4.4	7.32	5.48

Viscosities (centipoises) and relaxation times (10^{-11} sec) at 60°C.

Substance	η	τ_M	τ_μ	Substance	η	τ_M	τ_μ
Pyridine	0.58	0.48	0.36	Naphthalene	....	....	....
2,4,6-$(CH_3)_3$	0.58	2.33	1.82	1-CH_3	1.40	2.45	2.36
				2-CH_3	1.26	3.32	3.25
Trioxane	0.94	0.82	0.59	1-Cl	1.34	2.49	2.06
Paraldehyde	0.60	4.35	3.22	1-Br	2.05	3.61	3.01
				1-NO_2	3.57	6.95	5.00

In these two molecules the molecular moment lies in the plane of the ring, but in s-trioxane and paraldehyde it is perpendicular to the ring. The difference produces a 64% difference in relaxation times at 60° for the spheroidal pyridine and trioxane molecules and a larger difference for the trimethyl derivatives. The relaxation time of paraldehyde is 2.5 times that of 2,4,6-trimethylpyridine at 20° and 77% longer at 60°, presumably because the roughly triangular molecules of paraldehyde have to turn over in order to orient in an applied electric field, thereby necessitating more displacement of neighboring molecules than is necessary in the case of the 2,4,6-trimethylpyridine molecules, which can orient by turning in the plane of the ring instead of out of it.

The results listed in Table 1 show a tendency of the molecular relaxation time and the viscosity to increase with increase in molecular size in a pure liquid and of the relaxation time to increase with viscosity. However, many exceptions to this tendency occur. Although the attachment of a methyl group to a ring may not impede viscous flow and may even facilitate it, its protrusion impedes the molecular rotation necessary for orientation in an applied field and thus lengthens the relaxation time. The orientation of a dipole in an unsymmetrical molecule may determine the most probable direction of rotation of the molecule and thus may influence the relaxation time. When polar molecules are surrounded by nonpolar ones, their relaxation times are influenced by the nature of the nonpolar molecules as well as by the viscosity of the liquid as a whole.

Another approach to the problem of the relations between molecular character, viscosity and relaxation time is illustrated in Table 2, which compares the macroscopic and molecular relaxation times, τ_M and τ_μ within groups of molecules having the same size and shape[13]. The comparison is made first at constant viscosity η and then at constant temperature. The agreement among the τ_μ values at constant viscosity is generally better than that among the values at constant temperature,

Table 2

Effect on Viscosity and Internal Field on Relaxation Times

Substance	t, °C	Constant viscosity			Constant tcmp.			
		η	τ_M	τ_μ	t, °C	η	τ_μ	τ_μ/η
Toluenc	20	0,59	0,65	0,64	20	0,59	0,64	1,09
α-Picoline	46		0,93	0,70		0,81	0,95	1,17
γ-Picoline	55		0,91	0,67		0,94	1,02	1,09
Ethylbcnzenc	20	0,68	1,17	1,17	20	0,68	1,17	1,72
2-Ethylpyridinc	45		1,04	0,79		0,93	1,13	1,21
4-Ethylpyridinc	33		1,53	1,16		1,03	1,64	1,59
p-Chlorotoluenc	38	0,72	2,05	1,64	20	0,89	2,06	2,31
					60	0,56	1,30	2,32
(in *p*-xylenc)	11		2,15	2,15	20	0,64	1,95	3,00
					60	0,42	1,04	2,67
(in benzenc)	13		2,22	2,22	20	0,65	1,84	2,88
					60	0,39	1,03	2,45
(in *p*-dichlorobenzenc)	60		1,56	1,56	60	0,72	1,56	2,17

which are comparable, in agreement, to the macroscopic values at constant viscosity. The correlation of τ_μ values at constant viscosity is equivalent to the correlation of τ_μ/η values at constant temperature. For *p*-chlorotoluene in solution the values are calculated from the viscosities of the solvents. Good agreement is obtained for the three methyl-substituted compounds and also for ethyl-benzene and 4-ethylpyridine. Some discrepancies evident among other values may arise from a variety of causes, such as inadequacy of the macroscopic viscosity as a description of the frictional forces hindering molecular orientation.

It has been common practice, as above, to compare relaxation times measured in solution with those in pure liquids or in other solvents by using values of τ/η, assuming that η equals the solvent viscosity. If the mutual viscosity[14] η_{AB} is used instead of the solvent viscosity, a better agreement might be expected. Table 3 shows the excellent agreement which is thus obtained for three molecules. The first row gives values of τ_μ/η for the pure liquid substances. The second row shows the benzene solution relaxation times reduced by the mutual viscosities, and the third row gives for comparison the ratio of the solution relaxation time to the solvent viscosity. The agreement for *p*-dimethoxybenzene and 1-methoxynaphthalene is very good.

The value of τ_μ/η for 2-methoxynaphthalene is for 80°, and an extrapolation to 22° should yield a higher value in better agreement with the solution value at 22°.

Table 3

Substance:	*p*-Dimethoxybenzene	1-Methoxynaphthalene	2-Methoxynaphthalene
Temperature:	60°	22°	22°
τ_μ/η	0.64	1.84	0.90 at 80°
τ/η_{AB}	0.66	1.88	1.12
τ/η_1	1.17	3.78	2.37

Relaxation times have recently been measured[15] for benzene or dioxane solutions of seven large flat molecules: acenaphthenequinone, acepleiadylene, anthrone, fluorenone, phenanthrenequinone, and two porphyrazines. The relaxation times for six of these molecules were of the magnitude to be expected on the basis of values previously found for slightly smaller, rigid molecules, but were, as usual, shorter than predicted by the Debye theory with the use of the value of the macroscopic viscosity for that of the internal friction coefficient. The two porphyrazines were chosen to see if their large sizes in comparison with the solute molecules would reduce the departure from Debye behavior generally observed for small molecules. In several measurements published after the conclusion of this investigation Meakins[16] found that, when the solute molecule was at least three times as large as that of the solvent, the solutions gave good agreement with Debye's equation written in the form

$$\tau = 3\, V\eta/kT$$

where V is the van der Waals volume of the solute molecule calculated as an additive quantity. With the exception of the porphyrazines, the solute molecules had volumes slightly more than twice that of the solute, e.g., anthrone - $184 \cdot 10^{-24}$ cm^3, phenanthrenequinone - $188 \cdot 10^{-24}$ cm^3 and benzene - $84 \cdot 10^{-24}$ cm^3. These volumes lead to calculated relaxation times at 20° of $86 \cdot 10^{-12}$ sec for anthrone and $88 \cdot 10^{-12}$ for phenanthrenequinone, much higher than the observed values: $25 \cdot 10^{-12}$ and $31 \cdot 10^{-12}$ sec. These discrepancies and those for the remaining molecules, other than the porphyrazines, resemble those found by Meakins for other solutions in about the same range of solute-to-solvent molecular volume ratios. The volume of the metal-free porphyrazine molecule was calculated to be $881 \cdot 10^{-24}$ cm^3, about 10.5 times that of the solvent molecule. This gives a calculated relaxation time of $410 \cdot 10^{-12}$ sec, in much better agreement with the observed $302 \cdot 10^{-12}$ sec than any of the values calculated for the smaller molecules, an agreement consistent with the conclusion of Meakins. The ferric porphyrazine molecule has nearly the same volume as the metal-free molecule, but its dipole moment is perpendicular to the molecular plane instead of parallel to it. Having about the same volume, it should have about the same relaxation time according to the simple Debye equation, but the observed value is ~2.3 times as large, for the same reason that the previously discussed relaxation time of paraldehyde is 2.5 times that of 2,4,6-trimethylpyridine. It appears, therefore, that the relaxation times of molecules at least three times as large as the molecules surrounding them may be roughly proportional to the macroscopic viscosity, as found in early work on protein solutions, but the dipole direction within the molecule and molecular shape must be taken into account. The use of mutual viscosity instead of macroscopic viscosity gives much worse agreement for these solutions of large molecules, although it has been found to lessen the discrepancies between theoretical and observed behavior for some solutions of smaller molecules.

Although a rough proportionality between molecular relaxation time and the macroscopic viscosity of the liquid frequently exists, the relaxation times of small molecules tend to be much shorter than the values calculated from the viscosity and molecular radius, probably because the molecular motion involved in dipole orientation requires less translation of the molecules than is required in viscous flow. The Debye equation has been applied to the nearly spherical molecules of tetrasubstituted methanes of known radius to calculate the internal friction coefficient or microscopic viscosity from the molecular relaxation time.[17] The values thus obtained for several liquids are only 0.008 to 0.06 of the macroscopic viscosity, and there appears to be little parallelism between the internal friction coefficient and the macroscopic viscosity. Indeed, for two crystalline solids, namely, *t*-butylchloride and dibromodichloromethane[18], the apparent coefficient of internal friction is lower than that of the substances in the liquid state[17].

In view of the small size of the ammonia molecule and hydrogen bonding in the liquid, liquid ammonia might not be expected to conform to simple Debye behavior. Because of the similarity in molecular size and character and the existence of hydrogen bonding in both liquids, it is natural to compare the relaxation time of liquid ammonia[19] with that of water[20]. The macroscopic relaxation time of ammonia, $1.3\cdot10^{-12}$ sec at -40°, is much shorter than that of water, $17.9\cdot10^{-12}$ sec at 0°. However, the much lower boiling point of ammonia, -33.4°, as compared to 100° for water, as well as the differences in other physical properties, indicate less hydrogen bonding, and, therefore, less hindrance in ammonia to molecular orientation in a field. The viscosity of water at 0° is 1.79 centipoises as compared to 0.266 for ammonia at -33.5°, a 7 to 1 ratio, while the corresponding ratio of relaxation times is 17.9 to about 1.3, or 15 to 1. If, however, the comparison is made by extrapolation to the boiling points of both liquids, the ratio of the viscosities is 0.381 to 0.266 or 1.43 and of the relaxation times $2.1\cdot10^{-12}$ to $1.2\cdot10^{-12}$ or 1.8; the $\tau(10^{-12}\ \text{sec})/\eta(\text{cps})$ ratio at the boiling point is 5.5 for water and 4.5 for liquid ammonia. An approximate determination in this laboratory of the relaxation time of water-saturated benzene at 22° gives $1\cdot10^{-12}$ sec, i.e., a value for water in the presumable absence of hydrogen bonding indistinguishable from that of liquid ammonia in the vicinity of the boiling point. *t*-Butyl chloride, which has about six times the molar volume of water, shows a relaxation time in solution 1.3 to 3 times that of water in benzene. The much shorter relaxation time of liquid ammonia as compared to that of water is attributable to its weaker hydrogen bonding, while the smaller size of the molecule accounts for its lower value as compared to those of most other substances which have been measured. The effect of molecular inversion, which would be smeared out by the intermolecular forces in the liquid, is not apparent in these values of the relaxation time.

For the study of small molecules and molecules possessing intramolecular group rotation, the desirability of measurements in the region of a few millimeters has become increasingly evident. When the work summarized here was undertaken, no oscillators were available which would operate in the frequency region of 100 000 Mc. It was, therefore, necessary to employ a crystal harmonic generator in conjunction with a lower frequency oscillator. The dielectric constant and loss of ethylbenzene, *p*-chlorotoluene, chlorobenzene, 6-methylquinoline and 8-methylquinoline were measured at 3.1 mm[21] and the results evaluated in terms of the data on the compounds at longer wavelengths. Since the latter can satisfactorily be represented on a Cole-Cole semicircular arc, it was possible to calculate what the dielectric constant and loss would be at 3.1 mm if this behavior persisted at the higher frequencies. Table 4 contains the observed and calculated values of the dielectric constant and loss at 3.1 mm, together with the optical dielectric constant ϵ_∞ of each compound as obtained from the arc plot.

The measured dielectric constants are close to the calculated values, but slightly lower, while the observed losses are much higher than the calculated values, which depend on the difference between the static and optical dielectric constants, the critical wavelength and the distribution parameter of the compound. Since the uncertainty in these quantities could account for an error of not more than 20%, the discrepancies in Table 4 cannot be attributed to experimental error. It would thus appear that a higher frequency absorption region exists as suggested by Poley's measurements[22] on monohalogenated benzenes at lower frequencies. However, further evidence, particularly at shorter wavelengths, is needed for a proper evaluation of the situation.

An interesting result is the approximate agreement between the 3.1 mm dielectric constant and the optical dielectric constant of these compounds. The steep descent of the arc in this region makes this possible, in spite of the apparent departure of the 3.1 mm points from the values predicted by the Debye or Cole-Cole dispersion formulae discussed above. The measured dielectric constant at 3.1 mm can, therefore, be of great assistance in locating the high frequency intercept of a Cole-Cole arc plot. This is especially true of unassociated liquids

Table 4

Dielectric Constant and Loss of Substituted Benzenes and Quinolines at 3.1 mm

Substance	ϵ_∞	ϵ'		ϵ''	
		Obs'd	Calc.	Obs'd	Calc.
Ethylbenzene	2.26	2.25	2.27	0.05	0.02
p-Chlorotoluene	2.56	2.54	2.58	0.44	0.24
Chlorobenzene	2.56	2.56	2.62	0.55	0.43
6-Methylquinoline	2.97	2.91	2.98	0.34	0.12
8-Methylquinoline	2.82	2.80	2.83	0.18	0.08

having long critical wavelengths, where the discrepancies in the small loss values will have little effect on the shape of the arc plot.

Arc plots for water and methyl alcohol have been constructed[21] from the data of a large number of workers. As in earlier work[23], the dielectric dispersion of water was found to follow a semi-circular plot throughout, with no distribution of relaxation times, the 3.1 mm point giving a critical wavelength of 1.88 cm, which is in good agreement with the accepted value[23] of 1.78 ± 0.3 cm. The high value, 6.0, given by the arc plot for ϵ_∞ is consistent with the values, 5.5-6.2, indicated by previous arc plots 23 and with the presence of further considerable absorption at shorter wavelengths. Methyl alcohol shows a marked departure from the arc plot at 3.1 mm, while in the case of ethyl alcohol and -octyl alcohol, the departure is even greater.

When the 3.1 mm values for ethyl alcohol and *n*-octyl alcohol are combined with other data in plots of ϵ' against $\omega\epsilon''$ and against ϵ''/ω, the straight lines characteristic of the distinct high-frequency dispersion regions are obtained, with curvature at the low-frequency ends in the regions of overlap with lower-frequency dispersion regions. For ethyl alcohol, the slope of the line gives a relaxation time of $3.0 \cdot 10^{-12}$ sec for the second or high-frequency absorption region, and for the *n*-octyl alcohol, the slope gives for the third absorption region a relaxation time of $2.7 \cdot 10^{-12}$ sec, which is in good agreement with Brot's value[24] of 0.47 cm. These are in contrast to the values for the first absorption regions: $145 \cdot 10^{-12}$ sec for ethyl alcohol and $1.6 \cdot 10^{-9}$ for *n*-octyl alcohol.

The variety of dispersion regions shown by the alcohols is due, in part, to the effect of hydrogen bonding and, in part, evidently to some very high-frequency intramolecular motion. Measurements have been carried out on solutions of molecules made up of benzene or naphthalene rings with movable polar groups, such as CH_3O-, $-CH_2Cl$ and $-NH_2$, attached. The values obtained for the relaxation times from measurements at 1.2 and 3.2 cm wavelength give evidence of two overlapping absorption regions, which cannot be properly distinguished until measurements have been made at shorter wavelengths.

Frick Chemical Laboratory
Princeton University

References

1. C.P.Smyth, Dielectric Behavior and Structure, McGraw-Hill, New York, 1955, Chap.IV.
2. C.P.Smyth, Proc.Nat.Acad.Sci., 42, 234 (1956).
3. A.J.Petro & D.A.Pitt, Tables of Dielectric Constants, Dipole Moments and Dielectric Relaxation Times, in "Digest of the Literature on Dielectrics", Nat. Acad. Sci. - Nat. Research Council, Washington, 1957, Chap.II.

4. J.J.O'Dwyer & R.A.Sack, Australian J.Sci.Research, A5, 647 (1952).
5. J.G.Powles, J.Chem.Phys., 21, 633 (1953).
6. R.C.Miller & C.P.Smyth, J.Am.Chem.Soc., 79, 3310 (1957).
7. Reference 1, pp.105-111; F.X.Hassion & R.H.Cole, J.Chem.Phys., 23, 1756, (1955).
8. Reference 1, pp.114-125.
9. G.B.Rathmann, A.J.Curtis, P.L.McGeer & C.P.Smyth, J.Chem.Phys., 25, 413 (1956).
10. J.H.Calderwood & C.P.Smyth, J.Am.Chem.Soc., 78, 1295 (1956).
11. Reference 1, pp.69,70.
12. R.C.Miller & C.P.Smyth, J.Phys.Chemi, 60, 1354 (1956).
13. A.J.Petro & C.P.Smyth, J.Am.Chem.Soc., 79, 6142 (1957).
14. N.E.Hill, Proc.Phys.Soc., B, 67, 149 (1954).
15. D.A.Pitt & C.P.Smyth, To be published.
16. R.J.Meakins, Trans.Faraday Soc., 54, 1160 (1958).
17. C.P.Smyth, J.Phys.Chem., 58, 580 (1954).
18. J.G.Powles, D.E.Williams & C.P.Smyth, J.Chem.Phys., 21, 136 (1953); D.E.Williams, Ph.D.Thesis, Princeton University, 1956.
19. K.Fish, R.C.Miller & C.P.Smyth, To be published.
20. Reference 1, p.128.
21. R.W.Rampolla, R.C.Miller & C.P.Smyth, to be published.
22. J.P.Poley, Thesis, Delft, 1955.
23. Reference 1, p.127.
24. P.C.Brot, Thesis, Université de Paris, 1956.

DISCUSSION

G.I.Skanavi (regarding the reports of R.H.Cole, M.Magat & C.Brot, and A. Piekara): The reports presented at this meeting were of great interest to me; all three reports are substantial contributions. But I would also like to mention the regret that I felt now in listening to the report of Prof.Cole and earlier in reading his papers. We know that it was the Brothers Cole who first proposed the method of describing experimental data by means of which one can obtain the dipole distribution function for a given substance.

This work is very fruitful and its results have been widely used for many years, but it is regrettable that the distribution functions obtained are not related with any definite physical concept in each specific case, although it is understandable that this is difficult to do and naturally this question in each specific case requires special examination.

At the same time, an attractive feature of Prof.Cole's report is that the experimental data are apparently entirely reliable, and hence, although the frequency intervals are rather large and the temperatures very low, there is no reason to doubt that there are actually obtained curves correctly reflecting the properties of the investigated substances.

The researches of Cole and Davidson are of great interest at present. I would like very much to have the authors of these studies give some physical concepts related to their interesting results and pertaining to the asymmetrical dipole distribution function deriving from the experimental data for some organic compound.

As for the report of Prof.Magat, whom, like Prof.Cole, we want to thank for an interesting report, I would like to note that here Prof.Magat put forth an interesting consideration regarding the physical concepts that he associates with different dispersion regions.

Regarding the report of Prof.Piekara, one must first emphasize that these problems have long been under study in the laboratory of Prof.Piekara and that many significant results have been obtained. Unfortunately, as I now understand from the responses of Prof.Piekara, one cannot unambiguously determine the variation of the dielectric constant of different liquids in strong fields owing to experimental difficulties. Of particular importance is the question of the dielectric constant of solutions in strong fields. Let us hope that this problem will soon be solved in the laboratory of Prof.Piekara.

E.M.Fradkina: It is apparent from the reports that we have just heard that the authors give particular attention to the question of rotational oscillation (libration) of molecules. Until now, the intertia of the molecules was not taken into account in considering rotational vibrations. In particular Debye in considering the behavior of particles with a dipole moment μ in an external electric field F considered that the force $\mu F \sin\vartheta$ due to the field is balanced by the friction force $\rho\dot{\vartheta}$, i.e.,

$$\rho\dot{\vartheta} = -\mu F \sin\vartheta,$$

in doing so he did not take into account the inertia $I\ddot{\vartheta}$ of the particles, which becomes increasingly significant with increase in the frequency of the external field.

The first attempt to take into account inertia in rotational oscillations of dipole particles was made by the Leningrad authors Dmitriev and Gurevich in 1946. But in their work they made a number of assumptions that restrict their deductions to the case of very low concentrations.

If we write the equation of motion for dipole particles in the form

$$I\ddot{\vartheta} = -\rho\dot{\vartheta} - \mu F^* \sin\vartheta,$$

where F^* is the field acting on the particles, it will enable us to establish the relation between ϑ and μ which is then used in the statistical problem of determining $\overline{\mu}$ in the direction of the field F and then from the equation $\mu = \alpha F$ determining the polarizability α of the particles. If we now use not the Clausius-Mosotti formula, which is applicable only in a limited range of low concentrations, but the universal Maxwell equation

$$\varepsilon = 1 + 4\pi N\alpha,$$

we obtain an expression for the macroscopic value of the dielectric constant ε of the medium.

A number of authors, and particular Prof.Piekara in 1932, have considered the question of the magnitude of the acting field. The results obtained by them, however, in my opinion, are somewhat lower than what might be expected. Thus, the maximum correction φ in the formula

$$F^* = F(1 + \varphi)$$

does not exceed 0.1 f, where f is the volume concentration of particles.

I used the following expression for the acting field:

$$F^* = \frac{F}{(1 - f)^{2/3}}$$

and obtained expressions for ε' and ε'' similar to the Debye equations; however, the dispersion band proved to be shifted to the side of higher frequencies.

Thus, if in the Debye formula, we substitute $a = 2 \cdot 10^{-8}$ cm and $\eta = 0.01$, i.e., the values for water, we obtain a dispersion band in the meter range, whereas the critical wavelength given by experiment for water is $\lambda = 1.6$ cm. Calculation by means of my formulas, on the other hand, gives a dispersion band in the centimeter range, which is in better agreement with the experimental data.

I think what Prof.Piekara has told us about the positive saturation effect as discovered by him is of great interest. It would be very desirable to continue these investigations and to carry out calculations for water. In particular, this would be of great interest from the standpoint of the theory of electrolyte solutions where the experimental data are not in accord. Thus I obtained a value of the dielectric constant greater than in water and appreciably greater than follows from the Debye-Falkengagen theory. I would be very pleased if this could be explained with the aid of the considerations set forth by Prof.Piekara.

R.L.Myuller: The reports of Prof.Cole and Prof.Magat are concerned with very interesting effects and in particular with the fact that at elevated frequencies there is observed suppression or cutting off of the rotational motion of molecules in alcohols and some other organic compounds. It seems to me that cutting off of the rotational motion of molecules at high frequencies should be accompanied by at least partial attenuation or cutting off of rotational oscillations. This must be evinced in the behavior of the specific heat of the compounds in question.

M.Magat: In connection with the statements of Prof.Myuller I would like to make the following remark: it is essential to distinguish between rotational oscillation (libration) and simply rotation of molecules. The rotation of molecules disappears as frequencies corresponding to wavelengths of 1 cm or 8 mm, whereas libration persists. According to the experiments of Prof.Errera, in the alcohols investigated by us libration dispersion obtains in the region of 100 μ. Prof.Errera reports on his results in the Soviet Union in 1936-7, if I'm not mistaken.

Many years ago Rubens and Ladenburg, investigating the infrared absorption spectrum of water, detected an absorption band in the 500-700 cm^{-1} region. At that time, however, these authors could not interpret their results. In 1935-6 Dr.Bolia in Italy and I in France investigated the spectra of water and detected Raman lines at frequencies equivalent to the frequency of the infrared absorption found in the experiments of Rubens and Ladenburg. Later we measured the shifts of these frequencies in isotopic molecules and established that these shifts do not correspond to vibrations of the molecules relative to each other. In other words, we established that in this case we are dealing with rotational oscillations - libration. The first and second degrees of freedom were very clear; the third degree was detected by Dr.Bolia; I did not find it. In water, the first and second degrees of freedom correspond to frequencies of 700 cm^{-1} and 500 cm^{-1}, the third degree to 60 cm^{-1}.

Thus in our experiments of dielectric dispersion what disappears is not libration but rotational motion. This is the point I wanted to emphasize again.

V.I.Odelevskii: I wholeheartedly agree that the reports of Prof.Magat and Prof.Piekara are of exceptional interest. The report of Prof.Piekara pleased me by the fact that he brought in a new physical viewpoint to the question of the dependence of the dielectric constant on the electric field in liquids. The positive saturation effect discovered by Prof.Piekara is highly interesting; it is significant that the author succeeded in relating this effect to the structural features of the molecules.

With regard to the report of Prof.Magat I want to say the following. It is difficult to imagine how in the "rigid" structure of ice a molecule can turn and assume some new position. It is known that in ice the water molecules are rather tightly held by hydrogen bonds to four other molecules. For this reason the water molecule in ice has only one position - the equilibrium position - and one cannot imagine its occupying any other position.

In disagreement with Prof.Magat I believe that the high dielectric constant of ice must be related not with rotation of the molecules as a whole but with the process of "proton transfer" in the hydrogen bonds. Prof.Magat believes the possibility of "proton transfer" in hydrogen bonds is disproved; he argues that a) the proton detachment energy is very high - about 40 kcal per mole, and b) the process of "proton transfer" has not been detected in investigation of the reactions of some complex molecules by the isotope method.

I feel that this view is not well taken since without recourse to the concept of proton transfer it is difficult to explain the high dielectric constant; moreover, it is precisely by express proton transfer that one can explain the anomalous mobility of $(H_3O)^+$ in water solutions. If one precludes transition of protons, one cannot explain the neutron diffraction data according to which in water there are two close positions of the protons with a separation of approximately 0.4 Å.

By way of more complicated examples I can point to proton ferroelectrics - Rochelle salt, KH_2PO_4, and others - in the theory of which the process of proton transfer plays a fundamental role. Even if it be assumed that this theory is incorrect and that rotation of the moment is not connected with proton transfer, it will be impossible to explain the exceptionally great increase of the Curie temperature when hydrogen is replaced by deuterium in KH_2PO_4.

Further, as I understand it, the high proton detachment energy was found not for transition of a proton from one molecule to another in the condensed phase, but for the emergence of a proton from a molecule into free space. These must be entirely different energies if only because the action of dipole forces in the condensed polar phase leads to "pulling out" of the proton into the surface zone of the polar molecule, and the energy barrier is greatly lowered.

In the paper of Prof.Magat there was also passing mention that there exist isolated protons. Physically this is incomprehensible inasmuch as an isolated proton, having a vanishingly small radius, must inevitably be pulled into a water molecule. Thus the facts would appear to indicate that the process of proton transfer can and does occur in water, alcohols and a number of other compounds.

M.Magat: V.I.Odelevskii understood me as though I asserted that there exist free protons; evidently I did not express my thought clearly. Ever since the spectrum of $(H_3O)^+$ was discovered, one cannot speak of a free proton.

I consider merely that in the present case one must speak of two different types of effects. One type consists of the following: if there is a proton, a water molecule and one more molecule, then there can occur transfer of the proton from the first molecule, where it formed a hydrogen bond, to the second with the formation of a new hydrogen bond. This is what is called proton transfer. But in ice there are fewer such protons than in water; hence we must consider the process of relaxation of water molecules without recourse to H^+ transfer and without the mechanism of formation of $(H_3O)^-$.

There are many experiments proving that there does not occur transfer of H atoms; in fact one of the most elegant of these was carried out in the Soviet Union by Grigorov and Maklukhov who investigated the transfer of hydrogen in the strongly associating system hydroquinone-quinone. These investigators found that the exchange can occur only upon addition of acid to the water. In my opinion this is a very effective experiment; it shows the difference between the transfer through the intermediary of a proton and the intermediary of a covalently bound hydrogen. This is also substantiated by the equality of the rates of diffusion of D_2O^{16} and H_2O^{18}, which indicates that the water molecule must diffuse as a whole.

The second question is the question of orientation. The energy necessary for orientation of a water molecule, i.e., the activation energy, is very large, namely, 12 kcal/mole. This is one of the highest activation energies for small molecules in dielectric dispersion. At present it is difficult to say what is the second position of the water molecule. However, V.I.Odelevskii correctly noted that in ice there exist two positions for water molecules because it follows from entropy considerations and the data of molecular spectroscopy that the position of water molecules is not uniform in the entire structure of ice. V.I. Odelevskii says that protons are transferred, while I assert that part of the water molecules may be rotated to one side and part to the other. The static effect is the same. I note that the model of orientational polarization of ice was developed some years ago by Pauls.

Yu.L.Khait (regarding the reports of R.H.Cole, M.Magat & C.Brot, C.P.Smyth and G.I.Skanavi): I would like to make a few remarks. The first remark pertains to the difficulties that arise in trying to explain the temperature dependences of relaxation times. This question was discussed in the reports of R.H.Cole, G.I.Skanavi and M.Magat.

On the basis of general statistical-thermodynamic and kinetic considerations we propose the following formula for the relaxation times:

$$\tau_l = \frac{l^3 \hbar}{d^3 kT}\, e\left(\frac{\Delta}{kT}\right) \mathrm{sh}^{-1}\left(\frac{\bar{u}_0 l^3}{kT}\right);$$

this formula I believe offers some new possibilities for explaining the temperature dependence of relaxation times at low and high temperatures and also of the jump in the magnitude of the relaxation time incident to crystallization of water, a point mentioned by Prof.Magat.

In view of the fact that l depends on the temperature and enters the formula both under the exponent and before it, the temperature dependence of the relaxation time proves to be more complex than is usually assumed.

The asymmetrical function proposed by Prof.Skanavi probably is preferable to the expedient suggested by Prof.Cole inasmuch as the statistical character of the distribution function allows of extending it correctly to low temperatures. The formula proposed by Prof.Cole seems doubtful to me because the somewhat arbitrary form of this expression does not have the clear physical meaning possessed by the distribution function proposed by Prof.Skanavi.

My second remark is that apparently at low temperatures, as follows from the general principles of statistical thermodynamics, one cannot apply detailed model concepts inasmuch as collective quantitative effects become significant; these are determined by quantum-statistical regularities and hence one cannot individualize separate particles. Hence the model concepts of Prof.Smyth cannot be transferred to low temperatures in condensed media.

Lastly, we showed that the dielectric losses due to motion of molecular ions and so on can be evaluated by means of the formula

$$\Delta\psi_l \approx \frac{\Delta_l C}{\omega a^3 \tau_l},$$

where C is the concentration of particles responsible for the given energy dissipation process, for example, weakly bound ions, and so on.

A similar formula can be written for the relaxation loss in the case of elastic molecular encounters. In this case

$$\Delta\psi_y = -\frac{\Delta_y}{d^3 \omega \tau_\sigma},$$

where τ_0 is determined in a manner similar to τ_l, but with replacement of U_0 by the elastic energy density.

If we invoke mechanical effects such that the volume density of the elastic energy will be equal to the volume density of the electric energy and the frequency of the mechanical and electrical forces are also identical, then having measured one of these for the same conditions as mechanical and electric losses, we can determine C, the relative concentration of ions or other particles responsible for the electric loss in the substance.

* * * * * * *

FIELD AND CURRENT DENSITY DISTRIBUTION INHOMOGENEITIES IN CdS SINGLE CRYSTALS

- K.W.Böer

It can be shown that the field and current density distribution in CdS single crystals is characterized by appreciable inhomogeneity. This homogeneity may be due to different factors, namely, 1) the boundary layer at the contact of the metal electrode with the semiconductor, 2) regions or domains of different conductivity inside the crystal, and 3) electron space charge inside the crystal.

In what follows, however, we shall not consider the familiar boundary layer effect.[1]

In weak fields the field and current density distribution in the crystal are determined primarily by the domains of different conductivity. We shall not examine here the reasons for the formation of such different conductivity domains in the process of preparation of the crystal; our primary aim is to show how inhomogeneities of the material can be detected and what experimental procedures can be used to investigate them.

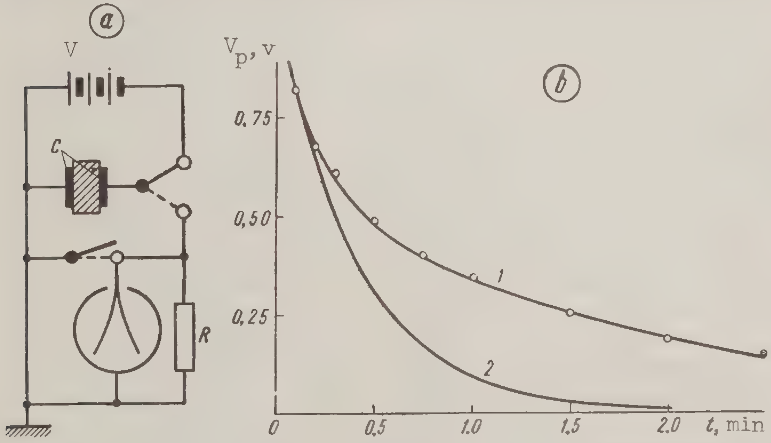

Fig.1. a) Circuit for determination of dielectric aftereffect; b) 1 - experimental decay of polarization voltage, 2 - exponential decay.

Indications that there do exist such regions of different conductivity are yielded by observations of the dielectric aftereffect. Assume that we have a CdS crystal serving as the dielectric in a capacitor which is charged from a dc source; then the discharge current through a not excessively high discharge resistance R is found to flow appreciably more slowly than might be expected from calculation of RC, where the capacitance C is found purely from the geometry of the capacitor and the known dielectric constant of CdS. Moreover, the voltage decay with time does not follow the simple exponential law (Fig.1).

The observed dielectric aftereffect can be explained[2] if we accept that the crystal consists of domains of different conductivity. Incident to passage of current there will form space charges at the interfaces between the domains with high and low conductivity. After cessation of current flow, the space charges

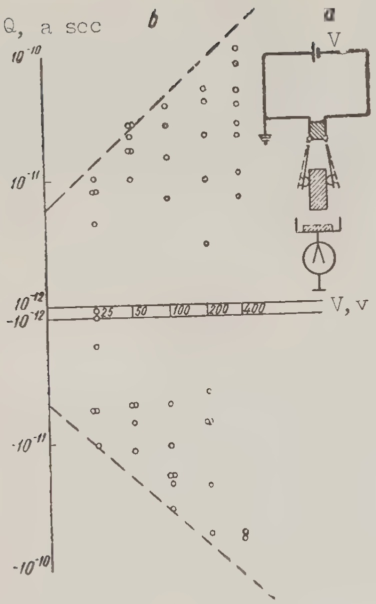

Fig.2. a) Experimental arrangement for measuring the electrostatic charge after passage of current through a CdS crystal; b) electrostatic charge on a CdS crystal as a function of the voltage applied to the contacting electrodes.

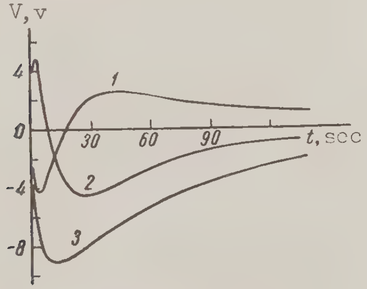

Fig.3. Time variation of the polarization voltage for three different crystals.

dissipate; the discharge occurs not only through the discharge resistance R but also through the resistances of a number of the crystal domains.

The space charges on the boundaries between the low and high conductivity domains will be positive or negative, depending on the direction of the applied field. The sum of these charges as a whole is nonzero owing to asymmetric geometric distribution, which leads to electrostatic charging of the crystal in relation to the surrounding medium[3] (Fig.2).

The magnitude of the measured charge increases with increase of the applied voltage in accord with the increase of the space charge with growth of the current. The great experimental scatter as regards the magnitude and polarity of the charge is explained by different positions of the crystal in the contact holder in successive measurements: as a result, different sets of domains occupy the space encompassed by the field.

The existence of a large number of different domains is satisfactorily explained by break-up of the internal space charge. This is observed particularly clearly if after cutting off the external voltage the charges on the metal plates of the capacitor are removed by briefly shorting them; then one can follow the re-establishment of the induced difference of potentials on the metal plates owing to equalization of the space charges. The equalization of the space charges occurs with a different time constant, depending on the conductivity and geometry of the domains so that there may finally obtain either one polarity or the other on the external electrodes. The process of establishment of the induced potential difference on the electrodes depends qualitatively and quantitatively on the distribution of differently conducting domains, which in turn depends on the nature of the crystal (Fig.3).

Indications pointing to the domain structure of CdS are also obtained in investigating the spectral distribution of the photocurrent, which differs a very appreciable amount for different regions of the same crystal. Fig.4 shows the spectral distribution of the photocurrent for a repeatedly cleaved crystal[4].

From the above mentioned experiments one cannot as yet judge to what extent the regions determining the photocurrent corresponds to the domains that influence the dark current and lead to the dielectric aftereffect and electrostatic charging. Nevertheless, it can be shown that in strong fields, when electric excitation begins in the low conductivity domains, there occur alterations of the domain structure.

Changes in the domain structure in high fields are characterized by an appreciable fluctuation of the current[5] which increases with increasing field strength. These fluctuations can readily be explained if we assume that upon

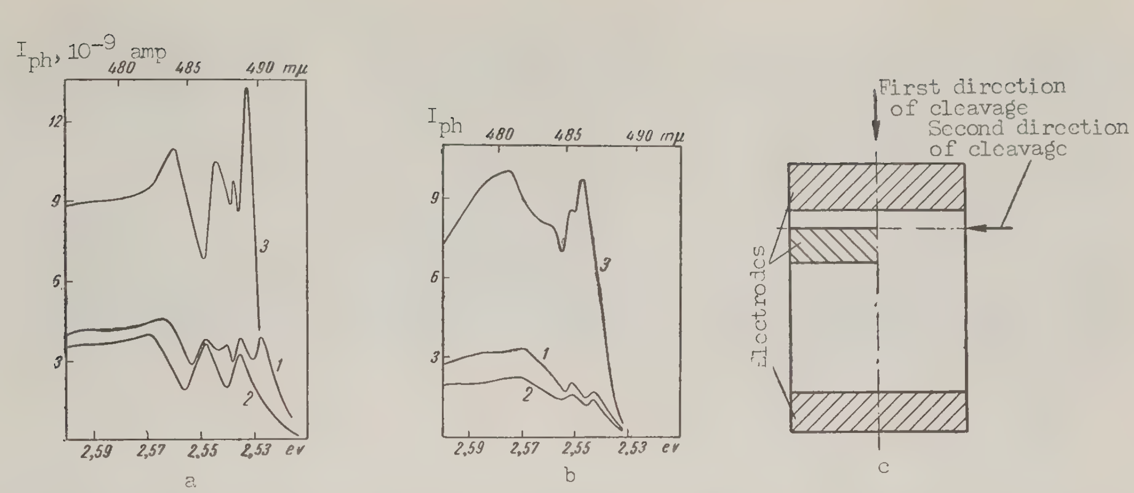

Fig.4. Spectral distribution of the photoconductivity of a CdS single crystal in polarized light incident parallel (a) and perpendicular (b) to the C axis at -180°: 1 - on the whole crystal (c); 2 - on the left-hand part of the crystal, and 3 - on the recleaved left-hand part of the crystal after application of a new electrode.

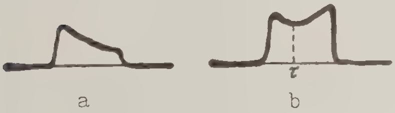

←Fig.5. Time variation of current upon application to a CdS single crystal of a square voltage pulse (pulse duration $3 \cdot 10^{-6}$ sec): a - applied voltage equal to 0.5 the breakdown voltage, b - applied voltage equal to 0.9 the breakdown voltage.

application of the external field the initial field distribution is primarily homogeneous but that with gradual build-up of space charges it slowly becomes inhomogeneous[6]. Increase of the field in the low conductivity domains may lead to increase in the number of electrons by electric excitation; the conductivity of these domains will then increase; the field in them will deteriorate but will increase in neighboring domains, in which now under the influence of electric excitation there may begin electron multiplication. At the same time the conductivity in the earlier excited electric domains falls off with a certain dielectric relaxation time, then the field intensity again increases to the point where there begins electron multiplication. The process is repeated quasi-periodically.

If there were present clearly defined discrete low conductivity regions one could expect regular periodicity of the current oscillations. The fact that such periodicity is not observed indicates that in the space occupied by the field there must exist a large number of domains with different conductivities.

One can readily follow the development with time of the effects of polarization and excitation if we apply to the crystal a short square voltage pulse and observe the current flowing through the crystal by means

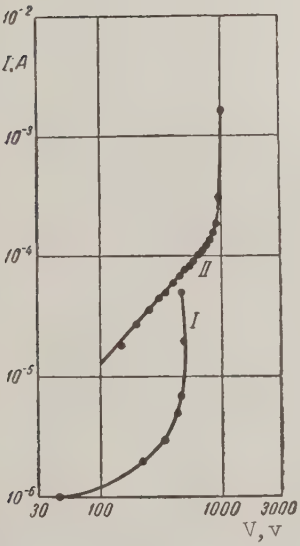

Fig.6. Variation of the current flowing through a crystal as a function of the applied voltage: I - dc voltage, II - pulse voltage (single $3 \cdot 10^{-6}$ sec voltage pulse).

of an oscilloscope[7]. At low values of the applied voltage the current quickly decreases with increase of the space charge[6] (Fig.5,a). At high voltages, the field, increasing in the low conductivity domains owing to formation of space charge, attains the critical value for the beginning of electric excitation. After an initial decrease over a period τ, during which there is attained the critical value of the field intensity, the current again increases owing to electron multiplication (Fig.5,b).

If the number of generated electrons is so great that the critical power necessary for thermal breakdown of the material is exceeded, we will have electric breakdown[8]. If the external field is applied to the crystal for such a short time that the elevated field due to the above described polarization effects cannot be fully attained, one may expect an increase of the dielectric strength. Fig.6 shows the current voltage characteristics for dc and pulse voltages which substantiate these inferences.

The described effects clearly show that the investigated CdS single crystals are characterized by appreciable inhomogeneities which substantially affect the character of the current flow. In view of the importance of the above described phenomenon for current measurements in solids, we developed a procedure which allows of direct observation of the field and current density distribution in crystals. Inasmuch as the absorption spectrum of crystals depends directly on the field strength or the effective current density, one can under a microscope observe the field or current distribution if the wavelength of the transmitted light is chosen at the edge of the principal absorption band of CdS, for the absorption in these regions varies with the field strength.

Changes in the absorption spectrum owing to variation of the field and current distribution may be accompanied by the following electron-optical effects.

	Direct effects	Side effect
Field distribution	Stark effect Franz effect	Inverse piezoelectric effect
Current distribution		Joule heating
Space charge distribution	Intrinsic absorption by free electrons. Absorption by defects with trapped electrons (for example, F band).	Disturbance of the absorption by the regular lattice in the vicinity of an electron (polaron).

Owing to the weakness of the indicated effects the experiment requires a high degree of monochromaticity and very low temperatures in order to eliminate interference from lattice vibrations. So far with the equipment available we have not succeeded in observing the expected effects in the region of very weak fields. (Possibly this is explained by the fact that we have not attempted to carry out measurements at temperatures below 40°K in our laboratory).

In very strong fields Joule heating becomes noticeable and under a microscope one can clearly distinguish a number of current lines in the region of the principal absorption peak (Fig.7). One must, however, exercise a certain caution in attempting to interpret this picture: owing to heat conduction, poorly conducting regions may influence the absorption so that the picture will seem more uniform than that corresponding to the true current density distribution.

In the range of weaker fields, but still in the breakdown region, there occurs a different spatially nonuniform absorption effect, which may or may not be

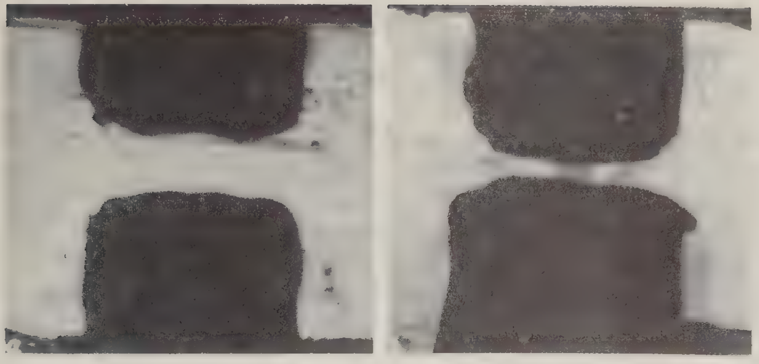

Fig.7

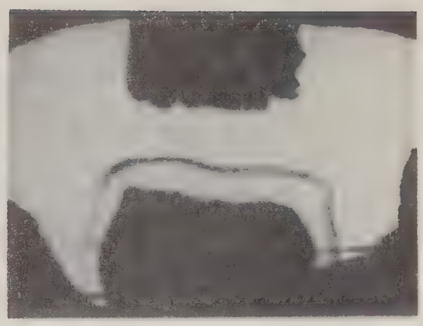

Fig.8

Fig.7. Photograph of a CdS single crystal in monochromatic light (λ = 520 mμ: a - no external field, b - in a field (distance between electrodes 1 mm; applied voltage 2000 v).

Fig.8. Photograph of CdS single crystal in monochromatic light (λ = 500 mμ) at -183°. Interelectrode distance 1 mm; applied voltage 1000 v.

explicable by one of the proposed mechanisms. Inasmuch as this effect involves an unusual field distribution which in many respects is reminiscent of the space charge distribution in discharge plasma, I would like to describe it in some detail and suggest some of the causes responsible for this effect.

Fig.8 shows a microphotograph of a CdS single crystal recorded in monochromatic light with a wavelength at the absorption edge. Characteristic here is the presence about the cathode of an annular darkened region which is separated from the cathode by an undarkened region and which has a distinct boundary on the side of the anode, particularly at low temperatures.

We established that the darkened annular region has the following physical properties.

1. The absorption spectrum of this region at -180° is devoid of structure and is evinced as a simple shift of the absorption edge. The shift is minimal in the vicinity of the cathode and increases in going towards the anode where at the line of the distinct boundary it may attain 40 Å.

2. The darkened region forms and disappears with a lag characterized by a time constant of the order 1 sec.

3. If the crystal is not illuminated upon application of the field or in case of removal of the field after formation of the annular darkening, the darkening forms and disappears with appreciably greater lag: the time constant increases by several orders of magnitude.

4. The darkened region forms a circle about the cathode, i.e., appears where on the basis of the electrode geometry one might not expect a high field intensity.

5. The distance of the annular darkened zone from the cathode may either remain constant or, particularly, in strong fields, may increase with time. At the same time the current through the crystal increases. If the ring reaches the anode, it breaks up under the influence of the appreciably enhanced current. Then there forms a new ring near the cathode which again begins to shift and grow. The process repeats periodically. The rate of displacement of the rings is of the order of 10^{-2} cm/sec.

6. Sometimes instead of monotonic growth of the ring there is observed "breathing" or fluctuation of either the entire ring or parts thereof. This is accompanied by current fluctuations.

7. The rate of displacement of the ring or the pulsation frequency increases with increase of the conductivity (under illumination).

8. Powder patterns revealing the field lines of force appear at exactly the same location as the darkened ring.

At the present stage of the investigation we can only assert that the observed effect cannot be explained solely by nonuniform heating.

If the experiments are carried out at low temperatures one can neglect the diffusion of heavy lattice ions under the influence of the field.

For the purpose of qualitative determination of the field distribution we are now carryong out measurements of the potential by the probe technique and also spectrographic investigations of the shape of the absorption edge. It is highly probable, however, that the observed darkening effect directly characterizes the field distribution.

At present we do not want to go much beyond communicating these first results, which, despite the fact that the causes of the phenomenon are still unclear, undoubtedly provide a means for investigating the process of conduction in the high field region.

In addition, it is to be hoped that with improvement of the sensitivity of the equipment it will be possible to detect other electron-optical effects for direct study of the field and current density distribution in weak fields as well.

I would like to sincerely thank my colleagues who participated in this research, particularly, Kümmel, Gutjahr, Hänsch & Dziesiaty. I also want to thank Prof.Rompe and Prof.Franz for interesting discussions.

Bereich Elektrischer Durchschlag,
Physikalisch-Technischen Institut
Deutsche Akademie der Wissenschaften zu Berlin

References

1. W.Schottky, Z.Phys., 113, 367 (1939); W.Schottky & W.Spenke, Wiss.Veröff. Siem.Konz., 18, 229 (1939); W.Schottky, Z.Phys., 118, 539 (1942); E.Oldekopp, Dissertation.-Göttingen, 1952; N.Mott, Proc.Cambridge Philos.Soc., 34, 568 (1938); N.F.Mott, Proc.Roy.Soc.A, 171, 27 u. 944 (1939); D.I.Blokhintsev & B.I.Davydov, Ber.Akad.Wiss. - Doklady, UdSSR, 20, 279 (1938); B.I.Davydov, Zhur.eksp.i teor. phys., 10, 1342 (1940); S.I.Pekar, Zhur.eksp.i teor.fiz., 10, 210 (1940); S.I. Pekar, Zhur.eksp.i teor.fiz., 9, 534 (1939); S.I.Pekar, Izvestiya AN SSSR, Ser. fiz., 5, 422 (1941); E.Spenke, Z.Phys., 126, 67 (1947); K.W.Böer, Arb.Tagung Festkörperphysik Dresden, 112 - Deutscher Verl. d. Wiss., Berlin, 1952.

2. K.Wagner in H.Schering, Die Isolierstoffe der Elektrotechnik - Berlin, 1924; K.W.Böer & U.Kümmel, Ann. Phys., 20, 303 (1957).

3. K.W.Böer & U.Kümmel, Naturforsch. a 12, 667 (1957); K.W.Böer & U.Kümmel, Ann.Phys., 2, 217 (1958).

4. K.W.Böer & H.Gutjahr, Z.Phys., 152, 203 (1958).

5. K.W.Böer & U.Kümmel, Ann.Phys., 16, 181 (1955).

6. K.W.Böer, International Conference on Solid State Physics in Electronics and Telecommunication. Brüssel, June, 1958. - London, 1960.

7. K.W.Böer, J.Dziesiaty & U.Kümmel, Z.Naturforsch., 13, 560 (1958).

8. K.W.Böer, U.Kümmel & R.Rompe, Z.Phys.Chem., 200, 180 (1952); K.W.Böer & U.Kümmel, Ann.Phys., 14, 341 (1954).

9. B.P.Gross, B.P.Zakharshenya & N.M.Reinov, Doklady AN SSSR, 97, 57 (1954).

SOME THEORETICAL CONSIDERATIONS CONCERNING INHOMOGENEOUS FIELD DISTRIBUTION IN ELECTRIC BREAKDOWN*

- K.W.Böer

Introduction

It was shown in the preceding paper[1] that with the aid of electron-optical effects one can observe inhomogeneities of electric conduction in crystals. Specifically, the crystals are observed under a microscope in monochromatic light at the principal absorption edge. Upon application of an electric field, there is observed in the crystals a spatially inhomogeneous displacement of the absorption edge to the side of longer wavelengths which is evinced by nonuniform darkening of the crystal. Of particular interest in these experiments is the frequent appearance around the cathode of a darkened annular region (see Fig.8 in the preceding article). This effect becomes apparent when the field applied to the electrode attains approximately 0.1 the breakdown value. With increase of the voltage the darkening becomes more intense and the distance of the darkened region from the cathode generally increases[2].

It was shown by powder pattern studies and probe measurements that the observed darkening presumably represents the actual spatial field distribution. However, since the powder patterns and probe measurements give the surface distribution, while the darkening effect involves a large part of the crystal volume, at present we can only tentatively assume this correlation between the darkening and the field distribution. In this paper we shall propose and discuss a mechanism that allows of explaining the inhomogeneous field distribution. We shall mention some of the inferences that are of particular interest from the standpoint of the physics of electric breakdown.

Potential, Field and Space Charge Distributions

Assuming that the variation of the darkening corresponds to the field distribution in the crystal, we note that the field is weakest at the cathode and increases rapidly with increasing distance from it. In the specific case of the crystal pictured in Fig.8 of the preceding article, the field intensity attains a maximum value at a distance of 0.5 mm from the cathode and then falls off sharply. There is no noticeable darkening between this sharp boundary and the anode; here the field intensity is very low.

Fig.1 shows the distributions of the potential, field and space charge as given by Poisson's equation on the basis of the above assumptions regarding the appearance of the darkened regions. The problem now is to propose a mechanism capable of explaining the distributions shown in Fig.1. The appearance of space charge indicates the influence of real structure. While the real structure should not determine the geometric shape of the effect, it can influence the minimum field intensity at which the effect appears and apparently determines the quantitative field distribution.

The space charge appearing in a real crystal is given by the difference between the concentrations of the positive and negative charge carriers:

$$\rho(x) = e\{n^{+}(x) - n^{-}(x)\}. \tag{1}$$

These charge carriers can either be free or trapped on defect levels. In CdS

---

*We take this opportunity to thank Prof.Böer for permission to publish his reports and for providing a copy of the German text. *Translation Editor.*

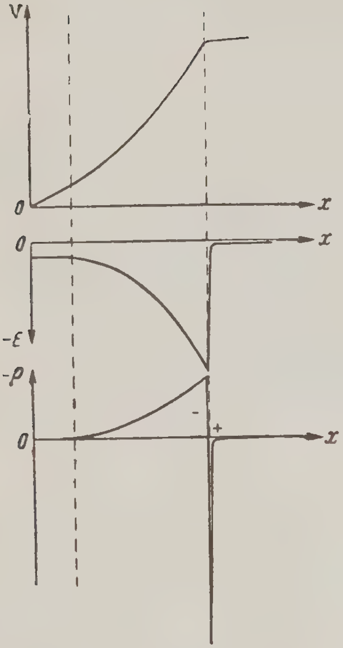

Fig.1. Potential, field and space charge distributions near the cathode.

the free charges with an appreciable concentration are conduction electrons (n-type conductivity). The other charges are "stationary" and are bound in activator levels and traps. In a vanishingly small external field the crystal as a whole is electrostatically neutral. In the first approximation this may also be assumed for each part of the crystal (condition of quasi-neutrality). In this case space charge does not appear (we neglect boundary layers and layers between domains with different conductivity in the crystal).

Electric excitation from defect levels

To explain the space charge distribution shown in Fig.1, we make the following assumptions.

1. Excitation of electrons from trapping levels into the conduction band and of holes from activator centers into the valence band occurs under the influence of the effective field. This excitation monotonically increases with the increasing field strength.
2. Recombination of electrons with holes is accelerated if the electrons or holes are free.
3. Under the influence of external fields the conduction electrons are displaced so that the spatial profile of the electron distribution is deformed in the direction of the electric field.
4. The locally variable field can attain a maximum value at which there occurs a sharp increase in conductivity owing to intensive electric excitation.
5. The field intensity at the cathode cannot exceed a certain maximum value depending on the contact conditions.

Spatially homogeneous case

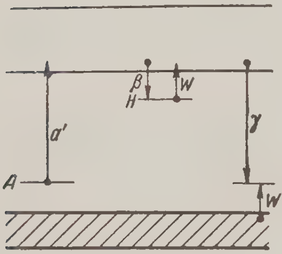

Fig.2. Reaction-kinetic model: a' = optical excitation probability; W and W' = electric excitation probabilities; A and H = level concentrations; β and γ = recombination coefficients.

To simplify the ensuing calculations we assume that there is only one trapping level and a group of activators with one energy level. The concentration of negative charge carriers is given by the sum of the concentration n of conduction electrons and the number h of electrons in the trap:

$$n^- = n + h. \tag{2}$$

The concentration of positive charge carriers is approximately equal to the number of holes trapped in activators:

$$n^+ = p. \tag{3}$$

The carrier concentration is calculated by means of the set of differential equations written for the reaction-kinetic model shown in Fig.2. The static concentration is obtained for

$$\frac{dn}{dt}=\frac{dh}{dt}=\frac{dp}{dt}\equiv 0. \qquad (4)$$

In the zero field case the probabilities W_{el} and W'_{el} vanish. The concentration will be expressed in terms of n_0, p_0 and h_0.

With increasing field strength p and h monotonically decrease since W_{el} and W'_{el} are monotonically increasing exponential functions of the field (we are not considering here the mechanism of electric excitation). By virtue of the fact that initially the electric excitation is constant over the volume, the quasi-neutrality of the crystal is not disturbed; hence

$$n+h=p. \qquad (5)$$

According to Eq.(5), owing to electric excitation with $n^+=p$, the negative carrier concentration $n^-=n+h$ decreases to the same extent as the concentration n^+ of positive charge carriers. Hence we can write

$$n^-=n^+\leqslant n_0^-=n_0^+, \qquad (6)$$

where the subscript o indicates zero field data.

Spatially inhomogeneous problem

As was shown above, the effective field in the range of high fields produces some decrease in the relative concentration of positive and negative carriers. By virtue of the fact that in a real crystal the conductivity is not uniform over the entire volume, the field intensity may undergo small variations. Let us consider a localized section of the crystal where the field is slightly stronger than in neighboring sections. Under the influence of the acting field there will be drawn into this region conduction electrons from the neighboring regions so that eventually this high field region will contain more negative carriers than positive ones. Hence in this region the condition of quasi-neutrality will be disturbed and there will appear a negative space charge.

By virtue of this, the acting field here increases, while the concentration of negative charge carriers decreases. This process leads, therefore, not to equalization of the disturbed equilibrium concentration but to further aggravation of the disequilibrium. The space charge increases with increasing distance from the cathode and according to Poisson's equation

$$\frac{d^2U}{dx^2}=-\frac{4\pi}{\varepsilon}\rho(x), \qquad (7)$$

the intensity of the acting field also increases monotonically (Fig.3).

Hence it may be expected that if the applied field is sufficiently strong to excite electrons or holes from levels in the forbidden band, there may begin the following process:

a) the concentration of positive and negative carriers will decrease, owing to enhanced recombination;

b) in regions where the field is comparatively high (due, for example, to statistical fluctuations) there will be a sharp decrease in the charge carrier concentration;

c) owing to the influence of the field, free negative charges will predominate and as a result there will form a negative space charge;

d) this space charge will result in an increase of the field in the field direction and hence the space charge and field will rise in the direction of the

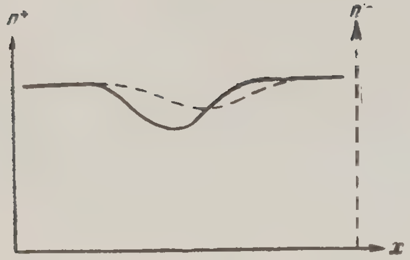

Fig.3. Spatial distribution of charge carrier concentration.

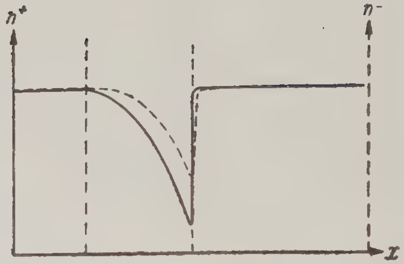

Fig.4. Spatial distribution of charge carrier concentration.

anode;*

e) this process is accentuated in the initially disturbed low carrier concentration regions and the inhomogeneities can attain a macroscopic magnitude.

The field can increase only to the value at which there begins rapid multiplication of the charge carriers owing to electric excitation; this results in a marked increase in conductivity and, consequently, leads to decrease of the field intensity.

The conduction electrons produced in this region will be drawn from their point of origin in the direction of the anode, thus favoring a growth in conductivity in a large region in the vicinity of the anode. This region of electron multiplication remains the region of positive space charge (double layer) (see Fig.4).

The space charge distribution shown in Fig.4, which is characterized by a pronounced field "peak" with a sharp boundary on the side of the anode, may occur initially only at one point in the crystal between the anode and the cathode, i.e., at a point where after application of the external field there happens to form a local high field region owing to statistical fluctuations.

The rapid displacement of this initial space charge zone in the direction of the cathode[2] can be explained if we assume that the part of the space charge region located near the anode has a higher conductivity than the entire space charge region or the part of it near the cathode. As soon as there is established in such a conducting system a state of minimum general resistance or maximum current, the high conductivity region will tend to expand towards the anode. It follows therefore that the space charge region should tend to shift in the direction of the cathode, which is what is observed experimentally.

With further approach to the cathode, the field intensity at the boundary between the metal and the CdS crystal increases. If at this point it attains a value greater than or equal to the maximum that can be attained in the crystal, the space charge region will be displaced to the cathode to such an extent that the point of maximum field strength will be located immediately at the boundary between the metal and the CdS. In this case, however, no field "peak" will be observed at the cathode.

The fact that there is a distinct space charge region at the cathode indicates that the maximum field intensity at the metal-CdS boundary is appreciably lower than the field intensity inside the crystal.

---

*The conduction electrons will not fully eliminate the dip in the carrier concentration; there will occur only a shift and some equalization of the curve (Fig.4). As a result, the space charge will be lower and the field increment in the direction of the cathode weaker than assumed.

Comparison of Theory with the Experimental Results

All the results described in the preceding paper[1] can be explained by means of the model proposed above. Furthermore one can infer a number of interesting physical effects.

1. It may be expected that the shape of the field "peak" near the cathode will depend on the distribution of the defect levels, inasmuch as it is assumed that build-up of the space charge depends on electric excitation of electrons and holes from defect levels. The fact that different field distributions are obtained for different crystals[2] substantiates this inference. It is reasonable to assume that one can draw certain conclusions regarding the distribution of defect levels by observation of the darkening distribution in a crystal.

2. One can judge of the spatial inhomogeneities of a crystal from the inhomogeneous darkening of sections of the annular darkened region.

3. The fact that there sometimes form two concentric darkened regions indicates that the region of enhanced conductivity does not occupy the entire space between the electron production zone and the anode. The electrons under the influence of the field drift from the point of their origin in the direction of the anode. Owing to trapping of electrons by lattice defects, the concentration of free electrons falls off with increasing distance from their point of origin. The field intensity increases accordingly and thus there may form a new space charge region and another field "peak". Thus a process analogous to that occurring at the cathode may also occur in the crystal. One can draw certain inferences regarding the drift path of the conduction electrons from the distance between the two darkening rings.

The large time constant obtained from the dielectric relaxation time,

$$\tau = \frac{\varepsilon - \varepsilon_0}{\sigma},$$

is difficult to understand; in order to explain its magnitude one must hypothesize the existence of regions with a conductivity five times lower than is obtained from the measured current, applied voltage and size of the crystal on the assumption of uniform conductivity. Inasmuch as the quotient obtained by dividing the applied voltage by the distance between electrodes is approximately 10^5 v/cm, in such regions the field strength would presumably attain 10^{10} v/cm, which is obviously impossible.

With the described mechanism the time constant must be evaluated from the time to attainment of a steady state (solution of the reaction-kinetic equation), which for the light intensity utilized is of the order of 1 sec. The settling time is strongly dependent on the conduction electron concentration; this was also found in observation of the darkening effect.

Influence on the Process of Electric Breakdown

Our experimental studies showed that in the region of high field strength there is also a marked current rise. This means that the field distribution in the breakdown region is not uniform over the volume. The breakdown field intensity will be attained only in a spatially localized, relatively small region of the crystal. Until the breakdown voltage on the electrode is attained, the high ohmic part of the crystal near the cathode acts as a stabilizing resistance hindering disruptive breakdown.

With increase of the applied voltage this stabilization becomes worse and finally fails at the breakdown voltage. Here in a relatively thin layer there is attained a high field intensity which, because of generation of conduction electrons, leads to a sufficiently heavy current to produce thermal disruption of the crystal. If we accept these assumptions, it becomes understandable why the breakdown voltage depends strongly on the real structure of the crystal[3].

The thickness dependence[4] of the breakdown field strength following from the theory of impact ionization can be explained otherwise. It has been reliably established that in thin layers one cannot obtain a high field intensity. Consequently, one must apply a higher voltage to thin layers in order to obtain a true breakdown field in a small crystal region. Finally, on the basis of the proposed mechanism one can readily understand the effects (described in the preceding paper[1]) obtained with a pulse voltage, particularly, the observed increase of the breakdown voltage with reduction of the pulse duration. In the case of short-term loads (brief pulses) there is not sufficient time for build-up of a space charge and for breakdown to occur the applied voltage must be relatively higher.

There follows from the above the important inference for the theory of electric breakdown that the breakdown voltages commonly accepted, at least for CdS, are at least one order of magnitude too low.

For qualitative evaluation of the applicability of the hypotheses advanced above one might be tempted to use the simplified model proposed in Fig.2. This, however, is impossible inasmuch as the proposed distribution of defect levels does not obtain in a real crystal, and moreover, it is impossible to determine the diffusion term in the equation.

Bereich Elektrischer Durchschlag,
Physikalisch-Technischen Institut,
Deutsche Akademie der Wissenschaften zu Berlin

References

1. K.W.Böer, Present issue of the Bulletin, p.35.
2. K.W.Böer, H.I.Hänsch & U.Kümmel, Naturwissenschaften, 45, 460 (1958); K.W.Böer, Congrès International sur le physique de l'état solide et ses applications. - Akad.Press, 1958.
3. K.W.Böer & U.Kümmel, Z.Naturforsch a, 9, 267 (1954); K.W.Böer, U.Kümmel & G.Ksoll, Ann.Phys. (in press).
4. W.Franz, Handbuch der Physik, XVII, S.244. - Springer, 1956; K.W.Böer, U.Kümmel & W.Misselwitz, Naturwissenschaften, 45, 331 (1958).

INFLUENCE OF FIELD EMISSION ON THE DISTRIBUTION OF STRONG FIELDS IN SOLIDS

- É.I.Adirovich

Introduction

In his reports to the present conference, Prof.Böer[1,2] described a new optical procedure for investigating strong electric fields in solid dielectrics and semiconductors. Being based on utilization of quantum-mechanical effect leading to displacement of the long wavelength absorption edge in the crystal under the influence of the electric field, this procedure allows of visual observation of the field distribution in solids. The absorption of light with a wavelength at the principal absorption edge increases with increasing field intensity. Hence the luminosity of the crystal observed in transmitted light is not uniform: the sample appears darker at points where the field E is stronger, and lighter where the field is weaker. Under appropriate experimental conditions the light and dark pattern in transmitted light coincides with the field distribution in the crystal.

The procedure proposed by Böer has obvious advantages over probe and similar techniques of investigating electric fields in solids. These advantages are particularly important in the case of nonsteady processes involving redistribution of fields and space charges. Interesting results regarding the field and space charge distributions were obtained by Böer for CdS single crystals[1].

Theoretical concepts regarding the processes in CdS single crystals, leading to the appearance of an E "peak" (field maximum) in the crystal and displacement of this maximum towards the cathode, were given by Böer in his second report[2]. Essentially, the electric field increases the probability of freeing of electrons from sticking levels into the conduction band and also the probability for filling of activator levels by electrons from the valence band. Recombination and redistribution of the majority of free current carriers (electrons in CdS) leads to the situation where deviations from field homogeneity due to inhomogeneities of the crystal or fluctuations do not relax but on the contrary build up to the point where the local field intensity is limited by breakdown considerations.

In our opinion, however, there is a difficulty as regards the concepts developed by Böer. Experiment shows that after formation in the crystal of a maximum field region, this region begins to migrate through the crystal towards the cathode; it does not reach it but stops at a certain distance from the cathode.[1] Instead of a physical explanation of this fact, Böer introduces two formal conditions, namely, the requirement of a minimum general resistance of the crystal and the requirement that the field at the cathode remain lower than the field in the maximum field region. The present paper is devoted to a consideration of this problem and the associated effect of oscillation of the maximum field region with a constant difference of potentials applied to the crystal[1]. In addition to a qualitative analysis of the transient effects, we give a calculation of the steady-state field distribution in the solid with local electronic states on the assumption that the influence of the field predominates over the thermal effects (high field case).

1. Influence of field emission on the kinetics of field redistribution

Let us consider a dielectric or, more accurately, a semiconductor with a low resistivity (for example, at low temperature) placed in a strong electric field. Let us assume that owing to the presence of impurities or defects, the semiconductor has primarily one type of conductivity; to be specific, let us assume that we are dealing with an n-type semiconductor.

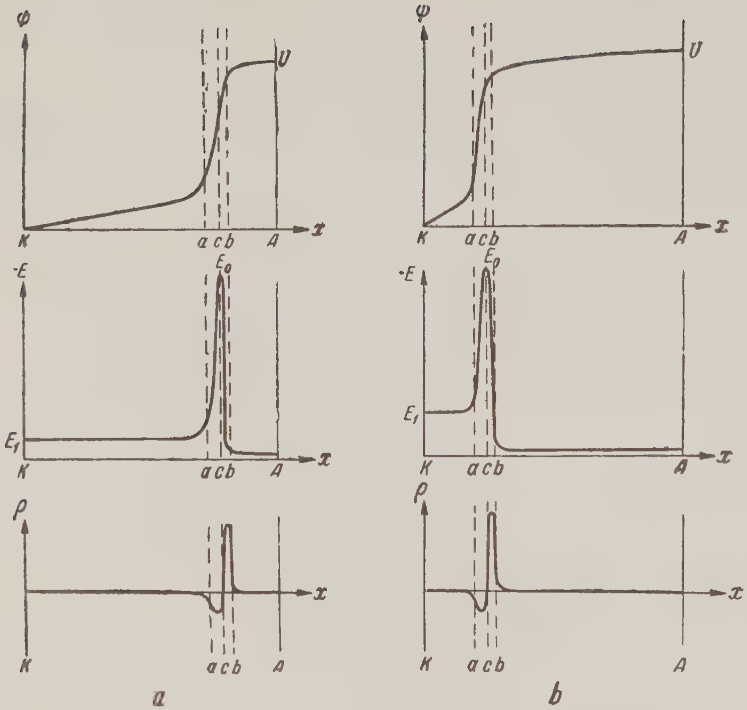

Fig.1. Distributions of potential, field intensity and space charge density at the beginning of the process of ionization of defects by the field (a) and in the steady state (b): K - cathode, A - anode, *a* and *b* - boundaries of the strong field region, *c* - position of the field maximum.

Let us assume that owing to volume inhomogeneities, fluctuation or other factors there has developed in the region *ab* (Fig.1) a field intensity appreciably exceeding the average field $E_{av} = -U/L$ and that this enhanced field intensity has substantially increased the local probability for transition of electrons from filled discrete levels to the conduction band. If such a strong field were produced from outside the semiconductor and were uniform throughout its volume, it would obviously produce no redistribution of space charges but would merely result in a change in the concentration of free and trapped electrons and holes. Under the conditions in question, relaxation of the conduction electrons produced by the field in the *ab* region will occur not only owing to recombination but also because of elimination or ejection of the electrons by the field through the boundary *b*. In a strong field this drift process will play a substantial role in the kinetics of the change in the number of free electrons in the *ab* region. As a result there will be a build-up of positive space charge in the region *cb*, which will lead to a decrease of the field intensity E inside *cb* and to an increase of E in the *ac* region*, i.e., to a displacement of the field "peak" and the whole region of localization of the strong field in the direction of the cathode.

The process of displacement of the *ab* region towards the cathode, illustrated in Fig.1, will be accompanied by increase of the field in the vicinity of the cathode and particularly in the immediate proximity of this electrode. This process must cease at the instant when the field and the metal-semiconductor interface attains a certain value $-E_1$, corresponding to the beginning of field emission from the cathode.

The reason for the displacement of the strong field region in the direction of the cathode is the transformation of negative space charge to positive charge

---

*The appearance of large positive values of $\rho(x)$ in the *cb* region will lead to a sharp decrease of the negative field in this region. It leads to a decrease of the potential drop between the cross section *c* and anode which (assuming a constant voltage between the electrodes) leads to an increase of the field to the left of *c*.

to the left of c, owing to the fact that ionization of the impurities by the field and the drift departure of the electrons through the cross section c are not compensated by the arrival of electrons from the side of the cathode (through cross section a). But at the instant when the field at the cathode attains the value $-E_1$, in addition to the earlier current distribution, there appears a field emission current from the cathode, which tends to balance the arrival and departure of electrons to and from the strong field region and leads to cessation of migration of this region through the semiconductor. Closer approach of the ab region to the cathode is impossible because, owing to the strong field dependence of the field emission current from the cathode, the electron flux into the strong field region from the side of the cathode would exceed the electron flux from this region to the anode, which would result in a displacement of the ab region in the opposite direction (i.e., towards the anode).

Let us now see what would occur if after attainment of the steady-state field distribution, we increase the potential difference applied to the semiconductor. Owing to increase of the field at the metal-semiconductor boundary, the field emission current from the cathode will increase. As a result the balance between incoming and outgoing electron fluxes will be disturbed, that is, the influx of electrons from the side of the cathode will come to exceed the departing flux to the anode. This will cause the strong field region to be displaced from the cathode towards the anode. This displacement of the ab region is a process with complex kinetics. Owing to the field dependence of the probability for freeing trapped electrons, the shift of the strong field region must lead to disturbance of the equality between the numbers of forward and reverse transitions, a change in the electron distribution in space and the appearance of additional diffuse fluxes. Consequently, the process of redistribution of fields and space charges produced by a change in the potential difference on the semiconductor may have noticeable aftereffects determined by the characteristic times of the processes of recombination, diffusion and so on.

The lagging component of the change in the field on the cathode, associated with the time dependent processes, may lead to the situation where even after the strong field region stops moving, the emission current from the cathode will continue to decrease, so that the balance of electron fluxes will be disturbed and the region ab will begin to move back towards the cathode. Under certain circumstances it may continue past the steady-state position and stop at a distance closer to the cathode; then, owing to continued increase of the delayed component of the cathode field and the resultant inverse imbalance of the electron fluxes, the entire process may begin anew.

We see that the internal (freeing of electrons from traps) and external (ejection of electrons from the cathode) effects associated with field emission and the kinetics of the processes of redistribution of electrons among quantum states and in the volume of the semiconductor can lead to self-oscillation of the field and space charge, for it is obvious that two different values of the field emission current from the cathode may correspond to the same position of the maximum field region in the semiconductor. As follows from the above analysis, the period of these oscillations will depend on the characteristic time of the semiconductor kinetics and not on the Maxwell relaxation time.

2. Steady-state distribution of a strong electric field

Böer proposes to represent the CdS single crystal by a band model containing local (trapping) levels of two types[2]. Illumination of the crystal is interpreted not only as a means for visualizing the field distribution but also as a physical agent determining the filling of upper levels by electrons. In our opinion such a special model is not necessary to obtain an inhomogeneous field distribution in the high field region. Hence we shall base our examination not on the specific band diagram of cadmium sulfide but on a general model encompassing the following fundamental features: 1) the presence of local (trapping) levels in the crystal, 2) field dependence of the probability for freeing of electrons from traps, and 3) field emission from the cathode with $E = -E_1$.

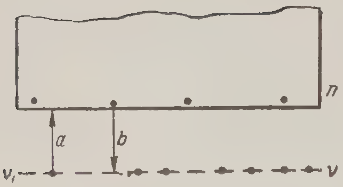

Fig.2. Energy diagram.

Let us consider the energy diagram for a crystal shown in Fig.2; it consists of a conduction band and local donor levels of one type. Electron processes in such a model may be described by the equations:

$$\left.\begin{aligned}&\frac{\partial n}{\partial t}-\frac{1}{q}\operatorname{div}\mathbf{j}=a\nu-bn(\nu_1-\nu),\\&\frac{\partial\nu}{\partial t}=-a\nu+bn(\nu_1-\nu),\\&j=q\mu n\mathbf{E}+qD\operatorname{grad}n,\\&\operatorname{div}\mathbf{E}=\frac{4\pi}{\varepsilon}\rho,\\&\rho=q(\nu_1-\nu-n).\end{aligned}\right\}\qquad(1)$$

Here ν_1, ν and n are the concentrations, respectively, of donors, electrons in trapping levels and electrons in the conduction bands; a and b are the probabilities for freeing and trapping of an electron by defects in a unit volume per unit time. The other designations are consistent with the conventional notation.

Let us analyze the steady-state case at a sufficiently low temperature when the thermodynamic equilibrium conductivity due to thermal freeing of electrons from traps is low. This is a necessary condition for producing a strong field in a semiconductor. For a crystal of macroscopic dimensions and not very high values of the average field $E_{av} = -U/L$, the current density $j = 0$*.

Writing the condition for a minimal current in the form $j \approx 0$ has different meanings for regions where there is a diffusion current and for regions where this current can be neglected: the first case, the total current j is small compared with the partial diffusion and drift currents ($j \ll j_{dr} \approx -j_{dif}$) in the latter case both the total current j and its drift component j_{dr} are small.

The probability for ejection of electrons from local states into the conduction band depends on the temperature and the field intensity: $a = a(T, E)$; at a sufficiently low temperature, however, we can write $a = a(E)$.

The field dependence of the probability for freeing of electrons from defects by the electric field must be very strong. We can approximate it by the function

$$a(E)=\begin{cases}0 & \text{for } |E|<E_0,\\ \infty & \text{for } |E|\geqslant E_0,\end{cases}\qquad(2)$$

where E_0 is the critical value of the field at which there beings intense freeing of electrons from defects (internal field emission). From the set of equations for the steady state:**

---

*Hereinafter for the sake of brevity, instead of "current density" we will simply say "current".

**We are considering the one dimensional problem and making use of the Einstein equation $D/\mu = kT/q$. As usual, $p = \nu_1 - \nu$ is the concentration of holes in the trapping levels.

$$\left.\begin{aligned} &\frac{dj}{dx}=0,\\ &p=\frac{\nu_1}{1+\frac{b}{a(E)}\,n},\\ &\frac{dn}{dx}+\frac{q}{kT}\,nE=\frac{j}{qD},\\ &\frac{dE}{dx}=\frac{4\pi}{\varepsilon}\,q\,(p-n), \end{aligned}\right\} \qquad (3)$$

it follows that with the probability for defect ionization given by Eq.(2), $E=-E_0$ will be the maximum possible value of the field intensity in the semiconductor; this value can be attained only at one or at most a few isolated points. Actually, in the limit as $x\to x_0-0$, E will tend to $-E_0$ in absolute value. Moreover, $\left.\frac{dE}{dx}\right|_{x_0-0}=-\frac{4\pi}{\varepsilon}qn<0.$ But at the point $x=x_0$ the concentration p abruptly changes its value from 0 to ν_1, and in consequence

$$\left.\frac{dE}{dx}\right|_{x_0+0}=\frac{4\pi}{\varepsilon}\,q\,(\nu_1-n)>0.$$

To find the inhomogeneous field distribution in a semiconductor we must solve the set of equations (3) to the left (cathode region) and right (anode region) of $x=x_0$ under conditions of continuity of the solution in the singular point x_0. The value of x_0 must be determined from the solution of the problem. The plane $x=x_0$ under these conditions represents the region of strong ionization of defects in which we cannot neglect the term j/qD in the third equation of the set (3) (the region cb in Fig.1). With $\nu_1\approx 10^{17}$ cm^{-3} a change in the field strength $\Delta E\approx 10^6$ v/cm occurs at a distance

$$l=\frac{\varepsilon\Delta E}{4\pi q\nu_1}\approx 10^{-5}\ \text{cm}, \qquad (4)$$

which is appreciably smaller than the distance L between electrodes. Hence this limit replacement of the region cb by a plane is admissible. The joining of the solutions for the cathode and anode regions is determined by the values set for the jumps in field strength and potential at $x=x_0$, i.e., by the value assumed for the charge and the thickness of the double layer in the vicinity of the singular point. Noting that the change in potential at the distance l is much less than the voltage between electrodes, we specify the boundary conditions at the singular point in the following form:

$$E|_{x_0-0}=-E_0;\ E|_{x_0+0}=0;$$
$$\psi|_{x_0-0}=\psi|_{x_0+0}=U. \qquad (5)$$

We shall return to a discussion of these conditions below. In the anode region $(x>x_0)$

$$\psi\approx U;\ E=n=p=\rho\approx 0. \qquad (6)$$

The carrier concentration, space charge density, partial current and field strength distributions in the cathode region are given by the equations

$$\left.\begin{aligned} &\frac{dn}{dx}+\frac{q}{kT}\,nE=0;\quad \frac{dE}{dx}+\frac{4\pi}{\varepsilon}\,qn=0;\\ &p=0;\quad \rho=-\frac{4\pi}{\varepsilon}\,qn;\ j_{\text{dr}}=q\mu nE;\ j_{\text{dif}}=qD\,\frac{dn}{dx}\,. \end{aligned}\right\} \qquad (7)$$

Introducing the potential ψ and setting $\psi|_{x=0} = 0$, we obtain

$$n = \frac{\varepsilon C_1}{8\pi kT} e^{\frac{q\psi}{kT}}, \tag{8}$$

where $\frac{\varepsilon C_1}{8\pi kT}$ is the electron concentration immediately at the cathode (for $x = 0$). The problem in the cathode region reduces to solution of the equation

$$\frac{d^2\psi}{dx^2} = \frac{qC_1}{2kT} e^{\frac{q\psi}{kT}}. \tag{9}$$

The first integral of this equation allows of expressing the field intensity as a function of the potential:

$$E = -\frac{d\psi}{dx} = -\sqrt{C_1 e^{q\psi/kT} + C_2}. \tag{10}$$

Second integration gives the potential distribution in the form of the inverse function

$$x = \int_0^{\psi} \frac{d\psi}{\sqrt{C_1 e^{q\psi/kT} + C_2}}. \tag{11}$$

The integration constants C_1 and C_2 and the position x_0 of the strong field region are determined from the conditions

$$\left.\begin{aligned} E|_{\psi=0} &= -\sqrt{C_1 + C_2} = -E_1, \\ E|_{\psi=U} &= -\sqrt{C_1 e^{qU/kT} + C_2} = -E_0, \\ x_0 &= \int_0^{U} \frac{d\psi}{\sqrt{G_1 e^{q\psi/kT} + C_2}}. \end{aligned}\right\} \tag{12}$$

Integrating in (11) and introducing the modified constants:

$$\lambda = \frac{C_1}{C_2} \quad \text{and} \quad r = \frac{kT}{q\sqrt{C_2}}, \tag{13}$$

we arrive at the following parametric form of the solution:

$$\begin{aligned} E &= -\frac{kT}{qr} z, \\ x &= r \ln \frac{(z-1)(z_0+1)}{(z+1)(z_0-1)}, \end{aligned} \tag{14}$$

the parameter being

$$z = \sqrt{\lambda e^{q\psi/kT} + 1}. \tag{15}$$

Solving the second equation (14) for ψ, we find the potential distribution between the cathode and singular point x_0, corresponding to the region of ionization of impurities

$$\psi = \frac{2kT}{q} \ln \frac{\operatorname{sh} \frac{R}{2r}}{\operatorname{sh} \frac{R-x}{2r}}. \tag{16}$$

For convenience of notation instead of λ, we have introduced here the constant R having the dimenionality of length:

$$R = r \ln \frac{\sqrt{\lambda+1}+1}{\sqrt{\lambda+1}-1}\,. \tag{17}$$

From (16) we find the field intensity distribution:

$$E = -\frac{kT}{qr}\,\mathrm{cth}\,\frac{R-x}{2r}\,. \tag{18}$$

Conditions (12) can now be written in the form

$$\left.\begin{aligned} &\frac{kT}{qr}\,\mathrm{cth}\,\frac{R}{2r} = E_1,\\ &\frac{kT}{qr}\,\mathrm{cth}\,\frac{R-x_0}{2r} = E_0,\\ &\frac{\mathrm{csch}\,\dfrac{R-x_0}{2r}}{\mathrm{csch}\,\dfrac{R}{2r}} = e^{\frac{qU}{kT}}, \end{aligned}\right\} \tag{19}$$

whence we determine the integration constants

$$\left.\begin{aligned} r &= \frac{kT}{qE_1}\sqrt{\frac{e^v-1}{e^v-\varkappa}}\,,\\ R &= \frac{kT}{qE_1}\sqrt{\frac{e^v-1}{e^v-\varkappa}}\,\ln\frac{\sqrt{e^v-1}+\sqrt{e^v-\varkappa}}{\sqrt{e^v-1}-\sqrt{e^v-\varkappa}} \end{aligned}\right\} \tag{20}$$

and the point of localization of the strong field:

$$x_0 = \frac{kT}{qE_1}\sqrt{\frac{e^v-1}{e^v-\varkappa}}\,\ln\frac{(\sqrt{e^v-1}+\sqrt{e^v-\varkappa})(\sqrt{\varkappa(e^v-1)}-\sqrt{e^v-\varkappa})}{(\sqrt{e^v-1}-\sqrt{e^v-\varkappa})(\sqrt{\varkappa(e^v-1)}+\sqrt{e^v-\varkappa})}\,. \tag{21}$$

Here

$$v = \frac{qU}{kT} \quad \text{and} \quad \varkappa = \frac{E_0^2}{E_1^2}\,. \tag{22}$$

The value of x_0 depends on U, E_1 and E_0 but does not depend on the dimensions of the semiconductor (specifically on L the distance between electrodes). The inhomogeneous field distribution due to the effects of internal and external field emission can be stationary only on condition that

$$x_0(U, E_1, E_0) < L. \tag{23}$$

Inasmuch as $\frac{kT}{q} \approx 0.025$ v at room temperature and ~0.01 v at liquid air temperature, the exponential $e^{qU/kT}$ may be regarded as much greater than not only unity but also the ratio E_0^2/E_1^2. This enables us to simplify the expressions for r, R and x_0:

$$\left.\begin{aligned} r &= \frac{kT}{qE_1}\,,\\ R &= \frac{U}{E_1} + \frac{kT}{qE_1}\ln\frac{4E_1^2}{E_0^2-E_1^2} \approx \frac{U}{E_1}\,,\\ x_0 &= \frac{U}{E_1} + \frac{kT}{qE_1}\ln\frac{4E_1^2}{(E_0+E_1)^2} \approx \frac{U}{E_1}\,, \end{aligned}\right\} \tag{24}$$

and to represent the potential, field and space charge density distributions in the cathode region (in the region between the cathode and the point of localization of the strong field) by the following formulas

$$\left.\begin{aligned}\psi &= \frac{2kT}{q}\ln\frac{\operatorname{sh}\frac{1}{2}\left[\frac{qU}{kT}+\ln\frac{4E_1^2}{E_0^2-E_1^2}\right]}{\operatorname{sh}\frac{1}{2}\left[\frac{q}{kT}(U-E_1x)+\ln\frac{4E_1^2}{E_0^2-E_1^2}\right]},\\ E &= -E_1\operatorname{cth}\frac{1}{2}\left[\frac{q}{kT}(U-E_1x)+\ln\frac{4E_1^2}{E_0^2-E_1^2}\right],\\ \rho &= -\frac{q\varepsilon E_1^2}{8\pi kT}\operatorname{csch}^2\frac{1}{2}\left[\frac{q}{kT}(U-E_1x)+\ln\frac{4E_1^2}{E_0^2-E_1^2}\right].\end{aligned}\right\}\qquad(25)$$

It follows from Eqs.(24) and (25) that the space charge and the inhomogeneous field are localized in the vicinity of the region of strong ionization of defects; the location of this region relative to the electrodes depends on the applied potential difference U and the magnitude of the field E_1 for field emission from the cathode, but virtually does not depend on the magnitude of the critical field E_0 for internal field emission from defects:

$$x_0 \approx U/E_1.$$

The physical meaning of this unexpected result is that the field $E \approx -E_0$ is localized in the region of high space charge density and, consequently, large values of dE/dx. Hence the difference as regards the positions of x_0 for two semiconductors with different E_0 (but the same E_1 must be small:

$$\Delta x_0 \approx \frac{\Delta E_0}{dE/dx} \ll x_0. \qquad (26)$$

For $U \approx 1000$ v and $E_1 \approx 10^5$ v/cm, we find $x_0 \approx 10^{-2}$ cm, which is in agreement with the experimental data of Böer[1].

In conclusion, we note that in the case when the positive space charge in the region of internal field emission does not produce complete screening of the field, instead of (5) there will obtain the following boundary conditions ($\psi_1 < \psi_2 < U$):

$$\left.\begin{aligned}E|_{x_0-0} &= -E_0; & E|_{x_0+0} &= -E_2;\\ \psi|_{x_0-0} &= \psi_1; & \psi|_{x_0+0} &= \psi_2.\end{aligned}\right\}\qquad(27)$$

The above solution remains valid for the cathode region except that U in all the formulas must be replaced by ψ_1. To the right of x_0 the field will again increase with distance and if the anode is located sufficiently far, and $U-\psi_2$ is not very small, the field may again attain the value $-E_0$ and give rise to a second region of ionization of defects.

I am indebted to Prof.Böer for communicating the results of his investigations and helpful discussion.

Note appended after the conference

After the conference we solved the problem of the steady-state distribution of the field and electron concentration in the dielectric both for thermionic and for field emission in the general form without neglecting the current term in the initial set of equations. For field emission and $x_0 < L$ the solution in the full range of real values of the current in dielectrics has the following form

$$\psi = 2\frac{kT}{q}\ln\frac{\operatorname{sh}(w_{x_0}+\eta-w_0)}{\operatorname{sh}(w_{x_0}+\eta-w)},$$

$$E = -\sqrt{E_1^2+\frac{8\pi|j|}{\mu\varkappa}x}\,\operatorname{cth}(w_{x_0}+\eta-w),$$

$$n = \left[\frac{\varkappa E_1^2}{8\pi kT}+\frac{|j|}{qD}x\right]\left\{\left[\frac{1+e^{-2(w_{x_0}+\eta-w)}+\dfrac{7}{72\,w}}{1-e^{-2(w_{x_0}+\eta-w)}-\dfrac{5}{72\,w}}\right]^2-1\right\}. \qquad (28)$$

Here

$$w = \frac{q}{3kT}\sqrt{\frac{8\pi|j|}{\varkappa\mu}}\,(x_1+x)^{3/2},$$

$$x_1 = \frac{\mu\varkappa E_1^2}{8\pi|j|} \text{ and } \eta = \frac{1}{2}\ln\frac{E_0+\sqrt{E_1^2+\dfrac{8\pi|j|}{\mu\varkappa}x_0}}{E_0-\sqrt{E_1^2+\dfrac{8\pi|j|}{\mu\varkappa}x_0}} \qquad (29)$$

are integration constants. For currents satisfying the inequality

$$|j|\,x_0 \ll \frac{\varkappa}{8\pi}\mu E_1^2, \qquad (30)$$

solutions (28) for ψ and E become (25). The influence on the current on the electron concentration n distribution in the dielectric is negligibly weak in the vicinity of the strong field region ($x\approx x_0$), while far from x_0 the concentration $n\approx\frac{|j|}{E_1}$.

"P.N.Lebedev" Physical Institute,
Academy of Sciences of the USSR

References

1. K.W.Böer, Present issue of the Bulletin, p.35.
2. K.W.Böer, Present issue of the Bulletin, p.41.

CURRENTS IN ALKALI HALIDE CRYSTALS DUE TO ELECTRON EMISSION FROM THE CATHODE IN STRONG ELECTRIC FIELDS

- E.A.Konorova

Introduction

Despite an appreciable number of experimental and theoretical investigations, the mechanism of electric breakdown of solid dielectrics is still not adequately understood. Whereas for semiconductor crystals with a narrow forbidden band (silicon, germanium), it has been established experimentally that breakdown is preceded by electron multiplication, for dielectrics (alkali halide crystals, mica, glass, etc.) electronic impact ionization appears to be more or less probable. Most experimental studies of electric breakdown of dielectrics consisted primarily of investigation of the dependence of the dielectric strength on different factors: temperature, time, etc. The value of the dielectric strength can be regarded as a true characteristic of the material only when the sample is perfect, i.e., if there is perfect contact between the electrodes and the crystal, if the crystal is free of microfissures, stresses and similar imperfections, and if the field inside the crystal is homogeneous.

In practice it is difficult or in some cases impossible to check whether these conditions are fulfilled, and since these factors influence the measured value of the dielectric strength comparison of experimental results is greatly hampered. On the other hand, it is perfectly clear that measurement of only the voltage corresponding to disruption of the sample cannot yield answers to the questions connected with the effect of electric breakdown. Hence we felt it would be of interest to investigate the processes that may occur in dielectrics in high fields immediately before breakdown, a matter that has not received due attention hitherto. From this standpoint, of particular importance is the variation of the current flowing through the dielectric in strong fields as a function of the applied voltage.

It has been established by a number of authors[1-3] that the current-voltage curve in strong fields deviates from Ohm's law (Fig.1). It has also been established that the currents at high voltages are predominantly electronic[4]; so far, however, the mechanism responsible for these currents remains unclear.

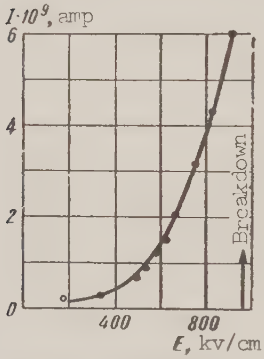

Fig.1. Variation of the current as a function of the field in a KCl single crystal[1].

Von Hippel[5] and his co-workers have advanced the hypothesis that in strong fields there begins emission of electrons from the metal into the dielectric. Inasmuch as the metal to crystal work function must be lower than the ordinary metal to vacuum work function, emission of electrons can begin in fields much lower than 10^7 v/cm.

The overall effect may be described as follows. When the field at the cathode attains a certain strength, electrons in large numbers cross the potential barrier and enter the crystal. Part of these electrons is trapped by defects and forms a negative space charge in the vicinity of the cathode, which acts to diminish the field at the cathode and limit the emission. If there were no thermal freeing of electrons from the defects, the steady-state current would be zero. In the presence of thermal excitation, however, the electron currents will be superposed on the ordinary ionic current and will give rise to deviation of the current-voltage curve from Ohm's law, which is observed experimentally. If the proposed explanation is correct, obviously upon application of a saw-tooth voltage pulse to the crystal, the pulse current must to an appreciable degree differ from the steady-state current. If the duration of the saw-tooth pulse is such that the field towards the end of the pulse remains virtually undistorted, the voltage dependence of the current will correspond to the Fowler-Nordheim or Zener formula for emission of electrons from the cathode. The pulse currents must be either completely or nearly temperature independent. With a dc voltage the electron current will be due to thermal freeing of electrons from traps. As regards absolute magnitude, this current cannot be large (this is confirmed by experiment), while its temperature dependence must be strong.

In the present work we investigated the currents in dielectrics in strong electric fields as a function of the duration of the applied voltage pulses and of the temperature.

Experiment

We assembled a special experimental set-up[6] for measuring the conduction currents in dielectrics subjected to voltage pulses. We used saw-tooth pulses of 50 to 1000 microsec duration and with an amplitude of up to 10 kv. The capacitive currents were compensated by the measurement circuit, and the conduction current pulse corresponding to the given voltage pulse was recorded by means of an oscillograph. The measurements were carried out with single pulses and also with periodic pulses with a repetition rate of 50 pps. With a sample capacitance of 15 to 25 pf, the sensitivity of the set-up was 10^{-7} amp/mm.

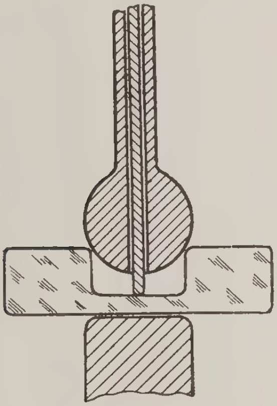

Fig.2. Crystal sample with electrodes.

The samples were specially prepared KBr single crystals. A cylindrical recess 7 mm in diameter was drilled in the single crystal plates measuring some 4-5 mm in thickness. The remaining sample thickness at the bottom of the recess equalled 0.1-0.2 mm (Fig.2). After preparation, the samples were washed in benzene and heated to a temperature 50° below the melting point with subsequent slow (0.5 degree/min) cooling. Part of the samples were cleaned ultrasonically in a water solution of KBr. The metal electrodes were applied by vacuum ($3\text{-}5\cdot10^{-6}$ mm Hg) evaporation. Prior to application of the electrodes, the sample surface was cleaned by a gas discharge in vacuum. Most of the experiments were carried out on samples with gold electrodes.

It should be noted that in the case of pulse measurements the way the electrodes are applied is even more important than in dc measurements. If the electrode does not make firm contact with the sample surface and there remain air layer "islets" between the electrode and the crystal, upon application of the pulse the voltage distribution over the area will be inversely proportional to the dielectric constants and the local voltage at one or more air layer "islets" may be sufficiently high for breakdown. Breakdown of an air "islet" gives rise to an instantaneous capacitive current pulse.

In the case of a large number of such local breakdowns, oscillographic current measurement becomes virtually impossible. The influence of the electrode application procedure on the appearance of the current oscillograms is illustrated in Figs.3,4 & 5.

We measured currents in crystals in fields ranging from 10^4 to $6\cdot10^5$ v/cm, at temperatures from 20 to 200° and with pulse durations from 100 to 1000 microsec. Actually, we carried out two series of measurements: measurements of the current with periodic pulses applied to the sample and current measurements under the same conditions but with single pulses. By single pulse measurements we mean that no

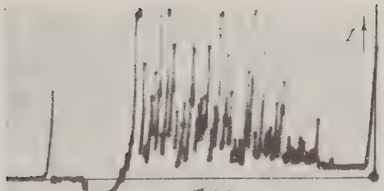

Fig.3

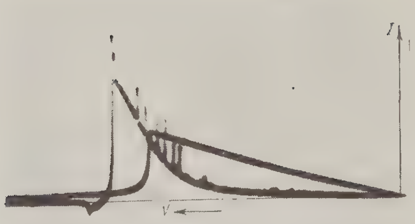

Fig.4

Fig.3. Current oscillogram for sample with sputtered gold electrodes applied without preliminary treatment.

Fig.4. Current oscillogram for sample with sputtered gold electrodes; surface cleansed by gas discharge in vacuum prior to application of the electrodes.

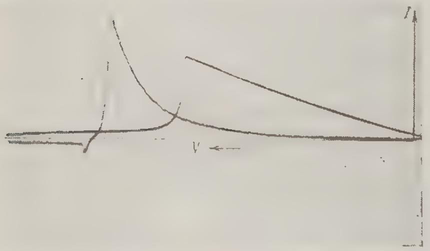

Fig.5. Current oscillogram for sample with sputtered gold electrodes; surface treated by ultrasound in KBr solution prior to application.

voltage was applied to the sample for a period of 3-4 hours prior to application of the test pulse.

Figs.6 & 7 show current oscillograms for relatively low amplitude (800 v peak) pulses of 100 and 1000 microsec duration at a temperature of 150°. Although obtained for the same sample, the oscillograms differ markedly. With a pulse duration of 100 microsec the shape of the current pulse virtually duplicates the shape of the voltage pulse, whereas in the 1000 microsec case the current has a maximum. As will be evident from these oscillograms, the absolute value of the current with a shorter rise time is greater. Neither the value of the current nor the shape of the curve depend to any appreciable extent on whether the measurements are made with a single pulse or with repeating pulses.

Fig.8 shows the variation of the pulse conductivity of the crystal at low field values as a function of the temperature: $\ln \sigma = f(1/T)$. For purposes of comparison, we also give the temperature dependence of the conductivity of KBr recorded with dc voltage. As will be evident from Fig.8, the two straight line plots are parallel. The variation of the pulse conductivity with the pulse dura-

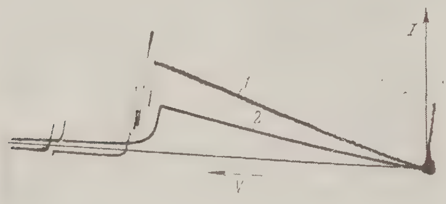

Fig.6

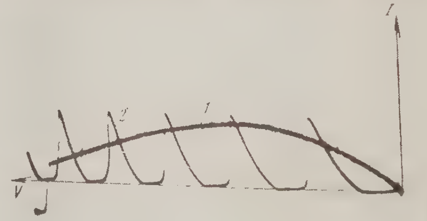

Fig.7

Fig.6. 1 - Current oscillogram for 100 microsec, 800 v peak value pulse; 2 - calibration.

Fig.7. 1 - Current oscillogram for 1000 microsec, 800 v peak value pulse; 2 - calibration.

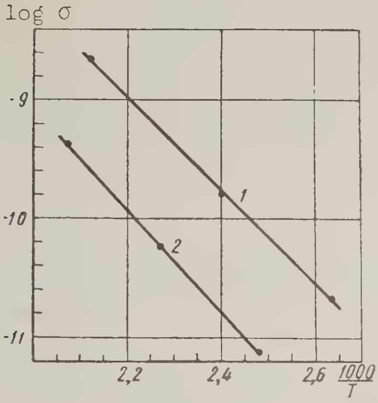

Fig.8. Variation of the conductivity with temperature: 1 - 100 microsec pulse; 2 - dc voltage.

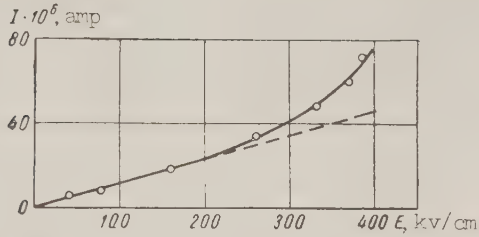

Fig.9. Variation of the current with the field strength at 150° with periodic 100 microsec pulses applied to the sample.

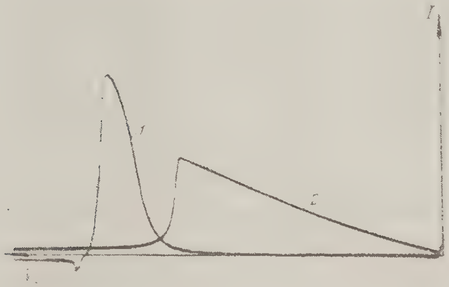

Fig.10. 1 - Current oscillogram for E = 400 kv/cm, single 100 microsec pulse (t = 150°); 2 - calibration.

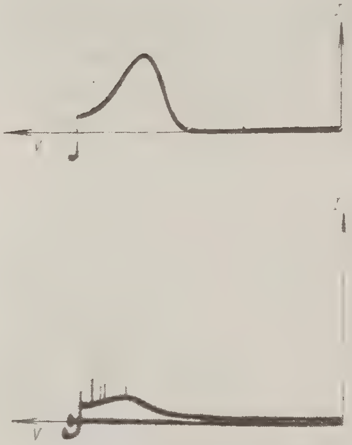

Fig.11. Current oscillogram for a pulse duration of 1000 microsec: above - for the first pulse; below - for the second pulse.

tion and the character of the temperature dependence give reason to infer that at the first instant of application of the voltage there occurs charging of the boundaries of the inhomogeneity regions in the crystal and of the layers in the vicinity of the electrodes. The current appears to be ionic as in the case of dc voltage; the difference in absolute values obtained with dc and pulse voltages is probably due to differences in field distribution inside the crystal.

In the case of measurements with periodic pulses, the picture remains substantially the same with increase of the field strength almost to the breakdown value. The variation of the current with the voltage for a pulse duration of 100 microsec at a temperature of 150° is shown in Fig.9. It will be evident that the current virtually obeys Ohm's law. The current also depends on the temperature just as in the range of low field values. The reproducibility of the measurement results for the same sample is in accord with the estimated experimental error.

Entirely different results were obtained when a single voltage pulse was applied to the sample. The current oscillogram corresponding to a maximum field strength of $4 \cdot 10^5$ v/cm, a single pulse duration of 100 microsec and a temperature of 150° is shown in Fig.10. It will be evident that at a certain field strength there occurs a sharp current rise; at the peak intensity of $4 \cdot 10^5$ v/cm the current through the sample attains a value of $0.8 \cdot 10^{-3}$ amp, i.e., exceeds the ionic conductivity current by several orders of magnitude. Upon application to the sample of a number of single pulses, the current gradually falls off and after 15-20 pulses the current oscillogram as regards general appearance and the absolute value of the current does not differ from the oscillograms obtained with periodic pulses. The initial picture (i.e., a sharp current rise on the oscillogram) is re-established only after the passage of an appreciable time (at least an hour) after application of the series of pulses.

A current oscillogram corresponding to a pulse of 1000 microsec duration is shown in Fig.11. Here also at a certain field strength the current begins to rise; it then goes through a maximum and falls off to a value only slightly exceeding the ionic current (Fig.11, above). The lower part of Fig.11 shows the current oscillogram corresponding to a second 1000 microsec pulse; while a current peak is still present it is much lower than for the first pulse.

The currents corresponding to the nonlinear part of the $I = f(V)$ curve increase with increasing temperature, but this increase is not described by any simple mathematical function. The results of measurements for four samples at different temperatures are shown in the accompanying table. It will be evident that the temperature dependence does not evince any definite regularity and in any case is appreciably weaker than the usual exponential dependence of the ionic conductivity of crystals.

Temperature dependence of the current

Sample No.	$E \cdot 10^{-5}$, v/cm	I, μamp			
		26° C	100°	150°	200°
50	2,7	—	34	37	158
84	3,25	—	22	244	500
84	3,25	—	—	200	274
84	3,75	—	102	—	1435
85	6	150	460	1900	—
94	3,2	—	273	420	1090

In conclusion, it may be noted that a characteristic of the current measurements with single pulses in the region of nonlinearity is poor reproducibility of the results even for the same sample. The results may differ by a factor of 2 under ostensibly identical experimental conditions. Better agreement of the results was obtained for the samples treated by ultrasound in KBr solution. In this case measurements even on different samples did not diverge by a factor of more than 1.5.

Conclusions

The results of our studies showed that the variation of current with voltage in strong electric fields in the case of pulse voltages differs substantially from the variation for dc voltages. Whereas in the case of dc measurements, the absolute value of the current equals 10^{-9} amp, in the case of pulse measurements the current attains the exceptionally high value for KBr of 10^{-3}-10^{-4} amp at the same field intensity.

The decrease of the current with increase of the pulse duration or with application of repeated pulses indicates that in the process of current flow there forms a space charge in the crystal, which weakens the field in the region where there are produced additional current carriers, and thereby limits the current.

Thus, the experimental results substantiate the assertions made in the introduction to this report.

At a certain field strength electrons are emitted into the crystal, giving rise to an appreciable current. Inasmuch as the concentration of defects in the KBr crystal apparently does not exceed 10^{-5} cm^{-3} and the field is rather strong, it may be assumed that the displacement of these electrons is appreciable - of the order of 10^{-2} cm, i.e., commensurate with the sample thickness. In view of this, during the time of a pulse (10^{-4} sec) only an insignificant part of the electrons can settle in defects and hence the field in the crystal remains undistorted. This is substantiated by the fact that upon application of a second and even third 10^{-4} sec pulse with relatively low currents flowing through the sample the magnitude of the current almost does not change. If this is the case, the field dependence of the current must satisfy the equation for cold emission. If one uses Zener's expression for the barrier penetration probability, the equation for the current density will have the form

$$j = \frac{e^3E^2}{8\pi h\varphi}\exp\left(-\frac{\pi^2 ma\varphi^2}{h^2eE}\right),$$

where e and m are the mass and charge of an electron, a is the lattice constant, φ is the metal to crystal work function and E is the electric field strength.

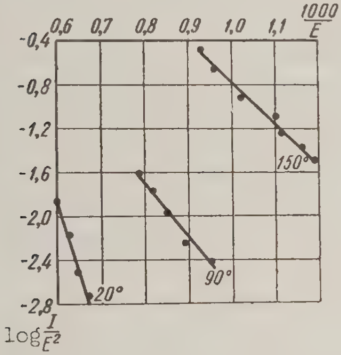

Fig.12. Variation of $\ln\frac{I}{E^2}$ with $\frac{1}{E}$ at different temperatures.

Fig.12 shows the variation of ln $(I/E^2) = f(1/E)$ for one of the samples at different temperatures. It will be seen that the experimental points fall on straight lines. The values of the work function calculated from the slope of the plots equal 0.6, 0.38 and 0.3 ev for 26, 90 and 150°, respectively. Analysis of a large number of oscillograms showed that the work function varies somewhat from sample to sample and even from experiment to experiment for one and the same sample. There is, however, evident a definite decrease of the work function with increasing temperature in all cases.

The deduced work function values are appreciably lower than those following from theoretical calculations. The gold to KBr crystal work function calculated as the difference between the minimum electron energy in the conduction band of the crystal and the metal to vacuum work function equals 4 ev.[7] However, the presence of a dielectric at the metal boundary may modify the properties of the surface (for example, due to formation of a monatomic layer of atoms of one of the crystal components). Hence the 4 ev value cannot be regarded as the only possible one.

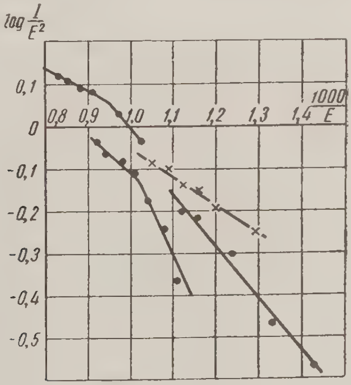

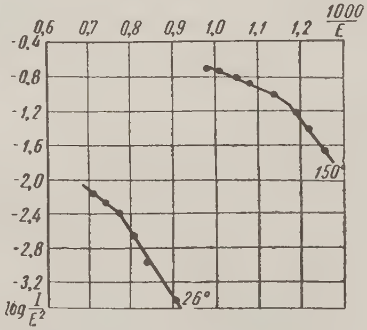

Fig.13. Variation of $\ln\frac{I}{E^2}$ with $\frac{1}{E}$ at 200° for different samples for a pulse duration of 200 microsec.

Fig.14. Variation of $\ln\frac{I}{E^2}$ with $\frac{1}{E}$ for a pulse duration of 100 microsec.

On the other hand, it may also be assumed that the field at the metal-dielectric interface differs from the mean calculated value (the potential difference divided by the thickness of the crystal) owing to unevennesses of the surface and/or the formation of ionic space charges. Thus the question of the true metal to crystal work function still remains open.

Fig.13 shows the variation of ln (I/E^2) as a function of $1/E$ for a pulse duration of 200 microsec; Fig.14 gives the same variation for a pulse duration of 100 microsec but with higher currents flowing through the sample. In both cases the curves exhibit a break: the slope changes towards the end of the pulse. It must be assumed that at high current values and long pulse durations, a space charge begins to form in the crystal; this limits the current rise and explains the character of the curves shown in Figs.13 and 14.

The character of the temperature dependence of the current corresponding to the nonlinear part of the current-voltage curve gives reason to think that this dependence is determined not by the nature of the current but is a consequence of secondary factors. The most probable reason for the observed variation is imperfect contact between the crystal surface and the electrode. The precautions taken to insure good contact (high vacuum in applying the electrodes, gas discharge cleansing of the crystal surface, washing of the crystal in solution after treatment, etc.) cannot guarantee complete absence of an intermediate layer between the electrode and the crystal. The density of this layer may vary with temperature and thereby change the value of the work function. The presence of an intermediate layer as well as inhomogeneities of the sample surface must obviously lead to some scatter of the experimental current values.

It will be evident from an examination of Fig.9 that at temperatures of 100-200° the current in high fields measured with periodic pulses applied to the sample almost follows Ohm's law. At the same time it was shown in the work of Val'ter & Inge[2] that with a dc voltage the field dependence of the current at the same temperatures deviates greatly from Ohm's law. This divergence may be explained by the following factors: first, the ionic current in the crystal with a pulse voltage exceeds the established current by an appreciable factor and, consequently, smooths out the field dependence due to the electronic current; second, at elevated temperatures and with voltages applied for an appreciable period, the current may heat the sample and, consequently, give rise to a stronger voltage dependence of the current.

I desire to express my gratitude to G.I.Skanavi for his interest in the work and valuable discussion of the results.

References

1. A.von Hippel, Phys.Rev., 54, 1096 (1938).
2. A.Val'ter (Walter) & L.Inge, Zhur.tekh.fiz., 6, 141 (1936).
3. B.V.Gorelik & V.T.Dmitriev, Ibid., 18, 333 (1948).
4. V.Pruzhnina-Granovskaya, Zhur.eksp.i teor.fiz., 7, 506 (1937).
5. A.von Hippel & R.S.Alger, Phys.Rev., 76, 127 (1947).
6. E.A.Konorova & D.G.Lebedev, PTE, No.4, 68 (1958). (Trans.Instruments and Experimental Techniques).
7. N.F.Mott & R.W.Gurney, Electronic Processes in Ionic Crystals, Oxford Univ. Press, 1948 (Cited in Russian trans.).

TEMPERATURE AND VOLTAGE DEPENDENCES OF THE CURRENT IN KBr SINGLE CRYSTALS IN PREBREAKDOWN FIELDS

- E.A.Afanas'eva, V.S.Vinogradov & E.A.Konorova

It was shown in the preceding report[1] that upon application of a single voltage pulse to a KBr crystal there flow through the crystal appreciable currents (10^{-3}-10^{-4} amp), exceeding by several orders of magnitude the currents obtained with an equivalent dc voltage. This substantiates the hypothesis of field emission from the cathode into the crystal in strong fields.

In the present work we shall show that with a dc voltage the current through a KBr crystal is due to thermal release of electrons in the space charge region.

Physics of the effect and calculations

The effects occurring in a dielectric to which a high voltage is applied may be briefly described as follows. Up to a certain field strength, ionic current flows through the dielectric. At a certain critical field value, however, there begins cold emission of electrons from the cathode into the dielectric. If there are present in the dielectric trapping levels, the electrons settling in the traps form a space charge which reduces the field at the cathode and thus hinders further emission. If the electrons are thermally freed from the traps, the current through the crystal will be determined by the conditions of their release, i.e., by the depth of the traps. It is usually assumed that in the presence of only one trapping level the current is proportional to the square of the voltage.[2,3] Our experimental data, however, as will be shown below, are not in agreement with this assumption.

If there is present in the crystal a spectrum of trapping levels, i.e., a distribution of traps in energy, the situation is more complex. With increase of the voltage, an additional number of electrons will be injected into the crystal, i.e., the space charge will increase. But, in addition, increase in the concentration of trapped electrons will lead to a rise of the Fermi level, i.e., to filling of the trapping levels closest to the conduction band. Thereby thermal release of the electrons is facilitated and the voltage dependence of the current becomes stronger than in the case of a single discrete trapping level. This can readily be demonstrated.

Fig.1 shows the schematic arrangement of energy levels behind the potential barrier. We shall assume that a quasi-steady state has been attained in the crystal. An analogous model for a dielectric was discussed by Rose[2] for the case when there is ohmic contact between the metal and an approximate formula was obtained for $I = f(V)$. Below we will show that a more precise formula can be deduced on the basis of field equations.

Let $\mathscr{E}(x)$ be the bottom of the conduction band, $\mathscr{E}_1(x)$ and $\mathscr{E}_2(x)$ - the energy levels between which the traps are located, and $F(x)$ - the energy level below which the traps are filled (Fermi quasi-level). Let us assume that the traps are uniformly distributed in the $\mathscr{E}_1-\mathscr{E}_2$ interval. We use $N_{t\mathscr{E}}$ to designate the number of traps per unit volume and unit energy interval.

Rigorously speaking, in order to find the current flowing through the dielectric in a strong field, one must solve the kinetic problem. But we shall use another approach, utilizing a set of equations analogous to that employed in the phenomenological theory of semiconductors. For the stationary problem the set of equations will have the form

$$j = e\mu nE - eD\frac{dn}{dx}\,; \tag{1}$$

$$\frac{dE}{dx} = \frac{4\pi e}{\varepsilon}(n + n_{\text{t}}); \tag{2}$$

$$n = N_{\text{cff}}\exp\left(-\frac{\mathcal{E} - F}{kT}\right); \tag{3}$$

$$n_{\text{t}\mathcal{E}} = \frac{N_{\text{t}\mathcal{E}}}{\exp\left(\frac{\mathcal{E}_{\text{t}} - F}{kT}\right) + 1}\,. \tag{4}$$

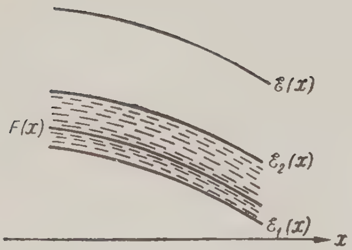

Fig.1. Diagram of energy levels.

Here n is the electron density in the conduction band, $n_{\text{t}\mathcal{E}}$ is the density of electrons held in traps, μ is the drift mobility, D is the diffusion coefficient, $e<0$ is the electron charge, F is the Fermi quasi-level, and $N_{\text{cff}} = \left(\frac{2\pi m_e kT}{h^2}\right)^{3/2}$ is the effective density of states in the conduction band.

Let us express $F(x)$ in terms of $n_{\text{t}}(x)$ using Eq.(4):

$$n_{\text{t}}(x) = \int\limits_{\mathcal{E}_1(x)}^{\mathcal{E}_2(x)} \frac{N_{\text{t}\mathcal{E}}\,d\mathcal{E}_{\text{t}}}{\exp\left(\frac{\mathcal{E}_{\text{t}} - F}{kT}\right) + 1} = N_{\text{t}\mathcal{E}}(F - \mathcal{E}_1) + kTN_{\text{t}\mathcal{E}} \times$$
$$\times \left\{\ln\left[1 + \exp\left(\frac{\mathcal{E}_1 - F}{kT}\right)\right] - \ln\left[1 + \exp\left(\frac{F - \mathcal{E}_2}{kT}\right)\right]\right\}. \tag{5}$$

If $F - \mathcal{E}_1 \gg kT$, then even in the most unfavorable case when $\exp\left(\frac{F - \mathcal{E}_2}{kT}\right) \approx 1$, we can write

$$n_{\text{t}}(x) \approx N_{\text{t}\mathcal{E}}(F - \mathcal{E}_1). \tag{6}$$

If $\exp\left(\frac{F - \mathcal{E}_2}{kT}\right) < 1$, then the accuracy of relation (6) is enhanced. Inserting (6) in (3), we obtain

$$n = N_{\text{cff}}\exp\left[\frac{-\Delta\mathcal{E} - \frac{n_{\text{t}}(x)}{N_{\text{t}\mathcal{E}}}}{kT}\right] = N_0\exp\left[\frac{n_{\text{t}}(x)}{n_0}\right], \tag{7}$$

where

$$\Delta\mathcal{E} = \mathcal{E} - \mathcal{E}_1,\ N_0 = N_{\text{cff}}\exp\left(-\frac{\Delta\mathcal{E}}{kT}\right),\ \text{and}\ \ n_0 = N_{\text{t}\mathcal{E}}kT.$$

Utilizing (7) we can express $n_{\text{t}}(x)$ in terms of n and substitute in Poisson's equation (2). We will assume that

$$n_{\text{t}} \gg n. \tag{8}$$

We then obtain:

$$\frac{dE}{dx} = \frac{4\pi e}{\varepsilon}n_0\ln\frac{n}{N_0}\,.$$

Let us neglect in Eq.(1) the diffusion current as compared to the conduction current (that this is justifiable will be shown below) and express n in terms of the current j and field E. Poisson's equation then assumes the form

$$\frac{dE}{dx} = \frac{4\pi e}{\varepsilon} n_0 \ln \frac{j}{e\mu N_0 E}\,. \tag{9}$$

Introducing the notation $\frac{4\pi e n_0}{\varepsilon} = \beta\,(\beta < 0)$ and $\frac{j}{e\mu N_0} = \sigma$, we can write (9) in the following form:

$$\frac{dE}{dx} = \beta \ln \frac{\sigma}{E}\,. \tag{10}$$

Our aim is to obtain an expression relating the experimentally observed quantities, i.e., to obtain an analytic expression for $j = f(V)$. The precise relation can be obtained by graphic integration of (10) taking into account the boundary conditions. We will not carry out this integration but will attempt to obtain an approximate relation between j and V on the basis of some simplifying assumptions. Integrating (10) from 0 to x, we obtain

$$\int\limits_{E(0)}^{E(x)} \frac{dE}{\ln \frac{\sigma}{E}} = \beta x. \tag{11}$$

Integrating in parts, we obtain for the left-hand part of (11):

$$\int\limits_{E(0)}^{E(x)} \frac{dE}{\ln \frac{\sigma}{E}} = \left(\frac{E(x)}{\ln \frac{\sigma}{E(x)}} - \frac{E(0)}{\ln \frac{\sigma}{E(0)}}\right) - \left(\frac{E(x)}{\ln^2 \frac{\sigma}{E(x)}} - \frac{E(0)}{\ln^2 \frac{\sigma}{E(0)}}\right) + 2\int\limits_{E(0)}^{E(x)} \frac{dE}{\ln^3 \frac{\sigma}{E}}\,. \tag{12}$$

By means of the relations

$$\int\limits_0^l \frac{E(x)\,dx}{\ln \frac{\sigma}{E(x)}} = \frac{V}{\ln \frac{\sigma}{E(a)}} \qquad 0 < a < l$$

and

$$\int\limits_0^l \frac{E(x)\,dx}{\ln^2 \frac{\sigma}{E(x')}} = \frac{V}{\ln^2 \frac{\sigma}{E(a')}} \qquad \begin{matrix} 0 < a' < l \\ (a < a') \end{matrix}$$

we obtain

$$\int\limits_0^l \int\limits_{E(0)}^{E(x)} \frac{dE}{\ln \frac{\sigma}{E}} = \left(\frac{V}{\ln \frac{\sigma}{E(a)}} - \frac{E(0)\,l}{\ln \frac{\sigma}{E(0)}}\right) - \left(\frac{V}{\ln^2 \frac{\sigma}{E(a')}} - \frac{E(0)\,l}{\ln^2 \frac{\sigma}{E(0)}}\right) + 2\int\limits_0^l \int\limits_{E(0)}^{E(x)} \frac{dE}{\ln^3 \frac{\sigma}{E}}\,. \tag{13}$$

After rearranging the terms in (13), we will have

$$\int\limits_0^l \int\limits_{E(0)}^{E(x)} \frac{dE}{\ln \frac{\sigma}{E}} = \frac{V - E(0)\,l}{\ln \frac{\sigma}{E(a)}} + \varphi, \tag{14}$$

where

$$\varphi = \frac{E_0 l}{\ln \frac{\sigma}{E(a)}} \left\{1 - \frac{\ln \frac{\sigma}{E(a)}}{\ln \frac{\sigma}{E(0)}}\right\} - \left\{\frac{V - E(0)\,l}{\ln^2 \frac{\sigma}{E(a')}} + \frac{E(0)\,l}{\ln^2 \frac{\sigma}{E(a')}} \left(1 - \frac{\ln^2 \frac{\sigma}{E(a')}}{\ln^2 \frac{\sigma}{E(0)}}\right)\right\} + 2\int\limits_0^l \int\limits_{E(0)}^{E(x)} \frac{dE}{\ln^3 \frac{\sigma}{E}}\,. \tag{15}$$

$$\varphi < \frac{E(0)\,l}{\ln \frac{\sigma}{E(a)}} \left(1 - \frac{\ln \frac{\sigma}{E(a)}}{\ln \frac{\sigma}{E(0)}}\right) - \left[\frac{V - E(0)\,l}{\ln^2 \frac{\sigma}{E(a')}} + \frac{E(0)\,l}{\ln^2 \frac{\sigma}{E(a')}} \left(1 - \frac{\ln^2 \frac{\sigma}{E(a')}}{\ln^2 \frac{\sigma}{E(0)}}\right)\right] + 2\,\frac{V - E(0)\,l}{\ln^3 \frac{\sigma}{E(l)}}$$

if $\ln\frac{\sigma}{E(l)} < \ln\frac{\sigma}{E(x)}$, i.e., the absolute magnitude of the electric field increases from 0 to l. We note that the second term in the brackets above cannot be greater than the first term:

$$\left|\frac{V}{E(0)\,l} - 1\right| \gtrsim \left|1 - \frac{\ln^2\frac{\sigma}{E(a')}}{\ln^2\frac{\sigma}{E(0)}}\right| \left(\ln\frac{\sigma}{E(0)} > \ln\frac{\sigma}{E(a')}\right).$$

For φ to be negligible compared with the first term in (14) it is sufficient that the following inequalities be fulfilled:

$$\frac{1}{\ln\frac{\sigma}{E(a)}} \gg \frac{1}{\ln^2\frac{\sigma}{E(a')}} > \frac{2}{\ln^3\frac{\sigma}{E(l)}}, \tag{16}$$

$$\left|\frac{V}{E(0)\,l} - 1\right| \gg \left|1 - \frac{\ln\frac{\sigma}{E(a)}}{\ln\frac{\sigma}{E(0)}}\right|. \tag{17}$$

One can also obtain weaker inequalities, which are more convenient for evaluation:

$$\frac{1}{\ln\frac{\sigma}{E(a)}} \gg \frac{1}{\ln^2\frac{\sigma}{E(l)}}; \tag{18}$$

$$\left|\frac{V}{E(0)\,l} - 1\right| \gg \left|1 - \frac{\ln\frac{\sigma}{E(l)}}{\ln\frac{\sigma}{E(0)}}\right|. \tag{19}$$

If equalities (16) and (17) are fulfilled, we obtain

$$\frac{V - E(0)\,l}{\ln\frac{\sigma}{E(a)}} = \frac{\beta l^2}{2}. \tag{20}$$

Whence we find

$$j = e\mu N_{\text{eff}} E(a) \exp\left[-\frac{\Delta\mathcal{E}}{kT} + \frac{\gamma(eV - eE(0)\,l)}{kT}\right], \tag{21}$$

where

$$\gamma = \frac{\mathcal{E}}{2\pi e^2 N_{t\mathcal{E}}\, l^2}, \quad E(a) \sim \frac{V}{l}. \tag{22}$$

In deriving Eq.(21) we neglected the diffusion current as compared with the conduction current. Let us show that this is permissible. Let us evaluate the diffusion current:

$$j_d = -eD\frac{dn}{dx},$$

utilizing the values of the density n and field E obtained without taking j_d into account. If $j_d \ll j$, the diffusion current can safely be neglected. By means of the Einstein equation

$$eD = \mu kT$$

we obtain

$$j_d = -\mu kT\frac{dn}{dx}$$

(we assume that in the range of fields in question μ does not depend on the field and that Einstein's equation is valid).

Substituting $n = \frac{j}{e\mu E}$ and utilizing (9), we obtain

$$j_d = \frac{4\pi}{\varepsilon} \cdot \frac{n_0 kT}{E^2} \ln \frac{\sigma}{E} \cdot j.$$

Thus there must be fulfilled the inequality

$$\frac{4\pi}{\varepsilon} \cdot \frac{n_0 kT}{E^2} \ln \frac{\sigma}{E} \ll 1.$$

Inserting in this equality the values obtained from experiment, we find

$$\frac{4\pi}{\varepsilon} \cdot \frac{n_0 kT}{E^2} \ln \frac{\sigma}{E} \approx 10^{-4}.$$

Consequently, the inequality $j_d \ll j$ does hold. Thus in the presence of a spectrum of traps the current depends exponentially on both the voltage and the temperature.

$E(0)$ can be obtained by equating the current through the crystal to the Zener current, i.e., setting

$$j = \frac{e^3 E^2}{8\pi h\varphi} \exp\left(-\frac{\pi^2 m a \varphi^2}{h^2 e E}\right), \tag{23}$$

where a is the lattice constant and φ is the metal to crystal work function.

In Eq.(21) the conditions obtaining at the metal-dielectric boundary determine the term $E(0)$; thus this is the term depending on the cathode to crystal work function. As was shown earlier, however, (see inequality (18)) $E(0)\,l \ll V$. This condition will obviously obtain at sufficiently high voltages. The Zener current is so strongly dependent on the field in the region of the potential barrier that a very small change in this field is sufficient for the current inequality condition to be fulfilled. It follows therefore that the work function cannot have an appreciable effect on the magnitude of the current.

Comparing (9) with (21), we see that

$$\frac{\sigma}{E(a)} = \exp\left\{\frac{\gamma\,[eV - eE(0)\,l]}{kT}\right\}. \tag{24}$$

Conditions (18) and (19) are fulfilled for $|\sigma| \gg |E(a)|$. For this γ must not be a very small quantity and V must be appreciably greater than $E(0)\,l$. The parameter γ can be evaluated by means of Eq.(24). Let

$$\gamma\,[eV - eE(0)\,l] \gtrsim 5kT. \tag{25}$$

Bearing in mind that $E(0)\,l \ll V$, for V = 4 kv we obtain

$$\gamma \gtrsim 3 \cdot 10^{-5}. \tag{26}$$

Thus for the density of trap levels, $N_{t\mathscr{E}}$, we obtain 10^{15} for l = 0.015 cm.

We see, therefore, that Eq.(21) is applicable in cases when the voltage is sufficiently high and the concentration of traps is not great.

Experimental procedure and discussion of the results

In order to obtain the effect in purest form it is obviously necessary to carry out the measurement under conditions when the ionic current is small, i.e., at low temperatures. Inasmuch as the measured currents may be very small (of the order of 10^{-14} amp) it was necessary to provide a high voltage set-up with a very sensitive measuring section and to provide for cooling of the specimen. We assembled a Bart type electric circuit with a sensitivity of $5 \cdot 10^{-15}$ amp per division; the high voltage was supplied by dry batteries and could be varied in 900-1200 v steps up to 10 kv; the temperature could be varied from room temperature to -150°.

With this sensitivity of the apparatus, the greatest difficulty was connected with elimination of weak corona formation in the high voltage part and polarization of the mounting fittings in the measuring chamber. It should be noted that only the use of fluoroplastic enabled us to eliminate interference connected with the polarization effect.

The specimen preparation procedure was described in the preceding article[1]. In addition, a grounded guard ring was mounted on the specimens (Fig.2). In order to minimize the influence of humidity the specimens were first dried in a thermostatic chamber at 200° for 6-8 hours. Then after being placed in the fluoroplastic cup (Fig.1), they were covered at 140° with "Kaloria-2", a silicone liquid with excellent dielectric characteristics. To check the operation of the set-up, control measurements of I as a function of V were carried out in a vacuum chamber and yielded identical results. From the very first measurements it was found that the current through the specimen depends on the magnitude of the high voltage applied to it beforehand.

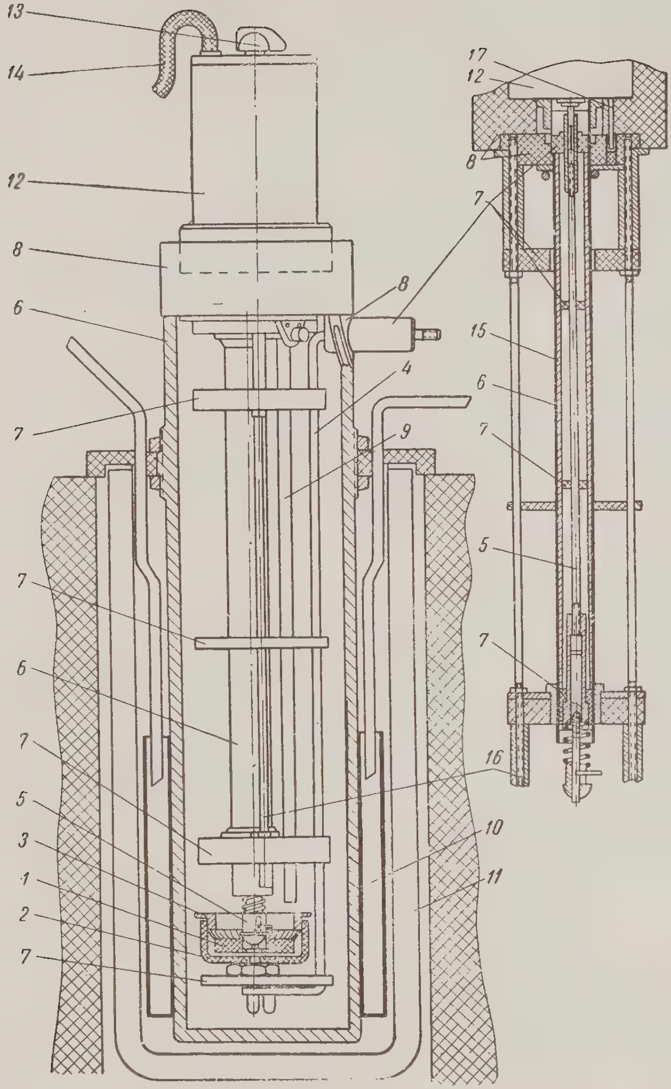

Fig.2. Section through measuring chamber: 1) specimen with drilled recess, 2) fluoroplastic cup, 3) metallic flange for grounding the specimen guard ring, 4) high voltage lead, 5) grid lead, 6) steel shields, 7) fluoroplastic bushings, 8) plexiglass bushing, 9) thermocouple leads, 10) cooling system, 11) Dewar, 12) steel case housing electrometric tube and measurement resistors, 13) measurement range selector switch, 14) lead from measuring circuit, 15) quartz tube, 16 & 17) grounding rods.

Fig.3 shows curves characterizing the variation of the current with time for different cases. It should be noted that the initial value of the current is not re-established even after heating of the specimen. The nature of this effect was

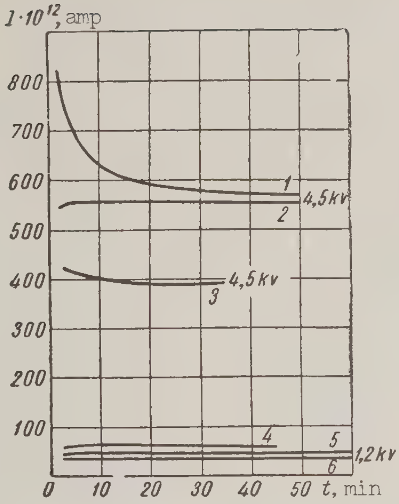

Fig.3

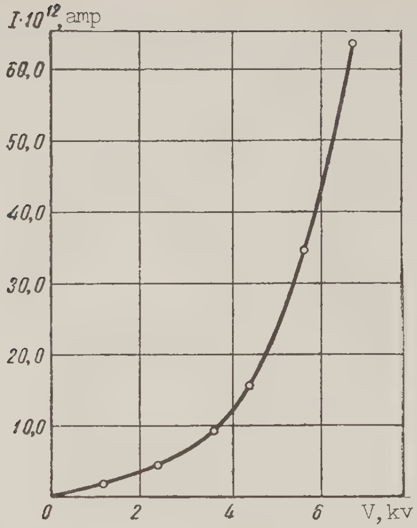

Fig.4

Fig.3. Variation of current with time: 1 & 4) high voltage applied to the specimen for the first time, 2 & 5) two corresponding repeat measurements, 3 & 6) two corresponding repeat measurements after application of a 7.5 kv potential to the specimen.

Fig.4. Variation of current with voltage at t = 0°C.

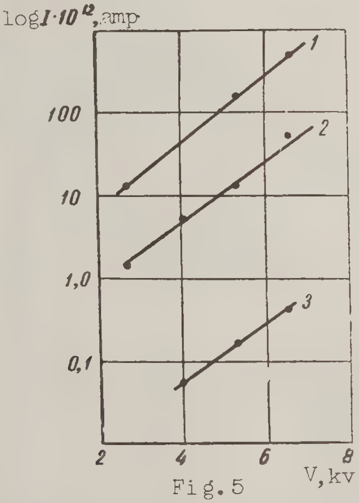

Fig.5

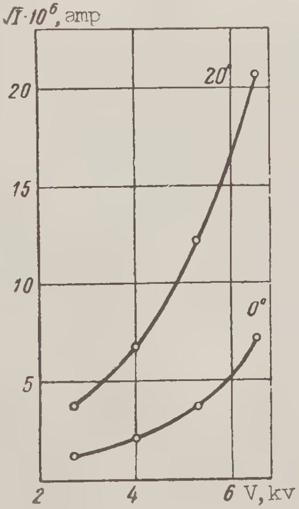

Fig.6

Fig.5. Variation of log I with voltage. The experimental curves correspond to measurements on the same specimen: 1) at 20°, 2) at 0°, 3) at -50°.

Fig.6. Variation of $\sqrt{I_{\text{nonlin}}}$ as a function of the voltage.

not clarified but it may be assumed that it is explained by electrical purification of the specimen, i.e., removal of impurities with a low activation energy.

Bearing this in mind, in order to obtain consistent results we "aged" the specimens before carrying out the measurements. First a potential of 6.5 kv was applied to the specimen and if no breakdown occurred it was covered with the silicone liquid as described above. Then 1-1.5 hours later the specimen was again subjected to 6.5 kv and then heated to 80°.

The current-voltage curves were recorded at temperatures from -50 to $+24^{\circ}$. Fig.4 shows a typical curve ($t = 0^{\circ}$). It will be evident that at any V one can represent the variation of I as a function of V in the form

$$I = \alpha V + I_{\text{nonlin}},$$

where α is given by the slope of the linear part of the curve which pertains to the ionic current, i.e., the current which is not of interest to us.

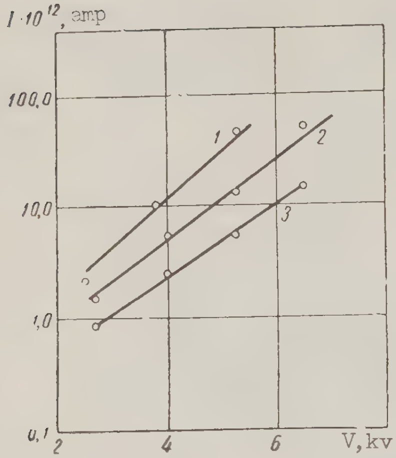

Fig.7. Variation of log I_{nonlin} as a function of V for three specimens at 0°. The figures at the curves refer to specimen numbers.

Values of γ_{cxp} and $N_{t\mathcal{E}}$ at different temperatures

t, °C	$\gamma_{cxp} \times 10^{5}$	$\frac{\gamma_{cxp}}{kT} \times 10^{4}$	$N_{t\mathcal{E}} \times 10^{-14}$
20	2,3	9,2	3,1
0	2,0	8,6	3,5
—50	1,6	8,4	4,4

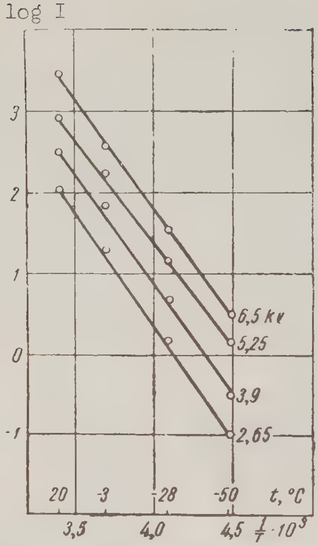

Fig.8. Variation of the current with temperature at a constant voltage for one specimen.

By means of the above formula one can readily determine I_{nonlin}; all further curves (see Figs.5-8) pertain to I_{nonlin}.

The variation of log I_{nonlin} as a function of the voltage at different temperatures is shown in Fig.5. We see that $I_{nonlin} = f(V)$ is well described by an exponential function. For purposes of comparison, in Fig.6 we give the variation of $\sqrt{I_{nonlin}}$ vs V.

From the slope of the log I_{nonlin} vs V plots one can determine γ_{cxp} (see table) and then using these values of γ_{cxp} calculate the trap concentration $N_{t\mathcal{E}}$. We see that the values of γ_{cxp} agree as regards order of magnitude with evaluations by means of Eq.(26). The value of γ depends to some extent on the temperature (Fig.5) and varies within a narrow range but in a somewhat random fashion from specimen to specimen (Fig.7). This can be explained on the assumption that the trap concentration varies with temperature and depends on the nature and history of the specimen.

Fig.8 shows the variation of log I_{nonlin} as a function of 1/T. It will be seen that the experimental points obtained for one specimen fit straight lines. From the slope of these plots we can determine the activation energy $\Delta\mathcal{E}$. It is equal to approximately 1 ev and varies somewhat from specimen to specimen. Inserting in Eq.(21) the experimentally determined values of γ and $\Delta\mathcal{E}$ and $\mu = 10$ $cm^2\ v^{-1}\ sec^{-1}$, $N_{eff} = 10^{19}$, $E(a) = 10^5$ v/cm, $V = 4 \cdot 10^3$ v and $l = 0.015$ cm, we obtain $j \approx 10^{-8}$ amp. This value is in satisfactory agreement with the experimental data.

Conclusions

Our experimental data can be explained on the basis of the proposed crystal model and the hypothesis of field emission. It should be noted that at present there are no experimental data indicating the existence of a wide band of trapping levels in alkali halide crystals. It may be assumed, however, that such a band or spectrum of levels does exist inasmuch as the edges of dislocations - always present in appreciable numbers in a crystal - can serve as relatively shallow electron traps. The fact that hitherto these trapping levels have not been detected in experimental work is not surprising inasmuch as their concentration must be relatively low.

References

1. E.A.Konorova, Present issue of the Bulletin, p.56.
2. A.Rose, Phys.Rev., 97, 1538 (1955).
3. M.A.Lampert, Ibid., 103, 1648 (1956).

DISCUSSION

A.E.Glauberman: I want to say a few words concerning the report of Afanas'eva, Vinogradov & Konorova. Although the calculations are not as rigorous as one might wish and there may be some question regarding the physical validity of the model, the report is interesting and the attempt to explain the described experimental facts merits attention.

In one of our papers published in 1959, we proposed a model which in a sense was the inverse of that discussed in the present report. If we consider the contact between a metal electrode and a crystal dielectric or a semiconductor in the presence of a strong uniform electric field F, then, ignoring for the sake of simplicity the influence of image forces and distortion of the bands of the dielectric near the point of contact, we obtain a scheme pictured in the accompanying figure.

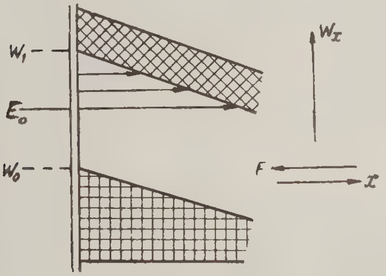

In calculating the electron current flowing from the metal into the conduction band of the dielectric by means of the tunnel effect, one must take into account both the electrons having an energy W_x of motion in the direction of the x-axis lower than the Fermi limit energy E_o in the metal and electrons with an energy greater than the Fermi limit. Taking into account electrons with $W_x > E_o$ is very important inasmuch as, despite the relatively small number of such electrons, the potential barriers penetration coefficient for them is very large.

As a result of calculations (A.E.Glauberman & I.I.Tal'yanskii, Doklady AN SSSR, 78, 661 (1951)) there were obtained three current components. The first two components, the usual cold emission current and a term of the type found by Hauston back in the 1930's, i.e., a term in which the field dependence is the same as for "cold" emission but which contains a temperature dependent factor in the exponent.

The third current component corresponds to the so-called Poole law; this third term in the formula for the total current depends on the electric field strength in the same way as the current obtained by the authors of the report under discussion and contains the requisite temperature dependence.

Thus one can describe the experimental data obtained by Afanas'eva, Vinogradov & Konorova without recourse to the questionable model of "distributed" traps merely by taking into account the temperature of the distribution of Fermi electrons in the metal.

Possibly the mechanism suggested by the authors of the report can obtain, but it may not be the determining mechanism, and in any case one must at the same time take into account the mechanism described above. Perhaps in developing their theory further the authors may reunite both viewpoints and supplement our old calculations by taking into account a number of factors we deliberately ignored.

K.B.Tolpygo: It must be noted that the problems discussed in the report of Afanas'eva, Vinogrado & Konorova are similar to some of the problems in the theory of semiconductors, problems that have been repeatedly discussed and partially solved some time ago.

In a number of his studies S.I.Pekar considered the problem of passage of current through the contact of a metal with a semiconductor. As is known, the difference between semiconductors and dielectrics is that in the former there are electrons due to thermal excitation, while in the latter these electrons are virtually absent. If there is a metal, the Fermi level in which lies below the conduction band of the dielectric, the electrons must overcome a high potential barrier to emerge. In this case one must first formulate appropriate boundary conditions, conditions which were not formulated in the report we have just heard, namely, that the current flowing from the metal to the dielectric minus the current flowing into the metal must be equal to the current flowing through the dielectric. This is necessary for consistence.

It should be noted that there is an appreciable disparity between the work function determined from the value of the current and the work function that might be expected. Thus, for example, if it is assumed that the work function for gold is 4 ev, while that for the dielectric is 1-1.5 ev, the gold to dielectric work function should be of the order of 2.5-3 ev, whereas the authors of the report obtained a value of the order of 0.5-1.5 ev.

A similar problem arose in studies of the photoconductivity of CdS in the laboratory of V.E.Lashkarev. In these experiments there was also obtained a very heavy current in weak fields. Lashkarev assumed that a substantial role is played by the formation of positive charge in the semiconductor and induction of a strong field in the gap between the metal and smiconductor. This new mechanism was called the "sluice" mechanism; without invoking this mechanism one cannot explain the relatively heavy current.

V.F.Pisarenko: First I would like to note that the idea of Lashkarev mentioned by K.B.Tolpygo, namely, that the space charge in the vicinity of the electrodes greatly enhances the electrode field, was advanced about a decade ago by M.S.Kosman for explaining the electric conductivity of glasses. In the opinion of Kosman the flow of electric current through a dielectric begins with displacement of electrons and holes inside the dielectric so that there form in the vicinity of the electrodes appreciable space charges which substantially distort the field in the dielectric. This idea was substantiated by many experimental studies carried out by Kosman and his co-workers.

My second remark pertains to evaluation of the concentration of defects made in the report of Afanas'eva, Vinogradov & Konorova. I think that this evaluation is an overestimate inasmuch as the filling of defects in the form of halide ion vacancies by electrons means the formation of F centers. A concentration of F centers equal to 10^{15} cm^{-3} would be superficially evident. Yet, Afanas'eva, Vinogradov & Konorova do not mention coloring. Thus if we assume that the space charge current limiting mechanism actually exists, one must evaluate the concentration as 10^{13} cm^{-3}, which corresponds to the equilibrium concentration of defects in the crystal.

One must also note that the mechanism of electronic conductivity in KBr proposed in the report cannot explain the magnitude of the conductivity of the crystal. We investigated the conductivity of KBr at elevated temperatures and strong fields. Tentative calculations based on the experimental results show that the observed conductivity of KBr cannot be assured by electrons thermally released from F centers. Evaluation of the thermal activation energy based on the observed variation of ln σ as a function of 1/T leads to a value of 0.4-0.6 ev, i.e., to an activation energy of the same order of magnitude as obtained by Afanas'eva, Vinogradov & Konorova. In order to explain the experimental facts, in our view, one must have recourse to the idea of long-range electrons appearing in the crystal as a result of emission from the cathode.

L.V.Keldysh: I would like to make a number of remarks regarding the formulas employed by the authors in processing the experimental data.

The question has already been discussed as to which formula one should use for describing cold emission from a metal into a dielectric: the usual Fowler-Nordheim formula or the Zener formula. The qualitative difference between these two laws rises mainly owing to certain assumptions made in deriving the Zener formula. If instead of this formula one uses the more consistent formula proposed by Franz, all the difference between it (except the numerical coefficients) and the Fowler-Nordheim formula reduce to the fact that the mass of a free electron is replaced by the effective mass of an electron in the dielectric. But one can scarcely doubt that the passage of electrons through a potential barrier lying wholly inside the dielectric is determined by the effective mass rather than the free electron mass.

Further, I think that one should not attach great significance to the value of the work function given in the report and to the divergence from the experimental data mentioned by K.B.Tolpygo. The numerical coefficient in the exponent can differ by an appreciable factor from that entering into the Franz formula for a number of reasons: first, this formula was derived in the effective mass approximation and is applicable only when the height of the potential barrier is sufficiently small compared with the width of the band and the band structure is sufficiently simple; second, it assumes that the field is uniform at distances of the order of the width of the barrier, i.e., of the order of 10^{-5} cm, which may or may not be true in the presence of space charge.

In connection with the remarks of F.F.Vol'kenshtein, I would like to note the following. The emission current from any level consists of two components: a thermionic emission and an autoionization (cold) emission. The latter, however, is very strongly (exponentially) dependent on the field; hence in sufficiently weak fields one can disregard this process, while beginning with a certain higher field, one may assume that it predominates and hence neglects thermionization. The field strength at which autoionization becomes the determining process increases with increase of the coupling energy of the levels from which the emission occurs. Hence there may be a situation where the current from the metal is determined primarily by cold emission, while the current from the levels is determined primarily by thermionization.

G.I.Skanavi (regarding the reports of Konorova and Afanas'eva, Vinogradov & Konorova): In my opinion the principal result of these researches is that it has been shown for the first time that in such "classical" dielectrics as KBr there may be created conditions under which the current attains an appreciable magnitude.

This research was undertaken in connection with the fact that in studies made abroad as well as in investigations of some of our scientists reporting at the present conference, it was established that the temperature dependence of the dielectric strength of crystal under a dc voltage is not equivalent to the temperature dependence with a pulse voltage. Thus, in the case of pulses the dielectric strength increases with increasing temperature, which is in agreement with the theory of impact ionization, while in the case of dc voltage there is observed a fairly clearly pronounced maximum. In connection with this von Hippel advanced the hypothesis that this kind of temperature dependence is due to the formation of space charge in the crystal: electronic space charge at low temperatures and ionic space charge at high ones.

In our laboratory we undertook to show experimentally the existence of electronic space charge is due to electrons emerging from the cathode and trapped by lattice defects; obviously, in this case the dc voltage and pulse voltage currents should differ substantially. In this respect the results of our studies are unambiguous: it was shown that electronic space charge is actually produced by the electric field.

The authors of the reports propose a qualitative interpretation of the temperature dependence of currents in strong fields. The calculations given are avowedly only approximate. Hence for the metal to dielectric work function, the calculated values are too low, as was emphasized by the authors. The reason for this is not clear so far and further research in this direction is indicated. I believe, however, that the hypothesis of cold emission developed by the authors is consistent with the experimental data.

REGULARITIES OF PULSE BREAKDOWN OF SOLID DIELECTRICS

- A.A.Vorob'ev & G.A.Vorob'ev

1. Voltage-time characteristics

During the 1930's there were obtained the voltage-time characteristics of many solid dielectrics. Most of the researches of the period suffered from shortcomings of the experimental techniques: the experimenters could not eliminate the influence of discharges in the surrounding medium (edge discharges) and did not have available cathode-ray oscillographs for recording the voltage and time of application thereof. It may be noted that the studies of Lemhaus[1] and Dittert[2] are free of these shortcomings.

In 1949 von Hippel & Alger[3] obtained the variation of the dielectric strength of KBr single crystals with the time of application of the voltage (Fig.1). The dielectric strength vs rate of rise of the applied field curve obtained by von Hippel & Alger is unusual. The authors attribute the minimum in the curve to the influence of ionic and electronic space charges; they do not discuss the question of the time lag of the discharge.

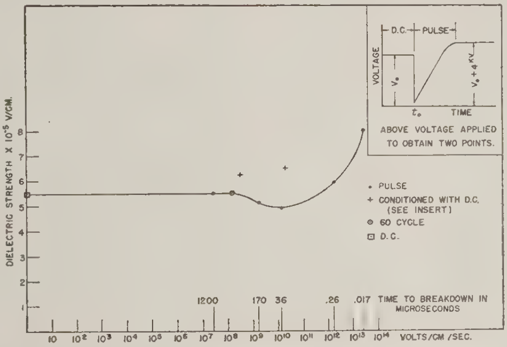

Fig.1. Dielectric strength of KBr vs rate of rise of applied field (after von Hippel & Alger[1]).

In the 1950's extensive studies of pulse breakdown of solid dielectrics were undertaken in Tomsk Polytechnic Institute. There was developed a technique for producing and recording pulse voltages with transient times down to 10^{-9} sec.

Vorob'ev[4] and Kuchin[5] obtained voltage rise time dependences of the dielectric strength of NaCl, KCl, KBr and KI crystals similar to the dependence obtained for KBr by von Hippel & Alger[3], but with the difference that the minimum was shifted approximately one order of magnitude to the side of shorter exposure times. As Mel'nikov[6] showed, this is connected with the fact that the crystal samples used by von Hippel & Alger were heat treated, whereas the samples of Vorob'ev and Kuchin were not so treated. Vorob'ev and Kuchin propose an explanation differing from that advanced by von Hippel & Alger for explaining the character of the voltage-time curve for alkali halide crystals. Vorob'ev and Kuchin hypothesize that in the investigated single crystals there forms only one type of space charge which leads to increase of the dielectric strength. That the space charge in question is ionic is indicated by the fact that the voltage-time characteristics of the investigated crystals at temperatures of 0° and lower, when ion motion is hindered, has no minimum.

Increase of the dielectric strength for exposures (rise times) of 10^{-7} sec and less may be explained by lag of the discharge. As was first established by Vorob'ev[7a], in the entire range of rise times the dielectric strength is proportional to the energy of the crystal lattice.

Mel'nikov[8] extended the voltage-time characteristics of NaCl, KCl, KBr and KI single crystals into the 10^{-9} sec exposure region. Fig.3 shows the voltage-time characteristics of NaCl, KCl, KBr and KI single crystals according to the data of Vorob'ev[4] and Mel'nikov[8].

At rise times of the order of $5 \cdot 10^{-9}$ sec, the dielectric strengths of NaCl, KCl, KBr and KI crystals tend to the same values. Plessner[9] obtained a continuous increase of the dielectric strength of thin films of KBr, NaF and CaF_2 with

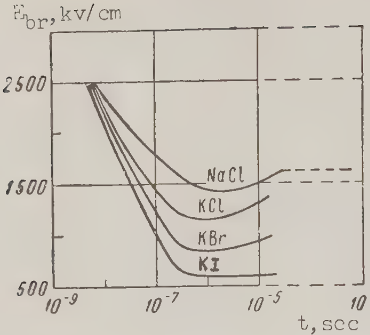

Fig.2

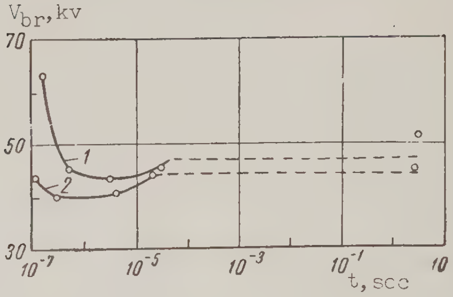

Fig.3

Fig.2. Variation of the dielectric strength of NaCl, KCl, KBr and KI single crystals with the time of application of the voltage; uniform field (after Vorob'ev[4] and Mel'nikov[8]).

Fig.3. Voltage-time characteristics of rock salt ([100] d = 0.7 mm) for breakdown in a nonuniform field (after Vorob'ev[7b]): 1 - point electrode negative; 2 - point electrode positive.

decrease of the rise time from several seconds to 10^{-6} sec; Plessner attributes this increase to thermal and polarization effects.

Fig.3 shows the voltage-time characteristics of rock salt for breakdown in a nonuniform field.[7b] In the region of short rise times the breakdown voltage increases appreciably faster with negative polarity of the point electrode. It was also found that in a nonuniform field the breakdown voltage is proportional to the energy of the crystal lattice.

Kevroleva[10] in our institute carried out experiments on the breakdown of crystal hydrates. She obtained a rise of the voltage-time characteristics in the region of short exposures similar to that observed for alkali halide salts.

Of great scientific and practical interest is investigation of the breakdown of mica and amorphous dielectrics characterized by a high dielectric strength and used in industry as insulating materials. Konorova[11] recorded the variation of the dielectric strength of $5 \cdot 10^{-4}$ cm thick mica sheets in the range of exposure times from $1 \cdot 10^{-6}$ to $5 \cdot 10^{-8}$ sec and found no variation of the dielectric strength with change in the rise time. Mel'nikov[12] in our institute found a variation of the dielectric strength of $4 \cdot 10^{-3}$ cm thick mica with the time of application of the voltage in the $1 \cdot 10^{-6}$ to $5 \cdot 10^{-9}$ sec range; he found that the dielectric strength of mica increases approximately 15% for the shortest rise time. Val'ter & Inge[13] investigated the voltage-time characteristics of glass and obtained the curves reproduced in Fig.4. They did not observe the influence of discharge lag, i.e., increase of the dielectric strength with decrease of the rise time.

Mel'nikov[12] investigated the voltage-time characteristics of a number of polymers. The curves obtained by him for lucite, polystyrene, teflon and films of styroflex and fluoroplastic-4 as well as for mica are reproduced in Fig.5. In all cases a significant increase (15-20%) of the dielectric strength was observed only for the shortest exposure time ($5 \cdot 10^{-9}$ sec).

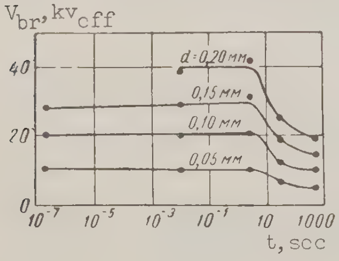

Fig.4. Voltage-time characteristics of glass; uniform field (after Val'ter & Inge[13]).

Astafurov[14] investigated the voltage-time characteristics of rock salt, river ice, paraffin and lucite in thick layers. The voltage-time characteristics obtained by him for

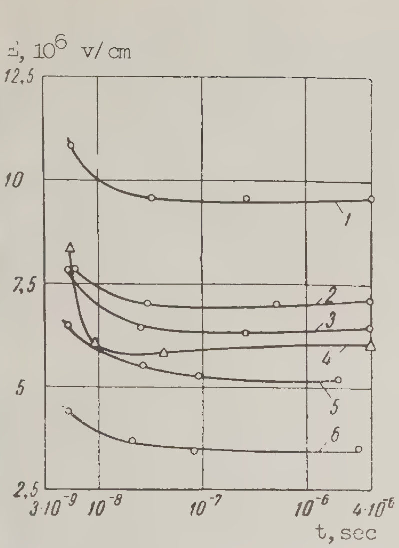

Fig.5. Variation of the dielectric strength of styroflex (1), teflon (2), mica (3), lucite (4), polystyrene (5) and bulk teflon (6) with the voltage rise time; uniform field (after Mel'nikov).

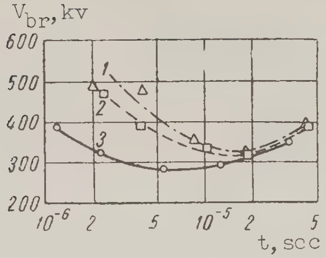

Fig.6. Voltage-time characteristics of ice (after Astafurov[14]): 1 - point electrode negative, d = 15 mm, 2 - uniform field, d = = 10 mm, 3 - point electrode positive, d = 15 mm.

ice are shown in Fig.6. For all the enumerated dielectrics he detected the influence of discharge lag, but only for exposures of the order of a few microsec, i.e., for appreciably longer voltage rise times than in the case of solid dielectrics in the form of samples having a thickness of some tenths of a millimeter.

The results of the studies carried out in the Tomsk Polytechnic Institute on solid dielectrics provide a basis for comparing the voltage-time characteristics of such solid dielectrics with the characteristics of liquid dielectrics and air. Fig.7 shows the voltage-time characteristics of mica, styroflex, rock salt, hexane and air. The vertical axis is laid off in values of the pulse strength factor β: the ratio of the dielectric strength at the given exposure to the dielectric strength with a rise of the order of 10^{-6} sec. The dielectric strengths of the enumerated dielectrics with a rise time of 10^{-6} sec are all of the order of 12-15 kv. It will be seen from the curves that as compared with the static dielectric strength the breakdown strength under voltage pulses with a steep rise increases in the following order: solid dielectrics, gas, liquid.

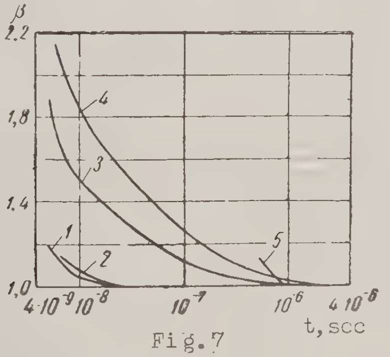

Fig.7

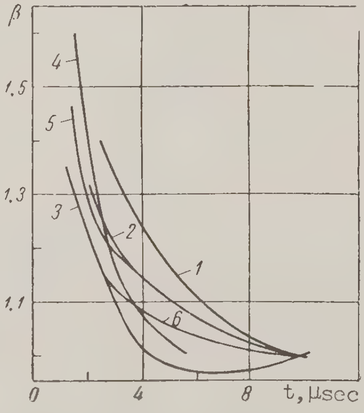

Fig.8

Fig.7. Variation of the pulse strength factor β of mica (1), lucite (2) (Ref.12), rock salt (3) (Ref. 12), hexane (4) (Ref.15) and air (5) (Ref.12) with the voltage rise time. Static breakdown voltages: 1 - 14.4 kv, 2 - 11.4 kv, 3 - 11.6 kv, 4 - 12.8 kv and 5 - 16 kv.

Fig.8. Variation of the pulse strength factor β for river ice (1,2,3) (Ref. 14), transformer oil (4) (Ref.16) and IShD-35 insulator (5,6) (Ref.17) with the voltage rise time. Static breakdown voltage 1 (point electrode negative) - 360 kv, 2 (uniform field) - 340 kv, 3 (point electrode positive) - 276 kv, 4 (point electrode negative) - 290 kv, 5 (negative pulse - 300 kv, 6 (positive pulse) - 250 kv.

Fig.8 shows the voltage-time characteristics of ice, transformer oil and IShD-35 insulator (air gap). It will be evident that the curves are similar. The pulse strength factor for transformer oil was calculated on the basis of the value corresponding to rise times of 10^{-5} to 10^{-1} sec. Upon increase of the exposure time above 10^{-1} sec the breakdown voltage of transformer oil falls off owing to the influence of impurities and thermal effects.

The data shown in Figs.7 and 8, of course, do not meet the extensive requirements of engineering. We still need experimental determination of the voltage-time characteristics of many commonly employed solid dielectrics (porcelain, ebonite, bakelite, micanite and so on) in layers of different thickness.

2. Discharge Lag

The discharge lag in general consists of the statistical delay time and the discharge formation time. The theory of the statistical delay time as it applies to solid dielectrics was developed by Seitz[18]. Kawamura et al[19] made an attempt to determine the statistical delay time in mica, glass and KCl single crystals. They applied square pulses of uniform amplitude and duration T to the solid dielectric sample until breakdown occurred; they determined the number n of pulses to breakdown. The product $n \cdot T$ was taken as the statistical delay time. They obtained the following values of $n \cdot T$: for glass, $< 3 \cdot 10^{-8}$ sec; for KCl $\sim 3 \cdot 10^{-7}$ sec with an overvoltage of 4% and $< 3 \cdot 10^{-8}$ sec with an overvoltage of 10%; for mica $\sim 10^{-4}$ sec with an overvoltage of 10%. Inasmuch as in these experiments the samples were subjected to a series of pulses, it is probable that what Kawamura et al measured was not the statistical delay time but the time of some cumulative effect.

Strigel[20] determined the discharge lag in many solid dielectrics. He made a formal separation of the delay time without determining clearly whether there really exists in solid dielectrics a statistical delay time or not. Similar formal separation of the discharge lag in KCl and sulfur single crystals was assumed by Inuishi & Suita[21].

Val'ter & Inge[22] investigated the voltage-time characteristics of x-irradiated and nonirradiated rock salt samples. They found no difference between the characteristics. They used a nonuniform field and did not succeed in eliminating edge discharges. As we showed in an earlier study, in a nonuniform field the influence of coloring is very weak. However, further experiments[23] on breakdown in a uniform field of x-rayed and nonirradiated rock salt crystals with an exposure time of $3 \cdot 10^{-8}$ sec also showed that nonirradiated rock salt samples as well as irradiated samples with and without illumination have virtually the same electric strength. This indicated that the statistical delay time in rock salt is appreciably shorter than $3 \cdot 10^{-8}$ sec. It was hypothesized that in solid dielectrics having an electric strength of the order of 10^6 v/cm or more the source of free electrons is cold emission from the cathode and electrostatic ionization of the dielectric material.

Mel'nikov[24], working in our institute on the breakdown of x-rayed and nonirradiated NaCl and KBr crystals, found a difference between the breakdown voltage values for x-rayed and nonirradiated samples and determined the statistical lag time to be of the order of $5 \cdot 10^{-10}$ sec.

Vorob'ev[4] determined the discharge delay time t_d in alkali halide crystals on the basis of the voltage-time characteristics taken off the breakdown oscillogram. Vorob'ev neglected the statistical delay time and hence assumed $t_d = t_f$, where t_f is the discharge formation time. He determined the mean discharge propagation rate:

$$v_{av} = \frac{d}{t_f}$$

where d is the thickness of the dielectric at the point of disruption.

The values of t_f and v_{av} were determined in an analogous fashion by Kevroleva[10] in crystal hydrates and by Astafurov[14] in some thick samples of solid dielectrics. The results of these measurements are summarized in the table below. Examination of the tabular data shows the following:

1) t_f decreases, while v_{av} increases with increase of the overvoltage,

2) t_f increases with increase of the sample thickness, and

3) v_{av} in experiments with a pointed electrode is greater with the point electrode positive.

Similar regularities were observed for the breakdown of gases. This similarity indirectly indicates that in the breakdown of solid dielectrics there also obtains electronic impact ionization or the streamer process.

If we assume that the thickness of the KBr plates used in the experiments of von Hippel & Alger was 0.1 mm (the authors did not specify the thickness), the mean discharge propagation velocity following from the voltage-time characteristics (Fig.2) is approximately $2\cdot10^6$ cm/sec. This rate, according to the concepts proposed by von Hippel & Alger[3], corresponds to the rate of formation of electronic space charge in KBr. The discharge process itself, in the opinion of these authors, occurs appreciably more rapidly.

Dielectric	Thickness, mm	Type of field	Overvoltage, %	t_f, 10^{-8} sec	v_{av}, 10^6 cm/sec	Ref.
NaCl	0,15	Uniform	14	1,7	0,88	[4]
	0,3		17,9	3	1,00	
KCl	0,15		16,2	1,6	0,94	
KBr	0,15		29,5	2,2	0,68	
KJ	0,15		28,4	2,1	0,72	
NaCl	0,7	Point −		5,1	1,37	
	0,7	Point +		0,9	7,77	
Talc	0,14	Uniform	50	1,91	0,79	[10]
Gypsum	0,15		18,8	2,18	0,69	
Rochelle salt	0,15		29,1	1,67	0,9	
NaCl	10	Point −	78	79	1,26	[14]
	10	Point +	12,5	5	18,5	
Ice	10	Uniform	20,5	69	1,45	
	15	Point −	30,5	92	1,63	
	15	Point +	18,5	38	3,96	
Paraffin	34	Uniform	12	18	18,9	
	34	Point −	29,5	25	13,6	
	34	Point +	32,5	18	18,6	

Mel'nikov[12] determined the discharge lag t_d in mica, lucite, polystyrene, teflon, styroflex and fluoroplastic-4. Determination of v_{av} by means of the above formula probably yields underestimated values inasmuch as with a rise time of $5\cdot10^{-9}$ sec in these dielectrics there may be a statistical delay time, as was obtained for NaCl and KBr single crystals. The statistical delay time in the solid dielectrics must, however, be shorter than in NaCl and KBr in view of their greater dielectric strength. The value of $v_{av}=d/t_d$ calculated by the author equals $4\text{-}7\cdot10^{-6}$ cm/sec, i.e., is appreciably greater than in alkali halide crystals, which is probably due to the high dielectric strength of the solid dielectrics.

Inuishi & Suita[21] determined the discharge lag for KCl and sulfur single crystals in breakdown by square pulses in nonuniform fields. Following Strigel[21] these authors formally divided the discharge delay time into a statistical delay time σ and a pulse formation time T_f. On the basis of the data for T_f, they determined the electron velocity, which it would be more correct to call the discharge propagation rate. The value deduced by them is appreciably smaller than that based on the data obtained in our institute[4,25].

Sonchik[25] determined the discharge delay time in NaCl, KCl, KBr and KI single crystals in breakdown by single square pulses. He found that the average discharge propagation velocity increases 1) with increase of the overvoltage, 2) with increase of the lattice energy and 3) for positive polarity of the point electrode.

Mel'nikov[26], using a voltage cut-off technique, obtained incomplete discharges in rock salt. By varying the instant of cut-off, he determined the velocity of propagation of the discharge channel through the thickness of the dielectric. This velocity, he found, increases with advance of the channel from the point electrode into the crystal plate and lies in the range from 10^5 to 10^6 cm/sec. Thus, the view of von Hippel & Alger[3] that the rise of the voltage-time characteristic in the range of short exposures (Fig.2) is due to lag in the formation of the electronic space charge rather than to delay of the discharge is disproved by the experiments of Mel'nikov.

3. Thickness dependence of the breakdown voltage

Astafurov[14] investigated the variation of the breakdown voltage of rock salt, ice, lucite and paraffin as a function of the sample thickness. He found that the breakdown voltage increases more slowly than the sample thickness both in uniform and nonuniform fields.

In all investigations of solid dielectrics there was observed the same effect of polarity: the breakdown voltage is higher with the point electrode negative. A similar polarity effect obtains for air. The variation of the pulse breakdown voltage with the thickness is satisfactorily described by an equation of the form

$$V_{br} = AKv^{0.25}d^n,$$

where A and n depend on the dielectric material, K is a coefficient dependent on the configuration of the field and the polarity of the point electrode, v is the rate of increase of the voltage at the 0.5 V_{max} point of the rising pulse (v takes into account the lagging of the discharge with decrease of the rise time), and d is the thickness of the sample. The deduced variation of V_{br} as a function of the thickness is of great practical interest. The further problem consists in experimental investigation of $V_{br} = f(d)$ and finding the analytical function for other solid dielectrics, particularly those employed in engineering.

4. Some other regularities of pulse breakdown of solid dielectrics

In the light of the concept of impact ionization, in considering the process of breakdown of solid dielectrics we can distinguish the following stages of breakdown: the stage of discharge formation which is evinced in the oscillograms as the discharge delay time (if it is legitimate to neglect the statistical delay time), a stage of very rapid (catastrophic) decrease of the specimen resistance, accompanied by a rapid falling off of the voltage across the specimen, and the true discharge stage in which the current through the specimen is determined primarily by the parameters of the test circuit. Above we have reviewed the available theoretical treatments and some of the experimental data pertaining to the first stage. At present there is a scarcity of data on the physical processes involved in the second and third stages.

Some data regarding the second stage have been obtained in the Tomsk Polytechnic Institute. Sonchik[25] and Vorob'ev[27] established that the time of the second, voltage drop stage, is approximately one order of magnitude shorter than the discharge formation time. In air also the duration of the second stage is appreciably shorter than that of the formation stage. According to the data of Sonchik[25], both the discharge formation time and the voltage drop time in alkali halide single crystals decrease with increase of the lattice energy.

Torbin^{28} measured the breakdown currents in rock salt. At the instant corresponding to the drop in voltage, the current trace (on the oscilloscope screen) shows a "throw" similar to the throw evinced during the principal discharge stage in the breakdown of wide air gaps.

Mel'nikov^{26} established that the diameter of the discharge channel in incomplete breakdown amounts to only 0.05-0.06 the channel diameter in complete breakdown. This shows that the principal destruction of the dielectric occurs during the second or third stage.

5. Conclusions

There have been established the following regularities concerning pulse breakdown of solid dielectrics:

1. For large thicknesses there becomes evident the effect of polarity in solid dielectrics: the breakdown voltage is greater with the point electrode negative.
2. The mean propagation velocity of the discharge is a) greater with the point electrode positive and b) increases with increase of the overvoltage.
3. The discharge formation time increases with increasing thickness of the dielectric.
4. The duration of the second discharge stage in alkali halide crystals is approximately one order of magnitude shorter than the discharge formation time.

These regularities are also characteristic of the breakdown of gases, which is indirect indication that impact ionization or the streamer mechanism are operative in solid dielectrics as well.

There has been established a correlation between some of the characteristics of breakdown of alkali halide crystals with the lattice energy: a) the dielectric strength in a wide range of rise times and temperatures is proportional to the lattice energy, and b) the discharge formation time and the duration of the second discharge stage are shorter in crystals having a high lattice energy.

Other regularities

1) The voltage-time curves for alkali halide crystals have a "dipper" shape due, on the one hand, to the influence of space charge and, on the other hand, to lagging of the discharge.

2) The average discharge propagation velocity in solid dielectrics is of the order of 10^6 cm/sec and decreases with rising temperature.

3) The breakdown voltage in uniform and nonuniform fields increases more slowly than the thickness of the sample; the thickness dependence of the breakdown voltage of many solid dielectrics is described by equations of the same type.

6. Some problems for further investigation

Improvements in the design of insulation in electric equipment and development of the theory of electric breakdown of solid dielectrics would be benefited by further experimental and theoretical studies such as the following:

1. Determination of the voltage-rise time characteristics of solid insulating materials subjected to breakdown under different conditions (different field configuration, layer thicknesses, temperatures, etc.) and also in the presence of such insulating agents as oil barrier insulation, air-dielectric and oil-dielectric interfaces, etc.
2. Investigation of the radiation from the discharge channel during discharge formation and complete breakdown. The radiation spectrum may yield information

on the character of the ionization processes involved.

3. Investigation of pre-breakdown currents; this is essential for better understanding of ionization processes during discharge formation.

4. Measurement of the pulse breakdown strength of solid dielectrics. Variation of the pulse conductivity with time may bring out the influence of space charge. Variation of the pulse conductivity with variation of the field strength should yield information on the character of the ionization processes.

It must be noted that present day theories of electric breakdown of solid dielectrics are far from adequate. Current theories do not consider the development of breakdown in space and time. As a result, the theories cannot predict the dependence of the breakdown voltage of solid dielectrics on such factors as the field configuration, the distance between electrodes, and the physical-chemical characteristics of the material. Hence in our institute, in attempting to explain the results obtained on the breakdown of solid dielectrics, we are forced to turn to analogies with breakdown of air.

In constructing a phenomenological theory of electric breakdown of solid dielectrics, in our opinion, one can borrow much from the theory of breakdown of gases. At the same time one must take into account the specific characteristics of solids. By way of example, one may indicate the following factors that may differ in solid dielectrics as compared with gases: 1) influence of space charge, 2) influence of cold emission from the cathode and electrostatic ionization in the dielectric, 3) high linear density of ionization which may give rise to strong influence of electrode polarity and possible transition to the streamer process, particularly in the case of small electrode separations, and 4) strong local fields, which may produce local mechanical destruction favoring propagation of the discharge.

Advances in theoretical treatment of electric breakdown of solid dielectrics taking into account the above mentioned factors would help give direction to further experimental research and this in turn would insure more thorough and rapid investigation of the entire complex phenomenon of electric breakdown of solid dielectrics.

Tomsk Polytechnic Institute

References

1. F.Lemhaus, Arch.Elektrotechnik, 32, 281 (1938).

2. L.Binder, Bluzhdaiyushchie volny v elektricheskikh setyakh (Stray waves in electric networks), M.-L., 1935.

3. A.von Hippel & R.S.Alger, Phys.Rev., 76, 127 (1949).

4. G.A.Vorob'ev, Zhur.eksp.i teor.fiz., 30, 256 (1956). (Trans.Soviet Physics - JETP).

5. V.D.Kuchin, Doklady AN SSSR, 114, 301 (1957). (Trans.Soviet Physics - Doklady.)

6. M.A.Mel'nikov, Izvestiya (Bulletin), Ministry of Higher Education, Physics, No.6, 173 (1958).

7a. A.A.Vorob'ev, Trudy (Proceedings), Siberian Physical-Technical Institute, 5, 234 (1939); b. G.A.Vorob'ev, Izvestiya (Bulletin), Tomsk Polytechnic Institute, 91, 89 (1956).

8. M.A.Mel'nikov, Izvestiya (Bulletin), Ministry of Higher Education, No.5, 12 (1958).

9. K.W.Plessner, Proc.Phys.Soc., 60, 243 (1948).

10. K.M.Kevroleva, Elektricheskaya prochnost' i nekotorye svoistva kristallogidratov (Dielectric strength and some properties of crystal hydrates), Thesis, Tomsk, 1956.

11. E.A.Konorova, Izvestiya, Tomsk Polytechnic Institute, 91, 73 (1955).

12. M.A.Mel'nikov, Elektrichestvo, 2, 64 (1959).

13. A.F.Val'ter & L.D. Inge, Zhur.priklad.fiz. (Journal of Applied Physics), 6, 3 (1929).

14. A.V.Astafurov, Issledovanie proboya tverdykh dielektrikov v bol'shikh tolshchinakh (Investigations of breakdown of solid dielectrics in thick layers), Thesis, Tomsk, 1958.

15. R.W.Crowe, J.Appl.Phys., 27, 156 (1956).

16. L.I.Sirotinskii (editor), Tekhnika vysokikh napryazhenii (High voltage engineering), Part II; 168, M., 1953.

17. A.M.Zalesskii, Apparaty vysokogo napryazheniya (High voltage equipment), p.254, M., 1954.

18. F.Seitz, Phys.Rev., 76, 1376 (1949).

19. H.Kawamura, H.Ohkura & T.Kikuchi, J.Phys.Soc., Japan, 9, 541 (1954).

20. R.S.Strigel, Elektrische Stossfestigkeit, Berling, 1939.

21. Y.Inuishi & T.Suita, J.Phys.Soc., Japan, 74, 150 (1954).

22. A.F.Val'ter & L.D. Inge, Doklady AN SSSR, 2, 65 (1934).

23. A.A.Vorob'ev & G.A.Vorob'ev, Izv.AN SSSR, Ser.fiz., 22, 397 (1958). (Trans.Bulletin 22, No.4, 399.)

24. M.A.Mel'nikov, Zhur.eksp.i teor.fiz., 36, 613 (1959). (Trans.Soviet Physics - JETP.)

25. K.K.Sonchik, Issledovanie zapazdyvaniya razryada v tverdykh dielektrikakh (Investigations of discharge lag in solid dielectrics), Thesis, Tomsk, 1958.

26. M.A.Mel'nikov, Tr.2-i Vsesoyuznoi konferentsii po fizike dielektrikov (Program of the Second All-Union Conference on the Physics of Dielectrics), M. 1960.

27. G.A.Vorob'ev, Izvestiya, Tomsk Polytechnic Institute, 91, 79 (1956).

28. N.M.Torbin, Tr.2-i (Program of the Second All-Union Conference on the Physics of Dielectrics), M., 1960.

BREAKDOWN VOLTAGE OF THICK INSULATING LAYERS IN A NONUNIFORM FIELD

- F.Obenaus

The proper employment of insulation in high voltage equipment is predicated on knowledge of the relation between the breakdown voltage V_{br} and the thickness of the insulating material. Thick insulation is used both for mounting current carrying components (for example, ceramic fittings) and for insulation in heavy electric equipment (for example, transformer oil).

We now have available tables of the breakdown strength of different technical materials in a uniform field. These tables, however, were compiled on the basis of data obtained for relatively thin (~2 mm) samples; hence they are not quite suitable for the design of insulating material components of appreciable thickness. For experimental determination of the breakdown strength of thick layers of insulators, one must have special high voltage equipment, and, what is more important, one must solve the difficult problem of providing a uniform field over a great thickness. As a result, the insulation of high voltage equipment does not always have a reliable breakdown strength, and this shortcoming is now particularly acutely felt when, in addition to familiar and thoroughly studied insulating materials, engineers are called upon to use a large number of newly developed insulators.

It may be assumed that as a result of overcoming these experimental difficulties the physics of electric breakdown will be amplified by new information, which will enable us to refine our concepts regarding the process of breakdown. It would, however, be overoptimistic to assume that in the near future we will be able to calculate the thickness dependence of the breakdown strength for complex insulating materials. For a long time yet, insulating engineering will have to depend on empirical methods of determining the insulating properties of materials.

Hence it is natural to turn to the experience gained from tests of air gaps. A wealth of data in this field has been accumulated and technical measurements of insulation have been possible even before we had any detailed knowledge of the physical processes occurring in gases. New information on the physics of electric breakdown must substantiate (or invalidate), first, the validity of the analogy between solid dielectrics and gases, and, second, the substantial role played by electrons in the development of breakdown.

Breakdown voltage of air gaps

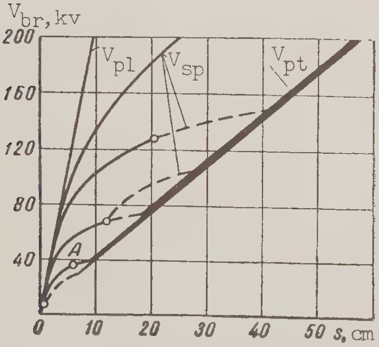

Fig.1. Ac voltage breakdown strength of air[1]: V_{pl} - uniform field, V_{sp} - nonuniform field (spheres 10, 5, 2 and 1 cm in diameter), V_{pt} - nonuniform field (needle electrodes).

Usually in investigating breakdown, the first thing studied is the variation of the breakdown voltage V_{br} with the separation s between the electrodes (Fig.1).[1] The limiting cases are $V_{pl} = f(s)$ for the case of a uniform field between plates and $V_{pt} = f(s)$ for the most nonuniform field between point electrodes. These functional dependences show what breakdown voltage for a given gap may be expected under conditions more or less favorable for breakdown. The $V_{sp} = f(s)$ curves, which lie between the curves for the limiting cases, were obtained for spherical electrodes. It will be seen that for small gaps these curves coincide with the $V_{pl} = f(s)$ curve, while for large gaps they approach and merge with the

$V_{pt} = f(s)$ curve. This transition occurs the later (i.e., for larger values of s), the greater the radius of curvature of the spherical electrodes. These intermediate characteristics are described up to a certain point (for example, point A in Fig.1) by the simple relation deduced by Schweiger[2]:

$$V_{sp} = V_a = E_a \eta s.$$

The breakdown voltage is equal to the initial voltage (V_a). It depends on the field geometry (η is the field inhomogeneity factor) and on the breakdown strength E_a of the insulating material. Inasmuch as with increase of s, the factor η decreases, the product $E_a\eta$ also decreases and the s dependence of V_{sp} changes, i.e., the characteristic is curved.

A different characteristic is obtained for a uniform field; in this case the thickness dependence of the breakdown voltage is described by

$$V_{pl} = E_{pl}s,$$

inasmuch as in a wide range of thicknesses the product $E_{pl}\eta$ is constant ($\eta = 1$, $E_a = \text{const}$). The slope of this straight line will depend only on the character of the insulating material (E_{pl} is the disruptive strength in a uniform field).

The same proportionality obtains between V_{br} and s for the point electrode case mentioned above.

Why is such a convenient linear dependence obtained from measurements on engineering materials? Schweiger[2] proposes the following explanation in his latest paper. He assumes that $V_{br} = f(s)$ is always linear if the space charge in the field forms so that the initial electrode shape is retained over the entire breakdown path. As soon as a certain initial voltage is exceeded, instead of the actual metal electrode there becomes effective an electrode formed by the space charge in the form of a luminous sheath or ramified discharge (Fig.2a). Usually the size of this effective electrode (r') differs from the size of the actual metal electrode (r_M), which has the effect of shortening the breakdown path. Instead of the initial inhomogeneity factor η, we have a new factor η' determined by the space charge. This factor always depends on the geometry of the initial arrangement of the electrodes; also, instead of s, we have s' (Fig.2b). The voltage necessary for further growth of the space charge electrode is

$$V = E\eta's'.$$

Inasmuch as the product $\eta's' = f(s)$ has a maximum (Fig.2c), the maximum voltage will be

$$V_{max} = E(\eta's')_{max}.$$

The voltage V_{max} is the breakdown voltage V_{br} for a spark gap. Upon attainment of this voltage, the electrode formed by the space charge grows very rapidly until it meets the opposite electrode. There arises an excess voltage. For stabilization of the rate of growth there must be a lower voltage corresponding to the descending branch of the $\eta's'$ curve. It has been shown that the function $(\eta's')_{max} = f(s)$ is linear for all electrodes which during growth of the space charge retain their initial shape (Fig.2 d & e):

$$(\eta's')_{max} = Bs = B(r_M + s') = Br_M + Bs' = A + Bs'.$$

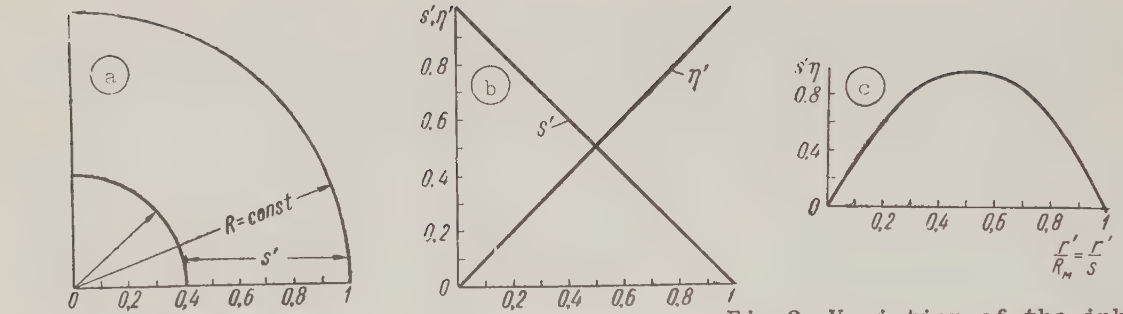

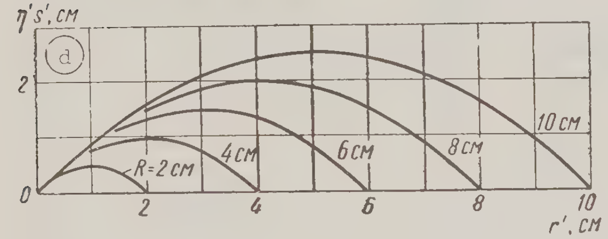

Fig.2. Variation of the inhomogeneity factor η' and gap width s' with growth of the space charge electrode; field between concentric circles with radii: internal metal electrode $r_м \to 0$ and external electrode $R_м = r_м + {}$ $+ \sim s$.

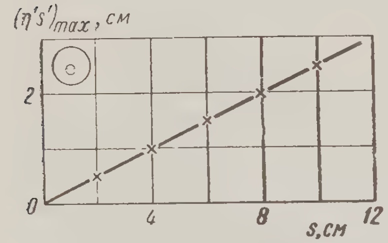

B depends on the shape of the electrode formed by the space charge. B is smaller in a three dimensional field (for example, in a spherical field) than in a two dimensional one (for example, the field between cylinders); A depends, in addition, on the size of the metal electrodes

In the case of a needle gap we can envisage the following physical situation: instead of a uniform charge distribution over the volume, there forms a filamentary channel, the point of which consists of one or more charge carriers. The field with such needle electrodes represents the extreme or absolutely nonuniform case. The radius of curvature of the electrodes in this case is small compared with the discharge gap so that the inhomogeneity factor does not vary with variation of the gap. In view of the fact that the radius of curvature is extremely small, the initial field strength is approximately the same as the constant field strength in the case of a uniform field between planar electrodes. In such a field the point of the pre-discharge channel may be thought of as an electrode with constant shape. The expression for V_{pt} in this case will be the following:

$$V_{pt} = A + Bs.$$

Inasmuch as the product of the field strength by the inhomogeneity factor for any discharge gap will have the same value, the dependence characterized by this relation is linear. As is known, for large (up to 3 meters) air gaps the constant A may be neglected. Then for a spark gap B will be the true "specific breakdown voltage" equal to 3.5 kv/cm. With the same justification, as in the case of the $V_{pl} = f(s)$ characteristic for a uniform field, it may be assumed that the slope of the $V_{pt} = f(s)$ characteristic is determined by the material, inasmuch as this characteristic depends only on the properties of the field. True, the factor B includes the inhomogeneity factor, but the latter depends not on the dimensions of the test set-up but only on the size of the predischarge channels, i.e., on the parameters of the insulating material. The lower bound of the $V_{pt} = f(s)$ characteristic is therefore suitable for evaluation and comparison of insulating materials.

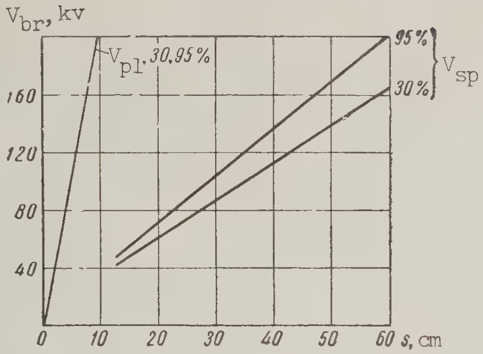

Fig.3. Ac disruptive strength of moist air (after Weiker[1]). Relative humidity - 30 and 95%.

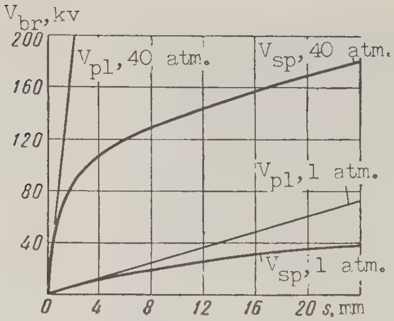

Fig.4. Ac disruptive strength of air at atmospheric and high pressure (after Gänger[3]).

This characteristic is very important, for in practice despite careful design to insure a uniform field, sections or areas of pronounced inhomogeneity are inevitable. We have in mind here inhomogeneities due to pores and cracks forming during fabrication of the insulator as well as microfissures formed under the influence of external mechanical forces and internal thermal stresses, etc.

Let us cite some examples which show how the V_{br} vs s curve depends on the state of the insulating substance. It is known that the breakdown voltage of air depends on its humidity. Fig.3 shows how the slope of the V_{sp} vs s plots increases with increase of the relative humidity. At the same time, it must be noted that the moisture content does not affect the V_{pl} vs s plots.

Fig.4 shows the characteristics change with change in air pressure (experimental results of Gänger[3] for the breakdown voltage in a point-plate field). It will be seen that the slope of the V_{pl} vs s lines increases sharply with pressure, while the s dependence of V_{sp} deviates from the V_{pl} vs s curve to the same extent as the intermediate curves in Fig.1.

From a comparison of the curves obtained in a uniform and nonuniform field at normal atmospheric pressure and also at high pressure (40 atm), it will be evident that in the former case the V_{pl} and V_{sp} plots are close, while in the latter case the V_{sp} plot beginning with small values of s deviates from the $V_{pl} = f(s)$ plot. Inasmuch as the metal electrodes in both cases were the same it is possible that at low pressures there become effective electrodes formed by the space charge due to the observed predischarges; with these electrodes the inhomogeneity factor is improved (for example, for p = 1 atm and s = 8 mm, $V_{pl} \approx V_{sp}$). At high pressures these space charges apparently cannot develop up to high values of the potential since the effect of η is unfavorable for metallic electrodes (for example, for p = 40 atm and s = 8 mm, $V_{pl} \gg V_{sp}$).

Thus at a pressure of 40 atm, air is a very good insulator in a homogeneous field; but in many actual devices and installations, where inhomogeneities are inevitable, its insulating characteristics are radically impaired. At the same time at a pressure of 1 atm air behaves in exactly the same way in uniform and nonuniform fields and has a low disruptive strength. This example shows that even if the s dependence of V_{pt} is nonlinear, one can still draw certain important inferences regarding the insulating properties of the substance from the appearance of the $V_{br} = f(s)$ curves for uniform and nonuniform fields. Here we might also refer to the similar deductions of Mikhailov[4] based on measurements of breakdown of very thin insulating materials (0.5 mm glass and 3 mm porcelain).

Predischarges in liquid and solid dielectrics

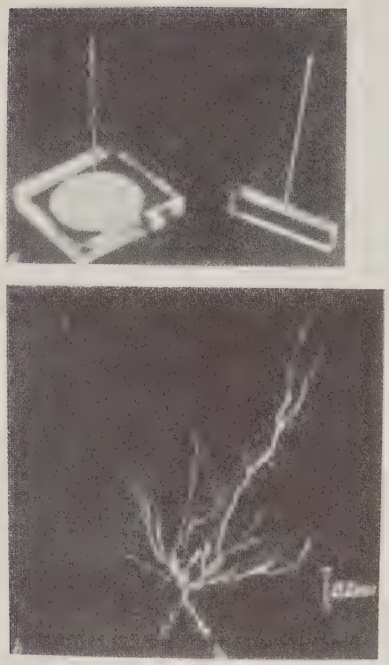

Fig.5. a - Specimens; b - predischarge in plexiglass under a pulse voltage (needle positive). Voltage = 53 kv, gap width = 3 mm, number of pulses = 6.

In considering the s dependence of V_{br} in gases, we spoke of space charge and predischarge channels. Do similar effects occur in liquid and solid dielectrics? Actually these effects have long been familiar in liquid dielectrics; in solid substances they are less well known inasmuch as they cannot be observed with the naked eye.

Many investigators[5] observed predischarges in solids in a uniform field. In recent experiments with plexiglass Müller[6] succeeded in observing and photographing under a microscope traces of predischarges both in the case of an alternating field and a pulse voltage (Fig.5,a & b). In all probability one can obtain s dependences of V_{br} for liquid and solid dielectrics similar to those that have been recorded for air.

Variation of the breakdown voltage with the gap width in liquid and solid insulating materials

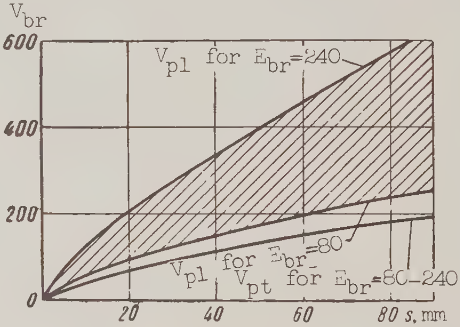

Fig.6. Distruptive strength of transformer oil under ac voltage (after Broszat[7]). E_{br} - disruptive strength (kv/cm) of the oil in a uniform field with s = 2.5 mm; V_{pt} - field between a needle electrode and a plate electrode perpendicular to it.

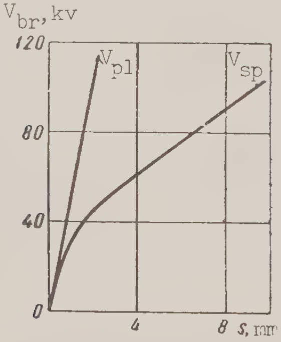

Fig.7. Disruptive strength of epoxy resin.

It must be noted that there have been as yet no systematic measurements for industrially important liquid and solid insulating materials similar to the exhaustive measurements available for air at atmospheric pressure.

Hence where liquid and solid dielectrics are concerned one can cite only a few examples. Figs.6 & 7 show the V_{sp} vs s curves for two isotropic materials, namely, transformer oil and epoxy resin. It will be seen that the plots are linear in the range of large thicknesses, but it is not clear whether the slope of these straight line plots correspond to the familiar s dependences of V_{pt} for air. Similar characteristics have been obtained for cable impregnating compounds, paraffin and plexiglass. The investigated range of gaps (thicknesses) is still rather small inasmuch as appropriately thick samples are not available. We give the curves for the above materials primarily

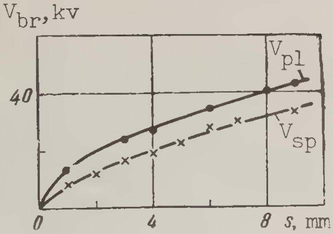

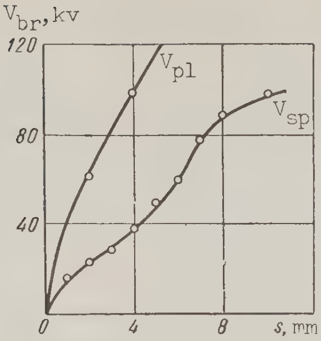

Fig.9

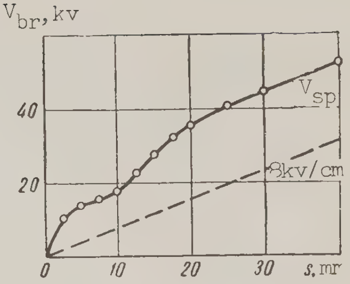

Fig.10

Fig.8. Disruptive strength of glass.

Fig.9. Disruptive strength of cardboard.

Fig.10 Variation of the breakdown voltage with gap width for a point-plate air gap with a layer of pressboard inserted into the gap.

because predischarge channels have been photographed in them. The V_{pl} vs s and V_{sp} vs s curves for isotropic materials (for example, glass) are usually close to each other (Fig.8). This is explained by the fact that the inhomogeneities of the material determine the value of the disruptive strength in a uniform field. For anisotropic materials with the layers oriented at right angles to the field lines (for example, cardboard - Fig.9), there is evident an irregular rise of the characteristic which is apparently connected with the structure of the material. Fig.10 shows that one can obtain an analogous change in the form of the characteristic for air by inserting, for instance, a sheet of pressboard at 90° to the field lines between the needle and plate electrodes.

Conclusions

In order to be able to evaluate the insulating properties of materials one must know the thickness dependence of the breakdown voltage not only in a uniform field but also in an extreme nonuniform field. From the character of the V_{br} vs s curve one can draw certain deductions regarding the nature of the electric process preceding breakdown. The character of the variation of V_{sp} as a function of the gap width for air indicates that in front of the actual metal electrodes there form space charge electrodes. There exists a minimum value of V_{pt} for the extreme inhomogeneous field in front of the needle of the discharge channel. The s dependence of V_{pt} is linear in a wide range of discharge gaps. For liquid and solid dielectrics of great thickness the V_{br} vs s characteristics are not always linear inasmuch as space charges also form in these materials. The predischarge channels observed in these substances are similar to the channels in air. Hence it may be assumed that knowledge of the character of the $V_{br} = f(s)$ curves for inhomogeneous fields in liquid and solid dielectrics may be just as important as for air[8]. The available curves show how low the breakdown voltage may fall in the case of unfavorable field distribution. Moreover, such curves help clarify the physical mechanism of breakdown and the structure of insulating material. It is essential to continue systematic investigations on solids and liquids similar to those carried out years ago for gases. These investigations should not be limited to point electrodes but should be carried out with electrodes of different shape and size.

Deutsche Akademie der Wissenschaften,
German Democratic Republic

References

1. W.Weicker, Elektrotechn.Z., 32, 436 (1911).
2. A.Schweiger, Elektrotechn.Z., Ausg.A, 75, 293 (1954).
3. B.Gänger, Arch.Elektrotechn., 34, 633 (1940).
4. M.M.Mikhailov, Elektromaterialovedenie (Characteristics and treatment of electrical engineering materials), p.89, M., 1953.
5. L.Juge & A.Walter, Arch.electrotechn., 24, 259 (1930); A.von Hippel, Z. Physik., 67, 707 (1931); R.Strigel, Elektrische Stossfestigkeit, S 80. - Springer-Verlag, Berlin, 1955.
6. U.Müller, Wiss.Z.Techn.Hochschule, Dresden, 4, 629 (1954/55).
7. Broszat, 4 Jahrestagung der Elektrotechniker.-Neimar, 1952.
8. F.Obenaus, Wiss.Z.Hochsch.Elektrotechn., Ilmenau, Jg.3, H.1, 53 (1957).

CHARACTERISTICS OF THE MOTION OF FAST CURRENT CARRIERS IN POLAR CRYSTALS

- Yu.I.Gorkun & K.B.Tolpygo

It was shown in the work of Pekar and his co-workers[1] that taking into account the interaction of conduction electrons with the longitudinal optical mode in polar crystals leads, in the zeroth approximation of the theory, to the inference that the polaron state rather than the band state is energetically more advantageous for the electrons. Evaluation of the mobility and concentration leads to the deduction that polarons are the majority current carriers in ionic (polar) crystals.

Usually theory treats the case of a slowly moving polaron[1] in which there is no resonance between the natural crystal frequencies and the frequencies of the moving charge field. In this case one can restrict the consideration to a quadratic relation between the polaron energy and velocity, and assume the polaron wave function and its effective mass to be velocity independent. The efforts of most investigators have been directed toward improvement of the methods of calculating the energy and ground state wave function of the polaron and its effective mass.

There remains, however, a gap in the theory; this stems from the fact that behavior of a polaron as its velocity increases has virtually not been investigated theoretically, i.e., we do not know how the polaron wave function, its effective mass, etc. depend on velocity. This question is very important because in the study of such phenomena as electric breakdown, field emission, thermionic emission, photoelectric and secondary emission, we are concerned with the motion of fast current carriers, which brings us into the region of resonance between the natural crystal frequencies and frequencies of the field of the moving charge. Here the slow (or "rigid") polaron approach becomes unsuitable. In a number of cases even thermal polarons are "fast".

In order to construct a systematic theory for the enumerated phenomena, it is necessary to study carefully the properties of polarons at high velocities. From the standpoint of this theory, therefore, we should consider polaron motion in the case when no limitations are imposed on its velocity. The Bogolyubov-Tyablikov method[2] makes possible such a treatment. This method, however, involves improper integrals. But here one can utilize the fact that the zeroth approximation of the Bogolyubov-Tyablikov method corresponds to the semiclassical polaron theory, in which the electron motion is described quantum mechanically and the motion of the lattice ions - classically. With such an approach the reason for the appearance of improper integrals becomes clear: at high polaron velocities, the harmonic approximation fails for describing the lattice vibrations because the polarization of the crystal becomes infinitely large. Consequently, in treating fast polarons it becomes essential to take into account the anharmonicity of the lattice vibrations.

This is most easily done on the basis of the Tolpygo theory[3] of the dynamics of a crystal lattice composed of deformable ions. Taking into account the anharmonicity leads to the appearance of an added imaginary term in the resonance expression for the amplitude of the forced vibrations of the ions, which precludes the appearance of improper integrals. If we assume that the polaron radius is large compared with the lattice constant (in this case we can take into account only the limiting wave lengths in the lattice and consider only interaction with the longitudinal optical mode) and that the adiabatic approximation is applicable (so that the ionic displacements are determined by the average electron field), then we obtain the following form of the Schrödinger equation for the wave function that describes the fluctuating motion of an electron in a polarized potential well, the center of which is moving with velocity v:

$$\left[-\frac{\hbar^2}{2m^*}\Delta+U(\mathbf{r})-W_0\right]\psi(\mathbf{r})=0, \tag{1}$$

where

$$U(\mathbf{r})=-\frac{4\pi e^2 c}{V}\sum_{\mathbf{K}}\frac{\omega_{\mathbf{K}}^2}{K^2}\,\frac{\int e^{-i\mathbf{K}\mathbf{r}'}|\psi(\mathbf{r}')|^2\,d\mathbf{r}'}{\omega_{\mathbf{K}}^2-(\mathbf{K}v)^2-i\mathbf{K}v\Gamma}\,e^{i\mathbf{K}\mathbf{r}}; \tag{2}$$

$c=\frac{1}{n^2}-\frac{1}{\varepsilon}$; n is the index of refraction, ε is the dielectric constant, m^* is the effective mass of a band electron, the $\omega_k\approx\omega$ are the natural frequencies of the longitudinal optical modes, **K** is the wave vector, V is the crystal volume, Γ is the anharmonicity "constant", which in principle can be calculated theoretically (for example, see Ref.3). This, however, entails cumbersome calculations, consequently, subsequently the value of Γ, where required, was taken from experiment^4. Assuming $\Gamma=0$ in (2), we obtain the results of the zeroth approximation in the Bogolyubov-Tyablikov theory.

Eq.(1) was solved by a direct variational method with trial wave functions

$$\psi_1=\sqrt{\frac{\alpha^3}{\pi}}\,e^{-\alpha r}, \tag{3}$$

$$\psi_2=\sqrt{\frac{\alpha^3}{\pi(1+9\beta^2/2\alpha^4)}}\,[1+\beta r^2 P_2(\cos\vartheta)]\,e^{-\alpha r}, \tag{4}$$

where P_2 is the field Lagrangian, ϑ is the angle between v and r and α and β are approximation parameters, the dependence of which on the dimensionless velocity $u=v/\omega r_0$, $r_0=\hbar^2/m^*e^2c$, was determined from the variational principle.

The results are given in Fig.1 (curves 1,2 & 3) from which it is apparent that the radius of the polaron initially decreases somewhat with increasing velocity, then begins to increase. This is related to the fact that as the velocity increases, we approach closer to the region of resonance between the natural crystal frequencies and most of the frequencies present in the Fourier series expansion of the field of the moving polaron. As the crystal polarization increases, the electron is localized in an ever smaller region of the crystal. With further increase in velocity such optimum conditions for resonance no longer obtain, the crystal polarization is diminished, the potential well is reduced and the polaron begins to "spread". In addition, the curve for the parameter β shows that as the velocity increases, the polaron is "flattened", stretching out in the direction of motion.

Data concerning the velocity dependence of the wave function can be used to calculate the energy of the system (crystal + electron) as a function of the translational velocity of the polaron; to this end it is necessary to average the Hamiltonian over one of the wave functions (3) or (4). For simplicity, this was done for (3), which gave:^{5,6}

$$E_0(u)=\frac{m^*e^4c^2}{\hbar^2}\left\{A(u)+\frac{\omega}{\Gamma}B(u)\right\}, \tag{5}$$

where $A(u)$ and $B(u)$ are functions of the dimensionless velocity u. For low velocities ($u\ll1$), the term $A(u)$ is dominant, giving the usual quadratic dependence; for high velocities ($u\gtrsim1$, i.e., of the order of the velocity of sound) the second term is dominant and $E_0=f(u)$ differs from a parabola, becomes considerably steeper (which can be interpreted as an increase in the polaron effective mass with velocity) and is strongly dependent on the anharmonicity constant. With further increase in velocity, a small drop in E_0 is observed. This behavior of the energy as a function of the velocity is also explained by the passage through the optimum

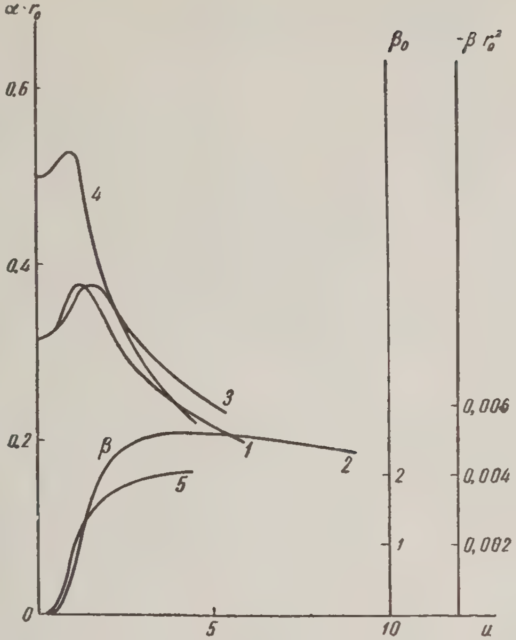

Fig.1

conditions for resonance and the corresponding behavior of the crystal polarization. Fig.2 shows the result of the calculation of $E_0(u)$ for NaCl (curve 1) with Γ taken from experiment[4]; for comparison purposes we also show the velocity dependences for a "rigid" polaron and a band electron (curves 2 & 3, respectively).

Because in the case of a fast polaron resonance occurs between the frequencies of the excitation force (the field of the moving polaron) and the natural frequencies of the crystal, lattice vibrations will be stimulated, and as a result the polaron will be retarded. The polaron energy loss per unit time was calculated as equal to the average increment in the lattice energy per unit time

$$\mathscr{E}(v) = \lim_{t\to\infty} \frac{1}{t} \int_0^t \frac{dA}{dt}\, dt, \tag{6}$$

where A is the lattice energy. Then, in the general case[7,5]

$$\mathscr{E}(v) = \frac{\pi\mu a^2}{v} \sum_{\alpha\mathrm{K}} \frac{1}{K} |D_{\alpha\mathrm{K}}|^2\, \delta\left(\cos\vartheta - \frac{\omega_{\alpha\mathrm{K}}}{Kv}\right), \tag{7}$$

where a is the lattice constant, μ is the reduced mass of an ion pair, ϑ is the angle between K and v,

$$D_{\alpha\mathrm{K}} = -\frac{4\pi i e^2 \sqrt{N}}{V\mu a} \frac{\mathbf{K}}{K^2}\, \pi^{\alpha\mathbf{K}} \int e^{i\mathbf{Kr}} |\psi(\mathbf{r})|^2\, d\mathbf{r}, \tag{8}$$

N is the number of unit cells, and $\pi^{\alpha\mathrm{K}}$ is the amplitude of the dipole moment of a unit cell, corresponding to the mode $\alpha\mathrm{K}$ (α is the number of the frequency branch).

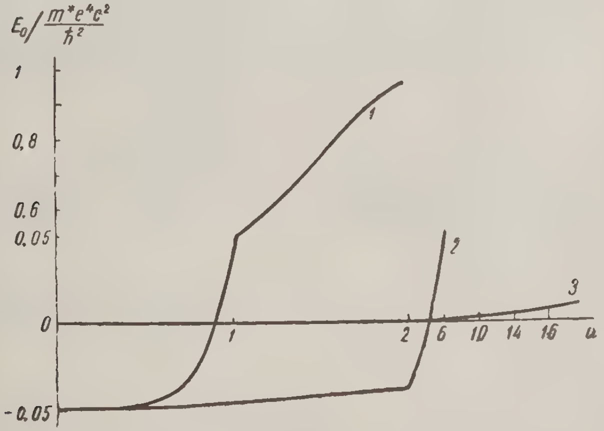

Fig.2

For a polaron of a large radius, when $u \approx 1$, dissipation for stimulation of longitudinal optical vibrations predominates[8]. In this case the loss is given by[5]

$$\mathscr{E}_1(v) = \frac{e^2\omega^2 c}{v} \int_{\omega/v}^{\infty} \frac{dK}{K} \left| \left(\int e^{i\mathbf{Kr}} |\psi(\mathbf{r})|^2\, d\mathbf{r} \right)_{\cos\vartheta = \frac{\omega}{Kv}} \right|^2. \tag{9}$$

The calculation of the losses by means of this formula for different wave functions of a "rigid" polaron shows[5] that the magnitude of the loss is not very sensitive to the choice of ψ (Fig.3, curves 1,2,3 & 4; Table 1). Taking into account polaron deformability leads to a significant decrease of the loss (in the given velocity region) (curves 5 & 6 of Fig.3), which is connected with the better "adaption" of the wave functions to the polarization of the surrounding crystal.

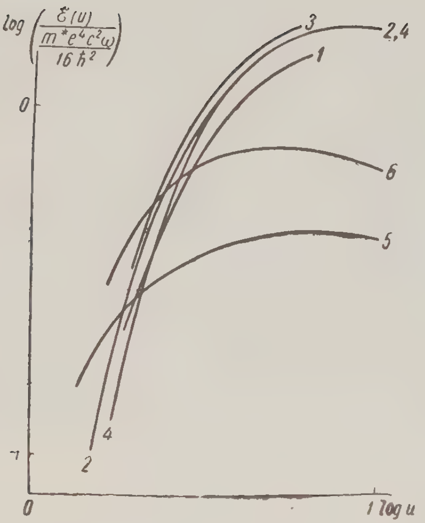

Fig.3

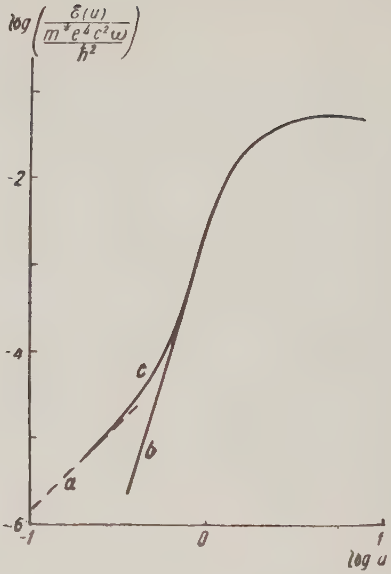

Fig.4

If we use the deduced loss values $\mathscr{E}_1(u)$ and evaluate the polaron mobility, we find that for $u<1$, we obtain greatly overestimated mobility values, i.e., $\mathscr{E}_1(u)$ yields an underestimate of the losses at low velocities. Actually, taking into account the anharmonicity of the lattice vibrations gives the following expression for the loss due to generation of longitudinal optical vibrations[9]:

$$\mathscr{E}^{\mathrm{an}}(u) = \mathscr{E}_1(u) + \frac{\Gamma}{\omega} B_1(u) . \tag{10}$$

When $u<1$, the second term ("anharmonic" retardation) dominates, while when $u \gtrsim 1$, the first term ("resonance" retardation) predominates. In the limit, as $u \to 0$, we obtain from (10) the result of Pekar[2], who took into account phenomenological absorption of equivalent electromagnetic waves. Fig.4 gives $\mathscr{E}_1^{\mathrm{an}}(u)$ for NaCl (curve a), and for comparison $\mathscr{E}_1(u)$ (curve b) and Pekar's result (curve c). The mobilities obtained therefrom are already of the order of magnitude of the experimental mobilities.

The results for the energy loss were used to evaluate the breakdown field strengths on the basis of the von Hippel criterion, according to which breakdown occurs when equality of energy lost and gained per unit time becomes impossible, i.e., when the electron goes over into the band state as a result of energy built-up and produces impact ionization. Then[7]

$$E_{\mathrm{br}} \equiv E_{\max}(v) = (\mathscr{E}_1(v)/ev)_{v=v_m}, \tag{11}$$

where v_m is determined from the condition $dE/dv = 0$. This gives:

$$E_{\mathrm{br}} = B \cdot 10^{-9} \frac{e}{r_0^2}\ \mathrm{v/cm}\ , \tag{12}$$

where the coefficient B depends on the choice of ψ-function. The values of B for several wave functions are given in Table 1. Table 2 gives the experimental and theoretical values of E_{br} for alkali halide crystals. It is apparent that in general the theoretical values of E_{br} exceed the experimental values; the agreement

Table 1

Curve No. in Fig. 3	ψ	B
1	$e^{-\alpha r}$	2,4
2	$(1+\alpha r)\, e^{-\alpha r}$	2,91
3	$(1+\alpha r+\beta r^2)\cdot e^{-\alpha r}$	3,12
4	$e^{-\alpha^2 r^2}$	2,3
5	$[1+\beta r^2 P_2(\cos\vartheta)]\, e^{-\alpha r}$	1,26
6	$e^{-\alpha r}$ (deformable)	2,1

Table 2

Crystal	$E_{br}\cdot 10^{-6}$ v/cm	$E_{exp}\cdot 10^{-6}$ v/cm (288°K)	$10 r_0$, Å	a, Å
RbI	1,4	0,49	13,6	3,66
RbBr	1,6	0,63	13,5	3,42
RbCl	2,5	0,83	11.3	3,27
KI	1,26	0,57	13,6	3,53
KBr	1,6	0,7	13,0	3,29
KCl	2,5	1,0	11,4	3,145
KF	10,5	1,9	6,69	2,66
NaI	3,4	0,8	8,5	3,23
NaBr	5,2	0,81	7,85	2,97
NaCl	5,9	1,5	7,4	2,82
NaF	14,4	2,4	5,8	2,3
LiF	70	3,1	2,7	2,0

improves as macroscopic consideration of the crystal becomes more valid (for which the condition $10\ r_0 \gg a$ should be fulfilled[1]). The divergence may be attributed to a number of factors, in particular to the neglect of the statistical scattering of polarons with respect to velocity and to use of an inaccurate value for the electron effective mass.

The properties of fast polarons considered hitherto can be evinced in photoelectric, thermionic and secondary emission. The use of these results for treatment of breakdown and field emission is quite justified, inasmuch as in the case of polaron motion in a strong electric field it is necessary to take into account the immediate influence of the external field on the shape of the potential well and the wave functions. Distortion of the potential may lead to a falling out of a discrete level and the "destruction" of the polaron.

Evaluation on the basis of the "rigid" polaron theory leads to apparent "destruction" of the polaron at fields of the order of E_{br}. We therefore investigated the self-consistent quasi-stationary motion of the polaron along the field when its velocity is constant in time and the energy loss is exactly compensated by the work of the external field:

$$e\mathrm{vE} = \mathscr{E}_1(v). \tag{13}$$

The corresponding Schrödinger equation is of the form:[10,6]

$$i\hbar\frac{\partial\psi}{\partial t} = \left[-\frac{\hbar^2}{2m^*}\Delta + U - e\mathbf{Er} - \mathscr{E}_1(v)\,t\right]\psi(\mathbf{r}, t); \tag{14}$$

it is distinguished by the presence of the term $-\mathscr{E}_1(v)\,t$, which takes into account the energy loss due to "friction" incident to motion in the crystal. U is given by Eq.(2). The solution of (14) can be written in the form

$$\psi(\mathbf{r}, t) = \psi_0(\mathbf{r}-\mathbf{v}t)\exp\frac{i}{\hbar}\left\{m^*\mathbf{vr} - t\left[W_0 + \frac{m^* v^2}{2} - e\mathbf{vE}t\right]\right\}, \tag{15}$$

where ψ_0 satisfies the equation

$$\left[-\frac{\hbar^2}{2m^*}\Delta + U - e\mathbf{Er}\right]\psi_0(r) = W_0\psi_0(\mathbf{r}), \tag{16}$$

which was solved by a variation method with the approximation

$$\psi_0(r) = A\,[1+\alpha r\,(1+\beta_0\cos\vartheta)]\,e^{-\alpha}, \tag{17}$$

where $\vartheta = (\hat{\mathbf{v}\mathbf{r}})$. Curves 4 & 5 in Fig.1 show the u-dependence of parameters α and β_0, which dependence is related to the field by Eq.(13). The maximum field intensity in which uniform translation of a polaron is possible (according to the von Hippel criterion it is equal to E_{br}) is given by Eq.(12) when $B \doteq 1$.

These results for the wave function were used to find the functional variation of the electron potential energy with the distance along the field direction.[6,10]

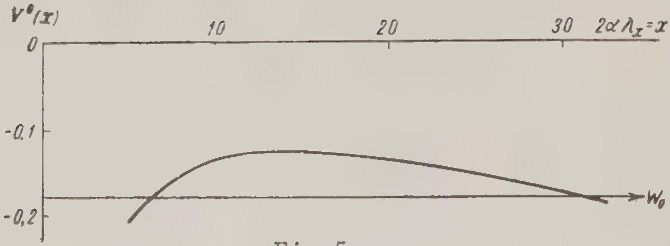

Fig.5

It was found (Fig.5) in the case of uniform motion of the polaron in the field, even in a field of the order of E_{br}, distortion of the potential well does not lead to falling out of a discrete electron level, i.e., "destruction" of a polaron can occur either due to the tunnel effect or because of acceleration and subsequent transition of the electron into the band state.

We note that this study suffers from the shortcoming that we did not take into account the weakening of the coupling with increasing polaron velocity, which Buimistrov and Pekar[11] showed, actually does occur.

Physics Institute,
Ukrainian SSR Academy of Sciences

References

1. S.I.Pekar, Issledovaniya po elektronnoi teorii kirstallov (Investigations on Electronic Theory of Crystals) M.-L., 1951.
2. N.N.Bogolyubov, Ukr.matem.zhur. (Ukrainian Math.Jour.), 2, 3 (1950).
3. K.B.Tolpygo, Trudy (Proceedings), Kiev State University, Math.Collection, 5, 99 (1951); Trudy Im-ta fiz. (Proc.Physics Inst.) Ukrainian SSR Ac. of Sci., 6, 102 (1955).
4. M.Szerny, Z.Phys., 65, 600 (1930).
5. Yu.I.Gorkun, Zhur.tekh.fiz., 27, 1764 (1957). (Trans.Soviet Phys.-Tech. Phys.)
6. Yu.I.Gorkun & K.B.Tolpygo, Doklady AN SSSR, 120, 491 (1958). (Trans. Doklady.)
7. Yu.I.Gorkun & K.B.Tolpygo, Izv.AN SSSR, Ser.fiz., 22, 377 (1958). (Trans. Bulletin 22, No.4, 377.)
8. K.B.Tolpygo & Z.I.Uritskii, Zhur.eksp.i teor.fiz., 30, 929 (1956). (Trans.Soviet Physics - JETP.)
9. Yu.I.Gorkun, Ukr.fiz.shur. (Ukrainian Phys.Jour.), 3, 289 (1958).
10. Yu.I.Gorkun, Ibid., 3, 1 (supplement), 32 (1958).
11. V.M.Buimistrov & S.I.Pekar, Zhur.eksp.i teor.fiz., 33, 1271 (1957). (Trans.Soviet Physics - JETP.)

NEW FORM OF POLAR CRYSTAL MODEL

- A.E.Glauberman

In the theory of weakly excited crystals, when the number of elementary excitations is small, for the so-called polar model it is convenient to use an approach allowing immediate separation of the part of the Hamiltonian containing the elementary excitations. In view of this the Shubin-Vonsovskii approach has been used in many theoretical investigations of metals, semiconductors and dielectrics.

At least two difficulties are encountered, however, in transformation of the second quantization Hamiltonian written in Fermi amplitudes to new quasi-particle operators in the method of Shubin-Vonsovskii. The first difficulty is that the quasi-particle operators are introduced as Bose type operators, which is scarcely admissible from the physical standpoint (if we have in mind current quasi-particles). The second difficulty is the complexity of constructing the Hamiltonian in the new operators, in which on the basis of qualitative (but incidentally sufficient) considerations it is necessary to express the bilinear groups of Fermi amplitudes in terms of groups of operators of the lattice point states. Thus, for example, for the popular model of an atomic crystal with one valence electron per atom the bilinear groups of Fermi operators $a_q{}^+a_{q'}$ must be replaced by the sum of quadruple products of the Shubin-Vonsovskii operators, determined as operators of the Bose type:

$$a_q^+a_{q'} \to \Psi_q^+\psi_q\Phi_{q'}\varphi_{q'} - \Psi_q^+\psi_q\psi_{q'}^+\Psi_{q'} + \varphi_q^+\Phi_q\Phi_{q'}^+\varphi_{q'} + \varphi_q^+\Phi_q\psi_{q'}^+\Psi_{q'},$$

where Φ_q, $\Phi_q{}^+$; Ψ_q, $\Psi_q{}^+$; φ_q, $\varphi_q{}^+$; ψ_q, $\psi_q{}^+$ are operators for dyads, holes, simple right and simple left points, respectively.

Further, for obtaining the excitation operator one must always go over to the quasi-classical approximation for operators not representing these excitations (for example, φ and ψ) in which the statistical averages for the corresponding occupation numbers depend on the number of excitations. All these steps are not mathematically self-evident so that the character of the corresponding transformations is not entirely clear from the standpoint of quantum mechanics.

In view of the above we propose the following scheme for transition to the excitation Hamiltonian in the polar model, which takes into account the distinctive features of the background and is essentially a canonical transformation. Bearing in mind the atomic crystal model mentioned above, let us consider the linear transformation of Fermi amplitudes:

$$a^+_{q\frac{1}{2}} = A\alpha_q^+ + B\beta_q, \quad a^+_{q-\frac{1}{2}} = C\alpha_q^+ + D\beta_q,$$

$$a_{q\frac{1}{2}} = A\alpha_q + B\beta_q^+, \quad a_{q-\frac{1}{2}} = C\alpha_q + D\beta_q^+, \tag{1}$$

where A, B, C and D are real numbers, the operators α_q^+ and α_q represent dyads, and the operators β_q^+ and β_q represent holes. Transformation (1) is a canonical one and defines the new operators as Fermi type operators.

From the commutation relations for Fermi amplitudes

$$a_\lambda^+a_{\lambda'} + a_{\lambda'}a_\lambda^+ = \delta_{\lambda\lambda'} \tag{2}$$

and the condition of conservation of the total number of electrons

$$\sum_q a^+_{q\frac{1}{2}}a_{q\frac{1}{2}} = M + S, \quad \sum_q a^+_{q-\frac{1}{2}}a_{q-\frac{1}{2}} = L + S, \tag{3}$$

where M is the number of simple right points, L is the number of simple left points, and S is the number of dyads, which is equal to the number of holes, and bearing in mind the requirement

$$\sum_q \overset{+}{\alpha}_q \alpha_q = S \quad \text{and} \quad \sum_q \overset{+}{\beta}_q \beta_q = S, \tag{4}$$

we obtain the following set of equations for the transformation coefficients:

$$A^2 + B^2 = 1, \quad AC + BD = 0; \quad n + s = (C^2 - D^2)\,s + D^2;$$
$$C^2 + D^2 = 1; \quad m + s = (A^2 - B^2)\,s + B^2, \tag{5}$$

whence

$$A^2 = \frac{n}{m+n}, \quad B^2 = \frac{m}{m+n}, \quad A^2 = D^2, \quad B^2 = C^2. \tag{6}$$

Here the concentrations $n = \frac{L}{N}$ and $m = \frac{M}{N}$; we have used the normalization condition $m + n + 2s = 1 \quad \left(s = \frac{S}{N}\right)$.

Owing to the fact that the constants A^2, B^2, C^2 and D^2 are expressed in terms of the relative concentrations of simple points, they do not contain the normalization constant of the statistical expressions for m and n and these last must be regarded as background concentrations.

Finally, transformation (1) is obtained in the form

$$\overset{+}{a}_{q^1/_2} = A_1 \overset{+}{\alpha}_q + B_1 \beta_q, \quad \overset{+}{a}_{q-{}^1/_2} = B_1 \overset{+}{\alpha}_q - A_1 \beta_q,$$
$$a_{q^1/_2} = A_1 \alpha_q + B_1 \overset{+}{\beta}_q, \quad a_{q-{}^1/_2} = B_1 \alpha_q - A_1 \overset{+}{\beta}_q, \tag{7}$$

where

$$A_1 = \sqrt{\frac{n}{n+m}}, \quad B_1 = \sqrt{\frac{m}{n+m}}. \tag{8}$$

Inversion of the above equations yields

$$\overset{+}{\alpha}_q = A_1 \overset{+}{a}_{q^1/_2} + B_1 \overset{+}{a}_{q-{}^1/_2}, \quad \overset{+}{\beta}_q = B_1 a_{q^1/_2} - A_1 a_{q-{}^1/_2},$$
$$\alpha_q = A_1 a_{q^1/_2} + B_1 a_{q-{}^1/_2}, \quad \beta_q = B_1 \overset{+}{a}_{q^1/_2} - A_1 \overset{+}{a}_{q-{}^1/_2}. \tag{9}$$

To illustrate the use of the method let us consider the problem of an atomic semiconductor with one valence s electron per atom in crossed electric and magnetic fields: $\mathbf{F} \parallel Oy$ and $\mathbf{H} \parallel Oz$, which we solved earlier[1] in the framework of the Shubin-Vonsovskii theory.

The Hamiltonian of the system, after transformation (7) and elimination of the constant terms pertaining only to the background, has the sense of an excitation Hamiltonian and equals

$$H_{\text{exc}} = eF \sum_q R_{qy} (\alpha_q^+ \alpha_q - \beta_q^+ \beta_q) + \mu_B H \frac{m-n}{m+n} \Big[N - \sum_q (\alpha_q^+ \alpha_q + \beta_q^+ \beta_q)\Big] +$$
$$+ \frac{1}{2}(A + I) \sum_q (\alpha_q^+ \alpha_q + \beta_q^+ \beta_q) + \sum_{q \neq q'} L_{qq'} (\alpha_q^+ \alpha_{q'} - \beta_q^+ \beta_{q'}) \tag{10}$$

in the approximation in which there are discarded as small higher order terms describing the interaction of quasi-particles (i.e., essentially there has been utilized the condition of smallness of the number of excitations $Sp \sum_q (\alpha_q^+ \alpha_q + \beta_q^+ \beta_q) \ll N$). For the "background" concentrations in the magnetic field we used the Boltzmann equation and obtain

$$\frac{m-n}{m+n} = \operatorname{th}\frac{\mu_{\mathrm{B}}H}{kT}. \tag{11}$$

The excitation operator in the Shubin-Vonsovskii method, after averaging over the background, was found by us earlier in the same "quadratic" approximation in the form

$$H_{\mathrm{exc}} = eF\sum_q R_{qy}(\Phi_q\Phi_q^+ - \Psi_q\Psi_q^+) + \mu_{\mathrm{B}}H\operatorname{th}\frac{\mu_{\mathrm{B}}H}{kT}\Big[N - \sum_q(\Phi_q\Phi_q^+ + \Psi_q\Psi_q^+)\Big] + \\ + \frac{1}{2}(A+I)\sum_q(\Phi_q\Phi_q^+ + \Psi_q\Psi_q^+) + \sum_{q\neq q'} L_{qq'}(\Phi_q\Phi_{q'}^+ - \Psi_q\Psi_{q'}^+). \tag{12}$$

Thus in the assumed approximation the difference in the final result is only that in the proposed scheme the dyad and hole operators appear as Fermi type operators. In the new scheme, construction of the Hamiltonian is exceptionally simple and clear at all stages.

The proposed scheme is universally applicable and can be extended to the case of a spin-closed background (germanium type crystals), to the case of impurity crystals and so on.

V.Vladimirov and I.Stasyuk participated in development of the scheme and in solution of a number of specific problems.

References

1. A.E.Glauberman & A.M.Muzychuk, Ukr.fiz.zhur. (Ukrainian Physics Journal), No.3, 178 (1958).

SOME ELECTROLUMINESCENT PROPERTIES OF ZINC OXIDE DOPED WITH BISMUTH OXIDE

- É.G.Pettsol'd

Losev[1] in his work discovered that there appears a glow at the point of contact of a metal with a semiconductor incident to flow of current. Subsequently, a number of investigators succeeded in observing the Losev effect in single crystals of zinc sulfide[2], cadmium sulfide[3,4], diamond[5], germanium[6] and other substances. There have apparently been no investigations of electroluminescence using sintered polycrystalline samples.

In principle, the Losev effect allows of obtaining a higher light yield as compared with the electroluminescence of substances suspended in a dielectric medium (Destriau effect[7]), which is important from the standpoint of practical utilization of this effect[8,9]. Hence investigation of the Losev effect is of interest not only from the scientific but also from the technological standpoint.

In the present work we investigated some of the electroluminescent properties of mixtures of zinc oxide, an n-type semiconductor, with bismuth oxide, a p-type semiconductor, incident to passage of a direct current through the sample. In the vicinity of the point electrodes there was observed either a yellow or a blue luminescence, depending on the conditions of heating of the samples and the bismuth oxide concentration.

Electric and electroluminescent properties of the samples

In preparing the samples, a mechanical mixture of zinc oxide and bismuth oxide (the amount of the latter was varied from 1 to 60% by weight) was compacted at a pressure of $5 \cdot 10^4$ kg/cm^2. It was found that the heating time and temperature, the rate of cooling and the impurity (i.e., Bi_2O_2) content all strongly affect the electric properties of the samples. Thus for example, sample No.102 had a conductivity of 10^{-8} mho/cm, while the conductivity of sample No.122 was of the order of 10^{-10} mho/cm. In general, samples with a higher conductivity are characterized by a more pronounced deviation from Ohm's law (curve 5 in Fig.1).

There can be no doubt that the electric properties of the samples determine their electroluminescent characteristics. Thus, samples with a high resistivity yielded a yellow emission, while samples with a low resistivity yielded a blue electroluminescence. The light emitted in the vicinity of both electrodes was picked up by an FEU-19 photomultiplier, the output of which was connected to a mirror galvanometer. The samples were mounted in a special holder which was then lowered into a suitable Dewar flask, so that measurements could be made at different temperatures. The sample temperature was measured by two copper-constantan thermocouples: one thermocouple was attached to one of the electrodes, the other was inserted into a recessed bored in the sample.

Fig.2 shows the variation of the electroluminescence intensity with the current passing through the sample. Reduction of the temperature to -100° leads to an even stronger dependence of the luminescence intensity on the current and also to a reduction of the initial current "igniting" the electroluminescence. In general, samples having a higher conductivity require a heavier "ignition" current (Fig.3).

The current-voltage characteristics (Fig.4) of the samples are definitely nonlinear. Reduction of the sample temperature to -100° leads to an insignificant alteration of the current-voltage characteristic (compare curves 3 & 4 in Fig.4).

It is interesting to note that the electroluminescence "ignition" current does not change with variation of the field strength over a wide range (Fig.5).

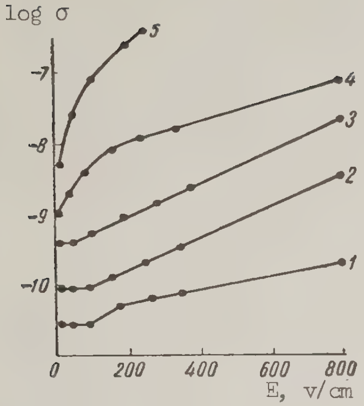

Fig. 1

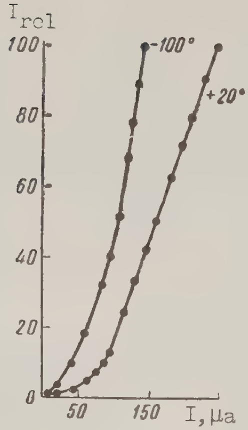

Fig. 2

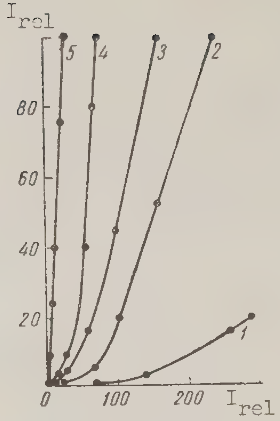

Fig. 3

Fig.1. Variation of the electric conductivity with the field strength: 1) 3% Bi_2O_3 (sample No.122), rapid cooling, $T = 900^{\circ}$; 2) 10% Bi_2O_3 (sample No.124), rapid cooling, $T = 900^{\circ}$; 3) 20% Bi_2O_3 (sample No.125), rapid cooling, $T = 900^{\circ}$; 4) 1% Bi_2O_3 (sample No.123), rapid cooling, $T = 900^{\circ}$; 5) 3% Bi_2O_3 (sample No. 102), slow cooling, $T = 1150^{\circ}$. (Heating time at indicated temperatures $t_h = 15$ min in all cases.)

Fig.2. Variation of the luminescence intensity with the current passing through the sample with 5% Bi_2O_3 (sample No.123), rapid cooling, $T = 900^{\circ}$, $t_h = 15$ min.

Fig.3. Variation of the luminescence intensity with the current passing through the sample: 1) sample No.102, 2) sample No.123, 3) sample No.124, 4) sample No.125, 5) sample No.122.

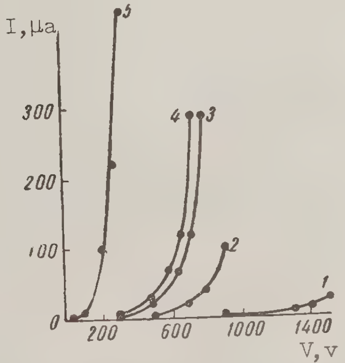

Fig. 4

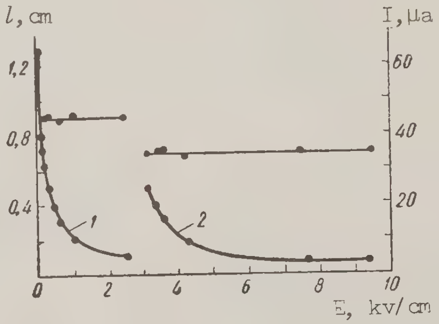

Fig. 5

Fig.4. Current-voltage characteristics of samples: 1) No.122, 2) No.124, 3) No. 123, $T = +20^{\circ}$; 4) No.123, $T = -100^{\circ}$, 5) No.102.

Fig.5. Variation of the field strength and current through the sample: 1) No.141, 30% Bi_2O_3, $T = 1100^{\circ}$, $t_h = 15$ min, rapid cooling, 2) No.124.

By means of a probe and a string galvanometer, we investigated the potential distribution over the surface of the samples. It will be evident from Fig.6 that the potential distribution is nonlinear; for some samples the depth of the "jump" attains several tenths of a millimeter. The distribution does become more uniform with increase of the applied voltage. The luminescence intensity distribution was determined by photometric scanning of photographs and was assumed to be

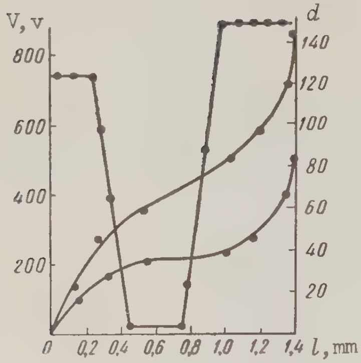

Fig.6. Distribution of the potential and electroluminescence intensity between electrodes (sample No.122).

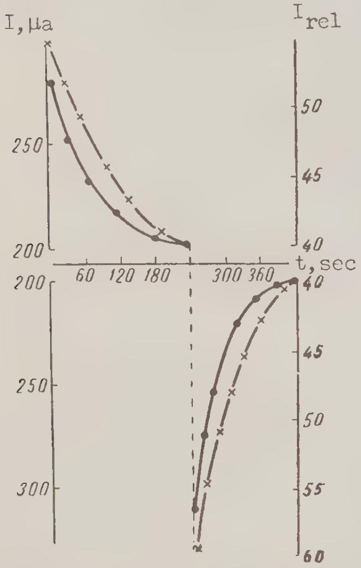

Fig.7. Variation of the current (●) and luminescence intensity (×) with time after application and reversal of the applied field (sample No.122).

proportional to the blackening. It will be apparent from Fig.6 that the electroluminescence is most intense at the point with the steepest field gradient.

If the field is reversed, both the current and luminescence intensity increase sharply at first and then fall off to the original value (Fig.7); the process is rather slow: some 2-3 min are required to attain equilibrium.

Discussion

A number of authors[10-14] consider that for electroluminescence to appear there must be an appreciable field concentration in a small volume of the sample and there must be present a source of carriers. It is assumed that a high field intensity of the order of 10^5 v/cm forms in a p-n junction having dimensions of the order of 10^{-5}-10^{-6} cm. One cannot, however, explain the experimental data set forth above solely by the effect of a p-n junction: first, because emission and potential discontinuities are observed at both electrodes, and, second, because the potential discontinuities extend to a depth of several tenths of a millimeter.

It has been repeatedly suggested in the work of Kosman and his collaborators[15-20] that the passage of an electric current through a dielectric or semiconductor is always accompanied by the build-up of space charge. The appearance of space charges in the vicinity of the electrode and extending to an appreciable depth[21,22] leads to a number of secondary effects.

Smith[23,24], Rose[25], Dacey[26], and Shockley & Prim (Ref.27) have also considered the influence of space charge on different properties of semiconductors.

The experimental facts described above are undoubtedly associated with space charges which, producing an appreciable alteration in the regions neighboring on the electrodes, give rise to the electroluminescence.

References

1. O.V.Losev, Telegrafiya i telefoniya bez provodov (Wireless telegraphy and telephony), No.18, 45 (1923); No.26, 403 (1924); No.5, (44), 485 (1927).
2. W.W.Piper & F.E.Williams, Phys.Rev., 87, 151 (1952).
3. K.M.Böer & H.Kümmel, Z.phys.Chem. (DDR), 200, 190 (1952).
4. P.W.Smith, Phys.Rev., 93, 347 (1954).
5. W.A.Thornton, J.Appl.Phys., 28, 313 (1957).
6. I.R.Haynes, Phys.Rev., 98, 1866 (1955).
7. G.Destriau, J.chim.phys., 33, 620 (1936).
8. R.E.Halsted & L.R.Koller, Proc.IRE, 43, 1911 (1955).
9. L.R.Koller, U.S.Patent, 2, 765 (5/81/55).

10. W.W.Piper & F.E.Williams, Phys.Rev., 98, 1809 (1955).
11. R.W.Smith, Phys.Rev., 105, 900 (1957).
12. A.K.Fischer, Z.Naturforsch., 8-a, 756 (1953).
13. D.Curie, J.Phys.Radium, 14, 672 (1953).
14. W.W.Piper & F.E.Williams, Brit.J.Appl.Phys.Supplement No.4, 39 (1955);
15. M.S.Kosman & V.F.Pisarenko, Proceedings of the (First) Conference on the Physics of Dielectrics), Dnepropetrovsk, 1956.
16. M.S.Kosman & V.S.Novosel'tsev, Uchenye zapiskii (Scientific notes), Leningrad State Pedagogical Institute, 148, 51 (1958).
17. M.S.Kosman & B.A.Tazenkov, Ibid., 148, 191 (1958).
18. M.S.Kosman & O.I.Kolesova, Ibid., 148, 227 (1958).
19. M.S.Kosman & I.V.Fedorov, Ibid., 148, 91 (1958).
20. M.S.Kosman & I.B.Stuken, Ibid., 148, 237 (1958).
21. M.V.Karev, Zhur.eksp.i teor.fiz., 7, 1018 (1937).
22. M.V.Karev, Ibid., 7, 1185 (1937).
23. R.W.Smith, Phys.Rev., 97, 1525 (1955).
24. R.W.Smith & A.Rose, Phys.Rev., 97, 1531 (1955).
25. A.Rose, Phys.Rev., 97, 1538 (1955).
26. G.C.Dacey, Phys.Rev., 90, 759 (1953).
27. W.Shockley & R.C.Prim, Phys.Rev., 90, 753 (1953).

DISCUSSION

G.I.Skanavi: Two years ago L.A.Tumerman and his co-workers in the Luminescence Laboratory of the Physical Institute (Academy of Sciences) observed luminescence in inhomogeneous media consisting of a powder and an organic binder. The color of this emission varied, depending on the type of material. The spectrum of the emission comprised a number of bands. Tumerman at first thought that this was a distinctive type of electroluminescence. Subsequently, it was found, however, that the radiation was emitted by vapors of different density held in the pores of the composite material. In the work of Pettsol'd there were obtained approximately the same results for ceramic samples of the zinc oxide-bismuth oxide system; these also probably had pores. I wonder whether one cannot attribute the observed emission in strong fields simply to some secondary effects, for example, ionization and excitation of gases occluded in pores or adsorbed on the surface.

E.G.Pettsol'd: No emission was observed in the case of sintered zinc oxide free of bismuth oxide. Although we did not specifically investigate the distribution of pores, it is hard to imagine that a small admixture of bismuth oxide would greatly increase the porosity or modify the pore distribution. Moreover, it must be noted that the luminescence remained unchanged even after outgassing of the samples in a vacuum of about 10^{-5} mm Hg. In fact, the same luminescence is observed in vacuum as at atmospheric pressure. The luminescence appears on the surface of the samples and its spectrum differs from the spectrum of a corona discharge. Our luminescence has a yellow color. The material of the electrode does not seem to matter; the electrodes were made in the form of points. We established that the luminescence depends on the impurity concentration and the heating conditions. The luminescence was observed not only in air and in vacuum but also in castor oil, benzene and liquid air. In all cases the emission spectrum was the same. An emission is also observed in the case of sintered zinc oxide doped with Cu_2O, but in this case the luminescence spectrum differs from that of zinc oxide with an admixture of bismuth oxide.

G.I.Skanavi: It is apparent from the answer given by E.G.Pettsol'd that the observed emission is not from occluded gases or vapors; the effect is definitely interesting.

We are omitting here a discussion pertaining to a two-part report by V. A. Chuenkov on the "Theory of Electric Breakdown in Semiconductors" which is published not in the Bulletin, but in Fizika tverdogo tela,No. 10, 1959 (Translation, Soviet Physics - Solid State). Without the report, the discussion is difficult to follow and presents little interest.

Translation editor

Bulletin of the Academy of Sciences of the USSR - Physical Series
Vol.24, No.1 - January 1960
Transactions of the Second All-Union Conference on the Physics of Dielectrics

TABLE OF CONTENTS

	Page Orig.	Page Trans.
Gregorii Ivanovich Skanavi (1910-1959)	2	2
Dielectric relaxation in liquid alcohols, alkyl halides and solutions - Robert H.Cole	4	3
On the dielectric dispersion of some aliphatic alcohols - M.Magat & C.Brot	10	9
Dielectric constant of dielectric liquids in strong electric fields - A.Piekara	19	17
Dielectric relaxation and molecular size and shape - C.P.Smyth	25	24
Field and current density distribution inhomogeneities in CdS single crystals - K.W.Böer	36	35
Some theoretical considerations concerning inhomogeneous field distribution in electric breakdown - K.W.Böer	43	41
Influence of field emission on the distribution of strong fields in solids - É.I.Adirovich	49	47
Currents in alkali-halide crystals due to electron emission from the cathode in strong electric fields - E.A.Konorova	58	56
Temperature and voltage dependences of the current in KBr single crystals in prebreakdown fields - E.A.Afanas'eva, V.S.Vinogradov & E.A.Konorova	66	63
Regularities of pulse breakdown of solid dielectrics - A.A. Vorob'ev & G.A.Vorob'ev	75	75
Breakdown voltage of thick insulating layers in a nonuniform field - F.Obenaus	84	84
Characteristics of the motion of fast current carriers in polar crystals - Yu.I.Gorkun & K.B.Tolpygo	94	91
New form of polar crystal model - A.E.Glauberman	101	97
Some electroluminescent properties of zinc oxide doped with bismuth oxide - É.G.Pettsol'd	104	100

To be continued in Vol.24, No.2

Translated in 1961 by
Columbia Technical Translations
5 Vermont Ave., White Plains, N.Y.

Transactions
# of the
Second All-Union Conference on the Physics of Dielectrics

(Moscow, 20-27 November 1958)

(Continued from Vol. 24, No. 1)

INVESTIGATION OF RELAXATION POLARIZATION AND THE PHASE COMPOSITION OF DIELECTRICS IN THE SYSTEM $SrTiO_3$—$Bi_2O_3 \cdot nTiO_2$ (n = 2,3)

- A.M.Kashtanova, N.N.Kurtseva & G.I.Skanavi

It was shown in earlier studies[1,2] that in polycrystalline dielectrics comprised in the system $SrTiO_3$—$Bi_2O_3 \cdot nTiO_2$ (n = 2,3) there occurs in a wide range of component concentrations relaxation polarization leading to a very high permittivity ϵ' without, however, the appearance of ferroelectric properties.

The present work was devoted to further investigation of the dielectric properties of $SrTiO_3$—$Bi_2O_3 \cdot 2TiO_2$ and $SrTiO_3$—$Bi_2O_3 \cdot 3TiO_2$ ceramics in correlation with the data of petrographic, chemical and x-ray diffraction analyses. This comprehensive investigation of the properties of the dielectrics enabled us to answer some of the questions raised in Ref.2.

It was noted in Ref.2 that dielectrics with a relatively low bismuth titanate concentration exhibit an anomalously high dielectric constant and a rather elevated value of the dielectric loss tangent. It was also noted that many of the ceramic samples were dark and were characterized by enhanced and field-dependent conductivity.

It was hypothesized that in sintering ceramic dielectrics of this type under conditions of high temperature (1400-1600°) and deficiency of oxygen there occurs dissociation of the TiO_2 or Bi_2O_3 with evolution of oxygen, as a result of which there are formed phases with different conductivities. Thus in these ceramic dielectrics, aside from relaxation polarization due to defect structure (strontium site vacancies), there may also obtain relaxation of the Maxwell type. This hypothesis was substantiated in the present work by the results of sintering the ceramic materials in an atmosphere of hydrogen and the results of heating the specimens. The ceramic specimens sintered in hydrogen were almost black.

In order to restore the oxygen lost owing to dissociation of the oxides we had recourse to heat treatment consisting of prolonged holding at a relatively high temperature in an atmosphere of oxygen or air. Restoration of the oxygen content in the ceramic materials and, consequently, liquidation of the heterogeneity of the microstructure was accompanied, as was to be expected, by reduction of the loss tangent, the dielectric constant and the conductivity, and also by bleaching of the specimens. An indication of the virtually complete restoration of the dissociated oxides was attainment of constant values of ϵ' and tan δ in the process of heat treatment.

We investigated some 10-12 ceramic specimens of the $SrTiO_3$—$Bi_2O_3 \cdot nTiO_2$ (n = = 2 and 3) system with different component concentrations. Sintering was realized without using flux. The well sintered specimens were subjected to prolonged heating in an atmosphere of air. The heating time and temperature were chosen depending on the composition of the samples and varied accordingly from 10 to 14 days and from 1050 to 1200°. In contrast to the results of annealing materials with a low bismuth titanate concentration, annealing of materials with a high bismuth titanate content leads only to a negligible decrease of ϵ' and tan δ and has almost no effect on the color of the ceramics.

Investigation of the phase composition

The ceramic samples obtained as a result of sintering were light yellow disks about 13 mm in diameter and 3-4 mm thick; they were subjected to chemical analysis and x-ray diffraction and microscopic examination. The specified batch proportions, the results of chemical analyses and the calculated proportions of the assumed components are listed in Tables 1 and 2.

Table 1

Composition and calculated percentages of the assumed components for the specimens of the $SrTiO_3$—$Bi_2O_3\cdot 3TiO_2$ system (percent by weight)

Ceramic No.	Basis batch proportions			Basis chemical analysis				Basis polarographic method		Calculated assumed components, molc %	
	Bi_2O_3	TiO_2	SrO	Bi_2O_3	TiO_2	SrO	sum	Bi_2O_3	TiO_2	$SrTiO_3$	$Bi_2O_3.3TiO_2$
1	—	43,70	56,30	1,90	42,20	55,60	99,70	—	—	100,0	0,0
2	8,08	42,42	49,50	7,89	42,35	49,75	99,99	7,84	42,70	96,5	3,5
3	10,97	42,03	47,00	10,36	42,00	46,90	99,26	10,50	41,28	95,1	4,9
4	13,70	41,60	44,70	13,25	42,35	44,40	100,00	13,50	42,60	93,6	6,4
5	19,10	40,80	40,10	18,48	40,77	40,75	100,00	—	—	90,4	9,6
6	20,80	40,60	38,60	20,35	40,50	38,70	99,55	—	—	89,3	10,7
7	32,00	38,90	29,10	31,75	39,00	29,25	100,00	—	—	80,3	19,7
8	38,45	37,93	23,52	37,96	38,36	23,68	100,00	—	—	73,3	26,7
9	61,55	34,50	4,05	Not determined						23,4	76,6
10	66	34	—							0,0	100,0

Table 2

Composition and calculated percentages of the assumed components for the specimens of the $SrTiO_3$—$Bi_2O_3\cdot 2TiO_2$ system (percent by weight)

Ceramic No.	Basis batch proportions			Basis chemical analysis				Basis polarographic method		Calculated assumed components, molc, %	
	Bi_2O_3	TiO_2	SrO	Bi_2O_3	TiO_2	SrO	sum	Bi_2O_3	TiO_2	$SrTiO_3$	$Bi_2O_3.3TiO_2$
1	—	43,70	56,30	1,90	42,20	55,60	99,70	—	—	100,0	0,0
14	8,02	41,70	50,28	6,66	42,00	50,60	99,26	6,58	42,10	96,5	3,5
15	11,70	40,65	47,65	7,50	43,00	47,60	98,20	—	—	95,1	4,9
16	14,18	40,15	45,67	11,00	40,65	48,00	99,65	—	—	93,6	6,4
17	19,80	38,60	41,60	18,12	38,60	44,72	101,44	18,11	38,62	90,4	9,6
18	33,80	35,20	31,0	29,00	39,00	32,10	100,10	29,00	39,00	80,3	19,7
19	41,33	33,46	25,21	37,95	35,33	27,20	100,48	—	—	73,3	26,7
20	55,5	29,95	14,55	54,00	30,50	14,60	99,10	—	—	54,0	46,0
21	68,54	26,82	4,64	67,40	27,20	4,50	99,10	—	—	23,4	76,6
22	74,50	25,50	—	73,50	25,80	—	99,30	—	—	0,0	100,0

The chemical analyses were performed in the IGEM by I.D.Borneman and O.A. Alekseeva*. Check polarographic determinations of Bi_2O_3 and TiO_2 were performed by N.M.Dyatlova* in the Institute of Pure Reagents.

It will be evident from Table 1 that in the case of the $SrTiO_3$—$Bi_2O_3\cdot 2TiO_2$ system (Table 2) the Bi_2O_3 content according to chemical analyses is appreciably lower than the content of the oxide in the initial batch. This is due to the observed effluence of the Bi_2O_3 during sintering. Nevertheless, the assumed component percentages were calculated on the basis of the batch composition.

Analysis revealed 1.90% Bi_2O_3 in material No.1, the initial batch for which consisted of pure strontium titanate. Unfortunately, the Bi_2O_3 entered this material owing to contamination of the Silit resistor furnace.

The investigated dielectrics, despite the prolonged annealing, proved to be fine-grained. The grain size varied within the range of a few microns and only individual crystals attained a diameter of 50-70 μ. The small size of the grains, the close values of the reflectivity of the phases involved and the high value of the index of refraction hampered microscopic analysis.

For purposes of phase diagnosis we used high refractive alloys of sulfur with selenium (over 70% Se). These mixtures according to the data of Larsen &

We take this opportunity to thank I.D.Borneman, O.A.Alekseeva and N.M. Dyatlova for the analyses.

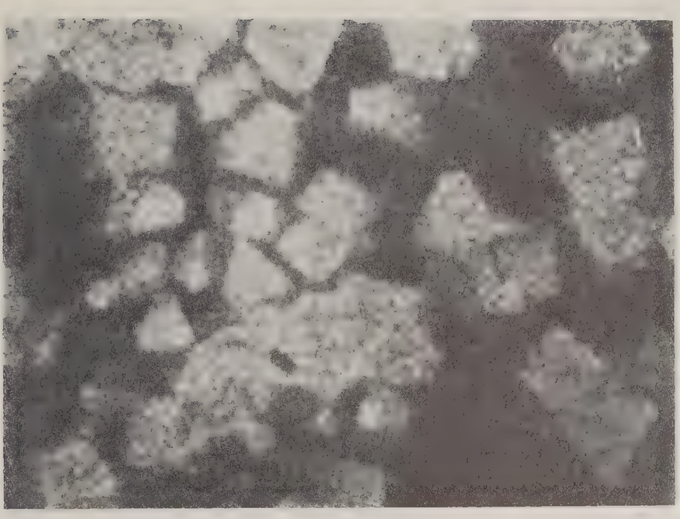

Fig.1. Ceramic material No.1. Inhomogeneous structure of strontium titanate. Magnification 150 X; without analyzer.

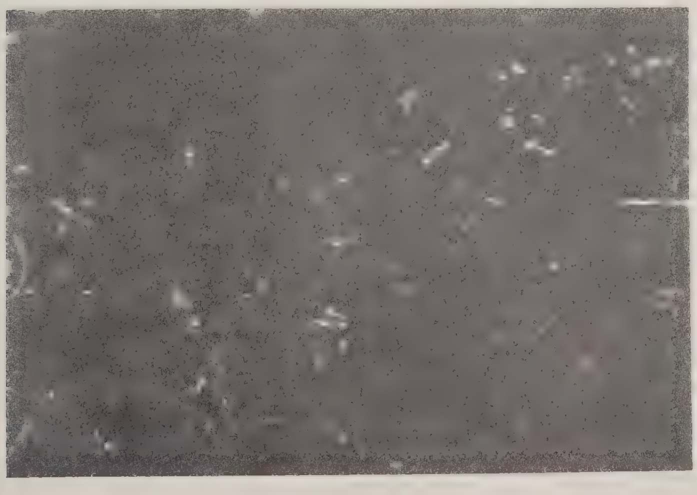

Fig.2. Ceramic material No.2. Incipient bismuth titanate. Magnification 290 X; with analyzer.

Berman[3] transmit mainly lithium light; measurements of the index of refraction performed in such mixtures in white light yield practically the same results as with lithium light. Hence in the present study we used white light in determining the constants of all the phases.

The ceramic material, the initial batch for which was designed to yield pure strontium titanate, had a monomineral phase composition. No glass in it was detected. The colorless isotropic grains of strontium titanate form an inhomogeneous structure, as may be seen in the micrograph of Fig.1.

According to the data of Levin, Field & Plock[5], strontium titanate single crystals are colorless, cubic and have $a =$ $= 3.904$ Å; the index of refraction lies in the range from 2.3756 to 2.3804. Our strontium titanate ($a = 3.900$ A and $n =$ $= 2.39$) had a somewhat higher index of refraction owing to incorporation of a minor amount of bismuth into its lattice (1.90% Bi_2O_3, see Tables 1 & 2). No discrete segregations of the bismuth phase were detected.

In ceramics Nos.2,3 and 4, despite the increase of Bi_2O_3 content (7.89, 10.36 and 13.25% by analysis, respectively), there is apparent only one phase consisting of a solid solution of strontium and bismuth titanates. The index of refraction increases to 2.42. The inference that only one phase is present in these ceramics is substantiated by the x-ray diffraction data.

A new phase appears in ceramic No.5, in which the $Bi_2O_3 \cdot 3TiO_2$ content is 9.6 mole percent; the amount of new phase is, however, minor. This phase is colorless and anisotropic; the refraction indices are $n_g = 2.50$ and $n_p = 2.40$ (Fig.2). This phase is still not evinced in the x-ray diffraction patterns. The principal component of material No.5 is a solid solution of strontium and bismuth titanates with $n = 2.42$.

In ceramic No.6 (10.7 mole percent $Bi_2O_3 \cdot 3TiO_2$) the amount of the new anisotropic phase increases sharply, although it is still not evinced in the x-ray patterns. The presence of the new phase becomes apparent in x-ray patterns only in ceramic No.7, containing 19.7 mole percent $Bi_2O_3 \cdot 3TiO_2$.

Inasmuch as ceramic No.8 (26.7 mole percent $Bi_2O_3 \cdot 3TiO_2$) consists entirely of this new phase and comprises no cubic solid solutions of strontium and bismuth titanates with $n = 2.42$, it may be inferred that the new anisotropic phase is a complex titanate of both bismuth and strontium.

Microscopic examination of ceramic No.9 (76.6 mole percent $Bi_2O_3 \cdot sTiO_2$) clearly shows the presence of two anisotropic phases with close values of the index of refraction (we were unable to determine the index of refraction separately for each phase). The appearance of these new phases is substantiated by the x-ray diffraction patterns.

Ceramic No.10, which according to the batch proportions should have consisted of 100% $Bi_2O_3 \cdot 3TiO_2$, proved to be inhomogeneous: it consisted of a highly refractive ($n_g = 2.64$ and $n_p = 2.56$), colorless anisotropic phase and a small amount of glass with a lower index of refraction. The presence of the glass does not allow of judging of the precise composition of the material, but it may safely be asserted that this phase is bismuth titanate, inasmuch as according to the x-ray and microscopic data, neither rutile nor Bi_2O_3 were present in the samples.

Optical investigation of the $SrTiO_3$—$Bi_2O_3 \cdot 2TiO_2$ system also showed the existence of cubic solid solutions of bismuth titanate and strontium titanate up to 9.6 mole percent $Bi_2O_3 \cdot 2TiO_2$ with increase of the index of refraction to 2.42 (see Table 2).

With increase of the Bi_2O_3 content there also appears in this system a new anisotropic phase, the amount of which increases with increase of Bi_2O_3. The refractive indices of this phase are $n_g = 2.56$ and $n_p = 2.50$. As regards x-ray diffraction, this phase is also different from the anisotropic phase forming in the $SrTiO_3$—$Bi_2O_3 \cdot 3TiO_2$ system.

Thus x-ray diffraction and microscopic investigation of the polycrystalline strontium-bismuth titanates shows the presence of cubic solid solutions of bismuth titanate ($Bi_2O_3 \cdot 3TiO_2$ or $Bi_2O_3 \cdot 2TiO_2$) in strontium titanate up to about 10 mole percent of each titanate, with increase of the index of refraction from 2.39 for $SrTiO_3$ to 2.42 for the limit solid solution.

With increase of the bismuth content a new phase appears in both systems; this phase appears to be a complex bismuth titanate with strontium ions incorporated into its lattice.

K.V.Filippova in our laboratory obtained Debye powder patterns of the strontium-bismuth titanate (in the region of solid cubic solutions of the titanate) in the temperature range from +20 to -120°. The invariance of the diffraction lines indicates that no phase transitions occur in the indicated temperature range; there is observed only a gradual change of the lattice parameter according to the law $a = a_0(1 + \alpha \Delta t)$, where $\alpha \approx 5 \cdot 10^{-6}$ degree^{-1}.

Dielectric properties

All the electric measurements were carried out in vacuum in a rather wide range of temperatures and frequencies.

Fig.3 shows the ϵ' and $\tan \delta$ vs barium titanate concentration curves for the ceramics in the $SrTiO_3$—$Bi_2O_3 \cdot 3TiO_2$ system. It will be evident from the figure that in the region of formation of strontium titanate-bismuth titanate solid solutions there is a sharp increase in ϵ' with increase of the $Bi_2O_3 \cdot 3TiO_2$ concentration. The pronounced peak in the ϵ' curve corresponds to the solid solution with the maximum barium titanate concentration (9.6 mole percent).

The formation in the given ceramics of a second phase (complex bismuth titanate with the strontium ions incorporated in its lattice) and the increase in the amount of this phase at the expense of decrease in the amount of strontium titanate

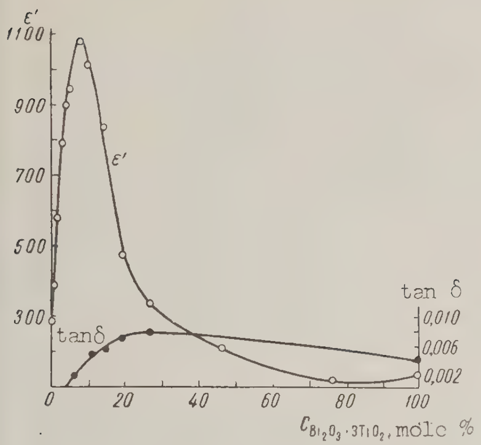

Fig.3. Concentration dependences of ϵ' and tan δ for the $SrTiO_3$—$Bi_2O_3 \cdot 3TiO_2$ system. ƒ = 1.1 Mc; t = 20° (measurements in vacuum).

bismuth titanate solid solution leads to a sharp decrease of ϵ'. It is significant that with increase of the bismuth titanate concentration there is evident an increase not only of the dielectric content of the material but also of the index of refraction of the solid solution (see above). This indicates that the bismuth ions actually do enter into the structure of the strontium titanate lattice. This is substantiated by the good agreement of the number of atoms per unit cell calculated from x-ray diffraction data and the density and the number of atoms determined from the equation for the solid solution formation reaction (Table 3). From the data of Table 3 it also follows that the number of atoms in a unit cell of the solid solutions decreases with increase of the bismuth titanate concentration, which indicates the formation of an omission solid solution of the second type. The marked reduction in the number of atoms per unit cell as compared with the number following from the reaction equation, noted in the work of Ref.2, is apparently connected with the presence in the investigated samples of a second phase, in addition to the main strontium titanate-bismuth titanate solid solution.

Table 3

Region of $SrTiO_3$—$Bi_2O_3 \cdot 3TiO_2$ solid solutions

Ceramic No.	Density, g/cm^3	No. of ions/cm^3 (x 10^{-21})				No. of ions per unit cell calculated by the formula		$Bi_2O_3 \cdot 3TiO_2$
		Bi	Ti	Sr	O	$N=\frac{Vd*}{A \cdot 1.65 \cdot 10^{-24}}$	**	content, mole, %
2	5,26	1,10	16,8	15,2	50,5	4,96	4,988	3,5
3	5,33	1,51	16,8	14,7	50,4	4,95	4,986	4,3
4	5,36	1,90	16,8	14,0	50,5	4,94	4,979	6,4
5	5,47	2,40	16,8	12,8	50,5	4,91	4,968	9,6

---

* V is the volume of the unit cell, A is the weighted mean atomic weight calculated from the composition of the samples and d is the density.

** $x\,SrTiO_3 + (1-x)\,Bi_{2/3}TiO_3 \rightarrow [Sr_x \cdot Sr^*_{1/3(1-x)} \cdot Bi_{2/3(1-x)}] \cdot TiO_3$, where Sr^* stands for the vacant sites in the strontium part of the lattice.

The temperature dependences of ϵ' and tan δ for different materials of the $SrTiO_3$—$Bi_2O_3 \cdot 3TiO_2$ system are shown in Figs.4a and 5a. The plots substantiate the relaxational character of the polarization in solid solutions of strontium titanate and bismuth titanate (ceramics Nos.2,3,4 and 5). It will be evident from the figures that increase of the bismuth titanate concentration leads to increase of the temperature maxima of tan δ and ϵ'. In the case of formation of an appreciable concentration of the second phase (ceramics Nos.6 and 7) the dielectric constant and loss tangent decrease, while the relaxational character of the polarization persists; the temperatures of the tan δ and ϵ' peaks do not change despite the increase in bismuth titanate concentration. As was noted earlier[2], relaxational polarization is not observed for materials with a predominant content of bismuth titanate (ceramics Nos.9 and 10).

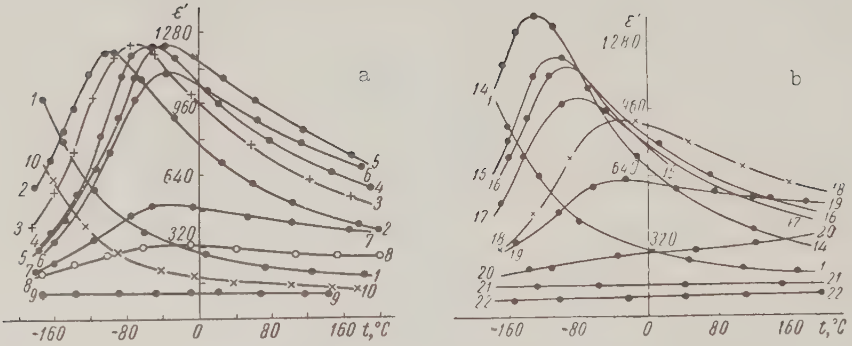

Fig.4. Variation of ε' with temperature for the systems $SrTiO_3$—$Bi_2O_3 \cdot 3TiO_2$ (a) and $SrTiO_3$—$Bi_2O_3 \cdot 2TiO_2$ (b) at f = 1.1 Mc. The figures at the curves identify the materials as listed in Tables 1 & 2.

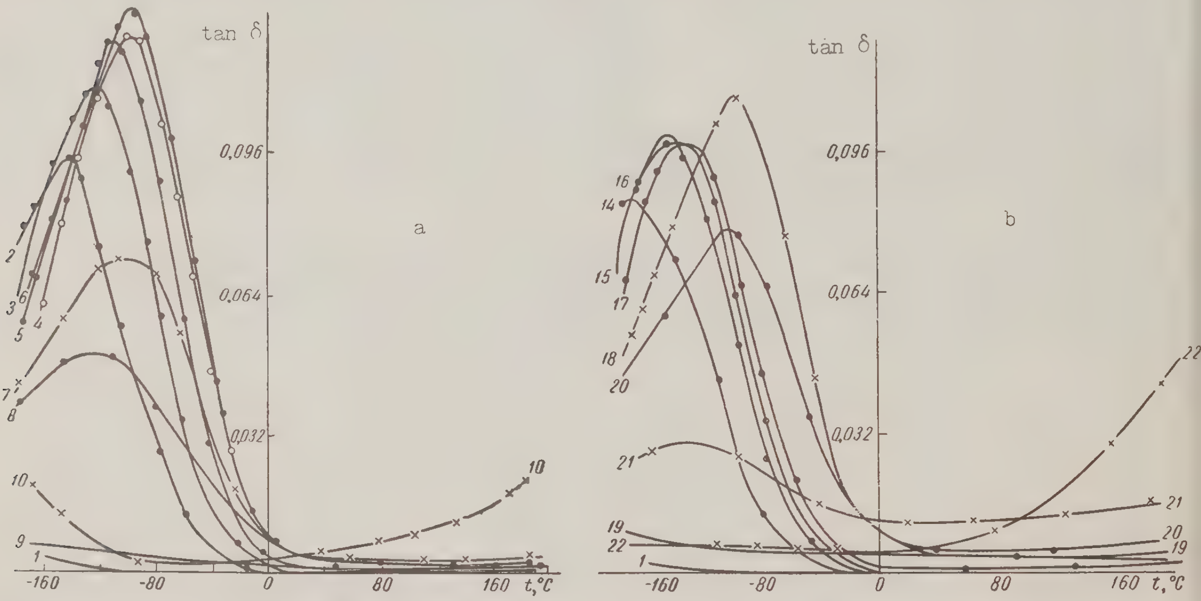

Fig.5. Variation of tan δ with temperature for the systems $SrTiO_3$—$Bi_2O_3 \cdot 3TiO_2$ (a) and $SrTiO_3$—$Bi_2O_3 \cdot 2TiO_2$ (b) at f = 1.1 Mc.

The polarization is relaxational in character also for most of the ceramics in the $SrTiO_3$—$Bi_2O_3 \cdot 2TiO_2$ system (see Figs.4b and 5b). The pronounced relaxational character of the polarization of solid solutions in this system is illustrated in Figs.6 & 7, which show the temperature dependences of ε', tan δ and ε" at different frequencies for ceramic No.5 (the solid solution with the maximum bismuth titanate concentration). It is significant that the ε' curves for different frequencies coincide in the range of higher temperatures.

From Fig.6 one can deduce the temperature dependence of the static dielectric constant (at high temperatures ϵ_s coincides with ε'); ϵ_{∞} can be obtained from the same plots by appropriate extrapolation into low temperatures.

Knowing the temperature dependence of ϵ_s we can make an approximate evaluation of the mean dipole moment $\overline{\mu_0}$ of the relaxing quasi-dipoles. According to

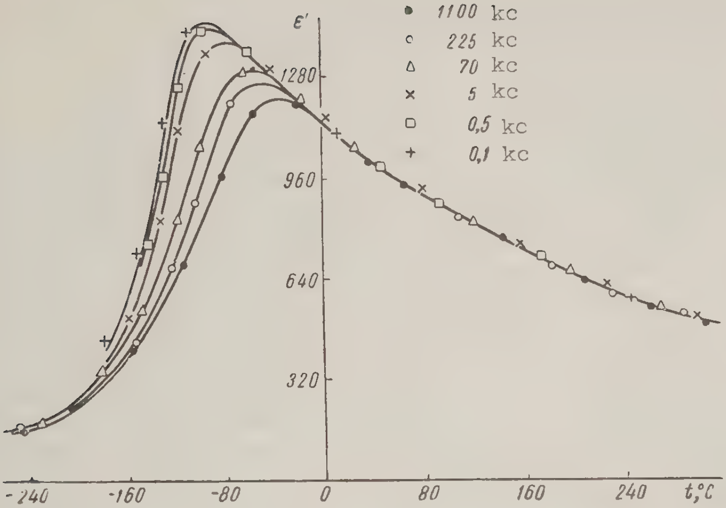

Fig.6. Temperature dependences of ε' for ceramic No.5 (molar composition 90.4% $SrTiO_3$ + 9.6% $Bi_2O_3 \cdot 3TiO_2$) at different frequencies.

the results of Refs.1 & 2, wherein the internal field coefficients were evaluated ($\beta_1 \approx 0$ and $\beta_2 = 4\pi/3$), there exists the following approximate relationship between the effective dipole moment and the static dielectric constant:

$$\frac{N\mu_0^2}{12kT} \approx \frac{4\pi(\varepsilon_s - \varepsilon_\infty)}{\beta_2\varepsilon_\infty} = \frac{3(\varepsilon_s - \varepsilon_\infty)}{\varepsilon_\infty},$$

where N is the concentration of quasi-dipoles, ϵ_∞ is the dielectric constant due to purely elastic polarization, and β_2 is the internal field coefficient associated with elastic polarization.

Fig.8 shows the variation of $\frac{4\pi(\varepsilon_s - \varepsilon_\infty)}{\beta_2\varepsilon_\infty}$ with 1/T for ceramic No.5 (β_2 is taken equal to $4\pi/3$.

We see that in the range of moderate temperatures this plot is nearly a straight line, from the slope of which one can determine the effective dipole moment: $\overline{\mu_0} \approx 20 \cdot 10^{-18}$ cgse units. In the range of higher temperatures the plot deviates from the straight line, which is presumably an indication of decrease in the number of quasi-dipoles. Calculations of $\overline{\mu_0}$ for solid solutions with a lower bismuth titanate content (ceramics Nos.2, 3 & 4) yields virtually the same value ($\sim 20 \cdot 10^{-18}$).

The appearance of the $\epsilon' = f(T)$, $\tan \delta = f(T)$ and $\epsilon'' = f(T)$ curves for the solid solution with the maximum bismuth titanate content at different frequencies is in qualitative agreement with the simplest Debye formulas containing one relaxation time. There are, however, substantial differences, namely, broadening of the experimental curve and decrease in the height of the tan δ and ε'' peaks, which indicate that there is actually a set of relaxation times in strontium titanate-bismuth titanate solid solutions.

The question of the distribution of relaxation times for solid solutions of strontium titanate and bismuth titanate and the question of the magnitude of the activation energy of relaxing ions and the temperature dependence of this activation energy will be discussed in future papers.

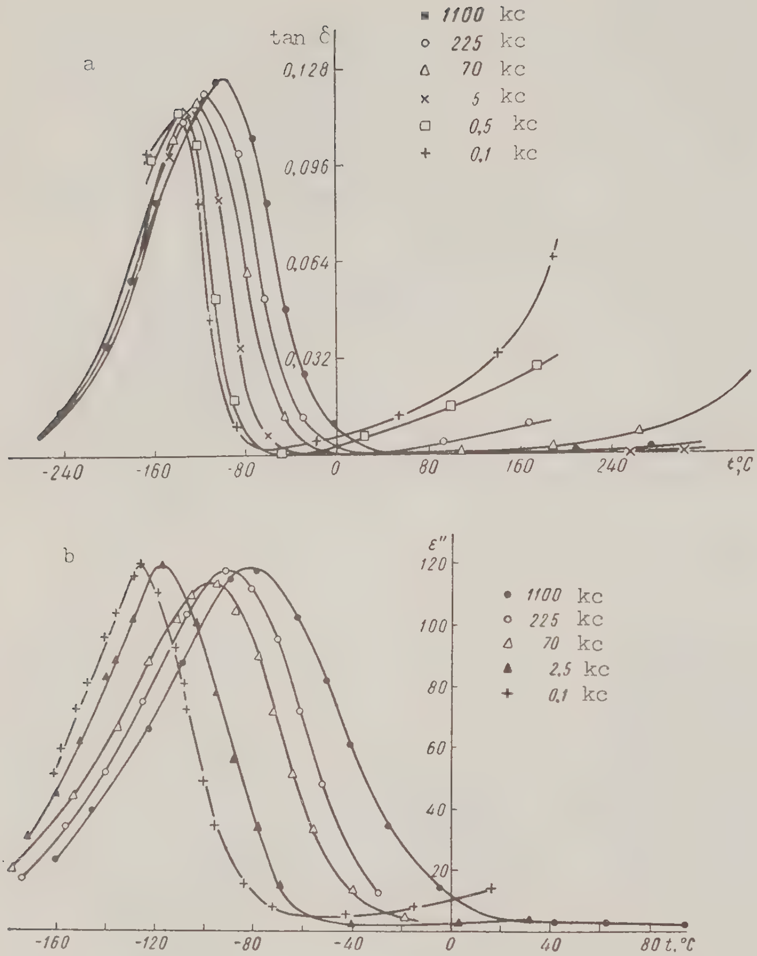

Fig.7. Temperature dependences of tan δ (a) and ε'' (b) for ceramic No.5 (90.4% $SrTiO_3$ + 9.6% $Bi_2O_3 \cdot 3TiO_2$) at different frequencies.

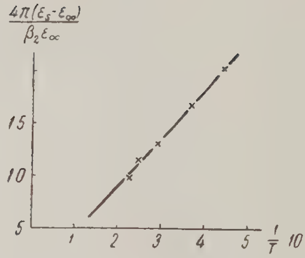

Fig.8. Variation of $\frac{4\pi(\varepsilon_s - \varepsilon_\infty)}{\beta_2\varepsilon_\infty}$ with $1/T \cdot 10^3$ for ceramic No.5.

References

1. G.I.Skanavi & E.N.Matveeva, Zhur.eksp.i teor.fiz., 30, 1047 (1956). (Trans.Soviet Physics - JETP).

2. G.I.Skanavi, Ya.M.Ksevdzov, V.A.Trigubenko & V.V.Prokhvatilov, Ibid., 33, 320 (1957).

3. E.Larsen & G.Berman, Identification of Transparent Minerals under the Microscope (Cited in Russian trans., 1937).

4. S.B.Levin, N.J.Field & F.M.Plock, J.Opt.Soc.Am., 45, 737 (1955).

5. P.Popper, S.N.Ruddlesden & T.A.Ingles, Trans.Brit.Ceram.Soc., 56, 356 (1957).

ON THE RELAXATION TIME AND DISTRIBUTION FUNCTION OF QUASIDIPOLES IN IONIC CRYSTALS WITH A DEFECT STRUCTURE

- G. I. Skanavi

It has been established in a number of studies that the presence of defects in a crystal lattice is often connected with enhancement of the dielectric loss and sometimes also with an exceedingly high dielectric constant. In such cases the dielectric polarization has a relaxational character. Relaxation dielectric losses are observed even in such relatively simple ionic crystals as the alkali halides.[1,2] In the presence of a large number of defects in perovskite type crystals relaxation polarization is clearly evinced and leads to very high values of the dielectric constant and to increased dielectric loss in the given frequency and temperature range.[3,5]

We, as well as other authors, up to the present, have used the simple Debye formulas in interpreting the experimental data, without taking into account the quasidipole distribution function, and we also attempted to find the distribution function from the experimental data.[3] We took into account the dipole interactions by means of the internal (local) field,[3,4] determining the generalized structural coefficients of the internal field on the basis of experimental data. However, this method of interpreting the experimental results is not satisfactory from the quantitative standpoint. The main difficulty is that evaluation of the relaxation time from the experimental data gives results which do not agree quantitatively with the formula

$$\theta = \frac{1}{2\nu} e^{\frac{U}{kT}}, \tag{1}$$

where U is the activation energy of a quasidipole, ν is the frequency of its natural oscillations at its fixed position, kT is the energy of thermal motion according to Boltzmann's statistics. In many cases we find that if we calculate θ from the condition of maximum dielectric loss

$$\omega\theta = 1 \tag{2}$$

(where ω is the angular frequency of the electric field), the activation energy U decreases greatly with increase in temperature. For example, upon increasing the temperature by 40-50°, U for strontium-bismuth titanates decreases by a factor of 2-3 (or the frequency ν has an absurdly high value).

It is obvious that such a great change in the activation energy with temperature cannot occur, particularly in solid dielectrics, where a temperature induced change in U can only be due to thermal expansion. (The temperature variation of the dipole activation energy in liquids can apparently be larger; see, for example, Ref.6). In the weak field region, taking into account the difference between the local field and the average field[3,4] leads only to the following modification of Eq.(1):

$$\theta = \frac{M}{2\nu} e^{\frac{U}{kT}}, \tag{1a}$$

where $M = \frac{4\pi + \beta_1(\varepsilon_s - 1)}{4\pi + \beta_1(\varepsilon_\infty - 1)}$; ε_s and ε_∞ are the static and high-frequency dielectric constants, β_1 is a coefficient which determines the contribution of the relaxation polarization to the local field. In all probability, β_1 lies between zero and $4\pi/3$, and, consequently, $1 < M \leqslant \frac{\varepsilon_s + 2}{\varepsilon_\infty + 2}$. Thus, when we allow for the difference between the local field and the average field, the conditions (2) for maximum loss should take the following form

$$\omega\theta = \frac{1}{M} < 1. \tag{2a}$$

Consequently, when $M > 1$, the magnitude of the activation energy calculated from the experimental values of ω and T, which correspond to the maximum loss, should decrease with rising temperature even more abruptly than in the $M=1$ case. Actually, by taking the logarithm of (2a), taking (1) into account, we obtain

$$U_{M>1} = kT(\ln 2\nu - \ln \omega) - kT\ln M = U_{M=1} - kT\ln M. \tag{3}$$

True, the coefficient M, generally speaking, decreases with temperature as a result of the decrease of ε_s. However, the coefficient M should be very large in order to compensate for the decrease of $U_{M=1}$ with temperature and in every case should decrease considerably more rapidly than the factor $e^{1/T}$. Neither of these conditions is realized in experiment. If we actually assume that β_1 has the maximum value of $4\pi/3$ in dielectrics with a very high dielectric constant, then $M \approx \frac{\varepsilon_s}{\varepsilon_\infty}$. Consequently, ε_s should exceed ε_∞ by approximately one order of magnitude and decrease considerably more sharply than in direct proportion to 1/T.* But the maximum of the ratio $\varepsilon_s/\varepsilon_\infty$ is 4-5 (for strontium-bismuth titanate), and, what is more important, ε_s does not decrease more rapidly with temperature than in proportion to 1/T. Thus, this manner of allowing for the dipole interaction in weak fields by means of the approximate internal field method does not provide a plausible explanation of the apparent decrease of the quasidipole activation energy with rising temperature nor does it explain the extraordinarily large values of ν, the natural quasidipole vibration frequency.

It is known that in the case of a strong field, when the field energy expended for the transition of a dipole (or weakly bound ion) from one of the equilibrium positions to a neighboring position is comparable with the energy of thermal motion kT, the kinetic equation for polarization is nonlinear with respect to the field[7], and the relaxation time is a function of the field and, consequently, of the polarization. In addition, the dielectric constant also becomes a function of the field strength, because the polarization ceases to be linear. This, however, is not realized experimentally for many crystals with a defect structure; the dielectric constant of such crystals is independent of the field almost up to breakdown. Therefore nonlinearity of the kinetic equation, due to a comparatively strong average field or local field (which is proportional to the average field), cannot be invoked to explain the above mentioned facts. Such a possibility can arise in principle if one assumes that the internal field is not proportional to the average field. But in the absence of spontaneous polarization it is difficult to think of a plausible reason for such non-proportionality.

An important problem in the theory of polarization in weak alternating fields is the rigorous calculation of dipole-dipole interaction, based on statistical laws, particularly for appreciable dipole concentrations. This problem is complicated because in the presence of a substantial dipole concentration, the kinetic equation which characterizes the time dependence of the relaxation polarization should, in general, become nonlinear. If we assume that the potential barrier which separates two local minima of the dipole (or weakly bound ion) potential energy does not depend on the polarization, then the kinetic equation for weak fields remains linear. Therefore every calculation of a dipole-dipole interaction, which does not include the polarization dependence of the potential barrier, for the weak field case, should in principle give the same result as the internal field method, i.e., should give a pre-exponential factor in Eq.(1) for the relaxation time.

---

*This requirement stems from the fact that the activation energy U in Eq.(1) should be much larger than kT, and consequently the term $kT \ln M$ in (3) will have a substantial value only when $\ln M \gg 1$.

Therefore it is important to find out whether there can be a solution of the nonlinear kinetic equation for polarization in weak alternating fields, in which the polarization dependence of the potential barrier is taken into account, the macroscopic values of ε' and ε'' are virtually field independent, and the relaxation time is determined by a formula differing from (1). If such a solution exists, then the experimental data for the relaxation polarization in ionic lattices could in principle be susceptible of satisfactory quantitative interpretation. This would mean that the discrepancies between the experimental data and the simplest Debye formulas and also expression (1) for the relaxation time are due to neglect in these formulas of dipole-dipole interaction for which the potential barrier depends on the polarization. The solution of this problem, however, must be left for the future.

On the other hand, the Debye formulas for ε' and ε'', as is known, do not include the dipole distribution in relaxation times. Yet, experimental data on relaxation polarization in crystals with a defect structure indicate that the dipoles are characterized not by a single relaxation time, but by a set of relaxation times.[3-5] The only exceptions, apparently, are alkali halide crystals.[1-2] The dipole distribution function with respect to relaxation time for polar liquids has been determined from experimental data in many papers. Extensively employed is the Cole-Cole[8] procedure, according to which the distribution function is found by means of the $\varepsilon''=f(\varepsilon')$ plot, which is the arc of a circle. In most cases the distribution functions found from the experimental data for polar liquids have a symmetrical character and the relaxation times are clustered around the most probable value θ_0.

In this case the condition for the maximum of the loss factor ε'' is of the form

$$\omega\theta_0 = 1. \tag{4}$$

It is obvious that the replacement of condition (2) by condition (4) cannot change the result of calculations of the activation energy, and the previously indicated difficulties remain. A different situation develops when the dipole distribution function is asymmetrical. The experimental data for strontium-bismuth titanates show that this can occur.

Fig.1 gives the curve

$$\frac{\varepsilon''}{\varepsilon_s-\varepsilon_\infty} = f\left(\frac{\varepsilon'-\varepsilon_\infty}{\varepsilon_s-\varepsilon_\infty}\right)$$

for strontium-bismuth titanates plotted on the basis of the experimental data of Ref.5. The static and high frequency dielectric constants ε_s and ε_∞ were obtained by extrapolation of the experimental data.

The curve in Fig.1 is plotted using the experimental values of ε'' and ε' obtained at different frequencies and temperatures. Plotting the curve in terms of $\frac{\varepsilon''}{\varepsilon_s-\varepsilon_\infty}$ vs $\frac{\varepsilon'-\varepsilon_\infty}{\varepsilon_s-\varepsilon_\infty}$ instead of ε'' vs ε' allows of a wider utilization of the experimental data, because the temperature dependence of ε_s does not affect the behavior of this curve.

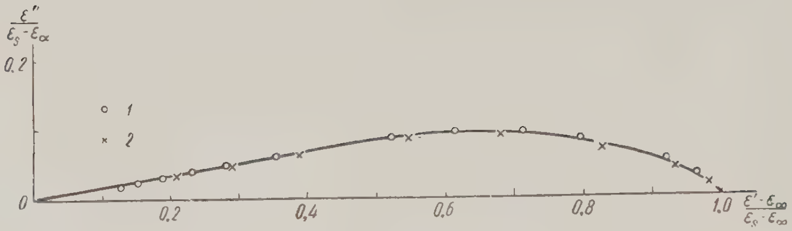

Fig.1. Variation of $\frac{\varepsilon''}{\varepsilon_s - \varepsilon_\infty}$ with $\frac{\varepsilon' - \varepsilon_\infty}{\varepsilon_s - \varepsilon_\infty}$: 1 - f = 1.1 Mc; 2 - f = 100 cps.

It is apparent from Fig.1 that the plot differs greatly from the arc of a circle, i.e., the distribution function is asymmetrical. It is easy to show that the quasidipole distribution function in ionic crystals with a defect structure can also be asymmetrical. Moreover, on the basis of simple physical considerations it is easy to obtain the form of this function and show that its asymmetry can be the reason for a great decrease in the effective activation energy with increasing temperature. It is necessary to keep in mind, however, that the considerations outlined below can be valid only in case of low quasidipole concentrations. If each defect (vacant site, interstitial ion or ionic group) creates a quasidipole, producing a corresponding distortion in the crystal lattice, then the number of such quasidipoles will be large. A defect in an ionic lattice bears a certain effective charge, the electric field of which acts not only on the nearest neighbors but also on more distant ions: the Coulomb field decreases comparatively slowly with distance. Therefore even unit cells relatively far from the defect can be distorted, although the degree of distortion will decrease with distance from the defect. The distortion may be such that some charges (ions) in the cell obtain a relatively large freedom of movement. For example, one of the ions may have several equilibrium positions, separated by a potential barrier.* The height of the potential barrier will determine the activation energy, and its width will determine the magnitude of the dipole moment of the quasidipole. It is obvious that under these conditions the activation energy U and the dipole moment μ of the quasidipoles should decrease with distance from the defect, but the number of quasidipoles with given values of U and μ should increase. As a result the distribution function becomes asymmetrical. On the basis of these assumptions, we can deduce the form of the distribution function.

It is necessary to note that usually the inverse problem is solved: by using the experimental data, one finds the form of the distribution function.[6,8,9] For ionic crystals of the type in question, and also several others, it is impossible to do this because the appropriate integrals are not taken. Besides, we feel it is of intrinsic interest to solve the problem of finding the distribution function on the basis of certain physical concepts, not particularly limited by the framework of any specific model. In order to solve this problem in our case, it is necessary to describe the height and width of the quasidipole potential barrier as a function of the distance from the defect. For example, let

---

*In the case of strontium-bismuth titanates, a vacant site in the strontium part of the lattice can cause a distortion of the oxygen octahedron surrounding the titanium ion, which therefore will have several equilibrium positions.

$$U = A_1 r^{-n_1}, \tag{5a}$$

$$\mu = qx = A_2 r^{-n_2}, \tag{5b}$$

where A_1, A_2, n_1 and n_2 are constants, q is the ion charge, and x is the width of the potential barrier. In addition, we specify that the height of the potential barrier U must lie within the limits $U_1 = A_1 r_1^{-n_1}$ to $U_2 = A_1 r_2^{-n_1}$, where r_1 is half the average distance between neighboring defects, and r_2 is the distance from a defect to the nearest quasidipole created by it.

If we assume that the distribution function is continuous, then the increment dN in number of quasidipoles corresponding to an increase dr of the distance from the defect will be given by

$$dN = Br^2 dr. \tag{6}$$

The relaxation time θ will be

$$\theta = \frac{M}{2\nu} e^{\frac{A_1 r^{-n_1}}{kT}} = \frac{1}{\nu'} e^{\frac{A_1 r^{-n_1}}{kT}}, \tag{7}$$

where M, as before, is a coefficient due to the difference between the actual (local) field and the average field. We will assume further that the difference $\varepsilon_s - \varepsilon_\infty$ is a function of $N\mu^2$. Then the distribution function $Y(\theta)$ satisfies the following equality:

$$Y(\theta)\,d\theta = \frac{\varepsilon_s - \varepsilon_\infty}{\int\limits_N d(N\mu^2)} d(N\mu^2). \tag{8}$$

Taking into account that

$$d(N\mu^2) = \mu^2 dN + 2\mu N d\mu,$$

and combining (5a), (5b), (6), (7) and (8), we obtain

$$Y(\theta) = \frac{(\varepsilon_s - \varepsilon_\infty) A_2^2 (kT)^{\frac{2n_2 - 3}{n_1}} (\ln\theta + \ln\nu')^{\frac{2n_2 - 3}{n_1} - 1} \left(\frac{2}{3} n_2 - 1\right)}{n_1 \theta \int\limits_N d(N\mu^2)} =$$

$$= \frac{(\varepsilon_s - \varepsilon_\infty) C (\ln\theta + \ln\nu')^{\frac{2n_2 - 3}{n_1} - 1}}{\theta} = A \frac{(\ln\theta + \ln\nu')^{n-1}}{\theta}, \tag{9}$$

where

$$A = (\varepsilon_s - \varepsilon_\infty) C \quad \text{and} \quad n = \frac{2n_2 - 3}{n_1}.$$

From the normalization condition $\int\limits_{\theta_1}^{\theta_2} Y(\theta)\,d\theta = \varepsilon_s - \varepsilon_\infty$ one can find the constant C, which turns out to be equal to

$$C = \frac{(2n_2 - 3)(kT)^{\frac{2n_2 - 3}{n_1}}}{n_1 \left(U_2^{\frac{2n_2 - 3}{n_1}} - U_1^{\frac{2n_2 - 3}{n_1}}\right)} = \left(\frac{kT}{U_2}\right)^n \frac{n}{1 - a^n}, \tag{10}$$

where $a = U_1/U_2$.

Knowing the distribution function, one can express ε' and ε'' for the case of sufficiently weak dipole interaction as

$$\varepsilon' - \varepsilon_\infty = \int\limits_{\theta_1}^{\theta_2} \frac{Y(\theta)\,d\theta}{1 + \omega^2\theta^2}; \tag{11a}$$

and

$$\varepsilon'' = \int_{\theta_1}^{\theta_2} \frac{\omega\theta Y(\theta)\, d\theta}{1+\omega^2\theta^2}. \qquad (11b)$$

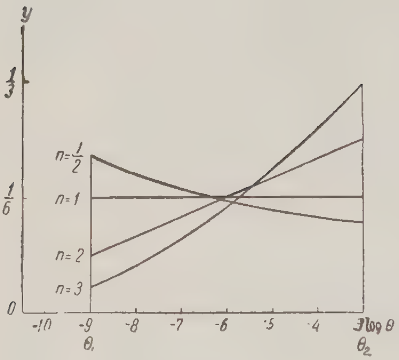

Fig.2. Variation of Y with ln θ for different n.
$\nu' = 10^{12}$; $U_2/kT = 9$; $U_1/kT = 3$.

Fig.2 gives qualitative plots of $Y(\theta)\cdot\theta = f(\theta)$ (which determines the dielectric loss) for different values of n. It can readily be shown that the experimental curve of Fig.1 corresponds to the curve of Fig.2 when $n>1$. The $n=1$ case corresponds to the one discussed by Fröhlich[10].

If we insert (9) into (11a) and (11b), we obtain integrals which can be evaluated only by numerical integration. However, even without integration, one can obtain the condition for the temperature maximum of ε'' at a given frequency, by differentiating (11b) with respect to temperature, taking into account the fact that θ_1, θ_2, ε_s and C are functions of the temperature. Simple transformations enable us to write out the above condition in the following form:

$$\frac{\omega\theta_2}{1+\omega^2\theta_2^2} - \frac{\omega\theta_1 a^n}{1+\omega^2\theta_1^2} = \frac{\varepsilon''_m(1-a^n)}{\varepsilon_s-\varepsilon_\infty}\left(1+\frac{T\frac{d\varepsilon_s}{dT}}{n\,(\varepsilon_s-\varepsilon_\infty)}\right) = C_1, \qquad (12)$$

where θ_1 and θ_2 are the limiting values of the relaxation times which correspond to the limiting values of the activation energy U_1 and U_2; $n = \frac{2n_2-3}{n_1}$, $a = \frac{U_1}{U_2}$; the derivative $\frac{d\varepsilon_s}{dT}$ can be determined from the experimental data, and ε''_m is the maximum value of ε'', known from the experimental data.

Thus the condition for maximum loss contains not only the most probable relaxation time θ_0, but the two limiting relaxation times θ_1 and θ_2. If the coefficients a and n are given, then from (12) one can find θ_1 and θ_2, and, consequently, U_1 and U_2 for a known value of the frequency $\nu' = 2\nu/M$ of the natural oscillations of the relaxing groups. One can assume that this frequency is close to 10^{12}-10^{13} sec^{-1}, although measurements in the far infrared region are necessary in order to evaluate this quantity.

The coefficient $n=\frac{2n_2-3}{n_1}>1$ can fluctuate within a comparatively narrow range, since n_1 and n_2 scarcely differ much from 1-3. The coefficient $a=\left(\frac{r_2}{r_1}\right)^{n_1}$ is a function of the dipole concentration N and the distance between the defect and the closest quasidipole created by this defect.

As was indicated earlier, in the particular case when $2n_2 = n_1+3$, the distribution function (9) is transformed into the hyperbolic function $Y(\theta) = A/\theta$, obtained by Fröhlich[10] for the distribution of the activation energy from U and $U+V$, under the assumption that the variation of the activation energy is directly proportional to the number of dipoles and that the moments of all the dipoles are identical. The use of this function gives the condition for maximum loss, which agrees with (4), if $\theta_0 = \sqrt{\theta_1\theta_2}$. Therefore, the hyperbolic function is not suitable for ionic crystals. Analysis of equation (12), obtained with the use of our distribution function (9), shows that the calculated values of U_1 and U_2 can be virtually independent of temperature for certain values of the parameters a and n, even in the case of a sharp temperature dependence of U determined from Eq.(1) using the experimental data.

This is easy to see for the following particular case. For a sufficiently wide interval $\theta_2 - \theta_1$, the temperature maximum of ε'' will occur where $\omega\theta_2 \gg 1$ and $\omega\theta_1 \ll 1$. Therefore in place of Eq.(12), we have approximately

$$\frac{1}{\omega\theta_2} - \omega\theta_1 a^n \approx C_1, \tag{12a}$$

or the frequency which corresponds to the maximum of ε'' equals

$$\omega \approx \frac{\sqrt{C_1^2 + 4a^n\theta_2/\theta_1} - C_1}{2a^n\theta_1}. \tag{13}$$

For a given value of $a = U_1/U_2$,

$$\theta_1 = \frac{1}{\nu'}\, e^{\frac{U_1}{kT}} = \frac{1}{\nu'}\, e^{\frac{aU_2}{kT}} = \theta_2\,(\nu'\theta_2)^{a-1},$$

or

$$\omega \approx \frac{\sqrt{C_1^2 + 4a^n\,(\nu'\theta_2)^{1-a}} - C_1}{2a^n\theta_2\,(\nu'\,\theta_2)^{a-1}} = \frac{D}{\theta_2}, \tag{14}$$

where

$$D = \frac{1}{2a^n\,(\nu'\theta_2)^{a-1}}\left[\sqrt{C_1^2 + 4a^n\,(\nu'\theta_2)^{1-a}} - C_1\right]$$

and the condition for the maximum of ε'' takes the form

$$\omega\theta_2 \approx D. \tag{15}$$

For certain values of a and n the magnitude of D is sufficiently large and increases with rising temperatures, but the limiting values of the activation energy $U_2 = kT(\ln\nu' + \ln D - \ln\omega)$ and $U_1 = a\,U_2$ prove to be virtually temperature independent.

Thus the asymmetry of the quasidipole distribution function in an ionic crystal with defects stems from specific physical concepts and makes it possible to explain quantitatively certain contradictions arising in attempts to interpret the experimental data concerning relaxation polarization in these crystals by means of the simple Debye formulas.

There remains, however, the main question concerning the effect of the quasidipole concentration. As previously noted, the above discussion was based on the assumption of a relatively low concentration of quasidipoles. As we know[3-5], however, the pronounced relaxational polarization of strontium-bismuth titanates is essentially polarization in a solid solution with a comparatively high concentration of bismuth titanate (up to 10 mole percent) and, consequently, in all probability, a high concentration of defects: vacancies in the strontium part of the lattice. Actually, there are several reasons for assuming that not all defects create quasidipoles. Fig.8 in Ref.5 gives a plot of $\frac{4\pi(\varepsilon_s - \varepsilon_\infty)}{\beta_2\varepsilon_\infty} = f(1/T)$. The slope of this plot should be proportional to the product of the quasidipole concentration N by the mean square of the dipole moment μ^2. In the high temperature region the plot deviates from a straight line. This can be understood if we assume that quasidipoles are produced only by associated defects, the number of which decreases with increasing temperature owing to dissociation. The concentration of associated defects, generally speaking, is considerably lower than the concentration of non-associated defects. Therefore, it is possible that the actual concentration of quasidipoles in strontium-bismuth titanates is not high.

In order to verify the quantitative results which have given us the asymmetrical distribution function, numerical integration of specific integrals in (11a) and (11b) was carried out on a "Ural" electronic computer. The values of the following integrals were found:

$$\frac{\varepsilon' - \varepsilon_\infty}{\varepsilon_s - \varepsilon_\infty} = \frac{n}{1 - a^n}\left(\frac{kT}{U_2}\right)^n \int_{\theta_1}^{\theta_2} \frac{(\ln\theta + \ln\nu')^{n-1}}{(1 + \omega^2\theta^2)\theta}\, d\theta$$

and

$$\frac{\varepsilon''}{\varepsilon_s - \varepsilon_\infty} = \frac{n\omega}{1 - a^n}\left(\frac{kT}{U_2}\right)^n \int_{\theta_1}^{\theta_2} \frac{(\ln\theta + \ln\nu')^{n-1}}{1 + \omega^2\theta^2}\, d\theta \qquad (16)$$

for different values of the parameters U_2, a and n over a wide temperature range (-200° to +300°) and the frequencies 1.1 Mc and 100 cps with $\nu' = 10^{12}$ and 10^{13}. The results of these calculations showed that it is impossible to choose a combination of the above listed parameters such that the calculated data would fit the experimental data simultaneously as regards the position of the temperature maxima of ε'' at different frequencies, the height of the maxima and width of the curves. The reason for this, apparently is the comparatively large dipole concentration in strontium-bismuth titanates and, consequently, the comparatively strong dipole-dipole interaction in these solid solutions.

For low quasidipole concentrations in ionic crystals with a defect structure this method of obtaining the distribution function is apparently practical.

I desire to thank A.M.Kashtanova, D.G.Sannikov and L.L.Sabsovich for assistance in processing the experimental data on the computer.

"P.N.Lebedev" Physical Institute,
Academy of Sciences of the USSR

References

1. R.G.Breckenridge, J.Chem.Phys., 16, 959 (1948).
2. B.N.Matsonashvili & G.I.Skanavi, Sb.tr.Vtoroi vsesyuznoi konferentsii po fizike dielektrikov (Program of the Second All-Union Conference on the Physics of Dielectrics). M.-L., 1960.
3. G.I.Skanavi & E.N.Matveeva, Zhur.eksp.i teor.fiz., 30, 1047 (1956). (Trans. Soviet Physics - JETP.)
4. G.I.Skanavi, Ya.M.Ksendzov, V.A.Trigubenko & V.V.Prokhvatilov, Ibid., 33, 320 (1957). (Trans. Ibid.)
5. A.M.Kashtanova, N.N.Kurtseva & G.I.Skanavi, Present issue of the Bulletin, p.109.
6. R.H.Cole & D.W.Davidson, J.Chem.Phys., 19, 1484 (1951).
7. G.I.Skanavi, Fizika dielektrikov - Oblast' slabykh polei (Physics of Dielectrics - Weak field region), M.-L., 1949.
8. K.Cole & R.Cole, J.Chem.Phys., 9, 341 (1941).
9. R.Fuoss & J.Kirkwood, J.Amer.Chem.Soc., 63, 385 (1941).
10. H.Fröhlich, Theory of Dielectrics, Oxford, 1949.

RELAXATION POLARIZATION OF THE $SrTiO_3 \cdot nMnO$ SYSTEM

- E.V. Sinyakov & A.M. Solok

Introduction

According to the hypothesis concerning ionic relaxation polarization, proposed by Skanavi and his co-workers[1,2], one can synthesize dielectrics with a high dielectric constant if one partially replaces the divalent cations in a perovskite type lattice by cations of a higher valence. For example, SBT* is such a dielectric, in which the substituent cation is trivalent bismuth.

We felt it would be of interest to study the effect of manganese ions on the dielectric polarization of strontium titanate. As is known[3], $MnCO_3$ decomposes into MnO and CO_2 when heated in air. The manganous oxide upon further heating in air can be oxidized to higher oxides: kurnakite (Mn_2O_3), hausmannite (Mn_3O_4), etc. Thus the presence of trivalent manganese ions in $SrTiO_3$ can bring about relaxation polarization. Analogously, one can expect the appearance of relaxation polarization in the $Bi_2O_3 \cdot nMnO$ system.

Sample Preparation

We investigated ceramic samples having the compositions listed in Table 1.

The samples were prepared according to the usual technology for ceramic dielectrics. Silver electrodes were applied by firing on. The values of ϵ and tan δ at frequencies of 1.5 Mc and 12 Mc were measured in a wide temperature range by means of a KV-1 Q-meter.

Table 1

Sample composition and sintering temperatures

$SrTiO_3$	Bi_2O_3 MnO	Bi_2O_3 2MnO	Bi_2O_3 3MnO	MnO	Sintering temp., °C (1 hr.)
100	—	—	—	-	1440
99	1	—	—	—	1440
97	3	-	—	—	1390
97	—	—	—	3	1420
95	5	—	—	—	1390
90	10	—	—	—	1360
—	100	—	—	-	720
—	—	100	—	—	740
—	—	—	100	-	840

Table 2

Composition	Density	$n = \frac{\rho a^3}{A_{av} \cdot 1.65 \cdot 10^{-24}}$
$SrTiO_3$	4.9	4.66
$97SrTiO_3 + 3MnO$	4.385	4.29

Experimental Results and Discussion

Fig.1 gives the variation of ϵ and tan δ of the 97 $SrTiO_3$ + 3 MnO samples as a function of the temperature at the two test frequencies. It will be seen that the maximum of the dielectric constant is shifted to the side of higher temperatures with increase of the frequency. The presence of a temperature maximum and also its shift with change in frequency are evidence of relaxation polarization in the 97 $SrTiO_3$ + 3 MnO system.

In order to determine the structural characteristics of the samples, x-ray diffraction patterns were recorded. From the x-ray data and measurements of the sample densities we could calculate the number of particles per unit cell (Table 2). It will be evident from Table 2 that the number of atoms per unit cell in the 97 $SrTiO_3$ + 3 MnO decreased markedly as compared with pure strontium titanate, i.e., an omission type solid solution was formed. The presence of vacant sites in the oxygen part of the lattice would appear most probable, because the radii of the trivalent manganese (0.62 Å) and of titanium (0.64 A) are very close[4]. But replacement of titanium ions by manganese ions should have led

---

*SBT (CBT) = solid solution of strontium and bismuth titanates.

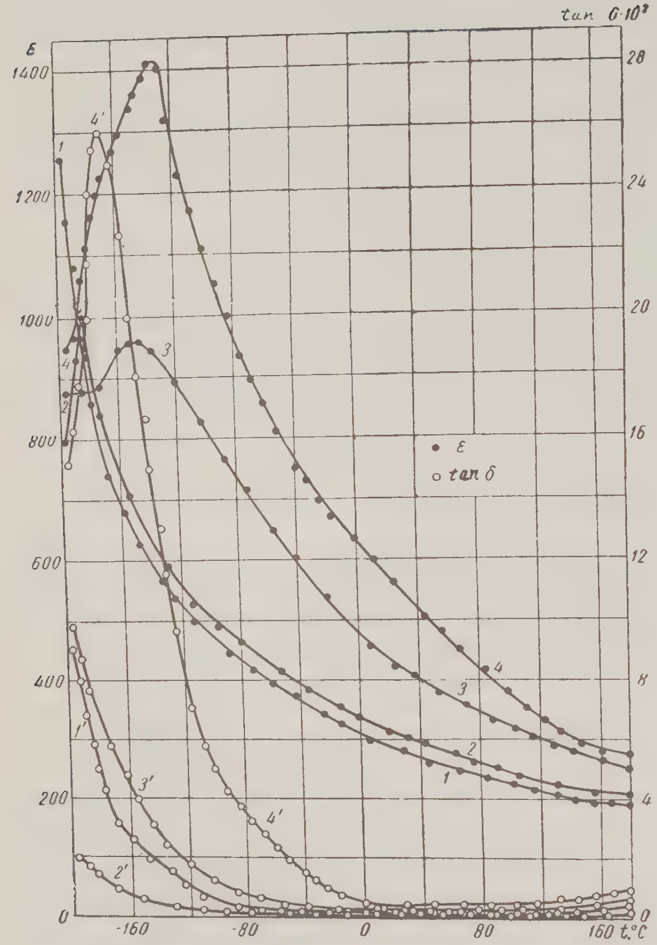

Fig.1. Temperature dependences of the dielectric constant and the dielectric loss tangent for the systems: 97 $SrTiO_3$ + 3 MnO (1 & 1' and 2 & 2') and 97 $SrTiO_3$ + $3(Bi_2O_3 \cdot MnO)$ (3 & 3' and 4 & 4'). 1, 1', 3 & 3' - ƒ = 1.5 Mc; 2, 2', 4 & 4' - ƒ = 12 Mc.

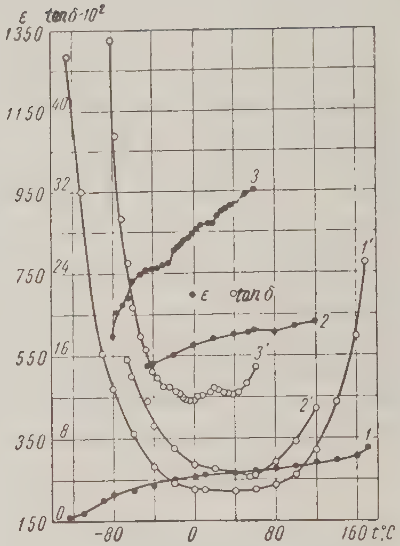

Fig.2. Temperature dependences of the dielectric constant and dielectric loss tangent in the $Bi_2O_3 \cdot nMnO$ system: 1) $Bi_2O_3 \cdot MnO$, 2) $Bi_2O_3 \cdot 2MnO$, 3) $Bi_2O_3 \cdot 3MnO$.

to an increase of the 97 $SrTiO_3$ + + 3MnO sample density as compared with pure strontium titanate; this was definitely not the case in reality. Therefore it must be assumed that the vacant sites are formed in the strontium part of the lattice.

Fig.2 gives the temperature dependences of ϵ and tan δ for samples of the $Bi_2O_3 \cdot nMnO$ system, wherein, as was noted above, the simultaneous presence of divalent and trivalent manganese in the $Bi_2O_3 \cdot nMnO$ system can lead to relaxation polarization, caused by electron transitions between divalent and trivalent manganese and divalent manganese and trivalent bismuth.

As will be evident from Fig.2, the dielectric constant in the $Bi_2O_3 \cdot nMnO$ system is strongly temperature dependent, and there is a marked increase of ϵ with increase in the number of MnO molecules. The large increase of tan δ with decrease of temperature is evidence of the presence of relaxation polarization. As the number of MnO molecules increases, the temperature of the sudden increase in tan δ shifts upward. The increase in the temperature of the tan δ rise may be associated with decrease of the relaxation time, if we assume that there simultaneously occur $Mn^{2+} \rightarrow Mn^{3+}$ and $Mn^{2+} \rightarrow Bi^{3+}$ electron transitions with different relaxation times. Then increase in the number of MnO molecules and also the increase in the sintering temperature connected with it lead to an increase in the

Table 3

Composition	−100°		20°		100°	
	ε	tan δ	ε	tan δ	ε	tan δ
$99SrTiO_3+1(Bi_2O_3 \cdot MnO)$	675	$0.35 \cdot 10^{-2}$	395	$2.2 \cdot 10^{-2}$	250	$3,1 \cdot 10^{-2}$
$97SrTiO_3+3(Bi_2O_3 \cdot MnO)$	825	$1.75 \cdot 10^{-2}$	445	$0.2 \cdot 10^{-2}$	380	$0.35 \cdot 10^{-2}$
$95SrTiO_3+5(Bi_2O_3 \cdot MnO)$	750	$3 \cdot 10^{-2}$	510	$0,3 \cdot 10^{-2}$	390	$0.7 \cdot 10^{-2}$
$90SrTiO_3+10(Bi_2O_3 \cdot MnO)$	386	$4,45 \cdot 10^{-2}$	420	$1,8 \cdot 10^{-2}$	375	$3.2 \cdot 10^{-2}$

number of trivalent manganese molecules, which enhances the probability of $Mn^{2+} \rightarrow Mn^{3+}$ transitions. From this one can conclude that the relaxation time of the $Mn^{2+} \rightarrow Mn^{3+}$ transitions is shorter than the relaxation time of the $Mn^{2+} \rightarrow Bi^{3+}$ transitions. The above serves to explain the observed increase of ε with increase of the MnO content in the $Bi_2O_3 \cdot nMnO$ system.

X-ray diffraction patterns of the $Bi_2O_3 \cdot MnO$ samples indicate the formation of a solid solution.

In order to check the effect of synthesized $Bi_2O_3 \cdot nMnO$ on the polarization of strontium titanate, we investigated samples of different compositions: (100-n) $SrTiO_3$ + n(Bi_2O_3 MnO). The values of ε and tan δ for four compositions at three temperatures are given in Table 3.

Fig.1 (curves 3 and 4) presents the temperature dependences of ε and tan δ for the 97 $SrTiO_3$ + 3($Bi_2O_3 \cdot MnO$) samples. It will be seen that the maximum of the dielectric constant is shifted in the direction of higher temperatures as the frequency is increased, and the absolute value of ε increases markedly. A comparison of curves 1 & 2 with 3 & 4 shows that the character of the relaxation polarization is different in the $SrTiO_3$ + nMnO and $SrTiO_3$ + n($Bi_2O_3 \cdot MnO$) systems.

If one can assume the presence of only ionic relaxation polarization in the $SrTiO_3 \cdot nMnO$ system, then in the $SrTiO_3 \cdot n(Bi_2O_3 \cdot MnO)$ system, in addition to ionic relaxation polarization, there is observed polarization connected with electron transitions. This is evinced by the ϵ_{max} temperature in the two systems, i.e., by the fact that the mean relaxation time in the $SrTiO_3 \cdot n(Bi_2O_3 \cdot MnO)$ system is considerably shorter than the time in the $SrTiO_3 \cdot nMnO$ system.

Conclusions

1. The introduction of manganese oxide into $SrTiO_3$ leads to the appearance of ionic relaxation polarization.
2. Relaxation polarization also occurs in the $Bi_2O_3 \cdot nMnO$ in which the relaxation of weakly bound electrons is possible owing to the presence of divalent and trivalent manganese, i.e., owing to the possibility of $Mn^{2+} \rightarrow Mn^{3+}$ electron transistors.
3. The simultaneous presence of weakly bound ions and electrons is possible in the $SrTiO_3 \cdot n(Bi_2O_3 \cdot MnO)$ system.

References

1. G. I. Skanavi, Dielektricheskaya polyarizatsiya i poteri v steklakh i keramicheskikh materialakh s vysokoi dielektricheckoi pronitsaimostvyu (Dielectric polarization and loss in glasses and ceramics with a high dielectric constant), M. 1952.
2. G. I. Skanavi, Ya.M.Ksendzov, V.A.Trigubenko & V.V.Prokhvatilov, Zhur.eksp. i teor.fiz., 33, 320 (1957). (Trans.Soviet Physics - JETP.)
3. Rode, Kisloradniye soedineniya margantsa (Oxygen compounds of manganese), M.-L. 1952.

4. C.Kittel, Introduction to Solid State Physics, N.Y. 1953. (Cited in Russian translation.)

DISCUSSION

Yu.N.Venevtsev: In explaining the high dielectric constant of SBT, Skanavi attributes an important role to vacancies in the crystal lattice of these solid solutions. It seems to me, however, that Skanavi does not give sufficient weight to the fact that the initial $SrTiO_3$ lattice is "loose".

As is known, the inference regarding the looseness of the $SrTiO_3$ lattice was made as a result of the experimental data obtained in the X-Ray Laboratory of the "L.Ya.Karpov" Physical-Chemical Institute and is in agreement with Megaw's evaluation of the t factor ($t = 0.97$). The strontium cations in the $SrTiO_3$ lattice are somewhat "free", while the titanium cations are "crowded", i.e., tightly held. Replacement of Sr cations by Bi cations, which are identical in size, leads only to a small increase in the looseness of the lattice owing to the appearance of vacancies.

The looseness of the $SrTiO_3$ lattice and its relatively small period are among the favorable features that lead to a noticeable increase of the dielectric constant as a result of a relatively small addition (substitution) of bismuth. Undoubtedly, a significant role here is played by the increased openness of the lattice owing to introduction of the bismuth and the fact that the Bi cation has a higher charge and apparently a higher polarizability as compared with the strontium ion.

It is of interest to study the $SrTiO_3$-"$BiAlO_3$" system. In this system, in a certain range of concentrations, there may exist $(Sr,Bi)(Ti,Al)O_3$ solid solutions having a lattice devoid of vacancies. At the same time in these solid solutions one can apparently expect a high dielectric constant.

Further, if we write the formula for perovskite type compounds as ABO_3, we can say that the relaxators in SBT are obtained as a result of replacement in $SrTiO_3$ of A type cations. It is, however, expedient partially to replace in the $SrTiO_3$ the B type cations (Ti) by complex cations B' = (Nb,Al) with a smaller mean radius ($R_{Al} < R_{Ti}$). In this case a part of the B' cations will have the geometric possibility for displacement. As a result, we assume that the dielectric constant may increase.

I.Ts.Lyast (regarding the reports of G.A.Smolenskii et al and E.V.Sinyakov & A.M.Solok): I have a number of remarks to make concerning the electron-relaxation mechanism discussed in the reports. From the standpoint of the electron-relaxation mechanism, in the case of a pure electron transition, we must assume that the transition occurs between some two states. For the transition to be relaxational, it is necessary that in addition to these two normal states there be a certain third intermediate excited state. The transition is relaxational in character if it occurs as follows: transition from one of the normal states to the excited state and then a reverse transition from the excited state to the other normal state. Such transitions can occur if the wave functions corresponding to these two states do not overlap. At the same time the two normal states have a common excited state.

On the other hand, it is essential that the wave functions of the excited states pertaining to different pairs of normal states do not overlap; otherwise, there will occur transitions corresponding to through conduction. It is also necessary that the separation of the excited level from the conduction band be large. The absence of through conduction corresponds therefore to fulfillment of the condition: $N_hV \ll 1$, where V is the volume occupied by the wave function of the excited state.

For an electron-relaxational transition to occur all these conditions must be fulfilled. I think, however, that fulfillment of all these requirements is rather difficult and hence the probability for electron-relaxational transitions is very low.

It may be assumed that the normal states have different energies, but in this case the expression for the dielectric constant must include a factor $e^{-\frac{\Delta U}{kT}}$, where ΔU is the separation between the normal state levels, and this means that if they differ from each other this difference must be small compared with kT.

N.P.Kalabukhov: I want to make a brief comment concerning the temperature dependence of polarization mentioned by Skanavi. According to the curve we were shown, there is deviation from linear dependence of B on 1/T in the range of higher temperatures. This apparently occurs as a result of elimination of vacancies at elevated temperatures. If this is the case, the temperature variation of the dielectric constant should differ for cooling as against heating inasmuch as the number of quasi-dipoles will not be re-established during cooling.

G.I.Skanavi: Repeated measurements both in heating and in cooling, in vacuum and in air, showed that the properties of SBT type dielectrics are stable and that the temperature dependence of the dielectric constant is the same in heating and in cooling. Our hypothesis is that the quasi-dipoles are created only by associated defects. At high temperatures the degree of association decreases, which is what results in the deviation of the B vs 1/T plot from a straight line.

CORRELATION BETWEEN THE DIELECTRIC LOSS AND THE STRUCTURE OF IONIC CRYSTALS

- N.P.Bogoroditskii, B.A.Kulik & I.D.Fridberg

Investigation of the physical processes occurring in dielectrics is becoming increasingly important. Such investigations bring to light new properties of dielectrics and thus open the way to new technical applications. By investigating the physics of effects taking place in dielectrics one can establish the regularities governing them and thus provide a means for controlling the technological operations involved in the fabrication of dielectric components.

The polarization of dielectrics, the character of which is indicated by the dielectric constant and the dielectric loss angle, is an important factor in determining the scope of possible applications of a given material. The nature of polarization determines the magnitude of the dielectric loss which is an inherent characteristic of the material. In this sense the dielectric losses occurring in the material owing to macroscopic inhomogeneity of this structure are a particularly important factor. The electric conductivity of ionic crystals is also intimately related with the thermal polarization.

Depending on the physical-chemical nature, either electronic or ionic polarization may predominate in ionic crystals and accordingly there are evinced electronic-relaxation or ionic-relaxation dielectric losses if the frequency of the field is not excessively high. Below we shall consider only ionic-relaxation dielectric losses.

It is known that such losses depend to a considerable degree on the structure of the dielectric. They are observed in loose (open) crystal lattices such as those of beryl and cordierite. It has been shown in a number of studies that a significant dielectric loss is evinced in solid solutions of the substitutional type, particularly those with omissions or extra ions, for example, in the $SrTiO_3$ —$Bi_2Ti_3O_9$ and ZrO_2—MgO systems[1,2,3]. Breckenridge[4], however, showed that in pure alkali halide crystals with a close packed lattice there may also occur ionic-relaxation dielectric losses. As is known, in pure alkali halide crystals there may be thermal Schottky defects, i.e., vacant anionic and cationic vacancies in equal numbers; also possible is the formation of dipole complexes - vacant sites of different polarity.

Matsonashvili[5] also established the existence of relaxation maxima of tan δ in alkali halide crystals.

Haven[6] observed a sharp increase of the dielectric loss in rock salt as a result of doping with CaO, MnO and other impurities generating cationic vacancies. The experimental results of Haven were explained theoretically by Lidiard[7].

Vodop'yanov & Galibina[8] compared the values of the dielectric loss, conductivity and dielectric constant of alkali halide crystals with the lattice energy.

The purpose of the present study was to investigate the electric loss in a large number of different alkali halide crystals and systems and thus supplement and amplify the extant data. We investigated almost all the halides of lithium, sodium, potassium and cesium. Part of the salts were investigated in the form of single crystals, others were studied in the form of polycrystalline formations obtained from melts of the chemically pure salts. In addition, we investigated various isovalent mixtures of alkali halide crystals with different ionic radii. We used either platinum or silver electrodes and carried out measurements at audio and radio frequencies in the temperature range from 200 to 300°.

Fig.1 shows the variation of tan δ for a number of alkali halide salts with octahedral and cubic coordination as a function of the ratio of the cation and anion radii. It will be evident from the figure that at values of r_c/r_a close to the critical, tan δ increases sharply. We recall that for the coordination

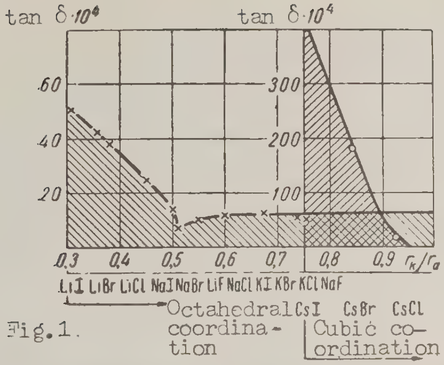

Fig.1.

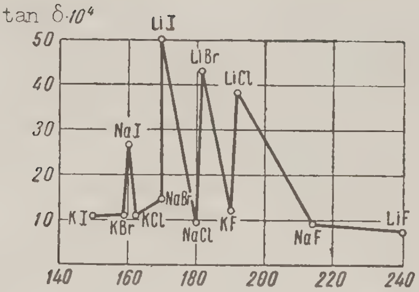

Fig.2

Fig.1. Variation of tan δ for different alkali halide crystals with the ratio of cation to anion radii at 200°.

Fig.2. Variation of tan δ with the lattice energy at 220°.

number 6 the lower bound of stability is 0.41, while for the coordination number 8 the lower stability bound is 0.73. It may be assumed that the increase of the dielectric loss in compounds of this type is due to increase in the number of thermal defects. The data of Fig.2, in which we have plotted measured values of tan δ for a large number of different alkali halide crystals against their lattice energy, show that there is no simple direct correlation between these two characteristics.

Analyzing the relation between tan δ and the structure of binary systems (KCl-NaCl, NaCl-CsCl, etc.) the components of which differ as regards ionic radii and which according to x-ray diffraction studies are either a mechanical mixture or form an isovalent substitutional solid solution, we noted that in a number of cases there is evident a maximum of tan δ in its concentration dependence curve (Figs.3 & 4).

According to the data of Devries et al[9], based on luminescence and radiographic analyses, it would appear that even at low temperatures one can detect the presence of a solid solution of components with markedly different ionic radii provided the impurity content is low.

Among the systems which are characterized by unlimited mutual solubility we investigated the concentration dependence of tan δ of KCl-KBr solid solutions. We established that tan δ in this case takes on values intermediate between those for pure KCl and KBr (Fig.5).

The regularity observed for the KCl-KBr system, wherein the anion radii are close, should be contrasted with the values for the NaCl-KCl system in which the cations differ appreciably as regards size. Inasmuch as the NaCl + KCl mixture

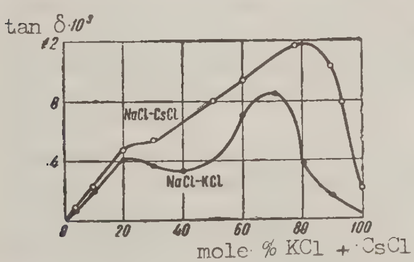

Fig.3

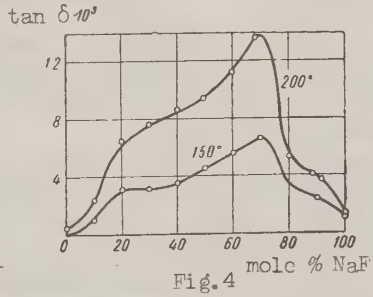

Fig.4

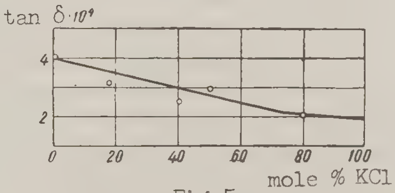

Fig.5

Fig.3. Concentration dependence of tan δ for the NaCl-KCl and NaCl-CaCl systems at 200°.

Fig.4. Concentration dependence of tan δ for the NaCl-NaF system.

Fig.5. Concentration dependence of tan δ for KBr-KCl system at 200°.

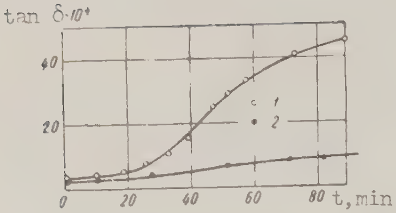

Fig.6. Variation with time of tan δ at 200°: 1) 35NaCl-65KCl, 2) 15NaCl-85KCl.

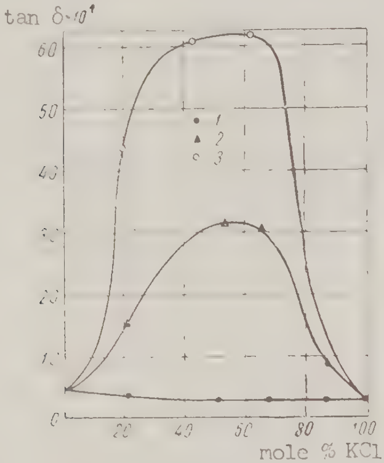

Fig.7. Concentration dependence of tan δ for the NaCl-KCl system at 200°: 1) immediately after preparation, 2) after 1 hour, 3) after 15 hours.

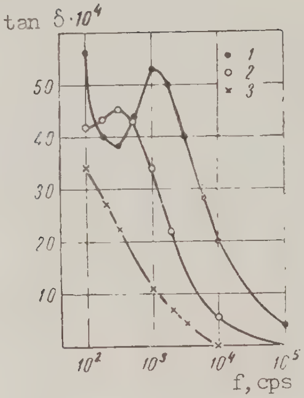

Fig.8. Frequency dependence of tan δ for KBr at 300°: 1) single crystal grown from the initial X 4 salt, 2) single crystal grown from salt purified by twofold recrystallization, 3) single crystal - threefold recrystallization.

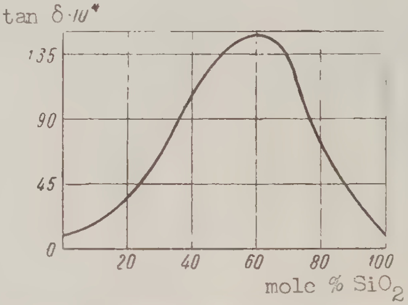

Fig.9. Concentration dependence of tan δ for the TiO_2-SiO_2 system at 100°.

is fully isomorphous at high temperatures and not isomorphous at low temperatures, we can assume the existence of a solid solution immediately after preparation and rapid cooling of the system.

Investigation of tan δ of the NaCl-KCl system showed that in the case of "quench" cooling the dielectric loss is small and has a value intermediate between the values characteristic of pure NaCl and KCl. With time, however, tan δ begins to increase (Fig.6), goes through a maximum and then gradually decreases. If the NaCl-KCl melt is cooled slowly, tan δ is small and does not change with time. Thus, the concentration dependences of tan δ of such mixtures will differ, depending when the dielectric loss is measured (Fig.7).

In the course of decomposition of the solid solution the number of imperfections in the lattice increases and tan δ rises. After completion of the decomposition, tan δ decreases. Finally, in the case of slow cooling, the process of decomposition forms part of the preparation procedure so that the measurements are carried out on what is essentially a mechanical mixture of the two components. The increase of the dielectric loss to a large extent is due to increase of the conductivity (on the average by one order of magnitude).

It may be assumed that in the process of decomposition of a solid solution the number of Schottky defects increases inasmuch as these are generated during the formation of the individual component crystals.

All the above curves pertain to data obtained at one frequency (1 Mc) and one temperature (200°), except Fig.2. Owing to the presence of peaks these data cannot be regarded as adequate for all purposes. In view of this we carried out measurements of the dielectric loss in a wide frequency range. In the investigated alkali halide crystals with less than 0.01% impurities there was observed a large relaxation loss maximum (Fig.8). This maximum is generally located in the range of high temperatures and yields an activation energy of from 0.65 to 1.5 ev for different salts. The observed loss is connected with the presence of impurities as is indicated by the gradual decrease of the tan δ maximum incident to purification of the salt by repeated recrystallization. At the same time the activation energy changes.

The 200° temperature and 1 Mc frequency lie in the range where tan δ of all the investigated salts is still far from its maximum value.

There is reason to assume that among metal oxides a similar loss mechanism operates in the SiO_2-TiO_2 system. The available physical-chemical data for the SiO_2-TiO_2 system are inadequate for precise determination of the region of existence of a solid solution of these oxides. Nevertheless, as will be evident from Fig.9, there is a clear maximum in the concentration dependence of tan δ.

Conclusions

We found that the dielectric loss associated with relaxation of ions is particularly noticeable in the following cases:

a) in the presence of a loose (open) crystal lattice; this includes crystalline materials of the beryl, cordierite and orthoclase type;

b) in omission type solid solutions, and in some cases in substitutional solutions with excess ions;

c) in substitutional solid solutions in the state of decomposition.

From the standpoint of practical utilization of ionic crystals in electronic engineering it is important to know, in addition to other characteristics, the structure of the pure substance and the type of solid solution formed.

In view of the instability characterizing certain technical dielectrics, for example, magnesium silicate ceramics, one must particularly emphasize the importance that should be attached to the nonequilibrium state of metallic oxide systems.

References

1. G.I.Skanavi, Ya.M.Ksendzov, V.A.Trigubenko & V.V.Prokhvatilov, Zhur.eksp. i teor.fiz., 33, 320 (1957). (Trans.Soviet Physics - JETP.)

2. N.P.Bogoroditskii, "Dielektricheskie poteri v radiokeramike". Doklady nauchno-tekhnicheskogo soveshchaniya po radiokepamike ("Dielectric loss in radioceramics" in Reports presented at the Scientific-Technical Conference on Radioceramics, Leningrad, 1955.

3. A.I.Avgustinnik & N.S.Antselevich, Zhur.fiz.khim., 27, 973 (1953).

4. R.G.Breckenridge, J.Chem.Phys., 16, 959 (1948).

5. B.N.Matsonashvili, Izv.AN SSSR, Ser.fiz., 22, 296 (1958). (Trans.Bulletin, 22, No.3, 294.)

6. Y.Haven, J.Chem.Phys., 21, 171 (1953).

7. A.B.Lidiard, Philos.Mag., 46, 815 and 1218 (1955).

8. K.A.Vodop'yanov & G.I.Galibina, Izvestiya (Bulletin), Tomsk Polytechnic Institute, 91, 269 (1956).

9. R.C.Devries, R.Roy & E.Osborn, Trans.Brit.Ceram.Soc., 53, 525 (1954).

10. V.I.Odelevskii & N.M.Verebeichik, Izvestiya (Bulletin), Tomsk Polytechnic Institute, 91, 247 (1956).

INVESTIGATION OF HIGH-FREQUENCY DIELECTRIC LOSS IN SOLID DIELECTRICS

- K.A.Vodop'yanov & G.I.Galibina

In this report we consider the experimental data relating to the frequency and temperature dependences of the dielectric loss angle in different ionic crystals with a view to elucidating the dielectric loss mechanism in solid dielectrics.

1. Relation between the dielectric loss angle in alkali halide crystals and their physical-chemical properties

Until recently there were no reliable values of the loss angle for alkali halide crystals, mainly owing to the lack of suitable procedures for measuring small dielectric loss angles. Yet the matter of establishing a correlation between the loss angle and the physical-chemical properties of alkali halide crystals has an important bearing on the problem of defining the dielectric loss mechanism not only in ionic crystals but also in the large group of solid inorganic dielectrics employed in electrical engineering. Such a correlation was found by us[1] for several ionic crystals in the high-frequency region by virtue of development of a more accurate technique[2] for measuring small loss angles. It was established that the absolute value of tan δ in alkali halide crystals is determined by their physical-chemical properties; we found that the lower the lattice energy, the melting point and the heat of formation and the larger the lattice constant, the greater the dielectric loss angle. This was shown by the temperature and frequency behavior of tan δ of the investigated alkali halide crystals in a wide range of temperatures and frequencies. The good agreement of the forward and reverse (heating and cooling) tan δ vs temperature curves for these crystals shows that at high frequencies under atmospheric conditions a small moisture content does not play any substantial role. Therefore, measurements need not be carried out in vacuo. When using vacuum apparatus the Q-factor of the circuit and the sensitivity of the measuring equipment are reduced. Owing to this in the work of Matsonashvili[3], for example, erroneously high values of tan δ were obtained and hence no clear correlation was found between the loss tangent and the physical-chemical characteristics of the tested alkali halide crystals.

Thus the dielectric loss at high frequencies in ionic crystals is associated mainly with weakly bound ions, which have a comparatively low activation energy.

2. Influence of heat treatment on the dielectric loss in alkali halide crystals

Heat treatment and mechanical deformation distort the crystal lattice and weaken the bonds, thereby increasing the probability of ions being released or dislodged by thermal motion. In a deformed crystal lattice conditions are favorable for the displacement of weakly bound ions in a finite volume, which leads to the appearance of relaxation dielectric losses.

Sikorskii[4] showed that annealing of a crystal at different temperatures has different effects on the magnitude of the loss angle. He found a relation between tan δ and the internal stresses in the crystal. In deformed crystals, tan δ was larger than in undeformed ones.

Krikov[5] investigated the influence of mechanical defects on the dielectric properties of rock salt crystals at high frequencies. The mechanical defects formed as a result of heating altered certain properties of the crystal. Prolonged annealing of a rock salt crystal at 600° relieved the internal stresses, while heating at temperatures above 600° led to a uniform distribution of impurities in the crystal. This in turn resulted in an increase of the effective impurity concentration per unit volume, which is equivalent to an increase in the number of defects.

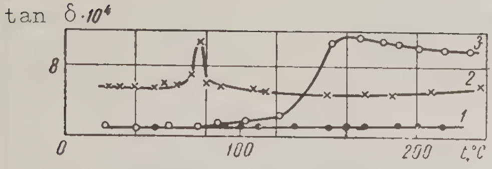

Fig.1. Temperature dependence of $\tan \delta$ in rock salt at 10^7 cps: 1) not heated, 2) heated, 3) compressed material (after Krivov[5]).

Gokhberg[6] discovered a considerable increase in the conductivity of NaCl after heating to 700°. He associates this increase with uniform impurity distribution throughout the crystal. Venderovich & Lapkin[7], in investigating the potential distribution in heated and unheated NaCl samples, demonstrated the absence of polarization in NaCl crystals heated to a high temperature, which is also evidence of uniform impurity distribution.

In connection with his investigation of the effect of deformation on the diffusion of sodium through NaCl, Popov[8] showed that the activation energy decreases with increase of the deforming stress.

Fig.1 shows the variation of $\tan \delta$ as a function of the temperature at a frequency of 10^7 cps for different NaCl samples: not heated crystals, crystals annealed for 10 hours at 700° and compressed pellets. In the unheated crystal, $\tan \delta$ is small and only weakly temperature dependent. In the annealed crystal, $\tan \delta$ is high and exhibits a maximum at 75°. For the compressed NaCl sample, at low temperatures $\tan \delta$ is comparable to that of the unheated crystal, but in the 80 to 240° range $\tan \delta$ goes through a maximum. It is interesting that for the annealed crystal the $\tan \delta$ maximum is well defined and sharp, while for the compressed sample the maximum is smeared out over a wide temperature interval. According to the data of Krivov[5], the temperature maxima of $\tan \delta$ in heated NaCl crystals are displaced towards higher temperatures with increase of frequency. This is due to ionic polarization of the weakly bound ions.

Thus in following the temperature dependence of $\tan \delta$ in annealed NaCl crystals and compressed salt pellets we note certain regularities substantiating the relaxational character of the dielectric losses. The existence of $\tan \delta$ maxima in annealed alkali halide crystals has also been reported by Breckenridge[9] and Matsonashvili[3]. In fact the latter even observed temperature maxima of $\tan \delta$ for individual nonannealed crystals in the frequency range from 10^3 to $7.5 \cdot 10^5$ cps.

In our ealier work[1] we showed that there were no $\tan \delta$ maxima in the temperature and frequency dependences of nonannealed crystals in the frequency range from 10^6 to 10^8 cps and temperature range from 20 to 200°. This indicates that in the given temperature and frequency ranges the conditions necessary for a maximum, namely, $\omega\tau = 1$, is not fulfilled. Possibly in the range of higher temperatures a low $\tan \delta$ peak is masked by conduction losses inasmuch as their relative importance increases at elevated temperatures.

Secondary effects, which are most pronounced at low frequencies, may influence the character of the temperature dependence of $\tan \delta$ in solid dielectrics. These secondary effects are primarily imperfect contact between the dielectric and the electrodes and possibly the penetration into the dielectric of metal ions incident to firing on the electrodes.

Nakamura[10] observed a temperature maximum of $\tan \delta$ for crystalline quartz; he explains this by poor quality of the contacts. Vorozhtsov[11] showed that in the high-frequency region there is no temperature maximum of $\tan \delta$ in quartz; in his experiments the contact effect was eliminated.

3. Influence of impurities on the dielectric loss in crystals

We studied the influence of nonisomorphous impurities on the dielectric loss in alkali halide crystals in the high frequency range. Specifically, we investigated NaCl and KCl crystals doped with $CaCl_2$, $BaCl_2$ and $MgCl_2$. Both the doped and undoped crystals were checked not only by chemical but also by spectroscopic analysis. Spectroscopic analysis showed the presence of traces of copper in the NaCl crystals and calcium in the KCl crystals. The doped crystals, in addition to the introduced impurities, contained the same impurities as those in the "pure" crystals.

Extensive x-ray diffraction and optical studies were carried out with a view to determining the influence of the impurities on the structure of the crystals. The lattice constant as determined from the x-ray diffraction patterns was the same for doped and undoped crystals; the lattice constant of the crystals containing the maximum amount of impurity differed from the constant of the undoped crystals by not more than 0.002 Å, which is within the limits of the experimental error. This result is in agreement with the data of Glover[12] who carried out measurements of the lattice parameters of KCl crystals with and without impurities in the temperature range from 20 to 600°. For the NaCl crystal containing the maximum $CaCl_2$ concentration we obtained a Laue diffraction pattern typical of NaCl single crystals.

There are no data in the literature on the structure of KCl crystals containing minor amounts of $CaCl_2$, $BaCl_2$ and $MgCl_2$. No evidence of these impurities was evident in the x-ray patterns for the investigated crystals. Hence we carried out additional optical studies of the crystals by the immersion technique. As a result of these studies, we detected in KCl crystals doped with $CaCl_2$ the existence of two phases, one with an index of refraction equal to that of pure KCl and a second phase with an index of refraction differing from that of KCl and $CaCl_2$. Similar results were obtained in investigating KCl crystals doped with $MgCl_2$.

In view of the above described results and the data of other authors[13] who investigated the structure of the KCl-$CaCl_2$ and KCl-$MgCl_2$ systems in the regions extending to higher concentrations of $CaCl_2$ and $MgCl_2$, we can assume that our KCl crystals doped with $CaCl_2$ and $MgCl_2$ were true KCl single crystals (this is indicated by the x-ray diffraction patterns) in which there was present in the form of an impurity a second phase differing from the introduced chloride. That this second phase could be a solid solution is contrary to the data in the literature and in fact is little probable owing to the great difference between the ionic radii of potassium, calcium and magnesium.

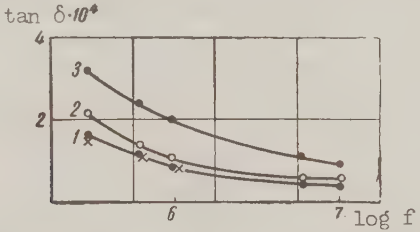

Fig.2

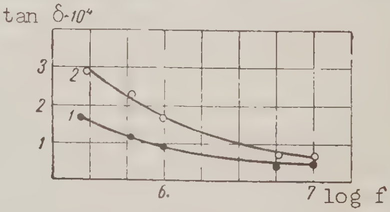

Fig.3

Fig.2. Frequency dependence of tan δ: 1) 100% KCl (solid circles) and KCl + 0.03% $MgCl_2$ (crosses), 2) KCl + 0.13% $MgCl_2$, 3) KCl + 0.55% $MgCl_2$.

Fig.3. Frequency dependence of tan δ: 1) 100% KCl and KCl + 0.13% $BaCl_2$, 2) KCl + 0.4% $BaCl_2$.

The frequency dependences of tan δ in crystals with the enumerated impurities are shown in Figs.2, 3 & 4. As will be evident from the figures, tan δ increases with decreasing frequency in all crystals, the increase being the more appreciable, the higher the impurity concentration. Consequently, it is clear that the impurities have a greater effect on the value of tan δ in the region of low frequencies. In the entire investigated frequency interval the greatest change in tan δ is observed as a result of doping KCl with $CaCl_2$. In the case of doping KCl with $BaCl_2$ and $MgCl_2$ there is a noticeable increase of tan δ only at impurity concentrations of several tenths of a mole percent. $BaCl_2$ and $MgCl_2$ impurities in amounts of up to ~0.1 mole percent have virtually no effect on tan δ at room temperature in the entire experimental frequency range.

We showed earlier[1] that the influence of low impurity concentrations on tan δ becomes more noticeable with increasing temperature. Whereas thousandths and even hundredths of a mole percent of impurity do not change tan δ in crystals at room temperature, they do change tan δ at high temperatures thereby altering the temperature dependence of tan δ: in crystals with impurities tan δ begins to rise earlier and more steeply with increasing temperature (see Figs.8 & 9 in Ref.1).

To clarify the role of conduction in the dielectric loss process in crystals with impurities, we measured the conductivity of a number of crystals with impurities; the values of tan δ measured at a frequency of 10^6 cps and the corresponding values calculated from the experimental conductivities of these crystals are listed in the accompanying table.

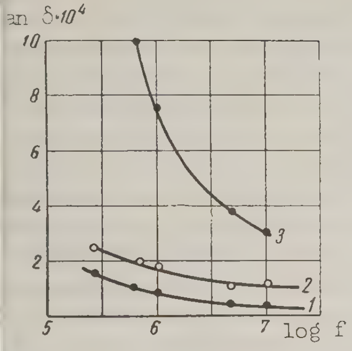

Fig.4. Frequency dependence of tan δ: 1) 100% KCl, 2) KCl + 0.11% $CaCl_2$, 3) KCl + + 0.4% $CaCl_2$.

T,°C	KCl+0.12% $BaCl_2$		T,°C	KCl+0.003% $CaCl_2$	
	tan δ_{cxp}	tan δ_{theo}		tan δ_{cxp}	tan δ_{theo}
56	$0,80\cdot10^{-4}$	$1\cdot10^{-7}$	100	$0.84\cdot10^{-4}$	$6.4\cdot10^{-7}$
124	$0,80\cdot10^{-4}$	$9\cdot10^{-7}$	130	$1.20\cdot10^{-4}$	$9.3\cdot10^{-6}$
170	$1,00\cdot10^{-4}$	$6\cdot10^{-5}$	180	$4.40\cdot10^{-4}$	$2.0\cdot10^{-4}$
200	$5,80\cdot10^{-4}$	$1,8\cdot10^{-4}$	200	$10\cdot10^{-4}$	$6,0\cdot10^{-4}$
210	$9.0\cdot10^{-4}$	$3,7\cdot10^{-4}$			
240	$21,0\cdot10^{-4}$	$11.0\cdot10^{-4}$			

As will be evident from the table, the experimental value of tan δ in the investigated crystals becomes comparable with tan δ as calculated from the conductivity only at 180-200°. The temperature and frequency dependences of tan δ for the investigated crystals with impurities are similar to the dependences for undoped crystals and differ only by the steeper increase of tan δ with decreasing frequency and the more appreciable rise of tan δ with increasing temperature. From this it may be inferred that the loss mechanism in undoped crystals is essentially the same as in doped ones.

Increase of tan δ in crystals as a result of doping is explained by the fact that the impurity distorts the crystal lattice, facilitating dissociation of the ions and thereby increasing the number of free and weakly bound ions. This also explains the steeper increase of tan δ in crystals with impurities as compared with undoped crystals. This becomes understandable if we recall the results of studies[14,15] on the influence of impurities on the electric conductivity of crystals. The energy required for release of an ion is reduced in the presence of impurities.

Frenkel'[16] pointed out that the greater the difference in size between the impurity ions and the host ions, the greater the decrease in "loosening" energy. As noted above, doping with $CaCl_2$ produces a greater increase in tan δ of KCl as compared with NaCl crystals. Probably the introduction of $CaCl_2$ loosens the KCl lattice to a greater extent. This is consistent with the ideas of Frenkel' regarding the influence of the size of the impurity ion on the decrease of the "loosening" energy. Structural studies also indicate a greater degree of loosening of the KCl lattice as compared with NaCl by the introduction of $CaCl_2$. According to Gromakov & Gromakova[13], KCl in mixture with $CaCl_2$ does not form solid solutions. In contrast, in the range of low $CaCl_2$ concentrations, NaCl does form solid solutions with this impurity, and the second phase forming at high $CaCl_2$ concentrations has much in common with the structure of NaCl and hence does not distort the NaCl structure to any appreciable extent.

The greater change in tan δ as a result of doping KCl with $CaCl_2$ as compared with doping with $BaCl_2$ can also be explained by the greater decrease of the "loosening" energy produced by calcium as compared with barium ions. The ionic radii of barium and potassium are close, which favors formation in a certain $BaCl_2$ concentration range of KCl-$BaCl_2$ solid solutions with an excess of KCl; hence the KCl lattice is less distorted by the introduction of $BaCl_2$ than by $CaCl_2$.

The introduction of $MgCl_2$ into KCl has the weakest effect on tan δ. The ionic radius of magnesium differs appreciably from the radius of potassium, which according to Frenkel' should make for an appreciable change of the "loosening" energy of the KCl lattice. Actually, however, this was not observed. Possibly, the weak influence of $MgCl_2$ impurity on tan δ in KCl is connected with the fact that the ionic radius of magnesium is small, so that the magnesium ions are distributed through the KCl lattice without producing an appreciable distortion in it

One can draw the following conclusions on the basis of our studies:

1. The temperature and frequency dependences of tan δ in doped crystals are similar to the dependences in "pure" crystals, which would appear to indicate that the same mechanism is responsible for dielectric losses in doped and undoped crystals.

2. The increase of tan δ in crystals with impurities is connected with loosening of the crystal lattice by the impurity and reduction of the energy of activation and dissociation of the crystal ions, which leads to increase in the number of free and weakly bound ions.

4. Dielectric loss in mixed crystals

On the basis of investigations of the dielectric loss in simple crystals and in solid solutions of alkali halides at high frequencies[1] it was established that in "pure" crystals tan δ increases with increase of the separation between ions in the crystal lattice, with decrease of the lattice energy and lowering of the melting point; these regularities change when it comes to solid solutions. In solid solutions there is an increase of energy loss as compared with "pure" single crystals. The temperature and frequency dependences of tan δ in solid solutions are characterized by a steeper rise of tan δ with decrease of frequency and increase of temperature.

A number of solid solution samples and their initial components were checked by spectroscopic analysis. It was found that there were present in the solid solution crystals only the impurities detected in the initial components. Hence the deviation of the temperature and frequency dependences of tan δ in the solid solutions from the dependences for the simple crystals cannot be explained by the influence of extraneous impurities or contamination. That extraneous impurities are not a factor is also indicated by the fact that the variation of tan δ as a function of the solid solution composition and the deviation of the temperature and frequency dependences of tan δ for solid solutions from the corresponding dependence for simple crystals obey certain regularities: the higher the concentration of the second component in the solid solution, the more tan δ differs in absolute value from tan δ in the initial component and the greater the departure of the temperature and frequency dependences from the corresponding dependences for simple crystals. All this indicates that the differences between the values and behavior of tan δ in solid solutions and in simple crystals must be attributed to the distinctive structural characteristics of the solid solutions.

As is known, the crystal lattice of solid solutions is looser than the lattice of simple, one-component crystals. The lattice of solid solutions differs from the lattice of simple single crystals by the presence of systematic distortions: imperfections or microdeformations. Microdeformations appear in the crystal lattice of solid solutions in the vicinity of sites occupied by ions of the second component with a radius differing from that of the host ions, and the number of such microdeformations increases with the increase of the second component concentration in the solid solution[17,18].

Distortion of the crystal lattice facilitates liberation or release of the ions from their position of equilibrium owing to reduction of the "loosening" energy.[16] This leads to increase in the number of ions participating in the conduction and increase in the number of weakly bound ions, more or less free to move in a limited volume of the crystal. Hence in solid solutions there is observed an increase of the energy loss. The number of distortions in the crystal lattice of solid solutions increases with increase in the concentration of the second component. This is accompanied by increase in the number of weakly bound and free ions, which is the factor responsible for the noted deviation of the dependences of tan δ in solid solutions from the corresponding dependences of tan δ in simple crystals.

The variation of tan δ in solid solutions with the composition in accord with the structureal characteristics of the solid solutions may be explained as follows: with increase in the concentration of the second component the number of microdeformations of the crystal lattice increases; this results in an increase in the number of weakly bound ions, the displacement of which within a small volume under the influence of the electric field is responsible for the relaxation losses. In addition, there is an increase in the number of ions participating in the conduction and hence responsible for the ohmic losses. The combination of the two factors explains the increase of tan δ with increase in the second component concentration. The conductivity of solid solutions is higher than that of simple crystals because the "loosening" energy of a lattice with extraneous impurities is lower than of a crystal lattice free of impurities. The observed increase of the conduction loss with decrease of frequency is explained by lowering of the maximum in the curve characterizing the variation of tan δ with the second impurity content (see Fig.4 in Ref.1). The earlier increase of tan δ in solid solutions as a function of the temperature is also connected with the greater conduction losses in solid solutions. The higher the concentration of the second component, the more distorted the crystal lattice, the greater the conduction losses, the greater the relative contribution to the total energy loss in the crystal, the lower the temperature at which the conduction losses become predominant and there becomes evident the sharp temperature dependence of tan δ characteristic of ohmic losses.

It is interesting to note that similar regularities in the behavior of tan δ as a function of the composition and temperature were also observed for solid solutions of ceramic type materials.[19,20] The lattice constant of solid solutions is approximately a linear function of their composition. The same is true of the crystal lattice energy, while the melting point of solid solutions as a function of the composition is characterized by a curve with a minimum. For alkali halide single crystals there is observed a parallel variation of the melting point and lattice energy. The mechanical strength, Brinnell hardness and microhardness increase with decrease of the separation between the ions forming the crystal lattice.[21] For solid solutions there is no analogy between the variation of their mechanical characteristics and their lattice constant: the lattice constant varies approximately as a linear function of the composition, while the mechanical characteristics are characterized by curves with a maximum.[22,23]

Consequently, the regularities governing the variation of the physical and chamical characteristics of solid solutions differ from the corresponding regularities for simple single crystals. In solid solutions tan δ as a function of the composition passes through a maximum. Consequently, the variation of tan δ in solid solutions varies more or less in parallel with the variation of their mechanical characteristics and inversely as regards the variation of the melting point. Actually tan δ in simple single crystals varies in the same manner, but in the case of solid solutions we do not have the correlation between the variation of tan δ and the variation of the lattice constant observed for simple single crystals.[1]

Conclusions

1. The dielectric loss mechanism in solid solution crystals is similar to the loss mechanism in simple crystals: the losses are made up of ohmic and relaxation losses associated with displacement of free and weakly bound ions in limited volumes under the influence of the applied electric field.

2. The dielectric loss in solid solution crystals is greater than the loss in simple crystals; this is connected with the structural features of the solid solutions, specifically with greater distortions of their crystal lattice.

3. The regularities governing the variation of the physical-chemical characteristics of solid solutions differ from the regularities for simple single crystals, which is also due to the distinctive characteristics of the structure of solid solutions.

G.F.Yarushevskaya participated in the experimental work in determining the influence of impurities on tan δ and the structure of the alkali halide crystals.

References

1. K.A.Vodop'yanov & G.I.Galibina, Izv.AN SSSR, Ser.fiz., 22, 288 (1958). (Trans.Bulletin 22, 287.)
2. K.A.Vodop'yanov & V.F.Ivlev, Zhur.tekh.fiz., 8, 1521 (1938).
3. B.N.Matsonashvili, Izv.AN SSSR, Ser.fiz.,22,296(1958). (Trans.Bull.22,294.
4. Yu.A.Sikorskii, Doklady AN SSSR, 54, 317 (1946).
5. M.A.Krivov, Trudy (Proceedings), Siberian Physical Technical Institute at Tomsk University, No.35, 3 (1956).
6. B.M.Gokhberg, Zhur.eksp.i teor.fiz., 1, 145 (1931).
7. A.Venderovich & B.Lapkin, Ibid., 9, 46 (1939).
8. D.N.Popov, Trudy (Proceedings), Siberian Physical-Technical Institute at Tomsk University, No.28, 379 (1949).
9. R.G.Breckenridge, J.Chem.Phys., 16, 959 (1948).
10. K.Nakamura, Sci.Rep.Tohoky, 25, 590 (1936).
11. B.I.Vorozhtsov, Izvestiya (Bulletin), Tomsk Polytechnic Institute, 91, 363 (1956).
12. E.V.Alekseevskii, Kolichestv. khimich. analiz (Quantitative chemical analysis), 138, 222 (1954).
13. S.D.Gromakov & L.M.Gromakova, Zhur.fiz.khim., 29, 36 (1955).
14. W.Lehfeld, Z.Phys., 85, 717 (1933).
15. R.Wagner & A.Hantelmann, J.Chem.Phys., 19, 17 (1951).
16. Ya.N.Frenkel', Kineticheskaya teoriya zhidkosti (Kinetic Theory of Liquids M., 1945.
17. H.Durham & B.Hawkens, J.Chem.Phys., 19, 44 (1951).

18. J.A.Wasastjerna, Phys.Rev., 55, 37 (1939).
19. A.I.Avgustinik & N.S.Antselevich, Zhur.fiz.khim., 27, 81 (1953).
20. N.S.Novosil'tsev & A.N.Khodakov, Zhur.tekh.fiz., 26, 215 (1956).
21. S.D.Dmitriev, Mikrotverdost' (Microhardness), Transactions of the Conference on Microhardness, M., 1956.)
22. A.P.Vrezhenevskii, Izvestiya SPb (Bulletin, St.Petersburg Polytechnic Institute), 14, 313 (1911).
23. A.N.Kislina, Bulletin, Tomsk Polytechnic Institute, 91, 125 (1956).

* * * * * * *

THERMAL EXPANSION, DIELECTRIC CONSTANT AND LOSS OF ALKALI HALIDE CRYSTALS

- V.V.Panchenko

Introduction

The theory of the dielectric constant of ionic crystals of the NaCl type encounters a number of difficulties. The principal ones are determination of the internal field in the crystal and evaluation of the constants which characterize the repulsive energy of the electron shells. The available experimental data are inadequate for correct calculation of these quantities and construction of a complete theory of permittivity.

Born was the first to deduce a formula relating the dielectric constant of a crystal with the square of the index of refraction and the polarization of the ionic displacement, which was found from the frequency of the natural vibrations of the ions. In 1934 Bretscher[1] obtained an expression for the temperature dependence of the dielectric constant. Bretscher measured the temperature coefficient of the dielectric constant (hereinafter TC of ϵ) for NaCl and compared it with the results given by his formula.

Eucken and Büchner[2] studied the dielectric constant of a large group of salts (including LiF, NaCl and KCl) in a wide temperature range. The results were compared with the values of ϵ given by the Born formula; the temperature coefficients of ϵ were determined and compared with the corresponding coefficients calculated according to the Bretscher formula. This check showed that the Bretscher formula, as a rule, yielded underestimates. The work of Eucken and Büchner is significant and important despite certain inadequacies (the experimental points were taken sparsely and no temperature dependence of TC of ϵ was detected).

Subsequently, the TC of ϵ of alkali halide crystals was measured by a number of investigators, but there were very few studies concerned with the temperature dependence of the coefficient itself and its relation to the other parameters and properties of the crystal. As shown by the calculations performed by Skanavi[6,7], the TC of ϵ for alkali halide crystals can be evaluated on the basis of the lattice constant, taking into account the mechanical and thermal properties of the crystal. It is apparent from these calculations that the TC of ϵ is temperature dependent.

Recently, there appeared two papers by Yamashita[8] in which a quantum-mechanical theory of the dielectric constant of ionic crystals is developed.

The present paper is devoted to a study of the temperature dependence of the dielectric constant and the coefficient of linear expansion of alkali halide single crystals and an analysis of the relation between these characteristics in a wide temperature range.

I. Some Problems of Theory

It is known that on the basis of the Lorentz expression for the effective field in the crystal

$$E = E_{\text{av}} + \frac{4}{3}\pi I, \tag{1}$$

where I is the electric moment per unit volume, one can obtain the Clausius-Mosotti equation

$$\frac{\varepsilon - 1}{\varepsilon + 2} = \frac{4}{3}\pi N(\alpha_1 + \alpha_2 + \alpha_i), \tag{2}$$

where α_1 and α_2 are the electronic polarizabilities of the ions, α_i is the ionic polarizability, and N is the number of ionic pairs per cm^3.

Mott and Gurney[9] infer that the nearest neighbor ions polarized by the field cannot interact like point dipoles; the fields acting on the cation and anion are found to be different. Setting the correction factor γ in the Mott formulas equal to zero, we obtain the following expression for the dielectric constant:

$$\varepsilon = \varepsilon_\infty + \frac{4\pi 2\,\dfrac{Nq^2}{k}}{1 - \dfrac{4}{3}\pi\,\dfrac{2Nq^2}{k}}, \tag{3}$$

where ε_∞ is the square of the index of refraction, k is the elastic coupling constant for unlike ions, and q is the ion charge.

We note, however, that these formulas are approximate, because they are based either on the point model of a crystal (the Clausius-Mosotti formula) or include undetermined parameters (Eq.(3)). In connection with this, Skanavi[6,7] subdivides all cubic ionic crystals into three groups.

The first group (lithium salt crystals) is characterized by a large difference between the radii and electronic polarizabilities of the anions and cations. The point model and all calculations based thereon are obviously not applicable to this group.

The second group (sodium salt crystals) is intermediate. A quantitative relation between the mechanical properties and the dielectric constant should exist only when the anions and cations are similar in size and electronic polarizabilities.

The third and largest group (potassium, rubidium and cesium salt crystals) is characterized by the fact that the anion and cation radii and electronic polarizabilities are close in magnitude. The point model is applicable to crystals of this group. For this group, calculations based on almost all variants of theory should lead to satisfactory agreement with experiment.

For crystals of the second and third groups of the Skanavi classification (i.e., sodium, potassium and rubidium salts), calculations of the TC of ϵ can be based on the Clausius-Mosotti equation either with the Mott correction (3) or without it (2). Differentiation of Eqs.(2) and (3) with respect to temperature gives

$$\frac{1}{\varepsilon}\cdot\frac{d\varepsilon}{dT} = \frac{(\varepsilon+2)^2}{3\varepsilon}\left[(n-1)\frac{\varepsilon-1}{\varepsilon+2} - (n+2)\frac{\varepsilon_\infty - 1}{\varepsilon_\infty + 2}\right]\cdot\alpha_l, \tag{4}$$

where ε_∞ is the square of the index of refraction, α_l is the coefficient of linear expansion (CLE), n is the exponent in the expression for the repulsive energy of electron shells, and

$$\frac{1}{\varepsilon}\cdot\frac{d\varepsilon}{dT}=\frac{4}{3}\pi\alpha l\left\{\frac{1.16\,(n-1)^2}{\left[1.16\,(n-1)-\frac{4}{3}\pi\right]^2}-\frac{3N\alpha_1}{\left(1-\frac{4}{3}\pi N\alpha_1\right)^2}-\frac{3N\alpha_2}{\left(1-\frac{4}{3}\pi N\alpha_2\right)^2}\right\}, \qquad (5)$$

As we see, there exists a relation between the CLE of a crystal and the TC of ϵ. It may be assumed that for crystals to which the point model is applicable, Eq.(4) will give the correct order of magnitude of the TC of ϵ.

Yamashita[8] calculated the crystal energy by applying the variational method of Slater and Kirkwood, and computed the dielectric constant, using the known relations

$$\Delta A=-\frac{1}{2}\chi E^2$$

and

$$\varepsilon-1=4\pi N\chi,$$

where ΔA is the change in energy caused by a uniform external field E, χ is the dielectric susceptibility and N is the number of ion pairs per unit volume.

In the presence of an external field, the wave function for the $2p$ electrons of the F^- ion was taken by Yamashita as

$$\psi=\psi_0(r)\,(1+\lambda r\cos\theta)=\frac{P(r)}{r}(1+\lambda r\cos\theta),$$

where

$$P(r)=A\,[e^{-3.05r}+0.095e^{-1.25r}]\,r^2,$$

λ is a variational parameter, and A is the normalization constant.

Yamashita neglected the variation of the $2s$ wave functions of the negative ion and the entire wave function of the positive ion, because the polarizability of the latter is small compared to that of the negative ion.

The calculations were carried out for a high-frequency field and for a static field. The value obtained for the dielectric constant of LiF (namely, 10.1) is close to the experimental value. The temperature variation of the dielectric constant was determined from the variation of the free energy. The TC of ϵ following from Yamashita's theory is also temperature dependent.

II. Experimental Part

1. Investigation of the coefficient of linear expansion

Measurements of the coefficient of linear expansion (CLE) and its temperature dependence were carried out in a specially constructed capacitive dilatometer, and also in a quartz dilatometer designed by Strelkov[10]. The elongation gage in the capacitive dilatometer is a capacitor, the capacitance of which varies with change in the linear dimensions of the crystal. The capacitance of the measuring capacitor was measured with the aid of a beat oscillator. The temperature was measured by means of chromel-alumel and platinum-platinrhodium thermocouples. The thermocouple emf was measured by a PP type potentiometer, a low-resistance dc PPTN-1 type potentiometer or a mirror galvanometer, the temperature being determined to within 0.5°. Temperature regulation was realized by means of a temperature control unit incorporating a thyratron.[10]

We investigated the CLE of LiF, NaF, NaCl, KCl, KBr and KI single crystals in the range from room temperature to 650-700°, i.e., up to temperatures close to the melting points. The crystals were grown from melts by the Kyropoulos technique.

The CLE of all the crystals increased with temperature. The temperature dependences of CLE for LiF, NaF and NaCl are presented in Fig.1; those for KCl, KBr and KI crystals are given in Fig.2. Our results for the temperature dependence

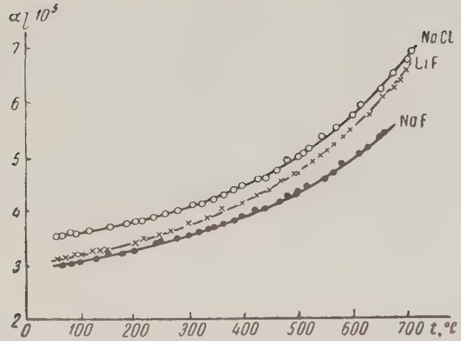

Fig.1. Coefficient of linear expansion as a function of temperature for LiF, NaF and NaCl crystals.

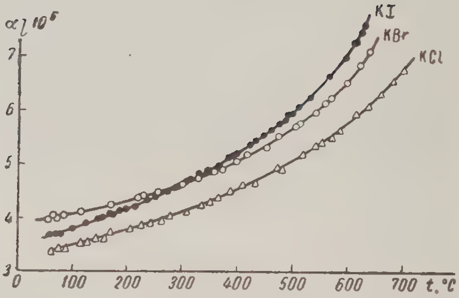

Fig.2. Coefficient of linear expansion as a function of temperature for KCl, KBr and KI crystals.

of the CLE of NaCl differ somewhat from those given in the literature[11,12]. In general, the values obtained with the capacitive dilatometer are in good agreement with those obtained on the Strelkov quartz dilatometer. Apparently, the discrepancy for α_l of NaCl, which exceeds the limits of the measurement error, is explained by the fact that crystals of different origins and hence with somewhat different properties were used in the two series of measurements. Strelkov[10] investigated natural crystals from the Bakhmut district; Dannöhl worked with crystals grown from a melt.

Analyzing the results, we note certain regularities. Thus comparing the temperature behavior of the CLE of the three potassium halides (Fig.2), we see that at low temperatures the CLE of KI is larger than the coefficient of KBr, which in turn is larger than that of KCl. In addition, the α_{KI} vs t curve is steeper than the α_{KCl} vs t curve which in turn is steeper than the α_{KBr} vs t curve. Consequently, among the potassium halides, the highest high-temperature CLE and strongest temperature dependence of the coefficient is exhibited by the compound with the anion having the highest atomic number or largest number of electron shells.

Strelkov[12] found a similar temperature behavior of the CLE in investigating AgCl and AgBr crystals. Comparing the coefficients of NaF and NaCl (Fig.1), we note a regularity similar to that for potassium halides: the CLE of NaCl is larger and its temperature dependence is steeper than those of NaF, although the differences are less marked than in the case of the potassium salts.

Inasmuch as the electronic polarizability in I is greater than in Br, and greater in Br than in Cl, we infer that the temperature dependence of the CLE in a series of halides of a given metal is stronger in the compounds in which the anion has the greater polarizability.

2. Investigation of the dielectric constant

The dielectric constant of the LiF, NaCl, NaF, KCl and KBr crystals was measured with a Q-meter by the null method and by the method of secondary beats. The plates and filaments of the beat oscillator tubes were supplied from storage batteries. An oscillograph was used as an indicator when employing the beat procedure. The measurements were carried out at different frequencies in the temperature range from 20 to 450-500°C.

We could not use mercury electrodes, since they can be employed only at low temperatures. It was impossible to use electrodes applied by cathode sputtering because the thin metal coating is corroded by halide ions at high temperatures. Fired on silver electrodes were also unsuitable because the crystal becomes contaminated in the process of application. Therefore, initially we used polished metal electrodes of nichrome or nickel in the form of disks 10 to 18-20 mm in diameter and 1 to 1.7 mm thick. Subsequently, we standardized on electrodes of chemically pure nickel, because it was found that they do not react with halides at high temperatures. The crystal samples were ground flat to within 3 μ and measured 20 x 20 x (1.3 to 0.8) mm. The dielectric constant was calculated by means of the following formula which takes into account the edge effect:

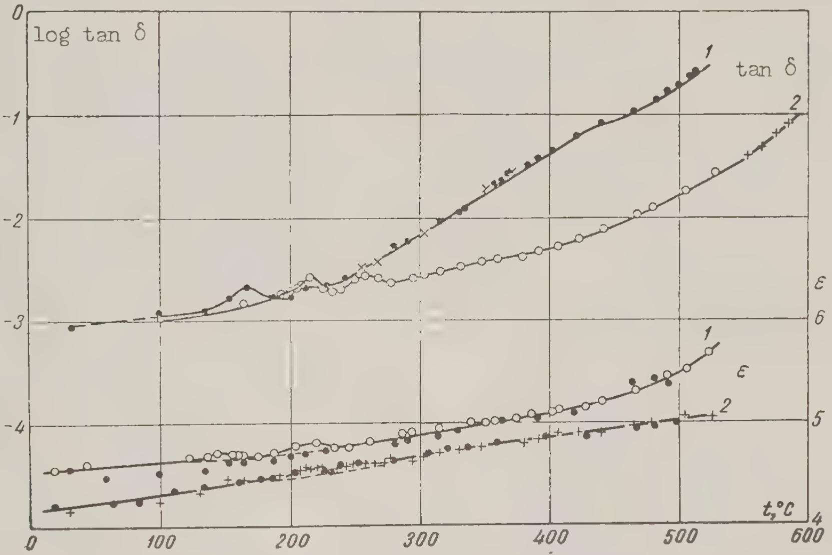

Fig.3. Variation of tan δ and ε with temperature for KCl: 1) 1 Mc, 2) 10 Mc. Tan δ: ● & O - heating, X - cooling; ε: + & ● - Q-meter measurements, O - measurements by the beat procedure.

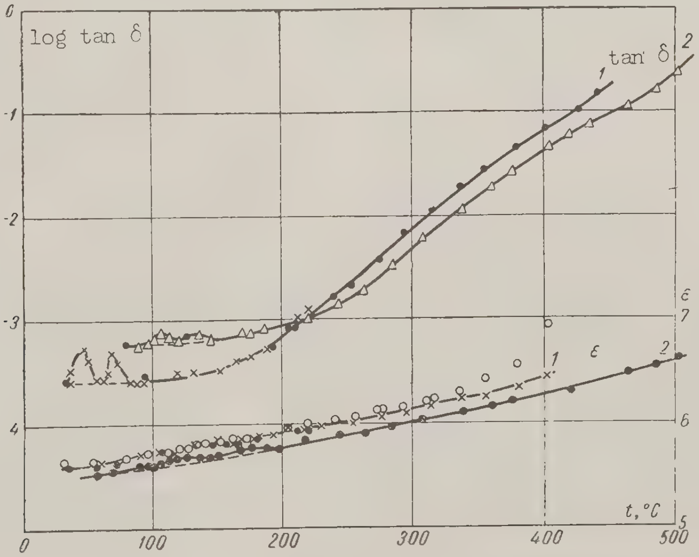

Fig.4. Variation of tan δ and ε with temperature for NaCl: 1) 1 Mc, 2) 3 Mc. Tan δ: ● & △ - heating, X - cooling; ε: X & ● - Q-meter measurements, O - measurements by the beat procedure.

$$C = \frac{\varepsilon R^2}{4d} + \frac{\varepsilon R}{4\pi}\left\{\ln\frac{16\pi(d+b)R}{d^2} + \frac{b}{d}\ln\frac{b+d}{b} - 3 + \frac{4}{\varepsilon}\right\},$$

where R is the electrode radius, b is the electrode thickness, and d is the thickness of the dielectric. The maximum error in determining ϵ did not exceed 10% in the measurements with the Q-meter and 2% in the measurements by the beat method.

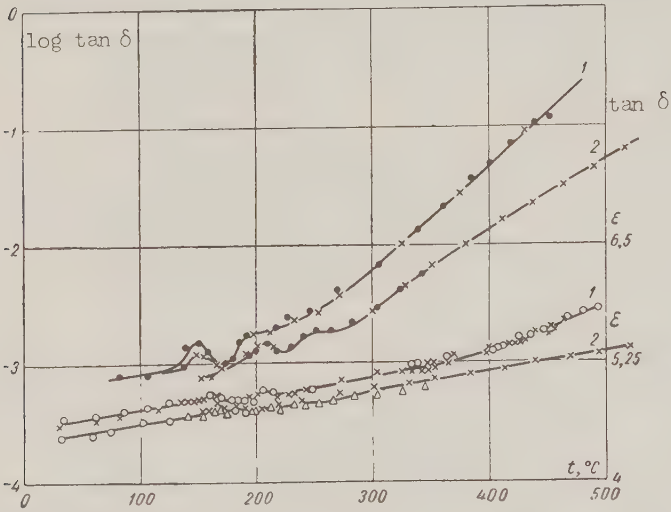

Fig.5. Variation of tan δ and ϵ for KBr: 1) 930 kc, 2) 3.5 kc. Tan δ: ● - heating, X - cooling; ϵ: X & Δ - Q-meter measurements, O - measurements by the beat procedure.

In order to eliminate the effect of moisture, all the samples were dessicated for 2-3 hours at 300° before the measurements. The results of the dielectric constant measurements are shown in Figs.3, 4 & 5. The dielectric constant of all the samples increased with temperature in the indicated temperature range. At low temperatures ϵ increases almost linearly with temperature. With a further increase of temperature, one observes a more rapid increase in the dielectric constant. Inasmuch as the conductivity of alkali halide crystals increases sharply with temperature, the beat method could be used only up to a certain temperature for each crystal. As is apparent from the figures, the beat procedure begins to yield incorrect results for NaCl from approximately 320°; for LiF from ~360°, etc. Below these "critical" temperatures the data obtained with the Q-meter and by the beat procedure agree satisfactorily. Small deviations from the smooth ϵ vs t curve (a sharp increase and then a small drop) are obtained for some samples, but these deviations for the most part lie within the limits of experimental error.

The experimental temperature coefficients of the dielectric constant were determined for all the enumerated halides.

3. Investigation of the loss tangent

One of the first investigations of dielectric losses in ionic crystals was that of Bogoroditskii & Malyshev[13], published in 1934. It was assumed for a long time thereafter that the losses in alkali halide crystals are conduction losses. Breckenridge[14] first discovered weakly defined maxima of relaxation losses in alkali halide crystals and silver halides after preliminary heat treatment of the samples. Subsequently, other investigators[15-21] obtained similar results.

One must particularly note the work of Matsonashvili[19] who investigated a large group of crystals in vacuum in a wide range of temperatures and frequencies. However, present data on losses in crystals are contradictory: some authors[22,23] did not observe the characteristic relaxation loss maxima for alkali halide crystals.

We investigated the temperature dependence of the loss tangent at two or more frequencies in the same temperature range as in the dielectric constant measurements. All the investigated samples exhibited two relaxation maxima in the

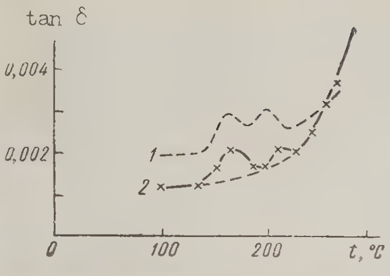

Fig.6. Variation of tan δ with temperature for KCl: 1) data of Konda & Suita[15] (2.6 Mc), 2) our data (1 Mc).

temperature variation of tan δ (Figs.3-5)*. None of the samples were subjected to preliminary heat treatment (other than drying at 300°). The maxima are shifted regularly towards higher temperatures with increase in frequency. Owing to appreciable hygroscopicity satisfactory results in measuring tan δ for some crystals (for example, NaCl) can be obtained only in the case of the reverse run (i.e., in cooling). The values of the higher tan δ maximum in almost all cases are well above the limits of the experimental error, so there can be no doubt regarding the existence of this maximum. The second maximum is always somewhat lower than the first and is often within the limits of the experimental error. The loss angle increases approximately exponentially with temperature; at high temperatures (400-500°), however, there is some deviation from the exponential law. The rises of tan δ are accompanied by changes of ϵ (as noted above), but in most cases the change is minor. In the reverse (cooling) curves for some crystals, the tan δ maxima are somewhat smoothed out.

Table 1

	LiF	NaF	NaCl	KCl	KBr
U_2	2,20	2,25	1,72—2,60	1,90—2,06	1,83—1,97
U	0,55	1,20	0,191	0,82	0,40
U_1	0,58	0,74	0,65	0,78	0,53

We calculated the activation energy U (in ev) of the relaxing groups from the shifts of the tan δ temperature maxima. The values deduced for U from the shift of the first maxima are compared with the values of the activation energy U_1 obtained by Breckenridge[14] and U_2 calculated by Lehfeld[20] on the basis of high temperature conductivity are juxtaposed in Table 1. It will be evident that the values of U obtained by us are close to the activation energies found by Breckenridge on the basis of measurements at audio frequencies (except for NaF).

As might be expected, the activation energy in the case of relaxation processes is 3-4 times lower than in the case of conduction. The values U calculated from the shift of the second maxima, as a rule, are slightly higher than the values computed from the shift of the first maxima.

The spectroscopic analyses of the crystals showed presence of various impurity elements (Ca, Mg, Sr, Si and Al), which were either inadvertently introduced in the process of crystal growth or were present as contaminants in the initial materials.

The relaxation losses observed by us can be explained in terms of reorientation of complexes comprised of either a) a cationic vacancy and a divalent impurity ion[14,19], or b) a cationic vacancy and an anionic vacancy[14,19,24]. Inasmuch as the activation energy calculated from the shift of the second maxima is always somewhat higher, one can assume, according to Grimley[24], that the first maximum is the result of reorientation of pairs of opposite-polarity vacancies, and the second maximum is the result of reorientation of pairs consisting of a cationic vacancy and an impurity ion. In view of the closeness of the activation energy values of different complexes, one may also assume that a dislocation mechanism[5,19] is involved.

---

*Two relaxation maxima in the temperature variation of tan δ were observed by Konda & Suita[15] for NaCl and KCl (Fig.6) and by Matsonashvili[5] for NaCl and CsBr.

III. Discussion

We carried out calculations of the temperature coefficient of the dielectric constant on the basis of the value of the lattice constant and the experimental coefficient of linear expansion of the crystals and taking into account the temperature dependence of the dielectric constant. The calculations were carried out by means of Eq.(4) based on the Clausius-Mosotti equation and Eq.(5) which was obtained by introducing the Mott correction.

The power law was used for the repulsion of electron shells. The values of the exponent n in the expression for the repulsive energy of the electron shells were taken from the calculations of Hildebrand[25] and Slater[26]. These values are probably the most reliable to be found in the literature. The electronic polarizabilities were taken from the work of Born & Heisenberg[27] and Pauling[28].

Table 2

t, °C	TC of $\varepsilon \cdot 10^5$				
	Exper.	$(4)_{Sl}$	$(4)_H$	$(5)_H$	$(5)_{Sl}$
40	34,7	21,12	29,93	25,29	36,60
100	44,7	21,94	30,88	25,42	36,80
200	61,4	24,00	33,74	26,19	37,89
300	87,6	27,40	38,37	28,18	40,80
400	101,0	32,49	45,40	31,00	44,97

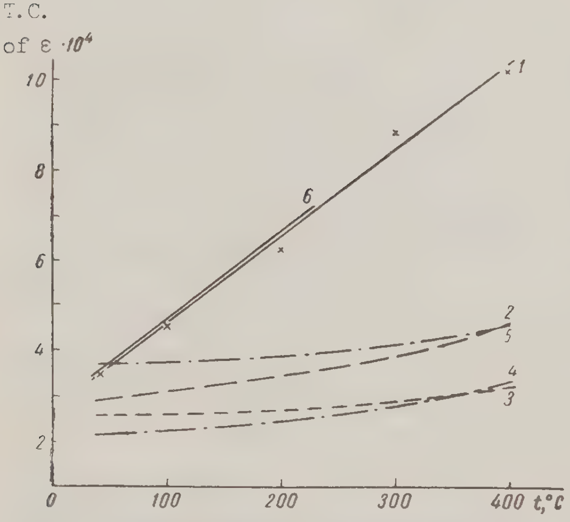

Fig.7. Comparison of the experimental temperature coefficient of ϵ for NaCl with the theoretical values: 1 - our data, 2 - $(4)_H$, 3 - $(5)_H$, 4 - $(4)_{Sl}$, 5 - $(5)_{Sl}$; 6 - Narasimhan's data. H = = Hildebrand's values, Sl = Slater's values of n.

We also made evaluations of the TC of ϵ using the exponential law for the electron shell repulsion, taking into account van der Waals forces. For LiF a comparison was made with the TC of ϵ obtained from the Yamashita theory.

In Table 2 and Fig.7 the experimental temperature coefficients of ϵ for NaCl are compared with the theoretical values obtained according to Eqs.(4) and (5) (the values of n were taken from the work of Hildebrand (H.) and Slater (Sl.). Figs.8,9 and 10 show the corresponding curves for KBr, KCl and LiF. It will be seen that the TC of ϵ varies linearly over a wide temperature range.

In the same figures, we have plotted the data of Narasimhan[4] for NaCl and LiF. It will be apparent that our values for NaCl are in good agreement with the results of Narasimhan. Our values for LiF are lower than those of Narasimhan and our rise of the TC of ϵ is less steep.

It will be evident that the experimental TC of ϵ in all cases increases more rapidly with temperature than the theoretical coefficient calculated by means of Eqs.(4) & (5), assuming the power law for shell repulsion. It will be noted, however, that the results obtained using the exponential law do not yield any better agreement with the experimental results.

Eq.(4) gives a steeper rise of the TC of ϵ. We see that for LiF, Eq.(4) gives results closer to the experimental values than does Eq.(5). Application of Eq.(5) containing the Mott correction to LiF gives unsatisfactory results for the TC of ϵ. Eq.(3), on which the derivation of Eq.(5) is based, rests on the assumption that neighboring ions polarized by the field cannot interact as point dipoles. Hence Eq.(5) should yield better

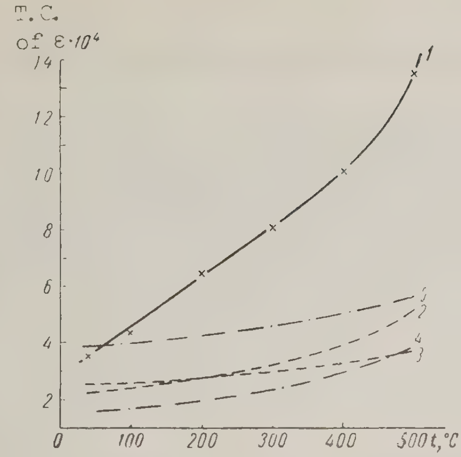

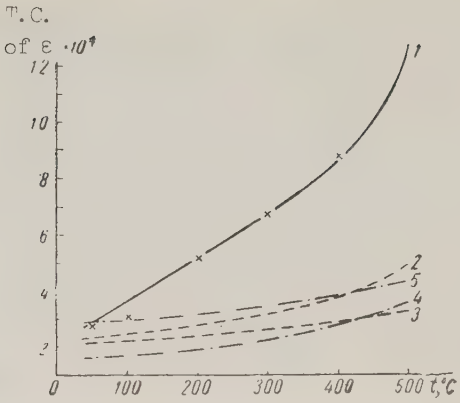

Fig.8. Comparison of the experimental TC of ϵ for KBr with the theoretical values: 1 - our data, 2 - $(4)_H$, 3 - $(5)_H$, 4 - $(4)_{S1}$, 5 - $(5)_{S1}$.

Fig.9. Variation of the TC of ϵ with temperature for KCl: 1 - experiment, 2 - $(4)_H$, 3 - $(5)_H$, 4 - $(4)_{S1}$, 5 - $(5)_{S1}$.

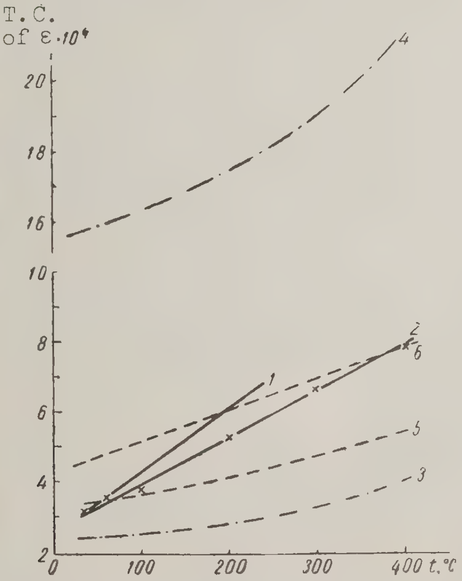

Fig.10. Variation of the TC of ϵ for LiF: 1 - Narasimhan's data, 2 - our data, 3 - $(4)_{S1}$, 4 - $(5)_{S1}$, 5 & 6 - Yamashita's results (5 - with the term $\Delta(K-TS)$ taken into account, 6 - the $\Delta(K-TS)$ term neglected).

results than (4), but actually the values of the TC of ϵ given by (5) are too high. We note that the introduction of the factor γ into the Lorentz internal field on the hypothesis that the nearest neighbors cannot interact as point charges is somewhat formal inasmuch as the Lorentz factor takes into account the field produced by distant ions.

The TC of ϵ for LiF obtained from the Yamashita theory, which takes into account ionic deformation, appears to be in closest agreement with experiment; but here, too, the calculated coefficient increases more slowly with temperature than the experimental coefficient. The TC of ϵ calculated taking into account the term $\Delta(K-TS)$ (K is the kinetic energy of the ionic vibrations, and S is the entropy) is closest to the experimental value at low temperatures, and increases more rapidly with temperature than the other calculated coefficients.

It will be evident that according to Eqs.(4) and (5) that the temperature dependence of the TC of ϵ is determined primarily by the temperature dependence of the CLE of the crystal. This is explained by the fact that Eqs.(4) and (5) were derived on the assumption that the polarization of the ionic displacement and, consequently, the elastic coupling constant vary only as a result of a change in the separation between ions.

Yamashita's results for the TC of ϵ are also determined mainly by the temperature dependence of the coefficient of thermal expansion. In practice, however, the TC of ϵ increases more rapidly with temperature than α_l.

Narasimhan suggests that the discrepancy between theory and experiment can also be explained by neglect of the long-range forces and by the fact that the calculation of the repulsive energy from the compressibility data may be inaccurate. Equations (4) and (5) were also derived taking into account the interaction only between the nearest (six) ions.

The numerical results obtained in using different values of n and ρ differ by 40 to 70%. Therefore the accuracy in evaluating the TC of ϵ depends on how precisely the constants n or ρ are determined from the compressibility data. On the other hand, the uncertainty introduced by inaccuracy in evaluating the repulsive energy can hardly have an appreciable effect on the character of the TC of ϵ.

I wish to express my gratitude to G. I. Skanavi for his interest in the work and discussion of the results.

Stalingrad Pedagogical Institute

References

1. E.Bretscher, Trans.Faraday Soc., 30, 684 (1934).
2. A.Eucken & A.Büchner, Z.phys.Chem. 13, 8, 27, 321 (1934).
3. M.S.Chmutin, Zhur.eksp.i teor.fiz., 26, 640 (1954).
4. P.T.Narasimhan, Proc.Nat.Inst.Sci.India A, 21, 133 (1955).
5. B.N.Matsonashvili, Izv.AN SSSR, Ser.fiz., 22, 296 (1958). (Trans.Bulletin, 22, 294.)
6. G.I.Skanavi, Dissertation, FIAN, M., 1945.
7. G.I.Skanavi, Zhur.eksp.i teor.fiz., 17, 390 (1947).
8. J.Yamashita, Progr.Theoret.Phys., 8, 280 (1952); Ibid., 12, 454 (1954).
9. H.Mott & P.Gurney, Electronic Processes in Ionic Crystals, Oxford Univ., 1940. (Cited in Russian trans.)
10. P.G.Strelkov, G.I.Kosourov & B.N.Samoilov, Izv.AN SSSR, Ser.fiz., 17, No.3 (1953).
11. A.Eucken & W.Dannöhl, Z.Electrochem., 40, 814 (1934).
12. V.F.Gaukovskii & P.G.Strelkov, Zhur.eksp.i teor.fiz., 7, No.4 (1937).
13. N.P.Bogoroditskii & V.N.Malyshev, Zhur.tekh.fiz., 4, 1306 (1934).
14. R.G.Breckenridge, J.Chem.Phys., 16, 959 (1948); 18, 913 (1950).
15. S.Konda & T.Suita, J.Phys.Soc.Japan, 5, 375 (1950).
16. I.Haven, J.Chem.Phys., 21, 171 (1953).
17. E.Burstein, J.Davisson & N.Sclar, Phys.Rev., 96, 819 (1954).
18. J.Dryden & N.Rao, J.Chem.Phys., 25, 222 (1956).
19. B.N.Matsonashvili, Zhur.eksp.i teor.fiz., 31, 1110 (1956). (Trans.Soviet Physics - JETP.)
20. W.Lehfeld, Z.Phys., 85, 717 (1933).
21. I.A.Voitsekhovskaya, L.A.Golubeva & E.V.Tyutyunnikova, Zhur.tekh.fiz., 27, 1591 (1957). (Trans.Soviet Physics - Technical Physics.)
22. G.Jacobs, Naturwissenschaften, 42, 575 (1955).
23. K.A.Vodop'yanov & G.I.Galibina, Izv. (Bulletin), Tomsk Polytechnic Institute, 91, 269 (1956).
24. T.B.Grimley, J.Chem.Phys., 17, 496 (1949).
25. J.Hildebrand, Z.Phys., 67, 127 (1931).
26. J.Slater, Phys.Rev., 23, 488 (1924).
27. M.Born & W.Heisenberg, Z.Phys., 23, 388 (1924).
28. L.Pauling, Proc.Roy.Soc.A, 114, 191 (1927).
29. G.I.Skanavi, Fizika dielektrikov (Physics of Dielectrics), M., 1949.

RELAXATION OF POLARIZATION AND LOSSES IN ALKALI HALIDE SINGLE CRYSTALS

- V.N.Lozovskii

Breckenridge[1] in 1948 discovered, and other authors[2-9] subsequently confirmed, the existence of relaxation dielectric losses in alkali halide crystals. At present it is generally accepted that the relaxation losses in such crystals are associated, in particular, with the presence of complexes consisting of divalent impurity cations and cationic vacancies. The process of reorientation of the complexes under the influence of an external electric field can be realized by a) interchange of the positions of the complex components, b) motion of the cationic vacancy about the impurity ion within coordination sphere II (unexcited complex) or c) motion of the vacancy about the impurity ion with transition of the vacancy into coordination sphere IV, VI, etc., (different degrees of excitation of the complex).

The relaxation of complexes can be described in the linear approximation by the set of equations (1), (see page 152) where $4n_1$ is the number of vacancies per cm^3 of the crystal, occupying any of four possible positions in the $x=a$ plane in coordination sphere II (Fig.1). Here a is the lattice constant. It is assumed that for the plane occupied by the impurity ion $x = 0$. $4n_2$ and $4n_3$ have the same meaning but pertain to the planes for which $x = 0$ and $x = -a$, respectively; m_1, $4m_2$ and m_3 are the numbers of vacancies per cm^3 located in coordination sphere IV and planes $x = 2a$, $x = 0$ and $x = -2a$, respectively; $4k_1$, $8k_2$, $8k_3$ and $4k_4$ are the numbers of vacancies in coordination sphere VI and planes $x = 2a$, $x = a$, $x = -a$ and $x = -2a$, respectively; ω_1 is the probability per second that a vacancy will transfer from one location in coordination sphere II to a neighboring location in the same coordination sphere; ω_2 is the probability for interchange of positions by a vacancy and a divalent impurity ion; ω_3 is the probability for transition of a vacancy from coordination sphere IV to one of the positions in coordination sphere II, and ω_4 is the probability for the reverse transition; ω_5 and ω_6 are the probabilities of forward and reverse transitions of vacancies between positions in coordination spheres VI and II; ω_7 and ω_8 are the probabilities for forward and reverse transitions of vacancies between positions in coordination spheres VI and IV; ω_9 and ω_{10} are the probabilities for transitions of vacancies from one position to any other position in coordination sphere VI (in the absence of an electric field $\omega_9 = \omega_{10}$); t is the time.

The set of equations (1) is based on the general principles of the theory of thermal ionic polarization.[10] Fundamental to construction of this set is not the process of polarization as such, but the inverse process of establishment of an equilibrium distribution of vacancies over all possible positions after sudden removal of the external field.

The number of equations in set (1) is very large. However, complexes with a high degree of excitation are encountered much less frequently than unexcited or slightly excited complexes. Moreover, in the case of a great separation between the vacancy and the divalent impurity ion their interaction energy becomes comparable to kT and such a pair can no longer be considered a complex[11]. Hence we can limit our consideration to transition of vacancies only to coordination spheres close to sphere II. The set as written out here takes into account single and double excitation of the complexes.

The purpose of the present work is to check the hypothesis of Lidiard[12] to the effect that the frequency broadening of the loss peak observed by Haven[2] can be explained by taking into account only single and double excitation of the complexes.

Preliminary consideration of the set of equations enclosed in the dashed-line rectangle (unexcited complexes) and the set enclosed in the solid line (singly

$$\begin{aligned}
\frac{dn_1}{dt} &= -n_1\omega_2 + n_3\omega_2 + 2n_2\omega_1 - 2n_1\omega_1 - 2n_1\omega_4 + m_1\omega_3 + m_2\omega_3 - 4n_1\omega_6 + 2k_2\omega_5 + 2k_1\omega_5 + \ldots \\
\frac{dn_2}{dt} &= 2n_1\omega_1 - 4n_2\omega_1 + 2n_3\omega_1 - 2n_2\omega_4 + 2m_3\omega_3 - 4n_2\omega_6 + 2k_2\omega_5 + 2k_3\omega_5 + \ldots \\
\frac{dn_3}{dt} &= n_1\omega_2 - n_3\omega_2 + 2n_2\omega_1 - 2n_3\omega_1 - 2n_3\omega_4 + m_2\omega_3 + m_3\omega_3 - 4n_3\omega_6 + 2k_3\omega_5 + 2k_4\omega_5 + \ldots \\
\frac{dm_1}{dt} &= -4m_1\omega_3 + 4n_1\omega_4 - 4m_1\omega_8 + 4k_1\omega_7 + \ldots \\
\frac{dm_2}{dt} &= -4m_2\omega_3 + 2n_2\omega_4 + n_1\omega_4 + n\omega_4 - 4m_2\omega_8 + 2k_2\omega_7 + 2k_3\omega_7 + \ldots \\
\frac{dm_3}{dt} &= -4m_3\omega_3 + 4n_3\omega_4 - 4m_3\omega_8 + 4k_4\omega_7 + \ldots \\
\frac{dk_1}{dt} &= -2k_1\omega_5 - k_1\omega_7 - 2k_1\omega_9 + 2n_1\omega_6 + m_1\omega_8 + 2k_2\omega_{10} + \ldots \\
\frac{dk_2}{dt} &= -k_2\omega_{10} + k_1\omega_9 - 2k_2\omega_5 + n_1\omega_6 + n_2\omega_6 + m_2\omega_8 - k_2\omega_7 + \ldots \\
\frac{dk_3}{dt} &= -k_3\omega_{10}k_4\omega_9 - 2k_3\omega_5 + n_3\omega_6 + n_2\omega_6 + m_2\omega_8 - k_3\omega_7 + \ldots \\
\frac{dk_4}{d} &= -2k_4\omega_9 + 2k_3\omega_{10} - 2k_4\omega_5 + 2n_3\omega_6 + n_3\omega_8 - k_4\omega_7 + \ldots \\
&\ldots\ldots\ldots\ldots\ldots\ldots\ldots\ldots\ldots\ldots \\
&\ldots\ldots\ldots\ldots\ldots\ldots\ldots\ldots\ldots\ldots
\end{aligned} \qquad (1)$$

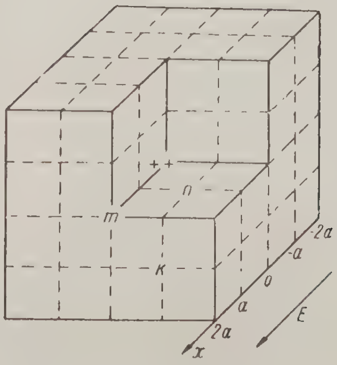

Fig.1. Diagram of the section of an NaCl type lattice containing a divalent impurity cation. ++ - position of the divalent impurity ion; *n* - one of the 12 positions closest to the impurity position which a vacancy can occupy as a result of reorientation of the complex (coordination sphere II); *m* - one of the 6 positions located in coordination sphere IV; *k* - one of the 24 positions in coordination sphere VI.

excited complexes) showed that taking into account the excitations leads to the maximum effect in the case of equality of all the parameters:

$$\omega_i\,(\omega_1 = \omega_2 = \omega_3 = \ldots).$$

This is fully understandable from the physical standpoint. Actually, equality of the probabilities for a vacancy jumping over different potential barriers corresponds to complete absence of distortion of the potential contour close to the impurity ion and, consequently, to equally probable distribution of the cationic vacancies over different positions in coordination spheres II, IV, VI, etc. This situation is possible only in the absence of interaction between the impurity ions and vacancies. Under actual conditions, however, the cationic vacancy tends to approach the divalent cation, and since it has an effective negative charge and moreover approaches an unlike ion, it partially relieves the local stresses produced by this ion in the lattice. The existence of interaction between impurity ions and vacancies leads to the fact that the probability of finding a vacancy at some position in coordination sphere II will be greater than the similar probability for finding it in spheres IV, VI, etc. The stronger the given interaction, the more appreciable will be this effect and the less important the role played by the excited complexes. This is illustrated by the curves of Fig.2. In this figure we have plotted the dielectrically active relaxation times τ_1 and τ_2 against the corresponding polarizabilities α_1 and α_2, and the total polarizability α_{tot} calculated per impurity atom. All these values were obtained by direct solution of the set of differential equations surrounded by the solid line. Specifically, we have

$$\alpha_1 = \frac{pa^2q^2\left[\exp\left(-\frac{V}{kT}\right)(B - 2\omega_3 + B_1) + 2\omega_4\right]\cdot[2\omega_4 - B + 2\omega_3 + B_1]}{6kT\cdot B_1\cdot\omega_4}, \tag{2}$$

$$\alpha_2 = \frac{pa^2q^2\left[\exp\left(-\frac{V}{kT}\right)\cdot(B - 2\omega_3 - B_1) + 2\omega_4\right]\cdot[B - 2\omega_3 + B_1 - 2\omega_4]}{6kT\cdot B_1\cdot\omega_4}, \tag{3}$$

$$\alpha_{\mathrm{tot}} = \frac{2pa^2q^2}{3kT}\cdot\left[1 + \exp\left(-\frac{V}{kT}\right)\right], \tag{4}$$

$$\tau_1 = \frac{1}{B + 2\omega_3 - B_1}, \qquad \tau_2 = \frac{1}{B + 2\omega_3 + B_1}, \tag{5}$$

where $$B = \omega_1 + \omega_2 + \omega_4, \quad B_1 = \sqrt{(B - 2\omega_3)^2 + 4\omega_3\omega_4},$$

V is the energy acquired by a vacancy in going from some position in coordination sphere IV to any position in coordination sphere II, q is the effective charge of a cationic vacancy, a is the lattice constant, p is the degree of association of the cationic vacancies and the divalent impurity ions $(0 \leqslant p \leqslant 1)$.

In plotting the curves of Fig.2 it was assumed that

$$\omega_1 = \omega_2, \tag{6}$$

$$\omega_3 = \omega_4\cdot\exp\left(\frac{V}{kT}\right) = \exp\left(\frac{V}{2kT}\right), \tag{7}$$

$$\omega = \frac{\nu}{3}\exp\left(-\frac{U}{kT}\right), \tag{8}$$

where ν is the frequency of vibration of cations neighboring on the vacancy, and u is the height of the potential barrier in the undistorted part of the lattice.

Under actual conditions, equality (6) is unlikely. However, for any values of $\omega_2 < \omega_1$ the results are virtually the same. With increase of ω_2 $(\omega_2 > \omega_1)$ we arrive in the limit to the case when the process of relaxation of a complex is realized only through interchange in the positions of the vacancy and the impurity ion and the loss peak is of the Debye type.

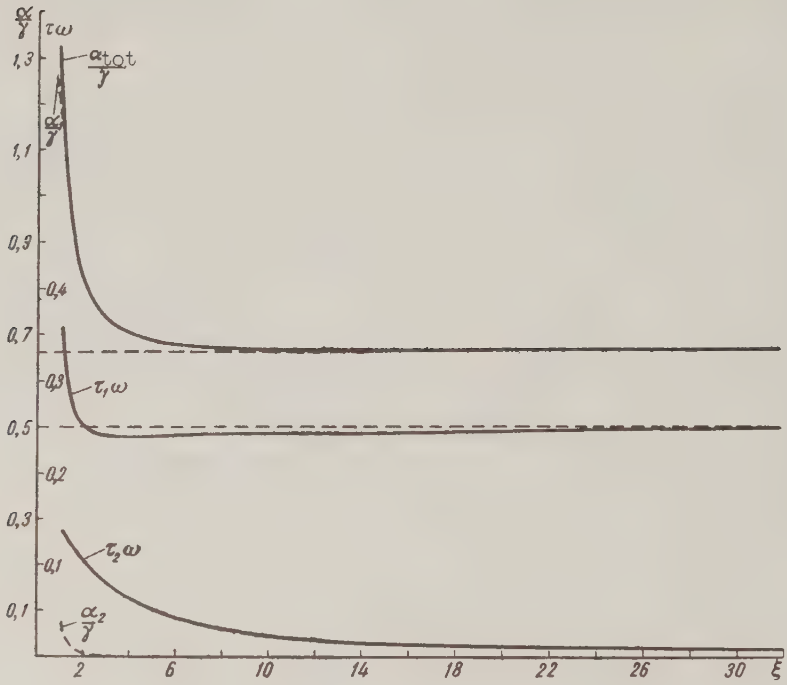

Fig.2. Variation of the polarizabilities (α_1, α_2, α_{tot}) and the relaxation times (τ_1, τ_2) for the case of singly excited complexes with the degree of coupling ξ of the vacancies with the divalent impurity ions $\left(\gamma = p\,\frac{a^2q^2}{kT}\right)$.

The strength of the coupling between the components of a complex is characterized in Fig.2 by the parameter $\xi = \exp\left(\frac{V}{2kT}\right)(T = 300°\mathrm{K})$.

For $\xi = 1$ the impurity ion-vacancy coupling is weakest, the distribution of vacancies over the sites of different coordination spheres is equally likely, the contribution of excited complexes to the process of polarization is comparable to the contribution of unexcited complexes and the total polarizability α_{tot} is relatively large (Fig.2). With increase of ξ the total polarizability α_{tot} rapidly decreases and becomes close to the polarizability of unexcited complexes (dashed line) when $\xi = 5$. For pure Coulomb interaction $\xi = 30.877$.

The principal results obtained in solving the set of equations taking into account both single and double excitation of the complexes are listed in the accompanying table. We have included in the table the values of the polarizabilities and relaxation times calculated for the two limiting cases, namely, a) when $\omega_1 = \omega_2 = \ldots = \omega_{10} = \omega$, and b) when the interaction between the vacancy and the impurity ion is described by Coulomb's law.

As will be evident from the table, the process of reorientation of the complexes in taking into account single and double excitation is described by four dielectrically active relaxation times. Even in the case of weakest coupling (a) between the vacancies and impurity ions the polarizability α_1, corresponding to the maximum relaxation time τ_1, is much greater than the polarizability corresponding to the other relaxation times. Consequently, taking into account double exci-

	Unexcited complexes	Taking into account single excitation		Taking into account double excitation	
		a	b	a	b
α_1/γ	0,6667	1,2629	0,66666	5,2469	0,666859
α_2/γ	—	0,0704	0,00015	0,0843	0,000179
α_3/γ	—	—	—	0,0025	0,000025
α_4/γ	—	—	—	0,0008	0,000001
$\tau_1\cdot\omega$	0,2500	0,3605	0,2481	0,5900	0,2483
$\tau_2\cdot\omega$	—	0,1286	0,0081	0,1971	0,0147
$\tau_3\cdot\omega$	—	—	—	0,1143	0,0129
$\tau_4\cdot\omega$	—	—	—	0,0871	0,0124
α_{tot}/γ	0,6667	1,3333	0,66681	5,3350	0,667064

tation does not lead to appreciable frequency broadening of the loss peak even in the case most favorable for this effect.

It will also be evident from the table that the total polarizability for excited complexes is greater than the polarizability of unexcited complexes; although the value of the polarizability cannot be precisely calculated without knowing all the parameters ω_i, we can assert that with weakening of the impurity cation-vacancy coupling the polarizability of the excited complex increases.

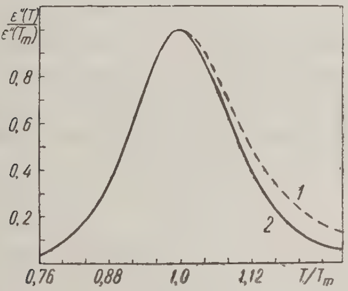

Fig.3. Variation of the dielectric loss factor $\varepsilon''(T)$ with temperature. T_m is the temperature at which $\varepsilon''(T)$ is maximal: 1) Debye temperature peak, 2) narrowed loss peak.

The table gives the polarizabilities calculated per divalent impurity ion. These polarizabilities are proportional to the degree of association p of the vacancies and impurity ions. The degree of association decreases with temperature in a certain temperature range.[13] This should obviously affect both the temperature dependence of the polarizability and the temperature dependence of the losses: the temperature peak must become narrower than predicted by Debye's theory. This is illustrated in Fig.3, where the narrowed loss peak is represented by the solid curve. In plotting this curve we used the following temperature dependence of the degree of association p for unexcited complexes:[14]

$$\frac{p}{(1-p)^2} = cz_0 \exp\left(\frac{\Delta G}{kT}\right),$$

where $z_0 = 12$ for an NaCl type lattice, c is the concentration of divalent impurity ions and ΔG is the energy increment associated with transporting a vacancy from infinity to the immediate proximity of an impurity ion.

The solid curve in Fig.3 is constructed for the case when $c = 10^{-3}\%$, $\Delta G/u = 1$, and the frequency of the alternating field is approximately 10^6 cps. Using other values of these parameters, one can obtain either a larger or smaller narrowing of the temperature peak of the dielectric loss. For example, at a lower frequency (and consequently, in the range of lower temperatures) the narrowing disappears completely.

Thus the temperature dependence of p, just like the temperature dependence of the activation energy,[9] leads to narrowing of the temperature peak of the dielectric losses. This effect was observed in the experimental work of Breckenridge[1,15] and Matsonashvili[9].

References

1. R.G.Breckenridge, Chem.Phys., 16, 959 (1948).
2. Y.Haven, J.Chem.Phys., 21, 171 (1953).
3. E.Burstein, J.V.Davisson & N.Sclar, Phys.Rev., 96, 819 (1954).
4. J.Suita, Phys.Rev., 94, 1497 (1954).
5. J.Meinnel, Conf.on Defects in Crystal Solids. Bristol, 1954.
6. M.Ishiguro, F.Oda & T.Fiyno, Phys.Rev., 95, 1347 (1954).
7. G.Jacobs, Naturwissenschaften, 42, 575 (1955); J.Chem.Phys., 24, 629 (1956)
8. B.N.Matsonashvili, Zhur.eksp.i teor.fiz., 31, 1110 (1956). (Trans.Soviet Physics - JETP).
9. B.N.Matsonashvili, Izv.AN SSSR, Ser.fiz., 22, 296 (1958). (Trans.Bulletin 22, 294.)
10. G.I.Skanavi, Fizika dielektrikov (Physics of Dielectrics), M., 1948.
11. R.M.Fuoss, Trans.Faraday Soc., 30, 967 (1934).
12. A.B.Lidiard, Conf.on Defects in Crystal Solids. Bristol, 1954.
13. A.B.Lidiard, Phys.Rev., 94, 29 (1954).
14. A.B.Lidiard, Phyl.Mag., 46, 1218 (1955).
15. R.G.Breckenridge, J.Chem.Phys., 18, 913 (1950).

DISCUSSION

V.I.Odelevskii: The results given in the report of Vodop'yanov are suspect from the standpoint of procedure. Absorption of moisture occurs rather rapidly and hence measurements of "dried" samples without evacuation and without the use of a moisture absorber may be distorted: they may simulate the effect of variation of tan δ with lattice energy, whereas actually hygroscopicity of the crystal plays an important role. It is also not proved that losses at or in the electrodes do not have an effect on the measurement results.

Unfortunately, in Vodop'yanov's work insufficient attention is given to the question of the loss mechanism in alkali halide crystals; typical relaxation losses at frequencies of 10^6-10^7 cps should develop at high temperatures, hence at room temperature one can at best observe the "tail" of the relaxation process.

In Panchenko's report, previously published studies are either ignored or viewed in a biased manner. He devotes much attention to the antiquated concept of Mott & Gurney and to Skanavi's classification of alkali halide crystals into artificial groups, which is also now out of date. At the same time Panchenko does not mention work of Tolpygo & Odelvskii regarding the influence of ionic deformation on the polarizability and does not use their results.

It should be noted that in calculating the temperature coefficients of the dielectric constant it is not necessary to carry out very complicated calculations such as those made in 1950 by Tolpygo; one can for simplicity introduce the assumption that the "crumpling" is temperature independent and then the calculations become much simpler. The use in the calculations of various "selected" functions for the repulsive energy, whether this be the Born function or an exponential function, in a number of cases is equivalent to further extrapolation and hence undesirable; it is better to expand the expression for the lattice energy into a Taylor series in displacements to as many terms as required by the conditions of the problem and to determine the coefficient from the experimental data, for example, from the pressure dependence of the volume.

If it is a question of calculating the temperature coefficient of linear expansion, for example, one must take into account terms containing second and third derivatives of the energy with respect to the displacement (or volume). This calculation procedure was used, for example, in Ya.I.Frenkel's book (1924) and in my article (1950).

The report does not propose any theoretical interpretation of the effect of abrupt increase of the expansion coefficient of crystals close to the melting point, yet explanation of this effect by hole formation was suggested some time ago (see the calculations in Frenkel's book "Kinetic Theory of Liquids" (1945)).

If the author of the report intends to extend his investigations, it would be desirable to pay greater heed to the theoretical aspects of the work.

I.D.Fridberg: In connection with the long standing discussion of the relation between the lattice energy and the dielectric properties, I would like to mention (at the author's request) some observations of S.M.Ariya of Leningrad State University regarding evidences of correlation between the lattice energy and dielectric properties. Most investigators relate both the semiconductor and dielectric properties of solids with the nature and concentration of defects in them.

This point of view is based on the general theoretical considerations according to which vacant sites, atoms in a state differing from their normal bulk state (in particular, atoms in a different valence state), atoms in interstitial positions and other lattice defects must insure increase of the electric conductivity and also give rise to a large number of experimental factors which indicate parallelism between the conductivity and dielectric losses, on the one hand, and the concentration of defects, on the other. True, these experimental facts cannot be regarded as direct proofs of correlation between the dielectric properties and imperfections of the crystal structure. However, most regularities observed in the variation of the electric properties of nonmetallic solids can be, if only qualitatively, explained on the assumption that they are dependent on or connected with lattice defects.

In our opinion it is a mistake to raise the question of whether these properties are connected with lattice defects or whether they are functions of the characteristics of an ideal crystal of some compound.

Actually, the energy of formation of a defect is finite, and hence, there is a definite nonzero probability for a defect forming at any temperature above absolute zero; consequently, if the crystalline substance is in a state of thermochemical equilibrium, it cannot at temperatures close to absolute zero have an ideal lattice: there must be some concentration of defects in the lattice. Consequently, it is incorrect to consider such electric properties as the conductivity and dielectric losses in complete neglect of the presence of inevitable defects.

At the same time, it is perfectly natural that the probability for the formation of defects and accordingly their concentration should be a function of the nature and composition of the solid; hence one cannot consider the properties of the material divorced from the specific structure of the material undisturbed by defects.

Great care must be taken, however, in searching for the causal (uncorrelated) relations between the electric properties and the characteristics of ideal structures, inasmuch as many of these characteristics may influence the electric properties by virtue of the fact that they are among the factors affecting the concentration of defects.

There are several investigations in which note has been taken of the relationship between some properties of a crystal substance and its other properties. It has been noted, for example, that there is a relation between such properties as the specific weight, melting point, and the compressibility, on the one hand, and the lattice energy on the other; there are frequently obtained smooth curves plotted in terms of a given property vs the lattice energy showing a consistent tendency of the given property to increase or decrease with the lattice energy. In most cases, however, such simple regularities will be observed only for compounds of elements of a certain group in the periodic table; this indicates that the existence of such a general tendency is not necessarily proof of an actual causal relation. The point is that all the properties of the elements vary over the periodic system in a regular fashion (since the periodic system is a natural system of the elements) and as a result there is often obtained a rather simple correlation between a number of different properties. This does not mean that there is a causal relationship between these properties.

It is obvious, for example, that the specific weight is not an actual function of the lattice energy. However, if we plot the specific weight of KI, KBr and KCl as a function of their lattice energies we obtain a descending curve; this occurs simply because the atomic weights of the halogens decrease more rapidly than the size of the ions.

The melting point is defined as the temperature at which the solid and liquid phases of the substance are in equilibrium. Accordingly, the melting point is a function of the properties of both the solid and liquid states. The thermodynamic characteristics of the liquid state in general are not directly related with the lattice energy of the compound in the crystal state, and consequently the melting point cannot in general be a simple function of the lattice energy.

The same thing applies to such properties as the dielectric strength of crystals. In this case one can plot fairly smooth curves in terms of the dielectric strength as a function of the heat of sublimation, the heat of formation or lattice energy. This does not mean that there is a causal relationship between these attributes; consequently, it is risky to attempt to predict the electric properties on the basis of such dependences. These are the comments I have been requested to express by S.M.Ariya.

I would like to add a few remarks concerning the report of Vodop'yanov. In the physics of dielectrics we are concerned primarily with the microscopic characteristics of the dielectric rather than its averaged macroscopic state. Among the data characterizing the microstate of a dielectric we have in particular the number of relaxators (and this, as has been noted here, is many orders of magnitude lower than the number of particles per unit volume) and the energy of defect formation. There are many examples when despite a high lattice energy an ionic dielectric contains a large number of defects - unoccupied sites, ions of different charge and so on - particularly, if some crystal phase forms a region of homogeneity with phases of different stoichiometric composition or when there occur delayed phase modifications. Such dielectrics are always distinguished by a high conductivity and a large dielectric loss.

Not only the energy of lattice formation but another fundamental thermodynamic function, namely, the free energy of the compound, cannot be uniquely related with electric properties of the material. Actually, the free energy depends both on the heat content and the entropy. Of particular importance to us is the component of the entropy associated with chaotic motion of the particles, so-called position entropy. With increase of the position entropy, the free energy decreases, but at the same time the conductivity and dielectric loss increase sharply. In connection with this when we consider not some one group of alkali halide crystals (with the same cation or the same anion) but a series of such crystals with different combinations of ions, no simple correlation between the electric properties and the lattice energy is evinced. In connection with this it may be useful to recall the remarks of the German theoretical chemist Hückel* regarding Pauling's concept of electronegativity:"In the graphic representation of electronegativity given by Pauling we are struck by the interrelation with the various groups and periods of the periodic system. It should not, however, be surprising. The different properties of similarly constructed compounds vary inside each group of the periodic table and the jump in going from the first to the second period is particularly great. Hence when the specific properties are utilized in calculations, in the final result there must always be evinced the same quantitative regularity, provided the calculation procedures are not illogical."

---

*W.Hückel, Die chemische Bindung, J.praktische Chemie, 5(4), 105, Dec., 1957.

K.A.Vodop'yanov: In measuring the dielectric loss in alkali halide crystals one must pay particular attention to the sensitivity of the equipment. In this respect the ordinary Q-meter is not a suitable instrument. At sufficiently high frequencies the influence of atmospheric humidity and of different secondary factors connected with the presence of space charges and poor contact between the electrodes and the sample is evinced to an appreciably lesser degree than at low frequencies. Hence high frequency measurements need not necessarily be carried out in vacuo. Unfortunately, in the work reported on by Bogoroditskii, Panchenko & Matsonashvili the measurements of the dielectric loss were carried out by means of a Q-meter. A pressing problem is development of sensitive apparatus for measuring the dielectric loss (to within 1 part in 10^5) in a wide frequency range.

The question of the relation between the electric properties of crystals and their physical-chemical attributes is very important. That there is a relation has been established in the work of A.A.Vorob'ev and his colleagues.

At present investigations should be continued in the direction of refining the experimental regularities (inasmuch as the electric properties and particularly the conductivity can vary a great deal, depending on external and chance factors), and in the direction of developing helpful theoretical concepts regarding the relation between the electric properties and the physical-chemical characteristics of crystals.

ON THE RELAXATION POLARIZATION OF CRYSTALS WITH THE STRUCTURE OF RUTILE AND PEROVSKITE

- I.Ts.Lyast

1. Calculation of the relaxation polarization of ionic crystals

The presence of a relaxation component in the polarization of ionic crystals is evidence of lattice distortions of some sort; therefore the "relaxing" elements responsible for the relaxation component can be called "relaxing defects". Regardless of the nature of the polarization mechanism, there arises the question of a method of calculating the polarization. In the case of relaxation processes we must use a statistical approach, the application of which to ionic crystals requires a generalization of the Kirkwood theory to a complex system consisting of relaxing and elastically polarizable elements.

It is convenient to divide relaxing defects into two groups:

1. Relaxing defects which have dimensions inferior to the interatomic separation; to this group one can partially attribute the ionic relaxation mechanism.
2. Relaxing defects which have dimensions greater than the distance between nearest ions; to this group one can attribute the Breckenridge and the electron-relaxation mechanisms.

Relaxing defects undoubtedly distort the lattice, but we can restrict ourselves to the case in which the number of defects is small, and the distortions produced in the immediate vicinity of the defects are insignificant. In this case we can represent the relaxing defects by rigid, freely rotating dipoles. The assumption of free rotation, adopted for convenience, should not seriously affect the results. Because the angular frequency of the dipoles is much lower than the ionic vibrational frequency, one can adopt the adiabatic hypothesis according to which the ionic states promptly follow the states of the dipoles. The interaction between the dipoles and the lattice ions leads to polarization of the ionic lattice by the dipoles, and the ionic lattice in turn exerts an orienting effect on the dipoles.

Calculations of the polarization of the relaxing defects of the first group were given in Ref.1. In order to compute the moment induced by the dipole in an ionic environment, the dipole is enclosed in a sphere, outside of which the medium is considered to be a continuous dielectric with the dielectric constant of the corresponding pure ionic crystal. The part of the crystal inside the isolated sphere will be called sphere B, while the entire sample will be referred to as sphere A. In calculating the moment induced by the dipole in the ionic lattice, we can disregard the other dipoles, because the lattice polarization is predominantly linear. In order to determine the moment induced by the dipole in sphere B, it is necessary to calculate the field due to the dipole and the other ions polarized by it, acting on each ion in the sphere:

$$E_{k\beta}^{(i)} = -\mathscr{E}_{k\beta\gamma}^{(i)} p_\gamma - \sum_{l=1}^{m} \sum_{j\,(\neq i)}^{I_l} \alpha_l \mathscr{E}_{kl\beta\gamma}^{(ij)} E_{l\gamma}^{(ij)}. \qquad (1)$$

The subscripts k and l designate the type of ion, and the superscripts $i, j = 1,2\ldots I_l$ pertain to the numbers of the l type ions; β and γ are the coordinate indices (the summation convention is implied for reiterative indices). The coefficients $\mathscr{E}_{kl\beta\gamma}^{(ij)}$ are tensors of the dipole-dipole interaction between corresponding ions:

$$\mathscr{E}_{kl\beta\gamma}^{(ij)} = (R_{kl}^{(ij)})^{-5}\{(R_{kl}^{(ij)})^2\delta_{\beta\gamma} - 3R_{kl\beta}^{(ij)}R_{kl\gamma}^{(ij)}\}; \quad \mathbf{R}_{kl}^{(ij)} = \mathbf{R}_k^{(i)} - \mathbf{R}_l^{(j)}, \qquad (2)$$

where the R are the radii vectors of the ions. The tensors E^{kl}_{ij} correspond to interaction between an ion and the dipole p. The solution of set (1) expressed in determinant form is

$$E^{(k_\nu i_\nu)}_{t_\nu \beta} = \frac{D^{(k_\nu i_\nu)}_{t_\nu r_\nu}}{D'}\, p_\gamma; \tag{3}$$

$$D'_{qr} = x_k E^{kl}_{ij\beta\gamma}(1-\delta_{ij}) + \delta_{ij}(1-\delta_{\beta\gamma}); \tag{4}$$

$$q = 3\sum_{\alpha=1}^{k-1} I_\alpha + 3(i-1) + \beta; \quad r = 3\sum_{\alpha=1}^{l-1} I_\alpha + 3(j-1) + \gamma. \tag{4'}$$

In determinant $D^{(k_\nu i_\nu)}_{t_\nu r_\nu}$ the column with $r_\nu = 3\sum_{\alpha=1}^{k_\nu-1} I_\alpha + 3(i_\nu-1) + \beta_\nu$ is replaced by the corresponding row of $E_{p\gamma}$.

Knowing the field (3), we can readily find the total moment, which in the case of an isotropic lattice equals

$$M = (1 + A_1)M_d; \quad A_1 = \sum_{k=1}^{m}\sum_{i=1}^{I_k} x_k \frac{D_k^{(i)}}{D'}. \tag{5}$$

Applying the Kirkwood equation to the dipole system and computing the moment induced by dipole p in the system of dipoles in sphere A, we obtain for the case when $\varepsilon, \varepsilon_1 \gg 1$ (Ref.1)

$$\varepsilon - \varepsilon_1 = \frac{2\pi N_d p^2}{kT}\,\frac{\varepsilon}{\varepsilon_1}(1 - A_2)\left(1 + \frac{\varepsilon_1}{\varepsilon}A_2\right)\left[1 - \frac{9}{2}\left(\frac{1}{\varepsilon_1} - \frac{1}{\varepsilon}\right)(1 + A_1)\right] \times \left(1 + \frac{N_d p^2}{3kT}A_3\right). \tag{6}$$

The coefficient A_2 characterizes the field acting on the dipole and due to the lattice polarized by the external field:

$$A_2 = \sum_{k=1}^{m} x_k C_k, \tag{7}$$

where the C_k are structure factors. The coefficient A_3 characterizes the moment M_3 induced by dipole p in the dipole system in sphere B:

$$\overline{M}_3 = \left(1 + \frac{N_d p^2}{kT}A_3\right)p; \quad A_3 = \frac{1}{N_l}\sum_{i=1}^{I_l}\frac{D_i''}{D_l'}. \tag{8}$$

Expression (8) is obtained under the assumption that the relaxing defects are formed at the site of l type ions. Determinant D_l' differs from determinant (4) in that it lacks terms corresponding to the interaction of the i-th ion of the l type with the other ions.

2. Ionic relaxation polarization in the perovskite lattice

According to the hypothesis of Skanavi[2,3], relaxation polarization in crystals having the rutile or the perovskite structure is caused by titanium ions that acquire the capacity for relaxational motion owing to loosening of the lattice by impurity atoms. In order to resolve the question whether relaxing ions can sharply increase the dielectric constant, one must find the coefficients A_1, A_2 and A_3. We will determine them for the perovskite lattice.

We assume that the titanium ions not located in the vicinity of impurity atoms are elastically coupled and that the number of the latter is much larger than the number of dipoles. The metal ions, which we assume to be ions of Group II of the periodic table, can be disregarded inasmuch as the dipole-dipole interaction of Me-Ti ions is zero, while for the Me-O ions it is very weak.

Coefficient (7) is obtained by means of straight-forward calculations:[4]

$$A_2 = \frac{0.438g\,(56.0g_2 + 21g)}{1 - 3.5\,(-0.20 + 5.3g_2 + 0.1g)}; \tag{9}$$

$$g = \frac{\alpha}{r^3}, \quad g_2 = \frac{\alpha_2}{r^3}, \tag{10}$$

where $r = a/2$ (half the lattice constant), and α and α_2 are the polarizabilities of the oxygen and titanium ions, respectively.

In the case of the perovskite lattice, it is not difficult to show that all the ions are polarized in one direction, therefore, in calculating the coefficient A_1 we can restrict ourselves to an evaluation of one field component, and hereinafter we take the interaction tensor to mean the component ε_{zz}. Inasmuch as by virtue of symmetry the equalities $E_1 = E_2$ and $E_3 = E_4 = E_5 = E_6$ hold for the fields (3) acting on the oxygen ions, the fields E_1 and E_3 are determined from the set

$$\begin{aligned} E_1 &= -\mathscr{E}_1 p - 4\alpha\mathscr{E}_{13}E_3, \\ E_3 &= -\mathscr{E}_3 p - 2\alpha\mathscr{E}_{31}E_1 - 2\alpha\mathscr{E}_{35}E_3, \end{aligned} \tag{11}$$

where $\mathscr{E}_1$ and $\mathscr{E}_3$ are tensors of the dipole-oxygen ion interaction, and $\mathscr{E}_{13}$ and $\mathscr{E}_{35}$ are interaction tensors of the oxygen ions located in one octahedron. In the first approximation with respect to α/r^3, we obtain

$$E_1 = -a_1 p = -\mathscr{E}_1\left(1 - \frac{\alpha}{2\sqrt{2}\,r^3}\right)p, \quad E_3 = -a_3 p = -\mathscr{E}_3\left(1 - \frac{\sqrt{2}\alpha}{r^3}\right). \tag{12}$$

When calculating the field E^i acting on the i-th titanium ion, it is necessary to take into account the effect of the neighboring I oxygen ions. For simplicity, one can neglect the interaction of the oxygen ions with each other in the case when the field source lies outside the given oxtahedron, therefore we can separate the set of $I + 1$ equations into two parts:

$$\begin{aligned} E^i &= -\mathscr{E}^i_0 p - \alpha\mathscr{E}^1_i E_1 - \ldots - \alpha\mathscr{E}'_{I^*}E_{I^*} - \alpha a^i_{I^*+1}E_{I^*+1} - \ldots - \alpha a^i_I E_I; \\ E_j &= -a_j p - \alpha_2\mathscr{E}^i_j E^i \qquad (j = 1,2,\ldots,I^*); \\ E_j &= -\mathscr{E}_j p - \alpha_2 a^i_j E^i \qquad (j = I^* + 1.\ldots, I), \end{aligned} \tag{13}$$

where the $j = 1,2,\ldots,I^*$ ions are located in the same octahedron with the dipole p, and the $j = I^* + 1,\ I^* + 2,\ldots,\ I$ ions are located in the same octahedron with the titanium ion; $\mathscr{E}^i_0$ designates the interaction tensor of the i-th titanium ion with the dipole, and $\mathscr{E}^i_j$ the interaction tensor with an oxygen ion.

The determinants of the set are

$$D' = 1 - \alpha\alpha_2 \sum_{j=1}^{6} \alpha_j\mathscr{E}_j, \tag{14}$$

$$D^i = -\mathscr{E}^i_0 + \alpha \sum_{j=1}^{I^*} a_j\mathscr{E}^i_j + \alpha \sum_{j=I^*+1}^{I} \mathscr{E}_j\mathscr{E}^i_j. \tag{14'}$$

When calculating the field acting on ions I and II (Fig.1), one can neglect the influence of the other titanium ions. Having calculated the field acting on ions I and II, it is easy to determine the field produced by these ions at the locations of the more distant ions:

$$E^i = \left(\frac{D^i}{D'} + \alpha_2 \sum_{i'} \frac{D^{ii'}D^i}{D'^2}\right)p \qquad (i' = \mathrm{I} \text{ or } \mathrm{II}), \tag{15}$$

Taking into account the effect of the nearest titanium ions, we obtain (Fig.1

$$E^I = \frac{D^I}{D'}p; \quad E^{\mathrm{II}} = \frac{D^{\mathrm{II}}}{D'}p; \tag{16}$$

$$E^{\mathrm{III}} = \frac{1}{D}\left\{D^{\mathrm{III}} + 2\alpha_2 \frac{(D^{I})^2}{D'}\right\} p; \quad E^{\mathrm{IV}} = \frac{1}{D'}\left\{D^{\mathrm{IV}} + 2\alpha_2 \frac{D^{\mathrm{I}}D^{\mathrm{II}}}{D'}\right\} p. \tag{16'}$$

After determining the tensors $\mathscr{E}_j$ and $\mathscr{E}_j^i$ and their corresponding coefficients a_j and a_j^i (12), we compute determinant (14):

$$\sum_{j=1}^{6} a_j \mathscr{E}_j = \frac{12}{r^6}(1 - 0.7\,g), \tag{17}$$

$$D' = 1 - 12\,gg_2(1 - 0.7\,g); \tag{17'}$$

$$D^{\mathrm{I}} = \frac{1}{r^3}(-0.125 + 1.1\,g - 1.15\,g^2); \quad D^{\mathrm{II}} = \frac{1}{r^3}(0.25 + 3.0\,g - 1.25\,g^2), \tag{18}$$

$$D^{\mathrm{III}} = \frac{1}{r^3}(-0.044 + 0.28\,g - 0.3\,g^2); \quad D^{\mathrm{IV}} = \frac{1}{r^3}(0.022 - 0.44\,g + 0.22\,g^2). \tag{18'}$$

Summing over the I to IV titanium ions and over the oxygen ions of one octahedron, we obtain

$$A_1 = \frac{g_2}{1 - 12\,gg_2(1 - 0.7\,g)}\left\{8.0\,g - 6.5\,g^2 + \frac{g_2(-0.38 - 3.8\,g + 62\,g^2)}{1 - 12\,gg_2(1 - 0.7\,g)}\right\} + 4.2\,g^2, \tag{19}$$

wherein $4.2\,g^2$ corresponds to the contribution of the oxygen ions.

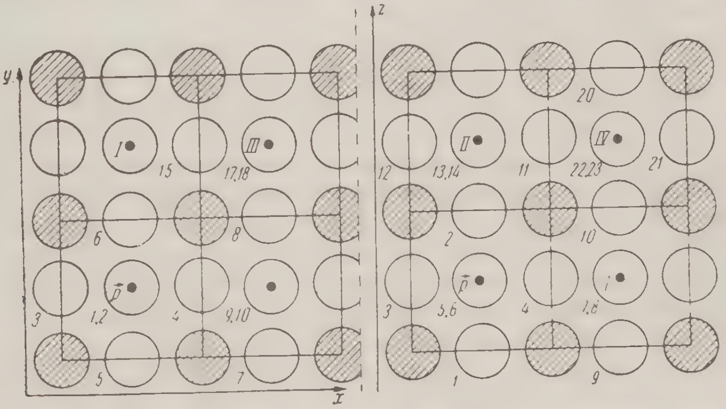

Fig.1. Perovskite lattice. The open circles are oxygen ions; the hatched circles are metal ions; the black dots are titanium ions. The Arabic numerals identify the oxygen ions; the Roman numerals - the titanium ions. The symmetrically located titanium atoms are designated by identical numbers.

It can readily be shown that in our case $D_i^{\mathrm{II}} = 1$; therefore it follows from a comparison of Eqs.(5) and (8) that coefficient (19), after subtraction of $4.2\,g^2$ equals $\alpha_2 N_l A_3/D'$, whence

$$A_3 = 64\,g - 52\,g^2 + \frac{8\,g_2(-0.38 - 3.8\,g + 62\,g^2)}{1 - 12\,gg_2(1 - 0.7\,g)}. \tag{20}$$

We assume $\alpha = 3\cdot10^{-24}$ and $\alpha_2 = 1\cdot10^{-24}$ cm^3 for the polarizabilities of the ions. Since $2r = 3.9\cdot10^{-8}$ cm for $SrTiO_3$, coefficients (10) are $g = 0.42$ and $g_2 = 0.14$. From Eqs.(9), (19), (21) and (17'), we find $A_2 = 12.2$, $A_1 = 3.8$, $A_3 = 63$ and $D' = 0.5$. Assuming that the number of relaxing defects is $N_g = 9\cdot10^{20}$ cm^{-3} (Ref.3), the dielectric constant of the ionic lattice is $\varepsilon_l = 100$, and that of the sample is $\varepsilon = 1000$, we obtain from Eq.(6):

$$\frac{p^2}{3kT} = 1.4 \cdot 10^{-22};$$

when T = 300°K, p has the value $4.2 \cdot 10^{-18}$ cgs units, which corresponds to a displacement of the Ti^{4+} ion a distance $z = 0.22 \cdot 10^{-8}$ cm. Calculations, performed disregarding the mutual interaction of the oxygen ions,[4] give approximately the same result.

The above calculation is based on an assumption of the possible existence of relaxing titanium ions in the perovskite lattice. It is desirable to justify this assumption from the molecular standpoint. The nature of the Ti ion motion is also important where the molecular theories of ferroelectricity are concerned. We will start from a purely ionic lattice model, and as a basic premise we will use the hypothesis that in the barium titanate lattice the space inside the oxygen octahedron is larger than the titanium ion volume[5]. The displacement z of the titanium ion will be assumed to be small, and its intrinsic electronic polarizability will be neglected.

The forces acting on the titanium ion can be divided into three parts: F_1, the Coulomb force, F_2, the short-range interaction, and F_3, the force due to the reactive field appearing as a result of polarization of the surrounding ions incident to displacement of the titanium ion.

When a center of symmetry exists, one can express the Coulomb interaction energy in terms of the tensors $\mathcal{E}$:

$$U_1 = -\frac{1}{2} q_0 z^2 \sum_{k=1}^{m} q_k \sum_{i=1}^{I_k} \mathcal{E}_k^i. \tag{21}$$

Because the Ti-Ba interaction tensors vanish and the sum of the Ti-O interaction tensors over all the ions of the octahedron is also zero, the Coulomb interaction energy can be neglected ($U_1 \doteq 0$). Without going into detail, we assume that the short-range forces begin to appear only incident to displacements of the titanium through distances greater than the half-sum of the Ba^{2+} and O^{2-} radii minus the Ti^{4+} radius. For $BaTiO_3$ this difference d equals 0.03 Å (Ref.5). For $z > d$, the force F_2 will be considered elastic;

$$F_2 = \begin{cases} 0, & z \leqslant d \\ -c(z-d), & z > d. \end{cases} \tag{22}$$

Incident to displacement of the titanium ion, the oxygen ions are polarized and acquire a moment $-\alpha a_j qz$, as a result of which the titanium ion will experience a reactive force, which, according to (17), is equal to

$$F_3 = bz; \quad b = \frac{12\, q^2}{r^3} g\,(1 - 0.7\, g). \tag{23}$$

From Eqs. (22) and (23), we obtain the following expression for the total energy:

$$U = \begin{cases} -\frac{1}{2} bz^2, & z \leqslant d \\ \frac{1}{2} c\,(z-d)^2 - \frac{1}{2} bz^2, & z > d. \end{cases} \tag{24}$$

It is apparent from this expression that the titanium ions have six equilibrium positions separated by barriers:

$$\Delta U = \frac{1}{2} d^2 \frac{bc}{c-b} = \frac{6\,(qd)^2\,(1 - 0.7\, g)\, g}{r^3} \tag{25}$$

(the last for $c \gg b$). The motion has a relaxational character, when $\Delta U \gg kT$, and the character of anharmonic oscillations, when $\Delta U \ll kT$. For $BaTiO_3$, $\Delta U = 7.3 \cdot 10^{-14}$ erg. The condition $\Delta U = kT$ is fulfilled at T = 520°K, which agrees in order of magnitude with the Curie point (T_c = 400°K) (Fig.2).

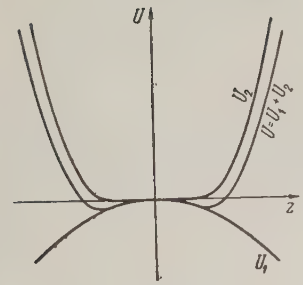

Fig.2. Configuration of the titanium ion potential well.

Calculations of the ionic energy in the barium titanate lattice were made by Syrkin[6]; according to these calculations the titanium ion cannot undergo relaxational motion. This disagreement with our results is due to the fact that in Syrkin's work the energy associated with the reactive field was evaluated to be of the order of z^4.

The appearance of relaxing ions in a nonferroelectric crystal after introduction of impurities can be explained from the standpoint of our results. Let us consider, for instance, the $SrTiO_3$ lattice doped with Bi. If the Bi ions form a substitutional solution[3], strontium ion vacancies appear in the crystal. In a cell with an Sr vacancy there should occur expansion of the oxygen octahedron and consequently, the titanium ion should be able to undergo relaxational motion. Expansion of the oxygen octahedra may also be caused by other types of defects.

3. The Breckenridge and electron-relaxation mechanisms

In the case of the Breckenridge mechanism, the relaxation polarization is caused by dipoles which have formed as a result of association of two oppositely charged defects. The defect ions or their vacancies can occupy certain positions in the unit cell; consequently, the resulting relaxing defects can be classed in the second group, where the dipole dimensions exceed the interatomic separations.

We calculate the polarization in the same way as for the case of point dipoles. The set of equations (1) preserves its form, with the difference that the moment p is replaced by the charge q, and tensors $\mathscr{E}^{(i)}_{k\beta\gamma}$ by the vectors $\vec{\mathscr{E}}^{(i)}_k$:

$$\vec{\mathscr{E}}^{(i)}_k = \frac{\mathbf{R}^{(i)}_{1k}}{\left(R^{(i)}_{1k}\right)^2} - \frac{\mathbf{R}^{(i)}_{2k}}{\left(R^{(i)}_{2k}\right)^2}, \tag{26}$$

where the $\mathbf{R}^{(i)}_{1k}$ and $\mathbf{R}^{(i)}_{2k}$ are the radii-vectors drawn from the poles of the dipole to the i-th ion of the k-th kind. Change of the dipole orientation results in change of the values of $\vec{\mathscr{E}}^{(i)}_k$, but this is not significant in cases when the lattice is isotropic or when the possible dipole orientations correspond to the lattice symmetry. The induced moment will be

$$\mathbf{M} = (\mathbf{d} + \mathbf{A}_1)\, q, \qquad \mathbf{A}_1 = \sum_{k=1}^{m} \sum_{i=1}^{I_k} \alpha_k \frac{\mathbf{D}^{(i)}_k}{D'}, \tag{27}$$

wherein $\mathbf{D}^{(i)}_k$ are obtained from the determinant D' by replacing the appropriate column by the row of (26). It is inconvenient to introduce $p = qd$ as a parameter, since it is impossible to determine the latter independently of the vectors $\mathscr{E}^{(i)}_k$. If rotation of the dipole corresponds to transition of one of its constituent ions to a position symmetrical relative to the initial one, it is not necessary to take into account the difference between the internal field and the average field, and Eq.(6) takes the form

$$\varepsilon - \varepsilon_i = \frac{4\pi N_d q^2}{kT} \frac{\varepsilon_i (\varepsilon + 2)(d + A_1)}{(2\varepsilon_i + 1)(\varepsilon_i + 2)} \left[d - \left(\frac{9\varepsilon_i}{(2\varepsilon_i + 1)(\varepsilon_i + 2)} - \frac{9\varepsilon}{(2\varepsilon + 1)(\varepsilon + 2)} \right)(d + A_1) \right]. \tag{28}$$

Equation (28) does not take into account the interaction of the dipoles with each other. Equation (28) is also useful for the calculation of relaxation polarization in crystal hydrates.[8] From the point of view of the accepted models, the electron-relaxation mechanism[9] gives two equilibrium positions for the dipole. If the internal field acting on the electron in both positions is the same, then Eq.(28) is valid. Otherwise the calculations become considerably more complicated.

In the simplest case electronic relaxation will occur if there are two states with the same energy, located sufficiently close to each other, but not so close that their wave functions ψ'_0 and ψ''_0 overlap:

$$I_0 = \int \psi'_0 \psi''_0 dx = 0. \tag{29}$$

A relaxation transition from the ψ'_0 state to the ψ''_0 state can occur through overlapping excited states ψ_n. A transition to an excited state corresponds to a polarization process and not to conduction, when the energy of the excited states is not too close to the bottom of the conduction band E_c $(E_c - E_n \gg kT)$ and if the dipole density is not so great that their excited states overlap:

$$\int \psi_n^i \psi_n^j dx = \delta_{ij}; \quad N_d v \ll 1 \tag{30}$$

(v is the volume of the region in which ψ_n is nonzero). The simultaneous fulfillment of conditions (29) and (30) is not difficult. It is also important to note that in using the usual formula for the relaxation time,

$$\frac{1}{\tau} = 2\nu \exp\left\{-\frac{E_n - E_0}{kT}\right\}, \tag{31}$$

under ν one must understand the frequency of the ionic lattice vibrations, and not the frequency of the electron itself. This applies not only to a quantum system, but to all cases where the vibrational frequency of the particle greatly exceeds the vibrational frequency of its surroundings, because this last determines the rate of change of the particle energy. Strictly speaking, Eq.(31) is not valid for a quantum system. However, in this case, when the number of excited levels is large and they are closely spaced, Eq.(31) should give the correct order of magnitude of the relaxation time.

References

1. I.Ts.Lyast, Fizika tverdogo tela, 2, No.6 (1960). (Trans.Soviet Physics - Solid State.)
2. G.I.Skanavi & E.I.Matveeva, Zhur.eksp.i teor.fiz., 30, 1047 (1956). (Trans.Soviet Physics - JETP.)
3. G.I.Skanavi, Ya.M.Ksendzov, V.A.Trigubenko & V.G.Prokhvatilov, Ibid., 33, 320 (1957). (Trans.Soviet Physics - JETP.)
4. I.Ts.Lyast, Fizika tverdogo tela, 2, No.6 (1960). (Trans.Soviet Physics - Solid State.)
5. A.V.Rzhanov, Usp.fiz.nauk, 38, 461 (1949).
6. L.N.Syrkin, Kristallografiya (Crystallography), 1, 274 (1956).
7. R.G.Breckenridge, J.Chem.Phys., 16, 959 (1948).
8. I.Ts.Lyast, Zhur.tekhn.fiz., 26, 2293 (1956). (Trans.Soviet Physics - Tech.Phys.); I.Ts.Lyast, Izv.AN SSSR, Ser.fiz., 22, 276 (1958). (Trans.Bulletin 22, 274.)
9. N.P.Bogoroditskii, I.D.Fridberg & N.M.Tsvetkov, Zhur.tekhn.fiz., 26, 1890 (1956). (Trans.Soviet Physics - Tech.Phys.)

APPLICATION OF THE THEORY OF VIBRATIONS OF A CRYSTAL LATTICE WITH DEFORMABLE IONS TO TREATMENT OF THE PHYSICAL PROPERTIES OF BINARY CUBIC CRYSTALS

- K.B.Tolpygo

1. Potential Energy of the Crystal

Solution of a large number of problems in the theory of solids is predicated on knowing the characteristic frequencies and amplitudes of vibration of the crystal lattice. This allows of introducing explicitly the normal coordinates of the crystal and writing the Hamiltonian of their interaction with any arbitrary external fields, electrons, etc. Frequency calculations have been carried out for NaCl (Kellermann[1]), KCl (Iona[2]), diamond (Smith[3]) and Si & Ge (Hsieh[4]) in accord with the early work of Born[5] on the assumption that the potential energy U of the crystal is equal to the sum of the interaction energies of all the ion pairs:

$$U = \frac{1}{2} \sum_{ss'll'} \varphi_{ss'}(\mathbf{R}_{ss'}^{l-l'}), \tag{1}$$

where $\mathbf{R}_{ss'}^{l-l'} = \mathbf{R}_s^l - \mathbf{R}_{s'}^{l'}$ is the radius vector connecting the s-th atom of the l-th cell with the s'-th atom of the l'-th cell. For ionic crystals, $\varphi_{ss'}$ is comprised of the Coulomb, exchange and van der Waal's forces. The first are taken into account for all $\mathbf{R}_{ss'}^{ll'}$, the second and third only for nearest neighbors and are assumed to be central.

In an earlier paper[6] the writer emphasized that it is inconsistent to ignore the polarizability of ions because the dipole moments $\mathbf{P}_s^l$ of the electronic shells and, consequently, the fields associated with them are of the same order of magnitude as the dipole moments $\mathbf{p}_s^l = e_s \mathbf{u}_s^l$ and the field produced by the displacements of the nuclei. In the work of Ref.6 the theory of vibrations of ionic crystals was based on the introduction of a potential energy U, assumed to be a function of the coordinates $\mathbf{R}_s^l$ and the dipole moments $\mathbf{P}_s^l$ of all the ions:

$$U = \frac{1}{2} \sum_{ss'll'} \varphi_{ss'}(\mathbf{R}_s^l \mathbf{P}_s^l \mathbf{R}_{s'}^{l'} \mathbf{P}_{s'}^{l'}). \tag{2}$$

The form of $\varphi_{ss'}$ was determined from consideration of one pair of ions, which was inconsistent. In later contributions[7,8] the author obtained U from calculation of the energy of all the electrons of the crystal in the adiabatic approximation.

The electron wave function for arbitrary small displacements of all the nuclei $\mathbf{u}_s^l = \mathbf{R}_s^l - \mathbf{r}_s^l$ ($\mathbf{r}_s^l$ is the position of the ^l_s-th site) was approximated by the antisymmetrized product of the ψ functions of the individual ions. Accordingly,

$$\Psi = Ac \prod_{sl} \psi_s^l (\vec{\rho}_{sn_s}^{\,l} \ldots \mathbf{R}_s^l), \tag{3}$$

where $\vec{\rho}_{sn_s}^{\,l}$ is the radius vector and spin of the n_s-th electron of the ^l_s ion; ψ_s^l was assumed to differ little from the ψ function of an isolated ion ψ_{s0}:

$$\psi_s^l = \psi_{s0} + \sum_{i=1}^{\infty} c_{si}^l \psi_{si} (\vec{\rho}_{sn_s}^{\,l} \ldots \mathbf{R}_s^l); \quad |c_{si}^l| \ll 1; \tag{4}$$

the ψ_{si} are the excited states of the s-th ion.

The approximation parameters c_{si}^l were determined from the variational principle - the minimum of the average Hamiltonian $\hat{H}$ of the crystal:

$$\min \overline{H} = \min \int \Psi^* \hat{H} \Psi \, d\tau \tag{5}$$

for arbitrary fixed dipole moments:

$$\mathbf{P}_s^l = -e \sum_{n_s=1}^{N_s} \int \vec{\rho}_{sn_s}^{\,l} \, |\psi_s^l|^2 \, d\tau_s^l; \tag{6}$$

here the $(c_{si}^l)^2$ were retained in the leading terms of the Hamiltonian, but only c_{si}^l in the secondary terms. The sought potential energy $U(\mathbf{R}_s^l \ldots \mathbf{P}_s^l)$ was identified with $\min \overline{H}$. Inasmuch as the true state of the electrons must be determined by the absolute rather than by the relative minimum of $\overline{H}$, $\mathbf{P}_s^l$ must be found from the conditions of minimization of $U = U^0$ in the absence of an external field and from the conditions for minimum $U = U^0 - \sum_{sl} \mathbf{E}^0(\mathbf{R}_s^l)\mathbf{P}_s^l$ in the presence of an external field $\mathbf{E}^0(\mathbf{r})$:

$$\frac{\partial U^0}{\partial \mathbf{P}_s^l} = 0 \text{ or } \frac{\partial U^0}{\partial \mathbf{P}_s^l} - \mathbf{E}^0(\mathbf{R}_s^2) = 0. \tag{7}$$

After elimination of $\mathbf{P}_s^l$ from (7), U^0 in the harmonic approximation decomposes only into a sum of terms[9] each of which depends on the displacement of not more than two nuclei, in full agreement with the more general theory of Born[10]; however, the individual terms $\sim \mathbf{u}_s^l \mathbf{u}_{s'}^{l'}$ no longer have the meaning of the interaction energy between atoms. This is particularly clearly evident in the case of homopolar crystals, where such a theory naturally explains the presence of "long-range forces"[11] (i.e., $\sim \mathbf{u}_s^l \mathbf{u}_{s'}^{l'}$ terms for large $\mathbf{R}_{ss'}^{ll'}$), which could not occur only in exchange interaction of neutral atoms but are necessary for agreement of theory with experiment[4].

In the indicated approximation the expression for $U^0(\mathbf{R}_s^l \ldots \mathbf{P}_s^l)$ comprises:

1) the Coulomb interaction of ions regarded as point charges and dipoles;

2) corrections to the Coulomb interaction owing to finite ionic size and exchange interaction of ions in $\psi_{s0}\, u_{12}(r)$ states (these forces are central and significant only for nearest neighbors);

3) the polarization energy $(\mathbf{P}_s^l)^2/2\alpha_s$ (α_s is the polarizability of the s-th ion);

4) the so-called exchange dipole interaction $\sum_s \mathbf{P}_s^l \vec{\beta}_{ss'}(\mathbf{R}_{ss'}^{ll'})$, describing the change in exchange energy owing to polarization of the ions;

5) the deformation terms U_1, appearing owing to mutual deformation of the ions; they are of the order of c_{si}^l with respect to the terms under 2), and depend also on the coordinates of the three neighboring ions, and in the harmonic approximation yield noncentral forces. These terms did not appear in the work of Ref.6.

In the harmonic approximation

$$\begin{aligned} U^0 = \sum_{sl} \Bigg\{ & \frac{(P_s^l)^2}{2\alpha_s} + \sum_{s'l'}^{(n)} \mathbf{P}_s^l \Big[(\mathbf{u}_s^l - \mathbf{u}_{s'}^{l'}) \frac{\beta_{ss'}(r)}{r} + \mathbf{r}\,(\mathbf{u}_s^l - \mathbf{u}_{s'}^{l'})\mathbf{r} \frac{1}{r} \frac{d}{dr} \frac{\beta_{ss'}(r)}{r} \Big]_{r = r_{ss'}^{l-l'}} + \\ & + \frac{1}{4} \sum_{s'l'}^{(n)} \Big[f_{ss'} (\mathbf{u}_s^l - \mathbf{u}_{s'}^{l'})^2 + \frac{d_{ss'}}{|r_{ss'}^{ll'}|^2} \langle (\mathbf{u}_s^l - \mathbf{u}_{s'}^{l'})^2 \cdot \mathbf{r}_{ss'}^{ll'} \rangle^2 \Big] + \\ & + \frac{1}{2} \sum_{s'l'} \Big[\frac{(\mathbf{p}_s^l + \mathbf{P}_s^l)(\mathbf{p}_{s'}^{l'} + \mathbf{P}_{s'}^{l'})}{|r_{ss'}^{ll'}|^3} - \frac{3(\mathbf{p}_s^l + \mathbf{P}_s^l) \cdot \mathbf{r}_{ss'}^{ll'} \, (\mathbf{p}_{s'}^{l'} + \mathbf{P}_{s'}^{l'}) \cdot \mathbf{r}_{ss'}^{ll'}}{|r_{ss'}^{ll'}|^5} \Big] \Bigg\}. \end{aligned} \tag{8}$$

In taking into account the forces under 2) and 5) above, the coefficients $f_{ss'}$ and $d_{ss'}$ are independent. If we neglect the terms under 5) above, we have

$$f_{12} = \frac{1}{r} \frac{du_{12}(r)}{dr} \Big|_{r = r_{1s}^{ll'}}; \quad d_{12} = \Big\{ -\frac{1}{r} \frac{du_{12}(r)}{dr} + \frac{d^2 u_{12}(r)}{dr^2} \Big\}_{r = r_{12}^{ll'}} \tag{9}$$

(here $\sum\limits_{s'l'}^{(n)}$ denotes summation over the n nearest neighbors of the $\substack{l\\s}$-th ion).

Below we shall consider the harmonic vibrations of lattices of the NaCl and CsCl type for maximum wavelengths, determine the parameters of theory and compare them with experiment.

2. Crystal Vibration Equations in the Form of Expansions in Powers of a/λ

The equations describing the natural vibrations of crystals:

$$m_s \ddot{u}^l_{sx} = -\frac{\partial U^0}{\partial u^l_{sx}} \text{ and } 0 = -\frac{\partial U^0}{\partial P^l_{sx}} \tag{10}$$

are solved by means of the substitutions

$$p^l_{sx} = p_{sx} e^{-i\omega t + i\mathbf{K}\mathbf{r}^l_s} \text{ and } P^l_{sx} = P_{sx} e^{-i\omega t + i\mathbf{K}\mathbf{r}^l_s}. \tag{11}$$

The electric field of the system of dipoles (11) was calculated by the method of Ewald[12]. After this, Eq.(10) was expanded in powers of the dimensionless wave vector $\mathbf{k} = a\mathbf{K}$ (a is the separation between nearest ions along the edge of the cube) to terms in $\sim k^2$. For a lattice of the NaCl type Eqs.(10) thereupon become

$$\begin{aligned}\mu_s \mathbf{p}_s \Omega^2 = &-\frac{2\pi}{3}\mathbf{P} + 2\pi\frac{(\mathbf{P}\mathbf{k})\,\mathbf{k} - \mathbf{P}\Omega^2/M}{k^2 - \Omega^2/M} + \mathscr{E}(\mathbf{p}_s + \mathbf{P}_s, \mathbf{k}) + \\ &+ \mathscr{E}'(\mathbf{p}_{3-s} + \mathbf{P}_{3-s}, \mathbf{k}) + H\mathbf{p}_{3-s}k^2 + G(\mathbf{p}_s + \mathbf{p}_{3-s}) - (\tfrac{1}{2}G + 3H)\,\mathbf{p}_{3-s};\ \mathbf{kk} + \\ &+ g\mathbf{P}_2 + \delta_{s1}\left[h\mathbf{P}_2 k^2 - \left(\frac{1}{2}g + 3h\right)\mathbf{P}_2;\ \mathbf{kk}\right];\end{aligned} \tag{12}$$

$$\begin{aligned}O = \frac{\mathbf{P}_s}{A_s} &- \frac{2\pi}{3}\mathbf{P} + 2\pi\frac{(\mathbf{P}\mathbf{k})\,\mathbf{k} - \mathbf{P}\Omega^2/M}{k^2 - \Omega^2/M} + \mathscr{E}(\mathbf{p}_s + \mathbf{P}_s, \mathbf{k}) + \mathscr{E}'(\mathbf{p}_{3-s} + \mathbf{P}_{3-s}, \mathbf{k}) + \\ &+ \delta_{s2}\left[g(\mathbf{p}_1 + \mathbf{p}_2) + h\,\mathbf{p}_1 k^2 - \left(\frac{1}{2}g + 3h\right)\mathbf{p}_1;\ \mathbf{kk}\right].\end{aligned} \tag{13}$$

Here $\mu_s = \frac{m_s}{\mu}$ is the dimensionless mass; $\mu = \frac{m_1 m_2}{m_1 + m_2}$; $\mathbf{P} = \mathbf{p}_1 + \mathbf{p}_2 + \mathbf{P}_1 + \mathbf{P}_2$ is the total amplitude of the dipole moment of the unit cell; $A_s = \frac{2\alpha_s}{\Delta}$ is the dimensionless polarizability of the s-th ion; Δ is the volume of the unit cell ($2a^3$ for NaCl); r_0 is the separation between nearest ions (in NaCl $r_0 = a$);

$$\begin{gathered}h = -\frac{\Delta}{2e_1 r_0}\beta_{21}(r_0); \quad g = \frac{n}{6}\frac{\Delta}{e_1}\frac{d\beta_{21}(r)}{dr}\bigg|_{r=r_0} - 4h; \\ H = -\frac{\Delta}{2e_1^2}f_{12};\ G = \frac{n}{6}\cdot\frac{\Delta}{e_1^2}(d_{12} + f_{12});\ \Omega^2 = \frac{\mu\Delta}{2e_1^2}\omega^2; \\ M = \frac{\mu c^2 \Delta}{2a^2 e_s^2} \approx 10^9 - 10^{11}.\end{gathered} \tag{14}$$

In view of the appreciably greater deformability of the anion, we neglected the β_{12} as compared with β_{21}. This yields an advantage over the other limiting case when $\beta_{12} = -\beta_{21}$.[6] For term Ω^2/M appears only when one takes into account lag in the electrostatic interaction and must be retained only for vibration wavelengths $\frac{2\pi}{|K|}$, comparable with the wavelength of the same frequency ω, i.e., $\lambda_0 = \frac{2\pi c}{\omega}$:

$$\begin{aligned}\mathscr{E}_{\mathrm{NaCl}}(\mathbf{p},\mathbf{k}) &= 0.2371\,\mathbf{p}k^2 - 0.2900\,(\mathbf{pk})\,\mathbf{k} - 0.4213\,\mathbf{p};\ \mathbf{kk};\\ \mathscr{E}'_{\mathrm{NaCl}}(\mathbf{p},\mathbf{k}) &= -0.4020\,\mathbf{p}k^2 - 0.9856\,(\mathbf{pk})\,\mathbf{k} + 2.191\,\mathbf{p};\ \mathbf{kk},\end{aligned} \tag{15}$$

where $\mathbf{p}_1;\ \mathbf{kk}$ denotes the vector $\mathbf{e}_x p_x k_x^2 + \mathbf{e}_y p_y k_y^2 + \mathbf{e}_z p_z k_z^2$. Quadratic expansion in $\mathbf{k}$ is allowable when $k^2 \leqslant 1$.

For CsCl crystals the vibration equations are fully analogous to (12) and (13), but

$$\begin{aligned}\mathscr{E}_{\mathrm{CsCl}}(\mathbf{p},\mathbf{k}) &= -0.0824\,\mathbf{p}k^2 - 0.6377\,(\mathbf{p},\ \mathbf{k})\,\mathbf{k} + 0.8850\,\mathbf{p};\ \mathbf{kk};\\ \mathscr{E}'_{\mathrm{CsCl}}(\mathbf{p},\mathbf{k}) &= 0.2680\,\mathbf{p}k^2 + 0.4024\,(\mathbf{pk})\,\mathbf{k} - 1.2065\,\mathbf{p};\ \mathbf{kk}.\end{aligned} \tag{16}$$

Moreover, the terms containing G, H, g and h have a somewhat different form: in Eq. (12) we must have

$$\begin{aligned}&G(\mathbf{p}_1 + \mathbf{p}_2) - \frac{1}{8}G\mathbf{p}_{3-s}k^2 - \left(\frac{1}{4}G + 2H\right)[(\mathbf{p}_{3-s},\mathbf{k})\,\mathbf{k} - \mathbf{p}_{3-s};\ \mathbf{kk}] +\\ &\quad + g\mathbf{P}_2 - \delta_{s1}\left\{\frac{1}{8}g\mathbf{P}_2k^2 + \left(\frac{1}{4}g + 2h\right)[(\mathbf{p}_2\mathbf{k})\,\mathbf{k} - \mathbf{P}_2;\ \mathbf{kk}]\right\},\end{aligned} \tag{17}$$

and in Eq. (13)

$$\delta_{s2}\left\{g(\mathbf{p}_1 + \mathbf{p}_2) - \frac{1}{8}g\mathbf{p}_1\mathbf{k}^2 - \left(\frac{1}{4}g + 2h\right)[(\mathbf{p}_1,\mathbf{k})\,\mathbf{k} - \mathbf{p}_1,\ \mathbf{kk}]\right\}. \tag{18}$$

Below we shall solve Eqs. (12) and (13) by the method of successive approximations - by expansion in powers of $\mathbf{k}$.

3. Optical Mode. Determination of the Parameters of Theory

We set

$$\Omega^2 = \Omega_0^2 + k^2\Omega_2^2 + \ldots;\ \mathbf{p}_s = \mathbf{p}_s^0 + \mathbf{k}^2\mathbf{p}_s^{(2)} + \ldots;\ \mathbf{P}_s = \mathbf{P}_s^0 + \mathbf{k}^2\mathbf{P}_s^{(2)} + \ldots. \tag{19}$$

In the zeroth approximation in $\mathbf{k}$ the equations for both types of lattice have the same form:

$$\begin{aligned}\mu_s\mathbf{p}_s^0\Omega_0^2 &= -\frac{2\pi}{3}\mathbf{P}^0 + 2\pi\frac{(\mathbf{P}^0\mathbf{s})\mathbf{s} - \mathbf{P}^0/n^2}{1 - 1/n^2} + g\mathbf{P}_2^0 + G(\mathbf{p}_1^0 + \mathbf{p}_2^0);\ s = 1,2,\ldots\\ O &= \frac{\mathbf{P}_s^0}{A_s} - \frac{2\pi}{3}\mathbf{P}^0 + 2\pi\frac{(P^0\mathbf{s})\mathbf{s} - \mathbf{P}^0/n^2}{1 - 1/n^2} + \delta_{s2}g(\mathbf{p}_1^0 + \mathbf{p}_2^0);\end{aligned} \tag{20}$$

where $n = \sqrt{k^2M/\Omega_0^2} = \frac{kc}{\omega}$ is the index of refraction for the given wavelength and $\mathbf{s} = \frac{\mathbf{k}}{|\mathbf{k}|}$ is the unit vector in the direction of the wave vector.

From the first pair of equations (20) we deduced the usual conditions for vibrations: for the optical mode $\Omega_0^2 \neq 0$ and $\mu_1\mathbf{p}_1^0 - \mu_2\mathbf{p}_2^0 = 0$, and for the acoustical mode $\Omega_0^2 = 0$ and $\mathbf{p}_2^0 = -\mathbf{p}_1^0;\ \mathbf{P}_s^0 = 0$.

For the first, the condition for the set (20) being solvable is

$$\left[\left(1 - \frac{2\pi}{3}A\right)(G - A_2g^2 - \Omega_0^2) - \frac{2\pi}{3}\beta^2\right]\mathbf{P} + 2\pi\left[A(G - A_2g^2 - \Omega_0^2) + \beta^2\right]\frac{(\mathbf{P}^0\mathbf{s})\,\mathbf{s} - \mathbf{P}^0/n^2}{1 - 1/n^2} = 0, \tag{21}$$

where $A = A_1 + A_2$ and $\beta = 1 - A_2g$.

Thus there may be longitudinal vibrations $\mathbf{P}^0 \parallel \mathbf{k}$ with

$$\Omega_0^2 = \Omega_{11}^2 = G - A_2g^2 + \frac{4\pi}{3}\frac{\beta^2}{1 + (4\pi/3)A} \tag{22}$$

and transverse vibrations $(\mathbf{P}^0\mathbf{k}) = 0$. For the last, Eq.(21) can readily be solved for n^2. As a result we obtain

$$n^2 = \frac{1+\frac{4\pi}{3}A}{1+\frac{2\pi}{3}A} + \frac{2\pi\beta^2}{\left(1-\frac{2\pi}{3}A\right)^2} : (\Omega_g^2 - \Omega_0^2), \tag{23}$$

where

$$\Omega_g^2 = G - A_2 g^2 - \frac{\frac{2\pi}{3}\beta^2}{1-\frac{2\pi}{3}A}.$$

Eq.(23) agrees with the usual dispersion formula

$$n^2 = n_0^2 + \frac{(\varepsilon - n_0^2)\,\omega_g^2}{\omega_g^2 - \omega^2}, \tag{24}$$

while Ω_g is a dimensionless dispersion frequency equal to $\sqrt{\frac{\mu\Delta}{2e_s^2}}\,\omega_g$.

We determine the parameters of theory from Eqs.(22), (23) and (25):

$$A = \frac{3}{2\pi}\frac{n_0^2-1}{n_0^2+2};\ \beta^2 = \frac{9}{2\pi}\frac{(\varepsilon - n_0^2)}{(n_0^2+2)^2}\Omega_g^2 \text{ and } g = \frac{1-\beta}{A_2};\ G = A_2 g^2 + \frac{\varepsilon+2}{n_0^2+2}\Omega_g^2. \tag{25}$$

Moreover, as will be evident from (22), (23) and (25).

$$\Omega_{11}^2/\Omega_g^2 = \varepsilon/n_0^2.$$

Vibrations in the range of long wavelengths $\Omega^2/M \sim k^2$ are mixed optical-mechanical vibrations, and the functional dependence $\omega(k)$ is described not by three but by five optical branches. With increase of k they all split into three purely mechanical and two purely optical modes. The $\Omega_g^2 < \Omega^2 < \Omega_{11}^2$ region (see figure) is a forbidden region: in it we have complete internal reflection. These results, which were deduced by the writer in Ref.6, were independently arrived at by Huang[13] and incorporated in this form in the monograph listed under Ref.10.

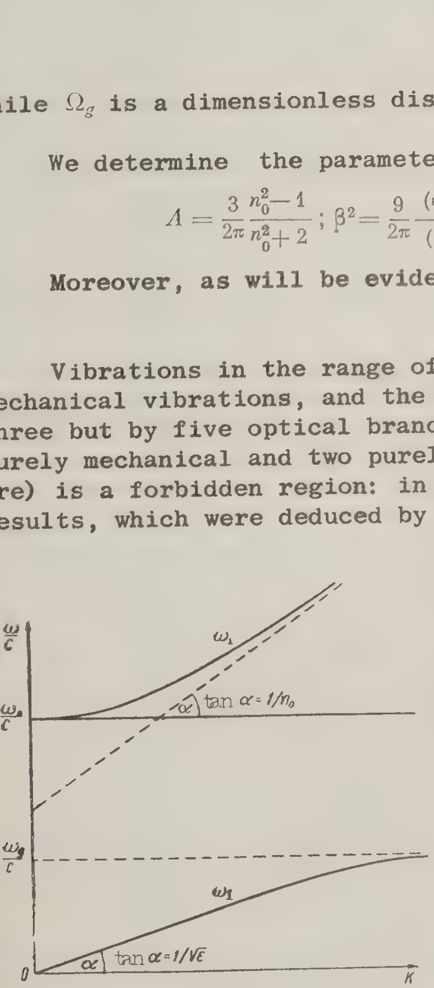

Equations (25) allow of determining the three parameters A, g and G of theory, if the experimental ω dependence of n^2 in the region of infrared dispersion is available, or if the values of n_0^2, ε and ω_g are known (the last is found from the peak of the infrared absorption). The magnitude of A_2 can be determined from $A_2 = A - A_1$, if $A_1 = 2\alpha_1/\Delta$ is taken on the basis of the theoretical values of the polarizability of the cation.[14] The parameter H of theory is determined from the condition of equilibrium of the lattice with respect to elongation. This condition gives

$H = \frac{\alpha_M}{n}\frac{\Delta}{2r_0^3}$ (α_M is Madelung's constant).

In Table 1 we have assembled the values of the parameters of theory for 25 crystals for which there are adequate experimental data. For the crystals identified by asterisks (*) we use the data on dispersion, for the crystals by degree signs (°) we used the data on ε, n_0^2 and the compressibility χ and for all other crystals the data on ε, n_0^2 and ω_g^2. It is interesting to note that despite the appreciable scatter of n_0^2, ε and ω_g^2, the values of the dimensionless parameters

Table 1

Values of the parameters of theory for 25 ionic binary crystals

Crystal	$a\cdot10^8$	n_0^2	ε	$\omega_g^2\cdot10^{-28}$	$\alpha_1\cdot10^{21}$	$\alpha_2\cdot10^{24}$	$A\cdot10^5$	$A_1\cdot10^5$	$A_2\cdot10^5$	$\alpha_2\text{theo}\cdot10^{24}$	Ω_g^2	g	G	β^2
LiF*	2,013	1,9216	8,923	33,3	0,025	0,98—1,04	11263	306	10956	0,89	0,9938	1,7902	3,116	0,6462
LiCl°	2,565	2,75	11,05			3,05—3,66	17590	150	17440	2,94	0,863	1,867	2,98	0,454
LiBr°	2,745	3,16	12,1			4,17—4,77	19990	120	19870	4,11	1,138	1,309	3,45	0,548
LiI°	3,00	3,80	11,03			6,28—7,55	2050	90	22960	6,20	0,826	2,158	2,93	0,255
NaF*	2,31	1,7440	5,468	19,6	0,17	6,28—7,55	9488	1380	8109	1,09	1,8093	2,099	3,966	0,6886
NaCl*	2,820	2,3303	5,851	9,410			14668	758	13970	3,12	2,1189	1,762	4,274	0,5699
NaBr	2,980	2,62	5,99	6,375			16742	642	16100	4,26	2,169	1,862	4,31	0,4904
NaI	3,230	2,91	6,60	4,853			18069	504	18570	6,09	2,292	1,57	4,47	0,5023
KF°	2,665	1,85	6,05				10541	4727	6315	1,20	1,656	2,85	3,98	0,672
KCl*	3,145	2,1748	4,870	6,950	0,80		13436	2569	10867	3,38	2,8935	1,836	5,128	0,6409
KBr*	3,2966	2,3615	4,825	4,580			14905	2233	12672	4,54	3,1007	1,907	5,313	0,5752
KI*	3,532	2,6481	5,20	3,340			16930	1827	15103	6,62	3,1473	1,790	5,359	0,5325
RbCl	3,270	2,19	5,0	4,934	1,5		13560	4290	9270	3,24	3,112	1,68	5,46	0,7134
RbBr	3,425	2,33	5,0	2,730			14670	3730	10930	4,39	3,261	1,69	5,58	0,6651
RbI	3,665	2,63	5,0	2,115			16810	3090	13760	6,77	3,829	1,61	6,14	0,6064
CsCl	4,11	2,60	7,20	3,410	2,35		16610	6770	9840	3,41	2,385	1,41	4,96	0,7426
CsBr*	4,29	2,7844	6,50	1,944			17808	5965	11842	4,665	2.751	1,691	5,226	0,6396
CsI°	4,56	3,03	5,65				19270	4957	14312	6,78	Complex	4,155—0,59i	4,03	Complex
TlCl	3,83	5,10	31,9	2,592	4,78		27570	17016	10556	2,97	1,583	—0,924	7,65	1,2057
TlBr	3,978	5,41	29,8	1,352			28420	15187	13230	4,16	1,760	—0,438	7,58	1,1194
AgCl*	2,77	4,0088	12,0	3,904	1,72		23908	8072	15816	3,36	1,5940	1,828	1,242	0,5053
AgBr	2,885	4,62	13,1	2,067			26110	7163	18950	4,55	1,640	1,72	4,30	0,4547
MgO*	2,10	2,9564	8,476	68,85	0,10	2,75—3,88	18847	1080	17767	1,645	1,1073	2,268	3,255	0,3564
CaO	2,40	3,28	11,8	48,67	0,54		20620	3906	16710	2,31	1,384	1,33	3,91	0,6060
SrO	2,67	3,31	13,3	16,06	1,0		20770	5891	14880	2,53	0,664	2,82	3,10	0,3363

Table 2

Experimental and theoretical values of the elastic moduli for 25 crystals in the rigorous heteropolarity approximation and in the $e^*=\beta e$ approximation in the absence of exchange-dipole forces

Crystal	Experiment				Theory with $e_s=\pm e^*$, $g\neq 0$			Theory with $e^*=\beta e^*$ in the absence of exchange-dipole forces			
	$C_{11}\cdot 10^{-11}$	$C_{12}\cdot 10^{-11}$	$C_{44}\cdot 10^{-11}$	$\chi\cdot 10^{12}$	$C_{11}\cdot 10^{-11}$	$C_{44}=C_{42}(\times 10^{-11})$	$\chi\cdot 10^{12}$	e^*/e	$C_{11}\cdot 10^{-11}$	$C_{12}=C_{44}(\times 10^{-11})$	$\chi\cdot 10^{12}$
LiF	9,8—11,8	4,0—4,4	5,5—6,3	1,4—1,5	12,12	4,885	1,371	0,804	13,11	3,157	1,545
LiCl				3,78		1,853		0,674		0,841	
LiBr				4,28		1,413		0,740		0,774	
LiI				7,2		0,990		0,504		0,252	
NaF				2,11	10,43	2,817	1,867	0,830	10,74	1,940	2,052
NaCl	4,7 — 5,1	1,2—1,3	1,2—1,3	4,1—4,14	5,256	1,268	3,85	0,755	5,559	0,7226	4,283
NaBr	3,02 — 3,25	1,22—1,31	1,33	5,09	4,266	1,017	4,76	0,700	4,487	0,4987	5,470
NaI				7,07	3,26	0,737	6,33	0,709	3,500	0,3702	7,057
KF				3,3		1,590		0,820		1,068	
KCl	3,6—4/1	0,6—0,7	0,6—0,7	5,1—5,5	4,405	0,820	4,96	0,801	4,512	0,5255	5,346
KBr	3,3—3,4	0,5—0,6	0,5—0,6	6,5—6,7	3,828	0,679	5,78	0,758	3,955	0,3905	6,333
KI	2,68	0,43	0,36—0,42	8,37—8,6	2,964	0,520	7,50	0,730	3,088	0,2769	8,237
RbCl				7,4	4,10	0,702	5,45	0,845	4,24	0,5008	5,72
RbBr				7,65	3,51	0,503	6,41	0,816	3,64	0,3346	6,79
RbI				9,58	3,04	0,445	7,64	0,779	3,16	0,2698	8,11
CsCl				5,9	4,27	0,873	4,98	0,862	3,61	1,086	5,19
CsBr				6,92—7,20	3,699	0,827	5,60	0,800	2,893	1,056	5,99
CsI				9,3—8,566							
TlCl				4,8	7,11	2,60	2,44	1,098	7,68	2,242	2,47
TlBr				5,2	6,07	2,20	2,87	1,058	6,37	2,034	2,88
AgCl	6,05	3,64	0,624	2,25	5,585	1,363	3,61	0,711	5,897	0,688	4,124
AgBr	5,622	3,28	0,729	2,8	4,845	1,158	4,189	0,675	5,175	0,5265	4,186
MgO	29,0	8,75	15,5	0,59—0,7	44,20	16,50	0,388	1,200	43,75	5,880	0,546
Cao				4,57	35,0	9,67	0,551	1,557	38,53	5,860	0,596
Sro					18,0	7,36	0,917	1,160	15,93	2,475	1,435

---

*2e for MgO, CaO and SrO.

A, Ω_g^2, G and, particularly, the exchange-dipole parameter g fall within a considerably narrower range. This indicates the great similarity of the properties of crystals if for the unit of length we take a, for the unit of mass μ, and for the unit of energy e_s^2/a.

It will also be apparent from Table 1 what a significant step forward the present theory represents. In the theory of rigid ions we would have $A_1 = A_2 = 0$ and $n_0^2 = 1$, which, of course, is highly erroneous. In the "classical" theory of lattices with deformable ions, i.e., in the case of neglect of exchange-dipole forces, we would have $g = 0$ and $\beta = 1$. Yet from Eq.(25) β^2 is found to be of the order of 0.5-0.7. Thus these forces prove to be appreciable. Finally, one could assume that $g=0$, but then reject the concept of complete heteropolarity of the compound. Then to obtain agreement of ε, n_0^2 and ω_g with experiment it would be necessary to assume that the charge e^* is equal to $e\beta$ which is apparently too low a value, and as we shall see below, worsens the agreement with experiment.

4. Acoustical Vibrations and Elastic Properties of Crystals

For the acoustical branches, considering Eq.(12) in the approximation in $\sim k^2$ and subtracting these from each other to eliminate $\mathrm{p}_s^{(2)}$ and $\mathrm{P}_s^{(2)}$, we obtain

$$\frac{\mu_1 + \mu_2}{2} \Omega_2^2 \mathrm{p}_1^{(0)} = (0.6390 - H)\mathrm{p}_1^0 + 0.6956\,(\mathrm{p}_1^0 s)\,\mathrm{s} + \left(\frac{1}{2} G - 2.6126\,\mathrm{p}_1^0;\ \mathrm{ss}\right), \tag{26}$$

which agrees with the macroscopic theory of elasticity equation

$$\rho\omega^2 \mathbf{u} = C_{44}\,\mathbf{u}k^2 + (C_{12} + C_{44})(\mathbf{u}\cdot\mathbf{k})\,\mathbf{k} + (C_{11} - C_{12} - 2C_{44})\ \mathbf{u};\ \mathbf{kk} \tag{27}$$

(u is the displacement vector and ρ is the density). Whence, comparing, in the approximation of central forces $H_{\mathrm{NaCl}} = \alpha_M/6 = 0.29126$,

$$C_{44} = C_{12} = \frac{e_s^2}{a^4}\,0.3478 \text{ and } C_{12} = \frac{e_s^2}{a^4}\left(\frac{1}{2} G - 0.6955\right). \tag{28}$$

Proceding analogously for the case of CsCl type crystals, we find in the case of central forces $H = \dfrac{\alpha_M}{6\sqrt{3}}$;

$$C_{12} = C_{44} = \frac{e_s^2}{a^4}\left(\frac{1}{2} G - 1.4018\right) \text{ and } C_{11} = \frac{e_s^2}{a^4}\left(\frac{1}{2} G + 0.2036\right). \tag{29}$$

In Table 2 we have given the values of the moduli C_{ik} and the compressibility $\chi = \dfrac{3}{C_{11} + 2C_{12}}$ and indicated the ranges of the corresponding experimental values.

For NaCl and CsCl type crystals

$$\frac{3}{\chi} = \frac{e_s^2}{a^4} \cdot \frac{1}{2} G \text{ and } \frac{e_s^2}{a^4}\,\frac{3}{2}\,G. \tag{30}$$

If the values of ω_g are known, we can find G from the above and then from the last two equations under (25) the value of g, defined by the quadratic equation

$$\frac{G - A_2 g^2}{(1 - A_2 g)^2} = \frac{2\pi}{9}\,\frac{(\varepsilon + 2)(n_0^2 + 2)}{\varepsilon - n_0^2}.$$

Where adequate experimental data for checking the theory are not available, we can test the theory indirectly by seeing whether the calculated values of g are close to the values for other crystals. From this standpoint LiCl gives best agreement, while the agreement for LiBr, LiI and KF is worse. For CsI we obtain a complex g, which, of course, is meaningless. The poorest results are obtained for thalium halides.

If we reject the assumption of central forces, H may also be regarded as a parameter of theory. If, in addition, we supplement the theory by introduction of the unknown van der Waal's forces for the second configuration sphere

$u_{ss}(r) = -\frac{\alpha_{ss}}{r^6}$ (for the first sphere they may be regarded as included in $u_{12}(r)$),

then for an NaCl type lattice we obtain

$$C_{44} = \frac{e_s^2}{a^4}[0.6390 - H - (a_{11} + a_{22})]; \; C_{12} = \frac{e_s^2}{a^4}[0.0565 + H - 3(a_{11} + a_{22})];$$

$$C_{11} = \frac{e_s^2}{a^4}\left[\frac{1}{2}G + 2H - 3(a_{11} + a_{22}) - 1.2780,\right] \tag{31}$$

where

$$a_{ss} = \frac{3d_{ss}}{4e_s^2 a^5}.$$

In the particular case of central forces $H = \frac{\alpha_M}{6} + a_{11} + a_{22}$, elimination of a_{ss} leads to the relations

$$C_{12} = C_{44} \quad \text{and} \quad C_{11} - \frac{1}{4}(C_{12} + C_{44}) = \frac{e_s^2}{a^4}\left(\frac{1}{2}G - 0.8693\right); \tag{32}$$

on the contrary, if we neglect van der Waal's forces with noncentral forces, elimination of H yields

$$C_{12} + C_{44} = \frac{e_s^2}{a^4} \cdot 0.6956 \quad \text{and} \quad C_{11} + 2C_{44} = \frac{e_s^2}{a^4}\frac{1}{2}G. \tag{33}$$

Finally, in the case of arbitrary a_{ss} and H there must obtain the relation

$$\frac{3}{4}C_{44} - \frac{5}{4}C_{12} + C_{11} = \frac{e_s^2}{a_4}\left(\frac{1}{2}G - 0.8693\right). \tag{34}$$

Table 3 gives the values of the right and left parts of Eqs.(32), (33) and (34) for the central force and van der Waal's force approximations, the noncentral force approximation and the approximation of nearest neighbors and, finally, for the more general case of Eq.(34). In the last columns of Table 3 we give the values of H and $a_{11} + a_{22}$, calculated by means of Eq.(31).

Lastly, we can consider the variant of the theory neglecting exchange-dipole forces, which assumes a constant fractional charge (complete disregard of ionic polarization is inadmissible inasmuch as $n_0^2 \sim 2$-2.5). Then, setting $e^* = \beta e$, we see that G becomes $\frac{1}{\beta^2}(G - A_2 g^2)$, while H retains its initial value. In the central force approximation for crystals of the NaCl type, we obtain

$$C_{12} = C_{44} = 0.3478\frac{e^2}{a^4}\beta^2; \; C_{11} = \frac{e^2}{a^4}\left(\frac{1}{2}G - \frac{1}{2}A_2 g^2 - 0.6955\beta^2\right);$$

$$\frac{3}{\chi} = \frac{e^2}{2a^4}(G - A_2 g^2), \tag{35}$$

and for crystals of the CsCl type,

$$C_{12} = C_{44} = \frac{e^2}{a^4}\left(\frac{1}{2}G - \frac{1}{2}A_2 g^2 - 1.4018\beta^2\right); \; C_{11} = \frac{e^2}{a^4}\left(\frac{1}{2}G - \frac{1}{2}A_2 g^2 + 2.8036\beta^2\right);$$

$$\frac{1}{\chi} = \frac{e^2}{2a^4}(G - A_2 g^2). \tag{36}$$

Table 3

Comparison with experiment of the elastic constants of theory taking into account noncentral forces as well as van der Waal's forces between like ions

Crystal	Noncentral forces $(a_{11} + a_{22} = 0)$				Central forces $(a_{11} + a_{22} \neq 0)$; $\left[C_{11} - \frac{1}{4}(C_{12} + C_{44})\right] \cdot 10^{-11}$ * experiment	Central & noncentral forces $(a_{11} + a_{22} \neq 0)$; $\left[\left(\frac{1}{2} G - 0.86934\right) \times \frac{e_s^2}{a^4}\right] \times 10^{-11}$ * theory	Noncentral forces $(a_{11} + a_{22} \neq 0)$		
	$(C_{12} + C_{44}) \cdot 10^{-11}$		$(C_{11} + 2C_{44}) \cdot 10^{-11}$				$\left(\frac{3}{4} C_{44} - \frac{5}{4} C_{12} + C_{11}\right) \cdot 10^{-11}$ * experiment	$a_{11} + a_{22}$	H
	Experiment	Theory	Experiment	Theory					
LiF	9,5—11,7	9,77	20,8—24,4	19,9	7,42—9,11	9,68	8,92—11,02	0	—0,054
NaCl	2,4—2,6	2,54	7,1—7,7	7,79	4,1—4,45	4,62	4,1—4,45	0	0,29126
NaBr	2,55—2,64	2,034	5,68	6,30	2,381	2,758	2,495	—0,0441— —0,0518	0,2096—0,2327
KCl	1,2—1,4	1,64	4,8—5,5	6,05	3,3—3,75	4,00	3,3—3,75	0,0396	0,328
KBr	1,0—1,2	1,36	4,3—4,6	5,186	3,05—3,1	3,488	3,05—3,10	0,0320	0,324
KI	0,79—0,85	1,04	3,40—3,52	4,00	2,48—2,74	2,704	2,41—2,45	0,0418—0,0318	0,3799—0,3297
AgCl	4,264	2,726	7,3	8,31	4,98	4,904	1,97	—0,098	0,0995
AgBr	4,01	2,306	7,08	7,151	4,62	4,266	1,704	—0,127	0,0902
MgO	24,25	33,00	60,0	77,2	4,75	35,95	29,67	0,046	—0,0635

---

* $C_{11} - \frac{1}{4}(C_{12} + C_{44}) = \left(\frac{1}{2} G - 0.86934\right) \frac{e_s^2}{a^4} = \frac{3}{4} C_{44} - \frac{5}{4} C_{12} + C_{11}$.

The corresponding values of the moduli are given in the next to the last columns of Table 2.

5. Comparison of Theory with Experiment and Discussion

Comparison of the theoretical moduli C_{ij} with experiment (Table 2) for nine crystals shows that the theory is best applicable to alkali halide compounds with ions not differing greatly as regards size and is not as well suited for treatment of AgCl, AgBr and MgO. The same thing is indicated by comparison of the compressibility for other crystals. The results are poorer for rubidium and, particularly, cesium crystals and very poor indeed for TlCl, TlBr, CaO and SrO. Refinement of the theory (see Table 3) shows that for NaCl the initial variant is adequate. For NaBr, KCl and KBr, the central force approximation is suitable, but $a_{11} - a_{22} \neq 0$. For LiF on the contrary, $a_{11} + a_{22}$ may be neglected, but the noncentral forces are significant, as in the case of MgO (only the agreement with experiment for MgO is poorer). For AgCl and AgBr both refinements of theory appear to be wholly inadequate. The alternative assumption of fractional charge of ions neglecting exchange-dipole forces leads to better agreement with experiment for the compressibility (Table 2), but then for most crystals the agreement with experiment as regards C_{ij} is impaired. This theory gives still larger values of C_{11}, while for C_{12} and C_{44} excessively low values are obtained. It would seem that better agreement with experiment for part of the crystals could be attained by retaining the exchange-dipole forces and fractional charges, for example, taking $\frac{e^*}{e} \approx \sqrt{3}$ in agreement with this writer's earlier deductions[15]. However, in this case, theory gives consistently high values of C_{11}. For crystals where the agreement with experiment is poor, introduction of the parameter e^* gives no improvement. Apparently for oxides, for AgCl, AgBr, TlCl and TlBr and partially for cesium crystals the assumption of rigid heteropolarity is inadequate even in the zeroth approximation. Examination of Table 2 leads us to conclude that exchange-dipole forces are significant and that the given theory has the advantage over the theory with constant fractional ionic charges. A more perfect theory should take into account not only the deformation of ions but also the change in their charges incident to displacement.

Physical Institute,
Academy of Sciences of the Ukrainian SSR

References

1. E.W.Kellermann, Phil.Trans.Roy.Soc., A238, 513 (1940).
2. M.Iona, Phys.Rev., 60, 822 (1941).
3. Helen Smith, Phil.Trans.Roy.Soc., A241, 105 (1948).
4. C.J.Hsieh, J.Chem.Phys., 22, 306 (1954).
5. M.Born & M.Göppert-Mayer, Theory of Solids in Handbuch der Physik (1934). (Cited in Russian trans., 1938.)
6. K.B.Tolpygo, Zhur.eksp.i teor.fiz., 20, 497 (1950).
7. K.B.Tolpygo, Ukr.fiz.zhur. (Ukrainian Physics Journal), 2, 242 (1957).
8. K.B.Tolpygo, Ibid., 4, 72 (1959).
9. K.B.Tolpygo, Trudy (Proceedings), Kiev State University, Math.Collection, No.5, 99 (1951).
10. M.Born & Kun Huang, Dynamical Theory of Crystal Lattices, Oxford, 1954.
11. V.S.Mashkevich & K.B.Tolpygo, Zhur.eksp.i teor.fiz., 32, 520 (1957). (Trans.Soviet Physics - JETP.)

12. P.P.Ewald, Ann.Phys., 64, 253 (1921).
13. Kun Huang, Proc.Roy.Soc., A208, 352 (1951).
14. Landolt-Bornstein, Phys.-Chem. Tabellen, 1950.
15. K.B.Tolpygo, Trudy (Proceedings), Inst.of Physics, Ac.of Sci. of the Ukrainian SSR, No.5, 28 (1954).

* * * * * * *

CONTRIBUTION TO THE THEORY OF THE PERMITTIVITY OF AN ANISOTROPIC MEDIUM POLARIZED AT A FINITE RATE

- R.A.Suris & B.N.Finkel'shtein

Earlier one of us in collaboration with Fastov[1] elaborated a thermodynamic theory of electric polarization of an isotropic homogeneous dielectric. In the present paper, this theory will be extended to the case of isothermal polarization of an anisotropic dielectric. In the case of change of the electric field E_i $(i = 1, 2, 3)$ at a finite rate, the thermodynamic equilibrium in the dielectric is disturbed, and as a result there occur in it one or more relaxation processes characterized by definite relaxation times. For small deviations from the equilibrium state there remain valid the usual thermodynamic relationships, for example,

$$D_i = -4\pi\partial\Phi/\partial E_i, \tag{1}$$

where D_i is the component of the electric induction vector, and Φ is the unit volume thermodynamic potential, which is related to the free energy by

$$\Phi = F - \frac{1}{4\pi} D_i E_i \tag{2}$$

(summation is implied over repeated indices).

Without invalidating the generality of the discussion, we shall limit our present consideration to one relaxation process. In the case of nonequilibrium state of the system, for describing it, in addition to the usual thermodynamic variables, one must introduce a relaxation variable, in the given case, the vector ξ_i.

In the approximation of Ref.1, the thermodynamic potential may be written in the form

$$\Phi = \Phi_0 - \frac{1}{4\pi}\left(\frac{1}{2}\alpha_{ik}E_iE_k + \beta_{ik}E_i\xi_k + \frac{1}{2}\gamma_{ik}\xi_i\xi_k\right), \tag{3}$$

where $\alpha_{ik} = \alpha_{ki}$, $\gamma_{ik} = \gamma_{ki}$ and β_{ik} are temperature and pressure dependent constants for the material, and Φ_0 is the thermodynamic potential of the dielectric for zero field. We write the following kinetic equation for the variable ξ_i:

$$\frac{\partial\Phi}{\partial\xi_i} = \frac{\partial\Omega}{\partial\dot{\xi}_i}, \tag{4}$$

where the dissipative function Ω is defined by

$$\Omega = \frac{1}{2} h_{ik}\dot{\xi}_i\dot{\xi}_k. \tag{5}$$

The kinetic coefficients h_{ik} satisfy the Onsager relation

$$h_{ik} = h_{ki}.$$

By appropriate transformation of the coordinates we bring (5) to the form

$$\Omega = \xi'_i \xi'_k; \tag{5'}$$

thereupon (3) becomes

$$\Phi = \Phi_0 - \frac{1}{4\pi}\left(\frac{1}{2}\gamma'_{ik}\xi'_i\xi'_k + \beta'_{ik}E'_i\xi'_k + \frac{1}{2}\alpha'_{ik}E'_iE'_k\right), \tag{3'}$$

and the kinetic equation assumes the form

$$\frac{\partial\Phi}{\partial\xi'_i} = \dot{\xi}'_i. \tag{4'}$$

Hereinafter we omit the primes. Insertion of (3') in (4') yields

$$\dot{\xi}_i + \frac{1}{4\pi}\gamma_{ik}\xi_k = -\frac{1}{4\pi}\beta_{ki}E_k, \tag{6}$$

or in symbolic form

$$\dot{\xi} + \Gamma\xi = f, \tag{6'}$$

where Γ is an operator defined by the matrix elements

$$\frac{1}{4\pi}\gamma_{ik}; \quad f_i = -\frac{1}{4\pi}\beta_{ki}E_k.$$

Introducing by way of initial condition the requirement that in the infinitely remote past $\xi_i = 0$, if $f(-\infty) = 0$, we obtain the following solution of Eq.(6') satisfying this condition:

$$\xi(t) = f(t) - \int_{-\infty}^{t} e^{-(t-t')\Gamma}\dot{f}(t')\,dt'. \tag{7}$$

Below it will be shown that the eigenvalues of the operator determine the inverse relaxation times.

Let us transform to the system of coordinates the axes of which coincide with the eigenvectors $e^{(k)}$ of the operator defined by the equations

$$\Gamma e^{(k)} = \gamma_k e^{(k)} \qquad (k = 1, 2, 3). \tag{8}$$

In view of the relationship

$$\gamma_{ik} = \gamma_{ki} = \gamma^{*}_{ki}$$

(here the * indicates transition to a complex conjugate quantity), the operator Γ is Hermitian. Invoking the familiar property of a function of an operator

$$e^{\alpha\Gamma} e^{(k)} = {}^{\alpha\gamma k} e^{(k)}$$

and transforming back to the old coordinate axes, we obtain

$$\xi_i = -\frac{1}{4\pi}\sum_{p,i,k} b_{pj}b_{pi}\beta_{kj}\tau_p E_k(t) + \frac{1}{4\pi}\sum_{p,i,k} b_{pj}b_{pi}\beta_{kj}\tau_p \int_{-\infty}^{t} e^{-\frac{t-t'}{\tau_p}}\dot{E}_k(t')\,dt'. \tag{9}$$

Here we have introduced the notation

$$\tau_p = 1/\gamma^{(p)};$$

$b_{pi} = (e^{0(i)}, e^{(p)})$ is the scalar product of a unit vector in the direction of the old i-th coordinate axis and a unit vector along the new p-th axis.

It follows from Eq.(1) that

$$D_i = \sum_k \Big(\alpha_{ik} - \frac{1}{4\pi} \sum_{q,p,j} \beta_{iq} b_{pq} b_{pj} \beta_{kj} \tau_p \Big) E_k + \frac{1}{4\pi} \sum_{q,p,j,k} \beta_{iq} b_{pq} b_{pj} \beta_{kj} \tau_p \int_{-\infty}^{t} \exp[-(t-t')/\tau_p]\, \dot{E}_k(t')\, dt'. \quad (10)$$

The results obtained show that the inverse eigenvalues of the operator Γ represent relaxation times. The number of independent values of $\gamma^{(p)}$ depends on the symmetry properties of the anisotropic medium.

Thus the number of relaxation times and directions of the principal axes of the operator Γ in the case of a single relaxation process is determined by the symmetry class of the crystal in question (see table).

Crystal system	Properties of the principal axes of the operator Γ	Relation between the τ^p
Triclinic	Principal axes not uniquely related with the crystallographic directions.	$\tau^{(1)} \neq \tau^{(2)} \neq \tau^{(3)}$
Monoclinic	One of the principal axes coincides with a second order symmetry axis or is perpendicular to the symmetry plane of the crystal.	$\tau^{(1)} \neq \tau^{(2)} \neq \tau^{(3)}$
Orthorhombic	All three axes determined.	$\tau^{(1)} \neq \tau^{(2)} \neq \tau^{(3)}$
Tetragonal	One of the axes coincides with a fourth order axis; the other two are arbitrary.	$\tau^{(1)} = \tau^{(2)} \neq \tau^{(3)}$
Rhombohedral	One of the axes coincides with a third order axis; the other two are arbitrary.	$\tau^{(1)} = \tau^{(2)} \neq \tau^{(3)}$
Hexagonal	One of the axes coincides with a sixth order axis; the other are arbitrary.	$\tau^{(1)} = \tau^{(2)} \neq \tau^{(3)}$
Cubic	All three axes arbitrary inasmuch as $\gamma_{ik} = \gamma\delta_{ik}$.	$\tau^{(1)} = \tau^{(2)} = \tau^{(3)}$

A dielectric with a cubic axis behaves as an isotropic substance. Of specific interest is the behavior of an anisotropic dielectric in a periodic field

$$E_i = E_i^{(0)} e^{i\omega t}. \quad (11)$$

Inserting (11) in (10), we obtain

$$D_j = [\varepsilon'_{jk}(\omega) - i\varepsilon''_{jk}(\omega)]\, E_k, \quad (12)$$

where

$$\varepsilon'_{jk}(\omega) = \alpha_{jk} - \sum_p \frac{C_{jkp}}{1 + (\omega\tau^{(p)})^2};$$

$$\varepsilon''_{jk}(\omega) = c \sum_p {}_{jkp} \frac{\omega\tau^{(p)}}{1 + (\omega\tau^{(p)})^2};$$

$$C_{jkp} = \sum_{in} \frac{1}{4\pi} \beta_{jn} b_{pn} \tau_p b_{pi} \beta_{ki}.$$

From these definitions it follows that

$$\varepsilon'_{ik} = \varepsilon'_{ki} \text{ and } \varepsilon''_{ik} = \varepsilon''_{ki}.$$

Thus the permittivity tensor is the sum of two components: an Hermitian component $\varepsilon'_{ik} = \varepsilon'_{ki}$ and an anti-Hermitian component $i\varepsilon''_{ik} = i\varepsilon''_{ki} = -(i\varepsilon'')^{*}_{ik}$. The last, anti-Hermitian part of the permittivity determines the dielectric loss, inasmuch as the amount of energy dissipated in a unit volume of the dielectric per cycle is proportional to $\varepsilon''_{ik} E_i E_k$.

Department of Physics,
Moscow Steel Institute

References

1. N.S.Fastov & B.N.Finkel'shtein, Izv.AN SSSR, Ser.fiz., 22, 249 (1958). (Trans.Bulletin 22, 246.)

TOWARDS A THEORY OF INCOMPLETELY POLAR CRYSTALS

- K.B.Tolpygo

Introduction

According to Born's general quantum-mechanical description of crystals, in the first stage of the adiabatic approximation one must find the mean energy $\overline{H}$ of all the electrons as a function of the nuclear positions R_s^l. This function then serves as the potential energy $U(\ldots R_s^l \ldots) = \overline{H}$ from which one obtains the motion of the nucleii. In the harmonic approximation U is expanded in a power series of the displacements $u_s^l = R_s^l - r_s^l$ (where r_s^l is the position of the s-th site in the l-th cell of the lattice), and contains only quadratic terms of the form $u_s^l u_{s'}^{l'}$, pertaining to no more than two different atoms. The actual expression for U, which is necessary if one wants to make detailed calculations, requires making certain supplementary assumptions.

Born's[2] early representation of U as the sum of the interaction energy of electron pairs is well known. The assumption that this interaction energy contains a Coulomb term of the form $e_s e_{s'}/R$, an exchange term, and a van der Waals term may be interpreted as a neglect of the ionic deformations and the resultant additional Coulomb forces. This approximation is therefore clearly not an adequate one.

In several of the writer's works[3-6] the atomic deformations accompanying lattice vibrations are described in terms of the dipole moments P_s^l of the electron shells, serving as additional variables. From the more general point of view[1] this is equivalent to approximating the Ψ function of the crystal electrons by antisymmetrized products of individual ion functions and taking into account small virtual electron excitations, which do not affect the ion charges. Careful comparison of the results of this theory with experiment[4,6] leads one to believe that this approximation is not good enough. It is clear that incident to virtual excitations of the ionic electronic shells there may occur electron transitions betwee different ions. Further, it would seem that the average equilibrium ion charges should be somewhat less than e for monovalent, and less than $2e$ for divalent compounds.

Indeed, when one determines the parameters of the theory from the values of the static ε and high-frequency dielectric constant n_0^2 and the dispersion frequency ω_d, the theoretical values for the elastic moduli C_{ik} usually turn out to be too high. In order for reduction of the "rigidity" of the crystal not to be accompanied by an increase in ε, the ionic charges must be less than e (or $2e$). On the other hand, as the writer has shown elsewhere[6], lattice-vibration theory with fractional, although constant, charges does not lead to better agreement with experiment than does the theory of a lattice with deformable ions and charges $\pm e$. Hence attempts, such as those of Czigetti,[7] Lundquist,[8] and Tenerz[9], to improve the point-lattice theory by using constant but fractional charges cannot be considered successful. One may object even to the way in which Czigetti and Lundquist introduce the charge e^* on the basis of the dipole moment P, resulting from the displacement of the ions a distance u (namely, $P = e^* u$): the difference between P and eu arises not only because $e^* \neq e$, but also because of the dipole moments P_s of the electron shells. Hence one should in fact write $P = eu + \sum_s P_s$.

The idea of variable ion charges was first suggested in the theory of crystals by Eucken and Buchner[10] in an attempt to explain the large values of ε and $d\varepsilon/dT$ in weakly polar crystals. Eucken & Buchner used the theoretical dependence of the molecular dipole moment on the internuclear distance as given by Kirkwood and Bartholome[11,12]. It is found, however, that this method cannot be used for quantitative calculations since the charge of each ion in a crystal will depend on the displacements of all of its neighbors and on the electric field. The writer found[4], as a rough estimate, that the ion charge in KCl and KBr crystals is $0.9e$; elsewhere,[13] he proposed a method for dealing with partially polar crystals. In the present work this method will be extended in order to obtain the approximate potential energy of the crystal and to find the equations describing the crystal vibrations.

1. Choice and normalization of crystal wave functions

Consider a NaCl type crystal, and assume that the charge of each ion is nearly $\pm e$. The anions spend most of their time in the ionic state ψ_2^l , and a small part of their time in the atomic state ψ_3^l. In the latter state their extra electron goes over to one of the neighboring cations in the state $\psi_4^{l'}$. We shall formally assign all these states to the $_2^l$ anion, writing its ψ function as

$$\Phi_2 = A_l\,[\psi_2^l(\vec{\rho}_1\,\vec{\rho}_2\ldots\vec{\rho}_{N_2'}\,\mathrm{R}_2^l) + \sum_{l'}^{(6)} \delta^{ll'}\,\psi_3^l(\vec{\rho}_2\ldots\vec{\rho}_{N_2},\mathrm{R}_2^l)\,\psi_4^{l'}(\vec{\rho}_1-\mathrm{R}_1^{l'})], \tag{1}$$

and we shall assume that the transfer of the electron has virtually no effect on the state $\psi_1^{l'}(\vec{\rho}_1'\,\vec{\rho}_2'\ldots\vec{\rho}'_{N_1},\mathrm{R}_1^{l'})$ of all the other electrons of the cation.

We approximate the crystal wave function by the antisymmetrized product of single-ion functions:

$$\Psi = \frac{1}{\sqrt{\mathfrak{N}}}\sum_{\nu}(-1)^{\nu}P_{\nu}\prod_{l}\psi_1^l\,\Phi_2^l. \tag{2}$$

The electron coordinates $\vec{\rho}$ include the spin but we shall neglect the spin dependence of the Hamiltonian. Then Ψ automatically excludes states with two extra electrons with the same spin at a single cation, but it will contain terms in which two extra electrons with different spins will be found at a single cation (which thus becomes an anion!). These excitations, however, are highly improbable from the energy standpoint, and we shall therefore eliminate them artificially from each product $\prod_l \psi_1^l\Phi_2^l$ in all the calculations. We shall consider the pairs of functions $\psi_1^{l'}\psi_2^l$; $\psi_1^{l'}\psi_3^l$; $\psi_1^{l'}\psi_4^{l''}$; $\psi_2^l\psi_4^{l'}$; $\psi_3^l\psi_4^{l'}$ orthogonal in the sense that integrals of $\psi_s^{*l}\psi_{s'}^{*l'}P_{\nu}\psi_s^l\psi_{s'}^{l'}$ vanish for all permutations P_{ν}, except the identity. Even with these assumptions, however, it is quite difficult to calculate $\overline{H}$ and the normalization integral

$$N = \int \Psi^*\,\Psi\,d\tau\,.$$

S.I.Pekar calculated N for a one-dimensional chain containing M ion pairs, using recursion formulas. In the limit as $M\to\infty$ (assuming all $|\delta^{ll'}|^2 = \delta$ to be equal), he obtains

$$N = \frac{1 + 3\delta + \delta^2 - x_2(1+\delta)}{x_1(x_1 - x_2)}\,(Ax_1)^M,$$

where

$$x_{1,2} = \frac{1}{2}\,\{1 + 2\delta \pm \sqrt{1 + 4\delta}\}; \tag{3}$$

then the mean charge of each ion turns out to be

$$e^* = e\,\frac{x_1 - \delta}{x_1 + \delta} \quad (\text{all } A_l = A). \tag{4}$$

It has proven impossible to generalize this method to a three-dimensional lattice. The difficulty lies in calculating quantities of the form

$$N=\prod_{l}|A_l|^2\Big[1+\sum_{l'}^{(6)}|\delta^{ll'}|^2\Big], \tag{5}$$

in which products $|\delta^{ll'}|^2|\delta^{l''l'}|^2$ with equal l' and different l and l'' are to be dropped. This can be done statistically in the limiting case when $\delta\ll 1$.

Let us temporarily write $|\delta^{ll'}|^2=\delta_1,\delta_2\ldots\delta_6$ for the position of the $\substack{l'\\1}$ ion with respect to the $\substack{l\\2}$ ion in the $x, -x, y, -y, z, -z$ directions. From the product in (5), we take out n_1 factors of type δ_1, n_2 factors of type δ_2, etc., and $M-n_1-n_2-\cdots-n_6$ factors of unity. If $n_i\ll M$, the probability is very low that two cations $\substack{l'\\1}$ and $\substack{l''\\1}$ "occupied" by electrons are neighbors along one of the coordinate axes. The choice of the n_1 factors can be made in just $\frac{M!}{(M-n_1)!\,n_1!}$ ways. Since, when the $\delta_1=|\delta^{ll'}|^2$ term is taken out of the factor $1+\sum_{i=1}^{2}\delta_i$, it is no longer possible to take δ_2 from this factor or to get $\delta_2=|\delta^{l''l'}|^2$ with the same l' from any other factor, the choice of the n_2 factors δ_2 can be made in only $\frac{M_1!}{(M_1-n_2)!\,n_2!}$ ways, where $M_1=M-2n_1$. Continuing in this way, and not going into the complications of the combinatorial analysis resulting from electrons on neighboring cations, we arrive at the formula

$$N=\sum_{n_1n_2\ldots n_6}|A|^{2M}\prod_{i=1}^{6}\frac{M_{i-1}!\,\delta_i^{n_i}}{(M_{i-1}-n_i)!\,n_i!}\equiv|A|^{2M}\sum_{n_1n_2\ldots n_6}N_{n_1n_2\ldots n_6}, \tag{6}$$

where $M_i=M_{i-1}-2n_i$ and $M_0\equiv M$.

One can now find the most probable value n_i of $\bar{n}_i$ for which $\ln N_{n_1n_2\ldots n_6}$ is maximum, and then by expanding $\ln N_{n_1n_2\ldots n_6}$ in a power series in $n_i-\bar{n}_i$ and dropping all terms beyond the quadratic, one can write N in terms of six Poisson integrals. In the asymptotic formula, when $\ln N\sim M$, one may neglect any finite number of factor of the order of M in the formula for N (we require only $A=1:\sqrt[2N]{N}$).

Using Stirling's formula, we have

$$\bar{n}_6=M_5\frac{\delta}{1+\delta}.$$

Setting $n_6=\bar{n}_6$ in the last factor, we see that $\frac{M_4!}{(M_4-n_5)!\,n_5}(\delta^{(5)})^{n_5}$ is to be varied with respect to n_5, where we have written $\delta^{(5)}=\frac{\delta}{(1+\delta)^2}$. Then $\bar{n}_5=M_4\frac{\delta^{(5)}}{1+\delta^{(5)}}$. Continuing this procedure, we arrive at

$$\bar{n}_i=M_{i-1}\,\frac{\delta^{(i)}}{1+\delta^{(i)}},$$

where

$$\delta^{(i-1)}=\frac{\delta^{(i)}}{(1+\delta^{(i)})^2}\quad\text{and }\delta^{(6)}\equiv\delta. \tag{7}$$

Finally, the maximum expression under the summation sign in (6) is

$$\prod_{i=1}^{6}(1+\delta^{(i)})^{M}\approx N \quad \text{and} \quad A=1:\sqrt{\prod_{i=1}^{6}(1+\delta^{(i)})}; \tag{8}$$

and the resulting mean charge on the ion is

$$e^{*}=\pm e\left\{1-\frac{1}{M}\sum_{i=1}^{6}\bar{n}_i\right\}. \tag{9}$$

Comparison of the statistical formulas (8) and (9) with the exact equation (3) for a one-dimensional chain shows that even for $\delta = 0.5$ the error in A^2 is no greater than 1.5%, while that in e^* is no greater than 5%. This is quite permissible when one recalls that $e^*/e \approx 0.6$ and that the bonding is far from heteropolar. In the following calculation of $\bar{H}$ we shall consider the $|\delta^{ll'}|^2$ all nearly equal to each other, but not equal to δ, although in the normalizing factors A_l and in calculating the combinatorial coefficients we shall not distinguish between $|\delta^{ll'}|^2$ and δ.

2. Calculation of the mean Hamiltonian of the crystal

The Hamiltonian $\hat{H}$ of the electrons in the crystal is made up of a sum of the kinetic and potential energies of each electron with coordinates $\vec{\rho}$ in the field of all the nuclei, namely, terms of the form

$$\hat{h}_{\rho}=-\frac{\hbar^2}{2m}\Delta_{\vec{\rho}}-\sum_{s'l'}\frac{e^2 Z_{s'}}{|\vec{\rho}-\mathrm{R}_{s'}^{l'}|}$$

plus the interaction energy of the electrons

$$\hat{h}_{\rho\rho'}=\frac{e^2}{|\vec{\rho}-\vec{\rho}'|}.$$

One may include also the constant interaction energy of the nuclei

$$K_{\mathrm{n}}=\frac{e^2}{2}\sum_{ss'll'}\frac{Z_s Z_{s'}}{|\mathbf{R}_s^l-\mathbf{R}_{s'}^{l'}|}.$$

We then have

$$\hat{H}=\sum_{sl}\sum_{n_s=1}^{N_s}\hat{h}_{\vec{\rho}^{\,l}_{sn_s}}+\frac{1}{2}\sum_{ss'll'}\sum_{n_s n_s'}\hat{h}_{\vec{\rho}^{\,l}_{sn_s}\vec{\rho}^{\,l'}_{s'n_s'}}+K_{\mathrm{n}}. \tag{10}$$

On integrating any of the $\hat{h}_{\rho}$ terms between wave functions Ψ^* and Ψ, we will obtain contributions only when the electron permutations and displacements in Ψ^* and Ψ are the same for all the electrons except that whose coordinates are $\vec{\rho}$. If this electron belongs to the ${}^{l}_{2}$ ion, the integral over all other electrons will differ, depending on whether we have the $\psi_2^l(\vec{\rho}\ldots)$ or the $\delta^{ll'}\psi_3^l(\ldots)\psi_4^{l'}(\rho)$ term in the $\Phi_2^l(\vec{\rho}\ldots)$ factor. In the first case we obtain simply the normalization integral N_{M-1} (one of the factors in Φ_2^l is eliminated), whereas in the second case, since the ${}^{l'}_{1}$ cation cannot be occupied by the electrons of the five neighboring ${}^{l''}_{2}$ anions $(l''\neq l)$, the integral will be somewhat smaller. Let us write its value as γN_{M-1}. Since the integration over $\vec{\rho}$ (without $\hat{h}_{\vec{\rho}}$) should give unity, we have

$$N_{M-1}(1+6\gamma\delta)=N_M,$$

whence it follows that

$$1+6\gamma\delta=\prod_{i=1}^{6}(1+\delta^{(i)})=\frac{1}{A^2}$$

and

$$\bar{\hat{h}}_{\vec{\rho}} = |A|^2 \left\{ \int \psi_2^{*l}\, \hat{h}_{\vec{\rho}} \psi_2^l\, d\tau_2^l + \gamma \sum_{l'}^{(6)} \left[\delta^{*ll'} \int \psi_3^{*l} \psi_4^{*l}(\vec{\rho})\, \hat{h}_{\vec{\rho}}\, \psi_2^l(\vec{\rho}\dots)\, d\tau_2^l + \right.\right.$$
$$\left.\left. + \delta^{ll'} \int \psi_2^{*l}(\vec{\rho}\dots)\, \hat{h}_{\vec{\rho}} \psi_3^l \psi_4^{l'}(\vec{\rho})\, d\tau_2^l + |\delta^{ll'}|^2 \int \psi_4^{*l'}\, \hat{h}_{\vec{\rho}} \psi_4^{l'}\, d\tau \right]\right\}. \tag{11}$$

We may neglect transitions of the $\vec{\rho}$ electron from the ${}^{l'}_{1}$ site in Ψ^* to the ${}^{l''}_{1}$ site in Ψ, because of the small overlap of the $\psi_4^{*l'}$ and $\psi_4^{l''}$ functions as well as because $\delta^{*ll'}\delta^{ll''}$ is small. Similar considerations hold also for calculating the average $\hat{h}_{\vec{\rho}\vec{\rho}'}$ except that in addition to the same permutations in Ψ^* and Ψ (Coulomb integrals), we must also consider permutations of different electrons with coordinate $\vec{\rho}$ and $\vec{\rho}'$ (exchange integrals). Further, we must include possible different displacements of the $\vec{\rho}$ and $\vec{\rho}'$ electrons in Ψ^* and Ψ (for instance, both to ψ_2^l or one to ψ_3^l and the other to $\psi_4^{l'}$, etc.).

It is seen also from the above discussion that $\gamma \sum_{l'}^{(6)} |\delta^{ll'}|^2 |A_l|^2$ is the fraction of the charge of the ${}^{l}_{2}$ ion which has been displaced onto the neighboring cations, while $\gamma \sum_{l'}^{(6)} |A_{l''}|^2 |\delta^{l''l'}|^2$, on the contrary, is the fraction of the charge arriving at the ${}^{l'}_{1}$ cation from the neighboring ${}^{l''}_{2}$ anions. Thus the resulting ion charges will be

$$\varepsilon_2^l = e_2 \left[1 - \gamma |A_l|^2 \sum_{l''}^{(6)} |\delta^{ll''}|^2 \right]; \quad \varepsilon_1^{l'} = e_1 \left[1 - \gamma \sum_{l''}^{(6)} |A_{l''}|^2 |\delta^{l''l'}|^2 \right]. \tag{12}$$

We introduce the dipole moments of the electron shells in the ψ_1, ψ_2, ψ_3, and ψ_4 states by

$$\mathbf{P}_s^l = -eN_s \int \vec{\rho}\, |\psi_s^l(\vec{\rho}\dots)|^2\, d\tau_s^l \quad (s = 1, 2, 3, 4). \tag{13}$$

and define the resulting dipole moments of the lattice sites by

$$\vec{\pi}_1^{l'} = a_1^{l'} \mathbf{P}_1^{l'} + a_4^{l'} \mathbf{P}_4^{l'}; \quad \vec{\pi}_2^{l} = a_2^l \mathbf{P}_2^l + a_3^l \mathbf{P}_3^l, \tag{14}$$

where

$$a_1^{l'} = 1; \; a_4^{l'} = 1 - \varepsilon_1^{l'}/e_1; \; a_2^l = \varepsilon_2^l/e_2; \; a_3^l = 1 - \varepsilon_2^l/e_2.$$

Further, we collect terms in $\bar{H}$ pertaining to the individual sites in the states $\psi_1, \dots, \psi_4$ in $\bar{H}_1^l$, $\bar{H}_2^l$, $\bar{H}_3^l$ and $\bar{H}_4^l$, and similarly for the terms describing interactions between the sites. We then obtain

$$\bar{H} = \sum_l \sum_{s=1}^{4} a_s^l \bar{H}_s^l + \frac{1}{2} \sum_{ll'} \sum_{s,s'=1,2} \left\{ \frac{\varepsilon_s^l \varepsilon_{s'}^{l'}}{|\mathbf{R}_{ss'}^{l-l'}|} + \frac{2\varepsilon_s^l \mathbf{R}_{ss'}^{l-l'} \vec{\pi}_{s'}^{l'}}{|R_{ss'}^{l-l'}|^3} + \frac{\vec{\pi}_s^l \cdot \vec{\pi}_{s'}^{l'}}{|R_{ss'}^{l-l'}|^3} - 3\, \frac{\vec{\pi}_s^l \cdot \mathbf{R}_{ss'}^{l-l'}\, \vec{\pi}_{s'}^{l'} \cdot \mathbf{R}_{ss'}^{l-l'}}{|R_{ss'}^{l-l'}|^5} \right\} -$$
$$- \sum_l \sum_{l'}^{(6)} \{ a_1^{l'} a_2^l I_{12} + a_1^{l'} a_3^l I_{13} + a_2^l a_4^{l'} I_{24} + a_3^l a_4^{l'} I_{34} +$$
$$+ \gamma [a_2^l (1 - a_4^{l'}) (I_{34} - I_{24}) |\delta^{ll'}|^2 + a_2^l (f_{12} \delta^{ll'} + f^*_{12} \delta^{*ll'})]\}, \tag{15}$$

where

$$I_{ss'} = I_{ss'}(\mathbf{R}) = e^2 \iint \psi_s^{*l}(\vec{\rho}\dots)\, \psi_{s'}^{*l'}(\vec{\rho}'\dots)\, \frac{1}{|\vec{\rho} - \vec{\rho}'|}\, \psi_s^l(\vec{\rho}'\dots)\, \psi_{s'}^{l'}(\vec{\rho}\dots)\, d\tau_s^l\, d\tau_{s'}^{l'}$$
$$(s, s' = 1, 2, 3, 4); \tag{16}$$

$$f_{12} = f_{12}(R_{21}^{l-l'}) = -\int \psi_2^{*l}(\vec{\rho}\dots)\, \psi_1^{*l'}(\rho'\dots)\, [\hat{H}_2^l + \hat{H}_{21}^{ll'}]\, \psi_3^l(\dots)\, \psi_4^{l'}(\vec{\rho})\, \psi_1^{l'}(\vec{\rho})\, d\tau_2^l\, d\tau_1^{l'},$$

$\hat{H}_2^l$ is the Hamiltonian of all the electrons of the ${}_2^l$ ion, and $\hat{H}_{21}^{ll'}$ is the interaction Hamiltonian for the ${}_2^l$ and ${}_1^{l'}$ ions.

3. Minimizing the mean Hamiltonian

We shall treat the mutual deformation of the ions, as in previous work,[3-6] by expanding ψ_s^l in excited-state wave functions ψ_{si}:

$$\psi_s^l(\vec{\rho}\ldots\mathbf{R}_s^l)=\psi_{s0}(\vec{\rho}\ldots\mathbf{P}_s^l)+\sum_{i=1}^{\infty}c_{si}^l\psi_{si}(\vec{\rho}\ldots\mathbf{R}_s^l)\quad(s=1-4); \tag{17}$$

in so doing, we will retain terms of order $|c_{si}^l|^2$ in the $\overline{H}_s^l$, whereas in the exchange integrals $I_{ss'}$ and in the transition matrix elements f_{12} we will keep only first powers of c_{si}^l. We shall consider the c_{si}^l to be approximation parameters for the ψ function, and we shall find their values from the condition that $\overline{H}$ be a minimum for constant $\mathbf{P}_s^l$.[13] Then, as in Ref.5, we have

$$\overline{H}=\sum_l\left\{\sum_{s=1}^{4}a_s^l\left[E_{s0}+\frac{1}{2\alpha_s}(\mathbf{P}_s^l)^2+\sum_{l'}^{(6)}\vec{\beta}_{ss'}(\mathbf{R}_{ss'}^{ll'})\mathbf{P}_s^l\right]+\frac{1}{2}\sum_{l'}\sum_{ss'=1,2}K_{ss'}^{ll'}+\sum_{l'}^{(6)}\omega_{12}^{ll'}\right\}+U_1; \tag{18}$$

here the $\vec{\beta}_{ss'}$ are certain functions of the distances $R_{ss'}^{ll'}$, the charges ε_s^l, and the $\delta^{ll'}$ coefficients, $K_{ss'}^{ll'}$ is the Coulomb energy of the ${}_s^l$ and ${}_{s'}^{l'}$ sites (the expression in the first braces in (15)), and $\omega_{12}^{ll'}$ is the expression in the second braces in (15) with all the $I_{ss'}$ and f_{12} evaluated for the unperturbed ψ_{s0} functions. The terms lumped together in U_1 are of order $(c_{si}^l)^2$, and are independent of the dipole moments. They arise from other than two-body interactions and noncentral forces between the atoms. In the first approximation they may be dropped.[5] Finally,

$$E_{s0}=\int\psi_{s0}^{*}\hat{H}_s^l\psi_{s0}\,d\tau_s^l.$$

Since only the first term in (18) depends separately on $\mathbf{P}_s^l$, we can minimize (18) with respect to $\mathbf{P}_s^l$ with the condition that $\vec{\pi}_1^{l'}$ and $\vec{\pi}_2^l$, defined in (14), remain constant. Then (18) simplifies, becoming

$$\overline{H}=\sum_l\left\{\sum_{s=1}^{4}a_s^lE_{s0}+\sum_{s=1,2}\left[\frac{1}{2\bar{\alpha}_s}(\vec{\pi}_s^l)^2+\sum_{l'}^{(6)}\vec{\bar{\beta}}_s\cdot\vec{\pi}_s^l\right]+\frac{1}{2}\sum_{l'ss'=1,2}K_{ss'}^{ll'}+\sum_{l'}^{(6)}\omega_{12}^{ll'}\right\}+U_1, \tag{19}$$

where

$$\bar{\alpha}_1=\alpha_1a_1^l+\alpha_4a_4^l;\quad\bar{\alpha}_2=\alpha_2a_2^l+\alpha_3a_3^l;\quad\vec{\bar{\beta}}_1=\frac{1}{\bar{\alpha}_1}(a_1^l\alpha_1\vec{\beta}_{12}+a_4^l\alpha_4\vec{\beta}_{42});\quad\vec{\bar{\beta}}_2=\frac{1}{\bar{\alpha}_2}(a_2^l\alpha_2\vec{\beta}_{21}+a_3^l\alpha_3\vec{\beta}_{31}). \tag{20}$$

We have obtained the mean Hamiltonian as a function of the distances $\mathbf{R}_{21}^{l-l'}$ between the nuclei, the dipole moments $\vec{\pi}_s^l$, charges ε_s^l, and the parameters $\delta^{ll'}$, (which enter into all the $\vec{\bar{\beta}}_s$ and $\omega_{12}^{ll'}$). In what follows we shall eliminate these parameters and write the equations for the crystal vibrations in the harmonic approximation and assuming U_1 to be negligible.

4. Equations for the vibrations of a lattice with variable charges

We assume that the charges ε_s^l undergo small amplitude oscillations about mean values $\varepsilon_s=e_s|A_l|^2$, and accordingly write

$$\varepsilon_s^l=\varepsilon_s+\eta_s^l\quad\text{and}\quad\delta^{ll'}=\delta_0+\delta_1^{ll'}. \tag{21}$$

The equilibrium charges, determined uniquely by the equilibrium position δ_0, are determined by minimizing the Hamiltonian $\overline{H}$ in the absence of displacements, external fields, and dipole moments, i.e., from

$$\min \overline{H}_0 = -\frac{\alpha_M \varepsilon_1^2}{a} - 6\{a_1 a_2 I_{12}^0 + a_1 a_3 I_{13}^0 + a_2 a_4 I_{24}^0 + a_3 a_4 I_{34}^0 +$$

$$+ \gamma[a_2(1-a_4)(I_{34}^0 - I_{24}^0)\delta_0^2 + a_2(f_{12}^0 \delta_0 + \overset{*}{f}{}_{12}^0 \overset{*}{\delta}_0)]\} + E_{10} + E_{20} + (1-\varepsilon_1/e_1)(E_{30} + E_{40} - E_{20}). \quad (22)$$

Here the index ^{0} indicates that the quantities are evaluated at the equilibrium ion positions and in the absence of dipole moments, and α_M is Madelung's constant. If instead of ε_1, we introduce the degree of deviation from heteropolarity $\varepsilon = 1 - \varepsilon_1/e_1$, we have

$$a_2 = 1 - \varepsilon; \; a_3 = a_4 = \varepsilon; \; \gamma\delta_0^2 = \frac{1}{6}\frac{\varepsilon}{1-\varepsilon},$$

and differentiation of (20) with respect to ε gives

$$\frac{2\alpha_M e_1^2}{a}(1-\varepsilon) + E_{30} + E_{40} - E_{20} + 6(I_{12}^0 - I_{13}^0) -$$

$$- 5I_{24}^0 - I_{34}^0 + 10\varepsilon(I_{24}^0 - I_{34}^0) - \frac{2f_{12}^0}{\delta_0}\left[1 - \frac{d\ln\delta_0}{d\ln\varepsilon}\right] = 0. \quad (23)$$

As δ_0 increases from zero, ε first increases as $6\delta_0^2$ and then its growth becomes slower. Thus the expression in square brackets in (23) varies between 1/2 and $-\infty$ as δ_0 is allowed to increase. Since the Madelung energy is much greater than the energy of the exchange forces, it follows from (23) that for small values δ_0 varies as $\dfrac{af_{12}^0}{2\alpha_M e_1^2}$. Thus when a heteropolar crystal is compressed, its polari ty should decrease somewhat, for as the distances are decreased f_{12}^0 will grow at a greater rate than $1/a$. As f_{12}^0 increases further, both $1 - \dfrac{d\ln\delta_0}{d\ln\varepsilon}$ and $1-\varepsilon$ decrease, and ε increases more slowly.

Let us now assume that we have solved Eq.(23) together with the relation $\varepsilon = 1 - 1/A^2$, and that we have found the equilibrium values ε and δ_0. We now vary the Hamiltonian of (18) with respect to the $\delta_1^{ll'}$ with the condition that the charges given by (12) remain constant; rather than the charges, we may speak of the constancy of the quantities

$$\sum_{l''}^{(6)} |\delta^{ll''}|^2 = \frac{6\delta_0^2}{\varepsilon}(1-\varepsilon_2^l/e_2) \quad \text{and} \quad \sum_{l''}^{(6)} |\delta^{l''l'}|^2 = \frac{6\delta_0^2}{\varepsilon}(1-\varepsilon_1^{l'}/e_1). \quad (24)$$

In this calculation we need only vary the terms

$$\sum_l \sum_{l'}^{(6)} \left\{\overline{\beta}_s \pi_s^l - \frac{1}{6}\frac{\varepsilon_2^l \varepsilon_1^{l'}}{e_2 e_1}(I_{34} - I_{24})\left(1 + \frac{2}{\delta_0}\delta_1^{ll'} + \frac{1}{\delta_0^2}(\delta_1^{ll'})^2\right) - \frac{\varepsilon}{3\delta_0(1-\varepsilon)}\frac{\varepsilon_2^l}{e_2} f_{12}^0(\mathbf{R}_{21}^{l-l'})\left(1 + \frac{1}{\delta_0}\delta_1^{ll'}\right)\right\}. \quad (25)$$

Since we consider the dipole moments $\vec{\pi}_s^l$ to be small quantities of the first order, we need maintain in the $\vec{\overline{\beta}}_s$ only first order terms in $\delta_1^{ll'}$:

$$\vec{\overline{\beta}}_s = \vec{\overline{\beta}}_{s0} + \frac{d\overline{\beta}_{s0}}{d\delta_0}\delta_1^{ll'}.$$

We vary (25) with the condition given by (24), using the Lagrange multipliers

$$\Lambda_1^{l'} = \Lambda_1 + \lambda_1^{l'} \quad \text{and} \quad \Lambda_2^l = \Lambda_2 + \lambda_2^l,$$

and arrive, in the first approximation in $\mathbf{u}_s^l$ and $\vec{\pi}_s^l$, at the equation

$$\frac{d\bar{\beta}_1}{d\delta_0}\cdot\vec{\pi}_1^{l'}+\frac{d\bar{\beta}_2}{d\delta_0}\vec{\pi}_2^{l}-\frac{(\mathbf{u}_2^l-\mathbf{u}_1^{l'})\cdot\mathbf{r}_{21}^{l-l'}}{|r_{21}^{l-l'}|}\left[\frac{\varepsilon}{3\delta_0}\frac{df_{12}^0}{dr}+\frac{(1-\varepsilon)^2}{3\delta_0}\frac{d}{dr}(I_{34}^0-I_{24}^0)\right]-$$

$$-\frac{1-\varepsilon}{3\delta_0}(I_{34}^0-I_{24}^0)\left(\frac{\eta_2^l}{e^2}+\frac{\eta_1^{l'}}{e_1}\right)-\frac{\varepsilon}{3(1-\varepsilon)\,\delta_0^2}f_{12}^0\frac{\eta_2^l}{e_2}-\frac{2}{\delta_0}(\lambda_2^l+\lambda_1^{l'})-$$

$$-\left[\frac{2(\Lambda_1+\Lambda_2)}{\delta_0^2}+\frac{(1-\varepsilon)^2}{3\delta_0^2}(I_{34}^0-I_{24}^0)\right]\delta_1^{ll'}-\frac{(1-\varepsilon)^2}{3\delta_0}(I_{34}^0-I_{24}^0)-\frac{\varepsilon f_{12}^0}{3\delta_0^2}-\frac{2(\Lambda_1+\Lambda_2)}{\delta_0}=0. \qquad (26)$$

Here the terms which are of zeroth order in $\delta_1^{ll'}$ should cancel, since we determined δ_0 from the condition that $\bar{H}$ be a minimum, and the expansion for $\bar{H}$ must start with terms of order $(\delta_1^{ll'})^2$, so that $\delta\bar{H}$ must start with terms of order $\delta_1^{ll'}$. From this we obtain

$$\Lambda_1+\Lambda_2=-\frac{(1-\varepsilon)^2}{6}(I_{34}^0-I_{24}^0)-\frac{\varepsilon}{6\delta_0}f_{12}^0.$$

Hence the $\delta_1^{ll'}$ turn out to be linear functions of the $\mathbf{u}_s^l$, $\vec{\pi}_s^l$, η_s^l and the λ_s^l, namely,

$$\delta_1^{ll'}=\mathrm{K}_1\vec{\pi}_1^{l'}+\mathrm{K}_2\vec{\pi}_2^{l}+L\frac{(\mathbf{u}_2^l\mathbf{u}_1^{l'})\,\mathbf{r}_{21}^{l-l'}}{|r_{21}^{l-l'}|}+m_1\eta_1^{l'}+m_2\eta_2^l+l(\lambda_1^{l'}+\lambda_2^l). \qquad (27)$$

The λ_s^l are found from Eq.(24), i.e., from

$$\sum_{l'}^{(6)}\delta_1^{ll'}=-\frac{3\delta_0}{\varepsilon}\frac{\eta_2^l}{e_2}\quad\text{and}\quad\sum_{l'}^{(6)}\delta_1^{l'l}=-\frac{3\delta_0}{\varepsilon}\frac{\eta_1^l}{e_1}. \qquad (28)$$

Now Eqs.(27) and (28) give chains of relations between the λ_s^l and η_s^l for all the ions. Insertion of (27) into (28) leads to $2M$ "equations of motion" for the λ_s^l. They are sufficient to determine the λ_s^l in terms of the $\mathbf{u}_s^l$, $\vec{\pi}_s^l$, and η_s^l. Equations (27) are used in all the terms of the Hamiltonian (20) which depend explicitly on the $\delta^{ll'}$, that is, in the $\bar{\beta}_s\cdot\vec{\pi}_s^l$ and in ω_{12}. Then $\bar{H}$ becomes a function only of $\mathbf{u}_s^l,\vec{\pi}_s^l$, η_s^l and λ_s^l. The next group of equations of motion is obtained from the relations

$$\frac{\partial\bar{H}}{\partial\eta_s^l}=0 \qquad (29)$$

$$\frac{\partial\bar{H}}{\partial\pi_{sx}^l}=0\quad(s=1,2;\ x=x,y,z). \qquad (30)$$

In these differentiations the $\delta_1^{ll'}$ are treated as constants given by (27), since we use the minimum value of the Hamiltonian $\bar{H}$ with respect to all the $\delta_1^{ll'}$. Finally, the displacements $\mathbf{u}_s^l$ must satisfy the equations

$$m_s\ddot{u}_{sx}^l=-\frac{\partial\bar{H}}{\partial u_{sx}^l}. \qquad (31)$$

The total number of equations (28)-(31) is then $M(2+2+6+6)=16\,M$, which is the number of the unknowns λ_s^l, η_s^l, $\vec{\pi}_{sx}^l$ and $\mathbf{u}_{sx}^l$.

When differentiating $\bar{H}$ with respect to one of the variables, all the others must be treated as constants. In conclusion, we write out the equations for the crystal vibrations in the presence of an external electric field $\mathrm{E}^0(\mathbf{r})$ whose potential is $v^0(\mathbf{r})$. For this case the Hamiltonian $\bar{H}$ requires, in the first approximation, the additional terms

$$\bar{H}^{(e)}=\sum_{sl}[v^0(\mathbf{r}_s^l)\,\varepsilon_s^l-\mathrm{E}^0(\mathbf{r}_s^l)(\vec{\pi}_s^l+\varepsilon_s\mathbf{u}_s^l)], \qquad (32)$$

and equations (29)-(31) become

$$\frac{\partial \overline{H}}{\partial \eta_s^l} + v^0(r_s^l) = 0; \ \frac{\partial \overline{H}}{\partial \pi_{sx}^l} - E_x^0(\mathbf{r}_s^l) = 0; \ m_s \ddot{u}_{sx}^l = -\frac{\partial \overline{H}}{\partial u_{sx}^l} + \varepsilon_s E_x^0(\mathbf{r}_s^l). \qquad (33)$$

Eq.(33) implies that in the presence of an external field not only the displacements and dipole moments of the ions change, but also their charges. This gives the crystal an additional dipole moment caused both directly by the external field (noninertial or prompt polarization) and by the secondary process in which the charges ε_s^l change when the nuclei are displaced (inertial or lagging polarization).

Eq.(28) and (33) can be solved by expanding all the unknowns in Fourier series. This leads to a set of sixteen equations for the Fourier components, and these are not very much more complicated than the set of twelve equations one obtains in the theory of crystal vibrations with deformed ions as presented in the author's previous works.[3-6]

Institute of Physics,
Academy of Sciences of the Ukrainian SSR

References

1. M.Born & Kun Huang, Dynamical Theory of Crystal Lattices, Oxford, 1954.
2. M.Born & M.Geppert-Mann, Theory of Solids. (Cited in Russian translation.
3. K.B.Tolpygo, Zhur.eksp.i teor.fiz., 20, 497 (1950).
4. K.B.Tolpygo, Trudy (Proceedings), Phys.Inst., Ukrainian SSR Academy of Sciences, No.5, 28 (1954).
5. K.B.Tolpygo, Ukr.fiz.zhur., 4, 72 (1959).
6. K.B.Tolpygo, Present issue of the Bulletin,p.167.
7. C.Czigetti, Trans.Faraday Soc., 45, 155 (1949).
8. S.O.Lundquist, Arkiv fisik., 12, 263 (1957).
9. E.Tenerz, Arkiv fisik., 12, 277 (1957).
10. A.Eucken & A.Z.Buchner, Phys.Chem., 27, 321 (1934).
11. J.G.Kirkwood, Phys.Z., 33, 259 (1932).
12. Z.Bartholome, Phys.Chem., 23, 131 (1933).
13. K.B.Tolpygo, Izv.AN SSSR, Ser.fiz., 21, 48 (1957). (Trans.Bulletin 21, 44.)

ON THE KINETICS OF ION CONDUCTIVITY AND ELECTRIC POLARIZATION IN CONDENSED SUBSTANCES

- Yu.L.Khait

Finkel'shtein and Fastov[1] studied relaxation processes in varying electric fields, basing their considerations on phenomenological thermodynamics, without recourse to any specific model. The methods of statistical thermodynamics with the concepts of the mean free path and mean free time[2] can be combined with the principle of detailed equilibrium based on the concept of "macroscopic states"[3] to develop a quasistatistical method for determining the activation rates of processes in condensed substances in an external field. Essentially the method involves ignoring the dynamics of individual strongly coupled particles, replacing it with a two-step statistical description by means of certain specially chosen, more or less independent, macroscopically small subsystems of volume l^3. First, each such sybsystem is treated by the procedures of statistical thermodynamics, and then the set of these $N=\frac{V}{l^3}\gg 1$ microcontinua is also treated statistically. The calculations will be carried out only to order of magnitude.

1. Quasistatistical calculation of activation rates

Both in physical kinetics[2] and in statistical physics when one introduces the concept of incomplete or partial equilibrium,[3] the nonequilibrium system is broken up into macroscopically small parts whose relaxation times τ satisfy the inequalities

$$\tau \ll \Delta t \ll T_0, \tag{1}$$

where Δt is a time during which only macroscopically small changes occur in the system, and T_0 is the relaxation time of the process in the body as a whole.

We shall deal only with processes so slow that they can be treated in line with the concept of partial equilibrium, which is defined by giving the mean values of physical quantities for macroscopically small volumes l^3. To choose the l^3 volumes, we make use of the observation due to Leontovich[4] that the separation of phenomena into "thermodynamic" and "fluctuational" depends rather on the formulation of the problem than on any inherent nature of the phenomena. Let us evaluate l on the basis of two competing requirements: (1) the subsystems must have many degrees of freedom for a statistical description to be valid; (2) their volumes l^3 must at the same time be small enough to be useful in a detailed description of fluctuational and activational processes.

Statistical thermodynamics is applicable to the subsystems if (a) they are quasi-closed systems, and (b) the quantum mechanical uncertainties of the thermodynamic functions (entropy, etc.) in them are negligibly small. Requirement (a) is satisfied if we take[2]

$$l = al_0\,(a > 1) \tag{2}$$

with the condition

$$l \gg \frac{\alpha}{\varepsilon_0 + \varepsilon_0'}, \tag{3}$$

where αl^3 is the energy of surface interaction between the subsystems, ε_0' is the energy per unit volume at absolute zero, ε_0 is the mean energy of the thermal excitation per unit volume,* and l_0 is the mean free path of the particles (or quasiparticles) which are responsible for the energy transfer in the substance.[2,5] Condition (b) will be satisfied if we require that $\tau \gg \hbar / kT$.[3] The time τ can be found by treating the energy carriers (say, phonons) as diffusing particles with a diffusion constant $D_\varepsilon = l_0^2 / \tau_0$, where τ is the mean free time. Then to order of magnitude $\tau = l^2 / D_\varepsilon$, or

$$\tau = a^2 \tau_0. \tag{4}$$

Requirement (b) will then be fulfilled if we take

$$a\tau_0 \gg \frac{\hbar}{kT}. \tag{5}$$

If the subsystems satisfy the inequalities in (2), (3) and (5), they may be handled by the methods of statistical thermodynamics. The accuracy of this method depends on the mean relative energy fluctuation γ. If m is the number of degrees of freedom of the subsystem, then $\gamma \sim m^{-1/2}$, and in condensed substance $m \approx \beta \frac{l^3}{d^3}$. Therefore the condition that $\gamma \ll 1$ becomes

$$\gamma \approx \left(\frac{d}{\beta^{1/3} a l_0} \right)^{3/2} \ll 1. \tag{6}$$

We must now find an upper bound for l. Since a condensed substance is a system of strongly interacting particles, each elementary act of breaking the bonds at a single particle is a cooperative effect involving not one, but many particles; in fact, strictly speaking, it involves the entire body. But since the interaction between particles propagates with a finite velocity, it is possible to choose a small region which, by virtue of rapid energy transfer, "takes part" in a single act. We then neglect the influence of the rest of the substance (macroscopic body). In order to apply statistical methods to calculate the probability for an elementary act of the process, it is necessary that between two successive bond breakages our subsystem has enough time to reach equilibrium. It takes a time of order $a\tau_0$ to establish equilibrium in a volume l^3. We therefore choose l^3 so small that in a time $a\tau_0$ there takes place on the average no more than a single elementary act of the activation process, i.e., such that

$$\tau' \gg a\tau_0, \tag{7}$$

where τ' is the mean time between successive bond ruptures in the subsystem. We arrive at the same condition by using the finite interaction propagation velocity and the uncertainty condition, since

$$kT > \frac{\Delta}{m} \gtrsim \frac{h}{a\tau_0} \quad \text{or} \quad l^2 \lesssim \frac{\Delta d^3}{\beta \hbar l_0} \tau_0; \ \frac{l^3}{d^3} > \frac{\Delta}{\beta kT}. \tag{8}$$

From this we get the condition for "slowness" of the process:

$$\left(\frac{l}{l_0} \right) \ll \left(\frac{\tau'}{\tau_0} \right), \tag{9}$$

which, when satisfied, allows of quasistatistical description of the process. We will not consider more rapid processes.

The mean number of elementary acts per unit time in a homogeneous system of volume V is

---

*For solids, at temperatures which are not too low $\varepsilon_0 \approx \frac{kT}{d^3}$, where d^3 is the atomic volume, and k is Boltzmann's constant.

$$N_1 = w\frac{V}{l^3}, \tag{10}$$

where V/l^3 is the number of subsystems in the volume V, and w is the probability (per unit time) for an elementary act in one of the subsystems.

To calculate w we assume that each elementary act occurs in two steps:

1. The energy of the entire volume l^3 undergoes a slight fluctuational increase, and the subsystem goes over into a state C, characterized by an excitation energy $\varepsilon_c > \bar{\varepsilon}$, where $\bar{\varepsilon} = \varepsilon_0 l^3$ is the mean thermal energy of the subsystem. This step of the process may be treated rigorously by a thermodynamic theory of fluctuations.
2. The excited state C of the subsystem decays according to

$$C \to A + b, \tag{11}$$

where A is a lower state of the subsystem, and b is a state of the particle (or quasiparticle) which carries off an energy Δ' per atomic volume d^3.

The physical meaning of the process described by (11) is the following. Having undergone a transition to the state C, the microcontinuum of volume l^3 remains in this excited state for a time long compared with the periods of vibration of the individual particles. There is therefore a finite probability that in the time $a\tau_0$ the excess thermal energy $\Delta' > \Delta$ will concentrate in a random manner on one or several of the bonds within the subsystem, giving rise to a new state A of this sybsystem. This process is similar to the concentration of energy and subsequent breaking of bonds in large molecules,[6] and to decay of a compound nucleus.[7] Therefore the position and time at which each elementary process (11) takes place are known only with an accuracy l^3 and $a\tau_0$, respectively. Finally, since these are very small quantities from the macroscopic standpoint, such accuracy is quite sufficient for the purposes of physical kinetics.

Let us calculate the probability for (11). It is quite clear that this problem is completely analogous to that involving the decay of a compound nucleus in the statistical theory of nuclear reactions. Let us therefore apply the results known from nuclear theory.[7] We assume that the entire subsystem of volume l^3 participates in the elementary process (11), and neglect the influence of the rest of the substance. To the set of elementary processes in the V/l^3 subsystems we apply the principle of detailed equilibrium

$$g_C w^C_{Ab}(\varepsilon_b) = g_A g_b w^{Ab}_C(\varepsilon_b), \tag{12}$$

where $w^C_{Ab}(\varepsilon_b)$ is the probability per unit time and per unit energy interval for (11), $w^{Ab}_C(\varepsilon_b)$ is the probability of the inverse process, and g_C, and $g_A g_b$ are the statistical weights of states C and A of the subsystem. Let each subsystem have entropy $S(\varepsilon)$ and temperature $T(\varepsilon)$. We express $w^{Ab}_C(\varepsilon_b)$ in terms of the cross section for the inverse process, insert the usual expressions for the statistical weights, and proceed with the calculation in complete analogy with the nuclear case.[7] Then for the integral "decay" probability for (11) we obtain the formula

$$w' = \int w^C_{Ab}(\varepsilon_b)\, d\varepsilon_b = \frac{kT}{\hbar}\exp\left\{\frac{S(\varepsilon_c - \Delta) - S(\varepsilon_c)}{k}\right\}. \tag{13}$$

In obtaining this result we have used the relations

$$\varepsilon_C = \varepsilon_A + \varepsilon_b + \Delta \text{ and } \varepsilon_b \ll \varepsilon_C.$$

To actually obtain w, we must multiply w' by the probability that the subsystem will undergo transition to the excited state C as a result of fluctuations, i.e., by a Boltzmann factor. Then

$$w = \frac{kT}{\hbar} \exp\left\{\frac{S(\varepsilon_C - \Delta) - S(\varepsilon_C)}{k}\right\} \exp\left\{\frac{F_C - F}{kT}\right\}, \tag{14}$$

where F and F_C are the free energies of the initial and excited states. Since the dependence of w on ε_C has a sharp maximum (it is a δ-like function), expression (14) need not be integrated over all states C. This sharp maximum in (14) means that the great majority of the elementary acts occurs in subsystems whose energy is equal to or greater than the fixed value ε_C, corresponding to the state of the microcontinuum in which the excess energy is Δ.

Now we add the effect of an external field, using thermodynamic "perturbation theory."[3] The condition under which this may be done can be written

$$U_0 \ll \varepsilon_0, \tag{15}$$

where U_0 is the energy density of the external field.

For an electric field this becomes

$$U_{0e} = \frac{\mu E^2}{8\pi} \ll \varepsilon_0 \tag{16}$$

(where μ is the dielectric constant, and E is the field strength).

Since the difference between ε_0 and U_0 is great, in the first approximation the probabilities w' for bond rupture, corresponding to the value of ε_C obtained from the maximum of (14), are those of the unperturbed system. The external field will merely destroy the symmetry in the frequency of occurrence of the C states favorable for the forward and inverse processes. This is because there is a slight change in the mean energy $\bar{\varepsilon}$ of the subsystem about which the fluctuations occur. It is in this way that the process becomes irreversible. Recalling that $\Delta \ll \bar{\varepsilon}$, in the first approximation we obtain

$$w = \frac{kT}{\hbar} \exp\left\{-\frac{\Delta - \bar{U}_0 l^3}{kT}\right\}. \tag{17}$$

Inserting this into (10) we arrive at

$$N_1 = \frac{V_k T c}{l^3 \hbar} \exp\left\{-\frac{\Delta - \bar{U}_0 l^3}{kT}\right\}, \tag{18}$$

$$\bar{U}_{0e} l^3 = \frac{E_0 l^3}{2} (P_c - P) \sim E_0 \tag{19}$$

(c is the relative concentration of those particles which are affected by the field, i.e., of ions, polar molecules, or the like). Condition (9) can be written in the form

$$\left(\frac{l}{l_0}\right) \ll \left(\frac{\hbar}{kT\tau_0}\right) \exp\left\{\frac{\Delta}{kT}\right\}. \tag{20}$$

The restriction imposed by this requirement is a weak one, inasmuch as it holds for $\Delta \sim 3kT - 4kT$. According to (5), (7) and (17), this method may be used with external fields such that

$$\bar{U}_0 < \frac{\Delta}{l^3}. \tag{21}$$

Equations (17) and (18) imply that we may treat as "weak" those fields which satisfy the inequality

$$\overline{U}_0 l^3 \ll kT. \tag{22}$$

The value of l_0 can be found from the thermal conduction[2,5] and the parameter a is of order of magnitude one (its exact value must be found from experiment). For $kT \approx 4 \cdot 10^{-14}$ erg and $l^3 \approx 10^{-18}$-10^{-19} cm^3, (22) is satisfied up to fields E of about 10^4-10^5 v/cm. It follows from (22) that the concept of a "weak" field is relative and depends strongly on T: as the temperature decreases the values of E which satisfy (22) also decrease, and for low T and large l the field may have to be small. Since the external field is only a small perturbation which produces something in the nature of a "drift" in relation to the overall fluctuational "background", the way to obtain the number N_2 of elementary acts responsible for the irreversible process is to subtract from N_1 the number $N_1' = \frac{V}{l^3} w_-$ of inverse processes, where w_- is obtained from (17) by replacing $\overline{U}_0$ by $(-\overline{U}_0)$, i.e.,

$$w_- = \frac{kT}{\hbar} \exp\left\{-\frac{\Delta + \overline{U}_0 l^3}{kT}\right\}. \tag{23}$$

Then

$$N_2 = \frac{2VkTc}{l^3 \hbar} \exp\left\{-\frac{\Delta}{kT}\right\} \operatorname{sh}\left\{\frac{\overline{U}_0 l^3}{kT}\right\}. \tag{24}$$

For fields satisfying (22) we obtain

$$N_2 = \frac{2V\overline{U}_0 c}{\hbar} \exp\left\{-\frac{\Delta}{kT}\right\}\left[1 + \frac{1}{3!}\left(\frac{\overline{U}_0 l^3}{kT}\right)^2 + \dots\right]. \tag{25}$$

We remark that the method here described can be used not only with constant external fields, but also with variable fields provided

$$t_0 \gg a^2 \tau_0, \tag{26}$$

where t_0 is a time characterizing the rate of change of the external field (if the field is periodic with angular frequency ω, then $t_0 = 1/\omega$). Since, from the macroscopic point of view, $a^2\tau_0$ is very small, the above formulas will hold to frequencies of the order of 10^9 cps. If the rate of change of the electric field satisfies (26), and if the inhomogeneity of the field and of the particle concentration may be ignored in volumes of the order of l^3, the substance can be described in terms of partial equilibrium, which we define by giving the mean values of the physical quantities (field gradients, concentrations, etc.) pertaining to the subsystems. These average values can then be handled by the electrodynamics of continuous media.[9]

2. Ion Conductivity

Consider ions of a given type with a charge q and let their number per unit volume be n. Using the usual formula

$$\lambda = \frac{\mathbf{J}}{\mathbf{E}} = \frac{q^2 n}{kT} D_e \tag{27}$$

for ion conductivity, we can find the diffusion constant D_e in an electric field.

Now c/w is the time between two successive ion displacements in a volume l^3. But this volume contains l^3/d^3 particles, and in view of the fluctuations, the probabilities of displacement are the same for all the particles. From such statistical considerations, therefore, it follows that before two successive displacements of a given ion take place, there will take place l^3/d^3 displacements of other ions Therefore the mean time τ_1 between two successive displacements of a single ion through a distance δ is

$$\tau_1 = \frac{l^3}{d^3 w}.$$

Using (17), we have

$$\tau_1 = \frac{l^3 kT}{d^3 \hbar} \exp\left\{\frac{\Delta - \overline{U}_0 e l^3}{kT}\right\}. \tag{28}$$

From this equation, and recalling[2] that $D_e = \frac{\delta^2}{\tau_1}$, we obtain

$$D_e = D_0 \exp\left\{\frac{\overline{U}_0 e l^3}{kT}\right\}, \tag{29}$$

where

$$D_0 = \frac{\delta^2 d^3 kT}{l^3 \hbar} \exp\left\{-\frac{\Delta}{kT}\right\} \tag{30}$$

is the diffusion constant in the absence of a field. Inserting (29) into (27), we arrive at

$$\lambda = \frac{q^2 n D_0}{kT} \exp\left\{\frac{\overline{U}_0 e l^3}{kT}\right\}. \tag{31}$$

If the field satisfies (22), this reduces to

$$\lambda = \frac{q^2 n D_0}{kT} \left\{1 + \frac{\overline{U}_{0e} l^3}{kT} + \ldots\right\}. \tag{32}$$

If E_0 is sufficiently small and we may neglect all terms other than the first in the brackets, λ will be independent of E and we obtain Ohm's law. Otherwise Ohm's law will not hold.

Let us use (31) to study the temperature dependence of the ion conductivity. Inserting (30) and $n = n_0 \exp\left\{-\frac{\Delta_1}{kT}\right\}$ into (31), we obtain

$$\lambda = \frac{q^2 n_0 \delta^2 d^3}{\hbar l^3} \exp\left\{-\frac{\Delta + \Delta_1 - \overline{U}_0 e l^3}{kT}\right\}, \tag{33}$$

where Δ_1 is the work required to produce a single ion, and n_0 is a number independent of T.

It is well known that in many ionic crystals the temperature dependence of $\ln \lambda$ has a break in it. Usually this break in the curve is explained by assuming the presence of several different kinds of ions. Eq.(33), however, gives us this break without any such assumption. In solids l_0 first decreases rapidly with rise of temperature, and then more slowly.[5] Therefore l^3 will also first decrease rapidly, and for higher temperatures it will become virtually constant (since condition (8) must be fulfilled in any case). Now according to (33), λ depends on several competing exponentials: whereas

$$\exp\left\{\frac{\overline{U}_0 l^3}{kT}\right\}$$

decreases with increasing T, both $1/l^3$ and the other exponentials increase, and both competing sets of factors depend rather strongly on T. Thus since the decrease in l^3 slows down in a rather narrow temperature interval, a bend in the $\ln \lambda$ curve should be observed. The curvature of this bend differs for different substances; it depends on the way l_0 decreases with temperature and, in general, on the field strength. In some cases there will appear not a break but a more gradual bend. For liquid dielectrics a bend is not observed if there is only one type of ion, since in liquids $l_0 \sim d$.

The methods proposed here can also be used to explain the effect of pressure on ion conductivity. If the substance is subjected to mechanical stress, it is, again, in a state of incomplete equilibrium.[3] This state may be defined by specifying the mean values of the energy of elastic deformation

$$U_{0\sigma} l^3 = \frac{\sigma_{ik} u_{ik}}{2} l^3$$

(where σ_{ik} and u_{ik} are the components of the stress and strain tensors) in the microcontinua of the l^3 subsystems.[10] We assume these subsystems to be deformed homogeneously. Hence under the simultaneous application of an electric field and a mechanical stress, Eqs.(17) and (33) become

$$w_e = \frac{kT}{\hbar} \exp\left\{- \frac{\Delta - \overline{U}_{0e} l^3 - \overline{U}_{0\sigma} l^3}{kT}\right\} \qquad (34)$$

and

$$\lambda = \frac{q^2 n_0 \delta^2 d^3}{l^3 \hbar} \exp\left\{- \frac{\Delta + \Delta_1 - \overline{U}_{0e} l^3 - \overline{U}_{0\sigma} l^3}{kT}\right\}. \qquad (35)$$

It has been shown[10] that $\frac{\overline{U}_{0\sigma} l^3}{kT}$ can be written in the form

$$\frac{U_{0\delta} l^3}{kT} = \sigma B \sqrt{\frac{l^3}{kTK}}, \qquad (36)$$

where K is the modulus of compressibility, σ is the mean stress in the subsystem, and B is a quantity of order of unity. Equations (34)-(36) can be used as a new approach to study of the effect of pressure and temperature on ion conductivity, even at low temperatures. As the temperature decreases, the factor multiplying σ in (36) increases. This general inference is in agreement with the experimental data. The degree to which pressure affects ion conductivity depends on the ratio given in (36) and this is a function not only of σ, but also of the properties of the substance itself and of the temperature.

3. Some relaxation processes in electric fields

The present method can also be used to study phenomena resulting from thermal motion of molecules, ions, etc., in varying fields satisfying (26). The free energy per unit volume of a substance in an electric field can be written

$$\Psi = \Psi_0 + \Psi_e,$$

where Ψ_0 and Ψ_e represent, respectively, the thermal and electrical parts[9]. If there is no energy dissipated when the field changes, then $\delta\Psi = \delta\Psi_e$, while $\delta\Psi_0 = 0$. In actual substances energy dissipation causes Ψ_0 to change, so that in fact $\delta\Psi_0 \neq 0$. Therefore we may write $\delta\Psi = \delta\Psi_0 + \delta\Psi_e$. Since the substance is in incomplete equilibrium, its free energy must have a relative extremum, so that we may write

$$\delta\Psi = \left(\frac{\partial \Psi_0}{\partial t} + \frac{\partial \Psi_e}{\partial t}\right) \delta t = 0, \qquad (37)$$

where t is the time. The quantity $\frac{\partial \Psi_0}{\partial t}$ can be evaluated from kinetic considerations. Each individual act involves the expenditure of an amount of work Δ. The number of such elementary acts responsible for the irreversible process (per unit volume and per unit time) is, according to (24), (23) and (17), $\frac{(w_e - w_-)}{l^3} c$.

Hence the work expended irreversibly per unit time is

$$\frac{c\Delta (w_e - w_-)}{l^3}.$$

To order of magnitude this is the desired quantity, namely,

$$\frac{\partial \Psi_0}{\partial t} \approx \frac{c\Delta}{l^3} (w_e - w_-). \tag{38}$$

Inserting (38) into (37), we arrive at

$$\frac{\partial \Psi_e}{\partial t} \approx - \frac{c\Delta}{d^3 \tau_e}, \tag{39}$$

where

$$\tau_e = \frac{l^3}{d^3 (w_e - w_-)} \tag{40}$$

plays the role of a relaxation time. We may interpret τ_e physically as the minimum amount of time needed for all the particles to take part in the "drift" impose on the overall "background" of fluctuational displacements (or rotations). In substances in which the value of Δ is the same for diffusion and losses, one may use (23) and (30) to obtain a simple relation between τ_e and the diffusion constant D_0, namely,

$$\tau_e = 2\tau_2 \operatorname{sh}^{-1} \left\{ \frac{\overline{U}_{0e} l^3}{kT} \right\}, \tag{41}$$

where

$$\tau_2 = \frac{\delta^2}{D_0}. \tag{42}$$

If the field satisfies (22), we may write

$$\tau_e = \frac{\tau_3 kT}{2\overline{U}_{0e} d^3} (1 - x + x^2 - \ldots), \tag{43}$$

where

$$\tau_3 = \frac{\hbar}{kT} \exp \left\{ \frac{\Delta}{kT} \right\}, \tag{44}$$

and

$$x = \frac{1}{3!} \left(\frac{\overline{U}_{0e} l^3}{kT} \right)^2 + \frac{1}{5!} \left(\frac{\overline{U}_{0e} l^3}{kT} \right)^4 + \ldots$$

Equations (40)-(44) show that τ_e depends on the field strength and on the temperature. For constant temperature and as $\overline{U}_{0e} \to 0$, we find that $\tau_e \to \infty$. Conversely, as $\overline{U}_{0e}$ increases, τ_e decreases. Using (41) and (42) and recalling that the viscosity coefficient $\eta \sim \frac{kT}{D_0}$, we obtain

$$\tau_e \sim \frac{\delta^2 \eta}{kT} \operatorname{sh}^{-1} \left\{ \frac{\overline{U}_{0e} l^3}{kT} \right\}. \tag{45}$$

Eq.(39) is easily solved if we assume that one can neglect all terms other than unity in the parentheses of Eq.(43). We shall not go through this solution, but shall discuss qualitatively and generally the question of energy dissipation. Three different cases are possible:

$$\omega \gg \frac{1}{\tau_e}; \quad \omega \ll \frac{1}{\tau_e} \text{ and } \omega\tau_e \sim 1. \tag{46}$$

The energy dissipated in a single period can be evaluated from the formula

$$\Delta\Psi \approx \frac{\partial\Psi_e}{\partial t}\cdot\frac{1}{\omega} = -\frac{\Delta c}{d^3\tau_e\omega}\,. \tag{47}$$

If $\tau_e\omega \gg 1$, the losses are small. Physically this means that the "drift" responsible for energy dissipation cannot be established in the time $1/\omega$. We note that if E_0 is increased (for constant ω and T) the product $\tau_e\omega$ decreases, and the losses therefore increase. This explains why dielectrics heat up in strong fields, even at high frequencies. The third of the possibilities in (46) corresponds to a unique kind of "resonance" in which all of the particles involved in the "drift" are able to keep up with the field, while there is no compensating effect of polarization to interfere with this "drift". This effect can be substantial when $1/\omega \gg \tau_e$. Then the "efficiency factor" $\beta_e < 1$ appears in Eq.(27); this factor decreases rather slowly with decreasing frequency. Thus, the maximum loss occurs when $\tau_e\omega \approx 1$. Increasing the field shifts this maximum towards higher frequencies (for constant T or lower temperatures (for constant ω). Increasing T shifts the maximum towards lower fields (for constant ω) or towards higher frequencies (for a constant field amplitude).

The results obtained can be used to relate phenomena taking place in dielectrics in an electric field to their thermal conductivity and other nonelectric quantities. In solid dielectrics this means that the theory of activation processes is related to the principal problems of the quantum theory of solid state.

The parameter l entering the deduced formulas must be found from experiment. It can be found, for instance, by analyzing one set of phenomena in a system (say, for instance, the ion conductivity), and then used for calculation of some other type of effect (for instance, loss due to ion transfer).

The above applications of our method for calculating the rates of activation processes does not exhaust its possibilities. It can also be used to study other phenomena connected with the motion and regrouping of particles and requiring an activation energy.

I desire to express my deep gratitude to B.N.Finkel'shtein for his constant attention to and interest in the work and for valuable suggestions. I am also grateful to A.S.Kompaneits and G.I.Skanavi for discussions and comment.

Note added in proof. It has been shown by Roginskii[11] that our method leads to a Δ-dependent factor multiplying the exponential in (17) and (18). We obtain this result if we assume that in an equilibrium homogeneous system the energy ε (and the internal parameters f) of N subregions of volume l^3 form an N-dimensional stationary ergotic Gaussian process[12] $\vec{\varepsilon}\,(t, \Omega)$ (and $\mathbf{f}\,(t, \Omega)$ with components $\varepsilon_p(t, \Omega)\cdot$ $\cdot(f_p(t, \Omega),\ p=1, 2, \dots, N)$ and finite mean $\bar{\varepsilon}$ (and $\bar{f}$) and deviations α^2. Its spectrum is bounded by the frequency $\omega_0 < \frac{l_0}{\tau_0 l}$. Then $\vec{\varepsilon}\,(t,\Omega)$ (and $\mathbf{f}\,(t, \Omega)$) are fully defined by their values at points spaced at intervals of $1/2\omega_0$.[13] Let us divide the range of variation E of ε into segments $\Delta\varepsilon$ equal to the mean variation of ε in a time $^1/_2\omega_0$. By $\varepsilon_p(t, \Omega)$ we understand a quantity defined in terms of a generalized process[14] given on the space of functions vanishing outside of the $1/2\,\omega_0$ intervals and normalized to unity. We characterize the state of a system over the time interval $\Delta\tau \lesssim \omega_0^{-1}$ by the occupation numbers b_k of the intervals $\Delta\varepsilon_k$. We then place the set of single acts of the activation process in correspondence with a finite (countable) set of increments of a continuous stationary process.[15] We choose l so that the variation of ε in the time $\frac{l}{l_0}\tau_0$ be less than Δ. We describe a nonequilibrium system satisfy-condition (1) in terms of processes with stationary incerments,[12,14] which we consider stationary in the time intervals Δt. The effect of an external field $U_0(f, g)$ which does not change the Gaussian nature of the process, leads in the first approx mation to the appearance of the factor

$$\exp\left\{\frac{U_0(\overline{f}_c, g) - U_0(f, g)}{\alpha^2}\, l^3(\varepsilon_c - \overline{\varepsilon})\right\},$$

where g is an external parameter.

References

1. N.S.Fastov & B.N.Finkel'shtein, Izv.AN SSSR, Ser.fiz., 22, 249 (1958). (Trans.Bulletin, 22, 246.)

2. L.É.Gurevich, Osnovy fizicheskoi kinetiki (Fundamentals of physical kinetics), M. 1940.

3. L.D.Landau & E.M.Lifshits, Statisticheskaya fizika, M. 1951. (Trans. Statistical Physics.)

4. M.A.Leontovich, Vvedenie v termodinamiku (Introduction to thermodynamics), M. 1951.

5. R.E.Peieris, Quantum Theory of Solids, Oxford, 1955. (Cited in Russian trans.)

6. L.Landau, Phys.Z.Sow., 10, 67 (1936).

7. A.Akhiezer & I.Pomeranchuk, Nekotorye voprosi theorii yadra (Some problems in the theory of the nucleus), M. 1948.

8. S.Glasstone, K.Laidler & H.Eyring, The Theory of Rate Processes, etc., N.Y., 1941. (Cited in Russian trans.)

9. L.D.Landau & E.M.Lifshits, Elektrodinamika sploshnykh sred (Electrodynamics of continuous media)., M., 1958.

10. Yu.L.Khait, Report at the First Conference on Relaxation Effects in Metals and Alloys, Moscow, 1958; Report at the All-Union Conference on the Physics of Strength, Kharkov, 1958.

11. S.Z.Roginskii & Yu.L.Khait, Doklady AN SSSR, 130, 366 (1960).

12. A.M.Yaglom, Usp.mat.nauk, 7, 3 (1952).

13. Yu.K.Belyaev, Teoriya veroyatnostei i ee primeneniya 4, 437 (1959). (Tran Theory of probabilities.)

14. I.M.Gel'fand, Doklady AN SSSR, 100, 853 (1955); K.Ito, in "Matematika" (Collected articles -"Mathematics"), No.1:3, p.139, M. 1957.

15. M.S.Bartlett, Stochastic Processes, Cambridge, 1955. (Cited in Russian translation.)

DISCUSSION

V.I.Odelevskii: I.Ts.Lyast in his report speaks of strontium-bismuth titanates, which in the simplest case can be represented in the form of an omission solid solution with deficiencies in the strontium-bismuth part of the lattice. Qualitative comparison of the theory with experiment was carried out for the strontium-bismuth titanate composition with 10% substitution (i.e., with $x = 0.1$); it was assumed that the dipole concentration is low, i.e., does not exceed 1%, and this assumption proved significant. Actually, however, with $x = 0.1$ the dipole concentration should be high. Thus the concentration of vacancies calculated with respect to the sum of the large cations and vacancies equals

$$C_B = \frac{x}{3} = \frac{0.1}{3} \approx 3.3\%.$$

In the theory under consideration, however, it is a question not of holes but of relaxators formed by titanium ions adjacent to a hole, the number of which equals 8.

Thus the dipole concentration referred to the number of large cations equals $3.3 \times 8 \approx 26\%$. Obviously, such a concentration cannot be regarded as low.

Furthermore, it is not clear to me to what extent the calculations of Lyast correspond to the ideas of Kirkwood's theory of polarization; they are probably closer to the theory of Onsager; in Kirkwood's theory a significant role is played by association of rigid dipoles, whereas in Lyast's report interaction of this type was not taken into account.

G.I.Skanavi: The most difficult question in the theory of polarization of condensed media is the question of taking into account dipole-dipole interaction, particularly in alternating fields.

In the case of a low dipole concentration, this interaction can with some degree of success be taken into account in the theory of polarization in static fields. Extant theories of polarization in alternating fields take into account the dipole interaction by means of the method of local fields. This method, however, cannot be applied in the case of a high dipole concentration. An urgent theoretical problem is a procedure for rigorously taking into account dipole-dipole interaction in alternating fields in the range of high dipole concentrations.

In the specific case of polarization of strontium-bismuth titanates, as I indicated in my report, the concentration of quasi-dipoles may be lower than the concentration of vacancies in the strontium part of the lattice, if the quasi-dipoles are produced only by associated vacancies. In this case the assumption regarding low quasi-dipole concentration, made by Lyast, is allowable. Then in an alternating field one can use the method of local fields and the concept of an asymmetrical quasi-dipole distribution function.

I.Ts.Lyast: It seems to me that in my work I took adequate account of the theory of Kirkwood; in the report, however, owing to lack of space, I could not dwell on this matter at sufficient length.

K.B.Tolpygo: (Regarding the report of V.L.Ginzberg*): I think there is a close analogy between the direction taken in the work of Ginzberg and that in the work of Pekar in which there was also considered the spatial dispersion of $\epsilon(k)$ (k is the wave number) and some other investigations in which the propagation of a wave in a crystal is discussed in connection with vibrations of the crystal lattice taking into account the lagging interaction. If we replace the plot of lattice vibration frequency vs wavelength by a plot of the square of the index of refraction vs the the frequency: $n^2(\omega)$, one can obtain the corresponding formula for spatial dispersion. Actually, in taking into account the higher terms of the expansion of $\omega = \omega(k)$, the formula for the frequency dependence of n^2 will include spatial dispersion as well. This method is, of course, a particular one as compared with the phenomenological method, which is based on utilizing the expansion of D in terms of E, $\partial E/\partial x$, etc. If, however, we want to carry out quantitative comparisons or make quantitative evaluations of the effects of spatial dispersion, it is easier to use the particular method of considering lattice vibrations, which naturally requires taking into account the specific interaction of atoms. It must be said, however, that what I have succeeded in doing in this direction leads to rather unpromising inferences. It is found that the next tensors, beginning with tensors of the third rank, are very small.

---

*The report of V.L.Ginzberg, "Electromagnetic waves in isotropic and crystalline media characterized by dielectric permittivity with spatial dispersion" has been published in Zhur.eksp.i teor.fiz., 34, 1593 (1958). (Trans.Soviet Phys.-JETP, 7, 1096.)

Actually, $\epsilon(k)$ must be expanded in powers of the ratio of the lattice constant to the wavelength, and for the infrared region of the spectrum this quantity is only of the order of 10^{-4}-10^{-5}.

Thus for dispersion in the infrared region in crystals with central symmetry, for example, in NaCl, the effect will be of the second order, of the order of 10^{-8}--10^{-10}. I attempted to compute birefringence in NaCl. It proved to be so small that to detect it one must have a crystal several meters thick.

If we go over to crystals without a symmetry center, for example, to diamond, the expansion of $\omega(k)$ will begin with a term of the first order. Hence birefringence in such a cubic crystal proves to be more significant. The difference between the refractive indices for the beams is found to be of the order of 10^{-5}, which is at the lower bound of experimental accuracy. Unfortunately, however, this effect may be noticeable only in the region of natural frequencies of the crystal, where the absorption becomes appreciable.

B.N.Finkel'shtein: I want to say a few words regarding that part of the work of K.B.Tolpygo which pertains to the introduction of fractional charges in binary dielectrics. The consistent microscopic theory for a heteropolar lattice would give, in addition to ionic binding, some contribution as regards homopolar binding. i.e., would lead to a result which here was obtained on the basis of a certain model.

Similar concepts were developed with regard to metallic alloys by N.F.Mott and A.G.Samoilovich in their work on the electronic theory of double metallic systems (α-brass). The theory of dielectrics is in a more advantageous situation than the theory of metals. At present in the study of metallic alloys there is a definite need of a dynamic theory of the crystal lattice even for understanding equilibrium properties. The last for its description requires taking into account not only the configuration energy but also the vibrational energy. In this respect where dielectrics are concerned considerable success has been achieved, as witness the report we have just heard.

POSSIBILITY OF THERMAL POLARIZATION OF ELECTRONS IN ZINC SULFIDE CRYSTAL PHOSPHORS

- F. I. Vergunas & P.E. Ramazanov

Introduction

When a crystal phosphor serving as the dielectric of a capacitor is exposed to ultraviolet light the dielectric loss tangent and the capacitance increase. This phenomenon is termed the photodielectric effect (hereinafter pde).

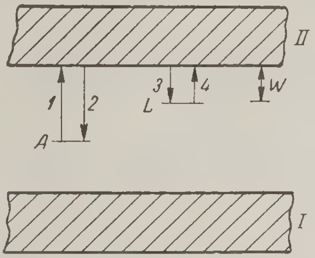

Fig.1. Band model of simple phosphor: I - valence band, II - conduction band, A - activator levels, L - trapping levels.

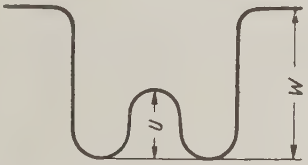

Fig.2. Potential energy curve of a trapping level.

Fig.1 shows the energy diagram for a simple crystal phosphor containing traps of one depth and luminescence centers of one type only. Upon excitation of the phosphor, the luminescence centers are ionized (transition 1). The conduction electrons appearing as a result of this ionization may recombine, emitting luminescence (transition 2), or may be localized on sticking levels (transition 3). Both free and trapped electrons appearing as a result of excitation of the phosphor may be responsible for the pde.

In the case of single crystals it is relatively easy to determine whether free or trapped electrons are responsible for the pde. In the case of fine-grained powders (and crystal phosphors are generally obtained in this form), however, the problem becomes much more difficult. Conduction electrons produce polarization of the phosphor grains, while trapped electrons give rise to centers capable of polarization. In both cases upon excitation of the phosphor the capacitance increases, which may be formally associated with increase of the dielectric constant ϵ.

Different models of polarizing centers have been proposed. In the opinion of Garlick & Gibson[1], for example, in an electric field the electrons are elastically displaced within the center, giving rise to additional dipole moments, and thermal motion plays no role in the process; on the other hand, Roux[2] proposed a model of a polarizing center in the form of a potential well of depth W with an internal potential barrier of height U, separating two possible equilibrium positions of the trapped electron (Fig.2). In an electric field the electrons are displaced primarily in one direction, giving rise to an additional dipole moment. This situation is analogous to thermal ionic polarization[3], only in this case the electrons play the part of weakly bound ions.

If the trapping centers are elastically polarized, one can easily determine whether conduction or trapped electrons are responsible for the pde. If, on the other hand, the centers give rise to thermal polarization, this question is difficult to resolve, particularly if we take into account the variation in the concentrations of free and trapped electrons with the temperature T and the intensity E of the exciting light. Thus, if the pde is due to conductivity in the grainy material, the phosphor consisting of conducting grains separated by insulating layers can be replaced by an equivalent circuit of two capacitors connected in series, one of which is shunted by an ohmic resistance that decreases with increasing concentration of the conduction electrons[4]. The increments of tan δ and capacitance C in such a system, taking into account the functional dependences of the free electron concentration N on T and E in the form

$$N = ME^{1/2}\exp\left(-\frac{W}{2kT}\right), \tag{1}$$

may be described by the following formulas[5]:

$$\Delta \tan \delta = \frac{(B/\omega)E^{1/2}\exp(-W/2kT)}{1+\frac{AE}{\omega^2}\exp\left(\frac{W}{kT}\right)}; \tag{2}$$

$$\frac{\Delta C}{C_0} = \frac{1}{1+\frac{\omega^2}{AE}\exp\left(\frac{W}{kT}\right)}. \tag{3}$$

Here M, B and A are constants, ω is the angular frequency of the electric field, E is the intensity of the exciting light, T is the temperature and W is the depth of the traps from which the electrons are thermally released at the given temperature (transition 4 in Fig.1).

It follows Eqs.(2) and (3) that with increase of ω, T or E the loss tangent increment $\Delta \tan \delta$ goes through maxima, the locations of which can be found from the relations

$$\omega_m = A^{1/2}E^{1/2}\exp\left(-\frac{W}{kT}\right); \tag{4}$$

$$T_m = \frac{W}{K}\frac{1}{\ln\frac{EA}{\omega}}; \tag{5}$$

$$E_m = \frac{\omega^2}{A}\exp\left(\frac{W}{kT}\right). \tag{6}$$

In the region of these maxima ΔC changes sharply: increases or decreases with increase of frequency, and attains a constant value with further increase of T or E (see Eq.(3)); it is noteworthy that the change in capacitance is not connected with change in the dielectric constant ϵ.

In the case of electronic thermal polarization, the increase in capacitance is proportional to the increase in dielectric constant. The increase of $\tan \delta$ and ϵ incident to excitation of the phosphor may be determined by means of the equations deduced for ionic thermal polarization by Skanavi[3], if we take into account the variation in the concentration n of filled traps with E and T in the form[6]

$$n = FE^{1/2}\exp\left(\frac{W}{2kT}\right), \tag{7}$$

where $F = \text{const.}$

In view of Eq.(7), the Skanavi equations[3] become

$$\Delta \tan \delta = \frac{\frac{\omega}{T}SPE^{1/2}\exp\left(\frac{2U+W}{2kT}\right)}{\frac{\varepsilon_\infty\omega^2}{4\pi}S^2\exp\left(\frac{2U}{kT}\right) + \frac{PE^{1/2}\exp\left(\frac{W}{kT}\right)}{T}}; \tag{8}$$

$$\Delta\varepsilon = \varepsilon_\infty + \frac{4\pi PE^{1/2}\exp\left(\frac{W}{2kT}\right)}{T\left[1+\omega^2S^2\exp\left(\frac{2U}{kT}\right)\right]}. \tag{9}$$

Here $S = 1/2\nu$; ν is the frequency of oscillation of the electron in the potential minimum, and P is a constant. We have neglected $\varepsilon_\infty/4\pi$ in the denominator of Eq.(9).

It follows from Eq.(8) that in contrast to the pde due to conductivity, in the case of thermal polarization $\Delta \tan \delta$ with increase of E does not go through a maximum but tends to a constant value. Temperature and frequency maxima, however, still obtain in this case. They can be determined from the following conditions:

$$\omega_m = \frac{4\pi E^{1/2} \exp\left(\frac{W-4U}{2kT}\right)}{\varepsilon_\infty T S^2}, \tag{10}$$

$$\frac{\omega}{E^{1/2}} \exp\left(\frac{U-W/4}{kT_m}\right) = \ln\left[\frac{U}{k}\frac{P}{T_m^2}\frac{4\pi}{\varepsilon_\infty S^2\left(\frac{2U-W}{2kT_m}-1\right)}\right] \tag{11}$$

or

$$T_m = \frac{U\frac{W}{P}}{k\left(L-\ln\frac{\omega}{E^{1/4}}\right)}, \tag{12}$$

where
$$L = \ln\left[\frac{U}{k}\frac{P}{T_m^2}\frac{4\pi}{\varepsilon_\infty S^2\left(\frac{2U-W}{2kT_m}-1\right)}\right]^{1/2}.$$

Comparing Eqs.(4) with (10) and (5) with (12), we see that in the case of conductivity and in the case of thermal polarization the position of the frequency and temperature peaks of Δ tan δ depends on the intensity E of the exciting light. With decrease of E, these maxima are shifted to the side of lower frequencies or higher temperatures. The shift of T_m with change in E in the case of thermal polarization is due to the temperature variation of the concentration of polarizing centers.

It is interesting to note that $\Delta\epsilon$ in the case of thermal polarization (Eq.(9)) does not tend to a constant saturation value, as $\Delta C/C_0$ does in the case of conductivity, but goes through a maximum. This maximum can be found from the condition

$$\omega \exp\left(\frac{U}{kT_m}\right) = \left[\frac{1+W}{2kT_m S^2\left(\frac{4U-W}{2kT_m}-1\right)}\right]^{1/2}, \tag{13}$$

from which it will be evident that the temperature of the $\Delta\epsilon$ maxima does not depend on the light intensity E.

Two interesting inferences follow from Eqs.(11) and (13):

1. Maxima for Δ tan δ and $\Delta\epsilon$ will be observed only so long as $W < 2U$ (Eq.(11)) or $W < 4U$ (Eq.(13)). In the case of deep levels, when $W > 2U$ or $W > 4U$, Δ tan δ and $\Delta\epsilon$ will be characterized by monotonic temperature dependences. This is due to the temperature variation of the concentration of trapped electrons.

2. For Δ tan δ and $\Delta\epsilon$, the plots of $\ln\omega$ vs $1/T_m$ are straight lines, the slope of which is equal to $\frac{U-W/4}{k}$ in the case of Δ tan δ (Eq.(11)) and U/k in the case of $\Delta\epsilon$ (Eq.(13)). Consequently, the temperature maxima for $\Delta\epsilon$ must be displaced to the side of higher temperatures relative to the T_m for Δ tan δ.

Thus the pde due to conductivity may be distinguished from the pde associated with thermal polarization from the character of the temperature dependences of $\Delta\epsilon$ obtained at different ω and E, from the character of the E dependences of Δ tan δ and from comparison of the $\ln\omega$ vs $1/T_m$ plots for Δ tan δ and $\Delta\epsilon$. The other dependences and relationships are the same in the case of both conductivity and thermal polarization.

The purpose of the present study was to elucidate the nature of the pde mechanism in ZnS:Cu:Fe phosphor. In the work of Ref.7 there were obtained data indicating that at least part of the pde in this phosphor is not due to conductivity. To check this and provide a definitive answer to the problem a more thorough investigation was indicated.

Experimental results and discussion

The pde in the ZnS:Cu:Fe phosphor was measured by means of a KV-1 Q-meter. The measurement procedure has been described earlier[8]. The capacitor was of the sandwich type. A 0.3 mm phosphor layer some 5 cm^2 in area was deposited by settling from acetone on a thin (0.03 mm) mica plate, covered with a similar mica plate and inserted between the two electrodes, one of which was a brass disk, and the other a framed copper screen (500 mesh per cm^2). The transparent screen electrode provided for UV illumination of the phosphor and observation of its phosphorescence. Thus we had a sandwich capacitor consisting of the phosphor, mica and air. From the data cited above it follows that the phosphor had the lowest capacitance; consequently, it determined the capacitance of the system. The dark capacitance C_0 showed no variation with frequency or temperature; consequently, the character of the variation of $\Delta C/C_0$ for the system was determined by the character of the variation of ΔC of the phosphor. The dark value of tan δ of the system also was frequency and temperature independent. Upon excitation of the phosphor, tan δ of the system increased by an order of magnitude; consequently, the

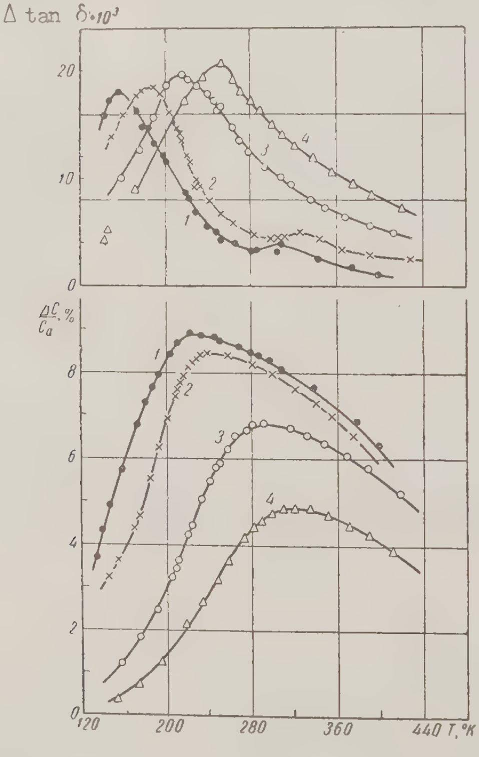

Fig.3

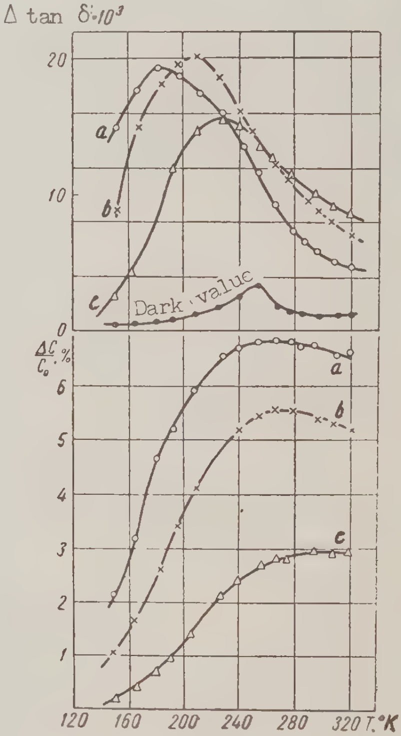

Fig.4

Fig.3. Variation of Δ tan δ and $\Delta C/C_0$ with temperature with excitation of the phosphor to equilibrium; curves recorded at different field frequencies: 1) 90.2 kc, 2) 282 kc, 3) 2.94 Mc, 4) 9.69 Mc.

Fig.4. Variation of Δ tan δ and $\Delta C/C_0$ with temperature at different intensities of the exciting light: a) E = 100%, b) E = 13.2%, c) E = 1.39%.

character of the variation of $\Delta \tan \delta$ of the phosphor determined the character of the variation for the system.

We recorded the temperature dependences of the pde at different frequencies with the phosphor excited to equilibrium by $\lambda = 365$ mμ light (Fig.3) and the temperature dependences at different intensities E of the exciting light (Fig.4). It will be evident from the figures that both $\Delta \tan \delta$ and $\Delta C/C_0$ exhibited temperature peaks. This in itself indicated that the pde is due to electronic thermal polarization, inasmuch as if the pde were due to conductivity, the $\Delta C/C_0$ curve should not have temperature maxima: with increasing temperature $\Delta C/C_0$ should tend to a constant value (Eq.(3)). True, in the case of ZnS:Cu phosphor[5], the pde in which is due wholly to conductivity, the plateau begins to droop, but for all frequencies and all values of E the beginning of the falling section of the curve coincided with the beginning of temperature quenching. In the case of the ZnS:Cu:Fe phosphor the character of the temperature dependences of $\Delta C/C_0$ is entirely different: there is no plateau and the temperature of the beginning of decrease of $\Delta C/C_0$ depends on the frequency, and the decrease is not connected with temperature quenching. Consequently, the curves of Fig.3 cannot be interpreted as indicating that conductivity is responsible for the pde; rather they are evidence in favor of electronic thermal polarization. In accord with the polarization character of the loss mechanism is the displacement of the $\Delta C/C_0$ peaks to the side of higher temperatures relative to the $\Delta \tan \delta$ maxima (Fig.3), the E independence of the $\Delta C/C_0$ maxima and the displacement of the $\Delta \tan \delta$ maxima to the right (side of higher temperatures) with decrease of E (Fig.4).

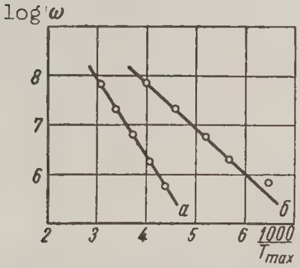

Fig.5. Variation of T_m with ω: a) for $\Delta C/C_0$ with U = 0.31 ev, b) for $\Delta \tan \delta$ with (U - - W/4) = 0.18 ev.

In the case of thermal polarization the $\ln \omega$ vs $1/T_m$ plots for $\Delta C/C_0$ and $\Delta \tan \delta$ should be straight lines (Eqs.(11) and (13)) with a slope corresponding to U in the case of $\Delta C/C_0$ and to U - W/4 in the case of $\Delta \tan \delta$. In order to determine whether this is the case for our phosphor, we constructed these plots on the basis of the data shown in Fig.3. It will be evident from Fig. 5 that there were obtained linear dependences in $\ln \omega$ vs $1/T_m$ coordinates. Assuming that the slopes of these lines are determined by Eqs.(11) and (13), we obtained U = 0.31 ev, (U - W/4) = 0.18 ev and, consequently, W = = 0.52 ev.

Nuvar'eva[9] detected in ZnS:Cu:Fe phosphor three groups of trapping levels with depths of 0.17, 0.3 and 0.52 ev. According to our data, only the deepest of these traps are responsible for the pde, while the shallower traps (0.17 and 0.3 ev) are not polarizing centers. Probably this is explained by the fact that their depth $W < U$. Consequently, the destruction probability for these traps is higher than the polarization probability.

In view of our result it is clear why in ZnS:Cu phosphor there was observed a pde due only to conductivity[5]. According to the measurements of Lukantsever & Krasovskaya[10], there are present in this phosphor only shallow traps having depths of 0.17 and 0.3 ev. Such traps cannot be polarizing centers if in the given phosphor the barrier height U is also 0.3 ev.

Gorki Physical-Technical Research Institute at
Gorki State University

References

1. G.F.J.Garlick & A.F.Gibson, Proc.Roy.Soc., A188, 485 (1947).

2. J.Roux, L'effet photodielectrique dans le sulfure et dans l'oxyde de zinc, Paris, 1956.

3. G.I.Skanavi, Fizika dielektrikov (Physics of Dielectrics), M., 1949.

4. H.Kallman, B.Kramer & A.Perlmutter, Phys.Rev., 89, 70 (1953).

5. F.I.Vergunac & O.V.Agashkin, Optika i spektroskopiya, 3, 338 (1957).

6. A.V.Yastrebov, Trudy (Proceedings), Physical Inst. of the USSR Ac. of Sci., 3, 123 (1946).

7. O.V.Agashkin & F.I.Vergunac, Trudy Pervoi vsesoyuznoi konferentsii po fizike dielektrikov (Transactions of the First All-Union Conference on the Physics of Dielectrics), 1958.

8. P.E.Ramazanov, Izvestiya (Bulletin), Institutions of Higher Learning, Physics, No.2, 39 (1958).

9. V.V.Nuvar'eva, Thesis, Tomsk, 1956.

10. Yu.L.Lukantsever & L.R.Krasovskaya, Izv.AN SSSR, Ser.fiz., 21, 511 (1957). (Trans.Bulletin 21, 509.)

ABSORPTION SPECTRA OF DEFECTS IN IONIC LATTICES

- O.Stasiw

Introduction

The ionic conductivity in heteropolar ionic crystals is determined by the concentration and mobility of the free charged defects. Two or more such defects, located close to each other, form associated complexes (dipoles, quadrupoles, etc.) with a definite orientation in the lattice. Upon application of an external electric field the presence of these dipoles leads to the appearance of one or more maxima in the loss angle curve when the frequency of the defect skips agrees with the frequency of the applied field. The physical nature of the forces, which are the cause of formation of such dissociated and associated effects (to which electrons can also be attached) have been investigated by many authors. Hence we decided to restrict our study to one special case which has been observed in silver halides with impurity O^{2-}, S^{2-}, Se^{2-} and Te^{2-} ions in measurements of the optical absorption in such mixed crystals.

Long Wavelength Absorption Bands

Recently we succeeded in observing in alkali halides with impurity O^{2-}, S^{2-}, Se^{2-} and Te^{2-} ions (the concentration of the impurity ions was $2 \cdot 10^{-4}$ relative to the concentration of Br^- ions) at low temperatures long wavelength absorption bands (Figs.1-4), located ahead of the principal absorption band. The absorption band of O^{2-} ions lies on the short wavelength side of the absorption of Te^{2-} ions. The positions of these bands can be represented by means of the following relation established by Koswig[1,2]:

$$h\nu d^2 = aR - bR^2, \tag{1}$$

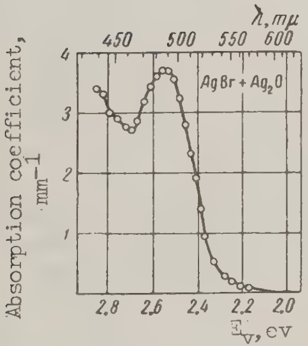

Fig.1

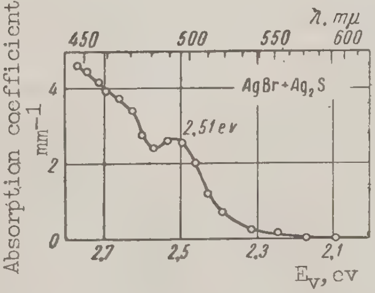

Fig.2

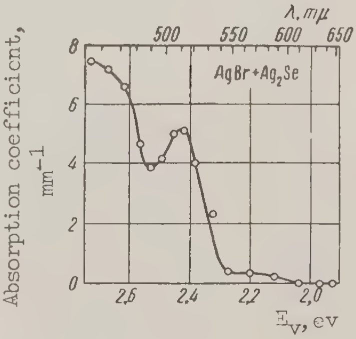

Fig.3

where $h\nu$ corresponds to the maximum of the absorption band, d is the lattice constant, and R is the ionic radius of the extraneous divalent ion introduced into the crystal. The constants a and b can be determined from the measured wavelengths of the absorption peaks and the corresponding ionic radii. If along the vertical axis we lay off values of $h\nu d^2/R$ and along the horizontal axis the values of the ionic radii, we obtain a straight line, at least in the given range of radii (Fig. 5). On the other hand, if we plot the data in $h\nu$ vs R coordinates, we obtain a parabola passing through the origin (Fig.6). It follows therefore that for a definite ionic radius, which corresponds to $a/2b$, there is a limiting value of the

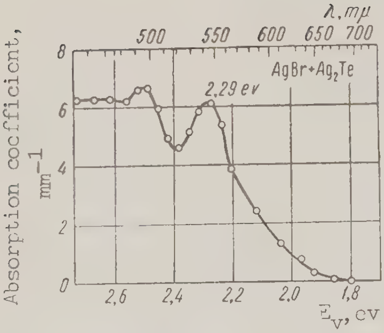

Fig.4

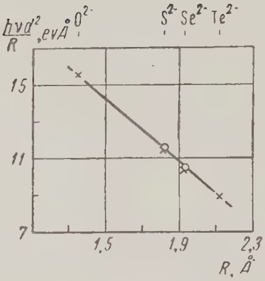

Fig.5

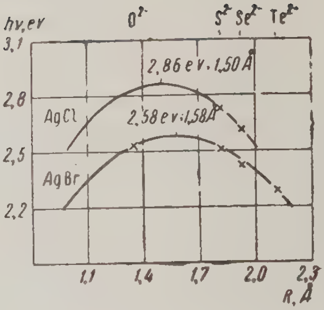

Fig.6

energy of the absorbed photons. This photon energy bound is determined from the maximum of the parabola. It can be shown that if we introduce into an alkali halide crystal a color center with a fictitious radius $a/2b$, there is fulfilled the following relation established by Mollwo[3]:

$$h\nu d^2 = \text{const} = \frac{a^2}{4b}.$$

Discussion of the Results

If we construct a theoretical lattice of bromine and silver ions, i.e., an AgBr crystal, according to the Heitler-London model the distance from the top of the valence band to the bottom of the conduction band will be approximately 4 ev. This value is in good agreement with the experimental data. The absorption edge in silver halide lies in this region. If in our silver bromide crystal we replace a bromine atom with a uninegative S^- ion then, owing to the weaker electron affinity of the S^- ion as compared with the Br^- ion (if we disregard volume and polarization effects incident to introduction of the S^- ion), the distance from the bottom of the conduction band to the level of the S^- ion will be reduced. Thus, owing to the negative electron affinity of the second electron, introduction into the crystal lattice of an excess electron does not lead to formation of an S^{2-} ion. The above also obtains in the case of introduction of O^{2-}, Se^{2-} or Te^{2-} ions into the silver halide lattice. If, however, we assume that the position of the absorption band corresponds to transition of an electron from a divalent anion to a neighboring cation, and determine the energy of the absorbed photons from the cyclic Born-Habersch process, then for the position of the absorption band we obtain the following relation

$$h\nu = G_A + P_A + E + G_K - P_K - J \pm A; \tag{2}$$

here ν corresponds to the position of the band peak, G_A is the energy of the lattice with the extraneous ion removed, P_A is the energy of polarization about the extraneous ion upon attachment of an electron (it is added to the electron binding energy), E is the electron affinity of the extraneous ion, G_K is the lattice energy upon removal of the cation (obviously here $G_K = G_A$), P_K is the polarization energy liberated incident to formation of a neutral atom, J is the ionization energy of a silver ion, and A is the energy due to volume effects, the precise value of which cannot be determined.

If in Eq.(2) instead of P_A and P_K, in accord with the Franck-Condon principle[4], we substitute the value of the electronic polarization, and instead of the other quantities (except A) insert known values, then we obtain a positive value for the binding energy of the second electron. Hence by means of this relation we can show that O^{2-}, S^{2-}, Se^{2-} and Te^{2-} ions can exist in silver halides. According to this formula, one should expect the position of the absorption band to depend on the electron affinity. This, however, was not observed experimentally. In order to explain the experimental data it must be assumed that the polarization energies P_A and P_K, the volume-effect-determined value of A and the electron affinity energy compensate each other and that experimentally they cannot be observed independently of each other. This explanation was first proposed by Schottky[5].

The fact that one can describe the absorption of color centers in alkali halide crystal by means of the relation valid for the absorption of divalent extraneous ions in silver halides enables us to draw certain inferences regarding the nature of defects. According to the relation established by Koswig[1], electron affinity plays no significant role in the process of light absorption by extraneous ions. The constants a and b are determined only by the character of the defects and the fact that the excess electrons in divalent anions are associated with the defects in the same way as electrons in color centers. At the same time it is found that the equation deduced by Mollwo is actually a particular case of the more general equation

$$h\nu d^2 = f(R), \tag{3}$$

where $f(R)$ is a function of the ionic radius of the introduced defect. In the case of a color center this means that the electron trapped by a halogen vacancy assures itself an appropriate ionic radius. This radius corresponds to the equilibrium state with the strongest electron binding and is determined by the maximum of the parabola (Fig.6). The Mollwo constant, which from Eq.(1) is found to be equal to $a^2/4b$, is a quantity that is independent of the lattice constant. This must be true not only of alkali halide crystals but also of silver halides.

The wavelength of the absorption band of color centers cannot be determined in this approximation from the macroscopic dielectric constant, as was done by Mott & Gurney[6] and Pekar[7]. The wavelength of the absorption band is determined only by the lattice constant and the size of the defect, which can be characterized by the ionic radius. From the theoretical standpoint certain difficulties are encountered in constructing this model. In formation of a color center we have a case of attachment or trapping of an electron at a defect with a positive excess charge. In the case of an extraneous ion, on the contrary, the electron is presumably attached to a neutral lattice defect.

These difficulties can be circumvented in the following manner. The attachment of an electron to a neutral defect of the crystal is connected with a polarization energy. This energy is added to the electron binding energy. In attachment of an electron at a defect with a positive excess charge there must be expended a polarization energy which is determined by the displacement of the ion and displacement of the center of gravity of the charge. Hence we must require that both these polarization energies exactly compensate the charge difference between the two forms of defects. At present it is not feasible to evaluate these energy contributions theoretically.

We were, however, able to obtain a rough experimental check. If, instead of a silver ion near the Se^{2-} ion, we introduce a Cd^{2+} ion, there will occur absorption of the Se^{2-} ion in the immediate proximity of an excess positive charge. In this case we are dealing with an electron associated with a positive effect.

Scheidler[8] experimentally showed that the absorption band of such a defect is shifted approximately only 0.06 ev to the short wavelength side of the spectrum relative to the absorption of an isolated Se^{2-} ion. This means that the association energy for formation of a $Cd^{2+} + Se^{2-}$ complex is very low. Thus it can be experimentally shown that the polarization energy contribution approximately compensates the charge difference at the location of the defect.

Thus the formula deduced by Koswig establishes the relation between the absorption spectrum of a color center and that of a divalent anion, at least for silver halides.

Institut der Kristallphysik
Deutsche Akademie der Wissenschaften zu Berlin

References

1. H.D.Koswig, Z.Phys., 149, 204 (1957).
2. H.D.Koswig & O.Stasi, Z.Phys., 149, 210 (1957).
3. E.Mollwo, Gott.Nachr.Math.-phys.Kl., 97, (1931).
4. F.K.Du Pré, R.A.Hunter & E.S.Rittner, J.Chem.Phys., 18, 379 (1950).
5. W.Schottky, Halbleiterprobleme, IV, s. 130, Verlag Viewig, Braunschweig, 1958.
6. N.F.Mott & R.W.Gurney, Electronic Processes in Ionic Crystals. Oxford, 1948.
7. S.I.Pekar, Zhur.eksp.i teor.fiz., 16, 335 (1946); 17, 868 (1947); 19, 746 (1949); 20, 510 (1950).
8. G.Scheidler (in press).

DIELECTRIC AND OPTICAL PROPERTIES OF SOME ZINC SULFIDES

- E.V. Stauer & V.P. Izotov

Introduction

In connection with the accelerated development of technical applications of electroluminescence, we are faced with the problem of detailed investigation of the dielectric properties of zinc sulfide, which is at present the base material for the brightest and best electroluminescent phosphors. There have been relatively few studies of the dielectric properties of ZnS and many of these contain contradictory data; there is as yet no consensus regarding the character of and reasons for variation of the dielectric constant of zinc sulfides under the influence of different factors.

The present work is concerned with the variation of the complex dielectric constant of some electroluminescent and nonelectroluminescent zinc sulfides as a function of the strength and frequency of the applied field, the ambient temperature and the surface treatment of the specimen. We also consider the temperature dependence of the intensity and spectral composition of the electroluminescence.

Apparatus and Measurement Procedure

For measuring the complex dielectric constant we used a KV-1 Q-meter and a bridge of the type described by Ince & Oatley[1] by means of which one can measure the capacitance and equivalent parallel resistance of the capacitor containing the phosphor. The source of the sinusoidal voltage for the bridge was a ZG-10 audio oscillator. The intensity of the electroluminescence was recorded by an FEU-19M photomultiplier connected either to a microammeter or a mirror galvanometer. The emission spectra were recorded by means of a Zeiss spectroscope.

The dielectric specimens were mounted in a special holder designed to permit simultaneous measurements of the optical and electrical properties of the phosphors in the temperature range from liquid air temperature to +200°C.

In view of the fact that we studied powdered phosphors, for measurement of their dielectric characteristics we used the somewhat approximate procedure proposed by Lehman[2]. The powdered phosphor was mixed in a certain proportion by volume with a liquid dielectric and placed between the plates of a capacitor. Under the influence of the electric field the phosphor particles arranged themselves into rather compact bridges between the electrodes.

Such a capacitor to good approximation may be thought of as consisting of two parallel connected capacitors, one of which is entirely filled by the phosphor, the other by the liquid dielectric. Knowing the proportion by volume and the dielectric characteristics of the liquid, we can calculate the dielectric properties of the investigated phosphor from the test results.

By way of liquid dielectric we used silicone oil. As compared with castor oil, a liquid frequently used in such experiments, silicone oil has more constant dielectric properties in a wide range of frequencies and temperatures, and moreover in it phosphor particles tend to form more compact bridges.

We investigated zinc sulfide phosphors activated by Zn, Cu, Mn, Al and other elements. Some of the phosphors were obtained from other scientific institutions; the others were prepared in our laboratory by two procedures, namely:

a) heating luminescence pure ZnS simultaneously with the activator and flux in a stream of hydrogen sulfide, and

b) two-stage heating of the zinc sulfide, first with flux in a covered quartz tube and then with the selected activator.

Experimental Results and Discussion

It has been reported by Lehman[2], Roberts[3] and other investigators that many electroluminophors at low frequencies exhibit an appreciable increase of the real (ϵ') and imaginary (ϵ'') parts of the complex dielectric constant, or as is sometimes said, are characterized by low frequency dispersion. In fact, Ince & Oatley[1] even assert that this low frequency dispersion is connected with electroluminescence and is not exhibited by nonelectroluminescent phosphors. We found, however, that low frequency dispersion is observed in both electroluminescent and nonelectroluminescent phosphors and hence is not directly related with electroluminescence.

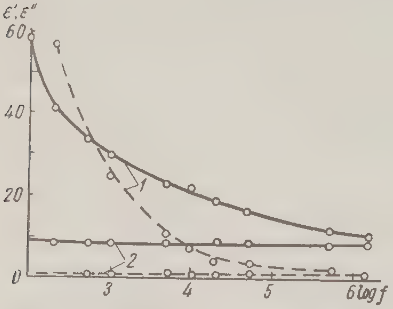

Fig.1. Variation of the complex dielectric constant of photoluminescing zinc sulfide with the frequency (solid line - ϵ'; dashed line - ϵ''): 1 - unwashed phosphors as initially prepared with flux, 2 - phosphor washed with hot acetic acid.

In investigating a series of nonelectroluminescing phosphors we established that many of them do not have low frequency dispersion of ϵ. However, some photoluminescent phosphors prepared so that the grain particles have a well conducting component on their surface, have pronounced low frequency dispersion of the real and imaginary parts of the complex dielectric constant, although they are not electroluminophors.

As a result of washing the phosphor with hot acetic acid, which removes the conducting component ZnO, the dielectric loss is sharply reduced and the low frequency dispersion disappears (Fig.1). At the same time we found that a number of strongly electroluminescing phosphors after thorough washing to remove the conducting component from the surface of the phosphor particles have an insignificant dispersion, although their dc conductivity, due to volume conduction of the particles, may be an order of magnitude higher than that of a phosphor exhibiting appreciable low frequency dispersion.

In fact one can start with a phosphor that does not have dispersion and by producing a conducting component consisting of a layer of zinc oxide or copper sulfide on the surface of the phosphor particles, obtain a product exhibiting low frequency dispersion. Consequently, low frequency dispersion of the dielectric constant in zinc sulfide phosphors is characteristic not only of electroluminescent phosphors and depends largely on the degree of surface conductivity of the phosphor particles.

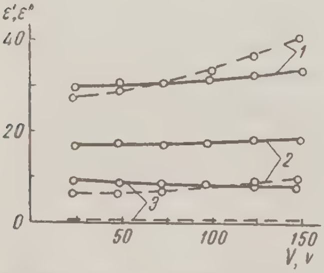

Fig.2. Variation of the dielectric constant of ZnS:Zn phosphor with the applied voltage: 1) 2 kc, 2) 20 kc (unwashed phosphor), 3) 2.5 and 20 kc (washed phosphor).

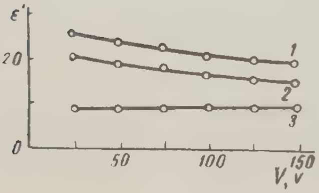

←Fig.3. Variation of the dielectric constant of ZnS:Cu phosphor with the applied voltage with the phosphor illuminated with visible light: 1) 0.2 kc, 2) 20 kc; 3) 0.2 and 20 kc in the dark.

The surface conductivity of the phosphor grains also affects the character of the field dependence of the complex dielectric constant. We were able to obtain different field dependences for the same phosphor by varying its surface conductivity and the experimental conditions. Thus, for electroluminescing and nonelectroluminescing

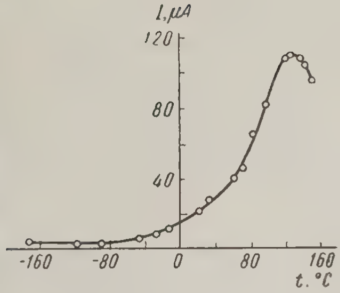

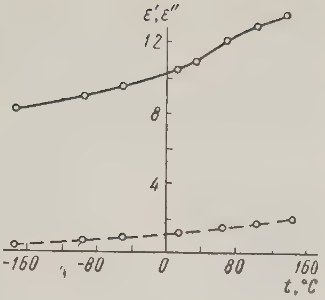

Fig.4. Variation of the electroluminescence intensity of ZnS:Cu:Al electroluminophor with temperature.

Fig.5. Variation of the dielectric constant of ZnS:Cu:Al with temperature.

phosphors having a conducting layer on the particle surface there is observed an increase of ϵ' and ϵ'' with increase of the applied electric field. After elimination of the conducting component by washing with an appropriate solution, the voltage dependence of the dielectric constant is greatly weakened (Fig.2). In the case of phosphors exhibiting the photodielectric effect (electroluminescing phosphors may also exhibit the photodielectric effect), the frequency and voltage dependences of the dielectric constant change under the influence of illumination. Some phosphors characterized by a very weak frequency and voltage dependence of ϵ in the dark, when illuminated, exhibit an appreciable low frequency dispersion. With increase of the field intensity the real part of the complex dielectric constant decreases (Fig.3), while the imaginary part increases.

In the case of phosphors with a strong dark dependence of ϵ on the field strength, as a result of illumination there may be observed extreme values of the dielectric constant. Thus, in zinc sulfide phosphors there may occur either a decrease or an increase of the dielectric constant with increase of the applied field.

The decrease of ϵ' with increasing field strength may be explained on the basis of the concepts of Garlick & Gibson[4], according to which the photodielectric effect is explained by enhanced polarizability of the trapped electrons. A strong electric field favors emptying of the traps, and as a result ϵ' decreases and ϵ'' increases. This interpretation is substantiated by the following experiment. If the applied voltage is rapidly increased and then at once reduced to the initial value, the magnitude of ϵ' remains the same as before the voltage increase. If, however, the phosphor is subjected to a high voltage for several minutes, during this period part of the traps will be emptied under the influence of the field, and hence when the voltage is again reduced the lower value of ϵ' will persist for some time.

We investigated simultaneously the temperature dependences of the electroluminescence intensity and the dielectric constant with a view to determining whether there is a correlation between these characteristics. We established that the electroluminescence intensity increases with increasing temperature owing to thermal release of the electrons that enter into the electroluminescence process. At the same time there occurs temperature quenching of the luminescence of the phosphor. At a certain instant it begins to predominate, and as a result the electroluminescence intensity curve falls off after passing through a maximum (Fig.4). The position of this maximum depends on the type of activator and the strength and frequency of the applied field.

We also found that both parts of the complex dielectric constant of electroluminophors continuously increase with increasing temperature (Fig.5), but do not go through a maximum in contrast to the electroluminescence intensity.

The emission spectrum of many electroluminophors consists of several bands, which sometimes overlap to form a single wide band. Each of these component

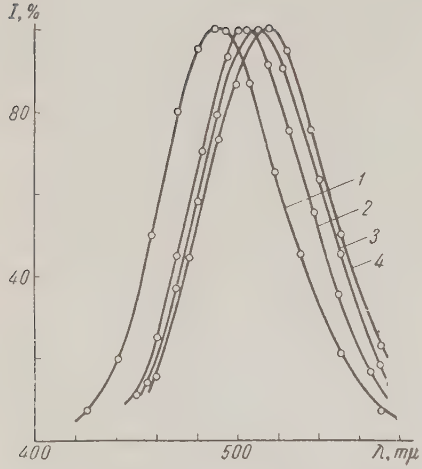

Fig.6. Shift of the electroluminescence peak of ZnS:Cu:Al phosphor with increase in temperature: 1) -72°, 2) 0°, 3) 50°, 4) 100°.

bands may be characterized by its own temperature dependence of the electroluminescence excitation and temperature quenching of the emission, as a result of which the emission spectrum may vary with temperature.

It has been variously reported in the literature that the emission peaks of photoluminescing zinc sulfide phosphors shift with increasing temperature to the side of shorter or to the side of longer wavelengths.[5] In the case of our zinc sulfide electroluminophors, ZnS:Cu, ZnS:Cu:Al and ZnS:Cu:Mn, which emit blue, green and orange, respectively, we observed consistent displacement of the emission peak to the side of longer wavelengths with increasing temperature (Fig.6). The magnitude of the displacement depends on the type of phosphor and also on the frequency and intensity of the applied field. The shift of the emission peak occurs due to more intense temperature quenching of the short wavelength band and greater stimulation of the long wavelength part of the luminescence.

Conclusions

1. Both parts of the complex dielectric constant of all zinc sulfide phosphors in the range of low frequencies are enhanced if the surfaces of the phosphor particles are coated with a conducting component.

2. With increase in the strength of the applied field, zinc sulfide phosphors may exhibit either an increase or a decrease of the dielectric constant: the increase is observed for phosphors with a large surface conductivity and in strong fields; the decrease for phosphors that exhibit a photodielectric effect.

3. The frequency and voltage dependences of the complex dielectric constant may be weakened by washing the phosphor in a solvent that removes the conducting surface layer from the phosphor particles.

4. Both the real and imaginary parts of the complex dielectric constant of zinc sulfide phosphors increase with increasing temperature.

5. The spectral emission peak of zinc sulfide electroluminophors shifts to the side of longer wavelengths as a result of heating.

Dnepropetrovsk State University

References

1. A.N. Ince & C.W. Oatley, Phil.Mag., 48, 1081 (1955).
2. W.Lehmann, J.Electrochem.Soc., 103, 24 (1956).
3. S.Roberts, J.Opt.Soc.Am., 42, 850 (1952).
4. G.F.Garlick & A.F.Gibson, Proc.Roy.Soc.A,188, 485 (1947).
5. R.E.Shrader & S.Larach, Phys.Rev., 103, 1899 (1956).

ON THE NATURE OF STIMULATED LUMINESCENCE IN KCl CRYSTALS

- N.P.Kalabukhov

Luminescence in crystal phosphors is determined by the presence in them of activator and electron-trapping centers, having energy levels located close to the bottom of the conduction band. Fig.1 shows the simplest energy diagram for such a crystal phosphor.

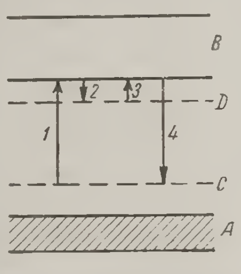

Fig.1. Energy level diagram: A) normally filled band, B) conduction band, C) activator levels, D) electron trapping levels.

The process of luminescence unfolds as follows: under the influence of light, electrons are stripped from the activation centers and go over into the conduction band (transitions 1); then the electrons are captured by impurity atoms serving as traps (transitions 2). The electrons are then freed from the trapping levels D by thermal agitation (transitions 3), go over into the conduction band and there, recombining with ionized activator ions (transitions 4), yield luminescence.

Potassium chloride crystals as a result of irradiation with x-rays or far ultraviolet are colored; immediately after coloring they phosphoresce for some time. If a crystal colored in this manner after extinction of the phosphorescence is illuminated for a brief period by visible or long wavelength ultraviolet light, the crystal again begins to luminesce, and this emission continues almost to complete bleaching of the crystal. Such luminescence-inducing illumination with visible or ultraviolet light is called stimulation and the resultant emission is termed stimulated luminescence. Luminescence of colored crystals is also observed when these are heated; the effect in this case is known as thermostimulated luminescence or thermal de-excitation.

Irradiation with x-rays brings the crystals to an excited state. As a result of this excitation there are formed in the crystals F-centers; at the same time vacancies are also formed in the crystals.[1] As was noted above, stimulating light produces luminescence of colored KCl crystals. This action of light may be represented as a process favoring the formation of M-centers, i.e., centers consisting of an F-center and two vacancies.

Investigation of thermostimulated emission of colored crystals may help understand this process, hence we undertook an investigation on a special set-up designed to record automatically the thermal stimulation (glow) curves on photographic paper.

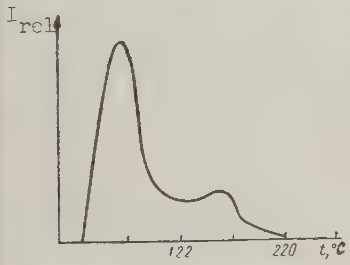

Fig.2. Thermostimulated emission.

The results of investigation of thermostimulated emission of KCl crystals without impurities are shown in Fig.2 (the curves were recorded by graduate student N.M.Magulariya). Before being heated the crystals were x-rayed for 9 min with the tube operated at 45 kv and 5 ma. The heating rate was 0.106 degrees per sec. It will be evident from the figure that the curve has two peaks: one at a temperature of about 70°; the second at about 130°. Calculation of the energy yields a value of 0.86 ev for the first peak and 1.17 ev for the second peak. Similar curves are given by Lushchik[2].

We note that the maximum of the absorption band for F-centers in KCl crystals lies at 555 mμ (2.22 ev); that for M-centers at 825 mμ (1.49 ev). From these data it may be inferred that the de-excitation occurs primarily owing to dissociation of M-centers which form at 70° from F-centers by association of these with two vacancies (Fig.3). Thus owing to approach of the vacancies to F-centers, the energy levels of the electrons in the F-centers are displaced (raised) towards the bottom of the conductio band (Fig.4).

It is interesting to note that at 70° additively colored crystals having a pronounced M absorption band lose this band entirely. The thermostimulation and thermal bleaching curves for the M band (based on data obtained by G.S.Ramishvili) are reproduced in Fig.5.

Additively colored KCl crystals that do not have an M absorption band do not yield thermostimulated luminescence. The colored KCl crystals possessing additional absorption bands in the long wavelength region (so-called R, R' and M bands) exhibit dark conduction. In view of what has been said above, it may be expected that with increase of temperature KCl crystals having an absorption band will exhibit an increase of dark current at 70°, i.e., at the temperature corresponding to dissociation of M-centers.

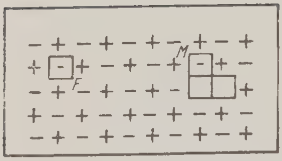

Fig.3. Formation of M-centers.

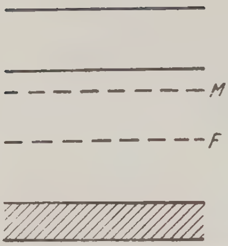

Fig.4. Level diagram.

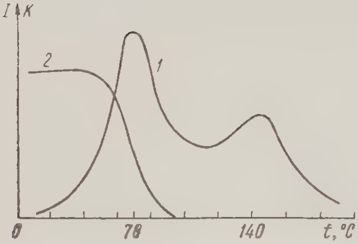

Fig.5. M-band thermal stimulation (1) and thermal bleaching (2) curves.

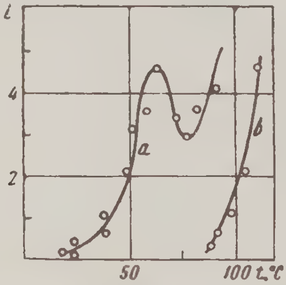

Fig.6. Temperature dependence of the current in colored crystals (a) and the ionic current in transparent crystals (b).

A.A.Shkol'nik carried out experiments on the temperature variation of the dark current in KCl crystals. The curves obtained by her are shown in Fig.6. Curve a shows the variation of the current in colored KCl crystals with temperature. It will be seen that at 70° there is a pronounced peak, which may be attributed to dissociation of M-centers. Thus the expected increase in dark current (conductivity) has been confirmed by experiment. For comparison, we also give the temperature variation of the ionic current in transparent KCl crystals (curve b).

P.A.Yurachkovskii and V.N.Romankevich investigated the spectral composition of the thermostimulated luminescence of the KCl crystals. This investigation showed that the luminescence is due to recombination of electrons with hole centers.

Tbilissi (Georgian SSR) State University &
Kiev Polytechnic Institute

References

1. N.P.Kalabukhov, Zhur.eksp.i teor.fiz., 27, 347 (1954).
2. Ch.B.Lushchik, Trudy (Proceedings), Inst.of Physics & Astronomy, Estonian SSR Ac. of Sci., 3, 120 (1955).
3. N.P.Kalabukhov, Zhur.eksp.i teor.fiz., 26, 242 (1954).

INFLUENCE OF THE ELECTRIC FIELD STRENGTH ON THE PHOTOCONDUCTIVITY OF LIQUID ORGANIC SYSTEMS

- P.K.Mitskevich & V.G.Bobyl'

I. As regards their electric properties weakly polar organic systems belong in the class of liquid ionic semiconductors.[1] The conductivity of this group of substances falls in the range from 10^{-2} to 10^{-10} mho/cm and in this respect they occupy an intermediate position between electrolytic conductors and liquid dielectrics.

In recent years the electric properties of liquid semiconductors have attracted the attention of scientists here and abroad. This is explained not only by theoretical considerations but also by purely practical necessity. On the one hand, the design and operation of liquid scintillation counters, bubble chambers, and various other detectors for investigation of different types of radiation is predicated on an understanding of the electric properties of the liquids employed in such devices; on the other hand, proof that the electric properties of solid semiconductors are determined primarily by the short-range, rather than the long-range, order[2] serves as a stimulus for investigation of the communal properties of liquid and solid dielectrics.

Over the past few years we have engaged in a systematic study of the electric properties of polyhalogen derivatives of methane, halogen derivatives of benzene, phenol, alcohols and other liquids and of two- and multiple-component liquid systems belonging to the class of semiconductors.[3-5] Our experiments have demonstrated that the enumerated liquids and systems as regards their electric properties are reminiscent of solid semiconductors. Recently attempts were made to utilize liquid semiconductors as diodes, triodes and photoresistors.

It has been established that an extensive group of the investigated liquid semiconductors have pronounced photoconductivity.[5] Under the influence of a certain range of radiation the conductivity of these liquid systems increases; after cessation of irradiation the conductivity falls off, tending to the initial pre-irradiation value. It has also been noted that under the action of radiation, in addition to increase of the conductivity, there occur changes in the dielectric properties of these systems; that is, these compounds and liquids exhibit the photodielectric effect.

II. Incident to study of the effects of light on thoroughly purified organic liquids and liquid two-component systems, we also investigated the influence of the electric field strength on the electric and photoconductivity of solutions of bromoform, iodoform, propyl bromide, ethyl iodide, bromophenol and other liquids in ethyl ether, anisole and other solvents. The chemically pure and analytic grade reagents were further purified by double vacuum distillation. The quality of the purified samples was determined by measuring the electric conductivity σ and the index of refraction n; if the measured values of σ and n of the purified materials exceeded the corresponding values for the pure substances as listed in the literature by as much as 10%, the purification operation was repeated.

The dc conductivity and photoconductivity were measured by means of a vacuum tube electrometer.[3] The ultraviolet sources were an SVDSh-250 quartz tube and an IG spark unit. For discrimination of the requisite narrow spectral ranges we used appropriate filters for the ultraviolet and an UM-2 monochromator for the visible region of the spectrum.

III. In general, the current-voltage characteristics of pure liquids are represented by a curve of the type shown in Fig.1. In such curves one can distinguish three sections:

1. Section ab corresponds to nonautonomous (by analogy with gases) conductivity of the liquid; this section is characterized by linear variation of the

current density with the electric field strength.

2. Section bc in which the current does not vary with the field strength. The field strength at which saturation is attained differs for different liquids. According to the theoretical calculations of Skanavi[1], saturation may occur at $E \approx 10^5$ v/cm. This inference, however, is in conflict with the experimental data of some investigators, for example, Nikuradze[6], who observed leveling off of the curve for pure hexane at field values of the order of 400 to 800 v/cm. No saturation current is observed in the case of solutions and liquids containing impurities.

3. Section cd corresponds to autonomous or intrinsic conductivity; here the current increases exponentially with the field strength.

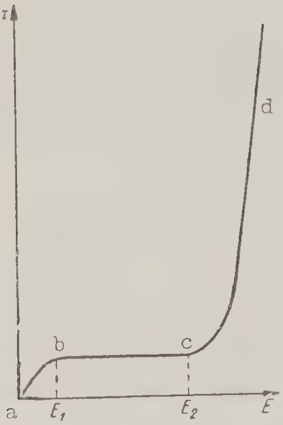

Fig.1. Current-voltage characteristic of a pure liquid.

IV. In weak fields ($E < E_1$ - Fig.1) the current carrier velocity due to the field is appreciably lower than the velocity of thermal motion, i.e., the field energy $\Delta U = q\delta E/2$ is negligibly small compared with the thermal agitation energy kT. This is the reason for the linear field dependence of the current density:

$$j = \sigma E; \tag{1}$$

here σ is the conductivity which may be expressed as

$$\sigma = q n_i U_i , \tag{2}$$

where q is the charge, n_i is the concentration and U_i is the mobility of the current carriers.

For Ohm's law to be obeyed the conductivity σ must be independent of the field strength, i.e., n_i and U_i must be independent of E.

Many experimenters have shown that U_i in the weak field region ($<10^5$ v/cm) does not depend on E.[1,2] The current carrier concentration n_i also does not depend on the field strength in the $E < 10^5$ v/cm region, inasmuch as the binding energy of current carriers held in neutral atoms is greater than the thermal agitation energy and consequently appreciably greater than the energy due to the applied field.

The physical basis of Ohm's law for thermal conductivity can, in our opinion, be utilized for investigation of the field dependence of photoconductivity.

V. Fig.2 shows the experimental data characterizing the influence of the field strength on the photoconductivity of solutions of propyl bromide and bromophenol in ethyl ether. We do not give the data on the other liquids listed above inasmuch as the curves for them do not differ qualitatively from the curves shown in Fig.2.

Illumination of the samples in all cases was started only when the falling off of the current under the influence of the field ceased, i.e., when the initial dark current attained a stable value. Upon illumination of the sample with ultraviolet the current increases. The lower the field strength, the slower the growth of the photocurrent in the initial period. After a certain time, which differs for different liquids, the growth of the photocurrent ceases, i.e., saturation is attained. When the light is turned off the current decreases and tends to the initial value.

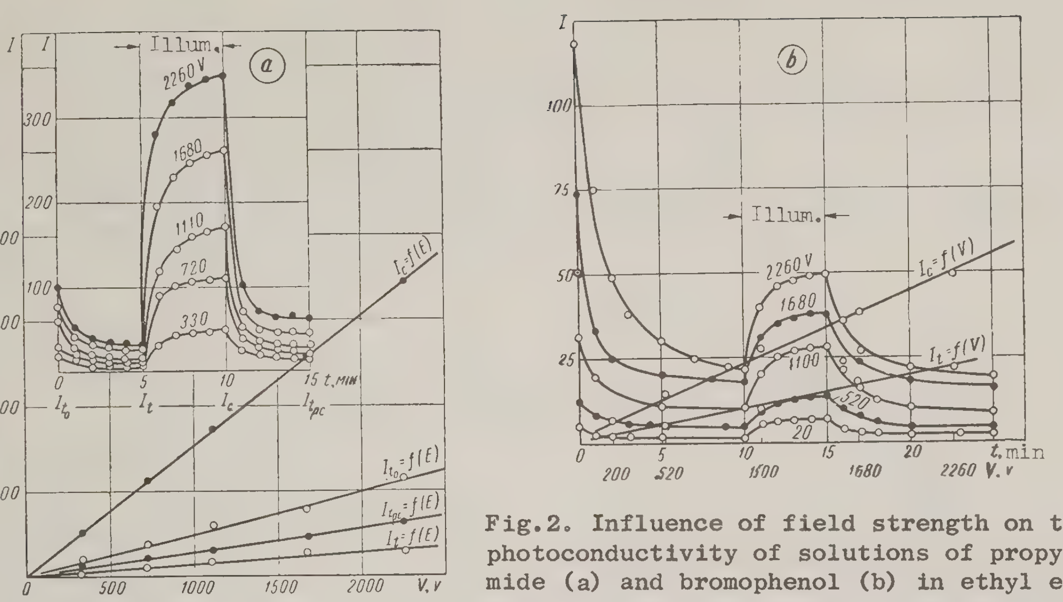

Fig.2. Influence of field strength on the photoconductivity of solutions of propyl bromide (a) and bromophenol (b) in ethyl ether. I_t = dark current, I_c = current under illumination, I_{pc} = post illumination current.

The current rise under illumination and decrease after cessation of illumination follows the exponential law.[5] Only ultraviolet light is photoactive. Visible light produces no noticeable effect. The photoconductivity for each of the investigated liquids occurs only in a certain definite spectral region, namely, in the region of absorption. However, for some samples (for example, solutions of iodoform in ether) we found that the "red limit" of the photoconductivity lies not in the region of self-absorption but is somewhat shifted to the long wavelength side.

Both the dark current and the photocurrent increase with increase of the applied field. The increase in the magnitude of the photocurrent and dark current is linear, i.e., obeys Ohm's law. No tendency to saturation was observed for either the photocurrent I_c or the dark current I_t with increase of the field strength up to 5 kv/cm.

The slope of the $I_t = f(E)$ and $I_c = f(E)$ lines for different samples differs (compare Figs.2a and 2b). The slope of the $I_c = f(E)$ plots for the same compound depends primarily on the concentration of the solution, which determines the short-range order, i.e., the number and nature of nearest neighbors (Fig.3). For most materials the slope of the straight line plots passes through a maximum (Fig.4), which coincides with the concentration maximum of the photoconductivity[5].

We carried out a thorough investigation of the same sample over a prolonged period with different light and dark intervals. It was natural to expect that under the influence of irradiation there would occur destructive changes in the solution, changes that might alter the photoelectric properties and hence impair the reproducibility of the results of successive measurements. To this end we investigated the bromobenzene-ethyl ether system. The experiments were repeated with different intervals over a period of 8 months. It was found that the qualitative behavior of the sample remained the same. True, there was observed an insignificant decrease of the photocurrent with time (the slope of the $I_c = f(E)$ line decreased somewhat), but the linear dependence of the photocurrent on the field strength persisted in all cases.

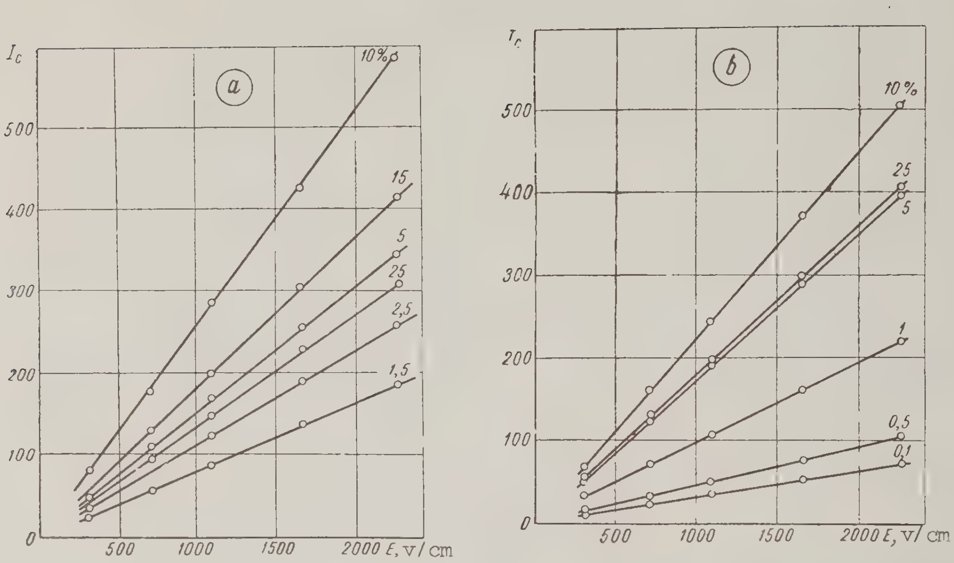

Fig.3. Influence of concentration (indicated in % at the curves) and the field strength on the magnitude of the photocurrent in solutions of propyl bromide (a) and bromophenol (b) in ethyl ether.

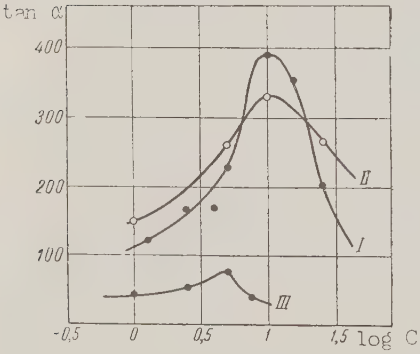

Fig.4. Variation of the slope of the $I_c = f(E)$ lines with the solution concentration: I - propyl bromide, II - bromophenol, III - ethyl iodide. Solvent in all cases - ethyl ether.

Comparing the experimental data for liquid semiconductors with similar data for solid semiconductors and dielectrics, we note that as regards photoconductivity in the weak field region liquid semiconductors exhibit a behavior quantitatively similar to that of solids.$^{1,7-9}$

The fact that the functions $I_t = f(E)$ and $I_c = f(E)$ are linear indicates that the dark conductivity and the photoconductivity are independent of the field strength. Consequently, the dark and light mobilities and concentrations of the "free" current carriers in the field region up to 10^4 v/cm do not depend on the electric field strength.

Department of Physics,
Dnepropetrovsk Engineering-Construction
Institute

References

1. C.I.Skanavi, Fizika dielektrikov (Physics of Dielectrics), M., 1949.

2. A.F.Ioffe, Fizika poluprovodnikov (Physics of Semiconductors), M., 1957.

3. V.G.Bobyl' & Yu.A.Kopylov, Trudy Pervoi mezhvuzovskoi konferentsii po sovermennoi tekhnike dielektrikov i polyprovodnikov (Transactions of the First Intercollegiate Conference on Modern Technology of Dielectrics and Semiconductors) Leningrad, June, 1956.

4. V.G.Bobyl' & Yu.A.Kopylov, Trudy konferentsii po fizike tverdykh i zhidkikh dielektrikov (Transactions of the Conference on the Physics of Solid and Liquid Dielectrics), Pub.AN SSSR, M., 1956.
5. V.G.Bobyl', Trudy (Proceedings), Dnepropetrovsk Eng.-Const.Inst., 1958.
6. A.Nikuradze, Zhidkie dielektriki (Liquid Dielectrics), M., 1936.
7. F.I.Kolomoitsev, Thesis, M., 1952.
8. A.T.Vartanyan, Zhur.fiz.khim., 20, 1065 (1946); 24, 11, 1961 (1950).
9. F.I.Kolomoitsev & A.Ya.Yakunin, Nauchn.zap. (Scientific notes), Dnepropetrovsk State University, 45, 3 (1956).

* * * * * * *

INVESTIGATION OF THE PHOTOCONDUCTIVITY OF ETHER SOLUTIONS

- Yu.A.Kopylov

The theoretical inference drawn by Ioffe[1] that the concentration of free electrons is determined by the short-range rather than by the long-range order in the substance was experimentally substantiated by Regel'[2] in investigating the conductivity of molten semiconductors. This inference is also upheld by the data of Kolomoitsev[3] on the influence of γ-irradiation on the conductivity of dielectrics. Additional support for the predominant importance of short-range order is furnished by investigations of the photoconductivity of substances in the liquid state under normal conditions. Such substances, for example, are halogen derivatives of some hydrocarbons and their solutions in ethyl ether. The electric conductivity of such substances and solutions increases appreciably under the influence of ultraviolet radiation.

In our investigation of this effect we used the ultraviolet radiation from an SVDSh-250 quartz mercury vapor tube; the sample liquids were placed in an electrolytic cell of fused quartz, provided with platinum electrodes for measuring the dc conductivity.

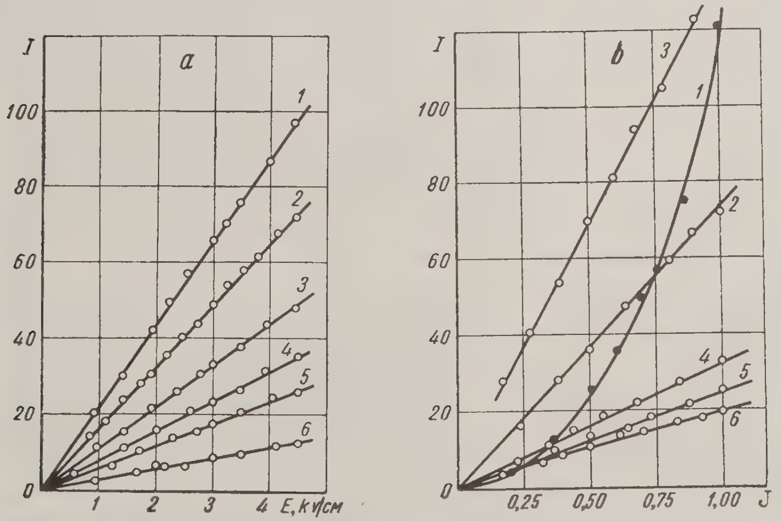

Fig.1. Variation of the photocurrent: a) with the field strength and b) the intensity of UV irradiation for solutions of different hydrocarbons in ethyl ether: I - 1% ethylene bromide ($I \cdot 1.5 \cdot 10^{-9}$ amp); 2 - 0.12% bromobenzene ($I \cdot 10^{-8}$ amp); 3 - 0.5% bromophenol ($I \cdot 10^{-9}$ amp); 4 - 5% propyl bromide ($I \cdot 10^{-8}$ amp); 5 - 1% ethyl iodide ($I \cdot 10^{-9}$ amp); 6 - 0.1% chlorophenol ($I \cdot 10^{-9}$ amp).

The relaxation of photoconductivity and re-establishment of the initial dark current are satisfactorily described by exponential regularities. The duration of relaxation does not depend on the solution concentration, field strength E or irradiation intensity J in a wide range of concentrations, fields and intensities.

The equilibrium

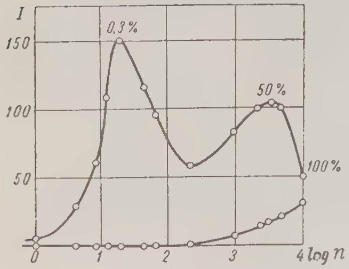

Fig.2. Variation of the photoconductivity (upper curve) and electric conductivity (lower curve) of solutions of bromobenzene in ethyl ether with the bromobenzene concentration (n = number of bromobenzene molecules per cm^3 of the mixture.

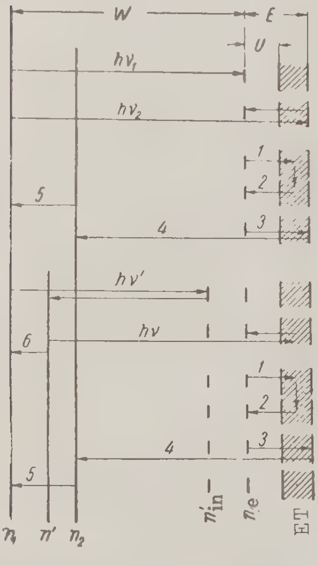

Fig.3. Scheme of energy levels: n_1 - molecular level, n_2 - ionic level, n_e - metastable electronic level, ET - zone of electronic transitions ("courier"), n' - first stage product level, and n'_{in} - intermediate first stage level.

value of the photoconductivity depends linearly on both E and J (Fig.1). The concentration dependence of the effect as a rule passes through a maximum, while in the case of the binary system bromobenzene-ether there are two maxima. Fig.2 shows the concentration dependence of the photoconductivity for this system. The presence of the maxima is explained by displacement of the photoactive wavelength region with increasing concentration. Thus for solutions of bromobenzene in ethyl ether the photoactive wavelength shifts from approximately 2650 Å (0.3% bromobenzene) to 2950 Å (50% bromobenzene). At concentrations corresponding to the maximum of the effect, the photoactive regions are those which comprise the group of the most intense lines in the emission spectrum of the mercury vapor tube. At concentrations corresponding to the minimum of the photocurrent, the photoactive regions are those corresponding to the low intensity lines in the tube spectrum. With increase of the solution concentration there also occurs a shift of the "red" absorption limit to the side of longer wavelengths. The indicated regularities cannot be explained in the framework of the ionic photoconductivity mechanism, but can be interpreted from the standpoint of the electronic mechanism if we assume the presence of metastable levels of the electrons near the liquid molecules.[4]

The energy level scheme proposed for explaining the photoconductivity mechanism is pictured in Fig.3. If as a result of absorption of a photon by a molecular complex (we use n_1 to designate the concentration of such complexes in the liquid), the electron undergoes a transition to a metastable level, where its lifetime is τ sec, the equilibrium concentration n_e of electrons on the metastable level is determined by equality of the forward and reverse transition rates:

$$\gamma n_1 = \frac{1}{\tau} n_e \,. \tag{1}$$

Here the photoionization parameter $\gamma = aJ$ is proportional to the illumination intensity.

If equality (1) is disturbed, the equilibrium will be shifted and the process of relaxation of the new equilibrium state will be described by the following differential equation:

$$\frac{dn_e}{dt} = \gamma n_1 - \frac{1}{\tau} n_e \,. \tag{2}$$

The solution of this equation sill give the time variation of the electron concentration:

$$n_e = \tau\gamma n_1 \left(1 - e^{-\frac{t}{\tau}}\right). \tag{3}$$

The current is proportional to the concentration of electrons, their charge and mobility and the intensity of the electric field. Bearing this in mind and inserting the value of the parameter γ, we obtain time variation of the current:

$$I = kEJ\,(-e^{-\frac{t}{\tau}}). \qquad (4)$$

The coefficient k in Eq.(4) includes all the quantities independent of E and J.

The equilibrium value of the photocurrent, i.e., the value in the limit as $t \to \infty$, is proportional to the field strength and illumination intensity:

$$I = kEJ. \qquad (5)$$

The decay or decrease of the current after cessation of illumination is given by

$$I = kEJe^{-\frac{t}{\tau}}. \qquad (6)$$

The current rise and decay times are equal and do not depend on E and J, in accord with experimental results.

The level scheme shown in Fig.3 can also serve to explain other effects. The closeness of the photoactive radiation to the "red" absorption limit may be interpreted as follows. Photons of energy less than W are not absorbed. If the photon energy lies in the range $W \leqslant h\nu \leqslant W + E$, absorption results in transition of electrons to metastable levels and into the band of intermolecular transitions.

Photons of energy exceeding W + E, when absorbed, produce more profound changes in the liquid; specifically, there may form new electrically neutral complexes. Increase of the bromobenzene concentration in the solution affects the molecular interaction and reduces W, the height of the metastable level, and at the same time the transition band. The "red" absorption limit is shifted to the side of longer wavelengths. This is accompanied by a corresponding displacements of the photoactive region. In case of nonuniform intensity distribution between the different sections of the emission spectrum, there occurs a corresponding change in the concentration of the metastable electrons and, consequently, in the photocurrent.

The scheme of Fig.3 implies the removal of electrons from the metastable level by thermal excitation (transitions 3-4), as a result of which there appear ions which recombine with the cations and form molecules of the initial substance. The fact that the conductivity due to these ions is disregarded in Eqs.(4)-(6) stems from their relatively low mobility. The movement of electrons can be represented in the form of electronic "couriers" dispatched from one molecule to another upon approach of sections of the transition band corresponding to separate molecules of the liquid (transitions 1-2). The duration of participation of electrons in the "courier" and the transition frequency are determined by thermal motion. This explains why the observed period of relaxation of the photocurrent is independent of E and J. The fact that the lifetime τ is apparently independent of the concentration may be explained by the assumption that the conditions for attachment of electrons to molecules of both components of the binary mixture are identical.

In accord with what has been said above, increase of temperature should be accompanied by increase of the mobility but decrease of the mean lifetime τ of the electrons in the metastable state, and, consequently, of their concentration. Depending on which of these processes has the strongest effect on the conductivity, we will observe either a positive or negative temperature coefficient.

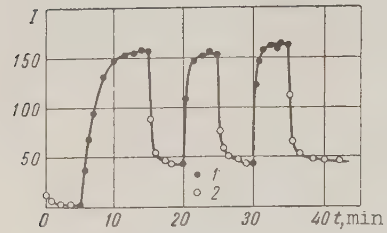

Fig.4. Variation of the conductivity of ethyl ether solutions of bromobenzene during irradiation with UV (1) and after illumination (2).

An investigation of the temperature dependence of the photoconductivity of ethyl ether solutions of bromobenzene, carried out by Bobyl'[5], showed that such solutions have a positive temperature coefficient of photoconductivity. Consequently, increase of the electron mobility is a stronger factor where the photocurrent is concerned than decrease in the electron concentration. The lack of data on relaxation processes precludes judging of the variation of τ with temperature and qualitative evaluation of the sign and relative importance of the above mentioned effects in the general temperature dependence.

In some cases, however, the above scheme is inadequate for explaining the experimental data. Thus we found that the duration of relaxation of the photoconductivity of ether solutions of bromobenzene differs in subsequent irradiations as compared with the first one (Fig.4). The illumination intensity dependence of the photocurrent in solutions of ethylene bromide is nonlinear (Fig.1b), and is described rather by $I = bJ^2$. These results indicate that the process of photoionization occurs in two stages. If the products of the first irradiation do not participate in charge transfer, but upon absorption of a photon serve as electron donors, their concentration will have a substantial influence on the variation of the photocurrent during subsequent illumination intervals.

The variation of the concentration n' of the products of the first stage as a result of absorption of a photon $h\nu'$ (first part of the scheme of Fig.3) will be described by the differential equation

$$\frac{dn'}{dt} = \gamma' n_1 - \left(\gamma + \frac{1}{\tau'}\right) n', \qquad (7)$$

where $\gamma' n_1$ is the rate of formation of the first stage products, $\gamma n'$ is the rate of photoionization, and τ' is the mean lifetime of the first stage products. The solution of this equation for n' is

$$n' = \frac{\gamma' n_1}{P'}\left(1 - e^{-P't}\right), \qquad (8)$$

where the relaxation parameter

$$P' = \gamma + \frac{1}{\tau'}. \qquad (9)$$

To find the variation in electron concentration we must solve the equation

$$\frac{dn_e}{dt} = \gamma \frac{\gamma' n_1}{P_1}\left(1 - e^{-P't}\right) - Pn_e\,, \qquad (10)$$

where $\gamma n'$ is the rate of photoionization and the relaxation parameter

$$P = \frac{1}{\tau}, \qquad (11)$$

here τ is the mean lifetime of an electron on the metastable level. The solution is of the form

$$n_e = \frac{\gamma\gamma' n_1}{P'P}\left(1 - \frac{P}{P - P'} e^{-P't} + \frac{P'}{P - P'} e^{-Pt}\right). \qquad (12)$$

Which term in the parentheses in Eq.(12) will have the predominant influence on the process will depend on the relative magnitude of the two relaxation parameters. If $P' \ll P$, then from Eq.(12), we obtain

$$n_e = \frac{\gamma\gamma' n_1}{P'P}(1 - e^{-P't}). \tag{13}$$

If the first illumination stage products are stable and one can neglect variations in their concentration in the dark interval up to the second irradiation, the variation in electron concentration during the second irradiation will be described by Eq.(3) but with n_1 replaced by n':

$$n_e = \tau\gamma n' \left(1 - e^{-\frac{t}{\tau}}\right). \tag{3a}$$

The value of n' from (8) equals $\frac{\gamma' n_1}{P'}$. Invoking Eq.(11), from the last equation we obtain

$$n_e = \frac{\gamma\gamma' n_1}{P'P}(1 - e^{-Pt}) \tag{14}$$

for values of the relaxation parameter greater than the parameter for the first irradiation. The change in the electron concentration results in a corresponding change in the current. Hence Eqs.(12)-(14) describe the time variation of the current characterized by the curves of Fig.4. The equilibrium electron concentration from Eq.(12) in the limit as $t \to \infty$ equals

$$n_e = \frac{\gamma\gamma' n_1}{P'P}. \tag{15}$$

When in Eq.(9) $\gamma \ll \frac{1}{\tau'}$, we have $P' \approx \frac{1}{\tau'}$. Then in view of (11), instead of Eq.(15), we obtain

$$n_e = \gamma\gamma'\tau\tau' n_1. \tag{16}$$

The equilibrium concentration is proportional to the product $\gamma\gamma'$, i.e., to the square of the irradiation intensity (inasmuch as each factor is proportional to J). This corresponds to the variation of I as a function of J observed for ethylene bromide.

Thus the proposed scheme of electron levels and "couriers" is consistent with the experimental data. Where the investigated liquids are concerned, there is a profound analogy with the behavior of solid semiconductors. The similarities are the following: 1) the relaxation process is described by exponential laws, 2) the photoconductivity maximum lies near the long wavelength absorption limit, 3) one of the necessary conditions for photoconductivity is a certain value of the dielectric constant[5], 4) the variations of the photocurrent with the field strength and illumination intensity, as a rule, are linear, and 5) the concentration dependence of the photoconductivity of binary systems has a maximum.

In contrast to solid semiconductors, however, liquids are characterized by a positive temperature coefficient of photoconductivity.[5] The similarity of the properties of different substances in the condensed state (i.e., semiconductors, dielectrics and liquids) is evinced in the properties that are determined by the charge carrier concentration, which, in turn, is determined by the short-range order. Differences between the properties become apparent where the decisive factor is the charge carrier mobility, which depends on the long-range order.

References

1. A.F.Ioffe, Fizika poluprovodnikov (Physics of Semiconductors), M., 1957.
2. A.R.Regel', Thesis, Leningrad, 1956.
3. F.I.Kolomoitsev, Thesis, Moscow, 1952.
4. Yu.A.Kopylov, Trudy (Proceedings), Dnepropetrovsk Eng.-Const.Institute, Department of Physics, Dnepropetrovsk, 1957.
5. V.G.Bobyl', Ibid.

DISCUSSION

I.G.Vorozhtsova: In connection with the report of Bogoroditskii, Volokobinskii & Fridberg* which explains some of the divergence between experiment and theory as regards the temperature dependence of the number of relaxators in dielectrics, I would like to say a few words about certain other deviations of the experimental data from theory, known for crystal hydrates. Thus, for example, mica is known to have two temperature maxima of tan δ. According to theory, the low temperature tan δ maximum is shifted with increasing frequency to the side of higher temperatures, while the high temperature maximum is shifted in the opposite direction. This unusual regularity for the dielectric loss in mica was observed by Izergin[1] and Van Keymeulen[2].

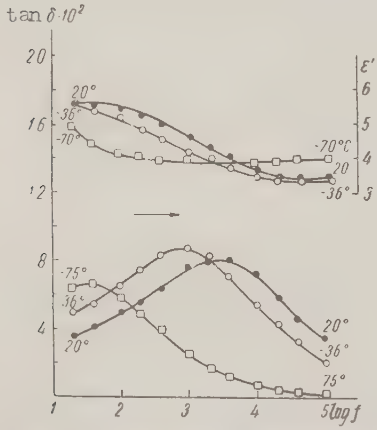

Fig.1. Frequency dependences of tan δ and ϵ' for muscovite at low temperatures.

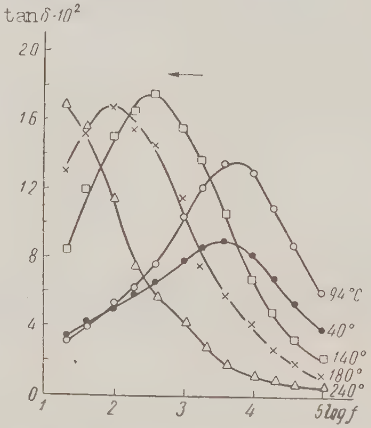

Fig.2. Frequency dependences of tan δ at high temperatures.

I obtained similar results for muscovite preheated at 600° at atmospheric pressure (Figs.1 & 2). I believe that this unusual behavior of the high temperature maximum of the loss in mica may be connected not with increase in the number of relaxators with increasing temperature as suggested by Bogoroditskii et al, but on the contrary, with decrease in the number of relaxators (mica is characterized by reversible desorption in the temperature range of the high temperature tan δ maximum.[3])

One can judge of the variation in the number of relaxators with temperature in muscovite from Figs.3 & 4; it will be apparent that in the case of the low temperature tan δ maximum the angle α characterizing the "set" of relaxation times does not change with increase of temperature, while in the case of the high temperature tan δ maximum α decreases. According to the mechanism for dielectric loss in crystal hydrates proposed by Lyast[4], there occurs a shift of the tan δ maximum to the side opposite to that required by theory if the number of relaxators in the dielectric decreases.

---

*This report by N.P.Bogoroditskii, Yu.M.Volokobinskii & I.D.Fridberg was published in Doklady AN SSSR, 120, 487 (1958). (Trans.Soviet Physics - Doklady.)

Thus if we invoke this mechanism and accept the idea that the dielectric loss in mica is connected with orientation of the water molecules, the disparity between experiment and theory becomes understandable.

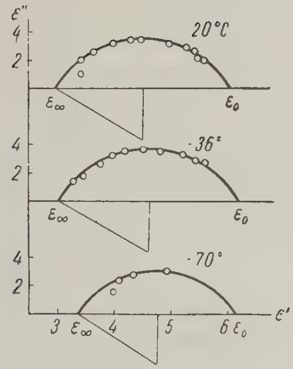

Fig.3. Variation of ϵ'' with ϵ' at low temperature.

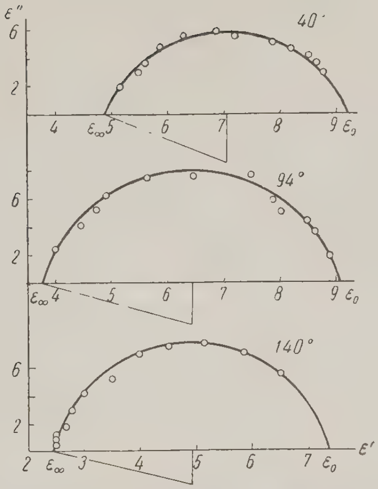

Fig.4. Variation of ϵ'' with ϵ' at high temperatures.

G.I.Skanavi: The variation in the number of relaxators with temperature must naturally affect the shape of the dielectric loss vs temperature curves. It must be recalled, however, that at present one cannot regard Debye's simple formulas for the relaxation losses in solid dielectrics as satisfactory. These formulas fail to take into account the dipole or quasi-dipole distribution function and, what is particularly important, the dipole-dipole interaction.

The variation in the number of relaxators is taken into account more consistently in the work of Lyast, pertaining to the dielectric loss in crystal hydrates. A new experimental substantiation of Lyast's calculations will be found in the work of Vorozhtsova, briefly mentioned at this conference.

Ya.N.Pershits: Kalabukhov in his results on the question of the mechanism of luminescence measured the variation of current with temperature in additively colored KCl crystals. It is apparent from the curve shown by Kalabukhov that at a temperature of the order of 100° the electronic conductivity greatly exceeds the ionic conductivity. At the same time it is known that in KCl crystals containing F-centers, at higher temperatures (500°) electronic conductivity is not more than two times greater than the ionic conductivity.

For a comparison of the electronic conductivity with the ionic, particularly in the case of different samples, one must use crystals that have been subjected to the same number of coloring cycles.[5] Often there is no increase in current as a result of the first coloring, i.e., the electronic current is masked by the influence of the electronic conductivity on the ionic. The ionic conductivity of a bleached crystal proves to be lower than that of the control sample. It should be noted that changes in the conductivity as a result of coloring and bleaching are not accompanied by changes in the activation energy, in any case, in the structure-sensitive region, i.e., in the temperature range below the point of the break in the conductivity vs temperature curve.

Crystals containing F-centers, in the absence of illumination, may be regarded as semiconductors only at relatively high temperatures, when the value of kT is sufficiently high to raise electrons from the local "trapping" levels into the conduction band. Special experiments show that at lower temperatures (220-300°) the conductivity of colored crystals is even lower than that of crystals not subjected to coloring. Thus we see that there is a significant difference between the results obtained by Kalabukhov at the temperatures employed in his experiments and the results that are obtained in investigating the conductivity of colored crystals containing F-centers.

N.P.Kalabukhov: I have been asked to describe the technique employed in measuring currents in the crystals. All the measurements were carried out in vacuum with a guard ring so that surface conductance was precluded. As for the dark electronic conduction in colored KCl crystals, the situation is the following: in such crystals dark electronic conductivity is observed only when there are present in these crystals additional absorption bands in the long wavelength region of the spectrum, i.e., so-called R and R' bands.

In the case of x-irradiated KCl crystals dark electronic currents are observed only after preliminary illumination of the crystals by light in the F band. As a result of this illumination, there form R, R' and M absorption bands. Additively colored KCl crystals always have dark conductivity inasmuch as it is difficult to eliminate the R, R' and M bands from such crystals. If, however, one succeeds in doing this, the dark conductivity vanishes. The conductivity appears in such crystals only after irradiation with x-rays. In irradiated crystals there appear ionic vacancies of both polarities, and as a result of this there form complex centers yielding absorption bands in the long wavelength part of the spectrum.

V.G.Pisarenko: I am engaged in investigation of the spectral distribution of photoconductivity in KBr as a function of the preliminary treatment. Specifically, in our work we are comparing the absorption spectra of KBr single crystals subjected to the following treatments: 1) colored by the Artsybyshev technique, 2) colored by electrolysis with flat aluminum electrodes, 3) x-irradiated, and 4) brought to the so-called "altered" state.[6] The absorption spectra of the samples are being measured on an SF-4 spectrometer by the usual procedure.

The spectral distribution of the photoconductivity was measured in the following manner. The crystal was illuminated at right angles to the field by a monochromatic light beam of known energy. The current was measured by a Compton electrometer (sensitivity 10^{-12} amp/mm). Polarization of the samples was precluded.

On the basis of the measured photocurrent, the difference of potentials on the sample and the intensity of the incident light, we calculated the product of the quantum yield by the displacement of the electrons according to the formula

$$i = \eta \omega e V \frac{N}{d^2},$$

where η is the quantum yield of photoelectrons, ω is the displacement of an electron in a 1 v/cm field, V is the difference in potentials applied to the sample, d is the distance between electrodes, and N is the number of photons incident on the sample per second.

The absorption spectra of KBr samples subjected to different treatments are shown in Fig.1. It will be noted that regardless of the treatment, the light absorption in the 2.8 to 3.8 ev region is virtually nil. Moreover, the absorption of samples in the "altered" state is very low over almost the entire spectral range. Fig.1 also shows the qualitative character of the absorption spectra.

The results of investigating the spectral distribution of the photoconductivity are shown in Fig.2 together with data taken from the work of Inchauspé[7] for additively (K vapor) colored samples (according to Inchauspé, the absorption spectrum of these crystals consists of only one F band). From a comparison of the data of Figs.1 and 2 we arrive at the following conclusions:

1. Samples colored by electrolysis and x-irradiation have one photosensitivity band corresponding to the F band.

2. Samples in the "altered" state have the greatest photosensitivity although the absorption in them is negligibly low. The region of photosensitivity extends over almost all the entire investigated spectrum; the photosensitivity maximum in

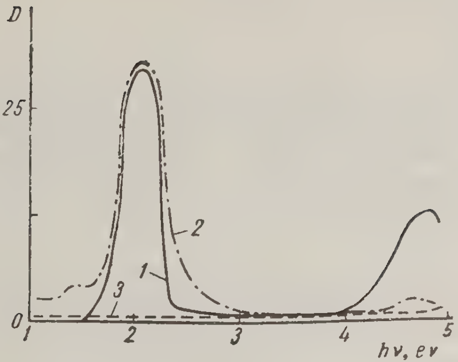

Fig.1

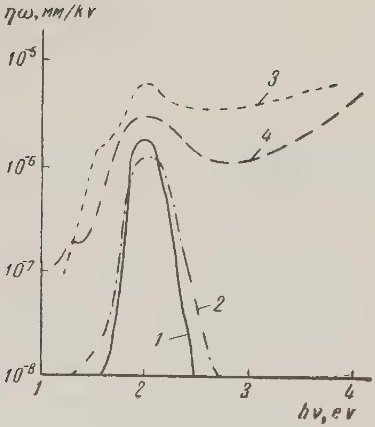

Fig.2

Fig.1. Absorption spectrum of KBr treated in different ways: 1) x-irradiated, 2) colored by electrolysis, 3) brought into the "altered" state.

Fig.2. Spectral distribution of the photoconductivity of KBr treated in different ways: 1) x-irradiated, 2) colored by electrolysis, 3) brought into the "altered" state, 4) colored in potassium vapor[7].

these samples corresponds to the location of the F band.

3. Additively colored samples, according to the data of Inchauspé[7], have a photosensitivity similar to that of samples in the "altered" state.

The above results may be interpreted as follows: the investigated samples have an equilibrium (10^{13} cm^{-3}) concentration of vacancies, which are the primary sticking or recombination centers in KBr; hence the carriers excited by the light will be long range ones: in the 1 to 1.8 ev range the carriers are probably electrons, while in the short wavelength range they are probably holes.

This is also evinced by the distribution of the photoconductivity in additively colored crystals. Shamovskii[8] showed that in the case of vapor coloring the formation of cation vacancies is improbable, and in this case the traps are F-centers, particularly in the range of low temperatures when there form stable F'-centers. Hence we assume that in the case of alteration of state and additive coloring there forms in the crystal a low concentration of centers with an absorption band in the 2.8-3.8 ev region, and that the carriers released by light from these centers are holes, analogous to the case of ionization of V-centers. These holes will be long-range carriers inasmuch as in additively colored samples and particularly in samples in the "altered" state there are very few such centers. This leads to a high photosensitivity of such samples.

References Mentioned in the Discussion

1. A.P.Izergin, Dissertation, Siberian Phys.-Tech.Institute at Tomsk State University, 1954.
2. I.Van Keymeulen, Naturwiss., 44, 326 (1957).
3. M.S.Metsik, Trudy (Proceedings), Siberian Phys.-Tech.Inst., No.35, 60 (1956).
4. I.Ts.Lyast, Zhur.tekh.fiz., 26, 2293 (1956). (Trans.Soviet Physics - Technical Physics.)
5. Ya.N.Pershits & G.D.Tarasenko, Izvestiya vyssh.uchebn.zavedenii. Fizika (Bulletin of the Institutions of Higher Learning, Physics)., No.5, 1958.
6. V.F.Pisarenko, Dokl.AN SSSR, 115,898 (1957). (Trans.Soviet Phys.-Doklady.)
7. N.Inchauspé, Phys.Rev., 106, 898 (1957).
8. L.M.Shamovskii, L.I.Rybakova & M.I.Gosteva, Doklady AN SSSR,91,67 (1953).

PIEZOELECTRIC EFFECT IN ELECTRETS

- A.N.Gubkin & V.S.Sorokin

Introduction

Adams[1] was the first to surmise that the piezoelectric effect should be observed in electrets. Later this question was investigated by Meissner & Beckmann[2] and then Gemant[3]. In 1936 Thiessen, Winkel & Herrman[4] came to the conclusion that the piezoelectric effect in electrets is presumably connected with changes in the shape of the specimen and, consequently, the capacitance of the system comprised by the specimen and the electrodes.

The electrets studied by the above mentioned authors were prepared mainly of carnauba wax. Hence no more than 5 kg/cm^2 pressure could be applied to the electrets, inasmuch as the specimens cracked under higher pressures. In view of this the observed effect could not be large and frequently barely equalled the sensitivity of the electrometer[3].

The fact that there are now available ceramic electrets[5] makes it possible to investigate this problem without serious restriction as to pressure inasmuch as ceramic specimens are capable of withstanding much higher loads. Moreover, ceramic electrets have a number of properties which distinguish them from carnauba wax electrets[5-6]. In particular, they have a higher value of the polarization semiconstant (see table below). If the polarization semiconstant is susceptible of change with change in mechanical pressure, the electret will be piezoelectric.

The question of the piezoelectric effect in electrets is intimately related with the question of the physical nature of heterocharge of electrets. Hence investigation of the piezoelectric effect in electrets, aside from its intrinsic interest, is also important from the standpoint of understanding in the electret effect in general.

Phenomenological description

Consider the scheme of a shorted electret, i.e., an electret mounted between two metallic electrodes at the same potential (Fig.1). As a rule, such an electret has both surface and volume (space) charges which may be either bound or free. It may be assumed that in ceramic electrets the bound charge is primarily heterocharge, while the free charge is primarily homocharge.

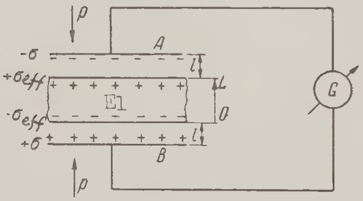

Fig.1. Diagram of electret and electrodes for investigating the piezoelectric effect: El - electret, A & B - electrodes, D - galvanometer.

We introduce the following notation: σ_1^0 and σ_2^0 are the surface charge densities of the electret on its top and bottom faces; these are described by

$$\sigma_1^0 = \sigma_{1f}^0 + \sigma_{1r}^0 \text{ and } \sigma_2^0 = \sigma_{2f}^0 + \sigma_{2r}^0,$$

where σ_{1f}^0 and σ_{2f}^0 are the surface densities of the bound charge and σ_{1r}^0 and σ_{2r}^0 are the surface densities of the free charge, $\rho_r(x)$ is the free charge volume density, $\rho_f(x)$ is the bound charge volume density, and $\rho_f = -\operatorname{div} P$, where P is the polarization semiconstant.

We shall consider the case when $\sigma_1^0 = -\sigma_2^0 = \sigma^0$, $\sigma_{1f}^0 = -\sigma_{2f}^0 = \sigma_f^0$ and $\int_0^L \rho_r(x)\,dx = 0$, i.e., the case when the electret as a whole is neutral.

Let $E(x)$ be the field inside the nonshorted electret, and E the field between the electret surfaces and the metallic electrodes in the case of shorting; then as shown in Ref.6, we can write

$$\sigma = \frac{E}{4\pi} = \frac{\sigma_{cff}}{\left(\frac{2\varepsilon l}{L}+1\right)}, \tag{1}$$

where σ is the surface density of the charge induced on the electrodes, is the dielectric constant of the electret material, and σ_{cff} is the effective surface charge density of the electret equal to[6]

$$\sigma_{cff} = \frac{\varepsilon}{4\pi L}\int\limits_0^L E(x)\,dx = \sigma^0 + \frac{1}{2L}\left\{\int\limits_0^L\left(\int\limits_0^x \rho_r(x)\,dx\right)dx - \int\limits_0^L\left(\int\limits_x^L \rho_r(x)\,dx\right)dx - 2\int\limits_0^L P(x)\,dx + 2PL\right\}. \tag{2}$$

The external manifestation of the piezoeffect in electrets will be the variation of σ as a result of application or removal of a mechanical stress, that is, the characteristic of the piezoeffect will be the quantity $d\sigma/dp$. In the general case, changes in mechanical pressure p may bring about changes in all the quantities entering into Eq.(1), namely σ_{cff}, l, L and ε.

Differentiating Eq.(1) with respect to p and assuming that $\frac{d\varepsilon}{dp} \approx \frac{dN}{dp}$, where N is the number of molecules per cm^3, we obtain,

$$\frac{d\sigma}{dp} = \frac{1}{\left(\frac{2\varepsilon l}{L}+1\right)}\left\{\frac{d\sigma_{eff}}{dp} - \frac{2\sigma_{eff}}{L\left(\frac{2\varepsilon l}{L}+1\right)}\left(\varepsilon\frac{dl}{dp} + \frac{l}{3}\alpha\left[3\varepsilon - 2\gamma(\varepsilon-1)(\varepsilon+2)\right]\right)\right\}; \tag{3}$$

here α is the reciprocal of Young's modulus and γ is Poisson's ratio.

Let us consider two particular cases.

1. $\frac{2\varepsilon l}{L} \ll 1$ Case

It follows from Eq.(1) that

$$\frac{d\sigma}{dp} = \frac{d\sigma_{eff}}{dp}. \tag{4}$$

Thus, in this case the effect is due only to change in the effective surface charge density σ_{eff}. To distinguish it from the effect described below we call this the "true piezoelectric effect" of electrets. In practice this case obtains for electrets having electrodes in intimate contact with the surface of the specimen, for example, in the case of electrodes applied by firing on or vacuum sputtering of silver (silvered specimens).

2. $\frac{d\sigma_{cff}}{dp} = 0$ Case

In this case the effect is connected with the presence of a gap between the surfaces of the electret and the electrodes. In this case we call the effect the "quasipiezoelectric effect". In general, according to Eq.(3), in the case of an electret having conventional laid-on electrodes there may be observed both the quasipiezoelectric effect and the true piezoelectric effect.

Let us consider the true piezoelectric effect in more detail. Let us assume for simplicity of calculation that $\operatorname{div} P = 0$. It is known[4] that the homocharge of electrets is usually located only in the thin surface layers next to the electrodes. Consequently, the variation of ρ with the

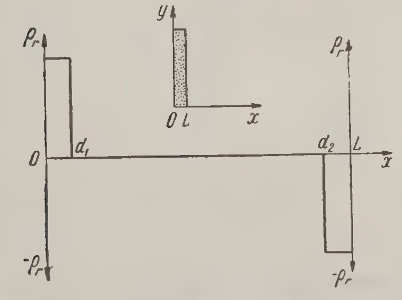

Fig.2. Location of homocharge in electrets: $d_1 = L - d_2$ and $(\rho_r)_0 = -(\rho_r)_L = \rho_r$.

distance x from one of the electret surfaces will have the approximate form shown in Fig.2. Then by means of Eq.(2) we obtain

$$\sigma_{eff}=\sigma^0+\frac{P_r}{L}d_1(L-d_1). \qquad (5)$$

Making the natural assumption that the homocharge may vary upon application of a mechanical load only owing to change in the geometric size of the specimen, from Eqs.(3) and (5) we obtain

$$\frac{d\sigma}{dp}=-2\alpha\gamma\sigma_{eff}-\frac{dP}{dp}. \qquad (6)$$

Let us evaluate the first term in Eq.(6). Inasmuch as $\alpha\approx 10^{-6}$ cm^2/kg (for porcelain, $\sigma_{eff}\approx 10^{-8}$ coulomb/cm^2 (for ceramic electrets) and $\gamma = 0.25$, we obtain $2\alpha\gamma\sigma_{eff}\approx 0.5\cdot 10^{-14}$ coulomb/kg. This is a very small quantity, too small to be measured experimentally by means of a ballistic galvanometer. Consequently, the true piezoelectric effect in electrets is due wholly to changes in the polarization semiconstant (heterocharge) and does not depend on the presence of homocharge.

Now let us consider the quasipiezoelectric effect in electrets. Let us evaluate the product

$$\frac{2\sigma_{eff}}{L\left(\frac{2\varepsilon l}{L}+1\right)^2}\left\{\frac{l}{3}\alpha\left[3\varepsilon-2\gamma(\varepsilon-1)(\varepsilon+2)\right]\right\},$$

taken from Eq.(3). For $l = 10^{-3}$ cm, $\alpha = 10^{-6}$ cm^2/kg, $\varepsilon = 100$, $L = 1$ cm and $\sigma_{eff} = 10^{-8}$ coulomb/cm^2, this product equals 10^{-13} coulomb/kg, i.e., is not sufficiently great to be experimentally measurable even at a maximum pressure of 300 kg/cm^2. Consequently, from Eq.(3) we have

$$\frac{d\sigma}{dp}=-\frac{2\sigma_{eff}}{L\left(\frac{2\varepsilon l}{L}+1\right)^2}\varepsilon\frac{dl}{dp}, \qquad (7)$$

that is, we see that the quasipiezoelectric effect in electrets is due primarily to changes in the electrode-electret gap (l in Fig.1) with variation of the mechanical load. In the case of laid-on electrodes this gap is inevitable; only in the case of ideal smoothness of the specimen and electrode surfaces does $l\to 0$. However, as experiments show, in practice even very careful polishing of the surfaces reduces the magnitude of the quasipiezoelectric effect very little. It will be evident from what has been said above and from the available experimental data that the variation of l under mechanical pressure is highly complex in character.

It follows from Eq.(7) that $d\sigma/dp$ in the case of the quasipiezoelectric effect is proportional to the surface charge density σ_{eff} and the dielectric constant of the material ε. The last will of course be true only when the denominator in Eq.(7) is not strongly dependent on ε.

It follows from Eqs.(3), (6) and (7) that the general formula describing the piezoelectric effect in electrets has the form

$$\frac{d\sigma}{dp}=\frac{1}{\left(\frac{2\varepsilon l}{L}+1\right)}\left\{\frac{dP}{dp}-\frac{2\sigma_{eff}}{L\left(\frac{2\varepsilon l}{L}+1\right)}\varepsilon\frac{dl}{dp}\right\}. \qquad (8)$$

Experimental Results

The piezoelectric effect was investigated experimentally in electrets made of titanates of Group II elements.[5] The investigated electrets are listed in the accompanying table together with the values of the polarization semiconstant P obtaining for these electrets under the indicated polarization conditions.

Characteristics of the investigated electrets

Electret material	ε	$P \cdot 10^8$, coul/cm^2			$\delta \cdot 10^{11}$ coul/kg
		20 kv/cm 20°	2 kv/cm 200°	20 kv/cm 200°	
I	II	III	IV	V	VI
$MgTiO_3$	15	<1	13	380	—***
$ZnTiO_3$	22	<1	—**	140	—***
$BaO \cdot 4TiO_2$	28	<1	—**	—**	—***
$Bi_2O_3 \cdot 2TiO_2$	80	14	—**	870	—***
$CaTiO_3$	150	10	93	690	—***
$SrTiO_3$	175	23	67	610	—***
CBT*	750	71	38	240	1.5
$BaTiO_3$	1200	100	—**	—**	60

*SBT = $SrTiO_3$–$Bi_2O_3 \cdot 2TiO_2$ or $SrTiO_3$–$Bi_2O_3 \cdot 3TiO_2$ solid solution. **No data obtained to date. *** Piezoeffect not detected.

The values in column III of the table correspond to polarization of the specimens in a 20 kv/cm field at room temperature for 6 hours; the values in columns IV and V are for the following polarization regimes: the specimens were heated to 200° in zero field, then the field was switched on, the specimens were held in it for 2 hours at 200°, during the next 4 hours the temperature was gradually reduced to 30°, after which the field was switched off. The field intensity was 2 kv/cm and 20 kv/cm, respectively. The magnitude of the polarization semiconstant was determined by the method of depolarization of the electrets.[7]

The electrets were polarized with heating to 200°. The polarization field was 5 kv/cm for the SBT (see under table) electrets and 10 kv/cm for the others. By way of exception some of the specimens were polarized at room temperature; this polarizing procedure is referred to as "cold polarization".

The piezoelectric effect was investigated by the static procedure. Compressive stresses of up to 300 kg/cm^2 were applied to the specimens (diameter from 30 to 60 mm, thickness 5 mm) in a lever press. The charge was measured by a ballistic galvanometer. All the measurements were carried out on two different lots of specimens, one of which had electrodes applied by vacuum evaporation of silver (silvered specimens) and the other had ordinary laid-on electrodes.

Silvered specimens

The experiments with the silver-electrode specimens showed that in all the investigated electrets except those of SBT (strontium-bismuth titanate) no detectable current is observed in the external circuit with change in load. On the other hand, electrets of SBT exhibit a proportional variation of the charge Q with the applied pressure p. The values of the piezoelectric coefficient differ somewhat for electrets prepared of different batches. On the average the piezoelectric coefficient δ equals $1.5 \cdot 10^{-11}$ coulomb/kg. No noticeable change in δ was observed over the period of a year. The piezoelectric coefficient of electrets prepared by a cold polarization is approximately one tenth the above value.

The experimental results for the SBT specimens are shown

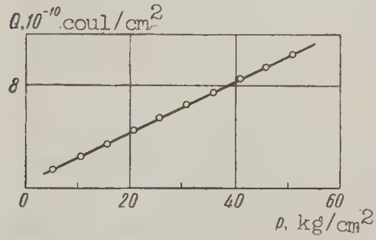

Fig.3. Variation of the charge developing under pressure with the pressure for SBT electrets (silvered specimens). Pressure range 0 to 60 kg/cm^2.

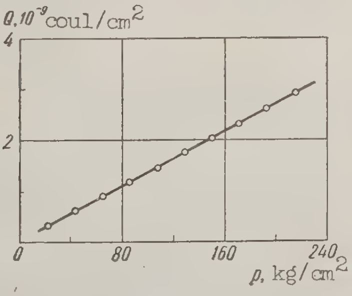

Fig.4. Same as Fig. 3 but for the pressure range from 0 to 240 kg/cm^2.

in Figs.3 & 4. The values of Q obtained in loading and unloading are equal in magnitude but opposite in sign. For purposes of comparison, similar experiments were carried out with polarized specimens of $BaTiO_3$, which were also electrets[5]. In the case of polarization in a 5 kv/cm field, the piezoelectric coefficient of $BaTiO_3$ equals $6 \cdot 10^{-10}$ coulomb/kg for cold and hot polarization (see table).

It may be stated therefore that both SBT and $BaTiO_3$ electrets exhibit the true piezoelectric effect associated with changes in the polarization semiconstant.

Specimens with laid-on electrodes

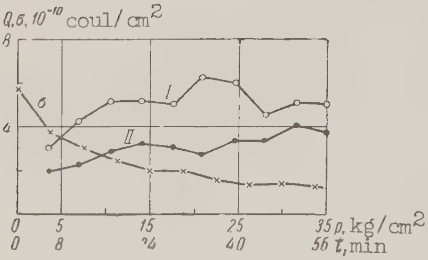

Fig.5. Variation of the charge Q with the pressure for electrets of SBT (laid-on electrodes): I - loading, II - unloading. σ - variation of σ_{eff} during the period of the experiment.

In the case of SBT electrets with laid-on electrodes there is observed a very complex pressure dependence of Q. Fig.5 gives the absolute values of Q (the polarities are opposite in loading and unloading) and the variation of σ_{eff} during the period of the experiments. It is known[5] that σ_{eff} of electrets changes if it is measured by the method of electrostatic induction a large number of times in succession. This was observed in our case. However, the decrease of σ_{eff} here is greater than usual, which is apparently connected with the influence of the mechanical loads. It will be evident that the results shown in Fig.5 are in qualitative agreement with Eq.(8). A similar picture is obtained for $BaTiO_3$ electrets.

For all the other investigated electrets we observed the quasipiezoelectric effect, the magnitude of which was proportional to σ_{eff} and ε of the material, as follows from the calculations (Eq.(7)). By way of illustration, in Figs.6 & 7 we give the experimental data for electrets of $CaTiO_3$ and $SrTiO_3$. In addition to the variation of the charge with mechanical load and time, these figures give the variation of the surface charge density of the investigated electret (σ_{eff}) and of a control specimen (σ_c) during the period of the experiment. The surface charge density of the control specimens was measured simultaneously with σ_{eff} of the test specimens by the method of electrostatic induction; the control specimens were not subject to pressure. For the other electrets the quasipiezoelectric effect was weaker, in accord with their smaller dielectric constant.

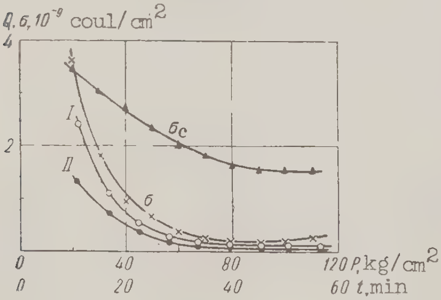

←Fig.6. Variation of the charge with the pressure for $CaTiO_3$ electrets (laid-on electrodes): I - loading, II - unloading. σ - variation of σ_{eff}; σ_c - variation of the surface charge density of the non-loaded control specimen during the period of the experiment.

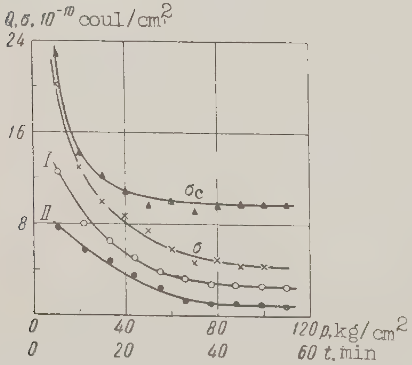

←Fig.7. Same as Fig.6 but for $SrTiO_3$ electrets.

It will be evident from Figs.6 and 7 that whereas during the first application of the load the quasipiezoelectric effect is appreciable ($d\sigma/dp \approx 10^{-11}$ coulomb/kg), it then falls off sharply and that the decrease follows the decrease of σ_{eff}. Our experiments showed that when the electret is acted on by a mechanical load of the same magnitude more than 10 times in succession, the decrease of σ_{eff} is slowed down and, accordingly, the magnitude of the quasipiezoelectric effect becomes more stable.

Assuming purely formally that $\frac{dl}{dp} = -\alpha' l$, where $E' = 1/\alpha'$ is an "effective" Young's modulus characterizing the variation of the gap l, we can from Eq.(7) calculate E'. For electrets of $CaTiO_3$, $E' \approx 10$ kg/cm^2; E' is also the same order of magnitude for the other electrets.

Conclusions

At present it is still difficult to say anything definite regarding the physical nature of the polarization semiconstant detected by us in titanates of Group II elements (see table). If, however, we assume that all the investigated titanates have spontaneous polarization with a coercive force that decreases with increase of the dielectric constant, many of the properties of these dielectrics can be explained. Thus, for example, in this case one can readily understand the existence of an appreciable polarization semiconstant and a large dielectric constant in the investigated dielectrics and also the presence of the piezoelectric effect in SBT (strontium-bismuth titanates).

According to this hypothesis, the coercive force in $BaTiO_3$ is minimal, hence even at room temperature this ceramic exhibits the nonlinearity of ε and hysteresis loops typical of ferroelectrics. Dielectrics with smaller ε must, we believe, manifest their ferroelectric properties at higher temperatures. In connection with this they cannot be polarized at room temperature (see table). In view of this hypothesis, the physical nature of heterocharges in the investigated inorganic electrets becomes clearer: it would appear that heterocharges form owing to spontaneous polarization.

In conclusion, it must be noted that the conductivity of the new piezoelectric material SBT is 2-4 orders of magnitude lower than the conductivity of barium titanate. Hence in a number of cases of practical application it may be advantageous to use SBT as a piezoelectric material in preference to barium titanate despite the fact that the piezoelectric coefficient of SBT is only a fraction of that of $BaTiO_3$ (see table).

We desire to thank G.I.Skanavi for valuable discussions.

"P.N.Lebedev" Physical Institute
Academy of Sciences of the USSR

References

1. E.P.Adams, J.Franklin Inst., 204, 469 (1927).
2. A.Meissner & R.Beckmann, Z.Techn.Phys., 9, 430 (1928).
3. A.Gemant, Phil.Mag., 20, 929 (1955).
4. P.Thiessen, A.Winkel & K.Herrman, Phys.Z., 37, 511 (1936).
5. A.N.Gubkin & G.I.Skanavi, Zhur.eksp.i teor.fiz., 32, 140 (1957). (Trans. Soviet Physics - JETP.); Izv.AN SSSR, Ser.fiz., 22,330 (1958). (Trans.Bull.22, 327.)
6. A.N.Gubkin, Zhur.tekh.fiz., 27, 1955 (1957). (Trans.Sov.Phys.-Techn.Physics.)
7. A.N.Gubkin, V.S.Mitronina, V.F.Sergienko & M.I.Subbotin, PTE, No.4, 113 (1959). (Trans.Instruments and Experimental Techniques.)

EFFECT OF SLOW-NEUTRON IRRADIATION ON THE DIELECTRIC PROPERTIES OF POLYCRYSTALLINE TITANATES

- L.K.Vodop'yanov & G.I.Skanavi

It has been shown in a number of papers published in recent years that the presence of defects in dielectrics affects their dielectric properties. For example, with a high concentration of vacant sites in the cationic part of a perovskite lattice there appears, as has been shown in Ref.1 & 2, a pronounced relaxation polarization due to extremely high permittivity and enhanced losses. In the studies referred to, the defects (cationic vacancies) were produced by preparing solid solutions in which part of the divalent strontium cations was replaced by trivalent bismuth ions, which have the same radius.

In connection with these results it occurred to us that one might obtain relaxation polarization in ionic structures by producing a sufficiently high concentration of defects by some physical procedure, for example, by bombardment with heavy particles.

Consequently, we undertook an investigation of the dielectric properties of a number of titanates before and after irradiation with slow neutrons in a pile. The fact that titanium nuclei are present in all titanates gave reason to hope that there would form a high concentration of defects in the crystals, inasmuch as the slow-neutron capture cross section for titanium is relatively large (5.6 barns). Actually, we did observe an appreciable change in the dielectric properties of the investigated titanates as a result of neutron irradiation.

The titanate samples were inserted into special research channels located close to the thermal column of the reactor. We used both dry channels and channels filled with water which cooled the samples. The average temperature in the channels was maintained in the range between 70 and 80°; however, the temperature of the samples themselves could be appreciably higher owing to heating by the nuclear reactions occurring in the sample material. The neutron energy distribution in a pile is characterized by a gaussian curve with a maximum at 0.025 ev. Thus it could be assumed that most of the neutrons are thermal.

We felt it essential first to determine what type of radiation is responsible for the observed effect inasmuch as in addition to slow neutrons there are present in the reactor fast neutrons (tail of the distribution curve), fission fragments, β-particles and γ-rays. As regards the fission fragments, it could be assumed that they did not even enter the investigated samples, inasmuch as in view of their large mass and charge (i.e., strong interaction with matter) their range is short (a few microns) and they are all stopped in the nuclear fuel. Low and medium energy β-radiation can also play no significant role in view of its low penetrating power.

By special experiments we established that the hard β-components, penetrating γ-rays and fast neutrons also play no significant role. To this end we wrapped the samples in cadmium foil, which absorbs slow neutrons but freely passes fast neutrons and penetrating β- and γ-radiation. Inasmuch as when cadmium foil was used the effect in question was not observed, we could safely assume that primarily slow neutrons are responsible for the observed effect.

The energy of a thermal neutron is too low for the formation of defects by direct neutron scattering from the nuclei, hence the defects can form only as a result of nuclear reactions. The only possible reaction with thermal neutrons is a reaction of the (n,γ) type. This reaction can occur on all the elements forming the investigated compounds. In the case of titanium the (n,γ) reaction with the formation of an unstable nucleus occurs on the isotope Ti^{50} and is characterized by the following formulas:

$$\text{I} \quad {}_{22}\text{Ti}^{50} + {}_{0}n^{1} \rightarrow {}_{22}\text{Ti}^{51} + \gamma$$

$$\text{II} \quad {}_{22}\text{Ti}^{51} \xrightarrow{(72\ \text{d}\ )} {}_{23}V^{51} + {}^{-}\beta\,(0.45\ \text{Mev}) + \gamma\,(1\ \text{Mev})$$

$$\Big| \xrightarrow{(3\,\text{min})} {}_{23}\text{V}^{51} + {}^{-}\beta\,(1.6\ \text{Mev}).$$

The gamma-spectrum in the first stage of the reaction incident to disintegration of the compound nucleus has been determined by Groshev et al[3]. This spectrum contains γ-rays of energies 1.39, 1.6, 4.8, 6.42 and 9.17 Mev. Knowing the γ-ray energy and invoking the law of conservation of momentum, we can determine the nuclear recoil energy. The recoil energy of the Ti nucleus in the case of emission of the lowest energy (1.39 Mev) gammas is ~30 ev.

On the other hand, the energy necessary for knocking out an atom from the crystal lattice, according to the evaluations of Seitz, is of the order of 25 ev. Thus the energies of the γ-rays emitted by the Ti nucleus are sufficiently high for formation of Frenkel defects. Similarly, knowing the β-particle energy, one can determine the recoil energy of the nucleus, which in this case also proves to be sufficiently high for formation of defects.

In accord with the above reaction, the formation of defects occurs in two stages, distinctly separated in time. The first stage of defect formation - disintegration of the compound nucleus with emission of γ-rays - occurs only during the irradiation in the reactor and ceases the instant the sample is withdrawn from the active zone. The second stage - decay of the unstable isotope with emission of β-particles and γ-rays - can occur both during irradiation and after withdrawal of the samples from the pile. The duration of the second stage of defect formation will be the longer, the longer the lifetime of the given element.

It must be noted that concurrently with formation of the defects there occurs annealing (healing) of the samples, a process which depends substantially on the sample temperature: the higher the temperature, the greater the defect mobility and the more probable their recombination.

We investigated the effect of irradiation on magnesium, zinc, calcium, strontium, bismuth and barium titanates and strontium-bismuth titanate. The polycrystalline samples were prepared in the form of 12 mm diameter disks, 0.5, 0.8 and 1 mm thick. By way of electrodes we used chemically pure aluminum which was applied by vacuum sputtering. Aluminum was chosen because it does not undergo any significant changes in a pile. After irradiation in the pile, the samples exhibited induced β- and γ-activity ranging from tens to hundreds of millicuries, depending on the integral radiation dose and the material.

We carried out a series of irradiations of the titanate samples at integral fluxes of 10^{17}, 10^{18} and 10^{19} n/cm^2. With an integral flux of 10^{18} n/cm^2 and higher we observed a strong increase of the dielectric loss angle for all the titanates (see table). We also found that in the case of irradiation of the sample in the water filled channel the effect is much stronger: this can be explained by the less intense anneal-healing of the defects as a result of cooling.

As for the dielectric constant, it increases noticeably as a result of irradiation only for zinc and magnesium titanates. For these materials we determined the frequency dependences of ϵ and tan δ at room temperature; the results are shown in Figs.1 & 2. Fig.3 shows the frequency dependences of ϵ and tan δ in the range of audio frequencies for zinc titanate samples irradiated with different slow-neutron fluxes.

Owing to heating of the samples in the pile there occur in them irreversible processes connected with annealing of the defects, as a result of which the actual change in the temperature dependences of ϵ and tan δ due to irradiation per se cannot be determined. Measurements of ϵ and tan δ of the investigated titanates were carried out both a few hours after irradiation (see Figs.1-3) and after the passage of an appreciable period (up to two years). It was found that the net change in properties produced by irradiation slowly decreases but does not wholly disappear even after the passage of 2 years. Heating of the samples to 300° followed by slow cooling eliminates the radiation induced changes in properties. This substantiates our inference that the change in dielectric properties is connected with the formation of defects.

Titanate	tan δ			
	Before irradiation	After irradiation		
		in dry channel 10^{18} n/cm^2	in water filled channel, 10^{18} n/cm^2	in dry channel 10^{19} n/cm^2
Bi	0.0013	0.034	0.06	----
Ca	0.0017	0.0028	0.10	0.30
Sr	0.002	0.0085	0.027	----
Ba	0.011	0.02	---	0.12
Sr-Bi	0.003	0.0076	---	0.08

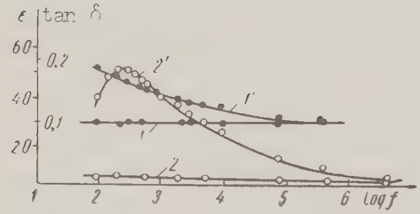

Fig.1. Frequency dependences of ϵ and tan δ of zinc titanate at room temperature before and after irradiation with an integral flux of 10^{18} n/cm^2 in the water filled channel. 1 & 2 - variation of ϵ and tan δ before irradiation; 1' & 2' - after irradiation.

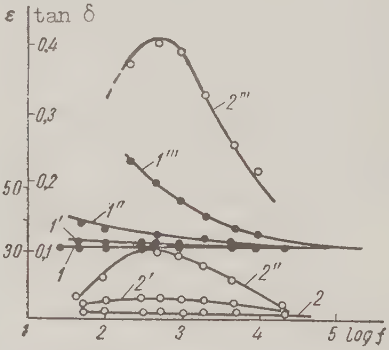

Fig.3. Frequency dependences of ϵ and tan δ of zinc titanate at room temperature after different doses of radiation in the dry channel. 1 & 2 - variation of ϵ and tan δ before irradiation, 1' & 2' - after irradiation with an integral flux of 10^{17} n/cm^2, 1'' & 2' - 10^{18} n/cm^2 flux, 1''' & 2''' - 10^{19} n/cm^2 flux.

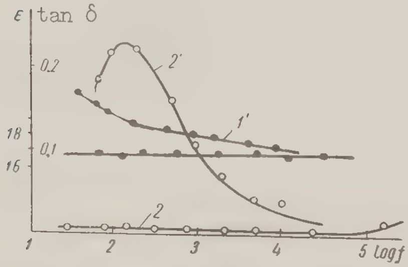

Fig.2. Same as Fig.1 but for magnesium titanate.

It follows from the character of the frequency dependences of ϵ and tan δ of magnesium and zinc titanates that the irradiation induced polarization is relaxational: tan δ has a pronounced frequency maximum, while the dielectric constant consistently decreases with increasing frequency.

It might be thought that neutron irradiation also results in an increase of the electric conductivity, which for titanates is primarily of the n-type. However, the increase of the dielectric loss cannot be explained only by increase of the conductivity, inasmuch as in this case tan δ should monotonically decrease with frequency with the dielectric constant remaining at the same value.

From the conditions of maximum loss $\omega\theta = 1$ (θ is the relaxation time and ω is the frequency corresponding to the maximum loss) one can evaluate the activation energy of the relaxing groups by means of the formula

$$U = kT(\ln\nu - \ln\omega),$$

where ν is the frequency of the natural oscillations of the relaxing groups. For $\nu = 10^{12}$ sec^{-1}, the energy $U = 0.5$ ev; for $\nu = 10^{13}$ sec^{-1}, the energy $U = 0.6$ ev. The fact that the observed change of ϵ and tan δ is very large indicates the presence of a very high concentration of defects.

Thus we have shown that by irradiation of ionic polycrystalline materials with a heavy flux of slow neutrons one can produce a high concentration of Frenkel defects; particularly if the material comprises elements with a large cross section for slow neutron capture. The formation of defects leads to the appearance of relaxation polarization, which is responsible for increase of the dielectric loss and also of the dielectric constant in cases when the dielectric constant before irradiation is not excessively high (specifically, in the cases of magnesium and zinc titanates).

We desire to thank F.L.Shapiro for helpful discussions.

"P.N.Lebedev" Physical Institute,
Academy of Sciences of the USSR

References

1. G.I.Skanavi & E.N.Matveeva, Zhur.eksp.i teor.fiz., 30, 1049 (1956). (Trans.Soviet Physics - JETP.)

2. G.I.Skanavi, Ya.M.Ksendzov, V.A.Trigubenko & V.V.Prokhvatilov, Ibid., 33, 320 (1957). (Trans.Ibid.)

3. L.V.Groshev, B.P.Ad'yasevich & A.M.Demidov, Report at the First International Conference on the Peaceful Uses of Atomic Energy, Geneva, 1955; B.D.Ad'yasevich, L.V.Groshev & A.M.Demidov, Atomnaya energiya No.2, 40 (1956). (Trans. Soviet Journal of Atomic Energy.)

Bulletin of the Academy of Sciences of the USSR - Physical Series
Vol. 24, No.2 - February 1960

Transactions of the Second All-Union Conference on the Physics of Dielectrics

TABLE OF CONTENTS

	Page Orig.	Page Trans.
Investigation of relaxation polarization and the phase composition of dielectrics in the system $SrTiO_3$—$Bi_2O_3 \cdot nTiO_2 (n = 2,3)$ - A.M.Kashtanova, N.N.Kurtseva & G.I.Skanavi	114	109
On the relaxation time and distribution function of quasidipoles in ionic crystals with a defect structure - G.I.Skanavi	124	117
Relaxation polarization of the $SrTiO_3 \cdot nMnO$ system - E.V.Sinyakov & A.M.Solok	132	125
Correlation between the dielectric loss and the structure of ionic crystals - N.P.Bogoroditskii, B.A.Kulik & I.D.Fridberg	137	130
Investigation of high-frequency dielectric loss in solid dielectrics - K.A.Vodop'yanov & G.I.Galibina	142	134
Thermal expansion, dielectric constant and loss of alkali halide crystals - V.V.Panchenko	150	141
Relaxation polarization and losses in alkali halide single crystals - V.N.Lozovskii	161	151
On the relaxation polarization of crystals with the structure of rutile and perovskite - I.Ts.Lyast	170	160
Application of the theory of vibrations of a crystal lattice with deformable ions to treatment of the physical properties of binary cubic crystals - K.B.Tolpygo	177	167
Contribution to the theory of the permittivity of an anisotropic medium polarized at a finite rate - R.A.Suris & B.N.Finkel'shtein	189	178
Towards a theory of incompletely polar crystals - K.B.Tolpygo	192	182
On the kinetics of ion conductivity and electric polarization in condensed substances - Yu.L.Khait	202	191
Possibility of thermal polarization of electrons in zinc sulfide crystal phosphors - F.I.Vergunas & P.E.Ramazanov	214	203
Absorption spectra of defects in ionic lattices - O.Stasiw	220	209
Dielectric and optical properties of some zinc sulfides - E.V.Stauer & V.P.Izotov	224	213
On the nature of stimulated luminescence in KCl crystals - N.P.Kalabukhov	229	217
Influence of the electric field strength on the photoconductivity of liquid organic systems - P.K.Mitskevich & V.G.Bobyl'	232	219
Investigation of the photoconductivity of ether solutions - Yu.A.Kopylov	237	223
Piezoelectric effect in electrets - A.N.Gubkin & V.S.Sorokin	246	232
Effect of slow-neutron irradiation on the dielectric properties of polycrystalline titanates - L.K.Vodop'yanov & G.I.Skanavi	253	238

Translated in 1961 by
Columbia Technical Translations
5 Vermont Ave., White Plains, N.Y.

Number 3 Volume 24 1960

BULLETIN

of the

ACADEMY OF SCIENCES OF THE USSR

— PHYSICAL SERIES —

(Izvestiya Akademii Nauk SSSR)
(Seriya fizicheskaya)

Reproduction rights reserved
by
Columbia Technical Translations
5 Vermont Avenue
White Plains, New York

Single Issues
$20

Annual Subscription
$215

Transactions
# of the
Tenth All-Union Conference on Nuclear Spectroscopy

(Moscow, 19–27 January 1960)

Lithoprinted in U.S.A.
EDWARDS BROTHERS, INC.
Ann Arbor, Michigan

ALPHA-RADIATION FROM U^{233}

- B.S.Dzhelepov, R.B.Ivanov, V.G.Nedovesov & Yu.T.Puzynovich

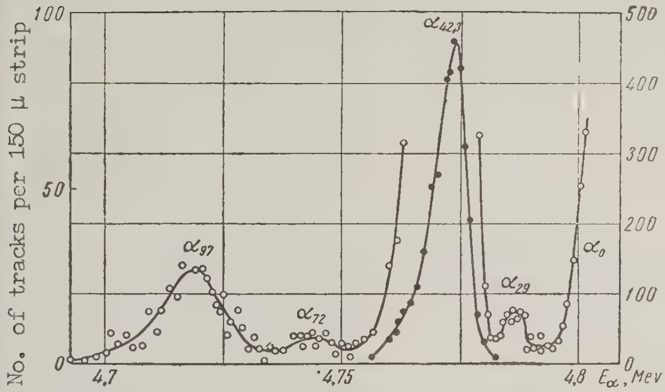

Fig.1. 4.7 to 4.8 Mev section of the α-spectrum of U^{233} (series I). The scale on the right is for the $\alpha_{42.3}$ line.

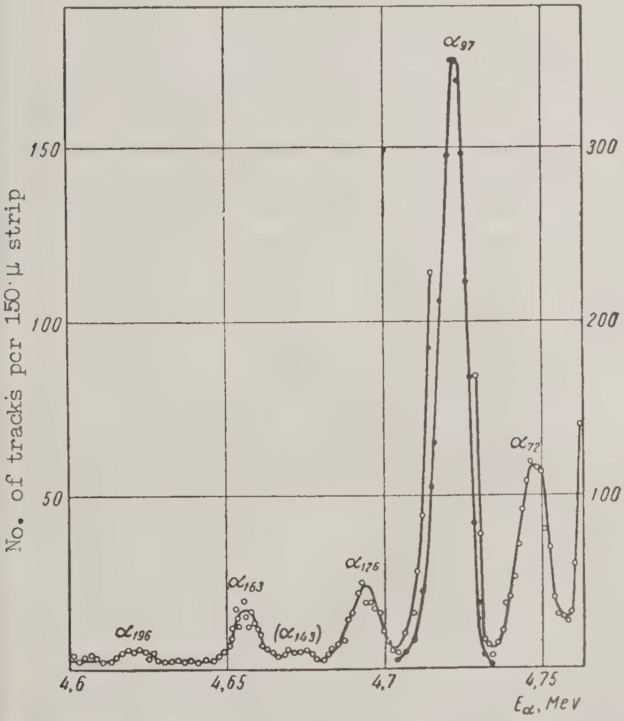

Fig.2. 4.6 to 4.75 Mev section of the U^{233} spectrum (series V). The scale at the right is for the α_{97} line.

In the present work we continued our earlier investigation[2] of the α-spectrum of U^{233} on the magnetic α-spectrometer described in Ref.1. In all we carried out six series of measurements with exposure times of 46, 80, 50, 80, 120 and 90 hours. For the measurements we used two U^{233} sources prepared by vacuum evaporation. In the first three series of measurements the line half-width was 8 kev (source dimensions - 0.5 x 10 mm). In using the second source under the same conditions the half-width increased to 10 kev, and the counting rate at the line peak increased by a factor of 2.5. The fifth and sixth measurement series were carried out under new operating conditions of the spectrometer: the photographic plate was located along the focal surface of the instrument (at an angle of 40° to the spectrometer radius). As a result the extent of the spectral region simultaneously recorded by the plate was increased from 130 to 400 kev. The sixth series of measurements was carried out with a 3 x 15 mm source; the line half-width in this case was 22 kev. The transmission factor of the instrument was 0.21% of 4π in all cases.

The sections of the U^{233} α-spectrum recorded in the first, fifth and sixth measurement series are shown in Figs.1,2 & 3. In addition to the already known α-transitions - α_0, α_1, α_2, α_3, α_4, (α_5), α_6 and (α_7) (see Ref.2) - we observed lines corresponding to transitions to levels with energies 29, 72, 126 and 195 kev in the daughter nucleus Th^{229}. Furthermore, we noted a slight rise above the background in the α-particle energy region corresponding to a transition to a level at 145 kev.

The results, namely, the Th^{229} level energies, the α-transition intensities, the assignments for these levels and the values of the inhibition factor F for the α-transitions, are listed in the accompanying table.

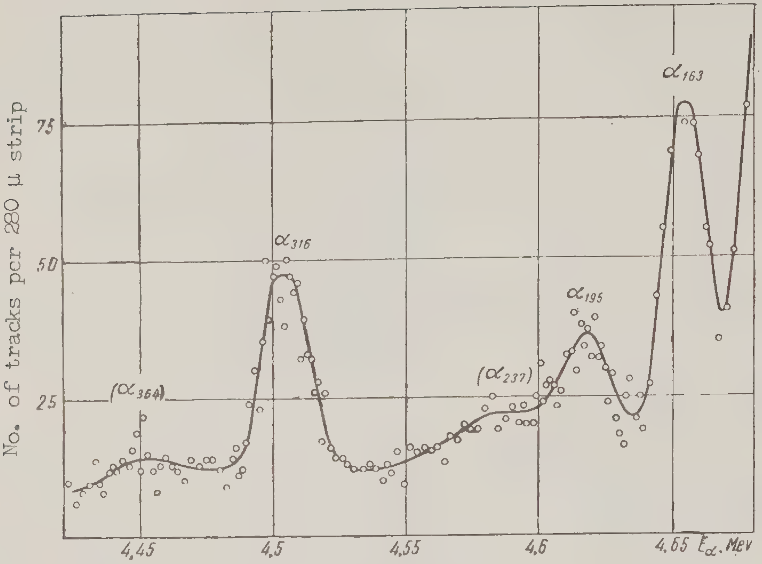

Fig.3. 4.4 to 4.7 Mev section of the U^{233} spectrum (series VI)

The 29, 72, 126 and 195 kev levels may be assumed to form a rotational band with quantum number K = 5/2, based on the 29 kev level. The experimental excitation energy ratios for this band are 1:2.26:3.87, while the theoretical ratios for the given spin are 1:2.28::3.86. It is interesting to note that for this band the moment of inertia J of the nucleus is equal to the moment of inertia of the ground state rotational band (K = 5/2+).

From analysis of the Nilsson[3] level scheme for deformed odd nuclei it follows that in the region of weak excitations there can be only one single-particle level in Th^{229}, a level with spin 5/2 and odd parity. Hence our assignment for the 29 kev level is 5/2-, and our assingments for the 72, 126 and 195 kev levels are 7/2-, 9/2- and 11/2-, respectively. Increase of the inhibition factor F for the transitions to these levels is not in conflict with the assignments. The proposed decay scheme for U^{233} is shown in Fig.4.

Transition intensities in U^{233} decay and Th^{229} level assignments

Th^{229} levels, kev	α-transition intensity, %	Assignment			Inhibition factor F
		K	I	π	
0	83	5/2	5/2	+	1,9
29±2	0,48±0,08	5/2	5/2	—	200
42,3	14,6	5/2	7/2	+	5,8
72±2	0,28±0,06	5/2	7/2	—	190
97	1,5	5/2	9/2	+	24
126±2	0,08±0,02	5/2	9/2	—	280
(145±5)	⩽0,01	—	7/2	(—)	~ 1700
163±2	0,06±0,02	5/2	11/2	+	200
195±3	0,015±0,05	5/2	11/2	—	500
(240±5)	⩽0,004	(5/2)	(13/2)	(+)	~ 1200
316±2	0,033±0,006	—	(3/2)	(+)	30
(364±5)	⩽0,004	—	(5/2)	(+)	130

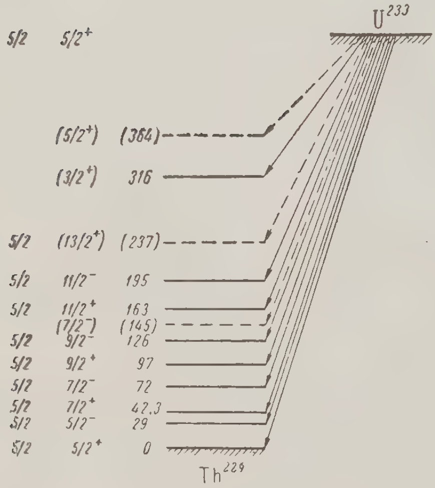

Fig.4. Decay scheme for U^{233}.

We are deeply grateful to L.L.Gol'din and G.I.Novikov for making available the U^{233} sources, L.K.Peker for discussion of the results and V.A. Belyakov and V.N.Delaev for assistance in carrying out the measurements.

"V.G.Khlopin" Radium Institute,
Academy of Sciences of the USSR

References

1. B.S.Dzhelepov, R.B.Ivanov, V.G.Nedovesov & V.G.Chumin, Izv.AN SSSR, Ser. fiz., 23, 782 (1959). (Trans.Bulletin 22, 780.)
2. B.S.Dzhelepov, R.B.Ivanov, V.G.Nedovesov & B.P.Shishin, Ibid., 23, 788 (1959). (Trans.Ibid., 22, 785.)
3. B.R.Mottelson & S.G.Nilsson, Mat.-fys. Skr.dansk. vid.selskab, 1, 8 (1959).

* * * * * * *

RADIOACTIVE DECAY OF Th^{231}*

- S.A.Baranov, R.M.Polevoi, Yu.F.Rodionov, G.V.Shishkin & V.M.Shubko

Introduction

Radioactive Th^{231} is a well-known β-emitter with a period of 25.6 hours. Most studies of Th^{231} decay were carried out using sources separated from a natural or U^{235} enriched mixture of uranium isotopes. Some information on the decay of this nuclide will be found in Refs.1-6.

Two different decay schemes for Th^{231} have been proposed by Freedman et al[4] and Mize and Starner[5] on the basis of experimental data.

In our work, as the initial material for obtaining the Th^{231} source we used thorium greatly enriched with Th^{230}. We undertook this further investigation of the decay of this β-emitter for the purpose of constructing the energy diagram of Pa^{231}. This diagram is of interest both from the standpoint of the unified (Bohr) nuclear model and the theoretical level diagrams of Nilsson.

In carrying out the present study we used the β- and γ-spectrometric equipment described in our earlier papers (see, for example, Ref.7).

1. Preparation of the Th^{231} source

The requisite Th^{231} activity was obtained by slow-neutron irradiation of Th^{230} in a reactor for physical and engineering research. The irradiated thorium was fused in a quartz tube with $NaHSO_4$ and after solution in 2N HNO_3 was deposited on lanthanum hydroxide, which was twice reprecipitated. For elimination of the protactinium, there was carried out three-fold precipitation of MnO_2 from HNO_3 by addition to the initial solution of a small amount of 5% solution of $KMnO_4$ and a drop of a dilute solution of sodium nitrite with subsequent heating of the solution in a boiling water bath for 5-10 min. The lanthanum hydroxide precipitate obtained by centrifuging was washed with water and dissolved in 2N HCl. For separation of the activity from the lanthanum carrier we used the cation exchange resin Dowex-50 followed by further washing out of the lanthanum with 6N HCl.

The remaining unweighable Th^{231} was washed off with 3-4 ml 1.25 M $NaHSO_4$ solution. To the solution there were added 5-10 mg Fe^{3-} and the hydroxide precipitated; this after two-fold precipitation was dissolved in 1 ml 8 N HCl. The solution was passed through a column containing Dowex-1 resin. The eluate was evaporated to dryness in a test tube; the dry residue was dissolved in two drops of 2N HCl and this solution was then used for preparing the sources for the β- and γ-spectrometric measurements.

---

*This report was presented at the Ninth All-Union Conference on Nuclear Spectroscopy (Khar'kov, 26 Jan - 2 Feb. 1959).

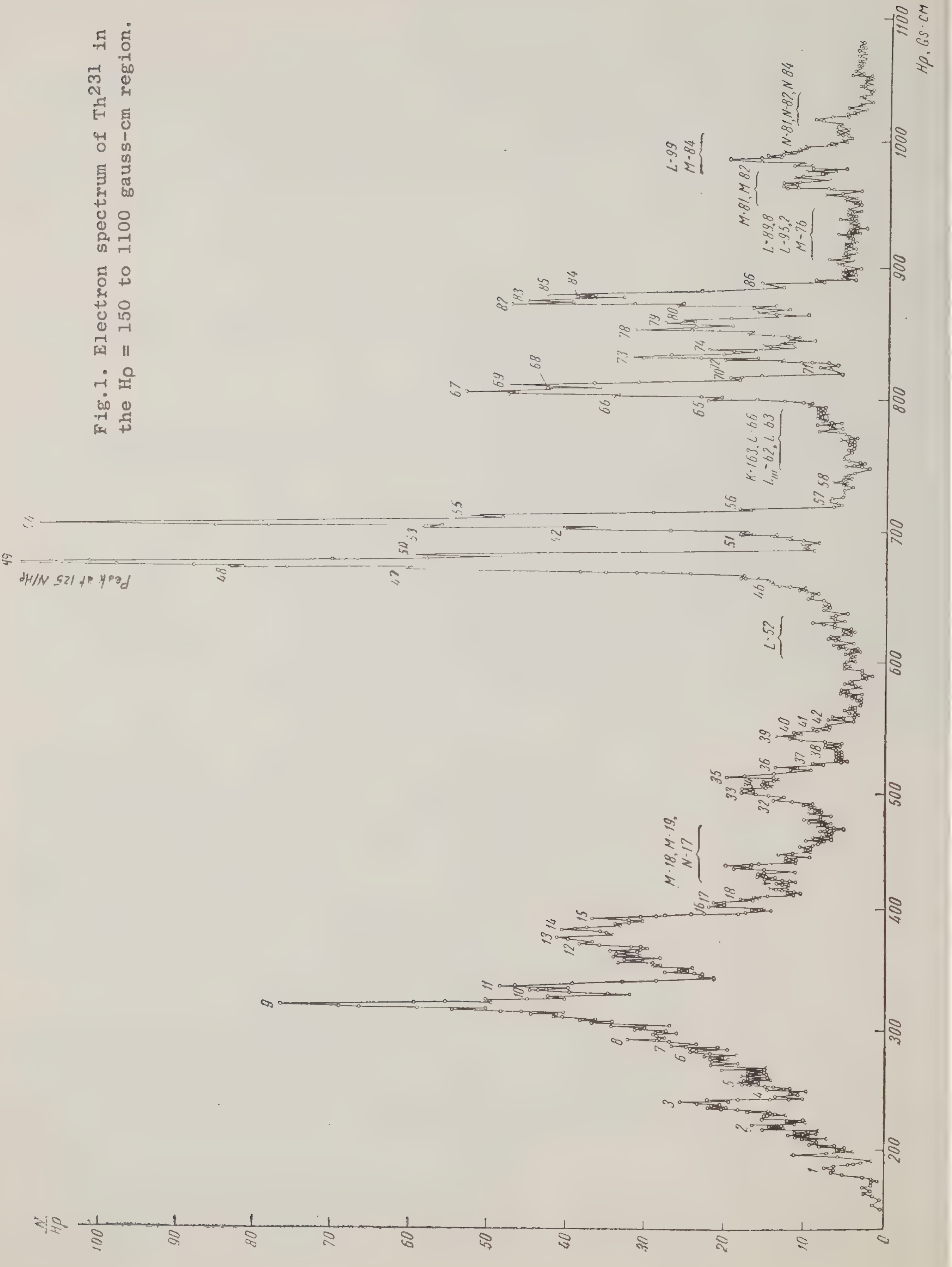

Fig.1. Electron spectrum of Th^{231} in the Hρ = 150 to 1100 gauss-cm region.

2. Electron spectrum

For investigating the β-decay of Th^{231} by means of a magnetic spectrometer we used very thin sources (1-5 μg/cm^2). Since in addition the film over the electron detector window was only 10^{-5} cm thick, we were able to investigate thoroughly the electron spectrum beginning with the very low electron energies.

The most interesting part of the electron spectrum, i.e., the spectrum in the Hρ range from 150 to 1100 gauss-cm, is reproduced in Fig.1. As will be evident from the figure, in the low energy part of the spectrum (up to about 550 gauss-cm) interpretation of the individual lines is hampered by the presence of Auger electron groups. Nevertheless a careful analysis of the observed lines does not preclude the possibility that there exist low energy γ-transitions in Pa^{231}. Thus, for example, there apparently occur in this nucleus γ-transitions with energies ~11.0, 17.1, 18.1, 19.8 and 30.6 kev. This inference is not in conflict with the results of investigation of the soft γ-radiation by means of a proportional counter, although in this case the γ-rays of the indicated energies are also masked by intense x-radiation of almost the same energy.

The most intense conversion lines (Nos.49 and 54) in the electron spectrum consist of several components. Line No.49 is the result of surposition of the following four monoenergetic electron groups: L_I-58.5, L_I-59.0, L_{II}-58.5 and L_{II}-59.0. The other intense line, No.54, comprises at least six groups, namely, L_I-62.0, L_{II}-62.0, L_{III}-58.5, L_{III}-59.0, L_I-63.4, L_{II}-63.4 and K-153(?). In this and the preceding complex case it is feasible to determine the multipole order only of the 25.6, 58.5 and 59.0 kev γ-transitions: E1, E2 and E2, respectively.

In the Hρ range from 750 to 950 gauss-cm, in addition to some M and N lines associated with the 58.5 and 59.0 kev γ-rays and L conversion lines of 81.1 and 84.2 kev transitions, we detected L lines of transitions having energies of 73.2(?), 76.0(?), 82.0, 85.0, 89.8, 95.2 and 99.1 kev and the K lines of ~163, ~169 and ~177 kev transitions.

Determination of the multipole orders of these γ-transitions involves a number of difficulties and a degree of arbitrariness. Hence we have restricted ourselves to assignments only for the 81.1 and 84.2 kev transitions: E1 in both cases.

More detailed information on the conversion lines is listed in Table 1 together with the intensities of some of the lines (I_{rel}) and the multipole orders of individual γ-transitions. We must emphasize that the interpretation of the individual low intensity lines is not unambiguous.

The Kurie plot based on the experimental data brought out four partial β-components with end-point energies: $E_{01} = 302 \pm 5$, $E_{02} = 218 \pm 5$, $E_{03} = 138 \pm 5$ and $E_{04} \approx 90$ kev. The relative intensities of these partial spectra are 52, 20, 22 and 6%, respectively. Although it cannot be definitively proved from the Kurie plot, we believe that the β-radiation comprises other partial spectra.

3. Gamma measurements

The experimental x-ray and soft γ-radiation spectrum of Pa^{231} recorded by means of proportional counters filled with heavy gases (Kr + CH_4 and Xe + CH_4) is shown in Fig.2.

The method of analysis applicable to such spectra has been described earlier[7]. The use of copper and aluminum absorbers enabled us to analyze the spectra shown in Fig.2 in some detail and this in conjunction with the β-spectrometric data made it possible to establish definitely the existence of a number of low energy γ-transitions in Pa^{231}.

Table 2 lists the energy values of the γ-transitions in Pa^{231} determined by means of the two above procedures and measurements with a scintillation γ-spectrometer.

Table 1

Interpretation of the electron lines observed in β-decay of Th^{231} to Pa^{231}

Line No.	Observed electron energy, kev	Shell	E_{γ}, kev
1	2	3	4
4	5,6	M_I	10,96
5	6,0	M_{II}	11,00
6	6,8	M_{III}	10,96
7	7,4	M_{IV}	11,00
8	7,6	M_V	11,03
			Average 11,03 ?
12	11,6	M_I	16,96
13	11,95	M_{II}	16,95
15	12,97	M_{III}	17,13
16	13,5	M_{IV}	17,10
17	13,7	M_V	17,13
22	15,7	N_I	17,07
24	16,0	N_{II}	17,21
25	16,2	N_{III}	17,19
26	16,4	N_{IV}	17,14
			Average 17,12 ?
14	12,59	M_I	17,95
18	13,9	M_{III}	18,1
19	14,45	M_{IV}	18,0
20	14,7	M_V	18,13
			Average 18,05 ?
1	3,2	L_{III}	19,92
19	14,45	M_I	19,81
21	14,9	M_{II}	19,90
23	15,75	M_{III}	19,91
25	16,2		19,80
26	16,4		19,83
29	18,4	N_I	19,77
30	18,5	N_{II}	19,87
31	18,9	N_{III}	19,89
32	19,1	N_{IV}	19,84
			Average 19,85
2	4,5	L_I	25,60
3	5,4	L_{II}	25,70
9	8,9	L_{III}	25,62 (I_{rel}= 109)
33	20,3	M_I	25,66
34	20,55	M_{II}	25,55
35	21,4	M_{III}	25,56
36	22,1	M_{IV}	25,70
37	22,2	M_V	25,63
39	24,2	N_I	25,57
40	24,4	N_{II}	25,61
41	24,7	N_{III}	25,69
42	24,9	N_{IV}	25,64
			Average 25,64 (*E*1)

Line No.	Observed electron energy, kev	Shell	E_γ, kev
1	2	3	4
10	9,5	L_I	30,6
11	10,4	L_{II}	30,7
18	13,9	L_{III}	30,6
			Average 30,64
43	31,0	L_I	52,10
44	31,7	L_{II}	52,00
46	35,5	L_{III}	52,22
			Average 52,14
47	37,4	L_I	58,5
49	28,2	L_{II}	58,5 ($I_{rel} \approx 146$)
54	41,8	L_{III}	58,5 ($I_{rel} \approx 113$)
66	53,2	M_I	58,56
67	53,5	M_{II}	58,50
69	54,35	M_{III}	58,46
70	54,9	M_{IV}	58,50
73	57,3	N_{II}	58,51
74	57,6	N_{III}	58,59
75	57,9	N_{IV}	58,64
			Average 58,53 ($E2$)
48	37,9	L_I	59,0
50	38,7	L_{II}	59,0 ($I_{rel} \approx 48$)
55	42,3	L_{III}	59,00 ($I_{rel} \approx 39$)
68	54,0	M_{II}	59,00
70	54,9	M_{III}	59,06
76	58,3	N_V	59,00
			Average 59,01 ($E2$)
51	41,05	L_I	62,15
53	41,8	L_{II}	62,10
58	45,2	L_{III}	61,9
			Average 62,05
56	42,3	L_I	63,4
57	43,0	L_{II}	63,3
59	46,6	L_{III}	63,3
			Average 63,33
58	45,1	L_I	66,2
59	45,9	L_{II}	66,2
62	49,7	L_{III}	66,4
			Average 66,3
60	47,4	L_I	68,5
61	48,2	L_{II}	68,5
63	51,8	L_{III}	68,5
			Average 68,5
64	52,1	L_I	73,3
65	52,9	L_{II}	73,2
72	56,5	L_{III}	73,2 (Coinc.with K-169)
			Average 73,23

Line No.	Observed electron energy, kev	Shell	E_γ, kev
1	2	3	4
70	54,9	L_{I}	76,0
71	55,7	L_{II}	76,0
77	59,4	L_{III}	76,12
91	70,5	M_{I}	75,86
92	71,0	M_{II}	76,00
93	71,8	M_{III}	75,96
94	72,6	M_{V}	76,03
			Average 76,0
78	60,1	L_{I}	81,20 (I_{rel}= 9,47)
79	60,8	L_{II}	81,10 (I_{rel}= 7,66)
85	64,4	L_{III}	81,12 (Coinc.with K-177
99	75,8	M_{I}	81,16
100	76,2	M_{II}	81,20
102	77,0	M_{III}	81,16 (Coinc.with M_{II}-82.03)
103	77,6	M_{IV}	81,20
104	77,8	M_{V}	81,23 (Coinc.with L_{I}-99.07)
108	79,7	N_{I}	81,07
109	80,0	N_{II}	81,21 (Coinc.with M_{III}-84.16)
			Average 81,16 (*E*1)
80	61,1	L_{I}	82,20
81	62,0	L_{II}	82,30
86	65,1	L_{III}	81,82
101	76,7	M_{I}	82,06
102	77,0	M_{II}	82,00 (Coinc.with M_{III}-81.16)
104	77,8	M_{III}	81,96
105	78,4	M_{IV}	82,0
112	80,6	N_{I}	81,97
113	81,3	$N_{IV}-N$	82,0—82,04
			Average 82,03
82	63,1	L_{I}	84,20 (I_{rel}= 18,4)
83	63,8	L_{II}	84,10 (I_{rel}= 18,0)
88	67,4	L_{III}	84,12 (I_{rel}= 0,87)
106	78,8	M_{I}	84,16
107	79,1	M_{II}	84,10
109	80,0	M_{III}	84,16 (Coinc.with N_{II}-81)
112	80,6	M_{IV}	84,20
115	82,8	N_{I}	84,17
116	83,0	N_{II}	84,21
117	83,4	N_{III}	84,39
			Average 84,16 (*E*1)
84	63,9	L_{I}	85,0
87	64,95	L_{II}	85,25
89	68,3	L_{III}	85,0
			Average 85,1
90	68,7	L_{I}	89,8
91	69,5	L_{II}	89,8
96	73,2	L_{III}	89,92
			Average 89,84

Line No.	Observed electron energy, kev	Shell	E_{γ}, kev
1	2	3	4
97	74,2	L_{I}	95,4
98	74,9	L_{II}	95,2
105	78,4	L_{III}	95,12
			Average 95,24
104	77,8	L	99,00 (Coinc. with M_{V}-81.16)
106	78,8	L_{II}	99,10
114	82,4	L_{III}	99,12
			Average 99,07
38	23,4	K	136
47	33	K	145,6
52	41,2	K	153,8
62^{a}	50,7	K	163,28
72	56,5	K	169,2 (Coinc. with L_{III}-73)
85	64,4	K	177,1 (Coinc. with L_{III}-81)

The sum of the partial β-spectrum intensities equals 506.

Table 2

Energies of γ-transitions in Pa^{231} (kev)

β-spectrometer	Proportional counter	Scintillation spectrometer	β-spectrometer	Proportional counter	Scintillation spectrometer
(11,1)	11,0		81,2	81,0	
(17,2)	17		82,1	(82)	
(18,1)			84,2	84,1	~ 84
19,8	19,8		85,1	?	
25,6	25,6	25	89,8		
30,6	(30,6)		—	~ 92	
52,1	52,0	~ 51	95,2		
58,5	58,5		99,2	99	95—99
59,0			106,5	106,5	
62,0			135,8		(136)
63,3	(63)		145,6		145
(66,0)	(66)		153,8		
			163,3		163
68,5	(68)		169,2		
(73,2)			177,1		180
(76,0)					218
					~ 250
					~ 310

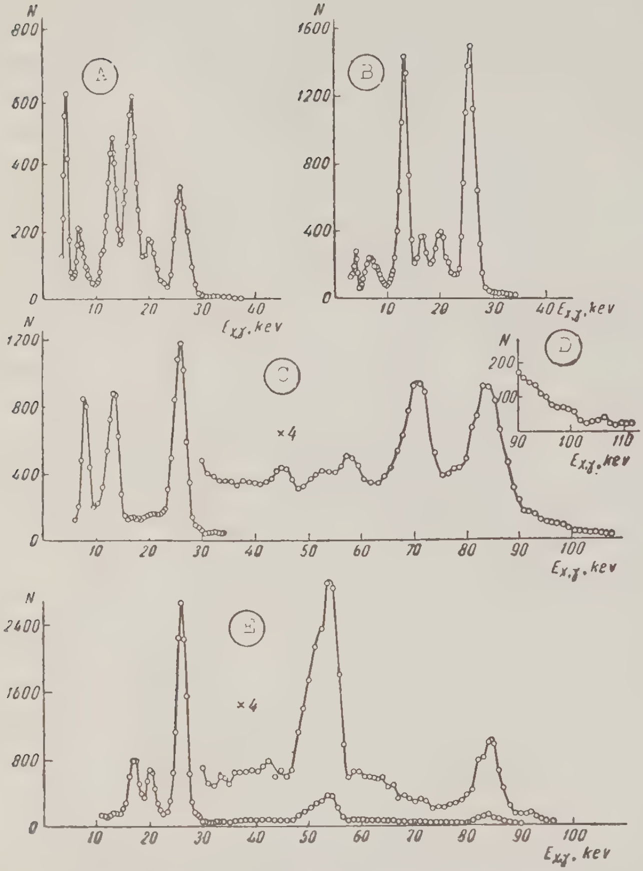

Fig.2. Spectrum of x- and low-energy γ-radiation from Pa^{231}: A-D - counter filled with Kr + CH_4 mixture (760 mm Hg), E - counter filled with Xe + CH_4 (380 mm Hg). Absorbers: A - 1 mm Al, B - 2 mm Al, C - 0.2 mm Cu, D - 1 mm Cu, E - 2 mm Al.

In addition to the straigh spectrometric measurements, in the present investigation we al had recourse to the γ-γ coincidence technique. These measurements were carried out by means of two scintillation spectromet with NaI(Tl) crystals connected in coincidence ($2\tau \approx 5\cdot10^{-6}$ sec

These measurements showed that the most intense γ-rays, t 25.6 and 84.1 kev γ-rays, are n in cascade. However, the 25.6 kev γ-rays do coincide in time with the 58, 95, 145, 163 and 2 kev γ-radiations. The experime al results also give reason to assume that the 250 kev γ-rays are not in coincidence with the most intense γ-rays (25.6 and 8 kev).

It may be inferred from co parison of the coincidence hist grams with the single γ-spectru that there exist γ-rays of 170-180 kev energy. Apparently the γ-rays do not coincide with any of the intense γ-rays.

We used the above data for constructing the decay scheme f Pa^{231}.

4. Multipole order assignments for some γ-transitions

On the basis of the experi mental data we evaluated the re tive and absolute conversion co efficients for some of the tran tions in Pa^{231}. The procedure for evaluating the absolute conversion coefficie has been described in Ref.7. As usual, the multipole orders were determined through comparison of the experimental coefficient with the theoretical coeffic ents given in the tables of Sliv & Band[8].

In Table 3 we list the experimental and theoretical values of the absolute (η_0) and relative ($\eta_1 = L_I/L_{II}$ and $\eta_2 = L_{II}/L_{III}$) conversion coefficients for t 25.6, 58.5, 59.0, 81.2 and 84.2 kev transitions. In the last column of the tab we list the inferred multipole orders.

It will be noted that the absolute conversion coefficients for the 81.2 an 84.2 kev transitions are anomalously high. The experimental L_I and L_{II} subshel conversion coefficients are approximately one order of magnitude greater than t corresponding theoretical coefficients. These anomalies cannot be explained so ly by an admixture of magnetic quadrupole radiation, although admittedly there be some fraction of M2 radiation involved in these cases.

Table 3

Absolute and relative conversion coefficients of the γ-transitions in Pa^{231}

E_γ, kev	Shell	Experimental values of η			Theoretical values of η									Multipole order
					E1			E2			M1			
		η_0	η_1	η_2	η_0	η_1	η_2	η_0	η_1	η_2	η_0	η_1	η_2	
25,6	L_I				0,606	0,541		96,5	0,030		168	9,1		
	L_{II}				1,12		0,732	3230		0,965	18,5		16,8	E 1
	L_{III}	$1,42^{+0,1}_{-0,15}$			1,53			3350			1,1			
58,5	L_I				0,14	1,138		2,3	0,033		15,5	8,8		E 2
	L_{II}	70^{+6}_{-10}		1,2	0,12		0,949	70		1,209	1,7		18,5	
	L_{III}	53^{+5}_{-8}			0,13			58			0,09			
59,0	L_I				0,14	1,138		2,3	0,033		15,5	8,8		E 2
	L_{II}	70^{+5}_{-10}		1,2	0,12		0,946	70		1,209	1,7		18,5	
	L_{III}	55^{+5}_{-8}			0,13			58			0,09			
81,2*	L_I	1.6 ± 0,4	1,4		0,07	1,505		0,55	0,046		5,5	8,45		E 1
	L_{II}	1,2 ± 0,3		1,25	0,046		1,048	12,0		1,2	0,65			
	L_{III}	1,0 ± 0,5			0,044			10,0			0,036			
84,2	L_I	1,77 ± 0,25	1,6		0,065	1,569		0,49	0,049		4,9	8,45		E 1
	L_{II}	0,76 ± 0,25		13,3	0,042		1,038	10,0		1,053	0,58		19,3	
	L_{III}	0,036 ± 0,01			0,040			9,5			0,030			

---

*The value of $\eta_{OL_{III}}$ = 1.0 obtained in this case gives reason to assume that the intensity of the L_{III}-81 line is due mainly to the fact that the K-177 line coincides with it.

It has been reported[9] that for the ~85 kev γ-rays (El) emitted by Pa^{231} there were obtained the following anomalously high values of the conversion coefficients: 1.32 (L_I), 0.84 (L_{II}) and 0.047 (L_{III}). We do not know the accuracy of these values, but we note that they are close to the coefficients listed in the table for E_γ = 84.2 kev.

Vartapetian[10,11] and Nilsson & Rasmussen[9] in their papers suggest a possible explanation of the anomalously high conversion coefficients for the El and M2 class multipoles. It must be borne in mind, however, that there is necessarily some degree of arbitrariness in the experimental evaluations of the absolute coefficients for the 81.2 and 84.2 kev γ-rays. In the highly complex level scheme of Pa^{231} there may exist other γ-transitions with energies differing only slightly from 81.2 and 84.2 kev. In view of the inadequate resolving power of the equipment employed, there may naturally arise errors in evaluating the experimental coefficients owing to disregard of such hypothetical close transitions. Naturally, also, the theoretical coefficients calculated by Sliv and by Rose may be in need of more or less substantial correction.

5. Pa^{231} level diagram

The detected four β-spectra ($5 \leqslant \log ft \leqslant 5.8$) and the results of Coulomb excitation experiments on Pa^{231} (Ref.12), the ground state spin of which $I_o = 3/2$ (Ref.13), unambiguously indicate that there exist in this nucleus levels with energies of 58.5, 84.2, ~169, ~248 and ~300 kev. Analysis of all the experimental data, however, gives reason to infer that the level scheme for Pa^{231} must comprise an additional number of levels. The fact that many (over 30) γ-transitions have been observed in this nucleus in the present and other studies[12] (see also Refs.4 & 5) substantiates this inference.

A possible decay scheme for Pa^{231} constructed on the basis of the available experimental data is shown in Fig.3a. Naturally, the spins and parities of most of the Pa^{231} levels cannot be unambiguously established on the basis of the present experimental data: hence the spin and parity assignments are either omitted or where a questionable value is available, indicated in parentheses. On the left in the scheme we have arbitrarily numbered the levels in sequence. Fig.3b shows the Pa^{231} level diagram predicted by Nilsson* on the basis of theoretical studies described in Refs.14 & 15, and, apparently, in other data. The predicted values of I and K and approximate energies are indicated for each level.

It is significant that the experimental level diagrams for Pa^{231} and Pa^{233} ($I_o = 3/2$) are very similar.

---

*Private communication from B.Mottelson.

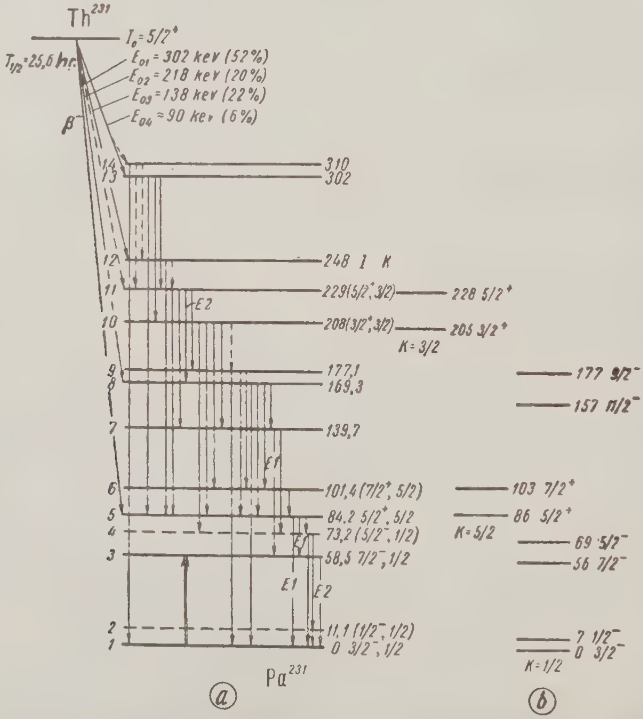
Th^{231}
$I_o = 5/2^+$
$T_{1/2} = 25{,}6$ hr.
$E_{01} = 302$ kev (52%)
$E_{02} = 218$ kev (20%)
$E_{03} = 138$ kev (22%)
$E_{04} \approx 90$ kev (6%)
β^-
14
13
12
11
10
9
8
7
6
5
4
3
2
1
310
302
248 I K
229(5/2⁺, 3/2)
208(3/2⁺, 3/2)
K = 3/2
177,1
169,3
139,7
101,4 (7/2⁺, 5/2)
84.2 5/2⁺, 5/2
73,2 (5/2⁻, 1/2)
58,5 7/2⁻, 1/2
11,1 (1/2⁻, 1/2)
0 3/2⁻, 1/2
E2
E1
E1
E1
E2
228 5/2⁺
205 3/2⁺
177 9/2⁻
157 11/2⁻
103 7/2⁺
86 5/2⁺
K = 5/2
69 5/2⁻
56 7/2⁻
7 1/2⁻
0 3/2⁻
K = 1/2
Pa^{231}
ⓐ
ⓑ

Fig.3. a - Decay scheme for Th^{231} based on the experimental data. b - level diagram for Pa^{231} after S.Nilsson.

Levels Nos.2,3 & 4 belong to a ground state rotational band and are associated with collective motion of the nucleons. Two of these levels (Nos.2 & 4) have not been definitively established and more certain proof of their actual existance is highly desirable.

If we assume that the energies and spins of these levels are as indicated in the scheme, then making use of the familiar formula of Bohr & Mottel'son[16] for the energy of levels in nuclei with K = 1/2,

$$E_I = E_0 + \frac{\hbar^2}{2J}[I(I+1) + a(-1)^{I+1/2}(I+1/2)],$$

(we omit second order terms) one can evaluate the constants E_0, $\hbar^2/2J$ and a. Our calculations yielded the following values: E_0 = -1.06 kev, $\hbar^2/2J$ = 5.79 kev and a = -1.36.

Some of the other levels shown in the scheme are single-particle levels or members of corresponding rotational bands. Thus, for example, level No.5 (84.2 kev, I = 5/2+, K = 5/2) is a single-particle excitation level, while level No.6 (101.4 kev, I = 7/2+, K = 5/2) is apparently a member of its rotational band. If these two levels are the first and second levels of a rotational series, the moment of inertia of the nucleus increases substantially (by a factor of ~2.5) as compared with the ground state.

The proposed decay scheme is neither complete nor definitive. However, qualitatively it is reminiscent of the scheme proposed by Nilsson and it does differ from the schemes given by Freedman et al[4] and Mize & Starner[5].

We desire to express our gratitude to P.E.Nemirovskii for valuable discussion of the results.

References

1. G.B.Knight & R.L.Macklin, Phys.Rev., 75,34 (1949).
2. P.H.Stoker, Ong Ping Hok & G.J.Sizoo, Physica, 17, 164 (1951).
3. A.H.Jaffey & Warshaw Lerner, Phys.Rev., 82, 498 (1951).
4. M.S.Freedman, A.H.Jaffey, F.Wagner & J.May, Phys.Rev., 89, 302 (1953).
5. J.P.Mize & J.W.Starner, Bull.Amer.Phys.Soc., Ser.II, 1, 171 (1956).
6. D.Strominger & J.O.Rasmussen, Phys.Rev., 100, 844 (1955).
7. S.A.Baranov, Yu.F.Rodionov, G.V.Shishkin & L.V.Chistyakov, Zhur.eksp.i teor.fiz., 34, 1367 (1958). (Trans.Soviet Physics - JETP.)
8. L.A.Sliv & I.M.Band, Tablitsy koeffitsientov vnutrennei konversii γ-izlucheniya (Tables of internal conversion coefficients) Part II, L shell, M.-L. 1958.
9. S.G.Nilsson & J.O.Rasmussen, Nucl.Phys., 5, 617 (1958).
10. H.Vartapetian, Thesis, Univ.de Paris, 1957.
11. H.Vartapetian, Compt.rendu., 224, 65 (1957).
12. D.Strominger, H.M.Hollander & G.T.Seaborg, Table of Isotopes, Revs.Mod. Phys., 30, 585 (1958).
13. H.Schüler & H.Callnow, Naturwissenschaften, 22, 511 (1934); see also J.Mack Revs.Mod.Phys., 22, 64 (1950).
14. B.R.Mottelson & S.G.Nilsson, in Probl.sovr.fiz. (Problems of Modern Physics), 1, 186 (1956).
15. S.Nilsson, Kgl.danske vid.selskab. Mat.-fys. medd., 29, 16 (1955).
16. A.Bohr & B.R.Mottelson, in Beta- and Gamma-Ray Spectroscopy, K.Siegbahn, (editor), Amsterdam, 1955.

CONVERSION ELECTRONS AND GAMMA-RAYS FROM Tm^{165}

- K.Ya.Gromov, B.S.Dzhelepov, A.G.Dmitriev, V.A.Morozov & K.I.Yakovlev

The conversion electron spectrum of Tm^{165} was investigated by means of a Ketron type[1] magnetic spectrometer. The relative line half-width was 0.4%; the transmission factor 0.4%. The γ-ray spectrum was investigated by means of a scintillation spectrometer. The half-width of the Cs^{137} 661 kev γ-line was 12%.

For the measurements we used a thulium activity (fraction) obtained by chromatic separation of the products of spallation of tantalum which had been bombarded for four hours with 660 Mev protons on the synchrocyclotron of the Join Institute for Nuclear Research. The separation of the group of rare earth elements was completed within 15-20 hours after the end of bombardment. Under these conditions the following isotopes were comprised in the thulium fraction: 7.7 hour Tm^{166}, 29 hour Tm^{165} and 9.6 day Tm^{167}. Tm^{165} has been investigated previously by a number of authors[2-8]. It was established that Tm^{165} transforms by K capture to Er^{165} which, also by K capture, with a period of 10 hours, converts to stable Ho^{165}.

No γ-radiation is emitted in the disintegration of Er^{165}.[7,9,10] All the γ-rays emitted by the equilibrium mixture of Tm^{165} + Er^{165} must therefore be attributed to Tm^{165}. The nuclear radiation emitted in the decay of Tm^{165} has been studied in detail only in the energy region up to 350 kev. The purpose of the present work, therefore, was investigation of the spectrum of Tm^{165} in the energy region above 350 kev.

1. Conversion electrons

The sections of the experimental conversion electron spectrum in the range from 85 to 1200 kev are shown in Figs.1,2 & 3. Each section of the spectrum was recorded at least three times with an interval of 24-35 hours between runs. Thus on the basis of the period we were able to distinguish the conversion lines of Tm^{16} from the lines of the other isotopes. The main interfering lines were the 208 and 530 kev conversion electron lines of 9.6 day Tm^{167}. In view of this we could not resolve the L line of the 219 kev γ-transition and could not determine the relative intensities of the conversion lines in the 470 to 480 and 515 to 525 kev intervals.

The line intensities were evaluated relative to the intensity of the strongest line, namely, the K-243 line, the intensity of which was arbitrarily taken as 100. The measurement results are listed in Table 1. We were able to detect a large number of new lines with intensities less than 2% the intensity of the K-243 line.

On the basis of the conversion electron data one can identify a number of new γ-transitions: 279.0, 312.1, 366.0, 378.4(?), 389.4, 457.2, 460.4, 471.6, 488.2, 543.5(?), 566.0, 807.1, 1133, 1179 and 1187 kev.

2. Gamma-rays

In view of the fact that the resolving power of our scintillation spectrometer was not high, only the most intense γ-lines stand out clearly in the γ-spectrum, which is shown in Fig.4. The γ-line energies and intensities are listed in Table 2. In view of the complex nature of the γ-spectrum there is an appreciable uncertainty in evaluating the relative γ-ray intensities. Many of the γ-lines are undoubtedly complex, consisting of two or more components.

The experimental data show that the actual decay scheme of Tm^{165} is appreciably more complex than that given in the literature[11,12]: in reality there are many more γ-transitions, some of which have an appreciable intensity.

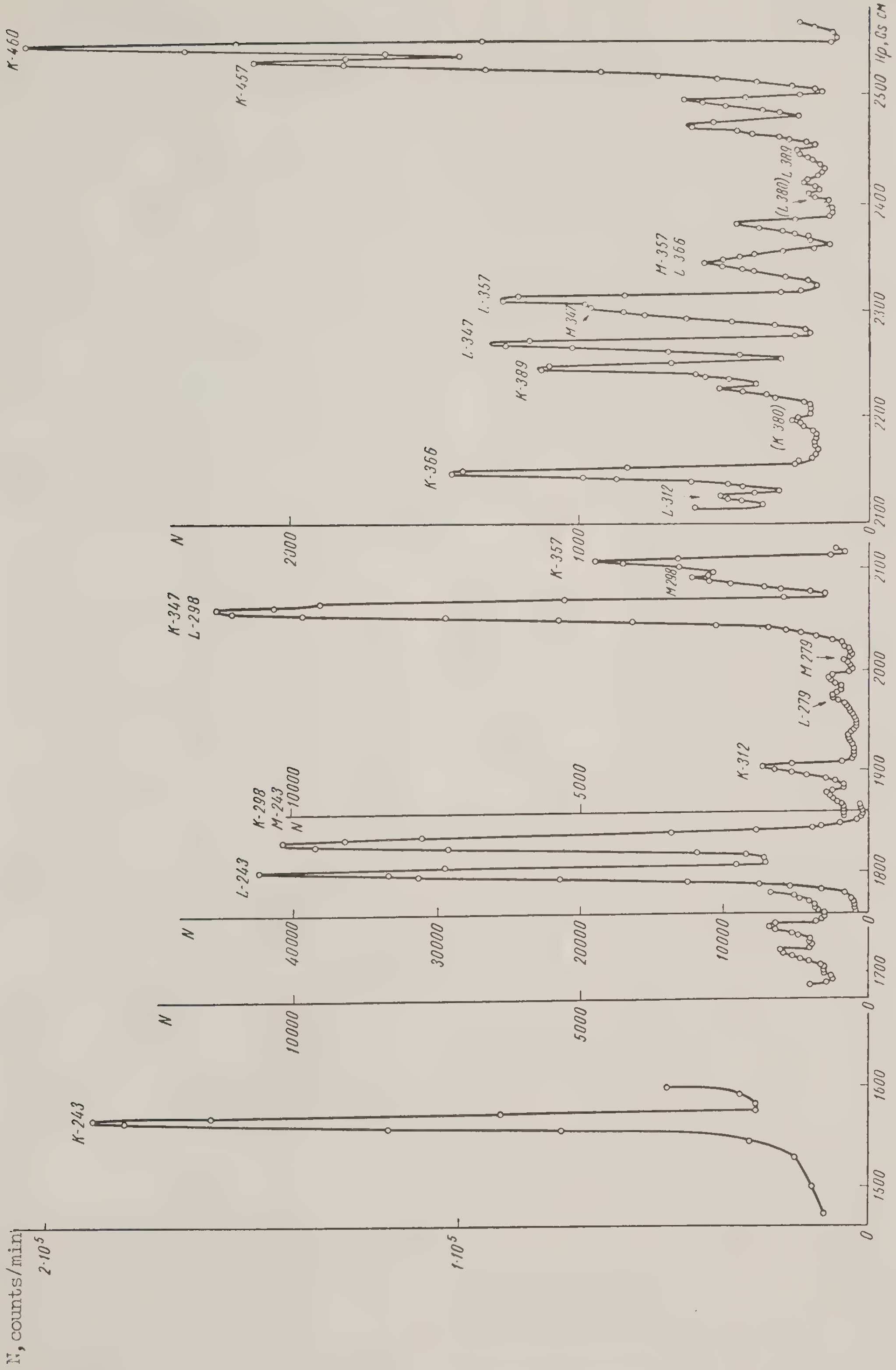

Fig.1. Conversion electron spectrum of Tm^{165} in the 190 to 420 kev region.

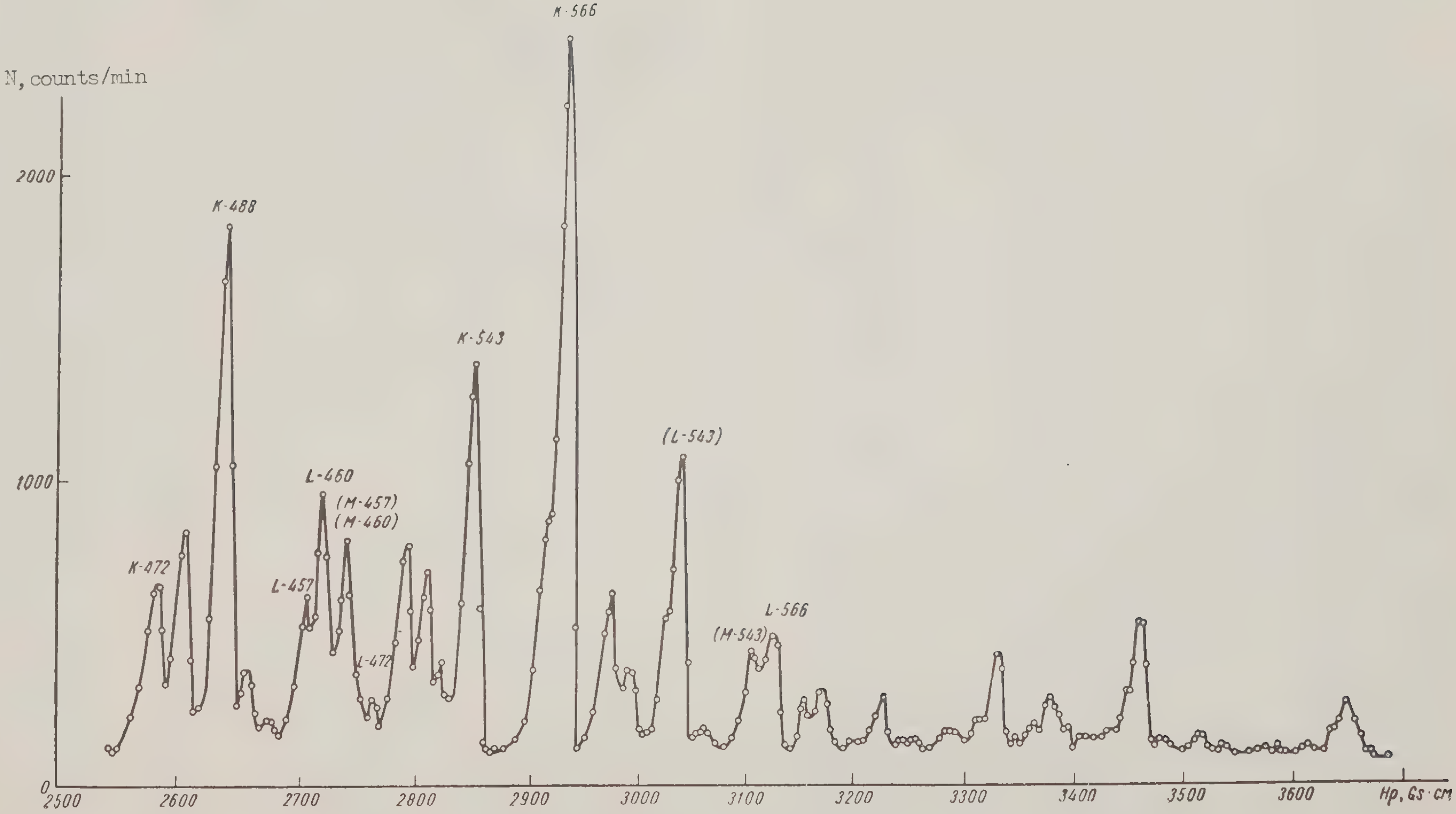

Fig.2. Conversion electron spectrum of Tm^{165} in the 420 to 700 kev region.

Table 1

Results of investigation of the Tm^{165} conversion electron spectrum

E_e, kev	$H\rho$, gauss-cm	Relative intensity	Identification	E_γ, kev
103,0 ± 0,4	1136	5,9 ± 0,5	*L*-113	112,8 ± 0,4
107,9 ± 0,5	1165	0,7 ± 0,2		
111,1 ± 0,4	1183	1,8 ± 0,3	*M*-113	
162,0 ± 0,4	1461	15,7 ± 1,0	*K*-219	219,5 ± 0,4
185,2 ± 0,4	1577	100	*K*-243	242,8 ± 0,4
216,6 ± 0,4	1728	0,8 ± 0,2		
218,3 ± 0,4	1736			
221,5 ± 0,4	1751	0,7 ± 0,1	*K*-279	279,0 ± 0,4
233,2 ± 0,4	1805	19,6 ± 1,0	*L*-243	
239,2 ± 0,4	1832	22,8 ± 1,0	*K*-298 *M*-243	
249,5 ± 0,6	1878	0,4 ± 0,1	*K*-307	307,0
254,6 ± 0,5	1902	1,0 ± 0,2	*K*-312	312,1 ± 0,5
261,7 ± 0,5	1931	0,1 ± 0,02		
270,0 ± 0,5	1970	0,4 ± 0,04	*L*-279	
273,2 ± 0,5	1985			
277,2 ± 0,5	2002	0,06 ± 0,01	*M*-279	
288,7 ± 0,5	2052,2	7,9 ± 0,4	*L*-298; *K*-347	
295,4 ± 0,5	2081,2	3,4 ± 0,4	*M*-298	
299,4 ± 0,5	2098,4		*K*-357	356,9 ± 0,5
302,8 ± 0,5	2113	0,09 ± 0,02	*L*-312	
308,5 ± 0,5	2137	0,6 ± 0,1	*K*-366	366,0 ± 0,5
314,8 ± 0,5	2164			
320,9 ± 1,0	2187	0,04 ± 0,02	(*K*-380)	(378,4)
327,1 ± 1,0	2216	0,1 ± 0,03		
331,9 ± 0,5	2236	0,43 ± 0,05	*K*-389	389,4 ± 0,5
337,6 ± 0,5	2260	0,49 ± 0,05	*L*-347	
344,4 ± 0,6	2288	0,69 ± 0,07	*M*-347	
347,3 ± 0,5	2301		*L*-357	
354,8 ± 0,5	2332	0,24 ± 0,03	*M*-357	
355,8 ± 0,5	2336		*L*-366	
364,2 ± 0,5	2370	0,15 ± 0,06		
370,5 ± 0,5	2396	0,03 ± 0,01	*L*-380	
373,7 ± 0,6	2409	0,04 ± 0,01		
380,0 ± 0,8	2435	0,04 ± 0,01	*L*-389	
386,1 ± 0,5	2460	0,22 ± 0,04		
391,6 ± 0,6	2482	0,24 ± 0,03		
399,7 ± 0,5	2514	1,7 ± 0,1	*K*-457	457,2 ± 0,5
402,9 ± 0,6	2528		*K*-460	460,4 ± 0,6
414,1 ± 1,0	2573	0,27 ± 0,05	*K*-472	471,6 ± 1,0
421,0 ± 0,7	2600	0,28 ± 0,05		
430,7 ± 0,5	2639	0,60 ± 0,05	*K*-488	488,2 ± 0,5
434,7 ± 0,5	2655	0,12 ± 0,03		
439,7 ± 0,4	2675	0,04 ± 0,01		
448,1 ± 0,7	2707	0,40 ± 0,08	*L*-457	
452,4 ± 1,0	2725		*L*-460	
457,6 ± 1,5	2745	0,30 ± 0,05	*M*-457 *M*-460	
462,6 ± 0,6	2765	0,04 ± 0,02	*L*-472	
471,3 ± 0,7	2799	*		
474,7 ± 0,5	2812			
478,3 ± 0,5	2826			
486,0 ± 0,5	2868	0,51 ± 0,06	(*K*-543)	(543,5)
491,8 ± 0,5	2879	0,09 ± 0,03		
~ 495				
503,2 ± 0,7	2923	1,0 ± 0,1	*K*-566	566,0 ± 0,8
508,5 ± 0,8	2943			
518,1 ± 0,7	2980	*		
522,6 ± 0,8	2998			
530,4 ± 0,5	3028	0,42 ± 0,04	*L*-543	
533,8 ± 0,5	3040			
539,8 ± 0,9	3063	0,04 ± 0,01		
551,1 ± 0,9	3106	0,30 ± 0,03	*M*-543	
555,7 ± 0,5	3124		*L*-566	

Table 1 cont.-

E_c, kev	Hρ gauss-cm	Relative intensity	Identification	E_γ, kev
563,9 ± 0,9	3155	0,11 ± 0,01		
566,7 ± 0,5	3165			
572,7 ± 0,9	3188	0,05 ± 0,02		
581,5 ± 0,8	3221,8	0,08 ± 0,02		
588,2 ± 1,0	3247	0,05 ± 0,2		
598,7 ± 1,0	3286	0,02 ± 0,01		
604,0 ± 0,8	3306	0,12 ± 0,02		
608,7 ± 0,8	3327			
619,0 ± 1,5	3362	0,08 ± 0,02		
620,4 + 1,5	3367			
625,8 ± 1,0	3388			
657,3 ± 0,7	3505	0,02 ± 0,005		
690,1 ± 1,0	3626	0,07 ± 0,02		
692,7 ± 1,0	3636			
749,6 ± 0,6	3845	1,7 ± 0,1	*K*-807	807,1 ± 0,6
780,8 ± 0,9	3958	0,12 ± 0,01	*K*-838	838,3 ± 1,0
798,4 ± 0,7	4022	0,27 ± 0,03	*L*-807	
805,2 ± 0,7	4047	0,075 ± 0,008	*M*-807	
1075,4 ± 1,5	5011	0,03 ± 0,005	*K*-1133	1132,9 ± 1,5
~ 1089	~ 5060	~ 0,01		
~ 1097	~ 5087	~ 0,01		
1121±1,5	5173	0,05 ± 0,005	*K*-1179	1179 ± 1,5
1129±1,5	5201	0,05 ± 0,005	*K*-1187	1187 ± 1,5

---

*Evaluation of the intensity of the lines in these sections of the spectrum is hampered by the K and L lines of the 530 kev γ-transition in Tm^{167}.

The γ-transitions given in parentheses are doubtful.

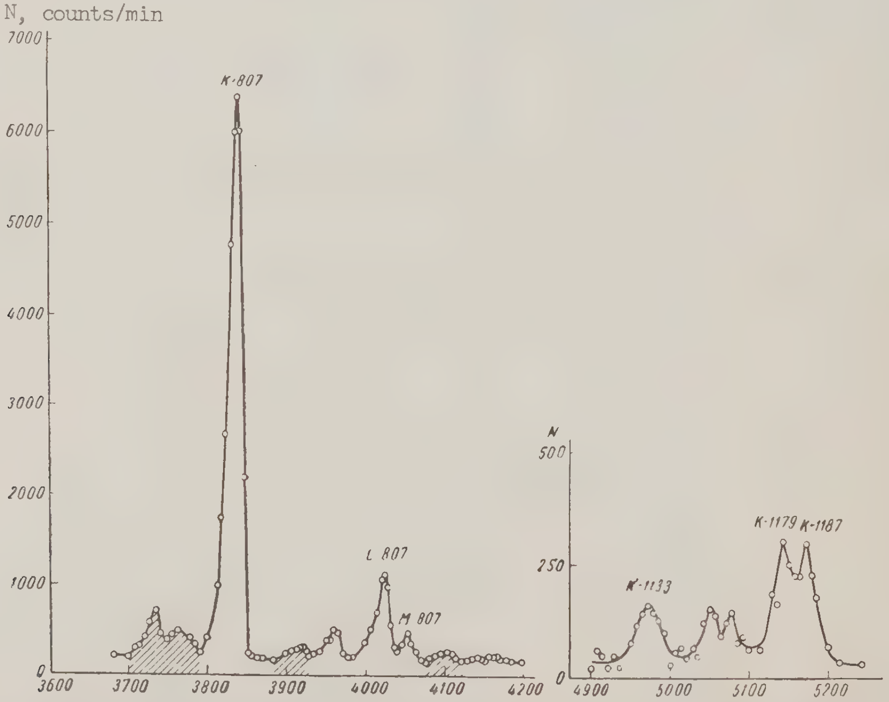

Fig.3. Conversion electron spectrum of Tm^{165} in the 700 to 1200 kev region. The sections of the spectrum characterized by a different period are indicated by hatching.

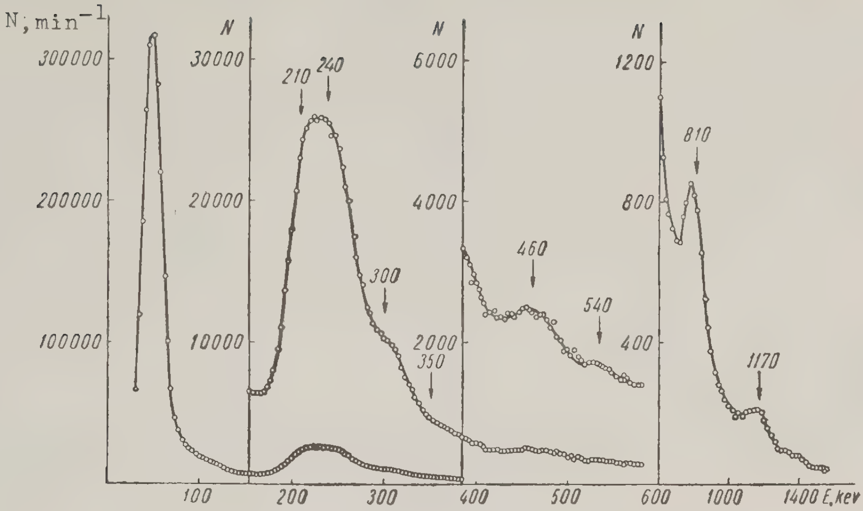

Fig.4. Tm^{165} γ-ray spectrum.

Table 2

E_γ, kev	Relative intensity
(219 ÷ 240)	1,0
296	1,0±0,3
350	0,32±0,10
450	0,23±0,07
540	0,21±0,06
810	0,37±0,10
1170	0,19±0,06

References

1. P.P.Zarubin, Izv.AN SSSR, Ser.fiz., 18, 563 (1954). (Trans.Bulletin 18, No.5, 244.)

2. T.H.Handley & E.L.Olson, Phys.Rev., 96, 1003 (1954).

3. M.C.Michel & D.H.Templeton, Phys.Rev., 93, 1422 (1954).

4. W.E.Nervik & G.T.Seaborg, Phys.Rev., 97, 1092 (1955).

5. J.W.Mihelich, B.Harmatz & T.H.Handley, Phys.Rev. 108, 989 (1957).

6. K.Ya.Gromov, B.S.Dzhelepov & B.K.Preobrazhenskii, Izv.AN SSSR, Ser.fiz., 21, 918 (1957). (Trans.Bulletin 21, 920.)

7. G.M.Gorodinskii, A.M.Murin, V.N.Pokrovskii & B.K.Preobrazhenskii, Ibid., 21, 1004 (1957). (Trans.Ibid., 21, 1005.)

8. B.S.Dzhelepov & V.A.Sergienko, Materialy II Soveshchaniya po neitronodefithitnym izotopam redkikh zemel' (Transactions of the Second Conference on Neutron-Deficient Rare Earth Isotopes), Dubna, 1959.

9. F.D.Butement, Proc.Phys.Soc., London, A64, 775 (1950).

10. O.I.Grigor'ev, B.S.Kuznetsov, N.S.Shimanskaya & I.A.Yutlandov, Izv.AN SSSR, Ser.fiz., 22, 850 (1958). (Trans.Bulletin 22, 845.)

11. B.S.Dzhelepov & L.K.Peker, Skhemy raspada radioaktivnykh yader (Decay schemes of radioactive nuclei), M.-L., 1958.

12. B.R.Mottelson & S.G.Nilsson, Mat.fys.Skr.Dansk.Vid.Selsk., 1, 8 (1959).

REGARDING THE 75-MIN YTTERBIUM ACTIVITY

- A.A.Abdurazakov, K.Ya.Gromov, B.S.Dzhelepov, Yu.V.Norseev,
G.Ya.Umarov & V.G.Chumin

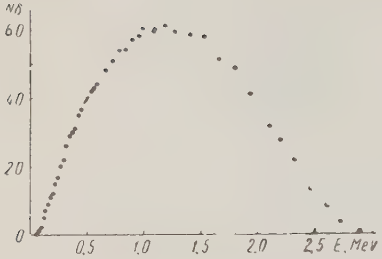

Fig.1. Positron spectrum of the 75-min Yb activity.

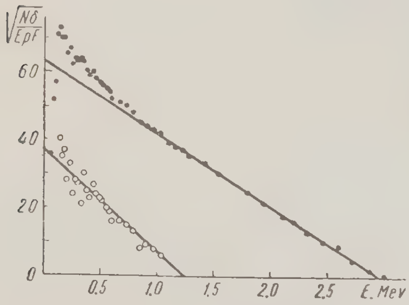

Fig.2. Fermi plot for the positron spectrum.

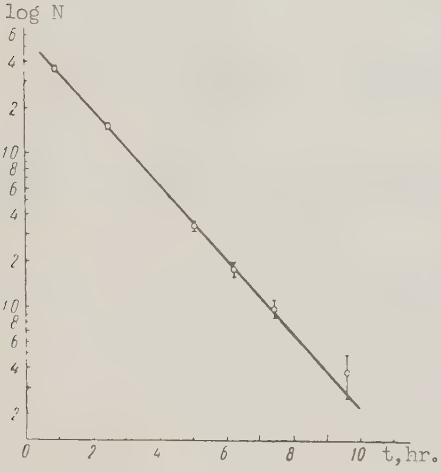

Fig.3. Positron spectrum decay curve.

We studied the electron and positron spectrum emitted in the decay of the 75-min ytterbium isotope[1,2] by means of a homogeneous field magnetic β-spectrometer. The half-width of the Cs^{137} K line was 0.8%. The electrons were detected by means of an MST-17 type counter, the window of which transmitted >60 kev electrons.

The ytterbium source was obtained by spallation of tantalum. The proton bombardment time varied from 15 min to 2 hours. The chemical operation of separating the ytterbium fraction was usually completed approximately 2 hours after the end of bombardment. The time required for preparing the source and installing it in the spectrometer was 15-20 min. Thus the measurements began 2-2.5 hours after the end of the bombardment.

Examination of the positron spectrum (Figs. 1 & 2) shows that its intensity falls off with a period of 75 ± 2 min at all points. One of the decay curves is shown in Fig.3. Analysis of the positron spectrum by the Fermi-Kurie plot (Fig.2) procedure shows that there is no deviation from rectilinearity in the 1300 to 2940 kev region. The end-point energy of the β^+-spectrum is 2940 ± 20 kev. This value is in good agreement with the results of Kalyamin et al[2]. In the energy range under 1300 kev there is deviation from the Fermi shape for allowed transitions.

If we assume that the deviation is connected with the presence of a second component in the β^+-spectrum, its end-point energy is found to be 1300 ± 100 kev and its intensity about 4% relative to the intensity of the high energy component (see Figs.1 & 2).

In the conversion electron spectrum we detected the L and M lines of a 915 kev transition and the K and L lines of a 211 kev transition. The data on the conversion lines are shown in Table 1.

The mass number of the 75-min Yb isotope has not been reliably established. Nervik & Seaborg[1] assigned the 74-min activity observed by them to Yb^{167} on the basis of build up of Tm^{167} in their thulium fraction. Later Aron et al[3] established the existence of the following series: $Lu^{167} \xrightarrow{55\ min} Yb^{167} \xrightarrow{18\ min} Tm^{167} \xrightarrow{9.6\ d} Er^{167}$. In view of this Dzhelepov & Peker[4] hypothesized the existence of a 75-min isomer of Yb^{167}.

Kalyamin et al, comparing the positron energy with the mass difference given by Levy's empirical formulas, inferred that the 75-min activity is due to Yb^{161}.

Table 1

Data on the conversion electrons from 75-min Yb

Hρ, gauss-cm	Electron energy, kev	Relative* intensities, %	Identification
1003±5	81,9±0,7	14±3	*L*-91,5
1050±5	89,2±0,7	5±1	*M*-91,5
1420±10	154±2	—	*K*-211
1655±5	201,2±2	0,1	*L*-211

*Intensity of the positron spectrum taken as 100%.

In order to establish the mass number we attempted to detect the conversion electron lines of possible daughter isotopes of the 75-min ytterbium activity. To this end we chose the most intense and convenient for observation conversion lines of possible daughter isotopes. Specifically, we chose the following lines: Tm^{167} L-208.3 (Refs.5 & 6), Tm^{165} K-243.3 (Refs. 5-7), Tm^{163} L-104 and Tm^{161} L-211 (Ref.8). The Tm^{163} L-104 line was observed in our preliminary experiments with the thulium fraction. The intensity of this line fell off with a period of 2 hr 15 min. This period was attributed by Mihelich et al[9] to Tm^{163}. The transitions energy is given according to the data of Abdurazakova et al[10].

Inasmuch as in carrying out these experiments the conversion lines of Tm^{167}, daughter of 18-min Yb^{167}, form an interfering background, subsequent experiments were carried out with an ytterbium source from which the thulium was separated 1.5 hours after separation of the ytterbium fraction.

Not a single one of the above enumerated lines was detected. For all the lines we obtained values of the upper intensity bound with reference to the intensity of the β-spectrum of the 75-min ytterbium. Using these data we could calculate the upper intensity bound of the corresponding conversion electrons in percent per disintegration of the hypothesized daughter isotope. The results of these calculations are shown in Table 2.

Table 2

Evaluation of the upper intensity bounds of the lines of different hypothesized daughter isotopes

Hypothesized series	Line chosen for evaluation	Upper intensity bound in percent per disintegration	
		According to our data	According to the data in the literature
Yb $\xrightarrow{75min}$ Tm^{167} $\xrightarrow{9.6d}$ Er^{167} (stable)	L-208 Tm^{167}	2	29
Yb $\xrightarrow{75min}$ Tm^{165} $\xrightarrow{29hr}$ Er^{165} $\xrightarrow{10hr}$ Ho^{165} (stable)	K-243 Tm^{165}	0.2	Prob.> 2
Yb $\xrightarrow{75min}$ Tm^{163} $\xrightarrow{2hr\ 15m}$ Er^{163} $\xrightarrow{75min}$ Ho^{163} $\longrightarrow$ Dy^{163}	L-104 Tm^{163}	0.1	--
Yb $\xrightarrow{75min}$ Tm^{161} $\xrightarrow{45min}$ Er^{161} $\xrightarrow{3.5\ hr}$ Ho^{161} $\xrightarrow{2.5hr}$ Dy^{161} (stable)	L-211 Er^{161}	0.1	--

As will be evident from Table 2, despite the fact that we chose the most intense lines of the hypothesized daughter isotopes, the upper intensity bounds for these lines prove to be very low. In two cases these bounds can be compared with those known from the literature and thus wholly preclude the possibility of the 167 and the 165 mass number assignments for the 75-min ytterbium activity. The 163 and 161 mass number assignments can also be excluded on the basis of the preliminary data on the intensities of the Tm^{163} L-104 and Er^{161} L-211 groups.

Thus of all possible mass numbers there remain only the assignments 164 and 162.

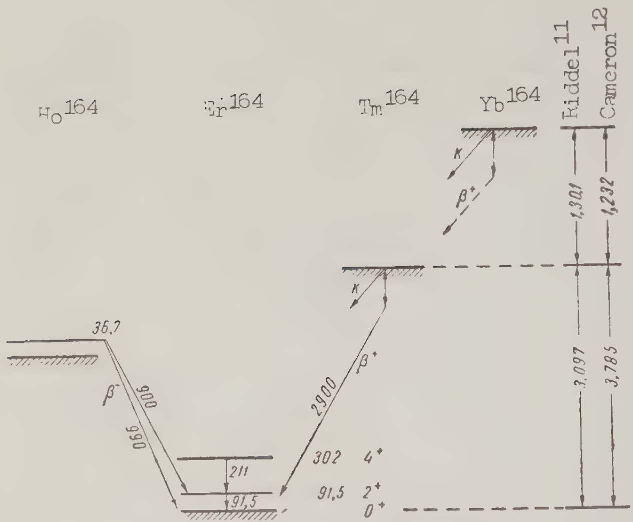

Fig.4. Proposed decay scheme for Yb^{164}.

The inference that the 75-min isotope has an even mass number is supported by the fact that the energy ratio of the two detected γ-transitions is in good agreement with the theoretical ratio for transitions between the first levels (4^+, 2^+, 0^+) of a rotational band based on the ground state, namely, 2.33 (the experimental ratio is 2.3).

The 91.5 ± 0.7 kev transition energy is consistent within the limits of the experimental error with the energy of the transition detected in Er^{164} in β^--decay of Ho^{164}.[5] In connection with this it is probable that the 75-min ytterbium isotope has the mass number 164. A possible decay scheme for this isotope is shown in Fig.4. In this scheme we indicate the empirical mass difference values according to Riddel[11] and Cameron[12].

To check the above inference, the conversion electron spectrum of the ytterbium fraction was studied by means of a β-spectrograph with a uniform magnetic field and photographic recording. Our purpose was to determine the atomic number Z of the nucleus in which the 91.5 kev transition occurs and to obtain a more accurate value of the energy of this transition. Accordingly, the magnetic field of the spectrometer was adjusted so that the photographic plate would record electrons with energies from 10 to 190 kev, i.e., so there would be recorded all the conversion electrons of the 91.5 kev transition. In the preparation of this source the tantalum target was bombarded for 15 min, the chemical separation operation was carried out within 2 hours, the source was prepared within 40 min. The exposure time was 20 hours. The following conversion lines arising in the decay series $Yb^{166} \xrightarrow{56\ min} Tm^{166} \xrightarrow{7.7\ hr} Er^{166}$ (Ref.4) were detected in the spectrogram: Er^{166} K-80.7 + Tm^{166} K-81, Er^{166} (L_I + L_{II})-80.7, Er^{166} L_{III}-80.7, Er^{166} L_{III}-80.7 + + Tm^{166} (L_I + L_{II})-81, Er^{166} M-80.7 + Tm^{166} M-81 and Er^{166} K-184.7. There were also detected the L_I + L_{II}, L_{III} and M lines of the ~91.5 kev transition occurring in the decay of the 75-min ytterbium activity. Other, weaker lines emitted in the decay of Yb^{166} were not detected. Also, unfortunately, we did not succeed in detecting the K line of the 91.5 kev γ-transition. For evaluating the energy of the conversion lines of the 91.5 kev transition by way of references we chose the energies of the Er^{166} (L_I + L_{II})-80.7 and K-184.7 lines which had been measured by Mihelich et al[5]. The resultant data are listed in Table 3.

Inasmuch as the K line of the 91.5 kev transition was not detected, we could not determined the atomic number of the nucleus in which this transition occurs from the K - L_{II} or K - L_{III} difference. We could only compare the experimental energy difference between the L_{II} and L_{III} lines, which is equal to 0.91 kev, with the tabular data: 0.85 for Ho, 0.91 for Er and 0.96 kev for Tm.

It will be evident that the experimental L_{III} - L_{II} difference is in best agreement with the tabular data for Er. Although we do not estimate the accuracy in determining the energies of the conversion lines to be better than 0.1 kev, we assume that the energy difference for such close lines as the L lines of the 91.5 kev transition was determined with sufficient accuracy for us to be able to assert with reasonable certainty that this transition occurs in Er. If this is the case we can readily determine the precise transition energy: it is 91.5 ± 0.1 kev.

Photometric measurements of the ($L_I + L_{II}$) and L_{III} conversion lines of the 91.5 kev γ-transition showed that their intensity ratio is 1.08. This is in good agreement with the theoretical ratio of 1.05 for an E2 transition.

These data again support our inference that the mass number assignment for the 75-min ytterbium activity should be 164.

Table 3

Experimental data on the conversion electron lines associated with the 91.5 kev γ-transition

Line	Electron energy, %	γ-transition energy, kev
$(L_I + L_{II})$-91,5	82,26	(91,5±0,1)
L_{III}-91,5	83,17	(91,5±0,1)
M-91,5	89,99	

Laboratory of Nuclear Problems,
Joint Institute for Nuclear Research &
Central Asian Polytechnic Institute

References

1. W.Nervik & G.Seaborg, Phys.Ref., 97, 1092 (1955).

2. a.v.Kalyamin, I.Yu.Levenberg & V.A.Yakovlev, Atomnaya energiya, 5, 582 (1959). (Trans.Soviet Journal of Atomic Energy.)

3. P.M.Aron, A.V.Kalyamin & V.A.Yakovlev, Izv.AN SSSR, Ser.fiz., 22, 817 (1958). (Trans.Bulletin 22, 811.)

4. B.S.Dzhelepov & L.K.Peker, Skhemy raspada radioaktivnykh yader (Decay schemes of radioactive nuclei), M.-L., 1958.

5. J.W.Mihelich, B.Harmatz & T.H.Handley, Phys.Rev., 108, 989 (1957).

6. K.Ya.Gromov, B.S.Dzhelepov & B.K.Preobrazhenskii, Izv.AN SSSR, Ser.fiz., 21, 918 (1957). (Trans.Bulletin 21, 920.)

7. K.Ya.Gromov, B.S.Dzhelepov, A.G.Dmitriev, V.A.Morozov & K.I.Yakovlev, Present issue of the Bulletin, p.260.

8. I.S.Dniprovskii & G.M.Kolesov, Izv.AN SSSR, Ser.fiz., 22, 935 (1958). (Trans.Bulletin 22, 927.)

9. J.W.Mihelich, B.Harmatz & T.H.Handley, Bull.Amer.Phys.Soc., 3, 358 (1958).

10. A.Abdurazakov, B.S.Dzhelepov, G.Ya.Umarov & I.A.Yutlanlov, Materialy II Soveshchaniya po neitronodifitsitnym izotopam redkikh zemel' (Transactions of the Second Conference on Neutron-Deficient Rare Earth Isotopes), Dubna, 1959.

11. J.Riddel, A Table of Levy's Empirical Atomic Masses, CRP 654, Chalk River, 1957.

12. A.G.W.Cameron, A Revised Semi-Empirical Atomic Masses Formula, CRP 690, Chalk River, 1957.

INVESTIGATION OF THE POSITRON SPECTRA OF NEUTRON-DEFICIENT ISOTOPES

- N.A.Bonch-Osmolovskaya, B.S.Dzhelepov & O.E.Kraft

The present study was concerned with the positron spectra of some neutron-deficient isotopes obtained as a result of bombardment of tantalum targets with fast (680 Mev) protons. The spectra were investigated by means of a triple focusing β-spectrometer[1].

Lutetium

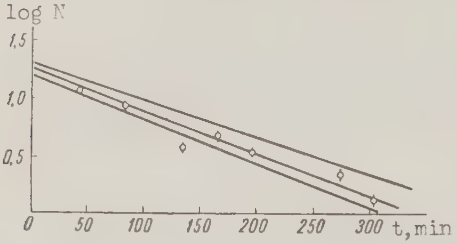

Fig.1. Determination of the period of the Lu β^+-spectrum with 2800 kev end-point energy. T = 85 ± 18 min.

The lutetium was separated from a tantalum target bombarded for 15 min. The measurements were started 2 hours after irradiation and showed that the spectrum is highly complex. The highest energy component had an end-point energy 2800 kev. Observation of the decay of the spectrum showed that all sections in the range above 1500 kev have the same period, namely, 85 ± 18 min. The decay curves for E = 1800 kev are shown in Fig.1.

The large uncertainty in determining the period is explained by the low satistical accuracy of the measurements: the maximum counting rate in this energy region at the beginning of measurement was only 20 pulses per min. The Kurie plot of the high energy β^+-spectrum is shown in Fig.2; it will be apparent that the end-point energy is 2800 ± 200 kev. After subtraction of this component (assuming the Fermi shape) from the total β^+-spectrum of lutetium, we determined on the basis of two series of measurements the period corresponding to the remaining parts of the spectrum (at different positron energies, 200 to 1400 kev). It proved to be 56 ± 12 min. This period is in good agreement with the half-life (55 min) reported for Lu^{167} (Refs.2 & 3).

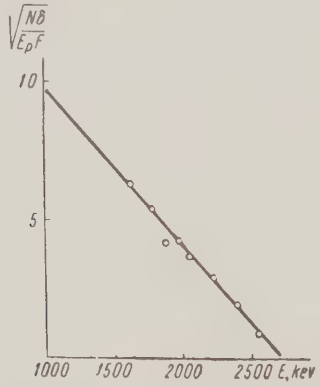

Fig.2

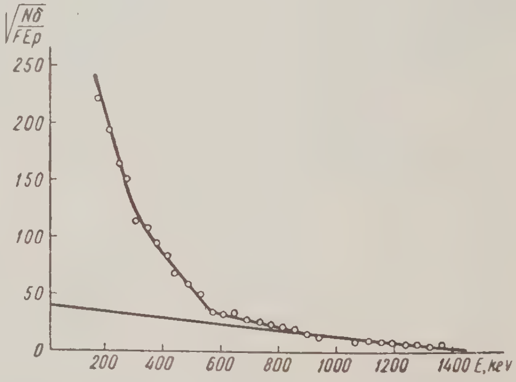

Fig.3

Fig.2. Kurie plot for the high energy part of the β^+-spectrum of Lu with T = 85 min.

Fig.3. Kurie plot for the β^+-spectrum of Lu with T = 56 min.

After determination of the period, the spectrum was processed in the usual manner. Fig.3 shows the Kurie plot; it will be evident that the spectrum is complex. Resolution of the spectrum showed that it consists of at least three components with end-point energies 1530 ± 200, 1110 ± 100 and 600 ± 50 kev and relative intensities 1:1:5. It is known[2] that Lu^{167} gives rise to the following decay series:

$$Lu^{167} \xrightarrow{55\ min} Yb^{167} \xrightarrow{18\ min} Tm^{167} \xrightarrow{9\ d} Er^{167}\ (stable).$$

Hence at present we cannot say definitely whether the observed 55-min β^+-spectrum belongs to Lu^{167} or Yb^{167}. According to the data of Cameron[4], the Yb^{167} - - Tm^{167} mass difference is 1.69 Mev, while the Lu^{167} - Yb^{167} mass difference is 3 Mev. The mass difference according to our data is $\geqslant 1.53 + 1.022 \approx 2.5$ Mev. This value of the disintegration energy would appear to indicate that the 1110 and 1530 kev end-point energy components belong to Lu^{167}. The 600 kev end-point energy component of the β^+-spectrum can be attributed with equal probability to either Lu^{167} or Yb^{167}.

We attempted to evaluate the number of positrons per disintegration for Lu^{167}. A 207 kev L conversion line of Tm^{167}, according to Gromov et al[6], appears in 29% of the decays. Having measured this line on our instrument and determined its area S_{e^-}, we were able, knowing the area occupied by the positron spectrum of Lu^{167}, to evaluate the number of positrons per disintegration. This was found to be 0.5--1%.

Knowing the number of positrons per disintegration and assuming that the entire T = 55 min β^+-spectrum belongs to Lu^{167}, we determined the ft values for the three β^+-components and found $ft = 3 \cdot 10^7$, $1 \cdot 10^7$ and $1.4 \cdot 10^5$ for the 1530, 1110 and 600 kev end-point energy components, respectively.

There remains the question of the assignments for the T = 85 min β^+-spectrum with 2800 kev end-point energy. No lutetium isotope with this half-life is known. Two possible explanations for the presence of this component in the spectrum of the lutetium fraction may be suggested:

1. It is possible that this spectrum belongs to some as yet unknown Lu isotope, for example, Lu^{168}. Then there must be observed γ-rays decaying with the same period. So far, no such γ-rays have been detected.

2. The second possibility is that there was present in the lutetium fraction some ytterbium impurity. It is known[3] that there is a Yb isotope with a close period (T = 75 min) and a β^+-spectrum end-point energy of 2.95 Mev. While, as indicated above, our experimental value for the end-point energy is somewhat different (2.8 Mev), it must be admitted that the uncertainty in determining both the period and the value of the end-point energy is such that one cannot entirely exclude the possibility of an admixture of ytterbium. Thus pending the completion of further experiments the question remains open.

Thulium

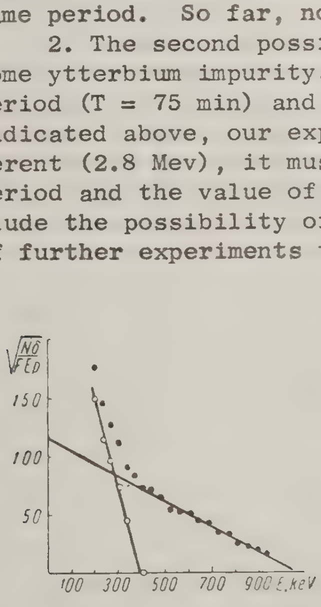

Fig.4. Kurie plot for the β^+-spectrum of Tm with T = = 137 min. o - Kurie plot for the low energy component of the Tm β^+-specimen.

The conditions of bombardment of the Ta target and subsequent separation of the Tm fraction were the same as described above. We detected a positron spectrum with a period of 7.3 hours and an end-point energy of 2.1 Mev, which can be attributed to Tm^{166} (Ref. 6), and a positron spectrum with T = 137 min. Conversion lines with the same period were observed by Mihelich et al[7] in investigating a thulium fraction and were attributed by these authors to Tm^{163}. The Kurie plot of the 137 min β^+-spectrum obtained in the present study is shown in Fig.4, from which it will be evident that the spectrum is complex and consists of two components with end-point energies 1050 ± 80 and 400 ± 50 kev and relative intensities 1:0.7.

According to our experimental data the Tm^{163} -

- Er^{163} mass difference is $\geqslant 1050 + 1022 = 2070$ kev. Levy's empirical formulas yield a value of 2.1 Mev for this mass difference; according to the data of Cameron it is 2.4 Mev.

Erbium

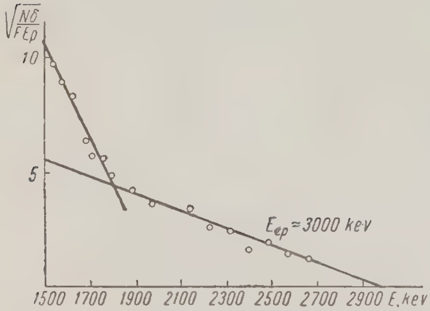

Fig.5. Kurie plot for the high energy part of the β^+-spectrum of the erbium fraction.

Investigation of the positron spectrum of the Er fraction obtained by chromatographic separation of the erbium from the other rare earth elements showed that in addition to the earlier observed[8,9] intense positron radiation with $T \simeq 2.5$ hours and 1300 kev end-point energy, there is a low intensity positron "tail" extending to ~3 Mev. We followed the decay in the intensity of this hard spectrum for 8 hours and found that its period is 115 ± 15 min. After being normalized to this period, the experimental points for five series of measurements fitted a single curve.

The Kurie plot for the high energy β^+-spectrum is shown in Fig.5; it will be evident that the spectrum is complex and consists of two components with end-point energies 1900 ± 100 and 2980 ± 100 kev and relative intensities 5:1. In investigating the electron spectrum of the Er fraction we observed a conversion line with ~900 kev energy and a period of 2 hours. This line was first observed in the work of Dneprovskii[9]. Assuming that this line and the β^+-spectrum with ~3000 kev end-point energy belong to the same isotope, we determined their relative intensities.

To this end the 3000 kev end-point energy β^+-spectrum was extrapolated to the low energy region assuming a Fermi shape. The ratio of the area of this line to the area of the ~900 kev conversion line, $S_{\beta+}/S_{e\text{-}900}$, was found to be 0.5. The β^+-spectrum observed by us may belong to either some erbium isotope or to some daughter holmium isotope. The Er - Ho mass difference according to our data is $\geqslant 4$ Mev; according to the data of Cameron this value may pertain to Er isotopes with mass numbers, 152, 153 or 155. The same Ho - Dy mass difference according to the tables of Cameron may be observed for Ho^{156} or Ho^{158}. Certain considerations set forth by Dneprovskii[9] give reason to think that the 3000 kev end-point energy β^+-spectrum belongs to Ho^{158}. This, however, is only a hypothesis. For a definite isotope assignment one must separate the Ho from the Er and see which component emits the hard β^+-spectrum.

Dysprosium

We started measurements on the dysprosium fraction 3.5 hours after the end of irradiation and 1 hour after separation of the dysprosium from the target. Different parts of the observed β^+-spectrum behaved in different ways.

The intensity of the spectrum in the 1000-2700 kev interval increased. The build-up occurred for a period of 9-10 hours after the time of separation of the dysprosium fraction; thereafter the intensity began to fall off with T = 18 hours. Analysis of this spectrum showed that it is complex and consists of two components with end-point energies 2700 ± 100 and 1650 ± 100 kev and relative intensities of 3:1.

One can advance two hypotheses regarding the origin of this spectrum:

1. The period, end-point energy and shape of the spectrum give reason to assume that this is the β^+-spectrum observed in the investigations of Refs.10 and 12

and attributed to Tb^{154}. If this assumption is correct, then inasmuch as the Tb^{154} β^+-spectrum was observed in the radiation from a dysprosium fraction and increased in intensity with a period of about 3 hours, it might be concluded that there exists the decay series $Dy^{154} \xrightarrow{3hr} Tb^{154} \xrightarrow{18hr} Gd^{154}$.

The following arguments can be adduced against this assumption:

a) Toth & Rasmussen[13] in bombarding targets enriched with different gadolinium isotopes with α-particles observed α-decay of Dy with a period of 13 hours; this was attributed by the authors to Dy^{154} on the basis of analysis of the (α,xn) reactions. According to our data, the period of the dysprosium parent is ~3 hours.

b) If one assumes that the 2700 kev end-point energy β^+-spectrum belongs to Tb^{154}, the Tb^{154} - Gd^{154} mass difference should be $\geqslant 3700$ kev, whereas according to the data of Cameron this mass difference is only 2700 kev.

c) No transition of 123 kev energy was detected in the conversion electron spectrum of the dysprosium spectrum investigated by Basina & Dzhelepov[14]; a transition of this energy could be expected in the decay of Tb^{154} to Gd^{154} (this transition is well known from $Eu^{154} \rightarrow Gd^{154}$ decay and was also observed in $Tb^{154} \rightarrow Gd^{154}$ decay by Henry et al[15]).

2. Toth & Rasmussen[13] observed α-decay of Dy^{152} with a period of 2.5 hours. It may be assumed that the build-up of the β^+-spectrum with a period of ~3 hours, observed in our work, is due to this isotope. The Tb^{152} - Gd^{152} mass difference, according to the data of Cameron, should be 3.3 Mev, which is close to our value for the disintegration energy, namely, 3.7 Mev. Basina & Dzhelepov[14] in investigating their dysprosium fraction on a lens spectrometer detected a 344 kev γ-transition, the intensity of which increased with a period of ~2.5 hours for some 6-8 hours after separation of the fraction and then fell off with a period of 17 ± ± 5 hours. Apparently, this transition belongs to the same Tb isotope as the β^+-spectrum observed by us.

It must be noted that the 344 kev γ-transition was observed in β^--decay of Eu^{152} to Gd^{152}. This is evidence in favor of the assumption that the observed increase in activity is associated with conversion of Dy^{152} to Tb^{152}. Recently Toth et al[17] reported detecting a new terbium isotope, Tb^{152}, which was obtained by the $Eu^{151}(\alpha,3n)$ and $Gd^{152}(p,n)$ reactions on enriched europium isotopes. According to Toth et al, the half-life of Tb^{152} is 18 hours. Thus we have further evidence in favor of the existence of the decay series $Dy^{152} \xrightarrow{3hr} Tb^{152} \xrightarrow{18hr} Gd^{152}$.

In addition to the above mentioned T = 18 hr, 2700 end-point energy β^+-spectrum component, we observed a β^+-spectrum with an end-point energy of ~900 kev and a period of 10 hours. It may be assumed that this β^+-spectrum belongs to Dy^{155}; it was observed in the work of Ref.1.

We desire to thank I.A.Yutlandov and V.M.Khalkin for the chemical separation and K.Ya.Gromov and L.K.Peker for discussion of the results.

Note added in proof. To clarify the origin of the T = 85 ± 18 min high energy component in the β^+-spectrum of the lutetium fraction, the lutetium was again purified to remove ytterbium. The T = 85 min, E_{ep} = 2800 kev β^+-component was not observed in the radiation from the purified lutetium, while the β^+-spectrum with T = 56 min was still evident. Thus it was shown that the 2800 kev end-point energy β^+-spectrum belongs to ytterbium impurity.

References

1. B.S.Dzhelepov & O.E.Kraft, Izv.AN SSSR, Ser.fiz., 20, 318 (1956). (Trans. Bulletin, 20, 293.)

2. P.M.Aron, A.V.Kalyamin, A.N.Murin & V.A.Yakovlev, Ibid., 22, 817 (1958). (Trans.Bulletin 22, 811.)

3. A.V.Kalyamin, I.Yu.Levenberg & V.A.Yakovlev, Atomnaya energiya No.5, 682 (1959). (Trans.Soviet Journ. of Atomic Energy.)

4. A.A.Cameron, A Revised Semi-Empirical Atomic Masses Formula, ACEL, No.433 (1956).

5. K.Ya.Gromov, B.S.Dzhelepov & B.K.Preobrazhenskii, Izv.AN SSSR, Ser.fiz., 21, 918 (1957). (Trans.Bulletin 21, 920.)

6. G.Wilkinson & A.Hicks, Phys.Rev., 75, 1370 (1949).

7. J.Mihelich, B.Harmatz & T.Handley, Bull.Amer.Phys.Soc., 28, 719 (1958).

8. W.Nervik & G.Seaborg, Phys.Rev., 97, 1092 (1955).

9. I.A.Dneprovskii, Materialy II Soveshchnaiya po neitronodefitsitnym izotopam redkikh zemel' (Transactions of the Second Conference on Neutron-Deficient Rare Earth Isotopes), Dubna, 1958.

10. B.S.Dzhelepov, O.E.Kraft, B.K.Preobrazhenskii & G.F.Yushkevich, Izv.AN SSSR, Ser.fiz., 22, 208 (1958). (Trans.Bulletin 22, 205.)

11. N.M.Anton'eva, A.A.Bashilov, B.S.Dzhelepov & B.K.Preobrazhenskii, Doklady AN SSSR, 119, 241 (1958). (Trans.Soviet Physics - Doklady.)

12. G.Wilkinson & H.Hicks, Phys.Rev., 79, 815 (1950).

13. K.Toth & J.Rasmussen, Ibid., 109, 121 (1958).

14. A.S.Basina & B.S.Dzhelepov, Materialy II Soveshchaniya po neitronodefitsitnym izotopam redkikh zemel' (Transaction of the Second Conference on Neutron-Deficient Rare Earth Isotopes), Dubna, 1958.

15. R.Henry, L.Dillman, N.Gove & R.Becker, Phys.Rev., 113, 1090 (1959).

16. D.Strominger, J.Hollander & G.Seaborg, Tables of Isotopes, Revs.Mod.Phys., 30, 585 (1958).

17. K.S.Toth, K.T.Faler & J.O.Rasmussen, Phys.Rev., 115, 158 (1959).

BETA-DECAY OF La^{140}

- B.S.Dzhelepov, B.A.Emel'yanov, K.P.Kupriyanova & Yu.N.Podkopaev

The data on the decay of La^{140} available hitherto was inadequate for making a definitive spin assignment for the ground state of this isotope. In view of this we felt it would be of interest to investigate the possible β-transition from the ground state of La^{140} to the ground state of Ce^{140}.

Accordingly, we recorded the electron emission from La^{140} in the energy range from 1800 to 4000 kev on the new β-spectrometer of the Scientific-Research Physical Institute of Leningrad State University, the β-hodoscope.

The operating principle of this spectrometer is similar to that of the γ-hodoscope[1], with the difference that in this case the electron source is the investigated radioactive material mounted in the spectrometer chamber, rather than a target. A description of the counters, magnets and associated electronic equipment of the γ-hodoscope will be found in Ref.2. Another difference between the hodoscopes is that in the β-hodoscope the plane of the source, passing through the vertical axis of the instrument, is oriented at an angle of 135° to the plane of the first row of counters. The electron source measuring 2 x 36 mm is located at a distance of 110 mm from the vertical axis of the instrument and parallel to it. The use of a narrow source (the fourth point on the electron trajectory) and employment of triple coincidences virtually eliminates all background due to scattered electrons and chance coincidences, which makes it possible to investigate very weak electron groups.

In all we carried out seven series of measurements with different values of the magnetic field H and with different sources: neutron irradiated La_2O_3, La^{140} separated from Ba^{140}, and Ba^{140} in equilibrium with La^{140}. Each series of measurements encompassed a ~1000 kev energy interval, the location of which in the energy scale depended on H. The results of all the series were joined and matched so that

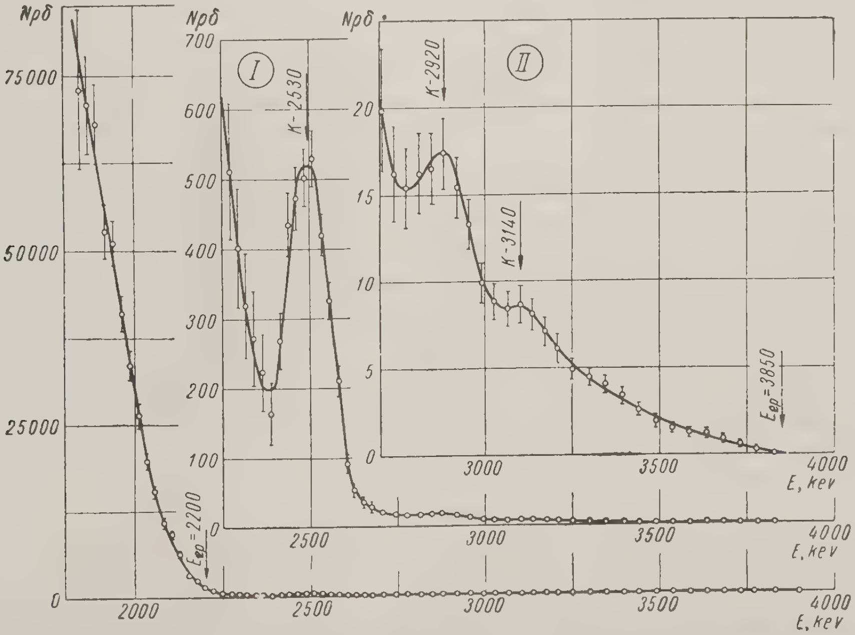

Fig.1. Beta and conversion electron spectrum in the energy range from 1800 to 4000 kev. The experimental results were obtained in the form of histograms; in the figure we show the envelopes. Inserts: I - enlarged 100 X, II - 2500 X.

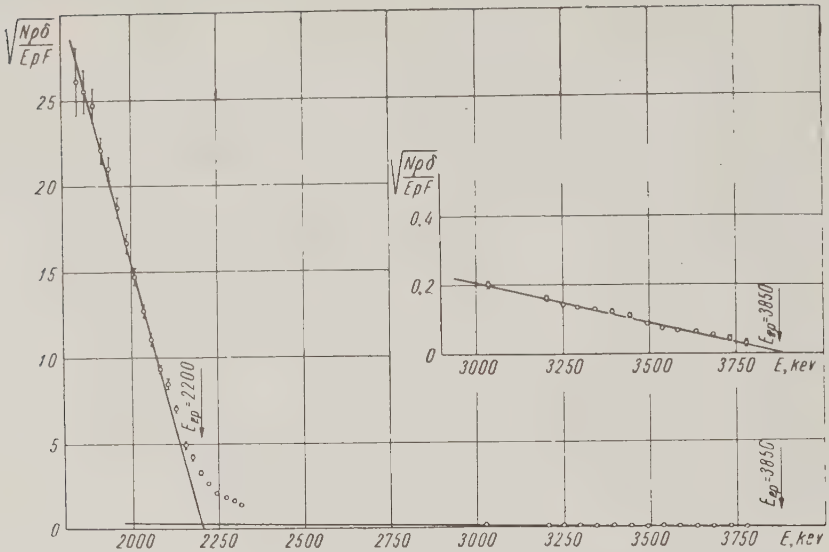

Fig.2. Kurie plot for the La^{140} β^--spectrum in the 1800 to 4000 kev range.

as a result we obtained the electron distribution in the energy range from 1800 to 4000 kev. This is shown in Fig.1.

1. At the left in Fig.1 we show the known[3] section of the La^{140} β-spectrum adjacent to ~2200 kev end-point energy. Our value for the end-point energy E_{ep} is 2200 ± 40 kev.

2. In the 2200 to 3850 kev energy region there is an electron distribution which we identified as the continuous spectrum of a β-transition between the ground states of La^{140} and Ce^{140} and conversion lines of γ-transitions in Ce^{140}.

As determined by extrapolation of the Kurie plot (Fig.2) the end-point energy, E_{ep} = 3850 ± 100 kev coincides within the limits of the experimental error with the mass difference following from the decay scheme given in the literature[4] and agrees with the value of the mass difference given by Riddel.[5] The intensity of the 3850 kev end-point energy β-transition is $(8 \pm 2)\cdot 10^{-4}\%$, assuming the intensity of the 2200 kev end-point energy β-transition to be 10% relative to the number of disintegrations[4] and further assuming that both these spectra have the Fermi shape. The reduced lifetime $ft = 1.4\cdot 10^{14}$ ($\log ft = 14.2$).

From the available data on the parity of the La^{140} and Ce^{140} ground states, the results of investigation of β_{2200}-γ_{1597} angular correlation in the decay of La^{140} and our ft value, it follows that the observed β-transition is thrice forbidden. The most probable spin assignment for the ground state of La^{140} is 3.

3. We detected conversion lines with energies of 2490 ± 30, 2880 ± 30 and 3100 ± 50 kev. The first two were observed earlier[6], the last line was detected for the first time in the present study.

The conversion line intensities and the energies of the corresponding γ-transitions are listed in the accompanying table.

We evaluated the relative line intensities and the numbers of conversion electrons per disintegration by comparing the areas of the lines with the continuous β-spectrum (E_{ep} = 2200 kev) normalized to equal energy intervals.

We computed the conversion coefficients using the intensity values for the 2525 and 2910 kev γ-transitions given by Prikhodtseva & Khol'nov[7]. We obtained

$\alpha_{K\text{-}2530} = 3.4\cdot10^{-4}$ and $\alpha_{K\text{-}2920} = 3.1\cdot10^{-4}$.

Comparison of the experimental coefficients with the theoretical values[8] shows that the 2530 kev γ-transition is M1. It is impossible to make an unambiguous multipole order assignment for the 2920 kev transition on the basis of the available data.

K line energy, kev	γ-transition, kev		Intensity K line referred to β-2200	n_e per 10^5 decays	
	Ref.6	Our data		Ref.6	Our data
2490	2525	2530	$1,2\cdot10^{-4}$	4,24	1,21
2880	2910	2920	$2,2\cdot10^{-6}$	0,013	0,022
3100	—	3140	$6,2\cdot10^{-7}$	—	0,0062

We note that the presence of a K line corresponding to a 3140 kev γ-transition indicates the existence of an excited level with this energy in Ce^{140}. The existence of excited levels at 2920 and 3140 in Ce^{140} is not surprising inasmuch as the La^{140}-Ce^{140} mass difference is approximately 3800 kev.

We desire to thank N.D.Novosil'tseva for providing the sources and L.V.Gustova for assistance in carrying out the measurements.

Scientific-Research Physical Institute,
"A.A.Zhdanov" Leningrad State University

References

1. B.Dzhelepov, Izv.AN SSSR, Ser.fiz., 21, 1580 (1957). (Trans.Bulletin 21, 1569.)
2. O.Chubinskii, Ibid., 21, 1583 (1957). (Trans.Bulletin 21, 1572.)
3. A.Bashilov, B.Dzhelepov & L.Chervinskaya, Ibid., 18, 88 (1954).
4. B.Dzhelepov & L.Peker, Skhemy raspada radioaktivnykh yader (Decay schemes of radioactive nuclei), M.-L., 1958.
5. J.Riddel, A Table of Levy's Empirical Atomic Masses, Chalk River, Reprinted April, 1957.
6. B.Dzhelepov, V.Prikhodtseva & Yu.Khol'nov, Doklady AN SSSR, 121, 995 (1958). (Trans.Soviet Physics - Doklady.)
7. V.Prikhodtseva & Yu.Khol'nov, Izv.AN SSSR, Ser.fiz., 22, 176 (1958). (Trans.Bulletin 22, 173.)
8. I.Band & L.Sliv, Tablitsy koeffitsientov vnutrennei konversii gamma-izlucheniya (Tables of internal conversion coefficients), Part I, K Shell, M.-L., 1956.

INVESTIGATION OF THE GAMMA-RADIATION OF Ag^{110m} IN THE ENERGY RANGE FROM 0.2 TO 2.0 Mev

- N.A.Voinova, B.S.Dzhelepov & N.N.Zhukovskii

Introduction

In 1957 we investigated[1] the γ-radiation from Ag^{110m} by means of an Elotron (magnetic spectrometer utilizing recoil electrons) and determined the relative intensities of 12 γ-lines in the energy range from 650 to 1600 kev. Owing to the relatively strong background in these experiments, the energy ranges below 650 kev and above 1600 kev were not investigated in detail.

Yet in the 400 to 730 kev region, Cork et al[2], working with photographic spectrometers, in addition to the 446, 619, 656 and 680 kev γ-transitions known at that time (1950), reported observing six weak transitions with energies of 438, 441, 499, 541, 575 and 723 kev.

In the energy region above 1600 kev in the γ-spectrum of Ag^{110m} Gustova et al[3] detected six γ-lines: 1760 ± 40, 1910 ± 30, ~2030, ~2090 (?), ~2220 and 2460 ± ± 5 kev with intensities $\leqslant 6 \cdot 10^{-4}$ gammas per disintegration. Capeller & Ganssauge[4] indicate the existence of a 1800 ± 50 kev line with an intensity of $\sim 7 \cdot 10^{-4}$ gammas per disintegration.

I. Experimental Results

We carried out a repeat investigation of the γ-spectrum of Ag^{110m} in the energy region from 0.2 to 2.0 Mev by means of the Elotron under improved conditions, i.e., the same conditions that were employed in investigating[5] the γ-spectrum of Ra in equilibrium with its decay products. In addition, the energy region above 1500 kev was investigated by means of the Ritron under the usual conditions for this instrument.[6]

By way of source we used a neutron activated silver chip weighing ~11 g. At the beginning of the experiments the activity of the source was ~0.9 curie.

The experimental recoil electron spectrum is shown in Fig.1. At the line peaks we indicate their energies according to our calibrations for which the energies of the 656 and 885 kev lines were taken as the references, inasmuch as these have been precisely determined by means of a crystal spectrometer[7]. After subtraction of the background, the experimental curve was resolved into components in accord with the usual instrument line shape.

In the energy range from 440 to 1600 kev we resolved 14 γ-lines, the intensity of which is >1% the intensity of the 656 kev γ-line.

Analysis of the experimental curve (Fig.1,a) obtained on the Elotron gives reason to affirm that in the 300 to 430 and 450 to 600 kev intervals there are lines with intensities >1% and >0.8%, respectively, the intensity of the 656 kev line. We found no evidence of the existence of the 723 (722.6) kev γ-line reported by Cork et al[2]. If this line exists, its intensity cannot exceed 1% the intensity of the 656 kev γ-line. We found no lines with an intensity exceeding 0.3% the intensity of the 656 kev γ-line in the 950 to 1350 kev energy interval.

The experimental curves for the 1600 to 1900 kev region, both those obtained on the Elotron and those obtained by means of the Ritron, definitely indicate that there are no γ-lines in this energy region with intensities exceeding 0.05% the intensity of the 656 kev line. There are virtually no noticeable rises above the background in the higher energy region.

In the first two columns of Table 1 we list our energy and relative intensity values for the 14 observed γ-lines. For purposes of comparison in columns 3 & 4 we list the results of Anton'eva et al[8] obtained by observation of photoelectrons

Table 1

Energies, relative intensities and multipolarities of the γ-transitions in Cd^{110}

Our data		Anton'eva et al[8]		Relative intensities of K conversion lines[9]	Experimental $\alpha_K \cdot 10^3$	Theoretical coefficient $\alpha_K \cdot 10^3$ (Ref. 10)					Multipole assignment
hν, kev	Relative intensities	hν, kev	Relative intensities			E1	E2	E3	M1	M2	
1	2	3	4	5	6	7	8	9	10	11	12
447±2	6±1	447±2	7±1	17	8,1±1,9	2,45	7,91	23,4	7,58	25,7	E2; M1; E2+M1 (E1+M2)
620±2	5±1	618±2	4±1	3,5	1,9±1,0	1,12	3,16	7,75	3,39	9,55	E2; E1+M2
656	100	655±1	100	100	2,76*	—	2,76	—	—	—	E2
680±3	15±2**	677±2	10±1	—	—	—	—	—	—	—	—
		686±2	7±2	8	2,5±0,9	0,93	2,51	6,89	2,76	7,59	E2; M1; E2+M1 (E1+M2)
706±2	18±2	706±2	21±2	16	2,4±0,4	0,85	2,34	5,25	2,57	6,92	E2; M1; E2+M1 (E1+M2)
742±2	5±2	740±2	—	3	1,6±1,2	0,78	2,04	4,57	2,34	6,02	E2; M1; E2+M1 (E1+M2)
764±2	23±2	763±2	24±2	16	2,0±0,3	0,73	1,95	4,26	2,14	5,62	E2; M1; E2+M1 (E1+M2)
818±2	6±1	816±2	10±2	3,7	1,6±0,3	0,63	1,62	3,54	1,86	4,57	E2; M1; E2+M1 (E1+M2)
885	74±4	883±2	71±5	32	1,2±0,1	0,59	1,32	2,88	1,51	3,71	E2; (E1+M2)
936±2	33±2	935±2	34±3	13	1,1±0,1	0,48	1,17	2,46	1,35	3,26	E2; (E1+M2)
1385±2	24±1	384±3	20±2	6,5	0,7±0,1	0,23	0,51	0,96	0,56	1,23	M1; M1+E2 (E1+M2)
1476±3	4±1	1480±5	3,6±1,0	0,8	0,5±0,2	0,21	0,47	0,83	0,49	1,07	E2; M1; E2+M1 (E1+M2)
1506±2	13±1	1506±5	10±1	2,5	0,5±0,1	0,20	0,44	0,80	0,48	1,02	E2; M1; E2+M1 (E1+M2)
1565±2	1,2±0,3	1 —	—	—	—	—	—	—	—	—	—

---

*Value taken from Anton'eva et al[9] and Rohr & Birkhoff[18].

**If we divide the observed intensity in the same proportion as was done in the work of Anton'eva et al[8], then for hν = 677 and 886 kev we obtain 9 and 6, respectively.

on the Ketron. It will be evident that the two sets of values agree within the limits of the experimental error.

Using the relative intensities of the K conversion lines obtained in the work of Anton'eva et al[9] and our relative intensity values, we determined the multipole orders of 12 of the γ-transitions. That the multipole order of the 656 kev γ-transition is E2 is known from direct measurements of α_K (Refs. 8,9,11 & 18) and from determinations of the cross section for Coulomb excitation of the 656 kev level in Cd^{110}, corresponding to a lifetime of $\tau = (5.7 \pm 0.8) \cdot 10^{-12}$ sec for this level[12].

Comparison of our experimental values of α_K with the theoretical values shows that unambiguous E2 assignments can only be made for the two transitions with energies 885 and 936 kev. A mixture of E1 and M2 is little probable inasmuch as it is observed primarily in the case of strongly forbidden E1 transitions and only in the region of strongly deformed nuclei. (The available data on Cd^{110} indicate that this nucleus is not appreciably deformed). Moreover, an E1 + M2 assignment for the 885 and 936 kev transitions would be in conflict with the even parity of the 1541 and 2476 kev levels following from the concomitance of the data decay of Ag^{110m}.

It is impossible at present to make unambiguous multipole order assignments for the other transitions owing to the great uncertainty in the values of the relative intensities of the γ-lines and K conversion lines. It may be asserted, however, that the multipole orders of the other ten γ-transitions are not higher than quadrupole. This inference is substantiated by the fact that no isomeric states with lifetimes

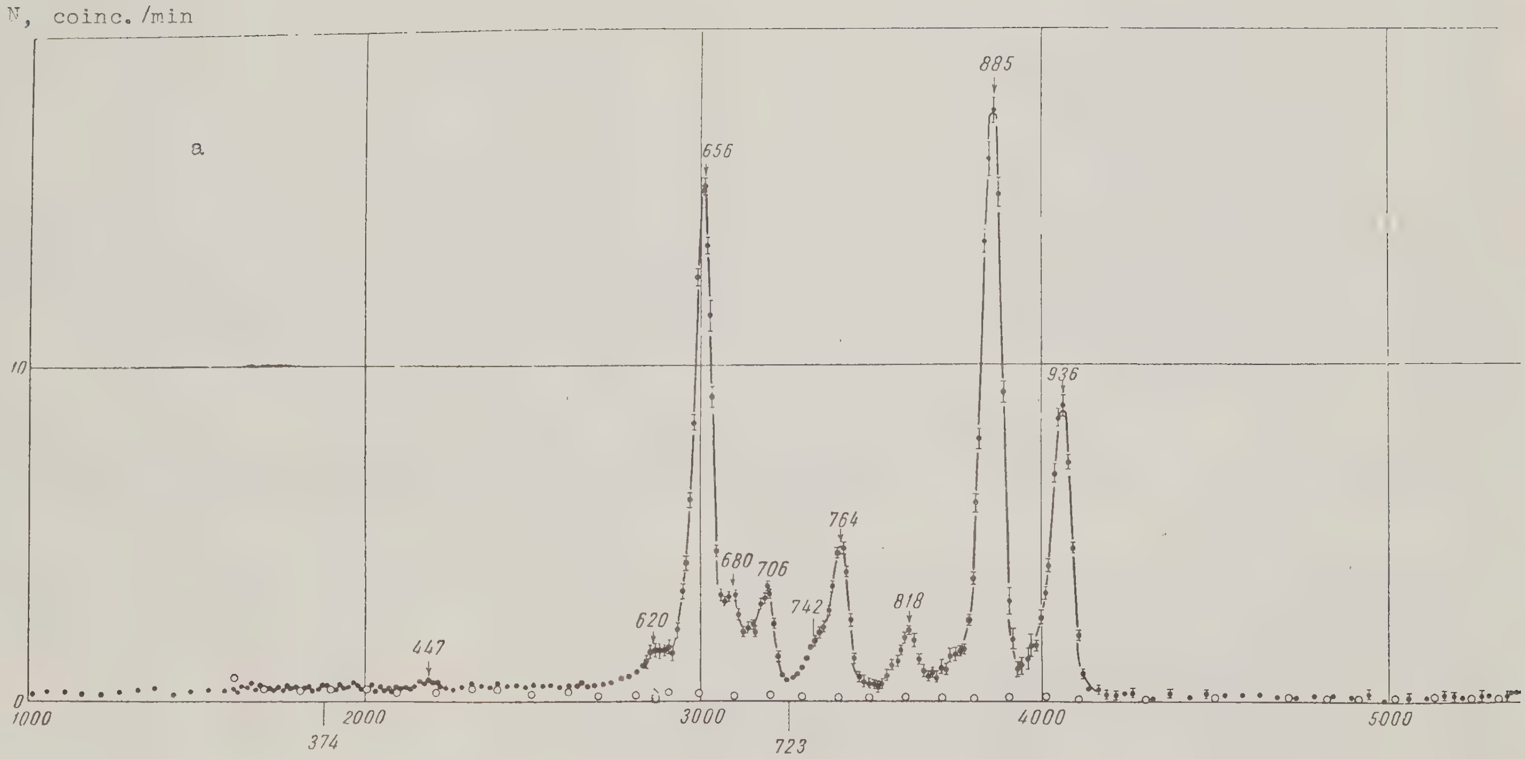

Fig.1. Experimental spectrum of recoil electrons from Ag^{110m} γ-rays: a - recorded on the Elotron using a polystyrene target with a superficial density of 2.34 mg/cm^2, b - recorded on the Ritron with a cellophane target with a superficial density of 6.15 mg/cm^2. Solid points - number of coincidences per min; open circles - background.

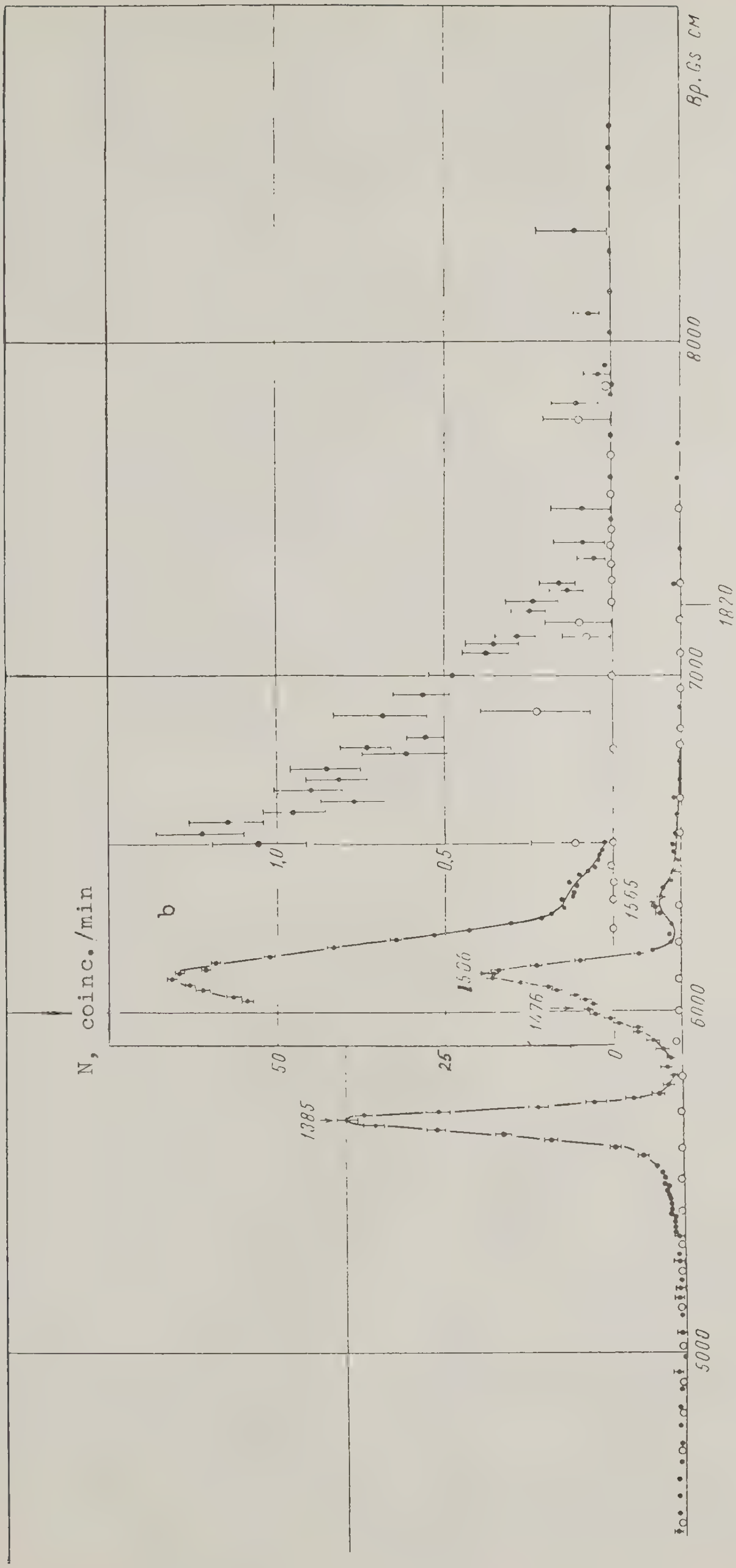

Fig.1, continued.

exceeding $3\cdot10^{-8}$ and $6\cdot10^{-10}$ sec were found in Cd^{110} (reported in Ref.13).

II. On the Decay Schemes for Isobaric Nuclei with A = 110

Since 1956 there have been published several studies[3,4,7,8,12-17,19], the results of which have substantially increased the available information on the decay of Ag^{110m}. These data have enabled us to justify the principal features of the decay scheme for Ag^{110m} and to accomodate in it all the γ-transitions for which the relative intensities are known.

Cd^{110} is the decay product of 253 day Ag^{110m}, 24.5 sec Ag^{110}, 5 hour In^{110m} and 66 min In^{110}. The decay schemes for these nuclei taking into account all the currently available experimental data are shown in Fig.2. In this scheme we have indicated the most probable energies of the β- and γ-transitions and excited levels and the relative intensities of the γ-transitions on the basis of our data. The values of log ft for the β-transitions in Ag^{110m} and Ag^{110} were calculated taking into account the relative intensities of these transitions obtained in the work of Anton'eva et al[8]. The value of log ft for orbital electron capture in In^{110m} to the 2475 kev level in Cd^{110} was calculated on the assumption that there is a direct transition of 120 kev energy[20,21] between In^{110m} and In^{110} (the energy of the transition involved in K capture in In^{110m} to the 2476 kev level in Cd^{110} was assumed to be 1570 kev). The experimentally determined spins of Ag^{110m} and In^{110m} are 6 and 7, respectively[22,23]. These spins, in accord with the "weak" rule of Nordheim[24] correspond to even configurations in which the last neutron and proton are, respectively, in $d_{5/2}$ and $g_{9/2}$ states. Thus, presumably the characteristics of Ag^{110m} and In^{110m} are, respectively 6+ and 7+. It must be noted, however, that the experimental data on the isomeric transitions (see below) in Ag^{110} and In^{110} are in conflict with these spin and parity assignments.

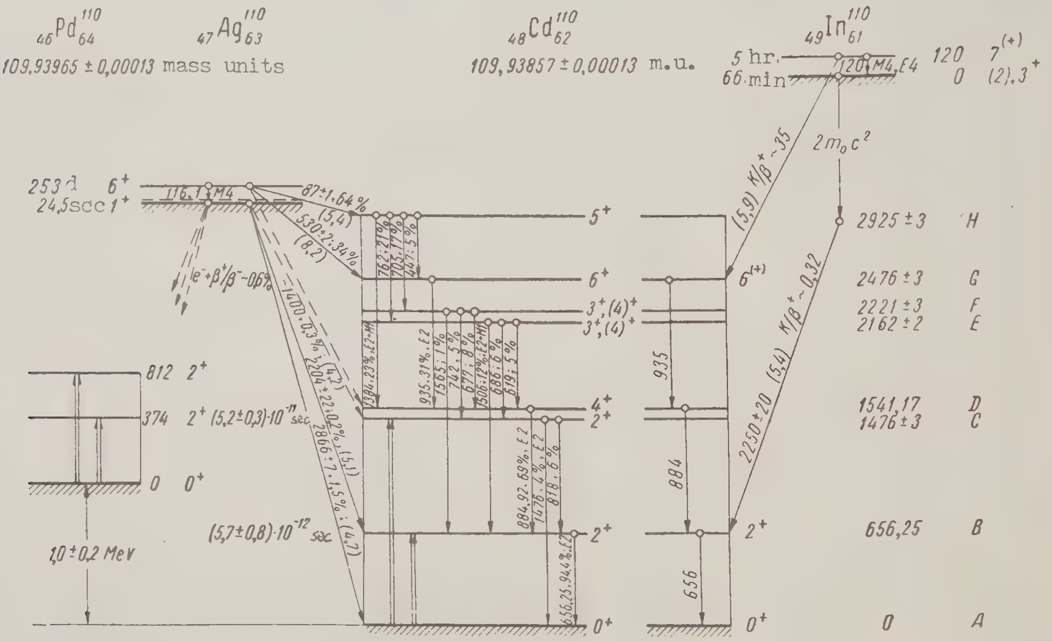

$_{46}Pd^{110}_{64}$
$_{47}Ag^{110}_{63}$
109,93965 ± 0,00013 mass units
$_{48}Cd^{110}_{62}$
109,93857 ± 0,00013 m.u.
$_{49}In^{110}_{61}$
5 hr.
66 min
120 M4,E4
120 $7^{(+)}$
0 (2),3^{+}
253 d 6^{+}
24,5 sec 1^{+}
116,1 M4
87±1,64 % (5,4)
530±2;34 % (8,2)
$e^{-}+\beta^{+}/\beta^{-}$ ~0,6%
1400;0,3%;(4,2)
2204±22;0,2%;(5,1)
2866±7;1,5%;(4,7)
762;21%
705;17%
447;5%
1384;23%;E2+M1
935;31%;E2
1565;1%
742;5%
677;8%
1506;12%;E2+M1
686;6%
619;5%
884,92;69%;E2
1476;4%;E2
818;6%
656,25;94,4%;E2
5^{+}
6^{+}
3^{+},$(4)^{+}$
3^{+},$(4)^{+}$
4^{+}
2^{+}
2^{+}
0^{+}
812 2^{+}
374 2^{+} $(5,2\pm0,3)\cdot10^{-11}$ sec
0 0^{+}
$(5,7\pm0,8)\cdot10^{-12}$ sec
1,0 ± 0,2 MeV
(5,9) K/β^{+} ~35
$2m_0c^2$
K/β^{+} ~0,32
2250±20 (5,4)
935
884
656
$6^{(+)}$
2^{+}
0^{+}
2925 ± 3 H
2476 ± 3 G
2221 ± 3 F
2162 ± 2 E
1541,17 D
1476 ± 3 C
656,25 B
0 A

Fig.2. Decay scheme for isobaric nuclei with A = 110.

1. Spin assignments for the excited levels of Cd^{110}

We assume that like all even-even nuclei Cd^{110} in the ground state has spin and parity 0+.

The assignment for the first excited level of Cd^{110} at 656 kev (level B in Fig.2) is assumed to be 2+. This follows from the data on the cross section for Coulomb excitation of this level[12,25], and from the E2 multipole order assignment for the 656 kev transition[9,11,18].

The next level, level C at 1476, was also obtained in Coulomb excitation of Cd^{110} (Ref.13) and apparently has spin and parity 2+.

From the data on angular correlation[13] of the (γ-1384)-(γ-885) and (γ-935)-(γ-885) cascades there follow the unambiguous spin values I = 5 for level H (2925 kev) and I = 4 for level D (1541 kev). Level G (2476 kev), in accord with the correlation in these cascades, may have I = 4 or 6. The correlation in the (γ-762)-(γ-1506) cascade is not in conflict with I = 3 or 4 for level E (2162 kev).

In view of the fact that the multipole order of the 885 kev and 936 kev γ-transitions is E2, levels D and C must have even parity. Level H must also have even parity inasmuch as the 87 kev end-point energy β-transition in Ag^{110m} (6+) to this level is allowed (log ft = 5.4). The 1384 kev transition between level H (5+) and level D (4+) must be a mixture of E2 + M1.

Of the possible assignments, 4± and 6±, for level G one must give preference to 6+. If the assignment were 4+, the 530 kev end-point energy β-transition would be twice forbidden, but since for it log ft = 8.2, it cannot be more than once forbidden, i.e., the spin of level G must in any case be $\geqslant 5$. Further, in the decay of 5 hour In^{110m} (7+) there is observed only the cascade (γ-935)-(γ-884)-(γ-656). Level H (5+) is not excited in the process: no γ-line at 1384 kev has been observed. No other levels in Cd^{110} with energies above 2476 kev are known, and no transitions with energies above 935 kev are evinced in the conversion electron spectrum[20]. This gives reason to infer that decay of In^{110m} proceeds primarily to level G. Inasmuch as for this decay log ft = 5.9, the decay is allowed and, consequently, the spin of level G cannot be less than 6. The 6- assignment is precluded by the fact that in this case the multipole order of the 935 kev transition would be M2. The experimental value of α_K (Table 1) corresponds to either E2 or E1 + M2.

Thus we conclude that the spin and parity of level G are 6+. In accord with the experimental data, the 935 kev transition departing from this level is E2. It is also understandable why there are no transitions from level G to the lower lying levels except D (4+). The β-transition with E_{ep} = 530 kev in Ag^{110} (6+) to the (6+) level must be allowed. The anomalously high value of log ft for this transition remains unexplained; apparently this transition is a rare case of allowed transitions of the type observed in C^{14} and Cd^{114}.

There have been no γ-γ angular correlation studies for the γ-transitions associated with level F (2221 kev). Nevertheless, the possible multipolarities and intensities of the γ-transitions associated with this level give reason to assert that this level has even parity and spin 3 or 4. Thus there arrives at this level the 705 kev transition from level H (5+); inasmuch as the multipole order of this transition is E2, M1 or E2 + M1, the possible assignments for level F may be 3+, 4+, 5+, 6+ or 7+. From level F there are relatively intense γ-transitions to levels D (4+), C (2+) and B (2+), the multipole orders of which are not greater than E2. Consequently, the assignments 5+, 6+ and 7+ are excluded and there remain only 3+ or 4+. These assignments are consistent with the fact that no β-transitions to level F are observed in the β-spectrum of Ag^{110m}.

2. Intensity balances for the excited levels of Cd^{110}

Check of the transitions for which relative intensities are known shows generally satisfactory balances for the levels of Cd^{110}. On the average the discrepancy between the transitions arriving and departing from a given level is less than 5%. The greatest divergence (~9%) is observed for levels F and G. In the case of level F one might question the location of the 677 kev transition, but there is no other way of accommodating this transition without introducing additional levels. It should be noted, moreover, that this transition was observed only in one investigation[8].

For level G the discrepancy between arriving and departing transitions is probably due to errors in evaluating the relative intensities of the β-components with end-point energies 87 and 530 kev.

3. Isomeric transition in Ag^{110}

In view of the allowed character of the 2886 and 2204 kev β-transitions in Ag^{110} (the log ft values are 4.7 and 5.1, respectively) and the fact that the first β^--transition does not yield β-γ coincidences[26] and that consequently it goes to the ground state of Cd^{110}, we infer that the spin and parity of the ground state of Ag^{110} must be 1+.

Since the assignment for Ag^{110m} is 6+, the isomeric transition $Ag^{110m} \rightarrow Ag^{110}$ must occur with $\Delta I = 5$ and no change in parity.

In the conversion electron spectrum of Ag^{110m} there was observed only one group of lines corresponding to a transition of 116.1 kev energy[14,16,27] and belonging to Ag; from the most reliable experimental value of K/L, namely, 2.1 ± 0.1 (Ref.27) (the theoretical values of K/L are 1.2 for E3, 3.58 for M3, 0.57 for E4, 2.09 for M4, 0.245 for E5 and 1.16 for M5 - Ref.10), the fact that the half-life of Ag^{110m} is 253 days, and the relative intensity of the isomeric transition, namely, 2-5% of the disintegrations of Ag^{110m} (Refs.9, 11 & 26), it may be inferred that the multipole order of the 116.1 kev transition must be M4. This means that the $Ag^{110m} \rightarrow Ag^{110}$ transition must be characterized by $\Delta I = 4$ (yes). Thus the spin assignments for Ag^{110m} and Ag^{110} and the multipole order assignment for the 116.1 kev γ-transition lead to conflicting results.

This conflict can be resolved only if we hypothesize that between Ag^{110} and Ag^{110m} there is an intermediate level that serves as the arrival level for the 116.1 kev transition. This level must have spin and parity 2- and must de-excite by an E1 transition in cascade with the 116.1 kev transition.

An indirect indication that there may exist such an intermediate level is furnished by the fact that the Ag^{110m} - Cd^{110} energy difference derived from the data pertaining to the isomeric branch is less than the corresponding value deduced from the data on the β-decay branch of Ag^{110m}. Thus, on the assumption that there occurs a transition of 116.1 kev energy between Ag^{110m} and Ag^{110}, the Ag^{110m} - Cd^{110} energy difference equals 116.1 + 2866 = 2985 ± 7 kev. On the other hand, on the basis of the (β-87)—(γ-1384)—(γ-885)—(γ-656) and (β-530)—(γ-935)—(γ-885)—(γ-656) cascades there are obtained the mass differences 3012 ± 5 and 3006 ± 5 kev, respectively.

The discrepancy amounting to 20-30 kev is substantially greater than the total uncertainty (±12 kev) in determining the β- and γ-transition energies. It is possible therefore that there exists a 20-30 kev γ-transition following the 116.1 kev transition. A transition of this energy is obviously difficult to detect against the background of the K x-radiation from Ag and Cd. There is only one reference[28] in the literature to a ~20 kev line in the γ-spectrum of Ag^{110}.

4. Isomeric transition in In^{110}

The radiation from 66 min In^{110} consists only of a β^+-transition with E_{ep} = 2250 ± 20 kev and a γ-transition of 656 kev energy; the transitions are in coincidence[20]. It is natural to assume that the β^+-transition feeds level B (2+). his β^+-transition is apparently allowed (log $ft = 5.4$); consequently, the assignents for 66 min In^{110} may be 2+ or 3+ (the assignment 1+ is excluded, inasmuch as n this case there should be observed a β^+-transition to the ground state of Cd^{110} vith an intensity not inferior to that of the β^+-transition with E_{ep} = 2250 kev).

In the conversion electron spectrum of 5 hour In^{110} (7+) there were observed[20] wo lines which may be identified as the K and L lines of a 119-121 kev γ-transiion[20,21]. The accuracy with which the energy difference between these lines is nown is inadequate for definitely determining Z of the decaying nucleus. McGinis[21] and Bleuler et al[20] assumed that this is the isomeric transition $In^{110m} \rightarrow In^{110}$. If this is the only isomeric transition, it must occur with change of spin: 7+ → (2+ or 3+), i.e., must have a multipole order not less than E4.

The K/L ratio for the 120 kev transition is 4.5 ± 1 (Ref.20) and the partial eriod based on the intensity ratio of the 120 and 656 kev conversion lines is $\approx 4 \cdot 10^5 - 6 \cdot 10^6$ sec (Refs.20 & 21). Comparison of the experimental and theoretial (Table 2) values of K/L and T shows that the multipole order assignment for he ~120 kev transition cannot be made unambiguously. The experimental value of /L is closest to the theoretical values for E2, M2 and M3; even with the most avorable assignment (M3), however, the half-life of this isomer cannot be greater han 20 sec.

Table 2

Theoretical values of K/L and T for the ~120 kev γ-transition in In^{110}

	E1	M1	E2	M2	E3	M3	E4	M4	E5	M5
K/L	8,0	7,9	4,1	5,8	1,4	3,4	0,49	1,9	0,25	1,1
$T_{1/2}$, sec	$1 \cdot 10^{-13}$	$1 \cdot 10^{-11}$	$3 \cdot 10^{-5}$	1.10^{-5}	1,5	20	$1 \cdot 10^{4}$	$7 \cdot 10^{7}$	$9 \cdot 10^{14}$	$4 \cdot 10^{14}$

On the basis of the period, the isomeric transition should be classed as E4 r M4, but in this case there is a great divergence between the theoretical and xperimental values of K/L. It is possible that the experimental value of K/L omprises a greater error than estimated by Bleuler et al[20]. In view of the even arity of In^{110m} and In^{110} one should favor the E4 assignment for this transition. hen the spin and parity of In^{110} should be 3+. It is not impossible, however, hat the ~120 kev transition departs from some level in Cd^{110}. Then the experiental value of K/L agrees within the limits of the experimental error with the heoretical values for multipole orders E2 + M1 or M3, and the lifetime of this evel can be much shorter than 5 hours, i.e., of the order of seconds or fractions f a second.

5. Possibility of β^+-decay and orbital electron capture in Ag^{110m} and Ag^{110}

Two stable isobars with A = 110 are known, namely, Pd^{110} and Cd^{110}; naturally, here arises the question of possible conversion of Ag^{110m} and Ag^{110}, in addition o β^--decay, by β^+-decay and orbital electron capture.

According to mass spectroscopic measurements[29,30], the mass difference beween Pd^{110} and Cd^{110} equals 1.0 ± 0.2 Mev. On the other hand, it follows from the data on β^--decay of Ag^{110m} and Ag^{110} that the mass differences Ag^{110m} - Cd^{110} and Ag^{110} - Cd^{110} are 3.009 ± 0.005 and 2.985 ± 0.007 kev, respectively. Consequently, the mass difference between the two isomers of Ag^{110} and Pd^{110} is ~2 Mev, i.e., conversion of Ag^{110m} and Ag^{110} to Pd^{110} by β^+-decay and orbital electron capture is feasible from the energy standpoint.

In even-even Pd^{110}, which in the ground state has spin and parity 0+, there are known to be two excited levels with 2+, located at 374 (Refs.12,24 & 31) and 812 kev (Ref.24). Decay of Ag^{110m} to these levels of Pd^{110} must be strongly forbidden owing to the great change in spin, inasmuch as the spin of Ag^{110} is 6. In contrast, decay of Ag^{110} to the ground state and the 374 and 812 kev excited state of Pd^{110} must be allowed inasmuch as the spin and parity of Ag^{110} are 1+. In the process there should appear γ-rays with energies of 374 and 438 kev and β^+-transitions with end-point energies of ~850, ~470 and ~30 kev.

On the assumption that the transitions of Ag^{110} to the levels of Pd^{110} are allowed, the total function $f_1 = 14.3$. At the same time, in the β^--spectrum of Ag^{110} there are three known β^--transitions to levels of Cd^{110}: 0 (0+), 656 (2+) and 1476 (2+) kev with end-point energies of 2866, 2204 and ~1400 kev, respectively.

In view of the spins and parities of the excited levels fed by these β-transitions, all these β^--groups should be allowed. In this case the total function $f_2 =$ $= 2.25\cdot10^3$. Consequently, the Ag$^{110}\!\rightarrow$Pd^{110} transitions should account for $f_1/(f_1 + f_2) = 14.3/(2.25\cdot10^3 + 14.3) \approx 0.6\%$ of the disintegrations of Ag^{110}. More than half these decays involve transitions to the ground state of Pd^{110}, and the intensity of the 374 kev γ-rays which appear in β^+-decay and orbital electron capture in Ag^{110} to the 374 and 812 kev levels, should not exceed 2% the intensity of the 656 kev γ-transition in the decay of Ag^{110}.

In the case of decay of Ag^{110m} in which the isomeric transition accounts for 2-5% of the disintegrations, the intensity of the 374 kev γ-line should amount to not more than 0.03% the intensity of the 656 kev line. In view of this relatively low probability for Ag$^{110}\!\rightarrow$Pd^{110} transitions, they should be very difficult to detect. Direct investigation of the β^+- and γ-spectra of Ag^{110} is hampered by the short half-life of Ag^{110} (24.5 sec). Detection of the conversion lines associated with γ-transitions in Pd^{110} in investigating the β^--spectrum of Ag^{110m} is impossible owing to superposition of the intense β^--spectrum of the silver isomer.

The first attempt to detect x-rays associated with orbital electron capture in Ag^{110m} was made by Deutsch[32]. This author failed to detect any x-rays in the γ-radiation from Ag^{110m} and came to the conclusion that K capture cannot amount to more than 3% referred to the total number of disintegrations. Emmerich & Kurbatov[33] searched for positron tracks in a Wilson cloud chamber and as a result of their experiments set an upper bound of $2\cdot10^{-3}$ for the ratio β^+/β^-.

Convincing results indicating the absence of any appreciable number of positrons in the radiation from Ag^{110m} were obtained by Mims & Halbap[34]. The Ag^{110m} source was mounted between two crystals 65 cm apart. There were recorded coincidences between pulses induced in the crystals by annihilation γ-radiation. The conditions of the experiment virtually excluded the possibility of detecting Ag^{110} cascade γ-rays. On the basis of the experimental data, Mims & Halbap give $(\beta^+ + + e^+)/\beta^- = (4.8 \pm 1.0)\cdot10^{-4}$. The results of Emmerich & Kurbatov and Mims & Halbap are in good agreement with the ratio $\beta^+/\beta^- \approx 3\cdot10^{-4}$ adduced above.

We made a search for a 374 kev γ-line which could be connected with the Ag$^{110}\!\rightarrow$Pd^{110} transition; analysis of the experimental results showed, however, that if this line does exist its intensity is <1% the intensity of the 656 kev γ-line. In our experiments it was difficult to observe the 438 kev line owing to surposition of the 447 kev line belonging to Cd^{110}.

We desire to thank V.P.Prikhodtseva and Yu.V.Khol'nov for making it feasible for us to investigate the 1.5 to 2.0 Mev section of the Ag^{110m} γ-spectrum on the Ritron.

"V.G.Khlopin" Radium Institute,
Academy of Sciences of the USSR

References

1. B.Dzhelepov, N.Zhukovskii & Yu.Kondakov, Izv.AN SSSR, Ser.fiz., 21, 973 (1957). (Trans.Bulletin,21, 975); B.Dzhelepov & N.Zhukovskii, Nucl.Phys.,6,665 (1958).
2. J.Cork, W.Rutledge, C.Branyan, A.Stoddard, W.Childs & J.LeBlanc, Phys.Rev., 80, 286 (1950).
3. L.Bustova, L.Timofeeva & O.Chubinskii, Zhur.eksp.i teor.fiz., 35, 1317 (1958) (Trans.Soviet Physics - JETP.)
4. U.Cappeller & E.Ganssuage, Z.Phys., 153, 592 (1959).
5. B.Dzhelepov, N.Zhukovskii, S.Shestopalova & I.Uchevatkin, Izv.AN SSSR, Ser. fiz., 22, 841 (1958) (Trans.Bulletin 22, 835); B.Dzhelepov, N.Zhukovskii, S.Shestopalova & I.Uchevatkin, Nucl.Phys., 8, 250 (1958).
6. B.Dzhelepov, V.Prikhodtseva, A.Feoktistov & Yu.Khol'nov, Izv.AN SSSR, Ser. fiz., 20, 1361 (1956). (Trans.Bulletin, 20, 1245; also see Bulletin,18, 285.)
7. P.Marmier, Nucl.Sci.Abstrs. 11, 350 (1957).
8. N.Anton'eva, A.Bashilov & E.Kulakovskii, Zhur.eksp.i teor.fiz., 37, 1497 (1959). (Trans.Soviet Physics - JETP.)
9. N.Anton'eva, A.Bashilov & B.Dzhelepov, Doklady AN SSSR, 77, 41 (1950).
10. L.Sliv & I.Band. Tablitsy koeffitsientov vnutrennei konversii (Tables of internal conversion coefficients) Part I, K Shell, M.-L., 1956.
11. K.Siegbahn, Phys.Rev., 77, 233 (1950).
12. G.Temmer & M.Heydenburg, Phys.Rev., 104, 967 (1956).
13. H.Taylor & W.Friskin, Phys.Rev., 114, 127 (1959).
14. M.Sakai, H.Omura & T.Momota, J.Phys.Soc.Japan, 12, 985 (1957).
15. E.Boschitz, Z.Phys., 154, 90 (1959).
16. H.Taylor & S.Scott, Phys.Rev., 114, 121 (1959).
17. A.Knipper, Proc.Phys.Soc., 71, 77 (1958).
18. K.Rohr & R.Birkhoff, Phys.Rev., 98, 1266 (1955).
19. E.Funk, Jr. & M.Wiedenbeck, Phys.Rev., 112, 1247 (1958).
20. E.Bleuler, J.Blue, S.Chowdary, A.Johnson & D.Tendam, Phys.Rev., 90, 464 (1953).
21. C.McGinnis, Phys.Rev., 81, 734 (1951).
22. W.Ewbank, W.Nierenberg, H.Shugart & H.Silsbec, Phys.Rev., 110, 595 (1958).
23. L.Marino, W.Ewbank, W.Nierenberg, H.Shugart & H.Silsbec, Phys.Rev., 111, 286 (1958).
24. L.Nordheim, Revs.Mod.Phys., 23, 322 (1951).
25. P.Stelson & F.McGowen, Phys.Rev., 110, 489 (1958).
26. R.Thomas,Jr., W.Whittaker & C.Peacock, BAPS, 1, 2, 86 (1956); Nucl.Sci. Abstrs., 10, 24 B, 70 (1956).
27. A.Bashilov, Nucl.Phys., 1, 629 (1956/57).
28. Yu Fu-Chung, Cheng Lin-Sheng & J.Kurbatov, Phys.Rev., 75, 1287 (1949).
29. R.Halsted, Phys.Rev., 88, 666 (1952).
30. H.Dackworth, Progr.Nucl.Phys., 6, 138 (1957).
31. H.Mark, C.McClelland & G.Goodman, Phys.Rev., 98, 1245 (1955).
32. M.Deutsch, Phys.Rev., 72, 527 (1947).
33. W.Emmerich & J.Kurbatov, Phys.Rev., 75, 1446 (1949).
34. W.Mims & H.Halbap, Proc.Phys.Soc. (London), 64, 311 (1951).

GAMMA-SPECTRUM OF $Eu^{152,154}$ IN THE 245 TO 500 AND 1450 TO 200 kev ENERGY INTERVALS

- B.S.Dzhelepov & Yu.V.Khol'nov

The complex γ-spectrum of Eu^{152} and Eu^{154} has been the subject of numerous investigations carried out both with sources consisting of a mixture of these two isotopes and with sources enriched in one of them. A detailed review of the studies published up to 1958 will be found in Zhukovskii's thesis[1].

We carried out an investigation of the 245 to 500 and 1450 to 2000 kev intervals of the γ-spectrum of these isotopes by means of a magnetic γ-spectrometer utilizing recoil electrons - the Ritron[2]. The source was a mixture of Eu^{152} and Eu^{154} with a total activity of ~800 mC.

The same mixture had been used earlier[1,3,4] in investigating the γ-spectrum of $Eu^{152,154}$. Using the data of Zhukovskii[1] on the numbers of 1280 (Eu^{154}) and 1411 (Eu^{152}) kev gammas per disintegration, we evaluated the Eu^{154} to Eu^{152} activity ratio and obtained a value of 0.21 ± 0.03.

The results of our experiments are shown in Figs.1 & 2 (background subtracted) and in the accompanying table, wherein the values have been corrected for absorption in the source and the instrument window and also for the spectral sensitivity of the instrument[2].

$Eu^{152,154}$ γ-ray energies and relative intensities

Our data		Zhukovskii		Nathan & Hultberg	
E_γ, keV	γ	E_γ, keV	I_γ	E_γ, keV	I_γ
245	35±4	—	—	—	—
344	100	344	100	344	100
415±4	10,1±2	440	19±5	411	8±2
450±4	11,4±2			444	17±2
496±10	2,6±1	—	—	—	—
(1480)	(2,3)	—	—	—	—
1526±15	1,2±0,3	—	—	—	—
1610±7	1,6±0,2	—	—	—	—

The 245 kev γ-line (Fig.1) is complex; it consists of two unresolved lines: 244.7 kev (Eu^{152}) and 248 kev (Eu^{154}). The principal contribution to this peak is from Eu^{152}. This follows from the work of Bobykin & Novik[6] who investigated the conversion electron spectrum of a similar Eu^{152} + Eu^{154} mixture. The intensity ratio of the L lines of the 245 kev (Eu^{152}) and 248 kev (Eu^{154}) transitions is 21.1 : 5.9. Both transitions are E2. If we take into account the small difference between the L shell conversion coefficients of these transitions (α_L = 0.0212 and 0.0228, respectively), we find that the contribution of the Eu^{152} γ-rays to this peak is approximately 3.8 times higher than the contribution of Eu^{154} γ-rays.

The 344 kev γ-line was used as the reference line in the present and earlier investigations.

The 440 kev γ-line was observed in the spectrum of $Eu^{152,154}$ earlier by Zhukovskii[1]. At the same time, in the work of Bobykin & Novik[6] there were observed conversion lines due to transitions of 411.23 and 444.23 kev energy. Gamma-rays of these energies were also detected by Nathan & Hultberg[5] in observing photoelectrons from a source enriched with Eu^{152}. Zhukovskii did not succeed in resolving the 411 and 444 kev lines, apparently owing to inadequate systematic accuracy of the measurements in this energy region; hence the relative intensity given by Zhukovskii for his 440 kev line is the total intensity of the two lines. Our data are in good agreement with the data of Zhukovskii. We believe that the divergence between our data and the data of Nathan & Hultberg[5] regarding the in-

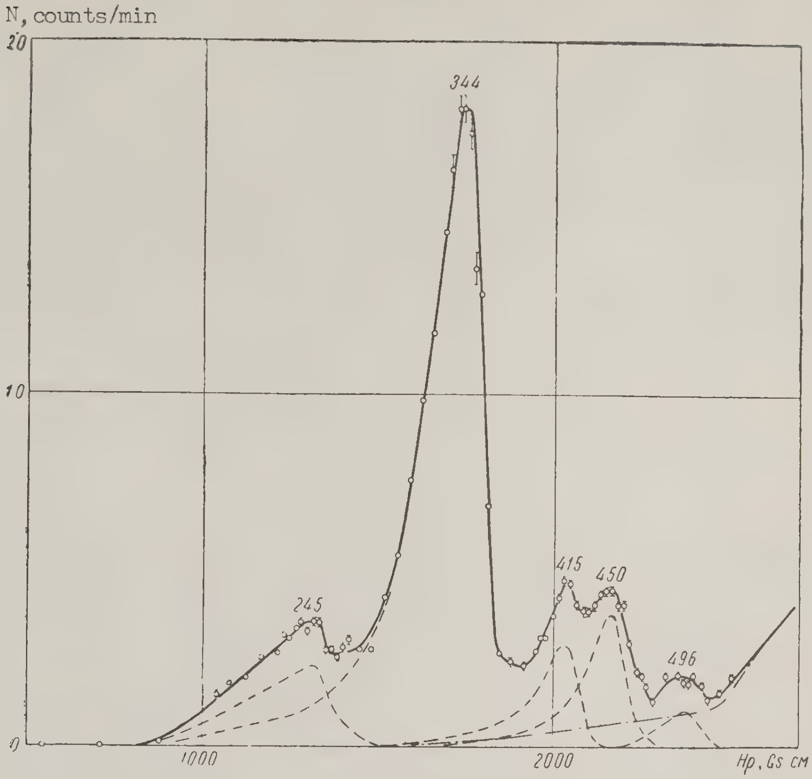

Fig.1. Recoil electron spectrum due to $Eu^{152,154}$ γ-rays with energies from 245 to 500 kev. The dashed line indicates the resolution of the spectrum into components; the dash-dot line denotes the low energy tail of harder lines.

tensity of the 444 kev line can be explained by the fact that in the work of Nathan & Hultberg the photoelectron lines were observed against a strong recoil electron background and the K-444 line was not separated from the intense L-344 line.

The 496 ± 10 kev γ-line was not observed earlier. The corresponding transition can be inserted in the decay scheme between the levels at 1577 and 1088 kev (in this case the transition energy is 489 kev) or, possibly between the 1533 and 1050 kev levels (transition energy - 483 kev) of Eu^{152} (Fig.2,b). There is no other possibility of accomodating this transition in the decay schemes for Eu^{152} and Eu^{154} (Fig.2, b & c).

In view of the fact that the Eu^{152} - Gd^{152} and Eu^{152} - Sm^{152} mass differences are about 1800 kev and the Eu^{154} - Gd^{154} mass difference is about 2000 kev, while the highest energy radiation detected on magnetic spectrometers was the 1411 kev γ-rays, we made a detailed investigation of the section of the spectrum from 1450 to 2000 kev. The results are shown in Fig.2,a. The high energy side of the intense 1411 kev line (it is not shown in Fig.2,a; its height corresponds to 82 pulses/min) is indicated by the dashed line. To determine this contour we made a special study of the high energy tail of the "pure" Co^{60} 1331 kev γ-line. It will be evident from Fig.2,a that the experimental points lie appreciably higher than the tail. After subtraction of the tail from the experimental curve, the remainder was resolved into components using standard line shapes (light solid lines). One can readily distinguish γ-lines of 1610 ± 7 and 1526 ± 15 kev energy.

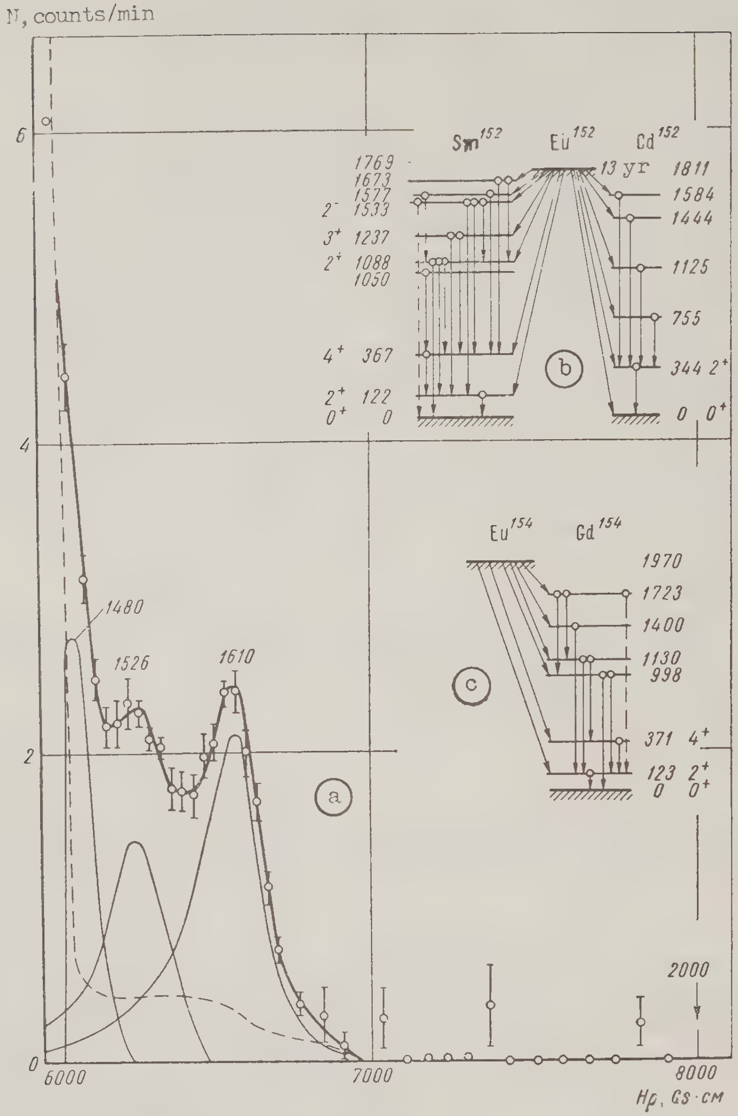

Fig.2,a - Spectrum of recoil electrons due to γ-rays with energies from 1450 to 2000 kev. Dashed line - high energy side of the 1411 kev line; light solid lines - resolution of the spectrum into components; heavy solid line - integral spectrum after subtraction of background. b - decay scheme for Eu^{152} (Ref.1), c - decay scheme for Eu^{154} (Ref.1).

Hitherto a 1600 kev γ-line was observed only by Juliano & Stephens[7] who investigated the γ-spectrum of Eu^{154} on a scintillation spectrometer. Juliano & Stephens do not show the ~1.6 Mev peak in their figures and give its intensity only approximately; hence it is difficult to evaluate the reliability of their results. In addition to the observation of Juliano & Stephens, further evidence that this transition occurs in Gd^{154} is the presence of levels at 1723 and 123 kev in Gd^{154} (1723 - 123 = 1600 kev). Moreover this transition cannot be inserted between any of the known levels of Sm^{152} and Gd^{152} (Fig.2,b).

The 1526 ± 15 kev γ-rays were not observed earlier. These γ-rays may correspond to a cross-over transition from the 1533 (2-) level to the ground level (0+) of Sm^{152} (Fig.2,b).

After subtraction of the 1526 and 1610 kev γ-lines and the tail of the 1411 kev line from the experimental curve, there still remains a certain excess of recoil electrons in the 1450 to 1490 kev region. This section of the spectrum, however, lies in the region of the steep high energy side of the 1411 kev line; hence one cannot unequivocally assert that there exist ~1480 kev γ-rays.

In the 1670 to 2000 kev interval we detected no γ-rays with intensities exceeding 0.1 in the units of the table ($I_{\gamma-344} = 100$).

We take this opportunity to thank students A.Ushakova and V.Rumyantsev for assistance in carrying out the measurements.

"V.G.Khlopin" Radium Institute,
Academy of Sciences of the USSR

References

1. N.N.Zhukovskii, Thesis, Radium Institute, Leningrad, 1958.

2. B.S.Dzhelepov, N.N.Zhukovskii & Yu.V.Khol'nov, Izv.AN SSSR, Ser.fiz., 18, 599 (1954), (Trans.Bulletin,18, 285); B.S.Dzhelepov, V.P.Prikhodtseva, A.I.Feoktistov & Yu.V.Khol'nov, Ibid., 20, 1361 (1956), (Trans.Bulletin,20, 1245); I.B.Golovanov, B.S.Dzhelepov, L.S.Lebedev, V.P.Prikhodtseva & Yu.V.Khol'nov, Ibid., 21, 985 (1957), (Trans.Bulletin,21, 987.)

3. B.S.Dzhelepov, N.N.Zhukovskii, V.G.Nedovsevo & G.E.Shchukin, Ibiz., 21, 966 (1957). (Trans.Bulletin,21, 968.)

4. B.S.Dzhelepov & N.N.Zhukovskii, Nucl.Phys., 6, 655 (1958).

5. O.Nathan & S.Hultberg, Nucl.Phys., 10, 118 (1959).

6. B.V.Bobykin & K.Novik, Izv.AN SSSR, Ser.fiz., 21, 1556 (1957). (Trans. Bulletin, 21, 1546.)

7. J.O.Juliano & F.S.Stephens, Phys.Rev., 108, 341 (1957).

RESONANCE FLUORESCENCE IN Ce^{140} EXCITED BY La^{140} GAMMA-RAYS

- B.S.Dzhelepov & M.A.Dolgoborodova

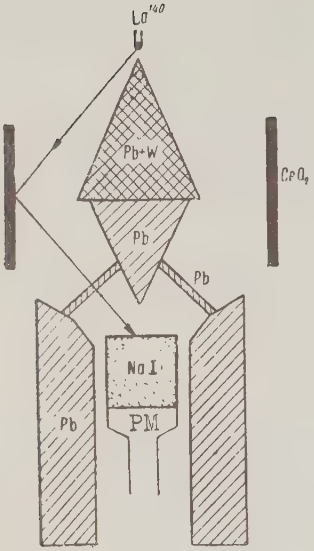

Fig.1. Experimental arrangement for investigation of resonance fluorescence.

We investigated nuclear resonance fluorescence excited in Ce^{140} by γ-rays from La^{140}. The geometry of the experiment is shown in Fig.1. The La^{140} source (activity 50 millicurie) was in the form of a solution $La(NO_3)_3$ in nitric acid.

Ce^{140} has a high-lying first excited level: 1597 kev. Hence it was natural to assume that the lifetime of this excited state is short and that one can use a condensed source (rather than a gaseous one). The scatterers were cylinders of CeO_2 and La_2O_3 having a height of 16 cm, a diameter of 28.5 cm, a wall thickness of 1.2 cm and weighing ~3 kg each. The CeO_2 and La_2O_3 scatterers were approximately equivalent as regards ordinary scattering. The La_2O_3 was free of radioactive impurities, but the CeO_2 contained traces of thorium salts that gave rise to a certain background, which was duly taken into account. The energy spectrum of this background had a peak in the region of the ThC'' 2615 line, but in the energy region of interest to us, i.e., near 1597 kev, the background varied smoothly (see Fig.2). The average scattering angle was 81°.

The radiation detector was a cylindrical 80 x x 80 cm NaI(Tl) crystal coupled to an FEU-24 photomultiplier and a single channel pulse height analyzer. The half-width of the total absorption peak for the 1597 kev line was 13%. A 12 mm thick shielding layer of lead was mounted between the crystal and the scatterer to protect the counting system from soft scattered rays.

In all we carried out 11 series of measurements in which the scatterers were alternately CeO_2 and La_2O_3. The curves for one series are shown in Fig.2. In the curves obtained with the CeO_2 scatterer there always is evident a peak in the 1597 kev region which is absent from the curves for scattering by La_2O_3 and in measurements of the background with a cerium scatterer. After subtraction of curves 2 and 3, there remain the resonance fluorescence curves, such as curve 5 in Fig.2. The resonance fluorescence curves for all 11 series of measurements are shown in Fig.3.

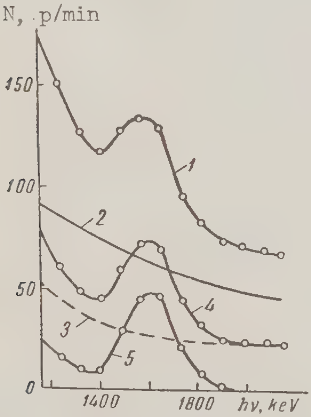

Fig.2. Resonance fluorescence curves obtained in one series of measurements: 1) La^{140} + CeO_2 (background), 3) La^{140} + La_2O_3, 4) scattering from Ce (difference between curves 1 & 2), 5) final resonance fluorescence curve (difference between curves 4 & 3).

From the intensity of the resonance fluorescence effect one can determine the radiation width of the level excited in the process. To this end one can use the formula[1]

$$\bar{\sigma} = \frac{2I^* + 1}{2I_0 + 1} \frac{\lambda^2}{4} m\Gamma_\gamma, \qquad (1)$$

where $\bar{\sigma}$ is the cross section for resonance fluorescence averaged over the microspectrum of the radiation from the source, I_0 is the spin of the ground state and I^* is the spin of the excited state, λ is the wavelength of the scattered rays, m is the fraction of the microspectrum per 1 ev width band in the region of resonance and Γ_γ is the sought radiation width (more accurately in Eq.(1) we should have Γ_γ^2/Γ, where Γ is the total width of the level, but $\Gamma_\gamma \approx \Gamma$).

For the case in question, $I_0 = 0$, $I^* = 2$, and $\lambda = 7.8 \cdot 10^{-11}$ cm. Thus in order to find Γ_γ, we must determine $\bar{\sigma}$ and m.

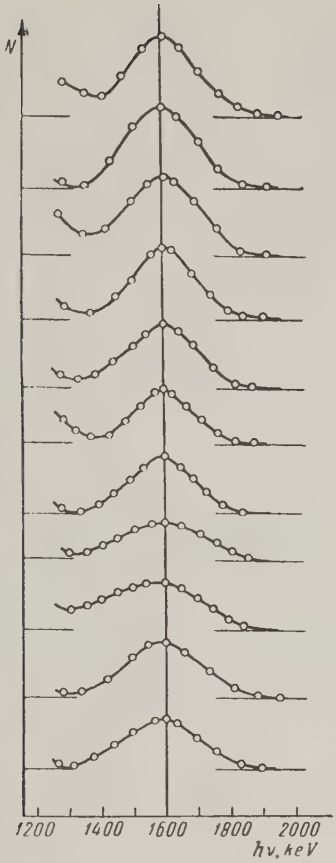

Fig.3. Resonance fluorescence curves for all 11 series of measurements. The scale for all the curves is the same; the curves have been displaced vertically for clarity.

Determination of $\bar{\sigma}$

The experimentally observed effect is proportional to $\bar{\sigma}$:

$$A = \frac{N_1 \bar{\sigma}}{4\pi} \sum_n \frac{k(\theta)\,\omega}{r^2} \varepsilon e^{-(\mu_1 x_1 + \mu_2 x_2)}. \qquad (2)$$

Here A is the number of pulses per second in the scintillation counter at the total absorption peak, N_1 is the number of 1597 kev γ-rays emitted per second from the source, n is the number of Ce^{140} atoms in the scatterer, r is the distance of the given atom from the source, ω is the solid angle under which the crystal is seen from the given point in the scatterer, ε is the efficiency of the crystal in detecting 1597 kev γ-rays (i.e., the number of pulses at the total absorption peak divided by the number of photons incident on the given surface of the crystal) and $k(\theta)$ is a factor taking into account angular anisotropy of the resonance radiation. This factor can be calculated for different points of the scatterer inasmuch as the angular distribution of the resonance radiation for $0^+ \rightarrow 2^+ \rightarrow 0^+$ transitions is described by the formula

$$W(\theta) = 1 - 3\cos^2\theta + 4\cos^4\theta.$$

The angular distribution described by this formula is shown in Fig.4; it will be seen from the figure that angles $\theta \approx 90$ and 180° are most favorable for investigating resonance fluorescence. With our angle of 81° the fluorescence intensity is also higher than it would be with isotropic scattering. For different points of the scatterer $k(\theta)$ has values from 1.07 to 1.24; the mean value is 1.15 and as such can be taken out from under the summation sign in (2).

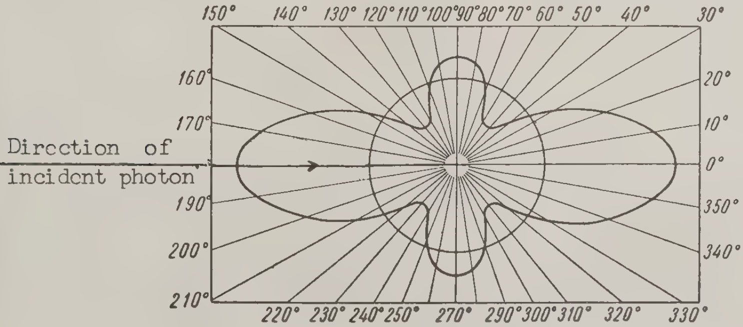

Fig.4. Angular distribution of resonance fluorescence radiation for $0^+ \rightarrow 2^+ \rightarrow 0^+$ transitions.

Further, $e^{-(\mu_1 x_1 + \mu_2 x_2)}$ in Eq.(2) is a factor taking into account the attenuation of the primary and scattered radiation in the scatterer; μ_1 is the attenuation coefficient for the primary radiation in CeO_2, x_1 is the path traversed by the primary radiation in the CeO_2 up to the scattering atom in the scatterer, μ_2 is the attenuation coefficient for the resonance fluorescence radiation in CeO_2 (this includes the photoeffect, pair production and scattering deviating the photon outside the solid angle ω), and x_2 is the path travelled by the resonance radiation in the CeO_2 after scattering (fluorescence). The factor $e^{-(\mu_1 x_1 + \mu_2 x_2)}$ also differs little from unity for all points of the scatterer. Resonance fluorescence makes an insignificant contribution to the attenuation coefficient μ_1: as will be shown below for Ce^{140} atoms (accounting for 88.5% of all the cerium) $\bar{\sigma}$ is equal to approximately 8 millibarns, whereas the cross section associated with the photoeffect, pair formation and the Compton effect is about 10.7 barns; this value was obtained by interpolation of the values given by Davisson^2. We assume $\mu_1 = 0.083$ cm^{-1}. In evaluating μ_2 one must take into account only the processes that deflect the photon outside the solid angle ω. According to our calculations $\mu_2 = 0.080$ cm^{-1}.

For these values of μ_1 and μ_2 and the values of x_1 and x_2 given by the geometry of the experiment, the correction factor $e^{-(\mu_1 x_1 + \mu_2 x_2)}$ is found to lie between 0.844 and 0.849 for different points of the scatterer; its averaged value of 0.846 can also be taken out from under the summation sign.

The product $\omega\varepsilon$ in (2) varies very little from point to point, but one cannot readily take this variation into account by calculation inasmuch as, aside from the geometric factors that determine ω, one must deal with such a difficult to calculate quantity as the efficiency of the crystal for different trajectories of the γ-rays. Hence we determined the product $\omega\varepsilon$ experimentally.

We held the La^{140} source, weakened a known factor by decay, or an auxiliary La^{140} source in an identical packing at different points in place of the scatterer and measured

$$B_h = N_2 (\varepsilon \cdot \omega)_h , \tag{3}$$

where B_h is the number of pulses per second at the peak of total absorption with the auxiliary source at a distance h along the vertical from the center point of the scatterer, N_2 is the number of 1597 kev photons emitted by the auxiliary source per second, and the other notation is the same as before. We use B_0 to designate the number of pulses per second at the total absorption peak with the auxiliary source in the center of the scatterer at its inner surface; for this point the distance from the center of the source is $r_0 = 20.2$ cm.

Inserting the above values of $k(\theta)$ and $e^{-(\mu_1 x_1 + \mu_2 x_2)}$ in Eq.(2) we can readily bring this equation to the following form

$$\bar{\sigma} = 4\pi e^{\overline{(\mu_1 x_1 + \mu_2 x_2)}} r_0^2 \cdot \frac{A}{B_0} \cdot \frac{N_2}{N_1} \cdot \frac{1}{\sum\limits_n \left(\frac{r_0}{r_h}\right)^2 \frac{B_0}{B_h}} = 5270 \frac{A}{B_0} \cdot \frac{N_2}{N_1} \left[\sum_n \left(\frac{r_0}{r_h}\right)^2 \cdot \frac{B_0}{B_h} \right]^{-1} . \tag{4}$$

Use of the above described procedure has the following advantages: dealing with the ratio A/B_0, we need not consider all the questions connected with the width of the amplifier channel, with absorption of γ-rays in the crystal covering and the lead shielding, etc., and can simply use the ratio of the total absorption peaks (ПП) in the γ-spectrograms.

Inasmuch as the total absorption peak is not fully resolved from the Compton distribution, for the sake of definitiveness we inscribed a gaussian curve with a half-width of 13% and took its area to be equal to $A_{\text{пп}}$ or $B_{0\text{пп}}$.

Finally we must determine $\sum\limits_n$. In view of the fact that the scatterer is thin

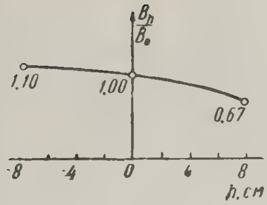

Fig.5.

(~1.2 cm) the functional dependence $B_h/B_0 = f(h)$ is virtually the same at different depths in the scatterer. The measurements were carried out along two verticals just inside and outside the scatterer. The average dependence of B_h/B_0 is shown in Fig.5. The accuracy of these measurements is admittedly not high, but in view of the weak h dependence of B_h/B_0, one can still determine the requisite values of B_h/B_0 from Fig.5 to within 5%.

Subdividing the scatterer into small volumes, we calculated $(r_0/r_h)^2 \cdot B_0/B_h$ for each of the elementary volumes and averaged the results. We obtained

$$\overline{\left(\frac{r_0}{r_h}\right)^2 \left(\frac{B_0}{B_h}\right)} = 0.90$$

and, consequently,

$$\sum_n = 0.90n.$$

Thus the correction for the finite dimensions of the scatterer and its displacement relative to the point B_0, owing to mutual compensation of the different factors, amounts to only 10%; the uncertainty in this value is also 10%. We used 2.8 kg of CeO_2 in which there were 2.03 kg of Ce^{140}. Thus there were $n = 8.7 \cdot 10^{24}$ Ce^{140} atoms in the scatterer.

Inserting the above value into (4), we obtain

$$\bar{\sigma} = 673 \frac{A_{\text{пп}}}{B_{0\text{пп}}} \cdot \frac{N_2}{N_1} \text{ barn.} \qquad (5)$$

The following are the values of $\frac{A_{\text{пп}}}{B_{0\text{пп}}} \cdot \frac{N_2}{N_1} \cdot 10^5$ obtained in the 11 series of measurements: 1.31, 0.82, 1.13, 0.93, 1.17, 1.10, 1.38, 1.09, 1.26, 1.67 and 1.86. The average value, accordingly, is $(1.25 \pm 0.06) \cdot 10^{-5}$ (the indicated uncertainty is the probable error). Inserting this in (5) we obtain $\bar{\sigma} = (8.4 \pm 1.0)$ millibarn (the uncertainty is comprised of the uncertainties in determining $\frac{A_{\text{пп}}}{B_{0\text{пп}}} \cdot \frac{N_2}{N_1}$, $\frac{B_h}{B_0}$ and $k(\theta)$ and the correction for absorption).

Value of m

The fraction m is determined by the shape of the microspectrum of the γ-rays from the source, while the microspectrum in turn is determined by the velocity distribution of the Ce^{140} atoms at the instant of emission of the 1597 kev γ-rays. The initial velocity distribution of the recoil nuclei is the result of β-decay of La^{140}. Subsequently, this distribution can change sometimes owing to repeat recoil incident to emission of γ-rays preceding the 1597 kev gammas, and sometimes owing to collisions with other atoms during the interval between the initial recoil and the emission of the 1597 kev photon.

The β-spectrum of La^{140} consists of several components; the end-point energies and relative intensities of the low energy components are known only approximately. After β-decay with a low energy, there occur different γ-transitions; although the limits of the microspectra associated with all these cascades are the same, their shape is different and all the cascades must be considered separately.

The cascades that we took into account are listed in the accompanying table and shown in the decay scheme for La^{140} pictured in Fig.6.

β-γ cascades in the decay of La^{140}

No.	Beta end-point energy, kev	Relative intensity of the β-component, %	Cascade preceding the 1597 kev γ-rays	Relative intensity of the cascade
1	2200	10	β	10
2	1714	17	β (γ-486)	17
3	1385	39+18	β (γ-815)	19
4			β (γ-328) (γ-486)	20+18
5	1277	16	β (γ-923)	9
6			β (γ-436) (γ-486)	3

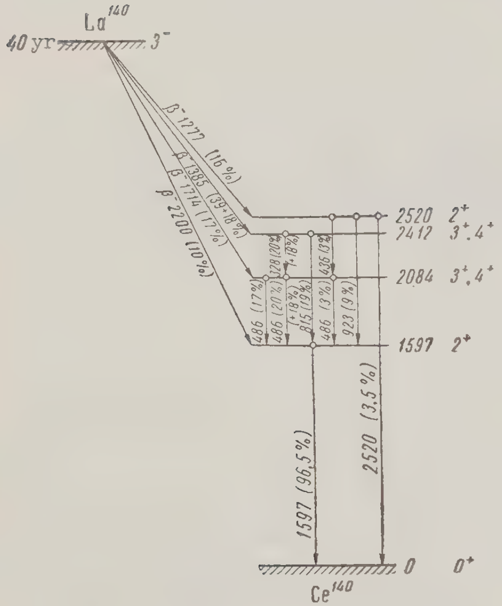

Fig.6. Decay scheme for La^{140}.

Only the hard component of the β-spectrum is not associated with a β-γ-γ cascade; all the other β-components are connected with cascades. The component with end-point energy 1277 kev has an intensity of 16%, but ~4% is accounted for by cascades not involving the 1597 kev γ-transition.

There are also probably softer component with a total intensity of 18%. At present, however, we do not know their energies or what γ-rays follow them; we therefore added these 18% to the (β-1385)-(γ-328)-(γ-486) cascade.

All four β-transitions in La^{140} are first forbidden inasmuch as for all of them $\Delta I \leq 1$ (yes). Thus there may be involved both Fermi and Gamow-Teller matrix elements with a total number to 4.

It is impossible at present to calculate the microspectrum accurately inasmuch as there are the following three sources of uncertainty:

1. The velocity distribution of the recoil nuclei depends on the value of the matrix elements involved in the β-decay.

2. There are angular β-γ, β-γ-γ, and β-γ-γ-γ correlations; they cannot be calculated for La^{140} inasmuch as the necessary matrix elements of the transitions and the multipole order mixtures are not known.

3. In any cascade of the β-γ, β-γ-γ, or β-γ-γ-γ type one of the intermediate excited states may have so appreciable a lifetime that the microspectrum will be distorted due to collisions.

For purposes of calculation, we made the following simplifying assumptions: there is no correlation, all the transitions are prompt and there is no distortion of the spectrum due to collisions.

A.A.Tkachenko calculated the shape of the microspectrum on the basis of different assumptions

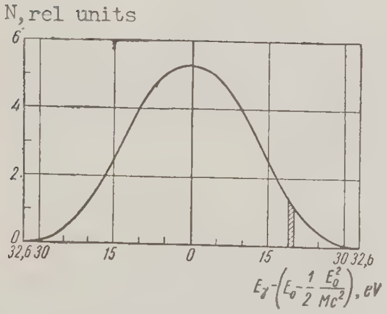

Fig.7. Microspectrum of γ-rays incident on the scatterer.

regarding the relative values of the matrix elements. He showed that for $\Delta I = 1$ (yes) transitions the true microspectrum must lie between the microspectra corresponding to allowed A and S type transitions, while for $\Delta I = 0$ (yes) transitions, the microspectrum must lie between the microspectra corresponding to allowed S and V transitions (wider range). For cascades Nos.1, 5 & 6 (see table) we plotted microspectra intermediate between A and S, while for cascades Nos.2, 3 & 4 we constructed microspectra intermediate between A and V. In the former case the error as regards ordinates does not exceed 10%, while in the second it may be as large as 40%.

Under these conditions we obtained the microspectrum shown in Fig.7; for it $m = 0.0083$. It is obviously difficult to evaluate the error in m. However, taking into account the averaging of the microspectra and neglect of possible correlations and collisions, we estimate that the error is about 40%, i.e., $m = 0.008 \pm$ $\pm\ 0.003$.

Calculation of T

Inserting $\bar{\sigma}$, m, I_0, I^* and λ in Eq.(1), we find

$$\Gamma_\gamma = 1.4 \cdot 10^{-4} \text{ ev}$$

and

$$T_{1597} = (3.3 \pm 1.3) \cdot 10^{-12} \text{ sec.}$$

Discussion

The above value of the half-life T was deduced on the assumption that interaction of the recoil atom with neighboring atoms does not alter the microspectrum. It is not clear how such interaction can change the shape of the microspectrum and the value of m associated with it. It may be assumed that these changes can occur for the following reasons:

1. The Ce^{140} atom at the instant of β-decay may be bound with some of the other atoms; in this case some of the recoil energy will be expended on rupturing the bonds. Consequently, the microspectrum (Fig.7) will be "compressed" and m will be reduced. On the other hand, the presence of bonds will to an extent increase the effective mass of the atom and, consequently, reduce the energy loss due to recoil, i.e., will shift the microspectrum in the direction to E_0, which should increase m.

2. After the recoil atom is freed of the molecular bonds, it undergoes collisions with other atoms and expends some of its energy. This should also lead to compression of the microspectrum and decrease of m

It is not clear at present what the composite effect of all these factors might be at the beginning of motion of the recoil nucleus. The fact that we are concerned here precisely with the beginning of motion is obvious, inasmuch as if the recoil atoms had time to come to rest, m would be equal to zero and no resonance fluorescence would be evinced.

It should be noted that some uncertainty is also introduced by the physical state of the scatterer. A free and stationary Ce^{140} atom should be excited by γ-rays with energy

$$E_0 + \frac{1}{2}\frac{(E_0)^2}{Mc^2},$$

but an atom bound in the crystal lattice may also be excited by γ-rays of lower energy down to E_0 (the momentum of the photon is taken up by the entire crystal). This circumstance may also lead to increase of the effective value of m. Judging from the value of T obtained by us the listed effects have little influence on the result.

We note that (γ-486)-(γ-1597) angular correlation is in good agreement with the theoretical angular correlation for $3^+ \rightarrow 2^+ \rightarrow 0^+$ type transitions. This means that during the lifetime of the 1597 kev level the spatial orientation of the recoil nucleus also does not have time to change significantly.

After completion of our experimental work and draft of the report, we learned of the contribution by Colleman[3], devoted to the probability of transitions in even nuclei, which contains data on the lifetime of the level under consideration. These data were obtained by observation of delayed (γ-815 + 923)-(γ-1597) coincidences. Colleman obtained $T = (17 \pm 14) \cdot 10^{-12}$ sec. There is obviously an appreciable divergence between Colleman's half-life value and ours, but the uncertainties involved are so great that they overlap the divergence.

The Weisskopf-Moszkowski formulas for single-particle transitions give $T = 0.6 \cdot 10^{-12}$ for our case. Thus the 1597 kev transition appears to be retarded by a factor of 6. We do not know of a single other case of comparable retardation in the de-excitation of a 2+ first excited level in even nuclei.[3] It must be noted, however, that more accurate determination of the microspectrum may substantially reduce the calculated lifetime, i.e., the apparent retardation.

References

1. F.Metzger, Phys.Rev., 101, 286 (1956).
2. C.Davisson, Revs.Mod.Phys., 24, 79 (1952).
3. C.Colleman, Nucl.Phys., 7, 488 (1958).

GAMMA-SPECTRUM OF W^{187}

- B.S.Dzhelepov, V.L.Rumyantsev, Yu.V.Khol'nov & G.E.Shchukin

We investigated the γ-radiation from W^{187} by means of the Ritron[1] (a magnetic γ-spectrometer utilizing recoil electrons). We carried out three series of measurements with ~1000 mC sources.

The accompanying figure (see next page) shows the average (for the three runs) recoil electron spectrum. The curve has been corrected for absorption in the source and the entrance window. The energies and relative intensities of the γ-rays (adjusted for the spectral sensitivity of the instrument) are listed in the table. The spectrum was resolved into components on the basis of the instrument line shape. The individual peaks are indicated by the light lines in the figure.

Whereas the energies in the γ-spectrum of W^{187} have been determined in a number of investigations[2-6], the relative line intensities have been evaluated only in the work of Dubey et al[3] who observed the spectrum of photoelectrons ejected from a gold target. It will be evident from the table that the values of Dubey et al differ from our data by appreciably more than our experimental uncertainties. Particularly surprising is the order of magnitude divergence for the intensity of the 864 kev line and the appreciable divergence for the 691 and 558 kev lines. Dubey et al do not give their experimental error. Apparently, their data comprise errors connected with incorrect estimation of the spectral sensitivity of their instrument (they did not take into account the angular distribution of the photoelectrons).

Energies and relative intensities of the γ-rays from W^{187}

Our data		Muller et al	Dubey et al	
E_γ, kev	I	E_γ, kev	E_γ, kev	I
488	100	479,52	482	100
—	—	—	510	12
558	22,5 ± 1,7	—	552	40
		618,89	621	30
622	31,2 ± 2,5	—	627	15
691	119 ± 7	686,06	686	185
778	22,2 ± 1,5	—	775	20
864 ± 9	1,4 ± 0,3	—	866	12
891 ± 9	1,1 ± 0,3	—	—	—

The highest energy line, which according to Dubey et al[3], and Cork et al[4] was located at 866 kev, proved to be double. Its experimental width is appreciably greater than the instrument width of lines in this region. This may be explained by the presence of hitherto undetected γ-rays with an energy of 891 ± 9 kev.

A search of the 950 to 1350 kev region revealed no γ-rays with intensities $>0.3\%$ the intensity of the 488 kev line.

"V.G.Khlopin" Radium Institute,
Academy of Sciences of the USSR

References

1. B.S.Dzhelepov, N.N.Zhukovskii & Yu.V.Khol'nov, Izv.AN SSSR, Ser.fiz., 18, 599 (1954) (Trans.Bulletin 18, 285); B.S.Dzhelepov, V.P.Prikhodtseva, A.I.Geoktistov & Yu.V.Khol'nov, Ibid., 20, 1361 (1956) (Trans.Ibid. 20, 1245); I.B.Golovanov, B.S.Dzhelepov, L.S.Lebedev, V.P.Prikhodtseva & Yu.V.Khol'nov, Ibid., 21, 985 (1957) (Trans.Ibid., 21, 987.)
2. D.Muller, H.Hoyt, D.Klein & J.DuMond, Phys.Rev., 88, 775 (1952).
3. V.Dubey, C.Mandeville, A.Mukerji & V.Potnis, Phys.Rev., 106, 785 (1957).
4. J.Cork, M.Brice, W.Nester, J.Le Blanc & D.Martin, Ibid., 89, 1291 (1953).
5. A.Sunyar, Ibid., 90, 387 (1953).
6. E.Germagnoli, A.Malvicini & L.Zappa, Nuovo cimento, 10, 1388 (1953).

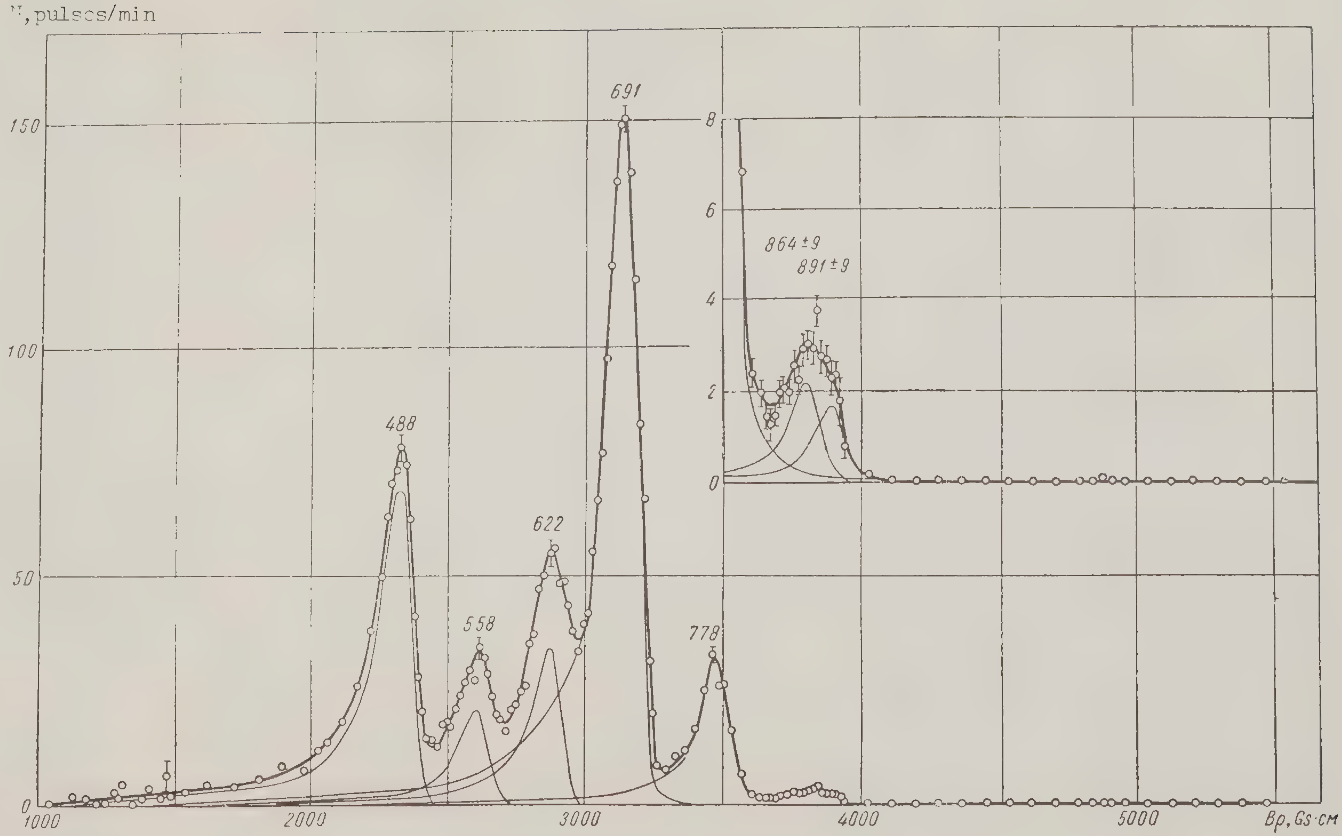

Spectrum of recoil electrons ejected from a cellophane target by W187 γ-rays.

DETERMINATION OF THE NUMBER OF DISINTEGRATION EVENTS IN ELECTRON-CAPTURE MATERIALS BY MEANS OF A 4π SCINTILLATION COUNTER

- V. I. Baranovskii & G. M. Gorodinskii

Introduction

The problem of counting the absolute number of disintegrations in the case of isotopes decaying by electron capture is very complicated. In this case one cannot, in contrast to the case of β- and α-emitters, base the procedure on the fact that each decay is accompanied by the emission of a particle.

The disintegration of electron-capture materials is accompanied by diverse radiations both electromagnetic (γ-rays, K and L and other x-radiation) and corpuscular (internal conversion and Auger electrons). The relation between the number of disintegrations and the number of emitted photons (and/or electrons) depends on the decay scheme and is statistical in character.

The most suitable hypothetical detector for determining the number of disintegrations of electron-capture materials would be an instrument capable of detecting with 100% efficiency in a 4π solid angle all the corpuscular and electromagnetic radiations of all energies including the radiation due to valence electrons. Given such hypothetical perfect detector, we could assert that each and every decay event is recorded inasmuch as every disintegration is accompanied by some sort of radiation. Such an instrument could be, for example, a counter filled with liquid scintillator in which the sample is dissolved; actually, however, the intrinsic (dark) noise of the photomultiplier precludes the possibility of detecting very low energy (<3-4 kev) radiation.

Procedures involving the use of a certain limited solid angle[1,2] yield errors of the order of 30-40% (before correction with reference to the decay scheme), and their sensitivity is generally low.

More advantageous is the method of determining the activity in a 4π proportional counter filled with a heavy noble gas.[3] Actually in view of the design characteristics of such counters measurements are made in 2π geometry, and the inadequate absorbing power of the heavy gas precludes recording K x-rays and γ-radiation with an efficiency close to 100%. This makes it difficult to obtain the absolute count and leads to errors of 6-8% (in the most favorable cases).

Below we describe a procedure for determining the number of disintegration events in isotopes undergoing electron capture based on the use of a CsI(Tl) crystal with the sample inserted into the crystal. Such a counter is capable of recording radiation with energy $\geqslant 30$ kev. The proposed method of taking into account coincidences between different forms of radiation makes it possible, in the case of elements with $Z \geqslant 55$, to reduce the uncertainty in determining the total number of disintegrations to 2-3%.

Counter Design

The principal component of the counter is a CsI(Tl) crystal 30 mm in diameter and 25 mm thick (Fig.1). A hole 3 mm in diameter and 13 mm deep was drilled in one face of the crystal. Thus the sample, when lowered to the bottom of the hole, is in the center of the crystal which insures 4π geometry (the effective solid angle occupied by the opening does not exceed 1-2% of 4π).

To protect the crystal against possible contamination by the sample activity, we prepared special "containers", i.e., tubes of 3.4 mg/cm^2 thick aluminum foil tightly closed at one end. The sample was placed in the bottom of the container which was then inserted into the hole in the crystal. Most of the measurements were made with neutron-deficient isotopes of the rare earth elements formed by fast proton bombardment of Ta. The rare earth elements were separated chromatographically; drops of the fractions were collected on aluminum foils (3.4 mg/cm^2) and dried. Then the section of foil (measuring 7 x 7 to 10 x 10 mm) with the activity was cut out, folded and dropped into the container.

In measurements of milligram amounts of active material the powder was first placed in a small tube 3-4 mm in length which in turn was lowered into the container. Our experiments showed that one can neglect absorption of x- and γ-rays in the packing walls. Thus, for example, less than 0.5% of the K x-radiation of the Tb (45 kev) was stopped in the aluminum foil and container walls, having a total thickness of ~10 mg/cm^2.

All measurements were carried out by means of the automated single-channel γ-spectrometer described in Refs.4 & 5. In carrying out measurements by the described procedure, it is essential that the single-channel differential discriminator operate accurately and reliably and that it be possible to switch rapidly from differential to integral pulse counting.

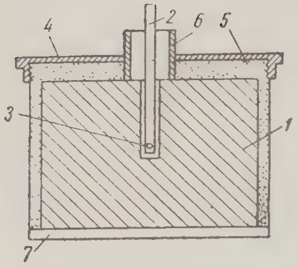

Fig.1. CsI(Tl) crystal (1) with hole drilled to its center. The container (2) with the sample (3) is inserted into the hole; 4 - cover, 5 - MgO powder, 6 - protective sleeve, 7 - glass base.

Fig.2 shows the γ-spectrum obtained for a Tm^{167} sample placed in the crystal. Region 6 of the spectrum represents pulses due primarily to photomultiplier noise. The part of the spectrum to the right of A-A, which includes the K x-radiation 1 and the harder γ-radiation 2-3, is separated from the noise region by a low count interval. Thus by setting the discriminator threshold at A-A, we will obtain a count of the K x-radiation and the γ-radiation emitted by the sample (radiations with energies $\geqslant$25-30 kev in the case of a CsI(Tl) crystal).

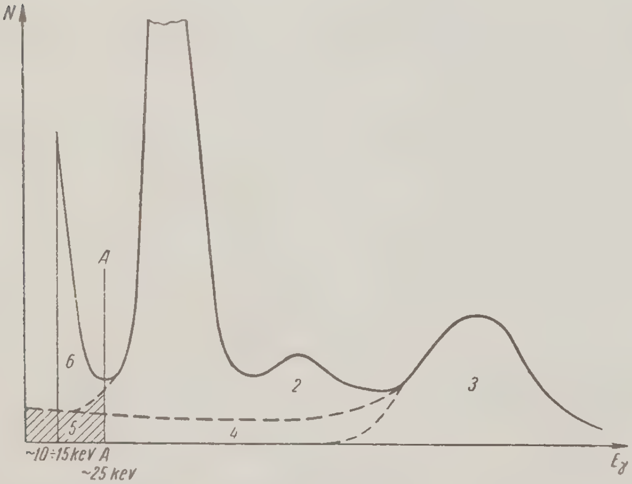

Fig.2. Gamma-spectrum of Tm^{167}: 1 - K x-radiation peak, 2 - peak due to coincidences between x-rays and 57 kev γ-rays, s - 207 kev γ-line (isomeric transition), 4 - Compton distribution from the 207 kev γ-rays, 5 - (hatched area) - soft part of the Compton distribution and the x-ray photopeak, 6 - region of photomultiplier noise. A-A - level of pulse height discrimation.

Taking into Account Coincidences in the Crystal

In general, the decay scheme for an electron-capture isotope can be represented by a diagram of the type shown in Fig.3. Let us call the mode of decay of nucleus X_Z^A to the ground state of nucleus X_{Z-1}^A a "channel". Thus each channel will include:

1) capture of an orbital electron by the X_Z^A nucleus with resultant conversion to nucleus X_{Z-1}^A in one of its possible excited states (or the ground state); hereinafter we shall refer to this process as "transition to the *i*-th level" or simply the "*i*-th transition"; and

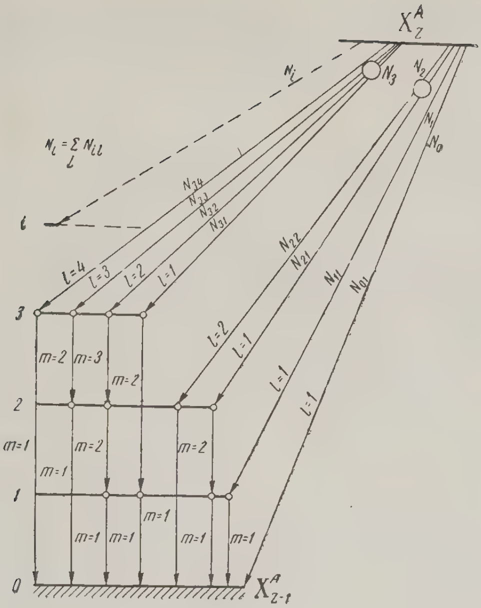

Fig.3. General $X_Z^A \xrightarrow{e} X_{Z-1}^A$ decay scheme.

2) a transition from the excited state of X_{Z-1}^A to the ground state by successive emission of one or more γ-rays.

We denote the levels of nucleus X_{Z-1}^A by the indices i; further we attribute an index l to each channel of the i-th transition (thus each channel will have two indices i and l). Let us assume for example that after electron capture the nucleus X_{Z-1}^A is left in the excited state with $i = 3$. Then the transition to the ground state may occur in one of four ways by one, two or three γ-transitions. Thus the transition with $i = 3$ can have no more than four channels. It will be evident that the same γ-transition (for example, the transition between levels 3 and 2) may pertain to different channels (in Fig.3 - to channels with $i = 3$ and $i = 4$). Assume that of the total number N_0 of disintegrations N_i transitions feed level i; $\left(N_0 = \sum N_i\right)$.

We are interested in the ratio between the total number N_0 of disintegrations occurring in the material and the number N_c of decay events counted by our instrument:

$$N_c = \xi N_0 \tag{1}$$

(the factor ξ characterizes the probability that a given decay of the isotope will be detected by the counter).

Let us consider the channel with indices i, l. After the initial transition to the i-th level, the nucleus will de-excite a number of γ-transitions, each of which we shall denote by an appropriate index m.

We assume that our counter detects:

1) K x-radiation accompanying the orbital electron capture (K radiation from capture),

2) the γ-rays of the succeeding cascade,

3) the K x-ray photons emitted in the conversion of the γ-transitions (conversion K radiation), and

4) all possible coincidences between the radiations listed under 1, 2 and 3 above.

We denote the probability that the K radiation from capture will be detected by W. Obviously, this probability depends on the ratio of K captures to the total number of captures (w_K), the K shell fluorescence yield (ω_K) and the efficiency of the crystal as regards detection of the x-radiation from the Z - 1 atom (p_K); in other words

$$W = p_K \omega_K w_K.$$

Let W_{ilm} be the probability that our counter will detect the m-th transition in the il-th channel. Since there can be no coincidences between the photons of this transition and the K rays from its conversion, we can write

$$W_{ilm} = \frac{p_K \omega_K \alpha_{Kilm} + p_{\gamma ilm}}{1 + \alpha_{ilm}}, \tag{2}$$

where α_{ilm} is the total conversion coefficient and α_{Kilm} is the K shell conversion coefficient for the transition with indices i, l, m; $p_{\gamma ilm}$ is the efficiency of the crystal for the γ-rays of the i, l, m transition. Thus we have

$$N_{Kilm} = \frac{\alpha_{Kilm} N_{ilm}}{1+\alpha_{ilm}}$$

and

$$N_{\gamma ilm} = \frac{N_{ilm}}{1+\alpha_{ilm}},$$

where N_K is the number of conversions on the K shell, and N_γ is the number of nonconverted γ-transitions.

The number of detected γ-rays will be $\frac{\gamma N_{ilm}}{1+\alpha_{ilm}}$, the number of converted transitions $\frac{p_K \omega_K \alpha_{Kilm} N_{ilm}}{1+\alpha_{ilm}}$, and the total number of counted events will be

$$N^c_{ilm} = \frac{p_K \omega_K \alpha_{Kilm} N_{ilm} + p_\gamma N_{ilm}}{1+\alpha_{ilm}}. \tag{3}$$

Equation (2) for W_{ilm} is obtained by dividing both parts of (3) by N_{ilm}.

Now let us calculate the probability W_{il} that at least one of the transitions in the i, l, m channel will be detected by the counter. This probability is equal to unity minus the probability that not a single one of the m transitions will be detected. Inasmuch as all the transitions in a channel occur within a time that is short compared with the resolving time of the apparatus, they will be recorded as a single pulse with an amplitude corresponding to the sum of the individual pulse amplitudes. Hence the probability of no detection will be equal to the product of the probabilities of type $(1-W_{ilm})$, each of which represents the probability that the given transition will not be detected. Thus

$$W_{il} = 1 - \prod_m (1 - W_{ilm}). \tag{4}$$

The initial orbital electron capture is also included in the channel; the radiation accompanying it also virtually coincides in time with the succeeding γ-transitions. Consequently, the probability that a decay event going through the il-th channel will not be detected is given by

$$(1-W)(1-W_{il}).$$

This means that the probability for detection of a decay through channel i, l is $1-(1-W)(1-W_{il})$.

Thus of N_{il} transitions the apparatus will detect and record

$$N_{il}[1-(1-W)(1-W_{il})] = N_{il} - N_{il}(1-W)(1-W_{il}) \tag{5}$$

transitions.

We obtain the total number of detected disintegrations by summing (5) over all i and l:

$$N_c = \sum_{i,l} N_{il} - \sum_{il} N_{il}(1-W)(1-W_{il}) = N_0 - (1-W)\sum_{il} N_{il}(1-W_{il}) \tag{6}$$

here $(1-W)$ is taken out of the summation inasmuch as it is assumed that the fraction of K captures does not depend on the arrival level of the transition (this is true in all cases when the decay energy is appreciably greater than the potential energy of the K electron[6]).

Dividing (6) by N_0, we obtain

$$\frac{N_c}{N_0} = \xi = 1 - (1 - W) \sum_{il} \frac{N_{il}}{N_0} (1 - W_{il}) = 1 - (1 - W) \sum_{il} \frac{N_{il}}{N_0} \prod_m (1 - W_{ilm}), \tag{7}$$

where $W = p_K \omega_K w_K$, and

$$W_{ilm} = \frac{p_K \, \omega_K \, \alpha_{Kilm} + p_\gamma}{1 + \alpha_{ilm}} \; (i \neq 0); \; W_{0lm} \equiv 0 \text{ for } i = 0;$$

$$i = 0, 1, 2, \ldots; \; l = 1, 2, 3, \ldots, 2^{i-1}; \; m = 1, 2, \ldots, i.$$

Determination of the Crystal Efficiency as Regards Detection of γ-Radiation

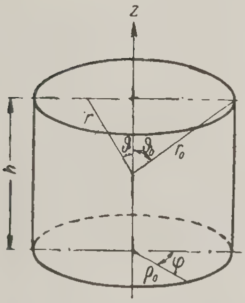

Fig.4. Diagram used in calculating the efficiency of the crystal.

Eq.(7) includes the parameters $p_\gamma (p_K)$ characterizing the efficiency of the crystal as regards γ-radiation. To calculate p_γ, we must know the absorption coefficient for γ-radiation in the material of the crystal. In Table 1 we list the values of the linear absorption coefficient μ and the mass absorption coefficient μ/ρ for CsI and NaI crystals calculated on the basis of the tables given in Ref.7. The values of μ and μ/ρ are given for the γ-ray energy range from 0.05 to 3.0 Mev.

A cylindrical crystal with the radiation source located at its center is diagrammed in Fig.4. We use h to denote the height of the crystal, ρ_0 to denote its radius and r to designate the radial distance from the center of the crystal to the face at an angle ϑ to the z-axis. Finally, r_0 is the angular radius from the center of the crystal to the intersection of the cylindrical surface with the end face; ϑ_0 is the angle between r_0 and the z-axis. We have the following obvious geometrical relationships

$$r = \frac{h}{2 \cos \vartheta} \quad (0 < \vartheta < \vartheta_0);$$

$$r = \frac{\rho_0}{\sin \vartheta} \quad \left(\vartheta_0 < \vartheta < \frac{\pi}{2} \right);$$

$$r_0 = \sqrt{\left(\frac{h}{2} \right)^2 + \rho_0^2}.$$

The minimum path travelled by γ-rays in the crystal is obviously $h/2$; the maximum path is r_0. We use J_0 to denote the intensity of the γ-rays of energy E in the 4π solid angle, and J for the intensity of the same γ-rays attenuated by the crystal; for the sake of brevity we introduce the notation $a = \mu h/2$ and $b = \mu \rho_0$. Then for J we can write

$$J = \frac{J_0}{2\pi} \int_0^{2\pi} d\varphi \left[\int_0^{\vartheta_0} e^{-\frac{a}{\cos \vartheta}} \sin \vartheta \, d\vartheta + \int_{\vartheta_0}^{\pi/2} e^{-\frac{b}{\sin \vartheta}} \sin \vartheta \, d\vartheta \right]. \tag{8}$$

Integrating over the azimuth and defining the fraction of radiation absorbed in the crystal in the form $p_\gamma = \frac{J_0 - J}{J_0}$, we obtain

$$p_\gamma = \frac{J_0 - J}{J_0} = 1 - (I_1 + I_2), \tag{9}$$

where

Table 1

E_γ, Mev	μ/ρ, cm^2/g		μ, cm^{-1}		E_γ, Mev	μ/ρ, cm^2/g		μ, cm^{-1}	
	CsI	NaI	CsI	NaI		CsI	NaI	CsI	NaI
0,05	12,82	10,3	57,7	36,7	0,50	0,0961	0,0936	0,432	0,343
0,06	7,86	6,34	35,4	23,3	0,60	0,0825	0,0813	0,371	0,298
0,08	3,65	2,96	16,4	10,9	0,80	0,0670	0,067	0,302	0,246
0,10	2,02	1,65	9,08	5,9	1,00	0,058	0,058	0,261	0,213
0,15	0,712	0,603	3,23	2,21	1,50	0,0467	0,047	0,208	0,172
0,20	0,376	0,326	1,69	1,19	2,00	0,0407	0,041	0,183	0,150
0,30	0,180	0,165	0,808	0,59	3,00	0,0364	0,036	0,0164	0,132
0,40	0,122	0,116	0,547	0,414					

$$I_1 = \int_0^{\vartheta_0} e^{-\frac{a}{\cos\vartheta}} \sin\vartheta\, d\vartheta; \quad I_2 = \int_{\vartheta_0}^{\pi/2} e^{-\frac{b}{\sin\vartheta}} \sin\vartheta\, d\vartheta. \tag{10}$$

These integrals can only be evaluated numerically.

Fig.5 shows the p_γ vs E curve for a cylindrical CsI crystal (h = 2.5 cm and ρ_0 = 1.5 cm). The values of μ were taken from Table 1. The efficiency p_γ was calculated on the assumption that the CsI crystal is spherical, the radius R of the sphere being taken so that the volume of the sphere will be equal to the volume of the cylindrical crystal.

In this case we have

$$p_\gamma = \frac{J_0 - J}{J_0} = 1 - e^{-\mu R}, \tag{11}$$

where

$$R = \left(\frac{3\rho_0^2 h}{4}\right)^{1/3}.$$

The results obtained by means of formula (11) and calculated using Eqs.(9) & (10) for a crystal of the indicated dimensions virtually coincide, so that the curves plotted on the basis of Eqs.(9) & (11) merge (Fig.5).

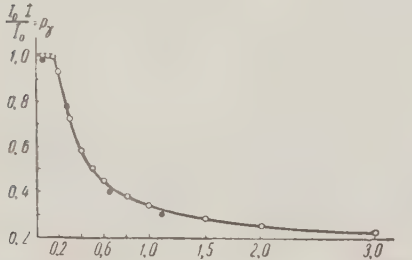

Fig.5. Efficiency curve for the CsI(Tl) crystal. Solid circles - experimental points.

We carried out an experimental verification of the computed p_γ vs E curve for E = 72, 282, 661 and 1120 kev. The activities of the sources used - Hg^{203}, Cs^{137} and Zn^{65} - were determined by the method of absolute β-counting with an accuracy of 1-2%. The results are shown by the solid circles in Fig.5. In connection with the fact that these sources are β-emitters (rather than K capture materials) there is no coincidence in time between the x- and γ-radiations (for example, in the case of Hg^{203} the 72 kev x-rays do not coincide with the 282 kev γ-rays). Hence an additional error creeps into the determination of p_γ due to failure to detect the part of the Compton distribution lying below the discrimination threshold (section 5 of the spectrum in Fig.2). Presumably this is the reason why the 661 and 1120 kev experimental points lie slightly below the theoretical curve.

Analysis of Equation (7)

Let us first consider Eq.(7) as it applies to isotopes in which the disintegration energy is appreciably greater than the K electron potential energy. In

Table 2

Isotope	ω_K	w_K	i	$\frac{N_i}{N_0}$	I	$\frac{N_{il}}{N_i}$	m	α_{Kilm}	α_{jlm}	$p_{\gamma ilm}$	ξ
Hf^{175}	0,935	0,88	1	0,86	1	1	1	0,105	0,13	0,62	0,94
					1	0,12	1	0,061	0,07	0,52	
			2	0,14	2	0,88	1	0,105	0,13	0,62	
							2	2,2	2,7	1	
							—	—	—	—	
Yb^{169}	0,93	0,88	0	0,08	1	1	1	0,06	0,07	0,67	0,97
			1	0,19	1	1	1	0	0,2	1	
			2	0,62	1	1	2	0,06	0,07	0,67	
							1	2,4	2,9	1	
			3	0,11	1	1	2	0,08	0,09	0,77	
							3	2	2,3	1	
Eu^{147}	0,9	0,89	0	0,16	1	1	—	—	—	—	0,955
			1	0,48	1	1	1	1,34	1,54	1	
			2	0,36	1	1	1	0,195	0,24	0,935	
Eu^{147}	0,9	0,89	0	0,16	1	1	—	—	—	—	0,946
			1	0,36	1	1	1	1,34	1,54	1	
			2	0,48	1	1	1	0,195	0,24	0,935	
Eu^{147}	0,9	0,89	0	0,18	1	1	—	—	—	—	0,942
			1	0,47	1	1	1	1,34	1,54	1	
			2	0,35	1	1	1	0,195	0,24	0,935	
Eu^{147}	0,9	0,89	0	0,16	1	1	—	—	—	—	0,945
			1	0,48	1	1	1	0,88	1,02	1	
			2	0,36	1	1	1	0,16	0,202	0,935	

this case for nuclei with Z > 55 the quantities ω_K and w_K are approximately equal to 0.9, so that their product $\omega_K w_K \approx 0.8$. Consequently,

$$\xi \approx 1 - 0{,}2 \sum_{il} \frac{N_{il}}{N_0} \prod_m (1 - W_{ilm}).$$

Inasmuch as $W_{ilm} \leqslant 1$, the detection probability ξ will clearly lie between the limits 0.8 and 1.0. If as a result of radioactive decay the nucleus is left in an excited state, the decay will be followed by the emission of one or more successive γ-rays. Let us take the extreme case when after electron capture the X^A_{Z-1} nucleus de-excites from the i-th state to the ground state by only one γ-transition. Then W_{ilm} (for E_γ = 400 to 700 kev) will be of the order of 0.5, i.e., $\xi \approx 0.9$-1.0.

Thus, if we know that the disintegration energy is high (and that the number of captures to the ground level is zero or negligibly small), we can convert from the number of pulses counted to the number of disintegrations with an accuracy of ±5%, taking $\xi = 0.95$.

The situation is even better if the decay scheme for the isotope is known (even approximately). For purposes of illustration we carried out calculations for three isotopes, namely, Hf^{175}, Yb^{169} and Eu^{147} (the decay schemes are shown in Figs.6,7 & 8). The results given in Table 2 (in all cases p_K was taken equal to unity).

In the case of Yb^{169}, we made the assumption that after electron capture the de-excitation from the i-th level to the ground state occurs with the minimum number of γ-transitions (this results in an underestimate for ξ). For Eu^{147} the value of ξ was calculated for different values of N_{il} and α_{Kilm}. As will be evident from Table 2, ξ varies within a range of less than 1%.

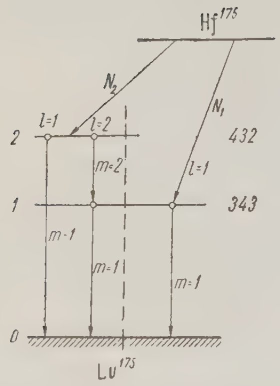

Fig.6. Decay scheme for Hf^{175}.

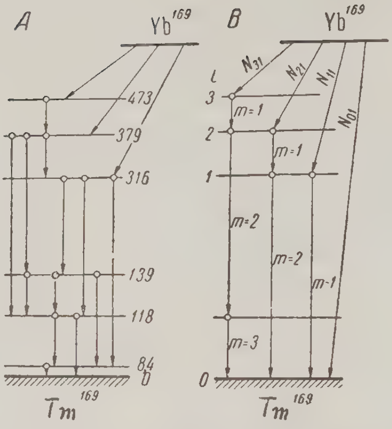

Fig.7. Decay scheme for Yb^{169}: A) detailed scheme, B) simplified scheme utilized for calculating ξ.

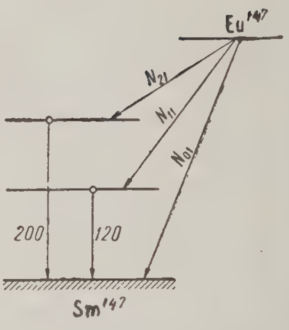

Fig.8. Decay scheme for Eu^{147}.

It will be seen that in all cases ξ lies between 0.94 and 0.97, despite the fact that the decay schemes for these isotopes differ appreciably. They have only two features in common: the presence of excited states and the fact that the number of captures directly to the ground state of the daughter nucleus is small.

The situation is somewhat different if the disintegration energy is comparable to the K electron potential energy. In this case the fraction of K captures (referred to the total number of captures) varies from isotope to isotope, depending on the disintegration energy. The fraction of captures to the ground level is usually large and in some cases may be 100%. An example is furnished by the disintegration of Er^{165}: capture occurs solely to the ground level, and the ratio L/K = 1.2 (Ref.8). For this nucleus, therefore, $\xi = 0.42$. For such isotopes the L/K ratios for capture to different levels may not be the same, which must be taken into account in carrying out the calculations.

An obvious question is whether one cannot in addition measure the L radiation accompanying electron capture and internal conversion? This can be done, for example, by means of an NaI(Tl) crystal (for $Z > 55$). Actually, even leaving aside isotopes in which capture in the L shell has an appreciable probability, the emission of a K x-ray photon leads to formation of a vacancy in the L shell. But the fluorescence yield for L radiation is small (0.1-0.2 for $Z > 55$); hence taking the L radiation into account would not significantly enhance the accuracy.

An NaI(Tl) crystal can be utilized for measuring the activity of electron-capture materials with $Z < 55$ (with K x-ray energies ~10-30 kev). There is, however, the practical inconvenience resulting from the hygroscopicity of NaI, so that in working with a drilled crystal special measures would have to be taken to preclude contact of the exposed surface of the crystal with atmospheric moisture.

Thus as regards accuracy of determining the absolute activity by means of a 4π scintillation counter, all electron-capture isotopes can be roughly divided into two classes:

1. Isotopes with a disintegration energy appreciably greater than the K electron potential energy and with a minor fraction of decays to the ground level of the daughter nucleus. For such isotopes, even if the decay scheme is not known, one can assume $\xi = 0.95 \pm 0.05$. If the decay scheme is reasonably well known the uncertainty can be reduced to ±1-2%. It will be evident that the described set-up

for measuring the activity of electron-capture isotopes of class 1 detects more than 95% of all the disintegrations, i.e., approaches the hypothetical instrument described in the introduction.

2. Isotopes with a low disintegration energy and a large branching ratio to the ground state of the product nucleus. Here the accuracy in determining ξ depends on knowledge of the details of the decay scheme. Even in this case, however, the described procedure has substantial advantages over the procedures based on the use of gas counters or measurements in a certain solid angle $< 4\pi$.

Determination of ξ in the Case of an Isomeric Transition

Next let us consider the case when one of the excited levels involved in the decay of the nucleus is a metastable one. If the lifetime τ' of the isomeric state is appreciably greater than the resolving τ of the scintillation spectrometer, the radiation accompanying the isomeric transition will obviously not be in coincidence as far as detection is concerned with the radiation emitted in the decay to the isomeric level. The transition to the isomeric level may be realized either directly as a result of electron capture or through the intermediary of a number of higher lying excited levels. Assume that N_0' of the total number N_0 of the decays go through the isomeric level and that N_0'' of the decays bypass the isomeric level; $(N_0 = N_0' + N_0'')$. One can calculate the value of ξ corresponding to each of these transition groups:

$$\left(\xi' = \frac{N_c'}{N_0'}\ ;\ \xi'' = \frac{N_c''}{N_0''}\right),$$

In the calculations the isomeric level must be regarded as the "ground level" for the first group. The transitions from the isomeric level to the actual ground state will also be detected by the crystal with a certain probability characterized by the coefficient ξ_{it}, which can readily be calculated by means of Eq.(7), taking into account the fact that in this case there is no K capture x-radiation:

$$\frac{N_{it}^c}{N_{it}} = \xi_{it} = 1 - \sum_{il} \frac{N_{il}^{it}}{N_{it}} \prod_m (1 - W_{ilm}), \tag{12}$$

where N_{it} is the total number of transitions from the isomeric level (obviously, $N_{it} = N_0'$); N_{il}^{it} is the number of transitions from the isomeric level to one of the lower lying levels with index i, accompanied by decay through a channel with the index l. The probability W_{ilm} is defined under Eq.(7).

The total number of counted transitions will be

$$N_c = N_0'\xi' + N_0''\xi'' + N_{it}\xi_{it} = N_0'\xi' + N_0'\xi_{it} + N_0''\xi''. \tag{13}$$

Dividing both parts of Eq.(13) by N_0 and inserting $\xi_0 = \frac{N_c}{N_0}$, we obtain

$$\xi_0 = \frac{N_0'}{N_0}(\xi' + \xi_{it}) + \frac{N_0''}{N_0}\xi''. \tag{14}$$

Precise determination of ξ', ξ'' and ξ_{it} is difficult, but it will be evident that they are of the same order of magnitude and therefore we can make use of the equation obtained from (14) by making the substitution $\xi' = \xi'' = \xi_{it} = \xi$:

$$\xi_0 = \left(\frac{2N_0'}{N_0} + \frac{N_0''}{N_0}\right)\xi = \left(1 + \frac{N_0'}{N_0}\right)\xi.$$

If $N'_0 = N_0$ (i.e., if all the decays are realized through the isomeric level), obviously $\xi_0 = 2\,\xi$.

All the above inferences are valid for the case when the lifetime of the isomeric state is short compared with the period of the parent isotope and when radioactive equilibrium has been attained. In all other cases one must take into account the laws governing the decay and build up of the genetically related radioactive substances.

If the lifetime of the isomeric state is of the same order of magnitude as the resolving time of the scintillation equipment it is clearly inadmissible to use the equations adduced above. Since, as a rule, the lifetime of the isomeric level is only approximately known and the resolving time of the equipment is not a rigorously constant quantity but depends on the specific experimental conditions, evaluation of the coincidence probability and hence ξ is difficult. An obvious expedient in such cases is to increase artificially the resolving time of the equipment so that there will be realized the inequality $\tau' \ll \tau$, so that use of Eq.(7) becomes legitimate. The simplest procedure for increasing τ is increasing the load (resistance) in the plate circuit of the photomultiplier. One can also shunt the photomultiplier anode by a small capacitor (this, however, results in reduction of the pulse height). By these procedures one can reduce τ by 2-3 orders of magnitude. At the same time one must limit the allowable load (pulse rates) accordingly

Conclusions

A 4π scintillation counter has the following principal advantages for purposes of determination of the number of disintegrations in electron capture materials:

1. High detecting efficiency for x- and γ-radiation in a wide energy interval.
2. High sensitivity: one can measure the decay of activities as weak as 10^{-10} Curie with a statistical accuracy of ±5%.
3. High accuracy in determining the number of disintegrations: the statistical accuracy varies from ±1% to ±5% depending on the specific measurement conditions and the characteristics of the decay scheme.
4. Simplicity and reliability of operation.

We desire to thank A.N.Murin and B.K.Preobrazhenskii for discussion of the results.

"V.G.Khlopin" Radium Institute,
Academy of Sciences of the USSR

References

1. W.S.Lyon, Phys.Rev., 87, 1126 (1952).
2. M.Ya.Kuznetsova & V.N.Mekhedov, Izv.AN SSSR, Ser.fiz.,21,1020 (1957). (Trans. Bulletin,21, 1021.)
3. A.A.Konstantinov, Pribory i tekhnika eksperimenta, No.1, 67 (1959). (Trans. Inst. & Experimental Techniques.)
4. G.M.Gorodinskii & V.N.Kochevanov, Ibid., No.4, 81 (1959).
5. G.M.Gorodinskii, A.N.Murin, V.N.Pokrovskii & B.K.Preobrazhenskii, Izv.AN SSSR, Ser.fiz., 21, 1004 (1957). (Trans.Bulletin,21, 1005.)
6. B.S.Dzhelepov & L.N.Zyryanova, Vliyanie elektricheskogo polya atoma na beta-raspad (Influence of the Electric Field of the Atom on Beta-Decay), M., 1956.
7. Beta- and Gamma-Ray Spectroscopy, K.Siegbahn, editor, Amsterdam, 1955. (Cited in Russian trans.)
8. O.I.Grigor'ev, B.S.Kuznetsov, N.S.Shimanskaya & I.A.Yutlandov, Izv.AN SSSR, Ser.fiz., 22, 850 (1958). (Trans.Bulletin,22, 845.)
9. B.S.Dzhelepov & L.N.Zyryanova, Vliyanie elektricheskogo polya atoma na beta-raspad (Influence of the Electric Field of the Atom on Beta-Decay), M.-L.,1956; B. L.Robinson & R.W.Fink, Revs.Mod.Phys.,27,424 (1955); Beta- and Gamma-Ray Spectr., Amsterdam, 1955; N.M.Lazar & W.S.Lyon, O.R.N.L.2430, Physics Division, Sept.10,1957

COMPARISON OF THE THEORY OF NONAXIAL NUCLEI WITH EXPERIMENT

- E.P.Grigor'ev & M.P.Avotina

I. Theory

The theory of deformed nuclei developed by Bohr & Mottelson[1] has proved very useful for explaining a number of regularities characterizing the distribution of energy levels of nuclei in the $150 < A < 190$ and $A > 222$ regions. Based on relatively simple concepts, this theory allows of determining with excellent accuracy the energies of rotational bands based on both the ground state and on other nonrotational levels[2-5]. The theory is in good agreement with experiment for deformed nuclei. By relatively simple calculations one can determine the ratio of probabilities for E2 or E1 transitions from a given level with known I and K to the levels of one rotational band. In many cases there is obtained excellent agreement of the predictions of theory with the experimental data.

The theory does not agree with experiment, however, at the extremes of the deformed nuclei region. In the level spectra of Sm^{152}, Gd^{154}, Os^{186}, Os^{188} and Os^{190} there is observed an appreciable deviation from the predictions of theory, although the rotational character of these spectra is beyond doubt.[2]

Davydov, Filippov & Rostovskii[6-9] considered the rotational levels of even-even nuclei on the assumption that these nuclei have an equilibrium shape lacking axial symmetry. The parameter of transverse deformation of the nucleus is the angle γ, which can vary from 0° to 60°. For $\gamma = 0°$ and 60°, the nucleus has axial symmetry; for $\gamma = 30°$, we have the greatest deviation of the nuclear shape from an ellipsoid of revolution. Below we give the relative values of the ellipsoid axes as functions of γ for a deformation parameter $\beta = 0.3$:

γ	R_1	R_2	R_3
0	1.189	0.906	0.906
10	1.183	0.935	0.879
20	1.177	0.967	0.857
30	1.163	1.000	0.837

In a number of contributions[7,10,11,etc.], Davydov and Zaikin attempted to show that the potential energy has a minimum with deviation of the nucleus from the axially symmetric shape if the nucleus has several nucleons outside the filled shells. This can be demonstrated, however, only on the basis of certain assumptions.

1. Levels of nonaxial nuclei

In addition to levels with total angular momentum 0+, 2+, 4+, 6+, etc. the theory of nonaxial nuclei yields a series of rotational levels with odd and even spins, which are not encompassed by the Bohr-Mottelson theory. Davydov and his co-workers have termed these levels anomalous levels in distinction to the 0+, 2+, etc. levels of the main rotational band based on the ground state.

The energy ratios of the ground state band levels differ from the ratios 1:3.3:7:12... found for the rotational levels of axially symmetric even-even nuclei. Only in the limiting cases $\gamma = 0°$ and $\gamma = 60°$ do the above ratios obtain.

Davydov & Filippov[6] derived formulas for determining the level energy as a function of γ. The energy in these formulas is given in $\frac{\hbar^2}{4B\beta^2}$, units, where B is an inertial parameter, and β is the usual deformation parameter. Below we give

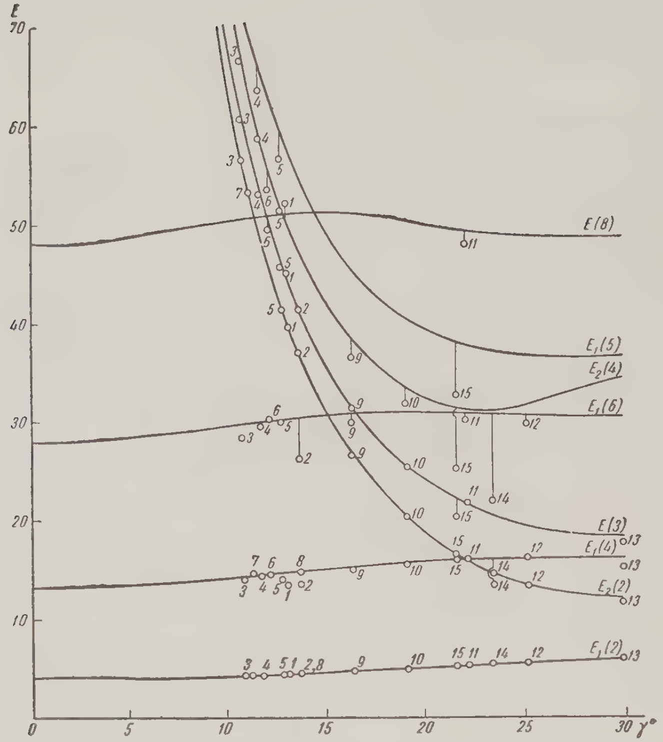

Fig.1. Variation of the level energy in $\frac{\hbar^2}{4B\beta^2}$ units as a function of γ according to the theory of nonaxial nuclei and comparison with the experimental data: 1 - Sm^{152}, 2 - Gd^{154}, 3 - Gd^{156}, 4 - Dy^{160}, 5 - Er^{166}, 6 - Er^{168}, 7 - W^{182}, 8 - W^{184}, 9 - Os^{186}, 10 - Os^{188}, 11 - Os^{190}, 12 - Os^{192}, 13 - Pt^{192}, 14 - Hg^{198}, 15 - Mg^{24}.

the formulas for the levels with spins 2+, 5+ (there are two of each) and 3+:

$$E_{1,2}(2)=\frac{9}{\sin^2(3\gamma)}\cdot\left[1\pm\sqrt{1-\frac{8}{9}\sin^2(3\gamma)}\right]; \tag{1}$$

$$E_{1,2}(5)=\frac{1}{\sin^2(3\gamma)}\left[45\pm 9\sqrt{9-8\sin^2(3\gamma)}\right]; \tag{2}$$

$$E(3)=\frac{18}{\sin^2(3\gamma)}. \tag{3}$$

The energies of the levels with spins 4+, 6+ and 8+ are determined as the roots of 3rd, 4th and 5th degree equations, respectively:

$$E^3-\frac{90E^2}{\sin^2(3\gamma)}+\frac{48\,[27+26\sin^2(3\gamma)]\,\varepsilon}{[\sin^2(3\gamma)]^2}-\frac{640\,[27+7\sin^2(3\gamma)]}{[\sin^2(3\gamma)]^2}=0; \tag{4}$$

$$E^4-\frac{252E^3}{\sin^2(3\gamma)}+\frac{1764\,[9+4\sin^2(3\gamma)]\,E^2}{[\sin^2(3\gamma)]^2}-\frac{2592\,[81+235\sin^2(3\gamma)+24\sin^4(3\gamma)]\,E}{[\sin^2(3\gamma)]^3}+$$
$$+\frac{36288\,[162+163\sin^2(3\gamma)]}{[\sin^2(3\gamma)]^3}=0; \tag{5}$$

$$E^5 - \frac{540\,E^4}{\sin^2(3\gamma)} + \frac{108\,[819+232\sin^2(3\gamma)]\,E^3}{[\sin^2(3\gamma)]^2} - \frac{864\,[5535+7362\sin^2(3\gamma)+452\sin^4(3\gamma)]E^2}{[\sin^2(3\gamma)]^3} +$$
$$+ \frac{248832\,[243+1413\sin^2(3\gamma)+599\sin^4(3\gamma)]E}{[\sin^2(3\gamma)]^4} - \frac{17915904\,[162+363\sin^2(3\gamma)+50\sin^4(3\gamma)]}{[\sin^2(3\gamma)]^4} = 0. \quad (6)$$

The calculated variation of the level energy as a function of γ is shown by the solid lines in Fig.1.

The value of γ, which characterizes the degree of deviation of the nucleus from the axially symmetric shape, can most simply be determined from the energy ratio of the two levels with I = 2.

The coupling between the single-particle motion and the collective motion in the nucleus can be taken into account by introduction of the corrections for nonadiabaticity. The Bohr-Mottelson correction term is of the form

$$BI^2(I+1)^2. \quad (7)$$

In the Davydov theory, fulfillment of the equality

$$E_1(2) = E(3) - E_2(2) \quad (8)$$

serves as the criterion for applicability of the adiabatic approximation.

2. Probability of transitions between levels

For axially symmetric nuclei one can determine the ratio of the probabilities for electric transitions to the rotational levels of one band[5] (Alaga's rules).

The theory of nonaxial nuclei allows of determining the probabilities for E2 transitions between all rotational levels. These probabilities depend on γ and for $\gamma = 0$ coincide with the results of Alaga. Davydov & Filippov[6,8] deduced the following formulas for the transition probabilities:

$$b(E2;\, 2_1^+ \to 0) = \frac{1}{2}\left[1 + \frac{3-2\sin^2(3\gamma)}{\sqrt{9-8\sin^2(3\gamma)}}\right]; \quad (9)$$

$$b(E2;\, 2_2^+ \to 0) = \frac{1}{2}\left[1 - \frac{3-2\sin^2(3\gamma)}{\sqrt{9-8\sin^2(3\gamma)}}\right]; \quad (10)$$

$$b(E2;\, 2_2^+ \to 2_1^+) = \frac{10\sin^2(3\gamma)}{7\,[9-8\sin^2(3\gamma)]}, \quad (11)$$

wherein

$$b = \frac{B}{e^2 Q_0^2\, 16\pi^2}$$

(here B is the reduced transition probability).

These authors also give the probability for transitions between other rotational levels.

The variation of the transition probability ratios

$$\frac{b(E2;\, 2_2^+ \to 2_1^+)}{b(E2;\, 2_2^+ \to 0)} \quad \text{and} \quad \frac{b(E2;\, 3^+ \to 4_1^+)}{b(E2;\, 3^+ \to 2_1^+)}$$

as a function of γ is shown by the solid lines in Figs.2 & 3.

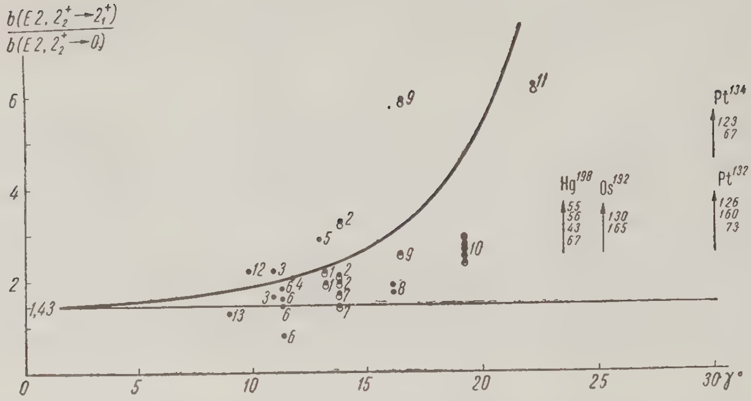

Fig.2. Comparison of the experimental values of the reduced transition probability ratio $b(E2;\,2_2^+\to 2_1^+)/b(E2;\,2_2^+\to 0)$ with the theories of Bohr & Mottelson and Davydov et al: 1 - Sm^{152}, 2 - Gd^{154}, 3 - Gd^{156}, 4 - Dy^{160}, 5 - Er^{166}, 6 - W^{182}, 7 - W^{184}, 8 - W^{186}, 9 - Os^{186}, 10 - Os^{188}, 11 - Os^{190}, 12 - Th^{228}, 13 - Th^{230}.

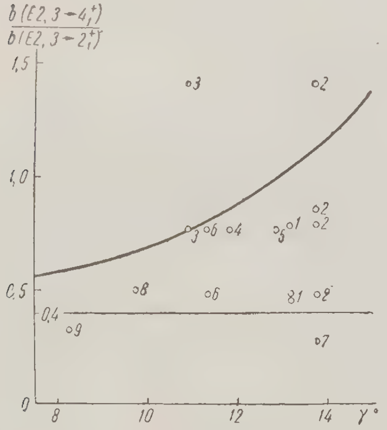

Fig.3. Comparison of the experimental values of the reduced transition probability ratio $b(E2;\,3^+\to 4_1^+)/b(E2;\,3_2^+\to 2_1^+)$ with the theories of Bohr & Mottelson and Davydov et al: 1 - Sm^{152}, 2 - Gd^{154}, 3 - Gd^{156}, 4 - Dy^{160}, 5 - Er^{166}, 6 - W^{182}, 7 - W^{184}, 8 - Th^{228}, 9 - Pu^{240}.

3. Fraction of E2 and M1 multipoles in $2_2^+\to 2_1^+$ transitions

At present only the theory of nonaxial nuclei allows of numerical determination of the ratio between M1 and E2 multipolarities in transitions between 2_2^+ and 2_1^+ levels. Davydov & Filippov[9] give the following formula for determining $\delta^2 = I(E2)/I(M1)$:

$$\delta^2 = \frac{0{,}21E_\gamma^2}{80h^2c^2}\left(\frac{eZR_0^2}{\mu_0 g_R}\right)^2, \tag{12}$$

where $\mu_0 = 5{,}05\cdot 10^{-24}$ erg/gauss, $g_R = 0{,}4$ and $R_0 = 1{,}2\,A^{1/3}\cdot 10^{-13}$ cm, and E_γ is measured in kev. Inserting these values into (12), we obtain

$$\delta^2 = 8{,}1\cdot 10^{-11}E_\gamma^2\cdot Z^2\cdot A^{4/3}. \tag{13}$$

For heavy nuclei and not excessively low γ-ray energies the fraction of M1 is small. Qualitative evaluations on the basis of the unified nuclear model also indicate the predominance of E2 transitions between 2_2^+ and 2_L^+ levels.[12]

At present there are three principal studies devoted to comparison of the experimental data with the theory of nonaxial nuclei.[13-15] The results of these studies are utilized in the present report.

II. Comparison with Experiment

1. Level energies

The known decay schemes for radioactive isotopes[2,3,16,17] were examined and analyzed from the standpoint of the theory of nonaxial nuclei. The deformation parameter γ was determined from the energy ratio of the spin 2+ levels. The energies of the rotational levels of different nuclei are plotted in Fig.1. It will be seen that there is good agreement between theory and experiment for the nuclei from Gd^{156} to Pt^{192}. We note that the levels of nuclei from Gd^{156} to W^{184} are satisfactorily explained by the Bohr-Mottelson model by means of introduction of two parameters A and B according to the formula

$$E^* = AI(I+1) + BI^2(I+1)^2.$$

For Os^{188}, Os^{190}, Os^{192} and Pt^{192}, however, no possible choice of the parameters A and B can reconcile the theory with the experimental data (Table 1). It will be apparent from Fig.1 that the position of the levels in these nuclei is rather close to the energies predicted by the theory of Davydov et al.

The energies of the levels of Mg^{24} and Hg^{198} differ appreciably from the values predicted by theory. The level scheme for these nuclei can be explained from the same standpoint, although in this case the conditions for applicability of the hydrodynamic and adiabatic approximations are only partially fulfilled and the necessary corrections are substantial.

There are many nuclei in which there are two levels with angular momentum 2+ and an energy of the first level equal to approximately half that of the second. These nuclei are commonly regarded as spherical. One might attempt to explain the distribution of levels in these nuclei by means of the nonaxial nuclei theory, assuming that for them $\gamma \approx 30^\circ$. So far, however, there are not known any levels in these nuclei with other spins, which as regards energies and quantum characteristics would correspond to this theory. Definitive deductions regarding these

Table 1

Corrections to level energies*

Nucleus	γ	$B(4)$	$B(6)$	$B(8)$	$\frac{B(4)}{B(6)}$	$E(3)-E_2(2)$	$E_1(2)$	$\frac{\Delta E}{E_1(2)}$, %
1	2	3	4	5	6	7	8	9
Sm^{152}	13,2	0,143	—	—	—	138	122	13
Gd^{154}	13,8	0,125	0,078	—	1,67	132	123	9,0
Gd^{156}	11,0	0,036	0,022	—	1,63	94	89	5,6
Dy^{160}	11,8	0,018	0,011	—	1,63	83	86,6	—5
Er^{166}	12,9	0,011	0,006	—	1,84	74	80,7	—7
Er^{168}	12,3	0,004	0,002	—	1,75	75	80	—6
Hf^{178}	0	0,008	0,012	0,011	—	—	93	—
Hf^{180}	0	0,006	0,006	—	—	—	93	—
W^{182}	11,35	0,023	—	—	—	110	101	9,0
W^{184}	13,8	0,018	—	—	—	102	111	—8
Os^{186}	16,5	0,039 (0,079)	0,017 (0,054)	—	2,3	141	137	3
Os^{188}	19,2	0,039 (0,079)	—	—	—	162	155	-4,5
Os^{190}	22,2	0,037 (0,25)	0,014 (0,17)	0,010 (0,12)	2,6	193	186	3,8
Os^{192}	25,2	0,034 (0,31)	0,022 (0,25)	—	1,55	—	206	—
Pt^{192}	30,0	0,20 (0,95)	—	—	—	308	316	2,5

---

* $B(I)$ is determined from the formula $E(I) + I^2(I+1)^2 B = \left[\frac{\varepsilon(1)}{\varepsilon(2)}\right]_{\text{theo}} [E(2) + 2^2 3^2 B]$, where I = 2, 4, 6 or 8. The corrections B calculated according to the Bohr-Mottelson theory are given in parentheses.

nuclei must be reserved pending accumulation of more complete experimental data and development of a method of introducing corrections into the theory.

As a result of analysis of the experimental data we established that the corrections to the level energies calculated according to the theory of nonaxial nuclei must have a form different from $BI^2(I+1)^2$. In Table 1 we list the corrections calculated for the 4_1^+ and 6_1^+ levels of a number of nuclei (columns 3 & 4). The correction for 4_1^+ levels is on the average 1.7 times greater than for 6_1 levels (column 6). For Hf^{178} and Hf^{180} the corrections are the same for the 4_1^+, 6_1^+ and 8_1^+ levels. The corrections B calculated according to the Bohr-Mottelson theory are given in parentheses. These corrections are appreciably larger than the corrections computed according to the theory of nonaxial nuclei for $\gamma > 13^{o}$. For $\gamma < 13^{o}$ the corrections virtually coincide for both theories. It must be emphasized that for $Os^{186-192}$ and Pt^{192} no choice of B allows of reconciling the experimental data with the theory of axial nuclei.

We also checked the relation between the energy of the first level and the energy difference $E(3)-E_2(2)$; these values calculated according to the theory of nonaxial nuclei should agree if the adiabatic approximation is applicable.

The values of the energy difference $E(3)-E_2(2)$ and the first level energy $E_1(2)$ are listed in columns 7 and 8, respectively; while column 9 lists the difference between the deduced values divided by $E_1(2)$. It will be seen that $\Delta E/E_1(2)$ varies over a wide range and does not depend on the corrections $B(4)$ and $B(6)$. It follows therefore that fulfillment of equality (8) cannot be regarded as a good criterion for applicability of the adiabatic approximation. It also follows from the data of the table that the corrections to the level energies can be connected not only with disturbance of the condition of adiabaticity but also with some other factors.

2. Transition probabilities

At present it is feasible to compare experimental data on relative transition probabilities with theory primarily for transitions from $E_2(2)$ and $E(3)$ levels to 0^+, 2_1^+ and 4_1^+ levels. Plots of the ratio of reduced transition probabilities

$$\frac{b\,(E2;\ 2_2^+ \to 2_1^+)}{b\,(E2;\ 2_2^+ \to 0)}\,.$$

as a function of γ are shown in Fig.2. According to the calculations of Alaga[5], this ratio equals 1.43. The solid rising line gives the ratio according to the theory of nonaxial nuclei; the points represent the experimental data. It will be evident from Fig.2 that almost all the experimental points lie between the nonaxial theory curve and the 1.43 horizontal line. In the theory of axial nuclei the relatively high probability for $2_2^+ \to 2_1^+$ transitions was explained by admixture of 2_2^+ states to the 2_1^+ state which has the same total momentum. In Davydov's theory this admixture is already taken into account. Moreover, M1 transitions are possible between these states; an admixture of such transitions would also increase the observed abundance of the $2_2^+ \to 2_1^+$ transitions and thereby lead to divergence between experiment and the theory of nonaxial nuclei.

For a more rigorous comparison of theory with experiment one should take the E2 component of the $2_2^+ \to 2_1^+$ transition, taking into account the M1 admixture on the basis of measurements of the conversion coefficients and γ-γ angular correlation. The cases where the M1 admixture was taken into account are indicated by crosses in Fig.2.

Evidence in favor of the theory of nonaxial nuclei is the fact that the experimental value of the ratio

$$\frac{b\,(E2;\,2_2^+ \to 2_1^+)}{b\,(E2;\,2_1^+ \to 0)}$$

increases appreciably with γ and for nuclei with $\gamma > 15^\circ$ differs substantially from 1.43.

The points in Fig.3 give the values of the experimental ratio of reduced transition probabilities from levels with spin 3^+ to 4_1^+ and 2_1^+ levels. Here we have somewhat better agreement of experiment with the new theory (solid curve). The above mentioned reasons for divergence of the Davydov theory from experiment do not pertain in this case.

The values of the reduced probability ratio

$$\frac{b\,(E2;\,4_2^+ \to 2_1^+)}{b\,(E2;\,4_2^+ \to 4_1^+)}$$

are known for Er^{166} and Dy^{160}:

Nucleus	Experiment[18,19]	Davydov	Alaga
Er^{166}	0.20	0.10	1.34
Dy^{160}	0.14	0.10	

In this case there may be an admixture of M1 in the $4_2^+ \to 4_1^+$ transitions, which would tend to increase the ratio of probabilities for the E2 components of these transitions. An admixture of the 4_2^+ state to the 4_1^+ state should decrease this ratio.

Thus at present it is difficult to decide in favor of one theory or the other on the basis of the relative transition probabilities. Nevertheless, the experimental data, although admittedly not very accurate at present, are not in conflict with the theory of nonaxial nuclei.

3. The $\delta^2 = I(E2)/I(M1)$ ratio in $2_2^+ \to 2_1^+$ transitions

In a recent publication Malik et al[15] give a comparison of the experimental data with formula (12). In Table 2 we list the values of the ratio $\delta^2_{exp}/\delta^2_{theo}$ which should obviously be equal to unity when experimental data agree with theory. In addition to the data taken from Malik et al, Table 2 contains some additional information on the multipole order ratio for $2_2^+ \to 2_1^+$ transitions, also obtained from data on γ-γ angular correlation. The very great discrepancy between the experimental data of different authors and the substantial uncertainty in the experimental values preclude definite inferences regarding the agreement or disagreement of theory with experiment in a number of cases. In fact the experimental data can tentatively be divided into three groups:

In the first part of Table 2 there are listed values of $\delta^2_{exp}/\delta^2_{theo}$ differing greatly from unity. Apparently the 2_2^+ levels in these nuclei are single-particle levels and the nuclei themselves are spherical; their shells are close to being closed.

The second group is comprised of nuclei for which the experimental value of δ^2 is close to the value following from the theory of Davydov et al; this group includes Fe^{58}, Ni^{60}, Te^{126}, Os^{186}, Os^{188} and Pt^{192}.

The third group consists of nuclei for which δ has not been measured with sufficient accuracy to permit conclusive comparison. It must be noted, however, that within the limits of experimental accuracy there is no conflict with the theory of nonaxial nuclei.

Table 2

Comparison of the experimental values of $\delta^2 = \frac{I(E2)}{I(M1)}$ with the theoretical values for $2_2^+ \to 2_1^+$ transitions

Nucleus	E_γ, kev	δ^2 exp	δ^2 theo	$\frac{\delta^2 \text{exp}}{\delta^2 \text{theo}}$	Data from Ref. No.
1	2	3	4	5	6
S^{34}	1160	0,016	3,1	0,005	[20]
		0,017+0,011		0,005±0,004	[21]
Fe^{56}	1810	0,026	38	0,0007	[22]
		0,004		0,0001	[23]
		0,023±0,020		$0{,}0006^{+0{,}00005}_{-0{,}00002}$	[15, 24]
	2100	0,087	53	0,0017	[24]
		0,036		0,0007	[25]
		0,078±0,017		0,0015±0,0003	[22]
		0,073		0,0014	[23]
	2490	0,017	73	0,0002	[22]
Zr^{92}	900	<0,002	43	<0,00005	[26]
		<0,008		<0,0002	[15,21]
Pd^{106}	1045	0,04	94	0,00043	[27]
Ce^{140}	920	<0,015	170	0,00009	[21]
Hg^{198}	675	0,92±0,4	270	0,0034±0,0015	[15, 28]
		1,5		0,0055	[29]
Po^{214}	1238	0,014	1100	0,00012	[30]
Fe^{58}	805	5,3±1,0	8,0	0,66±0,12	[15, 31]
Ni^{60}	850	≥9,0	11	≥0,84	[22]
Te^{126}	740	41±6	75	0,54±0,07	[32]
Os^{186}	627	100±40	200	0,50±0,20	[33]
Os^{188}	480	250±20	120	2,1±0,2	[15, 34]
Pt^{192}	296	42±16	48	0,9±0,4	[15, 35]
		19±7		0,40±0,15	[36]
Ge^{72}	630	≥32	9,9	≥3,3	[37]
Se^{76}	640	<14	13	<1,1	[15, 21]
		332		2,6	[38]
		49±20		4±2	[33]
Sn^{116}	800	12±8	73	0,17±0,1	[15, 39]
Te^{122}	686	10÷21	62	0,16÷0,34	[21]
		10		0,16	[15, 33]
Sm^{152}	970	≥80	240	≥0,3	[40, 41]
		50		0,2	[40, 41]
Gd^{154}	875	>10	210	>0,05	[42]
Dy^{160}	880	24	240	0,10	[43]
W^{182}	1122	>9	575	>0,02	[44]
Os^{190}	374	49	72	0,67	[45, 46]
Pt^{194}	293	850 (<3000)	47	18 (0,2—63)	[15, 47]
Pt^{196}	331	30±6	61	0,5±0,1	[15, 48]
		22±4		0,36±0,07	[49]

4. Range of applicability of the theory

It follows from the above analysis of the experimental data that the theory of nonaxial nuclei can be applied to nuclei which at present are regarded as deformed. The authors of the theory, however, also attempt to utilize it for interpreting the level spectra of such nuclei as Se^{76} and Te^{122}, which presumably are spherical. The available experimental data are at present inadequate to draw any conclusions regarding the rotational character of the levels in these nuclei. Actually the evidence in favor of the Davydov theory amounts only to the presence of two 2+ levels in these nuclei, the small admixture of M1 in the transitions between these levels and the large value of the transition probability ratio

$$\frac{b\,(E2;\,2_2^+ \to 2_1^+)}{b\,(E2;\,2_1^+ \to 0)} \approx 100.$$

Hitherto these levels have been explained by one-phonon and two-phonon excitation of the nuclei.[17] So far in none of these nuclei have there been detected levels (except 2_1^+ and 2_2^+) which could be interpreted and treated as rotational levels of nonaxial nuclei.

In our opinion the assertion made by Davydov & Zaikin in Ref.11 that γ-vibrational levels must always lie an order of magnitude higher than the usually observed 2_1^+ levels is not convincing.

Thus comparison of the theory of Davydov and his co-workers with the experimental data shows that this theory correctly describes some of the effects occurring in these nuclei. Undoubtedly the theory of nonaxial nuclei is a significant step forward in the development of nuclear model concepts.

We desire to express our gratitude to L.K.Peker and M.A.Listengarten for their help and constant interest in the work.

Scientific-Research Physical Institute,
"A.A.Zhdanov" Leningrad State University

References

1. A.Bohr & B.Mottelson, in Probl.sovrem.fiz.Sb.perev.i obz. in.period.lit. (Problems of Modern Physics. Collected translations and reviews from the foreign literature), No.9 (1955); Ibid., No.1 (1956).

2. B.S.Dzhelepov & L.K.Peker, Deformirovannye yadra v oblasti Nd-Os (Deformed nuclei in the Nd-Os region) Pub. OIYaI (Joint Inst. for Nucl.Res.), 1958.

3. B.S.Dzhelepov & L.K.Peker, Vozbuzhdennye sostoyaniya deformirovannykh yader (Excited states of deformed nuclei) OIYaI, 1959.

4. B.Mottelson & S.Nilsson, Intrinsic States of Odd-A Nuclei having an Ellipsoidal Equilibrium Shape. Copenhagen, 1959.

5. G.Alaga, K.Alder, A.Bohr & B.Mottelson, Dan.Mat.-fys.medd., 29, No.9 (1955).

6. A.S.Davydov & G.F.Filippov, Zhur.eksp.i teor.fiz., 35, 440 (1958). (Trans. Soviet Physics - JETP.)

7. A.S.Davydov & V.S.Rostovskii, Ibid., 36, 1788 (1959)(Trans.Ibid.); Nucl. Phys., 12, 58 (1959).

8. A.S.Davydov, Izv.AN SSSR, Ser.fiz., 23, 792 (1959). (Trans.Bulletin,23,788.)

9. A.S.Davydov & G.F.Filippov, Nucl.phys., 8, 237 (1958).

10. D.A.Zaikin, Zhur.eksp.i teor.fiz., 35, 529 (1958). (Trans.Sov.Phys. - JETP.)

11. A.S.Davydov & D.A.Zaikin, Ibid., 36, 233 (1959). (Trans.Ibid.)

12. K.Alder, A.Bohr, T.Huus, B.Mottelson & A.Winter, Revs.Mod.Phys., 28, 432 (1956).

13. D.M.Van Patter, Bull.Amer.Phys.Soc., 4, 233 (1959).

14. V.R.Potnis, S.Malik & C.E.Mandeville, Bull.Am.Phys.Soc., 4, 233, (1959).

15. S.S.Malik, V.R.Potnis & C.E.Mandeville, Nucl.Phys., 11, 691 (1959).

16. B.S.Dzhelepov & L.K.Peker, Skhemy raspada radioaktivnykh yader (Decay schemes of radioactive nuclei) M., 1958.

17. D.Strominger, J.M.Hollander & G.T.Seaborg, Table of Isotopes, Revs.Mod. Phys., 30, 585 (1958).

18. K.Ya.Gromov, B.S.Dzhelepov & V.N.Pokrovskii, Izv.AN SSSR, Ser.fiz., 23, 821 (1959).(Trans.Bulletin 23, 815.)

19. E.P.Grigor'ev, B.S.Dzhelepov, A.V.Zolotavin, B.Kratsik & G.Bitterlikh, Ibid., 23, 868 (1959). (Trans.Ibid.23, 859.)

20. G.G.Shute & P.S.Fisher, Phil.Mag., 3, 726 (1958).

21. C.F.Coleman, Nucl.phys., 7, 488 (1958).

22. N.Levine, H.Frauenfelder & A.Rossi, Z.Phys., 151, 241 (1958).

23. M.J.Stimac, W.L.Skeel & P.S.Jastram, Bull.Amer.Phys.Soc., 4, 56 (1959).

24. F.R.Metzger & W.B.Todd, Phys.Rev., 92, 904 (1953).

25. F.Asima, F.T.Kokoska, D.R.Cartwright & T.D.Kurbatov, Bull.Amer.Phys.Soc., 3, 103 (1958).

26. H.J.West, L.G.Mann & G.M.Iddings, Phys.Rev.,113, 881 (1959).

27. E.D.Klema & F.K.McGowan, Phys.Rev., 92, 1469 (1953).

28. C.D.Shrader, Phys.Rev., 92, 928 (1953).

29. D.Schiff & F.R.Metzger, Phys.Rev., 90, 849 (1953).

30. G.R.Bishop & F.Madaule, J.Phys.et radium, 19, 41 (1958).

31. H.Frauenfelder, N.Levine, A.Rosi & S.Singer, Phys.Rev., 103, 352 (1956).

32. M.Sakai, Cited in Ref.14.

33. T.Lindquist & J.Marklund, Nucl.Phys., 4, 189 (1957).

34. V.R.Potnis, V.S.Dubey & C.E.Mandeville, Phys.Rev., 102, 459 (1956).

35. J.Mraz, Nucl.Phys., 4, 457 (1957).

36. W.H.Kelly & M.L.Wiedenbeck, Phys.Rev., 102, 1130 (1956).

37. R.G.Arns & M.L.Wiedenbeck, Phys.Rev., 112, 229 (1959).

38. E.G.Funk & M.L.Wiedenbeck, Phys.Rev., 109, 922 (1958).

39. R.P.Scharenberg, M.G.Stewart & M.L.Wiedenbeck, Phys.Rev., 101, 689 (1956).

40. S.Ofer, Nucl.Phys., 4, 477 (1957).

41. R.W.Side & M.L.Wiedenbeck, Phys.Rev., 113, 840 (1959).

42. C.D.Hickman & M.L.Wiedenbeck, Phys.Rev., 111, 539 (1958).

43. R.G.Arns, R.E.Sund & M.L.Wiedenbeck, Nucl.Phys., 11, 410 (1959).

44. R.C.Williams & K.J.Roulston, Canad.J.Phys., 34, 1087 (1956).

45. F.Coopelani, U.Farinelli, F.Ferrero & R.Malvano, Physica, 24, 765 (1958).

46. O.Nielsen, Roy Poulsen,et al, Nucl.Phys., 10, 475 (1959).

47. C.E.Mandeville, J.Varma & B.Saraf, Phys.Rev., 98, 1185 (1955).

48. V.R.Potnis, Indian J.Phys., 30, 375 (1956).

49. R.M.Steffen, Phys.Rev., 89, 665 (1953).

50. L.Grodzins & H.Kendall, Bull.Amer.Phys.Soc., 1, 163 (1956); NSA, 10, 24 B (1956).

51. B.S.Dzhelepov, N.N.Zhukovskii, V.G.Nedovseov & G.E.Shchukin, Izv.AN SSSR, Ser.fiz., 21, 966 (1957). (Trans.Bulletin 21, 968.)

52. B.S.Dzhelepov, N.N.Zhukovksii & V.G.Nedovesov, Ibid., 19, 296 (1955). (Trans.Ibid., 19, 269.)

53. S.K.Bhattacherjee, T.D.Nainan, S.Raman and B.Sahai, Nuovo Cimento,7,501, (1958).

54. J.O.Juliano & F.S.Stephens, Jr., Phys.Rev., 108, 341 (1957).

55. B.V.Bobykin & K.M.Novik, Doklady AN SSSR, 115, 263 (1957). (Trans.Soviet Physics - Doklady).

56. O.Nathan, Nucl.Phys., 5, 401 (1958).

57. P.G.Hansen, O.B.Nielsen & R.K.Sheline, Nucl.Phys., 12, 389 (1959).

58. K.P.Jacob, J.W.Mihelich, B.Harmatz & T.H.Handley, Bull.Amer.Phys.Soc., 3, 358 (1958).

59. C.J.Gallagher & J.O.Rasmussen, Phys.Rev., 112, 1730 (1958).

60. J.J.Murray, F.Boehm, P.Marmier & J.W.M.DuMond, Phys.Rev., 97, 1007 (1955).

61. B.V.Bobykin & K.M.Novik, Izv.AN SSSR, Ser.fiz., 21, 1556 (1957). (Trans. 21, 1546.)

62. C.J.Gallagher,Jr., D.Strominger & J.P.Unik, Phys.Rev., 110, 725 (1958).

63. A.J.Poë, Phil.mag, 46, 1165 (1955).

64. M.W.Johns, C.C.McMuller, I.R.Williams & S.V.Nablo, Canad.J.Phys., 34, 69 (1956).

65. F.T.Porter, M.S.Freedman, T.B.Novey & F.Wagner, Jr., Phys.Rev., 103, 921 (1956).

66. C.C.McMallen & M.W.Johns, Phys.Rev., 91, 418 (1953).

67. V.R.Potnis, Phys.Rev., 104, 722 (1956).

68. P.S.Fisher & R.A.Naumann, Phys.Rev., 112, 1717 (1958).

69. M.W.Johns & S.V.Nablo, Phys.Rev., 96, 1599 (1954).

70. L.L.Baggerly, P.Marmier, F.Boehm & J.W.M.DuMond, Phys.Rev., 100, 1364 (1955).

71. V.Shiel, L.D.Wyly & C.H.Braden, Phys.Rev., 105, 1521 (1957).

72. M.L.Thieme & E.Bleuler, Phys.Rev., 102, 195 (1956); ibid., 99, 1646 (1955).

73. L.G.Elliot, M.A.Preston & J.L.Wolfson, Canad.J.Phys., 32, 153 (1954).

74. B.S.Dzhelepov, N.N.Zhukovskii, V.P.Prikhodtseva & Yu.V.Khol'nov, Nuovo cimento, 3, suppl.1, 49 (1956); Izv.AN SSSR, Ser.fiz., 19, 271 (1955). (Trans. Bulletin 19, 247.)

75. J.Volpe & G.Hinman, Phys.Rev., 104, 753 (1956).

76. S.Bjorholm, O.Nathan, O.B.Nielsen & R.K.Sheline, Nucl.Phys., 4, 313 (1957).

77. S.Bjorholm, O.Nathan, O.B.Nielsen & R.K.Sheline, NSA, 11, 24B (1957).

78. T.O.Passel, NSA, 9, 24B (1955).

Appendix

Experimental data on nuclei the level spectra of which can be explained by the theory of nonaxial nuclei (level energies are given in kev)

Nucleus	γ	$E_1(2)$	$E_1(4)$	$E_1(6)$	$E_1(8)$	$E_2(2)$	$E(3)$	$E_2(4)$	$\frac{b(E2; 2_2^+ \to 2_1^+)}{b(E2; 2_2^+ \to 0)}$	$\frac{b(E2; 3^+ \to 4_1^+)}{b(E2; 3^+ \to 2_1^+)}$	Data from Ref.
Sm^{152}	13,2	121,8	366	—	—	1087	1235	1423	1,96	—	[50]
									2,2	0,46	[51]
									2,2	0,78	[52]
									—	0,48	[53]
Gd^{154}	13,8	123,02	371,06	718,1	—	996,6	1128,4	—	1,94±0,27	0,85±0,12	[42]
									—	0,48	[54]
									2,11	0,78	[55]
									3,29	—	[51]
									—	1,4	[56]
Gd^{156}	10,95	89	288	584	—	1152	1246	1365	1,64	1,4	[57]
									2,2	0,77	[56]
Dy^{160}	11,85	86,6	283	580	—	966	1049	1156	2,04+0,04	0,77	[19]
Er^{166}	12,90	80,7	264,9	546	—	787,4	861	966	2,9	0,2	[18, 58]
										0,76	
Er^{168}	12,28	80	265	548	—	822	897	996	—	—	[58]
W^{182}	11,35	100,9	329,36	—	—	1222	1333	1481	0,8	—	[59]
									1,6	0,48	[60]
									1,8	0,77	[51]
W^{184}	13,81	111,2	364	—	—	899	1006	—	—	—	[16]
									1,72	0,28	[62]
									1,45	—	[59]
W^{186}	16,55	125	—	—	—	730	—	—	1,75	—	[63]
									1,9	—	[59]
Os^{186}	16,5	137	434	869	—	769	910	1060	2,6	—	[64]
									5,9	—	[65]
Os^{188}	19,2	155	479	—	—	634	796	987	2,56	—	[64]
									2,71	—	[66]
									2,92	—	[34]
									2,79	—	[67]
Os^{190}	22,2	186	548	1048	1662	557	754	956	2,5	—	[68]
									6,2	—	[46]
Os^{192}	25,2	206	580	1065	—	489	—	—	—	130,0	[69]
										165	[70]
Pt^{192}	30	316,5	784	—	—	613	921	—	160,5	22,9	[71]
									73	—	
Pt^{194}	30	327	—	—	—	621	—	—	127,5	—	[69]
									66,9	—	[72]
Hg^{198}	23,5	411,8	999	1636	—	1090,7	—	—	54,8	—	[73]
									42,5	—	[74]
									66,5	—	[75]
Th^{228}	9,75	58	187,0	—	—	966	1018	—	2,2	—	[76]
										0,5	[77]
Th^{230}	9,0	52,8	174	—	—	1060	—	—	1,3	—	[78]
Ra^{224}	22,3	84,47	253	487	—	—	—	—	—	—	[16,17]
Ra^{226}	19,9	67,76	210	416	—	—	—	—	—	—	
U^{232}	9,3	47	156	321	—	869	943	—	—	—	
U^{234}	14,4	43,5	143,3	296,4	499	—	—	—	—	—	
Pu^{238}	8,4	44,2	145,8	303,4	514,0	1032	1076	—	—	—	
Pu^{240}	8,3	42,87	141,77	292	—	1020	—	—	—	0,329	

ON SOME APPLICATIONS OF THE COINCIDENCE TECHNIQUE IN NUCLEAR SPECTROSCOPY

- É.E.Berlovich

Introduction

In the coincidence procedure experimental physicists have acquired a potent means of investigating processes correlated in time. By way of some of the important applications of this procedure in nuclear physics one can cite, for example, time-of-flight neutron spectroscopy, determination of the lifetimes of unstable particles, various studies in the field of nuclear spectroscopy and investigation of the problems involved in β-decay.

Among the last one can list in particular:

a) resolution of partial β-spectra, investigation of their shape and determination of their correlation with γ-rays,

b) determination of the internal conversion coefficients for γ-transitions accompanying β^-, β^+ and α-decays,

c) identification of γ-transition cascades,

d) determination of the lifetimes of nuclear levels formed in radioactive transformations,

e) measurement of the annihilation time for positrons in different media,

f) investigation of the angular distribution of annihilation quanta,

g) investigation of angular correlation of cascade radiations,

h) investigation of disturbance of angular correlation of cascade radiations under the influence of intra-atomic, intracrystalline or external fields as a function of time,

i) investigation of β-neutrino angular correlation,

j) investigation of plane and circular polarization of γ-rays,

k) investigation of longitudinal polarization of β-particles, and

l) discrimination of resonance fluorescence γ-rays by means of coincidences.

The list can be continued, but the cited examples are sufficient to give an idea of the importance of the coincidence technique in the fields of nuclear spectroscopy and β-decay.

During the last decade the potentialities of the coincidence procedure have been greatly extended thanks to the development of scintillation techniques and means of employing the coincidence procedure in conjunction with the methods of magnetic analysis.

In the present report we shall describe some applications of the coincidence procedure in the fields of nuclear spectroscopy involving the use of special equipment including a twin scintillation spectrometer, a twin magnetic spectrometer and a twin β-γ coincidence spectrometer. Many of the physical investigations carried out by means of these instruments have been described in print, while others are still in the laboratory stage.

Before turning to a description of the instruments, let us consider some of the general problems involved in employing the coincidence procedure.

General remarks concerning the coincidence technique

In essence the coincidence procedure consists of simultaneous detection of two or more time correlated events, i.e., events either occurring simultaneously or one following the other with a certain lag subject to statistical fluctuations. Here we shall restrict ourselves to the case of double coincidences, i.e., to the detection of only two events. Where nuclear spectroscopy is concerned, the two events may be the emission of two radiations or particles of the same type (for example, e-e or γ-γ) or of different types (for example, e-γ or β-γ). Where the radiation is not monoenergetic, these radiations can in general be discriminated in energy by some procedure. Here we shall deal with the case when the resolving time of the coincidence circuit (2τ) is greater than the lifetime of the intermediate level so that both radiations are detected simultaneously. The case when the resolving time is shorter than the lifetime of the intermediate level has been examined, for example, in Ref.1.

The number of true coincidences registered by the coincidence circuit per unit time, i.e., the number of cases in which the two detected radiations arise in the same elementary event, may be written

$$N_{1,2} = N_0 \omega_1 \varepsilon_1 \omega_2 \varepsilon_2 \sum_{i,k} p_{ik} \Phi_{1i} \Phi_{2k}, \tag{1}$$

where N_0 is the total number of radiative events occurring in the source per unit time (for example, the number of disintegrations in the radioactive source), ω_1 and ω_2 are the solid angles of acceptance (in fractions of 4π) subtended by the detectors of the first and second radiations, ε_1 and ε_2 are the efficiencies of the radiation detectors, p_{ik} is the intensity (number per disintegration) of the weakest of the two radiations, and Φ_{1i} and Φ_{2k} are functions connected with the nature of the first and second radiations and the fraction of the radiations incident on the instrument; these functions have different forms for different specific types of radiation and for different types of instruments (and adjustments of these instruments).

The sum is taken over the functions corresponding to all possible radiations that can be detected by each of the detectors with the given setting or adjustment and yield coincidences with the radiation being detected by the second detector. The situation where there are simultaneously registered several types of coincidences obtains, for example, in the case of a twin scintillation spectrometer when the gates (operating intervals) of the pulse height analyzers are set for the spectral regions which correspond to recoil electrons from several γ-rays forming cascade pairs. An analogous situation obtains in recording e-β coincidences by means of a twin magnetic spectrometer when for the given setting of the magnetic field there may occur coincidences of the conversion electrons simultaneously with several partial β-spectra.

In general in spectroscopic investigations there may be observed the following types of coincidences: β-γ, β-e, β-X_e, β-A_e, β-p, β^+-γ, β^+-e, β^+-X_e, β^+-A_e, β^+-p, β^+-a, a-a, a-γ, a-e, a-X_e, a-A_c, a-p, γ-γ, γ-e, γ-X_e, γ-X_c, γ-A_e, γ-A_c, γ-p, e-e, e-X_e, e-X_c, e-A_e, e-A_c, e-p, X_c-X_e, X_e-X_c, X_e-A_e, X_e-A_c, X_e-p, X_c-A_e, X_c-p, A_e-A_e, A_e-A_c, A_e-p, A_c-p, α-γ, α-e, α-X_e, α-A_e, α-p and p-p.

Here β, β^+, α and γ, as usual, stand for decay electrons and positrons, alpha-particles and gamma-rays; e = internal conversion electrons, X_c = characteristic x-ray accompanying internal conversion, X_c = characteristic x-rays accompanying electron capture, A_c = Auger electrons accompanying internal conversion, A_c = Auger electrons accompanying electron capture, p = pair conversion positrons, and a = annihilation quanta.

Thus the eleven different types of radiation yield 47 possible double coincidence combinations. Naturally this number does not agree with the binomial coefficient $C_{11}^2 = 11 \cdot 10/1 \cdot 2 = 55$, inasmuch as, first, from this one must subtract the 14 combinations devoid of physical significance: β-α, β-X_c, β-A_c, β-a, β^+-α, β^+-X_c, β^+-A_c, β^+-β, A_c-X_c, X_c-α, A_c-α, a-α, a-X_c, and a-A_c, and, second, add the six like radiation pairs: γ-γ, e-e, X_e-X_e, A_e-A_e, p-p and a-a, which are not included in the coefficient but do correspond to coincidences realized in practice. The specific forms of the Φ functions for different types of radiation and instruments are listed in the accompanying table.

Type radiation	Type of instrument	Form of the function Φ	Remarks
β,β^+	Mag.or scint.spect.	$f(E)\Delta E$	$f(E)$ is the decay electron distribution function normalized so that $\int_0^{E_{ep}} f(E)dE = 1$
γ	Mag.or scint.spect. obs. photoeffect	$\delta(1-K_t)$	δ is the fraction of the photopeak taken in by the instrument; K_t is the fraction of the total number of de-excitations of the excited state by emission of ordinary and pair conversion electrons
	Mag.or scint.spect. obs. Compton effect	$(1-K_t)\varphi(E)\Delta E$	$\varphi(E)$ is the recoil electron distribution function normalized so that $\int_0^{E_{ep\ Comp}} \varphi(E)dE = 1$
	Mag.or scint.spect. obs. pairs	$\delta(1-K_t)$	
e	Mag.or scint.spect.	δK	$K = \alpha/(1+\alpha)$ is the number of de-excitations of the excited state by emission of conversion electrons of the given group (K, L or M); α is the conversion coefficient
X_e	Mag.or scint.spect. obs. photoeffect	$\delta K f_x$	f_x is the fluorescence yield
	Mag.or scint.spect. obs. Compton effect	$K\varphi(E)\Delta E f_x$	
X_c	Mag.or scint.spect. obs. photoeffect	δf_x	
	Mag.or scint.spect. obs. Compton effect	$\varphi(E)\Delta E f_x$	
A_e	Magnetic or scintillation spectrometer	$\delta K(1-f_x)$	
A_c		$\delta(1-f_x)$	
α		δ	
π		$\pi\psi(E)\Delta E$	π is the fraction of de-excitations occurring along the pair conversion branch; $\psi(E)$ is the distribution function in the pair conversion positron spectrum normalized so that $\int_0^{E_{ep}} \psi(\sigma)dE = 1$
a	Mag.or scint.spect. obs. photoeffect	δ	
	Mag.or scint.spect. obs. Compton effect	$\psi(E)\Delta E$	

Note: E_{ep} = end-point energy

The load on a single (for example, the first) detector is given by

$$N_1 = N_0 \omega_1 \varepsilon_1 \sum_i p_{1i} \Phi_{1i}. \tag{2}$$

The number of chance coincidences per unit time is characterized by

$$N_c = 2\tau N_1 N_2 = 2\tau N_0^2 \, \omega_1 \omega_2 \, \varepsilon_1 \varepsilon_2 \left(\sum_i p_{1i} \Phi_{1i} \right) \left(\sum_k p_{2k} \Phi_{2k} \right). \tag{3}$$

Then the ratio of true to false coincidences is equal to

$$\frac{N_{1,2}}{N_c} = \frac{A}{2\tau N_0}, \tag{4}$$

where

$$A = \frac{\sum\limits_{i,k} p_{ik} \Phi_{1i} \Phi_{2k}}{\left(\sum\limits_i p_{1i} \Phi_{1i} \right) \left(\sum\limits_k p_{2k} \Phi_{2k} \right)}. \tag{4a}$$

A similar expression for the more particular case of β-γ coincidences and a simple decay scheme was deduced by Mitchell[2].

It follows from Eqs.(1), (3) and (4) that

1) the true coincidence counting rate is proportional to the solid angles ω_1 and ω_2, the efficiencies of the detectors as regards the coinciding radiations and the intensity of the source;

2) the chance coincidence counting rate is proportional to the solid angles, the detector efficiencies and the square of the source intensity;

3) the ratio of the true to chance coincidence counting rates is inversely proportional to the intensity of the source and the resolving time of the coincidence circuit. This means that to obtain good statistical accuracy one cannot simply increase the source intensity N_0 inasmuch as this leads to a quadratic increase of the chance coincidence background. Hence it is more expedient to obtain the desired level of true coincidences by increasing the solid angles (the product $\omega_1 \omega_2$). The source intensity permissible from the standpoint of a good $N_{1,2}/N_c$ ratio will be the greater, the shorter the resolving time 2τ of the coincidence circuit. These considerations are important in designing coincidence equipment.

Twin scintillation coincidence spectrometer

A description of the scintillation coincidence spectrometer will be found in Ref.3. It is designed to register β-γ, β-e, β-X_e, β-A_e, e-e, e-γ, e-X, γ-X and γ-A coincidences. The greatest advantage of this spectrometer as compared with other arrangements for measuring coincidences is the high "luminosity" or effective transmission, which is limited by pure geometric factors. The solid angle of each of the spectrometer branches can in principle be as large as 0.2-0.3 of 4π.

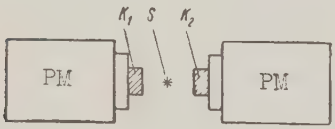

Fig.1. Experimental arrangement employed in the twin scintillation spectrometer: S - source, K_1 and K_2 - crystals, PM - photomultipliers.

Fig.1 shows the usual experimental arrangement in spectrometers of this type. Differential pulse height analyzers connected into the side arms of the triple coincidence circuit provide for energy selection of the radiation. Separation of radiations of different types (for example, electromagnetic and corpuscular) is realized by means of absorbers. The fast-slow coincidence circuit similar to the circuit described by Bell, Graham & Petch[4], includes a variable delay line, which makes it possible to measure the lifetimes of nuclear states.

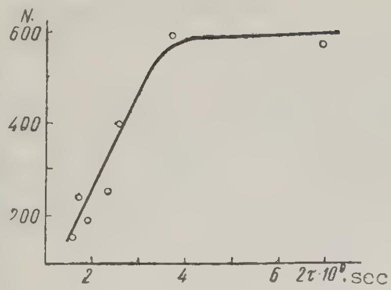

Fig.2. Coincidence counting efficiency as a function of the resolving time.

With FEU-33 type photomultipliers and stilbene crystals the resolving time of the coincidence circuit can be brought down to 1.5-2 nanosec.

Fig.2 shows the variation of the coincidence counting efficiency for the middle parts of the energy spectrum of recoil electrons from 1.33 and 1.17 kev γ-rays, obtained with FEU-33 photomultipliers, stilbene crystals and limiters assembled about 6Zh9P tubes. It will be evident from the figure that saturation of the efficiency is attained with a resolving time of $2\tau = 4 \cdot 10^{-9}$ sec. The limiter tubes are blocked by 1.5 v pulses. Such pulses with the given multipliers and crystals can be obtained from 6-8 ev electrons. It follows from the formula of Post & Shiff[5] that the time spread for the appearance of the first electron on the PM cathode for a stilbene crystal ($\tau_p = 6 \cdot 10^{-9}$ sec) and 100 kev electrons with the efficiency of the cathode being 0.1 photons per electron amounts to $2.6 \cdot 10^{-9}$ sec. The resolving time of the coincidence circuit in the range of low energies is determined primarily by the intrinsic rise time of the photomultiplier, which for FEU-33 type tubes is of the order of 1.5-2 nanosec.

Measurements of β-γ, e-γ and γ-γ coincidences on the given scintillation coincidence spectrometer for the purpose of determining the lifetimes of excited nuclear states have been described in Refs.1,6 & 7 and measurements of X-γ, X-e and X-A (electron capture) coincidences in Refs.8,9 & 10. A description of measurements of the photomultiplier pulse rise time and the scintillation decay time of crystals will be found in Ref.11. In many cases of measurement it is advantageous to use sodium iodide single crystals inasmuch as these allow of distinguishing individual gammas although these crystals are admittedly inferior to organic crystals as regards the phosphor decay time ($\tau_p = 0.25$ μsec). A specific investigation, involving measurements of the lifetimes of excited levels in Tm^{169}, by means of a spectrometer employing NaI crystals is described in Ref.12. With appropriate design of the pulse limiting circuit and selection of individual photomultiplier tubes with good cathodes, the resolving time of the coincidence circuit in working with NaI crystals can be brought down to under 10 nanosec.

Twin magnetic coincidence spectrometer

Despite their merits as regards high luminosity and so on, scintillation spectrometers cannot be used for investigating complicated conversion schemes owing to their inadequate resolution. In this respect twin magnetic spectrometers present definite advantages. Usually these are lens spectrometer[13] which are, as a rule, characterized by a higher transmission factor than magnetic spectrometers with transverse focusing[14]. Apparently, of all the instruments of this type described in the literature, the one with the best characteristics is the double spectrometer of Gerholm[15] which employs two lenses in magnetic shielding; the transmission factor of each part is 3.1% with a line half-width of 1.3%.

The instrument described below does not have such good properties: the transmission factor of each branch is 1%, the resolution 1.8-2%. Its merit is that belonging to the class of transverse spectrometers and having all the advantages of instruments of this class, it has a transmission factor characteristic of lens instruments. At the same time, as compared with other transverse type spectrometers, it is small in size, light in weight and requires a relatively low current for supplying the magnets. Thus a current of only 100 ma is required for focusing 2 Mev electrons.

Our twin magnetic spectrometer is a combination of two wide angle spectrometers of the sector (wedge) type with improved focusing[16]. In each of the two spectrometers the angle of divergence of the beam in the horizontal plane $2\alpha = 45^\circ$; the angle of divergence in the vertical plane $2\varepsilon = 10^\circ$.

Let us calculate the line half-width in a ordinary sector spectrometer for these angles of divergence. We write the formula for the aberration S and the dispersion D for the case of nonsymmetrical passage of the beam through the sector field, i.e., for the case when the angles θ and γ of inclination of the axial beam relative to the straight line passing through the source, the apex of the sector and the focus are not equal (Fig. 3):

$$S = \frac{a\alpha^2}{2}\left(\frac{\sin^2\theta}{\sin\gamma} + \frac{\sin^2\gamma}{\sin\theta}\right); \tag{5}$$

$$D = a\frac{\sin\theta}{\sin\gamma}(\sin\theta + \sin\gamma). \tag{6}$$

In our case the distance from the apex of the center to the focus $(2a)$ is twice the distance from the apex to the source (a), and there obtains the following relationship between angles θ and γ, the magnitude of a and the radius ρ of curvature of the electron trajectory:

$$\rho = a\sin\theta = 2a\sin\gamma; \tag{7}$$

$$\sin\gamma = \frac{\sin\theta}{2}. \tag{7a}$$

Simplifying the expressions for S and D by means of (7) and (7a), taking into account the aberration connected with the finite size of the vertical angle ε and utilizing the relation from electron optics for the case when the widths of the slit and image are equal,

$$\frac{\Delta(H\rho)}{H\rho} = \frac{2S}{D}, \tag{8}$$

we obtain for the line width

$$\frac{\Delta(H\rho)}{H\rho} = \frac{3}{4}(\alpha^2 + \varepsilon^2); \tag{9}$$

which for our particular angles of divergence gives

$$\frac{\Delta(H\rho)}{H\rho} \approx 0{,}13.$$

Thus with the transmission factor realized in the given instrument, the resolution of a conventional sector spectrometer would be very poor.

The procedures and measures employed to improve the focusing were mainly the following:

1. The entrance edge of the sector was chosen in the form of the arc of a circle.
2. From the focal point (on the extension of the straight line passing through the source and the apex of the sector) there was drawn a family of tangents to the circular electron trajectories in the central plane of symmetry. The locus of these points of tangency determined the selected shape of the exit edge of the sector. Inasmuch as the selected shape of the sector edge presupposes an ideal magnetic field configuration with a sharp cut-off, additional measures were indicated.
3. Correcting plates (shims) were introduced into the gap at the edges of the pole pieces and a shielding window was mounted outside the gap for compensation of the edge effect.

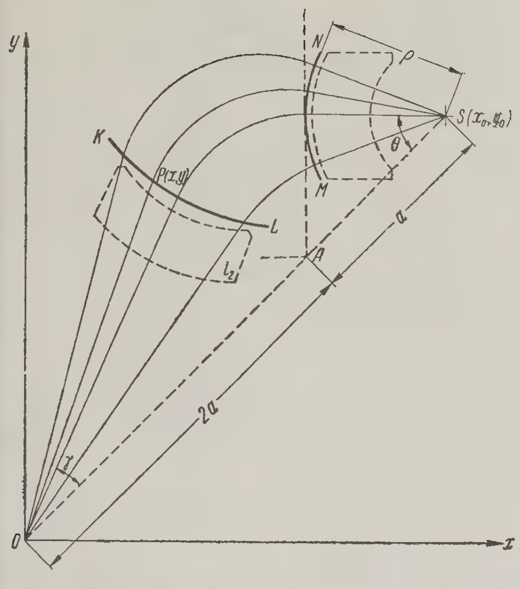

Fig.3. Diagram for derivation of the equation for the curve of the exit edge of the pole pieces: $S(x_0, y_0)$ - source, MN - entrance edge, $P(x, y)$ - point of contact of the tangent drawn through the focal point 0 (at the coordinate origin) to the trajectory, KL - sought curve for the exit edge.

4. A special device, provided for in designing the spectrometer, was used to investigate the focusing of narrow beams over the entire 45° region, and the electron detector was shifted in the counter chamber to the position of optimum intersection of these beams.

5. The final refinement of the focusing was realized by experimental modification of the stray field in the space between the exit edge of the sector and the shielding window of armco iron (l_2 in Fig.3) by gradual successive filing of the edges of the window (the design of the instrument provided for ready removal of the window from the instrument). The use of all these procedures was justified by the resultant 7-fold improvement of the instruments characteristics.

The analytic expression for the shape of the exit edge can be obtained from Fig.3, where S is the source and 0 is the coordinate origin, located at the chosen focal point. Let us use $P(x, y)$ to designate the point of contact of the tangent drawn from the focus to the circular electron trajectory in the gap (in the central plane of symmetry) and find the equation for the coordinates of this point.

We write the equation for the circular trajectory (radius ρ) passing through the point $P(x, y)$ and the equation for the tangent to this circular trajectory from the origin:

$$(x-a)^2+(y-b)^2=\rho^2, \tag{10}$$

$$a(x-a)+b(y-b)=-\rho^2. \tag{11}$$

In addition, we write the equation taking into account the fact that the coordinates of the centers a,b of all the circular trajectories lie on the circumference of a circle of radius $\rho\sqrt{2}$ with its center at the point S:

$$(a-x_0)^2+(b-y_0)^2=2\rho^2, \tag{12}$$

where x_0 and y_0 are the coordinates of point S (in our case $x_0=3\rho$ and $y_0=3\rho$).

Determining the variable coordinates a and b of the centers of the trajectories from Eqs.(10) & (11) and inserting the resultant expressions in (12), we obtain the equation for the sought locus of the points of tangency in the following form:

$$\left[\frac{x(x^2+y^2)+\rho y\sqrt{x^2+y^2}}{x^2+y^2}-x_0\right]^2+\left[\frac{y(x^2+y^2)-\rho x\sqrt{x^2+y^2}}{x^2+y^2}-y_0\right]^2=2\rho^2. \tag{13}$$

In practice it is more convenient to find the shape of the sought curve by geometric construction.

The photographic image of the focus (Fig.4) obtained by means of a conversion electron line associated with the 238 kev transition in ThC (F line) consists of

Fig.4. Photograph of focus.

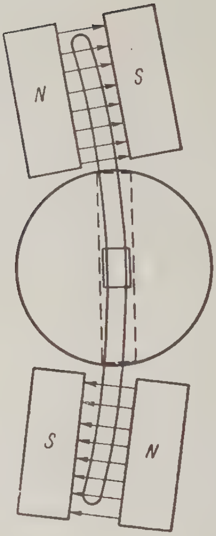

Fig.5. Diagram showing the installation and effect of the auxiliary magnets. The electrons arriving from under the plane of the drawing are focused on the rectangular region in the center and on the curved slit. The plane of the photocathode (circle) is located above the plane of the drawing (at a distance of 25 mm). The dashed lines indicate the region of the cathode to which the crystal is cemented. The electrons from the part of the slit extending beyond the cathode are deflected into the central region by the two magnets.

a pale elongated arc and a bright rectangle in the region of the top of this arc. This rectangle represents the focus of electrons, the trajectories of which form positive angles with the axial trajectory (effect of vertical focusing); the arc represents the focus of electrons, the trajectories of which form negative angles with the axial trajectory (effect of vertical defocusing). The fraction of electrons corresponding to the parts of the arc extending outside the boundaries of the photocathode equals ~20%.

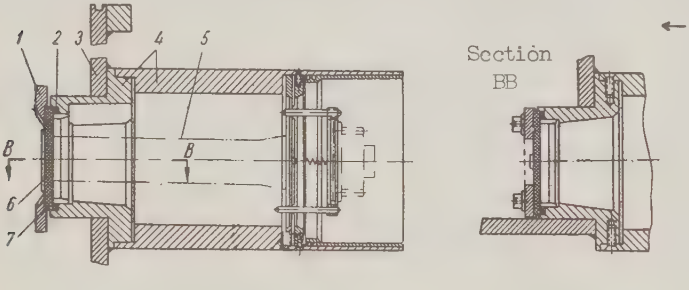

←Fig.6. Coupling of the photomultiplier and magnetic shielding with the chamber. The brass plate (1) with a cut out for the crystal (6) holds the plexiglass disk (7) to the rubber gasket (2). The photomultiplier (5) is mounted inside the magnetic shielding (4), part of which is welded into the chamber wall (3).

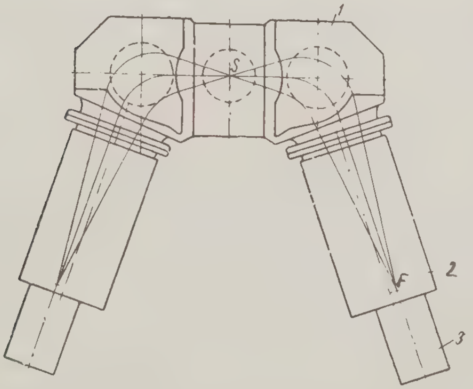

←Fig.7. Chamber of the twin magnetic spectrometer: 1 - pole piece, 2 - counter chamber, 3 - magnetic shielding of photomultiplier, S - source, F - focus.

In working with gas discharge counters, the slit in the counter was cut to the shape of the focus. In working with scintillation counters, small auxiliary magnets located inside the counter chamber were installed to collect the electrons from the regions corresponding to the projecting ends of the focal arc (see Fig.5). The slit of the receiving aperture was curved to conform to the focal arc and in the central portion was

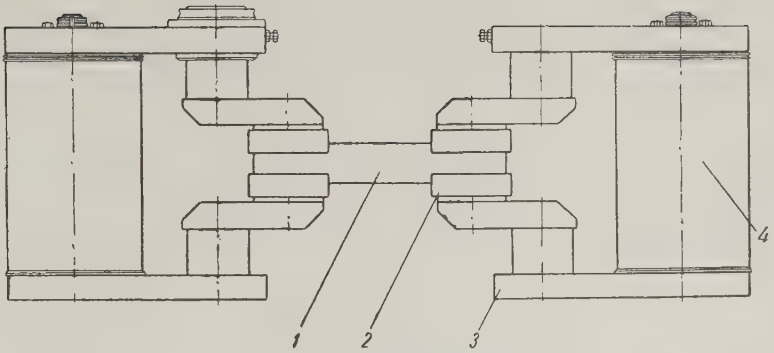

Fig.8. Coupling of the magnets with the chamber of the twin spectrometer (back view): 1 - chamber, 2 - pole piece, 3 - magnet yoke, 4 - coil.

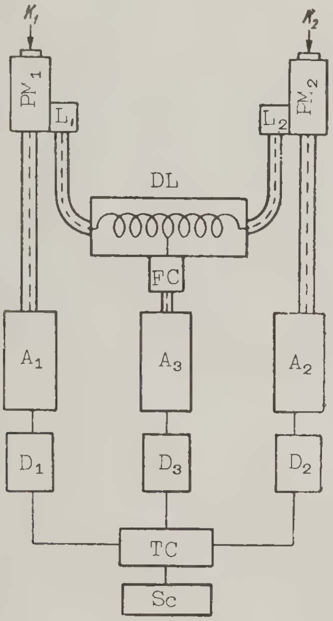

Fig.9. Block diagram of the electronic equipment associated with the twin magnetic spectrometer: K_1 & K_2 - crystals, PM_1 & PM_2 - photomultipliers in magnetic shielding, L_1 & L_2 - limiters, DL - variable delay line, FC - fast coincidence circuit, TC - triple coincidence circuit, A_1, A_2 & A_3 - amplifiers, D_1, D_2 & D_3 - discriminators, Sc - scaler.

enlarged to insure collection of the electrons deflected by the auxiliary magnets.

A thin phosphor plate, the width of which is sufficient to insure acceptance of all the electrons passing through the receiving slit, is cemented with Canada balsam to the surface of a flat plexiglass disk 5 mm thick which simultaneously serves as the chamber window and a light pipe. The outer surface of the disk is coupled to the photocathode by means of vaseline oil. There is a suitable rubber gasket between the disk and the chamber wall. Magnetic shielding of the photomultiplier is realized by means of a thick armco iron cylinder welded into the chamber wall. This cylinder encloses the photocathode and adjacent parts of the photomultiplier. The remaining part of the photomultiplier is surrounded by two coaxial cylinders.

The connection of the magnetic shielding with the chamber and the coupling of the photocathode with the chamber window are shown in Fig.6; a general diagram of the spectrometer chamber is given in Fig.7; a view of the magnet seen from the back is given in Fig.8. The given design insures magnetic independence of the two parts of the spectrometer. Fig.9 gives a block diagram of the associated electronic equipment. In contrast to the scintillation coincidence spectrometer, the magnetic spectrometer does not have differential pulse height analyzers in the side arms of the triple coincidence circuit.

The first version of the twin magnetic spectrometer, which had a smaller transmission factor, was used for investigating the RaB→RaC conversion scheme.[17] For the purpose of calibrating the spectrometer, we recorded the partial β-spectrum emitted in the decay of ThB and leading to the 238 kev excited state in ThC. The measurement results are shown in Fig.10. This spectrum was investigated earlier by a similar procedure by Feather et al[14] on a double

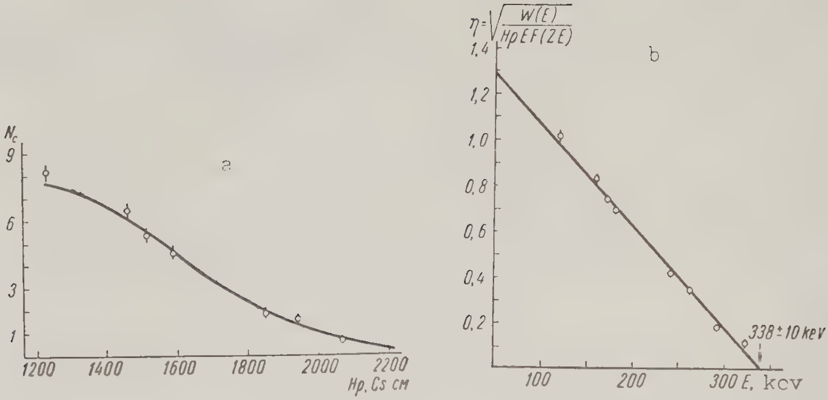

Fig.10. a - Partial β-spectrum of ThB, feeding the 238 kev level of ThC. b - Fermi plot for the partial β-spectrum.

spectrometer consisting of two 180° focusing spectrometers and by Groshev & Shavtvalov[13] on a twin lens spectrometer.

Fig.11 shows the coincidence curve obtained for the 296 and 230 kev γ-rays emitted by Eu^{147}; from this curve it may be inferred that the lifetime of the 230 kev level is less than one nanosecond.

The results of further measurements by means of this instrument will be published in the future.

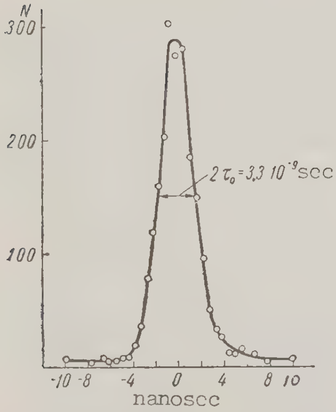

Fig.11. Coincidences of 396 and 230 kev γ-rays from Eu^{147}.

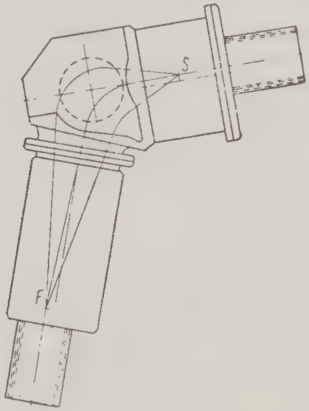

Fig.12. Diagram of the β-γ coincidence spectrometer: S - source, F - focus.

Twin β-γ coincidence spectrometer

The β-γ coincidence spectrometer has only one magnetic branch; the other branch is a scintillation spectrometer for detecting γ-rays. A number of similar coincidence spectrometers have been described in the literature.[18-20]

Either sodium iodide single crystals or organic scintillators can be used in the scintillation part of the instrument. The magnetic part consists of a single wide angle magnetic spectrometer with improved focusing of the type described above. The β-γ coincidence spectrometer as regards transmission factor and energy resolution is intermediate between the twin scintillation spectrometer and the twi magnetic spectrometer. When a sodium iodide crystal is used, the energy resolutio is better than with an organic phosphor: however, in this case the time resolution of the coincidence circuit is somewhat impaired.

As in the magnetic branch, the coupling of the photomultiplier cathode, which is enclosed by an armco iron shield outside the spectrometer chamber, with the crystal, which is located inside the chamber in the immediate proximity of the source, is realized by means of a light pipe passing through a suitable opening in the chamber wall. In this case the light pipe has a length of 50 to 80 mm and is a solid of revolution, starting with a cylinder in the region of the chamber wall and flaring out towards the scintillator to the shape most advantageous for light collection.

A diagram of the β-γ coincidence spectrometer is reproduced in Fig.12. The associated electronic equipment is similar to that employed in conjunction with the twin scintillation and magnetic spectrometers. It includes a variable delay line to provide for measurements of level lifetimes. A differential pulse height analyzer is connected only into the scintillation arm of the triple coincidence circuit.

This spectrometer can be used for investigation of β-γ, e-γ, A-γ, e-X, A-X, A-γ, e-α and β-e coincidences. In the case of the last, the decay electrons can be detected in the scintillation branch and the internal conversion electrons in the magnetic branch.

Fig.13 shows the results of measurements of the partial β-spectrum of Rb^{86}, going to the 1080 kev level in Sr^{86}. Other measurements carried out by means of this instrument will be described in a separate article.

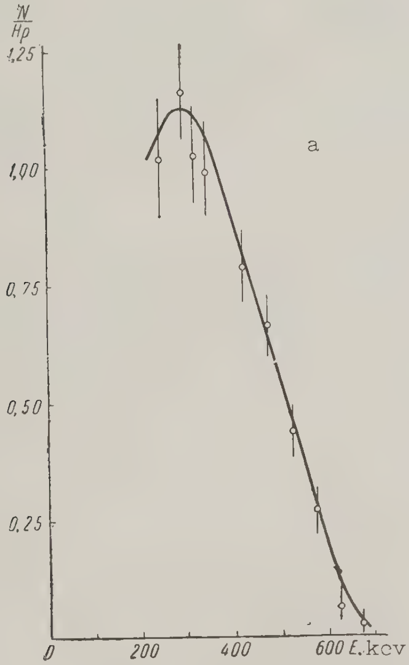

Fig.13. a - Partial β-spectrum of Rb^{86}, feeding the 1080 kev level in Sr^{86}.
b - Fermi plot for the β-spectrum.

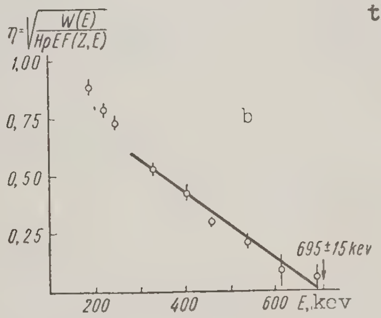

Conclusions

It will be clear from what has been said above that the three spectrometers complement each other for purposes of spectrometric investigation. Each of the spectrometers has advantages and disadvantages as compared with the others. Thus, the twin scintillation spectrometer, which has the greatest acceptance angle and thus the best $N_{1,2}/N_c$ ratio and therefore allows of carrying out studies with sources having a low specific activity, is appreciably inferior to the twin magnetic spectrometer as regards energy resolution. In view of this, in investigating complex conversion schemes one must give preference to the magnetic coincidence spectrometer.

The β-γ coincidence spectrometer occupies an intermediate position. In some cases, however, it may be the preferable instrument, for example, when the decay scheme under investigation is not very complex or if in discriminating coincidences of a given type there is no need in detailed energy analysis in both branches, for instance, because one of the radiations is the hardest component in the spectrum.

In this case there is no need to use the magnetic spectrometer and lose the higher transmission provided by the β-γ spectrometer.

In choosing between the three instruments for work on a specific problem, one must also take into account the γ-ray energies involved and the relation obtaining between the cross sections for the photoeffect and the Compton effect and the internal conversion coefficients.

Inasmuch as it is desirable that any apparatus utilizing the coincidence technique have a good transmission factor, good energy resolution and good time resolution, one can tentatively introduce the following qualitative characteristic for equipment of this type:

$$\xi = \frac{\omega_1\omega_2}{2\tau\eta_1\eta_2}. \tag{14}$$

The quantity ξ increases with improvement of all the enumerated parameters: with increase of the acceptance angle, with decrease of the line half-width, and with decrease of the resolving time of the coincidence circuit. It is assumed that the resolving time 2τ corresponds to the total coincidence counting efficiency. It is easiest to determine ξ for a twin magnetic spectrometer for which the transmission factor and the half-width have definite values. In the case of our twin magnetic coincidence spectrometer, we have

$$\xi = \frac{\omega_1\omega_2}{2\tau\eta_1\eta_2} = \frac{10^{-2}\cdot 10^{-2}}{2\cdot 10^{-2}\cdot 2\cdot 10^{-2}\cdot 4\cdot 10^{-9}} \approx 6\cdot 10^{7}.$$

It is more difficult to evaluate ξ for a twin scintillation spectrometer inasmuch as in this case the energy resolution is a function of the energy and the values of η_1 and η_2 differ for different energies. Assuming very approximately that for small energies the photopeak half-width is 20% and the solid angle is 0.2 of 4π, we have

$$\xi = \frac{0{,}2\cdot 0{,}2}{0{,}2\cdot 0{,}2\cdot 2\cdot 10^{-8}} \approx 5\cdot 10^{7}.$$

Obviously, in the high energy region, where the resolution is better, the value of ξ will be higher.

Lastly, a similar rough approximation for the β-γ spectrometer yields

$$\xi = \frac{10^{-2}\cdot 0{,}2}{2\cdot 10^{-2}\cdot 0{,}2\cdot 2\cdot 10^{-8}} \approx 2{,}5\cdot 10^{7}.$$

If in the last two instruments we use organic crystals instead of sodium iodide crystals as the scintillators, the resolving time is decreased, but on the other hand, the energy resolution is impaired.

Despite the approximate nature of the evaluations of ξ for the twin scintillation and β-γ coincidence spectrometers, it is apparent that all three spectrometers have close values of ξ (of the same order of magnitude). This must be understood in the sense that spectroscopic investigations by means of all three types of instruments will have an approximately equal value as regards the sum and quality of the resultant information. Consequently, the three instruments supplement each other in approximately the same measure.

I desire to thank A.V.Kamaev for assistance in adjusting the β-γ coincidence spectrometer and measurements of the Rb^{86} β-spectrum, I.M.Belousov for participating in the adjustment of the twin magnetic spectrometer and measurements of the ThB partial β-spectrum, A.I.Kislyakov, V.V.Il'in and T.Bedike for adjustment of the high vacuum system of the twin magnetic spectrometer and investigation of

the photoelectric multipliers and measurement of the Eu^{147} γ-γ coincidence curve.

Leningrad Physical-Technical Institute,
Academy of Sciences of the USSR

References

1. E.Berlovich, Izv.AN SSSR, Ser.fiz., 19, 343 (1955). (Trans.Bulletin,19, 305.)
2. A.Mitchell, in Beta- and Gamma-Ray Spectroscopy, K.Siegbahn, ed.Amst. 1955.
3. E.Berlovich, PTE, No.1, 68 (1958). (Trans.Inst. & Exp.Techniques).
4. R.Bell, R.Graham & H.Petch, Canad.J.Phys., 30, 35 (1952).
5. R.Post & L.Shiff, Phys.Rev., 80,1113 (1950).
6. E.Berlovich, Izv.AN SSSR, Ser.fiz., 20, 1438 (1956). (Trans.Bulletin,20, 1315.)
7. E.Berlovich, Zhur.eksp.i teor.fiz., 33, 1522 (1957). (Trans.Sov.Physics - JETP.)
8. E.Berlovich, K.Grotovskii, M.Bonits & G.Gorodinskii, Ibid., 33, 1523 (1957). (Trans.Ibid.)
9. E.Berlovich, K.Grotovski, M.Bonitz, K.Breslav & B.Preobrazhensky, Nucl. Phys., 6, 672 (1958).
10. E.Berlovich, V.Fleisher, V.Breslav & B.Preobrazhenskii, Zhur.eksp.i teor. fiz., 36, 1589 (1959). (Trans.Soviet Physics - JETP.)
11. E.Berlovich & B.Shilyaev, PTE, No.1, 62 (1958). (Trans.Inst. & Exp.Techniques.)
12. E.Berlovich, V.Klement'ev, V.Fleisher, O.Larionov, F.Murtazin & D.Apostolov, Zhur.eksp.i teor.fiz., 37, 1202 (1959). (Trans.Sov.Phys. - JETP.)
13. L.Groshev & L.Shavtvalov, Doklady AN SSSR, 68, 257 (1949); V.Sergienko, Izv.AN SSSR, Ser.fiz., 22, 198 (1958). (Trans.Bulletin,22, 195.)
14. N.Feather, J.Kyles & R.Pringle, Proc.Phys.Soc. (London), 66, 466 (1948).
15. T.Gerholm, Rev.Sci.Instr., 26, 1069 (1955).
16. E.Berlovich, Izv.AN SSSR, Ser.fiz., 18, 589 (1954). (Trans.Bulletin, 18, 274.)
17. E.Berlovich, Ibid., 16, 314 (1952).
18. H.Muether & S.Ridgway, Phys.Rev., 80, 750 (1950).
19. B.Ketelle, H.Zeldes, A.Brosi & R.Dandl, Phys.Rev., 84, 585 (1951).
20. S.Björnholm, O.Nielsen & R.Sheline, Nature, 178, 1110 (1956).

IONIZATION CHAMBER IN A MAGNETIC FIELD

- G.E.Kocharov & M.A.Yamshchikov

Pulse ionization chambers are finding increasing use in the study of nuclear reactions and investigation of the α-spectra of both long-lived isotopes and of short-lived ones, which are often available only in small amounts. This increased use is explained by the large acceptance angle of ionization chambers. Moreover, the improved energy resolution achieved in recent years[1,2] has also expanded the potentialities of ionization chambers. In particular, there have been developed techniques for investigations of coincidences between α-particles and conversion electrons[3], the last being detected by means of a proportional counter located inside the ionization chamber.

In order to extend the detected electron energy range and reduce the background due to low energy electrons the proportional counter may be installed in a magnetic field.[4] In this case the ionization chamber will also be in a magnetic field. In connection with this, it is of interest to determine the characteristics of operation of ionization chambers in magnetic fields. Investigation of the operation of chambers in a magnetic field is necessary for correct selection of the experimental geometry and operating conditions of the chamber. Moreover, by installing the ionization chamber in a magnetic field one can reduce the influence of conversion electrons on the α-spectrum. As is known[2,5] conversion electrons accompanying α-decay distort the α-particle energy distribution: specifically, several energy values correspond to each α-particle group. When the ionization chamber is placed in a magnetic field the conversion electrons (which in general move along helical trajectories) are curved back to the source and, consequently, the ionization produced by them is reduced owing to shortening of the effective path in the working volume of the chamber. As a result the conditions for observing the fine structure of α-spectra are enhanced.

Influence of the magnetic field on the associated electronic equipment

Installation of the ionization chamber in a magnetic field ($H_{max} = 3500$ oersted) made it necessary to take certain measures to minimize its influence on the operation of the associated electronic equipment. The preamplifiers, which were mounted directly on the chamber housing, were in the strongest stray field (up to 1 koe). As a first step, the preamplifier units were housed in shields of sheet iron. This proved to be insufficient. Then the preamplifier tubes (6Zh1P) were enclosed in shielding cups of armco iron (wall thickness 1.5 mm). Without this shielding the plate current and amplification factor were substantially reduced under the influence of the magnetic field. The remaining units of the electronic equipment were moved to a distance of 3 meters from the magnet. To check the effectiveness of the above measures, standard pulses from an oscillator were applied to the preamplifier input. The output pulse amplitude did not change by more than 0.05% upon switching on the magnetic field. Also there was no noticeable change in the rms value of the radio noise.

Electron motion in the presence of a magnetic field

Let us consider the influence of a magnetic field on the electron trajectories. This is important from the standpoint of correct choice of the chamber geometry. Knowledge of the electron trajectories is also necessary for explaining the effect of the magnetic field on the pulse height.

In the presence of a magnetic field directed perpendicular to the electric lines of force, the electrons will be subjected to the action of two mutually

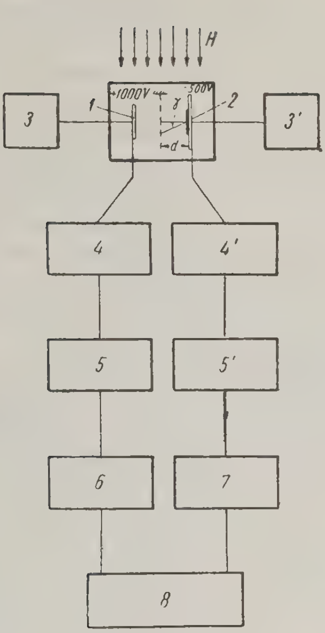

Fig.1. Block diagram of the experimental equipment: 1) collecting electrode, 2) high voltage electrode, 3 & 3') VSE-2500, 4 & 4') preamplifiers, 5 & 5') amplifiers, 6) limiter, 7) single-channel analyzer, 8) 28-channel analyzer. γ - angle between the direction of motion of the electrons in the presence of a magnetic field and the normal to the high voltage electrode.

perpendicular forces: electric and magnetic. As a result the electrons will drift at a certain angle γ relative to the electric lines of force (Fig.1). Consequently, the electron travel time will be increased, which will lead to an increase of the pulse rise time. Having measured this time, we can determine the direction of motion of the electrons.

It can readily be shown that the electron drift velocity in the gas filling the chamber in the presence of a magnetic field is given by

$$W_H = \frac{W_E}{1+\gamma^2\tau^2}, \tag{1}$$

where $\gamma = \frac{eH}{mc}$; τ is the mean time between successive collisions of an electron with gas atoms, and W_E is the electron drift velocity in the absence of a magnetic field.

It follows from Eq.(1) that the electron travel time from the high voltage electrode to the grid is

$$t_H = \frac{d}{W_H} = t_E\,(1+\gamma^2\tau^2), \tag{2}$$

where t_E is the travel time in the absence of a magnetic field.

For the purpose of experimental determination of t_H we used the pulses appearing on the high voltage electrode. The pulses from the output of a wide band amplifier were applied to an IO-4 oscillograph and photographed. A whole set of pulses ("rectangle") appeared in the photograph. The pulses with the maximum amplitude correspond to α-particles emitted parallel to the plane of the source; those with minimum amplitude correspond to α-particles emitted normal to the plane of the source. We determined the rise time of the maximum pulses and their amplitude as a function of E/p (E is the electric field strength, and p is the gas pressure in the chamber).

One of the pulse oscillograms is shown in Fig.2. One can clearly see the effect of the magnetic field (increase of the pulse rise time and decrease of the pulse height). The results of these experiments are shown in Figs.3 & 4. It follows from the experimental data that in a certain range of E/p values the electron travel time in the magnetic field increases noticeably. When narrow passband amplifiers are employed (i.e., under the usual operating conditions) this leads to impairment of the resolution in energy.[5,6] As will be evident from Fig.4 in a magnetic field saturation is attained at higher values of E/p.

From the pulse rise time and the separation between the electrodes one can calculate the electron drift velocity (Figs.5 & 6). Fig.6 also shows the variation of the electron drift velocity as a function of E/p in a magnetic field calculated according to Eq.(1). It will be evident that the agreement between the experimental dependence and the calculated curve is good. Thus having established that the drift velocity decreases in a magnetic field, we can suggest a quantitative explanation for the decrease of the pulse height (Fig.4). The decrease presumably occurs due to increase of recombination. In a magnetic field the electrons remain for a longer time in the vicinity of the positive ions and hence the probability for recombination increases.

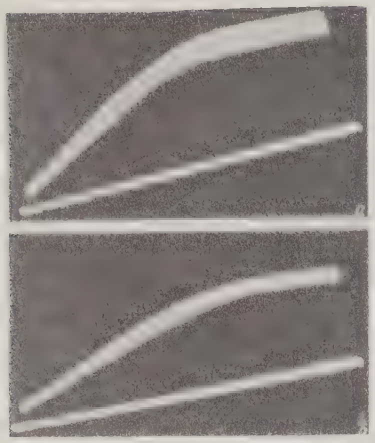

Fig.2. Oscillograms of pulses on the high voltage electrode: a) H = 0, b) H = 3500 oersted.

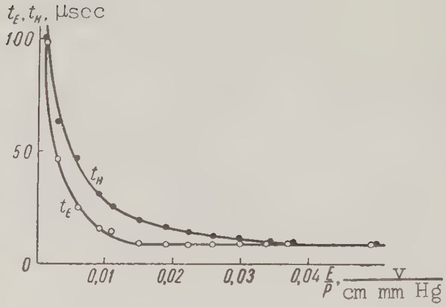

Fig.3. Variation of the electron travel time (from the high voltage electrode to the grid) as a function of *E*/*p*.

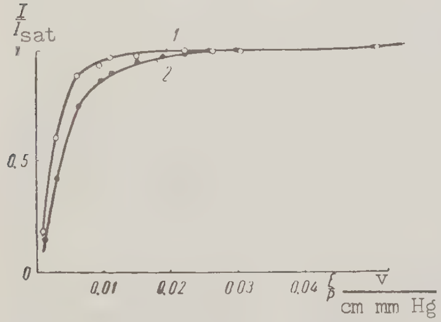

Fig.4. Variation of the pulse height on the high voltage electrode as a function of *E*/*p* : 1) H = 0, 2) H = 3500 oersted.

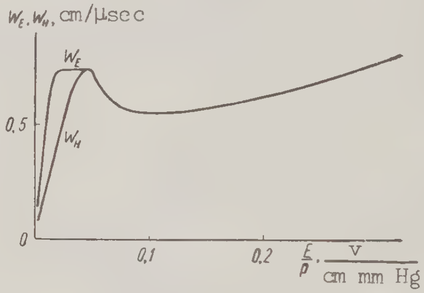

Fig.5. Variation of the electron drift velocity with *E*/*p* in chemically pure argon: W_E - H = 0, W_H - H = 3500 oersted.

When an ionization chamber is used in a magnetic field, diffusion becomes important: electrons in the region between the high voltage electrodes and the grid are "blown" off to the chamber walls. Thus, for example, for *d* = 5.5 cm (Fig.1) the amplitude of the pulses on the collecting electrode in the presence of a magnetic field fell off by a factor of almost two and the resolution was seriously impaired. It should be noted that at the same time the amplitude of the pulses on the high voltage electrode virtually did not change. This is understandable. The settling of electrons on the chamber walls does not effect the height of the pulses on the high voltage electrode inasmuch as the pulses on this electrode are due to positive ions.

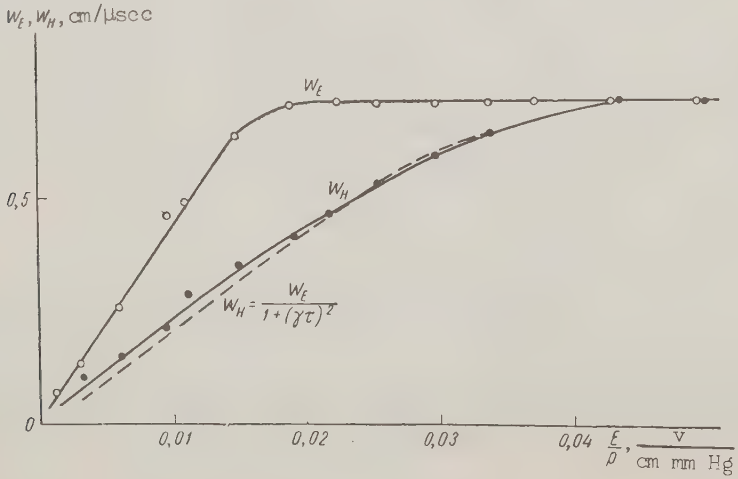

←Fig.6. Same as Fig.5. The dashed line represents the calculated dependence.

When the distance d was reduced to 3 cm, no significant decrease of the pulse amplitude on the collecting electrode was observed.

Effect of a magnetic field on conversion electrons

Precise analysis of the influence of a magnetic field on conversion electrons is complicated, hence for our consideration we introduced the following simplifying assumptions:

1. The ionization is uniform over the track.
2. The electric field does not effect the conversion electron trajectories.
3. The electron motion can be treated as though it occurs in vacuum, i.e., the electron energy is assumed to remain constant.

On the basis of assumption 1, we can regard the pulse due to a conversion electron as proportional to the residual range. Actually, of course, the specific ionization increases towards the end of the range. This leads to deviation from linearity of the decrease of pulses due to conversion electrons with increase of the magnetic field, but does not change the character of the dependence.

For rigorous solution of the problem one must consider the motion of the conversion electrons in crossed electric and magnetic fields. In such crossed fields the electrons move along a trochoid. It can be shown, however, that in our case (E_e = 30-50 kev, E = 100-200 v/cm, and H ≈ 3 koe) each period of the trochoid differs little from a circular arc. This explains the second assumption.

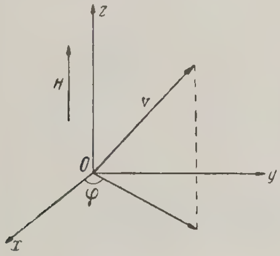

Fig.7. Diagram used in calculating the electron trajectory in a magnetic field. The magnetic field is directed along the Oz axis; the electric field, opposite to Oy; φ is the angle between the projection of the electron velocity on the xOy plane and the Ox axis.

The third assumption is the most serious. In moving through a material medium the electrons gradually lose energy. At the same time the radius of curvature of the electron trajectory gradually decreases and the electron moves along a spiral. Thus the greatest deviation along the electron trajectory from the arc of a circle occurs towards the end of its range. However, with increase of the magnetic field there remains within the working volume of the chamber the part of the range which corresponds to a smaller energy loss and the actual deviation of the trajectory from the arc of a circle decreases. Thus with increase of the magnetic field our assumption becomes increasingly valid.

From the equation of motion of an electron in a magnetic field one can obtain the magnetic field dependence of the residual range:

$$R = 2\rho(\pi - \varphi), \qquad (3)$$

where ρ is the radius of curvature of the electron trajectory in the magnetic field (the directions of the magnetic and electric fields are shown in Fig.7).

Assuming that the electron emission is isotropic, we can use (3) to construct the conversion electron energy spectrum for any given value of the magnetic field. Then knowing the electron energy spectrum, we can plot the α-particle spectrum taking into account the effect of conversion electrons. The respective curves are shown in Fig.8.

In constructing the spectrum we assumed that the half-width of the individual α-lines is 30 kev and that the shape is gaussian. It follows from Fig.8 that the intensity of the α_1 group must increase in the presence of a magnetic field (the dashed line represents the α-spectrum in the complete absence of the effect of conversion electrons).

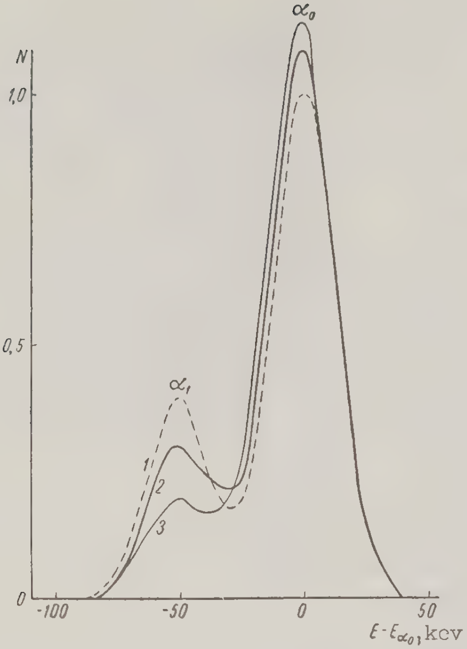

Fig.8. Alpha-spectrum of U^{234} (calculated taking into account the resolution of the instrument). The separation between the α_0 and α_1 lines is 50 kev: 1 - α-spectrum in the complete absence of the effect of conversion electrons, 2 & 3) α-spectrum taking into account the effect of conversion electrons: 2 - H = 3500 oersted, 3 - H = 0.

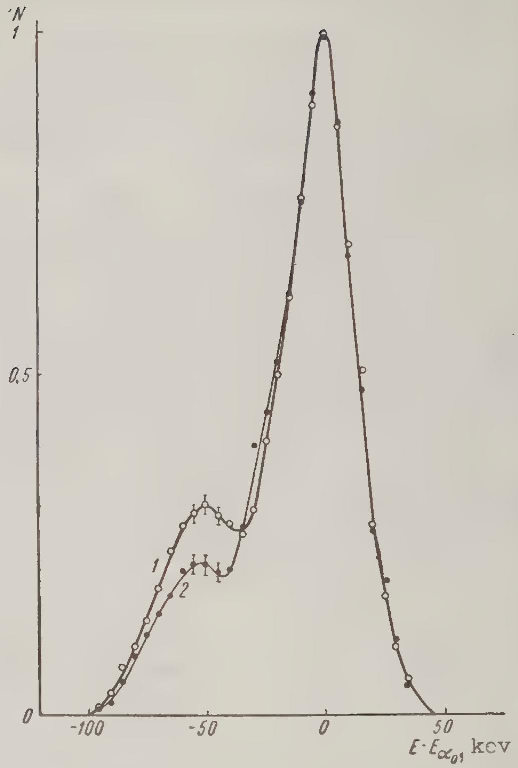

Fig.9. Experimental α-spectrum of U^{234}: 1 - H = 3500 oersted, 2 - H = = 0.

The experimental U^{234} α-spectrum is shown in Fig.9. It will be seen that upon application of a 3500 oersted field the intensity of the α_1 group does increase and that the relative increase in intensity agrees with the calculated value.

Effect of the magnetic field on δ-electrons

In the process of ionization, an α-particle, in addition to slow electrons, also produces fast electrons, so-called δ-electrons, the maximum energy of which for 5 Mev α-particles is about 2.5 kev. Almost 70% of the α-particle energy is expended on the formation of δ-electrons. These electrons also ionize the gas. The quantity measured in an ionization chamber is the total ionization. When the ionization chamber is placed in a magnetic field, the total ionization can be reduced owing to deflection of the δ-electrons back to the source, which leads to decrease of the pulse height due to α-particles. Obviously, the greatest decrease in ionization will occur for particles emitted parallel to the source.

To evaluate this effect we recorded the pulses from the collecting electrode that corresponded to α-particles emitted at angles from 90° to 90° - β, where β equals a few degrees (the angle was reckoned from the normal to the particle source). The decrease in pulse height with application of a magnetic field was less than 1%. Thus in practice the effect of a magnetic field on δ-electrons can be neglected. It should be noted that with the field used in our experiments the α-particle trajectories remained virtually unchanged.

Conclusions

1. The results of our experiments should be of help in specifying the geometry and operating conditions of ionization chambers to be used in a magnetic field.

2. With the chamber geometry and operating conditions correctly specified, the magnetic field does not affect the resolution of the instrument.

3. The effect of conversion electrons can be reduced by using a magnetic field.

4. It should be noted that operation of an ionization chamber in a magnetic field is particularly useful in working directly with a beam of accelerated particles and also in investigating α-spectra in the presence of a strong β-background.

I desire to thank A.P.Komar for his interest in the work.

Physical-Technical Institute,
Academy of Sciences of the USSR

References

1. D.W.Engelkemeir & L.B.Magnusson, Rev.Sci.Instr., 26, 295 (1955).
2. B.A.Bochagov, A.P.Komar & G.E.Kocharov, Zhur.eksp.i teor.fiz., 32, 5 (1957). (Trans.Soviet Physics - JETP.)
3. A.P.Komar, G.A.Korolev & G.E.Kocharov, Izv.AN SSSR, Ser.fiz., 22, 824 (1958). (Trans.Bulletin,22, 818.)
4. S.C.Curran, A.L.Cocroft & G.M.Insch, Proc.Phys.Soc.A, 63, 845 (1950).
5. G.E.Kocharov, A.P.Komar & G.A.Kocharov, Zhur.eksp.i teor.fiz., 36, 68 (1959). (Trans.Soviet Physics - JETP.)
6. B.G.Harvey, H.G.Jackson, T.E.Eastwood & G.S.Hanna, Canad.J.Phys., 35, 3 (1957).

INVESTIGATION OF PULSES ARISING ON THE GRID OF AN IONIZATION CHAMBER

- G.A.Korolev & G.E.Kocharov

Introduction

Pulse ionization chambers are now extensively used for investigating nuclear reactions, α-spectra and so on. The introduction of a grid made it possible to go over to recording electron pulses, which enhanced the time and energy resolution of ionization chambers. The use of pulses from different electrodes in different combinations (in coincidence and anticoincidence) makes it possible to record not only the energy of particles but also their angular distribution and point of emergence (in the case of nuclear reactions) and allows of reducing the background. The introduction of a second grid, which becomes a screening grid, allows of utilizing pulses from the first grid, the amplitude of which depends on the angle of emergence of the particles.[1,2]

The questions of the shape of the pulses from the collecting and high voltage electrodes and of the choice of the best passband of the amplifier have been examined in detail by Gillespie[3], Elmore[4] and other authors. The usual principal criterion in selecting the amplifier passband is the maximum value of the signal to noise ratio. Below we will show that in the case of pulses from the grid the optimum passband is determined primarily by the condition of conservation of the angular distribution function.

Shape of ionization chamber grid pulses

Let us consider an ionization chamber with two grids and find the shape of the voltage pulse arising on the first grid (the second grid is grounded) (Fig.1).

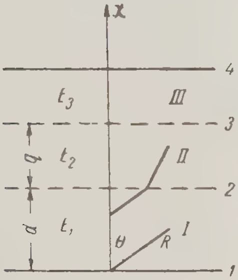

Fig.1. Diagram of ionization chamber with two grids: 1) high voltage electrode with the particle source, 2) first grid, 3) second (screening) grid, 4) collecting electrode. The potentials on the electrode are chosen so that $E_3 > E_2 > E_1$. The particle range R is assumed to lie within the volume between the high voltage electrode and the grid.

Assume that at instant $t = 0$ there was emitted from the source located on the high voltage electrode an α-particle at an angle θ relative to the normal to the electrode and that this particle produced N ion pairs in the volume of the chamber. In moving to the collecting electrode, the electrons induce a charge on the grid (accordingly, a voltage pulse arises on the grid capacitance C).

Let us calculate the magnitude of this pulse under the following assumptions: 1) there is no diffusion of the "electron track", 2) the ionization density along each α-particle track is constant, and 3) there are no electronegative impurities in the gas filling the chamber.

For convenience of calculation, let us consider the induced potential during successive time intervals:

1. The interval during which the electrons move towards the grid and the first of them reaches the grid:

$$0 \leqslant t \leqslant \frac{d - R\cos\theta}{w_1},$$

where R is the α-particle range, d is the distance between the high voltage electrode and the grid, and w_1 is the electron drift velocity in region I (Fig.1).

The space between the high voltage electrode and the grid can be regarded as a two-electrode chamber, where the grid plays the part of the collecting electrode. In replacing the grid by an equivalent solid conducting plane, the potential of the plane should be taken different from the potential of the grid by the amount $\Delta V = l(E_2 - E_1)$ (Ref.5), where l is a parameter depending on the grid geometry, and E_1 and E_2 are the field intensities in regions I and II. For the usual grid and chamber geometry the potential of the equivalent conducting plane virtually does not differ from the grid potential. Hence in determining the potential induced on the grid by a unit charge e one can make use of the formula derived by Wilkinson[6] for a two-electrode chamber:

$$\varphi = \frac{ex}{Cd},$$

where x is the distance from the high voltage electrode to the unit charge e.

At the initial instant the electrons and positive ions produced by the α-particle are at the same distance from the grid; hence the total induced potential is zero. During the electron collection time the ions remain virtually stationary, so that the positive potential induced by the ions remains constant, while the negative potential induced by the electrons increases as they approach the grid.

Hence in the time interval under consideration the total potential induced on the grid is negative and decreases linearly:

$$\varphi_1 = -\frac{Ne}{C} \cdot \frac{w_1 t}{d}.$$

2. The interval from the instant when the first electron reaches the grid to the instant when the last electron passes behind (above in Fig.1) the grid:

$$\frac{d - R\cos\theta}{w_1} \leqslant t \leqslant \frac{d}{w_1}.$$

To preclude the possibility of electrons settling on the grid, the electric field intensities in regions I and II (Fig.1) are chosen so that $E_2 > E_1$. As a result the electrons in region II move w_2/w_1 times faster* (w_2 is the drift velocity in region II). The electron track is "refracted", i.e., the angle relative to the normal changes.

The potential induced on the grid is determined by the aggregate effect of the positive ions and electrons in regions I and II and varies with time as a parabolic function, passing through a minimum:

$$\varphi_2 = -\frac{Ne}{C}\left(1 - \frac{R}{d}\cos\theta + \frac{w_1}{d}t' - \frac{w_1^2 m}{2dR\cos\theta}t'^2\right),$$

where

$$m = 1 + \frac{T_1}{T_2}; \quad T_1 = \frac{d}{w_1}; \quad T_2 = \frac{q}{w_2}; \quad t' = t - \frac{d - R\cos\theta}{w_1};$$

q is the distance between the first and second grids.

3. The interval from the instant when the last electron passes behind the first grid to the instant when the first electron reaches the second grid:

$$\frac{d}{w_1} \leqslant t \leqslant \frac{d}{w_1} + \frac{q}{w_2} - \frac{R\cos\theta}{w_1}.$$

---

*It must be noted that w_2 is not always greater w_1, although $E_2 > E_1$ (see, for example, Ref.7).

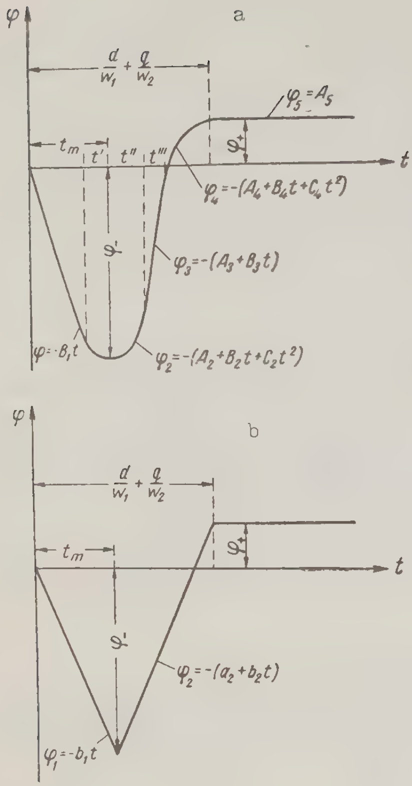

Fig.2. Shape of grid pulses: a) precise, b) approximate.

The potential increases linearly with time:

$$\varphi_3 = -\frac{Ne}{C}\left(1 - \frac{R\cos\theta}{2dm} - \frac{w_2}{q}\,t''\right),$$

where

$$t'' = t - \frac{d}{w_1}\,.$$

4. The interval during which the electron track passes through the second grid:

$$\frac{d}{w_1} + \frac{q}{w_2} - \frac{R\cos\theta}{w_1} \leqslant t \leqslant \frac{d}{w_1} + \frac{q}{w_2}\,.$$

The potential varies with time as a parabolic function, attaining a maximum:

$$\varphi_4 = -\frac{Ne}{C}\left(\frac{mR\cos\theta}{2d} - \frac{w_2}{q}\,t''' + \frac{w_1 w_2}{2qR\cos\theta}\,t'''^2\right),$$

where

$$t''' = t - \frac{d}{w_1} - \frac{q}{w_2} + \frac{R\cos\theta}{w_1}\,.$$

5. The interval after all the electrons have passed behind the second grid:

$$t \geqslant \frac{d}{w_1} + \frac{q}{w_2}\,.$$

The potential induced on the grid is due only to the positive ions:

$$\varphi_5 = \varphi_+ = \frac{Ne}{C}\cdot\frac{X}{d}\cos\theta, \qquad (1)$$

where X is the distance from the center of gravity of the ions to the beginning of the α-particle track. In the case of uniform ionization $X = R/2$.

The general shape of the pulse on the grid is shown in Fig.2,a. The pulse consists of two parts: a negative part φ_- and a positive part φ_+. The negative pulse attains a maximum value at the time

$$t_m = \frac{d - R\,(1 - {}^1/m)\cos\theta}{w_1}\,, \qquad (2)$$

and its amplitude is a linear function of $\cos\theta$:

$$\varphi_- = -\frac{Ne}{C}\left[1 - \frac{R}{d}\left(1 - \frac{1}{2m}\right)\cos\theta\right]. \qquad (3)$$

Thus the dependence of the pulse amplitude on the angle of emission of the α-particle is evinced both in the positive (1) and in the negative (3) parts of the grid pulse.

Choice of the passband in working with negative grid pulses

As a rule, one strives to obtain the maximum signal to noise ratio in pulse amplifiers. This ratio depends both on the parameters of the first preamplifier tube and on the passband of the amplifier, which is determined by the differentiating and integrating circuits. In the case of negative grid pulses, the choice of the passband is particularly important in view of the fact that the differentiating and integrating circuits have a substantially different influence on the pulses associated with particles emitted at different angles. If the passband is not properly chosen, the angular distribution of pulses may be distorted.

Calculation of the pulse at the output of the differentiating and integrating circuits showed that the output pulse attains a maximum during the time T_M which is given by the equation

$$e^{-\frac{T_M}{T_i}} \cdot \frac{1-\frac{T_i\,dm}{TR\cos\theta}\cdot e^{\frac{T_1}{T_i}\left(1-\frac{R}{d}\cos\theta\right)}}{\frac{T_i\,dm\,(p-1)}{T_1R\cos\theta}} - \frac{T_1R\cos\theta}{T_i\,dm\,(p-1)} \times \left\{1-\frac{T_i\,dmp}{T_1R\cos\theta}\cdot e^{\frac{T_1}{T_ip}\left(1-\frac{R}{d}\cos\theta\right)}\right\} e^{-\frac{T_M}{T_ip}} = 1, \qquad (4)$$

where $p = T_d/T_i$; T_d and T_i are the time constants of the differentiating and integrating circuits. The pulse amplitude equals

$$U = -\frac{Ne}{C}\left\{p\left[\frac{T_i md}{T_1R\cos\theta}\left(1-\frac{R}{d}\cos\theta\right)+\frac{md\,(p+1)}{p^2R\cos\theta}-\frac{T_i}{T_1}\right]+\right.$$
$$+\frac{T_ip^2}{T_1(p-1)}\left[1-\frac{T_i\,mdp}{T_1R\cos\theta}e^{\frac{T_1}{T_ip}\left(1-\frac{R}{d}\cos\theta\right)}\right]e^{\frac{T_M}{T_ip}} -$$
$$\left.-\frac{T_i\,p}{T_1(p-1)}\left[1-\frac{T_i md}{T_1R\cos\theta}e^{\frac{T_1}{T_M}\left(1-\frac{R}{d}\cos\theta\right)}\right]e^{\frac{T_M}{T_i}}-\frac{T_i\,mdp}{T_1^2R\cos\theta}T_M\right\}. \qquad (5)$$

It will be evident that determination of the pulse rise time and amplitude by means of Eqs.(4) and (5) is rather complicated. Hence it is expedient to make certain approximations. It may be assumed that the grid pulse decreases linearly to the true value φ_- as given by (3) during the true time t_m (2), and then linearly increases to the value φ_+ (1), so that the total duration is equal to $\frac{d}{w_1}+\frac{q}{w_2}$ (Fig.2,b). For an α-particle emitted at an angle $\theta = 90^\circ$, the approximated pulse coincides with the true pulse. The greatest error obtains for the pulses of α-particles emitted at $\theta = 0^\circ$.

Thus, we have

1. $\varphi_1=\frac{\varphi_-}{t_m}t$ for $0\leqslant t\leqslant t_m$;
2. $\varphi_2=\varphi_-+\frac{\varphi_+-\varphi_-}{\frac{d}{w_1}+\frac{q}{w_2}-t_m}(t-t_m)$ for $t_m\leqslant t\leqslant\frac{d}{w_1}+\frac{q}{w_2}$,

where φ_+, φ_- and t_m are determined from (1), (3) and (2).

The pulse rise time t_0 to the maximum and the maximum amplitude U_- at the output of the differentiating and integrating circuits are given by

$$t_0 = \frac{p}{p-1}T_i\ln\frac{(A+B)\,e^{\frac{t_m}{T_i}}-A}{(A+B)\,e^{\frac{t_m}{pT_i}}-A}, \qquad (6)$$

$$U_- = pT_1\left\{B-\frac{\left[(A+B)\,e^{\frac{t_m}{T_i}}-A\right]^{\frac{1}{1-p}}}{\left[(A+B)\,e^{\frac{t_m}{pT_i}}-A\right]^{\frac{p}{1-p}}}\right\}, \qquad (7)$$

where

$$A=\frac{Ne}{C}\cdot\frac{1-\frac{R}{d}\left(1-\frac{1}{2m}\right)\cos\theta}{\frac{d-R\left(1-\frac{1}{m}\right)\cos\theta}{w_1}}; \quad B=\frac{Ne}{C}\,\frac{1-\frac{R}{2d}\left(1-\frac{1}{m}\right)\cos\theta}{\frac{q}{w_2}+\frac{R}{w_1}\left(1-\frac{1}{m}\right)\cos\theta}.$$

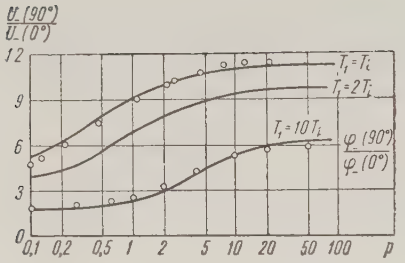

Fig. 3

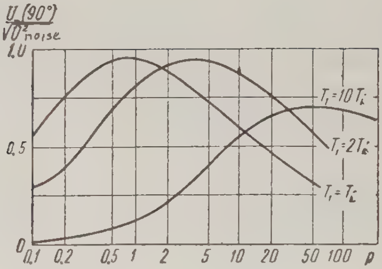

Fig. 4

Fig.3. Variation of $\frac{U_-(90°)}{U_-(0°)}$ with the amplifier passband. The curves were calculated for the case when $R = d$ and $T_1 = 2T_2$; the points represent experimental data.
Fig.4. Variation of the signal to noise ratio in arbitrary units as a function of the amplifier passband for α-particles emitted at an angle $\theta = 90^\circ$.

It is known that in the case of isotropic emission of α-particles the differential pulse height distribution on the grid, as on the high voltage electrode, should have the form of a rectangle. As analysis of Eq.(7) shows, the shape of the angular distribution at the amplifier output depends on the passband and in general is not rectangular. We find that the ratio $\frac{\varphi_-(90°)}{\varphi_-(0°)}$ at the amplifier output depends on the geometry and operating conditions of the chamber and equals $1 - \frac{R}{d}\left(1 - \frac{1}{2m}\right)$. The ratio $\frac{U_-(90°)}{U_-(0°)}$ at the amplifier output differs from $\frac{\varphi_-(90°)}{\varphi_-(0°)}$, and the greater this difference, the more appreciable the distortion of the differential pulse distribution. This imposes certain limitations on choice of the amplifier passband. On the other hand, as was noted above, the general approach is to choose the passband so as to obtain the best signal to noise ratio. By way of illustration in Figs.3 & 4 we show the curves characterizing the variation of $\frac{U_-(90°)}{U_-(0°)}$ and the signal to noise ratio with the passband $(p = T_d/T_i)$ for some particular cases. It will be evident from the curves that the angular distribution is not distorted for certain definite values of p.

In Fig.3 we also show the experimental data for two particular cases, which are in good agreement with the calculated data. The values of w_1 and w_2 were determined from the experimental field dependence of the electron drift velocity^8. Thus to retain the true angular distribution one must choose the passband so that $\frac{U_-(90°)}{U_-(0°)} = \frac{\varphi_-(90°)}{\varphi_-(0°)}$. In this case the signal to noise ratio may not be the maximum attainable. Moreover, one must know the variation of the electron drift velocity with the electric field intensity.

The fact that the optimum passband depends on the chamber geometry, the operating conditions and the gas filling the chamber complicates the matter of recording angular distributions and limits the range of usefulness of negative grid pulses.

Influence of diffusion on negative grid pulses

In considering the motion of electrons to the collecting electrode one must take into account the influence of diffusion, owing to which the electron tracks are elongated and thickened. The pulse magnitude is affected by electron diffusion only in the direction of the axis (Fig.1). Increase in the length of the electron tracks, as will be evident from Eq.(3), leads to reduction of the negative pulse amplitude. It can be shown that the relative decrement in pulse amplitude due to diffusion is described by

$$\frac{\Delta\varphi_-}{\varphi_-} = \frac{0{,}178 \sqrt{\frac{\eta}{\Delta V}\left[1 - \frac{R}{d}\left(1 - \frac{1}{m}\right)\cos\theta\right]}\left(1 - \frac{1}{m}\right)}{1 - \frac{R}{d}\left(1 - \frac{1}{2m}\right)\cos\theta} \tag{8}$$

where η is the mean electron energy in thermal agitation units (corresponding to $3.7 \cdot 10^{-2}$ ev at 15°), and ΔV is the potential difference between the grid and the high voltage electrode.

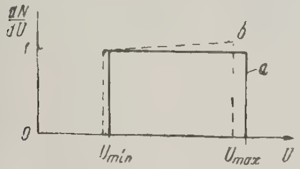

Fig. 5

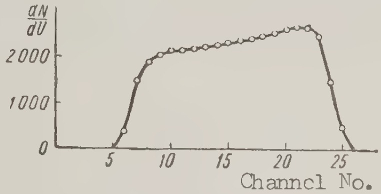

Fig. 6

Fig.5. Differential pulse height distribution for isotropic emission of α-particles: a) disregarding diffusion, b) taking diffusion into account.

Fig.6. Experimental differential distribution of negative grid pulses due to U^{234} α-particles in argon.

As will be evident from Eq.(8), the relative decrement in pulse amplitude is a nonlinear function of the cosine of the angle of emission of the α-particles, which means that there is distortion of the angular distribution. In the case of isotropic emission of α-particles, the differential pulse height distribution will be distorted as shown in Fig.5. The experimentally recorded distribution of α-particles in argon does show this distortion (Fig.6). In recording the angular distribution the passband was chosen with reference to the curves of Fig.3 so that $\frac{U_-(90^\circ)}{U_-(0^\circ)}$ would be equal to $\frac{\varphi_-(90^\circ)}{\varphi_-(0^\circ)}$. This eliminated distortion of the rectangle associated with choice of the amplifier passband.

It also follows from Eq.(8) that the decrement of the pulse amplitude depends (through η) on the type of gas used in the chamber. The values of $\Delta\varphi_-/\varphi_-$ in different gases for the case $\theta = 90°$, $\Delta V = 520$ v and $m = 3$ are listed below:

Gas	$\frac{\Delta\varphi_-(90^\circ)}{\varphi_-(90^\circ)}$	Gas	$\frac{\Delta\varphi_-(90^\circ)}{\varphi_-(90^\circ)}$
H_2	0,009	He	0,017
O_2	0,012	Ne	0,041
N_2	0,014	A	0,057

Obviously, use of pure monatomic gases (in which θ is large) leads to the greatest distortion of the angular distribution owing to diffusion. The distorted α-particle angular distribution recorded in pure argon (Fig.6) is corrected and becomes a regular rectangle if 3% methane is added to the argon. This is explained by the fact that the addition of methane results in a sharp decrease of the mean electron energy[7] and $\Delta\varphi_-/\varphi_-$ also decreases.

Thus, when negative grid pulses are used for recording the angular distribution it is important to choose a gas in which the mean electron motion energy is low.

Positive grid pulses

According to Eq.(1), the amplitude of a positive grid pulse is

$$\varphi_+ = \frac{Ne}{C} \cdot \frac{X}{d} \cos\theta .$$

As noted above, the positive pulse φ_+ is produced by positive ions. Inasmuch as the diffusion coefficient for positive ions is small, the amplitude of φ_+ is virtually not affected by diffusion of ions. Electron diffusion can influence only the shape of the positive grid pulses.

If we consider positive grid pulses alone, i.e., divorced from negative pulses, we find that the angular distribution of the positive pulses does not depend on the amplifier passband. Actually each positive pulse φ_+ is always preceded by a negative pulse φ_-, which in passing through the differentiating circuit yields a positive "throw" or overshoot. The subsequent positive grid pulse is superposed on this overshoot so that its amplitude is not rendered correctly.

For the positive pulse per se the best signal to noise ratio is obtained if the passband is chosen so that $T_d = T_i$ (i.e., $p = 1$). If, however, one takes into account the overshoot due to φ_-, the total positive pulse height at the amplifier output will be given by

$$U_+ = \alpha e^{-\frac{\alpha - \beta}{\alpha}}, \tag{9}$$

where

$$\alpha = T \frac{\varphi_-(T_1 + T_2) - \varphi_+ t_m}{T_1 + T_2 - t_m} e^{\frac{t_m}{T}} + T \frac{\varphi_+ - \varphi_-}{T_1 + T_2 - t_m} e^{\frac{T_1 + T_2}{T}} - \frac{T\varphi_-}{t_m},$$

$$\beta = \frac{T_1 + T_2 + T}{T_1 + T_2 - t_m} (\varphi_+ - \varphi_-) e^{\frac{T_1 + T_2}{T}} + (T - t_m) \left(\frac{\varphi_-}{t_m} - \frac{\varphi_+ - \varphi_-}{T_1 + T_2 - t_m} \right) e^{\frac{t_m}{T}} - \frac{T\varphi_-}{t_m}.$$

$T = T_d = T_i$ and φ_-, φ_+ and t_m are given by Eqs.(3), (1) and (2).

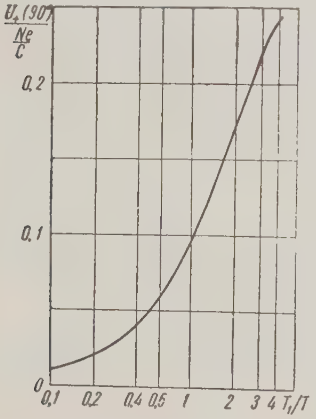

Fig.7. Variation of the negative pulse overshoot with the ratio T_1/T for α-particles emitted parallel to the electrode. Ne/C is the negative pulse amplitude; C is the grid-ground capacitance.

It will be evident that in (9) the variation of U_+ with $\cos\theta$ is nonlinear. This means that the negative pulse overshoot will distort the angular distribution of positive pulses and that consequently one must eliminate or at least reduce this overshoot.

Fig.7 shows the variation of the positive pulse amplitude for an α-particle emitted at an angle $\theta = 90°$ with the ratio T_1/T (this is essentially the negative pulse overshoot, inasmuch as for $\theta = 90°$, $\varphi_+ = 0$). Since the choice of T is limited by the noise characteristics of the output tube, the obvious way to decrease the overshoot is to reduce T_1, i.e., to use a gas in which the electron drift velocity is high. In our case addition of 3% methane to the chemically pure argon led to a reduction of T_1 from 10 to 1 μsec, as a result of which the magnitude of the overshoot was reduced by a factor of 10. It must be noted, however, that the overshoot is reduced but not wholly eliminated by this expedient.

The negative pulse overshoot can be eliminated by blocking out the negative pulses by means of a discriminator passing pulses of only one polarity. The discriminator should be introduced at the input of the differentiating circuit. For good pulse selection and to avoid overloading the amplifier tubes by high pulses, the discriminator with the differentiating circuit should be coupled into the amplifier at the point where the pulse heights are 5-10 v. The angular distribution obtained with this arrangement was not distorted.

In a number of cases, for example, in working with particle accelerators, difficulties are encountered owing to overloading of the amplifier tubes by microphonics. In such cases one can couple in at the amplifier input an auxiliary differentiating circuit with a time constant several times greater than that of the main differentiating circuit following the discriminator. The auxiliary differentiating circuit gives almost no negative pulse overshoot and at the same time substantially reduces overloading due to microphonic oscillations.

Conclusions

In using negative grid pulses for angular distribution measurements one must:

1) fill the chamber with a gas for which the diffusion coefficient is small, and

2) choose an amplifier passband for which the angular distribution is not distorted.

When positive grid pulses are used for recording the angular distribution one must:

1) use a gas in which the electron drift velocity is high, and

2) reduce or eliminate the negative part of the grid pulse before feeding the positive pulse into the differentiating circuit.

References

1. B.A.Bochagov, A.A.Vorob'ev & A.P.Komar, Izv.AN SSSR, Ser.fiz., 20, 1455 (1956). (Trans.Bulletin,20, 12a, 1331.)
2. B.A.Bochagov, Thesis, Physical-Technical Inst., USSR Acad.of Sci., 1956.
3. A.B.Gillespie, Signal, Noise and Resolution in Nuclear Counter Amplifiers. London, 1953.
4. W.C.Elmore, Nucleonics, 2(3), 16 (1948).
5. O.Bunemann, T.E.Cranshaw & J.A.Harvey, Can.J.Research, A 27, 191 (1949).
6. D.H.Wilkinson, Ionization Chambers and Counters, Cambridge, 1950.
7. W.N.English & G.C.Hanna, Can.J.Phys., 31, 768 (1953).
8. G.E.Kocharov & M.A.Yamshchikov, Present issue of the Bulletin, p.336.

ROTATIONAL LEVELS IN DEFORMED ODD-ODD NUCLEI

- L.K.Peker

According to published data, rotational levels have been detected only in one odd-odd nucleus, namely, Lu^{176}.[1] In the present contribution we show that such levels are evinced in a number of other odd-odd nuclei and evaluate the probable level energies. These are calculated by means of an equation of the form

$$E_I = \frac{\hbar^2}{2J}[I(I+1) - I_0(I_0+1)]. \qquad (1)$$

Inasmuch as usually the ground state spin I_0 of the nucleus is known, for calculating the energy one must evaluate the moment of inertia $J_{\text{o-o}}$ of the odd-odd nucleus. This can be done as follows.

It is evident from analysis of the properties of odd-A nuclei that the odd nucleon makes an appreciable contribution (to 50-70%) to the moment of inertia. The magnitude of this contribution δJ depends substantially on the quantum state of the extra nucleon;[2,3] δJ is defined as the difference between the moment of inertia $J_{\text{o-e}}$ of the odd-even nucleus and the moment of inertia $J_{\text{e-e}}$ of the neighboring even-even nucleus, lacking the unpaired nucleon:

$$\delta J_{p \text{ or } n} = J_{\text{o-e}} - J_{\text{e-e}},$$

The index p corresponds to an odd proton; n - to an odd neutron.

Inasmuch as in deformed nuclei the coupling between the outer nucleons is appreciably weaker than the coupling of the outer nucleons with the nuclear surface, in the first approximation the odd proton and neutron in odd-odd nuclei may be assumed to move independently of each other. Hence it is expedient to assume that each of them makes an independent contribution to the total moment of inertia. In the given approximation the moment of inertia of an odd-odd nucleus can be written

$$J_{\text{o-o}} = J_{\text{e-e}} + \delta J_p + \delta J_n. \qquad (2)$$

The values of $J_{\text{e-e}}$, δJ_p and δJ_n can be found from the energies of the rotational levels in neighboring even-even and odd-even nuclei in which the odd nucleon is in the same quantum state as in the odd-odd nucleus under consideration.

Rotational levels in odd-odd nuclei

Nucleus	I_0	δJ_p, %	δJ_n, %	$\delta J_p + \delta J_n$, %	E_1		E_2/E_1		Method of excitation	Data of Ref.
					theo	exper	theo	exper		
$_{63}Eu^{152}_{89}$	3—	~31	~41	~72	94	92	—	—	(n, γ)	[6,7]
$_{63}Eu^{154}_{91}$	3—	~31	~41	~72	~79	75	2,25	2,21	(n, γ)	[6,7]
$_{71}Lu^{174}_{103}$	1—	~ 7	~13	~20	45	44,7	—	—	Isomer decay	[4]
$_{71}Lu^{176}_{105}$	7—	~ 8	~18	~26	~181	184	2,12	2,14	Coulomb excitation	[1]
$_{73}Ta^{182}_{109}$	3—	~ 6	~10	~16	116	113	2,25	2,29	(n, γ)	[6,8]
$_{75}Re^{188}_{113}$	1—	~18	~51	~69	61	~60	—	—	Isomer decay	[5]

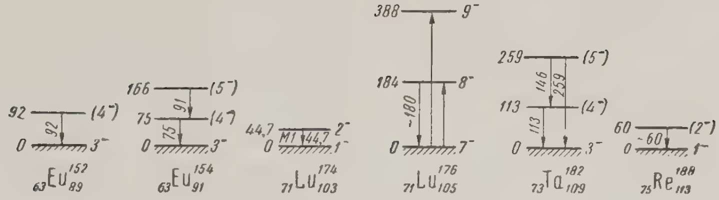

Rotational levels in odd-odd nuclei.

In the accompanying table we list the experimental values of δJ_p and δJ_n for a number of nuclei, taken from Mottelson & Nilsson[3], and the values, calculated by means of Eqs.(1) and (2), of the energy E_1 of the first rotational level and the ratio E_2/E_1 of the energies of the second and first rotational levels.

Actually comparison of the calculated values of E_1 and E_2 with the experimental data is not as simple a matter as one could wish. The rotational level energies E_1 and E_2 have been accurately determined by the method of Coulomb excitation only in $_{71}Lu^{176}$.[1] The table shows that these experimental data are in good agreement with the calculated values. The situation is somewhat more complicated in the case of the other nuclei. The spins of the rotational levels follow in the order $I_0+1; I_0+2\ldots$ and are always greater than unity. Hence these levels are virtually not excited in β-decay of even-even nuclei with spin 0.

Levels with spin $I>1$ can be excited in the decay of isomeric states of odd-odd nuclei, the spin of which is greater than the spin in the ground state. Isomeric states of this type have been observed for $_{71}Lu^{174}$ (Ref.4) and $_{75}Re^{188}$ (Ref. 5). In their decay there are excited levels with spin and parity 2- and energies 44.7 and ~60 kev in the former and latter, respectively. Comparison of these energies with the calculated values of E_1 indicate that these levels can be interpreted as the first rotational levels of Lu^{174} and Re^{188} (see figure).

Another method of detecting rotational levels is connected with analysis of the β-spectra accompanying the (n,γ) reaction on odd-Z nuclei. Unfortunately, the available data on these γ-spectra are so scanty that one cannot precisely establish the energies of the excited levels in the nuclei of interest to us. However, comparison of the γ-transition energies in these spectra with the calculated values of E_1 (see table) shows that some of them can be interpreted as transitions between the first and second rotational levels. In this way one can at least tentatively establish the heights of rotational levels in such odd-odd nuclei as Eu^{152}, Eu^{154} and Ta^{182} (see figure).

Next let us consider the multipolarities of the γ-transitions between rotational levels with $\Delta I=1$. As is known, these transitions are mixed M1 + E2 transitions. According to the unified nuclear model, the reduced M1 transition probability is given by the formula[2]

$$B(M1)=f(I_i, I_f, K)\ (g_K-g_R)^2. \tag{3}$$

Inasmuch as the gyromagnetic ratio, $g_R \approx Z/A$, due to collective nuclear motion, is approximately the same in neighboring nuclei and, according to the experimental data[2], equals 0.2-0.6, the fraction of M1 transitions in the mixture depends on the magnitude of the geomagnetic ratio, g_K, due to motion of the unpaired nucleon.

The admixture of E2 in rotational transitions with $\Delta I=1$ in odd-even nuclei is usually small (except for the case when $g_K \approx g_R$) and does not exceed 20%; according to Alder et al[2], however, it is not less than 2-3%.

In odd-odd nuclei the fraction of E2 transitions of this type can be substantially smaller than in odd-even nuclei. For such nuclei[9]

$$g_K = \frac{1}{K}(\Omega_p g_{Kp} + \Omega_n g_{Kn}); \quad K = |\Omega_p \pm \Omega_n|, \tag{4}$$

where the terms in the parentheses describe the contributions of the odd proton and odd neutron separately, and can be obtained from analysis of the experimental data on neighboring odd-even nuclei with the same odd nucleons. For large Ω_p and Ω_n, these terms appreciably exceed g_{Kp} and g_{Kn}. If g_{Kp} and g_{Kn} have the same sign and $K = |\Omega_p - \Omega_n|$ is small, g_K becomes large. Inasmuch as it may be expected that for odd-odd nuclei $g_R \approx 0.2\text{-}0.4$, the difference $(g_K - g_R)^2$ in such states is large and $I+1 \rightarrow I$ rotational transitions must be virtually pure M1 (whereas the reverse $I \rightarrow I+1$ transitions occurring in Coulomb excitation must be pure E2). Evaluations show that in the most unfavorable cases when g_{Kp} and g_{Kn} have opposite signs, the fraction of E2 transitions is very small and their effect virtually unnoticeable. Lu^{174} can serve as an example of such an odd-odd nucleus. Measurements of the internal conversion coefficients show that the fraction of E2 in the rotational 44.7 kev transition does not exceed 0.7-0.3%.[4]

Such a small admixture of E2 can readily be explained if we recall that in Lu^{174} $\Omega_p = 7/2+$, $\Omega_n = 5/2-$, $K = |\Omega_p - \Omega_n| = 1$, $g_{Kp} \approx (0.76\text{-}0.9)$ (calculated on the basis of Lu^{175}), and $g_{Kn} = -0.5$ (basis Yb^{173}). Insertion of these data in Eq.(4) gives $g_K = 1.1\text{-}1.9$.

Let us compare the admixture of E2 in the rotational transition in Lu^{174} with the admixture of E2 in the rotational transitions in odd-even nuclei with approximately the same values of g_K and g_R. It follows from the table given by Alder et al[2] that in Ho^{165} $\Omega_p = 7/2-$, $g_K = 1.12$, $g_R \approx 0.33$. In this nucleus the 95 kev rotational transition is characterized by 96% M1 + 4% E2.

If we assume that g_K and g_R in Ho^{165} and Lu^{174} are identical, we find that the E2 transition in Lu^{174} is retarded as compared with the E2 transition in Ho^{165} for the following reasons.

1. The 2.1-fold energy difference leads to retardation of the E2 transition by a factor of $(2.1)^5$ and of the M1 transition by a factor of $(2.1)^3$. Consequently, the E2 transition in Lu^{174} is retarded by a factor of 4.4 relative to the M1 transition.

2. The difference between the values of the internal quadrupole moment Q_o (equal to 8.0 in Ho^{165} and 7.6 in Lu^{174}) leads to retardation of the E2 transition in Lu^{174} by a factor of ~1.1.

3. Lastly, the difference in the respective values of K leads to retardation of the E2 transition in Lu^{174} by a factor of ~1.1. As a result of the aggregate effect of all three factors the E2 transition in Lu^{174} is slowed down by a factor of 5.3 as compared with the E2 transition in Ho^{165}, and, consequently, the fraction of E2 in the rotational transition is reduced from 4% in Ho^{165} to 0.7% in Lu^{174}. This last value is in good agreement with the experimental data. Naturally, our initial assumption regarding the equality of g_K and g_R for both nuclei, upon which the evaluations are based, is not entirely valid, and these evaluations are given here only by way of illustration. They do show, however, that the fraction of E2 transitions in Lu^{174} must be very small.

In the odd-odd nucleus $_{71}Lu^{176}$, $\Omega_p = 7/2+$, $g_{Kp} = (0.66\text{-}0.9)$ (basis Lu^{175}), $\Omega_n = 7/2-$ and $g_{Kn} = -0.1$ (basis Hf^{177}).

For this nucleus, however, $K = (\Omega_p + \Omega_n) = 7-$. Insertion of these values in Eq.(4) gives $g_K \approx 0.4$. Inasmuch as $g_R \approx 0.3\text{-}0.4$, the difference $(g_K - g_R)^2$ in the case of Lu^{176} is small. Hence there must be an appreciable admixture of E2 in the $I+1 \rightarrow I$ type γ-transitions between the rotational levels of Lu^{176}.

Similar evaluations can readily be carried out for the rotational transitions in other odd-odd nuclei.

I desire to express my sincere gratitude to L.A.Sliv, M.A.Listengarten and G.M.Shklyarevskii for helpful discussions.

Scientific-Research Physical Institute,
"A.A.Zhdanov" Leningrad State University

References

1. B.Elbek, M.C.Olesen & O.Skilbreid, Nucl.Phys., 10, 294 (1959).
2. K.Alder, A.Bohr, T.Huus, B.Mottelson & A.Winther, Revs.Mod.Phys., 28, 432 (1956).
3. B.R.Mottelson & S.G.Nilsson, Mat.-fys. Skr.Dan.Vid.Selsk., 1, 8 (1959).
4. V.A.Romanov, M.G.Iodko & V.V.Tuchkevich, Materialy II Soveshchaniya po neitronodefitsitnym yadram v OIYaI (Transactions of the 2nd Conference on Neutron-Deficient Nuclei held at the Joint Institute for Nuclear Research), Dubna, June, 1959.
5. J.W.Mihelich, Phys.Rev., 89, 907 (1953); A.Flammersfeld, Z.Naturforsch. a, 8, 274 (1953).
6. V.V.Sklyarevskii, E.P.Stepanov & B.A.Obinyakov, Atomnaya energiya, 4, 22 (1958). (Trans.Soviet Journ.Atomic Energy).
7. J.E.Draper and A.A.Fleischer, Nucl.Phys., 13, 53 (1959); Phys.Rev., 114, 268 (1959); E.T.Patronis & H.Marshak, Nucl.Phys., 13, 53 (1959).
8. G.A.Bartholomew, P.J.Campion, J.W.Knowles & G.Manning, Proceedings of the International Conference on Neutron Interaction with the Nucleus, p.252, 1957.
9. A.Bohr & B.Mottelson, Kgl.Danske Fys.-mat.medd., 27, No.16, (1953).

CONTRIBUTION TO THE INTERPRETATION OF THE HIGH-LYING LEVELS OF W^{182}

- L.K.Peker

Recently there became available data on the high-lying excited levels in deformed even-even nuclei, in particular, in Sm^{152}, Dy^{160}, Er^{166}, Er^{168}, Yb^{170}, Yb^{172} and W^{182}. In connection with this, we are faced with the problem of interpretation of these levels from the standpoint of the unified nuclear model. As the first step, it is essential to identify the rotational levels and to establish the bands to which they belong. The present note is devoted to this question in the specific case of W^{182}.

The level density increases rapidly in deformed even-even nuclei in the region of excitation energies above 1 Mev. Decrease of the intervals between the levels leads to enhancement of the coupling of the rotational motion with the vibrational and single-particle motions. Hence in the given high excitation energy region rotational motion cannot be wholly separated from the other forms of motion, and to some degree the concept of pure rotational levels loses meaning. States with spin I will be described by a complex wave function $\Psi(I)$, which may be expanded in a series $\Psi(I) = \Sigma a_K \Psi_K(I)$ in wave functions of pure states with given values of K and I (K is the projection of the total angular momentum of the nucleus on the symmetry axis). Each level will be characterized by its own set of coefficients a_K. Inasmuch as the γ-transition probability is highly sensitive to small changes in the wave function, the simple rules of Alaga et al[1] for determining the relative intensities of γ-transitions to the levels of one rotational band, which were deduced on the assumption of pure states, cannot be applied to the γ-transitions between high-lying levels.

Thus the relative γ-transition intensities cannot serve as a criterion for assigning high-lying levels to a given rotational band. The level energies are not so sensitive to the coupling between different types of nuclear motion. If the separations between the levels are not very small, their "interaction" can be regarded as a perturbation. It can be shown[2,3] that in the second approximation of perturbation theory the interaction of levels with equal I and $\Delta K = \pm 2$ leads to an energy shift

$$\Delta E_1 = A_1[I(I+1) - I_0(I_0+1)] - B_1[I(I+1) - I_0(I_0+1)]^2.$$

Interaction of levels with the given I and $\Delta K = \pm 1$ leads (in the second approximation of perturbation theory[4]) to the same spin dependence of the level shift. The nature of ΔE_2 is such that the parameter B_2 may be either greater or smaller than zero:

$$\Delta E_2 = A_2[I(I+1) - I_0(I_0+1)] \pm B_2[I(I+1) - I_0(I_0+1)]^2.$$

As a whole the correction to the energy of rotational levels in the particular case under consideration (when the separations between the levels are not very small and the interaction between levels with $\Delta K > 2$ is neglected) is of the form

$$\Delta E = \Delta E_1 + \Delta E_2 = A[I(I+1) - I_0(I_0+1)] - B[I(I+1) - I_0(I_0+1)],$$

where $$A = A_1 + A_2, \text{ a } B = B_1 \pm B_2.$$

The rotational formula in this case can be written as

$$E_I = A_0[I(I+1) - I_0(I_0+1)] + \Delta E.$$

Substituting for ΔE and collecting similar terms, we finally obtain

$$E_I = A[I(I+1) - I_0(I_0+1)] - B[I(I+1) - I_0(I_0+1)]^2.$$

The structure of this formula agrees precisely with the structure of the usual rotational formula for relatively pure rotational formula for relatively pure rotational levels in the lower part of the spectrum[5], despite the fact that the wave functions of the high-lying levels under consideration differ substantially from the wave functions of pure rotational levels.

If the parameter $B = B_1 - B_2$, the level shift may prove to be small, despite the strong interaction of the levels. In the case of small intervals between "interacting" levels the above considerations obviously lose force. The shifts of such levels may prove to be very appreciable.[6] The possibility of identifying rotational bands by comparison of the level energies with the energies given by the formula for E makes it useful to retain the concept of rotational levels in analysis of high-lying excited levels, at least in the excitation energy range from 1 to 2 Mev.

The considerations set forth above apparently can help in interpretation of the high-lying levels of W^{182}.

The level arrangement in W^{182} is shown in the accompanying figure.[7-9] The levels have been distributed between the rotational bands on the basis of energy considerations and the experimental spin values (for clarity the different rotational bands have been displaced horizontally). Of greatest interest in this scheme is the band with K = 2- inasmuch as it comprises six terms up to a level with spin 7. The levels with spins 2-, 3-, 5- and 7- are satisfactorily described by the rotational formula with A = 14.2 kev and B = 0.016 kev. The parameter B proves to be approximately the same as for the ground state rotational band. These results serve to substantiate the arguments set forth above.

The spin 6- levels in the rotational bands with K = 2- and K = 4- according to the formula should have the same energy: ~1781 kev. Hence there should be strong "interaction" between them as a result of which they should repel each other. Possibly these two levels are the experimentally observed levels at 1769 kev and 1810 kev, both of which have spin and parity 6-. Obviously, one cannot at present assign each of these levels to its particular specific band.

The 1488 kev level[4], which belongs to the rotational band with K = 2-, is shifted upward 2.4 kev relative to the expected energy value. Possibly this shift is due to the influence of the close 4- level with somewhat lower energy (1481 kev) which can be introduced into the scheme on the basis of the experimental data on γ-transitions.

It should be noted that hitherto there have been two attempts to interpret the high-lying levels of W^{182}. The first of these[1] dates back to 1955 when only seven high-lying levels were known (whereas today 19 are known). The second attempt was undertaken in 1958 by Gallagher & Rasmussen[7] and cannot be regarded as successful inasmuch as the authors chose as the criterion for a level belonging to a given rotational band the requirement that the relative intensities of the γ-transitions from the levels under consideration conform to the simple rules of Alaga et al. These rules, as was noted above, were established for transitions to pure rotational levels; it follows from the considerations set forth above, however, that these rules cannot hold for transitions between high-lying excited levels.

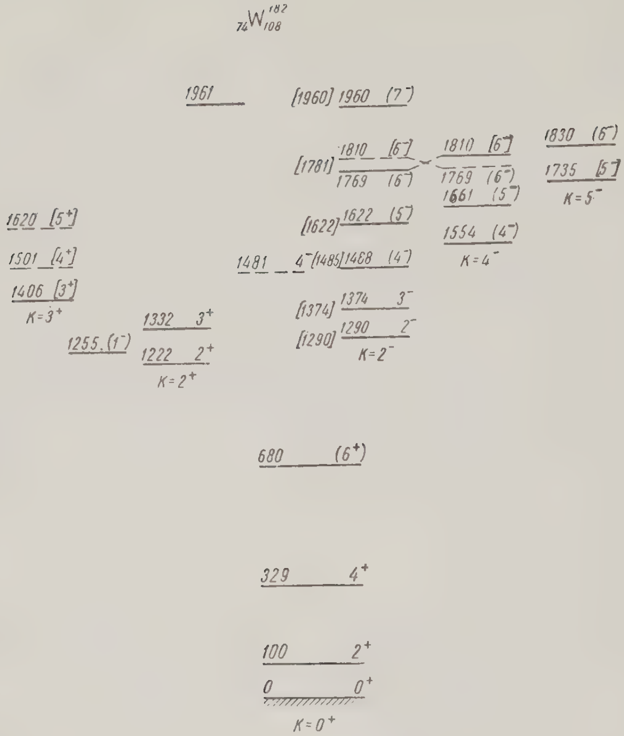
$_{74}W^{182}_{108}$
1961
[1960] 1960 (7-)
1830 (6-)
[1781] 1810 [6-]
1769 (6-)
1810 [6-]
1769 (6-)
1661 (5-)
1735 [5-]
K=5-
1620 [5+]
[1622] 1622 (5-)
1554 (4-)
1501 [4+]
1481 4-
[1485] 1468 (4-)
K=4-
1406 [3+]
K=3+
[1374] 1374 3-
1332 3+
1255 (1-)
[1290] 1290 2-
1222 2+
K=2-
K=2+
680 (6+)
329 4+
100 2+
0 0+
K=0+

Level diagram for W^{182}. The spins in parentheses are the values listed by Gallagher & Rasmussen[7]; the spins given in brackets are the values assumed in the present study (they are not in conflict with the experimental data[7,8]). The energy values given in brackets near the levels of the band with K = 2- were calculated by means of the formula for E_I with A = 14.2 kev and B = 0.0157 kev.

Scientific-Research Physical Institute
"A.A.Zhdanov" Leningrad State University

References

1. G.Alaga, K.Alder, A.Bohr & B.Mottelson, Kgl.Danske Mat.-fys.medd., 29, No.9 (1955).
2. A.Bohr, Kgl.Danske Mat.-fys.medd., 26, No.14 (1952).
3. B.L.Birbrair, L.K.Peker & L.A.Sliv, Zhur.eksp.i teor.fiz., 36, 803 (1959). (Trans.Soviet Physics - JETP).
4. A.Kerman, Kgl.Danske Mat.-fys.medd., 30, No.15 (1956).
5. A.Bohr & B.Mottelson, Kgl.Danske Mat.-fys.medd., 27, 16 (1953).
6. L.K.Peker, Izv.AN SSSR, Ser.fiz., 23, 1511 (1959). (Trans.Bulletin, 23, 1493.)
7. C.J.Gallagher & J.O.Rasmussen, Phys.Rev., 112, 1730 (1958).
8. C.J.Gallagher, J.O.Newton & V.S.Shirley, Phys.Rev., 113, 1298 (1959).
9. J.Murray, F.Boehm, P.Marmier & J.DuMond, Phys.Rev., 97, 1007 (1955).

MAGNETIC MOMENTS OF DEFORMED NUCLEI WITH K = 1/2

- L.K.Peker & D.A.Varshalovich

It is a known fact that deformed nuclei in the $K = {}^1/_2$ state have a number of distinctive attributes.[1] Such nuclei, for example, have an anomalous rotational band characterized by not one but two parameters $3\hbar^2/J$ and a. The magnetic moments and M1 transition probabilities between the levels of the rotational band with $K = {}^1/_2$ are determined not only by the single particle and collective motion gyromagnetic ratios g_K and g_R, but also by the parameter b:[1] *

$$\mu(I) = \frac{1}{4(I+1)}(g_K - g_R)\left[1 - (2I+1)(-1)^{I-{}^1/_2}b\right] + Ig_K; \tag{1}$$

$$B(M1, I+1 \to I) = \frac{3}{64\pi}\left(\frac{e\hbar}{2Mc}\right)^2 \frac{2I+1}{I+1}(g_K - g_R)^2\left[1 + b(-1)^{I-{}^1/_2}\right]^2. \tag{2}$$

According to the collective nuclear model, g_R = Z/A ≈ 0.4. However, owing to the fact that the single-particle and collective motions of the nuclear nucleons are not wholly independent, g_R differs somewhat from the above value, i.e., takes on values from +0.2 to +0.6.[3] The parameters g_K and b depend on the details of the internal motion of the nucleons and are determined by the single-particle wave functions. However, the parameter b is connected with the parameter a characterizing the positions of the levels of the $K = {}^1/_2$ rotational band. In view of this we can write the expression for the magnetic moment of the nucleus in the ground state of the band with $I = K = \Omega = {}^1/_2$ as follows:[1]
for $K = {}^1/_2{}^+$

$$3\mu_0 = g_K + g_R(1-a) - g_l(1-a) + \frac{g_s}{2}, \tag{3}$$

for $K = {}^1/_2{}^-$

$$3\mu_0 = g_R(1-a) + g_l(1+a) - \frac{g_s}{2}, \tag{4}$$

where g_s and g_l are the spin and orbital gyromagnetic ratios of the unpaired proton or neutron. The commonly assumed[1,4] values of the ratios are g_s = 5.58 (for the proton) and -3.82 (for the neutron), and g_l = 1 (for the proton) and 0 for the neutron). It is not impossible, however, that in a nucleus the values of g_s and g_l may differ substantially from the above ratios for free nucleons. In the present note we shall show that to explain the experimental values of the magnetic moment of Yb^{171} and W^{183}, it is essentially to renormalize the gyromagnetic ratios g_s and g_l.

The validity of relation (3) with nonrenormalized values of g_s and g_l and g_R = Z/A was checked by Mottelson & Nilsson[4] for the case of Tm^{169}. However, at that time all the necessary values for independent determination of g_K and g_R were not available. At present, there are four nuclei, namely, Tm^{169}, Yb^{171}, W^{183} and Pu^{239}, having rotational bands with $K = {}^1/_2$ for which the magnetic moment μ_0 has been measured and the parameter a determined.

First, let us consider Tm^{169} and Pu^{239} in which the rotational band is characterized by even parity. The following quantities have been determined experimentally for Tm^{169} (see Appendix):

$$a = -0.77;$$
$$\mu_0 = -0{,}21 \text{ nm};$$

---

*Deformed nuclei with K = 1/2 were considered by Zaretskii & Shut'ko[2] assuming a different coupling scheme for the angular momenta. However, the coupling scheme assumed by Nilsson is in better agreement with the experimental data.

$$\mathfrak{M}_1 \equiv (g_K - g_R)(1 + b) = -2.67 \text{ nm};$$

$$\mathfrak{M}_2 \equiv (g_K - g_R)(1 - b) = -2.34 \text{ nm}.$$

These data enable us to calculate the values of the parameters:

$$b = \frac{\mathfrak{M}_1 - \mathfrak{M}_2}{\mathfrak{M}_1 + \mathfrak{M}_2} = 0.067;$$

$$g_K = 2\mu_0 + {}^2/_3\,\mathfrak{M}_1 = -2.20,$$

$$g_R = 2\mu_0 + {}^1/_6\mathfrak{M}_1 - {}^1/_2\mathfrak{M}_2 = +0.30.$$

Knowing the empirical values of g_K and g_R, we readily see that for Tm^{169} relation (3) is actually fulfilled for the nonrenormalized values of g_s and g_l.

The experimentally determined quantities for Pu^{239} are (see Appendix):

$$a = -0.58;$$

$$\mu_0 = \pm 0.02 \text{ nm} \quad \text{or} \quad \pm 0.4 \text{ nm};$$

$$\mathfrak{M}_2 \equiv (g_K - g_R)(1 - b) = \pm 0.304 \text{ nm};$$

unfortunately these data are inadequate for independent determination of the necessary parameters. They do, however, relate the numerical values of g_K and g_R:

$$g_K = 2\mathfrak{M}_2 - 6\mu_0 + 4g_R.$$

Inserting this expression for g_K in relation (3) and using the nonrenormalized values for g_s and g_l, we can determine g_R. Owing to the fact that the experimental values of μ_0 and $\mathfrak{M}_2$ are not unique, we obtain several possible values of g_R. For $\mu_0 = \pm 0.02$ nm, the values of g_R are close to $Z/A = 0.39$ (0.20, 0.26, 0.41 or 0.47). But for $\mu_0 = \pm 0.4$ nm, we obtain $g_R = 0.86$, 1.08, -0.40 or -0.19. Hence one cannot draw any definitive conclusion regarding the values of g_s and g_l in Pu^{239}.

The other two nuclei, Yb^{171} and W^{183}, have rotational bands with $K = {}^1/_2$ characterized by odd parity. Eq.(4) for the magnetic moment of the ground state band in the $K = {}^1/_2{}^-$ case does not depend on g_K. The entire dependence on the single-particle wave functions is included in the parameter a, which can readily be determined from the level diagram for the nucleus.

For Yb^{171} we have available the following experimental data (see Appendix):

$$a = +0.86;$$

$$\mu_0 = +0.45 \text{ nm};$$

$$\mathfrak{M}_1 \equiv (g_K - g_R)(1 + b) = \pm 0.642 \text{ nm}.$$

These data yield $g_K = +1.38$ for $\mathfrak{M}_1 = +0.642$ or $g_K = +0.42$ for $\mathfrak{M}_1 = -0.642$, but do not give g_R. The value of g_R can be determined by means of Eq.(4), inserting the nonrenormalized values of g_s and g_l. In this case, however, g_R proves to be -4.0, which is very far from the experimental values of g_R for other nuclei and in conflict with our concepts regarding the collective motion of nucleons in a nucleus. On the other hand, if we take $g_R = Z/A = 0.40$, then for relation (4) to be fulfilled for Yb^{171} one must take either $g_s = -2.59$ with $g_l = 0$, or $g_l = -0.32$ with $g_s = -3.82$, or else one must renormalize both ratios. Nonfulfillment of relation (4) can in general be due to a change in the parameter a owing to shift of the rotational bands with $K = {}^1/_2$ and $K = {}^3/_2$. As has been shown by Kerman[5], however, even an appreciable shift of the rotational levels does not result in a substantial change of the parameter a, so that one cannot explain the experimental value of μ_0 without renormalizing g_s and g_l.

The empirical values of the parameters a, b, g_K and g_R for W^{183} were determined by Kerman[5], taking into account the shift of the rotational levels. He obtained the following values: $a = +0.17$, $b = +0.46$, $g_K = +0.16$, $g_R = +0.28$ and $\mu_0 = +0.115$ nm. If we take the free nucleon values for the gyromagnetic ratios, it follows from relation (4) that $g_R = -1.9$. This value differs radically from the experimental value for g_R given above and is in conflict with the collective nuclear model. Inasmuch as the shift of the rotational levels was taken into account in determining the above parameters, in the case of W^{183} the divergence can be eliminated only by renormalization of g_s and g_l. Relationship (4) will be satisfied for $g_s = 0.226$ and $g_l = 0$ or for $g_s = -3.82$ and $g_l = -1.52$.

Thus the experimental values of the magnetic moments of Yb^{171} and W^{183} require modification (renormalization) of the free nucleon spin and orbital gyromagnetic ratios g_s and g_l.

APPENDIX

Experimental data on Tm^{169}, Yb^{171} and Pu^{239}

Tm^{169}

In the ground state Tm^{169} has spin I = 1/2 and a magnetic moment $\mu_0 = -0.21$ nm (Refs.6 & 7). The levels of the rotational band based on the ground state are characterized by $3\hbar^2/J = 74$ kev and $a = -0.77$ (Ref.8). The lifetime of the first rotational level at 8.42 kev was measured[9] by the delayed coincidence procedure and found to be $(3.7 \pm 0.5)\cdot 10^{-9}$ sec. This state decays primarily by internal electron conversion. The M and N shell conversion coefficients for the 8.42 kev transition are $\alpha_M + \alpha_N = 106 \pm 6$, and the multipole order of the transition is M1 (E2 < 1%) (Ref.10). Assuming the total conversion coefficient to be 130, we obtain for the reduced transition probability $B(M1, {}^3/_2 \to {}^1/_2) = 1.58\cdot 10^{-5}\ e^2$ barn^2, which corresponds to

$$\mathfrak{M}_1 \equiv (g_K - g_R)(1 + b) = \pm 2.67 \text{ nm.}$$

The probability for excitation of the second rotational level at 118.20 kev is known from Coulomb excitation experiments[3]: $B(E2, {}^1/_2 \to {}^5/_2) = 3.8\ e^2$ barn^2. The intensity ratio of the γ-rays corresponding to the ${}^5/_2 \to {}^3/_2$ and ${}^5/_2 \to {}^1/_2$ transitions is $\frac{I_\gamma(109{,}78)}{I_\gamma(118{,}20)} = \frac{22}{2{,}6}$ (Ref.11). The 109.78 kev radiation is mixed 98% M1 + 2% E2. These data give the reduced M1 transition probability: $B(M1, {}^5/_2 \to {}^3/_2) = 1.43\cdot 10^{-5}\ e^2$ barn^2, which corresponds to

$$\mathfrak{M}_2 \equiv (g_K - g_R)(1 - b) = \pm 2.34 \text{ nm.}$$

Yb^{171}

The ground state of Yb^{171} has spin I = 1/2 and $\mu_0 = +0.45$ nm (Refs.6 & 7). The ground state rotational band levels are characterized by $3\hbar^2/J = 72$ kev and $a = 0.86$ (Ref.8).

From the data on Coulomb excitation we have the reduced probability $B(E2, {}^1/_2 \to {}^3/_2) = 2.48\ e^2$ barn^2 (Ref.12). The 66.72 kev γ-radiation is mixed 68% M1 - 32% E2 (Ref.13). The calculated reduced M1 transition probability is $B(M1, {}^3/_2 \to {}^1/_2) = 0.90\cdot 10^{-6}\ e^2$ barn^2, which corresponds to

$$\mathfrak{M}_1 \equiv (g_K - g_R)(1+b) = \pm 0{,}642 \text{ nm.}$$

Pu^{239}

Pu^{239} in the ground state has spin I = 1/2 and $\mu_0 = \pm 0.02$ nm or ± 0.4 nm (Refs.6 & 7). The levels at the ground state rotational band are characterized by $3\hbar^2/J = 37$ kev and $a = -0.58$ (Ref.8).

From Coulomb excitation measurements, we have $B(E2,\ {}^1/_2 \rightarrow {}^5/_2) = 4.2\ e^2$ barn^2 (Ref.3). The intensity ratio for the γ-rays corresponding to the ${}^5/_2 \rightarrow {}^3/_2$ and ${}^5/_2 \rightarrow {}^1/_2$ transitions is $\frac{I_\gamma(49{,}47)}{I_\gamma(57{,}31)} = 1.8$ (Refs.6 & 7).

The 49.47 kev radiation is mixed 78% M1 + 22% E2 (Refs.6 & 7). Using the above experimental data we obtain $B(M1,\ {}^5/_2 \pm {}^3/_2) = 2.42 \cdot 10^{-7}\ e^2$ barn^2, which corresponds to

$$\mathfrak{M}_2 \equiv (g_K - g_R)(1-b) = \pm 0{,}304 \text{ nm.}$$

Scientific-Research Physical Institute
"A.A.Zhdanov" Leningrad State University

References

1. S.G.Nilsson, Kgl.danske vid.selskab.Mat.-phys.medd., 29, 16 (1955).
2. D.F.Zaretskii & A.V.Shut'ko, Zhur.eksp.i teor.fiz., 32, 370 (1957). (Trans.Soviet Physics - JETP.)
3. K.Alder, A.Bohr, T.Huus, B.Mottelson & A.Winter, Rev.Mod.Phys., 28, 432 (1956).
4. B.Mottelson & S.G.Nilsson, Z.Phys., 141, 127 (1955).
5. A.K.Kerman, Kgl.danske vid.selskab.Mat.-phys.medd., 30, 15 (1956).
6. D.Strominger, J.M.Hollander & G.T.Seaborg,Revs.Mod.Phys., 30, No.2, Part II (1958).
7. B.S.Dzhelepov & L.K.Peker, Skhemy raspada radioaktivnykh yader (Decay schemes of radioactive nuclei), M.-L., 1958.
8. B.Mottelson & S.G.Nilsson, Kgl.danske vid.selskab.Mat.-phys.Skrif., 1, 8 (1959).
9. H.Beekhuis & H.de Waard, Physica, 24, 767 (1958).
10. G.Charpak & F.Suzor, J.Phys.et radium., 20, 513 (1959).
11. F.Hatch, F.Boehm, P.Marmier & J.DuMond, Phys.Rev., 104, 745 (1956).
12. B.Elbek, K.O.Nielsen & M.C.Olesen, Phys.Rev., 108, 406 (1957).
13. V.A.Romanov, V.V.Tuchkevich, M.G.Iodko & O.M.Kresin, Trudy Soveshchaniya po yadernoi spektroskopii (Transactions of the Conference on Nuclear Spectroscopy), Joint Inst. for Nucl.Research, Dubna, 1959.

VARIATION OF THE GAIN OF PHOTOMULTIPLIERS WITH THE PULSE HEIGHT AND TIME INTERVALS BETWEEN PULSES

- A.G.Berkovskii & V.G.Pol'skii

Introduction

Bell et al[1] and Caldwell & Turner[2], in investigating scintillation counters, noted that in the case of some photomultipliers the pulse height varies with the integral counting rate. These authors also observed that the photomultiplier gain varies with the pulse height.

In many cases the dependence of the photomultiplier gain on the current load seriously hampers energy measurements of the detected radiation. For purposes of quantitative evaluation of the possible measurement errors in a wide counting rate range and investigating the said dependence we developed some special equipment and used it to study several dozen photomultiplier tubes (primarily FEU-33 photomultipliers).

Equipment and Procedure

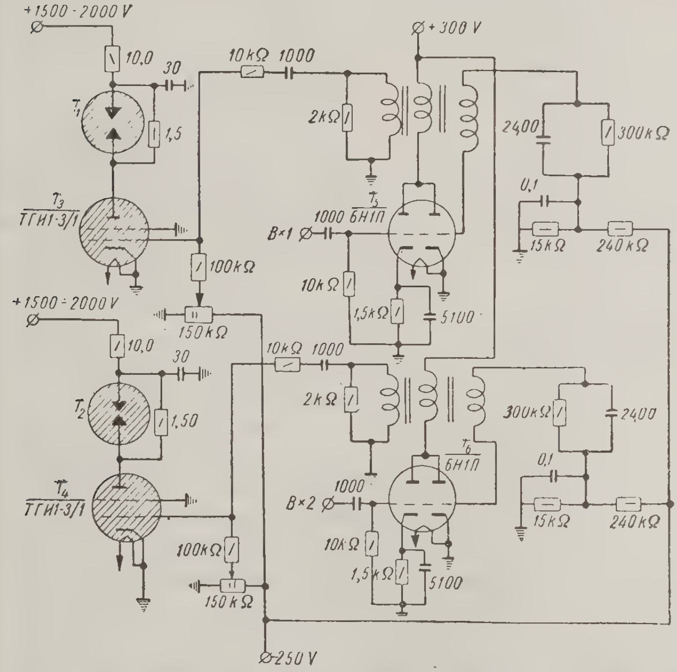

Fig.1. Circuit of controlled light pulse sources.

It is more convenient to investigate the variation of photomultiplier gain as a function of the load current not under the usual scintillator counter conditions but by means of a pulsed light source with provision for regulating the periodicity and flux intensity. We used two independently regulated uniform sources with provision for simple control of the interval between flashes, ranging up from approximately one nanosecond.

In the experimental setup, two pulsed light sources controlled by a driving oscillator periodically illuminate the cathode of the investigated photomultiplier, the output pulses from which are applied to an oscillograph. With variation of the interval between the pulses observed on the oscillograph screen or of the intensity of the "first" flashes (i.e., the amplitudes of the first pulses on the screen) one can readily measure the corresponding changes in the amplitude of the "second" pulses.

The electric circuit controlling the pulse light sources is shown in Fig.1. Pulses from the GIS-1 staggered pulse type generator are fed to Bx1 and Bx2 at a frequency of 2 kc. The positive polarity output pulses from the blocking oscillators assembled about tubes T_5 and T_6 (6N1P tubes) trigger the thyratrons T_3 and T_4 (TGI1-3/1). The discharge tubes T_1 and T_2 (RB-2), filled with hydrogen to 100 mm Hg pressure, are connected into the plate circuits of the thyratrons. The indicated hydrogen pressure in the given tubes insures a minimum duration of the light flashes (~1 nanosec[3]).

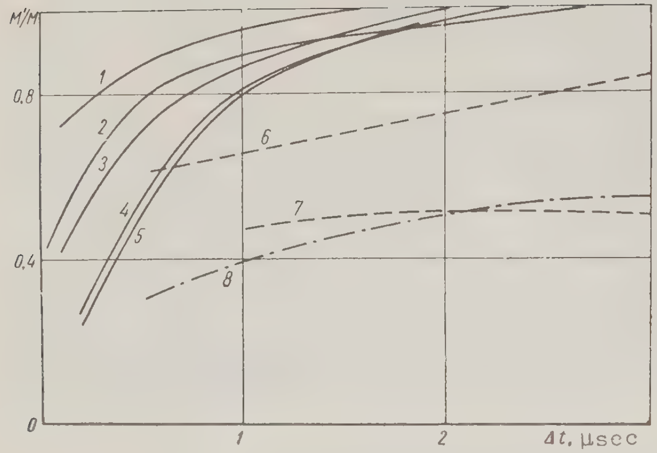

Fig.2. Recovery of the amplification factor of photomultipliers with variation of the interval between pulses (solid lines - FEU-33; dashed lines - RCA-6810A): 1) No.193, I_1 = 480 ma, I_2 = = 420 ma, 2) No.227, I_1 = 530 ma, I_2 = 340 ma, 3) No.288, I_1 = 500 ma, I_2 = 480 ma, 4) No.335, I_1 = 840 ma, I_2 = 810 ma, 5) No.337, I_1 = 480 ma, I_2 = 480 ma, 6) No.308, I_1 = 140 ma, I_2 = 170 ma, T_B = 15 μsec; 8) RCA-6810A, I_1 = 600 ma, I_2 = = 600 ma; T_B = 20 μsec, I_1 = the amplitude of the first pulse, I_2 = amplitude of the second pulse with $\Delta t \gg T_B$; Δt is the interval between pulses; M is the amplification factor with $\Delta t \gg T_B$, M' is the amplification factor with $\Delta t < T_B$.

Upon discharge of the distributed capacitances of the anode circuits through the thyratrons, a pulse voltage of the order of 1500 v is applied to the discharge tubes, giving rise to breakdown accompanied by a light flash. Smooth regulation of the time interval between light pulses (to 0.5 μsec) is realized by varying the negative voltage on the control grid of the thyratrons.

In carrying out measurements in the nanosecond range, we used a special high-speed oscillograph^4, while in the wider range of longer time intervals, we employed an IO-4 oscillograph.

Measurement Results

We investigated the variation in the height of the "second" pulse with the time interval between pulses for a large number of tubes: 30 FEU-33, 2 FEU-11, 2 FEU-13, 1 RCA-6810A and 3 RCA-6342 tubes. The overall supply voltage was set in the range from 3 to 4 kv. No time dependence of the second pulse amplitude was observed in the case of the FEU-11 and FEU-13 tubes, but a very strong dependence was observed for the RCA-6810A and RCA-6342 tubes.

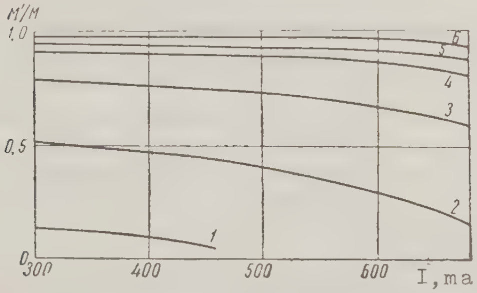

Fig.3. Variation of M'/M as a function of the amplitude of the "first" pulse with Δt = const: 1) Δt = 0.1, 2) 0.5, 3) 1.0, 4) 1.5, 5) 2.0, and 6) 2.5 μsec.

The results of our measurement in the form of the variation of the amplification factor of the photomultipliers as the function of the interval between the pairs of pulses (i.e., recovery curves) are shown in Fig.2. It will be apparent from the curves that all the tested FEU-33 tubes have a recovery time (time to re-establishment of the rated amplification factor) $T_B \leqslant 3$ microsec, while for the RCA-6810A and RCA-6342 tubes T_B = 15-20 microsec.

The fact that the FEU-11 and FEU-13 photomultipliers do not exhibit a time interval dependence of the second pulse is explained by the appreciably greater (as compared with other types of photomultipliers) width of the output pulse. In the case of the FEU-33 tubes, in the absence of the optimum voltage distribution over the first stages, leading to an appreciable increase in the duration of the output pulses, the investigated dependence was also not observed.

Using the same set-up we also investigated the variation in the amplitude of the "second" pulse as a function of the amplitude of the "first" pulse with different intervals between the pulses (from 0.1 to 2.5 microsec). The results of these measurements for one of the FEU-33 tubes are shown in Fig.3. As might have been expected, the amplitude of the "second" pulse decreases with increase of the amplitude of the "first" pulse. The slope of these curves may differ substantially for different individual photomultiplier tubes.

References

1. R.Bell, R.Davis & W.Bernstein, Rev.Sci.Instr., 26, 726 (1955).
2. R.Caldwell & S.Turner, Nucleonics, 12, 47 (1954).
3. J.Malmberg, Rev.Sci.Instr., 28, 1027 (1957).
4. V.G.Pol'skii, Sbornik materialov po vakuumnoi tekhnike (Collected articles on vacuum techniques), No.21, Gosenergoizdat, 1959.

Bulletin of the Academy of Sciences of the USSR - Physical Series
Vol.24, No.3 - March 1960
Transactions of the Tenth All-Union Conference on Nuclear Spectroscopy
(To be continued in Vol.24, Nos. 7 and 9)

TABLE OF CONTENTS

	Page Orig.	Page Trans.
Alpha-radiation from U^{233} - B.S.Dzhelepov, R.B.Ivanov, V.G.Nedovesov & Yu.T.Puzynovich	258	247
Radioactive decay of Th^{231} - S.A.Baranov, R.M.Polevoi, Yu.F.Rodionov, G.V.Shishkin & V.M.Shubko	261	249
Conversion electrons and gamma-rays from Tm^{165} - K.Ya.Gromov, B.S.Dzhelepov, A.G.Dmitriev, V.A.Morozov & K.I.Yakovlev	272	260
Regarding the 75-min ytterbium activity - A.A.Abdurazakov, K.Ya.Gromov, B.S.Dzhelepov, Yu.V.Norseev, G.Ya.Umarov & V.G.Chumin	278	266
Investigation of the positron spectra of neutron-deficient isotopes - N.A.Bonch-Osmolovskaya, B.S.Dzhelepov & O.E.Kraft	283	270
Beta-decay of La^{140} - B.S.Dzhelepov, B.A.Emel'yanov, K.P. Kupriyanova & Yu.N.Podkopaev	288	275
Investigation of the gamma-radiation of Ag^{110m} in the energy range from 0.2 to 2.0 Mev - N.A.Voinova, B.S.Dzhelepov & N.N.Zhukovskii	291	278
Gamma-spectrum of $Eu^{152,154}$ in the 245 to 500 and 1450 to 2000 kev energy intervals - B.S.Dzhelepov & Yu.V.Khol'nov	300	288
Resonance fluorescence in Ce^{140} excited by La^{140} gamma-rays - B.S.Dzhelepov & M.A.Dolgoborodova	304	292
Gamma-spectrum of W^{187} - B.S.Dzhelepov, V.L.Rumyantsev, Yu.V. Khol'nov & G.E.Shchukin	311	299
Determination of the number of disintegration events in electron-capture materials by means of a 4π scintillation counter - V.I.Baranovskii & G.M.Gorodinskii	313	301
Comparison of the theory of nonaxial nuclei with experiment - E.P.Grigor'ev & M.P.Avotina	324	311
On some applications of the coincidence technique in nuclear spectroscopy - É.E.Berlovich	336	323
Ionization chamber in a magnetic field - G.E.Kocharov & M.A.Yamshchikov	350	336
Investigation of pulses arising on the grid of an ionization chamber - G.A.Korolev & G.E.Kocharov	357	342
Rotational levels in deformed odd-odd nuclei - L.K.Peker	365	350
Contribution to the interpretation of the high-lying levels of W^{182} - L.K.Peker	369	354
Magnetic moments of deformed nuclei with $K = 1/2$ - L.K.Peker & D.A.Varshalovich	372	357
Variation of the gain of photomultipliers with the pulse height and time intervals between pulses - A.G.Berkovskii & V.G.Pol'skii	377	361

Translated in 1961 by
Columbia Technical Translations
5 Vermont Ave., White Plains, N.Y.

Number 4 Volume 24 1960

BULLETIN

of the

ACADEMY OF SCIENCES OF THE USSR

— PHYSICAL SERIES —

(Izvestiya Akademii Nauk SSSR)
(Seriya fizicheskaya)

Reproduction rights reserved
by

Columbia Technical Translations
5 Vermont Avenue
White Plains, New York

Single Issues
$20

Annual Subscription
$215

Lithoprinted in U.S.A.
EDWARDS BROTHERS, INC.
Ann Arbor, Michigan

Transactions

# of the

Fourth All-Union Conference on X-Ray Spectroscopy

(Rostov-on-the-Don, 29 June - 6 July 1959)

SELECTION OF CRYSTALS FOR X-RAY SPECTROSCOPY

- J.Bačkovský

For investigating the fine structure of x-ray spectra and the width and shape of emission lines and absorption edges it is essential to have instruments with a high resolution, a parameter which can easily be measured only for double crystal x-ray spectrometers. In order to insure high resolution of a double crystal spectrometer one must employ perfect crystals. Perfect in this sense are crystals the natural reflection widths of which are close to the width calculated according to the theory of Ewald & Darwin and Prino & Keller.

Where one can restrict the reflection to a sufficiently small area, most crystals satisfy this condition. Even sodium chloride[1] and potassium chloride[2] crystals grown from a melt are close to perfect crystals if very small areas are used.

When, however, a high luminosity is required, one must use wider x-ray beams. Moreover, the point of reflection shifts along the crystal and it is very difficult to find crystals that are perfect over a sufficiently large area. A given crystal can be perfect at one point on its surface and defective at another. Perfect sections could be sought by gradually covering both crystals in a double crystal spectrometer with parallel orientation of the crystals and obtaining the reflection curves for combinations of different sections of both crystals. This procedure is obviously laborious and time consuming.

The method of photographing the structure of the surface proposed by the writer[3] some twenty years ago and used by Gogberidze[4] makes it possible to determine the location, size and shape of good reflecting regions and even to measure the relative inclination of the mosaic blocks. However, this procedure allows of detecting only such distortion of the crystal surface which correspond to the natural angular width of the radiation employed, i.e., equal to approximately half an angular minute for the lines usually investigated. This is completely inadequate for the selection of crystals for double crystal spectrometers. Hence we made an attempt to improve this procedure with a view to enhancing its resolving power.

The test set-up is diagramed in Fig.1. The cross (F) indicates the point focus of the x-ray tube. The rays fall on a calcite crystal oriented in the position for second order reflection. After reflection from this crystal, the beam falls on the investigated crystal mounted in the antiparallel position relative to the first crystal. Inasmuch as the distance between the crystals is 3 meters, in order to reduce absorption the beam is directed through a tube filled with hydrogen. The test crystal is mounted on a movable stage so that it can be displaced parallel to the reflecting plane. The x-rays reflected from this crystal are incident on the photographic plate which is located as close as possible to the crystal.

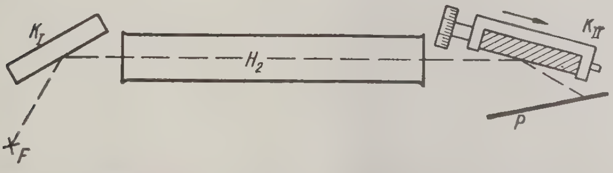

Fig.1. Test set-up: K_I and K_{II} - crystals, F - source, P - photographic plate.

In view of the fact that the crystals are oriented antiparallel, reflection from the second crystal occurs only in a very narrow zone, the structure of which appears on the photographic plate. In order to obtain an extended picture of the entire surface of the crystal, one must gradually displace the crystal and make repeated exposures in successive positions.

By way of illustration the surface structure of a calcite crystal is shown in Fig.2. One can discern a number of reflection zones indicating which sections of the crystal have perfect structure and which have distortions. It is evident

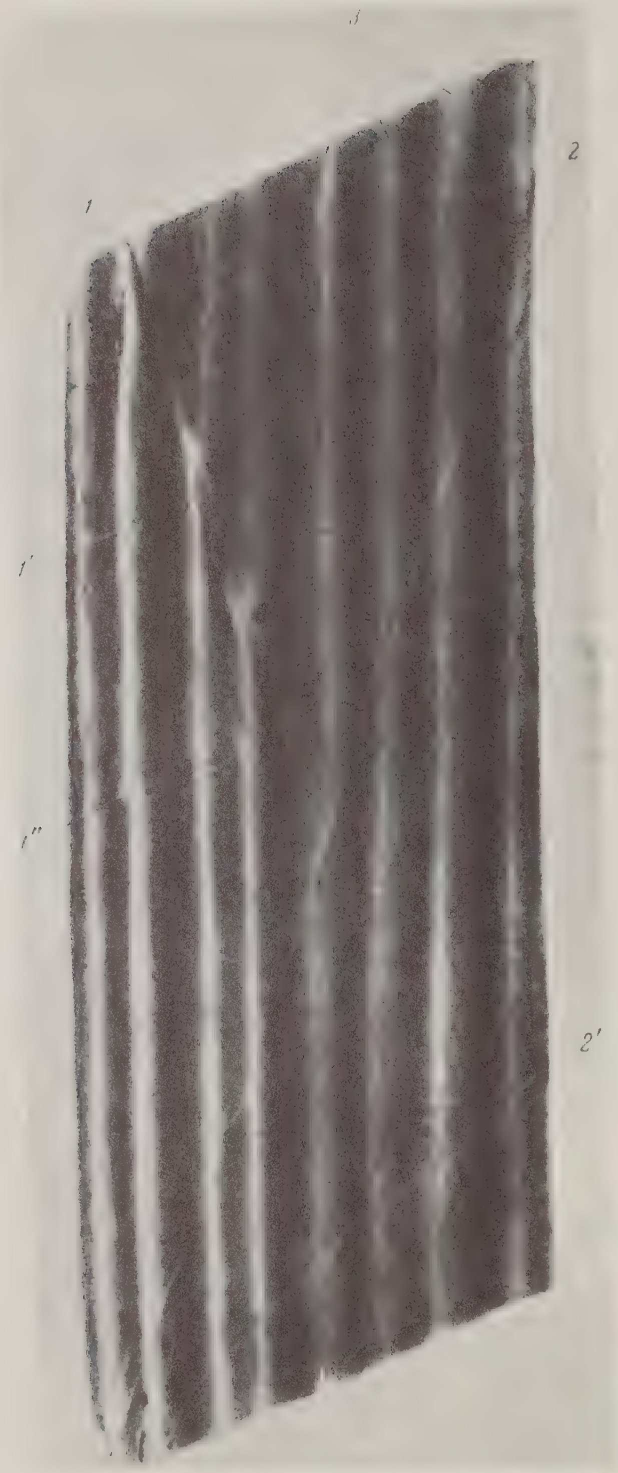

Fig.2. Surface structure of a calcite crystal: 1, 1' & 1" - mosaic block boundaries, 2 & 2' - steps, 3 - region with different lattice constants.

from the photograph that some of the reflection zones have breaks and are shifted sideways. This indicates that the crystallographic planes at these points are slightly skewed. Connecting these discontinuities one can determine the location of the boundaries between two neighboring mosaic blocks. On the other hand, the step-like character of the crystal surface has no influence on the location and width of the reflecting zone. (This crystal, which was kindly presented by Prof. Borovskii, was already etched.)

The widening of the reflection zones indicates imperfection of the crystal due to variation in the separation between the crystallographic planes (for example, owing to contamination). The regions where the reflection zones are narrow and parallel pertain to sections with a perfect surface structure; these are suitable for use in a high resolution double crystal spectrometer.

Thus by means of the described procedure one can readily locate on the surface of the crystals sections with a perfect structure, the boundaries of mosaic blocks and local variations of the lattice constant. The angular resolution obtainable by this procedure is better than 3". This means that it is of approximately the same order of magnitude as the theoretical width of the reflection curve.

Institute of Technical Physics
Czechoslovakian Academy of Sciences

References

1. M.Renninger, Naturwissenschaften, 22, 334 (1934).
2. J.Bačkovský & R.Bubáková, Českosl. časop. Fys., 6, 647 (1956); Chekhosl. fiz.zh., (Czechosl.Phys.Journ.) 7, 80 (1957).
3. J.Bačkovský, J.Phys., 9, 471 (1938).
4. D.B.Gogberidze, Zhur.eksp.i teor.fiz., 10, 96 (1940).

NUCLEAR X-RAY GENERATOR FOR FLUORESCENT ANALYSIS

- K. I. Narbutt, R. L. Barinskii & I. S. Smirnova

In recent years the question of replacing x-ray tubes by an artificial radioactive source has attracted the attention of many authors. A number of contributions devoted to this question have appeared in the foreign periodic literature. Particular attention has been given to the use of β-sources as "generators" of x-radiation. Liden & Starfelt[1], for example, propose a β-source by means of which one can excite characteristic x-radiation both directly by β-particles (analog of an x-ray tube with primary excitation) and by bremsstrahlung emitted incident to stopping of the β-particles in the shielding screen surrounding the source (analog of fluorescence x-ray excitation). These authors investigated the problem of excitation of the characteristic K x-radiation of lead and tin by β-particles from S^{35} (170 kev) and P^{32} (1700 kev). Reiffel & Hamfriz[2] give a comprehensive review of attempts to use sources of x-rays excited by β-particles. X-ray sources excited by β-radiation from $Sr^{90} \rightarrow Y^{90}$ and Eu^{155} were used by these authors for radiography, for determining the density of flowing liquids and the thickness of photographic emulsions. These authors also propose using such x-ray sources for fluorescent analysis of some simple chemical systems. The x-radiation appearing as a result of K capture in the artificial isotope Fe^{55} has been used in practice for determining the sulfur content in petroleum products[3], and chlorine and bromine in organic liquids[4]. In these studies the content of the element in question was determined from the mass absorption coefficient of the x-rays from the Fe^{55} source. Moreover, Fe^{55} can be used for excitation of the characteristic x-radiation of light elements.[5] Yakubovich[6] gives a brief description of the use of radioactive Tm^{170} and Tl^{204} for purposes of analysis for tantalum and niobium.

We used the γ- and x-radiation from a Tm^{170} source for fluorescences excitation of the K radiation of the elements from $_{30}Zn$ to $_{92}U$. Thulium^{170} disintegrates by β-γ decay. The radiation from this source comprises 1) 968 and 884 kev β-particles, 2) 84 kev γ-rays, 3) ytterbium and thulium x-radiation (primarily Yb $K\alpha_{1,2}$ and Tm $K\alpha_{1,2} \approx 52$ kev), and 4) bremsstrahlung due to stopping of the β-particles in the source (Refs.7,8 & 9).

Originally it was our intent to obtain mixed excitation of the characteristic x-radiation both by β-particles (primarily excitation) and by γ- and x-rays (fluorescent excitation). However, soon the evident need for reducing the background with a view to enhancing the analytic sensitivity forced us to concentrate on the fluorescent method of excitation. The β-particles were eliminated from the excitation process; complete suppression of the β-particles was realized by means of a set of aluminum absorbers installed between the thulium source and the specimen. As will be described below, this suppression of the β-particles resulted in an appreciable reduction of the background.

The Tm^{170} source was prepared of thulium oxide: powdered Tm_2O_3 was compacted in a corrugated cell of 50 micron aluminum foil and subjected to a heavy dose of neutron radiation. The artificial radioactive source obtained in this manner, which had an initial activity of 12 curie*, was loaded into a special container. Adequate radiation protection was assured by the 4.5 cm thick walls of the container. The design of the container provides for insertion and removal of the samples with complete safety for the operator. Photographs of the container, disassembled and assembled, are shown in Figs.1 & 2.

In view of the low intensity of the excited fluorescence x-radiation it was

---

*It should be noted that the work was continued over the period of a year so that most of the results described below were obtained with a source activity of $\leqslant 1.5$ curie.

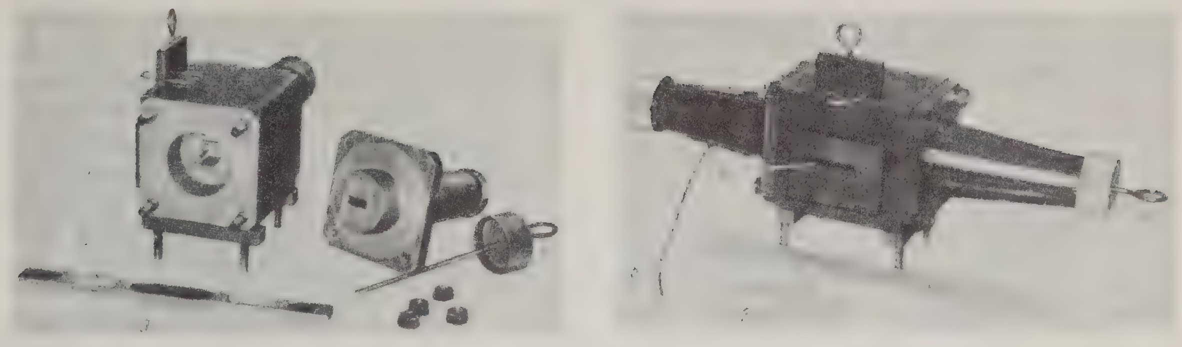

Figs.1 & 2. Container disassembled and assembled: 1 - lead container, 2 - thulium source compressed in its aluminum foil cell, 3 - sample slide, 4 - sample holder, 5 - cable for ejecting sample, 6 - slit for exit of x-radiation, 7 - shutter, 8 - sample slide handle.

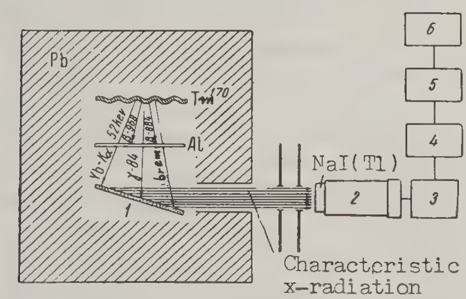

Fig.3. Block diagram of apparatus: 1) sample, 2) FUE-29 photomultiplier, 3) cathode follower, 4) amplifier, 5) differential pulse height analyzer, 6) scaler.

obviously impossible to investigate the spectral composition of the radiation by the crystal diffraction procedure. Hence we had recourse to the procedure based on the use of a scintillation counter and a pulse height analyzer. A block diagram of the set-up is shown in Fig.3. The scintillation counter consists of a 20 x 5 x 1.5 mm NaI(Tl) crystal coupled to an FEU-29 photomultiplier. The amplification factor of the linear amplifier is 500; the channel width of the single channel pulse height analyzer is 1 v; the resolving time is 1-2 μsec.

In view of the fact that the intensity of the scattered background depends on the method of preparation of the sample, we standardized on the procedure described earlier by Narbutt & Bespalova[10] but modified as follows. The samples were prepared in the form of tablets or pellets by compressing sheets of paper coated with the test material and polystyrene (the plastic serves as a reinforcing backing). About 100 mg of material are required to obtain a pellet of 6 cm^2 area.

In the very first experiments we encountered the serious problem of reducing the background due to radiation from the source, scattered inside the container, and x-radiation generated in the lead walls of the container. The initial measure, provided for in the design, consisting of making all the inner parts of the container of aluminum, proved to be inadequate. In the first experiments, the background intensity was higher than the intensity of the characteristic radiation from the samples. We were able to obtain an appreciable reduction of the background by the following means:

1) thorough collimation of the beam emerging from the container,
2) proper choice of the procedure for preparing the samples, which insured minimal scattering in the sample itself,
3) proper selection of the sample holder material, insuring better absorption of the radiation scattered from the back wall of the container, and
4) complete absorption of the β-particles.

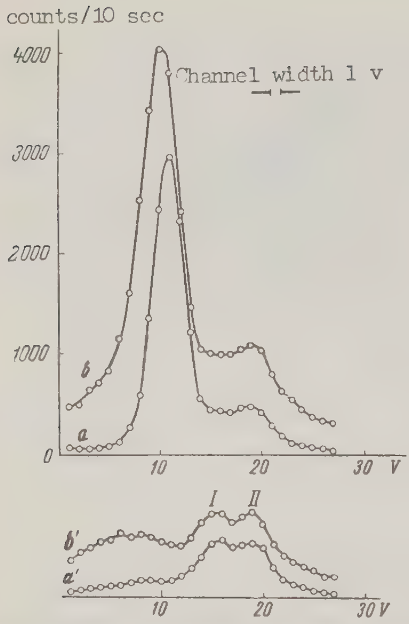

Fig.4. Experimental pulse height distribution curves (radiator - iodine). Below - similar amplitude distribution curves for the backtround pulses. a & a' - complete absorption of β-particles; b & b' - partial filtration.

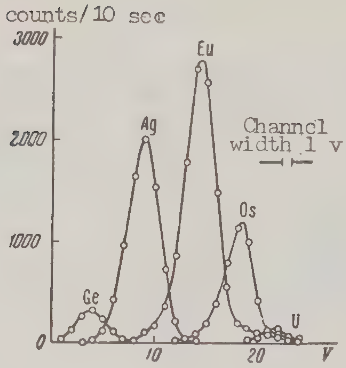

Fig.5. Pulse height distribution curves from the characteristic K radiation of Ge, Ag, Eu, Os and U under different excitation conditions.

The effect of β-particle absorption is illustrated in Fig.4. This figure gives the pulse height distribution curves obtained for the K series of iodine and the background pulse curves obtained with complete (a') and partial (b') absorption of the β-particles. Peak I corresponds to an energy of 52 kev and is the result of scattering of the x-rays from the Tm^{170} source in the walls of the container. Peak II corresponds to the energy of Pb $K\alpha$ radiation and is the result of excitation of the characteristic radiation of lead by the nuclear radiation (mainly in the wall of the container opposite the exit slit). With introduction of the sample pellet into the container, the shape and height of the background spectral distribution curves changes somewhat, but the Z dependence of this change is insignificant, and for close values of Z the background is virtually identical. This circumstance makes it feasible to subtract the background graphically. In view of the nonuniform character of the background this possibility is a decisive factor where investigation of the energy composition of the characteristic radiation of specimens is concerned. All the energy distribution curves given below are the results obtained after subtraction of the background distribution curve from the experimental curves of the pulse height distribution from the fluorescence radiation of the samples.

The efficiency of excitation of the characteristic radiation of different elements is determined by the energy composition of the radiation from the Tm^{170} source. Fig.5 shows the pulse height distributions for the K series lines of a number of elements.

The K series of Ge is located under unfavorable excitation conditions inasmuch as the energy of the primary radiation greatly exceeds the excitation energy: 11.1 kev.

The K series of Ag (excitation energy 25.5 kev) is intermediate between the K series of Ge and Eu. The K series of Eu (excitation energy 48.6 kev) is effectively excited by the 52 kev radiation; it is also excited by the 84 kev γ-rays and the bremsstrahlung.

The K series of Os (excitation energy 78.1 kev) is excited by the 84 kev γ-radiation and the bremsstrahlung but is not excited by the 52 kev $K\alpha_{1,2}$ x-rays.

The K series of U (excitation energy 115 kev) is excited only by the bremsstrahlung.

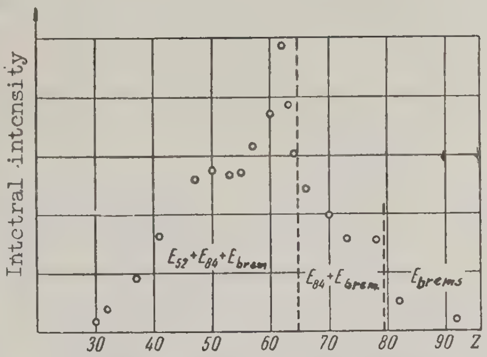

Fig.6. Efficiency of the excitation of the K radiation of elements by x- and γ-radiation from Tm^{170} as a function of Z. The vertical dashed lines indicate the boundaries separating elements characterized by different excitation conditions.

Fig.6 shows the Z dependence of the efficiency for excitation of the K radiation of elements from Z = 30 to Z = 92 by the x- and γ-radiation of the Tm^{170} source. As will be evident from the figure our nuclear generator is most efficient for elements from Z = 47 to Z = 64.*

In cases when the characteristic radiation detected by the scintillation spectrometer has an energy greater than 33 kev, there appear in the pulse height distribution curve additional peaks associated with the excitation of the characteristic radiation of iodine, contained in the NaI(Tl) crystal.[12] Fig.7 shows the pulse height distribution observed in the case of a tantalum radiator. Peak A corresponds to the K radiation of tantalum; peak C to the L radiation of this element. Peak B is due to the pulses from the photons of the Ta K radiation that have lost 33 kev on excitation of the characteristic radiation of iodine and the pulses due to the said K radiation of iodine. The appearance of such "spurious" peaks, which are associated only with the scintillator crystal and do not correspond to any radiation actually emitted from the container, greatly hinder interpretation of the experimental pulse height distribution. Possibly this hindering effect can be reduced by using scintillators with light elements, for example, such as LiF, or organic crystals.

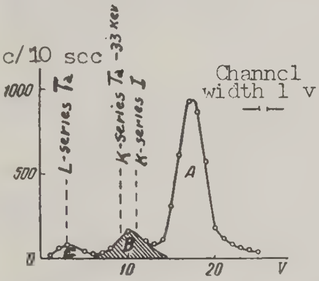

Fig.7. Pulse height distribution observed in detecting the characteristic radiation of tantalum. The spurious peak B is hatched.

The dispersion curve for our scintillation spectrometer is shown in Fig.8. It will be seen that this curve in the 0 to 100 kev energy region consists of two rectilinear sections; a break in the dispersion curve has also been observed by other investigators[13,14], who infer that it is connected with the properties of the NaI(Tl) crystal. In the same figure we give the curves characterizing the resolution of our scintillation spectrometer (ratio of the line half-width to the energy). It will be seen that the resolution curve has a discontinuity at the energy of the break in the dispersion curve.

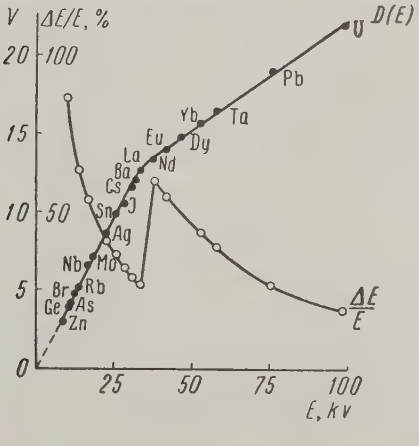

←Fig.8. Curves characterizing the dispersion D(E) and resolution $\Delta E/E$ of the scintillation spectrometer.

---

*The given data in Fig.6 differ from those presented earlier in Ref.11 in that they are the result of more refined measurements obtained in the course of our research.

Fig.9. Pulse height resolution curves for the characteristic K radiations of niobium and tantalum. ↓

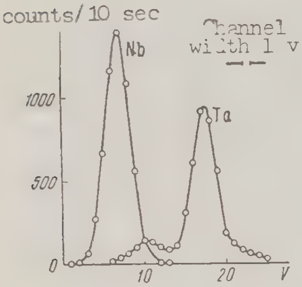

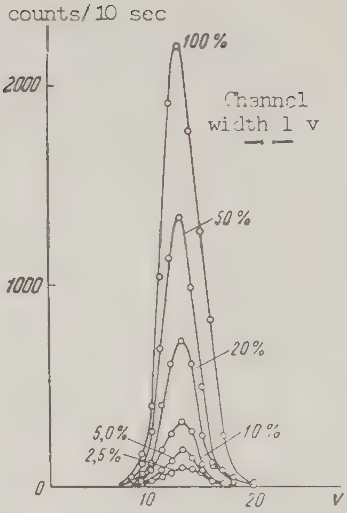

←Fig.10. Pulse height resolution curve associated with the K radiation of elements of the cerium group of rare earths obtained with different total contents of the rare earth elements.

Despite the relatively low resolution of our scintillation spectrometer (see Fig. 5), it can still be used for the solution of certain analytic problems. It must be noted that the possibilities as regards improvement of the resolution have not been exhausted (use of higher quality crystals and possibly employment of a proportional counter). By way of one of the possible applications of the equipment (with the attained resolving power) one can propose the classical example of analysis for pairs of elements such as Ta & Nb and Hf & Zr. As will be apparent from Fig.9, the characteristic lines of Ta and Nb are fully resolved.

For the first practical use of the described nuclear generator we tackled the problem of quantitative determination of the total content of rare earths in different minerals. The presence of a nonuniform background, mentioned above, sets a limit on the sensitivity and accuracy of the analytic procedure. Hence further measures aimed at reducing the background are important where extension of the potentialities of the given equipment and procedure are concerned. Promising on this respect is replacement of thulium^{170} by a more appropriate radioactive source and certain modifications in the design of the container. Fig.10 shows the K series lines obtained for artifical mixtures having different total concentrations of cerium group rare earth elements ranging from 2.5 to 100%.

The sensitivity of the proposed analytic procedure as regards the total content of cerium group rare earths is 0.5%; the error in the 5 to 100% total concentration range is 5%. For lower contents - from 5 to 0.5% - the error increases to 20% of the determined quantity, also the counting time for each point increases from 10 to 100 sec.

Fig.11 shows the pulse height distribution curves associated with the characteristic x-radiation obtained for different rare earth minerals. In the case of monazite and orthite (= allanite), which contain only the cerium group rare earths, the above described procedure was used for quantitative determination of the total content of the rare earth elements. The results obtained by this method are compared in the accompanying table with those obtained by the conventional x-ray spectroscopic procedure involving excitation of the characteristic L radiation of the rare earths by the primary radiation from the x-ray tube and crystal diffraction investigation of the spectral composition of the radiation.

As will be apparent from Fig.11, each of the minerals has its own characteristic pulse height distribution curve corresponding to the spectral composition of the characteristic x-radiation, which makes it possible to use the procedure for identification of these minerals. From the shape of the curve, one can immediately, without further processing of the results, obtain information on the qualitative elemental composition of the mineral. For example, it follows from

Mineral	$(\Sigma TR)_C$	%
	Nuclear generator and scintillation counter	X-ray tube & crystal diffraction procedure
Monazite	65 ± 3	68 ± 3
Orthite	24 ± 1	26 ± 1
Unknown mineral	20 ± 1	22 ± 1

the curves reproduced in Fig.11 that monazite contains only cerium group rare earths; orthite contains primarily cerium group elements; fergusonite contains both cerium and ytterbium group elements and uranium; euxenite contains elements of the ytterbium group and uranium; wiikite contains ytterbium group rare earths. Approximately one hour is needed for carrying out the entire analysis, most of this time being expended on preparation of the sample pellet. The actual measuring operation and processing of the results require less than 20 min. The compactness of the equipment and the fact that there is no need for a great deal of electric power (electricity is used only for supplying the associated electronic-counting equipment) makes this procedure suitable for use in the field.

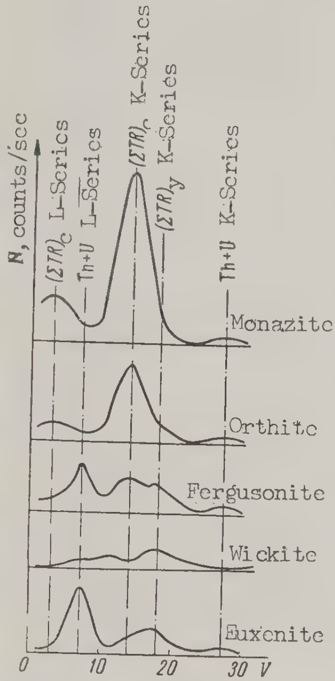

Fig.11. Amplitude distribution of pulses from the characteristic x-radiation of different minerals. $(\Sigma TR)_c$ - total of rare earth elements of the cerium group; $(\Sigma TR)_y$ - total of rare earth elements of the ytterbium group.

IGEM and IMGRÉ,
Academy of Sciences of the USSR

References

1. K.Liden & N.Starfelt, Arkiv Fys., 7, 18,193 (1953).
2. L.Reiggel & R.F.Hamfriz, Reports presented by foreign scientists at the International Conference on Peaceful Uses of Atomic Energy: "Applications of radioactive isotopes in industry, medicine and agriculture", M., 1956.
3. H.K.Hughes & J.W.Welczewski, Anal.Chem., 26, 1889 (1954).
4. W.Seaman, H.C.Lawrence & H.C.Craig, Anal.Chem., 29, 1631 (1957).
5. L.Reiffel, Nucleonics, 13, 3, 22 (1955).
6. A.L.Yakubovich, Razvedka i okhrana nedr. (Prospecting and conservation of mineral resources), No.8, 29 (1958).
7. A.N.Nesmeyanov, A.V.Lapitskii & N.P.Rudenko, Poluchenie radioaktivnykh izotopov (Preparation of radioactive isotopes), M., 1954.
8. K.Liden & N.Starfelt, Arkiv Fysik, 7, 9, 109 (1954).
9. P.P.Day, Phys.Rev., 102, 1572 (1956).
10. K.I.Narbutt & I.D.Bespalova, Zavodsk, laboratoriya, No.5, 617 (1958). (Trans.Industrial laboratory.)
11. K.I.Narbutt, R.L.Barinskii & I.S.Smirnova, Doklady AN SSSR, 130, 291 (1960). (Trans.Soviet Physics - Doklady.)
12. H.I.West, W.E.Meyerhof & R.Hofstatter, Phys.Rev., 81, 141 (1951).
13. J.G.Kereiakes & G.K.Kraft, Nucleonics, 16, 1, 80 (1958).
14. P.I.Cooper & G.A.Morton, Nucleonics, 14, 4, 46 (1956).

INSTRUMENT FOR X-RAY SPECTROSCOPIC MICROANALYSIS

- A.M.Solov'ev & V.N.Vertsner

The technique of local x-ray spectroscopic analysis has been undergoing vigorous development in recent years particularly as regards investigation of chemical composition in mocrovolumes of diverse samples.

Since the American scientist Hillier[1] in 1947 patented an instrument for x-ray spectroscopic microanalysis, investigators in different countries have worked on furthering this technique. At present instruments for "point" x-ray-chemical analysis have been constructed in France, England, the United States and the Soviet Union[2-6].

The developed instruments and installations can be divided into two groups. The first of these comprises instruments intended for investigation of the content of different elements at a chosen "point" of the sample or study of the variation in the content of a given element over the sample in a chosen direction. The second group of instruments, which utilizes the principle of scanning the object with an electron probe, allows of obtaining a "map" of the distribution of different elements over the surface of the sample.

In 1954 we began work on the design of the equipment for x-ray spectroscopic microanalysis and development of analytic techniques. There was realized in our laboratory an experimental model of an x-ray microanalyzer.[7,8] This equipment utilized the basic electron-optical components of an EM-3 electron microscope as well as the vacuum system and power supply of this microscope. This first model was used primarily to develop the electron optics forming the electron probe, the spectrograph and the recording system. The chemical composition of different phases in a number of metal alloys was investigated by means of this experimental model.

In 1956 we started the design and early in 1959 constructed an instrument for local spectroscopic analysis. This new instrument is now in the stage of laboratory tests and improvement. The instrument consists of four basic components: an electron-optical system forming the electron probe, an x-ray spectrograph diffracting the x-radiation excited in the specimen in a 1-2 μ diameter zone, a recording system, and an optical system for visual observation of the object and selection of the area to be investigated.

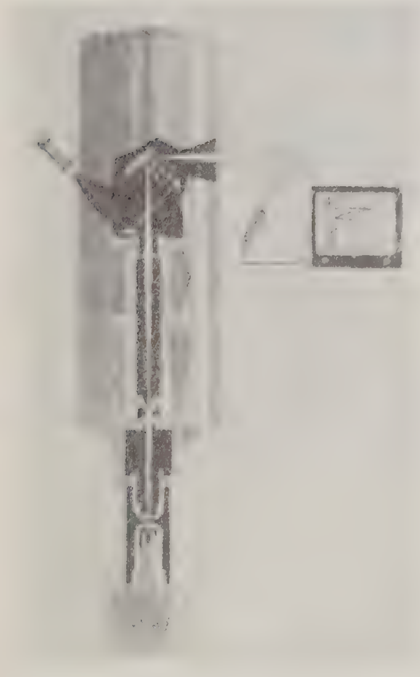

Fig.1. Principle of operation of the instrument.

The electron optical system consists of an electron gun and an assembly of two electromagnetic lenses (Fig.1). The electron gun is a three-electrode gun with negative bias on the cathode cylinder; it produces a narrow electron beam down to 20-25 μ in diameter. The shape of the electrodes, their arrangement and the bias potential are chosen so that the gun will operate with maximum brightness.

The two electromagnetic lenses serve to form a demagnified (diameter - 0.5-1 μ) image of the electron source. This image - the electron probe - is focused on the specimen, which is mounted in the object chamber on a special drum type stage which has room for four specimens. Usually instead of one of the specimens there is

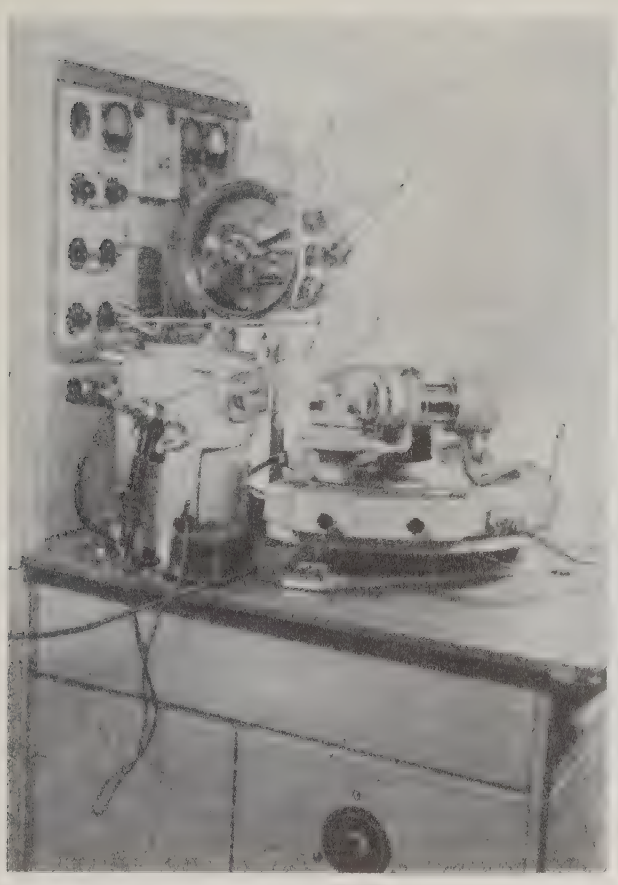

Fig.2. View of the instrument with the object chamber cover thrown back: 1) electromagnetic lens assembly, 2) x-ray spectrograph, 3) optical microscope, 4) microscope objective with holder in raised position, 5) specimen stage, 6) specimen stage motion control knobs.

installed a luminescent crystal which serves to monitor the point of incidence of the demagnified electron beam. We use a special high resolution single crystal capable of withstanding high electron beam densities without damage.

The design of the stage allows of interchanging specimens (four or three and the above mentioned crystal) without disturbing the vacuum by means of an external knob, and also of displacing the specimen under the electron beam in two mutually perpendicular directions with an accuracy of 1 μ by means of appropriate control knobs (see Fig. 2). In addition, for automatic scanning, the specimen can be translated in one of the directions by means of a motor operating through a 5-speed reduction gear.

Tests with the model showed that the minimum diameter of the electron probe obtainable in the instrument is limited by astigmatism. This is due primarily to contamination along the path of the electron beam, in particular owing to deposits forming on the defining apertures. Hence for correction of the astigmatism, the instrument was supplied with a stigmator (compensator) with a rotating magnetic field.

Since precise alignment of the point of incidence of the electron beam on the object at the center of the field of view of the optical microscope is not always obtainable by simple mechanical displacement of the microscope objective, the instrument is equipped with an electromagnetic deflecting system consisting of two pairs of deflecting coils by means of which the electron beam can be deflected to bring its point of incidence to the center of the field of view.

The microscope objective and two mirrors are mounted inside the vacuum chamber; the other components of the light microscope - the tube with eyepiece and illuminator - are located outside the vacuum (Fig.2). The mirror-lens microobjective was specially prepared for this instrument and has a magnification of 43 X, a numerical aperture of 0.5 and a working distance of 7 mm. By virtue of the large working distance (focal length) of the microscope objective, one can observe the specimen during analysis. The microscope provides for examination of the surface of the specimens in reflected light with a magnification of up to 500 X.

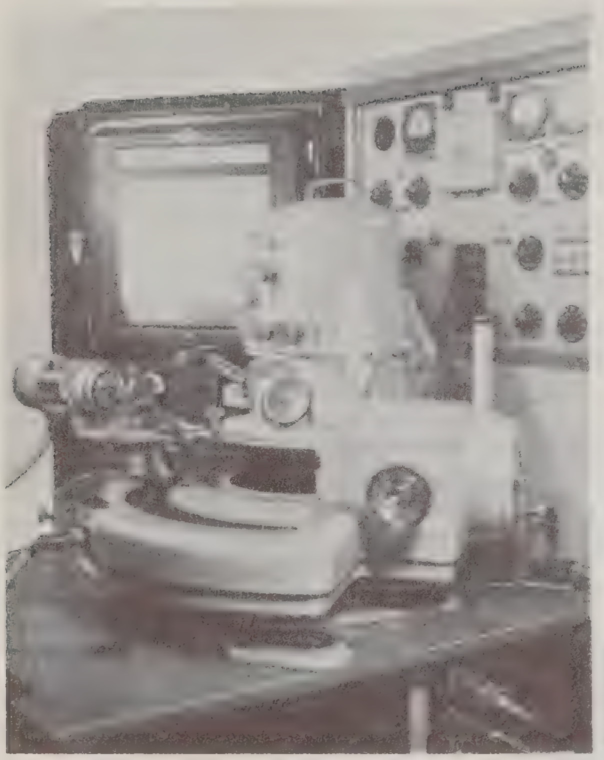

Fig.3. View of instrument with recording unit in place.

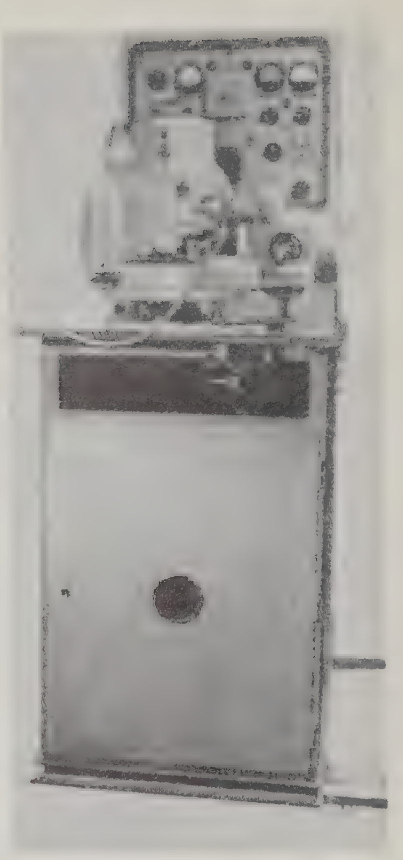

Fig.4. View of instrument with vacuum spectrographic attachment.

The spectrograph, which is located on the instrument bench, consists of a heavy base on which are mounted all its basic components, including the rotating arm carrying the crystal holder and crystal and the Geiger-Müller counter mounting, an appropriately graduated glass dial and an optical system projecting an enlarged image of the dial on a screen, and a reduction gear for varying the rate of rotation of the crystal.

The crystal and the x-ray source are located on the circumference of a Rowland circle with a radius of 250 mm; the center of the circle coincides with the center of rotation of the arm carrying the crystal. The design of the spectrograph allows of working either by the "transmission" or the "reflection" method. The spectrograph base also has provision for mounting a vacuum spectrographic attachment (Fig.4) by means of which one can carry out analyses for light elements. Thus the instrument can be used for local spectroscopic analysis for elements ranging from magnesium to uranium.

By way of analyzer crystals the instrument uses bent (R = 500 mm) quartz plates with reflection from the $(13\bar{4}0)$ planes in using the "transmission" method and from the (0001) planes in using the "reflection" method and mica plates (reflection from the (100) planes). Experiments have also been carried out with LiF crystals ((200) planes) which, utilizing the first and second orders, can be used in the entire nonvacuum region of the x-ray spectrum.

The x-radiation is detected by means of Geiger-Müller counters. The radiation intensities can either be read on the scale of a pulse integrator or recorded by means of an electromagnetic register. Continuous recording of the spectrum or variation in the intensity of some line of the spectrum is realized by means of a recording electronic potentiometer.

The instrument consists of two subassemblies (Fig.3): the first comprises the electron-optical system, the spectrograph, the high voltage circuit, the lens current supply and the vacuum system; the second includes all the instruments of the detecting and recording system and the voltage regulator.

References

1. J.Hillier, U.S.Patent No.2,418,029, 25 March 1947.
2. R.Castaing & A.Guinier, Proceedings of the Conference on Electron Microscopy, Delft, 1949. Delft, 1950.
3. R.Castaing & A.Guinier, Spectrochemica Acta, 6, 509 (1953).
4. V.E.Cosslett & P.Duncumb, Nature, 177, 1172 (1956).
5. L.S.Birks & E.J.Brooks, Rev.Sci.Instr., 28, 709 (1957).
6. I.B.Borovskii & N.P.Il'in, Doklady AN SSSR, 106, 655 (1956). (Trans. Doklady).
7. V.N.Vertsner & A.M.Solov'ev, Optika i spektroskopiya, 5, 83 (1958).
8. A.M.Solov'ev & V.N.Vertsner, Izv.AN SSSR, Ser.fiz., 23, 750 (1959). (Trans. Bulletin 23, 744.)

UNIVERSAL X-RAY SPECTROGRAPH FOR INVESTIGATION OF THE CHEMICAL COMPOSITION IN MICROVOLUMES

- N.P. Il'in

The x-ray spectroscopic procedure for investigating the chemical composition in microvolumes is being ever more extensively employed and is attracting the attention of investigators working on diverse problems connected with study of the structure of solids, particularly alloys. The high degree of localization of analysis in conjunction with the possibility of carrying out quantitative determinations of most elements with an average sensitivity of 0.1% gives this procedure distinct advantages over other methods of local chemical analysis. In fact, many of the results obtained with this procedure[1-3] could not be duplicated by any other method of physical-chemical analysis. In view of the wide range of applications of the x-ray microspectroscopic procedure for the solution of diverse problems in the fields of metal physics and metallurgy, technology and mineralogy, it may be asserted that in the near future this procedure will be as widely used in scientific institutes and plant laboratories as electron diffraction studies are now. Hence an important current problem is the development of simple and reliable equipment for x-ray spectroscopic microanalysis. Accordingly, there was recently developed the new RSASh-3DS equipment taking into account the said requirements of simplicity and reliability; essentially the equipment is based on the time tested units and subassemblies of the RASAh-2 quipment[4]. The new apparatus allows of analyzing for a wide range of elements from magnesium ($Z = 12$) to uranium ($Z = 92$) with localization in a region of 2-3 μ and an average sensitivity of 0.1%.

The RSASh-3DS equipment utilizes the following basic components of the RSASh-2: the electron-optical system with the object chamber and object stage (microfocus x-ray tube), all the power supply units, the recording-detecting column, and the vacuum system.

New in principle and design in the RASAh-3DS equipment is the x-ray spectrograph. For spectral dispersion of the radiation and focusing of the monochromatic beam by a bent crystal the spectrograph utilizes the "transmission" method, which has the advantage of eliminating absorption of the x-ray radiation by the crystal-analyzer plate. The kinematic system of the spectrograph has been modified accordingly. The stationary x-ray tube and the radiation detector are situated on the same side of the crystal, symmetrically relative to its radius of curvature. The crystal is located on the focusing circle (Rowland circle) with the radiation detector being displaced along the same circle at twice the rate of the crystal. With the tube stationary on the Rowland circle, this kinematic system assures constant equality of the angles of incidence and reflection, i.e., detection in each position of the crystal of a certain definite wavelength corresponding to the Bragg reflection condition.

In practice it is impossible to cover a very wide wavelength range (0.7 to 10 A) by means of one crystal. Hence the spectrograph design provides for three single crystals; for simplicity of design all the crystals operate in the same range of glancing angles (20 to 40°). The spectrum in the wavelength range from 0.7 to 1.5 Å is covered by a quartz plate with $(13\bar{4}0)$ reflecting planes and a lattice constant $d = 1.174$ Å. The wavelength interval from 1.4 to 5.4 Å is covered by a quartz crystal with reflection from the $(10\bar{1}0)$ planes and $d = 4.245$ Å. The remaining wavelength range to 10 Å is covered by means of a mica crystal with (001) reflecting planes and $d = 9.928$ Å. These three crystals provide for the determination of all elements ranging from magnesium ($Z = 12$) to uranium ($Z = 92$) on the basis of the K and L series in the first or higher orders of reflection.

Use of the "reflection" method without providing a vacuum over the entire path of the x-ray beam from the x-ray tube to the radiation counter precludes the possibility of analyzing with adequate accuracy radiation with a wavelength exceeding 2.5 Å. In conventional vacuum spectrographs the vacuum is provided in the entire volume of the spectrograph including the kinematic system and the radiation detector; very often, therefore, the vacuum volume amounts to tens and even hundreds of liters and to evacuate it one must employ a powerful pump or provide a separate forevacuum section, which in turn leads to the necessity of installing foil windows that absorb soft radiation.

In the RASAh-3DS spectrograph this design problem has been solved in a new and different way: a high vacuum is provided only in the x-ray tube and over the immediate path of the x-ray beam from the tube anode to the detector. All the units of the kinematic system and recording assembly are located in air, i.e., outside the vacuum volume. The vacuum is "localized" by the use of flexible vacuum "pipes" which connect the crystal holder chamber with the object chamber (tube) and with the radiation detector. These "pipes" are flexible sylphon bellows cylinders which allow of 2-2.5-fold variation in length and the necessary bending. Their bacuum packing is realized by means of flanges and rubber gaskets. By virtue of the hydrostatic pressure of the atmosphere these sylphon conduits always assume the shortest length and in any position of the kinematic linkages are located along the chord of the kinematic circle, i.e., along the path of the x-ray beam. With the chosen range of glancing angles, the sylphon conduits in addition to expansion and contraction, rotate relative to the middle position through an angle of up to 10^{o}; this rotation is provided for by flexure of the end 3-4 corrugations.

Two crystals, bent to a radius of 550 mm, are mounted in the crystal holder chamber; these crystals can be displaced in the chamber under vacuum along the radius of curvature and can be rotated about their vertical axis thus assuring the necessary adjustment of the crystals. The third crystal - the mica crystal - which is used for determination of a few light elements, is removable and is installed prefocused in its own crystal holder instead of one of the quartz crystals.

The radiation detector - an end window Geiger-Müller counter - is introduced into the vacuum volume only at the window end; the counter is installed on a special flange made vacuum tight with picein. The rest of the counter envelope including the terminals and leads is located in a protective shield outside the vacuum. The counters for different wavelength intervals are interchanged together with their mounting flanges. The total volume of the vacuum system of the spectrograph is about 0.5 liter, which makes it possible to join its vacuum system to that of the microfocus x-ray tube without the use of a foil window and to use a common evacuating system (TsVL-100 and VN-461 vacuum pumps).

The arrangement of the principal spectrograph components is shown in Fig.1.

The kinematic system of the spectrograph was designed taking into account the fact that the sylphon conduits are under atmospheric pressure. Hence it was necessary to provide a sufficiently rigid construction. The main components* are two heavy arms rotating about a common center located at the center of the Rowland circle at a distance of 275 mm from the axis of the electron-optical column.

One arm (A_k in Fig.1) carries the crystal holder chamber; the other arm (A_c) - the counter chamber. Arm A_c is rigidly connected to a worm pair which transmits the rotary motion from a reduction gear; the arm can be rotated either manually or by means of a motor. The lever linkage P_1-P_2 insures synchronous motion of

---

*The kinematic components were developed in collaboration with Design Engineer I.M.Mogilevskii.

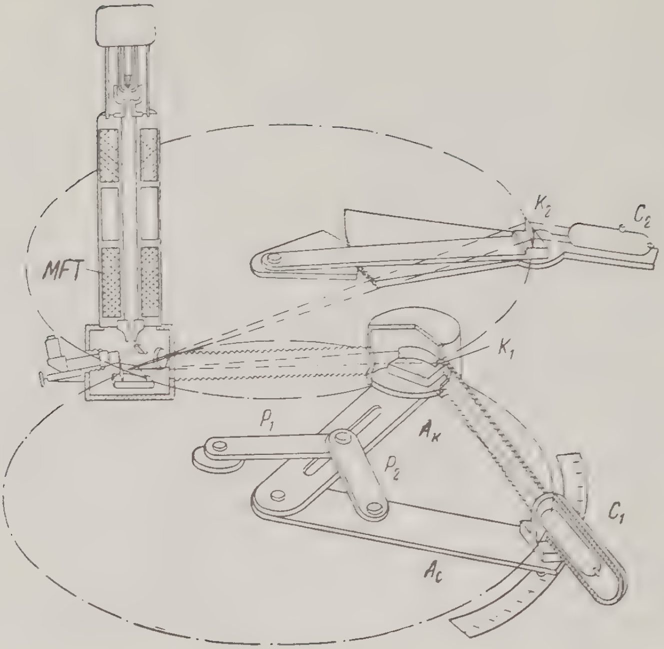

Fig.1. RSASh-3DS spectrograph: MFT - microfocus x-ray tube, K_1 - replaceable crystal of the long wavelength spectrograph, K_2 - crystal of the short wavelength spectrograph, C_1 and C_2 - radiation counters, A_k, A_c, P_1 and P_2 - linkages of the kinematic system of the long wavelength spectrograph.

Fig.2. RSASh-3DS spectrograph with microfocus x-ray tube.

both arms. The two levers, which differ in length, have a common axis of rotation on the carriage (pivot) moving in a slot in arm A_k. The other ends of the levers are pivoted on axes mounted symmetrically relative to arm A_k (see Fig.1). This circular type mechanism insures synchronous motion of arms A_k and A_c with the requisite 1:2 speed ratio. To bring the axis of the counter in line with the axis of the monochromatic beam at any angle of reflection, the counter chamber with its slit can be rotated through the requisite angle by means of a bar connecting the counter chamber with the central vertical axis of the crystal holder. The design of the kinematic linkage has provision for the necessary adjustments of the tube, crystals and counter slit on the Rowland circle. A general view of the RSASh-3DS x-ray spectrograph is shown in Fig.2.

The compact design of the x-ray spectrograph and its convenient location relative to the object chamber make it possible to bring out a second x-ray beam from the tube and direct it into a simple x-ray spectrographic attachment, specifically a short wavelength x-ray spectrograph operating by the DuMond "transmission" method (crystal K_2 and counter C_2 in Fig.1).

This spectrograph analyzes and detects the spectrum in the wavelength range from 0.7 to 2.0 Å, i.e., the radiation of the 40 heavy elements which could be determined on the earlier RSASh-2 equipment. Thus these elements can be simultaneously detected in two channels, i.e., in the short wavelength and long wavelength spectrographs, which offers great advantages in investigating the distribution of elements, for with one passage of the electron "probe" over a given part of the section one can simultaneously detect two elements and record their distribution curves. This is of particular interest in studying mutual diffusion. The fact that an appreciable range of elements is detectable in each of the spectrographs makes it possible to carry out concurrent analyses in the two channels for a wide range of alloy compositions and to vary the experimental procedure as dictated by the problem involved. The availability of two spectrographs simultaneously operating from one x-ray tube allows of choosing the most advantageous operating conditions and analytic lines for detection of heavy elements yielding short wavelength characteristic x-rays.

The location of the radiation detectors in both spectrographs outside the vacuum is convenient for carrying out experiments on selection of the most efficient radiation intensity detectors and in particular allows of replacing the Geiger-Müller counters by photomultipliers with crystal phosphors or secondary electron tubes without modifying the basic design of the spectrograph. Thus potentially one can greatly increase the sensitivity of analysis by means of the described equipment.

"A.A.Baikov" Institute of Metallurgy,
Academy of Sciences of the USSR

References

1. I.B.Borovskii, N.P.Il'in, L.E.Loseva, I.D.Marchukova & A.N.Deev, Izv.AN SSSR, Ser.fiz., 21, 1415 (1957). (Trans.Bulletin 21, 1404.)

2. A.A.Yavnel', I.B.Borovskii, N.P.Il'in & I.D.Marchukova, Doklady AN SSSR, 123, 256 (1958). (Trans.Soviet Physics - Doklady.)

3. I.B.Borovskii, N.P.Il'in, L.E.Loseva & I.D.Marchukova, Sb. Nauchnye issledovaniya IMET AN SSSR v 1957 (Scientific investigations of the Institute of Metalurgy at the USSR Acad. of Sci., in 1957), M., 1958.

4. I.B.Borovskii & N.P.Il'in, Zavodsk.laboratoriya (Industrial laboratory), No.10, 1234 (1957).

DEVELOPMENT OF THE FIRST AUTOMATIC X-RAY SPECTROGRAPH IN CZECHOSLOVAKIA

- R.Rotter & M.Klapuch

Four years ago work began in our Institute on the development of an automatic x-ray spectrograph based on the principle of secondary emission. The spectrograph with appropriate auxiliary instruments is built into a special cabinet-bench (Fig. 1).

The spectrometer proper (Fig.2) is based on the design realized earlier by Blokhin[1], i.e., the specimen, crystal and radiation detector are located along the periphery of a focusing (Rowland) circle of constant radius. This arrangement assures precise focusing for each and every wavelength in the x-ray spectrum, as was theoretically shown by Johann[2]. The radius of the focusing circle is 200 mm. By way of crystal we provisionally use a quartz plate 0.2 mm thick cut parallel to the $(1\bar{3}40)$ planes. The crystal is bent so that its radius of curvature is twice the radius of the focusing circle. By way of detector we used a Millard Type MS-118 Geiger counter which is very sensitive in the frequency range employed in the instrument.

The entire spectrometer is assembled on a heavy steel plate which is attached to the top of the bench-cabinet. The linkages governing the motion of the detector, crystal and secondary emitter are arranged so that the normal to the tangent to the surface of the crystal always bisects the angle between the incident and reflected rays. Two levers connecting the crystal with the secondary emitter and the detector insure conditions under which the incident beam during motion of the mechanism continuously follows the crystal, while the reflected beam is always directed on the slit of the detector. The arm carrying the detector is mounted on a common shaft with a circular scale engraved on silver; the scale is projected by means of a simple optical system onto a ground glass screen built into the control panel of the instrument. The silver scale is enclosed in an air-tight box to protect it against dust, tarnishing, etc.

The instrument is completely mechanized; one can, for example, mechanically change the specimens in the secondary emitter by means of a special revolver head, which carries twelve interchangeable specimens. The number of the specimen in the working position is automatically indicated on the control panel.

Raising of the x-ray tube incident to replacement of the cell with the specimen is also mechanized. As the tube is moved, its window is automatically covered. Thus the operator is protected against accidental exposure to the primary radiation.

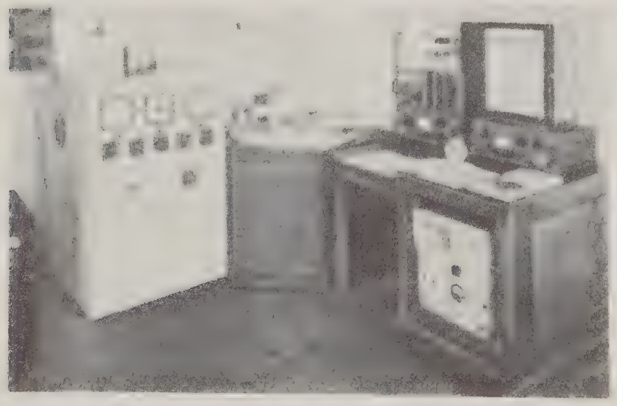

Fig.1. General view of spectrograph.

The entire spectrographic assembly can be displaced in the direction of increasing or decreasing angles of reflection at two angular velocities: a low velocity (analytic) and a high velocity (used for setting the system to a desired spectrum line).

The Geiger counter can be switched by one movement of the selector switch to an integrator, which is used in qualitative analysis, or to a decimal scaling system which is used for a precise measurement of line intensities.

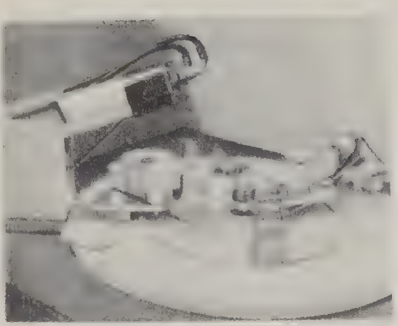

Fig.2. Spectrometer assembly.

In view of the fact that in designing the instrument we had in mind its complete automation, a spectrometer with a crystal located at the center of the main circle seemed to us to be disadvantageous: for remote control it would require a very complex mechanism. Hence we used a spectrometer with peripheral location of the crystal despite the fact that as regards absorption of x-rays in air it is less advantageous than a spectrometer with a crystal located at the center of the circle. The disadvantages ensuing from the adopted arrangement in working with long wavelengths can be eliminated by using suitable crystals which substantially reduce the path of the incident and reflected rays.

In developing the automatic control system for the instrument we attached great weight to determining the magnitude of the mean error in carrying out certain operations on our spectrograph.

In the accompanying table we give the percentage errors for some operations that are important in the choice of a suitable automatic measuring process. In contrast to quantitative x-ray spectroscopic analysis, which was not carried out automatically and in which the intensity of the spectrum line was expressed by the number of pulses from the decimal scaler circuit during a given interval, in automatic x-ray analysis it is more advantageous to express the spectrum line intensity in terms of time during which the scaler circuit records a set number of pulses. Automation of quantitative x-ray analysis presupposes automatic performance of the following three operations:

1) measurement and recording of the time necessary for attaining a predetermined number of pulses,

2) rotation through 30° of the cell with the analyzed specimen and advance of the next specimen to the working position, and

3) switching off of the automatic system after measurement of the 12 specimens with appropriate indication that the cycle of measurement has been completed.

The list of automatic operations does not include initial setting on the spectrum line inasmuch as manual setting is more accurate. Moreover, given the appreciable time required for measurement of all 12 samples, we assumed that automatic setting on the line maximum would be an unnecessary luxury.

The automatic devices provided include the following elements:

1) A central control mechanism (provides automatic control of individual operations).

2) Pulse counter (measures each 1000 pulses by means of a decimal scaler to a preset number).

3) Timer (allows of setting, by means of a push-button, the desired number of total pulses to be counted: 1000, 2000, 5000 or 8000, and cuts off the counter when the given count is attained).

4) Automatic register (automatically records the time at the beginning and end of measurement of the set number of pulses; prints out the numerical values on a paper tape).

5) Sample indicator (counts and indexes the measured samples and switches off the automatic mechanism at the end of a measurement cycle and signals the end of measurement).

6) Decimal scaler (counts the pulses from the Geiger counter and transmits each thousandth pulse to the final pulse counter; we used a standard Tesla scaler).

7) Automatic device for changing samples (actuated by a control pulse, this device automatically cycles the samples).

Table 1

Errors in different operations

Operation or source of error	Absolute magnitude of the relative error, %
Raising of the x-ray tube	0.44
Instability of the instrument	0.23
Rotation of the specimen cell to the working position	0.20
Successive rotation of the different parts of the carrying cell in the working position	0.61
Measurement of the intensity of the spectrum lines (initially all the peaks are measured, then the background corresponding to each line)	0.16
Measurement of the intensity of the spectrum lines (simultaneous measurement of the peaks and corresponding background)	0.27
Alignment on the line peak from the same direction	0.07
Alignment on the line peak alternately from two directions	0.88
Filling the cell without weighing or measuring the specimen	0.32
Error due to exposure (at an intensity of 7000 pulses/min):	
30 sec	1.06
1 min	0.96
3 min	0.63
10 min	0.94

In addition to automation of the process of measuring the intensity of any selected spectrum line, which is essentially automation of quantitative analysis, our instrument has an automatic device for carrying out quantitative analysis with reference to two spectrum lines. By means of the instrument one can also make a continuous record of the x-ray spectrum by means of an integrator and milliammeter.

Using a quartz crystal (reflection from the $(13\bar{4}0)$ plane) one can, by means of this instrument, carry out analyses for all elements from cobalt to ytterbium with reference to the K series and from hafnium to uranium with reference to the L series. With reference to the L series one can also analyze for the group of transuranium elements, as we demonstrated by measurement of several lines of plutonium and americium.

Of the large number of measurements that we carried out by means of this instrument, we shall cite here only two series, one of which (Table 2) represents determination of copper in lead-copper concentrate from Zolotye Gory with continuous servicing of the instrument by an operator, while the other (Table 3) represents determination of copper in other concentrates from the same origin but using the automatic device for measuring the line intensity.

It will be evident from comparison of the results given in the two tables that automatic measurements yield more accurate results than measurements carried out by an operator and that the time required for automatic analysis is appreciably shorter. An experienced operator requires 20-25 min for carrying out an analysis of one of a series of 12 samples; one automatic analysis is accomplished in 10 min. The indicated times in both cases include repetition of all measurements.

Experimental measurements carried out in our Institute showed that automation of x-ray spectroscopic analysis is feasible and that such automated analysis

Table 2

Quantitative determination of Cu in lead-copper concentrates*

Sample No.	Maximum average pulses	Background average pulses	Intensity, pulses	% Cu according to		Difference
				x-ray analysis	chemical analysis	
224	2074	462	1612	11.7	11.0	0.7
227	2092	493	1599	Standard I	11.70	—
230	1760	469	1291	10.0	10.0	0.0
233	1611	464	1147	Standard II	9.26	—
236	1721	433	1288	10.0	9.8	0.2

---

*The sample is excited by Mo radiation at 40 kv and 20 ma. The measuring time was 3 min. The peak of the Cu $K\alpha_1$ line was monitored at 40°40'; the background at 40°00' for each sample. These measurements were not automated.

Table 3

Automatic quantitative determination of Cu in lead-copper concentrates*

Sample No.	Time to record 1000 counts, sec	Number of pulses per 100 sec	% Cu according to		Difference
			x-ray analysis	chemical analysis	
1	32	3125	Standard I	21.5	—
2	34	2941	20.2	19.9	0.3
3	80.5	1242	7.6	7.6	0.0
4	179.5	557	Standard II	2.5	—
5	37.5	2667	18.3	18.6	0.3

---

*The sample was excited by Mo radiation at 40 kv and 20 ma. Only the peak of the Cu $K\alpha_1$ line at 40°40' was measured.

can replace conventional chemical analysis in many branches of industry with resultant economies. The above described automatic x-ray spectrograph is scheduled for batch production at the Hiran Plant in Modjana near Prague.

Institute for the Investigation of Ores,
Czechoslovakia

References

1. M.A.Blokhin, Zavodsk. laboratoriya (Industrial laboratory), 16, 181 (1950).
2. H.H.Johann, Z.Phys., 60, 185 (1931).
3. R.Rotter & M.Klapuch, Vyvoj roentgenoveho spectrografu pró sekundarni emisi k analyse rudnich mineralu. (Development of a secondary emission x-ray spectrograph for analysis of ores and minerals.)
4. R.Rotter & M.Klapuch, Vyzkum automatisace rtg. spectrografu a jeho aplikace v praxi, automatisace kvantitativni analysy.(Tests of an automatic x-ray spectrograph and its application for purposes of automatic quantitative analysis.)

REFLECTION OF X-RAYS FROM A BENT CRYSTAL IN THE CASE OF A MICROFOCUS SOURCE

- S.A.Ditsman

The development of point focus x-ray spectroscopy for analysis of the chemical composition in microvolumes[1] and study of the fine structure of x-ray spectra[2] calls for special investigation of the distinctive features of reflection of x-radiation from a bent crystal in the case of a microsource. Most studies devoted to the geometric theory of focusing of radiation by bent crystals in x-ray spectrographs are limited to consideration of the conditions of focusing in the plane of the Rowland circle. Johansson considered the case of spatial focusing in the mounting proposed by him for the case of a wide focal spot x-ray tube.[3] In the present report we give the results of theoretical and experimental investigation of the reflection of x-radiation from a bent crystal in the case of a microsource.

Let us consider the conditions of reflection of a ray from a point source F (Fig.1) on a circle of radius $R/2$ incident on an arbitrary point P of the crystal curved to a cylinder of radius R (Kapitsa-Johann mounting). We shall define the point P by its coordinates in the plane of the crystal: l and h. We denote the glancing angle at the point P_1 of the crystal and the tangent to the Rowland circle by ϑ_0. Then the glancing angle ϑ_x of the ray FP at the point P can be found from the following geometric relationships (Fig.1,a and b):

$$\sin\vartheta_x = \frac{FM}{FP} = \frac{FP_2}{FP}\sin(\vartheta_0+\varphi) = \sin(\vartheta_0+\varphi)\left(1-\frac{h^2}{2PF^2}\right);$$

$$FP_2 = \sqrt{FP^2+h^2} \approx FP\left(1-\frac{h^2}{2FP^2}\right).$$

Usually in x-ray spectrographs $l, h \ll R$ and $FP \approx R\sin\vartheta_0$. Using the expression for the geometric broadening of spectrum lines given by Borovskii & Blokhin[4], we determine the angle φ:

$$\varphi = \frac{FK}{FP} = \frac{l^2}{2R^2}\operatorname{ctg}\vartheta_0,$$

inasmuch as

$$FK = \frac{l^2}{2R}\operatorname{ctg}\vartheta_0\sin\vartheta_0.$$

After substitution of the deduced expression and simple transformations, we obtain

$$\sin\vartheta_x = \sin\vartheta_0 + \frac{l^2}{2R^2}\operatorname{ctg}\vartheta_0\cos\vartheta_0 - \frac{h^2}{2R^2\sin\vartheta_0} \qquad (1)$$

Let us determine the locus of the points with an equal glancing angle ϑ_0 on the surface of the crystal; setting $\vartheta_x = \vartheta_0$, we obtain

$$h = l\cos\vartheta_0. \qquad (2)$$

This expression defines the points on the surface of an ideal crystal* reflecting monochromatic radiation of wavelength λ_0 (corresponding according to the Bragg equation, to a glancing angle ϑ_0). It also follows from Eq.(1) that condition (2) divides the surface of the crystal into regions in which the glancing angles will be greater than and smaller than ϑ_0. These regions will, accordingly, reflect wavelengths longer than and shorter than λ_0 (Fig.2).

---

*An ideal crystal is understood to be one reflecting monochromatic radiation from a point source in perfect conformity with the Bragg equation.

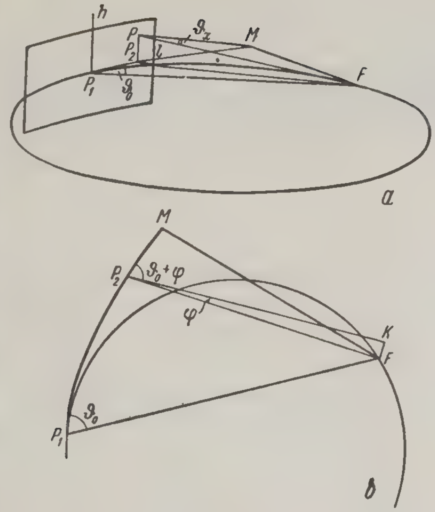

Fig.1.

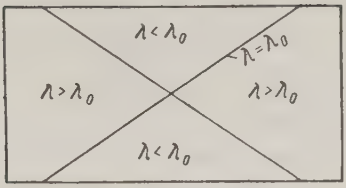

Fig.2.

Let us find the part of a surface of a real crystal (a crystal which has a reflection curve of width δ for the given wavelength) reflecting monochromatic radiation from a source of diameter d. The radiation will be reflected by those points of the surface for which there is fulfilled both the geometric condition for reflection of the rays incident from all points of the source and the condition of reflection arising owing to finite width of the reflection curve of the crystal. This last obtains in the case when the angle of incidence of the λ_0 beam at the point in question differs from ϑ_0 by not more than $\delta/2$. The radiation from a source of diameter d incident on the point P of the crystal is in the angular interval

$$\vartheta_x + \frac{d}{2R\sin\vartheta_0}, \quad \vartheta_x - \frac{d}{2R\sin\vartheta_0}.$$

The radiation will be reflected from this point if the following relation obtains for the angle ϑ_x:

$$\vartheta_x - \vartheta_0 = \Delta\vartheta \leqslant \frac{d}{2R\sin\vartheta_0} + \frac{\delta}{2}; \tag{3}$$

from Eq.(1), we have

$$\Delta\vartheta = \frac{l^2}{2R^2}\operatorname{ctg}\vartheta_0 - \frac{h^2}{R^2\sin 2\vartheta_0}.$$

The case of equality in (3) corresponds to the condition of reflection from points on the surface of the crystal bounding the region reflecting the radiation. After substitution in (3) and transformation for these points, we obtain

$$h^2 = l^2\cos^2\vartheta_0 \pm \left(Rd\cos\vartheta_0 + \frac{R^2}{2}\delta\sin 2\vartheta_0\right).$$

The appearance of this reflecting region is shown in Fig.4. In considering the conditions of reflection for a wavelength interval $\Delta\lambda$, there is obtained a similar shape of the radiation reflecting region.

In investigations of the fine structure of x-ray spectra by means of a microfocus spectrograph the principal factor determining the resolving power of the instrument is correct choice of the dimensions of the working surface of the crystal with the given radius of curvature, the size of the source and the wavelength region. As was shown in Ref.2, for small size of the working surface of the crystal and a microsource (2-3 mm and ~10 μ, respectively, in the ~2 Å wavelength region) there is discriminated from the investigated spectral interval (emission line) by the conditions of reflection a monochromatic pencil of rays. Resolving the investigated spectral interval into such pencils by varying the conditions of reflection of the radiation (by displacing the crystal along the Rowland circle) and detecting the intensities, we can reproduce the intensity distribution of the radiation in the investigated region of the spectrum. Accordingly, the resolution of a microfocus spectrograph is determined by the monochromaticity of the reflected pencil of rays and the corresponding resolution of a conventional x-ray spectrographic instrument.

Let us evaluate the monochromaticity of the radiation reflected by a crystal with dimensions $2h \times 2l$. From (3) and (5) it follows that the minimum angle for radiation reflected from the point $l = 0$ will be

$$\vartheta_{\min} = \vartheta_0 - \left(\frac{d}{2R\sin\vartheta_0} + \frac{h^2}{R^2\sin 2\vartheta_0} + \frac{\delta}{2}\right).$$

Analogously, the maximum angle for radiation reflected from the point $h = 0$ is

$$\vartheta_{\max} = \vartheta_0 + \frac{d}{2R\sin\vartheta_0} + \frac{l^2}{2R^2}\operatorname{ctg}\vartheta_0 + \frac{\delta}{2};$$

hence the total angular interval of the radiation reflected by the given surface of the crystal will be

$$\vartheta_{\max} - \vartheta_{\min} = \frac{l^2}{2R^2}\operatorname{ctg}\vartheta_0 + \frac{h^2}{R^2\sin 2\vartheta_0} + \frac{d}{R\sin\vartheta_0} + \delta.$$

Utilizing the Bragg condition, we readily obtain

$$\Delta\lambda = \lambda\operatorname{ctg}\vartheta\cdot\Delta\vartheta,$$

where $\Delta\vartheta$ is the full angular interval of the reflected radiation. For a wavelength interval $\Delta\lambda$ reflected from the crystal surface under consideration we finally obtain

$$\Delta\lambda = \lambda\operatorname{ctg}\vartheta_0\left(\frac{l^2}{2R^2}\operatorname{ctg}\vartheta_0 + \frac{h^2}{R^2\sin 2\vartheta_0} + \frac{d}{R\sin\vartheta_0} + \delta\right). \qquad (4)$$

By choice of appropriate parameters of the instrument one can in a given wavelength region obtain a pencil of rays with monochromaticity $\sim 10^{-2}$ X.

In the above calculations we consider the conditions of reflection of radiation from the surface of the crystal tangent to the Rowland circle. The geometric condition of reflection for internal planes are somewhat different.

Our experimental investigation of the reflection of radiation from a bent crystal was carried out for a Kapitsa-Johann mount in a microfocus x-ray spectrograph[2]. We used a quartz crystal with reflection from the $(10\bar{1}0)$ plane, curved to a radius of 500 mm, and a 10-20 μ diameter radiation source. There was imaged on the photographic film located in the immediate proximity of the crystal (Fig. 3) the surface of the crystal reflecting the investigated line of the x-ray spectrum. Fig.4 shows the results of investigation of reflection of the Fe $K\alpha_1$ line. These results are in good agreement with the above calculations. The cross-shaped form of the reflecting region of the crystal corresponds to the position of the crystal on the Rowland circle when for the central part of the crystal there is fulfilled the condition for reflection of the $K\alpha_1$ radiation. Upon displacement of the crystal from this position, the reflection region is shifted over the surface of the crystal. Displacement of the crystal along the Rowland circle in the direction towards the source (Fig.4, a & b) shifts the region of reflection of the $K\alpha_1$ line into the range $\lambda > \lambda_0$ (Fig.2) inasmuch as the wavelength of the radiation reflected from the central part of the crystal is shorter than the investigated

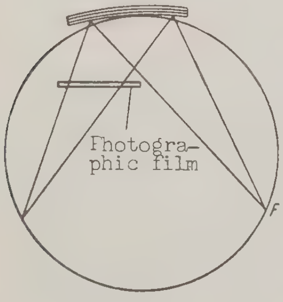

Fig.3.

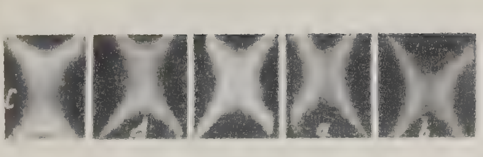

Fig.4.

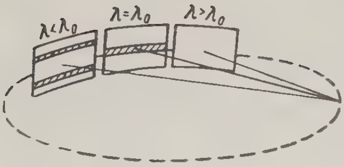

Fig.5.

wavelength. Upon displacement of the crystal further away from the source (Fig.4, c & d), the conditions for reflection of the $K\alpha_1$ line are fulfilled in the range $\lambda < \lambda_0$.

It follows from the results obtained that with a microsource located on the focusing circle of a crystal bent by the method of Kapitsa-Johann, the selected line of the x-ray spectrum is reflected by a section of the crystal surface with a complex configuration.

For purposes of chemical analysis in microvolumes one must regard as optimal choice of a cross-shaped working surface of the crystal. The dimensions and angular dependence of this region can be evaluated by means of Eqs.(2) and (4). Further increase of the working surface of the crystal leads to decrease in the sensitivity of the instrument.

The character of reflection in the case of focusing of the radiation according to Johansson with a microsource is shown in Fig.5. In this case Eq.(1) obtained for a Kapitsa-Johann type mount transforms into the analogous expression for a Johansson mount, if in Eq.(1) we set $l = 0$.

The results obtained can also be utilized in investigating problems connected with the resolution and the character of the distortions introduced by a crystal in wide focus x-ray spectrographs. Obviously, the image of a line in the x-ray spectrum obtained on the Rowland circle, formed of monochromatic pencils with a small working surface of the crystal, will contain less distortion than the same line image formed of nonmonochromatic pencils with a larger working surface of the crystal. The question of determining the optimal working surface for a crystal requires separate investigation.

I desire to thank I.B.Borovskii for valuable suggestions and helpful discussion.

"A.A.Baikov" Institute of Metallurgy,
Academy of Sciences of the USSR

References

1. I.B.Borovskii, Sb. Problemy metallurgii, Akad. I.P.Bardiny k 70-letiyu (Collected articles on Problems of Metallurty, publication dedicated to the 70th anniversary of Academician I.P.Bardin), M.-L., 1953; I.B.Borovskii & N.P.Il'in, Doklady AN SSSR, 106, 655 (1953); R.Castaing & A.Guinier, Anal.Chem., 25, No.5, 724 (1953).

2. I.B.Borovskii & S.A.Ditsman, Doklady AN SSSR, 124, 1042 (1959). (Trans. Soviet Physics - Doklady.)

3. T.Johansson, Z.Phys., 82, 507 (1933).

4. I.B.Borovskii & M.A.Blokhin, Rentgeno-spektral'nyi analiz (X-ray spectroscopic analysis), M., 1939.

OPTIMUM CORRECTION OF X-RAY SPECTRA FOR DISPERSIVE DISTORTION

- I.Ya.Nikiforov

An x-ray spectrum obtained with dispersive distortion can be represented in the form of the sum of the true spectral curve $\varphi(x)$, the systematic errors $r(x)$, arising as a result of distortion, and the chance experimental errors Δf, i.e.,

$$f(x)=\varphi(x)+r(x)+\Delta f(x). \tag{1}$$

The true shape is found by solution of the integral equation

$$f(x)=\frac{1}{\pi}\int_{-\infty}^{+\infty}\varphi(t)\,\gamma\,dt\,/\,[(t-x)^2+\gamma^2], \tag{2}$$

where γ is the half-width of the distorted dispersion curve. The solution by the method successive approximations is of the form

$$\varphi_n(x)=\int_{-\infty}^{+\infty}f(t)\,\Phi_n(t-x)\,dt,$$

where $\Phi_n(x)$ is the reversal function[1] found in the n-th approximation. With increase in the order n of the approximation the systematic error, i.e., the difference $\varphi(x)-\varphi_n(x)=r_n(x)$ will decrease. In the absence of systematic errors, $r_n(x)$ could be made arbitrarily small. Actually, however, with increase of n the chance errors Δf after correction increase. This occurs for all methods of correction and for distortions of all types. Beginning with a certain n, the increase in the chance error may exceed the decrease of the systematic error $r_n(x)$ so that further increase of n becomes not simply useless but actually harmful. There is, therefore, a value of n for which the correction will be optimal.

By way of measure of the correspondence of the corrected spectrum $\varphi_n(x)$ with the true spectrum $\varphi(x)$ one can take the quantity

$$\delta=\delta_1+\delta_2,$$

where

$$\delta_1=\int_a^b[\varphi(x)-\varphi_n(x)]^2\,dx$$

is the square of the systematic error integrated over the section ab of the spectrum being corrected, and

$$\delta_2=\int_a^b\left[\int_a^b\Delta f(t)\,\Phi_n(t-x)\,dt\right]^2dx$$

is the square of the corrected chance error Δf integrated between the same limits.

The optimum n leading to minimum δ is found from the condition

$$\partial\delta/\partial n=\partial\delta_1/\partial n+\partial\delta_2/\partial n=0. \tag{3}$$

A similar problem regarding the optimum correction is encountered in optical spectroscopy[2] and in radiophysics, where it was approximately solved by Bracewell[3] for the case of diffractive distortion of radiosignals in a radiotelescope. The results of Bracewell were utilized by Porteus & Parratt[4,5] for correcting x-ray spectra. The problem of finding the optimum approximation was solved by Bracewell[3] for the correction method developed by him.[6,7] In the present work we solved the problem of the optimum n for the correction methods developed by Blokhin[8] and the writer[1].

Values of the coefficient $p_j \cdot 10^4$

x/γ	n								
	1	2	3	4	5	6	7	8	9
0,0	18440	26114	33280	39277	46566	52815	58865	65285	70414
0,5	—1269	—3060	—5142	—7011	—9799	—12277	—14823	—17406	—20026
1,0	—804	—1776	—2756	—3688	—4551	—5336	—6042	—6670	—7223
1,5	—495	—976	—1356	—1624	—1792	—1871	—1874	—1814	—1700
2,0	—321	—565	—699	—745	—742	—642	—534	—398	—228
2,5	—221	—352	—394	—376	—325	—256	—183	—118	—83
3,0	—160	—234	—243	—218	—178	—138	—102	—76	—58
3,5	—121	—165	—163	—142	—117	—96	—82	—76	—76
4,0	—94	—122	—117	—101	—87	—77	—74	—74	—78
4,5	—75	—94	—88	—77	—69	—65	—65	—67	—72
5,0	—61	—74	—69	—62	—55	—56	—57	—59	—60
5,5	—51	—60	—56	—51	—50	—48	—49	—50	—51
6,0	—43	—50	—46	—43	—41	—41	—43	—44	—44
6,5	—37	—42	—39	—36	—35	—36	—36	—37	—38
7,0	—32	—36	—33	—31	—31	—31	—32	—32	—33
7,5	—28	—31	—29	—27	—27	—28	—28	—29	—29
8,0	—24	—27	—25	—25	—25	—25	—25	—25	—26
8,5	—22	—24	—22	—22	—22	—22	—22	—23	—23
9,0	—19	—21	—20	—20	—20	—20	—20	—20	—20
9,5	—17	—19	—18	—17	—17	—18	—18	—18	—18
10,0	—16	—16	—16	—16	—16	—16	—16	—16	—16

The optimum number of approximations in correcting for dispersive distortion, as in any other similar case, depends on the shape of the spectrum and the ratio of the half-width γ of the uncorrected dispersion curve to the half-width β of the corrected spectrum, i.e., γ/β, on the root mean square chance error Δf and on the character of its distribution over the spectrum. In the present work the optimum approximation was sought for the case of a spectrum having a classical dispersion shape; this example was chosen in view of the relative simplicity of the calculations in this case.

The spectrum was corrected by the method of columns[8] which readily allows of calculating how the chance error varies in the process of correction. Inasmuch as the method of columns derives directly from the method of steps, the deduced dependences of optimum n on Δf and γ/β presumably pertains to both methods of correction. In the method of columns the ordinates of the $\varphi_n(x)$ curve are found by multiplying the heights $f(x_i)$ of the columns (into which the curve $f(x)$ is divided) by certain correction coefficients p_j that depend on the number of the approximation. The chance errors Δf are also multiplied by the same coefficients. Hence

$$\delta_2 = \sum_{ij} p_j \, \Delta f(x_i).$$

The problem was solved for the case when the relative root mean square error $\Delta f(x)/f(x)$ is constant over the spectrum (method of equal accuracy measurements). The dispersion curve, having a base width 6β, was divided into $N = 21$ columns for $\gamma/\beta = 0.6$, 31 columns for $\gamma/\beta = 0.4$ and 61 columns for $\gamma/\beta = 0.2$. Then by means of the coefficients p_j, computed beforehand for approximations 1 to 9 (see table), using the value of p_j for $n = 14$ taken from Ref.8*, we calculated the corrected shapes of $\varphi_n(x)$ for different γ/β and n, and also the values of δ_1 (by summation of $r_n(x_i)$) and of δ_2. Fig.1 shows how δ_1 and $\delta_2/\Delta f^2$ for one column vary with variation in the number of the approximation for the case $\gamma/\beta = 0.4$. Using the graphically determined $\partial\delta_1/\partial n$ and $\partial\delta_2/\partial n$, we found the values of Δf corresponding to each n. On the basis of these results we constructed the graph (Fig.2) relating

---

*In the notation of Ref.8 this n equals 15.

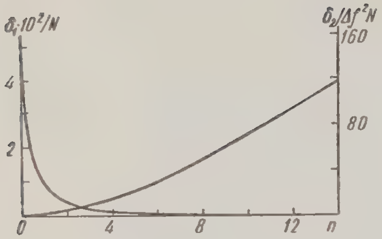

Fig.1

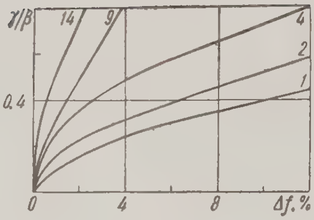

Fig.2

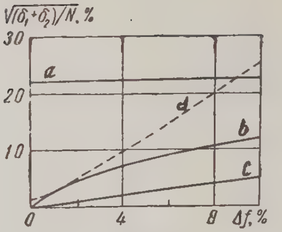

Fig.3

Fig.1. Variation of the mean systematic error δ_1/N and the chance error $\delta_2/\Delta f^2 N$ with increase in the order of the approximation.

Fig.2. Optimum approximation number n as a function of the chance experimental error Δf and the ratio γ/β of the half-widths of the distorted and corrected curves.

Fig.3. Root mean square error in the uncorrected spectrum (a), in the spectrum corrected in the optimum approximation (b) and in the ninth approximation (d) as a function of the chance experimental error Δf.

n, γ/β and Δf. By means of this graph, one can, knowing the experimental root mean square error Δf and having determined γ/β from the spectrum, find the optimum n, and then correct the spectrum using the tabulated values of p_j corresponding to the determined n. Determination of the precise optimum number of approximations by means of the graph of Fig.2 is possible for a simple emission spectrum. In the case of spectra of more complex shape the curves of Fig.2 allow of only approximate determination of the optimum n.

We calculated the averaged (over the spectrum) relative (to the maximum ordinate) mean square error in the spectrum corrected in the optimum approximation, i.e., $\sqrt{(\delta_1 + \delta_2)/N}$, where N is the number of columns. The calculations were carried out for different values of Δf and γ/β. Curve b in Fig.3 shows the variation of this error as a function of Δf for $\gamma/\beta = 0.4$. Curve a in this figure shows the total mean error of the uncorrected spectrum. Curve d characterizes the increase of the total error in the corrected spectrum with increase of Δf when the correction is made not in the optimum approximation but in the ninth approximation regardless of the magnitude of Δf. In plotting all the curves we took into account the variation in the process of correction of the peak ordinate with respect to which the total error is evaluated for each column.

It will be seen that curves b and d are tangent at the point $\Delta f = 1.5\%$ for which $n = 9$ is the optimum approximation. Inasmuch as curves a and b intersect at $\Delta f = 9\%$, it is obvious that for $\Delta f > 9\%$ and $\gamma/\beta \geqslant 0.4$ the spectrum corrected in the nineth approximation will be further from the true spectrum than the initial experimental (uncorrected) spectrum. For this region ($\gamma/\beta \approx 0.4$ and $\Delta f \approx 9\%$) one should, as is evident from Fig.2, use the first approximation. It is clear that for small chance experimental errors, the systematic error $r_n(x)$ in the spectrum corrected in the optimum approximation is very small. But with increase of Δf the optimum number n decreases and $r_n(x)$ increases. Thus the "artificial" increase of the resolution of the instrument that is attained in the process of correction is limited by the magnitude of the chance experimental error. One should strive simultaneously to obtain the maximum resolution and the greatest recording accuracy.

I wish to acknowledge my indebtedness to M.A.Blokhin for his guidance in the work.

Rostov-on-the-Don State University

1. I.Ya.Nikiforov, Izv.AN SSSR, Ser.fiz., 21, 1362 (1957). (Trans.Bulletin, 21, 1351.)

2. S.G.Rautian, Usp.fiz.nauk, 66, 475 (1958). (Trans.Soviet Physics - Uspekhi.)

3. R.N.Bracewell, Proc.I.R.E., 46, 106 (1958).

4. J.O.Porteus & L.G.Parratt, Bull.Amer.Phys.Soc., Ser.II, 3, 263 (1958).

5. L.G.Parratt, Electronic Band Structure of Solids by the Method of Experimental X-Ray Spectroscopy, Cornell, 1958.

6. R.N.Bracewell & J.A.Roberts, Austral.J.Phys., 7, 615 (1954).

7. R.N.Bracewell, Austral.J.Phys., 8, N 1, 61 (1955).

8. M.A.Blokhin, Metody rentgenospektral'nykh issledovanii (Methods of x-ray spectroscopic investigation). Fizmatgiz, M., 1959.

ON ALLOWING FOR APPARATUS DISTORTION AND THE WIDTH OF DISPERSION TYPE INNER LEVELS IN EMISSION SPECTRA

- Ya.E.Genkin & I.A.Rumyantsev

The interaction of the x-ray photons with the instrument leads to distortion of the spectrum lines. The experimental spectrum shape $F(x)$ is related to the true shape $f(x)$ by

$$F(x) = \int_{-\infty}^{\infty} f(z)\,\varphi(x-z)\,dz, \tag{1}$$

where $\varphi(x-z)$ is the distortion function.

In the case of a bent crystal spectrograph the distortions are very close to the classical dispersion (Lorentzian) shape.

The distortion function is normalized as follows:

$$\int_{-\infty}^{\infty} \varphi(x-z)\,dz = 1, \tag{2}$$

with this normalization the distortion function is written

$$\varphi(x-z) = \frac{1}{\pi\beta}\cdot\frac{1}{1+\left(\frac{x-z}{\beta}\right)^2}, \tag{3}$$

where β is the distortion parameter, and Eq.(1) assumes the following form:

$$F(x) = \frac{1}{\pi\beta}\int_{-\infty}^{\infty}\frac{f(z)\,dz}{1+\left(\frac{x-z}{\beta}\right)^2}. \tag{4}$$

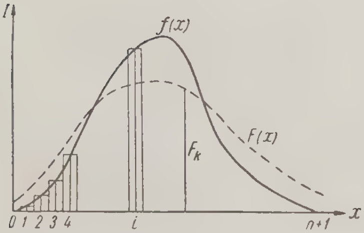

Fig.1.

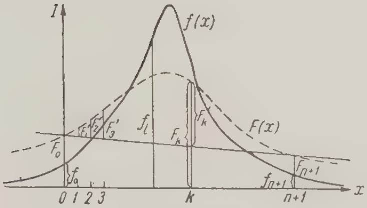

Fig.2.

There are a number of methods (for example, see Refs.1-5) of approximate solution of Eq.(4). Below we give a method based on approximation by second degree polynomials of the internal function $f(x)$ inasmuch as approximation of the sections of the external function $F(x)$ by functions that are not analytic over the entire correction interval cannot in principle yield a solution for the integral equation (4). Moreover, the proposed method takes into account the ambiguity in the position of the origin of the ordinates of the experimental curve, which was not taken into account in earlier investigations.

2. Method of columns

Let $f(x)$ be the true function characterizing the intensity distribution over the energy scale (Fig.1; the photon energies are laid off in the $\pi\beta/2 = 1$ scale along the horizontal axis).

Let there be n points with integral values of x $(1, 2, 3..., i,..., n)$ in the interval under consideration. We assume that $f(x)$ is constant and equal to $f(i)$ over the entire range from $i - {}^1\!/_2$ to $i + {}^1\!/_2$, i.e., we approximate the true function $f(x)$ by columns of unit width and height $f(i)$. We assume that $f(x) = 0$ for $x \leqslant 0$ and $x \geqslant n+1$.

Then by integration Eq.(4) is brought to the form

$$F_k = \sum_{i=1}^{n} C_{ki} f_i, \tag{5}$$

where f_i and F_k are values of the true and distorted function, respectively, at the points with integral x, and

$$C_{ki} = \frac{1}{\pi}\left(\operatorname{arc\,tg}\frac{k-i+{}^1/_2}{\beta} - \operatorname{arc\,tg}\frac{k-i-{}^1/_2}{\beta}\right).$$

Solution of the set (5) reduces to finding the inverse matrix

$$f_i = \sum_{k=1}^{n} p_{ik}F_k; \tag{6}$$

finding the inverse matrix is facilitated by the fact that the coefficients of the initial matrix rapidly decrease with increase of the difference $|k-i|$ and are also symmetric $(C_{ki} = C_{ik})$ and equivalent along any diagonal $(C_{k+1,\, i+1} = C_{ki})$.

The inverse matrix $\| p_{ik} \|$ of linear transformation (6) allows of finding the true shape of the spectrum from the experimental shape. However, it must be noted that approximation of the true curves by columns of finite width involves an appreciable error.

3. Method of parabolas

Let us expand $f(x)$ in a series in powers of $x-i$ near points with integral values of x:

$$f(x) = f(i) + (x-i)f'(i) + \frac{(x-i)^2}{2}f''(i) + \ldots . \tag{7}$$

In the case of approximation by columns we restrict ourselves to the first term of this expansion. Approximation by parabolas of the second order takes into account the first three terms of the expansion (7). We draw a parabola through every three neighboring points of the $f(x)$ curve and carry out integration between the initial limits (from $i-{}^1/_2$ to $i+{}^1/_2$). As before, we assume that $f(x)=0$ for $x \leqslant 0$ and $x \geqslant n+1$.

Then

$$F_k = \sum_{i=1}^{n} a_{ki}f_i, \tag{8}$$

where the coefficients a_{ki} are found by means of the following formulas:

$$\begin{aligned}
a_{k1} = {} & -\frac{\beta}{\pi} + \frac{\beta m}{\pi}\ln\frac{\beta^2+(m+1)^2}{\beta^2+(m-{}^1/_2)^2} - \frac{(m+1)(m-1)-\beta^2}{\pi} \times \\
& \times\left(\operatorname{arc\,tg}\frac{m+1}{\beta} - \operatorname{arc\,tg}\frac{m-{}^1/_2}{\beta}\right) - \frac{\beta(m-{}^3/_2)}{2\pi}\ln\frac{\beta^2+(m-{}^1/_2)^2}{\beta^2+(m-{}^3/_2)^2} + \\
& + \frac{(m-1)(m-2)-\beta^2}{2\pi}\left(\operatorname{arc\,tg}\frac{m-{}^1/_2}{\beta} - \operatorname{arc\,tg}\frac{m-{}^3/_2}{\beta}\right) \quad (m=k-1); \\
a_{k2} = {} & \frac{\beta}{4\pi} - \frac{\beta(m+{}^3/_2)}{2\pi}\ln\frac{\beta^2+(m+2)^2}{\beta^2+(m+{}^1/_2)^2} + \frac{(m+2)(m+1)-\beta^2}{2\pi} \times \\
& \times\left(\operatorname{arc\,tg}\frac{m+2}{\beta} - \operatorname{arc\,tg}\frac{m+{}^1/_2}{\beta}\right) + \frac{\beta m}{\pi}\ln\frac{\beta^2+(m+{}^1/_2)^2}{\beta^2+(m-{}^1/_2)^2} - \frac{(m+1)(m-1)-\beta^2}{\pi} \times \\
& \times\left(\operatorname{arc\,tg}\frac{m+{}^1/_2}{\beta} - \operatorname{arc\,tg}\frac{m-{}^1/_2}{\beta}\right) - \frac{\beta(m-{}^3/_2)}{2\pi}\ln\frac{\beta^2+(m-{}^1/_2)^2}{\beta^2+(m-{}^3/_2)^2} + \\
& + \frac{(m-1)(m-2)-\beta^2}{2\pi}\left(\operatorname{arc\,tg}\frac{m-{}^1/_2}{\beta} - \operatorname{arc\,tg}\frac{m-{}^3/_2}{\beta}\right) \quad (m=k-2); \\
a_{ki} = {} & -\frac{\beta(m+{}^3/_2)}{2\pi}\ln\frac{\beta^2+(m+{}^3/_2)^2}{\beta^2+(m+{}^1/_2)^2} + \frac{(m+2)(m+1)-\beta^2}{2\pi} \times \\
& \times\left(\operatorname{arc\,tg}\frac{m+{}^3/_2}{\beta} - \operatorname{arc\,tg}\frac{m+{}^1/_2}{\beta}\right) + \frac{\beta m}{\pi}\ln\frac{\beta^2+(m+{}^1/_2)^2}{\beta^2+(m-{}^1/_2)^2} - \frac{(m+1)(m-1)-\beta^2}{\pi} \times
\end{aligned} \tag{9}$$

	1	2	3	4	5	6	7	8	9	10	11
1	0,66310	0,06580	0,01729	0,01239	0,00793	0,00552	0,00405	0,00312	0,00246	0,00200	0,00165
2	0,56650	0,23180	0,02700	0,02140	0,01239	0,00793	0,00552	0,00405	0,00312	0,00246	0,00200
3	0,20990	0,45950	0,15540	0,04366	0,02140	0,01239	0,00793	0,00552	0,00405	0,00312	0,00246
4	0,07660	0,17460	0,42350	0,16520	0,04366	0,02140	0,01239	0,00793	0,00552	0,00405	0,00312
5	0,04450	0,04770	0,16410	0,42610	0,16520	0,04366	0,02140	0,01239	0,00793	0,00552	0,00405
6	0,02980	0,02300	0,04350	0,16520	0,42610	0,16520	0,04366	0,02140	0,01239	0,00793	0,00552
7	0,02190	0,01310	0,02130	0,04366	0,16520	0,42610	0,16520	0,04366	0,02140	0,01239	0,00793
8	0,01660	0,00859	0,01213	0,02140	0,04366	0,16520	0,42610	0,16520	0,04366	0,02140	0,01239
9	0,01370	0,00606	0,00770	0,01239	0,02140	0,04366	0,16520	0,42610	0,16520	0,04366	0,02140
10	0,01130	0,00485	0,00540	0,00793	0,01239	0,02140	0,04366	0,16520	0,42610	0,16520	0,04366
11	0,00950	0,00348	0,00400	0,00552	0,00793	0,01239	0,02140	0,04366	0,16520	0,42610	0,16520
12	0,00800	0,00290	0,00303	0,00405	0,00552	0,00793	0,01239	0,02140	0,04366	0,16520	0,42610
13	0,00690	0,00236	0,00240	0,00312	0,00405	0,00552	0,00793	0,01239	0,02140	0,04366	0,16520
14	0,00610	0,00195	0,00196	0,00246	0,00312	0,00405	0,00552	0,00793	0,01239	0,02140	0,04366
15	0,00550	0,00163	0,00160	0,00200	0,00246	0,00312	0,00405	0,00552	0,00793	0,01239	0,02140
16	0,00480	0,00140	0,00135	0,00165	0,00200	0,00246	0,00312	0,00405	0,00552	0,00793	0,01239
17	0,00440	0,00124	0,00115	0,00139	0,00165	0,00200	0,00246	0,00312	0,00405	0,00552	0,00793
18	0,00380	0,00105	0,00099	0,00118	0,00139	0,00165	0,00200	0,00246	0,00312	0,00405	0,00552
19	0,00340	0,00092	0,00086	0,00102	0,00118	0,00139	0,00165	0,00200	0,00246	0,00312	0,00405
20	0,00300	0,00082	0,00076	0,00089	0,00102	0,00118	0,00139	0,00165	0,00200	0,00246	0,00312
21	0,00270	0,00073	0,00067	0,00078	0,00089	0,00102	0,00118	0,00139	0,00165	0,00200	0,00246
22	0,00250	0,00065	0,00060	0,00069	0,00078	0,00089	0,00102	0,00118	0,00139	0,00165	0,00200
23	0,00230	0,00059	0,00054	0,00062	0,00069	0,00078	0,00089	0,00102	0,00118	0,00139	0,00165
24	0,00210	0,00054	0,00049	0,00056	0,00062	0,00069	0,00078	0,00089	0,00102	0,00118	0,00139
	1	2	3	4	5	6	7	8	9	10	11

$$\times\left(\operatorname{arc\,tg}\frac{m+{}^1/_2}{\beta}-\operatorname{arc\,tg}\frac{m-{}^1/_2}{\beta}\right)-\frac{\beta\,(m-{}^3/_2)}{2\pi}\ln\frac{\beta^2+(m-{}^1/_2)^2}{\beta^2+(m-{}^3/_2)^2}+$$
$$+\frac{(m-1)\,(m-2)-\beta^2}{2\pi}\left(\operatorname{arc\,tg}\frac{m-{}^1/_2}{\beta}-\operatorname{arc\,tg}\frac{m-{}^3/_2}{\beta}\right)\quad(m=k-i;\ i>2). \tag{9}$$

The matrix $\|a_{ki}\|$ of linear transformation (8) is given in Table 1 (internal part of the table) for $n = 20$.

Solution of the set of equations (8) reduces to finding the inverse matrix

$$f_i=\sum_{k=1}^{n} b_{ik}F_k. \tag{10}$$

In determining the inverse matrix $\|b_{ik}\|$ of linear transformation (10), the inverse matrix $\|p_{ik}\|$ found earlier was taken as the approximate inverse matrix which was then corrected by the usual procedure (see, for example, Ref.6).

Matrix $\|b_{ik}\|$ is given in Table 2. With an experimental error ε in determining F_k the maximum error in determining f_i amounts to from 4ε (at the edges of the correction interval) to 6ε (inside the interval). It is assumed that the level (origin) from which the ordinates F_k are measured is known.

4. Refinement of the method

Let us now assume that the true intensity distribution function $f(x)$ does not vanish at the edges of the interval under consideration but assumes the values f_0 and f_{n+1} (Fig.2). Assume further that outside this interval $f(x)$ monotonically

Table 1

12	13	14	15	16	17	18	19	20	21	22	
0,00139	0,00118	0,00102	0,00089	0,00078	0,00069	0,00062	0,00056	0,00049	0,00054	0,00210	1
0,00165	0,00139	0,00118	0,00102	0,00089	0,00078	0,00069	0,00062	0,00054	0,00059	0,00230	2
0,00200	0,00165	0,00139	0,00118	0,00102	0,00089	0,00078	0,00069	0,00060	0,00065	0,00250	3
0,00246	0,00200	0,00165	0,00139	0,00118	0,00102	0,00089	0,00078	0,00067	0,00073	0,00270	4
0,00312	0,00246	0,00200	0,00165	0,00139	0,00118	0,00102	0,00089	0,00076	0,00082	0,00300	5
0,00405	0,00312	0,00246	0,00200	0,00165	0,00139	0,00118	0,00102	0,00086	0,00092	0,00340	6
0,00552	0,00405	0,00312	0,00246	0,00200	0,00165	0,00139	0,00118	0,00099	0,00105	0,00380	7
0,00793	0,00552	0,00405	0,00312	0,00246	0,00200	0,00165	0,00139	0,00115	0,00121	0,00440	8
0,01239	0,00793	0,00552	0,00405	0,00312	0,00246	0,00200	0,00165	0,00135	0,00140	0,00480	9
0,02140	0,01239	0,00793	0,00552	0,00405	0,00312	0,00246	0,00200	0,00160	0,00163	0,00550	10
0,04366	0,02140	0,01239	0,00793	0,00552	0,00405	0,00312	0,00246	0,00196	0,00195	0,00610	11
0,16520	0,04366	0,02140	0,01239	0,00793	0,00552	0,00405	0,00312	0,00240	0,00236	0,00690	12
0,42610	0,16520	0,04366	0,02140	0,01239	0,00793	0,00552	0,00405	0,00303	0,00290	0,00800	13
0,16520	0,42610	0,16520	0,04366	0,02140	0,01239	0,00703	0,00552	0,00400	0,00348	0,00950	14
0,04366	0,16520	0,42610	0,16520	0,04366	0,02140	0,01239	0,00793	0,00540	0,00485	0,01130	15
0,02140	0,04366	0,16520	0,42610	0,16520	0,04366	0,02140	0,01239	0,00770	0,00606	0,01370	16
0,01239	0,02140	0,04366	0,16520	0,42610	0,16520	0,04366	0,02140	0,01213	0,00859	0,01660	17
0,00793	0,01239	0,02140	0,04366	0,16520	0,42610	0,16520	0,04366	0,02130	0,01310	0,02190	18
0,00552	0,00793	0,01239	0,02140	0,04366	0,16520	0,42610	0,16520	0,04350	0,02300	0,02980	19
0,00405	0,00552	0,00793	0,01239	0,02140	0,04366	0,16520	0,42610	0,16410	0,04770	0,04450	20
0,00312	0,00405	0,00552	0,00793	0,01239	0,02140	0,04366	0,16520	0,42350	0,17460	0,07660	21
0,00246	0,00312	0,00405	0,00552	0,00793	0,01239	0,02140	0,04366	0,15540	0,45950	0,20990	22
0,00200	0,00246	0,00312	0,00405	0,00552	0,00793	0,01239	0,02140	0,02700	0,23180	0,56650	23
0,00165	0,00200	0,00246	0,00312	0,00405	0,00552	0,00793	0,01239	0,01729	0,06580	0,66310	24
12	13	14	15	16	17	18	19	20	21	22	

decreases. We approximate $f(x)$ outside the interval by hyperbolas, i.e., $y = \left(\frac{x_m - x_0}{x - x_m}\right)^2 f_0$ (for $x \leqslant 0$) and $y = \left(\frac{x_{m_1} - x_{n+1}}{x - x_{m_1}}\right) f_{n+1}$ (for $x \geqslant n+1$). We set $x_m = 10$, $x_{m_1} = 11$, $x_0 = 0$, and $x_{n+1} = n+1$. Then, integrating Eq.(4), we obtain

$$F_k = \sum_{i=0}^{n+1} a_{ki} f_i. \tag{11}$$

The matrix $\|a_{ki}\|$ of linear transformation (11) is given in Table 1 (for $n = 20$); the coefficients a_{k0} and $a_{k,\,n+1}$ are given, respectively, in columns 1 and 22, while rows 1, 2, 23 and 24 allow of calculating F_{-1}, F_0, F_{n+1} and F_{n+2}, respectively.

In this case we draw a straight line through points F_0 and F_{n+1} and reckon the ordinates from this level, i.e., transfer the ordinate origin to this line. Then the new ordinates of F'_k can be written

$$F'_k = F_k - \frac{F_0\,(n+1-k) + F_{n+1} \cdot k}{n+1}. \tag{12}$$

It is possible to introduce this transfer of the ordinate origin directly into the matrix $\|a_{ki}\|$ of transformation (11):

$$a'_{ki} = a_{ki} - \frac{a_{0i}\,(n+1-k) + a_{n+1,\,i} \cdot k}{n+1}. \tag{13}$$

Table 2

	1	2	3	4	5	6	7	8	9	10	11	12	13	14	15	16	17	18	19	20	
1	2,538	—0,982	0,154	—0,084	—0,001	—0,014	—0,006	—0,006	—0,004	—0,003	—0,003	—0,002	—0,002	—0,002	—0,001	—0,001	—0,001	—0,001	—0,001	—0,001	1
2	—1,106	3,219	—1,216	0,235	—0,097	0,007	—0,013	—0,004	—0,004	—0,003	—0,002	—0,002	—0,002	—0,001	—0,001	—0,001	—0,001	—0,001	—0,001	—0,001	2
3	0,178	—1,209	3,255	—1,228	0,237	—0,098	0,007	—0,013	—0,005	—0,004	—0,003	—0,002	—0,002	—0,002	—0,002	—0,001	—0,001	—0,001	—0,001	—0,001	3
4	—0,092	0,231	—1,228	3,261	—1,229	0,237	—0,098	0,007	—0,013	—0,004	—0,004	—0,003	—0,002	—0,002	—0,002	—0,002	—0,001	—0,001	—0,001	—0,001	4
5	0,002	—0,098	0,237	—1,229	3,262	—1,229	0,237	—0,098	0,007	—0,013	—0,004	—0,004	—0,003	—0,002	—0,002	—0,002	—0,001	—0,001	—0,001	—0,002	5
6	—0,016	0,009	—0,099	0,238	—1,229	3,262	—1,229	0,237	—0,098	0,007	—0,013	—0,004	—0,004	—0,003	—0,002	—0,002	—0,002	—0,002	—0,001	—0,002	6
7	—0,006	—0,012	0,007	—0,098	0,237	—1,229	3,262	—1,229	0,237	—0,098	0,007	—0,013	—0,004	—0,004	—0,003	—0,002	—0,002	—0,002	—0,001	—0,002	7
8	—0,009	—0,003	—0,013	0,007	—0,098	0,237	—1,229	3,262	—1,229	0,237	—0,098	0,007	—0,013	—0,004	—0,004	—0,003	—0,002	—0,002	—0,001	—0,002	8
9	—0,003	—0,005	—0,004	—0,013	0,007	—0,098	0,237	—1,229	3,262	—1,229	0,237	—0,098	0,007	—0,013	—0,004	—0,004	—0,003	—0,003	—0,002	—0,003	9
10	—0,005	—0,002	—0,004	—0,004	—0,013	0,007	—0.098	0,237	—1,229	3,262	—1,229	0,237	—0,098	0,007	—0,013	—0,004	—0,004	—0,003	—0,002	—0,003	10
11	—0,003	—0,002	—0,003	—0,004	—0,004	—0,013	0,007	—0,098	0,237	—1,229	—3,262	—1,229	0,237	—0,098	0,007	—0,013	—0,004	—0,004	—0,002	—0,005	11
12	—0,003	—0,002	—0,003	—0,003	—0,004	—0,004	—0,013	0,007	—0,098	0,237	—1,229	3,262	—1,229	0,237	—0,098	0,007	—0,013	—0,004	—0,005	—0,003	12
13	—0,002	—0,001	—0,002	—0,002	—0,003	—0,004	—0,004	—0,013	0,007	—0,098	0,237	—1,229	—3,262	—1,229	0,237	—0,098	0,007	—0,013	—0,003	—0,009	13
14	—0,002	—0,001	—0,002	—0,002	—0,002	—0,003	—0,004	—0,004	—0,013	0,007	—0,098	0,237	—1,229	3,262	—1,229	0,237	—0,098	0,007	—0,012	—0,006	14
15	—0,002	—0,001	—0,002	—0,002	—0,002	—0,002	—0,003	—0,004	—0,004	—0,013	0,007	—0,098	0,237	—1,229	3,262	—1,229	0,238	—0,099	0,009	—0,016	15
16	—0,002	—0,001	—0,001	—0,001	—0,002	—0,002	—0,002	—0,003	—0,004	—0,004	—0,013	0,007	—0,098	0,237	—1,229	3,262	—1,229	0,237	—0,098	0,002	16
17	—0,001	—0,001	—0,001	—0,001	—0,002	—0,002	—0,002	—0,002	—0,003	—0,004	—0,004	—0,013	0,007	—0,098	0,237	—1,229	3,261	—1,228	0,231	—0,092	17
18	—0,001	—0,001	—0,001	—0,001	—0,001	—0,002	—0,002	—0,002	—0,002	—0,003	—0,004	—0,005	—0,013	0,007	—0,098	0,237	—1,228	3,255	—1,209	0,178	18
19	—0,001	—0,001	—0,001	—0,001	—0,001	—0,001	—0,001	—0,002	—0,002	—0,002	—0,003	—0,004	—0,004	—0,013	0,007	—0,097	0,235	—1,216	—3,219	—1,106	19
20	—0,001	—0,001	—0,001	—0,001	—0,001	—0,001	—0,002	—0,002	—0,002	—0,003	—0,003	—0,004	—0,006	—0,006	—0,014	—0,001	—0,084	0,154	0,982	2,538	20
	1	2	3	4	5	6	7	8	9	10	11	12	13	14	15	16	17	18	19	20	

Applying transformation (13) to the elements of the matrix $\| a_{ki} \|$, we obtain the matrix $\| a'_{ki} \|$, to which the ordinate origin has been transposed:

$$F'_k = \sum_{i=0}^{n+1} a'_{ki} f_i. \tag{14}$$

The matrix $\| a'_{ki} \|$ of linear transformation (14) is given in Table 3. Rows 1 and 22 allow of calculating F'_{-1} and F'_{22}, respectively. As will be evident from (12), $F'_0 = F'_{21} = 0$. Solution of the set of equations (14) reduces to finding the inverse matrix

$$f_i = \sum_{k=-1}^{22} b'_{ik} F'_k, \tag{15}$$

the index k takes on the following values: -1, 1, 2, ...19, 20, 22.

$$f(x) = \frac{100}{1 - \left(\frac{x-7}{1.5}\right)^2} + \frac{80}{1 + \left(\frac{x-11}{3}\right)^2}$$

$$F(x) = \frac{1.5}{0.64 + 1.5} \cdot \frac{100}{1 + \left(\frac{x-7}{0.64+1.5}\right)^2} + $$

$$+ \frac{3}{0.64 + 3} \cdot \frac{80}{1 + \left(\frac{x-11}{0.64+3}\right)^2}$$

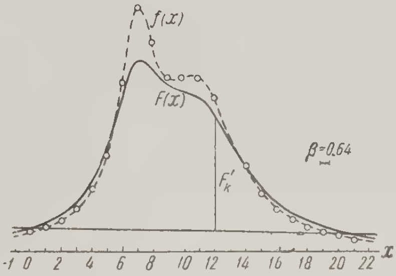

Fig.3.

The inverse matrix $\| b'_{ik} \|$, calculation of which involves certain difficulties, is given in Table 4. For calculating f_0 one inserts the values of F'_k in the first row of matrix $\| b'_{ik} \|$; for calculating f_1 the same values are inserted in the second row, etc.

For an experimental error ε in determining F'_k, the maximum error in determining f_i amounts to from 26 ε (at the edges of the interval) to 20ε (inside the correction interval).

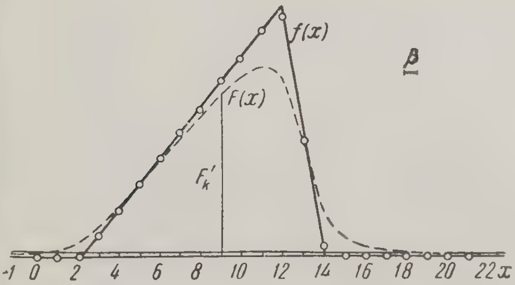

Fig.4.

Figs.3 and 4 show examples of correcting curves by means of the matrix $\| b'_{ik} \|$ of the linear transformation (15). In the case of superposition of the dispersion curves (Fig.3), the points obtained by means of the matrix $\| b'_{ik} \|$ lie close to the true curve (the error does not exceed 1%). In the case of an abrupt drop of the emission curve, the corrected values of the ordinates (Fig. 4) differ from the true values by not more than 5% at the points close to the steep side of the peak and by not more than 1% in the rest of the corrected section of the curve.

In the case of wide bands (width at half-height of the corrected section of the curve greater than one third the entire corrected section), one must use the matrix $\| b'_{ik} \|$. For narrow bands use of the matrix $\| a'_{ik} \|$ is not expedient owing to the great experimental uncertainty. In this case one should use the matrix $\| b_{ik} \|$.

I desire to acknowledge my indebtedness to M. I. Korsunskii for his interest in the work and valuable advice.

"V. I. Lenin" Kharkov Polytechnic Institute

	1	2	3	4	5	6	7	8	9	10	11
1	0,06973	—0,17701	—0,01106	—0,01000	—0,00502	—0,00275	—0,00169	—0,00107	—0,00075	—0,00051	—0,00037
2	—0,032973	0,23871	0,12966	0,02325	0,00957	0,00480	0,00263	0,00161	0,00102	0,00071	0,00048
3	—0,43617	—0,03518	0,39902	0,14578	0,03238	0,01415	0,00731	0,00417	0,00258	0,00169	0,00115
4	—0,44140	—0,15107	0,14088	0,40767	0,15448	0,03675	0,01654	0,00877	0,00509	0,00321	0.00210
5	—0,42923	—0,16476	0,02154	0,14776	0,41594	0,15863	0,03902	0,01793	0,00964	0,00567	0,00359
6	—0,41027	—0,16365	0,00060	0,02721	0,15560	0,41987	0,16078	0,04033	0,01874	0,01018	0,00601
7	—0,38870	—0,15715	—0,00731	0,00594	0,03461	0,15931	0,42190	0,16202	0,04110	0,01925	0,01049
8	—0,36473	—0,14867	—0,01048	—0,00208	0,01291	0,03811	0,16122	0,42306	0,16273	0,04156	0,01952
9	—0,34027	—0,13887	—0,01152	—0,00555	0,00446	0,01619	0,03990	0,16230	0,42372	0,16315	0,04179
10	—0,31520	—0,12923	—0,01166	—0,00697	0,00055	0,00752	0,01786	0,04091	0,16291	0,42410	0,16335
11	—0,28983	—0,11880	—0,01137	—0,00745	—0,00130	0,00340	0,00907	0,01879	0,04146	0,16325	0,42427
12	—0,26407	—0,10833	—0,01074	—0,00740	—0,00221	0,00134	0,00484	0,00993	0,01930	0,04176	0,16338
13	—0,23800	—0,09773	—0,00994	—0,00707	—0,00258	0,00021	0,00265	0,00561	0,01038	0,01955	0,04186
14	—0,21173	—0,08703	—0,00902	—0,00654	—0,00269	—0,00038	0,00140	0,00335	0,00601	0,01059	0,01962
15	—0,18557	—0,07626	—0,00801	—0,00590	—0,00259	—0,00070	0,00069	0,00202	0,00369	0,00618	0,01062
16	—0,15910	—0,06544	—0,00695	—0,00517	—0,00238	—0,00082	0,00025	0,00123	0,00232	0,00382	0,00618
17	—0,13283	—0,05459	—0,00585	—0,00439	—0,00209	—0,00083	0,00001	0,00072	0,00148	0,00241	0,00379
18	—0,10637	—0,04371	—0,00472	—0,00356	—0,00174	—0,00075	—0,00012	0,00040	0,00091	0,00153	0,00233
19	—0,07990	—0,03280	—0,00356	—0,00270	—0,00134	—0,00062	—0,00016	0,00020	0,00054	0,00092	0,00142
20	—0,05333	—0,02188	—0,00239	—0,00182	—0,00091	—0,00044	—0,00015	0,00008	0,00029	0,00051	0,00078
21	— 0,02667	—0,01095	—0,00120	—0,00092	—0,00047	—0,00023	—0,00009	0,00002	0,00012	0,00021	0,00033
22	0,02667	+0,01096	0,00121	0,00093	0,00049	0,00025	0,00011	0,00001	—0,00007	—0,00016	—0,00024
	1	2	3	4	5	6	7	8	9	10	11

	1	2	3	4	5	6	7	8	9	10	11
1	—10,43413	—7,71665	2,46775	—0,75176	0,16405	—0,05552	0,00275	—0,00512	—0,00386	—0,00222	—0,00096
2	— 8,77015	—2,36106	0,63372	—0,31114	0,03021	—0,02955	—0,00689	—0,00561	—0,00464	—0,00340	—0,00173
3	— 8,52414	—6,45704	4,95961	—1,72721	0,35255	—0,13098	0,01184	—0,01276	—0,00608	—0,00347	—0,00324
4	— 8,07960	—4,78737	0,40944	2,78065	—1,11764	0,20562	—0,09332	0,00675	—0,01339	—0,00516	—0,00324
5	— 7,73964	—4,89463	1,79475	—1,68446	—3,36486	—1,25812	0,24113	—0,09815	0,00595	—0,01250	—0,00474
6	— 7,37642	—4,57023	1,39142	—0,19992	—1,12790	3,23208	—1,22431	0,23666	—0,09890	0,00692	—0,01196
7	— 7,04978	—4,39536	1,43532	—0,51675	0,33349	—1,25578	3,26441	—1,22849	0,23582	—0,09802	0,00788
8	— 6,70438	—4,17192	1,34481	—0,39045	—0,00728	0,21140	—1,22488	3,26027	—1,22937	0,23675	—0,09801
9	— 6,36907	—3,96789	1,28700	—0,39133	0,09408	—0,12252	0,24033	—1,22841	3,25942	—1,22845	0,23728
10	— 6,04375	—3,76566	1,22168	—0,36502	0,06978	—0,01557	—0,09475	0,23726	—1,22942	3,26014	—1,22898
11	— 5,71811	—3,56658	1,15627	—0,34123	0,07078	—0,03345	0,01015	—0,09776	0,23567	—1,22853	3,25991
12	—5,39606	—3,36555	1,09203	—0,32282	0,06805	—0,02515	—0,00915	0,00710	—0,09921	0,23646	—1,22843
13	—5,06977	—3,16701	1,02970	—0,30375	0,06434	—0,02258	—0,00240	—0,01203	0,00661	—0,09821	0,23704
14	—4,75912	—2,96800	0,96535	—0,28518	0,06102	—0,02165	—0,00108	—0,00514	—0,01316	0,00696	—0,09854
15	—4,44278	—2,77309	0,90096	—0,26409	0,05555	—0,01851	—0,00160	—0,00326	—0,00609	—0,01259	0,00694
16	—4,11622	—2,57025	0,83585	—0,24552	0,05206	—0,01733	0,00010	—0,00353	—0,00449	—0,00547	—0,01248
17	—3,80512	—2,37885	0,77341	—0,22616	0,04704	—0,01528	—0,00063	—0,00172	—0,00493	—0,00369	—0,00585
18	—3,47411	—2,17180	0,70447	—0,20454	0,04197	—0,01366	—0,00030	—0,00179	—0,00294	—0,00439	—0,00366
19	—3,16136	—1,98078	0,65370	—0,18644	0,03764	—0,01201	—0,00034	—0,00088	—0,00336	—0,00259	—0,00423
20	—2,84349	—1,78042	0,57879	—0,16838	0,03374	—0,01105	—0,00005	—0,00118	—0,00253	—0,00256	—0,00264
21	—2,51325	—1,57476	0,51299	—0,14961	0,03027	—0,00954	—0,00046	—0,00058	—0,00503	—0,00181	—0,00228
22	—2,22118	—1,39957	0,45686	—0,13233	0,02427	—0,00764	—0,00075	—0,00024	—0,00244	—0,00185	—0,00266
	1	2	3	4	5	6	7	8	9	10	11

Table 3

12	13	14	15	16	17	18	19	20	21	22	
—0,00024	—0,00016	—0,00007	0,00001	0,00011	0,00025	0,00049	0,00093	0,00121	0,01096	0,02667	1
0,00033	0,00021	0,00012	0,00002	—0,00009	—0,00023	—0,00047	—0,00092	—0,00120	—0,01095	—0,02667	2
0,00078	0,00051	0,00029	0,00008	—0,00015	—0,00044	—0,00091	—0,00182	—0,00239	—0,02188	—0,05333	3
0,00142	0,00092	0,00054	0,00020	—0,00016	—0,00062	—0,00134	—0,00270	—0,00356	—0,03280	—0,07990	4
0,00233	0,00153	0,00091	0,00040	—0,00012	—0,00075	—0,00174	—0,00356	—0,00472	—0,04371	—0,10637	5
0,00379	0,00241	0,00148	0,00072	0,00001	—0,00083	—0,00209	—0,00439	—0,00585	—0,05459	—0,13283	6
0,00618	0,00382	0,00232	0,00123	0,00025	—0,00082	—0,00238	—0,00517	—0,00695	—0,06544	—0,15910	7
0,01062	0,00618	0,00369	0,00202	0,00069	—0,00070	—0,00259	—0,00590	—0,00801	—0,07626	—0,18557	8
0,01962	0,01059	0,00601	0,00335	0,00140	—0,00038	—0,00269	—0,00654	—0,00902	—0,08703	—0,21173	9
0,04186	0,01955	0,01038	0,00561	0,00265	0,00021	—0,00258	—0,00707	—0,00994	—0,09773	—0,23800	10
0,16338	0,04176	0,01930	0,00993	0,00484	0,00134	—0,00221	—0,00740	—0,01074	—0,10833	—0,26407	11
0,42427	0,16325	0,04146	0,01879	0,00907	0,00340	—0,00130	—0,00745	—0,01137	—0,11880	—0,28983	12
0,16335	0,42410	0,16291	0,04091	0,01786	0,00752	0,00055	—0,00697	—0,01166	—0,12923	—0,31520	13
0,04179	0,16315	0,42372	0,16230	0,03990	0,01619	0,00446	—0,00555	—0,01152	—0,13887	—0,34027	14
0,01952	0,04156	0,16273	0,42306	0,16122	0,03811	0,01291	—0,00208	—0,01048	—0,14867	—0,36473	15
0,01049	0,01925	0,04110	0,16202	0,42190	0,15931	0,03461	0,00594	—0,00731	—0,15715	—0,38870	16
0,00601	0,01018	0,01874	0,04033	0,16078	0,41987	0,15560	0,02721	0,00060	—0,16365	—0,41027	17
0,00359	0,00567	0,00964	0,01793	0,03902	0,15863	0,41594	0,14776	0,02154	—0,16476	—0,42923	18
0,00210	0,00321	0,00509	0,00877	0,01654	0,03675	0,15448	0,40767	0,14088	—0,15107	—0,44140	19
0,00115	0,00169	0,00258	0,00417	0,00731	0,01415	0,03238	0,14578	0,39902	—0,03518	—0,43617	20
0,00048	0,00071	0,00102	0,00161	0,00263	0,00480	0,00957	0,02325	0,12966	0,23871	—0,32973	21
—0,00037	—0,00051	—0,00075	—0,00107	—0,00169	—0,00275	—0,00502	—0,01000	—0,01106	—0,17701	0,06973	22
12	13	14	15	16	17	18	19	20	21	22	

Table 4

12	13	14	15	16	17	18	19	20	21	22	
—0,00266	—0,00185	—0,00244	—0,00024	—0,00075	—0,00764	0,02427	—0,13233	0,45686	—1,39957	—2,22118	1
—0,00228	—0,00181	—0,00503	—0,00058	—0,00046	—0,00954	0,03027	—0,14961	0,51299	—1,57476	—2,51325	2
—0,00264	—0,00256	—0,00253	—0,00118	—0,00005	—0,01105	0,03374	—0,16838	0,57879	—1,78042	—2,84349	3
—0,00423	—0,00259	—0,00336	—0,00088	—0,00034	—0,01201	0,03764	—0,18644	0,65370	—1,98078	—3,16136	4
—0,00366	—0,00439	—0,00294	—0,00179	—0,00030	—0,01366	0,04197	—0,20454	0,70447	—2,17180	—3,47411	5
—0,00585	—0,00369	—0,00493	—0,00172	—0,00063	—0,01528	0,04704	—0,22616	0,77341	—2,37885	—3,80512	6
—0,01248	—0,00547	—0,00449	—0,00353	0,00010	—0,01733	0,05206	—0,24552	0,83585	—2,57025	—4,11622	7
0,00694	—0,01259	—0,00609	—0,00326	—0,00160	—0,01851	0,05555	—0,26409	0,90096	—2,77309	—4,44278	8
—0,09854	0,00696	—0,01316	—0,00514	—0,00108	—0,02165	0,06102	—0,28518	0,96535	—2,96800	—4,75912	9
0,23704	—0,09821	0,00661	—0,01203	—0,00240	—0,02258	0,06434	—0,30375	1,02970	—3,16701	—5,06977	10
—1,22843	0,23646	—0,09921	0,00710	—0,00915	—0,02515	0,06805	—0,32282	1,09203	—3,36555	—5,39606	11
3,25991	—1,22853	0,23567	—0,09776	0,01015	—0,03345	0,07078	—0,34123	1,15627	—3,56658	—5,71811	12
—1,22898	3,26014	—1,22942	0,23726	—0,09475	—0,01557	0,06978	—0,36502	1,22168	—3,76566	—6,04375	13
0,23728	—1,22845	3,25942	—1,22841	0,24033	—0,12252	0,09408	—0,39133	1,28700	—3,96789	—6,36907	14
—0,09801	0,23675	—1,22937	3,26027	—1,22488	0,21140	—0,00728	—0,39045	1,34481	—4,17192	—6,70438	15
0,00788	—0,09802	0,23582	—1,22849	3,26441	—1,25578	0,33349	—0,51675	1,43532	—4,39536	—7,04978	16
—0,01196	0,00692	—0,09890	0,23666	—1,22431	3,23208	—1,12790	—0,19992	1,39142	—4,57023	—7,37642	17
—0,00474	—0,01250	0,00595	—0,09815	0,24113	—1,25812	3,36486	—1,68446	1,79475	—4,89463	—7,73964	18
—0,00324	—0,00516	—0,01339	0,00675	—0,09332	0,20562	—1,11764	2,78065	0,40944	—4,78737	—8,07960	19
—0,00324	—0,00347	—0,00608	—0,01276	0,01184	—0,13098	0,35255	—1,72721	4,95961	—6,45704	—8,52414	20
—0,00173	—0,00340	—0,00464	—0,00561	—0,00689	—0,02955	0,03021	—0,31114	0,63372	—2,36106	—8,77015	21
—0,00096	—0,00222	—0,00386	—0,00512	0,00275	—0,05552	0,16405	—0,75176	2,46775	—7,71665	—10,43413	22
12	13	14	15	16	17	18	19	20	21	22	

References

1. M.A.Blokhin, Doklady AN SSSR, 107, 33 (1956). (Trans.Doklady.)
2. M.A.Blokhin, Ibid., 107, 229 (1956).
3. M.A.Blokhin, Izv.AN SSSR, Ser.fiz., 20, 142 (1956). (Trans.Bulletin 20, 127.)
4. I.Ya.Nikiforov, Izv.AN SSSR, Ser.fiz., 21, 1362 (1957). (Trans.Bulletin 21, 1351.)
5. M.A.Blokhin, Metody rentreno-spektral'nykh issledovanii (Methods of x-ray spectroscopic investigation, Fizmatgiz, M., 1959.
6. I.M.Gel'fand, Lektsii po lineinoi algebre (Lectures on linear algebra), p.231, Second edition, M., 1951.

* * * * * * *

ON SPECIFYING THE ENERGY OF X-RAY PHOTONS AND THE ENERGY OF ELECTRON LEVELS

- N.D.Borisov & V.V.Nemoshkalenko

I

More accurate determination of the lattice constant of calcite led in 1947 to the decision[1] to introduce a new unit, the Seigbahn or X unit and its 10^3 multiple kX, retaining for the angstrom its metrical definition 1 Å = 10^{-8} cm.

According to the data of 1947,

$$1 \text{ kX} = 1.00203 \text{ Å}. \tag{1}$$

Adoption of this definition made it possible to retain all the earlier numerical values for the wavelength of the x-ray spectrum. On the other hand, in calculations involving wavelengths in CGS units, the requisite conversion was to be effected by means of the formula

$$\lambda(\text{cm}) = 1.00203 \cdot 10^{-11} \lambda(\text{XU}), \tag{2}$$

rather than by the formula $\lambda(\text{cm}) = 10^{11} \lambda(\text{XU})$ employed prior to 1947. It must be noted, however, that in the tables of Refs.2-16, which were published after 1947, the energy values for x-ray photons and electron levels are listed without taking the new relation (1) into account.

This makes it impossible to use the tabular data directly, i.e., without conversion, for obtaining the energy characteristics of x-ray photons and electron levels in atoms.

In the accompanying table we show an example of the discrepancy between the tabular data of Refs.3-6 and the energy values calculated by means of the formula

$$E = \frac{1}{\lambda R} \tag{3}$$

where R is the Rydberg constant in cm^{-1}, λ is the wavelength in cm and E is the energy corresponding to the $K\alpha_1$ lines of a number of elements in Rydbergs.

It will be evident from the table that the error in determining the photon energy owing to failure to take (1) into account increases in magnitude with increase of the photon energy.

K_{α_1}-line	λ, XU	E, R		ΔE, R
		Tabular	Calculated	
$_{13}$Al	8321,37	109,51	109,29	0,22
$_{29}$Cu	1537,400	592,74	591,53	1,21
$_{42}$Mo	707,831	1287,41	1284,79	2,62
$_{62}$Sm	308,54	2953,50	2947,49	6,01
$_{74}$W	208,571	4369,11	4360,24	8,87
$_{92}$U	125,686	7250,33	7235,66	14,68

For the same reason the formula given in Refs.2, 3 & 4 for conversion from wavelengths expressed in XU to photon energies expressed in Rydbergs is misleading. The correct formula is

$$\log E(R) = 5.9587650 - \log \lambda(XU), \quad (4)$$

[rather than $\log E(R) = 5.9596457 - \log \lambda(XU)$].

For convenience and to avoid possible errors we feel it would be expedient to express wavelengths of x-ray spectra only in angstroms (Å). In the range of medium and short wavelengths, where specification in angstroms becomes inconvenient owing to the smallness of the quantities involved, one can use the unit proposed by Merrill & DuMond[7], namely, the milliangstrom,

$$1\ \text{mÅ} = 10^{-3}\ \text{Å}. \quad (5)$$

II

Data on the energies of electron levels in various atoms are given in the tables of Refs.3-6. Apart from the fact that the energy values of the electron levels were calculated with reference to the wavelengths of the x-ray absorption spectra without taking relation (1) into account, we feel that the procedure employed in using these data for the above purpose is in need of revision.

Sokolovskii, Nordling & Seigbahn[8], using a new magnetic spectrometer, were able to determine with high accuracy the energy of the K level of copper. The value they give is 660.44 ± 0.07 R. The corresponding value for the energy of the K level of copper given in the tables of Ref.4 is 661.44 R.

It can easily be shown that the 1 R difference is due to the following two causes:

1) failure to take relation (1) into account in calculating the tabular value of the K level energy on the basis of the wavelength of the K absorption edge of copper, and

2) difference in the choice of the zero (datum) in the energy scale for the electron levels; in determining the level energies by the magnetic spectroscopy procedure the zero energy is taken to be the energy of the neutral atom, whereas in using the absorption edge data, the energy datum is assumed to be the energy of an atom with the outer valence electron removed.

It may be expected that after taking into account relation (1) all the electron level energies calculated on the basis of the tabular data for the absorption spectra will differ from the corresponding values obtained on the basis of magnetic spectrometer experiments by an amount equal to the work function in the case of metals or by the magnitude of the first stage ionization potential in the case of gases.

In our case, for the energy of the photon corresponding to the wavelength of the K absorption edge of copper we obtain 660.09 R which leaves a difference of 0.35 R between the values obtained by magnetic spectroscopy and x-ray spectroscopy. The work function of copper, according to the data in the literature[9], is 4.48 ev or 0.33 R, which is close to the difference 0.35 R found above.

Analogous comparisons for gases are precluded by the lack of magnetic spectrometer data on the energies of electron levels in gases. However, a number of authors[10] have worked out a procedure for calculating the fine structure of x-ray spectra by means of which one can distinguish the "true" absorption edge as the point of inflection of the arc tangent curve representing the absorption spectrum, which point corresponds to transition of the electron into the continuum.

Thus, Bačkovský[11], using this procedure, resolved the complex structure of the K absorption edge of neon into selective lines and the "true" absorption edge. The value deduced by Backovsky for the "true" K absorption edge of neon was 63.970 R.

The indicated method of determining the K level energy from the point of inflection of the arc tangent curve representing the "true" absorption edge, like the method of magnetic spectrometry, presupposes choice of the state of the neutral atom as the zero for the energy scale. Hence one can expect good agreement between the value obtained by Bačkovsky for the K level energy of neon and the value obtained by summing the data for the photon energy of the $K\alpha_{1,2}$ lines of neon[12] and the first stage ionization potential for neon[13]. In this case for the energy of the K level we obtain

$$62.355 \text{ R} + 1.585 \text{ R} = 63.940 \text{ R}.$$

The agreement may be regarded as fully satisfactory.

In view of the above one can understand the allusion made by Vainshtein[2,14] to "certain discrepancies" between theory and experiment, connected with the 2 to 5 ev difference between the position of the center of the short wavelength branch of the $K\beta_5$ band and the position of the "true" absorption edge of the same element. It can readily be shown that the center of the short wavelength side of the $K\beta_5$ peak of a transition element should not coincide with the "true" absorption edge but rather will be shifted to the side of longer wavelengths by the equivalent of the work function (3-5 ev), which is what was observed by the above mentioned author.

Thus at present we find that different authors in constructing the electron energy spectrum take as the datum or ground state either the state of the atom with the outer electron removed or the state of the neutral atom.

The choice of an atom with the outer valence electron removed as the zero state was dictated by the tendency of some investigators to obtain the values of the electron level terms directly from x-ray absorption spectra. In the present state of development of solid state physics - our understanding of the fine structure of absorption spectra and the dependence of this structure on the atomic bonds, the crystal lattice and other physical and physical-chemical properties - such choice of the energy scale can hardly be regarded as proper and convenient, particularly in view of the fact that in the case of dielectrics the energy of the absorption edge will not correspond with the energy of the atomic level but must be decreased by the magnitude of the energy gap between the vacant and occupied states; this, however, has not been taken into account in compiling the tables of Refs.2-6.

The second reference system, which takes as the datum the state of the neutral atom, is free of these shortcomings. Modern magnetic spectrometers make it possible to obtain reliable values for the electron term in this energy scale, values equal in accuracy to those based on x-ray spectroscopy and in no way dependent on the absorption spectrum data.

Summarizing the foregoing, we can draw the following conclusions.

1. The present tabular values for the energy of x-ray photons and absorption edges should be revised in the light of the latest data on the physical constants involved.

2. It is essential to obtain new data for electron level energies, taking as the datum (zero) of the energy scale the state of the neutral atom.

3. It is desirable to compile new reference tables for x-ray spectroscopy taking the above considerations into account.

Institute of Metal Physics,
Academy of Sciences of the Ukrainian SSR

References

1. W.L.Bragg, Scient.Instr., 24, (1947).
2. E.E.Vainshtein, Rentgenovskie spektry atomov v molekulakh khimicheskikh soedinenii i v splavakh (X-ray spectra of atoms in molecules of chemical compounds and in alloys), M.-L., 1950.
3. M.A.Blokhin, Fizika rentgenovykh luchei (Physics of x-rays), M., 1953.
4. E.E.Vainshtein & M.M.Kakhana, Spravochnye tablitsy po rentgenovskoi spektroskopii (Reference tables for x-ray spectroscopy), M., 1953.
5. I.B.Borovskii, Fizicheskie osnovy rentgenospektral'nykh issledovanii (Physical bases of x-ray spectroscopic investigations), Pub.Moscow State Univ., 1956.
6. M.A.Blokhin, Fizika rentgenovykh luchei (Physics of x-rays), Second revised edition, M., 1957.
7. J.J.Merrill & W.M.DuMond, Phys.Rev., 110, 79 (1958).
8. E.Sokolowski, C.Nordling & K.Siegbahn, Arkiv.fys., 12, 4, 301 (1957).
9. Landolt-Börnstein, Zahlenwerte und Funktionen aus Physik, Chemie, Astronomie, Geophysik und Technik, 1, 4 Teil, 760. -Berlin, 1955.
10. E.E.Vainshtein, R.L.Barinskii & K.Narbutt, Zhur.eksp.i teor.fiz., 23, 5939 (1952).
11. I.Bačkovsky, Českosl. časop. fys., 4, 118 (1954).
12. C.Moor, Proc.Phys.Soc., A 68, 717 (1955).
13. Amer.Institute of Physics Handbook, N.Y., 1957.
14. I.B.Borovskii & E.E.Vainshtein, Izv.AN SSSR, Otd.khim.nauk, (Bulletin, USSR Ac.of Sci., Div. of Chem.Sci.), 5, 309 (1942).

CONCERNING THE SHAPE OF ENERGY BANDS IN SOLIDS

- M.A.Blokhin & V.P.Sachenko

The observed shape of x-ray emission bands agrees only very roughly with the shape given by theoretical calculations. The emission bands of metals of the third period have low- and high-energy tails which were assumed not to be connected with the actual shape of the conduction band and were therefore "cut off" by different, more or less arbitrary procedures. Even neglecting the tails, however, the shape of the emission bands of these elements is at best only in quantitative agreement with the deductions of theory (for example, with the theoretical dependence for the K spectra).

As regards the emission bands of the transition elements, specifically, the $K\beta_5$ lines, their shape is even in poorer agreement with theory. Generally, the $K\beta_5$ line has a very large long wavelength tail. This tail makes the base width of the $K\beta_5$ line much greater than the width of the filled part of the $3d$-$4sp$ band computed theoretically. We showed in earlier contributions[1,2] that this discrepancy cannot be eliminated by correcting the shape of the $K\beta_5$ line for apparatus distortion and the width of the K level.

Skinner[3] indicated that the long wavelength tail of the emission bands of elements of the third period can be explained by broadening of the levels of the valence band or the conduction band of these elements. In the process of emission of an x-ray photon the solid undergoes a transition from an excited state characterized by the absence of an inner electron at some atom to a state characterized by the absence of an electron in the upper energy band.

The initial state has a definite energy width which virtually coincides with the width of the corresponding level of a free atom. This is the width for which we corrected the shape of the $K\beta_5$ line in the work of Ref.2.

The final state, however, also has some width owing to the finite lifetime of the vacancy in the upper energy band. Inasmuch as radiative transitions within the band are forbidden, the principal vacancy filling mechanism consists of nonradiative transitions.

Skinner[3] explained the appearance of the long wavelength tails of the emission bands of elements of the third period precisely by this mechanism of broadening of the levels in the upper energy band. It may be assumed that the shape of this broadening is Lorentzian. The broadening is very small for levels located close to the Fermi surface and increases for deeper lying levels, attaining, according to Skinner, ~1 ev. Accordingly, the broadening of the levels has almost no effect on the short wavelength part of the line but does substantially extend the long wavelength part, leading to the appearance of a tail.

Landsberg[4] calculated the shape of the L_{III} emission band of sodium taking into account the broadening of the conduction band levels. He calculated this in the free electron approximation, with a perturbation of the form $\exp(-\alpha r_{12})/r_{12}$. In his calculations, however, Landsberg did not fully take into account the restrictions imposed by the law of energy conservation on the number of possible transitions and, as will be shown below, did not properly allow for the influence of the x-ray transition probability on the shape of the emission lines.

Moreover, in the work of Skinner[3] and Landsberg[4] the broadening of the levels in the conduction band is associated only with emission of an x-ray photon. Actually, broadening of these levels should obtain in all investigations concerned with the energy bands of solids, inasmuch as in any experimental procedure, an electron is removed from the conduction band in one manner or another. Such experimental procedures, in addition to x-ray spectroscopy, include optical spectroscopy, investigations of the photoeffect and electric conductivity, etc.

In the present work we have carried out more rigorous calculations of the level broadening in the free electron approximation, investigated the influence of level broadening on the shape of the x-ray emission bands and the distribution of electrons in energy in the bands of the solid.

Let us consider two conduction band electrons with wave vectors $\mathbf{k}_2$ and $\mathbf{k}_3$. In the free electron approximation their wave functions will be

$$\psi_2(\mathbf{r}_1) = \frac{1}{L^{3/2}} e^{ik_2 r_1};$$

$$\psi_3(\mathbf{r}_2) = \frac{1}{L^{3/2}} e^{ik_3 r_2}.$$

The wave functions are normalized in the volume L^3.

After collision, one of the electrons fills a vacancy with wave vector $\mathbf{k}_1$, while the second electron goes over into the state $\mathbf{k}_4$ in the unoccupied part of the conduction band. Thus the following restrictions are imposed on the moduli of $\mathbf{k}_4$, $\mathbf{k}_3$ and $\mathbf{k}_2$:

$$\begin{gathered} k_4 \geqslant k_F, \\ k_1 \leqslant k_3 \leqslant k_F, \\ k_1 \leqslant k_2 \leqslant k_F, \end{gathered} \tag{1}$$

where k_F is the wave number characterizing the position of the Fermi surface; moreover, from the law of energy conservation

$$k_2^2 + k_3^2 = k_1^2 + k_4^2 \tag{2}$$

it follows that

$$k_4 \leqslant \sqrt{k_F^2 + k_2^2 - k_1^2},$$

if we assume that the vacancy is filled by the electron from state k_2 or

$$k_4 \leqslant \sqrt{k_F^2 + k_3^2 - k_1^2},$$

if we assume that the vacancy is filled by the electron from the k_3 state.

Consequently, the range of variation of the modulus of k_4 will be

$$k_F \leqslant k_4 \leqslant \sqrt{k_F^2 + k_i^2 - k_1^2}, \tag{3}$$

where $i = 2, 3$.

The transition probability between two states of the continuum is given by the familiar formula

$$W = \frac{2\pi}{\hbar} |H_{mn}|^2 \rho(k), \tag{4}$$

where H_{mn} is the matrix element of the perturbation producing the transition and $\rho(k)$ is the density of the final states (per unit energy interval).

The total transition probability P to the state k_1 taking into account exchange effects will be

$$P = \frac{2\pi}{\hbar} \rho(k_4) (|A - B|^2 + |A|^2 + |B|^2), \tag{5}$$

where

$$A = e^2 \int \frac{1}{|\boldsymbol{r}_1 - \boldsymbol{r}_2|} \psi_1^*(\boldsymbol{r}_1)\psi_4^*(\boldsymbol{r}_2)\,\psi_2(\boldsymbol{r}_1)\,\psi_3(\boldsymbol{r}_2)\,d\tau_1\,d\tau_2$$

and

$$B = e^2 \int \frac{1}{|\boldsymbol{r}_1 - \boldsymbol{r}_2|} \psi_1^*(\boldsymbol{r}_2)\,\psi_4^*(\boldsymbol{r}_1)\,\psi_2(\boldsymbol{r}_1)\,\psi_3(\boldsymbol{r}_2)\,d\tau_1\,d\tau_2.$$

The wave functions ψ_1 and ψ_4 of the final states in the free electron approximation will be similar in form to ψ_2 and ψ_3. Let us consider the integral

$$A = \frac{e^2}{L^6} \int e^{i(\boldsymbol{k}_3 - \boldsymbol{k}_4)\boldsymbol{r}_2}\,d\tau_2 \int \frac{1}{|\boldsymbol{r}_1 - \boldsymbol{r}_2|}\,e^{i(\boldsymbol{k}_2 - \boldsymbol{k}_1)\boldsymbol{r}_1}\,d\tau_1.$$

After integration over the coordinates of the first electron, we obtain

$$A = \frac{4\pi e^2}{L^6\,|\boldsymbol{k}_2 - \boldsymbol{k}_1|^2} \int e^{i(\boldsymbol{k}_3 - \boldsymbol{k}_4 + \boldsymbol{k}_2 - \boldsymbol{k}_1)\boldsymbol{r}_2}\,d\tau_2;$$

this integral does not vanish for

$$\boldsymbol{k}_2 + \boldsymbol{k}_3 = \boldsymbol{k}_1 + \boldsymbol{k}_4, \tag{6}$$

which follows from orthogonality of the wave functions and is a consequence of conservation of momentum in the transition. Thus

$$A = \frac{4\pi e^2}{L^3\,|\boldsymbol{k}_2 - \boldsymbol{k}_1|^2}; \tag{7}$$

a similar expression is obtained for :

$$B = \frac{4\pi e^2}{L^3\,|\boldsymbol{k}_3 - \boldsymbol{k}_1|^2}$$

For free electrons the density of states per energy interval in a solid angle element is given by the expression

$$\rho_1(\boldsymbol{k}_4, \theta, \varphi)\,d\theta\,d\varphi = \frac{mL^3}{8\pi\hbar^2}\,\boldsymbol{k}_4 \sin\theta\,d\theta\,d\varphi. \tag{8}$$

For fixed k_1 and k_2 the conservation laws (2) and (6) determine the vector k_3 and one component of the vector k_4. Moreover, conditions (1) and (2) impose restrictions on the values of the other two components of k_4. Determining k_3 from (6) and inserting this value in (2), we obtain

$$\boldsymbol{k}_2^2 - \boldsymbol{k}_4(\boldsymbol{k}_2 - \boldsymbol{k}_1) - (\boldsymbol{k}_1\boldsymbol{k}_2) = 0.$$

We choose the $\boldsymbol{k}_2 - \boldsymbol{k}_1$ direction for the z axis; then

$$k_4 = \frac{\boldsymbol{k}_2^2 - (\boldsymbol{k}_1\boldsymbol{k}_2)}{|\boldsymbol{k}_2 - \boldsymbol{k}_1|\,\cos\theta}. \tag{9}$$

Taking into account (1) and (2), we obtain the restriction imposed on the values of the angle θ:

$$\frac{\boldsymbol{k}_2(\boldsymbol{k}_2 - \boldsymbol{k}_1)}{|\boldsymbol{k}_2 - \boldsymbol{k}_1|\sqrt{k_F^2 + k_2^2 - k_1^2}} \leqslant \cos\theta \leqslant \frac{\boldsymbol{k}_2(\boldsymbol{k}_2 - \boldsymbol{k}_1)}{|\boldsymbol{k}_2 - \boldsymbol{k}_1|\,k_F}.$$

No restrictions are imposed on the values of φ.

Inserting (9) in (8) and integrating over all possible values of θ and φ, we obtain the following expression for the density of states taking into account the restrictions imposed by (1), (2) and (6):

$$\rho(k_4)=\frac{mL^3}{8\pi^2\hbar^2}\,\frac{\mathbf{k}_2(\mathbf{k}_2-\mathbf{k}_1)}{|\mathbf{k}_2-\mathbf{k}_1|}\ln\frac{k_F^2+k_2^2-k_1^2}{k_F^2}\,. \tag{10}$$

Inasmuch as expressions (1), (2) and (6) are symmetrical with respect to the vectors $\mathbf{k}_2$ and k_3, the expression for $\rho(k_4)$ can also be written in the form

$$\rho(k_4)=\frac{mL^3}{8\pi^2\hbar^2}\,\frac{\mathbf{k}_3(\mathbf{k}_3-\mathbf{k}_1)}{|\mathbf{k}_3-\mathbf{k}_1|}\ln\frac{k_F^2+k_3^2-k_1^2}{k_F^2}\,.$$

The total probability for transition to the k_1 level is determined by integrating (5) over all possible values of k_2 and k_3 allowed by (1).

The integrals for $|A|^2$ and $|B|^2$ will be equal inasmuch as the expressions for A and B, like the expressions for ρ, are symmetrical relative to the vectors k_2 and k_3. The integral for $|A-B|^2$ is very complex; hence it was not calculated in this work.

Let us calculate the result of integration of

$$\frac{2\pi}{\hbar}|A|^2\rho(k_4)$$

over all possible states of the second electron characterized by the wave vector $\mathbf{k}_2$:

$$W_A(k_1)=\frac{L^3}{(2\pi)^2\hbar}\int_{k_1}^{k_F}k_2{}^2\,dk_2\int_0^{\pi}\sin\theta\,d\theta\int_0^{2\pi}|A|^2\rho(k_1)\,d\varphi.$$

Substituting the expressions for A and $\rho(k_4)$ from (7) and (10) and carrying out the integration over φ, we obtain,

$$W_A(k_1)=\frac{me^4}{\pi\hbar^3}\int_{k_1}^{k_F}k_2{}^2\ln\frac{k_F^2+k_2^2-k_1^2}{k_F^2}\,dk_2\int_0^{\pi}\frac{\mathbf{k}_2(\mathbf{k}_2-\mathbf{k}_1)}{|\mathbf{k}_2-\mathbf{k}_1|^5}\sin\theta d\theta; \tag{11}$$

this integral diverges logarithmically for all values of k_1, except $k_1 = 0$. For $k_1 = 0$ the integral does not depend on k_1 and equals

$$W_A(0)=\frac{\pi me^4}{12\,\hbar^3}\,,$$

which corresponds to an energy width of 7.0 ev. Consequently, neglecting the integral for $|A-B|^2$, the width of the level $k_1 = 0$ equals 14.0 ev.

In the work of Landsberg[4], owing to inaccuracy in the calculations, the integral determining $W_A(k_1)$ diverges as $1|k_1-k_2|$ in the limit as $k_2\to k_1$, and a finite value is not obtained even for $k_1 = 0$.

The divergence of the integral (11) for $k_1 \neq 0$ is due to choice of the Coulomb expression for the interaction energy of the two electrons. Actually, the interaction of the two electrons in the conduction band will be weakened by the screening effect of the other electrons in the band.

Following Cauchois & Mott[5], we choose the expression for the interaction energy of two electrons in the conduction band in the form

$$U(\mathbf{r}_1,\mathbf{r}_2)=e^2\,\frac{e^{-\alpha(|\mathbf{r}_1-\mathbf{r}_2|)}}{|\mathbf{r}_1-\mathbf{r}_2|}\,,$$

where the parameter α, according to Cauchois & Mott, is of the order of 1-2 Å^{-1}. Then for A in (5) we obtain

$$A=\frac{e^2}{L^6}\int e^{i(k_3-k_4)r_2}\,d\tau_2\int\frac{1}{|r_1-r_2|}e^{i(k_2-k_1)r_1}\,e^{-\alpha(|r_1-r_2|)}\,d\tau_1.$$

Integrating over the coordinates of the first and second electrons, we find

$$A = \frac{4\pi e^2}{L^3 (|\boldsymbol{k}_2 - \boldsymbol{k}_1|^2 + \alpha^2)} \tag{12}$$

for

$$\boldsymbol{k}_2 + \boldsymbol{k}_3 = \boldsymbol{k}_1 + \boldsymbol{k}_4.$$

The expression for $W_A(k_1)$ is obtained analogously to (11) from Eqs.(10) and (12) by integration over all possible states of the second electron:

$$W_A(k_1) = \frac{me^4}{\pi\hbar^3} \int_{k_1}^{k_F} k^2{}_2 \ln \frac{k_F^2 + k_2^2 - k_1^2}{k_F^2} dk_2 \int_0^{\pi} \frac{[\boldsymbol{k}_2^2 - (\boldsymbol{k}_2 \boldsymbol{k}_1)] \sin\theta}{(|\boldsymbol{k}_2 - \boldsymbol{k}_1|)\,[|\boldsymbol{k}_2 - \boldsymbol{k}_1|^2 + \alpha^2]^2}\, d\theta.$$

Integrating over θ, we obtain

$$W_A(k_1) = \frac{me^4}{\pi\hbar^3} \int_{k_1}^{k_F} \frac{k_2^2}{2} \left\{ \frac{4k_2}{[(k_2 - k_1)^2 + \alpha^2]\,[(k_2 + k_1)^2 + \alpha^2]} - \frac{1}{k_2\alpha^2} + \right.$$

$$\left. + \frac{\alpha^2 + k_2^2 - k_1^2}{2k_2k_1\alpha^3} \operatorname{arctg} \frac{2k_1\alpha}{\alpha^2 + k_2^2 - k_1^2} \right\} \ln \frac{k_F^2 + k_2^2 - k_1^2}{k_F^2}\, dk_2. \tag{13}$$

Eq.(13) is finite for all values of k_1. The total transition probability to the k_1 level, neglecting exchange effects, will be equal to $2W_A(k_1)$.

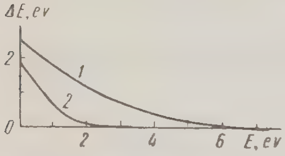

Fig.1. Variation of the width of the levels as a function of their energy.

Fig.1 shows the variation of the broadening of the levels as a function of their position in the band. The probability $W_A(k_1)$ was calculated by numerical integration of (13). Curve 1 was obtained for $E_F = \hbar^2 k_F^2/2m$ = 7 ev and $E_\alpha = \hbar^2\alpha^2/2m$ = 4 ev, which corresponds to the position of the Fermi surface in copper and α = 1 Å^{-1}. Curve 2 corresponds to E_F = 3.2 ev (position of the Fermi surface in sodium) and α = 0.75 Å^{-1}.

As will be evident from Fig.1, the broadening of the levels in the conduction band is very small at the top of the band and increases greatly for the low lying levels.

If broadening of the levels is neglected, the distribution $N(E)$ of states in energy agrees with the distribution $N_1(E)$ of electrons in energy. If there is broadening of the levels, however, $N_1(E)$ may differ substantially from $N(E)$. In the case of level broadening the values of $N_1(E)$ and $N(E)$ will be related by the following expression, which is a natural generalization of the integral expression of the curl type to which "correction" of the x-ray spectra reduces[1] for the case of a nucleus with a variable parameter:

$$N_1(E) = \frac{1}{\pi} \int_0^{E_F} \frac{N(t)}{a(t)\left[1 + \left(\frac{t - E}{a(t)}\right)^2\right]} dt, \tag{14}$$

where the shape of the broadened level E is assumed to be Lorentzian and $a(E)$ is its half-width. Moreover, it is assumed that $N(E)$ vanishes outside the interval 0 to E_F, where E_F is the energy of the Fermi surface.

If there is no broadening of the levels, $a(E)$ = 0 for all E and from (14) it follows that

$$N_1(E) = N(E).$$

It must be emphasized that in most physical effects it is important to know the distribution $N_1(E)$ of electrons in energy and not the distribution $N(E)$ of states in energy, inasmuch as $N_1(E)$ is the distribution evinced in experiments on investigation of the shape of the energy bands in solids. In contrast to $N(E)$, the function $N_1(E)$ given by (14) is nonzero for all finite values of E. Hence the concept of the width of the electron distribution curve, as given by the base of the curve, is somewhat arbitrary. One can legitimately speak of the width of the $N_1(E)$ curve having in view the energy interval in which $N_1(E)$ differs appreciably from zero. The width determined in this manner will exceed the width of the distribution of states in energy curve.

In experimental determination of the distribution $N(E)$ of states, an electron is removed in one way or another from the energy band. Hence what is determined experimentally is not the function $N(E)$, but actually the product of $N(E)$ by the transition probability $P(E)$. The latter is evaluated on the basis of different considerations and may be substantially different for different effects.

The influence of the transition probability should be taken into account also in determining the electron distribution $N_1(E)$. When the transition probability $P(E)$ is taken into account, Eq.(14) should be replaced by the more general expression

$$N_1(E) = \frac{1}{\pi}\int_0^{E_F} \frac{N(t)\,P(t)}{a(t)\left[1+\left(\frac{t-E}{a(t)}\right)^2\right]}\,dt. \qquad (15)$$

It is important to emphasize that now the x-ray transition probability is under the integral. In the work of Landsberg[4] the intensity of the emission band was found by multiplying $N_1(E)$, found by means of Eq.(14), by the transition probability, which is not correct.

According to (15), the function $N_1(E)$ characterizes the energy distribution of the electrons participating in the given effect. Inasmuch as the probability $P(E)$ is different for different effects, obviously, the distribution $N_1(E)$ will also be different. Thus for any given physical effect the significant quantity is $N_1(E)$ and comparison of data on the shape of energy bands, obtained in different experiments becomes nontrivial.

In such comparisons one must exclude the influence of the transition probability. Consequently, the problem reduces first to finding the product $N(E)\cdot P(E)$ by solving Eq.(15), eliminating $P(E)$ by calculating this function and finally finding the density of state distribution $N(E)$. The functions determined in this manner can be compared. On the contrary, if $N(E)$ is known, then having $P(E)$ and $a(E)$, by means of (15) we can find the electron distribution $N_1(E)$, which should be compared with the experimentally observed curve. One should proceed analogously in comparing theoretical and experimental data.

In order to check the foregoing we calculated the shapes of the K, L and M x-ray emission bands in the free electron approximation. In this case $N(E) \sim E^{1/2}$. The probability for transition of electrons from the conduction band to a level of p type symmetry does not depend on E, but the probability for transition to a level of s symmetry is proportional to E. Strictly speaking, this energy dependence of the transition probability is valid only for the beginning of the band. For the sake of simplicity, however, we assume that this dependence is valid for the entire filled part of the conduction band.

Then $N(E)\cdot P(E) \sim E^{1/2}$ for transitions to a level of p type symmetry, i.e., for the L and M spectra, and $N(E)\cdot P(E) \sim E^{3/2}$ for transitions to a level of s type symmetry, i.e., for the K spectra. The integral (15) was evaluated numerically. The values of $a(E)$ were taken from curve 1 of Fig.1.

The results of our calculations are shown in Fig.2. The $N_1(E)$ curve corresponds to the $N(E)P(E) \sim E^{1/2}$ case, i.e., should characterize the shape of the L and M spectra. Curve $N_1'(E)$ corresponds to the $N(E)P(E) \sim E^{3/2}$ case, i.e., should represent the shape of the K spectra. The scales of the curves were chosen so that the areas bounded by the curves would be equal. It will be apparent from Fig.2 that

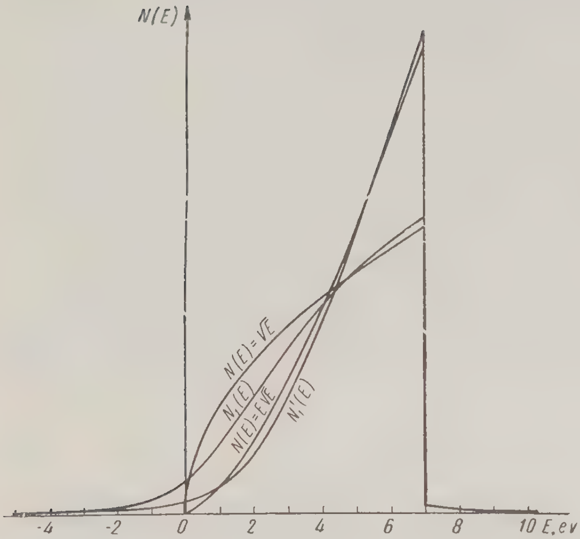

Fig.2. Character of the electron distribution in states for free electrons taking into account level broadening.

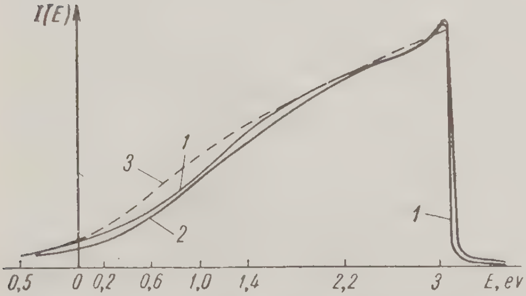

Fig.3. Experimental and theoretical (taking into account level broadening) shape of the L_{III} emission band of sodium.

the shape of the $N_1(E)$ curves differs substantially from the shape of the initial $N(E){\cdot}P(E)$ curves. Noteworthy is the absence in the case of the $N_1(E)$ curves of a rapid tendency to approach zero as $E\to 0$ (in contrast to the initial curves). The sections of the curves located in the negative energy region represent long wavelength tails corresponding to the tails actually observed on the low energy side of experimental emission bands. As will be evident from Fig.2, the K band tails should be less strongly evident than the tails attached to the L_{III} bands. This is substantiated by experiment[3].

Beginning from the Fermi surface the $N_1(E)$ curves show short wavelength tails. Such high energy tails are also familiar from experiment. It is interesting to note that in the optical absorption spectra of copper recorded by Biondi[6] (at 4.2°K) after a sharp absorption edge at ~0.55 μ, a distinct tail extends to the side of longer wavelengths (to ~2 μ). It may be assumed that this tail is also associated with broadening of the levels in the conduction band of copper.

As a whole the shape of the $N_1(E)$ curves is in much better agreement with the shape of the emission bands (for metals of the second and third periods) than the shape of the initial $N(E){\cdot}P(E)$ curves. Substantiation of this is also furnished by calculation of the shape of the L_{III} emission band of sodium. To a high degree of accuracy it may be assumed that the electrons on the conduction band of sodium are free. Hence it may be assumed that for sodium $N(E)\sim E^{1/2}$ and that the energy dependence of the level broadening is characterized by curve 2 in Fig.1. The results of calculation of the shape of the L_{III} band of sodium are shown in Fig.3. Curve 1 represents $N_1(E)$; curve 2 - the shape of the L_{III} band of sodium according to the data of Skinner[7]; curve 3 represents the theoretical shape of the L_{III} band of sodium calculated by Landsberg[4]. It will be evident from Fig.3 that curves 1 and 2 virtually coincide.

It may be noted that the level broadening effect allows of explaining the minor peak (spike) observed in the L_{III} band of sodium near the Fermi surface. Whereas $a(E)$ approaches zero as $E\to E_F$ more slowly than $(E-E_F)$, as follows from Eq.(15), $N_1(E_F)$ becomes infinite. It follows from Eq.(13) that $a(E)$ approaches zero as $(E-E_F)^2$ in the limit as $E\to E_F$. Thus $N_1(E_F)$ is finite but takes on large values which leads to the appearance of a peak near the Fermi surface. A peak at this point is observed in the experimental curve obtained by Skinner[7] and is not explained in the work of Landsberg[4]. It follows from the above said that the height of the peak is determined by the behavior of $a(E)$ near E_F. Consequently, the height of the peak will be substantially affected by thermal smearing of the Fermi surface and electron-phonon collisions. These considerations can explain why this peak is absent in the L_{III} spectra of Na obtained by other authors.

The idea of broadening of the levels in energy bands also allows of explaining the shape of the $K\beta_5$ emission band in the spectra of the transition elements. As is known, the $K\beta_5$ band has a large long wavelength tail with the result that its base width is anomalously great. It may be assumed that this effect is also connected with broadening of the levels in the $3d$-$4sp$ bands of the transition metals. Direct calculation of the magnitude of this broadening in the case of the transition metals is difficult. It may be assumed, however, that this broadening is in any case not less than that deduced above in the free electron approximation. It will be recalled that the $3d$-$4sp$ band of the transition metals contains from 8 to 11 electrons, whereas the conduction band in the metals of the second and third periods comprises only 1-2 electrons. The greater density of filled states in the former case (other conditions being equal) should increase the probability for filling of vacancies and, consequently, the width of the levels in the band. Thus it may be expected that the broadening of the levels in the $3d$-$4sp$ band will be of the order of 5 ev for the low lying levels. This value is sufficient to explain the presence of the great long wavelength tail at the $K\beta_5$ line.

It follows from general considerations[8], based on analysis of the symmetry of the lattices of Cu, Ni and Fe, that the $3d$ band of these elements must have two density of states peaks. This deduction in general is substantiated by all the theoretical calculations involving different approximations. Actually, however, two peaks are not observed in either the K, L and M spectra or the ultraviolet spectra of these elements. This discrepancy can be explained by great broadening of the levels in the region of the more deeply located peak, as a result of which it is virtually effaced from the $N_1(E)$ curves. In Ref.2 we gave the shape of the $K\beta_5$ band of the enumerated elements, corrected for the width of the K level. In nickel and iron, there is a "fluctuation" on the long wavelength side of the corrected curves, which may be regarded as manifestation of a second maximum of the density of states in the $3d$ band. The position of this "fluctuation" in the case of iron is in good agreement with the position of the second peak in the $N(E)$ curves as calculated by Manning[9].

The absence of a similar "fluctuation" in the corrected $K\beta_5$ band of copper is explained by the greater broadening of the levels in the region of the second maximum as compared with nickel and iron. The greater broadening is connected with the greater width of the filled part of the conduction band in copper (~7 ev) as compared with Fe and Ni (~4-5 ev).

For purposes of approximate evaluation of the magnitude of the broadening necessary for effacement of the second maximum in the density of states curve, we carried out the following calculations. The $N_1(E)$ curve was obtained by means of Eq.(15) from the $N(E)$ curve for the $3d$ band taken from the work of Koster[8] (curve 1 in Fig.4). The probability $P(E)$ was assumed to be constant. The variation of broadening of $a(E)$ with energy was taken to be

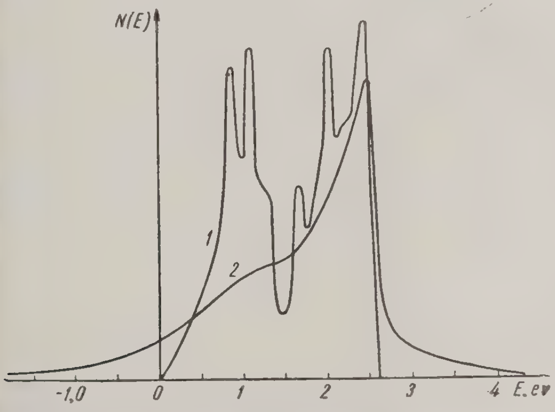

Fig.4. Influence of level broadening on the shape of the $3d$ band.

linear with $a(E)$ equal to zero at the end of the band. The results of our calculations are shown in Fig.4: curve 2 was obtained for $a(0) = 2$ ev, which corresponds to a total broadening of 4 ev. These calculations show that even such relatively minor broadening is sufficient for effacement of the second maximum from the $N_1(E)$ curve and appearance of a large long wavelength tail.

Above we indicated that broadening of the levels in the energy bands of a solid is common to any method of investigating the energy bands. By way of another example one can take the photoelectric effect. Dickey[10] gives the energy distribution of electrons for the external photoelectric effect in Na and K. He found that at photon energies $h\nu$ greater than the sum of the work function φ and Fermi energy E_F, there is observed a relatively large number of low velocity electrons with an energy lower than $h\nu - (\varphi + E_F)$. Thus below the bottom of the conduction band there is a continuous electron spectrum. Without going into detail regarding possible explanations of this effect (see Ref.10), it must be noted that the preponderance of such slow electrons can be explained in the light of the character of the $N_1(E)$ curves (Figs.2 & 3), the long wavelength tails of which correspond to electrons residing below the bottom of the band (before the beginning of the $N(E)$ curve).

There are mentions of the possible role of the effect of level broadening in the conduction band as regards the behavior of electric conductivity in the works of Peierls and Samoilovich (see Ioffe[11], p.229).

Thus we have shown that

1) broadening of the levels in the energy bands of solids can explain some of the features of experimental x-ray spectra, and

2) the broadening of the levels in the energy bands of solids has general significance in solid state physics.

Rostov-on-the-Don State University

References

1. M.A.Blokhin, Izv.AN SSSR, Ser.fiz, 20, 142 (1956). (Trans.Bulletin,20, 127.)
2. M.A.Blokhin & V.P.Sachenko, Ibid., 21, 1343 (1957). (Trans.Ibid., 21, 1333.)
3. H.W.B.Skinner, Phil.Trans.Roy.Soc., London, A239, 95 (1940).
4. P.T.Landsberg, Proc.Phys.Soc., A62, 806 (1949).
5. Y.Cauchois & N.F.Mott, Phil.Mag., 40, 1260 (1949).
6. M.A.Biondi, Phys.Rev., 96, 534 (1954).
7. H.W.B.Skinner, Repts.Progr.Phys., 5, 257 (1938).
8. G.F.Koster, Phys.Rev., 98, 901 (1954).
9. M.F.Manning, Phys.Rev., 63, 190 (1943).
10. J.Dickey, Phys.Rev., 81, 612 (1950).
11. A.F.Ioffe, Fizika poluprovodnikov (Physics of semiconductors), M.-L., 1957.

CALCULATION OF THE CHARGE OF ATOMS IN MOLECULES FROM THE K ABSORPTION SPECTRA

- R.L.Barinskii & E.G.Nadzhakov

In Ref.1 we proposed a new method for calculating the K absorption spectra of atoms in molecules, a method that makes it feasible, in principle, to determine the effective quantum number of the absorbing atom and its total charge in the field of which the electron ejected from the K shell moves. We succeeded[1] in carrying out such calculations in a few simple cases (the K absorption spectra of free A and Ne atoms, gaseous Cl_2 and B_2 molecules, and the Zn^{2+} ion in solution), which provided an effective check on the applicability of the calculation method, inasmuch as the magnitude of charge of the absorbing atom was known beforehand in these cases. The calculated values of the charge at the periphery* of the atoms of argon, neon, chlorine, bromine and Zn^{2+} agreed satisfactorily with these known values.

In the present work the proposed method is used to calculate the K absorption spectra of atoms in other, more complex molecules of gases and crystals for which the atomic charge is not known a priori. In so doing we chose compounds for which we could safely assume a not excessively great departure from central field symmetry in the neighborhood of the absorbing atom. In these cases (as in Ref.1) presumably the K absorption spectrum can be approximately represented by a Rydberg series of absorption lines and a true edge. Agreement of theory with experiment would serve as further substantiation of this assumption.

To calculate the main K absorption edge we used the following formulas:

$$\left.\begin{aligned} \mathcal{E}_n &= \mathcal{E}_\infty - \frac{\eta^2}{n^2}\,\mathrm{Ry}, \\ \mathcal{E}_{n+1} &= \mathcal{E}_\infty - \frac{\eta^2}{(n+1)^2}\,\mathrm{Ry}, \\ &\dots\dots\dots\dots \end{aligned}\right\} \qquad (1)$$

$$\left.\begin{aligned} \frac{\pi\Gamma\tau_n}{\tau_\infty} &= 4\eta^2\,\frac{n^2-1}{n^5}, \\ \frac{\pi\Gamma\tau_{n+1}}{\tau_\infty} &= 4\eta^2\,\frac{(n+1)^2-1}{(n+1)^5}, \\ &\dots\dots\dots\dots \end{aligned}\right\} \qquad (2)$$

from Ref.1, here the $\mathcal{E}_n$, $\mathcal{E}_{n+1}\dots$ are the energies of the successive absorption lines in the Rydberg series; $\mathcal{E}_\infty$ is the energy of the series limit, η is the total charge of the absorbing atom (equal to a unit positive charge in the K shell plus the effective charge (η') at the periphery of the atom); n is the effective quantum number, which increases by unity for each successive absorption line; τ_n, $\tau_{n+1}\dots$ are the peak heights of the successive absorption lines; τ_∞ is the intensity of continuous absorption (the peak height of the true edge); Γ is the total width (in Rydbergs) of the absorption lines at half-height; and Ry is the Rydberg constant.

Actually, formulas (1) and (2) constitute a set of several equations that enable one to reproduce the entire shape of the main absorption edge for given values of Γ, η and n. The value of Γ can be ascertained directly from experiment; the values of η and n, on the other hand, are determined so that the calculated shape of the edge will fit the experimental curve. Since calculation of K absorption spectra entails reproducing the shape of the main edge over its entire extent, the above procedure makes it possible to reduce the effect of various errors (experimental, as well as calculation errors due to inaccurate determination of the

---

*By the atom's periphery we understand the region outside its filled shells.

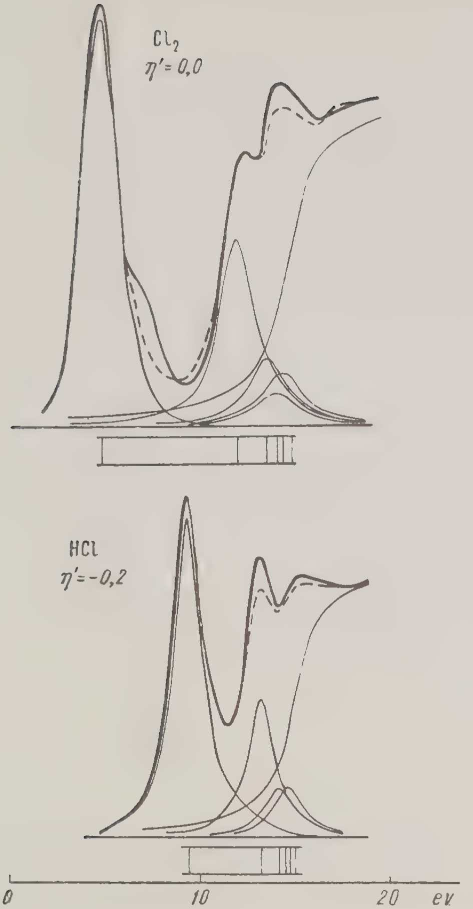

Fig.1. K absorption spectra of chlorine in Cl_2 and HCl. Here and in the following figures: heavy solid line = experimental absorption curve; dash line = integral theoretical curve; thin solid lines = true edge and absorption lines whose positions are indicated by the vertical strokes under the spectra.

edge parameters) on the determination of η and n. The method is particularly sensitive as regards determination of η (see Fig.1 in Ref.1).

The choice of values for Γ, η and n involves a certain arbitrariness (associated with the lack of definiteness in the structure of the experimental absorption curve). This does not mean, however, that just any shape of the absorption edge is reproduced by this method. Actually, our procedure for determining η and n (especially in those cases when the edge has clear structure) can be considered as approximate solution of several equations with two unknowns. Hence there can be reproduced only such curves as satisfy the condition of consistency of Eqs. (1) and (2). Thus we also obtain an experimental check on the theory. In practice, in calculating the main K absorption edge by means of Eqs.(1) and (2) with the aim of determining the values of η and n, we generally took into account four or five successive absorption lines (four or five equations in each set (1) and (2)), which were assumed to have a Lorentzian shape with the same width Γ. The shape of the true edge was chosen in the form of an arc tangent curve (of width Γ). A first approximation for η and n was found by means of the first two equations of the set.

The parameters Γ, τ_n/τ_∞ and $\mathscr{E}_\infty - \mathscr{E}_n$ in these two equations were measured as follows. The value of Γ was determined from the long wavelength branch of the experimental curve. For the second parameter we generally chose the ratio of the height of the first absorption line, standing out clearest in the experimental curve, to the height of the true edge, i.e., τ_n/τ_∞. In this connection it should be borne in mind that formulas (2) contain the ratio of the area (and not the height) of the absorption line to the height of the true edge $(\pi\Gamma\tau_n/\tau_\infty)$. For this reason the experimental errors arising from incorrect choice of absorber thickness and leading to especially pronounced distortion of the first absorption line, or the broadening of this line due to splitting of levels in the field of the molecule or crystal (see, for example, the spectrum of zinc in $Zn(C_6H_5)_2$ in Fig.4), affect the results of calculation much less than would be the case if Eq.(2) contained the ratio of the height of the line to that of the edge. For the third parameter we chose either the hypothetical distance between the first absorption line and the true edge $(\mathscr{E}_\infty - \mathscr{E}_n)$, or the distance between the first two absorption lines $(\mathscr{E}_{n+1} - \mathscr{E}_n)$, if the second absorption line stood out clearly enough in the experimental curve. The remaining equations of

Molecule	Absorbing atom	n	η'	Charge according to Pauling
Cl_2 gas	Cl	1,18	$+0,0_1$	0
HCl "	Cl	1,25	$-0,2$	$-0,17$
$GeBr_4$ "	Ge	1,9	$+0,7_5$	$+0,8$
	Br	1,33	$-0,1_5$	$-0,2$
GeH_4 "	Ge	2,1	$+0,2$	$+0,2$
$ZnBr_2$ "	Zn	1,9	$+0,5$	—
	Br	1,08	$-0,2_4$	—
$Zn(C_6H_5)_2$ crystal	Zn	1,12	$+0,2$	$+0,3$
$Zn(C_5H_7O_2)_2$ "	Zn	2,4	$+1,8$	$+1,0$
$K_3Fe(CN)_6$ "	Fe	1,7	$+1,0$	—
$Fe(CO)_5$ gas	Fe	1,3	$+0,4$	—
$Fe(CO)_5$ liquid		1,3	$+0,4$	—
K_2CrO_4 crystal	Cr	1,04	$\pm0,_1$	—
$Cr(CO)_6$ gas	Cr	1,4	$+0,4$	—
$Cr(CO)_6$ crystal		1,4	$+0,4$	—

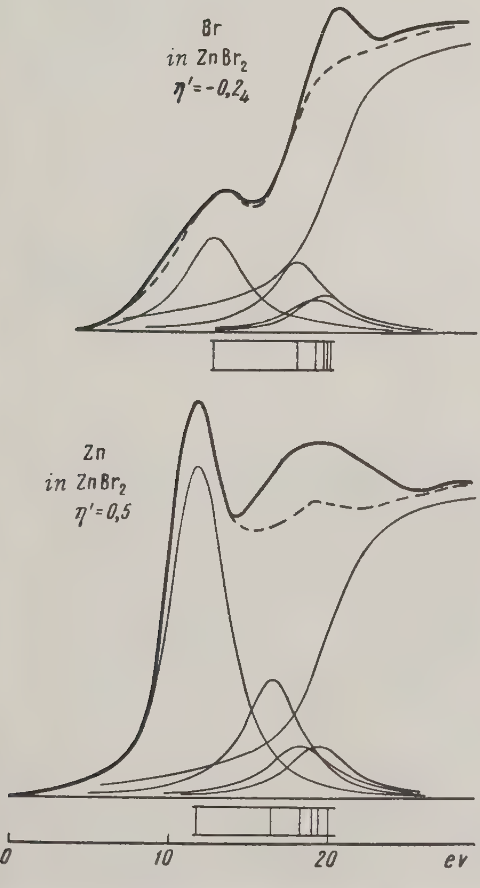

Fig.2. K absorption spectra of zinc and bromine in the gaseous $ZnBr_2$. The two spectra are plotted to make the limits of their Rydberg series coincide.

the set (1) & (2) were then used to evaluate all three parameters (as well as η and n) with the necessary accuracy to secure coincidence of the calculated and experimental curves. The error in determining the value of η by this method lies in the range 2 to 10%.

The results of calculating the K absorption spectra of some atoms in different chemical compounds are shown in Figs.1 through 6. The experimental K absorption curves are taken from Refs.2-6. The calculated values obtained for the effective quantum number n and effective charge $\eta' = \eta - 1$ are shown in the accompanying table.

In the last column of the table we list the values of the charge of these atoms in compounds as calculated by Pauling's method[7] from the electronegativity values. In the case of zinc the electronegativity was determined from the x-ray spectrum of zinc in $ZnBr_2$ and the resultant value (1.65) was used to calculate the charge of zinc in the compounds $Zn(C_6H_5)_2$ and $Zn(C_5H_7)_2)_2$. As will be evident from the table, in simple cases Pauling's method, despite its limitations, yields the same value for the charge of the atom as that obtained from the x-ray spectra. Since Pauling's method is apparently inapplicable to the last four compounds, the corresponding values have been omitted.

It is evident that in the case of the $ZnBr_2$ molecule the effective charge (+0.5) concentrated in the region of the Zn atom is approximately equal in absolute magnitude and opposite in polarity to the sum of the effective charges (-0.24 each) concentrated in

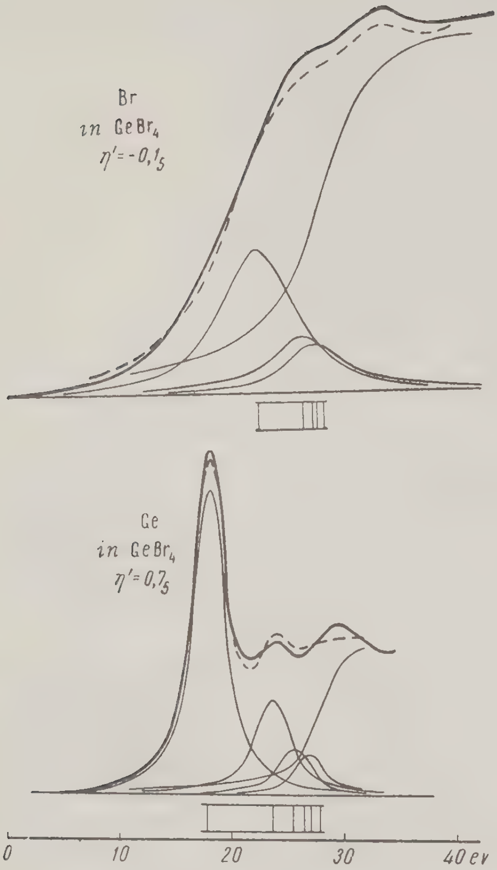

Fig.3

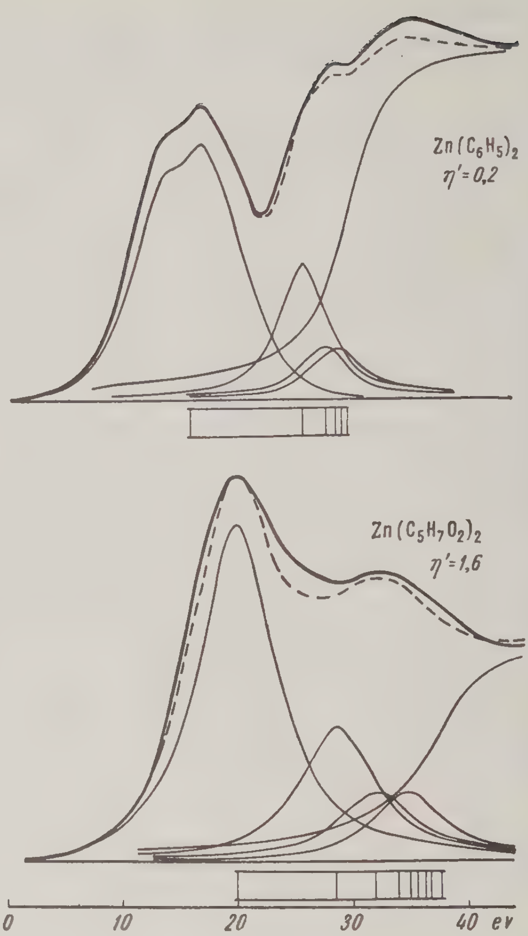

Fig.4

Fig.3. K absorption spectra of germanium and bromine in the gaseous $GeBr_4$. The spectra are plotted to make the limits of their Rydberg series coincide.

Fig.4. K absorption spectra of zinc in complex compounds. The relative location of the spectra was taken from Ref.5. In calculating the spectrum of $Zn(C_6H_5)_2$ the area of the first line (an unresolved doublet) was taken directly from the experimental curve. The widths of the remaining lines and true edge were taken so as to secure the best fit of the integral curve (dash line) with the remaining section of the spectrum. The value of η' (in this particular case) varies in the range from 0.2 to 0.3 for a factor of two variation in the area of the first line.

the environs of bromine atoms. The same situation (within the limits of the calculation error) obtains in the case of the $GeBr_4$ molecule. This leads to the natural conclusion that the whole molecule is electrically neutral, which again shows that the effective charges obtained for atoms in compounds by the present method have a genuine physical meaning.

The tabular data also show that the charge of the central atom in the complex practically does not depend on the state of aggregation of the substance and is determined primarily by the character of the immediate environment. The influence of the crystal field (as Joos & Peter[6] have pointed out) is evinced only in some degree of smoothing out of the structure of the spectrum.

Some K absorption spectra, for example, the spectrum of chlorine in Cl_2 (to the right of the first absorption line in Fig.1), zinc and bromine in $ZnBr_2$, and germanium in $GeBr_4$ exhibit an additional absorption peak, the origin of which cannot be interpreted within the framework of the simple model involving one Rydberg series. It is possible that the appearance of this peak is associated with the presence of a molecular level, upon arriving on which the K electron loosens one of the chemical bonds. One may assume that this level also appears owing to another cause, for example, splitting of the first levels of the Rydberg series in the field of the molecule.

The results of our calculations warrant sketching the following picture: in the process of K absorption the photoelectron from the K shell shifts over (if only for the first absorption lines) not to the periphery of the entire molecule, as was suggested earlier[8], but rather to the immediate vicinity of the absorbing atom. The electron moves in the field comprised of the unit positive charge of the atom (the hole in the K shell) plus effective charge at the atom's periphery; the effective charge is due the participation of the atom in the chemical bond and to redistribution of the density of its valence electrons. If the magnitudes of the radii* corresponding to the first free energy levels of the ejected K electron are rougly evaluated on the basis of the experimental data for η and n resulting from calculation of the K absorption spectra of the indicated atoms, it is found that the values for these radii are consistent with the picture we have been sketching. These values lie close to those for the covalent radii of chlorine and bromine in Cl_2 and Br_2 molecules and the ionic radius of the Zn^{2+} ion in solution. For atoms in other compounds the radii evaluated in this manner have values intermediate between those for the covalent and ionic radii of these atoms and reflect in the main correctly the tendency for the magnitude of the radius to vary with the charge of the given atom in different compounds.

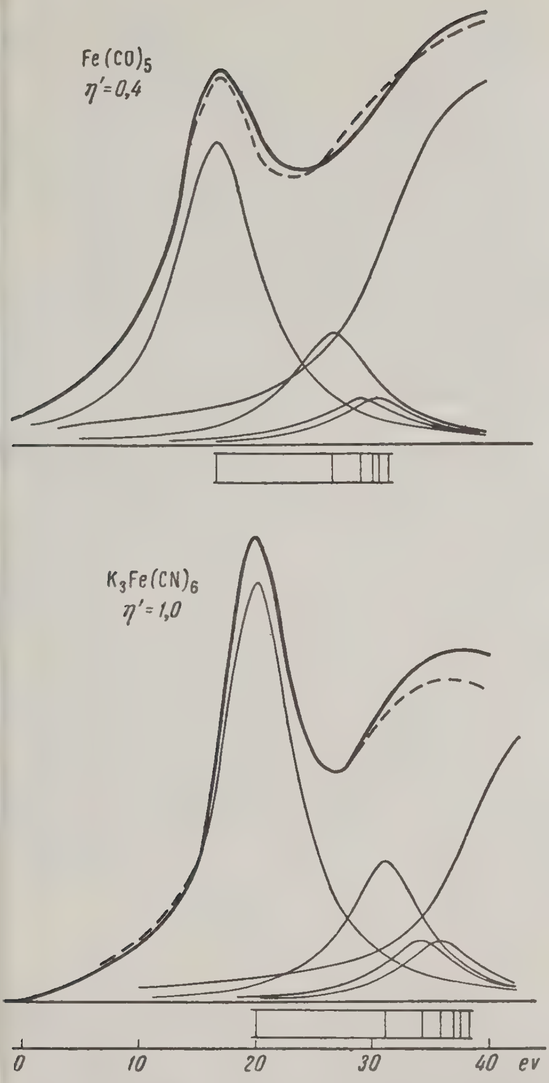

Fig.5. K absorption spectra of iron in complex compounds. The relative location of the spectra was taken from Ref.5.

---

*Roughly speaking, the radius of a sphere inside of which the effective charge of the atom is concentrated.

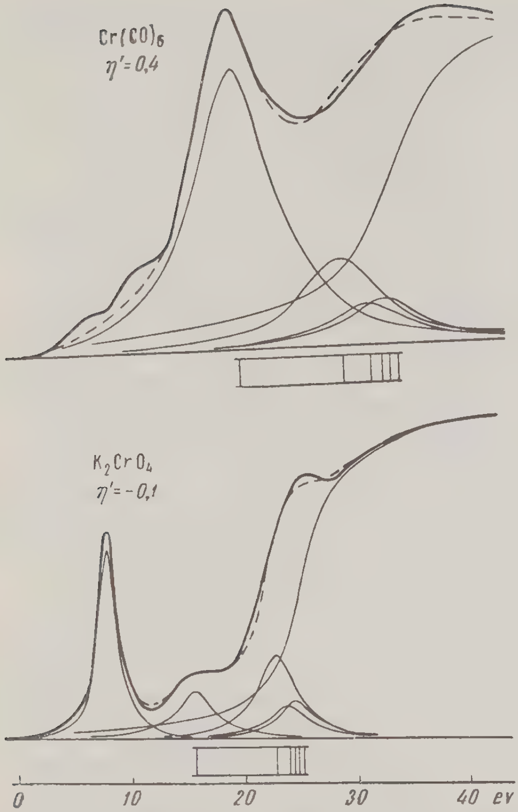

Fig.6. K absorption spectra of chromium in Cr(CO)$_6$ and K_2CrO_4. The relative location of the spectra was taken from Ref.5. Calculation of the spectrum of K_2CrO_4 using the first narrow absorption line is impossible. This result once again confirms the indirect inference regarding the origin of this line (hybrid *3d* level of chromium) drawn in Ref.9.

It is legitimate to conclude from the foregoing that, in a sense the electron ejected from the atom's K shell constitutes a "probe charge" located in that part of the molecule which is in the immediate proximity of the investigated atom, and as such enables us to determine the effective charge in this part of the molecule. By investigating the K absorption spectra of all components of the molecule, it is possible, as has been shown for the cases of zinc and bromine in $ZnBr_2$ and germanium and bromine in $GeBr_4$, to determine the effective charge in different parts of the molecule.

When comparing the present method with other methods for determining charges, for example, from the dipole moments or (recently) nuclear quadrupole interaction, it should be borne in mind that the application of the earlier methods is restricted to cases of the most simple, (primarily diatomic) molecules, inasmuch as the difficulty of charge determination by these methods increases with increasing complexity of the molecule. In contrast, in the case of the method considered here, the difficulty of determining the charge does not increase provided the symmetry of the molecule does not deviate too much from spherical; moreover, the method is suitable even for complex compounds.

Conclusions

1) The method proposed in our previous paper[1] has been used to calculate the K absorption spectra of atoms in gas and crystal molecules.

2) The calculations led to the determination of the values of the effective charges of atoms in compounds (see Table). In those cases where these values can be compared with other data, good agreement is obtained. It was also shown that the charge of the central atom in a complex compound is determined mainly by the character of its immediate ambiance.

3) The effective charge in different parts of a molecule can be determined by investigating the K absorption spectra of the components of the molecule.

Institute of Rare Elements of the
Academy of Sciences of the USSR and
Physical Institute of the
Bulgarian Academy of Sciences

References

1. E.G.Nadzhakov & R.L.Barinskii, Doklady AN SSSR, 129, 1279 (1959). (Trans. Soviet Physics - Doklady.)
2. S.T.Stephenson, R.Krogstad & W.Nelson, Phys.Rev., 84, 806 (1951).
3. K.I.Narbutt, Doklady AN SSSR, 93, 21 (1953); Izv.AN SSSR, Ser.fiz., 20, 780 (1956). (Trans.Bulletin,20, 710.)
4. H.Glaser, Phys.Rev., 82, 618 (1951).
5. K.Böke, Z.phys.Chem., BRD, 10, 59 (1957).
6. G.Joos & K.H.Peter, Ibid., 18, 74 (1958).
7. L.Pauling, The Nature of the Chemical Bond and the Structure of Molecules and Crystals, Cornell Univ.Press, 1942. (Cited in Russian trans.)
8. E.E.Vainshtein, R.L.Barinskii & K.I.Narbutt, Zhur.eksp.i teor.fiz., 23, 593 (1952).
9. R.L.Barinskii, E.E.Vainshtein & K.I.Narbutt, Doklady AN SSSR, 83, 199 (1952).

DETERMINATION OF THE CHARGE AND TYPE OF BOND OF OSMIUM IN COMPOUNDS FROM THE L_{III} ABSORPTION SPECTRA

- E.G.Nadzhakov & R.L.Barinskii

The question of the nature of the chemical bonds in complex compounds of the transition elements has long attracted the attention of numerous investigators. Particularly many studies have been devoted to the properties of compounds of the transition elements of the Third Period. Of late these studies have been supplemented by investigations of the x-ray absorption spectra of Cr, Mn, Fe, Co and Ni atoms in complex compounds.[1-5]

Apart from data on hybridization of the orbits of the metal atom, Kauer[1] and Böke[2] also tried to obtain information on the magnitude of the atomic charge in complex compounds. Using virtually the same experimental material on x-ray spectra, they arrived at contrary conclusions regarding the charge of the central atom in similar type compounds. Thus, Kauer[1] holds that the charge of Fe in $K_4Fe(CN)_6$ is approximately +1, whereas Böke[2] estimates the charge to be -4. Both authors use Kunzl's rule or the closed cycle for their evaluations. Neither author refers to any other objective data for gaging the magnitude of charge of the central atom.

In earlier contributions[6,7] we proposed a method for calculating the effective charge of the atoms bound in molecules and crystals from K x-ray absorption spectra. The accuracy in determining the magnitude of charge by this method is better than 10%. Application of this method to the calculation of the K absorption spectra of Fe, Cr and Zn in complex compounds of these elements made it possible to find the magnitude of the effective charge of the Fe, Cr and Zn atoms.

The present article contains experimental material on the L_{III} absorption spectra of Os in its complex compounds. It should be noted that in contrast to the x-ray spectra of transition elements of the Third Period, the x-ray spectra of elements of the palladium and platinum groups have scarcely been studied. We have almost no information on the type of chemical bonds formed by these elements in complex compounds.

Some data has recently been published by Belova & Syrkin[8] regarding the magnetic susceptibility of osmium complexes. From these data the authors arrive at certain deductions regarding the type of hybridization of the Os orbits in these compounds. They also discuss the possible charge of atoms of transition elements in complex compounds. In this connection we thought it might also prove interesting to apply the computational method of Refs.6 and 7 to the L_{III} absorption spectra of osmium (particularly, since no one has hitherto undertaken to resolve the L absorption spectra into a line series and a true edge).

Experimental Procedure

The L_{III} absorption spectra of Os were investigated on a vacuum x-ray spectrometer with quartz crystal bent to a radius of 0.5 m. The spectra were recorded by a Geiger counter in the fourth order. The dispersion was 3.85 X/mm; the resolution ~8000. Anode - silver. Reference lines - the Ni $K\beta_1$ and Cu $K\alpha_{1,2}$ lines in the third order of reflection. The anode current was stabilized by means of an electronic stabilizer within ±0.5%, while the voltage was not regulated. The main L_{III} absorption edge of Os was measured at points 0.05 mm apart with a 0.04 mm slit in front of the counter.

We carried out special experiments aimed at stabilizing the intensity and insuring reproducible results with the given equipment. Our tests showed that the usual unilateral shift in intensity, persisting over several hours, can be eliminated by arranging the collimating devices so that the entire effective x-ray beam is incident on the crystal without being cut off by the aperture edges.

This indicates that the variation in intensity is due to shifting of the focal spot over the anode of the demountable tube. With the proper collimating arrangement it is feasible to obtain reproducible intensity values (within ±2%) even after admitting air into the spectrometer tank.

Under the selected operating conditions for the x-ray tube (40 kv and 8 ma) the intensity amounted to $(5\text{-}6)\cdot10^3$ pulses per min. The edge of Os was recorded 10 times with a 2 minute reading at each point in each run. This procedure smoothed out the long term fluctuations associated with slow voltage variation and any residual shifting of the focal spot.

The root mean square error of the averaged curve (in pulses/2 min) was evaluated to be 46. For the purely statistical character of the fluctuations the rms error amounted to 37. For one of the spectra we calculated the minimal value of the rms error incident to a shift of the individual measurements along the vertical. It turned out to equal the purely statistical value. Thus the rms error in intensity amounts to 0.3-0.4%, while the error in the relative height of the spectrum amounts to 2%.

The intensity of the radiation passing through the sample equals

$$I = I_0 e^{-\mu_0-\mu} + \sum_\lambda I_\lambda e^{-\mu_\lambda},$$

where I_0 is the initial intensity in the fourth order of reflection, I_λ is the radiation intensity of the other wavelengths, μ_0 is the "absorption coefficient" for all electrons except those of the L_{III} shell of osmium (it is the product of the linear absorption coefficient by the thickness of the sample), μ is the coefficient for the L_{III} electrons of osmium and radiation in the fourth order of reflection, and μ_λ is the absorption coefficient of the whole substance for the spurious wavelength λ. In order to obtain from this equation an unambiguous relation between the known value of I and the coefficient μ that interests us, we must make a correction for the variation in the investigated 2.4 mm long region of the spectrum of the quantities $A = I_0 e^{-\mu_0}$ and $B = \sum_\lambda I_\lambda e^{-\mu_\lambda}$. The latter quantity represents the background, which in our case attains 60% of the total intensity as a consequence of operating in the fourth order of reflection. We can assume that in the working range, these variations are linear with a slight slope. They are due to variations of I_0 and I_λ because of geometric factors, as well as to variations of μ_0 and μ_λ with the wavelength.

First, we found the slope of $I_0 + \sum_\lambda I_\lambda$ (without an absorber) by drawing a straight line through the averaged points by the least-squares method. The slope amounted to 0.6% mm^{-1} (the variation in percent relative to the total intensity over the 1 mm focal circle). Next, we determined the slope of $A + B$ with 0.06 and 0.14 mm thick aluminum absorbers. In both cases it amounted to 1.5% mm^{-1} (the thicknesses of the Al absorbers were so selected that the absorption coefficients μ_0 for the wavelength of the L_{III} edge of osmium would encompass the entire range of values of μ_0 for the investigated compounds of Os; this being the case, the Al should yield approximately the same slope due to variation of μ_0 and μ_λ as the Os compounds). Thus experiments showed that the slope of $A + B$ hardly changes with the absorption coefficient within the indicated range. Moreover, theoretical calculations of the change in slope of A owing to a change of μ_0 lead to the conclusion that when the thickness of Al is changed from 0.06 to 0.14 mm, the slope of A changes from 1 to 1.4% mm^{-1}. Therefore we can assume (especially for thicknesses close to 0.14 mm) that A and B have the same slope and that both terms become constant if the value of I is corrected for this slope.

After this correction, we can write

$$\nu = \frac{I_l - I}{I_l - I_S} = \frac{1 - e^{-\mu}}{1 - e^{-\mu_S}},$$

where I_l is the intensity on the long wavelength side of the edge ($\mu = 0$), and I_S is the intensity on the short wavelength side ($\mu = \mu_S$). In Fig.1 the values of ν are laid off along the vertical axis. For small values of μ and μ_S we have $\nu = \mu/\mu_S$, for large values of μ and μ_S distortions set in. In order to ensure that the distortions and errors would be approximately the same, we took samples of the different Os compounds weighed out to contain the same amount of osmium (3 mg/cm^2). This quantity of the sample substance (rubbed into cigarette paper) secured a reasonable compromise between the distortions and measurement accuracy. By appropriate addition of Al the magnitude of μ_0 was reduced to the equivalent of ~0.12 mm of Al, which increased the accuracy by weakening the soft component of the background and provided greater accuracy in taking into account the slope. With this measurement procedure, the distortion in the value of the ratio of the peak of the discrete selective line ($\mu = \mu_d$) to the edge ($\mu = \mu_S$) equalled

$$\frac{(\mu_d/\mu_S) - \nu}{\mu_d/\mu_S} \cdot 100 = 10\text{-}20\%$$

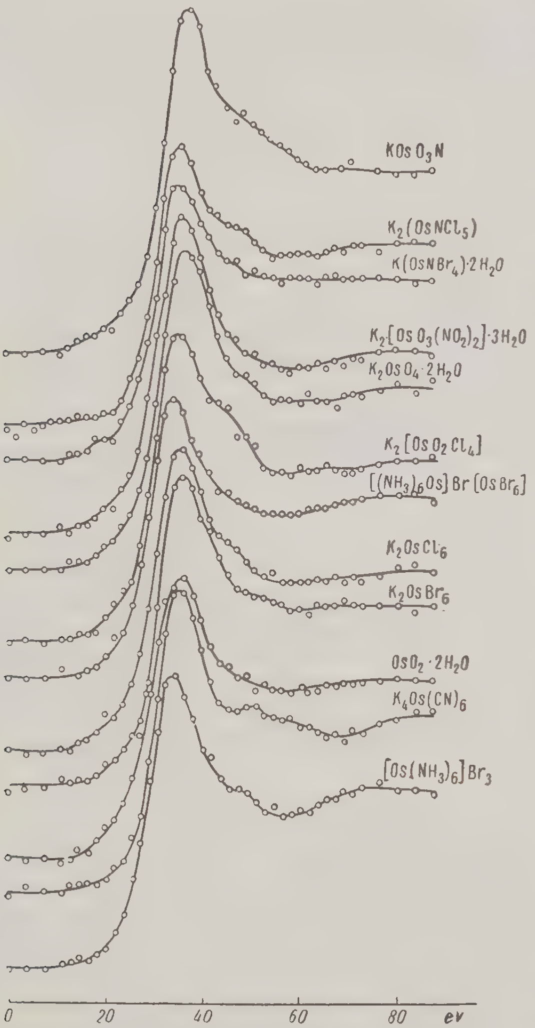

Fig.1. L_{III} absorption spectra of Os in complex compounds. The relative values of the absorption coefficient are laid off along the vertical axis (not shown in the figure).

Fig.1 shows the relative values of the absorption coefficient for the L_{III} shell of Os (the value ν) inasmuch as it is difficult to determine the absolute values with sufficient accuracy owing to the strong and varying background. Nevertheless (using the tabular value of the L_{III} absorption discontinuity), we can assume that the value of the L_{III} shell mass absorption coefficient corresponding to $\nu = 1$ is ~125 cm^2/g.

Results

Fig.1 shows the experimental data for the L_{III} absorption spectra of Os in complex compounds. The compounds were so chosen to cover the entire valence range of Os (from 8 to 2), and the inner coordination sphere of the complex contained different groups of elements.

As can be seen from Fig.1, the L_{III} absorption spectra of Os in complex compounds change very little for even a great change in valence and character of

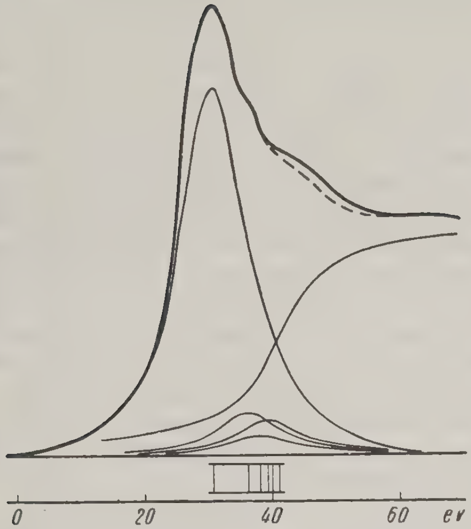

Fig.2. L_{III} absorption spectrum of Os in $KOsO_3N$ ($\eta' = 1$). Here and elsewhere the heavy solid line is the experimental absorption curve; the dashed line is the integral theoretical curve, and the light lines are the true edge and the absorption lines, whose positions are indicated by the vertical bars under the spectra.

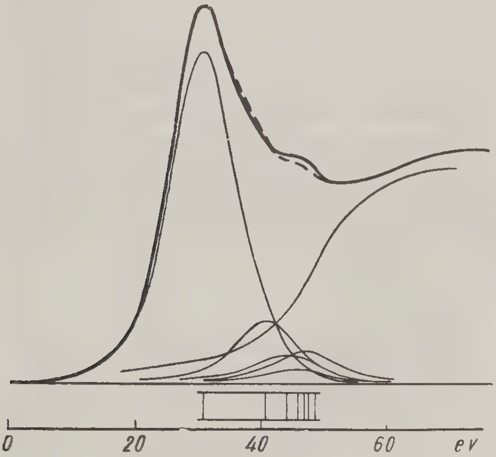

Fig.4. L_{III} absorption spectrum of Os in $(Os(NH_3)_6)Br_3$($\eta' = 1$).

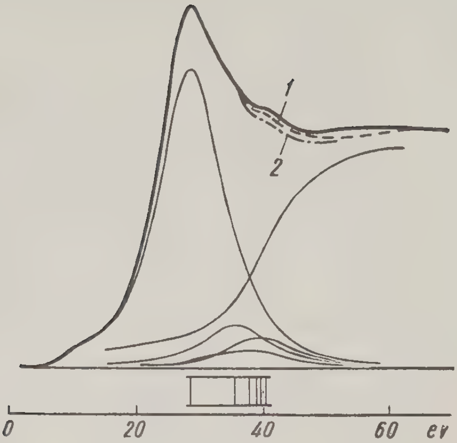

Fig.3. L_{III} absorption spectrum of Os in $K(OsNBr_4)\cdot 2H_2O$ ($\eta' = 0.7$). 1 is the integral theoretical curve corresponding to the best approximation of the spectrum ($n = 1.8$, $\eta = 1.7$); the dot-dash curve 2 ($n = 2$, $\eta = 2$) illustrates the attempt to approximate the spectrum for the given value of η. As can be seen, change of η by 0.3 significantly impairs the accuracy of approximation.

the immediate environment of Os. There is no noticeable shift of the first absorption line, nor are any substantial changes in the general form of the spectrum observed. On the whole, there are changes only in the height of the first absorption line and the depth of the minimum in the region of 60 ev.

We calculated the L_{III} absorption spectra of Os using the method described in Refs.6 and 7. We assumed that the $5d$ states of Os are responsible for the first absorption line in the L edge (dipole transition L_{III} — $5d$) and that by virtue of their special properties, associated with filling of the $5d$ levels in this group of elements, they may not belong to the Rydberg series. For this reason the calculation should be carried out beginning with the second absorption line. If we recall that the L_{III} electron of Os must go over to one of the s or d levels, we see that the direct use of Eq.(2) of Ref.7 cannot be justified a priori. Nevertheless, this formula yields a better result in the sense of approximation of the L_{III} edge than the corresponding formulas for the transition probability of an L_{III} electron. This is the very reason we settled in favor of using Eq.(2) even though admittedly there is less physical justification for this calculation method than in the case of K spectra.*

The calculation of the L_{III} absorption spectra of Os was carried out by the method described in Ref.7. We found that the values of η and n practically do not depend upon whether the position (but not the height) of the first absorption line is chosen as the first line of the Rydberg series, or whether the entire calculation is carried out beginning with the second line. Taking into account all that has been said above, it can be noted that the error in determining the value of η is greater than the error in calculating K absorption spectra and that this error can attain 15% (cf. Fig.3).

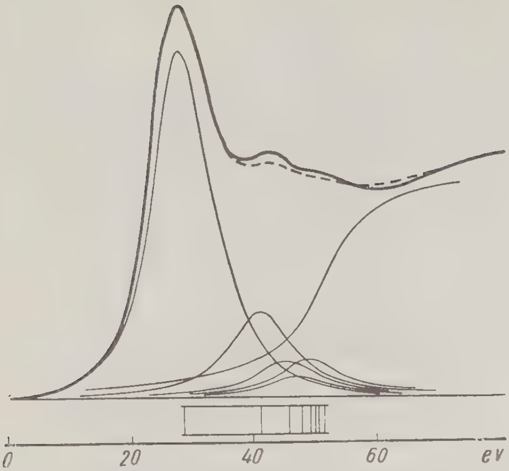

Fig.5. L_{III} absorption spectrum of Os in $K_4Os(CN)_6$ ($\eta' = 1.5$).

The results of calculating the L_{III} absorption spectra of Os in complex compounds are shown in Figs.2-5 and the table. Examination of the data in the second and third columns of the table enables one to understand the above-noted similarity as regards the appearance and position of the L_{III} spectra of Os regardless of its valence and the character of the environment (nearest neighbors) of the Os atom complex. When the valence of Os changes from 8 to 2, its effective charge (η') varies within the range +0.7 to +1.5. Therefore it follows that in complexes of octa- and hexavalent Os there predominates a covalent type of bond; this becomes increasingly ionic as we go to tri- and divalent compounds. A rough evaluation of the radius of the sphere in which the effective charge of Os is distributed, leads to the same conclusions. It turns out to lie close to the covalent radius of Os.

As has been pointed out above, in calculating the L_{III} absorption spectra of Os we did not take into account the height of the first absorption line. This height can, however, be determined from the calculation data on the assumption that the position of the first absorption line coincides with the position of the first line of the Rydberg series. This procedure can be justified as long as it does not affect the calculation results. It turned out that the height of the

Molecule	n	Charge	τ_{exp}/τ_{theo}	Molecule	n	Charge	τ_{exp}/τ_{theo}
$KOsO_3N$	2,3	1,0	3,5	$K_2[OsCl_6]$	1,9	0,8	2,7
$K[OsNBr_4]\cdot 2H_2O$	1,8	0,7	2,6	$K_2[OsBr_6]$	1,8	0,7	2,6
$K_2[OsO_2Cl_4]$	1,9	0,8	2,7	$OsO_2\cdot 2H_2O$	1,9	0,8	2,5
$K_2[OsNCl_5]$	1,8	0,7	2,6	$[(NH_3)_6Os]\ Br[OsBr_6]$	1,8	0,8	2,3
$K_2[OsO_3(NO_2)_2]\cdot 3H_2O$	1,9	0,8	2,7	$[Os(NH_3)_6]Br_3$	1,8	1,0	1,9
$K_2OsO_4\cdot 2H_2O$	1,9	0,8	2,7	$K_4[Os(CN)_6]$	2,0	1,5	1,5

---

*It would be possible to understand this on the assumption that apart from the Coulomb potential there exists another term proportional to r^{-2}, which would lead to a change in the form of the n-dependence in Eq.(2) of Ref.7.

first line calculated in this manner was in all cases less than the experimental height; the ratios of the experimental to calculated heights are listed in the last column of the table. It will be seen that this ratio decreases regularly (within the limits of the calculation error) as one goes from Os compounds with valence 8 to compounds with valence 2. This phenomenon can be understood on the assumption that it is associated with the screening of the $5d$ levels of Os by its valence electrons. Then with the increasing ionic character of the bond as the transition is made to the hexamines and hexacyanides of tri- and divalent Os, a balancing of the effective charge at the periphery of Os and in the region of its $5d$ levels should take place, which is associated with the withdrawal of the valence (in this case, obviously $6s,p$) electrons of Os in the direction of the ligands. In the case of complexes of Os with a predominantly covalent type of bond, the effective charge in the region of the $5d$ levels of Os is obviously greater than in the region of the second and following absorption lines; hence in this case, the ratio τ_{exp}/τ_{theo} also increases sharply.

Conclusions

1. We investigated the L_{III} absorption spectra of complex compounds of Os in different valence states (from 8 to 2) (the inner sphere of the complexes contained different groups of elements).
2. First we carried out a resolution of the L spectra into an absorption line series and a true edge.
3. Calculation of the L_{III} absorption spectra of Os showed that the variation of the effective charge of Os in complexes falls within the range +0.7 to +1.5. Thus in complexes of octa- and hexavalent Os there predominates covalent bonding, but the bonding becomes increasingly ionic in going over to compounds of tri- and divalent Os.
4. The height ratio τ_{exp}/τ_{theo} for the first absorption line decreases regularly with decreasing valence of Os, which is obviously associated with the increasingly ionic character of the bonds and, as a consequence, the decreasing degree of screening of the $5d$ levels of Os by its $6s, p$ electrons.

All the above indicated compounds of Os were obtained from V.I.Belovaya, whom we take this opportunity to thank. The authors are also obliged to I.B.Markusfel'd and S.L.Yakovskom for assistance in performing the measurements.

Physical Institute of the Bulgarian Academy of Sciences,
Institute of Rare Elements of the Academy of Sciences of the USSR

References

1. E.Kauer, Z.Phys.Chem., BRD, 6, 105 (1956).
2. K.Böke, Z.Phys.Chem., BRD, 10, 59 (1957).
3. K.Böke, Z.Phys.Chem., BRD, 11, 326 (1957).
4. G.Joos & K.H.Peter, Z.Phys.Chem., BRD, 18, 74 (1958).
5. E.O.Fischer, G.Joos & E.Vogg, Z.Phys.Chem., BRD, 18, 80 (1958).
6. E.G.Nadzhakov & R.L.Barinskii, Doklady AN SSSR, 129, 1279 (1959). (Trans. - Doklady.)
7. R.L.Barinskii & E.G.Nadzhakov, Present issues of the Bulletin, p.419.
8. V.I.Belova & Ya.K.Syrkin, Zhur.neorgan.khim. (Jour. inorganic chemistry), 3, 2016 (1958).

ON THE ORIGIN OF SOME SATELLITES IN X-RAY SPECTRA

- Z.Gorak

In the present note we consider the origin of the Kα' and Kα_4 lines in the spectrum of neon and neighboring elements ($Z \leqslant 14$) and the origin of the Kβ' line in the spectrum of trivalent iron (Fe^{3+}).

Some authors[1,2] associate the Kα' and Kα_4 lines with simultaneous excitation of vacancies in the $1s$ and $2p$ shells. As a result of electrostatic and exchange interaction with an additional $2p$ vacancy, the Kα line $(1s \to 2p)$ presumably splits into three lines

$$1)\ 1s\,2p\,{}^1P \to (2p)^2\,{}^1D;$$

$$2)\ 1s\,2p\,{}^1P \to (2p)^2\,{}^1S;$$

$$3)\ 1s\,2p\,{}^3P \to (2p)^2\,{}^3P,$$

of which 1) and 2) have the same initial state. This makes it possible in the case of neon to determine their precise separation, inasmuch as the energy difference between the final states $(2p)^2\,{}^1S$ and $(2p)^2\,{}^1D$ is known from optical spectra[3]. In addition, the theory of atomic spectra yields a relative intensity of $I_1/I_2 = 5$ (Table 3 in Ref.4). The experiments[5,6] show that within the limits of the measurement error these theoretical expectations are indeed fulfilled in the spectrum of neon for the two line pairs: α' & α_4 and α'' & α_3'.

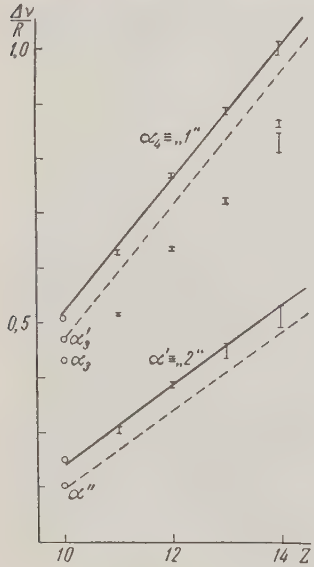

$$\frac{\Delta\nu}{R}(Z) = \frac{\nu_{\text{sat}}}{R} - \frac{\nu}{R}(K_\alpha).$$

The experimental data were taken from Refs.8-9. The uncertainties indicate the influence of the chemical bonds. The dashed lines show the incorrect positions of $\alpha_3' \equiv$ "1" and $\alpha'' \equiv$ "2".

To decide which one of the "doubtful" line pairs actually represents the "1" and "2" lines, it is necessary to use the following theoretical dependences:

$$\left(\frac{\Delta\nu}{R}\right)_1 = \left(\frac{\nu}{R}\right)_1 - \frac{\nu}{R}\,(K_\alpha) = 0.12093\ Z + b_1;$$

$$\left(\frac{\Delta\nu}{R}\right)_2 = \left(\frac{\nu}{R}\right)_2 - \frac{\nu}{R}\,(K_\alpha) = 0.07194\,Z + b_2.$$

The numerical values in these relations were obtained by means of the perturbation theory using hydrogen-like functions. Corrections for the influence of $3s\,p$ electrons were made by means of Slater's rules[7]. It was also assumed that one can disregard the multiplet structure that arises as a result of interaction between the unfilled $3sp$ shells and the vacancies in the $2p$ shell. The difference $b_1 - b_2$ can be determined for $Z = 10$ from the optical terms.[3]

The accompanying figure shows the straight line plots for $\left(\frac{\Delta\nu}{R}\right)_1$ and $\left(\frac{\Delta\nu}{R}\right)_2$ and their two possible positions. It is evident that the position for which $\alpha_4 \equiv$ "1" and $\alpha' \equiv$ "2" is more advantageous than the other position ($\alpha_3' \equiv$ "1", $\alpha'' \equiv$ "2"), inasmuch as it explains a greater number of experimental data[8,9].

The Kβ' line in the spectrum of Fe^{3+} arises in a manner analogous to that of the α' and α_4 lines. In this case it is assumed, in accordance with the ideas of Coster & Dryvesteyn[10], that the splitting of the Kβ line ($1s \rightarrow 3p$) is due to interaction of a $3p$ vacancy with the unfilled $(3d)^5$ shell. Instead of Kβ, there are obtained the two lines:

$$1)\ 1s\,(3d)^5\,{}^7S \rightarrow 3p\,(3d)^5\,{}^7P;$$

$$2)\ 1s\,(3d)^5\,{}^5S \rightarrow 3p\,(3d)^5\,{}^5P,$$

whose separation and relative intensity can be calculated theoretically. The order of magnitude obtained for these values by means of Slater's wave functions[7] agrees with the separation and relative intensity of the Kβ and Kβ' lines. Consequently, we can assert that Kβ ≡ "1" and Kβ' ≡ "2".

Institute of Technical Physics,
Czechoslovakian Academy of Sciences

References

1. E.H.Kennard & E.G.Ramberg, Phys.Rev., 46, 1034, 1040 (1934).
2. D.I.Candlin, Proc.Phys.Soc., A 68, 322 (1955).
3. Ch.E.Moore, Atomic Energy Levels, 1, 467, National Bureau of Standards, 1949.
4. E.V.Condon & E.G.Shortley, The Theory of Atomic Spectra. Cambridge, 1958.
5. H.R.Moore & F.C.Chalklin, Proc.Phys.Soc., A68, 717 (1955).
6. J.Drahokoupil, Vyzkumna zprava UTF, c.373, Ceskoslovensk. Akademie Ved, Praga, 1954.
7. J.C.Slater, Phys.Rev., 36, 57 (1930).
8. F.Tyren, Nova acta Regia soc.scient.upsaliensis, Ser.IV, 12, 1 (1940).
9. S.Flemberg, Z.Phys., 96, 167 (1935).
10. D.Coster & M.I.Dryvesteyn, Z.Phys., 40, 765 (1926).

CONCERNING INTERPRETATION OF X-RAY SPECTRA

- A.T. Shuvaev

Recently Karal'nik[1-3] and Varley[4] called attention to the possibility of explaining the shift of the last absorption lines and K edges of the transition elements of the iron group incident to change of the chemical bonds owing to displacement of the K level caused by change in the external screening in this level by $4s$ valence electrons. The K level shifts arising incident to removal of one $4s$ electron were evaluated by means of hydrogenic functions and proved to be of the order of a few electronvolts.

Hydrogenic functions, however, can only roughly characterize the density distribution of the valence electrons near the nucleus.[5] In connection with this, in the present work, we carried out evaluations of the external screening parameter by means of wave functions found by the method of the self-consistent field (Ref.6-8). The contribution of one $4s$ electron to the $1s$ level screening parameter was calculated by means of the expression

$$\sigma_{4s}(r_{1s}) = \int_{0}^{r_{1s}} \psi_{4s}^{2} r^{2}\,dr,$$

where ψ_{4s} is the wave function of the $4s$ level, and r_{1s} is the radius corresponding to the maximum in the density distribution of the $1s$ electron cloud. The results of our calculations for Ca, Fe and Zn atoms are listed in Table 1.

Table 1

Element	$\sigma_{4s}\cdot 10^4$	ΔE, ev
Ca	2,0	0,11
Fe	2,4	0,17
	1,5(av)	0,10
Zn	1,9	0,15

Table 2

Element	n_{4p}	$\sigma_{4p}\cdot 10^4$	$\Sigma_{4p}\cdot 10^4$
As	3	1,44	4,32
As^{+}	2	1,84	3,64
As^{2+}	1	2,26	2,26

For the iron atom we also calculated the mean external screening parameter for shielding of the $1s$ level by one $4s$ electron by means of the expression

$$\hat{\sigma}_{4s} = \int_{0}^{\infty} \psi_{1s}^{2}\sigma_{4s}(r)\, r^{2}\,dr.$$

The values of the shift ΔE of the K level owing to change in the screening parameter by the amount σ_{4s} were determined according to the formula

$$\Delta E = 13.6\cdot 2\,(Z - \sigma)\,\sigma_{4s},$$

where Z is the atomic number and $\sigma = 0.3$ is the internal screening parameter for the K level.

As will be evident from Table 1, the K level shift owing to removal of one $4s$ electron is very small and lies near the limit of measurement in x-ray spectroscopy. Moreover, incident to removal of a valence electron the external screening of the K level changes by an amount appreciably smaller than the contribution of this electron to the screening. This fact is illustrated in Table 2.*

Upon removal of one $4p$ electron in As the screening of the $1s$ level by all $4p$ electrons (Σ_{4p}) changes by an amount two times smaller than the screening by one $4p$ electron. This indicates that the possible K level shifts are appreciably

---

* n_{4p} is the number of $4p$ electrons in the atom or ion, and σ_{4p} is the manitude of the external screening of the $1s$ level by one $4p$ electron.

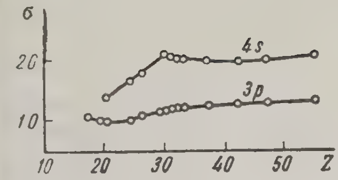

Fig.1. Variation of the internal screening parameter for the $4s$ and $3p$ levels in free atoms as a function of Z.

smaller than the values listed in Table 1. Thus the changes in potential in the region of the K shell produced by changes in the external screening by valence electrons have virtually no effect on the observed position of the K level.

In the present work we investigated the influence of changes in the internal screening parameter on the position of the Kβ_5 line in the spectra of transition elements of the iron group. Fig.1 shows the variation of the internal screening for the $4s$ and $3p$ levels according to the data of Hartree[5]. As will be evident from the figure, in the range of elements with Z = 20 to 29 the electron density between the $4s$ and $3p$ levels increases rapidly owing to filling of the $3d$ shell, which should have a substantial effect on the separation between these levels and in particular on the magnitude of $\sigma_{4s,3p}$, which is determined by means of Moseley's law:

$$E_{4s} - E_{3p} = E_{4s,\,3p} = \left(\frac{1}{n_1^2} - \frac{1}{n_2^2}\right)(Z - \sigma_{4s,\,3p})^2,$$

where E_{4s} and E_{3s} are the energies of the corresponding levels, and $n_1 = 3$ and $n_2 = 4$ are the principal quantum numbers of the respective levels. Fig.2 shows the variation of $\sigma_{4s,\,3p}$ and $\sigma_{4p,\,3p}$ with Z. Curves 1 and 2 were calculated using the theoretical values of the $3p$, $4s$ and $4p$ level energies calculated by the self-consistent field method for free atoms[6-11]. In plotting curve 3 the value of $E_{4p,\,3p}$ was determined from the energy difference between the K$\beta_{5,2}$ (K→N$_{II,III}$) and Kβ_1 (K→M$_{III}$) lines in the x-ray spectra of the pure elements in the solid state.* The data were taken from the tables of Ref.12.

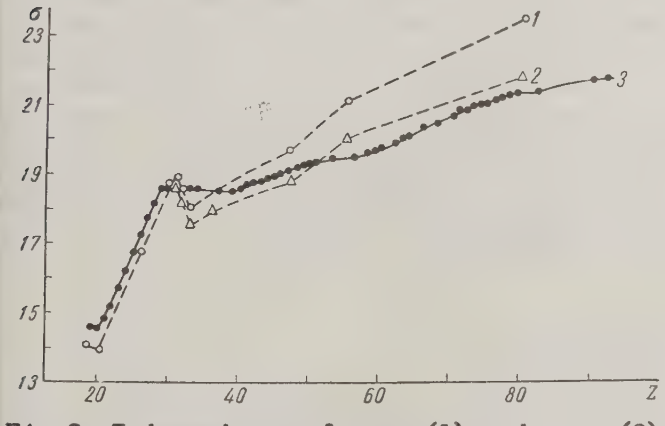

Fig.2. Z dependence of $\sigma_{4s,\,3p}$ (1) and $\sigma_{4p,\,3p}$ (2) for free atoms and for elements in the solid state (3).

It will be evident from Fig.2 that $\sigma_{4s\,,3p}$ and $\sigma_{4p,3p}$ increase with filling of the $3d$, $4d$, $4f$ and $5d$ shells, but in all other cases either remain constant or increase very slightly. If we assume that $\sigma_{4s,\,3p}$ and $\sigma_{4p,\,3p}$ in the Z = 20 to 29 region vary in direct proportion to number n_d of $3d$ electrons, then for a free iron atom we obtain $n_d = 6.05$ (curve 1), while for an iron atom in the metal we obtain $n_d = 6.8$ (curve 3). Calculations by the self-consistent field method[13] for metallic iron lead to $n_d = 7.2$.

Weiss & DeMarco[14] determined n_d from the atomic scattering factor for metallic iron and obtained a value of 2.3. Obviously, further investigation is necessary to determine which of these values is closest to the true one. From the shape of curve 3 in Fig.2 it follows that the separation between the K$\beta_{5,2}$ and Kβ_1 lines changes only incident to change in the number of $3d$ electrons; removal of a $3d$ electron leads to a shift of the Kβ$_{5,2}$ line to the short wavelength side inasmuch as the Kβ$_1$ line virtually does not change position. Change in the number of s,p electrons has practically no effect on the position of the Kβ$_{5,2}$ line.

---

*For Z > 40 the value of $E_{4p,\,3p}$ was determined from the energy difference between the Lγ_3 (L$_I$—N$_{III}$) and Lβ_3 (L$_I$—M$_{III}$) lines.

The above inference was checked experimentally for the case of the calcium compounds CaF_2, CaO and CaC_2. The number of s,p valence electrons in Ca in these compounds differs: the numbers are 0.2, 1.2 and 1.6, respectively as determined by Pauling's method. The position of the Kβ$_5$ line, however, remains the same in all these compounds. It must be noted that the above inferences are valid only for compounds with the same type of bonds. In the case of a radical change in the type of bond, changes in the character of atomic interaction will have an effect on the position of the last lines.

It is of interest to evaluate the shift of the Kβ$_{5,2}$ line incident to change in the number of d electrons in the atom. Inasmuch as upon removal of a $3d$ electron $\sigma_{4p,\,3p}$ changes by ~0.4 (see Fig.2), the corresponding change in energy will be

$$\Delta E_{4p,\,3p} = \frac{7}{72}(Z - \sigma_{4p,\,3p})\cdot 0.4 \approx 2.5 \text{ ev (for } Z = 26\text{)}.$$

In the event of redistribution of the valence electrons, for example, incident to transition of a d electron to the s state, $\sigma_{4p,\,3p}$ changes by a smaller amount than incident to removal of a d electron. Thus, for example, the values of $\sigma_{4p,\,3p}$ for the two configurations $3d_6\ 4s_2$ and $3d_7\ 4s_1$ in iron differ by 0.15.* The corresponding change: $\Delta E_{4p,3p} = 0.9$ ev. For manganese and copper the corresponding changes in $E_{4p,\,3p}$ incident to similar valence electron redistribution are 0.8 and 1.0 ev, respectively.

In many cases the above arguments and evaluations make it possible to interpret the changes observed in x-ray spectra. By way of example, one can offer interpretation of the results obtained in the work of Vainshtein & Kotlyar[15]. These investigators found that in Heusler alloy incident to transition through the ferromagnetic Curie point the Cu Kβ$_5$ line is shifted to the short wavelength side by 0.9 ev, and its width increases; the Mn Kβ$_5$ line is shifted 1.2 ev to the long wavelength side and becomes narrower. As was noted above, shift of the Kβ$_5$ line to the short wavelength side indicates decrease in the number of d electrons; increase in the width of the Kβ$_5$ line indicates increase in the number of p electrons (inasmuch as the Kβ$_5$ line characterizes the distribution of p states in the valence band). Thus in transition of the Heusler alloy from the ferromagnetic to the paramagnetic state, part (about one) of the copper d electrons go over into the p state In the Mn atom all the changes occur in the opposite direction, i.e., ~1.5 of the s,p electrons go over into the d state.

Conclusions

1. Change in the electron density in the region of the K shell of atoms owing to change in the external screening by the valence electrons incident to change in the character of the chemical bond has virtually no effect on the position of the K level.

2. Changes in the position of the Kβ$_{5,2}$ line (in elements with Z = 20 to 29) of atoms in compounds having bonds of the same type are determined primarily by changes in the number of d electrons. Removal of one d electron produces a ~2 ev shift of the Kβ$_{5,2}$ line to the short wavelength side. Redistribution of the valence electrons, i.e., $s \to d$ and $s \to p$ type transitions, lead to a similar but smaller (~1 ev) shift of the Kβ$_{5,2}$ line.

---

*In calculating $\sigma_{4s,\,3p}$ we used the level energies obtained by the method of the self-consistent field.[7,13]

References

1. S.M.Karal'nik, Izv.AN SSSR, Ser.fiz., 20, 815 (1956). (Trans.Bulletin, 20, 739.)
2. S.M.Karal'nik & S.Nizhnik, Ukr.fiz.zhur. (Ukrainian Physics Journal), 2, 333 (1957).
3. S.M.Karal'nik, Izv.AN SSSR, Ser.fiz., 21, 1445 (1957). (Trans.Bulletin, 21, 1432.)
4. J.H.Varley, Nature, 178, 939 (1956).
5. D.R.Hartree, Revs.Mod.Phys., 30, 63 (1958).
6. D.R.Hartree & W.Hartree, Proc.Roy.Soc., A149, 210 (1935).
7. M.Manning & L.Goldberg, Phys.Rev., 53, 622 (1938).
8. W.Hartree & D.Hartree, Phys.Rev., 59, 29 (1941).
9. D.R.Hartree, Proc.Roy.Soc., A143, 506 (1934).
10. D.R.Hartree, Phys.Rev., 46, 738 (1934).
11. B.H.Worsley, Proc.Roy.Soc., 247, 390 (1958).
12. E.E.Vainshtein & M.Kakhana, Spravochnye tablitsy po rentgenovskoi spektroskopii (Reference tables for x-ray spectroscopy)., M., 1953.
13. F.Stern, Phys.Rev., 104, 684 (1956).
14. R.Weiss & J.DeMarco, Revs.Mod.Phys., 30, 63 (1958).
15. E.E.Vainshtein & B.I.Kotlyar, Doklady AN SSSR, 110, 44 (1956). (Trans. Soviet Physics - Doklady.)

INVESTIGATION OF THE CORRELATION BETWEEN THE FINE STRUCTURE OF X-RAY ABSORPTION SPECTRA AND THE CHARACTERISTIC ELECTRON ENERGY LOSSES

- I.B.Borovskii & V.V.Shmidt

A number of investigators[1-4] have noted correlation between the characteristic energy losses of electrons in passing through thin films (or on being reflected from bulk samples) and the fine structure of the x-ray absorption spectrum. They sought a simple, unambiguous correspondence between the characteristic loss lines and the maxima or minima in the absorption on the short wavelength side of the main absorption edge. In this they were justified inasmuch as they considered the characteristic losses to be the result of inelastic pair collisions of incident fast electrons with the valence band electrons.[5,6]

If we assume that the characteristic losses are associated with excitation of plasma oscillations of the electrons in the sample (excitation of plasmons)[7], we can conceive of still another connection between the fine structure of the x-ray absorption spectrum on the short wavelength side of the main absorption edge and the characteristic electron energy losses[8].

In the present work, in the course of investigating the temperature dependence of the main K absorption edge of Fe, we obtained experimental proof of some correlation between the fine structure of the absorption edge and the characteristic losses. This has made it possible to refine the interpretation of the main absorption edge.

Our study was carried out on a double-crystal spectrometer with a resolution $\lambda/\delta\lambda = 11\,000$. The Fe absorber foil, held in a vacuum of $5 \cdot 10^{-6}$ mm Hg, was heated by passing an electric current through it. The experimental spectra are shown in Fig. 1. In the long wavelength part of the spectrum each point corresponds to recording of 12 000 pulses; in the short wavelength section to 6 000 pulses. The reproducibility was checked repeatedly.

In earlier measurements[9] of the reflection curve of the double-crystal spec-

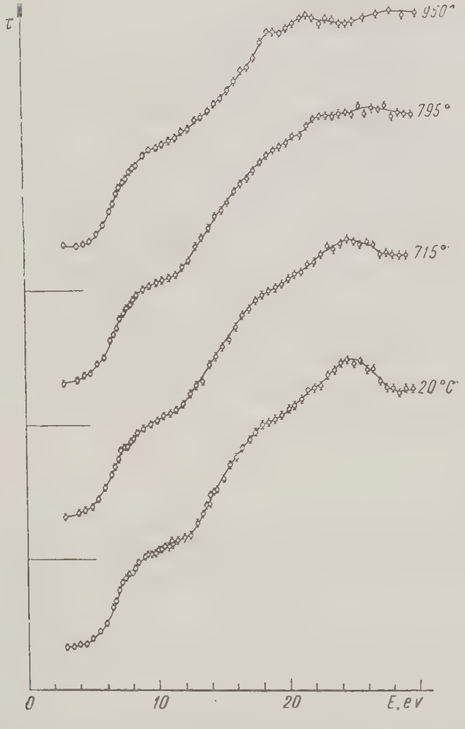

Fig.1

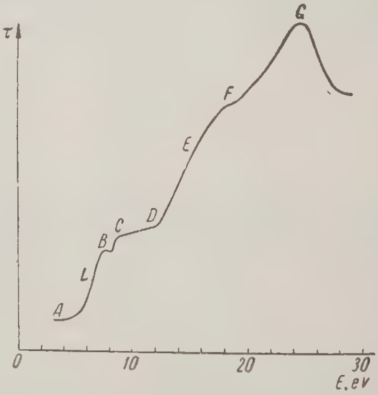

Fig.2

Fig.1. K absorption spectra of Fe at different temperatures; τ is the absorption coefficient.

Fig.2. Corrected absorption edge of Fe at room temperature.

trometer in the (1, -1) position, we showed that the distortion of the instrument has a Lorentzian shape. This made it feasible to correct the experimental curves by the method described in Ref.10. The corrected Fe absorption edge at room temperature is shown in Fig.2.

The long wavelength section of the absorption spectrum consists of a steep rise of the absorption coefficient (ALB), an absorption peak (B), and a horizontal plateau (CD). On the short wavelength side of the main edge, there is a hump (DEF) and a short wavelength peak (G).

The absorption curves are characterized by great stability of the shape of the initial absorption region ABCD, which undergoes no appreciable change even incident to Curie point transition (780°C) and the $\alpha \rightarrow \gamma$ transition (910°C). The inflection point L gives the location of the Fermi surface.

The shape of section DEF, on the other hand, changes markedly as a result of the $\alpha \rightarrow \gamma$ transition; the absorption maximum G goes down with increasing temperature and splits incident to the $\alpha \rightarrow \gamma$ transition.

We now turn to an interpretation of the experimental result. The absorption peak B, which is observed only for the transition elements of the Fe group[11] and coincides with Nilsson's h structure[12], corresponds to transitions of $1s$ electrons into the unfilled part of the $3d$ band.

According to Beeman and Friedman[13], the horizontal section CD is associated with transitions of $1s$ electrons into the unfilled part of the $4sp$ band, while the steep rise DEF is due to the beginning of transitions to the $4p$ band. According to Wilson[14], however, the absorption coefficient associated with transition of $1s$ electrons into the initial part of the $4p$ band, is proportional to $E^{3/2}$. This should yield a convexity in the direction of the energy axis in the absorption curve. Such a dip in the absorption coefficient curve is observed only for γ-Fe.

Beeman and Friedman[13] attribute the short wavelength absorption peak G to transitions of $1s$ electrons into the high density of states region N(E). However, as noted above, this peak has the following properties: it decreases with increasing temperature and turns into a col incident to the α-γ transformation; moreover, its position in the energy scale coincides well with the first long wavelength peak of the far short-wave structure calculated by Kostarev[15] and Shiraiwa et al[16]. In these studies the structure of the short wavelength part of the absorption spectrum is attributed to variation of the transition probability P(E) with the energy. The aforesaid properties of peak G convince us that it is associated with a variation of the transition probability P(E) and not with a variation of the density of states N(E).

We shall now show that the shape and temperature dependence of section DEF, can be explained by the effect of plasma oscillations of the electron gas in the metal, which distort the true shape of the absorption edge.

According to Sobel'man and Feinberg[8], it is highly probable that the absorption of an x-ray photon whose energy is close to that of the absorption edge will be accompanied by the simultaneous excitation of a plasmon. This means that if we observe a photon absorption peak, the spectrum should also exhibit another peak displaced to the short wavelength side of the first peak by an amount $\hbar\omega_p$ (the plasmon energy). Here

$$\omega_p = (4\pi n e^2 / m)^{1/2}$$

(where n is the number of electrons per unit volume participating in the plasma oscillations, and m is the effective electron mass). We shall call this peak the "plasma image" of the first peak.

Kleinn's work[17] on characteristic electron energy losses in Fe has shown that the first maximum is located some 7 ev from the line corresponding to elastically

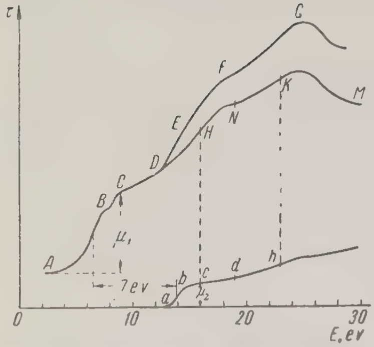

Fig.3. Separation of the true shape of the K absorption edge of α-Fe.

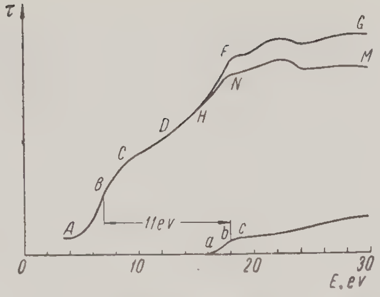

Fig.4. Separation of the true shape of the K absorption edge of γ-Fe.

scattered electrons. If we assume that this maximum is associated with plasmon excitation, it is natural to regard section DEF as a superposition of the true absorption edge and the plasma image of the initial section ABCD. The above noted stability of section ABCD, which does not vary materially either with temperature, crystal structure or introduction of Fe into some alloys, gives reason to infer that the true shape of the edge has a similar stability over the entire extent of the main absorption edge. In this case the change observed in shape of section DEF incident to the α→γ transformation can be explained on the assumption that $\hbar\omega_p$ changes incident to the α→γ transition, so that the plasma image is displaced to the higher energy side, thus "revealing" the true shape of the absorption edge.

On the basis of these considerations, we "resolved" the true shape of the K absorption edges of α- and γ-Fe (Figs.3 & 4). Curve ABCDEFG in Fig.3 is the experimental curve at 20°C. Section DH is a section of the experimental curve for γ-Fe. The difference between them is given by section *abc* of the difference curve. According to our hypothesis, this section represents the plasma image of section ABC. This construction enabled us to determine the relative scale μ_2:μ_1 for plotting the entire plasma image curve. Thus to section *abc* we added section *cdh*, corresponding to section CDH of the true curve. The resultant section *cdh* was subtracted from the experimental curve, giving section HK of the true curve. Proceeding in this manner, we obtained the hypothetical shape of the true absorption edge of Fe at 20°C (curve ADHKM).

Fig.4 shows the experimental curve for the K absorption edge of γ-Fe (ABCFG). Section DHN of the true edge of α-Fe is superposed on this curve. According to our hypothesis, the true edge of γ-Fe should have the same shape. In this case the difference curve *abc* again treated as the plasma image of section ABC, enables us to carry out the graphic analysis (as in the above case) and thereby bring out the true shape of the K absorption edge of γ-Fe (ABCHNM).

It is evident from Figs.3 and 4 that the plasma image is displaced to the higher energy side by 7 ev in the case of α-Fe and 11 ev in the case of γ-Fe.

Thus, by means of an internally consistent procedure (i.e., without adducing any data except the x-ray data), we obtained the true shapes of the absorption edges of α- and γ-Fe, as well as the values of $\hbar\omega_p$, namely, 7 ev for α-Fe and 11 ev for γ-Fe.

It is known that investigation of the characteristic energy losses of fast electrons in a metal essentially constitutes direct experimental determination of the plasmon energy for the metal. Therefore, in collaboration with Yu.M.Kushnir and A.N.Kabanov, we undertook special study of the variation of the characteristic electron energy losses in Fe as a function of temperature[18]. For this work we used an electrostatic electron-velocity analyzer[19] with a resolution of 0.5 ev. The electrons were reflected from samples prepared in the form of ~0.1 mm thick

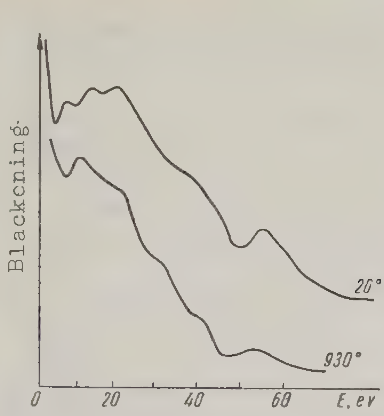

Fig.5. Photometric traces of the spectrum of characteristic electron losses in Fe.

plates, which could be heated by electric current in the vacuum ($\sim 5\cdot 10^{-6}$ mm Hg) chamber.

The photometric curves for α- and γ-iron are shown in Fig.5. Below we give the results of averaging of the photometric traces of 6 to 11 photographic plates.

These data show that a change in temperature from 20° to 800°C does not lead to any change in the characteristic loss, which amounts to 7.5 ev. The value of the characteristic electron energy loss does change abruptly incident to the $\alpha \to \gamma$ transition: it rises to 11 ev. In other words, we obtain complete agreement with the results from x-ray spectroscopy.

Thus, in the present work, we established the influence of plasma excitations of the electrons on the fine structure of the main K absorption edge of Fe; we clarified the interpretation of this structure and explained its variation with temperature.

Characteristic Loss Values in ev

$T = 20°$	7,5±0,7;	14,8±0,7;	21,5±0,6;	40±2;	55±2.
$T = 800°$	8,1±0,5;	13,2+0,7;	20,7±0,8;	43+2;	57±3.
$T = 950°$	11,0±0,6;	23±1;	33±0,5;	43±2;	54,4±0,7.

"A.A.Baykov" Institute of Metallurgy,
Academy of Sciences of the USSR

References

1. L.Leder, H.Mendlowitz & L.Marton, Phys.Rev., 101, 1460 (1956).
2. H.Watanabe, J.Phys.Soc.Japan, 9, 920; 1035 (1954).
3. H.Watanabe, Phys.Rev., 95, 1684 (1954).
4. Y.Coucois, Acta crystallogr., 5, 351 (1952).
5. A.Ya.Vyatskin, Zhur.tekh.fiz., 28, 2217 (1958). (Trans.Soviet Physics - Tech.Physics.)
6. A.Ya.Vyatskin, Ibid., 28, 2455 (1958). (Trans.Ibid.)
7. D.Pines, Solid State Physics, 1, 367 (1955).
8. I.I.Sobel'man & E.L.Feinberg, Zhur.eksp.i teor.fiz., 34, 494 (1958). (Trans., Soviet Physics - JETP.)
9. I.B.Borovskii & V.V.Shmidt, Izv.AN SSSR, Ser.fiz., 21, 1412 (1957). (Trans. Bulletin 21, 1400.)
10. I.Ya.Nikiforov, Ibid., 21, 1362 (1957). (Trans.Bulletin 21, 1351.)
11. I.B.Borovskii & V.A.Batyrev, Present issue of the Bulletin, p. 449.
12. A.Nilsson, Arkiv.fys., 6, 513 (1953).
13. W.W.Beeman & H.Friedman, Phys.Rev., 56, 392 (1939).
14. A.H.Wilson, The Theory of Metals, Cambridge 1936. (Cited in Russian trans.)
15. A.I.Kostarev, Zhur.eksp.i teor.fiz., 11, 60 (1941); Ibid., 19,413 (1949).
16. T.Shiraiwa, T.Ishimura & M.Sawada, J.Phys.Soc.Japan, 13, 847 (1958).
17. W.Kleinn, Optik, 11, 226 (1954).
18. I.B.Borovskii, A.N.Kabanov, A.N.Kushnir & V.V.Shmidt, Zhur.eksp.i teor. fiz., 38 (1960). (Trans.Soviet Physics - JETP.)
19. A.N.Kabanov & V.I.Milyutin, Radiotekhnika i elektronika, 4, 109 (1959). (Trans.Radio Engineering & Electronics.)

NOTE ON THE ASYMMETRY INDEX OF THE $K\alpha_{1,2}$ LINES OF THE TRANSITION ELEMENTS

- N.Malkovskaya

It is known that the $K\alpha_{1,2}$ lines of the transition elements are asymmetric. Snyder[1] and Wainstein[2] hold that this asymmetry is due to interaction of $3d$ and $2p$ electrons and that the asymmetry index of the $K\alpha_{1,2}$ lines is determined by the number of unpaired $3d$ electrons. We wish to call attention to certain facts which, in our opinion, compel a revision of the concept of the asymmetry index and the inferences drawn on the basis of this concept.

A comparison of the values of the asymmetry index obtained for the $K\alpha_{1,2}$ lines by different authors shows that the scatter of the values is much greater than the error in determining the magnitude of the asymmetry index. The inconsistency of data is probably due primarily to differences in apparatus line broadening. It is difficult to assess the magnitude and shape of such broadening. To facilitate reference we list the values of the asymmetry index found for the Mn and Fe $K\alpha_1$ lines by different authors in Table 1.

Table 1

Asymmetry indices of the $K\alpha_1$ lines of Mn and Fe

Authors, year & Ref.No.	Mn	Fe
Allison, 1933 [3]		1,8
Parratt, 1933 [4]	1,60	1,65
Bearden, Shaw, 1935 [5]	1,52	1,61
Parratt, 1936 [6]	1,43	1,60
Roseberry, Bearden, 1936 [7]	1,54	
Vainshtein, Borovskii, 1945 [8]		1,40
Nemnonov, Kolobova 1958 [9]		1,52
Malkovska, 1959		1,45

The tabulated data show that the variation of the asymmetry index precludes drawing physical inferences when the values were not obtained under identical experimental conditions.

But can such inferences be drawn even in the event of identical experimental conditions? An affirmative answer can be given only if it can be shown that the asymmetry index varies consistently with some other quantity. For example, the above-mentioned explanation implying dependence of the asymmetry index on the number of unpaired $3d$ electrons would require that the asymmetry index of the $K\alpha_1$ line of any element in its different chemical states should grow with increase in the number of unpaired $3d$ electrons. Roseberry and Bearden[7] give practically the same value of the asymmetry index for Fe (1.61), Fe_2O_3 (1.6), Fe_3O_4 (1.58), and FeS (1.58) although it is evident that the $3d$ level of iron in these substances is not equally populated. Snyder[10] obtained a greater value of the asymmetry index (1.89) for the $K\alpha_1$ line of $NiSO_4$ than for the $K\alpha_1$ line of $CoCl_3$ (1.65) even though the number of unpaired electrons is smaller in the case of $NiSO_4$. Nor could we detect proportionality between the asymmetry index and the number of unpaired $3d$ electrons or the magnetic moment of the substance in the case of iron and its compounds. We carried out measurements by the fluorescence method on a double-crystal spectrometer employing single crystals of germanium with reflection from the (111) plane. Table 2 gives the measured values of the asymmetry index of the $K\alpha_1$ line, as well as the magnetic moment of the substance and the number of unpaired $3d$ electrons of iron in the given compound.

In view of the foregoing, we feel that it is debatable whether the asymmetry index, as it is commonly defined, is a suitable characteristic or measure of the asymmetry of spectrum lines. Further, we feel that it is desirable to investigate in greater detail and with more precision the nature of the asymmetry of the $K\alpha_{1,2}$ lines of the transition elements. At any rate, we seriously question the assertions made by Nemnonov and Kolobova[9] to the effect that "by virtue of its intrinsic nature the asymmetry index apparently depends only on the number of uncompensated electron spins remaining in the $3d$ layer of the transition metal"

Table 2

Substance	Asymmetry index of $K\alpha_1$ line	No. of Bohr magnetons per atom	No. of unpaired 3*d* electrons
Fe^{3+} $[Fe_2(SO_4)_3;\ NH_4Fe(SO_4)_2]$	1,47	5,86	5
Fe^{2+} $[FeSO_4{:}\ (NH_4)_2\cdot(FeSO_4)_2]$	1,51	5,25	4
Fe	1,45	2,22	2,22
$K_3[Fe(CN)_6]$	1,21	2,33	1
FeS_2	1,36	0,6	—
$K_4[Fe(CN)_6]$	1,11	0	0

and that "the magnitude of the asymmetry index of the $K\alpha_1$ lines can be used to characterize the variation of the magnetic moment of transition metal atoms".

Institute of Technical Physics,
Czechoslovakian Academy of Sciences

References

1. T.M.Snyder, Phys.Rev., 59, 689 (1941).
2. E.E.Wainstein, Doklady AN SSSR, 40, 102 (1943).
3. G.Allison, Phys.Rev., 44, 63 (1933).
4. L.G.Parrat, Phys.Rev., 44, 695 (1933).
5. J.A.Bearden & S.H.Show, Phys.Rev., 48, 18 (1935).
6. L.G.Parrat, Phys.Rev., 50, 1 (1936).
7. H.H.Roseberry & J.A.Bearden, Phys.Rev., 50, 204 (1936).
8. E.E.Vainshtein & I.B.Borovskii, Doklady AN SSSR, 49, 342 (1945).
9. S.A.Nemnonov & K.M.Kolobova, Fiz.metallov i metallovedenie 6, 466 (1958). (Trans.Phys.of Metals & Metallography.)
10. T.M.Snyder, Phys.Rev., 59, 168 (1941).

INVESTIGATION OF THE FINE STRUCTURE OF THE K X-RAY SPECTRA OF SOME SULFIDES

- I.A.Ovsyannikova & I.B.Borovskii

The physical properties of the sulfides CuS, NiS and CoS give reason to infer that they are compounds of the intermetallic type. These sulfides have metallic conductivity, and their conductivity exhibits the temperature dependence characteristic of metals (CuS is a superconductor). A marked change in properties is evinced when we turn to zinc sulfide: ZnS is one of the best dielectrics. CuS is a diamagnetic. NiS and CoS are paramagnetic, but their paramagnetic susceptibility is considerably lower than that of the divalent ions of the corresponding metals in solution. These are the facts, which Klemm & Schüth[1] discovered in their magnetochemical investigations, that led to the hypothesis that the said compounds are not salts but intermetallic compounds.

Earlier x-ray spectroscopic studies[2,3] of CuS and NiS were confined to investigation of the absorption or emission spectrum of only one component. We investigated the fine structure of the K emission and absorption spectra of both components of CuS and NiS (the latter in two crystal modifications). For purposes of comparison we also investigated the fine structure of the spectra of the respective pure elements. All measurements for each element were carried out on one and the same instrument, using the same reference lines. This afforded the possibility of reliably detecting the relative changes in the spectra in going from the pure element to the element bound in a compound.

The spectra were recorded photographically on a Kapitsa-Johann focusing vacuum x-ray spectrograph with quartz crystal bent to a radius of 500 mm.

The sulfur spectra were recorded in the first order of reflection from the $(10\bar{1}1)$ rhombohedral planes; the copper spectra with reflection from the $(13\bar{4}0)$ planes. The sulfur emission spectra were produced by secondary excitation; the secondary anode was water-cooled to preclude decomposition of the compound due to heating. The fluorescence radiation was excited by the continuous spectrum of gold.

Calculations and experiments showed that the optimal absorber thickness for bringing out the details of the fine structure was 1-1.5 mg/cm^2 for sulfur and 4-5 mg/cm^2 for copper. Therefore, we chose for the CuS and NiS absorbers a thickness of 4 mg/cm^2 for observing the sulfur spectra and 6-7 mg/cm^2 for the copper and nickel spectra. In investigating the absorption spectra of sulfur, we took special care not to excite higher orders of the continuous spectrum; to this end the tube potential was not allowed to exceed 5 kv. Under these conditions the necessary exposure times extended to 16 hours. This led to build up of a considerable background and explains the relatively low accuracy in determining the position of the edge (±0.4 XU).

Table 1 gives the wavelength values (averages for 3-4 measurements). Fig.1 shows the absorption and emission spectra of pure copper and sulfur and of the same elements in CuS. The spectra of sulfur and copper in the compound are plotted so that the points of inflection of the long wavelength part of their respective edges are located on the same vertical; the other curves are plotted relative to this vertical. The energy scale is the same for all the spectra.

Comparison of the experimental results shows the following. Whereas in the K spectra of pure sulfur there exists an energy discontinuity between the center of the short wavelength branch of the last emission line and the point of inflection of the long wavelength part of the edge, such as is typical of dielectrics (1.4 ev), no such discontinuity appears in the spectrum of S in CuS. The beginning of the absorption edge of sulfur is shifted 2.4 ev to the low energy side. An additional peak appears in the long wavelength part of the edge (*abc*). The intensity ratio of the shortest wavelength $K\beta_x$ line to the $K\beta_1$ line in the spectrum

Table 1

Wavelengths of the components of the fine structure

Fine structure component	In the pure element, XU	In CuS		Uncertainty, XU
		XU	ΔY, ev	
K edge of S	5007,2	5012,1	2,4	±0,4
S-K_{β_1}	5019,4	5021,3	0,9	±0,2
S-K_{β_x}	5013,4	5013,1	0,15	±0,2
K edge of Cu	1377,9	1377,5	2,6	±0,1
Cu-K_{β_5}	1378,4	1378,2	1,3	±0,1
Cu-K_{β_1}	1389,65	1389,26	2,6	±0,05

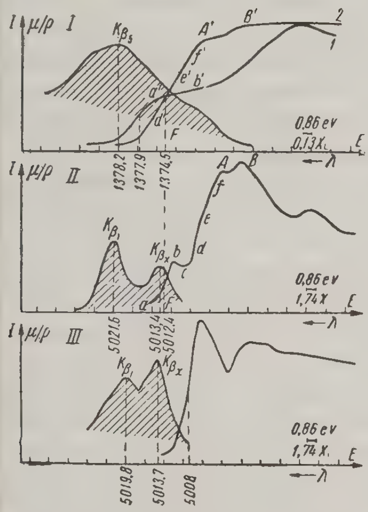

Fig.1. I - spectra of Cu: metallic (1) and in CuS (2); II - spectra of S in CuS; III - spectra of pure sulfur. The hatching represents the emission lines.

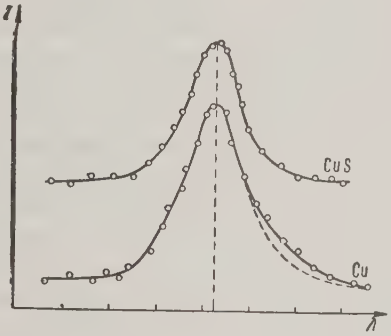

Fig.2. $K\beta_1$ line in the spectra of metallic Cu and CuS.

of S in CuS diminishes by a factor of two as compared with the case of pure sulfur.

The K absorption edge of copper in the compound differs markedly in shape from the edge of metallic copper: the long wavelength structure (plateau *a'b'*) disappears and the curvature is reversed in the region *d'e'f'* (Fig. 1). The K edge of copper becomes similar to the K edge of zinc. It is also important to note that the K edges of copper and sulfur, which are quite dissimilar in the case of the pure elements, acquire considerable similarity in the compound CuS: they have the same upward curvature in the region *def* and its counterpart *d'e'f'* and two peaks A and B and their counterparts A' and B', located at approximately the same distance from point F (the position of the Fermi surface).

The Cu $K\beta_1$ line was investigated on a microfocus spectrograph[4] by the ionization recording procedure (Fig.2). A weak satellite $K\beta'$ was detected in the spectrum of pure copper; this satellite does not appear in the spectrum of Cu in CuS.

Turning to discussion of the results, we note that a number of authors[2,3,5] have considered the possible causes of the splitting of the last emission line in the spectra of sulfur. Therefore we shall not dwell upon this question here.

The "white line" (the maximum of the absorption coefficient) in the absorption spectrum of sulfur is evidently associated with transitions of 1*s* electrons to the unfilled part of the 3*p* band. The appearance of additional structure in the long wavelength part of the edge of S in CuS, the shift of the edge to the long wavelength side, and the decrease of the intensity ratio of the $K\beta_x$ and $K\beta_1$ emission lines in the compound as compared with pure sulfur - all these effects indicate that part of the electrons, with transitions of which the $K\beta_x$ line in the spectrum of pure sulfur is associated, go over to a different state in the compound. Thus, absorption of a photon with resultant transition of electrons to the formerly

Table 2

Wavelengths of the components of the fine structure of nickel compounds

Fine structure component	In millerite		In NiAs type structure		Uncertainty, XU
	XU	$\Delta\gamma$, ev	XU	$\Delta\gamma$, ev	
K edge of S	5009,9	1,35	5011,4	2,1	±0,4
S-K_{β_1}			5019,4	0,0	±0,2
S-K_{β_x}			5012,0	0,7	±0,2
K edge of Ni	1483,89	6,17	1484,05	5,3	±0,04
K edge of metallic Ni	1484,99				±0,04
K edge of Ni in NiBi	1485,51	2,93			±0,04

occupied states becomes feasible. The spectrum of copper changes, becoming reminiscent of the spectrum of zinc, which has two *4s* electrons. Thus it is natural to conclude that part of the *3p* electrons of sulfur go over into the *4s* state and therefore are not evinced in the K spectra. In the crystal there exist two *4s* states per copper atom, and one of them is normally occupied by the *4s* electron of copper. So on the average one electron of sulfur goes over to the *4s* state. This electron is in fact a conduction electron of the whole compound with metallic properties, just like the above mentioned *4s* electron of the copper atoms. The copper in the compound is present in the form of Cu^+ ions, and hence there are two *4s* electrons in the conduction band for each copper atom. Moreover, it is evident from comparison of the absorption and emission spectra of sulfur that its *3p* electrons also participate in the conduction, inasmuch as there is no discontinuity between the filled and vacant parts of the *3p* band.

The fact that the Kβ' satellite is absent from the spectrum of Cu in CuS (as from the spectrum of Zn) lends further support to the view point set forth above. Recently another weighty argument in favor of the above interpretation of the spectrum of Cu in CuS was obtained by V.A.Batyrev, who investigated the K absorption edge of copper in an alloy of 30% Cu and 70% Zn. This alloy is an electron compound (Hume-Rothery phase) with an electron to atoms per cell ratio of 21/13. In this compound, wherein the number of conduction band electrons is known to be

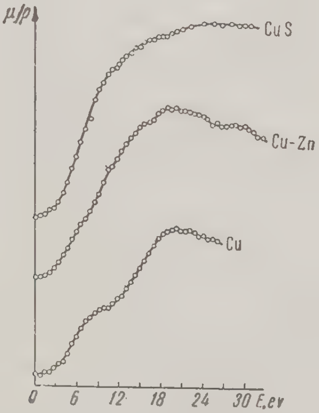

Fig.3. K absorption edge of Cu in the metal, in the γ-phase of a Cu-Zn alloy, and in CuS.

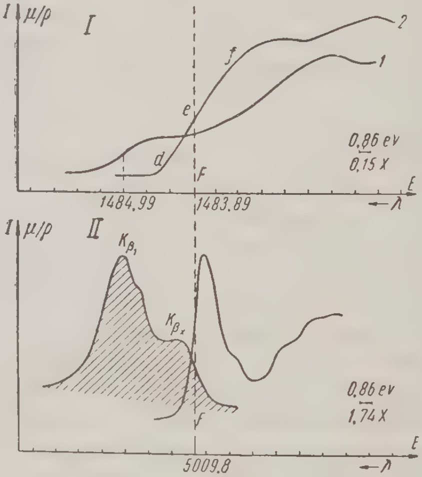

Fig.4. I - absorption edge of Ni: metallic (1) and in NiS (2); II - absorption edge and $K\beta_x$ line of S in NiS.

greater than in pure copper, the absorption edge of Cu is shifted in the same direction as that of Cu in CuS; although the fine structure in the long wavelength part of the edge is not smoothed out, inasmuch as the *4s* states are not completely filled (Fig.3).

Thus we conclude that CuS is a compound of the intermetallic type, in which both components give up their electrons to the conduction band and are left in the form of positive ions, as is generally the case for metals.

We note that the ionization energy of copper (for $Cu \to Cu^{2+}$) is high compared with other closely-related metals, while the sulfur atom is easily polarized (this is known from refraction data, for example). Both these factors favor the formation of the type of compound we have envisaged above.

We also investigated the x-ray spectra of nickel sulfide in two crystal modifications: millerite (class C_{3V}) and a hexagonal modification of the NiAs type. The experimental conditions and data processing were the same as for CuS.

Fig.4 shows the spectra of S and Ni in NiS, and Table 2 gives the wavelengths of the principal components of the fine structure of the K emission and absorption spectra. Comparison of the spectra reveals the following: the absorption edge of S in NiS is shifted to the long wavelength side by 1.35 ev in millerite and 2.1 ev in the hexagonal phase as compared with the spectrum of pure sulfur; the $K\beta_x$ line is reduced in intensity; the beginning of the edge of Ni is displaced to the short wavelength side and the edge changes shape in the same way as the edge of copper in CuS, i.e., the long wavelength structure disappears from the absorption edge of Ni and the curvature is reversed in the region *def*. On the other hand, the shape of the absorption edge of S in NiS hardly changes as compared with the spectrum of pure sulfur. Nor do we find any resemblance between the absorption edges of S and Ni in NiS (such as we discerned in the case of CuS). Thus, on the basis of examination of the fine structure of x-ray spectra we can assert that NiS belongs to the same type of intermetallic compounds as CuS. However, the facts at hand do not allow of unambiguously determining the electronic structure of the ionic Ni residue. The presence of unoccupied *3d* states in Ni hampers decipherment, so that interpretation must be predicated on further experimental investigation.

The spectra of S and Ni in the two crystal modifications differ as regards the position of the beginning of the absorption edge and the peaks of the emission lines, and also as regards the shape of the edge (Fig.5). Fig.5 shows the absorption edge of pure sulfur and sulfur in the two crystal modifications of NiS. In general, while the character of the spectra is identical, there exists a difference in the shape of the maximum of the absorption coefficient.

For CuS and NiS we obtained experimental proof of similarity between the K absorption edges of copper and nickel and the K absorption edge of zinc. One of these compounds (CuS) is a superconductor. Judging by its physical properties, NiS might be expected to exhibit superconducting properties at low temperature. But its electronic structure, as revealed by x-ray spectroscopy data (if we build on the conceptions one of

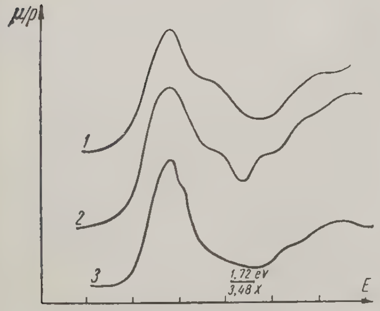

Fig.5

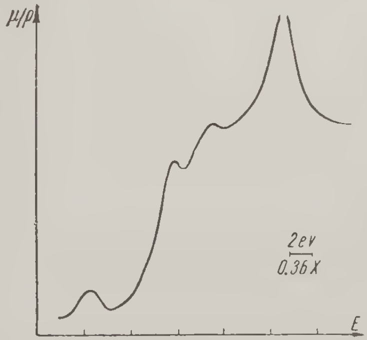

Fig.6

Fig.5. Absorption edge of sulfur: 1 - pure S; 2 - in the hexagonal structure of NiAs type; 3 - in millerite.
Fig.6. Absorption edge of nickel in NiBi.

us[6] developed elsewhere), indicates that NiS should not be a superconductor. Special measurements carried out in the laboratory of N.Ye.Alekseyevskii confirmed this deduction.

To obtain further proof, we investigated the fine structure of the K spectra of Ni in the superconducting compound NiBi. Here the fine structure of the absorption edge differs substantially from that observed for NiS. After correction for apparatus distortions there became evident a resemblance between the Ni edge and the edges of Ti and V. Hence the experimental results confirm the views expressed in Ref.6 to the effect that the electron energy spectrum of a non-superconducting metal in a superconducting compound should be similar to the spectrum of the superconductor closest to this metal in the same period of the Mendeleev periodic table. Thus, as noted above, the spectrum of copper in the superconducting compound CuS resembles the spectrum of the superconductor Zn; the spectrum of Ni in the superconducting compound NiBi resembles the spectra of the superconductors Ti and V. Such comparison is meaningful at any rate for compounds having the same lattice as the corresponding superconductor. The proposed hypothesis is based on the fact that the electron spectrum does not undergo substantial variation with temperature and maintains its character at room temperature, as well as temperatures close to that of the transition to the superconducting state.

The assumption of a correlation between superconducting properties and the structure of the entire electron spectrum would seem to contradict the present-day concepts of the theory of superconductivity[7,8] to the effect that only the structure of the electron spectrum in the immediate vicinity of the Fermi surface is important where the possibility of superconductivity is concerned. However, in any attempt to apply the theory to real metals in order to explain the presence of superconducting properties in some of them, as well as to explain the formation of superconducting compounds out of non-superconducting elements,[9] it is necessary to operate with the concepts of effective ionic charge and effective number of electrons, i.e., with quantities that are determined by the structure of the entire electron spectrum. It is precisely on these quantities that both Coulomb and phonon-induced interaction between electrons depend, i.e., in the final analysis, the presence or absence of superconductivity. The very fact that non-superconducting elements can combine to yield superconducting compounds speaks in favor of the views expressed above. These views[6] in fact imply that the conditions favorable to superconductivity may be sought in the special features of the electron spectrum of the compound.

"A.A.Baikov" Institute of Metallurgy,
Academy of Sciences of the USSR

References

1. W.Klemm & W.Schüth, Z.allg.Chemie, 203, 104 (1932).
2. Ya.M.Fogel', Zhur.eksp.i teor.fiz., 15, 545 (1945).
3. J.Valasek, Phys.Rev., 43, 612 (1933); 51, 832 (1937).
4. I.B.Borovskii & S.A.Ditsman, Doklady AN SSSR, 124, 1024 (1959). (Trans. Soviet Physics - Doklady.)
5. I.B.Borovskii, Referaty nauchno-issledovatel'skikh rabot otdeleniya geologo-geograficheskikh nauk AN SSSR (Abstracts of Scientific Reports of the Dept. of Geological-Geographic Sciences of the USSR Acad.of Sci.) p.151, Pub.USSR Acad. of Sci., 1944.
6. I.B.Borovskii, Trudy in-ta metallurgii AN SSSR (Proceedings of the Inst. of Metallurgy of the USSR Acad.of Sci.), Vol.VI, p.24, M., 1960.
7. N.N.Bogolyubov, V.V.Tolmachev & D.V.Shirkov, Novyi metod v teorii sverkhprovodimosti (New method in theory of superconductivity) Pub.USSR Acad.of Sci.,1958.
8. J.Bardeen, L.N.Cooper & J.R.Schrieffer, Phys.Rev., 108, 1175 (1957).
9. D.Pines, Phys.Rev., 109, 280 (1958).

NATURE OF THE FINE STRUCTURE OF THE MAIN K ABSORPTION EDGE OF ELEMENTS OF THE IRON GROUP

- I.B.Borovskii & V.A.Batyrev

There have been several investigations[1,2] devoted to the fine structure of the main K absorption edge of atoms of elements of the iron group. Until now, however, a number of distinctive features of these spectra have not received a satisfactory explanation.

We investigated the K absorption spectra of metals of the iron group on a bent quartz crystal spectrograph with high resolution (in the working range the ratio $\Delta\lambda/\lambda$ was about 10 000).

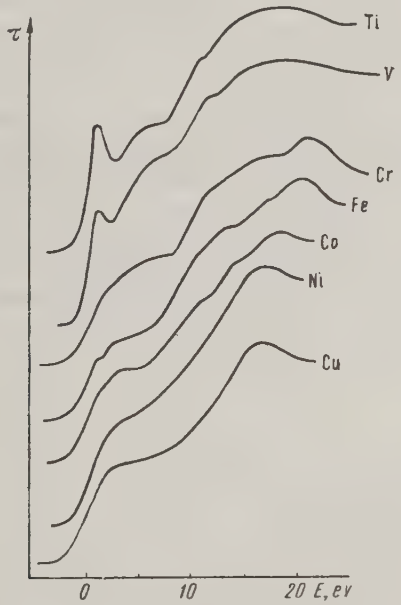

Fig.1. Experimental K absorption spectra of Ti, V, Cr, Fe, Co, Ni and Cu.

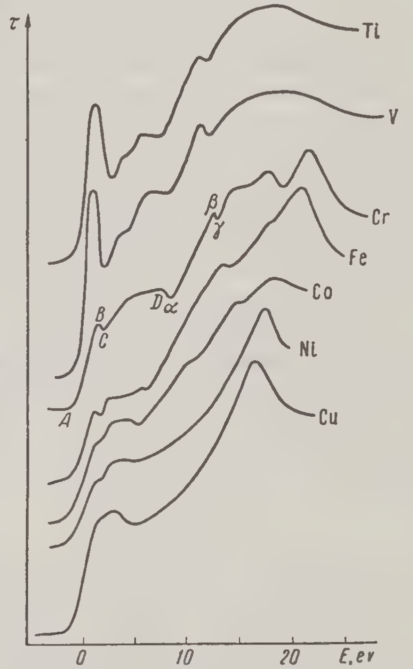

Fig.2. Same as Fig.1 but corrected for apparatus distortion.

The experimental K absorption spectra are given in Fig.1. Fig.2 shows the same spectra corrected for apparatus distortion by the method described in Ref.3. Examination of Figs.1 and 2 discloses the distinctive features characteristic of these edges: in the extreme long wavelength part of the main K absorption edge of the transition elements of the iron group there is evident a section (ABC) with structure, which is gradually smoothed out with increase of the atomic number of the element; to the short wavelength side of this structure there follows a horizontal plateau and then a steep rise of the absorption curve.

If we associate the extreme long wavelength structure ABC with photoelectron transitions to the unfilled part of the *3d* band, the gradual smoothing out of this structure with increasing atomic number can be correlated with filling of the *3d* band as one goes from vanadium to copper. It is then logical to associate the plateau CD with photoelectron transitions to the *4sp* band. In most investigations[1,2], however, the section of the curve that is linked with transitions to the unfilled part of the *3d* band, is section ABCD, which includes the plateau. This assumption cannot explain the presence of the section ACD in the edge of copper, in which the $3d$ band must be completely filled. The steep rise of the absorption curve after the plateau CD corresponds to an increase of the photoelectron transition probability to the region of $4p$ states.

Element	Separation between the characteristic points, ev			Separation betw. characteristic loss peaks, ev
	A & α	B & β	C & γ	
Ti	8,5	9,0	9,0	10
V	8,5	10,5	9,8	—
Cr	9,3	11,2	10,9	10
Fe	7,2	9,1	—	8
Co	7,8	8,2	9,6	8

The K absorption edges of Ti, V, Cr, Fe and Co (Fig.2) - particularly, the edge of Cr - clearly exhibit a repetition (section $\alpha\beta\gamma$) of the initial absorption structure (section (ABC).

The accompanying table shows the separations (in ev) between points A and α, B and β, C and γ in the K edge absorption curves of the listed elements. These distances are compared with the distances between the peaks of the characteristic electron energy losses in thin films[4]. According to Pines[4], the characteristic energy losses arise as a result of excitation of collective plasma oscillations of the free electrons in the solid. Characteristic electron losses may also occur due to excitation of single-electron transitions.

Thus, we hold that the main edge of the K absorption spectrum is a superposition of two absorption edges, one of which is associated with the ordinary photoeffect, while the other is due to the photoeffect with simultaneous excitation of plasma oscillations of the free electrons or excitation of electrons located in outer orbits of the metal atoms. It is natural that the second absorption edge should tend to duplicate the structure of the first. Complete identity of the two absorption edges is not realized, however, owing to a difference between the lifetimes of these two excited states.

"A.A.Baikov" Institute of Metallurgy,
Academy of Sciences of the USSR

References

1. W.W.Beeman & H.Friedman, Phys.Rev., 56, 392 (1939).
2. I.B.Borovskii, Doklady AN SSSR, 26 (1940).
3. I.Ya.Nikiforov, Izv.AN SSSR, Ser.fiz., 21, 1362 (1957). (Trans.Bulletin, 21, 1351.)
4. D.Pines, Solid State Physics, 1, 367 (1955).

INFLUENCE OF THE NICKEL CONCENTRATION ON THE STRUCTURE OF THE ELECTRON ENERGY SPECTRUM OF IRON-CHROMIUM ALLOYS

- N.D.Borisov, V.V.Nemoshkalenko & A.M.Fefer

I

In an earlier contribution[1] we gave experimental data on the structure of the energy spectrum of electrons in iron-chromium alloys. We left unanswered, however, a number of questions pertaining to the effect of addition to these alloys of a third component that improves their industrial properties without reducing their heat resistance.

The purpose of the present work was to determine such characteristic changes in structure of the electron energy spectrum of iron-chromium alloys as are due to the introduction of a third component, namely, nickel.

For the objects of our study we chose the chromium and iron $K\beta_5$ lines associated with electron transitions from the conduction band to the K level (together with the short wavelength $K\beta'''$ satellite), and the $K\beta_1$ lines associated with electron transitions from the to the K level.

These spectrum lines were recorded at 1000°C for samples of pure chromium and iron and samples of Fe-Cr-Ni alloys Nos.1, 2, 3, 4 and 5 containing (by weight) 40% iron and, respectively, 0, 2, 5, 7 and 10% of the alloying element nickel. The $K\beta$ group lines of nickel in alloys Nos.2, 3, 4 and 5 were not recorded owing to their low intensity.

The initial metals were electrolytic chromium, iron and nickel. All the alloys were prepared in a hf vacuum furnace. The alloys were subjected to a homogenizing anneal at 1150°C for 50 hours. Special plates were cut of each alloy and mounted on the primary target of the x-ray tube. The vacuum maintained in the system was of the order $8 \cdot 10^{-6}$-$2 \cdot 10^{-5}$ mm Hg and was monitored by a VI-3 ionization gage.

The Fe lines of the $K\beta$ group were recorded in the fourth order; the Cr $K\beta$ lines in the fifth order of reflection.

In order to check the constancy of composition of the alloys in the region of the focal spot up to and during detection, we recorded the Cr $K\alpha_{1,2}$ (III) and Fe $K\beta_1$ (IV) under optimal conditions. The invariance (within the experimental scatter) of the intensity ratio of these lines indicated that the composition of the alloys remained virtually unchanged during the recording operation.

The dispersion data in the region of the $K\beta$ lines of Cr and Fe are listed in Table 1. Resolution of the complex contour of the Fe $K\beta$ band into components was carried out by the method of successive subtraction at each point of the $K\beta_5$ band contour of the photographic densities of the $K\beta'''$ satellite.

Table 1

Line	λ, XU	$\frac{\Delta\lambda}{\Delta l}$, XU/mm	$\frac{\Delta\nu}{\Delta l}$, ev/mm	$\frac{\Delta(\nu/R)}{\Delta l}$, R/mm
Fe-$K_{\beta'''}$	1738,60	2,45192	10,02657	0,73698
Fe-K_{β_5}	1740,54	2,44631	9,98147	0,73366
Fe-K_{β_1}	1752,99	2,41003	9,68982	0,71222
Cr-$K_{\beta'''}$	2061,38	3,90399	11,35647	0,83473
Cr-K_{β_5}	2066,53	3,89294	11,26796	0,82822
Cr-K_{β_1}	2080,60	3,86247	11,02889	0,81065

The experimental procedure was analogous to that described in Ref.2. The width T_{max} of the $K\beta_5$ band was determined as the sum of two terms T_1 and T_2, which are respectively the widths of the short and long wavelength branches of the $K\beta_5$ band.

Table 2 summarizes the calculated data for

Table 2

T_1, T_2 and T_{max} at 1000°C for the pure metals and the Fe-Cr-Ni alloys with different nickel concentrations.

Substance	T_1, ev	T_2, ev	T_{max}, ev		Line
Chromium	1,8	8,9	10,7		Cr-$K\beta_5$
Iron	1,8	10,8	12,6		Fe-$K\beta_5$
Alloy No. 1 Fe-Cr	2,0	10,0	12,0	11,9	Cr-$K\beta_5$
(40% Fe)	1,9	9,9	11,8		Fe-$K\beta_5$
Alloy No. 2 Fe-Cr-Ni	2,1	9,8	11,9	11,9	Cr-$K\beta_5$
(40% Fe, 2% Ni)	1,9	10,0	11,9		Fe-$K\beta_5$
Alloy No. 3 Fe-Cr-Ni	2,1	9,8	11,9	12,1	Cr-$K\beta_5$
(40% Fe, 5% Ni)	1,9	10,4	12,3		Fe-$K\beta_5$
Alloy No. 4 Fe-Cr-Ni	2,1	10,4	12,5	12,4	Cr-$K\beta_5$
(40% Fe, 7% Ni)	1,9	10,3	12,2		Fe-$K\beta_5$
Alloy No. 5 Fe-Cr-Ni	2,1	10,7	12,8	12,6	Cr-$K\beta_5$
(40% Fe, 10% Ni)	1,9	10,5	12,4		Fe-$K\beta_5$

Tables 3 and 4 summarize the values for wavelengths and photon energies based on photometric measurements of the corresponding spectrograms.

Fig.1 shows the diagram of the $3d$ band of Fe-Cr-Ni alloys plotted on the basis of the data of Tables 2, 3, 4 and the energies of the chromium and iron K levels, which we took to be 5993.12 and 7115.10 ev, respectively. These values equal the sum of the energy values for the short wavelength edges of the chromium and iron $K\beta_5$ bands and the work function (cf. Ref.4).

Table 3

Substance	Line	λ, XU	E, ev	Position of short-wave edge, ev
Chromium	Cr-$K_{\beta'''}$	2061,00	6003,25	—
	Cr-K_{β_5}	2066,64	5986,87	5988,67
	Cr-K_{β_1}	2080,61	5946,67	—
Alloy №1	Cr-$K_{\beta'''}$	2060,89	6003,57	—
	Cr-K_{β_5}	2066,72	5986,64	5988,64
Alloy №2	Cr-$K_{\beta'''}$	2061,11	6002,93	—
	Cr-K_{β_5}	2066,71	5986,66	5988,76
Alloy №3	Cr-$K_{\beta'''}$	2061,02	6003,19	—
	Cr-K_{β_5}	2066,74	5986,58	5988,68
Alloy №4	Cr-$K_{\beta'''}$	2060,92	6003,49	—
	Cr-K_{β_5}	2066,76	5986,52	5988,62
Alloy №5	Cr-$K_{\beta'''}$	2061,11	6002,93	—
	Cr-K_{β_5}	2066,68	5986,75	5988,85
Alloys №№ 1—5	Cr-K_{β_1}	2080,63	5946,61	—

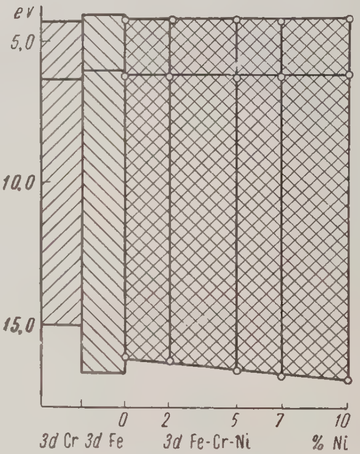

Fig.1. Diagram of the 3d band of Fe-Cr-Ni alloys.

II

It is easy to see that in plotting the energy diagram of the $3d$ band of alloys of the Fe-Cr-Ni system, we postulated that the energy values for the K levels of chromium and iron are constant within the limits of the experimental uncertainty, and that these values are practically independent of the degree of screening of the inner atomic electrons by the "outer" $4s$ electrons.

The results of measurements on magnetic spectrometers[7], as well as x-ray spectroscopy data, can provide a direct answer to the question as to what causes the experimentally observed shifts of the K edge and of the short and long wavelength branches of the last emission lines; in other words, the question as to whether these shifts occur owing to variation in the energy of the K level or to change in the Fermi energy.

In our case the high degree of accuracy in determining the positions of the line peaks permits an unequivocal answer to this question. Thus, if we subscribe to the view of Karal'nik[4-6], in the event of a shift of the K edge or the short

Table 4

Substance	Line	λ, XU	E, ev	Position of short-wave edge, ev
Iron	Fe-$K_{\beta'''}$	—	—	—
	Fe-K_{β_5}	1740,41	7109,07	—
	Fe-K_{β_1}	1752,97	7058,14	7110,87
Alloy № 1	Fe-$K_{\beta'''}$	1737,96	7119,09	—
	Fe-K_{β_5}	1740,45	7108,91	7110,81
Alloy № 2	Fe-$K_{\beta'''}$	1738,06	7118,68	—
	Fe-K_{β_5}	1740,47	7108,83	7110,73
Alloy № 3	Fe-$K_{\beta'''}$	1738,19	7118,15	—
	Fe-K_{β_5}	1740,53	7108,58	7110,48
Alloy № 4	Fe-$K_{\beta'''}$	1737,93	7119,22	—
	Fe-K_{β_5}	1740,49	7108,75	7110,65
Alloy № 5	Fe-$K_{\beta'''}$	1737,97	7119,05	—
	Fe-K_{β_5}	1740,48	7108,79	7110,69
Alloys №№ 1—5	Fe-K_{β_1}	1752,97	7058,14	—

wavelength branch of the last emission band, we should expect all the energy levels of the atom to be displaced by different amounts, dependent on the probability of the inner electrons being on these levels (which probability in turn depends on the different degrees of screening of the atom's inner energy levels by outer electrons).

In this case, in addition to the shift of the chromium and iron $1s$ levels, one might have expected a shift of their $2p$ and $3p$ levels by different amounts. However, control measurements relating to the position of the peaks of the Cr and Fe $K\beta_1$ lines, which are associated with transitions of $3p$ electrons to the K level, did not reveal any shift within the limits of scatter (±0.01 XU). By way of references in these measurements we chose the Co $K\alpha_1$ and Cu $K\alpha_1$ lines. Moreover, in determining the position of the Fe $K\beta_1$ line relative to the Cr $K\beta_1$ line of the alloys, which line is associated with electron transitions from the $2p$ to the K level, we found this to be constant with the same limits of scatter.

All this gives reason to believe that the diagram we have plotted for the $3d$ energy band of Fe-Cr-Ni alloys (Fig.1) is correct, and so we can draw the following conclusions:

1. Partial replacement of chromium by nickel in the 40% Fe + Cr alloy leads to a broadening of the narrow region of component concentration, referred to in the work of Ref.1, the $3d$ band of which is characterized by the presence of completely collectivized "outer" electrons of chromium and iron (Fig.2).

2. The $3d$ band broadens with increasing nickel concentration in the Fe-Cr alloy (40% Fe) owing to lowering of the bottom of this band.

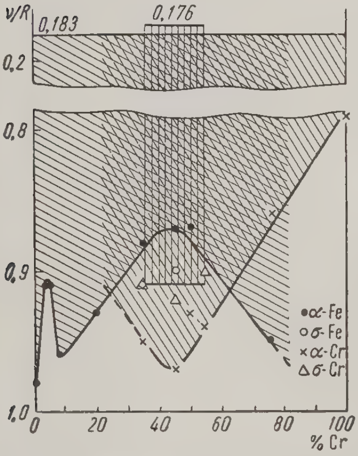

Fig.2. Overlapping of the Cr and Fe energy bands in Fe-Cr alloys.

Institute of Metal Physics,
Academy of Sciences of the Ukrainian SSR

References

1. N.D.Borisov, V.V.Nemoshkalenko & A.M.Fefer, Doklady AN SSSR, 121, 264 (1958). (Trans.Soviet Physics - Doklady.)

2. N.D.Borisov, V.V.Nemoshkalenko & A.M.Fefer, Izv.AN SSSR, Ser.fiz., 21, 1424, (1957). (Trans.Bulletin, 21, 1412.)

3. Landolt-Börnstein, Zahlenwerte und Functionen aus Physik, Chemie, Astronomie, Geophysik und Technik, 1 Band, 4 Teil, S.760, Berlin, 1955.

4. S.M.Karal'nik, Izv.AN SSSR, Ser.fiz., 21, 1445 (1957). (Trans.Bulletin, 21, 1432.)

5. S.M.Karal'nik, Ukr.fiz.zhur. (Ukrainian Physics Journal), 2, 333 (1957).

6. S.M.Karal'nik, Naukovi provid.Kiivs'k.un-t. (Scientific Notes, Kiev State University), Physics Section, No.1, 41, 1956.

7. E.Sokolowski, C.Nordling & K.Seigbahn, Arkiv.fys., 12, No.4, 301 (1957).

FINE STRUCTURE OF THE PRINCIPAL K ABSORPTION EDGE OF TRANSITION METALS OF THE IRON GROUP, THEIR ALLOYS AND COMPOUNDS

- S.A.Nemnonov

One of the fundamental problems in investigating the electronic structure of transition metals, their alloys and compounds, is that of establishing correlation between changes in the various x-ray spectroscopic characteristics, on the one hand, and changes in the electronic structure and character of the interatomic binding forces, on the other hand. The purpose of the present communication is to examine some experimental data that help reveal some regularities in the variation of the fine structure of the principal K absorption edge of the transition metals of the first long period as a function of the atomic binding in alloys and compounds and to formulate the most probable interpretation consistent with these data.

Let us start by considering the fine structure of the principal K absorption edge of one of the transition metals, for example, iron (curve 1 in Fig.1).[1] On the basis of the results of Beeman & Friedman[2], Koster & Kistra[3] and Nilsson[4], the principal components of the structure of the K absorption edge of the transition metals from scandium to copper may be interpreted as follows: the low energy rise in the absorption curve, i.e., the initial region of absorption (the region *abc* in our figures) corresponds primarily to transitions of *1s* electrons to unoccupied states of the *3d-4s* band, which may have some admixture of *p* states. The section *c*A of the principal absorption edge corresponds mainly to transitions of K electrons into the *4p* band (it may be noted that another inflection is observed in the absorption curves of chromium and iron between the points *c* and A, but we shall not consider the origin of this feature here). The fine structure of the principal K absorption edge of the transition metals is satisfactorily reproduced by the K excitation curves obtained by the method of "isochromates" of the characteristic spectrum.[4] In addition, in the K excitation curves of the transition metals from Ti to Ni there is evinced the so-called *h* structure, indications of which are observed in the initial absorption sections of the principal K edge of some metals (for example, chromium[5]). It is known that transitions of *1s* electrons to unoccupied levels of *d*, *s* and *p* symmetry contribute to the formation of the fine structure of the principal K edge of the transition metals. The spectral distribution of the absorption coefficient within the range of the principal edge will be determined both by the degree of filling of the *3d*, *4s* and *4p* bands, which have different densities of states, and by the degree of hybridization of the *d*, *s* and *p* orbits, which determines the probability of the corresponding transitions. Both these factors can change incident to formation of alloys, which leads to alteration of the principal absorption edge. By way of example, let us consider iron-aluminum alloys.

In earlier contributions[1,6] we cited data indicating that in alloying of aluminum with iron, part of the outer electrons of the aluminum atoms are drawn into the sphere of influence of the iron ions, as a result of which the degree of filling of the overlapping *3d* and *4s* bands of iron should increase with increasing aluminum concentration. Some of these earlier data are reproduced in Table 1, where point *b* indicates the position of the midpoint of the initial absorption curve, *f* stands for the position of the midpoint of the entire absorption edge (discontinuity), A is the first absorption maximum and

$$q = \frac{(\mu/\rho)_C}{(\mu/\rho)_A},$$

is the ratio of the initial absorption to the entire "jump" in the absorption coefficient.

Table 1

c_{Al}, at.%	*b*, ev	*f*, ev	*A*, ev	*q*
0 (pure iron)	7110,4	7117,1	7129,0	0,35
17	7110,0	7115,7	7128,9	0,39
25	7109,7	7114,8	7128,9	0,42
50	7109,3	7114,2	7129,4	0,48
75	7111,1	7113,9	7137,0	0,65

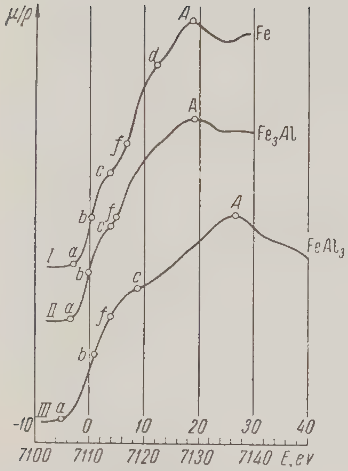

Fig.1. Structure of the principal K absorption edge of iron in Fe, Fe_3Al and $FeAl_3$.

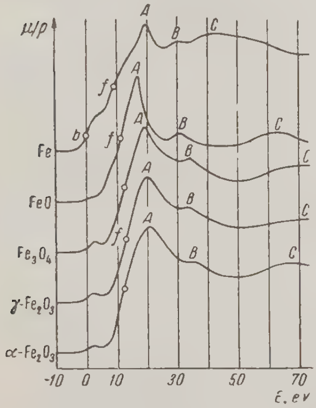

Fig.2. Structure of the principal K absorption edge of iron in its oxides.

It will be evident from Table 1 that the salient characteristics of the principal edge, i.e., the center of the initial absorption curve (*b*) and the midpoint of the entire jump (*f*) are shifted to the side of lower energies with increasing aluminum concentration. Here, however, we want to note another no less interesting fact, namely, that not all the sections of the principal edge are shifted to the same degree: the greatest shift with increasing Al concentration is exhibited by the point *f*; the point *b* is shifted much less (by not more than 1 ev), while the position of point A remains virtually the same up to 50 atomic percent aluminum. In the case of the intermetallic compound $FeAl_3$ there is observed not only an appreciable difference in the magnitude of the shifts, but also a difference in the direction of these shifts. If by analogy with the curves for pure iron and Fe_3Al (curves I and II in Fig.1) we take the section *abc* as the initial region of absorption in the edge curve for iron in $FeAl_3$ (curve III), we find that the midpoint of the initial absorption curve in the case of $FeAl_3$ is shifted not to the long wavelength side, as in the case of alloys with a lower aluminum concentration, but to the short wavelength side.

The peak A is shifted some 8 ev to the high energy side as compared with the position of point A for other alloys. In contrast to these two characteristics, the center of the entire absorption edge (point *f*) undergoes the greatest (for all the investigated iron-aluminum alloys) displacement to the long wavelength side (in the spectrum of $FeAl_3$ it is located at 7113.8 ev instead of 7117.1 ev for pure iron). Thus, different parts of the principal K absorption edge of a transition metal may shift with entry of it into a compound not only by different amounts but also to different sides.

It will be evident from the K absorption edge curves for iron given in Ref.1 that simultaneously with increase of the initial absorption with increase of the aluminum content in the alloy (up to 50%), there occurs smoothing out of the inflection designated by *c*. The K absorption edge of iron is transformed so that at elevated aluminum concentrations ($FeAl_3$ - Fig.1; FeAl (Ref.1)) there becomes evident a pronounced rise or hump in the curves. This change in the appearance of the principal edge may occur owing to increase in this energy region of the admixture of *p* states introduced by the valence-active *3p* levels of the aluminum atoms.

In contrast to the case of iron-aluminum alloys, in iron oxides (Fig.2 - Ref. 3), as well as in other ionic and ionic-covalent compounds of the transition elements, there is observed a sharp decrease of the initial absorption. This dip in the intensity of the initial absorption of transition elements in their oxides and other compounds can be explained by appreciable or complete disappearance of admixture of *p* states in the *3d* and *4s* bands. This factor is fundamental inasmuch as it determines the probability of the corresponding electron transitions. The K electrons will undergo transitions to the first allowed band (the *4p* band) missing one of the lower lying wholly or partially unoccupied bands (*4s* and *3d*) and the forbidden band between them, the width of which is determined by the character of the binding forces in the given material. As a result the center of the principal absorption edge can undergo strong displacement to the short wavelength side, as is observed in the spectra of the salts or oxides of the transition metals.[7]

The absence of *4p* states in the energy region of the *4s-3d* quasi-levels of transition element ions in strongly polar crystals is explained by the greater separation of the metal ions in such crystals, which leads to an appreciable decrease in the width of the *4s* and *4p* bands and, consequently, to increase of the gap between them, i.e., to the appearance of a forbidden band. This is substantiated by the fact that the first peak in the K absorption curves of the transition metals in compounds becomes narrower and more pronounced.

To this one must add another, no less important factor acting in the same direction. This factor is that the *np* levels of the valence band of negative ions, which usually extend to the octal configuration (taking into account *ns* levels) are apparently strongly localized and in contrast to the *3p* states of atoms of aluminum in Fe-Al alloys, cannot introduce an admixture of these *np* states to the unoccupied part of the *4s* and *3d* bands of the metal ions. In crystals with strongly polar bonds these factors lead to complete disappearance of the initial absorption region in the K edges of some of the transition elements, which is illustrated by the K absorption curves of the divalent ions of copper, nickel and cobalt in $CuSO_4 \cdot 5H_2O$, $NiSO_4 \cdot 7H_2O$ and $CoCl_2 \cdot 6H_2O$.[8]

In earlier investigations, owing to the relatively low resolution of the instruments then available and possibly inadequate techniques, the initial absorption region in the K edges of transition metals was not detected for many polar and polar-covalent substances, but subsequently it has been observed with reasonable certainty[5,8]. The initial or long wavelength region of the K absorption edge is evinced even more clearly in different oxides, fluorides and sulfides of the transition metals.[8] The fact that the true structure of the energy bands in these compounds is obscured by the selection rules and is not adequately evinced in the K absorption spectra led many investigators to erroneous comparison of two essentially and basically different points in the K absorption curves of transition metals. In one case the position of the boundary between the occupied and unoccupied states (the Fermi level) is characterized with some approximation by the energy of the midpoint of the initial absorption (point *b*), associated for the metallic state with transitions of K electrons into the unoccupied part of the communal *3d-4s* band. In the other extreme case, corresponding primarily to ionic crystals, experimenters have taken as corresponding to the beginning of the unoccupied states the center of the curve of the entire absorption discontinuity, i.e., the point *f*, the appearance of which is due to transition of K electrons into another higher lying band, namely, the *4p* band; in doing this the investigators failed to take into account that there is present a lower lying and entirely unfilled band - the *4s* band (and also the partially unoccupied *3d* band). Obviously, in attempting

Table 2

Position of the characteristic points in the K absorption edge of elements from $_{24}Cr$ to $_{30}Zn$ in different compounds

Substance	$(f-b)$, ev	$(A-b)$, ev	Δf, ev	ΔA, ev	q, %	Ref.
Cr	6,8	18,7	0	0	49	[5]
$Cr_2(SO_4)_3$	13,2	18,6	+6,4	—0,1	—	
$CrCl_3$	10,4	17(21)	+3,6		+	
Cr_2O_3	10,8	17,5(20,7)	+4,0		+	
Mn	10,0	17,0	0	0	33	[3]
$MnCl_2 \cdot 4H_2O$	7,5	12,5	—2,5	—4,5	+	[8]
$MnSO_4 \cdot H_2O$	7,4	12,6	—2,6	—4,4	+	
MnF_2	6,3	13,3	—3,7	—3,7	+	
MnO	9,2	15,5	—0,8	—1,5	+	[3]
Mn_3O_4	10,5	19,5	0,5	+2,5	+	
Mn_2O_3	12,0	19,7	+2,0	+2,7	+	
MnO_2	12,0	19,4	+2,0	+2,4	+	[8]
Fe	8,5	19,8	0	0	29	[2]
$FeCl_2 \cdot 4H_2O$	8,8	14,2	+0,3	—5,6	3	[8]
$FeSO_4 \cdot 7H_2O$	9,3	14,6	+0,8	—5,2	4	
FeF_2	11,1	20,0	+2,6	+0,2	6	
Fe_2O_3	10,8	20,0	+2,3	+0,2	10	
FeO	11,0	16,5	+2,5	—3,3	3	[3]
Fe_3O_4	12,0	19,2	+3,5	—0,6	8	
FeS	5,5	18,9	—3,0	—0,9	20	[8]
Co	7,0	20,0	0	0	36	[2]
$CoCl_2 \cdot 6H_2O$	9,1	13,8	+2,1	—6,2	—	
CoF_2	9,6	16,3	+2,6	+3,7	+	[8]
Co_2O	11,3	20,0	+4,3	0	+	
CoS	7,1	21,0	+0,1	+1,0	+	
Ni	8,0	17,3	0	0	42	[2]
$NiSO_4 \cdot 7H_2O$	11,0	16,2	+3,0	—1,1	—	[8]
NiF_2	11,7	16,2	+3,7	—1,1	—	
Ni_2O_3	11,1	17,4	+3,1	+0,1	+	
NiO	11,1	17,5	+3,1	+0,2	+	
NiS	7,9	?	—0,1	7	—	
Cu	6,0	14,7	0	0	48	[2]
$CuSO_1 \cdot 5H_2O$	10,0	17,9	+4,0	+3,2	—	
CuO	5,0	18,7	—1,0	+4,0	+	[8]
Cu_2O	3,0	17,4	—3,0	+2,7	—	
CuS	4,3	18,6	—1,7	+3,9	+	
Cu_2S	3,9	19,6	—2,1	+4,9	+	
Zn	0,8	10,1	0	0	73	[ ]
$ZnSO_4 \cdot 7H_2O$	2,8	7,4	+2,0	—2,7		
ZnO	0,4	8,4	—0,4	—1,7		[8]
ZnO_2	3,0	7,8	+2,2	—2,3		
ZnS	0,0	4,9(9,6)	—0,8	—5,2 (—0,5)		

comparison of such different (as regards both origin and position in the energy scale) points as points b and f, one can expect to observe a large "shift" of the K absorption edge of the transition element in ionic compounds.

The error in such juxtaposition of the K absorption edges of pure metals with the position of the K edges in ionic compounds is evident from the fact that if we compare the positions of points b and f in each of the K absorption curves of the transition elements, we find that the energy difference between these points for the pure metals is of the same order of magnitude as in many of their salts, oxides and similar compounds (see Table 2, column 2).

To clarify the actual changes that occur in the structure of the principal absorption edge of the transition metals in different compounds let us examine the magnitude and direction of the shifts of the three most characteristic points of the K edge, namely, points *b*, *f* and A.

Position of the center of the initial absorption curve (point *b*)

The magnitude of the initial absorption depends to an appreciably extent on the type of atomic bonds: in ionic compounds the region of initial absorption may decrease to the point where it vanishes. At present there have been investigated many diverse compounds with transition metals, in the K spectra of which there was observed an initial absorption region[1,3,5,8]. Analysis of these data shows that the position of the midpoint of the initial absorption curve (point *b*), regardless of its height, remains virtually the same for different compounds as compared with the position of this point for pure metals (see for example, Fig.2). Where there is a shift of point *b* (reported for some substances), it does not exceed 1-1.5 ev. The constancy of the position of point *b* for most compounds is illustrated by the K absorption spectra given in Refs.3,5 & 8. Consequently, one of the principal elements of the structure of the K absorption edge of the transition metals of the iron group, namely, the position of the midpoint of the initial absorption either does not shift at all in the energy scale with change in the character of the atomic bonds and the crystal structure in different compounds or undergoes only a very minor shift, although the region of initial absorption (in the μ/ρ scale) actually varies a great deal, to the point of vanishing completely (for example, in the case of $Cr_2(SO_4)_3$, $CoCl_2 \cdot 6H_2O$ and $NiSO_4 \cdot 7H_2O$).

In analyzing the data on the shift of the initial absorption curve, one must bear in mind, however, the fact that the initial absorption region itself has a fine structure (see Refs.4 & 5).

Midpoint of the entire K absorption discontinuity (point *f*)

The point *f* in the K absorption spectra of Cr, Mn, Fe, Co, Ni and Cu is located in the section of the absorption curve (above point *c*), which is associated primarily with transitions of K electrons into the *4p* band. In ionic or ionic-covalent compounds the position of the K edge of transition elements is usually characterized by the position of point *f*, the origin of which is not associated, as was noted above, with transitions of K electrons into the first unoccupied states immediately above the filled part of the valence band. Comparison of the energy position of point *b* (pure metals) with the position of point *f* (ionic compounds) naturally yields a difference between them, and this difference obtained for a given compound as compared with the pure metal is often taken as the magnitude of the "shift" of the principal K absorption edge. This spurious "shift" is directed to the side of higher energies and varies for most ionic compounds of transition metals from 7 to 15 ev.[7] So great an observed "shift" of the K edges of the transition metals in different compounds led in many cases to erroneous interpretation of this effect (we have in mind here explanations based on taking into account the so-called effect of external screening[9]).

In cases when the absorption spectra exhibit a section of initial absorption (Refs.5 & 8), the magnitude of which may vary for different compounds, but as a rule is less than in the pure element, there arises the question: at what value of the initial absorption should the position of the principal K edge of a transition element be characterized by point *f* rather than point *b*?

The results of analysis of the experimental data obtained in the investigations of Refs.2,3,5 & 8 are given in Table 2. The values in columns 2 and 3 represent the differences (in electron volts) between the points *f* and *b* and the points A and *b*, respectively, (the position of the point *b* in going from the pure metal to the compound may be regarded as constant in the first approximation); Δf is the difference between the positions of the midpoint of the principal K absorption edge in the given compound and its position for the pure metal; similarly ΔA represents the shift of the point A. It will be evident from the table that even for pure transition metals the energy difference $f - b$ amounts to 7-10 ev. This is the order of magnitude of the error introduced in determining the position of the principal K edge of transition elements in different ionic compounds when one compares the position of the point f in the compound with the position of point b in the spectrum of the pure metal.

As explained above, to obtain a correct idea of the direction and magnitude of the shift of the center of the entire K absorption edge, i.e., of the shift of point f, for different compounds, one must compare the position of this point in the K absorption curve of the compound with the position of the same point f in the K absorption edge of the pure metal. These values are given in column 4 of Table 2. Here the plus sign means that the shift Δf is to the side of higher energies; the minus sign - that the shift is to the side of lower energies. It will be apparent from the table, first, that the maximum value of the shift of point f for all the considered compounds (except $Cr_2(SO_4)_3$) does not exceed 4 ev and in all cases is appreciably smaller than the difference $f - b$ given in column 2 and, second, that for some ionic and ionic-covalent compounds of the transition metals the center of the principal K absorption edge is shifted to the short wavelength side as compared with its position for the pure metal, while in other substances of the same type the shift is in the opposite direction. The reason for the last effect is unclear.

As a rule, for most compounds of chromium, iron, cobalt and nickel, the point f is displaced to the side of higher energies. However, for the transition metals under consideration and their compounds, the center of the principal K absorption edge, i.e., point f, is associated primarily with transitions of $1s$ electrons to higher lying (as compared with the unoccupied $3d$ and $4s$ levels) $4p$ states, so that the shift of this point in going from the metal to its ionic compounds cannot serve as a criterion for determining the true magnitude of the displacement of the edge. The short wavelength shift of this point for polar substances is apparently due to appreciable narrowing of the $4p$ and $4s$ bands and the appearance of a forbidden band between them.

Thus the energy level corresponding to the center of the principal K absorption edge (point f) of a transition element in strongly polar compounds is separated from the highest lying occupied state (the $3d$ level) by a series of bands, namely, 1) the unoccupied part of the $3d$ band, 2) the wholly vacant $4s$ band, and 3) a forbidden band located between the $4s$ and $4p$ bands (it is not impossible that there may also form a forbidden band between the $3d$ and $4s$ bands). In view of this one can understand and explain the very appreciable "shifts" of the K edges of transition elements in ionic compounds observed by authors[7] who reckoned the position of point f from the center of the curve for the initial absorption of the pure metal. However, the physical meaning attributed to these effects is not identical with that implied when one speaks of the true magnitude of the displacement of the K absorption edge, i.e., of the change in energy of the first unoccupied state above the valence band as compared with the energy of the Fermi surface of the metal.

Position of point A

In column 5 of Table 2 we list the values of ΔA characterizing the position of the peak A in different compounds as compared with its position in the absorption edge of the respective pure metals. It will be apparent from these data that there is no consistent correlation between the shift of points f and A. The principal regularity that may be noted is that in almost all the substances listed in Table 2, except for the compounds of copper and three compounds of manganese, the position of point A as compared with its position in the spectra of the pure metals either remains the same or is shifted to the long wavelength side, which again may be taken as indication of narrowing of the *4p* band for most of the substances for which the point *f* is shifted to the side of higher energies.

The absorptions characterized by points *f* and A are due primarily to transitions of K electrons into a band of the same symmetry, i.e., into the *4p* band. For ionic crystals and the oxides of the transition metals, in accord with the earlier scheme of reckoning, the principal K absorption edge (point *f*) is shifted 8-15 ev to the side of higher energies as compared with the position in pure metals (Ref.7 and Table 2). If we assume that a shift of this order of magnitude is due, in accord with the theory of external screening[9], to lowering of the *1s* level (increase of its term), then one may naturally expect to observe an equal shift of point A in the same direction, inasmuch as the initial and final states for the two points are common. Actually, however, peak A is shifted in most substances to the side of lower energies or remains in the same position. Moreover, so appreciable (8-15 ev) a decrease in the energy of the inner *1s* level of the ions of the transition elements in different compounds should give rise to a strong shift of the center of the initial absorption (point *b*) to the side of higher energies. Actually, however, as we have shown above, the position of point *b* in going from the pure metal to different compounds remains virtually unchanged. Moreover the $K\beta_5$ band (line) for a number of oxides of the transition metals is shifted to the long wavelength side.[7] In order to explain these experimental data by taking into account the effect of external screening, Karal'nik[9] hypothesizes that in the oxides of the transition metals there also occurs a lowering of the levels of the *3d* band, which must not only compensate the appreciable (8-15 ev) decrease in the energy of the *1s* level, due to withdrawal of *4s* electrons (for formation of the interatomic bonds), but must also exceed this decrease by several electron volts. In final analysis the energy of the unoccupied part of the *3d* band, electron transitions from which to the *1s* level give rise to the $K\beta_5$ emission band, should, according to Karal'nik[9], be lowered by 11 ev in Ni_2O_3, 12 ev in Co_2O_3, 14.6 ev in Fe_2O_3, 15 ev in Cr_2O_3 and 20 ev in V_2O_5 (Ref.7), which, in our opinion, is doubtful. We do not in principle deny possible manifestation of the effect of external screening in x-ray spectra, but we find that the order of magnitude of this effect inferred by Karal'nik is open to question and in conflict with the experimental facts.

References

1. S.A.Nemnonov & K.M.Kolobova, Fizika metallov i metallovedenie, 6, 183 (1958). (Trans.Physics of Metals & Metallography.)
2. W.W.Beeman & H.Friedman, Phys.Rev., 56, 392 (1939).
3. D.Koster & S.Kistra, Physica, 14, 175 (1948).
4. A.Nilsson, Arkiv.Fys., 6, 513 (1953).
5. S.A.Nemnonov & A.Z.Men'shikov, Izv.AN SSSR, Ser.fiz., 23, 578 (1959). (Trans.Bulletin,23, 559.)
6. S.A.Nemnonov & K.M.Kolobova, Fizika metallov i metallovedenie, 6, 183 (1958). (See Ref.1).
7. Landolt-Börnstein, Atom- und Molekularphysik, 1, Teil 4, 1955.
8. H.Hanson & J.Knight, Phys.Rev., 102, 632 (1956).
9. S.M.Karal'nik, Izv.AN SSSR, Ser.fiz., 21, 1445 (1957). (Trans.Bulletin, 21, 1432.)

INVESTIGATION OF THE PRINCIPAL K ABSORPTION EDGE OF NICKEL IN NICKEL-ALUMINUM ALLOYS

- S.A.Nemnonov & M.F.Sorokina

The present work is one of a series of studies, the program of which includes x-ray spectroscopic investigation of compounds of metals of the first transition period with aluminum, silicon and some other elements and has as its purpose to elucidate the characteristics of the electron interaction in such compounds as a function of a degree of filling of the *3d* shell of the transition element and the valence of the other components.

The intermetallic compounds of nickel with aluminum chosen for the present investigation are of particular interest for the following reasons.

Judging from the phase diagram, these intermetallic compounds are characterized by extremely strong interaction between unlike elements. The melting point of NiAl (1638°C) is almost 200° higher than the melting point of the most refractive of the components. According to the data of Nikolaeva & Umanskii[1], the characteristic temperature of this compound (490°K) is appreciably higher than the characteristic temperature of aluminum (390°) and nickel (385°). This phase exhibits an ordered structure (CsCl type) up to the melting point. The compound Ni_3Al, which forms from the liquid state as a result of a peritectic reaction, is also ordered even at high temperatures.

Such strong interaction must necessarily involve appreciable changes in the outer electron shells of both metals. The character of this interaction is apparently highly complex. Ageev & Guseva[2] applied harmonic analysis to the x-ray data to investigate the steric distribution of the electron density in NiAl. They found that the electron density in the direction from the nickel atom to the aluminum atom is appreciably greater than the interatomic "background" and halfway between the Ni and Al atoms equals $0.9\ \mathrm{\AA}^{-3}$. In the Ni—Ni direction it amounts to only $0.4\ \mathrm{\AA}^{-3}$, and in the Al—Al direction only $0.2\ \mathrm{\AA}^{-3}$. The high electron density bridges are evidence of an enhanced interaction differing in character from purely metallic coupling.

Foëx & Wucher[3], in investigating the magnetic properties of the limiting-concentration intermetallic compounds of metals of the first transition period with aluminum, found that the $NiAl_3$ phase is characterized by weak and virtually temperature independent paramagnetism; the paramagnetic susceptibility of $NiAl_3$ is even lower than the susceptibility of pure aluminum at the same temperature. Foëx & Wucher explained this by the filling of the *3d* orbits of the nickel atoms so that in the aluminum, owing to loss of part of the free electrons, there occurs decrease of the already weak paramagnetism. These results are in agreement with the concepts of Raynor[4] that metals of the first long period in compounds with aluminum (at an appreciable concentration of the latter) exhibit a negative valence sufficient for complete (or almost complete) filling of the *3d* levels. It is difficult to judge of the validity of these concepts in general, but in the case of nickel, which lacks only 0.6 electrons per atom, they would appear to be applicable. Here it may be useful to recall that when only a few electrons are lacking for complete filling of a level the tendency to complete filling is enhanced. An example of this is furnished not only by the pronounced negative valence of the halogens, but also the filling of the *3d* levels by 10 electrons in the copper atom by the transfer of one of the *4s* electrons. If the *3d* levels of nickel in $NiAl_3$ are actually filled, there must exist in this compound a polar component of the bonding forces owing to different charge of the atomic polyhedra composed of nickel and aluminum atoms. Evidence of a polar component in the bonding of Ni-Al alloys is furnished by the exceptional stability of the superstructure in Ni_3Al and NiAl and also the higher electronegativity of nickel as compared with aluminum (1.8-1.9 as against 1.5).[5]

Thus there are a number of indications of the presence in Ni-Al alloys, in addition to the predominating metallic bonds, of a certain fraction of covalent-polar bonds. Hence a complete and thorough x-ray spectroscopic investigation of the electron structure of these alloys would be highly desirable. So far we have investigated only the K absorption edges of nickel in these alloys.

For the purposes of this investigation we used pure nickel and the intermetallic compounds Ni_3Al, NiAl and $NiAl_3$. X-ray diffraction phase analyses show that Ni_3Al and NiAl are free of extraneous phases, while $NiAl_3$ contains a small amount of pure aluminum which, however, is not an interfering factor in recording the K absorption edge of nickel.

The K absorption edge of nickel was recorded photographically in the first order on a Johann mounting vacuum spectrograph. The analyzer was a bent quartz crystal (R = = 915 mm) with reflection from the (1$\bar{3}$40) planes (d_I = 1173.98 XU). The linear dispersion in the region of the K edge of nickel under these conditions was 3.0 XU/mm; the resolving power of the spectrograph (determined with reference to the Kα doublet of zinc) was about 6500. The density values obtained as a result of photometric scanning of the spectrograms were converted by means of an appropriate sensitometric curve to quantities proportional to the mass absorption coefficient μ/ρ.

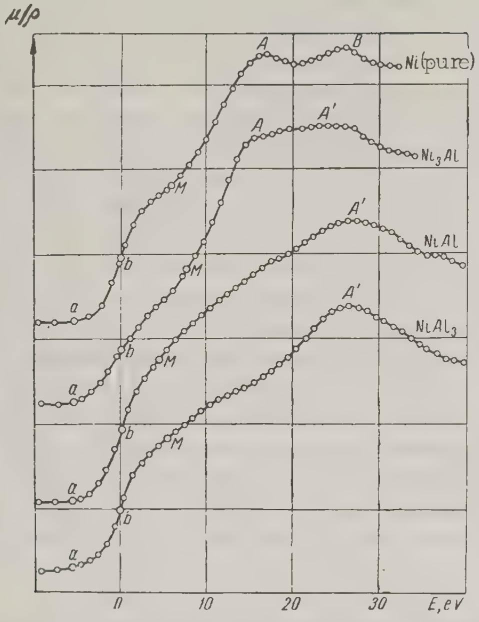

Fig.1. K absorption edges of nickel, pure metal and in the investigated alloys.

The K absorption edges of nickel in metal form and in the investigated compounds are shown in Fig.1. It will be evident that the structure of the edge undergoes alterations with increase of the aluminum content. The points identified by letters in Fig.1 have the following meanings: *a* - beginning of the rise of the absorption coefficient, *b* - center of the initial absorption region (the point of inflection of the rising absorption curve), M - midpoint or half-height of the whole absorption discontinuity, A - first absorption peak in the K edge of pure nickel, A' - first absorption peak in the altered edge of nickel in the compounds.

The structure of the initial region of the K absorption edge is determined primarily by the wave functions of the *3d* and *4s* states of the absorbing atom. An important role here, however, is also played by the nearest neightbor atoms: the symmetry of their outer wave functions and the degree of overlapping of these with the wave function of the *3d* and *4d* states significantly affect the probability for the transitions associated with the initial absorption.

Hence we shall simultaneously consider the changes occurring in the principal edge and the changes in the immediate ambiance of the nickel atom. Information on the crystallographic structure of the investigated compounds and on the immediate ambiance (nearest neighbors) of the Ni atoms in these compounds are presented below.

In Ni_3Al, as in pure nickel, each nickel atom has 12 nearest neighbors, but four of the Ni atoms are replaced by Al atoms, while the remaining 8 Ni atoms are displaced somewhat further from the central atom than in pure nickel (the distance $d^{(8)}_{Ni...Ni} = d^{(4)}_{Ni...Al} = 2.52$ Å as against 2.48 Å in pure nickel).

Phase	Type of symmetry	Distance to nearest neighbors of the Ni atom, A
Ni	f. c. c.	$d^{(12)}_{\mathrm{Ni}\ldots\mathrm{Ni}}=2{,}48$
Ni_3Al	f. c. c. (Cu_3Au)	$d^{(8)}_{\mathrm{Ni}\ldots\mathrm{Ni}}=d^{(4)}_{\mathrm{Ni}\ldots\mathrm{Al}}=2{,}52$
NiAl	b. c. c. (CsCl)	$d^{(8)}_{\mathrm{Ni}\ldots\mathrm{Al}}=2{,}44;\ d^{(6)}_{\mathrm{Ni}\ldots\mathrm{Ni}}=2{,}82$
$NiAl_3$	Rhombic	$\bar{d}^{(8)}_{\mathrm{Ni}\ldots\mathrm{Al}}=2{,}46;\ d^{(1)}_{\mathrm{Ni}\ldots\mathrm{Al}}=2{,}72$

If we assume that the initial absorption region is due to electron transitions to the *3d*-*4s* states and that it has an appreciable intensity only by virtue of overlapping of these states with the *4p* states, then the increase in the height of the initial absorption region in Ni_3Al can be explained by decrease of this overlapping owing to increase in the radius of the first coordination sphere. This reason also serves to explain the decrease in intensity in the absorption section next to the initial region, leading to effective shift of the point M to the side of higher energies. Because nickel atoms still predominate in the immediate ambiance, the structure of the principal absorption edge is in general similar to that of the K edge of pure nickel, although in the region ABA' there is already evident some modification of the structure in which one can discern new elements, i.e., some of the features characteristic of the absorption edge of nickel in NiAl and $NiAl_3$ (the A' region).

As regards fine structure, the K absorption edge of nickel in NiAl already differs appreciably from the edge in the spectrum of pure nickel. Although the point *b* persists in the same location (within ± 0.2-0.2 ev), the peak A is virtually effaced and a new peak A' appears some 10 ev to the short wavelength side of it. (A very similar rearrangement of the structure of the principal absorption edge of a transition element is observed in iron-aluminum[6], iron-silicon[7] and chromium-silicon[8] alloys.) NiAl has the CsCl type structure so that the immediate ambiance of each nickel atom consists of 8 aluminum atoms located at a distance of 2.44 Å from it. The second coordination sphere is comprised of six nickel atoms, each at a distance of 2.82 Å from the central Ni atom. Thus the immediate ambiance consists only of aluminum atoms (the nickel atoms are situated at an appreciably greater distance) and the *3p* wave functions of aluminum now apparently play the same role as the *4p* wave functions of nickel: they overlap with the *3d* and *4s* wave functions of nickel and thereby give rise to an appreciable absorption in the initial region and the neighboring section of the spectrum; this leads to an effective shift of the point M some 1.3 ev to the long wavelength side.

The crystallographic structure of $NiAl_3$ has a low order of symmetry (rhombic) and is extremely complex. But the immediate ambiance of each nickel atom here differs little from the ambiance in NiAl, so that the structure of the absorption edge of $NiAl_3$ is similar to that of NiAl. Each nickel atom is surrounded by 8 aluminum atoms located at an average distance of 2.46 Å (two Al atoms are at 2.42 Å, three at 2.44 Å, one at 2.46 Å and two at 2.52 Å), the ninth aluminum atom is located at a distance of 2.72 Å from the nickel atom. The new structure in the absorption edge of nickel, already evident in NiAl, becomes clearer and sharper in $NiAl_3$. The peak A' becomes more prominent but retains its position in the energy scale.

On the basis of examination and comparison of all the investigated absorption edges we arrive at the following deductions.

1. With increase in the aluminum content of the Ni-Al alloys the principal K absorption edge of nickel undergoes substantial modifications. The alterations occur mainly in the region of the principal peaks. Here we see evidence of gradual transition from the atomic interaction characteristic of pure nickel with its typical electron distribution in the conduction band to a new interaction with another

symmetry of the conduction band, a different electron density distribution in the band and a different probability for transitions from the *1s* state.

Comparison of the results obtained for the K absorption edges of nickel in NiAl alloys with the results for the transition metal in the Fe-Al (Ref.6), Fe-Si (Ref.7) and Cr-Si (Ref.8) systems shows that in all cases with increase of the second component there occurs a very complex alteration of the structure of the edge, which indicates that there is a certain degree of similarity in the interaction of different transition metal atoms with the atoms of aluminum or silicon in these systems.

It should be noted that in Ni-Al alloys the new peak A', located well to the short wavelength side of the peak A in the edge of pure nickel, already appears to a 50 atomic percent content of aluminum, whereas in Fe-Al alloys the corresponding peak is evinced only at appreciably higher aluminum concentrations.[6] Here undoubtedly we have the effect of the lower degree of defectiveness of the *3d* shells of nickel as compared with iron.

We note the following interesting fact. Although the intermetallic compounds NiAl and FeAl belong to the same crystallographic type (CsCl) and to the same group of electronic compounds (β-brass)[9], the structure of the principal K absorption edge of iron and nickel in these compounds is entirely different; this betokens a corresponding difference in the energy spectra of the free states. The nature of this effect is now being investigated.

2. As for the initial absorption region, it changes little and the point *b* undergoes little or displacement (Fig.1). In an earlier study[10] it was noted that the initial absorption region retains its energy position and changes only in height owing to change in the probability of the corresponding electron transitions. The results of the present investigation substantiate this fact. In the investigated compounds the initial absorption region is lowered slightly only in the spectrum of Ni_3Al, where the radius of the first coordination sphere is somewhat increased. When, however, the aluminum atoms (as in NiAl and $NiAl_3$) are located close enough to the nickel atoms to insure great overlapping of the Ni *3d-4s* wave functions with the Al *3p* functions, the intensity of the initial absorption again increases, attaining approximately the value for pure Ni. This is clearly evident from Fig.2, wherein we have superposed the K absorption edges of nickel in NiAl and of the pure metal.

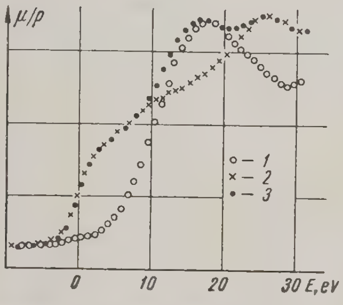

Fig.2. Superposition of the K absorption edges of nickel in NiO (1), $NiAl_3$ (2) and the pure metal (3).

We note that the results of measurements[11] of the magnetic moments of nickel atoms in Ni-Al alloys definitely show that the addition of 20 atomic percent aluminum to nickel already leads to appreciable filling of the *3d* band. It can therefore be safely assumed that in NiAl and $NiAl_3$ there can be no *3d* vacancies. This is substantiated by the experimental results of Foëx & Wucher[3].

The fact that the initial absorption region in the spectra of these alloys differs little from the same region in the spectrum of pure nickel gives reason to think that either in the case of nickel, despite the relatively high density of states in the *3d* band, $1s \rightarrow 3d$ transitions make no substantial contribution to the initial absorption region* or that the overlapping of the *3d-4s* wave functions of nickel with the *3p* functions of aluminum in NiAl and $NiAl_3$ leads

---

*The isochromate of the characteristic spectrum of nickel exhibits only a very low intensity *h*-structure peak, located on the steeply rising section of the excitation line.[12]

to a greater increase in the transition probability than the overlapping with the *4p* functions in pure nickel. The first alternative seems to be more likely.

3. The persistence of a significantly high transition probability corresponding to the initial absorption region in the spectra of Ni-Al alloys is evidence of the active role played by the *3p* wave functions of aluminum. In this respect it is interesting to compare the atomic separations and the K absorption edges of nickel in NiAl and NiO. In the oxide, as in NiAl, the nickel ions are forced further apart by the ions of the second component. But despite the fact that the number of unoccupied *3d* states increases owing to removal of part of the electrons, and the fact that the oxygen ions are located closer to the nickel atoms than the aluminum atoms in NiAl ($d_{\text{Ni}\ldots\text{O}} = 2.09$ Å as against $d_{\text{Ni}\ldots\text{Al}} = 2.44$ Å in NiAl), in the spectrum of nickel in NiO, the initial absorption rise is virtually effaced and there remains only a barely discernible hump (see Fig.2). This is apparently due to the fact that in the divalent oxygen ions there are no free *p* states close in energy to the *3d* and *4s* levels, and the occupied states in the oxygen ion form a more or less compact noble gas type configuration with negligibly small radial wave functions. In nickel-aluminum alloys, on the other hand, the wave functions of the outer (occupied and unoccupied) states in all probability strongly overlap and hybridize, as a result of which the initial absorption increases, although the number of unoccupied states in the *3d* band must be appreciably reduced in connection with its filling.

Comparison of the K absorption edges of nickel in Ni-Al alloys with the K absorption edge of iron in Fe-Al alloys, wherein x-ray spectroscopic data indicate the presence of a polar component in the bonding in addition to the predominant intermetallic bonding, gives reason to infer the presence of similar bonds in nickel-aluminum alloys. The validity of this inference is substantiated by the results of magnetic measurements[3] and the presence in nickel-aluminum alloys of a highly stable superstructure. In fact, judging by these attributes, the polar component in the bonds in nickel-aluminum compounds must be greater than in iron-aluminum alloys.

Projected investigations of the emission spectra of nickel and aluminum and studies of the corresponding emission and absorption characteristics of alloys of other transition metals of aluminum should provide the basis for more definite inferences.

Institute of Metal Physics,
Academy of Sciences of the USSR

References

1. S.M.Nikolaeva & Y.S.Umanskii, Izv.AN SSSR, Ser.fiz., 20,631 (1956). (Trans. Bulletin,20, 573.)
2. N.V.Ageev & L.N.Guseva, Izv.AN SSSR, Otd.khim.nauk, 3,225 (1949). (Trans. Bulletin, Ac. of Sci., Div.Chem.Sci.)
3. G.Foëx & J.Wucher, Compt.rend. 238, 1281 (1954).
4. G.V.Raynor, Progr.Metal.Phys., 1, 1 (1949).
5. L.Pauling, The Nature of the Chemical Bond and the Structure of Molecules and Crystals, Cornell, 1942. (Cited in Russian trans.)
6. S.A.Nemnonov & K.M.Kolobova, Fiz.metallov i metallovedenie, 6, 183 (1958). (Trans.Physics of Metals and Metallography.)
7. S.A.Nemnonov & K.M.Kolobova, Ibid. (In press).
8. S.A.Nemnonov & A.Z.Men'shikov, Fiz.metallov i metallovedenie, 9, 385 (1960). (Trans.Physics of Metals and Metallography.)
9. Ya.S.Umanskii et al, Fizicheskoe metallovedenie (Physical Metallography)M., 1955; W.Hume-Rothery & G.Raynor, Structure of Metals and Alloys (Cited in Russ.tr.)
10. S.A.Nemnonov & A.Z.Men'shikov, Izv.AN SSSR, Ser.fiz.,23,578 (1959). (Trans. Bulletin,23, 559.)
11. R.M.Bozorth, Ferromagnetism, N.Y., 1951 (Cited in Russian trans.)
12. A.Nilsson, Arkiv.fys., 6, 513 (1953).

FLUORESCENT L-SPECTRA OF NIOBIUM IN NbB_2, NbC, NbN AND PURE NIOBIUM*

- M. I. Korsunskii & Ya. E. Genkin

The L series fluorescent spectra of niobium - pure and in the nitride, carbide and diboride - were obtained on a bent (R = 1000 mm) quartz crystal x-ray spectrograph employing a Johann mounting ($d_\infty = 4246.02$ X). The spectrograph was equipped with a special fluorescence x-ray tube with interchangeable anodes. In order to insure a high intensity of the characteristic radiation of the primary target, the glancing angle of the cathode beam was made small (~28°).

The vacuum in the spectrograph was maintained at 10^{-5} mm Hg by means of MM-1000 and MM-40 pumps. Both the primary and secondary anodes were water cooled. The temperature of the secondary target did not exceed 25°. The speculum of the primary anode was made of silver.

The fluorescent L spectra of Nb were excited by the characteristic L radiation of silver. There were obtained the $L\alpha_1$, $L\alpha_2$, $L\beta_1$, $L\beta_2$, $L\beta_3$, $L\beta_4$ and $L\gamma_1$ lines of niobium as well as the satellites of the $L\alpha_1$ and $L\beta_1$ lines. The spectrograms were scanned on an MF-1 recording microphotometer.

Comparison of the spectrograms shows that entry of the niobium into the enumerated compounds is accompanied by changes in different parts of the spectrum: both the shape and intensity of individual spectrum lines and satellites change.

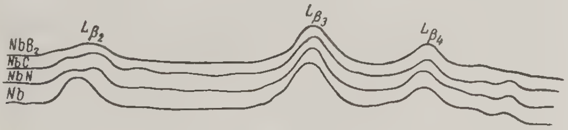

Fig.1

Photometric traces of the spectra of metallic niobium and niobium in the listed compounds in the region of the Nb-$L\beta_2$ - S-$K\alpha$ lines are juxtaposed in Fig.1. The exposure times were chosen so that the $L\beta_4$ line in each case would have the same density (for pure niobium - 14 hours, for the carbide and nitride - 16 hours and for the diboride - 17 hours). One can clearly discern variations in the shape and intensity of the $L\beta_2$ band. In pure niobium it has the shape of a normal spectrum line with an asymmetry index of 1.4. In the carbide and nitride, the band becomes a wide double-humped line. In the diboride, this band is distinctly asymmetric with a very flat slope on the short wavelength side.

To clarify the character of the changes, we superposed the spectrum of pure niobium upon the spectra of niobium in the compounds. Inasmuch as the relative intensity varies, an important factor in such superposition is choice of the "reference" line, i.e., the line, the contour of which is fully matched in superposing the spectra.

Obviously, when niobium enters into compounds there occur changes in the state of its outer electrons. These changes are accompanied by changes in the relative intensity of the lines associated with transitions competing with the L_{II}—N_{IV} and L_{III}—N_V transitions. For this reason one should not choose the $L\alpha_1$, $L\alpha_2$, $L\beta_1$ or any other similar line associated with such competing transitions as the "reference" for matching.

Among the lines associated with the noncompeting transitions L_I—M_{II}, L_I—M_{III}, etc. ($L\beta_4$ and $L\beta_3$, respectively), the $L\beta_4$ line represents transitions between deepest lying levels, so that changes in the outer shells should have the least effect on this line; hence in superposing the niobium spectra we equalized and matched the $L\beta_4$ lines.

This report was presented at the Sixth Scientific-Engineering Conference on the Application of X-rays to Investigation of Materials, held on June 24, 1958 in Leningrad.

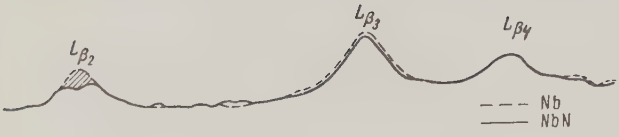

Fig.2

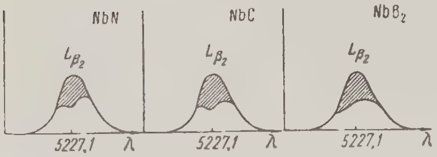

Fig.3

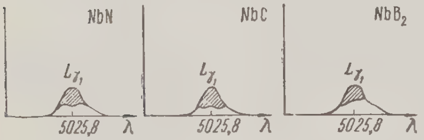

Fig.4

Table 1

Line	Nb	NbN	NbC	NbB$_2$
L_{β_2}	100	71,5	72,9	68,5
L_{γ_1}	37	26,3	27	27,6

Table 2

Line	Nb	NbN	NbC	NbB$_2$
L_{α_1}	100	100	100	100
L_{α_2}	11	11	11	11
L_{β_1}	60,0	60,5	61,0	62,0
L_{β_3}	9,9	9,5	9,9	10,2
L_{β_2}	5,3	4,0	4,0	3,5
L_{γ_1}	2,0	1,47	1,48	1,40
n_{IV}	0,56	0,39	0,39	0,36
n_V	1,27	0,91	0,90	0,77
$n_{IV}+n_V$	1,83	1,30	1,29	1,13

Fig.2 shows the superposition of the spectra of niobium and its nitride in the Nb-$L\beta_2$ - S-$K\alpha$ line region. It will be seen that with the proper intensity adjustment the $L\beta_4$ lines of Nb and NbN coincide over the entire contour; the $L\beta_3$ line retains its shape and changes very little in intensity.

In contrast, appreciable changes occur in the character of the $L\beta_2$ band. The $L\beta_2$ band of niobium in NbN lies wholly within the contour of this band in the spectrum of pure niobium. It may be said that part of the $L\beta_2$ band disappears incident to formation of the nitride (hatched area in Fig.2). It will be noted that the greatest change occurs in the central portion of the band.

Similar superpositions were carried out for the spectra of Nb & NbC and Nb & NbB$_2$. Enlarged views of the superposed $L\beta_2$ band sections are shown in Fig.3. It will be seen that in each case the $L\beta_2$ band is wholly inscribed in the contour of the emission band of pure niobium.

Thus in each case the change in the $L\beta_2$ band is characterized by the disappearance of part of the band. In the case of NbC and NbN the effect is strongest in the central part of the band, while in the case of NbB$_2$ the fading is greatest on the short wavelength side.

Inasmuch as the $L\beta_2$ emission band is complex in that it characterizes the density of a number of states (s, p, $d_{3/2}$ and $d_{5/2}$) the observed changes may be taken as evidence of changes in the density of the d states in the different compounds.

The $L\gamma_1$ band also undergoes pronounced changes incident to entry of Nb into compounds. Fig.4 shows the result of superposition of the $L\gamma_1$ band in pure niobium with the band in the enumerated compounds (as in the case of the $L\beta_2$ band the superposition was carried out for equal intensities of the $L\beta_4$ line). Here again we see that part of the band disappears in the compounds.

In Table 1 we list relative values characterizing the variation of the $L\beta_2$ and $L\gamma_1$ bands of NbB$_2$, NbC and NbN (for equal intensities of the $L\beta_4$ line). Table 2 lists the measured values of the integral L line intensities in the spectra of the nitride, carbide and diboride as compared with the intensity in the spectrum of pure niobium. It will be evident from the table that the $L\beta_1/L\alpha_1$ intensity ratio differs for different compounds, which may be taken as indication of redistribution of states in the *4d* band.

Satellites

The $L\alpha_1$ line in the spectra of all the investigated substances is accompanied by numerous satellites, which represent the radiation of doubly ionized atoms. The distribution in intensity among the satellites of the $L\alpha_1$ line in the spectra of niobium and its compounds differs. Whereas the intensity of most of the satellites changes very little, the intensity of the longest wavelength satellite $L\alpha_3$, which presumably is associated with L_{III}—M_V transitions in the absence of one of the N shell *d* electrons, undergoes an appreciable change. The intensity of this satellite is appreciably lower in all the compounds as compared with pure niobium. A particularly great change in the intensity of this satellite is observed in the spectrum of NbB_2.

The decrease in intensity of the $L\alpha_3$ satellite in going from pure niobium to the compounds substantiates our inference made above regarding the decrease in the density of *d* states incident to entry of niobium into the enumerated compounds.

Discussion

As was noted above, the intensity of the $L\beta_2$ and $L\gamma_1$ bands decreases appreciably incident to formation of niobium nitride, carbide and diboride. This decrease in intensity may partially be due to self-absorption. There is, however, no noticeable shift of the levels; hence the increase in self-absorption as compared with pure niobium can occur only as a result of decrease in the degree of filling of the *4d* states. The noticeable decrease of the relative intensity of the $L\beta_2$ and $L\gamma_1$ bands, therefore, may be taken as clear evidence of decrease in the density of *d* states in the communal band of all the investigated compounds.

Consequently, the hypothesis[1-5] regarding the transition of part of the valence electrons of nonmetallic atoms into the *d* band of the metallic atom in crystals incident to formation of interstitial phases of the transition elements is not substantiated in the case of stoichiometric niobium carbide, nitride and diboride.

The data of Table 2 bring out another interesting point. The fact that in going from pure niobium to the carbide, nitride and diboride, there occurs an increase in the intensity ratio $I\beta_1/I\alpha_1$ indicates that in these compounds there also occurs an increase of the ratio n_V/n_{IV}.[6]

The niobium compound samples used in the present investigation were made available by I.N.Frantsevich & G.V.Samsonov; we take this opportunity to thank them.

"V.I.Lenin" Kharkov Polytechnic Institute

References

1. E.Wigner & B.H.Huntington, J.Chem.Phys., 3, 764 (1935).
2. A.R.Ubbelohde, Proc.Roy.Soc., A,159, 295 (1937).
3. Ya.S.Umanskii, Karbidy tverdykh splavov (Solid solution carbide), p.60, M., 1947.
4. Ya.S.Umanskii, B.N.Finkel'shtein & M.E.Blanter, Fizicheskie osnovy metallovedeniya (Physical fundamentals of metallography), p.186, M., 1949.
5. Ya.S.Umanskii, Metallovedenie i termicheskaya obrabotka (Metallography and heat treatment), p.3, Collected Proceedings of the Moscow Steel Institute, No.XX, M., 1940.
6. M.I.Korsunskii & Ya.E.Genkin, Present issue of the Bulletin, p.470.

RELATIVE INTENSITIES OF THE Lβ_2, Lβ_{15} AND Lγ_1 LINES IN THE L SERIES SPECTRA OF SUBSTANCES WITH AN UNFILLED N SHELL*

- M. I. Korsunskii & Ya. E. Genkin

Removal of electrons from the L_{II} and L_{III} levels leads to the appearance of a number of the L series lines in the emission spectra.

We use $N_{L_{III}}$ and $N_{L_{II}}$ to designate the number of atoms with ionized L_{III} and L_{II}, respectively, levels formed per second in some constant excitation field. Let us consider the transitions L_{III}—M_V (Lα_1 line), L_{III}—M_{IV} (Lα_2), L_{II}—M_{IV} (Lβ_1), L_{III}—N_V (Lβ_2), L_{III}—N_{IV} (Lβ_{15}) and L_{II}—N_{IV} (Lγ_1). We designate the number of radiative transitions per second as a result of which there appear the enumerated L series lines lines by N_{α_I}, N_{α_2}, N_{β_I}, N_{β_2}, $N_{\beta_{15}}$ and N_{γ_I}, respectively. Further, we use a lower-case letter to indicate the number of electrons, and the same upper-case letter to indicate the shell to which the said electrons belong. The indices at the letters indicate the numbers of the sublevels.

Using the above notation we can write the following relations:

$$\begin{aligned}
N_{\alpha_I} &= N_{L_{III}} \frac{m_V \cdot \eta_{L_{III}M_V}}{\Sigma L_{III}}\ ; \quad N_{\beta_2} = N_{L_{III}} \frac{n_V \cdot \eta_{L_{III}N_V}}{\Sigma L_{III}}\ ; \\
N_{\alpha_2} &= N_{L_{III}} \frac{m_{IV} \cdot \eta_{L_{III}M_{IV}}}{\Sigma L_{III}}\ ; \quad N_{\beta_{15}} = N_{L_{III}} \frac{n_{IV} \cdot \eta_{L_{III}N_{IV}}}{\Sigma L_{III}}\ ; \\
N_{\beta_I} &= N_{L_{II}} \frac{m_{IV} \cdot \eta_{L_{II}M_{IV}}}{\Sigma L_{II}}\ ; \quad N_{\gamma_I} = N_{L_{II}} \frac{n_{IV} \cdot \eta_{L_{II}N_{IV}}}{\Sigma L_{II}}\ ,
\end{aligned} \tag{1}$$

where η_{fi} is the probability for the $f \to i$ transition, and

$$\begin{aligned}
\Sigma L_{III} &= \sum_{j,\,K} k_j \eta_{L_{III}K_j} \ (j = \mathrm{I},\ \mathrm{II},\ \mathrm{III},\ \mathrm{IV},\ \mathrm{V},\ \ldots); \\
\Sigma L_{II} &= \sum_{j,\,K} k_j \eta_{L_{II}K_j} \ (K = L,\ M,\ N,\ O,\ \ldots).
\end{aligned} \tag{2}$$

Taking Eqs. (1) in pairs and dividing, we readily obtain

$$\begin{aligned}
\frac{N_{\beta_2}}{N_{\alpha_1}} &= \frac{n_V}{m_V} \cdot \frac{\eta_{L_{III}N_V}}{\eta_{L_{III}M_V}}\ ; \\
\frac{N_{\beta_{15}}}{N_{\alpha_2}} &= \frac{n_{IV}}{m_{IV}} \cdot \frac{\eta_{L_{III}N_{IV}}}{\eta_{L_{III}M_{IV}}}\ ; \\
\frac{N_{\gamma_I}}{N_{\beta_I}} &= \frac{n_{IV}}{m_{IV}} \frac{\eta_{L_{II}N_{IV}}}{\eta_{L_{II}M_{IV}}}\ .
\end{aligned} \tag{3}$$

The lines under consideration form two triplets. The relative line intensity of such triplets satisfies the Burger-Dorgelo rule provided the levels are filled and the magnitude of their splitting is not great. Assuming that for elements with filled M and N shells the intensity distribution among the lines of the multiplets will be the same, we can write

$$\frac{\eta_{L_{III}N_V}}{\eta_{L_{III}M_V}} = \frac{\eta_{L_{III}N_{IV}}}{\eta_{L_{III}M_{IV}}} = \frac{\eta_{L_{II}N_{IV}}}{\eta_{L_{II}M_{IV}}}\ . \tag{4}$$

One part of this relationship can be checked on the basis of the experimental data given in the literature on the intensities of the $L\alpha_1$, $L\alpha_2$, $L\beta_2$, $L\beta_I$ and $L\gamma_1$ lines in the spectra of elements with a filled N shell. Inasmuch as the intensity I_j of a given line is equal to the product of the photon energy by the number of transitions $h\nu_j N_j$, we can write

---

*This report was presented at the Sixth Scientific-Engineering Conference on the Application of X-Rays to Investigation of Materials, held on June 24, 1958 in Leningrad.

$$\frac{\eta_{L_{\mathrm{III}}N_{\mathrm{V}}}}{\eta_{L_{\mathrm{III}}M_{\mathrm{V}}}} = \frac{N_{\beta_2}}{N_{\alpha_1}} = \frac{I_{\beta_2}\cdot\lambda_{\beta_2}}{I_{\alpha_I}\cdot\lambda_{\alpha_1}};$$

$$\frac{\eta_{L_{\mathrm{II}}N_{\mathrm{IV}}}}{\eta_{L_{\mathrm{II}}M_{\mathrm{IV}}}} = \frac{N_{\gamma_I}}{N_{\beta_1}} = \frac{I_{\gamma_I}\cdot\lambda_{\gamma_I}}{I_{\beta_I}\cdot\lambda_{\beta_I}}. \qquad (5)$$

The experimental data on $\frac{I_{\beta_2}\cdot\lambda_{\beta_2}}{I_{\alpha_1}\cdot\lambda_{\alpha_1}}$ (circles) and $\frac{I_{\gamma_1}\cdot\lambda_{\gamma_1}}{I_{\beta_1}\cdot\lambda_{\beta_1}}$ (crosses) are shown in Fig.1. Within the limits of scatter, which does not exceed the usual uncertainty in measuring line intensities, the crosses and circles fall on one horizontal straight line, which substantiates the equalities (4).

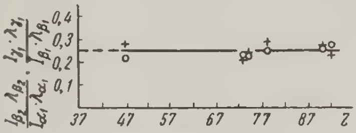

Fig.1

It follows from (3) and (4) that for elements with a filled M shell but an unfilled N shell,

$$N_{\beta_2} : N_{\beta_{15}} : N_{\gamma_1} = 6\,\frac{n_{\mathrm{V}}}{n_{\mathrm{IV}}} : 9\,\frac{N_{\alpha_2}}{N_{\alpha_1}} : 9\,\frac{N_{\beta_1}}{N_{\alpha_1}}, \qquad (6)$$

inasmuch as $m_{\mathrm{IV}} = 4$ and $m_{\mathrm{V}} = 6$.

The ratio

$$\frac{N_{\alpha_2}}{N_{\alpha_1}} = \frac{4}{6}\cdot\frac{\eta_{L_{\mathrm{III}}M_{\mathrm{IV}}}}{\eta_{L_{\mathrm{III}}M_{\mathrm{V}}}} \qquad (7)$$

must be constant for atoms with both a filled and an unfilled N shell.

As for the relation

$$\frac{N_{\beta_1}}{N_{\alpha_1}} = \frac{4}{6}\cdot\frac{\eta_{L_{\mathrm{II}}N_{\mathrm{IV}}}}{\eta_{L_{\mathrm{III}}M_{\mathrm{V}}}}\cdot\frac{N_{L_{\mathrm{II}}}}{N_{L_{\mathrm{III}}}}\cdot\frac{\Sigma L_{\mathrm{III}}}{\Sigma L_{\mathrm{II}}}, \qquad (8)$$

it depends not only on the ratio $\frac{\eta_{L_{\mathrm{II}}N_{\mathrm{IV}}}}{\eta_{L_{\mathrm{III}}M_{\mathrm{V}}}}$, but also on the ratio $\frac{\Sigma L_{\mathrm{III}}}{\Sigma L_{\mathrm{II}}}$. The last in atoms with an unfilled N shell will not remain constant but will vary with filling of the $d_{3/2}$ and $d_{5/2}$ states of the N shell, for, as can readily be shown,

$$\Sigma L_{\mathrm{III}} = \eta_{L_{\mathrm{III}}M_{\mathrm{V}}}\left(2\,\frac{\eta_{L_{\mathrm{III}}M_{\mathrm{I}}}}{\eta_{L_{\mathrm{III}}M_{\mathrm{V}}}} + 4\,\frac{\eta_{L_{\mathrm{III}}M_{\mathrm{IV}}}}{\eta_{L_{\mathrm{III}}M_{\mathrm{V}}}} + 6 + 2\,\frac{\eta_{L_{\mathrm{III}}N_{\mathrm{I}}}}{\eta_{L_{\mathrm{III}}M_{\mathrm{V}}}} + n_{\mathrm{IV}}\,\frac{\eta_{L_{\mathrm{III}}N_{\mathrm{IV}}}}{\eta_{L_{\mathrm{III}}M_{\mathrm{V}}}} + \right.$$

$$\left. + n_{\mathrm{V}}\,\frac{\eta_{L_{\mathrm{III}}N_{\mathrm{V}}}}{\eta_{L_{\mathrm{III}}M_{\mathrm{V}}}} + o_1\,\frac{\eta_{L_{\mathrm{III}}O_1}}{\eta_{L_{\mathrm{III}}M_{\mathrm{V}}}}\right); \qquad (9)$$

$$\Sigma L_{\mathrm{II}} = \eta_{L_{\mathrm{II}}M_{\mathrm{IV}}}\left(2\,\frac{\eta_{L_{\mathrm{II}}M_{\mathrm{I}}}}{\eta_{L_{\mathrm{II}}M_{\mathrm{IV}}}} + 4 + 2\,\frac{\eta_{L_{\mathrm{II}}N_{\mathrm{I}}}}{\eta_{L_{\mathrm{II}}M_{\mathrm{IV}}}} + n_{\mathrm{IV}}\,\frac{\eta_{L_{\mathrm{II}}N_{\mathrm{IV}}}}{\eta_{L_{\mathrm{II}}M_{\mathrm{IV}}}} + o_1\,\frac{\eta_{L_{\mathrm{II}}O_1}}{\eta_{L_{\mathrm{II}}M_{\mathrm{IV}}}}\right). \qquad (10)$$

The values of the probability ratios $\frac{\eta_{jk}}{\eta_{jf}}$, entering into Eqs.(9) and (10), can be determined from the experimental data for the relative intensities of the lines associated with the corresponding transitions in heavy atoms with a filled N shell. Analysis of the available data yielded the following numerical values:

$$\begin{aligned}
&\frac{\eta_{L_{\mathrm{III}}M_{\mathrm{I}}}}{\eta_{L_{\mathrm{III}}M_{\mathrm{V}}}} = 1/9; \quad && \frac{\eta_{L_{\mathrm{II}}M_{\mathrm{I}}}}{\eta_{L_{\mathrm{II}}M_{\mathrm{IV}}}} = 0.03;\\
&\frac{\eta_{L_{\mathrm{III}}M_{\mathrm{IV}}}}{\eta_{L_{\mathrm{III}}M_{\mathrm{V}}}} = 1/6; && \frac{\eta_{L_{\mathrm{II}}N_{\mathrm{I}}}}{\eta_{L_{\mathrm{II}}M_{\mathrm{IV}}}} = 0.01;\\
&\frac{\eta_{L_{\mathrm{III}}N_{\mathrm{I}}}}{\eta_{L_{\mathrm{III}}M_{\mathrm{V}}}} = 9/200; && \frac{\eta_{L_{\mathrm{II}}N_{\mathrm{IV}}}}{\eta_{L_{\mathrm{II}}M_{\mathrm{IV}}}} = 1/4;\\
&\frac{\eta_{L_{\mathrm{III}}N_{\mathrm{IV}}}}{\eta_{L_{\mathrm{III}}M_{\mathrm{V}}}} = 0.042; && \frac{\eta_{L_{\mathrm{II}}O_{\mathrm{I}}}}{\eta_{L_{\mathrm{II}}M_{\mathrm{IV}}}} = 0.00\ldots;\\
&\frac{\eta_{L_{\mathrm{III}}N_{\mathrm{V}}}}{\eta_{L_{\mathrm{III}}M_{\mathrm{V}}}} = 1/4; && \frac{\eta_{L_{\mathrm{III}}O_{\mathrm{I}}}}{\eta_{L_{\mathrm{III}}M_{\mathrm{V}}}} = 3/200.
\end{aligned} \tag{11}$$

Inserting these in (9) and (10), we find

$$\Sigma L_{\mathrm{III}} = (6.99 + 0.042 n_{\mathrm{IV}} + 0.25 n_{\mathrm{V}})\, \eta_{L_{\mathrm{III}}M_{\mathrm{V}}}; \tag{12}$$

$$\Sigma L_{\mathrm{II}} = (4.08 + 0.25 n_{\mathrm{IV}})\, \eta_{L_{\mathrm{II}}M_{\mathrm{IV}}}. \tag{13}$$

Invoking the fact that $\frac{N_{L_{\mathrm{II}}}}{N_{L_{\mathrm{III}}}} = \frac{l_{\mathrm{II}}}{l_{\mathrm{III}}} = 1/2$, we obtain from (8), (12) and (13)

$$\frac{I_{\beta_1}\cdot\lambda_{\beta_1}}{I_{\alpha_1}\cdot\lambda_{\alpha_1}} = \frac{N_{\beta_1}}{N_{\alpha_1}} = \frac{(6.99 + 0.042 n_{\mathrm{IV}} + 0.25 n_{\mathrm{V}})}{3\,(4.08 + 0.25 n_{\mathrm{IV}})}. \tag{14}$$

It follows from (14) that the intensity ratio I_{β_1}/I_{α_1} actually does depend on the degree of filling of the N shell. For a filled N shell ratio (14) takes on a value of 0.57, which virtually coincides with the value of 5/9 for this ratio following from the Burger-Dorgelo rule.

For evaluating n_{IV} and n_{V} from (14) we shall use the graph of Fig.2, which shows the variation of I_{β_1}/I_{α_1} as a function of n_{V} for different n_{IV}. Filling of the n_{V} and n_{IV} states in the ratio 3:2 yields values varying from 0.571 to 0.568 for I_{β_1}/I_{α_1} (dashed line in Fig.2).

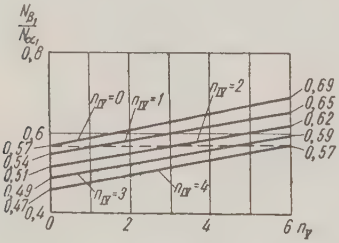

Fig.2

Larger values of I_{β_1}/I_{α_1} correspond primarily to filling of the $d_{5/2}$ state; smaller values to filling of the $d_{3/2}$ state. For example, if $I_{\beta_1}/I_{\alpha_1} = 0.6$, and there are only three electrons in the d state, it follows from the graph that $n_{\mathrm{IV}} \approx 0.5$ and $n_{\mathrm{V}} \approx 2.5$, i.e., $\frac{n_{\mathrm{V}}}{n_{\mathrm{IV}}} > 3/2$.

Converting in (6) to intensities and neglecting the difference between the photon energies for the $L\beta_2$ and $L\beta_{15}$ emission lines and for the $L\alpha_1$ and $L\alpha_2$ lines, we obtain, taking (11) into account:

$$I_{\beta_2} : I_{\beta_{15}} : I_{\gamma_1}\frac{\lambda\gamma_1}{\lambda\beta_2} = 6\,\frac{n_{\mathrm{V}}}{n_{\mathrm{IV}}} : 1 : 9\,\frac{I_{\beta_1}\cdot\lambda_{\beta_1}}{I_{\alpha_1}\cdot\lambda_{\alpha_1}}. \tag{15}$$

Inasmuch as the intensities of the $L\beta_2$, $L\beta_{15}$ and $L\beta_7$ lines in the spectra of substances with unfilled N shells are inseparable, in practice the intensity I'_{β_2} of the experimental line is comprised of the intensities $I_{\beta_7} + I_{\beta_{15}} + I_{\beta_2}$. However, according to (11), the intensity I_{β_1} is relatively low and hence can be neglected compared to $I_{\beta_{15}}$ and I_{β_2}.

From (3) and (11) we obtain

$$n_{\mathrm{IV}} = 16\frac{I_{\gamma_{\mathrm{I}}}\cdot\lambda_{\gamma_1}}{I_{\beta_1}\cdot\lambda_{\beta_1}}. \tag{16}$$

From (15) and (16) it follows that

$$n_{\mathrm{V}} = 24\frac{I'_{\beta_2}\cdot\lambda_{\beta_2}}{I_{\alpha_1}\cdot\lambda_{\alpha_1}} - 2.67\,\frac{I_{\gamma_1}\cdot\lambda_{\gamma_1}}{I_{\beta_1}\cdot\lambda_{\beta_1}}. \tag{17}$$

The ratios (15) represent the relative intensities I_{β_2}, $I_{\beta_{15}}$ and I_{γ_1} of the triplet for substances with an unfilled N shell. Together with (3) and (11), Eq.(15) allows of determining by means of formulas (16) and (17) the number of electrons in the $d_{3/2}$ and $d_{5/2}$ states for single atoms, i.e., in the gaseous state of the substance.

In the solid state the levels are hybridized. The symmetry of the wave function of the outer electron changes. The state of the outer electrons from being pure becomes primarily a mixture of s, p and d states. In this case, formulas (16) and (17) determine not the number of N shell electrons in the $d_{3/2}$ and $d_{5/2}$ states of an isolated atom but the relative weights of the $d_{3/2}$ and $d_{5/2}$ states in the outer band.

It will be noted that there enter into (16) and (17) the experimental values of the integral intensities of the L lines of substances with an unfilled N shell. Hence in using Eqs.(16) and (17) one must know the precise values of the integral intensities of these lines.

In view of the fact that the last emission lines of the substances under discussion may be distorted somewhat owing to self-absorption in the emitter, one must give preference to Eq.(14) which contains the ratio of the integral intensities of the $L\beta_1$ and $L\alpha_1$ lines. These lines are located at an appreciable distance from the main absorption edge; hence their relative intensities remain virtually constant.

In the accompanying table we give the relative line intensities $\frac{I_{\beta_1}}{I_{\alpha_1}}$, $\frac{I_{\gamma_1}}{I_{\beta_1}}$ and $\frac{I'_{\beta_2}}{I_{\alpha_1}}$ and the values of $n_{\mathrm{IV}}, n_{\mathrm{V}}$ and $n_{\mathrm{IV}}+n_{\mathrm{V}}$ calculated on the basis thereof. The values of the integral intensities were calculated on the basis of the data in the literature^1 and the results of our measurements^2.

	$_{41}$Nb	$_{42}$Mo	$_{45}$Rh	$_{46}$Pd	$_{47}$Ag
$\frac{I_{\beta_1}}{I_{\alpha_1}}$	0,6	0,54	0,565	0,536	0,546
$\frac{I_{\gamma_1}}{I_{\beta_1}}$	0,035	0,197	0,200	0,218	0,305
$\frac{I'_{\beta_2}}{I_{\alpha_1}}$	0,053	0,118	0,171	0,158	0,275
n_{IV}	0,56	2,9	3,0	3,2	4,5
n_{V}	1,27	2,1	3,2	3,0	5,28
$n_{\mathrm{IV}}+$ $+n_{\mathrm{V}}$	1,83	5	6,2	6,2	9,78

It follows from the tabular data that the distribution of $d_{3/2}$ and $d_{5/2}$ states differs in the listed elements. Whereas in Nb, Rh and Ag the weight of the $d_{5/2}$ states is greater than the weight of the $d_{3/2}$ states, in Mo and Pd the weight of the $d_{5/2}$ states is lower than that of the $d_{3/2}$ states. The weight of the $d_{3/2}$ and $d_{5/2}$ states in Mo is 5, which coincides with the number of electron on the N_{IV} and N_V levels in the free Mo atom; at the same time the weight of the $d_{3/2}+d_{5/2}$ states in Nb, Rh and Pd is appreciably lower than the number of electrons on the N_{IV} + N_V levels of the free atoms of these elements: specifically, in Nb 1.38 instead of 4; in Rh 6.2 instead of 8; in Pd 6.2 instead of 10. These data show that in the solid state the weight of the d states in the outer energy band of the substances under consideration is relatively low. The cited data indicate the possibility of determining the electron distribution in the $4d$ band of the transition metals. However, in connection with the fact that the data on the integral intensities are not characterized by particularly great accuracy, one must regard the values of n_{IV} and n_{V} listed in the table as only approximate.

In connection with the possibility of determining the values of n_{IV} and n_{V} from the data on the integral intensities of the L series line we are faced with the important problem of precise determination of the integral intensities of all the lines in the L spectra of the transition elements and their alloys and compounds with a view to determining the population of the $d_{3/2}$ and $d_{5/2}$ states.

"V.I.Lenin" Kharkov Polytechnic Institute

References

1. M.A.Blokhin, Fizika rentgenovskikh luchei (Physics of x-rays), Second edition, p.492, M., 1957.
2. M.I.Korsunskii & Ya.E.Genkin, Present issue of the Bulletin, p.467.

FLUORESCENT L SERIES OF NIOBIUM BOUND IN SOME COMPOUNDS

- M. I. Korsunskii & Ya. E. Genkin

In the present report we give some of the results of our investigation of the L series of niobium in compounds with nitrogen (6.32, 6.8, 8.1, 10.2, 11.9 and 12.6% N by weight), silicon and hydrogen. This investigation was a continuation of the work of Ref.1, wherein we described the experimental procedure and the method of processing the fluorescent spectra.

In the spectra of the enumerated substances, as in the earlier investigated spectra of niobium in NbB_2, NbN and NbC, there occur very appreciable changes in the $L\beta_2$ and $L\gamma_1$ emission bands (as compared with the spectrum of pure niobium). The other lines of the L series undergo no noticeable shift and change little in intensity.

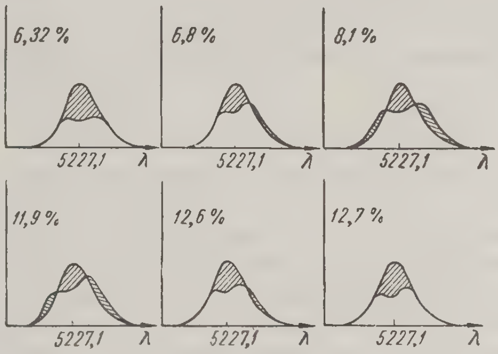

Fig.1

The change in the character of the $L\beta_2$ emission band in the niobium-nitrogen system for different nitrogen concentrations is shown in Fig.1, which represents a superposition of the $L\beta_2$ band of the indicated substances on the $L\beta_2$ band of pure niobium (the superposition was realized by matching the $L\beta_2$ lines). The noncoinciding parts of the bands are hatched. The two-humped character of the band in the spectra of the bound niobium is clearly evident.

The values of the integral intensity of the $L\beta_2$ band for different nitrogen concentrations are listed in the accompanying table (the intensity values are referred to the intensity in the spectrum of pure Nb, taken as unity).

Substance	c_N, %	Integral intensity
NbN	6,32	0,68
	6,8	0,79
	8,1	1,05
	10,2	1,10
	11,9	1,10
	12,6	0,74
Nb_5Si_3		0,60
$NbSi_2$ (with impurities)		0,99
NbH_x		1,06

The $L\gamma_1$ band undergoes analogous changes; it is two-humped.

In Fig.2 the $L\beta_2$ bands of Nb_5Si_3, $NbSi_2$ and NbH are superimposed on the $L\beta_2$ band of pure niobium. It will be seen that the $L\beta_2$ band of niobium in Nb_5Si_3 lies entirely within the contour of the $L\beta_2$ band of pure niobium. Again, this band is two-humped. The $L\gamma_1$ band exhibits similar changes.

In NbH the $L\beta_2$ and $L\gamma_1$ bands change appreciably as regards shape and position: in the NbH spectrum these become two-humped broad bands, the center of gravity of which is shifted to the long wavelength side relative to the center of gravity of the respective bands in the spectrum of pure niobium.

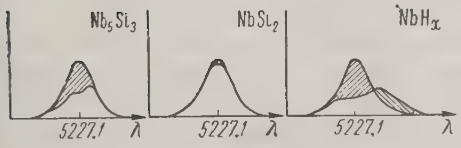

Fig.2

Our $NbSi_2$ samples contained an appreciable amount of impurities (up to 7% iron and ~1% sulfur). It is interesting to note that in this case, the shape, position and intensity of all the lines were the same, within the limits of the measurement error, as in the spectrum of pure niobium.

Discussion

Change in the shape of a given band in the fluorescent spectrum may to some extent be due to self-absorption in the secondary target. The influence of self-absorption is taken into account by the factor

$$\frac{1}{1+\frac{\mu_1\cdot\sin\varphi_2}{\mu_2\cdot\sin\varphi_1}},$$

where μ_1 is the coefficient of absorption of the secondary radiation in the material of the secondary target, μ_2 is the coefficient of absorption of the primary radiation in the material of the secondary target, φ_1 is the average angle of emission of the secondary radiation from the material of the secondary target to the analyzer (glancing angle) and φ_2 is the average glancing angle of the primary radiation relative to the surface of the secondary target.

Hence to determine the influence of reabsorption we obtained the L spectra of pure niobium and niobium in NbN for two different values of the angles, namely,

$$1)\ \varphi_1 = 30^\circ,\ \ \varphi_2 = 70^\circ;$$
$$2)\ \varphi_1 = 70^\circ,\ \ \varphi_2 = 30^\circ.$$

In the first case the ratio $\frac{\sin\varphi_1}{\sin\varphi_2}$ is 0.53; in the second case it is 1.88.

Despite this, the ratio of the spectral intensities over the entire $L\beta_2$ band in the spectra of NbN and pure niobium remains the same. This shows that in the case under consideration the influence of reabsorption on the shape of the band is virtually nil. Hence the observed change in the $L\beta_2$ and $L\gamma_1$ bands is not due to self-absorption, but indicates a change in the character of the bonds in the investigated substances.

In our opinion the investigated spectra may be divided into two groups.

The first group includes spectra of niobium in compounds with nitrogen at concentrations of 6.32, 6.8 and 12.6%, in Nb_5Si_3, and also the spectra of the earlier investigated[1] NbB_2, NbC and NbN. In these spectra the $L\beta_2$ band is not shifted relative to its position in the spectrum of pure niobium and its shape changes so that the contour of the $L\beta_2$ band in the spectrum of the compound lies wholly within the contour of the band in the spectrum of pure niobium.

The disappearance of different parts of the $L\beta_2$ emission bands in the spectra of the enumerated compounds indicates that the relative density of *d* states in the communal band is not constant, but differs in the different compounds.

It should be noted that the substances yielding spectra in the first group are compounds with a stoichiometric proportion of the components (NbB_2, NbC, NbN and Nb_5Si_3) or substances comprised in regions of phase homogeneity (the 6.32 and 6.8% nitrogen concentration range corresponds to the region of homogeneity of the Nb_2N phase, while the 12.6% nitrogen concentration corresponds to the region of homogeneity of the NbN phase).

From the fact that all the lines of niobium in substances of the first group are not shifted, it may be concluded that the charge of the niobium ions in these compounds does not undergo any substantial change.

The second group comprises the emission spectra of substances in which the $L\beta_2$ band is shifted and is not contained within the contour of the $L\beta_2$ band of pure niobium. Such spectra are exhibited by niobium nitrides with 8.1, 10.2 and 11.9% nitrogen by weight and also the investigated niobium hydride specimen.

The broadening of the $L\beta_2$ band of niobium in compounds indicates increase in the number of electrons in the communal band of these compounds as compared with pure niobium.

"V. I. Lenin" Kharkov Polytechnic Institute

Reference

1. M. I. Korsunskii & Ya. E. Genkin, Present issue of the Bulletin, p.467

HIGH TEMPERATURE X-RAY STUDIES OF INVAR ALLOYS

- S.M.Karal'nik, L.G.Nikolaeva & N.N.Nefedov

In an earlier investigation[1] of the characteristic x-ray absorption of components of iron-nickel alloys it was established that the most appreciable shift in the position of the K edges occurs in the concentration range wherein there occur the greatest changes in many of the physical properties of the alloy, including the coefficient of thermal expansion, i.e., in the region of formation of Invar type alloys. We felt it would be worthwhile to carry out a more precise investigation of the position of the K edge of components of alloys not only of the iron-nickel system but of some other system that also has an Invar region. Moreover, we felt it would be desirable to carry out this investigation not only at room temperature but with variation of the temperature to high values, inasmuch as Invar type alloys are characterized not only by low values of the thermal expansion coefficient but by an appreciable variation of the coefficient with increase of temperature.[2]

The basic experimental procedure was described in Ref.3; in the present work it was improved in the sense that the number of pulses per unit time was recorded by means of a B-2 scaler. In addition, in order to obviate possible oxidation of the samples incident to heating, these were placed under a small airtight hood, the space under which could be either evacuated or filled with an appropriate inert gas. This hood was provided with beryllium windows for passage of the x-rays. The walls and bottom of the hood were made double to form a water jacket. By this means we assured a constant temperature of the assembly at any temperature of the heating unit inside the hood and thus eliminated the possibility of heating the diffracting crystal, which could lead to distortion of the experimental results. That such heating may result in distortion can readily be shown by simple calculations. According to the Bragg law

$$\Delta\varphi = -\frac{\Delta d}{d}\tan\varphi,$$

inasmuch as $\Delta d = \alpha\Delta t\, d$, we have $\Delta\varphi = -\alpha\Delta t\tan\varphi$.

For an NaCl crystal $\alpha = 0.42\cdot10^{-4}$ degree^{-1}, and therefore for $\Delta t = 1^{\circ}C$

$$|\Delta\varphi_{1^{\circ}}| = 0.42\cdot10^{-4}\tan\varphi.$$

For the K edge of iron in the third order of reflection $\varphi \approx 67^{\circ}$, hence $|\Delta\varphi_{1^{\circ}}| = 9.9\cdot10^{-5}$. Thus a ~3° temperature rise of the analyzer crystal is sufficient to produce a noticeable displacement of the x-ray spectrum, i.e., a 1' shift of the edge to the short wavelength side, which for the specific case of Fe K III is equivalent to approximately 1 ev.

There can be no doubt that misleading results were obtained in experiments where this effect was not eliminated or taken into account. Apparently, this is the reason for the erroneous results obtained by Kazantsev[4] in determining the apparent shift of the K edge of nickel with increase of the sample temperature. The fact that in his work, Kazantsev recorded micrograms with reference lines did not eliminate the temperature distortion inasmuch as the reference line and the K edge of nickel were recorded in separate exposures, i.e., the reference line was recorded in the absence of the heated specimen. Thus the analyzer crystal in the exposures for the K edge of nickel was at a higher temperature, and with increase of the heater temperature the heating of the crystal undoubtedly increased more rapidly than according to the linear law inasmuch as in vacuum heating heat transfer occurs primarily by radiation. We believe that this heating effect led Kazantsev[4] to an erroneous inference regarding the shift of the K edge of nickel incident to heating through the Curie point. In our set-up the leads to the chromel-alumel thermocouple and to the heater were brought in through the bottom of the vacuum hood. The furnace was made in the form of two rectangular heating elements which were sandwiched over the sample foil. The foil was folded at one end to form a pocket which received the thermocouple. The indications of the thermocouple were checked with reference to the melting point of a number of metals and alloys placed in turn into the same pocket. These tests showed that our temperature measurements were accurate to within ±10°.

Table 1

Shift of the K absorption edge of Fe in alloys as compared with the position of the edge in Armco iron

Alloy	Composition	Shift, cv
№ 1	Fe + 25% wt.Pt	1,6±0,4
№ 2	Fe + 48% wt.Pt	2,3±0,2
№ 3	Fe + 56% wt.Pt	5,2±0,5
№ 4	Fe + 75% wt.Pt	7,0±0,4

Table 2

Shift of the K edge of Fe in alloys Nos.1,2 & 3

Alloy	t, °C	Shift[#], cv
№ 1	80	0±0,2
	205	+0,3±0,2
	270	—0,2±0,3
	350	+0,2±0,2
	390	+0,6±0,2
	470	+0,2±0,2
	500	+0,6±0,2
	550	+0,2±0,2
	660	+0,2±0,2
	695	+0,2±0,2
	765	—0,2±0,2
	855	—0,1±0,3
№ 2	70	0±0,0
	180	—1,0±0,4
	260	—0,4±0,3
	410	—0,7±0,3
	590	—0,5±0,4
	620	—1,0±0,3
	850	+0,6±0,2
№ 3	85	+0,3±0,5
	140	+1,1±0,6
	230	+0,4±0,6
	260	+0,9±0,6
	400	+0,8±0,6
	450	+0,7±0,7
	800	+2,0±0,8
	930	+1,2±0,6

The experimental results are listed in Tables 1 and 2.

All the K edge shifts listed in Table 1 were to the side of shorter wavelengths; as will be evident from the table, the maximum shift occurred for the alloy of stoichiometric composition (75% Pt[*]). A somewhat smaller shift of the K edge obtains for alloy No.3, characterized by the minimum expansion coefficient[2].

We carried out measurements of the temperature dependence of the position of the K absorption edge for Fe-Pt alloy samples Nos.1,2 and 3. As noted above, in order to check and refine our earlier results[1], employing our improved technique, we also carried out temperature measurements on samples of Fe + 34% Ni and Fe + 63% Ni alloys and on samples of Armco iron and electrolytic nickel. The magnitudes of the Fe K edge shift in the spectra of the Fe-Pt alloy samples at different temperatures are shown in Table 2. The sifts are referred to the position of the K edge at room temperature. In all cases we used the third order of reflection from the NaCl crystal.

As will be evident from Table 2 a measurable shift with increase of temperature was observed only for alloy samples Nos.2 and 3, the shift being primarily to the short wavelength side in the case of alloy No.3 and to the long wavelength side in the case of alloy No.2. We were unable to detect any significant shift of the Fe K edge in alloy No.1.

In the case of the Fe-Ni alloys, we were able to detect a shift of the absorption edge with increasing temperature only for the Fe + 34% Ni alloy. At temperatures above 200° the K edge of iron in this alloy is shifted approximately 0.7 ev (uncertainty ±0.2 ev). In the experiments with electrolytic nickel we observed no significant shift of the K edge of Ni in the entire range of investigated temperatures. The K edge of Armco iron is shifted 0.7 ± 0.2 ev to the short wavelength side relative to the room temperature position at temperatures above 900°. These results are in agreement with the data of Trapeznikov[6].

---

[*] All percentages here and below are by weight.

[#] The plus sign indicates shift of the K edge to the higher energy side; the minus sign - shift to the side of lower energies.

Our measurements show that the K edge of Fe and Ni in the pure metals does not shift in going through the Curie point. In alloys of iron with nickel and iron with platinum the K edge of Fe also does not change position in going through the Curie point. The K edge of iron does shift to a measurable extent with increase in temperature in alloys that are characterized by an anomalous value of the thermal expansion coefficient and increase of the coefficient with increase in temperature. This gives reason to assert that changes in the position of the K absorption edge should be correlated not with temperature-induced changes of the magnetic properties but with variation in the character of the interatomic bonds.

Moreover, it would appear that in Invar type alloys changes in the coefficient of thermal expansion are accompanied not only by change in the separation between the atoms but also by changes in the energy state of the atomic electrons, which change is evinced in the x-ray spectrum. Naturally, these changes can be accompanied by alteration of a number of physical properties including the magnetic properties.

Thus we are inclined to the view that direct correlation exists between the x-ray spectroscopic characteristics and the character and strength of the interatomic bonds (evinced in the distribution in state of the atomic electrons), but not between the x-ray characteristics and the magnetic state of the alloy or metal per se, although obviously one of the results of the change in the character of the bonds may be modification of the magnetic properties of the alloy. We came to a similar conclusion (but on the basis of other considerations) earlier in Ref.5.

In comparing our x-ray data with the phase diagrams for the iron-nickel and iron-platinum systems, it becomes evident that the shifts in the position of the K edge usually occur in the temperature region of the transition from the α to the γ-modification of the alloy. This again indicates that the energy state of the atomic electrons changes incident to this phase transition; this change is naturally evinced in the position of the K edge of iron.

"T.G.Shevchenko" Kiev State University

References

1. L.G.Nikolaeva & S.M.Karal'nik, Ukr.fiz.zhur. (Ukrainian Physics Journal), 4, 260 (1959).
2. K.P.Belov, Uprugie, teplovye i elektricheskie yavleniya v ferromagnitnykh metallakh (Elastic, thermal and electric effects in ferromagnetic metals) Chapter IV, M.-L.,1951.
3. S.M.Karal'nik, Ukr.fiz.zhur. (Ukrainian Physics Journal), 3, 678 (1958).
4. V.A.Kazantsev, Doklady AN SSSR, 123, 667 (1958). (Trans.Soviet Physics - Doklady.)
5. S.M.Karal'nik, I.Ya.Dekhtyar, D.M.Komskii, V.G.Chupryna & L.G.Nikolaeva, Izv.AN SSSR, Ser.fiz., 20, 811 (1956). (Trans.Bulletin,20, 736.)
6. V.A.Trapeznikov, Fiz.metallov i metallovedenie (Physics of Metals and Metallography), 3, 561 (1956).

USE OF THE METHOD OF EXTERNAL STANDARDS IN FLUORESCENT X-RAY SPECTROSCOPIC ANALYSIS

- N.F.Losev

Introduction

In employing the method of external standards the intensity of the analytic line for the sample is compared with the intensity of the same line, recorded before, after or simultaneously, for a standard sample with a known content of the determined element.

The simplicity and rapidity of the analytic procedure have attracted the attention of spectroscopists to this method. However, its general use in analytic practice is held back by serious difficulties connected with the influence of the chemical composition of the material on the intensity of the secondary lines. Attempts to eliminate or take into account this influence can be undertaken with any hope of success only if one knows the dependence of the line intensity of the analyzed for elements on their content in the sample. Determining this dependence is a serious and so far unsolved problem standing in the way of further development of fluorescent x-ray analysis.

A general solution can be obtained only by taking into account a number of important factors involved in excitation of the secondary spectrum of elements under the specific conditions of x-ray spectroscopic analysis: excitation is realized either by non-uniform or mixed primary radiation; the components of the analyzed sample (including the element being determined) absorb both the primary radiation penetrating into the secondary emitter and the secondary radiation emitted from the depth of the emitter; the secondary radiation of the other elements in the sample can in turn excite the lines of the determined element (selective excitation); the emitter is irradiated by a broad divergent beam of primary rays, the source of which is located in the immediate proximity of the secondary emitter and generally has dimensions comparable to the dimensions of the emitter.

So far in the literature we find only particular solutions of the problem, based to some degree on the assumption that the primary beam is monochromatic[1-3]. In the present contribution we shall examine the case of excitation of the secondary spectrum by heterogeneous radiation in the absence of selective excitation.

1. Intensity of the Secondary-Spectrum Lines

The expression for the intensity i of a line in the secondary spectrum of a given element A, excited by monoenergetic radiation of wavelength λ_1 from a primary source located at a distance R from the secondary emitter may be written in the form[4]

$$I_{2,\,i} = kI_1\tau^{\mathrm{A}}_{m1}\,\frac{\lambda_1/\lambda_i C_{\mathrm{A}}}{\dfrac{\mu_{m1}}{\sin\varphi}+\dfrac{\mu_{mi}}{\sin\psi}}\left[1-e^{-\left(\frac{\mu_{m1}}{\sin\varphi}+\frac{\mu_{mi}}{\sin\psi}\right)\rho d}\right], \tag{1}$$

where

$$k=\frac{1}{4\pi R^2}\,\omega^{\mathrm{A}}_q p_{qi} s\,\frac{S^{\mathrm{A}}_q-1}{S^{\mathrm{A}}_q};$$

I_1 is the intensity of the primary beam at the surface of the secondary emitter, τ^{A}_{m1} is the mass coefficient of true absorption of the primary radiation in the atoms of element A, λ_1 is the wavelength of the line i, C_{A} is the concentration of the element A, μ_{m1} is the mass absorption coefficient for the primary radiation of wavelength λ_i in the emitter material, μ_{mi} is the mass absorption coefficient for the secondary radiation of wavelength λ_i in the emitter material, φ is the angle of incidence of the primary beam on the emitter, ψ is the angle of emission of the secondary radiation from the emitter, ρ is the density of the emitter material in g/cm^3, d is the thickness of the emitting layer in cm, ω_q^A is the quantum yield of the q series of element A, $p_{q,i}$ is the probability for the transition responsible for the appearance of the i line of the q series of element A, s is the area (in cm^2) of the emitter irradiated by the primary beam, and S_q^A is the q absorption discontinuity of the element A.

When the secondary spectrum is excited by heterogeneous radiation there participate in the excitation process resulting in an intensity $I_{1,i}$ all the wavelengths of the primary beam from λ_0, the wavelength of the short wavelength edge of the primary spectrum to λ_q, the wavelength of the absorption edge of the excited element.

Obviously, the quantities I_1, τ_{m1}^A and μ_{m1} in Eq. (1) will be functions of these wavelengths:

$$I_{1\lambda} = CZi\frac{c^2}{\lambda_0}\cdot\frac{\lambda-\lambda_0}{\lambda^3}; \tag{2}$$

$$\tau_{m\lambda}^A = \frac{0.016}{A}\cdot Z_A^{3.94}\lambda^3 \quad \text{for } \lambda < \lambda_K, \tag{3}$$

where $C = (5 \pm 1.5)\cdot 10^{-50}$, Z is the atomic number of the element comprising the primary anode, i is the current density in the x-ray tube, A is the atomic weight of the excited element and Z_A is its atomic number. The value of the mass absorption coefficient for wavelengths in the interval $\lambda_0 - \lambda_q$ can be expressed in terms of the value of the absorption coefficient μ_{mi} for the investigated line i in the secondary spectrum. In doing so, one must take into account the absorption discontinuities of the elements the edges of which lie between the wavelength of the line i and the wavelength λ_0 of the primary radiation. If, for example, we are concerned with the Kα_1 line of the component being determined, such elements will be all elements with atomic number $Z_H \geqslant Z_{A-2}$.

Equation (1) can be applied only in cases when the emitter does not contain elements leading to selective excitation, i.e., when the atomic number Z_H of the elements in the mixture satisfies the condition $Z_H \leqslant Z_{A+1}$ (in excitation of the K series). Hence the condition for the elements, the absorption discontinuities of which it is worth taking into account, will be written in the form $Z_{A+1} > Z_H \geqslant$ $\geqslant Z_{A-2}$. If in analysis we consider the Kβ_1 line, one should take into account the K edge only of the determined element. In this case for the mass coefficient of absorption of wavelength λ of the primary radiation we obtain

$$\mu_{m\lambda} = (\lambda/\lambda_i)^3\,[C_A\mu_{mi}^A(S_K - 1) + \mu_{mi}]. \tag{4}$$

Invoking (2), (3) and (4), let us use Eq. (1) to determine the fraction of the intensity of the line of the secondary spectrum excited by the spectral interval $(\lambda, \lambda + d\lambda)$ of the primary continuous spectrum. Thus we obtain

$$dI_{2,i} = k'\frac{1}{\lambda_0}\cdot\frac{\lambda(\lambda-\lambda_0)\,C_A}{a\lambda^3+b}\cdot\left[1 - e^{-\frac{1}{\sin\varphi}[(\lambda/\lambda_i)^3 + b/\lambda_i^3]\rho d}\right]\cdot d\lambda, \tag{5}$$

where

$$k' = kCZic^2\frac{0.016}{A}Z_A^{3.94}\sin\varphi\cdot\lambda_i^2, \tag{6}$$

$$a = C_A\mu_{mi}^A(S_K^A - 1) + \mu_{mi}, \tag{7}$$

$$b = \frac{\sin\varphi}{\sin\psi}\cdot\lambda_i^3\mu_{mi}. \tag{8}$$

For "thick layers" the term in the brackets can be neglected. The thickness of such a critical layer can be evaluated by means of the expression

$$\frac{I^d_{2,\,i}}{I^\infty_{2,\,i}} = 1 - e^{-\frac{1}{\sin\varphi}[(\lambda/\lambda_i)^3 b/\lambda^3_i]\rho d}$$

by inserting into it a value of λ close to λ_0 and then taking the ratio of the intensity $I^d_{2,\,i}$ from a layer of finite thickness to the intensity $I^\infty_{2,\,i}$ from a layer of infinite thickness to be close to unity (with the requisite degree of approximation).

The total line intensity of the secondary K spectrum of element A excited by heterogeneous radiation will be determined by integrating Eq.(5) over the wavelengths of the continuous spectrum between the limits λ_0 and λ_K. In the case of a "thick" emitter we obtain

$$I_{2,\,i} = k'\frac{C_\mathrm{A}}{\lambda_0}\int\limits_{\lambda_0}^{\lambda_K}\frac{\lambda(\lambda-\lambda_0)}{a\lambda^3+b}\cdot d\lambda = k'\frac{C_\mathrm{A}}{\lambda_0}\left\{\frac{1}{3a}\cdot\ln\frac{\lambda_K^3+b/a}{\lambda_0^3+b/a}-\right.$$
$$-\frac{\lambda_0}{6a\sqrt[3]{b/a}}\cdot\ln\frac{\left[\lambda_K^2-\sqrt[3]{b/a}\,\lambda_K+\left(\sqrt[3]{b/a}\right)^2\right]\left(\lambda_0+\sqrt[3]{b/a}\right)^2}{\left[\lambda_0^2-\sqrt[3]{b/a}\,\lambda_0+\left(\sqrt[3]{b/a}\right)^2\right]\left(\lambda_K+\sqrt[3]{b/a}\right)^2}-$$
$$\left.-\frac{\lambda_0\sqrt{3}}{3a\sqrt[3]{b/a}}\arctan\frac{\sqrt{3}\,\sqrt[3]{b/a}\,(\lambda_K-\lambda_0)}{2\lambda_0\lambda_K-\sqrt[3]{b/a}\,(\lambda_K+\lambda_0)+2\left(\sqrt[3]{b/a}\right)^2}\right\}. \tag{9}$$

If our analytic line is the $K\alpha_1$ line, then in the presence in the sample of elements with atomic numbers $Z_{A+1} > Z_j \geqslant Z_{A-2}$ the quantity a will be given by

$$a = \sum_j C_j\,(S^j_K - 1)\,\mu^j_{mi} + \mu_{mi}, \tag{10}$$

where C_j is the concentration of the element with atomic number Z_j; S^j_K is its K absorption discontinuity and μ^j_{mi} is the coefficient of mass absorption of the $K\alpha_1$ line of element A by the element with atomic number Z_j.

Equation (9), deduced for the line intensity in the secondary K spectrum of element A, is a complex function of the concentration of this element, the absorbing power of the analyzed material, the potential on the x-ray tube and other parameters.

2. Experimental Verification of the Intensity Formula

Variation of the intensity with the concentration of the determined elements and the absorption power of the sample

Formula (9) was checked by comparing the values of the intensity of the $K\alpha_1$ line of zirconium calculated by means of this formula with the intensity of this line as measured on a KRUS spectrometer.

For the purpose of these measurements we prepared a series of samples with different proportions of zirconium and filler. The sample material was tamped into aluminum cells, the thickness of which in all cases assured a thick emitter layer.

The primary radiation was supplied by an x-ray tube with a tungsten anode operated at 41 ± 0.5 kev and 15 ma. The high voltage was provided by a VS-50-50 unit. Before using Eq.(9), we found the geometric characteristic of the spectrometer $\frac{\sin\varphi}{\sin\psi}$, which must be different from the calculated one, owing to divergence of the primary and secondary radiation beams. The value of this sine ratio was taken as such so as to insure coincidence of the theoretical (calculated according to (9)) ratio of the intensities of the $K\alpha_1$ line of Zr for two samples (with 5 and 100% ZrO_2) with the experimentally obtained ratio. Agreement of the experimental and calculated intensity ratio was obtained for $\frac{\sin\varphi}{\sin\psi} = 1.865$. This value was then used in further calculations by means of Eq.(9).

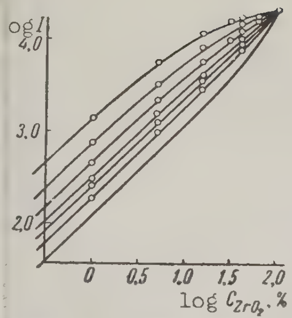

Fig.1. Comparison of the experimental (points) and calculated (solid lines) intensities of the $K\alpha_1$ line of zirconium.

The calculated intensities of the $K\alpha_1$ line of Zr as a function of the zirconium dioxide concentration in the samples with different amounts of filler (solid lines) are compared in Fig.1 with the experimental results (points). The mass coefficient of absorption for the analytic line in the filler varied from 5.1 cm^2/g for the upper curve to 64.6 cm^2/g for the lowest curve. In plotting the experimental points the scale was adjusted to match the theoretical and experimental values for 100% zirconium dioxide. It will be evident from Fig.1 that good agreement of experiment with theory was obtained.

Variation of the intensity with the tube potential

Equation (9) brings out the dependence of the secondary line dependence on the wavelength λ_0 of the short wavelength edge of the continuous spectrum, i.e., essentially on the voltage on the x-ray tube inasmuch as

$$V_{SW} = \frac{12.370}{\lambda_0\,(kX)}\,. \tag{11}$$

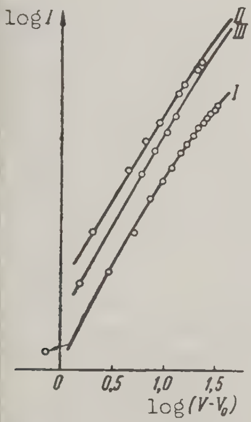

Fig.2. Variation in the intensity of the fluorescent lines with the tube voltage: I - Ni $K\alpha_1$, II - Zr $K\alpha_1$, III - Ag $K\alpha_1$.

The solid lines in Fig.2 show the calculated intensities of the $K\alpha_1$ lines of nickel, zirconium and silver as functions of the excess operating voltage V over the excitation potential V_0 for the K series of the enumerated elements. For purposes of calculation we took out from the constant factor multiplying k' the part $\frac{0.016\,Z_A^{3.94}}{A}\lambda_i^2$, which was taken into account in going from one element to another. In addition, for the pure elements we took $a = \mu_{mi}^A S_K^A$ and $b = 1.865\ \lambda_i^3 \mu_{m_i}^A$.

The intensities of the $K\alpha_1$ lines of the enumerated elements were recorded on a short wavelength KRUS spectrometer with a tungsten anode. The fluctuation of the rectified voltage did not exceed 5% the crest value. The points in Fig.2 give the experimental results. As in the previous case the experimental scale was adjusted to obtain coincidence for 100% zirconium dioxide concentration.

It will be evident from Fig.2 that the calculated relative variation of the $K\alpha_1$ line intensity as a function of the tube voltage is in good agreement with the observed variation. There is evident a more complex relationship than indicated by Blokhin[4]:

$$I_{2,i} \backsim (V - V_0)^{1,79}. \tag{12}$$

The exponent in our experiments varied with increase of the voltage from 1.9-2.0 to 1.45-1.5 and only its mean value for the entire voltage range was close to 1.79.

3. Effective Wavelength of the Primary Radiation

Some authors[2,5] in characterizing the exciting effect of heterogeneous primary radiation used the effective (mean weighted) wavelength from the interval (λ_0, λ_K). Formula (9) allows of determining this value. Thus from the left part of (9) according to the theory of means we have

$$I_{2,i} = k' \frac{C_A}{a\lambda_0} \int\limits_{\lambda_0}^{\lambda_K} \frac{\lambda(\lambda - \lambda_0)}{\lambda^3 + \frac{b}{a}} d\lambda = \frac{k'C_A}{a\lambda_0}(\lambda_K - \lambda_0)\frac{\lambda_1(\lambda_1 - \lambda_0)}{\lambda_1^3 + \frac{b}{a}}; \tag{13}$$

on the other hand, the right part of (9) can be written in the form

$$I_{2,i} = \frac{k'C_A}{a\lambda_0} \cdot D, \tag{14}$$

where D is the expression in the braces in Eq.(9) but without the factor $1/a$. Equating the right parts of (13) and (14), we obtain the following third degree equation for finding the weighted mean wavelength λ_1:

$$D\lambda_1^3 - (\lambda_K - \lambda_0)\lambda_1^2 + \lambda_0(\lambda_K - \lambda_0)\lambda_1 + D\frac{b}{a} = 0; \tag{15}$$

the root of this equation, satisfying the condition $\lambda_0 < \lambda_1 < \lambda_K$, is found in the form

$$\lambda_1 = -2\sqrt{|p|}\cos(60^\circ - \gamma/3) + \frac{\lambda_K - \lambda_0}{3D}, \tag{16}$$

where

$$\gamma = \arccos\frac{q}{r^3}, \quad r = \sqrt{|p|}, \tag{17}$$

$$p = \frac{3\lambda_0(\lambda_K - \lambda_0)D - (\lambda_K - \lambda_0)^2}{9D^2}, \tag{18}$$

$$q = -\frac{(\lambda_K - \lambda_0)^3}{27D^3} + \frac{\lambda_0(\lambda_K - \lambda_0)^2}{6D^2} + \frac{b}{2a}, \tag{19}$$

$$\frac{b}{a} = \frac{\lambda_i^3 \mu_{mi}}{C_A \mu_{mi}^A (S_K^A - 1) + \mu_{mi}} \cdot \frac{\sin\varphi}{\sin\psi}. \tag{20}$$

For a given operating condition of the x-ray tube (λ_0) the weighted mean wavelength λ_1 will be determined by the ratio b/a. The minimum value of b/a will obtain for pure elements and will equal

$$\left(\frac{b}{a}\right)_{\min} = \frac{\lambda_i^3}{S_K^A} \frac{\sin\varphi}{\sin\psi}, \tag{21}$$

and the maximum value, obtaining in the limit as $C_A \to 0$, will be

$$\left(\frac{b}{a}\right)_{\max} = \lambda_i^3 \frac{\sin\varphi}{\sin\psi}. \tag{22}$$

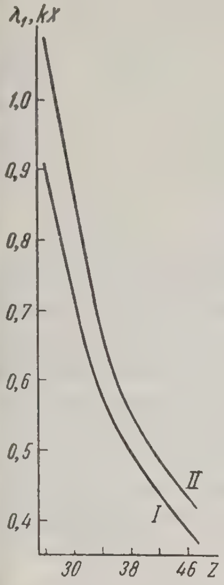

Fig.3. Limits of variation of the effective wavelength: I - for pure elements, and II - for mixtures as $C_A \to 0$.

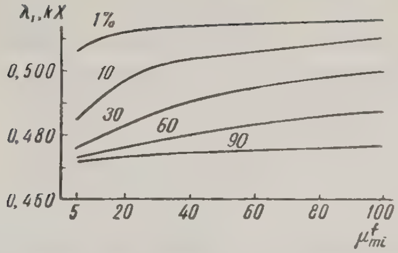

Fig.4. Values of λ_1 in the case of excitation of the Kα_1 series of zirconium for different contents of zirconium (indicated in percent at the curves).

Fig.3 shows the results of calculation by means of (16) of the effective minimum and maximum values of λ_1 for $\lambda_0 = 0.300$ kX (i.e., V = 41.3 kv) for the elements from $_{26}$Fe to $_{47}$Ag.

The calculations show that, depending on the composition of the analyzed material, the value of λ_1 in formula (13) can vary in a wide range, for example, for $_{40}$Zr from 0.472 to 0.515 kX, for $_{26}$Fe from 0.904 to 1.082 kX, etc.

Fig.4 shows the calculated variation of the effective wavelength of the primary radiation for the case of excitation of the Kα_1 line of zirconium in samples of different composition with an operating voltage V = 41.3 kv. The values of the mass absorption coefficient μ_{mi}^f of the filler were taken in the range from 5 to 100 cm^2/g, which corresponds approximately to its possible values in the analysis of actual samples.

For a given value of the mass absorption coefficient μ_{mi}^f of the filler the wavelength λ_1 will be determined by the degree of absorption of the primary radiation by the atoms of the determined element. The greater the content of this element in the mixture, the stronger will be the absorption of the wavelengths adjacent to λ_K in the continuous spectrum. They will be absorbed in the upper layers of the emitter, and the main mass of atoms of the determined element will be excited by the shorter wavelength part of the spectrum. Hence with increase of C_A the effective wavelength λ_1 decreases. At a given concentration C_A, decrease of μ_{mi}^f will be accompanied by increase of the relative absorption of radiation of wavelengths close to λ_K by the atoms of the determined element as compared with the atoms of the filler. Hence for the above reasons the effective wavelength λ_1 must decrease and in the limit as $\mu_{mi}^f \to 0$, λ_1 will approach its value for the pure element.

The above inferences regarding the effective wavelength of the primary continuous radiation were checked for the case of excitation of zirconium in the samples used for plotting the points in Fig.1. For each of the samples we determined the value of b/a and at a voltage of 41.3 kv found, by means of Eq.(16) the value of the effective wavelength λ_1. Using relation (13), we then calculated the intensity of the Kα_1 line of zirconium. The results obtained fit the curves calculated by means of formula (9) and are in good agreement with the experimental data.

If in formula (13) instead of the precise value, we take a constant value of λ_1 from within its range of possible values, for example, if we take its arithmetic mean value,

$$\lambda_1' = \frac{(\lambda_1)_{\min} + (\lambda_1)_{\max}}{2}, \tag{23}$$

there will be obtained a substantial difference between the calculated intensities and the experimental ones. Fig.5 shows the maximum value of the relative error in determining the intensity of the Kα_1 lines of the elements from $_{26}$Fe to $_{47}$Ag by means of Eq.(13), if in it, instead of the precise value λ_1, we take the arithmetic mean λ_1' given by (23). It will be evident from Fig.5 that for the elements from $_{38}$Sr to $_{42}$Mo the relative error does not exceed ±12%. In other cases, however, the deviation attains ±19-20%. Thus Eq.(13) with a constant value of λ_1 can be used only for qualitative evaluations of the line intensities in the secondary spectrum of the determined element.

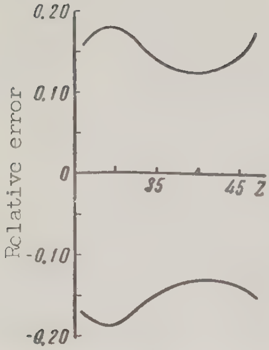

Fig.5. Maximum relative error in determining the intensity of the Kα_1 lines in the case when λ_1 is assumed to be constant and equal to the arithmetic mean value (Eq.(23)).

4. Tests of the Method of External Standards

Let us consider the case when analysis is carried out with reference to an analytic (working) curve, i.e., a graph of $I_{2,i} = f(C_A)$ plotted with reference to several standards. For determination of the element, the intensity I_x of the analytic line of the sample is matched with the intensity I_0 of the same line for the closest standard.

Let us multiply and divide the right part of (9) by b, the value of which is given by (8), take out the factor $1/a$ from the braces, and use $F(b/a)$ to denote the expression remaining in the braces. Then the intensity can be written in the form

$$I_x = \frac{k'}{\lambda_0} \cdot \frac{C_x}{b_x}\left(\frac{b}{a}\right)_x F\left[\left(\frac{b}{a}\right)_x\right]; \tag{24}$$

similarly, the intensity I_0 will be given by

$$I_0 = \frac{k'}{\lambda_0} \cdot \frac{C_i}{b_0}\left(\frac{b}{a}\right)_0 F\left[\left(\frac{b}{a}\right)_0\right], \tag{25}$$

where C_i is the concentration of the determined element, which is found from the working curve, and the index $0'$ refers the values of a and b to the standard with a concentration C_i of the element A.

Inasmuch as by definition the analytic condition is $I_x = I_0$, from (24) and (25) we have

$$\frac{C_x}{b}\left(\frac{b}{a}\right)_x F\left[\left(\frac{b}{a}\right)_x\right] - \frac{C_i}{b_0}\left(\frac{b}{a}\right)_0 F\left[\left(\frac{b}{a}\right)\right] = 0\,. \tag{26}$$

The sought quantity is the concentration C_x of the determined element. It can readily be shown that the root of Eq.(26) is the expression

$$C_x = C_i \frac{\mu_{mi}^x}{\mu_{mi}^0}\,. \tag{27}$$

Relation (27) was checked by us with reference to the Kα_1 lines of yttrium, zirconium, niobium and molybdenum, using samples the fillers in which were media with different mass absorption coefficients. The working curves in all cases were plotted with reference to standards with a constant mass absorption coefficient for the corresponding Kα_1 line.

The solid line in Fig.6 shows the theoretical variation of the ratio of the true concentration C_x of zirconium dioxide to the concentration C_i found from the working curve as a function of the ratio of the mass absorption coefficients of the analyzed samples and the standards (μ_{mi}^0 for the Kα_1 line of zirconium equal to 16.4 cm^2/g). The experimental results are indicated by the points in Fig.6. It will be evident that there is good agreement between the theoretical and experimental data. Similar fits were obtained for yttrium, niobium and molybdenum.

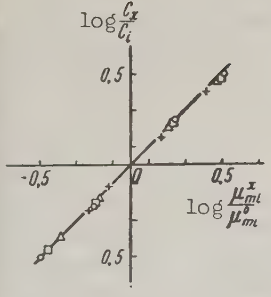

Fig.6. Variation of C_x/C_i with μ^x_{mi}/μ^0_{mi}.

Equation (27) opens new possibilities for carrying out quantitative determinations by the method of external standards. If for each sample we determine the mass absorption coefficient, then, knowing the absorption coefficient for the standards, we can always correct the concentration found from the working curve, i.e., take into account the influence of the composition of the sample on the analytic results. This must always give positive results when the sample is free of elements leading to selective excitation of the atoms of the element being determined. One must also bear in mind that in the presence in the sample of elements with atomic numbers $Z_A > Z_j \geqslant Z_{A-2}$ one must use the Kβ_1 rather than the Kα_1 line as the analytic line. For the standards, one can always have $\mu^0_{mi} = \text{const}$ if one prepared them using a filler with a mass absorption coefficient equal to the absorption coefficient of the medium (the pure element or its chemical compound) in or with which the determined element is introduced into the standard.

5. Examples of Analysis

Stages of Analysis

On the basis of our investigation, we propose the following sequence of operations for analysis by the method of external standards.

1. Plot the analytic curve

$$I_{2,i} = f(C_A). \tag{28}$$

with reference to standards with $\mu^0_{mi} = \text{const}$.

2. Using this curve, determine the concentration C_i of the element being determined in the samples submitted for analysis.

3. Determine the mass absorption coefficients μ^x_{mi} of the samples for the given analytic line.

4. Finally, find the ratio of the mass absorption coefficients of the samples and standards and calculate by means of (27) the sought concentration C_x.

It is also convenient to make use of the functional dependence of the ratio of the intensity I_i of the analytic lines of all the standards to the intensity I_0 recorded for one particular standard on the concentration C_A:

$$\frac{I_i}{I_0} = f(C_A). \tag{29}$$

The function (29) can be plotted beforehand by averaging a large number of experimental results. Then in the process of analysis it will be sufficient to record at appropriate time intervals the intensities I_0 only for one standard and then determine the intensity of the line of the sought element in the samples with reference to this intensity. If the determinations are being carried out in a wide range of concentrations, the working curve should be plotted in logarithmic coordinates since in this case it is possible to read off the values with an accuracy one order of magnitude higher than that characterizing the experimental error.

In our work we determined the mass absorption coefficients for the samples at the wavelength of the analytic line in the following manner. The samples were packed into special cells which by means of a massive sample holder were mounted in a vertical position on the stage attached to the vacuum tube of the spectrometer on the side of the x-ray tube. The irradiator (emitter) was the pure determined element or its compound. The spectrometer counter recorded the intensity of the analytic line undergoing absorption in the absorbent. The value of the absorption coefficients μ^x_{mi} of the samples was found by means of the familiar formula

$$\mu^x_{mi} = 2.3 \frac{\log \frac{I_0}{I_1}}{m} s, \tag{30}$$

where I_1 is the intensity of the analytic line undergoing absorption with the cell filled, I_0 is the intensity of the analytic line with the cell empty, m is the weight of the absorbent in grams, and s is the area of the absorbent in square centimeters.

All the cells used in our work had the same area. The material must be distributed uniformly in the cell so that the ratio of the weight of the whole absorbent to the total volume of the irradiated section would be equal to the ratio of the corresponding areas. This condition is best fulfilled if the area of the absorbent is equal or close to the area of the irradiated section. To satisfy this requirement the area of the cells used in our work was 1.1 x 0.5 cm. Their thickness was 1 mm.

The accuracy of determining the mass absorption coefficient was evaluated using samples of known composition. We measured the absorption of the $K\alpha_1$ lines of yttrium, zirconium, niobium and molybdenum. In all cases the results of consecutive determinations (not less than three for each sample) showed a scatter characterized by a mean relative error of 1.5-2%. The experimentally determined mean absorption coefficients differed from the calculated values by 2-3%.

The described procedure allows of carrying out 20-25 determinations of the absorption coefficients of the analyzed material within a period of 2-3 hours.

Determination of zirconium

The primary radiation was obtained from an x-ray tube with a tungsten anode operated at 40 ± 0.5 kv (VS-50-50 high voltage unit) and 15 ma. The analytic line was the $K\alpha_1$ line of Zr (λ = 784.3 X) in the first order. The Zr content was determined in ores, concentrates and processed materials. The results of determination by the method of external standards and the data obtained by other methods of analysis (μ^0_m = 16.4 cm^2/g) are shown in the accompanying table.

Results of determination of zirconium

Sample No.	μ^x_{mi}, cm^2/g	C_{ZrO_2}, %				Deviation $\Delta C/C_0$, %	
		C_i	C_x	C_0		from chemical analysis	from optical spectrum analysis
				Chemical analysis*	Optical spectrum analysis**		
1	15,4	68,0	64	62,0	—	3,2	
2	11,0	3,60	2,42	2,50	—	3,2	
12	9,30	0,65	0,37	0,38	—	2,6	
63	5,86	0,098	0,035	—	0,038		7,9
51	5,86	0,28	0,10	—	0,097		3,1
46	5,1	0,21	0,065	—	0,060		8,3

---

* The accuracy of chemical determination is characterized by a mean relative deviation of 3-4%.

** The accuracy of optical spectroscopic analysis is characterized by a mean relative deviation of 6-7%.

Numerous tests carried out with a view to evaluating the accuracy of determination of zirconium by the above described procedure showed that the deviation between the determined concentrations C_x and the true (calculated) values equaled 3.8% on the average. This figure also characterizes the mean deviation from the data of chemical analysis. The deviations from the results of spectroscopic analysis averaged 5-6%.

Experiments carried out for the purpose of evaluating the sensitivity of the procedure showed that for samples with a mass absorption coefficient from 5 to 30 cm^2/g the sensitivity equals 0.03 to 0.10%. The sensitivity was determined as the concentration which provided a counting rate at the analytic line exceeding the background by 40-50%. The accuracy of determination at the sensitivity threshold with a counting time of 10 min was characterized by a mean relative error of 10%. Some 15-20 determinations can be made during a normal working day.

During the period of testing and introduction of the described procedure there were carried out over 1000 determinations of zirconium in different materials. Part of these were checked by optical spectrum analysis. In rare cases the divergence between the results exceeded 13-15%, but on the average was 5-6%. We obtained similar results in determinations of yttrium, niobium and molybdenum in ores and concentrates.

Conclusions

1. We have derived a formula for the intensity of the fluorescent line excited by heterogeneous primary radiation for thick emitters in the case when there is no selective excitation. This formula gives the dependence of the line intensity on the x-ray tube potential and on the composition of the emitter; this dependence is substantiated by experiment.

2. We investigated the question of the possibility of using the mean weighted (effective) wavelength, i.e., a constant value, in calculating the intensity of the secondary spectrum lines. The results obtained for the elements from $_{26}Fe$ to $_{47}Ag$ show that, depending on the composition of the emitter, this wavelength varies in a wide range. If this variation is neglected, the relative error in calculating the intensity may attain 12-20%.

3. Tests of the method of external standards showed that the concentration of the determined element in a sample of complex composition is equal to the concentration given by the working curve multiplied by the ratio of the mass absorption coefficients for the analytic line in the sample and in the standard.

4. We propose a new procedure for carrying out analysis by the method of external standards, based on preliminary determination of the mass absorption coefficients of the samples. Application of this procedure is limited by the requirement of absence of selective excitation in the samples.

5. Extensive tests of the proposed analytic procedure for determination of yttrium, zirconium, niobium and molybdenum gave positive results. With an accuracy of 5-10% and a sensitivity of 0.02-0.10% (in terms of the oxides), the productivity of the procedure amounts to 15-20 determinations per normal working day.

Irkutsk State Institute of Rare Metals

References

1. M.A.Blokhin, Metody rentgeno-spektral'nykh issledovanii (Methods of x-ray spectroscopic investigation), 1959.
2. E.Gillam & H.T.Heal, Brit.J.Appl.Phys., 3, 353 (1952).
3. I.Scherman, Spectrochimica Acta, 7, 283 (1955).
4. M.A.Blokhin, Fizika rentgenovykh luchei (Physics of x-rays), M. 1953.
5. M.A.Blokhin, Dissertation, Moscow, 1951.

Bulletin of the Academy of Sciences of the USSR - Physical Series
Vol. 24, No. 4 - December 1960

Transactions of the Fourth All-Union Conference on X-ray Spectroscopy

TABLE OF CONTENTS

	Page	
	Orig.	Trans.
Selection of crystals for x-ray spectroscopy - J.Bačkovský	352	369
Nuclear x-ray generator for fluorescent analysis - K.I.Narbutt, R.L.Barinskii & I.S.Smirnova	354	372
Instrument for x-ray spectroscopic microanalysis - A.M.Solov'ev & V.N.Vertsner	362	378
Universal x-ray spectrograph for investigation of the chemical composition of microvolumes - N.P.Il'in	367	382
Development of the first automatic x-ray spectrograph in Czechoslovakia - R.Rotter & M.Klapuch	371	386
Reflection of x-rays from a bent crystal in the case of a microfocus source - S.A.Ditsman	376	390
Optimum correction of x-ray spectra for dispersive distortion - I.Ya.Nikiforov	380	394
On allowing for apparatus distortion and the width of dispersion type inner levels in emission spectra - Ya.E.Genkin & I.A. Rumyantsev	384	398
On specifying the energy of x-ray photons and the energy of electron levels - N.D.Borisov & V.V.Nemoshkalenko	393	406
Concerning the shape of energy bands in solids - M.A.Blokhin & V.P.Sachenko	397	410
Calculation of the charge of atoms in molecules from the K absorption spectra - R.L.Barinskii & E.G.Nadzhakov	407	419
Determination of the charge and type of bond of osmium in compounds from the L_{III} absorption spectra - E.G.Nadzhakov & R.L.Barinskii	415	425
On the origin of some satellites in x-ray spectra - Z.Gorak	422	432
Concerning interpretation of x-ray spectra - A.T.Shuvaev	424	434
Investigation of the correlation between the fine structure of x-ray absorption spectra and the characteristic electron energy losses - I.B.Borovskii & V.V.Shmidt	428	438
Note on the asymmetry index of the $K\alpha_{1,2}$ lines of transition elements - N.Malkovskaya	433	442
Investigation of the fine structure of the K x-ray spectra of some sulfides - I.A.Ovsyannikova & I.B.Borovskii	435	444
Nature of the fine structure of the main K absorption edge of elements of the iron group - I.B.Borovskii & V.A.Batyrev	441	449
Influence of the nickel concentration on the structure of the electron energy spectrum of Fe-Cr alloys - N.D.Borisov, V.V. Nemoshkalenko & A.M.Fefer	443	451
Fine structure of the principal K absorption edge of transition metals of the iron group, their alloys and compounds - S.A.Nemnonov	447	455
Investigation of the principal K absorption edge of nickel in nickel-aluminum alloys - S.A.Nemnonov & M.F.Sorokina	455	462
Fluorescent L spectra of niobium in NbB_2, NbC, NbN and pure niobium - M.I.Korsunskii & Ya.E.Genkin	461	467
Relative intensities of the $L\beta_2$, $L\beta_{15}$ and $L\gamma_1$ lines in the L series spectra of substances with an unfilled N shell - M.I.Korsunskii & Ya.E.Genkin	465	470

Fluorescent L series of niobium bound in some compounds - M.I.Korsunskii & Ya.E.Genkin 470 475
High-temperature x-ray studies of Invar alloys - S.M.Karal'nik, L.G.Nikolaeva & N.N.Nefedov 473 477
Use of the method of external standards in fluorescent x-ray spectroscopic analysis - N.F.Losev 476 480

Translated in 1961 by
Columbia Technical Translations
5 Vermont Avenue, White Plains, N.Y.

Number 5 Volume 24 1960

BULLETIN

of the

ACADEMY OF SCIENCES OF THE USSR

— PHYSICAL SERIES —

(Izvestiya Akademii Nauk SSSR)
(Seriya fizicheskaya)

Reproduction rights reserved
by

Columbia Technical Translations
5 Vermont Avenue
White Plains, New York

Single Issues
$20

Annual Subscription
$215

Transactions

# of the

Eighth Conference on Luminescence

(Molecular Luminescence and Luminescence Analysis)

(Minsk, 19-24 October 1959)

Part of the transactions of the Eighth Conference on Luminescence is being published in the present issue of the Bulletin and in Vol.24, No.6. The rest of the transactions on Molecular Luminescence will be published in Uspekhi Fizicheskikh Nauk (Trans. Soviet Physics - Uspekhi) and in Optika i Spektroskopiya (Trans. Optics & Spectroscopy). The transactions concerned with Luminescence Analysis will appear as a separate book to be published by the Academy of Sciences of the Belorussian SSR in 1960.

Lithoprinted in U.S.A.
EDWARDS BROTHERS, INC.
Ann Arbor, Michigan

OPENING ADDRESS

- V.L.Levshin

The last conference on molecular luminescence was held in February 1958 - just over a year and a half ago. Yet the number of reports published by Soviet investigators in this brief interval is very appreciable. These reports encompass the entire field of molecular luminescence. During this time there have been carried out serious theoretical investigations, new important experimental studies and research on the applications of molecular luminescence in diverse branches of the national economy.

The present conference will hear over one hundred communications. All this is evidence of the significant advances in the study of luminescence and its applications being made in the Soviet Union.

Our Conference is devoted to the luminescence of molecules. In other words, following established usage we shall not consider the luminescence of crystal phosphors. This tradition (of alternate conferences on molecular luminescence and on crystal phosphors) has a practical basis inasmuch as it is impossible at one conference to cover all the numerous and diverse researches on luminescence, but there is also an important reason of principle, stemming from the profound difference between the luminescence mechanisms of crystal phosphors and molecules.

At the same time, I feel it would be useful to say a few sords regarding the essence of investigations in the fields of molecular luminescence and molecular spectroscopy, on the profound relationship between these two fields of physical optics. In the very first works on molecular luminescence carried out in the Soviet Union, the particular attention of investigators - S.I.Vavilov and others - was directed to investigation of the energy processes involved in luminescence: investigation of the luminescence efficiency and different processes of quenching of luminescence, energy distribution in luminescence spectra, study of the kinetics of the processes of excitation energy migration and conversion. These processes, connected with the transfer and transformation of energy, required for their clarification investigation not only of the emission as such, but of other properties of matter, for example, absorption, and of processes competing with luminescence, such as conversion of excitation energy to heat, photochemical transformations, dissociation and ionization.

Thus luminescence, although it is the raison d'etre of the investigations in question, also served as the stimulus for comprehensive investigation of energy transfer and conversion in matter. This peculiarity of luminescence research has recently found reflection in the content of scientific conferences; thus, for example, a conference on transfer and conversion of light energy was held in Paris in 1958.

The predominant importance of investigation of energy processes in research on molecular luminescence distinguished, at least earlier, such studies from investigations in the field of molecular spectroscopy, the primary purpose of which was investigation of the frequency characteristics and structure of the absorption and emission spectra of molecules.

More recently, however, we see approach of these two fields. On the one hand, in studies of luminescence for investigating energy exchange one must have precise knowledge of the structure of the absorbing and emitting centers, the vibrations excited in molecules and the transition probabilities between individual states of molecules; on the other hand, the development of molecular spectroscopy has led to extensive study of intensity distribution in spectra and examination of the vibration of molecules as evinced in their luminescence spectra.

We even note a closer approach or identification of the subjects of investigation: whereas molecular spectroscopy as it develops turns to investigation of ever more complex molecules, in research on molecular luminescence, after investigation of the fundamental phenomena of luminescence in extremely complex molecules, for the purpose of detailed investigations of the mechanisms involved in energy conversion, investigators often have recourse to the simplest molecules. Thus, while remaining distinctive as regards content, experimental techniques and applications, these two fields of physical optics have recently come into intimate contact and, in a number of cases, are involved in the solution of common problems. One cannot but welcome this drawing together since its ultimate result should lead to a deeper understanding of the interaction of light with matter.

I now turn to a brief review of the development of research in molecular luminescence in the Soviet Union during the past year and a half.

There has been marked development of theoretical problems involving the relation of luminescence to light scattering and thermal radiation. We have a more accurate answer now to the question of the theoretically possible values of luminescence yield. There has been intensive work on the problem of energy conversion inside molecules in connection with the different types of molecular structure and the different strengths of the coupling between electron motion and nuclear vibrations, on the interaction of light with harmonic oscillators and so on. M.A. El'yashevich, B.S.Neporent and B.I.Stepanov have been particularly active in this field.

B.I.Stepanov examined another fundamentally important question - that of the relation between luminescence spectra and thermal radiation spectra and the possibility of obtaining the contours of the luminescence band from general considerations. One report on the subject will be presented at this Conference.

Many investigations have been devoted to intermolecular energy transfer by resonance and to questions of energy migration by means of excitons. There has been further development of theory of quenching by impurities: B.Ya.Sveshnikov and his co-workers clarified the role of diffusion and investigated the depolarization of luminescence incident to energy migration. A number of authors have emphasized the important role of energy migration from excited monomers to nonluminescing dimers and higher polymers, leading to luminescence quenching.

A new case of molecular resonance between triplet levels, leading to sensitized phosphorescence, and also intramolecular energy molecular transfer over triplet levels of complex molecules was investigated by A.N.Terenin and V.L.Ermolaev.

We note continuing widespread investigation of exciton processes. V.M.Agranovich and other authors have examined theoretically the problem of the free path and trapping of excitons in molecular crystals. N.D.Zhevandrov experimentally demonstrated the substantially different effect of free and trapped excitons and showed how to distinguish between the processes involved.

A.N.Sevchenko, G.P.Gurinovich and A.M.Sarzhevskii established mirror symmetry of polarization spectra. In a number of studies P.P.Feofilov continued his investigation by polarization techniques of the nature and orientation of luminescenc centers in cubic crystals.

N.G.Bakhshiev, V.V.Zelinskii and others carried out detailed investigations of the influence of the surrounding medium and the structure of organic molecules on their emission.

There have been many investigations devoted to the luminescence of organic scintillators under the influence of α- and β-particles and γ-rays; M.D.Galanin and his co-workers made a particularly thorough study of the luminescence yield under the influence of ionizing radiation and the reasons for the low efficiency under this type of excitation.

A great deal of attention has been given to detailed investigation of the frequencies and intensities in the absorption and luminescence spectra of organic compounds at liquid hydrogen temperature; fundamental research in this field has been carried out by A.F.Prikhot'ko and her school in the Ukrainian Academy of Sciences.

E.V.Shpol'skii and his co-workers made a detailed investigation of the structure of the spectra of aromatic compounds in frozen solutions of saturated hydrocarbons. Interesting studies of the structure of the spectra of anthracene and its derivatives in different solvents have been carried out by A.S.Charkasov. A.N.Sevchenko, L.V.Volod'ko and D.S.Umreiko investigated and interpreted the spectra of uranyl compounds.

In the laboratories of Kiev State University, A.A.Shishlovskii and M.U.Belyi continued their investigation of the luminescence and absorption of solutions of inorganic compounds. Important results have been obtained in the study of the luminescence of chlorophyll. These investigations have been successfully carried out by A.N.Terenin, A.A.Krasnovskii, A.V.Karyakin and V.B.Evstigneev, by many workers in the Belorussian Academy of Sciences and by G.N.Godnev, A.N.Sevchenko, L.A. Kravtsov and others.

The luminescence of vapors and gases and energy transfer in molecular collisions in a gaseous medium will be discussed at our Conference in only five reports (S.O.Mirumyants & B.S.Neporent, V.P.Klochkov, N.A.Borisevich & V.A.Tolkachev, P.A. Apanasevich & G.S.Kruglik and N.A.Borisevich & V.V.Gruzinskii) which, of course, does not correspond to the paramount importance of these problems.

At the first stages of investigation of luminescence there were carried out in the Soviet Union the classical studies of A.N.Terenin on optical excitation of vapors; at the same period, A.A.Shishlovskii carried out an extensive investigation of anthracene vapor. Since then work on the luminescence of vapors has been carried out primarily in the laboratory of B.S.Neporent and recently by N.A.Borisevich in the Belorussian Academy of Sciences. These investigations are of great interest, but I personally feel that there should be more research in this field. Investigation of luminescence in the gaseous phase allows of solving problems on the influence of the medium and clarifying the interaction of molecules and energy transfer between them under the most elementary conditions. Hence one could wish for an appreciable development of studies of the luminescence of vapors and gases with excitation both by light and fast particles.

Already at the last conference on molecular luminescence one could note indications of widespread introduction of the methods of luminescence analysis in engineering, biology, medicine and other fields of science and the national economy. Significant advances have been achieved here during the past two years. Particularly one must note the development of research in the field of biology, where, thanks to the initiative and insistence of M.N.Meisel, there has been achieved widespread acceptance of the techniques of luminescent microscopy; there have now been carried out by means of luminescence many studies of micro-organisms and viruses and pathological changes in different tissues.

A.V.Karyakin is responsible for the development of luminescence analysis techniques for the solution of important practical problems in the field of medicine.

Also worthy of note is the significant progress made in the application of luminescence analysis for detection of minor contaminants in high purity materials. A number of authors have developed procedures for determination of tellurium, thorium, indium and other elements from their interaction with luminescent dyes and other complex organic luminophors. E.A.Bozhevol'nov investigated the question of the relation between nonradiative transitions in intracomplex compounds and noncomplanar arrangement of the parts of the molecules; the results of his investigation enabled him to find new luminescent reagents for determination of aluminum and gallium. There has also been developed another method of detecting minor impurities in inorganic substances by means of preparation of crystal phosphors. Thus, for example, there was developed a procedure for analysis of antimony.

V.K.Matveev synthesized a new organic phosphor, lumogen orange-red, the emission color of which made it possible to use luminescence flaw-detection in the electrovacuum industry for locating points of leakage in the walls of glass equipment. The new method is simpler and in some cases more sensitive than the conventional methods of mass spectrometry.

Among the various technical applications of luminescence one must note the further development by V.K.Matveev and V.V.Patrikeev of the method of investigating sandy alluvia for purposes of hydroelectric engineering by means of sand colored with luminescent substances. This luminescence procedure in recent years has come into widespread use both in the USSR and abroad.

The above mentioned investigations will be reflected in the content of the reports to be presented at our Conference. At plenary sessions we shall consider problems of general significance; more particular problems, problems of procedure and industrial and scientific applications of luminescence and luminescence analysis will be discussed at sectional meetings.

There can be no doubt that consideration of the reports by so numerous an audience of specialists and the ensuing discussions will contribute greatly to the further development of research in luminescence.

I wish the Eighth Conference on Luminescence success in its work.

INTERNAL CONVERSION FROM THE FLUORESCENCE TO THE PHOSPHORESCENCE LEVEL IN NAPHTHALENE DERIVATIVES

- V.L.Ermolaev, I.P.Kotlyar & K.K.Svitashev

It is assumed that the triplet state of complex organic molecules participates in many important photochemical reactions;[1] hence investigation of the processes involved in population of this state is an important problem. One of the essential stages in investigation of the process of internal conversion to the triplet state is measurement of the ratio of the quantum efficiencies of phosphorescence and fluorescence of organic molecules in solid solutions at low temperature.[2] The present work is concerned with such measurements. Before describing the experimental results, however, it may be useful to outline the nature of the mechanism of internal conversion.

It is usually assumed that the transition to the triplet state is realized at the point of intersection of the potential hypersurfaces of the fluorescence and triplet states of the molecule. However, one can also attempt to explain internal conversion to the triplet state from a different standpoint.

In a brief note published in 1956 Franck & Sponer[3] proposed interpreting rapid nonradiative conversion of complex molecules from high-lying excited states to a low-lying state as an effect of intramolecular nonradiative energy transfer, similar to intermolecular nonradiative resonance energy transfer observed in the familiar effects of concentration depolarization or sensitized fluorescence. Inasmuch as in complex molecules, with a few rare exceptions, there is overlapping of the bands that are mirror images of the second or third absorption bands, (i.e., the bands corresponding to the spectrum of emission from the second or third electronic level; this emission is generally not seen) with the first or second electron absorption bands, the condition necessary for this process is fulfilled. In contrast to the case of sensitized fluorescence of organic compounds, where the oscillators of the energy donors and acceptors are separated in space so that the interaction is insignificant, in the given case the two oscillators are virtually adjoining if not merged, so the process must occur with high efficiency. The resultant excess of vibrational energy is rapidly transferred to the surrounding medium or to optically inactive vibrations of the molecule. The said process, leading to rapid conversion of part of the electron excitation energy to vibrational energy, cannot obtain for a transition from a low lying excited state to the ground state, inasmuch as in this case there is no overlapping of the emission and absorption spectra, which leads to the possibility for emission of luminescence.

A similar process will also occur in the case of excitation to high-lying triplet levels of an organic molecule. Franck & Sponer[3] do not distinguish between the mechanisms involved in transitions from high-lying singlet and high-lying triplet levels to low-lying excited levels of the same multiplicity.

We believe, however, that the mechanisms of conversion from high-lying singlet and high-lying triplet levels are different. In the case of transitions between singlet levels and consequently interaction of allowed electron transitions there is a high probability for inductive interaction analogous to the case of intermolecular resonance interaction[4]. On the other hand, in the case of conversion to triplet levels there must obtain an exchange-resonance interaction mechanism inasmuch as inductive interaction between the corresponding transitions is weak because these transitions are forbidden. That the interaction between two molecules leading to nonradiative transfer with excitation of the triplet level is of exchange-resonance character was shown earlier by Terenin and one of the present authors[5].

We now turn to a consideration of how one can from this standpoint characterize the process of conversion from a low-lying singlet excited level to the triplet level. As is known, intercombinational transitions in atoms and molecules are inhibited owing to weak spin-orbit coupling. Spin-orbit interaction in a molecule leads to a triplet state admixture in the singlet state and vice versa. From the model standpoint it may be said that there is a definite (in most cases, low) probability for molecules in the singlet excited state to go over into a state of the same energy but with the configuration of one of the triplet levels (T_i). From the T_i state the molecule rapidly goes over into the low-lying triplet state by means of the above-mentioned exchange-resonance mechanism. Thus the probability r for internal conversion from the fluorescent state to the phosphorescent state is equal to the product of the probability for realization of the intermediate state T_i, determined by the spin-orbit interaction, multiplied by the probability for nonradiative transition from this state to the low-lying triplet state, depending on the overlapping of the corresponding emission and absorption spectra. The probability for a radiative transition corresponding to phosphorescence can also be represented as the product of two probabilities, namely, the fraction of singlet states in the low-lying triplet state and the probability of radiative transition from this state to the ground state. The strength of the spin-orbital coupling in most cases is of the same order of magnitude in the fluorescence and phosphorescence states of the molecule. Consequently, the difference between the probabilities for interval conversion $S^* \rightarrow T$ and emission of phosphorescence, which attains a magnitude of 10^6-10^9, is due to the appreciably higher probability for nonradiative resonance transitions in the molecule as compared with the probability for radiative transitions.

In the experimental part of this work we shall consider the influence of certain factors on the strength of the spin-orbit interaction and consequently on the probability of internal conversion of the molecule to the triplet state. First, let us consider the effect of introducing a heavy atom into the molecule. There have been a number of studies of this effect[6]; in most of these primarily quantitative results were obtained. We investigated the ratio of the quantum efficiencies of phosphorescence and fluorescence in a series of monosubstituted derivatives of naphthalene, substances which proved very convenient for quantitative comparison of the influence fluorine, chlorine, bromine and iodine. The results of our measurements are given in the accompanying table.

Ratios of the efficiencies of phosphorescence and fluorescence of some derivatives of naphthalene in solutions at -196°*

Compound	η_{phos}/η_{fluo}		η_{tot}	$\frac{1}{\tau_{phos}}$, sec^{-1}	r, sec^{-1}
	$a+e$	$p.e.$	$a+e$		
1	2	3	4	5	6
Naphthalene	0,093±0,003	0,064±0,004	0,60	0,43	$(1\div8)\cdot10^5$
1-Fluoronaphthalene	0,068±0,004	—	0,90	0,66	$(2\div5)\cdot10^5$
1-Chloronaphthalene	5,2±0,5	—	0,36	3,4	$(1\div5)\cdot10^7$
1-Bromonaphthalene	160±20	190±25	0,27	50	$(5\div20)\cdot10^8$
1-Iodonaphthalene	>1000	—	0,38	500	$>3\cdot10^9$
1-Methylnaphthalene	0,053±0,002	—	0,89	0,48	$(1\div5)\cdot10^5$
1-Hydroxynaphthalene	0,047±0,002	0,056±0,004	0,80	0,52	$(1\div10)\cdot10^5$
1-Naphthaldehyde	>200	—	0,02	12	—
1-Nitronaphthalene	>1000	—	0,08	20	—
Quinoline	1,9±0,1	>100	0,29	0,73	—

---

*The experimental procedure was described earlier in Ref.7; $a + e$ = 2 to 1 mixture of alcohol and ether; $p.e$ = petroleum ether.

It will be evident from the table that the ratio of quantum efficiencies of phosphorescence and fluorescence in the series of halogen derivatives of naphthalene increases very rapidly in going from fluorine to iodine; in fact, the increase of this ratio (column 2) occurs more rapidly than the increase of the probability for emission of phosphorescence as evaluated from its lifetime (column 5). Inasmuch as the probability for emission of fluorescence in this series of halogen derivatives of naphthalene remains approximately constant, the more rapid increase of the phosphorescence efficiency as compared with the increase of the probability for emission of phosphorescence is indicative of the increasingly strong interaction of the halogen atom with the π-cloud of the naphthalene core in the singlet state as compared with the triplet state. A number of substituents (such as CH_3-, HO- and F-) have little effect on the yield and persistence of phosphorescence. The reasons for the increase of the relative yield of phosphorescence upon introduction of aldehyde and ketone groups was discussed in the work of Terenin and one of us[8]. Possibly a similar effect is produced by a nitro radical. The probability for internal conversion to the triplet state is greatly increased in going from naphthalene to its heteroanalog, quinoline.

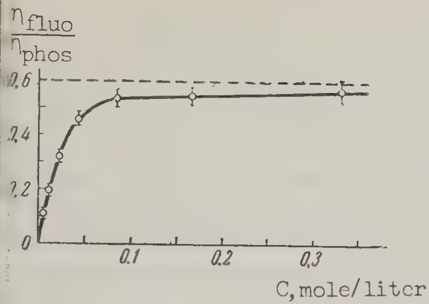

Variation of the ratio of the quantum efficiencies of fluorescence and phosphorescence of quinoline in petroleum ether at -196° with the concentration of isopropyl alcohol.

In the last column of the table we give quantitative evaluations of the minimum (when all the quenching is assumed to occur on the fluorescence level) and the maximum (when all the quenching is assumed to be on the triplet level) values of the probability for internal conversion to the triplet state. Change from a polar solvent (alcohol + ether) to a nonpolar solvent (petroleum ether) resulted in no appreciable change in the ratio of quantum efficiencies of phosphorescence and fluorescence in all the investigated cases except that of quinoline (see columns 2 & 3 of the table). Quinoline in petroleum ether emits no fluorescence (only phosphorescence).

We attribute the change in the probability for internal conversion from the fluorescence to the phosphorescence state in quinoline in going from alcohol + ether to petroleum ether to the presence in the former case of a hydrogen bond between the N atom of the quinoline and the HO group of the alcohol and the absence of this bond in the latter case. To check this inference we investigated the influence of different polar molecules on the luminescence of quinoline in petroleum ether. A number of polar molecules, such as pyridine, ethyl ether, diethylamine and formamide, do not affect the luminescence of quinoline in petroleum ether. A strong effect on this luminescence is exerted only by molecules possessing acid properties, in particular by alcohols. Thus, to insure fluorescence of quinoline with maximum efficiency it is sufficient to add 1-2% alcohol to the petroleum ether. The variation of the ratio of the fluorescence and phosphorescence efficiencies of quinoline in petroleum ether as a function of the concentration of isopropyl alcohol is shown in the accompanying figure. The observed variation is evidence of the association of the alcohol and quinoline molecules into complexes:

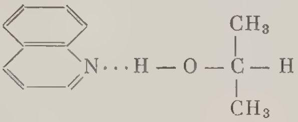

Conclusions

1. Internal conversion of organic molecules from the fluorescent to the phosphorescent state may be interpreted as a process of intermolecular excitation energy transfer operating by the exchange-resonance mechanism.

2. The probability for internal conversion in naphthalene derivatives increases greatly when the hydrogen is replaced by an atom of chlorine, bromine or iodine; the change in the spin-orbit interaction of molecules in the fluorescent state, leading to increase in the probability for internal conversion is greater than the corresponding change in the spin-orbit interaction in the triplet state. The spin-orbit coupling in this case does not change noticeably in going from a polar to a nonpolar solvent.

3. As compared with naphthalene, the strength of the spin-orbit coupling in the fluorescent state is much greater in quinoline, a heteroanalog of naphthalene comprising an N atom. The spin-orbit coupling decreases when the N atom of quinoline eneters into a hydrogen bond, which indicates the substantial role played by the free electrons of the N atom in the spin-orbit interaction in the fluorescent state.

In conclusion, we desire to express our deep gratitude to A.N.Terenin under whose guidance the work was performed.

References

1. A.N.Terenin, Fotokhimiya krasitelei i rodstvennykh organicheskikh soedinenii (Photochemistry of dyes and allied organic compounds), M. 1947; G.Oster & A.H.Adelman, J.Amer.Chem.Soc., 78, 913, 3977 (1956); A.N.Terenin, Fotokhimiya khlorofilla i fotosintez (Photochemistry of chlorophyll and photosynthesis), VI Bakhovskie chteniya, Pub.AN SSSR, 1951; J.Franck, Proc.Nat.Acad.Sci.U.S.A., 44, 941 (1958).
2. B.Ya.Sveshnikov, Dissertation, Physical Institute, USSR Ac.of Sci.M, 1951.
3. J.Franck & H.Sponer, J.Chem.Phys., 25, 172 (1956).
4. M.D.Galanin, Dissertation, Physical Institute, USSR Ac.of Sci., M., 1955; Th.Förster, Ann.phys., 2, 55 (1948).; D.L.Dexter, J.Chem.Phys., 21, 836 (1953).
5. V.L.Ermolaev & A.N.Terenin, J.Chim.phy., 55, 698 (1958); V.L.Ermolaev, Optika i spektroskopiya, 6, 642 (1959). (Trans.Optics and Spectroscopy.)
6. P.Yuster & S.I.Weissman, J.Chem.Phys., 17, 1182 (1949); M.Kasha, Disc. Faraday Soc., No.9, 14 (1950); E.H.Gilmore, G.E.Gibson & D.S.McClure, J.Chem.Phys. 20, 829 (1952); 23, 399 (1955); V.V.Zelinskii & V.P.Kolobkov, Optika i spektroskopiya, 1, 560 (1956); E.Clementi & M.Kasha, J.Chem.Phys., 26, 956 (1957).
7. V.L.Ermolaev & K.K.Svitashev, Optika i spektroskopiya, 7, 664 (1959). (Trans.Optics & Spectroscopy.)
8. V.L.Ermolaev & A.N.Terenin, Usp.fiz.nauk, 71, 137 (1960). (Trans.Soviet Physics - Uspekhi.)

LUMINESCENCE OF MATTER WITH ARBITRARY ABSORPTION AND EMISSION BANDS IN VOLUMES OF FINITE SIZE

- A.M. Samson

1. Investigation of resonance radiation from finite volumes[1] can be regarded as the first stage in the solution of the more general problem of propagation of light in matter with arbitrarily overlapping absorption and emission bands. In the present contribution we shall consider the applicability to this case of the results of the theory of propagation of resonance radiation and luminescence of an infinitely thick layer. Both these problems are important from the standpoint of investigation of substances with arbitrary absorption and emission bands in volumes of finite size.

2. The influence of secondary absorption and emission processes on the characteristics of the emitted radiation can be investigated by means of the following equation:[2,3]

$$\frac{dn_2}{dt} = -\frac{n_2}{\tau_0} + \frac{1}{4\pi\tau_0}\int\limits_V \frac{n_2(\mathbf{r})}{|\mathbf{r}-\mathbf{r}_0|^2}\,dV \int\limits_0^\infty \gamma(\nu)\,\varepsilon(\nu)\,\varkappa(\nu)\,e^{-\varkappa(\nu)|\mathbf{r}-\mathbf{r}_0|}d\nu + F(\mathbf{r}_0,\,t), \qquad (1)$$

where n_2 is the density of the emitting particles, τ_0 is the persistence of luminescence of an elementary volume, ν is the frequency, r_0 are the coordinates of the investigated point of volume V, $\varepsilon(\nu)$ is the emission band $\left(\int\varepsilon(\nu)\,d\nu = 1\right)$, $\varkappa(\nu)$ is the absorption coefficient, and $\gamma(\nu)$ is the quantum efficiency.

The density of the emitting particles excited without involving secondary absorption and emission processes is determined by the independent term. Equation (1) has been written without taking into account forced emission and is valid when the emission band $\varepsilon(\nu)$ and the persistence τ_0 do not depend on the frequency of the exciting light.

Analysis[4] shows that Eq.(1) can be reduced to the corresponding equation for resonance radiation[5] if, instead of $\gamma(\nu)$ and $\varkappa(\nu)$, we introduce the quantities:

$$k_{\mathrm{eff}} = \frac{\int\limits_0^\infty \gamma(\nu)\,\varepsilon(\nu)\,\varkappa^2(\nu)\,d\nu}{\int\limits_0^\infty \gamma(\nu)\,\varepsilon(\nu)\,\varkappa(\nu)\,d\nu} \quad \text{and} \quad \gamma_{\mathrm{eff}} = \frac{\left[\int\limits_0^\infty \gamma(\nu)\,\varepsilon(\nu)\,\varkappa(\nu)\,d\nu\right]^2}{\int\limits_0^\infty \gamma(\nu)\,\varepsilon(\nu)\,\varkappa^2(\nu)\,d\nu}. \qquad (2)$$

The introduction of these constants is effective and legitimate for relatively small volumes (optical thickness at the maximum of the emission band of the order of 2-3 units) and in the case when the excited particles are concentrated in a relatively small part of the volume. If the excited particles are distributed more or less uniformly through a large volume, better results should be obtained if $\gamma(\nu)$ and $\varkappa(\nu)$ are replaced by the constants:

$$\gamma_0 = \int\limits_0^\infty \gamma(\nu)\,\varepsilon(\nu)\,d\nu, \quad k'_{\mathrm{eff}} = \frac{1}{\gamma_0}\int\limits_0^\infty \gamma(\nu)\,\varepsilon(\nu)\,\varkappa(\nu)\,d\nu, \qquad (3)$$

where γ_0 is the yield (efficiency) of an elementary volume with excitation of it by radiation having a Planckian spectral distribution. Introduction of γ_{eff} and k_{eff} into the integral equation yields lower values (for large volumes), while the introduction of γ_0 and k_{eff} yields overestimates (for small volumes). Hence in some cases it is expedient to replace $\gamma(\nu)$ and $\varkappa(\nu)$ by average values intermediate between the above constants.

3. If we are investigating radiation emitted from an infinitely thick layer, reduction of the problem to the resonance case can be realized by the introduction of only one parameter, dependent on the properties of the medium and the conditions of illumination. It was shown in the work of Agranovich[3] and Sobolev[6] that the intensity (in photons) of the radiation emitted from a layer under steady state

conditions can be expressed by means of an auxiliary function φ:

$$I^{st}\left(\frac{\cos\theta}{b(\nu_1)}, \frac{\cos\theta'}{b(\nu)}\right) = \frac{\gamma(\nu_1)}{4\pi} I_{\nu_1}(\theta)\cos\theta \frac{\varepsilon(\nu)}{b(\nu)} \frac{\varphi(\cos\theta/b(\nu_1))\,\varphi(\cos\theta'/b(\nu))}{\cos\theta/b(\nu_1)+\cos\theta'/b(\nu)}, \tag{4}$$

where $b(\nu)$ is the shape of the absorption band normalized to unity at the maximum of the emission band ν_0*; θ and θ' are the angles of incidence and observation, $I_{\nu_1}(\theta)$ is the intensity of the external radiation, ν_1 is the frequency of the incident radiation, and ν is the frequency of the observed radiation.

The auxiliary function $\varphi\left(\frac{\cos\theta}{b(\nu_1)}\right)$ is proportional to the density of the emitting particles at the boundary of the layer and in the general case is determined by means of the following equation:

$$\varphi(x) = 1 + \frac{1}{2}\varphi(x)\,x\int\limits_0^\infty \gamma(\nu)\,\varepsilon(\nu)\,b(\nu)\,d\nu \int\limits_0^{1/b(\nu)} \frac{\varphi(y)}{x+y}\,dy, \tag{5}$$

where

$$x = \cos\theta/b(\nu_1); \quad y = \cos\theta'/b(\nu).$$

Knowing φ one can find not only the intensity of the radiation under steady state conditions, but also the shape of the band, the efficiency and the coefficients of "reflection" and "emission", etc. If the analytic form of φ is known, one can also obtain the intensity under nonsteady state conditions and determine the mean persistence of luminescence as a function of the properties of the medium and the experimental conditions. Actually, however, it is difficult to obtain a rigorous solution of (5) in final form.

Equation (5), like Eq.(1), reduces to the corresponding equation for the resonance case if we set $\varepsilon(\nu) = \delta(\nu - \nu_0)$ or $b(\nu) = 1$. For all other cases we write,

$$\varphi(x) \approx \varphi^{res}(x, \gamma_{eff}). \tag{6}$$

Expanding the right and left parts of (6) into series in orders of radiation (powers of γ) and equating the first terms of the expansion, we find

$$\gamma_{eff}(x) = \frac{\int\limits_0^\infty \gamma(\nu)\,\varepsilon(\nu)\,b(\nu)\ln\left(1+\frac{1}{xb(\nu)}\right)d\nu}{\ln\left(1+\frac{1}{x}\right)} = \gamma_0\alpha(x). \tag{7}$$

Thus for known φ^{res} one can readily find $\varphi(x)$. Calculations carried out for a Doppler shape of the emission and absorption lines show good agreement with the results of rigorous computation.

4. The above described method of determining $\varphi(x)$ is convenient when there are available tables giving values of φ^{res} or it is not required to know $\varphi(x)$ in final form. For calculation, for example, of the nonsteady state luminescence[7,8] one must have the analytic variation of φ with the efficiency γ_0. In an earlier contribution[9] we derived a simple expression for φ^{res} If in this expression we replace γ by $\gamma_{eff}(x)$, we obtain the following formula for the case of arbitrarily overlapping absorption and emission bands:

$$\varphi(x) \approx \frac{1+2x}{1+2x\sqrt{1-\gamma_{eff}(x)}}. \tag{8}$$

---

*This normalization of $x(\nu)$ serves to simplify the exposition.

Values of $\varphi(x)$

x	$\gamma_0 = 0{,}4$			$\gamma_\iota = 0{,}7$			$\gamma_0 = 1{,}0$	
	I	II	III	I	II	III	II	III
0,2	1,07	1,07	1,05	1,14	1,13	1,11	1,23	1,19
0,6	1,12	1,12	1,11	1,27	1,26	1,24	1,51	1,48
1,0	1,15	1,15	1,14	1,35	1,34	1,32	1,73	1,71
3,0	1,21	1,21	1,21	1,53	1,52	1,52	2,46	2,50
5,0	1,24	1,24	1,23	1,60	1,60	1,60	3,00	3,05
7,0	1,25	1,25	1,25	1,64	1,64	1,64	3,50	3,51
10,0	1,26	1,26	1,26	1,68	1,68	1,68	—	4,04
∞	1,29	1,29	1,29	1,83	1,83	1,83	∞	∞

In the accompanying table we list the values of $\varphi(x)$ for a Doppler line shape; the values in columns I and II are the precise values calculated by means of Eqs. (6) and (7), respectively; the values in column III were calculated by means of Eq.(8).

It will be evident in all cases close values are obtained. With increase of x the values in all the columns approach

$$\varphi(\infty) = 1/\sqrt{1-\gamma_0}, \tag{9}$$

which is identical with the corresponding rigorous value.

5. By means of the function φ determined in this manner one can solve a number of problems relating to the luminescence of an infinitely thick layer under steady state and nonsteady state conditions. By way of example let us consider the spectral dependence of the radiation emitted from a medium under steady state conditions when the emission and absorption bands have the Gaussian shape. The accompanying figure shows the values of the intensity for different frequencies

$$\omega \left(\omega = \frac{\nu - \nu_0}{\Delta\nu}\right),$$

normalized to unity at the maximum of the emission band ν_0. The curves were plotted according to Eq.(4) for different γ_0 and $\cos\theta/b\,(\nu_1)$ and for $\theta' = 0^\circ$.

It will be evident from the figure that the contour of the emission band in all cases differs greatly from the initial Doppler contour (curves 1). Only when the surface layer is excited exclusively by the external radiation $(\cos\theta/b\,(\nu_1) \ll 1)$ and γ_0 is low is the frequency dependence of the emitted radiation the same as for an elementary volume. With increase of $\cos\theta/b\,(\nu_1)$, i.e., when the external radiation excites increasingly deeper lying layers, the emission band becomes wider. At still higher values of $\cos\theta/b(\nu_1)$ there is obtained a self-reversed line with side peaks, which in the limit as $\cos\theta/b(\nu_1) \to \infty$ shift to infinity. Analysis of the above dependences shows that an infinitely thick layer does not always, when the concentration of excited particles decreases towards the layer boundaries, yield a self-reversed line. For example, with $\cos\theta/b(\nu_1) = 1$ there are no self-reversed lines, although as follows from Ref.1, for high γ_0 there is a noticeable decrease in the density of the emitting particles towards the boundary of the layer. Thus, decrease of the concentration of excited particles is not a sufficient condition for the appearance of self-reversed lines, which is in agreement with the deductions of Biberman[10].

6. If the γ_0 dependence of φ is known, one can readily find the radiation intensity under nonsteady state conditions:

$$I(t) = \frac{\gamma(\nu_1)}{\tau_0}\frac{\varepsilon(\nu)}{b(\nu)}\cos\theta \int\limits_{-\infty}^{t} I_{\nu_1}(\theta, t')\, e^{-\frac{t-t'}{\tau_0}} \sum_{k=1}^{\infty} \left(\frac{\gamma_0}{\tau_0}\right)^{k-1} \frac{(t-t')^{k-1}}{(k-1)!} \times R_k\left(\frac{\cos\theta'}{b(\nu)}, \frac{\cos\theta}{b(\nu_1)}\right) dt'. \tag{10}$$

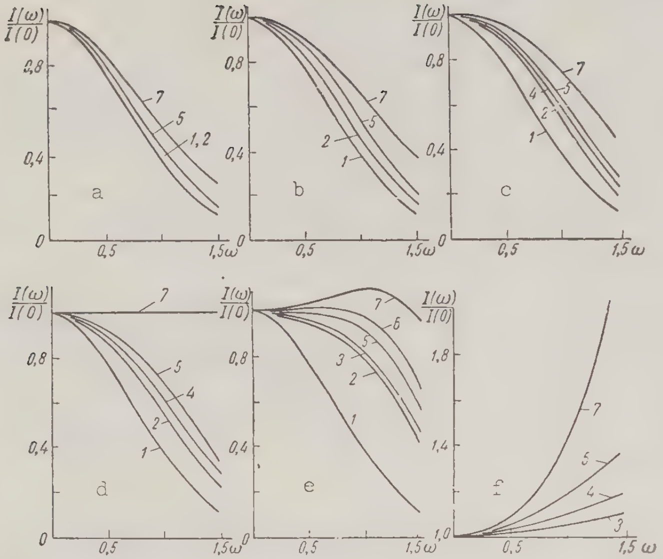

Variation of the radiation emitted from a layer as a function of the frequency with observation normal to the surface of the layer: a - $\cos\theta/b(\nu_1) \ll 1$, b - 0.5, c - 1.0, e - 5.0, f - ∞, d - excitation by equilibrium radiation; 1 - $e^{-\omega^2}$, 2 - $\gamma_0 \to 0$, 3 - $\gamma_0 = 0.4$, 4 - 0.6, 5 - 0.8, 6 - 0.9, 7 - 1.0.

Here the factor R_k is proportional to the intensity of the k-th order under steady state conditions. The factor can be determined by expanding (4) in a series in powers of γ_0. From Eq.(10) one can readily obtain the intensities under conditions of build-up, decay, etc. In some cases, one can sum instead of integrating in (10) and obtain a simple expression. It is evident from Eq. (10), for example, that the luminescence decay laws do depend not only on the angles of incidence and observation, but also on the frequencies involved. The variation of the decay laws as a function of the experimental conditions and the parameters of the layer can be investigated by means of the mean persistences:*

$$\bar{\tau}^{\mathrm{pu}} = \tau_0 \frac{\gamma_0}{I^{\mathrm{st}}} \frac{dI^{\mathrm{st}}}{d\gamma_0},$$

and

$$\bar{\tau}^{\mathrm{pr}} = \frac{\tau_0}{2} \frac{d^2(\gamma_0 I^{\mathrm{st}})}{d\gamma_0^2} \Big/ \frac{dI^{\mathrm{st}}}{d\gamma_0}, \tag{11}$$

here $\bar{\tau}^{\mathrm{pu}}$ and $\bar{\tau}^{\mathrm{pr}}$ are the mean luminescence persistences for short term (pulse - $\Delta t \ll \tau_0$) and prolonged excitation of the medium.

Substituting the value of I^{st} obtained from (4) in Eq.(11) and using Eq.(8) for φ, one can obtain the mean persistences under any conditions of excitation and observation.

7. For purposes of illustration we adduce below several rigorous formulas for the luminescence intensity under conditions of preliminary short term excitation of the system and for mean persistences defined by (11).

A. Excitation of the layer by a diffuse flux with the following frequency distribution of the incident energy:

$$I = I_0 \varepsilon(\nu_1) / b(\nu_1).$$

a) Observation conditions: $\cos\theta' / b(\nu_1) \ll 1$.

$$I^{\mathrm{pu}}(t) = I_0 \frac{\gamma_0}{2} \frac{\varepsilon(\nu}{b(\nu)} e^{-\frac{t}{\tau_0}\left(1-\frac{\gamma_0}{2}\right)} \left[I_0\left(\frac{\gamma_0 t}{2\tau_0}\right) - I_1\left(\frac{\gamma_0 t}{2\tau_0}\right) \right]^{**}, \tag{12}$$

---

*The mean duration is defined as $\bar{\tau} = \int_0^\infty I(t)\,t\,dt \Big/ \int_0^\infty I(t)\,dt.$

**See footnote on following page.

$$\bar{\tau}^{pu} = \tau_0 \frac{1+\sqrt{1-\gamma_0}}{2\sqrt{1-\gamma_0}}, \quad \bar{\tau}^{pr} = \tau_0 \frac{1-{}^3/_4\gamma_0}{1-\gamma_0}. \tag{13}$$

b) Observation conditions: $\cos\theta' / b(\nu) \gg 1$.

$$I^{pu}(t) = \frac{\gamma_0}{4\cos\theta'} \varepsilon(\nu) I_0 e^{-\frac{t}{\tau_0}\left(1-\frac{\gamma_0}{2}\right)} \left[I_0\left(\frac{\gamma_0 t}{2\tau_0}\right) + I_1\left(\frac{\gamma_0 t}{2\tau_0}\right)\right]^{*}, \tag{14}$$

$$\bar{\tau}^{pu} = \tau_0 \frac{1+\sqrt{1-\gamma_0}}{2(1-\gamma_0)}, \quad \bar{\tau}^{pr} = \tau_0 \frac{1-\gamma_0/4}{1-\gamma_0}. \tag{15}$$

It will be evident from the adduced formulas that, depending on the region of the spectrum wherein the luminescence is observed, we will obtain different values of the mean persistences. For example, for $\gamma_0 = 0.96$ in case (a) above, we have $\bar{\tau}^{pr} = 7\tau_0$, while in case (b) - $\bar{\tau}^{pr} = 19\tau_0$.

B. Excitation by weakly absorbed radiation: $\cos\theta / b(\nu_1) \gg 1$.

a) Conditions of observation: $\cos\theta' / b(\nu) \ll 1$.

$$I^{pu}(t) = \frac{\gamma(\nu_1) I_{\nu_1} b(\nu_1)}{4\pi} \frac{\varepsilon(\nu)}{b(\nu)} e^{-\frac{t}{\tau_0}\left(1-\frac{\gamma_0}{2}\right)} I_0\left(\frac{\gamma_0 t}{2\tau_0}\right)^{*}, \tag{16}$$

$$\bar{\tau}^{pu} = \tau_0 \frac{1-\gamma_0/2}{1-\gamma_0}, \quad \bar{\tau}^{pr} = \tau_0 \frac{8-8\gamma_0+3\gamma_0^2}{4(1-\gamma_0)(2-\gamma_0)}. \tag{17}$$

b) Conditions of observation: $\cos\theta' / b(\nu) \gg 1$.

$$I^{pu}(t) = \frac{\gamma(\nu_1) I_{\nu_1} b(\nu_1)}{4\pi} \frac{\varepsilon(\nu)}{b(\nu)} e^{-\frac{t}{\tau_0}(1-\gamma_0)}, \tag{18}$$

$$\bar{\tau}^{pu} = \bar{\tau}^{pr} = \tau_0 \frac{1}{1-\gamma_0}. \tag{19}$$

Analysis of Eqs.(16)-(19) shows that the increase in the persistence of luminescence owing to secondary excitation processes in the system is greater in the case of weakly absorbed radiation. For the same values of the efficiency ($\gamma_0 = 0.96$) the persistences τ^{pr} in cases (a) and (b) increase by a factor of 18.5 and 25, respectively. It should also be noted that weakly absorbed luminescence decays exponentially.

Here we have given only part of the rigorous formulas characterizing the luminescence decay laws under different experimental conditions. Analysis of the adduced formulas is sufficient, however, to judge of the general functional dependence of the persistence of luminescence on the spectral composition of the incident and observed radiations in the presence of secondary absorption and emission processes. It must also be noted that increase in the persistence of luminescence owing to secondary processes in volumes of finite size is determined, other conditions being equal, by $\varepsilon(\nu)$, $\gamma(\nu)$ and the product of the absorption coefficient $\varkappa(\nu)$ in the emission band by the size of the volume. The behavior of the absorption curve outside the emission band is immaterial. Moreover, for an infinitely thick layer the absolute magnitude of the absorption coefficient $\varkappa(\nu)$ in the band $\varepsilon(\nu)$ is also unimportant.

I desire to thank V.I.Stepanov for suggesting the topic and his interest in the work.

Institute of Physics
Academy of Sciences of the Belorussian SSR

---

*The I_0 and I_1 in the brackets are Bessel functions of an imaginary argument.

References

1. A.M.Samson, Vestsi AN BSSR, Ser.fiz.-tekhn.nauk (Bulletin of the Acad. of Sci. of the Belorussian SSR, Phys.-Tech.Series), No.3, 16 (1959).

2. L.M.Biberman, Zhur.eksp.i teor.fiz., 17, 416 (1947).

3. V.M.Agranovich, Izv.AN BSSR, Ser.fiz., (Belorussian Ac.of Sci., Phys.Series), 23, 40 (1959).

4. A.M.Samson, Doklady AN SSSR, 3, 479 (1959). (Trans.Doklady.)

5. A.M.Samson, Optika i spektroskopiya, 5, 500 (1958).

6. V.V.Sobolev, Perenos luchistoi energii v atmosferakh zvezd i planet (Transfer of radiant energy in the atmospheres of stars and planets), M., 1956.

7. A.M.Samson, Inzh.-fiz.zhur. (Engineering-Physics Journal), 2, No.8, 84 (1959).

8. A.M.Samson, Optika i spektroskopiya, 8, 89 (1960). (Trans.Optics and Spectroscopy.)

9. A.M.Samson, Inzh.-fiz.zhur. (Eng.-Physics Journal), 1, No.1, 65 (1958).

10. L.M.Biberman, Zhur.eksp.i teor.fiz., 19, 585 (1947).

SECONDARY LIGHT ABSORPTION AND EMISSION PROCESSES

- B. I. Stepanov & A. M. Samson

1. Spectroscopic investigations are generally concerned with a whole collective of particles occupying a finite volume. The radiation emitted by atoms in different internal parts of the volume does not always emerge. It may be absorbed by neighboring particles, which being excited by this radiation may again emit light. Secondary absorption and emission processes can therefore affect the intensity, efficiency, rate of decay and other characteristics of the excited radiation. This effect complicates the functional dependence of the emitted light on the experimental conditions and hampers interpretation of the experimental data. The matter of taking into account secondary absorption and emission processes is important in astrophysics, atmospheric and marine optics, investigation of the properties of light sources, the luminescence of substances with overlapping absorption and emission bands, and the like. The theory of radiant energy transfer as it was developed in the context of astrophysical problems virtually does not touch upon the problems of the luminescence of finite volumes under laboratory conditions. Only in recent years have a few authors[1-3] begun to apply this theory to the investigation of luminescence, the emission of flames and discharges, etc.

In the present report we give the results of investigation of resonance luminescence of matter in volumes of finite size.[4] In contrast to other studies, we investigated in detail the influence of secondary absorption and emission properties on the characteristics of resonance luminescence. The formulas deduced allow of calculating the luminescence under different conditions of irradiation and observation for volumes of different size.

Investigation of the propagation of resonance radiation in volumes of finite size may be regarded as the first stage in the solution of the more general problem, that of propagation of light in matter with arbitrary absorption and emission bands. It enables us to evaluate the influence of secondary processes on the characteristics of luminescence in the pure form without considering the structure of the bands in detail. Taking into account the shape of the absorption and emission bands complicates the problem but only slightly modifies the basic regularities.

2. Let us consider the distribution of excited particles inside a luminescent volume. The equation defining the number of excited particles at any point of a finite volume containing a system of particles with two energy levels is of the form:

$$\frac{dn_2(\mathbf{r}, t)}{dt} = -n_2(\mathbf{r}, t)(A + d) + nB[u_1(\mathbf{r}, t) + u_2(\mathbf{r}, t)], \quad (1)$$

where n_2 is the density of the excited particles, n is the total particle density, A and B are the Einstein probability coefficients, d is the nonoptical transition probability, u_1 is the radiation density due to the external source, and u_2 is the flux density due to the luminesce of the substance. When the complex functional dependence of u_1 and particularly u_2 on the coordinates of the volume is taken into account, Eq. (1) is an integro-differential equation. Its solution in the general case can be written as

$$n_2(\mathbf{r}, t) = \frac{Bn}{c}\int_{-\infty}^{t} I_{\text{es}}(t')\, e^{-\frac{t-t'}{\tau_0}} \sum_{i=0}^{\infty} \frac{\gamma^i (t-t')^i}{\tau_0^i\, i!}\, u^{(i)}(\mathbf{r})\, dt', \quad (2)$$

where $\gamma = \frac{A}{A+d}$ is the efficiency and $\tau_0 = \frac{1}{A+d}$ is the persistence of the luminescence of an elementary volume, and I_{es} characterizes the intensity of the light from the external source on the surface of the volume (specimen). Under steady

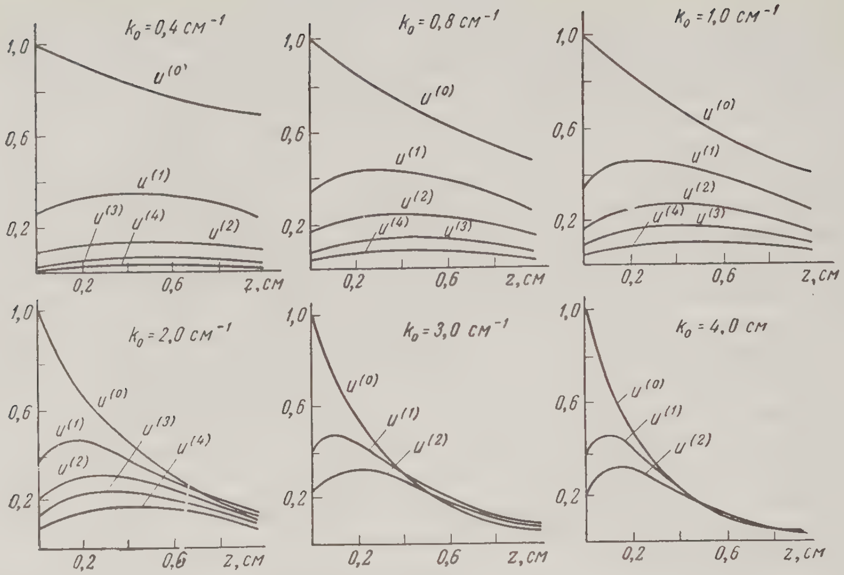

Fig.1. Variation of different orders of radiation (luminescence) with depth.

state conditions the $u^{(i)}(\mathrm{r})$ are proportional to the density of the radiations of different orders at the point r:

$$u^{(i)}(\mathrm{r}) = \frac{k_0}{4\pi}\int_V u^{(i-1)}(\mathrm{r}')\,\frac{e^{-k_0|\mathrm{r}-\mathrm{r}'|}}{|\mathrm{r}-\mathrm{r}'|^2}\,dV', \quad u^{(0)}(\mathrm{r}) = \frac{cu_1}{I_{\mathrm{es}}}, \tag{3}$$

where k_0 is the absorption coefficient, and V is the volume.

Eq.(2) gives the number of excited particles at the point r and the instant t for any time dependence of the intensity of the external source. Different particular cases (build-up, decay, steady state, etc.) are characterized by the corresponding form of the function $I_{\mathrm{es}}(t)$. If we set $I_{\mathrm{es}}(t) = I_{\mathrm{es}}$ (i.e., assume steady state excitation conditions), we have

$$n_2^{\mathrm{ss}}(r) = \frac{Bn\tau_0}{c}\,I_{\mathrm{es}}\,[u^0 + \gamma u^{(1)} + \gamma^2 u^{(2)} + \ldots] = \frac{Bn\tau_0}{c}\,I_{\mathrm{es}}\sum_{i=0}^{\infty}\gamma^i u^{(i)}. \tag{4}$$

The first term in the series (4) is proportional to the density of the radiation arriving from outside at the given point r; the second term is proportional to the density of the primary luminescence, i.e., the radiation due to the emission of the particles excited by the external radiation; the third term is proportional to the density of the secondary luminescence and so on.

3. We carried out calculations for the specific case of an infinite plane-parallel layer irradiated by a beam normal to its surface. The integrals were evaluated graphically. Fig.1 shows the curves characterizing the variation of $u^{(i)}$ as a function of the depth into the layer for different values of the absorption coefficient k_0 (for a layer thickness l = 1 cm). It will be evident from the curves that for small k_0 the density of the primary luminescence at each point is lower than the density of the radiation from the external source, the density of the secondary luminescence is lower than that of the primary, that of the third is lower than that of the secondary, and so on. For large k_0 and high γ the density of the radiation of the preceding order may become lower than the density of the radiation of the succeeding order.

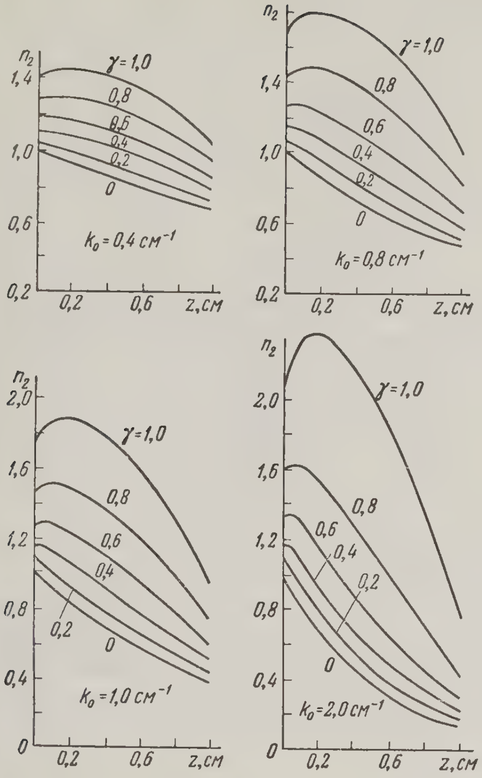

Fig.2. Variation of the density of excited particles with depth for different values of the absorption coefficient k_0.

If the $u^{(i)}$ are known, one can by means of (4) find the total luminescence density and also the number of excited particles for any given γ. Fig.2 shows curves characterizing the variation in the density of excited particles over the depth of the layer for different k_0 and γ. It will be seen that even for $\gamma = 0.2$ the distribution of excited particles differs substantially from the distribution that obtains in the absence of secondary processes ($\gamma = 0$ curve).

The excess of the actual number of excited particles over the number corresponding to direct excitation by the external source even for $k_0 = 0.4$ and $\gamma = 0.2$ amounts to 10%. With increase of k_0 the difference increases and may attain 100% or more. For high values of the absorption coefficient the density of the external radiation (and, consequently, the number of particles excited by it) near the back surface of the layer will amount to only a small fraction of the total density even at medium values of γ.

4. The formulas for determining n_2 under steady state conditions are rather complex even for a plane-parallel layer. However, convenient expressions for the radiation propagating inside and outside the medium can be obtained by using the so-called Schwarzschild-Schuster[4] approximation:

$$\frac{n_2 c}{Bn\tau_0 I_{\text{es}}} = \frac{1-4\cos^2\theta}{1-\beta^2\cos^2\theta}\, e^{-\frac{k_0 z}{\cos\theta}} + \frac{\gamma\cos\theta\,(1+R)}{1-\beta^2\cos^2\theta}\,\frac{1}{1-R^2 e^{-2\beta k_0 l}}\,\cdot$$

$$\{e^{-\beta k_0 z}[(2\cos\theta+1)-(2\cos\theta-1)\,Re^{-\beta k_0 l - k_0 l/\cos\theta}+$$

$$+e^{\beta k_0 z}[-(2\cos\theta+1)e^{-2\beta k_0 l l}+(2\cos\theta-1)\,e^{-\beta k_0 l+\frac{k_0 l}{\cos\theta}}]\}, \tag{5}$$

where θ is the angle of incidence of the exciting radiation, $\beta = 2\sqrt{1-\gamma}$ and $R = \frac{2-\beta}{2+\beta}$. In the same approximation one can also readily obtain the auxiliary functions of Ambartsumyan, φ and ψ, by means of which one can calculate the intensities of the "reflected" (observed from the front) and "transmitted" (observed from the back) radiation emitted by the layer at a given angle θ':

$$I_R^{\text{ss}}(\theta, \theta') = \frac{\gamma I_{\text{es}}\cos\theta}{4\pi}\cdot\frac{\varphi(\cos\theta)\,\varphi(\cos\theta') - \psi(\cos\theta)\,\psi(\cos\theta')}{\cos\theta+\cos\theta'},$$

$$I_T^{\text{ss}}(\theta, \theta') = \frac{\gamma I_{\text{es}}\cos\theta'}{4\pi}\cdot\frac{\varphi(\cos\theta)\,\psi(\cos\theta') - \varphi(\cos\theta')\,\psi(\cos\theta)}{\cos\theta'-\cos\theta}. \tag{6}$$

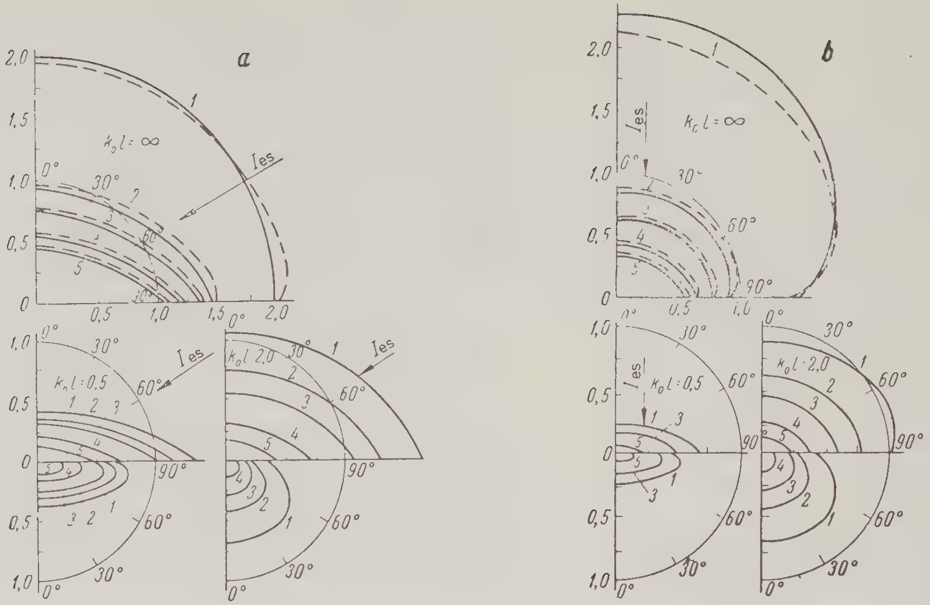

Fig.3. Angular distribution of the radiation emitted from the layer. The curves located above the horizontal axis correspond to observation "from the front"; those below the axis to observation "from the back"; a - excitation at an angle of 60°, b - at 90°; the dashed lines represent the precise curves. 1 - $\gamma = 1.0$, 2 - $\gamma = 0.9$, 3 - $\gamma = 0.8$, 4 - $\gamma = 0.6$, 5 - $\gamma = 0.4$.

These functions are in general defined by a set of nonlinear integral equations. Approximate expressions for them can be obtained using the rigorous relationships

$$\varphi(\cos\theta) = \frac{c}{BnI_{es}\tau_0} n_2(0, \theta), \qquad \psi(\cos\theta) = \frac{c}{BnI_{es}\tau_0} n_2(l, \theta), \tag{7}$$

and the approximate value of n_2 from (5). The values of φ and ψ obtained in this way are in good agreement with the corresponding precise values.

Knowing φ and ψ one can, by means of (6), investigate the angular distribution of the radiation emerging from the layer. The corresponding indicatrices for "reflected" and "transmitted" light are shown in Fig.3. The indicatrices depend on the luminescence efficiency, the absorption coefficient, the thickness of the layer, and the angle of incidence of the exciting radiation. In the presence of secondary processes a spherical indicatrix is obtained only for an infinitely thick layer with $\gamma = 1$ and irradiation of the layer by a diffuse flux. In all other cases the indicatrix differs substantially from spherical. For low values of γ, when a significant role is played by only one secondary process - reabsorption - the shape of the indicatrix is determined only by the angles of incidence and observation.

5. Above we have given the density distribution of radiation of different orders over the depth of the layer found by numerical integration. The intensities $\gamma^i R_i(\theta, \theta')$ and $\gamma^i T_1(\theta, \theta')$ of the i-th order of radiation emitted from the layer can be found by expanding (6) (for known φ and ψ) in a series in powers of γ. The values of R_i and T_i for several layer thicknesses and for $\theta = \theta' = 0°$ are listed in the accompanying table. In the last columns of the table we give the values of

k_0l	R_1	R_2	R_3	R_4	R_5	I_R/I_{es}	T_1	T_2	T_3	T_4	T_5	I_T/I_{es}	$T_0 = e^{-k_0l}$
0,4	0,022	0,007	0,002	0,001	—	0,032	0,021	0,007	0,002	0,001	—	0,031	0,670
2,0	0,039	0,025	0,018	0,013	0,010	0,140	0,022	0,018	0,015	0,012	0,010	0,110	0,135
4,0	0,040	0,027	0,020	0,016	0,015	0,217	0,006	0,006	0,006	0,007	0,007	0,118	0,018
∞	0,040	0,027	0,020	0,016	0,015	0,358	—	—	—	—	—	—	—

the corresponding intensities under steady state conditions for $\gamma = 1$. The values of R_i and T_i are comparable.

6. It follows from Eq.(2) that if the different orders of radiation under steady state conditions are known, one can readily calculate the luminescence under nonsteady state conditions as well. Sometimes the series (2) can easily be summed. From analysis of the deduced expressions and tentative calculations it follows that the variation of n_2 after cessation of excitation is nonexponential. At high quantum efficiencies γ the decrease of n_2 with time should be one-two orders of magnitude slower than for an elementary volume. At the back surface of the layer the variation of n_2 with time is slower than at the front (irradiated) surface. The thicker the layer (or the higher the absorption coefficient) the stronger will be the influence of secondary effects on $n_2 = f(t)$.

7. Knowing the spatial distribution of excited particles, one can readily calculate the radiation emerging from the volume. For example, the intensities of the radiation emitted from the front and back of the layer at a given angle θ' will be

$$I_R(t;\theta,\theta') = \frac{\gamma\cos\theta}{\tau_0}\int_{-\infty}^{t} I_{es}(t',\theta)\, e^{-\frac{t-t'}{\tau_0}} \sum_{k=1}^{\infty} \frac{(\gamma t-\gamma t')^{k-1}}{\tau_0^{k-1}(k-1)!} R_k(\theta,\theta')\,dt',$$

$$I_T(t;\theta,\theta') = \frac{\gamma\cos\theta}{\tau_0}\int_{-\infty}^{t} I_{es}(t',\theta)\, e^{-\frac{t-t'}{\tau_0}} \sum_{k=1}^{\infty} \frac{(\gamma t-\gamma t')^{k-1}}{\tau_0^{k-1}(k-1)!} T_k(\theta,\theta')\,dt'. \tag{8}$$

From the general equation (8) one can deduce expressions for the luminescence intensity in different particular cases (build-up, decay, steady state, etc.). Analysis of Eq.(8) shows that the rate of decay depends not only on the efficiency, layer thickness and mode of observation, but also on the duration of the excitation process (irradiation). Observation "from the back" in the case of short term ($\Delta t \ll \tau_0$) excitation may even show an increase in the luminescence intensity during the first instants. For example, for $k_0l = 4$ and $\gamma = 1$, using the tabular data, we obtain

$$I_T^{\text{pu}}(t;0,0) = \frac{I_{\text{es}}}{4\pi}\, e^{-\frac{t}{\tau_0}}\left[0.073+0.078\,\frac{t}{r_0}+\frac{0.081}{2!}\left(\frac{t}{\tau_0}\right)^2+\frac{0.083}{3!}\left(\frac{t}{\tau_0}\right)^3+\frac{0.084}{4!}\left(\frac{t}{\tau_0}\right)^4+\dots\right]. \tag{9}$$

For low values of t/τ_0 the expression in brackets in (9) increases more rapidly than $e^{-\frac{t}{\tau_0}}$ decreases, and consequently the pulse excitation intensity I_T^{pu} (observation "from the back") will also increase. At $t/\tau_0 = 2$ the luminescence intensity will be some 8-10% higher than the intensity at the initial instant.

8. For a semi-infinite layer ($k_0l = \infty$) the series in (8) can be summed in some cases. In the case of illumination of a layer by a diffuse flux (external source intensity direction-independent) we obtain the following rigorous expression for the intensity of the emerging radiation averaged over all directions:

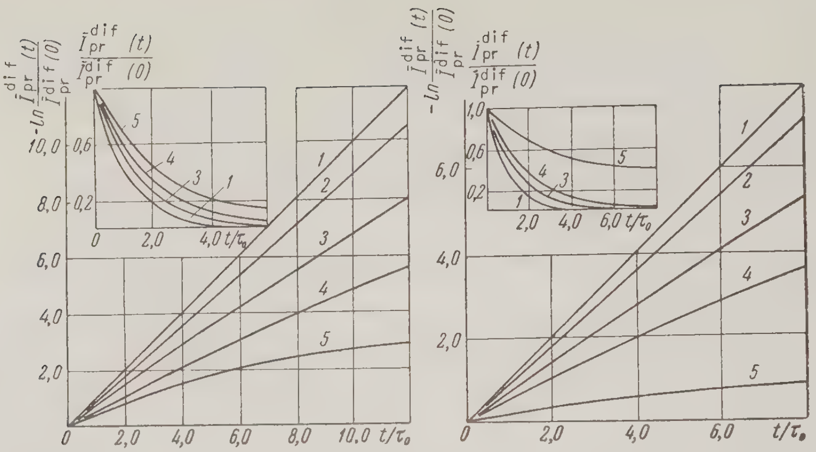

Fig.4. Luminescence decay curves after pulse or prolonged excitation of the system: 1 - $\gamma \to 0$, 2 - $\gamma = 0.20$, 3 - $\gamma = 0.50$, 4 - $\gamma = 0.75$, 5 - $\gamma = 1.0$.

$$\bar{I}^{\,\mathrm{dif}}(t) = \int\limits_{-\infty}^{t} I_{\mathrm{es}}(t')\,\frac{e^{-\frac{t-t'}{\tau_0}\left(1-\frac{\gamma}{2}\right)}}{t-t'}\,I_1\left(\frac{\gamma t-\gamma t'}{2\tau_0}\right)dt'\,^{*}. \qquad (10)$$

From Eq.(10) one can in turn deduce an expression for the average intensity during decay after preliminary short term (pulse) or prolonged excitation of the system.

Fig.4 shows the variation of the luminescence intensity with time for different γ. The slope of the curves is always less than unity, which corresponds to a more slow than exponential (e^{-t/τ_0}) decrease of the luminescence intensity. With increase of γ the slope of the curves decreases. In the range of low values of γ the variation of the logarithm of the intensity is approximately linear (curves 1, 2, 3), i.e., the luminescence decay is approximately exponential, although the persistence of the luminescence is somewhat greater than the persistence from an elementary volume. The slope of the curves for $\gamma = 1$ tends to 0 with increase of t/τ_0, which corresponds to a very slow increase in the luminescence intensity. For example, the intensity $I^{\mathrm{dif}}_{\mathrm{pr}}$ with $\gamma = 1$ at the instant $t = 8\tau_0$ amounts to 38% of the initial intensity. In the absence of secondary absorption and emission events the intensity would amount to only 0.03%.

9. It is sometimes convenient to investigate nonsteady luminescence of a layer in terms of average persistences given by the formula

$$\bar{\tau} = \frac{\int\limits_0^\infty I(t)\,t\,dt}{\int\limits_0^\infty I(t)\,dt}\,. \qquad (11)$$

Inserting into (11) the corresponding expressions for the intensities from (8), we obtain the persistences

$$\bar{\tau}_R^{\mathrm{pu}} = \tau_0\,\frac{\gamma}{I_R^{\mathrm{ss}}}\,\frac{dI_R^{\mathrm{ss}}}{d\gamma}\,, \qquad \bar{\tau}_T^{\mathrm{pu}} = \tau_0\,\frac{\gamma}{I_T^{\mathrm{ss}}}\,\frac{dI_T^{\mathrm{ss}}}{d\gamma}\,, \qquad (12)$$

---

*Here I_1 is a Bessel function of an imaginary argument.

$$\bar{\tau}_R^{\,\mathrm{pr}} = \frac{\tau_0}{2}\,\frac{d^2(\gamma I_R^{\mathrm{ss}})}{d\gamma^2}\Bigg/\frac{dI_T^{\mathrm{ss}}}{d\gamma}, \quad \bar{\tau}_T^{\,\mathrm{pr}} = \frac{\tau_0}{2}\,\frac{d^2(\gamma I_T^{\mathrm{ss}})}{d\gamma^2}\Bigg/\frac{dI_T^{\mathrm{ss}}}{d\gamma}. \qquad (13)$$

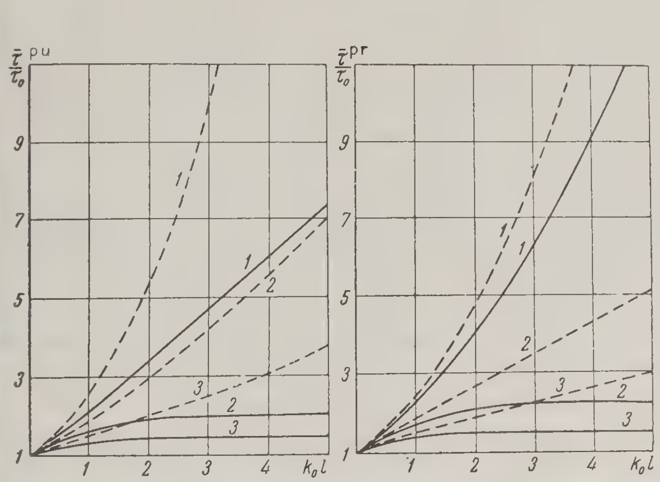

Fig.5. Variation of the luminescence persistence with the thickness of the layer with observation of the mean intensity "from the front" (solid lines) and "from the back" (dashed lines). Preliminary irradiation at an angle of 60°. 1 - $\gamma = 1.0$, 2 - $\gamma = 0.75$, 3 - $\gamma = 0.51$.

Here $\bar{\tau}_R^{\,\mathrm{pu}}$ and $\bar{\tau}_T^{\,\mathrm{pu}}$ are the afterglow persistences with pulse excitation of the system and observation "from the front" and "from the back", respectively; $\bar{\tau}_R^{\,\mathrm{pr}}$ and $\bar{\tau}_T^{\,\mathrm{pr}}$ are the corresponding persistences in the case of prolonged preliminary illumination by a constant radiant flux; I_R^{ss} and I_T^{ss} are the intensities "from the front" and "from the back" under steady state conditions. Inserting into (12) and (13) the expressions for the intensities determined through φ and ϕ and substituting for the last their approximate values, one can calculate the mean persistences for any θ and θ', any layer thickness and any efficiency γ. Curves characterizing the variation of the mean afterglow persistence with the optical thickness are reproduced in Fig.5. It will be evident from the figure that the phosphorescence persistence, particularly the persistence with observation "from the back" is strongly dependent on the absorption coefficient and the quantum efficiency γ. At large $k_0 l$ and high γ the luminescence persistence may be increased by one or two orders of magnitude.

Analysis shows that secondary absorption and emission processes play a significant role under nonsteady state conditions. Whereas under steady state conditions one can restrict the calculation of the luminescence intensity to one-two orders of luminescence, in calculating mean persistences one must extend the calculation to higher orders.

Institute of Physics
Academy of Sciences of the Belorussian SSR

References

1. L.M.Biberman, Dissertation, Moscow Power Institute, 1958.
2. V.M.Agranovich, Izv.AN SSSR, Ser.fiz., 23, 40 (1959). (Trans.Bulletin 23, 44.)
3. S.F.Kilin & I.M.Rozman, Optika i spektroskopiya, 6, 70 (1959). (Trans. Optics and Spectroscopy.)
4. A.M.Samson, Ibid., 5, 500 (1959); 8, 89 (1960); Inzh.-fiz.zhur. (Engineering-Physics Journal), 1, No.1 (1958); Ibid., 2, No.6 (1959); Ibid., 2, No.8 (1959); Doklady AN BSSR (Belorussian Ac.of Sci.) 1, No.2 (1958); Ibid., 3, No.5 (1959); Izv.AN SSSR, Ser.fiz., 22, 1399 (1958) (Trans.Bulletin 22, 1389); Vestsi AN BSSR, Ser.fiz.-tekhn.navuk (Bulletin of the Belorussian SSR Ac.of Sci. Phys.-Techn.Series), No.3, 16 (1959).

PROBABILITY METHOD OF CALCULATING ABSORPTION AND EMISSION PROPERTIES

- P.A. Apanasevich

For solution of many optical problems it is essential to know the transition probabilities and populations of the energy levels (distribution function) of the atoms or molecules involved. The transition probabilities are determined by the interaction of the radiation with the atoms and molecules and by the interaction between individual degrees of freedom of the matter. In each specific case they may be regarded as determined by the parameters of the system, which are assumed to be known from experiment or theory. The level populations N_i are complex functions of both the properties of the system and external conditions. If we accept that the number of transitions is equal to the product of the transition probability by the number of particles on the initial level, then from the condition that the change in the number of particles on level i per unit time is equal to the difference between the number of particles arriving at and departing from this level, we can readily write the set of equations describing the particle distribution over the energy levels:

$$\frac{dN_i}{dt} = -\sum_{j<i} f_{ij}N_i - \sum_{j>i} a_{ij}N_i - \sum_j d_{ij}N_i + \sum_{j>i} f_{ji}N_i + \sum_{j<i} a_{ji}N_j + \sum_j d_{ji}N_j, \tag{1}$$

where f_{ij} is the transition probability from level i to a lower lying level j with emission of a photon, a_{ij} is the transition probability from level i to a higher lying level j with absorption of a photon, and d_{ij} is the probability for nonradiative transitions due to interaction between individual degrees of freedom.

Equation (1) was first used in investigating a particular case by Einstein[1] in 1917. From considerations of thermodynamic equilibrium Einstein showed that the transition probabilities a_{ij} and f_{ij} depend on the radiative energy density $\rho(\omega)$ and can be represented in the form

$$\left.\begin{aligned} a_{ij} &= B_{ij}\rho(\omega_{ji}), \\ f_{ji} &= A_{ji} + B_{ji}\rho(\omega_{ji}), \end{aligned}\right\} \quad (j > i), \tag{2}$$

where ω_{ji} is the natural frequency of the substance, and B_{ij}, B_{ji} and A_{ji} are the familiar Einstein coefficients.

In the case of a simple system, the validity of (2) has been substantiated by quantum electrodynamics, which also allows of calculating the Einstein coefficients. In 1927 Landau[2] showed that in the absence of external radiation ($\rho(\omega) = 0$) and nonradiative transitions Eqs. (1) follow from Dirac's quantum theory. Nonradiative transitions have been taken into account in (1) only relatively recently. On the basis of the principle of detailed equilibrium Stepanov[3] established the following relationship between the probabilities for forward and reverse nonradiative transitions:

$$d_{ij} = d_{ji}e^{-\frac{\hbar\omega_{ji}}{kT}}. \tag{3}$$

Equations (1) together with relationships (2) and (3) have been successfully and extensively used by many authors for calculating the attributes of absorption and emission of light. We call the method of calculation based on these equations the probability method. By means of this method it has been proved feasible, for example, to investigate the behavior of quenching and the quantum yield of fluorescence and phosphorescence, to find the laws characterizing the build-up and decay of photoluminescence, and to analyze the kinetics of the processes involved in the interaction of light with matter. In general, the results obtained are in good agreement with experiment. A great advantage of the probability method is its simplicity and directness; it can be used as a semiempirical method of the transition probabilities are known from experiment. It should not be forgotten, however, that this method is not a rigorous one and that it can yield correct results only within certain limits.

Below we give a consistent derivation of equations (1) from the equations of quantum electrodynamics, indicate the limits of applicability of these equations and show that the probability method of calculation corresponds to the first approximation of perturbation theory.

For the solution of physical problems in the framework of quantum electrodynamics it is necessary to find the wave functions and then, using these, to determine the sought quantities. In practice the matter of finding the wave functions is fraught with serious mathematical difficulties. Hence it is of interest to evolve a method of calculation that would make it possible to find the sought properties without determining experimentally not observable quantities. The derivation of the equations of the probability method from the fundamental equations of quantum electrodynamics shows that in the first approximation the probability method is precisely such a method.

Let us consider a system consisting of a molecule (or atom) and a medium, interacting with each other, and a radiation field interacting with the molecule (atom). The behavior of such a system is described by the wave function Ψ satisfying the Schrödinger equation

$$(H_{\mathrm{m}} + H_{\mathrm{me}} + V + H_{\mathrm{f}} + U)\,\Psi = ih\frac{\partial}{\partial t}\,\Psi, \tag{4}$$

where H_{m}, H_{me} and H_{f} are the Hamiltonians of the molecule, the medium, and the radiation field, respectively, and V and U are interaction operators of the molecule with the medium and with the radiation field, respectively. We expand Ψ in terms of the wave functions of the substance $\psi_{i\alpha}$ and the field $\varphi_{(n_\varkappa)}$:

$$\Psi = \sum_{i\alpha\,(n_\varkappa)} C_{i\alpha(n_\varkappa)}\psi_{i\alpha}\varphi_{(n_\varkappa)}\,e^{-\frac{i}{n}(E_{i\alpha}+E_{(n_\varkappa)})t}. \tag{5}$$

The state of the system can be described by means of the coefficients $C_{i\alpha\,(n_\varkappa)}$ which have the meaning of amplitudes of the probabilities that the molecule will be in state i, the medium in state α, and that the field will contain photons n_1, $n_2, \ldots, n_\varkappa \ldots$ The probability of finding the molecule in the i-th state at a given instant t for any condition of the medium and the radiation field is given by

$$\sum_{\alpha(n_\varkappa)} \overline{|C_{i\alpha\,(n_\varkappa)}|^2} = b_i = \sum_{\alpha} b_{i\alpha} = \frac{N_i}{N}, \tag{6}$$

where $N = \sum_i N_i$ is the total number of molecules, and the bar over the modulus indicates averaging over an arbitrary phase[4]. On the basis of Eq.(4) one can readily derive a system of equations relating the different probability amplitudes $C_{i\alpha\,(n_\varkappa)}$.[5] Solving this system by the method of perturbation theory and using the first approximation solution one can show[6] that the probabilities b_i are related to each other by equations of the form

$$\frac{db_i}{dt} = -\sum_{j<i}\bar{f}_{ij}b_i - \sum_{j>i}\bar{a}_{ij}b_i - \sum_{j}\bar{d}_{ij}b_i + \sum_{j>i}\bar{f}_{ji}b_j + \sum_{j<i}\bar{a}_{ji}b_j + \sum_{j}\bar{d}_{ji}b_j. \tag{7}$$

Here the $\bar{a}_{ij}$, $\bar{f}_{ij}$ and $\bar{d}_{ij}$ are the averaged (over the states of the medium) probabilities for transition of the molecule from the state i to the state j incident to a change of the medium from α to β, and are described by the expressions

$$\bar{a}_{ij} = \frac{\sum\limits_{\alpha,\beta} a_{i\alpha}^{j\beta} b_{i\alpha}}{\sum\limits_{\alpha} b_{i\alpha}}, \tag{8}$$

$$\bar{f}_{ij} = \frac{\sum\limits_{\alpha,\beta} f_{i\alpha}^{j\beta} b_{i\alpha}}{\sum\limits_{\alpha} b_{i\alpha}},$$

$$\bar{d}_{ij} = \frac{\sum\limits_{\alpha,\beta} d_{i\alpha}^{j\beta} b_{i\alpha}}{\sum\limits_{\alpha} b_{i\alpha}}, \tag{9}$$

where

$$a_{i\alpha}^{j\beta} = \frac{4\pi^2}{3h^2} \mid p_{i\alpha}^{j\beta} \mid^2 \rho\,(\omega_{j\alpha}^{j\beta}); \tag{10}$$

$$f_{i\alpha}^{j\beta} = \frac{4\pi^2}{3h^2} \mid p_{i\alpha}^{j\beta} \mid^2 \left[\rho\,(\omega_{j\beta}^{i\alpha}) + \frac{h\,(\omega_{j\beta}^{i\alpha})^3}{\pi^2 c^3} \right]; \tag{11}$$

$$d_{i\alpha}^{j\beta} = 2\pi \frac{\mid M_{i\alpha}^{j\beta} \mid^2}{h^2}\, \delta\,(E_{j\beta} - E_{i\alpha}); \tag{12}$$

$p_{i\alpha}^{j\beta}$ is the matrix element of the dipole moment of the molecule interacting with the medium; $M_{i\alpha}^{j\beta}$ is the matrix element of the interaction operator of the molecule with the medium. The transition probabilities $\alpha_{j\beta}^{i\alpha}$ and $f_{j\beta}^{i\alpha}$ have been written here on the assumption that the molecules are oriented isotropically and have dimensions that are small compared with the wavelength of light.

In deriving Eqs.(7) from the fundamental equations of quantum electrodynamics it is necessary to assume that either there is no radiation at all or that its frequencies coincide with the natural frequencies $\omega_{i\alpha}^{j\beta}$ and that in the vicinity of the natural frequencies the radiation energy density $\rho(\omega)$ varies so slowly that it may be regarded as constant. This is essentially the only condition limiting the applicability of Eq.(7), and, consequently, the probability method (see Ref.6).

The derivation of equations (1) from quantum electrodynamics allows not only of determining the limits of applicability of (1) but also of establishing some of the attributes of the transition probabilities entering into them. It is evident from Eqs.(8) and (9) that there must enter into equations (1) transition probabilities averaged over all possible states of the surrounding medium. By inserting (12) into (9) one can show that the probabilities for nonradiative transitions of the molecule satisfy condition (3). The radiative transition probabilities $\bar{a}_{ij}$ and $\bar{f}_{ij}$ of the molecule interacting with the medium, as follows from (8), (10) and (11), in the general case do not satisfy condition (2), i.e., one cannot introduce the Einstein coefficient into the expressions for these probabilities. Inasmuch as the distribution of $b_{i\alpha}$ is a function of the temperature, $\bar{a}_{ij}$ and $\bar{f}_{ij}$ may also depend on the temperature.

Usually these properties of $\bar{a}_{ij}$ and $\bar{f}_{ij}$ are not taken into account and it is assumed that relations (2) are always fulfilled and that the temperature affects only the population of the levels. Actually, however, this is true only in the case of weak interaction of the molecule with the medium when the state of the medium is not changed as a result of radiative transitions. In this case, the radiative transition probabilities become

$$\bar{a}_{ij} = \frac{4\pi^2}{3h^2} \mid p_{ij} \mid^2 \rho\,(\omega_{ji}), \tag{14}$$

$$\bar{f}_{ij} = \frac{4\pi^2}{3h^2} | p_{ij} |^2 \left[\rho(\omega_{ij}) + \frac{h\omega_{ij}^3}{\pi^2 c^3} \right], \tag{15}$$

i.e., do not depend on the temperature and fully satisfy (2). In the case of strong interaction of the molecule with the medium, on the contrary, their temperature dependence may be substantial and relation (2) may be inapplicable. The experimentally observed approach of the absorption and emission bands of complex molecules with decreasing temperature, as Pikulik[7] showed, is explained precisely by this temperature dependence of the radiative transition probabilities.

It should be noted that in the case of strong interaction with the medium it is sometimes more convenient to use not Eq.(7), which was written for a molecule, but the following expression, which describes the distribution in the system molecule-medium as a whole:

$$\frac{db_{i\alpha}}{dt} = -\sum_{j,\beta}^{E_{i\alpha}<E_{j\beta}} a_{i\alpha}^{j\beta} b_{i\alpha} - \sum_{j,\beta}^{E_{i\alpha}>E_{j\beta}} f_{i\alpha}^{j\beta} b_{i\alpha} - \sum_{j,\beta} d_{i\alpha}^{j\beta} b_{i\alpha} + \sum_{j,\beta}^{E_{i\alpha}>E_{j\beta}} a_{j\beta}^{i\alpha} b_{j\beta} + \sum_{j,\beta}^{E_{i\alpha}<E_{j\beta}} f_{j\beta}^{i\alpha} b_{j\beta} + \sum_{j,\beta} d_{j\beta}^{i\alpha} b_{j\beta}. \tag{16}$$

Here the radiative transition probabilities $a_{i\alpha}^{j\beta}$ and $f_{i\alpha}^{j\beta}$ are defined by Eqs. (10) and (11), satisfying relation (2), and do not depend on the temperature, while the nonradiative transition probabilities $d_{i\alpha}^{j\beta}$ given by (12) satisfy the condition $d_{i\alpha}^{j\beta} = d_{j\beta}^{i\alpha}$.

Thus the probability method of calculation follows consistently from quantum electrodynamics and corresponds to the first approximation solution by the method of perturbation theory of problems involving the interaction of light with matter. In the absence of external radiation, the equations (1) of the probability method are always applicable regardless of the specific properties of the matter. In the presence of incident radiation they are applicable when this radiation contains frequencies coinciding with the natural frequencies of the matter and the energy density of this radiation in the vicinity of the natural frequencies is a slowly varying function of the frequency. If, however, the irradiation is realized by nonresonance radiation (scattering), the probability method is not applicable to problems involving the interaction of radiation with matter. However, in this case it is apparently feasible to develop a method of calculation similar to the probability method if one uses for this purpose the second approximation of the solution of the equations of quantum electrodynamics. Obviously, the probability method of calculation cannot be used for investigating questions of coherence.

The radiative transition probabilities entering into equations (1) in general can be expressed in terms of the Einstein coefficients only in the case of not excessively strong interaction of the molecule or atom with the surrounding medium. In the case of strong interaction with the medium these probabilities may be temperature dependent.

I wish to thank B.I.Stepanov for suggesting the topic and for his constant interest in the work.

Institute of Physics
Academy of Sciences of the Belorussian SSR

References

1. A.Einstein, Phys.Z., 18, 121 (1917).
2. L.Landau, Z.Phys., 45, 430 (1927).
3. B.I.Stepanov, Lyuminestsentsiya slozhnykh molekul (Luminescence of complex molecules), Pub.by Belorussian SSR Ac. of Sci., 1956; Doklady AN SSSR, 99, 971 (1954).
4. P.A.Apanasevich, Trudy (Transactions), Inst.of Physics-Mathematics, Belorussian SSR Ac. of Sci.), No.3, 187 (1959); Optika i spectroskopiya, 5, 97 (1958).
5. P.A.M.Dirac, The Principles of Quantum Mechanics, Oxford, 1935 (Cited in Russian trans.)
6. P.A.Apanasevich, Vestsi An BSSR, Ser.fiz.-tekhn.navuk (Bulletin of the Belorussian SSR Ac.of Sci., Phys.-Techn.Science Series), 2, 31 (1959).
7. L.G.Pikulik, Optika i spektroskopiya, 8, 338 (1960). (Trans.Optics and Spectroscopy.)

SPECTROSCOPIC INVESTIGATION OF VIBRATIONAL ENERGY TRANSFER IN COLLISIONS OF COMPLEX MOLECULES

(Summary of report)

- S.O.Mirumyants & B.S.Neporent

Investigation of energy transfer in molecular collisions, in view of the fact that it is closely related to the formation and evanescence of active molecules, is of substantial interest from the standpoint of chemical kinetics. Of primary importance here are the regularities governing the transfer of vibrational energy, which comprises the major part of the activation energy. This is particularly true of complex molecules possessing a large number of degrees of freedom.

One of the methods of investigating transfer and conversion of the vibrational energy of excited complex molecules is study of the variation of the fluorescence yield of vapors of aromatic compounds as a function of the pressure of extraneous gases, i.e., of the enhancement or weakening of fluorescence connected with stabilization[1,2] or labilization[3] of excited molecules owing to loss or acquisition by them of vibrational energy in encounters. This procedure allows of obtaining the most detailed information on the course of the phenomenon inasmuch as it permits direct determination of the mean amount of vibrational energy transferred in a collision.

In the report we consider the processes of vibrational energy transfer in both directions - loss and acquisition of energy by an excited molecule; we show that the experimental data now available is inadequate for evaluating the role of different degrees of freedom (translational, rotational and vibrational) of the acceptor molecule in the process of vibrational energy transfer from the donor molecule.

With a view to solving the formulated problem we investigated the stabilization of excited 3-dimethylamino-6-aminophthalimide molecules in collision with molecules of extraneous gases from their effect on the luminescence efficiency of the vapor of the investigated substance with excitation by different wavelengths in a wide spectral range. We tested a large group of extraneous gases: monatomic - He, Ne, A, Kr & Xe; diatomic - H_2, D_2, N_2 & CO, and polyatomic - H_2O, D_2O, NH_3 & C_5H_{12}.

On the basis of the experimental results, we determined, using the procedure described in Ref.2, the average amount of vibrational energy lost and acquired by an excited 3-dimethylamino-6-aminophthalimide molecule in a single collision with an extraneous gas molecule.

In agreement with the results of earlier studies, we found that the average amount of vibrational energy lost by an excited 3-dimethylamino-6-aminophthalimide molecule in a single kinetic encounter increases with increase of the mass and the complexity of the extraneous gas molecules. The results obtained, however, do not allow of establishing a common (for all extraneous gases) monotonic variation of the amount of vibrational energy lost by the excited 3-dimethylamino-6-aminophthalimide molecule in a collision as a function of the mass of the extraneous molecule. A consistent dependence is observed only for monotonic gases, but the observed dependence differs greatly from that calculated by the theory of elastic impact of spheres. This shows that the process of energy transfer in molecular collisions is not subject to the regularities governing the elastic impact of rigid spheres. Moreover, the mass dependence observed for inert gases can serve only for very rough evaluation of the role of different degrees of freedom of the colliding molecules in the process of energy transfer. The situation is further complicated by the fact that in a collision of a 3-dimethylamino-6-phthalimide molecule with particles of the extraneous gas there may occur energy exchange not only between the investigated molecule and the gas molecule, but also between internal and external degrees of freedom of the excited molecule. Such energy exchange becomes possible only in collisions with molecules of extraneous gases when conditions for conservation of momentum of the system are realized. Hence for more definitive judgment, using the experimental results and data on the specific heat of the investigated molecules, we found such values of the accommodation coefficient, which essentially represents the efficiency of the first stabilizing collision, that the process of energy transfer is characterized taking into account all the degrees of freedom of the molecules participating in the collision.

The values of the accommodation coefficient were calculated using the new expression deduced in Ref.4 in which there are taken into account the above observations regarding the participation of external degrees of freedom of the investigated molecule in the process of conversion of its excess of vibrational energy. The results are considered taking into account the different characteristics of the extraneous gas molecules. It is shown that the collision efficiency in the sense of energy exchange is a function of the coefficient of the van der Waals interaction of the extraneous gas molecules. We give an evaluation of the role of rotational and vibrational degrees of freedom of the diatomic and polyatomic extraneous gas molecules in the process of conversion and transfer of vibrational energy by an excited 3-dimethylamino-6-phthalimide molecule. It was established experimentally that the inverse process - conversion of energy from the extraneous gas molecule to vibrational energy of the investigated molecule - occurs with appreciably lower efficiency than in the case of the above considered "forward" process.

References

1. B.S.Neporent, Zhur.fiz.khim. (Journ.Phys.Chem.), 13, 965 (1939).
2. B.S.Neporent, Ibid., 24, 1219 (1950).
3. N.A.Borisevich & B.S.Neporent, Optika i spektroskopiya, 1, 536 (1956).
4. B.S.Neporent & S.O.Mirumyants, Ibid., 8, 483 (1960). (Trans.Optics and Spectroscopy.)

INVESTIGATION OF THE TEMPERATURE DEPENDENCE OF THE INTERACTION BETWEEN MOLECULES IN THE VAPOR STATE

- V.P.Klochkov

Neporent[1,2] in 1945 observed a decrease in the absorption of β-naphthylamine vapor upon the addition of light gases (helium, hydrogen, etc.) to the vapor. The first investigations of this important effect showed that there is a limit to the absorption decrease, dependent on the β-naphthylamine concentration. This indicated interaction between the β-naphthylamine molecules, an interaction that in some manner protects these molecules from the influence of the light gases. Subsequent studies[3-7] demonstrated that this effect, which is characteristic of compounds with conjugated bonds (except benzene), regardless of its mechanism, can serve as a sensitive method for studying long range (of the order of hundreds of angstroms) molecular interaction. It was found that below a certain vapor concentration c_0 , which depends on the nature of the compound and the temperature, the magnitude of the limiting absorption decrease $\varepsilon_\infty/\varepsilon_0$* does not change with further decrease of the concentration, i.e., at a certain sufficiently large separation between the molecules, their interaction virtually ceases. Hence by determining the limit concentration c_0 one can gage the degree of molecular interaction. As a measure of this interaction, therefore, we can take either the limit concentration c_0 or the corresponding vapor pressure p_0. This method was used to study the long range forces as a function of molecular structure. It was shown that the increase of conjugation in the phthalimide series there is a shift of the spectra to the long wavelength side and enhancement of the molecular interaction.[4,5] The present work is a continuation of these studies and is devoted to determining the temperature dependence of the interaction energy of aromatic molecules.

The measurements were carried out by means of the vapor absorption apparatus described earlier.[8] Specifically, we investigated the following compounds: anthracene, 1,4-diphenylbutadiene-1,3, phthalimide and its 3- and 4-amino derivatives. The light gas used was helium since it has the strongest effect on the absorption of aromatic compounds. The vapor pressure of these compounds as a function of the temperature was determined earlier.[9,10] The results of measurements of p_0 and the corresponding concentration c_0, obtained in the present study and in that of Ref.4, are summarized in the accompanying table. As will be evident from the data presented, the strength of molecular interaction as a function of the temperature varied in a different manner for different substances. With increase of the temperature the interaction between 3- and 4-aminophthalimide and anthracene molecules is weakened, while the rate of change of c_0 varies from molecule to molecule. The greatest change in c_0 for a 90° temperature rise is observed in the case of 4-aminophthalimide; the smallest change in the case of anthracene.

Compound	T, °C	p_0, mm Hg	$c_0 \cdot 10^{-15}$, cm^3
Naphthalene	200	1	20,4
Phthalimide	223	0,5	9,7
4-Aminophthalimide	260	0,15	2,7
	350	0,85	13,2
Anthracene	220	0,13	2,5
	311	0,22	3,6
3-Acetylaminophthalimide	223	0,05	0,97
3-Aminophthalimide	221	0,03	0,59
	310	0,12	2,0
1,4-Diphenylbutadiene-1,3	225	0,027	0,52
	250	0,039	0,72
	275	0,044	0,77
	300	0,027	0,46
3-Dimethylamino-6-aminophthalimide	230	<0,02	<0,38

---

* ε_0 is the absorption coefficient in the absence of the light gas; ε_∞ is the absorption coefficient in the presence of a large amount of the light gas.

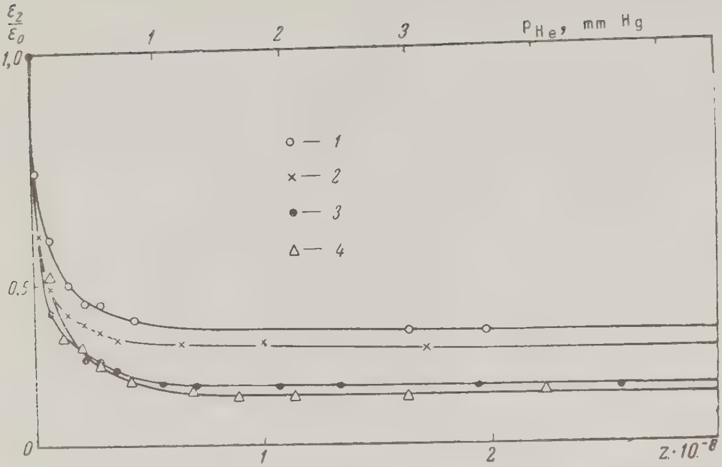

Fig.1. $\varepsilon_z/\varepsilon_0$ vs collision frequency and helium pressure for 1,4-diphenylbutadiene-1,3 (p = 0.011 mm Hg): T = 225°, 2) 250°, 3) 275°, 4) 300°.

The behavior of diphenylbutadiene differs somewhat from that of the other compounds and it was investigated in detail inasmuch as for it we observe an unusual temperature dependence of the limiting absorption weakening and temperature behavior of the $\varepsilon_z/\varepsilon_0 = f(\bar{z})$* curves (Fig.1).

It was found that in the case of diphenylbutadiene at relatively low temperatures (<275°) with increase of the temperature the interaction between the molecules is weakened (as for the other investigated compounds), while the rate of decrease of the interaction energy is high (the same as in the case of 4-aminophthalimide). With increase of the temperature this rate decreases and at temperatures above 275° changes sign, i.e., the interaction between molecules begins to increase. This behavior of the diphenylbutadiene spectra is not due to decomposition of the compound inasmuch as we observed no indications of decomposition (such as appearance of a deposit on the cell walls, variation of the absorption with time, or change in the nature of the spectra).

Other experimental facts also furnish evidence of change in the character of the interaction. In investigating the temperature dependence of $\varepsilon_\infty/\varepsilon_0$ we found that at low temperatures and concentrations below c_0, the ratio $\varepsilon_\infty/\varepsilon_0$ with increase in temperature at first decreases and then beginning at a certain temperature, (which depends on the compound and the concentration) begins to increase. This increase can be explained by enhancement of the molecular interactions, which, as is known[1,2,4,5], protect the molecules from the action of the light gas.

The described effect was observed in the case of diphenylbutadiene at temperatures above 360° (vapor pressure - 0.012 mm Hg, p_0 = 0.044 mm Hg at 275°) and in the case of phthalimide at temperatures above 460° (vapor pressure - 0.35 mm Hg, p_0 = 0.5 mm Hg at 223°). Although we did not perform corresponding experiments for the other investigated compounds, one may reasonably expect them to exhibit a similar behavior.

Furthermore, the temperature behavior of the $\varepsilon_z/\varepsilon_0 = f(z)$ curves (Fig.1) indicates that there occur substantial changes in the properties of the molecules at high temperatures. Fig.2 shows the result of conversion of these curves by means of the formula[6,7] characterizing the dependence of the absorption decrease on the collision frequency z. It will be evident from Fig.2 that the slope of the converted plots, which depends on the ratio c/c_0,[5] gradually decreases with temperature up to 275° (similar dependences were observed for the other investigated compounds). With further increase of the temperature, however, the slope begins to increase.

---

* ε_z - absorption coefficient depending on z, the number of molecular collisions per second.

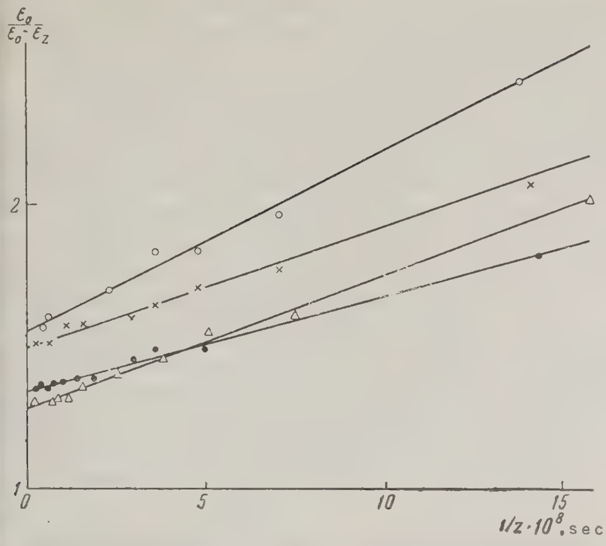

Fig.2. Curves of Fig.1 corrected taking into account the decrease in absorption as a function of the collision frequency (Ref.6 & 7). Designations same as in Fig.1.

The observed dependences can hardly be explained by changes in the structure of the molecules connected, for example, with decomposition of the substance. The experimental data gives reason to infer that at high temperatures, in addition to the interactions observed at "low" temperatures, there becomes operative a new type of interaction characterized by a different temperature dependence. It is probable that interactions of this type also occur at lower temperatures, but are masked in this range by the stronger interactions of the first type.

To differentiate between them we shall refer to the interactions evinced at "low" temperatures as interactions of the first type and to the interactions manifested at "high" temperatures as interactions of the second type. Interactions of the first type were investigated earlier by the writer in collaboration with Neporent.[4,5,11] It was shown that these long range interactions are connected with the properties of the electron shell of molecules with conjugated bonds, i.e., that these interactions may be interpreted as interactions of electronic oscillators. The interaction energy within a given class of compounds (phthalimides) increases concurrently with shift of the absorption spectra to the long wavelength side, with increase of conjugation and, consequently, polarizability of the molecules. These regularities are substantiated by the results obtained in the present study (see table): at equal temperatures, the limiting concentration c_0 for phthalimide and 4-aminophthalimide, the absorption spectra of which are located in the shortest wavelength region, is higher than for the other phthalimide derivatives investigated earlier[4,11] (3-acetylamino-, 3-amino- and 3-dimethylamino-6-aminophthalimide). The results of the present experiments show that interaction of the first type are weakened with increasing temperature. In our earlier studies (Ref.4 & 5) we attributed these interactions to dispersion forces which, according to the calculations of Coulson & Davies[12] for molecules with conjugated bonds (polyenes) can be very appreciable, the increase of the interaction energy $E_{\pi\pi}$ being due to sharp increase of the polarizability of the molecules with enhancement of the conjugation (or increase in the length of the conjugated chain):

$$E_{\pi\pi} = -16 \frac{e^4 a^4}{R^6 \pi^9 \beta} (2m+1)^5 \cos^2 \gamma \, (3 \sin^2 \gamma - 1)^2, \qquad (1)$$

where m is the number of double bonds in the molecule, γ is the angle characterizing the relative orientation of the interacting conjugated chains, R is the distance between molecules, e is the charge of an electron, a is the separation between the atoms in the molecule, and β is the resonance integral between neighboring atoms.

The hypothesis regarding the dispersion-force character of the observed interactions would seem to be in conflict with the known temperature independence of dispersion forces. This is true, however, only for spherically isotropic oscillators. It follows from Eq.(1) that the interaction energy of the π-electrons of two molecules depends on the relative position of the oscillators and, consequently, in this case, temperature dependence is not precluded. Nevertheless, it may be inferred that the strong temperature dependence observed by us is determined primarily not by this factor but by variation in the polarizability of the molecules which depends on the state of the conjugated system. Any - even small - disturbances of the conjugation, which can arise as a result of excitation of low frequency torsional or deformation vibrations with increasing temperature, have a substantial effect on the state of the conjugate system of π-electrons,[13-15] which should lead to change in the polarizability and, consequently, to weakening of the molecular interaction.

Owing to the paucity of experimental data it is difficult at present to draw any definitive inferences regarding the nature of the interactions of the second type. We only know at present that the interactions of this type are enhanced with increasing temperature. Recently there have been published a number of reports devoted to the problem of long range interaction of complex biological systems (macromolecules). Müller[16] assumes that the interaction in complex biological systems is due to the interaction of thermally excited identical or almost identical vibrational states.

Yos, Bade & Jehle[17,18] in considering the interaction between macromolecules come to the conclusion that the molecular interaction energy may be represented as the sum of two quantities, namely, interaction of electronic oscillators and interaction of low frequency classical oscillators, i.e., the oscillators responsible for infrared absorption. The increase in interactions of the second type with increase in temperature observed by us gives reason to infer that in this case there obtains interaction of excited vibrational oscillators. In very complex molecular systems the contribution of the interaction of vibrational oscillators to the total interaction energy of the molecules may be appreciable even at room temperature; in the case of less complex molecules, such as our phthalimides, these interactions become significant only at more elevated temperatures.

I desire to express my deep gratitude to B.S.Neporent under whose guidance the present work was performed.

References

1. B.S.Neporent, Dissertation, State Optical Institute, 1945.
2. B.S.Neporent, Doklady AN SSSR, 72, 35 (1950).
3. B.S.Neporent & A.A.Solodovnikov, Optika i spektroskopiya, 1, 951 (1956).
4. B.S.Neporent & V.P.Klochkov, Ibid., 3, 529 (1957).
5. V.P.Klochkov, Dissertation, State Optical Institute, 1958.
6. B.S.Neporent, Optika i spektroskopiya, 4, 703 (1958).
7. B.S.Neporent, Izv.AN SSSR, Ser.fiz., 22, 1051 (1958). (Trans.Bulletin 22, 1039.)
8. V.P.Klochkov, Zhur.fiz.khim. (Journal Phys.Chem.) 29, 1432 (1955).
9. V.P.Klochkov, Ibid., 30, 2823 (1956).
10. V.P.Klochkov, Ibid., 32, 1177 (1958).
11. B.S.Neporent & V.P.Klochkov, Doklady AN SSSR, 114, 524 (1957). (Trans. Doklady.)
12. C.A.Coulson & P.L.Davies, Trans.Faraday Soc., 48, 777 (1952).
13. A.N.Terenin, Izv.AN SSSR, Ser.fiz., 9, 305 (1945).
14. P.P.Feofilov, Doklady AN SSSR, 57, 447 (1947).
15. Primenenie spektroskopii v khimii (Applications of Spectroscopy in Chemistry), M., 1959.
16. H.J.Müller, Proc.Roy.Soc., B,134, 1 (1947).
17. J.Yos, W.L.Bade & H.Jehle, Proc.Nat.Acad.Sci., 43, 341 (1957).
18. H.Jehle, Ibid., 43, 847 (1957).

TEMPERATURE DEPENDENCE OF THE FLUORESCENCE EFFICIENCY OF COMPLEX MOLECULE VAPORS

- N.A.Borisevich & V.A.Tolkachev

1. The luminescence yield or efficiency is a significant characteristic of the process of conversion of absorbed light energy by complex molecules. Several studies[1-7] have been devoted to the fluorescence efficiency of complex organic molecules in the vapor state. In these studies there were determined the absolute and relative efficiencies and the variation of the quantum efficiency with the frequency of the exciting radiation. Neporent and his associates[3-6] also measured the fluorescence efficiency of β-naphthylamine and several phthalimide derivatives at two or three temperatures in the range to 100°. It was found that the fluorescence of these vapors is quenched with increase of temperature, as with increase in the frequency of the exciting radiation. According to the concepts developed by Neporent[3], the decrease in efficiency with increase in the frequency of the exciting radiation and rise of temperature is connected with increase of the probability for nonradiative transitions.

Later Kundzich[8] in a series of experiments varied the temperature in a wider range and obtained by visual observation a qualitatively different temperature dependence of the yield of Stokes fluorescence of phthalimide derivative vapors. According to Kundzich, with increase of the temperature the efficiency at first increased rapidly, passed through a maximum at a certain temperature, and then decreased. The temperature dependence observed by Kundzich was not satisfactorily explained.

In the present work we investigated the yield of Stokes and anit-Stokes fluorescence of 3,6-tetramethyldiaminophthalimide, 3-aminophthalimide and 1,4-dihydroxyanthraquinone (quinizarin) in the vapor state with variation of the temperature in a relatively wide range.

2. As is known, to determine the temperature dependence of the fluorescence efficiency one must measure the emission and the absorption of the substance at equal temperatures. The fluorescence intensity of the vapors was measured on a highly sensitive photoelectric spectrometer similar to that described in Ref.6. The superheated vapors were contained in a quartz cell connected to a vacuum system which could be pumped to 10^{-5} mm Hg. The vapor pressure was controlled by the temperature of the first heater which surrounded a branch of the cell, containing crystals of the test substance. The working part of the cell was surrounded by a second heater, which controlled the temperature of the vapor. In all experiments the temperature of the second heater was consistently higher than the temperature of the heater vaporizing the crystals. Particular attention was devoted to the matter of insuring good temperature control. The error in measuring the relative fluorescence intensity taking into account possible temperature and vapor pressure fluctuations is estimated to be less than 3%.

The absorption of the vapors was determined by means of a photoelectric set-up assembled about an SF-4 spectrophotometer. The thermostating and other arrangements were the same as in investigating the fluorescence intensity. The thickness of the absorption cell was 40 cm.

3. The lower experimental temperature bound for measuring the efficiency was determined by the possibility of measuring the absorption of the vapor. Fig.1 shows the results obtained in measuring the temperature dependence of the intensity I of the Stokes fluorescence of 3,6-tetramethyldiaminophthalimide (curves 1 & 2) and the optical density D of this vapor (curves I and II). Whereas measurements of I could be carried out without difficulty at a vapor pressure of $1\cdot10^{-4}$ mm Hg* so that one could start measurements from T = 80° with excitation of the fluorescence by $\lambda_{ex} = 405$ mμ light (curve 2), reliable measurement of D at the peak of the absorption

---

*The vapor pressure values were taken from Klochkov[9].

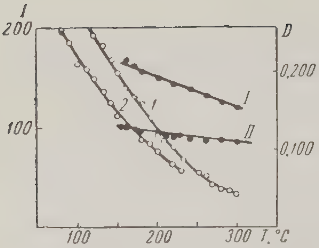

Fig.1. Temperature dependences of the fluorescence intensity I (1,2) and optical density D (I,II) of 3,6-tetramethyldiaminophthalimide vapor: 1 & I - λ_{ex} = 436 mμ; 2 & II - λ_{ex} = 405 mμ.

band (λ_{ex} = 436 mμ) was feasible only at vapor pressures above 10^{-3} mm Hg (curve I).

It will be evident from Fig.1 that the fluorescence intensity, beginning with relatively low temperatures (80-100°) monotonically decreases with increase of the temperature. The optical density of the vapor decreases slowly and virtually linearly. Hence the character of the temperature dependence of the efficiency is determined primarily by the intensity curve. Temperature quenching of the fluorescence of the vapors is fully reversible, i.e., with decreas of the vapor temperature the fluorescence intensity is re-established.

It should be noted that investigation of the temperature dependence of the coefficient of absorption is of independent interest. In view of the conditions of the experiment the vapor pressure remained constant despite variations in temperature and consequently the concentration of the vapor increased in proportion to T with increasing temperature. Calculation of the absorption coefficient from the measured optical density values showed that the coefficient at the maximum of the first absorption band for the investigated substances increases slowly with temperature. Thus for 1,4-dihyroxyanthraquinone increase of the temperature by 230° leads to only a 10% increase in the absorption coefficient. The absorption coefficient for anti-Stokes excitation wavelengths increases appreciably more rapidly with increase in temperature. For example, with increase of the temperature of 1,4-dihydroxyanthraquinone vapor by 200 the absorption coefficient of the vapor increased by a factor of more than 10. The absorption for anti-Stokes excitation wavelengths in the case of phthalimide vapors increases somewhat more slowly.

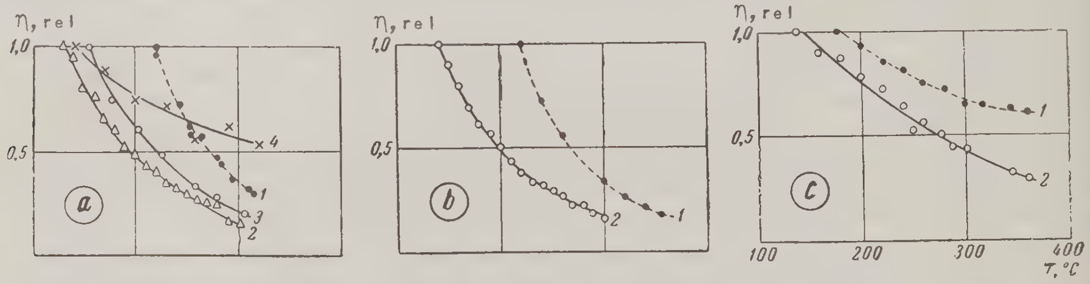

Fig.2. Temperature dependences of the relative fluorescence efficiency: a) 3,6-tetramethyldiaminophthalimide: 1 - λ_{ex} = 546 mμ, 2 - 436 mμ, 3 - 405 mμ, 4 - 313 mμ; b) 3-aminophthalimide: 1 - λ_{ex} = 405 mμ, 2 - 365 mμ; c) 1,4-dihydroxyanthraquinone: 1 - λ_{ex} = 546 mμ, 2 - 436 mμ.

4. The temperature dependences of the relative fluorescence yield of the vapors of the three investigated substances for different wavelengths of the exciting radiation are shown in Fig.2. The relative values are referred to the maximum yield at the given excitation wavelength λ_{ex}, obtained at the lowest temperature. The solid lines represent the yield of Stokes fluorescence; the dashed lines the efficiency of anti-Stokes fluorescence.*

---

*See footnote on following page.

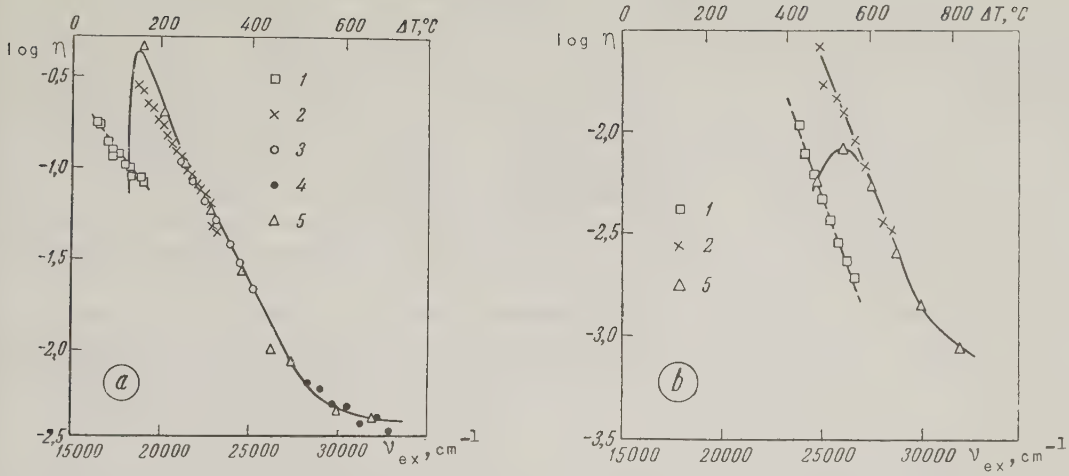

Fig.3. Variation of the fluorescence efficiency of phthalimide vapors as a function of the temperature (1-4) and the frequency of the exciting radiation (5): a) 3,6-tetramethyldiaminophthalimide: 1 - λ_{ex} = 546 mμ, 2 - 436 mμ, 3 - 405 mμ, 4 - 313 mμ; 5 - T = 285°C; b) 3-aminophthalimide: 1 - λ_{ex} = = 405 mμ, 2 - 365 mμ; 5 - T = 265°C.

It will be evident from Fig.2 that the efficiency of both Stokes and anti-Stokes fluorescence of the vapors monotonically decreases with increasing temperature. There is no evidence of any maximum in the curves.

Using the efficiency vs temperature curves obtained in the present investigation and the efficiency vs ν_{ex} curves from Ref.6, we calculated, by the method described by Neporent[3], the values of the heat capacity C_{vib} of the investigated phthalimides. Calculations for 3,6-tetramethyldiaminophthalimide and 3-aminophthalimide yielded 69 and 61 cal/mole degree, respectively, values which are in satisfactory agreement with those found earlier[6]. Knowing the molecular heat capacity one can readily plot the variation of the yield as a function of ν_{ex} and T. This has been done in Fig.3, where the horizontal axis has been laid off to a common scale, corresponding to the relative change in the vibrational energy stored by the molecule. The horizontal axes in both cases are laid off in terms of the logarithm of the absolute quantum efficiency. It was feasible to do this inasmuch as the absolute values of the quantum efficiency for different ν_{ex} at constant temperature are known for the investigated phthalimides.

It is evident from Fig.3 that increase in the store of vibrational energy of the molecule by thermal means leads to exponential decrease of the yield of both the Stokes and anti-Stokes fluorescence. Increase of the store of the vibrational energy of complex molecules by optical means leads to exponential decrease of the quantum efficiency only for Stokes excitation within the limits of the first absorption band. Increase of ν_{ex} in the case of excitation in the second absorption band of 3-aminophthalimide (λ_{ex} = 313 mμ) and 3,6-tetramethyldiaminophthalimide (λ_{ex} = 334 and 313 mμ) is accompanied by a slower decrease in efficiency. With

---

*The variation of the fluorescence efficiency of the vapors of the investigated phthalimides as a function of the wavelength of the exciting radiation was studied earlier[5,6]. In the case of 1,4-dihydroxyanthraquinone vapor excitation with λ_{ex} = 546 mμ lies at the maximum of the fluorescence band and the fluorescence emitted in this case may be regarded as anti-Stokes.

increase in the vapor temperature of 3,6-tetradiaminophthalimide the efficiency of fluorescence excited by $\lambda_{ex} = 313$ mμ also increases more slowly than of the fluorescence excited by $\lambda_{ex} = 405$ and 436 mμ. The deviation from the exponential law in the variation of the efficiency at high ν_{ex} should be linked with the deviation from the exponential variation of the probability d for nonradiative transitions at high values of the vibrational energy of the molecule. It is possible, however, that the probability f for radiative transitions also does not remain constant above a certain value of the molecular vibration energy.

Thus, one can speak of equivalence of the optical and thermal means of changing the store of vibrational energy of the molecule only in the case of Stokes excitation.

Both Stokes and anti-Stokes fluorescence excited within the range of the firs absorption band are characterized by a similar temperature dependence of the efficiency. This substantiates the inference[10] made earlier in investigating the influence of extraneous gases on the fluorescence efficiency that the molecules responsible for the appearance of anti-Stokes fluorescence are close in energy attributes to the molecules responsible for the appearance of the fluorescence excited in the adjacent Stokes region. Despite the sharp increase with increasing temperature of the absorption coefficient for anti-Stokes excitation, the efficiency of the anti-Stokes fluorescence of the vapors of the investigated substances decreases exponentially with rising temperature. If the hypothesis that the anti-Stokes decrease is connected with the presence of nonexciting absorption[6,11] were correct, then the efficiency of anti-Stokes fluorescence should increase rather than decrease with increasing temperature.

Institute of Physics,
Academy of Sciences of the Belorussian SSR

References

1. A.N.Terenin, B.S.Neporent & A.T.Vartanyan, Trans.Faraday Soc., 35, 39 (1939).
2. B.S.Neporent, Zhur.fiz.khimii (Journ.Phys.Chem.), 13, 965 (1939).
3. B.S.Neporent, Ibid., 21, 1111 (1947).
4. N.A.Borisevich, V.V.Zelinskii & B.S.Neporent, Doklady AN SSSR, 94, 37 (1954).
5. B.S.Neporent & N.A.Borisevich, Ibid., 94, 447 (1954).
6. B.S.Neporent & N.A.Borisevich, Optika i spektroskopiya 1, 143 (1956).
7. G.A.Kundzich & A.A.Shishlovskii, Doklady AN SSSR, 97, 429 (1954).
8. G.A.Kundzich, Dissertation, Kiev, 1955.
9. V.P.Klochkov, Zhur.fiz.khimii, 30, 2823 (1956).
10. N.A.Borisevich & B.S.Neporent, Optika i spektroskopiya, 1, 536 (1956).
11. L.A.Tumerman, Trudy (Proceedings), Physical Institute, USSR Ac.of Sci.1, No.4, 77 (1938).

ANGULAR DISTRIBUTION OF RESONANCE RADIATION FROM VAPORS

- P.A.Apanasevich & G.S.Kruglik

Wood[1] in 1909 was the first to observe mirror reflection of light by mercury apor. He found that with increase of the mercury vapor pressure in the vessel iffuse resonance emission of the 2537 Å line gradually transforms into mirror eflection similar to reflection from a specular surface. The maximum diffuse mission of the 2537 Å line is observed at a saturated Hg vapor pressure correponding to a temperature of about 100° (p = 0.3 mm Hg; a cube having the linear imensions of the wavelength contains approximately 125 Hg atoms). With increase f the temperature in the vessel and, consequently, the pressure of the saturated ercury vapor, the intensity of the diffuse resonance radiation decreases and aleady at a temperature of 270° (p = 124 mm Hg; about 35 000 Hg atoms in a cube havng the linear dimensions of the wavelength) diffuse emission is virtually absent nd all the resonance emission is observed only in the direction of mirror reflecion.

Subsequently reflection of radiation by metal vapors was investigated by a umber of authors[2-8]. It was observed for cadmium vapor[2,5,6,8] and for vapors of lkali metals[7,8]. It was established that reflection from metal vapors is selective n character, that it is quenched appreciably less than diffuse resonance radiation, hat there is no change in the frequency of the radiation in the process[3], that in he case of irradiation of the vapor with plane polarized light the reflected light s elliptically polarized. However, there cannot be found in the literature a conistent theoretical treatment of this effect, satisfactorily explaining its properies. In most cases investigators have used the concepts of classical theory for nterpreting the experimental data on mirror reflection, and such interpretations o not lead to satisfactory agreement with experiment. No quantum electrodynamical heory of this effect has been developed. There are only fragmentary remarks conerning treatment of coherent transformation of radiation in the framework of quanum electrodynamics.[9,10] At the same time, it is clear that detailed theoretical onsideration of this effect is of interest not only from the purely scientific tandpoint but also has practical value: it can be used for determining transition robabilities of atoms and for investigating the interaction between atoms. The urpose of the present communication is to consider in the framework of quantum lectrodynamics the angular distribution of resonance radiation at different densiies of the luminous vapor.

Diffuse resonance emission is a process of light conversion by the aggregate f the vapor atoms, the separation between which is so great that there is no contant phase relationship between them. To describe the process one can apply the heory of light conversion or transformation by a single atom.[11] Mirror reflection f resonance radiation by vapors shows that at a certain vapor density the indiviual atoms no longer act as independent entities in transforming the light. Hence n considering the process one must treat the conversion of light by a conjunction f identical particles forming a common system.

Assume that we have a system consisting of N identical atoms. For the sake f simplicity we further assume that the atoms have only two energy levels and that n the first approximation their interaction and thermal motion can be neglected. [f such a system is in a field of electromagnetic radiation, its behavior in the ccupation number representation is described by the following equation following rom the Schrödinger equation:

$$ih\frac{\partial C_{N_1 N_2(n_\varkappa)}}{\partial t} = \sqrt{\frac{N_2(N_1+1)}{N^2}} \sum_{\varkappa'} \frac{H_{21}^{(\varkappa')}\sqrt{n_{\varkappa'}+1}}{\sqrt{\omega_{\varkappa'}}} e^{i(\omega_{21}-\omega_{\varkappa'})t} C_{N_1+1,\, N_2-1(n_\varkappa+\delta_{\varkappa\varkappa})} +$$

$$+\sqrt{\frac{N_1(N_2+1)}{N^2}} \sum_{\varkappa'} \frac{H_{12}^{(\varkappa')}\sqrt{n_{\varkappa'}}}{\sqrt{\omega_{\varkappa'}}} e^{-i(\omega_{21}-\omega_{\varkappa'})t} C_{N_1-1,\, N_2+1(n_\varkappa-\delta_{\varkappa\varkappa'})}, \qquad (1)$$

where

$$H_{12}^{(\varkappa')} = (H_{21}^{(\varkappa')})^* = \sqrt{2\pi h}\, i\omega_{12} p_{12} \sum_{s=1}^{N} \cos(\widehat{\mathbf{p}_s \mathbf{e}_{\varkappa'}})\, e^{-i\mathbf{K}'\mathbf{R}_s} e^{i(\alpha_2^{(s)}-\alpha_1^{(s)})}. \qquad (2)$$

In the above equations $C_{N_1 N_2(n_\varkappa)}$ represent the probability amplitudes that N_1 atoms are in the first (ground) state, N_2 atoms are in the second (excited) and that in the field there are $n_1, n_2, \ldots n_\varkappa, \ldots$ photons; $n_\varkappa$ is the number, $\omega_\varkappa$ is the frequency, $\mathbf{K}$ is the wave vector and $\mathbf{e}_\varkappa$ is the polarization vector of photons of the $\varkappa$ kind; p_s is the dipole moment of the s-th atom and p_{12} is the matrix element of the absolute value of the dipole moment; ω_{21} is the natural frequency of the atom; $\alpha_i^{(s)}$ is the arbitrary phase of the s-th atom in the i-th state, and R_s is the radius vector of the center of gravity of the s-th atom.

Solving Eq.(1) for the transition process

$$N_1 N_2(n_\varkappa) \to N_1-1,\ N_2+1(n_\varkappa-\delta_{\varkappa\varkappa'}) \to N_1 N_2(n_\varkappa-\delta_{\varkappa\varkappa'}+\delta_{\varkappa\varkappa''}),$$

as a result of which the light is converted, by the method described in Ref.11, we can readily find the intensity of the converted light. If the primary radiation is propagating in the direction $\mathbf{K}'$, the energy flux of the secondary radiation, propagating in the direction $\mathbf{K}''$, will be given by

$$I(\mathbf{K}' \to \mathbf{K}'') = I_0 \cdot \sum_{s,\, r} \cos(\widehat{\mathbf{p}_s \mathbf{e}_{\varkappa''}}) \cos(\widehat{p_s \mathbf{e}_{\varkappa'}}) \cos(\widehat{p_r \mathbf{e}_{\varkappa'}}) \cos(\widehat{\mathbf{p}_r \mathbf{e}_{\varkappa''}})\, e^{i(\mathbf{K}'-\mathbf{K}'')(\mathbf{R}_s-\mathbf{R}_r)}, \qquad (3)$$

where $|\mathbf{K}'| = |\mathbf{K}''|$ and I_0 is the part of the expression independent of the direction of the propagation and polarization of the primary and secondary photons.

Expression (3) describes the intensity of the secondary radiation for a certain definite arrangement of the atoms in space. In order to obtain the intensity observed experimentally one must average (3) over all possible positions of the atoms and orientations of their dipole moments. In the general case such averaging is a complicated problem. However, in the case of a highly rarefied gas or in the case of one sufficiently dense, the results of averaging can be evaluated relatively easily. Let us consider these two cases.

1. Highly rarefied vapor (separation between atoms comparable to or greater than the light wavelength). If the gas is rarefied to the extent where the average distances between atoms are comparable or equal to the wavelength of the radiation, then as a result of thermal agitation of the atoms the phase factor in (3) can assume any values from -1 to +1. Hence averaging over the separations between atoms for $\mathbf{K}'$ different from $\mathbf{K}''$ gives

$$I(\mathbf{K}' \to \mathbf{K}'') = I_0 \sum_{s} \cos^2(\widehat{\mathbf{p}_s \mathbf{e}_{\varkappa''}}) \cos^2(\widehat{\mathbf{p}_s \mathbf{e}_{\varkappa'}}). \qquad (4)$$

Thus in this case the intensity of the secondary emission does not depend on the direction of propagation of the radiation, i.e., there is observed diffuse conversion of the light. Nevertheless, it still depends on the directions of the polarization vectors of the primary and secondary radiations. Assuming that the atoms are oriented isotropically and replacing each term in the sum (4) by its average value, we can readily show that

$$I(\mathbf{K}'\to\mathbf{K}'')=I_0N\frac{1}{15}[1+2\cos^2(\widehat{\mathbf{e}_{\kappa'}\mathbf{e}_{\kappa''}})]. \qquad (5)$$

This represents the case of diffuse resonance radiation observed, for example, in the case of saturated mercury vapor at 100°, when the average separation between atoms is equal to approximately one fifth the wavelength of the radiation.

2. Dense vapors (average distance between atoms appreciably smaller than the wavelength). It is known from experiment that in the case of a high vapor density in the test vessel resonance radiation is observed only from a thin layer adjacent to the front wall of the vessel. In this case there is no need to consider the entire gas in the volume, one need only take into account the conversion of light by atoms forming this thin surface layer. Hence we assume that the atoms of interest comprise a plane layer, the thickness of which is appreciably smaller than the wavelength.

In the case of dense packing of the atoms, the entire layer can be divided into elementary volumes, each containing a large number of atoms, but having dimensions small compared to the wavelength. In this case the summation in (3) can be carried out in two stages: first we sum over the atoms comprised in an elementary volume, within the limits of which the phase factor can be regarded as constant, and then sum over all the elementary volumes:

$$I(\mathbf{K}'\to\mathbf{K}'')=I_0\sum_{i,j}e^{i(\mathbf{K}'-\mathbf{K}'')(\mathbf{R}_i-\mathbf{R}_j)}\times\sum_{s}^{v_i}\cos(\widehat{\mathbf{p}_s\mathbf{e}_{\kappa'}})\cos(\widehat{\mathbf{p}_s\mathbf{e}_{\kappa''}})\sum_{r}^{v_j}\cos(\widehat{\mathbf{p}_r\mathbf{e}_{\kappa'}})\cos(\widehat{\mathbf{p}_r\mathbf{e}_{\kappa''}}), \qquad (6)$$

where R_i is the radius vector of the central point of the i-th elementary volume. Inasmuch as each elementary volume comprises a large number of atoms, the sum over the elementary volume v_i can be represented in the form

$$\sum_{s}^{v_i}\cos(\widehat{\mathbf{p}_s\mathbf{e}_{\kappa'}})\cos(\widehat{\mathbf{p}_s\mathbf{e}_{\kappa''}})=a(\mathbf{e}_{\kappa'},\,\mathbf{e}_{\kappa''})N_i, \qquad (7)$$

here $a(\mathbf{e}_{\kappa'},\mathbf{e}_{\kappa''})$ is the average over all orientations of p_s of the product of the cosines; N_i is the number of atoms in volume v_i, equal to

$$N_i=N_0v_i+\Delta N_i, \qquad (8)$$

where N_0 is the average particle density; ΔN_i is the deviation of the number of particles in volume v_i from the mean value N_0v_i. In the case of isotropic orientation of the atoms it can readily be shown that

$$a(\mathbf{e}_{\kappa'},\,\mathbf{e}_{\kappa''})=\frac{1}{3}\cos(\widehat{\mathbf{e}_{\kappa'}\mathbf{e}_{\kappa''}}).$$

Inserting (7) and (8) into (6) and averaging over the ΔN_i (fluctuations), we obtain

$$I(\mathbf{K}'\to\mathbf{K}'')=I_0a^2(\mathbf{e}_{\kappa'}\mathbf{e}_{\kappa''})\sum_{i,j}e^{i(\mathbf{K}'-\mathbf{K}'')(\mathbf{R}_i-\mathbf{R}_j)}(N_0v_iv_j+\Delta N_i^2\delta_{ij}). \qquad (9)$$

Thus the intensity of the secondary emission of a dense vapor consists of two parts. One part of the intensity is proportional to the fluctuations in the density of the atoms and does not depend on the directions of K' and K'', i.e., is due to diffuse radiation; taking into account the fact that the number of elementary volumes is V/v this intensity can be written in the form

$$I_{\text{dif}}(\mathbf{K}'\to\mathbf{K}'')=I_0a^2(\widehat{\mathbf{e}_{\kappa'}\mathbf{e}_{\kappa''}})V\frac{\overline{\Delta N^2}}{v}; \qquad (10)$$

The second part of the radiation is proportional to N_0^2. Replacing summation over elementary volumes by integration over the entire plane layer, we obtain

$$I_{\mathrm{mir}}(\mathrm{K}' \to \mathrm{K}'') = \begin{cases} I_0 a^2 V^2 N_0^2 & \text{for } [\mathrm{K}' - \mathrm{K}'', \mathrm{h}] = 0 \\ 0 & \text{for } [\mathrm{K}' - \mathrm{K}'', \mathrm{h}] \neq 0, \end{cases} \tag{11}$$

where the vector h represents the normal to the layer. It will be evident from (11) that this part of the emission can be observed only in the direction of the incident light (light passing through the layer) and in the direction of mirror reflection (vector $\mathrm{K}' - \mathrm{K}''$ parallel to h). If instead of $\overline{\Delta N^2}$, we substitute its value in the case of an ideal gas $(N_0 v)$, then from the relation $I_{\mathrm{dif}} : I_{\mathrm{mir}} \sim 1/VN_0$ it is apparent that the diffuse radiation will amount to an insignificant fraction of the mirror reflection. Mercury vapor at 270°, when there are on the average 33 atoms per wavelength, apparently may be regarded as a high density vapor. Hence the "conversion" of 2537 Å light by mercury vapor at 270° consists primarily of reflection.

Institute of Physics
Academy of Sciences of the Belorussian SSR

References

1. R.W.Wood, PhysZ., 10, 425 (1909).
2. R.W.Wood, Phys.Z., 13, 359 (1912); Phil.Mag., 44, 1105 (1922).
3. W.Rump, Z.Phys., 29, 196 (1924).
4. O.Schnettler, Z.Phys., 65, 55 (1930).
5. M.Spitzer, Compt.rend., 241, 631 (1953); Ibid., 244, 2036 (1957).
6. H.L.Welsh, J.Kastner & A.C.Lauriston, Canad.J.Research A, 28, 93 (1950).
7. A.C.Lauriston & H.L.Welsh, Canad.J.Phys., 29, 217 (1951).
8. J.A.Galt & H.L.Welsh, Canad.J.Phys., 35, 98 (1958); Ibid., 35, 114 (1957).
9. V.Weisskopf, Ann.Phys., 9, 23 (1931).
10. W.Heitler, The Quantum Theory of Radiation, Oxford, 1954. (Cited in Russian trans.)
11. P.A.Apanasevich, Trudy (Proceedings), Inst. of Phys. and Math., Belorussian SSR Ac. of Sci., No.2, 55 (1957); Optika i spektroskopiya, 5, 97 (1958).

ON AGREEMENT BETWEEN THE CLASSICAL AND QUANTUM THEORIES OF THE INTERACTION OF LIGHT WITH HARMONIC OSCILLATORS

- V.P.Gribkovskii & B.I.Stepanov

In considering the processes of absorption and emission of light, the quantum ystem of particles with two energy levels is frequently modeled on classical osillators. This is done in agreement with the principle of correspondence. Calulations[1,2] show, however, that a system of particles with two energy levels has number of purely quantum attributes (in particular, variation of the absorption ower and polarization with the temperature of the ambient medium and the density f the exciting light), which are wholly lost in treating classical oscillators.

The divergence between the results of classical and quantum theories is someimes regarded as a shortcoming of the classical theory. In the given case this iew is not well founded inasmuch as we are dealing here with the optical properies of entirely different models.

In order to clarify the limits of applicability of the classical theory of a armonic oscillator one must in the quantum theory as well consider the interaction f light with a quantum harmonic oscillator. This formulation of the problem is airly obvious and the only correct one. Yet, hitherto, investigators as a rule ave subdivided quantum oscillators into individual pairs of levels and investigaed the radiation emitted incident to transition of the oscillator between the disrete pair of levels. The approximate results obtained in this way were compared ith the precise results of classical theory, which led to the conclusion that the esults of the two theories agree only in the case when the oscillator is excited o a high-lying energy level.[3] So far there has been no consistent juxtaposition f the results of the classical and quantum theories.

Below we give the results of quantum mechanical calculations of the interacion of light with a harmonic oscillator. In all the calculations the oscillator ith its infinite set of energy levels is considered as a single whole. This made t possible to finalize the solution of the problem and obtain a number of new reults.

Absorption

Kravets[4] in the framework of the classical theory established that the freuency-integral coefficient of absorption (Kravets integral) does not depend on ither the temperature or the intensity of the exciting light. For calculating he integral absorption and emission of a harmonic oscillator in the framework of he quantum theory it is most convenient to use the probability method. The iniial equations of this method, the equations of particle balance at the energy levls, follow from the fundamental equations of electrodynamics.[5]

Let us consider the totality of n harmonic oscillators interacting with exernal radiation having an energy density s, and a frequency equal to the natural requency of an oscillator. In the general case, the absorption power is given by he sum

$$W_{\text{abs}} = \sum_{v=0}^{\infty} [n_v(s, T, t) B_{v,\, v+1} s - n_{v+1}(s, T, t) B_{v+1,\, v} s] h\nu_0, \tag{1}$$

here $n_v(s, T, t)$ is the number of oscillators on level v, and

$$B_{v+1,\, v} = B_{v,\, v+1} = (v+1) B_0 = (v+1) \frac{\pi e^2}{3mh\nu_0} \text{ —} \tag{2}$$

re the Einstein coefficients for forced transitions between the levels v and $+1$. The numbers $n_v(s, T, t)$ depend on the density of the exciting light, the temperature and the time t.

Following Stepanov[1] and Frish[6], we regard forced emission here as negative absorption. Taking into account the fact that according to (2), $B_{v,\,v+1} - B_{v,\,v-1} = B_0$, we obtain from (1) the absorption power of n harmonic oscillators:

$$W_{\text{abs}} = nB_0 sh\nu_0 = n\frac{\pi e^2}{3m}s. \tag{3}$$

As is evident from (3) the absorption power of a harmonic oscillator does not depend on the distribution function and, consequently, on the temperature of the surrounding medium. The linear dependence of W_{abs} on s indicates that Bouguer's law is rigorously observed. Equation (3) agrees exactly with the results of classical theory.

Luminescence: Growth and Decay Laws

In the presence of thermal radiation of density u the luminescence power may be represented in the form:[1]

$$W_{\text{lum}}(t) = \sum_{v=1}^{\infty}\left[n_v(s,\,T,\,t)\left(A_{v,\,v-1} + B_{v,\,v-1}u\right) - n_{v-1}(s,\,T,\,t)\,B_{v-,1v}u\right]h\nu_0, \tag{4}$$

where

$$A_{v,\,v-1} = vA_0 = v\frac{8\pi e^2\nu_0^2}{3mc^3} \text{ —} \tag{5}$$

is the probability for spontaneous transition from level v to level $v-1$. The distribution of the oscillators over the energy levels satisfies the following set of equations

$$\begin{aligned}\frac{d}{dt}n_v(s,\,T,\,t) = &-n_v(s,\,T,\,t)\left[A_{v,\,v-1} + B_{v,\,v-1}(u+s) + B_{v,\,v+1}(u+s)\right] + \\ &+ n_{v+1}(s,\,T,\,t)\left[A_{v+1,\,v} + B_{v+1,\,v}(u+s)\right] + n_{v-1}(s,\,T,\,t)\,B_{v-1,\,v}(u+s).\end{aligned} \tag{6}$$

Differentiating (4) with respect to time and using (5), we obtain after simple transformations:

$$\frac{d}{dt}W_{\text{lum}}(t) + A_0W_{\text{lum}}(t) = A_0 n\frac{\pi e^2}{3m}s. \tag{7}$$

Solving this equation, we obtain

$$W_{\text{lum}}(t) = Ce^{-A_0 t} + n\frac{\pi e^2}{3m}s, \tag{8}$$

where C is an integration constant which should be determined from the initial conditions. By means of (8) we find that the luminescence powers during the processes of growth of luminescence, steady state excitation and decay are given by the following formulas:

$$W^{\text{g}}_{\text{lum}}(t) = n\frac{\pi e^2}{3m}s\left(1 - e^{-2\gamma_0 t}\right), \tag{9}$$

$$W^{\text{ss}}_{\text{lum}} = n\frac{\pi e^2}{3m}s, \tag{10}$$

$$W^{\text{d}}_{\text{lum}}(t) = n\frac{\pi e^2}{3m}se^{-2\gamma_0 t}, \tag{11}$$

where $2\gamma_0$ is the classical decay constant. According to Eqs.(9)-(11) the results of classical and quantum theories pertaining to the integral emission during steady state excitation and to the laws characterizing the growth and decay of uminescence of a harmonic oscillator fully agree with each other.*

Polarization

According to the principle of correspondence, a classical harmonic oscillator orresponds to each pair of energy levels of the oscillator. The error inherent n this view becomes particularly obvious in considering the polarization of lumiescence. Assume that we have an aggregation of n harmonic oscillators which are rranged chaotically in space and cannot change the directions of their dipole moents. The oscillators are irradiated with linearly polarized light propagating long the x axis. The electric vector of the incident light is directed along the axis, and the luminescence is observed along the y axis. The distribution of he oscillators over energy levels in the given case will depend not only on the emperature of the ambient medium and the density of the exciting light, but also n the direction of the dipole moment of the oscillator, specified by the angles and φ. The number of oscillators on the level v with a given direction of the ipole moments (per unit solid angle) under steady state conditions is given by[2]:

$$n_v(s, T, t) = \frac{n}{4\pi}\,\frac{A_0}{A_0 + B_0u + 3B_0 s\cos^2\theta}\left[\frac{B_0u + 3B_0 s\cos^2\theta}{A_0 + B_0u + 3B_0 s\cos^2\theta}\right]^v. \tag{12}$$

The powers of the luminescence polarized along the z and x axes emitted incient to transition of the oscillator from level v to level $v-1$ are given by the ormulas

$$W^z_{v,\,v-1} = h\nu_0\int\limits_{\Omega}\{n_v(s,T,\Omega)\,[A^z_{v,\,v-1}(\Omega) + B^z_{v,\,v-1}(\Omega)\,u_1] - n_{v-1}(s,T,\Omega)\,B^z_{v-1,\,v}(\Omega)\,u_1\}\,d\Omega, \tag{13}$$

$$W^x_{v,\,v-1} = h\nu_0\int\limits_{\Omega}\{n_v(s,T,\Omega)\,[A^x_{v,\,v-1}(\Omega) + B^x_{v,\,v-1}(\Omega)\,u_1] - n_{v-1}(s,T,\Omega)\,B^x_{v-1,\,v}(\Omega)\,u_1\}\,d\Omega, \tag{14}$$

here $u_1 = \frac{1}{8\pi}u$ is the Planck radiation density, calculated per unit solid angle nd per polarization, and the differential Einstein coefficients are

$$A^z_{v,\,v-1}(\Omega) = \frac{3}{8\pi}vA_0\cos^2\theta, \qquad B^z_{v,\,v-1}(\theta) = 3vB_0\cos^2\theta,$$

$$A^x_{v,\,v-1}(\Omega) = \frac{3}{8\pi}vA_0\sin^2\theta\cos^2\varphi, \quad B^x_{v,\,v-1}(\Omega) = 3vB_0\sin^2\theta\cos^2\varphi. \tag{15}$$

On the basis of Eqs.(13) and (14) one can calculate the polarization of indiidual lines by means of the formula

$$P_{v,\,v-1} = \frac{W^z_{v,\,v-1} - W^x_{v,\,v-1}}{W^z_{v,\,v-1} + W^x_{v,\,v-1}}. \tag{16}$$

Calculations[2] show that $P_{v,v-1}$ is a function of the temperature of the ambient edium and the density of the exciting light. In particular, when $u = 0$ and $s \to 0$, he quantities P_{10}, P_{21}, $P_{32}, \ldots, P_{v,\,v-1}$ tend on the lower side to the limits 1/2, 2/3, /4,..., $v/v+1$. With increase of s the values of the $P_{v,v-1}$ decrease and in the imit $(s \to \infty)$ the polarization of a line with a small number v may be negative down to -1). If, on the other hand, $u \gg s$ the values of all the $P_{v,v-1}$ are close o 1/2.

In order to find the polarization of the total luminescence of the oscillators ne must sum (13) and (14) over all v from 1 to ∞. Carrying out, first, the sumation over v and then integration over Ω, we find z and x, the components of the total luminescence, the polarization of which, regardless of the values of s and T always equals 1/2. This agrees with the results of classical theory[8] and is not in conflict with the fact that the polarization of individual lines depends on both the density of the exciting light and on the temperature of the ambient medium.[2]

---

*It was shown in Ref.7 that the decay law for a harmonic oscillator is always xponential regardless of the initial conditions.

Natural Line Contour

It follows from the quantum theory of radiation that the natural width of the energy levels of a harmonic oscillator increases in proportion to the number of the level. From this it might be concluded that the natural width of a spectrum line will be the greater, the higher the energy level to which the oscillator is excited at the initial instant. As Weisskopf & Wigner[9] showed for a particular case, however, this inference is not correct. The harmonic oscillator occupies a special place among quantum systems, hence in considering its interaction with an electromagnetic field one must use a special mathematical approach. It is essential to take into account the fact that any given photon emitted by the oscillator cannot be attributed to a transition between any specific pair of levels inasmuch as the photon may appear incident to transition from any energy level to the neighboring lower-lying level. This indeterminacy is connected with the equal spacing of the energy levels and the fact that all the dipole moment matrix elements, which determine the anisotropy of the radiation, are parallel to each other.

Weisskopf & Wigner[9] calculated the line contour in the simplest case when the oscillator at the initial instant is on the second excited level, and obtained a result agreeing with the results of classical theory. We considered the general case when the system is excited to any energy level. As a result of our calculations, carried out consistently within the framework of quantum electrodynamics, we obtained the following expression for the energy distribution over the frequencies of all the emitted photons:

$$W(\omega_1, \omega_2, \omega_3, \dots \omega_N) = \left(\frac{\gamma_0}{\pi}\right)^N \prod_{j=1}^{N} \frac{1}{(\omega_j - \omega_0)^2 + \gamma_0^2}. \qquad (17)$$

If we integrate (17) over any $N-1$ frequencies, we obtain the following expression for the frequency distribution of the energy of one photon:

$$W(\omega) = \frac{\gamma_0}{\pi} \frac{1}{(\omega - \omega_0)^2 + \gamma_0^2}. \qquad (18)$$

According to (18), regardless of the excitation energy, the natural line contour of a harmonic oscillator always coincides with the line contour calculated in the framework of classical theory.

Conclusions

Summarizing the results of the above described calculations and comparing them with the results of Refs.1, 2 & 10, we arrive at the following conclusions:

1. In the dipole approximation all the results of quantum theory pertaining to the optical properties of a harmonic oscillator are in complete agreement with the results of classical theory.

2. A system with two energy levels is not identical with a classical harmonic oscillator.

3. Correspondence of the optical properties of the system with two energy levels or an arbitrary pair of levels of a more complex quantum system (with the exception of a quantum oscillator) with the optical properties of a classical

oscillator obtains only provided the population of the highest-lying level is negligibly small compared with the population of the lowest level and the arrival of particles on the higher level occurs only as the result of forced optical transitions from the lower level.

4. A quantum harmonic oscillator must always be considered as a unified whole, inasmuch as even in the case of fulfillment of the conditions formulated above, individual level pairs cannot be represented by the classical oscillator model.

Institute of Physics,
Academy of Sciences of the Belorussian SSR

References

1. B.I.Stepanov, Lyuminestsentsiya slozhnykh molekul (Luminescence of complex molecules), Minsk, 1956.
2. V.P.Gribkovskii & B.I.Stepanov, Optika i spektroskopiya, 8, 176 (1960). (Trans.Optics and Spectroscopy.)
3. E.V.Shpol'skii, Atomnaya fizika (Atomic physics), Vol.II, M.-L., 1950.
4. T.P.Kravets, Trudy po fizike (Works on physics), M., 1959.
5. P.A.Apanasevich, Vestsi AN BSSR, Ser.fiz.-tekh.navuk (News, Belorussian Ac. of Sci., Phys.-Tech. Science Series) No.2, 31 (1959).
6. S.E.Frish, Uspekhi fiz.nauk, 53, 582 (1951).
7. V.P.Gribkovskii, P.A.Apanasevich & B.I.Stepanov, Trudy (Proceedings), Inst.of Phys. and Math, Belorussian SSR Ac. of Sci., No.3 (1959).
8. V.L.Levshin, Fotolyuminestsentsiya zhidkikh i tverdykh veshchestv (Photoluminescence of liquids and solids), M.-L., 1951.
9. V.Weisskopf & E.Wigner, Z.Phys., 65, 18 (1930).
10. B.I.Stepanov & V.P.Gribovskii, Optika i spektroskopiya, 8, 224 (1960). (Trans.Optics and Spectroscopy.)

NONLINEAR OPTICAL EFFECTS IN A SYSTEM OF PARTICLES WITH THREE ENERGY LEVELS

- B.I.Stepanov & V.P.Gribkovskii

Vavilov in his work[1] repeatedly formulated different problems in nonlinear optics. Nonlinear effects are associated with transition of part of the molecules to an excited state and differences between the optical properties of unexcited and excited molecules. The nature of nonlinear effects is illustrated by the case of a particle with two energy levels at absolute zero. As is known, the variation in the distribution of particles as a function of the exciting radiation density is of the form[2]

$$n_2 = \frac{Bs}{A + 2Bs + d} n \quad \text{and} \quad n_1 = \frac{A + Bs + d}{A + 2Bs + d} n. \tag{1}$$

In the range of low radiation densities (small s) the s dependence of n_2 is linear, while n_1 is virtually constant. For large s the dependence departs from linear. In the limit as $s \to \infty$, $n_2 \to n_1 \to \frac{n}{2}$. The absorption power

$$W_{\text{abs}} = (n_1 - n_2) Bsh\nu = n \frac{Bs(A+d)h\nu}{A + 2Bs + d}. \tag{2}$$

If s is small, the absorption power is proportional to s; then with increase of density W_{abs}/s decreases, approaching a steady value in the range of large s. Thus increase in the intensity of excitation is not accompanied by increase in the amount of light absorbed. An analogous variation is exhibited by the luminescence power $W_{\text{lum}} = n_2 Ah\nu$. The absorption coefficient $\varkappa = W_{\text{abs}}/cs$ is constant for small s and then falls off to zero. In the limit as $s \to \infty$, the material becomes virtually transparent and Bouguer's (= Lambert's) law is no longer fulfilled.

Similar dependences should be observed for other optical effects: polarization of luminescence, dichroism, absorption and, as Vavilov noted, dispersion, birefringence, and rotary power.

The value of the radiation density at which deviation from linearity begins as regards order of magnitude is given by

$$s \sim \frac{A}{B} = \frac{8\pi h\nu^3}{c^3}.$$

These values in the visible region are very large and virtually unattainable under laboratory conditions.

At present the number of nonlinear effects actually observed is relatively small. We can mention the experiments of Vavilov & Levshin[1] and Sveshnikov[3]. The last observed violation of Bouguer's law and simultaneous depolarization of luminescence. Cherdyntsev[4] detected nonlinear effects in investigating dichroism.

The magnitude of nonlinear effects depends on the location and characteristics of the energy levels in the investigated substance. In principle, there can be no nonlinear effects for a harmonic oscillator.[5] For particles with two energy levels the effects should be minor. The nonlinear effects can be appreciable in special systems and particularly in the case of complex molecules with a metastable level. The existence and behavior of phosphorescence indicates that an appreciable number of particles may accumulate on the metastable level. This provides the basis for manifestation of nonlinear effects.

The purpose of the present work was simultaneous calculation of the variation of the absorption and luminescence powers, the polarization of luminescence, dichroism and the intensity of α-phosphorescence as functions of the incident radiation intensity. The calculations were carried out for particles with three energy levels (the second level - metastable; the third, higher-lying - labile) by the conventional probability method, neglecting thermal background, i.e., assuming T = 0. In all cases it was assumed that the incident radiation of frequency ν_{31} is linearly polarized (direction of propagation along the x axis; electric vector aligned with the z axis). The transition probabilities are designated by p_{ij}. The probabilities p_{13} and p_{31} depend on the density of the incident radiation and the angle θ between the direction of the electric vector of the exciting light and the dipole moment of the molecule:

$$p_{13} = 3B_{13}s\cos^2\theta \quad \text{and} \quad p_{31} = A_{31} + 3B_{31}s\cos^2\theta + d_{31}\,.$$

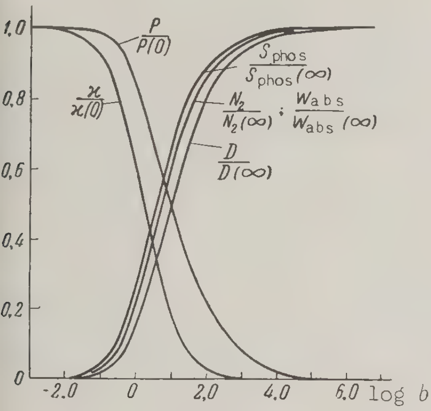

Fig.1

The probabilities p_{23}, p_{32} and p_{21} are associated with intramolecular processes; $p_{12} = 0$. As usual, it was assumed that unexcited molecules are distributed chaotically and that there is no rotation of the molecules.

The distribution of particles among levels under steady state conditions was calculated from the balance equation

$$\left(\Delta n_i = 0,\ n_1 + n_2 + n_3 = \frac{1}{4\pi}n\right).$$

The formal results of the calculations have been published elsewhere[6]. Analysis shows that under the influence of selective excitation the molecules acquire orientation. For small s, we have $n_2 \sim \cos^2\theta$ and $n_3 \sim \cos^2\theta$. In the range of large s, the orientation diminishes and in the limit $s \to \infty$ disappears completely. The total number of molecules on the metastable level (after integration over Ω) equals

$$N_2 = n\frac{p_{32}}{2p_{21} + 2p_{23} + p_{32}}\left(1 - \frac{1}{\sqrt{b}}\operatorname{arc\,tg}\sqrt{b}\right) = N_2(\infty)\left(1 - \frac{1}{\sqrt{b}}\operatorname{arc\,tg}\sqrt{b}\right), \tag{3}$$

where

$$b = \frac{3B_{13}(2p_{21} + 2p_{23} + p_{32})}{(A_{31} + d_{31})(p_{21} + p_{23}) + p_{21}p_{32}}\,s \approx \frac{3B_{13}}{A_{31} + d_{31}}\cdot\frac{p_{32}}{p_{23}}\,s. \tag{4}$$

The approximate equality in (4) is valid for $p_{21} \ll p_{23} \ll p_{32}$, i.e., in the absence of β-phosphorescence and with a relatively low α-fluorescence yield. The plot of N_2 as a function of log b is given in Fig.1. When s is small, N_2 is proportional to s, but then tends to $N_2(\infty)$. Saturation begins at $b \approx 1$, i.e., for $s \approx \frac{A_{31}}{B_{31}}\cdot\frac{p_{23}}{p_{32}}$. For fluorescein, for example, $p_{23}/p_{32} \approx 10^{-6}$. This means that nonlinear effects in a system of particles with a metastable level begin at incident radiation intensities some six orders of magnitude lower than the intensity marking the beginning of nonlinear effects in a system of particles with only two energy levels. In the case under consideration $N_2(\infty) \sim n$, i.e., an appreciable fraction of the particles goes over to the metastable state.

The absorption of the incident radiation is given by

$$W_{\text{abs}} = h\nu_{31}\int\limits_{\Omega}[n_1(\Omega) - n_3(\Omega)]\,p_{13}d\Omega = 3nB_{13}\,\text{sh}\,\nu_{31}\frac{1}{b}\left(1 - \frac{1}{\sqrt{b}}\operatorname{arc\,tg}\sqrt{b}\right) =$$

$$= W_{\text{abs}}(\infty)\left(1 - \frac{1}{\sqrt{b}}\operatorname{arc\,tg}\sqrt{b}\right). \tag{5}$$

It follows from a comparison of Eqs.(3) and (5) that W_{abs} and N_2 are characterized by the same s dependence in any system. A similar dependence obtains for the integral (over all angles) luminescence power. For $d_{31}=0$ and $p_{21}=0$, the luminescence power is equal to the absorption power.

From (5) one can readily deduce the expression for the absorption coefficient:

$$\varkappa = \frac{3B_{13}nh\nu_{31}}{c}\,\frac{1}{b}\left(1-\frac{1}{\sqrt{b}}\,\mathrm{arc\,tg}\sqrt{b}\right). \tag{6}$$

In the range of small s, the absorption coefficient is constant. When $b\approx 1$, it begins to decrease and rapidly approaches zero (Fig.1). The luminescence intensities observed along the y axis with the electric vectors aligned with the z and x axes are given by the formulas

$$W_{31}^{z}=\int\limits_{\Omega} n_3(\Omega)\,A_{31}^{z}(\Omega)\,h\nu_{31}d\Omega \quad\text{and}\quad W_{31}^{x}=\int\limits_{\Omega} n_3(\Omega)\,A_{31}^{x}(\Omega)\,h\nu_{31}d\Omega. \tag{7}$$

Here $A_{31}^{z}(\Omega)=\frac{3}{8\pi}A_{31}\cos^2\theta$ and $A_{31}^{x}(\Omega)=\frac{3}{8\pi}A_{31}\sin^2\theta\cos^2\varphi$ are Einstein's differential coefficients.

As a result of calculations, we obtained the following expression for the polarization of luminescence:

$$P=\frac{W_{31}^{z}-W_{31}^{x}}{W_{31}^{z}+W_{31}^{x}}=\frac{(3+b)\,\mathrm{arc\,tg}\sqrt{b}-3\sqrt{b}}{{}^{4}\!/_{3}\sqrt{b^3}-\sqrt{b}+(1-b)\,\mathrm{arc\,tg}\sqrt{b}}. \tag{8}$$

The b dependence of P is shown in Fig.1. In the region of small s, $P = 1/2$ while for $b = 1$, P decreases to 0.425. In the limit as $s\to\infty$, the polarization approaches zero. Depolarization of the luminescence appearing with increase of s is not connected with the occupation of the metastable state by part of the molecules per se, inasmuch as the probabilities p_{23} and p_{32} do not depend on the orientation of the electric vector of the incident radiation relative to the dipole moment of the molecule. The depolarization is associated only with build-up of the number of particles on the metastable level, decrease in the number of unexcited molecules and the resultant disorientation of the excited particles.

Anisotropy of the distribution of excited molecules over angles is also evinced in dichroism. If a previously excited system is irradiated by a new dose of radiation along the y axis (with density s_1), the absorption will differ for differently polarized beams. In this case the calculations were carried out by means of the formulas

$$\left.\begin{aligned} W_{\mathrm{abs}}^{z} &= 3B_{13}s_1h\nu_{31}\int\limits_{\Omega}[n_1(\Omega)-n_3(\Omega)]\cos^2\theta\,d\Omega,\\ W_{\mathrm{abs}}^{x} &= 3B_{13}s_1h\nu_{31}\int\limits_{\Omega}[n_1(\Omega)-n_3(\Omega)]\sin^2\theta\cos^2\varphi\,d\Omega.\end{aligned}\right\} \tag{9}$$

The calculations showed that the absorption powers W_{abs}^{z} and W_{abs}^{x} are characterized by different dependences on the density s of the exciting radiation. For $s = 0$ the two absorption powers are equal (given by Eq.(5)) and then, with increasing s fall off to zero.

In general, the dichroism is described by

$$D=\frac{\varkappa^{x}-\varkappa^{z}}{\varkappa^{x}+\varkappa^{z}}=\frac{(b+3)\,\mathrm{arc\,tg}\sqrt{b}-3\sqrt{b}}{(b-1)\,\mathrm{arc\,tg}\sqrt{b}+\sqrt{b}}. \tag{10}$$

In the range of small s the value of D is proportional to s. In the limit as $s\to\infty$, saturation sets in, and $D\to 1$ (Fig.1).

The afterglow appearing after cessation of excitation was investigated in detail by the same method by Sveshnikov[7,8]. Here we shall consider only the dependence of the afterglow on the intensity of the exciting radiation. The calculations were carried out for the light sums, i.e., for the energy emitted in the process of α-phosphorescence during the entire time after cessation of excitation (observation in a unit angle in the direction of the y axis). The pertinent equation is

$$S_{\text{phos}} = \alpha_2\tau_2 \frac{n}{4\pi} \frac{(p_{21}+p_{23})A_{31}}{2p_{21}+2p_{23}+p_{32}} h\nu_{31}\left[1-\frac{3}{4b}+\frac{3}{4}\left(\frac{1}{\sqrt{b^3}}-\frac{1}{\sqrt{b}}\right)\operatorname{arc\,tg}\sqrt{b}\right]. \tag{11}$$

Obviously for $s=0$, there is no α-phosphorescence. Linear increase of the phosphorescence light sum occurs only in the range of small s, then the value tends to saturation (Fig.1).

According to the results of our calculations (see Fig.1) the dependences of all the optical effects considered as the function of the incident radiation intensity are similar in character, which is connected with the common cause of the effects, namely, accumulation of molecules on the metastable level. All the nonlinear effects begin at values of the radiation density at which N_2 amounts to an appreciable fraction of n. The presence of noticeable α-phosphorescence indicates the possibility of nonlinear s dependence of the absorption power, dichroism and decrease in the polarization of fluorescence. The inverse, however, is not necessarily true, inasmuch as for small p_{23} and $p_{21} \neq 0$, α-phosphorescence may be absent even in the presence of strong nonlinear effects. In the case of a high nonoptical transition probability p_{21} accumulation of particles on the metastable level becomes impossible, which leads to quenching of the α-phosphorescence and effacement of all the nonlinear effects.

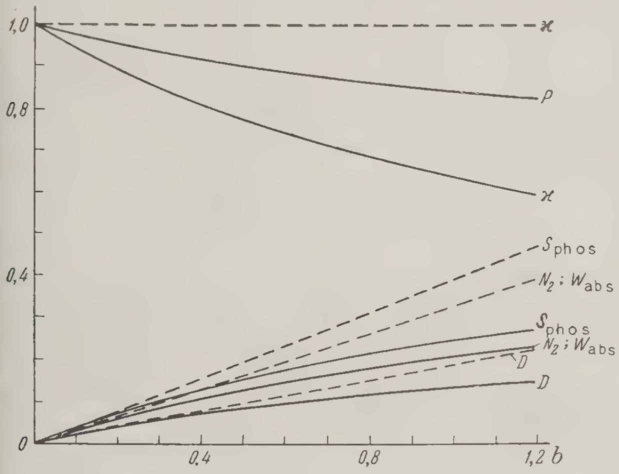

Fig.2

The initial sections of the curves of Fig.1 are shown to an enlarged scale in Fig.2. Here the horizontal axis is scaled in values of b (not log b). The dashed lines give the dependences that obtain in the absence of nonlinear effects. Thus the separations between the dashed and solid curves characterize the deviations from linearity.

As will be evident from Fig.2, all the nonlinear effects become noticeable at $b \approx 1$. For purposes of qualitative comparison of these effects it is convenient to use a dimensionless parameter that can serve as a measure of the nonlinear effects. By way of such parameter we have chosen the ratio of the deviation from linearity to the magnitude of the given physical quantity (effect) in the absence of nonlinear behavior. These parameters are obviously equal to zero for $b = 0$ and increase to 1 in the limit as $b \to \infty$. The values of these parameters for values of b from 0 to 1.4 are shown in Fig.3. Deviation from linearity should first be evidenced for the α-phosphorescence light sum, then for the absorption power and somewhat more weakly for dichroism. It will be seen that the nonlinearity of polarization is characterized by the smallest parameter (M_p).

In conclusion it must be noted that although the results of our calculations are in qualitative agreement with the experimental data in the literature, quantitative comparison of theory with experiment is at present difficult. Different nonlinear effects have been investigated separately, using different materials and

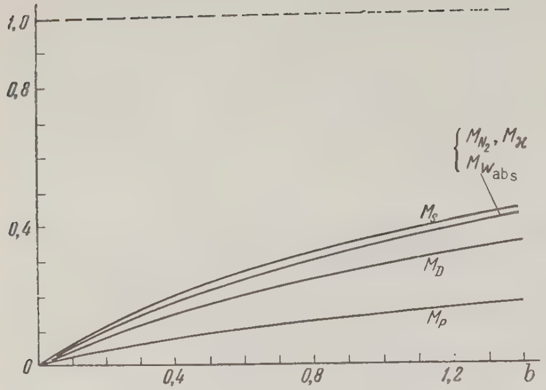

Fig.3

different techniques and as a rule there is a lack of data on the actual intensities of the exciting light. It would be desirable to carry out a systematic experimental investigation of all nonlinear effects.

Institute of Physics,
Academy of Sciences of the Belorussian SSR

References

1. S.I.Vavilov, Mikrostruktura sveta (Microstructure of light), M., 1950.
2. B.I.Stepanov, Lyuminestsentsiya slozhnykh molekul (Luminescence of complex molecules), Pub.Belorussian SSR Ac. of Sci., 1956.
3. B.Ya.Sveshnikov, Doklady AN SSSR, 51, 675 (1946).
4. S.V.Cherdyntsev, Zhur.eksp.i teor.fiz., 18, 352 (1948).
5. V.P.Gribkovskii & B.I.Stepanov, Optika i spektroskopiya, 8, 176 (1960). (Trans.Optics & Spectroscopy.)
6. B.I.Stepanov & V.P.Gribkovskii, Ibid., 8, 224 (1960). (Trans.Ibid.)
7. B.Ya.Sveshnikov, Zhur.eksp.i teor.fiz., 18, 878 (1948).
8. B.Ya.Sveshnikov, Izv.AN SSSR, Ser.fiz., 13, 67 (1949).

CALCULATION OF THE PROBABILITY OF ELECTRONIC-VIBRATIONAL TRANSITIONS FOR AN ANHARMONIC OSCILLATOR

- K.K.Rebane & O.I.Sil'd

The probability distribution for electronic-vibrational transitions over the vibrational levels is determined by the Franck-Condon integrals

$$W_{nm}=\Big[\sum_{l} A_l I_{nm}^{(l)}\Big]^2,\quad I_{nm}^{(l)}=\int \psi_n(x)\, x^l \psi_m(x)\, dx, \tag{1}$$

where x is the vibrational coordinate, and ψ_n and ψ_m are the vibrational wave functions of the nuclei; A_l is a constant in the expansion of the electronic matrix element in terms of the nuclear displacements.[1] In many cases the electronic matrix element is weakly dependent on the nuclear coordinates, and the zeroth order Franck-Condon integrals are of the greatest interest.

In our preceding paper[2] we carried out for the case of a harmonic oscillator a comparison of the quantum mechanical distributions $W_{nm}=[I_{nm}^{(0)}]^2$ (Refs.3-5) with three versions of semiclassical calculations. The principal results of this work are the following.

In treating transitions between individual vibrational levels, the coordinate distribution prior to the transition must be considered from the standpoint of quantum mechanics. If one retains the first part of the Franck-Condon principle (constancy of coordinates and momentum), there are obtained results that are close to the quantum mechanical ones. Attempts to improve the semiclassical treatment by modifying the first part of the formulation of the Franck-Condon principle[6] do not yield any substantial improvement and are not theoretically warranted.

In the present paper we calculate $W_{nm}=[I_{nm}^{(0)}]^2$ for a Morse oscillator.[*]

While in our treatment we have in mind primarily the parameters of oscillators encountered in considering luminescence centers, the results obtained should be applicable to other cases, in particular to diatomic molecules, and may also be useful in treating the single-oscillator model of complex molecules[8,9].

In the case of luminescence centers the single-oscillator model[10-14] has one distinctive feature, namely, the Stokes losses attain the magnitude of fifty vibrational quanta.[10] It follows from this that in calculating the Franck-Condon integrals one of the wave functions belongs to a very high vibrational level and accordingly has many nodes. Moreover, even the simplest wave functions - the wave functions of a harmonic oscillator - of such orders have not been tabulated. All this virtually precludes computation of the Franck-Condon integrals by simple numerical integration.

We consider an oscillator, the potential energy of which is given by the function

$$U(x)=D\,[(1-e^{-gx})^2-1], \tag{2}$$

where D is the dissociation energy. The vibration frequency in the harmonic approximation is $\omega=g\sqrt{2D/\mu}$. The potential energy minimum of the oscillator is located at the point $x=0$. The wave function is of the form[15]

---

[*] After completion of the present calculations we became aware of the contributions listed under Ref.7 in which there have also been calculated the corresponding integrals of overlapping of the vibrational wave functions of a Morse oscillator. But in these papers the results are obtained in a form that makes computation of the numerical values of $I_{nm}^{(0)}$ very difficult in general and virtually impossible for vibrational levels with high numbers.

$$\psi_n(u) = N_n e^{-u/2} u^s P_n(u), \tag{3}$$

where the dimensionless coordinate $u \equiv \frac{2\sqrt{2\mu D}}{g\hbar} e^{-gx}$; the parameter $s \equiv \frac{\sqrt{-2\mu E_n}}{g\hbar}$; μ is the reduced mass of the oscillator; E_n is the energy of the n-th vibrational level:

$$E_n \equiv -D\left[1 - \frac{g\hbar}{\sqrt{2\mu D}}\left(n + \frac{1}{2}\right)\right]^2;$$

$P_n(u)$ is a polynomial: $P_n(u) = F(-n, 2s+1, u)$, where $F(\alpha, \beta, z)$ is a confluent hypergeometric series. The problem reduces to calculating the overlapping of the wave functions:

$$I_{nm}^{(0)} = \int_{-\infty}^{\infty} \psi_n(x)\, \psi_m(x-a)\, dx = \frac{1}{g}\int_0^{\infty} \psi_n(u)\, \psi_m(ku)\, \frac{du}{u}, \tag{4}$$

where $k = e^{ga}\sqrt{D'/D}$ and a is the shift of the equilibrium position of the oscillator.

The primed quantities pertain to the final electronic state. Direct multiplication of the hypergeometric series and term by term integration of the resultant series yields*

$$I_{nm}^{(0)} = \frac{1}{g} k^{s'} N_n N_m \left(\frac{2}{1+k}\right)^{s+s'} \sum_{p=0}^{n} (-1)^p \binom{n}{p} \Gamma(s+s'+p) \times$$
$$\times \left(\frac{2}{1+k}\right)^p F\left(-m, s+s'+p, 2s'+1, \frac{2k}{1+k}\right), \tag{5}$$

where $F(\alpha, \beta, \gamma, z)$ is a hypergeometric series.

In principle Eq.(5) allows of calculating the distribution W_{nm} for a Morse oscillator. But in this form it is applicable in practice only for small quantum numbers n and m. For high n and m it becomes very inconvenient inasmuch as with increase of n (or m) the number of terms of the alternating series increases in proportion and to insure the requisite accuracy, the calculation must be extended to a very large number of significant figures.

Using the familiar recursion formulas for hypergeometric functions[16], one can establish the following recurrent relationship

$$F(\alpha, \beta, \gamma, z) = \left[\frac{(\gamma+1)(\gamma+2)}{\alpha\beta z}\left(1 + \frac{(\gamma+1)(\alpha+\beta-\gamma-1)}{(\gamma+1-\alpha)(\gamma+1-\beta)}\right)\right]^{-1} \times$$
$$\times \left\{\left[\frac{2(\gamma+1)}{\gamma} + \frac{(\gamma+1)(\gamma+2)[\gamma-(2\gamma+1-\alpha-\beta)z]}{\gamma z(\gamma+1-\alpha)(\gamma+1-\beta)}\right] F(\alpha+1, \beta+1, \gamma+2, z) - \right.$$
$$\left. - \frac{(\alpha+1)(\beta+1)z}{(\gamma+2)(\gamma+3)} F(\alpha+2, \beta+2, \gamma+4, z)\right\}. \tag{6}$$

By means of (6) one can calculate the hypergeometric series in (5) and thereby avoid the cumbersome computation of the alternating series for large m.

Using Eqs.(5) and (6) we calculated the following distributions:

$$n = 0 \rightarrow m = 0-30 \quad \text{and} \quad n = 1 \rightarrow m = 0-35$$

for $a = +\sqrt{15}\,x_0$ (absorption in the case of potential curves of the form shown in Fig.1) and

---

*We calculated the Franck-Condon integrals of any order l in a similar manner.

Fig.1. Morse oscillator and distribution of probabilities $W(E)$ for electronic-vibrational transitions from the initial $n=0$ vibrational level: 1) transition between Morse oscillators, 2) transition between parabolas approximating the Morse curves at their equilibrium points, 3) transition between parabolas approximating the Morse curves at the point of equilibrium of the initial oscillator. Stokes losses $p_0 = 10\,\hbar\omega$; shift of the oscillator equilibrium position $a=\sqrt{15}\,x_0$; E_0 - energy of the electronic-vibrational transition; $h\nu_e$ of a purely electronic transition.

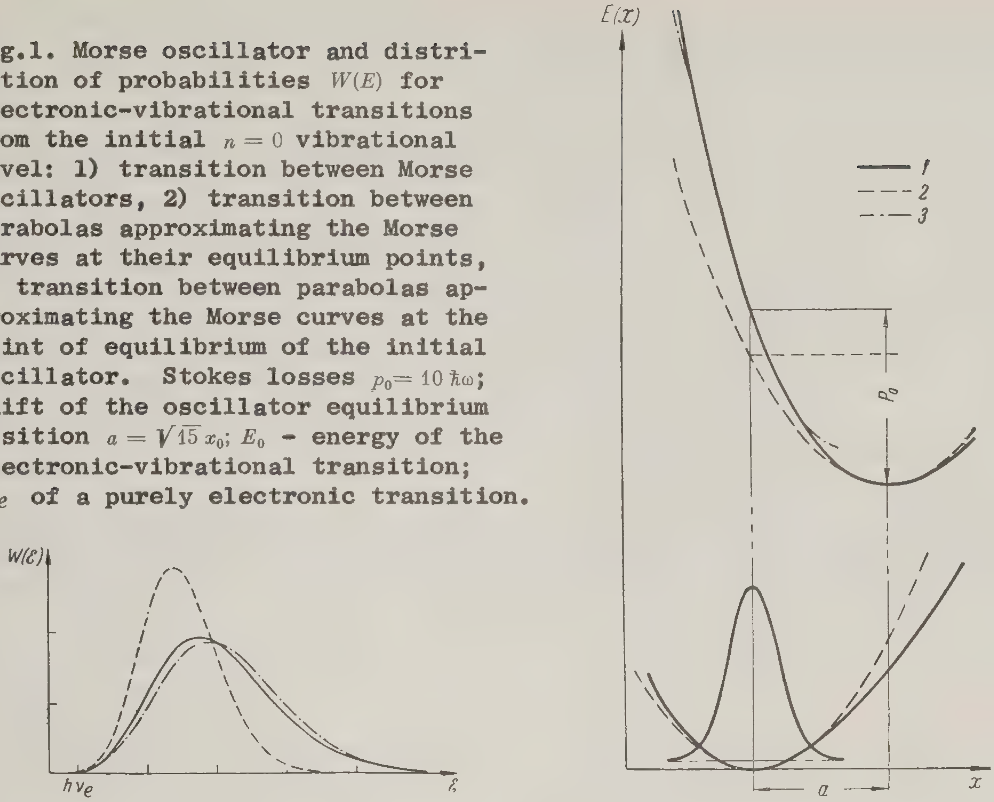

$$n=0 \to m=0-12 \text{ and } n=1 \to m=0-14$$

for $a=-\sqrt{15}\,x_0$ (radiation), where $x_0=\sqrt{\hbar/\mu\omega}$.

The parameters of the Morse oscillator were $D=D'=83.25\hbar\omega$ and $gx_0=1/\sqrt{2\cdot 83.25}$. The displacement of the minima and the anharmonicity of the curves were chosen so that the transition from the minimum of the potential curve for the initial state would occur to the 10-th vibrational level of the Morse oscillator in the final state and to the 7-th vibrational level of the approximating parabola (Fig.1).

To check the accuracy of the quantum mechanical calculations we used the formula $\sum\limits_m [I^{(0)}_{nm}]^2 = 1$, where the summation over m is extended over the entire energy spectrum.

The results are shown in Fig.2. For purposes of comparison, we give the results of semiclassical calculations carried out by means of the formula

$$W_n(x) \sim \frac{|\psi_n(x)|^2 \rho_n(x)}{\left|\frac{d}{dx}[U'(x)-U(x)]\right|}, \tag{7}$$

where $\rho_n(x)$ is the level density in the final state.* Equation (7) was derived on

---

*Bakhshiev[17] recently calculated the spectral contour for a Morse oscillator in the purely classical approximation, but he did not take into account the factor $\rho_n(x)$.

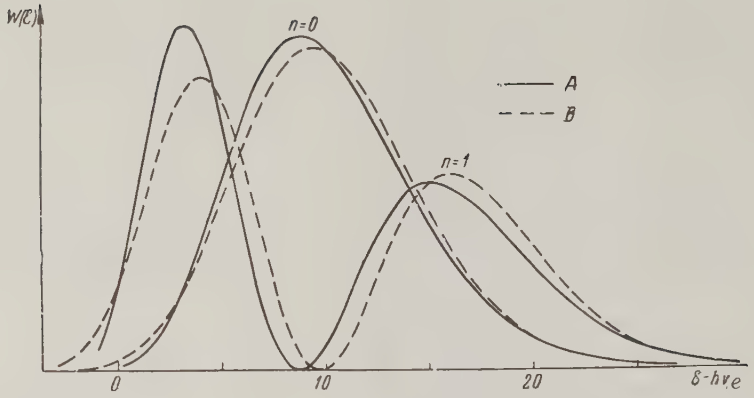

Fig.2. Probability distribution $W(E)$ for electronic-vibrational transitions from the initial vibrational levels with $n = 0$ and 1 in the case when $a > 9$: A - quantum mechanical distribution (according to Eq.(5)) converted to a continuous energy scale; B - semiclassical distribution (according to Eq.(7)).

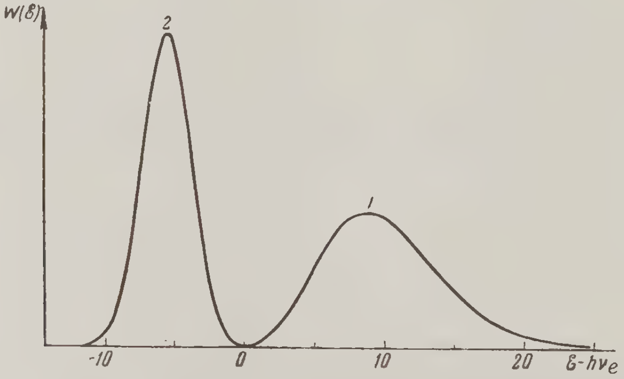

Fig.3. Quantum mechanical probability distributions $W(E)$ for electronic-vibrational transitions from the initial $n = 0$ level converted to a continuous energy scale: 1 - in the case when $a > 0$ (see Fig.1); 2 - in the case when $a < 0$. For the location of the potential curves shown in Fig.1, 1 corresponds to the absorption band at T = = 0; 2 corresponds to the emission band at T = 0 (strictly speaking for obtaining the contour of the emission band the ordinates of curve 2 should be multiplied by ν^3, where ν is the emitted frequency).

the assumption that the first part of the Franck-Condon principle (constancy of coordinates and momenta) is fulfilled exactly but that the coordinate distribution in the initial state is described by quantum mechanics (method B in Ref.2). Careful comparison of the curves substantiates the deductions arrived at in our preceding paper relative to the agreement betwen quantum mechanical and semiclassical calculations.

The role of anharmonicity is illustrated in Figs.1 and 3. It will be seen that the appreciable influence of anharmonicity is evinced in the potential curve of the final state. There are two possibilities as regards approximation of this curve by a parabola. If we replace it by a parabola obtained by expansion of the orse potential into a series about the point of equilibrium of the final state scillator, there obtain appreciable divergences (Fig.1). The agreement is ap- reciably better if the expansion is carried out about the point of equilibrium f the initial oscillator.

The results may be formulated as follows[2,18,19]. The principal influence of nharmonicity is evinced through change in the curvature of the section of the inal potential curve that is important in the classical treatment. Hence one an approximately take into account the anharmonicity by replacing both curves by arabolas, but in this case the absorption is determined by one pair of parabolas, hile the emission is characterized by a different pair.

It will be evident from Fig.3 that for equal true vibration frequencies (in dentical systems of vibrational levels) one can obtain an appreciable difference s regards the half-width of the spectra. For the chosen location of the potential urves (Fig.1) the normalized absorption spectrum is appreciably wider than the mission spectrum. It can be seen from Eq.(5) that for unequal dissociation ener- ies (different systems of vibrational levels) the point of intersection of the ormalized spectra does not coincide with the energy of a purely electronic transi- ion.

The third model that is of interest is the harmonic oscillator in which both he position of equilibrium and the frequency change incident to an electron transi- ion. The Franck-Condon integrals for this case were calculated by Hutchisson[3] and agner[5] (formulas for the spectra were also deduced by Ratner & Zil'berman[20]). he results of integration were obtained in very complex form unsuitable for prac- ical calculations, so that actually no final calculations were carried out by eans of these formulas.

Owing to the possibility of varying the dissociation energy D and D', one can ith high accuracy (in principle any desired degree) approximate the parabolas by orse curves and use the relatively simple formulas (5) and (6) for calculation.

We are sincerely grateful to B.I.Stepanov for his interest in the work and aluable discussions. We are also indebted to graduate students A.Purga and V. hizhnyakov for help in the calculation.

artu State University,
nstitute of Physics and Astronomy,
cademy of Sciences of the Estonian SSR

References

1. G.Herzberg, Spectra and Structure of Diatomic Molecules (Cited in Russian rans., M., 1949).
2. K.K.Rebane, A.A.Rentel' & O.I.Sil'd, Inzhenerno-fiz.zhur. (Engineering- hysics Journal), 2, 60 (1959).
3. E.Hutchisson, Phys.Rev., 36, 410 (1930); Ibid., 37, 45 (1931).
4. M.A.Krivoglaz, Zhur.eksp.i teor.fiz., 25, 191 (1953).
5. M.Wagner, Naturforsch., a, 14, 81 (1959).
6. D.L.Dexter, Nuovo Cimento, Supplemento, VII, Serie X, Nr.2, 245 (1958).
7. D.Bates, Monthly Notices Roy.Astron.Soc., 112, 614 (1952); R.W.Nicholls, .Chem.Phys., 24, 1104 (1956); P.Fraser, W.R.Jairman, Proc.Roy.Soc., A, (London) 6, 1145, 1153 (1953); W.R.Jairman, P.A.Fraser & R.W.Nicholls, Astrophys.J., 118, 28 (1953); Ibid., 119, 286 (1954); Ibid., 122, 55 (1955).
8. B.I.Stepanov, Lyuminestsentsiya slozhnykh moleku (Luminescence of complex olecules), Pub.Belorussian ASR Ac. of Sci., 1955.
9. B.S.Neporent, Trudy GOI (Proceedings, State Optical Institute), Session n commemoration of S.I.Vavilov, M., 1953.

10. F.Williams, J.Chem.Phys., 19, 457 (1951); F.Williams & M.Hebb, Phys.Rev., 84, 1181 (1951); C.Klick, J.Phys.Chem., 57, 776 (1953).

11. N.N.Kristofel', Optika i spektroskopiya, 7, 78 (1959) (Trans.Optics & Spectroscopy); Trudy (Proceedings), Inst. of Phys. & Astronomy, Estonian SSR Ac. of Sci., No.7, 85 (1958); No.7, 112 (1958); No.10, 3 (1959); No.10, 43 (1959).

12. Ya.Ya.Kirs,Ibid., No.4, 108 (1956).

13. K.K.Rebane, Ibid., No.7, 62 (1958).

14. N.E.Lushchik & Ch.B.Lushchik, Ibid., No.6,5 (1957); Ch.B.Lushchik, N.E. Lushchik & K.K.Shvarts, Ibid., No.8, 3 (1958).

15. L.Landau & E.Lifshits, Kvantovaya mekhanika (Quantum mechanics), Part 1, M., 1948.

16. I.M.Ryzhik & I.S.Gradshtein, Tablitsy integralov, summ, ryadov i proizvedenii (Tables of integrals, sums, series and products), M., 1951.

17. N.G.Bakhshiev, Optika i spektroskopiya, 6, 250 (1959). (Trans.Optics & Spectroscopy.)

18. E.-M.Simm, Thesis, Tartu State University, 1957.

19. A.Vernitskaya, Thesis, Tartu State University, 1959.

20. A.M.Ratner & G.E.Zil'berman, Doklady na III Soveshchanii po teorii poluprovodnikov (Report presented at the 3rd Conference on the Theory of Semiconductors L'vov, 1959.

ELECTRONIC SPECTRA OF ANTHRAQUINONE VAPORS

- N.A.Borisevich & V.V.Gruzinskii

1. Owing to their practical and scientific importance compounds of the anthrauinone series have long attracted the attention of spectroscopists. There are any publications on the electronic absorption spectra of solutions of anthraquione and its derivatives.[1-6] The available data on the luminescence of anthraquione solutions, however, are conflicting.[7,8] Förster[8] reported that luminescence is exhibited by those derivatives of anthraquinone in which intramolecular hydrogen bonds may form. Recently, Shigorin et al[9] investigated the luminescence of frozen solutions of anthraquinone by the method of E.V.Shpol'skii.

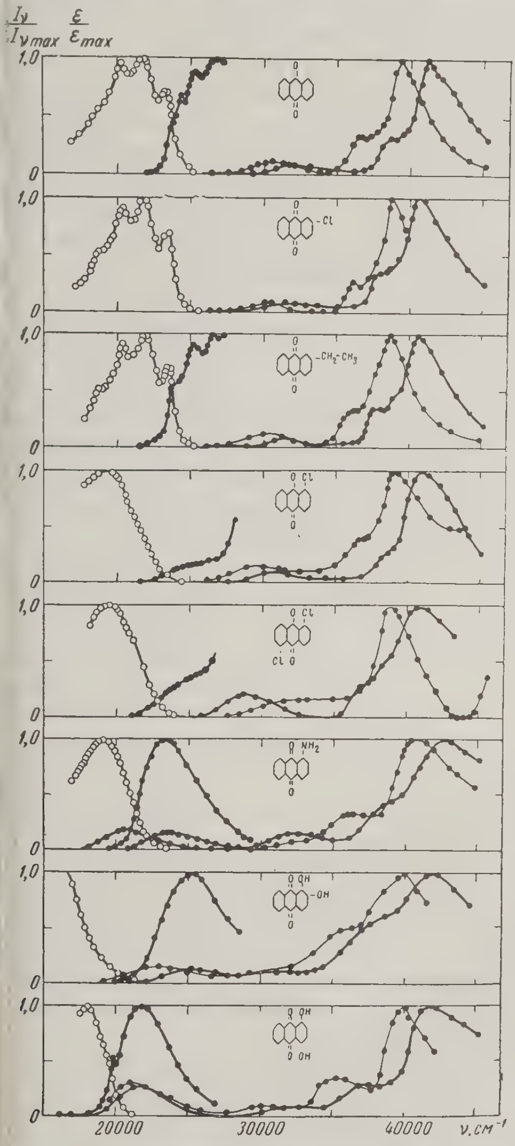

ig.1. Fluorescence spectra of the apors, and absorption spectra of he vapors (heavy lines) and soluions (light lines) of anthraquione and its derivatives: open oints - fluorescence; solid points absorption.

Fluorescence of anthraquinone vapor was observed back in 1895 by Wiedemann & Schmidt[10]. Karyakin & Terenin[3,11] list 24 anthraquinone derivatives that fluoresce in the vapor state; these authors made a careful study of the quenching effect of oxygen on the fluorescence of the vapors and adsorbates of these substances.

2. The present work was devoted to a systematic investigation of the fluorescence and absorption spectra of eight anthraquinones.

The fluorescence spectra was measured by means of a high sensitivity photoelectric spectrometer; the absorption spectra - by means of a photoelectric set-up assembled about an SF-4 spectrophotometer. The measurements were carried out under vacuum conditions (10^{-5} mm Hg). For the investigation we chose the following anthraquinones, differing as regards the position and character of the substituent groups: anthraquinone (I), 2-chloroanthraquinone (II), 2-ethylanthraquinone (III), 1-chloroanthraquinone (IV), 1,5-dichloroanthraquinone (V), 1-aminoanthraquinone (VI), 1,2-dihydroxyanthraquinone (alizarin) (VII), and 1,4-dihydroxyanthraquinone (quinazarin) (VIII). All the compounds were thoroughly purified by recrystallization and subsequent vacuum distillation.

3. The experimental results are shown in Figs.1 & 2. Fig.1 gives the luminescence spectra of the vapors and the absorption spectra of the vapors and solutions in ethyl alcohol; here we also give the structural formulas for each compound. The relative scale units are the values of the intensity at the peak of the fluorescence band of the vapors and the optical density at the peak of the shortest wavelength absorption band of the vapors and solutions. We note that anthraquinones I-V

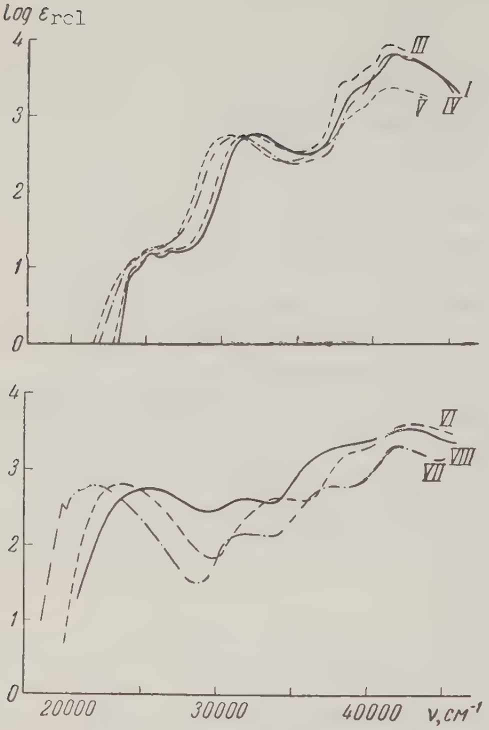

Fig.2. Relative absorption coefficients of anthraquinone vapors.

are characterized by exceptionally weak absorption in the long wavelength region, adjacent to the luminescence spectrum. Only by substantially increasing the concentration* can one obtain for these substances a long wavelength absorption band of noticeable intensity; this band overlaps greatly with the second absorption band. The long wavelength sections of the absorption spectra of the vapors of all the investigated compounds are shown to an enlarged scale in Fig.1. Here the unit value is the optical density at the peak of the long wavelength absorption band, if it is clearly evinced.

In Fig.2 the absorption spectra are plotted to a logarithmic density scale, which is convenient for comparing the relative values of the absorption coefficient over the spectrum.

It will be evident from Figs.1 and 2 that the investigated anthraquinones differ as regards their spectra. The fluorescence spectra of substances I, II and III exhibit structure, which is only slightly smeared out with increase of the vapor pressure (0.02-17 mm Hg) and temperature (160-350°). The long wavelength absorption band of the vapors also shows structure, which qualitatively repeats the structure of the fluorescence band.** In the fluorescence band and the long wavelength absorption band there appear four peaks with a frequency separation of 1600 cm^{-1} and 1400 cm^{-1}, respectively. In general the spectra of these three compounds are virtually identical.

No distinct structure is observed in the fluorescence spectra and the first absorption bands of compounds IV and V (at most there are discernable only traces of structure). The fluorescence spectra of these substances are shifted some 1600 cm^{-1} to the side of longer wavelengths relative to the spectra of compounds I, II and III.

A common characteristic of substances I through V is the relatively weak absorption in the range of the long wavelength absorption bands. The absorption coefficient at the peak of this (first) band is the spectra of both vapors and solutions is approximately two orders of magnitude lower than the coefficient at the peak of the second band. This may be why a number of authors[2,3,5] have mistakenly identified what is actually the second absorption band, peaking at a 325 mμ, as the long wavelength absorption band.

The weak long wavelength absorption band of anthraquinones should be attributed to $n \rightarrow \pi^*$ transitions.[13]

---

*The vapor pressure is given in the literature[12] only for anthraquinone and quinazarin. In measuring the long wavelength absorption band of these substances the pressures were 1.8 and 0.1 mm Hg, respectively. The short wavelength absorption bands of these substances are clearly evinced at a pressure of 0.01 mm Hg in each case.

**The long wavelength band of substance II was not studied in detail.

As regards their spectra substances VI, VII and VIII form a separate group. hey are characterized by intense fluorescence in the vapor state. In contrast o the foregoing compounds, these anthraquinones exhibit appreciable luminescence n ethyl alcohol solutions. The fluorescence spectra of the vapors and the adacent absorption band are shifted into the long wavelength region. The shortest avelength absorption band is shifted to the opposite side. The first absorption and in the spectra of vapors and solutions is evinced at ordinary concentrations. he coefficient at the peak of the long wavelength absorption band of quinazarin IV) vapor is approximately two orders of magnitude greater than the absorption oefficient at the peak of the same band in the spectrum of anthraquinone (I) (Fig.).

4. The above described differences in the spectra of the investigated anthrauinones can in general be associated with structural features of the molecules. haracteristic structure is evidenced in the spectra of anthraquinone and its deriatives in which the substituent is in the β-position. Shigorin, Shcheglova & Nurukhametov, investigating these compounds in frozen solutions, detected a line tructure and found that the frequency difference between the corresponding compoents and the principal bands averages 1664 cm^{-1}. They attributed this frequency o the CO group. The structure observed in the spectra of vapors (component sepaation 1600 cm^{-1}) may also be associated with the CO group.

If the substituent is in the α-position (compounds IV-VIII) then, owing to nteraction of the substituent with the CO group, the spectrum is shifted to the ong wavelength side (the height of the excited electronic level is lowered) and he structure is effaced. The strength of the interaction depends on the nature f the substituent group. In the case of OH and NH_2 groups, there forms an intraolecular hydrogen bond[14], which has a strong effect on the electronic configuration f a molecule. The above described features of the electronic spectra of compounds I, VII and VIII can be explained by formation of intramolecular hydrogen bonds in hese molecules.

We desire to express our gratitude to P. I. Petrovich for his interest in the ork.

nstitute of Physics,
cademy of Sciences of the USSR

References

1. Lewis & Calvin, Chem.Rev., 25, 273 (1939).
2. Morton & Earlam, J.Chem.Soc., 159 (1941).
3. A.V.Karyakin, Zhur.fiz.khim., 23, 1332 (1949).
4. Hartman, Z.Naturforsch., 7a, 36 (1952).
5. Labhart, Helv.chim.acta, 15, 1410 (1957).
6. Maran & Stonehill, J.Chem.Soc., 765 (1957).
7. J.A.de Ment, Fluorochemistry, N.Y. 1945.
8. Förster, Fluoreszenz organischer Verbindungen. Göttingen, 1951.
9. D.N.Shirogin, N.A.Shcheglova & R.N.Nurmukhametov, Izv.AN SSSR, Ser.fiz., 3, 37 (1959). (Trans.Bulletin, 23, 39.)
10. Wiedemann & Schmidt, Ann.Phys., 56, 18 (1895).
11. A.V.Karalnik & A.N.Terenin, Izv.AN SSSR, Ser.fiz., 13, 9 (1949).
12. Handbook of Chemistry & Physics, Chem.Rubber Co., 1955.
13. Sidman, J.Am.Chem.Soc., 72, 4567 (1956).
14. D.N.Shirogin & N.S.Dokunikhin, Doklady AN SSSR, 100, 323, 745 (1955); N.Shirogin, M.M.Shemyakin, L.A.Shchukina, M.N.Kolosov & F.A.Mendelevich, Doklady N SSSR, 108, 672 (1956). (Trans. - Doklady.)

Discussion

R.N.Nurmukhametov: The continuous character of the emission and absorption spectra of substances in the third group (with an intramolecular hydrogen bond) can be understood on the basis of the data obtained in our laboratory. The presence of an H bridge in a molecule of an α-derivative of anthraquinone leads not simply to shift of the electron levels but to a substantial redistribution of the molecular energy over electronic-vibrational sublevels. For example, the spectrum of 1,2-aminochloroanthraquinone consists of diffuse ($\Delta\nu \approx 150\text{-}200\ \mathrm{cm}^{-1}$) equidistant bands with a vibrational difference of 440 cm^{-1} in the emission spectrum and 420 cm^{-1} in the absorption spectrum. The presence of a resonance band indicates that the observed emission is fluorescence, whereas anthraquinone itself and a number of its derivatives in solid solutions phosphoresce. The spectra of compounds in the third group are also diffuse at low temperatures; their bands are separated by a small interval and generally overlap in the vapor state as a result of additional broadening.

V.V.Gruzinskii: As noted in our report, the spectra of anthraquinone derivatives IV through VIII in the vapor state are not only shifted to the long wavelength side but also are devoid of structure. The fact that the structure is effaced is obviously the result of redistribution of energy among the electronic-vibrational sublevels. According to the data of Karalnik, the luminescence persistence of the vapors of anthraquinone and some of its derivatives is of the order of 10^{-9} sec.

LUMINESCENCE OF ANTHRACENE SOLID SOLUTIONS

- V.L.Broude & V.S.Medvedev

A number of authors in investigating the variation of the luminescence intensiy of crystals as a function of the wavelength of the exciting light detected flucuations in the emission intensity for certain wavelengths.[1-4] Such fluctuation n the luminescence excitation curve is usually explained by the specific influence f the surface of the sample on radiative annihilation of the excitons diffusing owards it.

Hence of particular interest is investigation of the luminescence spectra of aterials in which the exciton mechanism of energy transfer is suppressed. We inestigated the luminescence of different solid solutions of anthracene excited in he region of absorption of anthracene and transmission of the solvent. The excitnt light from a DKSSh-1000 tube was discriminated by a DSF-8 monochromator (reiprocal dispersion 3 Å/mm). A second small monochromator (150 Å/mm) isolated the elected interval in the luminescence spectrum of the sample, which was mounted in n integrating sphere. The emission was detected by means of an FEU-19 photomultilier. In all cases the thickness of the sample was taken such as to insure 100% bsorption of the incident light.

By way of solvents we used styrene, polystyrene, dihydroanthracene and naphhalene. In the first case the anthracene was dissolved in fresh styrene directly fter its distillation. In the case of polystyrene and naphthalene the samples were repared by adding a weighed amount of anthracene to the molten solvent (polystyrene t 100-120°; naphthalene at 80°). In the case of anthracene in dihydroanthracene, e used a material containing approximately 1-2% anthracene as an impurity.

In the case of all the enumerated samples we observed a virtually constant uminescence yield over the entire region of absorption of anthracene, correspondng to the first electronic transition (3950-3300 Å); an abrupt fall-off of the ield was observed only at the long wavelength edge* (Fig.1).

An entirely different situation was encountered in investigating copolymers of nthracene and styrene obtained by polymerization of solutions of anthracene in styene at 150-170° for 5-6 hours. The spectral distribution of luminescence curve for uch a copolymer and the absorption curve for the same sample are shown in Fig.2.

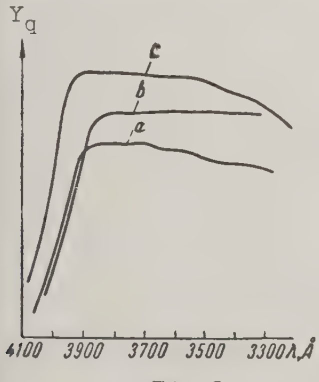

Fig.1

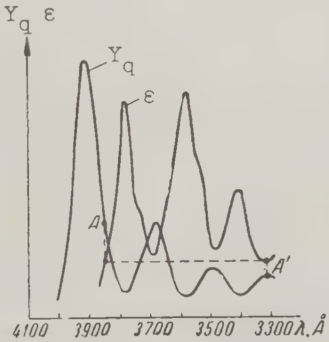

Fig.2

ig.1. Spectral distribution of the luminescence ield of solutions of anthracene in a) styrene, b) polystyrene, c) dihydroanthracene.

Fig.2. Spectral distribution of the luminescence yield and the absorption spectrum of anthracene-polystyrene copolymer.

As in the case of the excitation spectrum of anthracene crystals[2], in this case there is anticorrelation between the luminescence quantum efficiency and the absorption coefficient in the range of individual bands; in other words, in the wavelength scale a peak in the absorption spectrum corresponds to a minimum in the luminescence spectrum. On the other hand, as may be seen in Fig.2, concurrently with a general decrease of absorption in going to the short wavelength side (within the range of the first electron transition in the anthracene molecule) the luminescence yield decreases. Hence there is no unique, consistent relation between the absorption coefficient and the luminescence intensity: at different frequencies characterized by the same absorption coefficient the yield may differ appreciably (for example points A and A' in Fig.2).

---

*The nature of this abrupt decrease in luminescence has been repeatedly discussed in literature[5]; according to some authors, the fall-off is connected with increase of the effective wavelength owing to weak inactive secondary absorption.

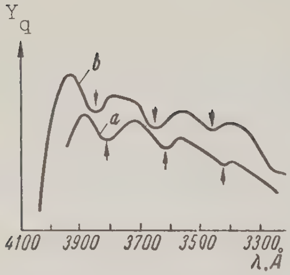

Fig.3. Spectral distribution of the luminescence yield of solid solutions of anthracene after irradiation of the sample: a) in polystyrene, b) in dihydroanthracene.

Analysis of the possible experimental errors and special control tests showed that the structure observed in the luminescence curve is not connected with or due to inactive absorption by some impurity, reabsorption of the luminescence light, anisotropy of the emission, inhomogeneity in the anthracene distribution through the sample, or selective absorption of the exciting light.

We obtained luminescence spectra at 20°K of both anthracene solutions in polystyrene and of the products of copolymerization of anthracene and styrene. From the fact that these spectra are similar as regards position of the peaks and general character to the luminescence spectrum of anthracene solutions in alcohol, it may be inferred that microcrystals of anthracene did not form in our samples.

Investigation of copolymer samples with anthracene concentrations from 0.05 to 10% (by weight) showed that the appearance of the luminescence curve (positions and relative intensities of the individual peaks) does not depend on the concentration. The absence of concentration dependence indicates that the observed structure in the luminescence yield curve cannot be explained by energy migration between anthracene impurity molecules.*

A similar structure in the excitation spectra of solid solutions of anthracene in polystyrene, naphthalene and dihydroanthracene became evident after prolonged irradiation of these samples through a Wood's filter (transmission peak at 3800 Å). Some of these excitation spectra after prolonged irradiation of the samples are shown in Fig.3 (compare with Fig.1). We found that irradiation leads to changes not only in the surface layer but virtually throughout the thickness of the sample, i.e., to the depth of penetration of the exciting light. This was verified by tests on samples from which we removed successive surface layers.

Our experimental results can be understood if we assume that in the course of copolymerization of anthracene with styrene, the anthracene molecule is somehow incorporated into the polystyrene chain[6,7] and hence finds itself in the copolymer under conditions differing from those in a conventional solid solution. Experiments show that such incorporation of a molecule into a chain or its association with other molecules is realized as a result of the photochemical influence of ultraviolet radiation. To check this inference, we carried out a special series of measurements of the luminescence yield of a solution of anthracene-polystyrene copolymer in liquid benzene. It was found that the luminescence yield curve in this case is virtually identical with the curve for the solid polymer (curve A in Fig.3). This indicates, first, that the anthracene molecule is actually incorpor-

---

*The absolute emission intensities were not measured; hence we cannot say anything definite regarding the concentration dependence of the integral luminescence intensity.

ed into the polystyrene chain and remains in the chain even upon solution of
e polystyrene and, second, that the reason for the appearance of structure in
e luminescence spectrum is the "interaction" between the anthracene molecule and
e polymer chain that arises incident to incorporation of the molecule into the
ain.

The character of the incorporation of the anthracene molecule into the polymer
ain and the nature of the forces retaining it in the chain are as yet unclear.
might be assumed[7] that the anthracene molecule forms a valence bond with the
yrene link. However, the observed small (<50 Å) shift of the absorption spectrum
solutions of the copolymer relative to the spectrum of a solution of anthracene
hexane may be taken as evidence against this hypothesis.*

It is known[9] that in copolymerization of anthracene and styrene part of the
thracene molecules (1 molecule per two polymer chains) is incorporated into the
lymer chain, forming a valence linkage in position 9 or 10. The effect observed
us is not connected with a small group of incorporated molecules; it is charac-
eristic for the entire amount of anthracene introduced into the copolymer. A di-
ect check of this was furnished by investigation of the excitation spectra of co-
lymers of styrene and 9,10-dimethylanthracene. It was found that the polymeriza-
ion product in which the possibility of a valence linkage of the 9,10-dimethyl-
thracene molecule with the polymer chain is precluded[9], exhibits pronounced struc-
ure in the luminescence spectrum, which may be taken as evidence of nonvalence
ype incorporation of the molecules into the chain.

Thus on the basis of the observed spectral distribution of the luminescence
ields of the copolymers and the behavior of their luminescence spectra it may be
sserted that the anthracene molecule forms labile nonvalence linkages with the
lymer chain, linkages that may be realized through the interaction of the π-
ectron systems (so far we have not been able to observe a similar clearly pro-
unced structure in the excitation spectrum of anthracene-polymethylacrilate co-
lymer).

The formation of such linkages may be responsible for partial diversion of
e excitation energy at different wavelengths and thus may be responsible for the
pearance of structure in the luminescence spectra. The nature of this energy
umping" and how it may be related to the structure and nature of the spectra re-
ains unclear. It is evident from the results obtained so far, however, that for
plaining the structure in the luminescence curves one can have recourse not only
the usual hypothesis of migration of excitons towards the surface of the sample
t also to the concept of some type of interaction of the molecule with the sur-
ounding medium (the polymber chain). The question of how such interactions can
use fluctuation of the luminescence yield over the wavelength scale is a subject
r further investigation. The observed effect of fluctuations of the quantum
ield in the presence of labile linkages between the luminescent molecule and the
dium may be interpreted as selective external quenching for different wavelengths
the exciting light.

It would be of interest to determine whether a similar selectivity as regards
citation wavelengths does not operate in other known cases of external quenching
luminescence such as concentration quenching and quenching by "luminescence
illers". Clarifying this matter, we believe, may help establish the nature of
ternal quenching of luminescence in general.

stitute of Physics,
ademy of Sciences of the Ukrainian SSR

---

*It is known that replacement of one hydrogen in the anthracene molecule by
CH$_3$ group results in an appreciably greater (120 Å) shift of the spectrum.[8]

References

1. G.T.Wright, Proc.Phys.Soc., B68, 701 (1955).
2. M.D.Borisov & V.N.Vishnevskii, Ukr.fiz.zh. (Ukrainian physics jour.), 1, 371 (1956).
3. C.C.Klick, Phys.Rev., 98, 274 (1953).
4. V.L.Broude, V.V.Eremenko & V.S.Medvedev, Zhur.tekh.fiz., 28, 2563 (1958). (Trans.Soviet Physics - Tech.Physics.)
5. B.I.Stepanov, Uspekhi fiz. nauk, 58, 3 (1956).
6. F.H.Krenz, Trans.Faraday Soc., 51, 172 (1955).
7. H.H.Hinrichs, Z.Naturforsch., a., 9, 617 (1954).
8. A.S.Cherkasov, Optika i spekro., 4, 496 (1959). (Trans.Optics & Spectroscopy.)
9. E.V.Anufrieva, M.V.Vol'kenshtein & M.M.Koton, Zhur.fiz.khim. (J.Phys.Chem), 31, 1532 (1957).

LUMINESCENCE OF CRYSTALLINE NAPHTHALENE CONTAINING MINOR IMPURITIES

- M.T.Shpak & E.F.Sheka

1. There have been numerous investigations of the luminescence of molecular rystals, but the question of the nature of the luminescence of such crystals is till open.

Analysis of the experimental data in the literature shows that in most cases he luminescence of molecular crystals is associated with the emission of impuriies or structural defects, which are inevitably present in actual crystals.[1] esonance (coincidence) of the short wavelength bands in the luminescence spectra ith the highly polarized long wavelength intrinsic absorption bands, which, acording to Davydov[2], are connected with the formation of free excitons in the crysal, was observed at low temperatures (77°K) only in the spectra of naphthalene rystals.[3]

2. The intense luminescence spectrum of crystalline naphthalene at 20.4°K beins with a band at 31 060 cm^{-1} that coincides with a weak band in the absorption pectrum.[4] The intensity of this weak absorption band differs in the absorption pectra of different batches of naphthalene. It was established by deliberate ntroduction of impurities that the band with ν = 31 060 cm^{-1} is due to β-methylaphthalene impurities.[5] This indicates that the familiar luminescence spectrum f crystalline naphthalene is essentially an impurity effect.

3. In the luminescence spectrum of crystalline naphthalene purified of β-ethylnaphthalene by zone melting, there was observed a weak band, polarized in he *a* direction, at 31 480 ± 3 cm^{-1} (A band), which virtually coincides with the ighly polarized A_1 band (ν = 31 476 cm^{-1}) in the crystal absorption spectrum.[6] he intensity of the A band increases for higher purity samples (Fig.1).

With increase of the temperature to 77°K there appears in the luminescence the crystal another band with ν = 31 623±3 cm^{-1} (B band), which is polarized the *b* direction and coincides with the second highly polarized B_1 band in the sorption spectrum of the crystal at 77°K (Fig.2).

Increase of the temperature to 200-210°K leads to smearing out and partial polarization of the A and B bands, and also to the appearance of a new short velength band at 31 900 cm^{-1} (I band), which may be matched with the band at 956 cm^{-1} in the absorption spectrum of crystalline naphthalene at 20.4°K (Fig.3).

Further increase of the naphthalene temperature to 20°C and higher leads to ticeable enhancement of all the short wavelength luminescence bands, to complete polarization of these bands and to the appearance of a broad weak band located the region of the strongly polarized A_2 and B_2 absorption bands (at 20.4°K).[6]

Moreover, in the absorption spectra of ~5-7 mm thick naphthalene single crysls at 77°K and higher there is observed a long wavelength band with ν = 31 100 $^{-1}$, the intensity of which increases with increasing temperature. Apparently is band is associated with 1→0 transitions.

4. If we accept that the strongly polarized A_1 and B_1 absorption bands are mponents of Davydov splitting of the 0→0 transition[7], the experimental results tained in the present study can be interpreted as follows.

The light energy absorbed by the crystal is transferred by excitons migrating rough the crystal from the host lattice to the impurity molecules, where the radiive de-excitation occurs. Obviously, with increase in the purity of the crystal e probability for collision of excitons with impurity molecules is reduced. This ads to the appearance of luminescence associated with transitions from exciton ates to the ground state, i.e., to the appearance of highly polarized intrinsic exciton luminescence of the crystal; it may be noted that at 20.4°K there is obrved in the luminescence spectrum only one component (the A band) associated with ansitions from the lowest lying exciton band to the ground state.

It was shown by Broude et al[1] that at low temperatures exciton luminescence must in general be highly hindered. Increase in the intensity of this luminescence compared with other forms of luminescence is possible with rise in temperature. This

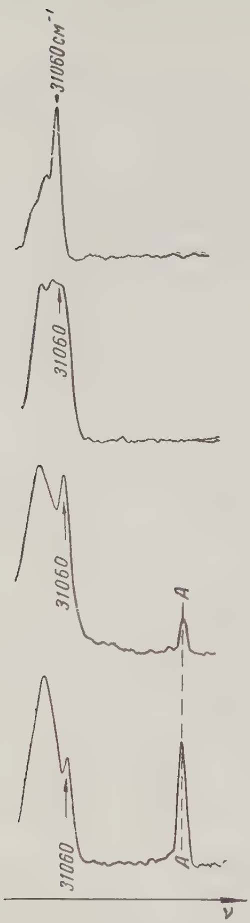

Fig.1

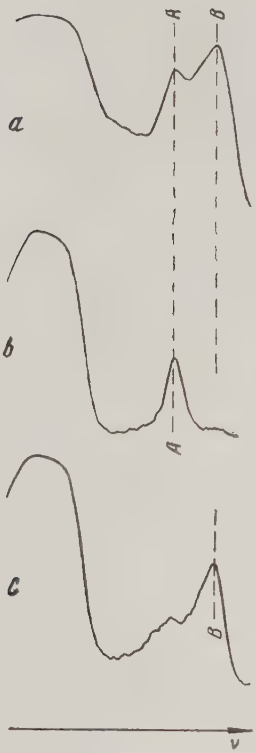

Fig.2

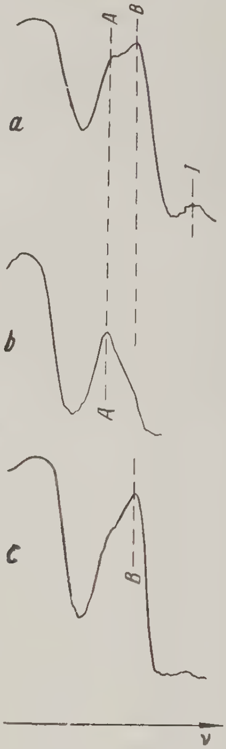

Fig.3

Fig.1. Microphotometric traces of the luminescence spectra of crystalline naphthalene at 20.4°K (nonpolarized light). The concentration of β-methylnaphthalene in the investigated samples decreases from the top to the bottom spectrum.

Fig.2. Traces of the luminescence spectra of crystalline naphthalene at 77°K: a) nonpolarized light, b) *a* component, c) *b* component.

Fig.3. Traces of the luminescence spectra of crystalline naphthalene at 200-210°K: a) nonpolarized light, b) *a* component, c) *b* component.

process will compete with enhancement of nonradiative transitions.

The experimental data given above indicate that with increase of the temperature the intrinsic luminescence of naphthalene crystals is stimulated (there appear new bands). This can be explained by the fact that in the case of crystalline naphthalene, the nonradiative transitions are compensated for by increase in the population of the exciton bands owing to increase of kT.

Depolarization of the strongly polarized A and B bands with increase in temperature is probably connected with disturbance of the translational symmetry of the lattice by thermal density fluctuations and the formation of a larger number of defects in the crystals at elevated temperatures.

5. Thus in the case of crystalline naphthalene with a minor impurity content

e have succeeded in observing luminescence which in view of its behavior may be alled "exciton luminescence".

nstitute of Physics,
cademy of Sciences of the Ukrainian SSR

References

1. V.L.Broude, A.F.Prikhot'ko & E.I.Rashba, Uspekhi fiz nauk, 67, 99 (1959). Trans.Soviet Physics - Uspekhi.)
2. A.S.Davydov, Teoriya pogloshcheniya sveta v molekularnykh kristallakh Theory of light absorption in molecular crystals), Kiev 1951.
3. D.Griessbach, G.Will & H.C.Wolf, Z.Naturforsch., 11a, 791 (1956).
4. I.V.Abreimov & K.G.Shabaldas, J.Phys., 7, 168 (1943).
5. A.F.Prikhot'ko & M.T.Shpak, Optika i spektro., 6, 119 (1959). (Trans. ptics & Spectroscopy.)
6. A.F.Prikhot'ko, Zhur.eksp.i teor.fiz., 19, 383 (1949).
7. D.S.McClure & O.Schnepp, J.Chem.Phys., 23, 1575 (1955).

CONCERNING THE LUMINESCENCE AND PHOTOCONDUCTIVITY OF ANTHRACENE CRYSTALS

- A.N.Faidysh

Owing to the migration of the excitation energy in organic crystals such as naphthalene and anthracene, the surface and diverse impurities and defects may exert an appreciable influence on the luminescence and photoconductivity. Investigation of this influence should be of help in clarifying the nature of the luminescence spectrum and serve to establish the actual overlapping of the absorption and luminescence spectra, which overlapping is indicative of the probability of electronic excitation energy transfer from one molecule to another.

1. Influence of the surface and impurities on the luminescence of anthracene

According to the phenomenological theory of the diffusive motion of excitons proposed earlier by the writer[1,2], the quantum yield of the host material is

$$B_Q = \frac{K}{1-K^2\lambda^2}\frac{1}{1+\gamma C_\rho}\left[H_0\alpha_0\left(-\frac{1}{\lambda}\frac{1+e^{-Kd}}{1-e^{-Kd}}\,th\,\frac{\lambda d}{2}+\frac{1}{K}\right)+\frac{s}{\lambda_0^2}\left(\lambda\frac{1+e^{-Kd}}{1-e^{-Kd}}\,th\,\frac{\lambda d}{2}-K\right)\right],$$

where λ is the reciprocal of the exciton diffusion length, K is the absorption coefficient for the exciting light, and d is the thickness of the crystal.

The first term in this formula characterizes the volume emission; the second, the emission of molecules located at the surface. Calculations by means of this formula show that in going from thick films ($d > 1\ \mu$) to thin ones ($d = 0.1\ \mu$) the relative percentage of surface radiation increases from 30 to 80%.

In the case of anthracene microcrystals, such as those obtained by recrystallization in a solid solution, virtually all the emission occurs from the surface. If one introduces such a defect-producing impurity as naphthalene into an anthracene crystal, as a result of migration of the excitation energy, an appreciable part of the emission will occur from anthracene molecules located near naphthalene molecules;[3] as a result the luminescence spectrum will approach the spectrum of anthracene microcrystals in naphthalene.

The above described effect has been observed experimentally. Fig.1 shows the distribution of the intensity in the luminescence spectra of crystals 10 μ and 0.1 μ thick, anthracene microcrystals in naphthalene ($c_a = 10^{-2}$g/g) and anthracene crystals doped with naphthalene ($c_n = 10^{-2}$g/g). The measurements were performed at 295° K (samples in vacuum); the intensities were normalized to the intensity at $\lambda = 428$ mμ, where the influence of reabsorption is minimal.[4] The principal differences between the spectra are due to shift of the bands and energy redistribution between some of the bands. The observed alterations are partially due to variation in reabsorption. However, the character of the shifts and the displacements of the long wavelength bands indicate that the changes are due primarily to the influence of the backing material (in case of thin films) and naphthalene molecules on the luminescence of anthracene. This inference is substantiated by the similarity of the energy distribution in the last three cases (the similarity would be even greater if one were to take into account reabsorption in the anthracene crystals doped with naphthalene and the luminescence of individual molecules in solutions of anthracene in naphthalene). It may be assumed that the great increase in the intensity of the short wavelength band is largely due to changes in the transition probability for molecules located at the surface of the crystal or near defects (naphthalene molecules).

As our experiments showed, the role of surface emission increases somewhat as a result of introduction into the anthracene crystal of exciton trapping impurities (naphthacene and phenazine).

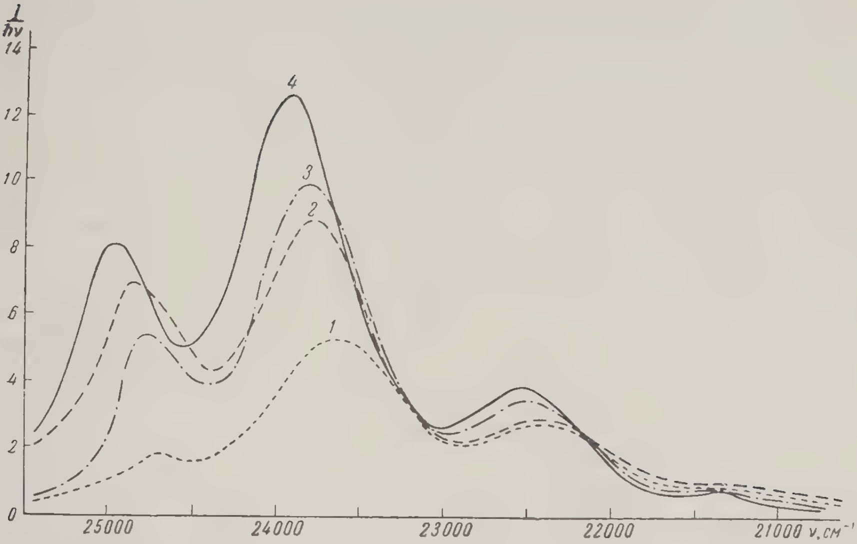

ig.1. Intensity distribution in the luminescence spectrum of anthracene at 290°K λ_{ex} = 365 mμ): 1) 11 μ thick anthracene film, 2) 0.1 μ anthracene film, 3) 5 μ nthracene film doped with naphthalene, 4) 12 μ naphthalene film doped with anthracene.

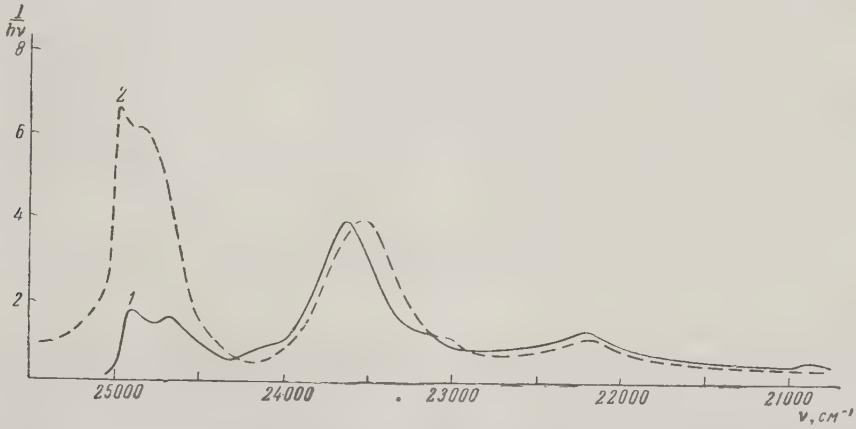

ig.2. Intensity distribution in the luminescence spectrum of anthracene at 90°K (λ_{ex} = 365 mμ): 1) 10 μ thick anthracene film, 2) 0.1 μ anthracene film.

Similar measurements were carried out at 90°K (Fig.2). The shifts with de- reasing temperature and decreasing thickness at the low temperature differ for ifferent bands. The increase in the intensity of the short wavelength band with eduction of the temperature is connected partially with increase in the proba- lity for different transitions (this is substantiated by experiments with a low ncentration of anthracene in naphthalene) and partially to decrease of reabsorp- on. The appreciable increase in intensity of the short wavelength band in going rom 10 μ to 0.1 μ thick crystals at 90°, when the influence of reabsorption is educed, is evidenced in favor of the inferred enhanced role of surface emission.

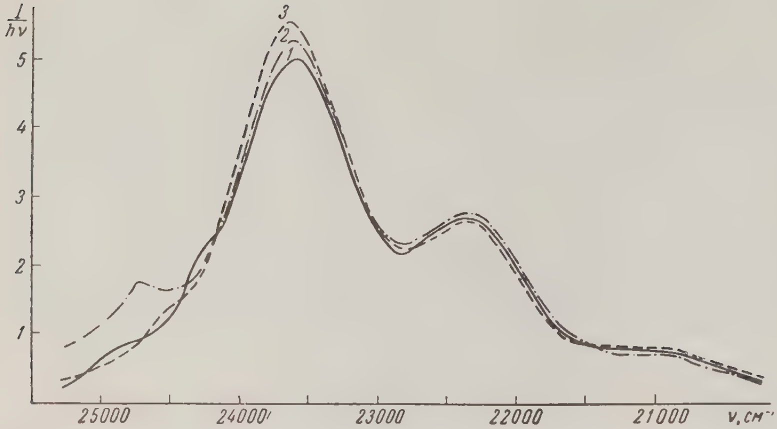

Fig.3. Intensity distribution in the luminescence spectrum of anthracene at 290°K: 1) 11 μ thick anthracene film, λ_{ex} = 313 mμ; 2) 11 μ thick anthracene film, λ_{ex} = = 365 mμ; 3) 10 μ thick anthracene film coated with phenazine, λ_{ex} = 365 mμ.

Doping anthracene crystals with phenazine or naphthalene has little effect on the luminescence spectrum at 90°K. The introductions of these impurities lead only to a change in the intensity ratio of the two peaks in the short wavelength band. That the influence of impurities is reduced at low temperatures is substantiated by our experiment which showed that the transfer of excitation energy from anthracene to phenazine diminished by an appreciable factor (~3) in going from 290° to 90°K.

In view of the hypothesized influence of the surface, the luminescence spectrum may be expected to depend on the absorption coefficient for the exciting light. Calculations show that in going from excitation at 365 mμ to excitation at 313 mμ, when the absorption coefficient falls off by a factor of about 4, the fraction of surface emission decreases from 30 to 6-7%.

As will be evident from Fig.3, this change in the excitation wavelength leads to an appreciable reduction of the intensity in the short wavelength region. This effect may be partially due to the difference between the energies of the exciting photons. If the influence of surface emission does have the importance indicated above, the application of a thin quenching film (phenazine[5]) to the surface of the anthracene crystal should have the effect of reducing the integral intensity and altering the spectrum in the short wavelength region. To check this hypothesis, we applied a 0.1 μ thick phenazine film to the surface of a 10 μ anthracene crystal (curve 3 in Fig.3).

Our measurements showed that without a phenazine coating the luminescence yield of anthracene does not change (to within 3-4%) in going from λ_{ex} = 365 mμ to λ_{ex} = 313 mμ. Application of a phenazine film, however, weakens the integral intensity in the first case by a factor of about 1.35, in the second case by a factor of 1.1. This is in fair agreement with the results of calculations by mean of the above formula. As might be expected, there is also observed a considerable weakening of the short wavelength band (in Fig.3 the intensities have also been normalized to that at 428 mμ).

The results of the above described experiments bear evidence to the appreciable influence of the surface and different impurities on the luminescence of anthracene. The influence of different lattice defects on the luminescence of anthracene crystals have been discussed by other authors[6-9].

2. Influence of oxygen and the conditions of preparation of anthracene crystals

If the sample is maintained under vacuum the photoluminescence intensity of anthracene does not change (within 2-3%) over a period of many hours. Irradiation with light in air, however, leads to the formation of photo-oxides which suppress the luminescence.[1,10,11] In our experiments we found that usually (occasional samples exhibit a markedly different behavior) at 90°K the intensity of photoluminescence remains constant. At 290°K, however, it falls off by approximately 20% after one hour of illumination, and at 360°K by 35-40%. It may be inferred, therefore, that a certain activation energy is necessary for the formation of photo-oxides; it may be assumed that some thermal agitation is necessary for sufficiently close approach of the anthracene and oxygen molecules.

The formation of photo-oxides probably occurs when an exciton approaches the point of direct contact between an anthracene and an oxygen molecule. Our experiments showed that the introduction of exciton trapping impurities (phenazine or naphthacene) greatly reduces the rate of photo-oxidation of anthracene; at a naphthacene concentration of 3.10^{-5} g/g the decrease in intensity is reduced by a factor of 5. In a number of cases at 360°K doping with phenazine or naphthacene leads to a certain increase in the intensity of photoluminescence of anthracene. This is due to decrease of energy transfer from the anthracene to the impurity molecules. The anthracene samples used in the above described experiments were prepared in air (melting or sublimation).

Samples prepared by vacuum sublimation strongly scatter light and their behavior differs appreciably from that of samples prepared in air. If one isolates the section of the luminescence spectrum near 4230 Å, it is found that the intensity in this region under irradiation with light increases by 15-30% over a period of two hours and by a factor of ~2 over a period of ten hours. Investigation of the spectra showed that in the case of samples prepared by vacuum sublimation there occurs a shift of the luminescence bands and appreciable redistribution in energy in the luminescence spectrum; specifically, the intensity of the 4230 Å band increases during irradiation.

It may obviously be inferred from the experimental results that under the influence of light there may occur structural changes in samples prepared under vacuum.

3. Photoconductivity

The photoconductivity in anthracene samples is of the impurity type and is strongly dependent on photo-oxidation.[12-14] The appearance of photoconductivity is probably due to the following processes (cf. Terenin[15]). As a result of absorption of light there are formed excitons in the crystal. Near photo-oxide formations there occur transitions from the singlet excited state to the triplet state, with subsequent trapping of the electron. The holes released as a result of this process are responsible for the photoconductivity.

If this hypothetical scheme is valid, exciton trapping impurities, such as naphthacene, should substantially reduce the photoconductivity in two ways: 1) by reducing the rate of formation of photo-oxides, and 2) by lowering the exciton concentration. Our experiments[14] substantiated the existence of these effects. Upon introduction of naphthacene into an anthracene crystal the rise of the photocurrent under illumination of the sample in air is greatly reduced owing to decrease of the rate of formation of photo-oxides. The magnitude of the photocurrent is also substantially decreased: at a naphthacene concentration of 3.10^{-5} mole/mole it falls off by a factor of ~4.5; at a naphthacene concentration of 6.10^{-4} mole/mole, by a factor of ~60 as compared with pure anthracene.

It should also be noted that the photoconductivity of single crystal films prepared by sublimation in air is strongly dependent on the crystallographic directions. Thus with the electrodes located along the *b* axis, the photoconductivity is 5 times greater than with the electrodes along the *a* axis. This obviously indicates that the effective mass of the current carriers in anthracene is strongly dependent on the field direction. This dependence, as well as the low mobility of the current carriers and the strong temperature dependence of the photocurrent, may be taken as an indication that the electric current in anthracene is due to transition of electrons from one molecule to another, the process involving surmounting of an energy barrier, the height of which depends on the separation between the molecules.

"T.G.Shevchenko" Kiev State University

References

1. I.Ya.Kucherov & O.M.Faidysh, Doklady AN Ukrainian SSR, No.1, 57 (1956).
2. A.N.Faidysh, Optika i spektroskopiya, 1, 595 (1958).
3. A.N.Faidysh, I.Ya.Kucherov & Ya.A.Tverskoi, Ibid., 1, 403 (1956).
4. I.Ya.Kucherov, A.N.Faidysh & Z.N.Fesendo, Ibid., 2, 462 (1957).
5. E.I.Bowen, E.Mikiewicz & F.W.Smith, Proc.Phys.Soc., A,62, 128 (1949).
6. A.F.Prikhot'ko & I.Ya.Fugol', Optika i spektroskopiya, 4, 375 (1958).
7. V.L.Broude, V.V.Eremenko, V.S.Medvedev, O.S.Pakhomova & A.F.Prikhot'ko, Ukr.fiz.zhur. (Ukrainian Physics Journal), 3, 232 (1958).
8. A.F.Prikhot'ko, Izv.AN SSSR, Ser.fiz., 22, 1312 (1958). (Trans.Bulletin, 22, 1304.)
9. J.W.Sidman, Phys.Rev., 102, 96 (1956).
10. M.D.Galanin & Z.A.Chizhikova, Zhur.eksp.i teor.fiz., 26, 224 (1954).
11. G.T.Wright, Proc.Phys.Soc., B,68, 701 (1955).
12. A.T.Vartanyan & I.A.Karpovich, Zhur.fiz.khim., 32, 178 (1958).
13. A.Bree, G.I.Carswell & L.E.Lyons, J.Chem.Soc., 23, 128 (1955).
14. O.M.Faidysh & Slobodyanik, Vistnik KDU (News, Kiev State Univ.), No.2, Phys. & Chem.Series, No.1, 3 (1959).
15. A.N.Terenin, Radiotekhnika i elektronika (Radio Eng. & Electronics), No.8, 1127 (1956).

EFFECT OF β-RADIATION ON THE PHOTOLUMINESCENCE OF MOLECULAR CRYSTALS

- Sh.D.Khan-Magometova, N.D.Zhevandrov & V.I.Gribkov

A number of authors[1-3] have observed and investigated the decrease in the intensity of photoluminescence of molecular crystals under the influence of ionizing radiations. This effect is termed degradation of luminescence. It can serve as a measure of the radiation damage to molecular crystals. The decrease in photoluminescence intensity is described by

$$\frac{I}{I_0} = \frac{1}{1+AD}, \qquad (1)$$

where A is a constant and D is the radiation dose. There is disagreement between the experimental results of Black[2] and Schulman et al[3]: the former detected no degradation of luminescence of anthracene as a result of β-irradiation, whereas the latter report observing degradation.

The above law (1) governing the decrease of photoluminescence was deduced theoretically by Rosenstock & Schulman[4]. These authors do not consider the damage mechanism but use a formal model of the phenomenon in which a significant role is played by long-range energy migration through the crystal. In view of agreement of the deduced law with the experimental data, these authors assert that migration of energy over large distances in the crystal is an important factor in the process of degradation of luminescence. This is consistent with the role currently attributed to free excitons in optical effects occurring in molecular crystals. In particular, apparently, free electrons are responsible for transfer of excitation energy from the base material to the impurity in mixed crystals of the anthracene-naphthacene type.

In the present work we investigated the influence of β-irradiation on the photoluminescence of mixed crystals. We studied the effect of β-radiation on crystals of pure anthracene and anthracene with different concentrations of naphthacene.

The β-radiation sources were radioactive strontium - Sr^{90} (activity 25 mC and 100 mC; mean electron energy 0.9 Mev; maximum electron energy 2.2 Mev) and tritium - H^3 (activity 0.37 C and 3.4 C; mean electron energy 5.5 kev; maximum energy 18 kev). The maximum radiation doses used were Sr^{90} $2 \cdot 10^6$ rad and H^3 $3.5 \cdot 10^{10}$ rad. One must, however, exercise caution in comparing the results obtained with strontium and tritium inasmuch as the electron mean free paths in the two cases are different. For the electrons from strontium the mean free path length is much greater than the thickness of the single crystals used in the investigation (several microns), while in the case of the tritium electrons the path length is of the same order of magnitude as the thickness. Hence in the case of Sr^{90} one can speak of the effect of the electrons on the entire volume of the crystal, whereas in the case of H^3 one can only speak of the dose impinging on the surface of the crystal and absorbed in the superficial layer.

In all we irradiated several series of samples of pure anthracene and anthracene with different concentrations of naphthacene from 10^{-5} to $5 \cdot 10^{-3}$ g/g. For each sample we recorded the photoluminescence spectrum before and after irradiation under identical geometric and optical conditions (λ_{excit} = 365 mμ). The irradiation time varied from three to six days. The measurements were carried out on a series of single crystals (in the course of these it proved feasible also to measure the polarization of the luminescence) on blocks consisting of several single crystals and on powdered specimens. In the last case the investigation was complicated by the effect of strong reabsorption.

Typical results, derived from one series of experiments with strontium, shown in Fig.1 (A and B). Irradiation of pure anthracene results in overall depression of the photoluminescence spectrum (I_1/I_0 = 16%); the luminescence decrement for

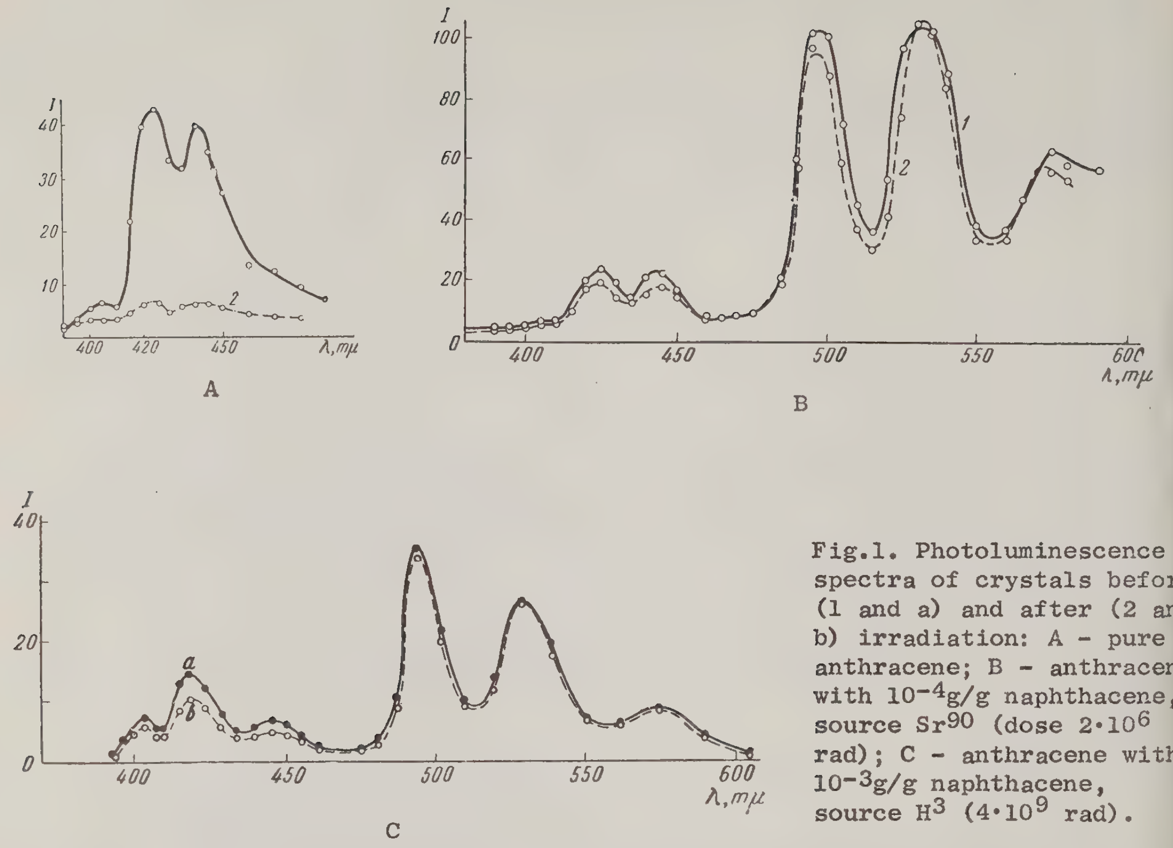

Fig.1. Photoluminescence spectra of crystals before (1 and a) and after (2 and b) irradiation: A - pure anthracene; B - anthracene with 10^{-4}g/g naphthacene, source Sr^{90} (dose $2 \cdot 10^6$ rad); C - anthracene with 10^{-3}g/g naphthacene, source H^3 ($4 \cdot 10^9$ rad).

anthracene in a mixed crystal with 10^{-4} g/g naphthacene is much smaller: $I'_1/I'_0 =$ $= 71\%$ (at a still higher naphthacene concentration, namely $5 \cdot 10^{-3}$g/g, I'_1/I'_0 amounts to 95%, i.e., there is virtually no degradation). The luminescence spectrum of naphthacene is virtually not altered by irradiation (with the doses used). A similar result was obtained in irradiating an anthracene single crystal with 10- g/g naphthacene with the 0.37 C tritium source (Fig.1,C).

A series of special experiments showed that the absorption of exciting light by the crystals does not change at all as a result of β—irradiation with a dose of $2 \cdot 10^6$ rad. Thus the observed effect is due to change in the luminescence efficiency. The degradation of luminescence is irreversible: tests showed that the intensity is not restored to any appreciable extent even a month after irradiation.

The significant result is that the degradation of luminescence of anthracene is diminished in the presence of naphthacene. This may explain the above-mentioned divergence between the results of Black[2] and Schulman et al[3]. Commercial anthracene is often contaminated with naphthacene and this may have been the reason why Black observed virtually no degradation.

Two hypotheses may be proposed for explaining the suppression of luminescence in molecular crystals: 1) formation under the influence of β-radiation of inactively absorbing, nonluminescent molecules, or 2) formation of exciton-trapping quenching centers.

The results of the theoretical work of Rosenstock & Schulman[4] mentioned above would appear to favor the second hypothesis. Actually, however, apparently both processes may occur in molecular crystals. The appearance of quenching centers leads to the competition of two quenching processes in anthracene, connected with trapping of excitons by the quenching centers and by the naphthacene impurity molecules. The time during which quenching by centers produced by β-radiation is feasible will be shortened owing to trapping of excitons by the naphthacene molecules.

Can this competition of quenching processes explain the observed decrease in the relative degradation of anthracene in the presence of naphthacene?

Quenching by extraneous quenching centers is described by the formula

$$\frac{I_1}{I_0} = \frac{1}{1+q_1},$$

where $q_1 = k_1c_1$ is a quenching constant proportional to the concentration c_1 of quenching centers (in our case c_1 is proportional to D, the radiation dose). Analagously, the quenching by naphthacene molecules is described by

$$\frac{I'_0}{I_0} = \frac{1}{1+q_2},$$

where $q_2 = k_2c_2$ (c_2 is the naphthacene concentration). The simultaneous operation of both quenching factors will therefore be characterized by

$$\frac{I'_1}{I_0} = \frac{1}{1+q_1+q_2},$$

and, consequently, the relative quenching in an anthracene crystal with naphthacene by centers produced by β-radiation will be described by the formula

$$\frac{I'_1}{I'_0} = \frac{1+q_2}{1+q_1+q_2}.$$

We can find the value of q_1 from the experimental data on the degradation of pure anthracene: I_1/I_0 = 16%; whence q_1 = 5.25. The value of q_2 (for a naphthacene concentration $c_2 = 10^{-4}$g/g) can be calculated from the data of Galinum & Chuzlikova[5] and Bowen et al[6] on the luminescence yield as a function of the naphthacene concentration (the data of these authors are in fairly good agreement): I'_0/I_0 = 17.5%, whence q_2 = 4.7. Knowing q_1 and q_2, we obtain I'_1/I'_0 = 52%. As noted above, experiment gives a value of 71% for this ratio.

Thus one cannot explain the entire regeneration of the luminescence of anthracene by the competition of quenchings. Moreover, it must be noted that the process of degradation does not consist entirely of formation of quenching centers. There may also occur formation of nonluminescent centers (first hypothesis) to which the competition of quenchings does not apply.

In discussing the competition of quenchings one must bear in mind yet another factor. If there occurs extinction of excitons on the surface of the crystal, this process must also participate in the competition. However, the probability for such exciton extinction will be included in the constants q_1 and q_2, if the luminescence is uniformly excited throughout the volume of the crystal. The condition for this will be $k\lambda \ll 1$, where k is the absorption coefficient for the exciting light, and λ is the diffusion length for an exciton in an anthracene crystal. For 365 mμ light $k = 3 \cdot 10^4$ cm^{-1} and $\lambda = \sqrt{D\tau}$ (D here is the diffusion coefficient and τ is the exciton lifetime); according to the data of Kucherov & Faidysh[7], $\lambda = 1.5 \cdot 10^{-5}$ cm, while according to the data of Galanin & Chizhkova[5], $\lambda = 1.4 \cdot 10^{-6}$ cm. Thus according to the data of the former $k\lambda < 1$, while according to the data of the latter $k\lambda \ll 1$. Thus the above-mentioned condition is undoubtedly fulfilled. Only when $k\lambda \gg 1$ will calculation taking into account extinction of excitons at the surface differ substantially from that given above.

Why then is the decrease in degradation of luminescence of anthracene in the presence of naphthacene greater than follows from calculations based on the competition of quenchings?

It may be assumed that some part of the β-particle energy, before it has time to inflict damage (regardless of the damage mechanism), is intercepted by the naphthacene molecules and emitted as luminescence. It is difficult at present to say anything definite regarding the mechanism of such "luminescent shielding", but that it exists is perfectly possible by analogy with the protective action of luminescent substances in plastics as regards photochemical damage[8] and the chemical shielding against radiation damage observed in polymers, complex molecules and biochemical systems[9].

Obviously, a significant role in the protective effect is played by energy migration through the crystal. The fact that the shielding is effective even at low impurity concentrations (lower than in the case of chemical shielding) is understandable inasmuch as in the case of luminescent shielding there occur no irreversible changes in the protecting impurity.

Hence it would be of interest to undertake experiments aimed at establishing the possibility of luminescent shielding against radiation damage and at elucidating its mechanism not only in molecular crystals but in plastics, polymers, solutions of complex molecules and biological systems.

In the range of heavy radiation doses yet another factor comes into play, namely, decrease in the luminescent intensity of naphthacene. As noted above, in these experiments we used a high-activity (3.4 C) tritium source. The electron range in this case is relatively short. Hence in contrast to the experiments with the strontium sources, the irradiation in this case was carried out on the same surface of the crystal as the excitation and observation of photoluminescence. The crystals were subjected to doses of up to $3.6 \cdot 10^{10}$ rad.

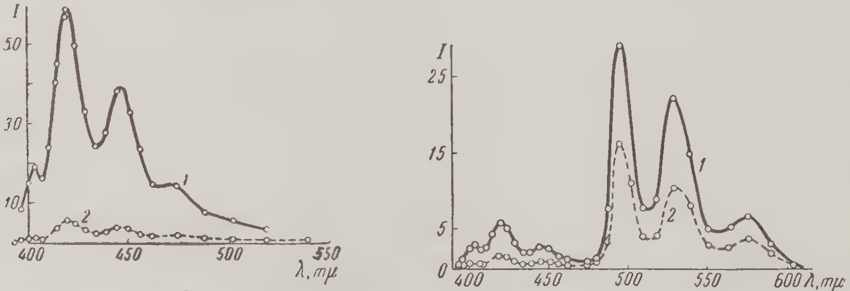

a b

Fig.2. Photoluminescence spectra of crystals before (1) and after (2) β-irradiation: a - pure anthracene; b - anthracene 10^{-4}g/g naphthacene. Source H^3; radiation dose $3.6 \cdot 10^{10}$ rad.

The results are shown in Fig.2. Pure anthracene exhibits degradation: $I_{1a}/I_{0a} = 10\%$. The difference from the case of a lower radiation dose - $I_{1a}/I_{0a} = 16\%$ - is not appreciable; this is understandable inasmuch as the degradation law is hyperbolic and hence increases at a slower rate for heavy doses. In this case, however, the restoration of luminescence of anthracene in the presence of naphthacene is appreciably smaller: 27% at an anthracene concentration of 10^{-4}g/g, instead of 71% (see above). At the same time, there begins degradation of the naphth cene luminescence: $I_{1n}/I_{0n} = 57\%$.

It can hardly be supposed that the luminescence intensity of naphthacene decreases owing to quenching at centers formed in the host lattice because energy transfer from naphthacene to anthracene is impossible. It is more logical to

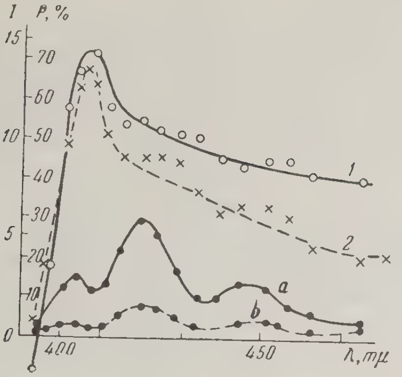

Fig.3

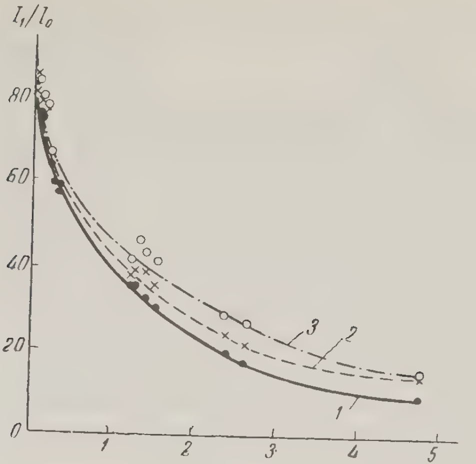

Fig.4

ig.3. Photoluminescence spectra (a & b) and spectral dependence of the polariza-
ion (1 & 2) of the luminescence of anthracene single crystals before (a & 1) and after (b & 2) β-irradiation. Source H^3; dose $3.6\cdot10^{10}$ rad.

Fig.4. Decrease in the intensity (degradation) of luminescence at the peaks of the spectrum of anthracene as a function of the β-radiation dose: 1 - 405 mμ, 2 - 420 mμ, 3 - 445 mμ.

ssume that there occurs direct damage of individual naphthacene molecules, as a esult of which they become nonluminescent. Regardless of the precise nature of ie damage mechanism, a consequence of its operation will obviously be decreased the regeneration of the anthracene luminescence, in agreement with the results our experiments (an obvious further result will be weakening of the luminescent ielding action).

It should be noted that in the process of degradation (decrease in intensity) the luminescence of anthracene under the influence of β-radiation the structure the spectrum remains virtually unchanged: the spectrum is lowered as a whole th almost no deformation (Fig.3). In other words, the quenching of luminescence individual peaks is nearly equal (Fig.4). The intensity decrement vs radiation se curves are consistent with Eq.(1). This indicates that the luminescence mechism per se does not undergo any substantial changes incident to β-irradiation.

The wavelength dependence of the polarization of the photoluminescence of thracene* also undergoes little change as a result of irradiation; there persist e abrupt changes in polarization at the short wavelength edge of the photolumiscence spectra, changes which are apparently connected with emission due to free citons[10].

This also shows that β-radiation does not produce any substantial changes in e mechanism of luminescence and the mechanism of exciton energy transfer in the ttice. Also there appear to be no substantial disturbances or distortions of e crystal lattice, although a minor decrease in polarization in the long wavegth region, where the polarization is intimately connected with the structure the crystal and orientation of the molecules in the lattice, would appear to dicate that some small alterations of the lattice may occur.

---

*These measurements were carried out on single crystals in a spectropolaritric set-up.

We desire to acknowledge our indebtedness to G.B.Radzievskii for assistance in the work.

"P.N.Lebedev" Physical Institute,
Academy of Sciences of the USSR

References

1. J.B.Birks & F.A.Black, Proc.Phys.Soc.A, 64, 511 (1951).
2. F.A.Black, Phil.Mag., 44, 263 (1953).
3. J.H.Schulman, H.W.Etzel & J.G.Allard, J.Appl.Phys., 28, 792 (1957).
4. H.B.Rosenstock & J.H.Schulman, J.Chem.Phys., 30, 116 (1959).
5. M.D.Galanin & Z.A.Chizhikova, Optika i spektroskopiya, 1, 175 (1959).
6. E.J.Bowen, E.Mikiewicz & F.W.Smith, Proc.Phys.Soc.A, 62, 26 (1949).
7. I.Ya.Kucherov & A.N.Faidysh, Izv.AN SSSR, Ser.fiz., 22, 29 (1958). (Trans. Bulletin 22, 27.)
8. L.W.A.Meyer & W.M.Gearhart, Industr. and Eng.Chem., 43, 1585 (1951); B.E. Geller, Khimiya i tekhnologiya khlorinovogo volokna (Chemistry & Technology of Chlorofibers) Chapt.8, M., 1958.
9. P.Alexander, Nature, 173, 578, 1954; P.Alexander & A.Charlsby, in Voprosy radiobiologii (Problems of Radiobiology), M., 1956; P.Alexander, in Yadernoe izluchenie i zhisn' (Nuclear Radiation & Life), M., 1959; H.N.Dunning, J.Amer. Chem.Soc., 79, 5320 (1957); M.Burton and others, Radiation Res., 8, 203 (1958); A.Lacassan, in Voprosy radiobiologii (Problems of Radiobiology), M., 1956; F.A. Bovey, The Effects of Ionizing Radiation on Natural and Synthetic High Polymers, N.Y., 1958 (Cited in Russian trans.).
10. N.D.Zhevandrov, V.I.Gribkov & V.N.Varfolomeeva, Izv.AN SSSR, Ser.fiz., 23, 57 (1959). (Trans.Bulletin, 23, 59.)

ON THE POSSIBLE ROLE OF TEMPERATURE QUENCHING IN SCINTILLATION OF ORGANIC SUBSTANCES

- I.M.Rozman

It is known that the specific scintillation efficiency or radioluminescence ield of organic substances with excitation by slow heavy particles is much lower han with excitation by fast electrons. Of particular importance in this connecion are the following experimental facts: 1) the decrease in yield for heavy paricles does not depend to any appreciable extent on the individual properties of he scintillator material: the ratio of the average yield for 5 MeV α-particles o the yield for fast electrons (or the α/β ratio $D_{\alpha\beta}$) for all tested crystalline, iquid and plastic scintillators lies in the range from 0.07 to 0.15 (Refs.1 & 2);) the mean scintillation persistence or decay time τ does not depend (or is only eakly dependent) on the type of exciting particles; according to the data of Kallan & Brucker, the decay time τ_α for α-scintillation does not differ appreciably rom the β-scintillation decay time τ_β (or at least equals not less than 0.5 τ_β), .e.,

$$\tau_\alpha/\tau_\beta \gg D_{\alpha\beta} .$$

Consequently, the rate of quenching at the high excitation density that obains along the track of slow particles must be much greater than the rate of emision of photons. With this ratio of the rates complete quenching does not occur ither because the process of quenching ceases rapidly or because part of the exited molecules are never involved in the process. The first possibility underies the theory relating quenching with the interaction of excited molecules. The uenching intensity is proportional to the concentration of excited molecules to he second (or a higher) power and rapidly decreases. So far, however, this aproach has not yielded satisfactory agreement with experiment.[1,3]

The second possibility has been utilized in the theory of Galanin[4], in which uenching is related with a local temperature rise along the particle track, i.e., ith so-called "thermal spikes". It is assumed that with a temperature wave ampliude exceeding a certain value ϑ there occurs complete quenching, while for lower mplitudes no quenching occurs. In view of this the scintillation persistence hould not depend on the exciting radiation, that is, the α and β excitation decay imes should be equal. Further, according to the evaluations of Galanin, all the racks of α-particles with energies under ~10 Mev should be fully quenched. Hence alanin introduces the hypothesis that the observed luminescence is produced only y fast secondary electrons, which leads to $D_{\alpha\beta}$ being independent of the scintilator material.

In view of the importance of these inferences, it would appear expedient to evelop the theory of temperature quenching further and to investigate theoreticaly and experimentally its basic premises, specifically, to investigate 1) temperaure quenching in different states of aggregation, 2) rate of conversion of excitaion energy to heat, and 3) the structure and dynamics of charged particle tracks, aking into account secondary electrons. Some of these questions will be discussed n the present paper.

Temperature dependence of the radioluminescence yield

Herforth & Kallmann[5] observed a sharp decrease in the radioluminescence yield with γ-excitation) as a result of melting of organic crystals. It is evident from he curves given by these authors that the yield falls off by a factor of at least) for naphthalene and 10-20 for biphenyl and phenanthrene. According to the data f Kulakova & Rozman[6], as a result of melting of dibenzil and stilbene the radio-

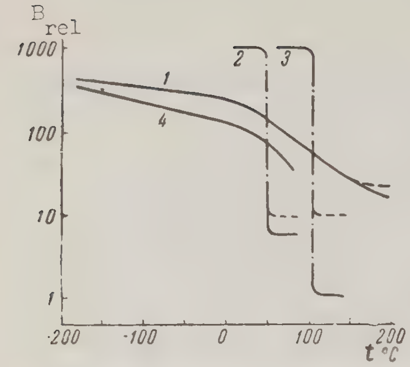

Fig.1. Temperature dependence of the relative luminescence yield of different scintillators. Solid curves - α-particle excitation; - dashed curves - β-particle excitation: 1) polyvinyltoluene, 2) dibenzil, 3) stilbene, 4) polystyrene.

luminescence yield for α-excitation decreases by a factor of 200 and 1000, respectively (Fig.1). It is important to note that up to the melting point the α/β ratio remains virtually constant.* Similar results were obtained by Chizhikova[7] for tolan (diphenyl acetylene).

Polystyrene[8] and polyvinyltoluene[9] exhibit a distinctive temperature dependence: the yield decreases gradually and by a relatively small factor (Fig.1). Moreover $D_{\alpha\beta}$ remains constant over the entire temperature range.

On the basis of the above results it was inferred in the work of Ref.6 that the particle energy dependence of the radioluminescence yield cannot be determined only by temperature quenching in the "thermal spikes". One can, however, draw a different deduction[4,7] namely, that the temperature quenching is the decisive factor and the individual properties of scintillators are suppressed or masked owing to complete quenching of the main track; this presumably explains the temperature independence of $D_{\alpha\beta}$.

Regarding the hypothesis of complete quenching of the main track

The hypothesis of complete quenching of the main track must be considered from two standpoints: first, whether the amplitude and lifetime of the "thermal spike" are sufficient to produce complete quenching within the interaction range R_0 of the particle, and, second, whether this assumption is in agreement with the experimental data on the luminescence yield with excitation by slow particles.

At an α-particle energy of 5 Mev the specific loss dE/dx in organic substances (anthracene, polystyrene) is approximately 850 Mev g^{-1} cm^2. Approximately 30% of the loss is accounted by the kinetic energy of the secondary electrons moving out of the interaction range $R_0 \approx 17$ Å, i.e., away from the main track.** The remaining 70% of the loss is accounted for mainly by the energy of electronic excitation of the molecules. The more rapidly this energy is converted to heat, the greater will be the amplitude of the "thermal spike". Hence a measure of the "rapidity" of the process is the rate of heat removal. If we assume that the excess energy of electron excitation above the first level is converted to atomic vibration energy within $\sim 10^{-13}$ sec, we find that in the section of the track under consideration there obtains virtually instantaneous evolution of about 300 Mev g^{-1} cm^2 heat energy. Possibly one should add to this ~200 Mev due to "inactive absorption".[12]

For the purposes of further calculation we assume that the energy of the instantaneous source on the α-particle track equals $Q = 0.5\, dE/dx$ for an initial emperature increment

---

*With excitation by β-particles (C^{144}--Pr^{144}) the scintillation intensity of the melts was due primarily to Cerenkov radiation.

**Herein below the values of dE/dx are taken in accord with the calculations of Ref.9, the results of which for polystyrene are in agreement with experiment[10]. R_0 was calculated by means of the formula given by Williams[10] for an electron binding energy of 6 ev.

$$\vartheta(r,0)=\vartheta_0\exp(-r^2/r_0^2),\ \vartheta_0=Q/\pi r_0^2c, \tag{1}$$

here c is the specific heat.* The parameter r_0 was determined from the condition that all the energy Q is released within a cylinder of radius R_0, i.e., r_0 = 0.5 R_0. The solution for the heat conduction equation for axial symmetry is of the form**

$$\vartheta(r,t)=\frac{\vartheta_0 r_0^2}{4at+r_0^2}\exp\left(-\frac{r^2}{4at+r_0^2}\right). \tag{2}$$

For $r \leqslant r_0$ the temperature falls off monotonically. For $r > r_0$ the temperature at first increases, attaining a maximum value

$$\vartheta_m(r)=\vartheta_0 r_0^2/er^2 \text{ at } t_m=\frac{r^2-r_0^2}{4a}. \tag{3}$$

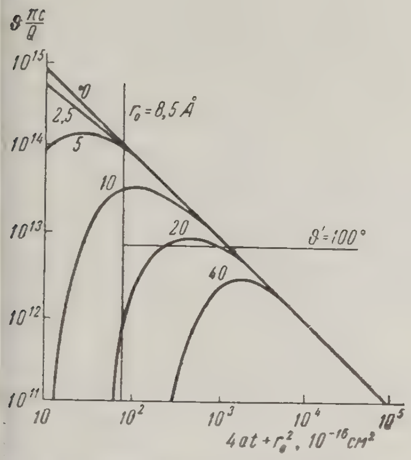

ig.2. Temperature wave in a ylindrical "spike". The igures at the curves denote he distance from the axis in . The horizontal and verti- al lines r_0 = 8.5 A and ϑ' = 100° outline the region of "spike" with an amplitude $> \vartheta'$ in the case of 5 Mev α-articles.

Fig.2 shows the $\vartheta(r,t)$ curves for a number of values of r. Let us now turn to an evaluation of the degree of temperature quenching in the main track, assuming that it is of second order and neglecting transfer of excitation energy[4]. Let η_0 be the yield and τ_0 the persistence of luminescence for ϑ_0 = 0°C (the temperature of the experiment) and $\eta(\vartheta)$ be the yield as a function of the amplitude of the "thermal spike". Then the effective yield at a distance r from the track axis will be given by

$$\eta_{\text{eff}}(E,r)=\eta_0\int_0^\infty \exp\left\{-\frac{\eta_0}{\tau_0}\int_0^{x\tau_0}\frac{dt}{\eta(\vartheta)}\right\}dx. \tag{4}$$

The dependence on E is contained in R_0 and ϑ_0. Averaging (4) over the iniial transverse distribution $n_0(r)$ of excited molecules and over the length of the hole track, we obtain the average yield for a particle with initial energy E_0:

$$\overline{B}=\int_0^{E_0}\frac{dE}{E_0}\int_0^{R_0}2\pi r n_0(r)\,\eta_{\text{eff}}(E,r)\,dr. \tag{5}$$

In the simplest case $\eta=\eta_0$ for $\vartheta<\vartheta'$ and $\eta=\eta'$ for $\vartheta\geqslant\vartheta$, (Fig.1) formula (4) ives

$$\eta_{\text{eff}}=\eta'+(\eta_0-\eta')\exp\left\{-\frac{\eta_0}{\eta'\tau_0}t_q(r)\right\}, \tag{4'}$$

here $t_q(r)$ is the lifetime of the state with $\vartheta(r,t)\geqslant\vartheta'$. Calculations show that for

---

*We are neglecting the temperature dependence of the specific heat c and the eat conduction λ. We have taken the value of 10^{13} Mev g^{-1} degree^{-1} for c, which orresponds to the value for organic substances at ~100°. For the temperature cofficient of conduction $a = \lambda/c$ we have taken its value at room temperature, i.e., $\cdot 10^{-3}$ cm^2/sec for crystals and $9\cdot 10^{-4}$ cm^2/sec for polymers.

** dE/dx remains virtually constant over the length of the track, which is much onger than the radial distance of interest to us.

Table 1

Some characteristics of α particle tracks

E, Mev	dE/dx, Mev g^{-1} cm 2	R_0, Å	ϑ_0, °C acc. to Ref. 1	$\vartheta_m(R_0)$, °C acc. to Ref. 3	R_m^* for $\vartheta_m = 185°$, Å	$4at_q$, 10^{-12} cm²				
						$r = r_0$		$r = R_0$		$r = R_m$
						$\vartheta' = 10$	$\vartheta' = 100$	$\vartheta' = 10$	$\vartheta = 100$	$\vartheta' = 100$
1	2	3	4	5	6	7	8	9	10	11
0,2	1820	3,4	$100 \cdot 10^3$	$100 \cdot 10^2$	24	2,9	0,29	2,9	0,29	0,23
0,4	2460	4,9	$65 \cdot 10^3$	$60 \cdot 10^2$	28	3,9	0,39	3,9	0,39	0,28
0,8	2480	6,9	$33 \cdot 10^3$	$31 \cdot 10^2$	28	3,9	0,39	3,9	0,39	0,32
1,6	1810	9,7	$12,2 \cdot 10^3$	$11,3 \cdot 10^2$	24	2,9	0,28	2,9	0,28	0,22
3,2	1140	14	$3,7 \cdot 10^3$	$3,4 \cdot 10^2$	19	1,8	0,17	1,8	0,16	0,14
6	720	19	$1,3 \cdot 10^3$	$1,2 \cdot 10^2$	—	1,15	0,10	1,12	0,05	—
12	450	27	390	36	—	0,67	0,04	0,62	—	—
20	320	35	166	15	—	0,44	—	—	—	—
5	850	17	2000	185	17	1,43	0,13	1,41	0,11	0,11

---

* R_m is the maximum distance from the axis of the track, where the amplitude of the "thermal spike" may attain 185°.

Table 2

Average luminescence yield $\overline{B}/\eta_0$ of the main track of a 5 Mev α-particle (calculated by means of Eq. (5'))

"Quenching" temperature spike amplitude, ϑ' °C	Stilbene* $\eta_0/\eta' = 1000$; $\tau_0 = 3 \cdot 10^{-9}$ sec	Dibenzil* $\eta_0/\eta' = 200$; $\tau_0 = 44 \cdot 10^{-9}$ sec
10	0,00	0,46
40	0,00	0,80
100	0,01	0,92
200	0,07	0,97

---

* η_0/η' from Fig. 1; τ_0 from Ref. 13.

Table 3

Maximum temperature rise ϑ_0 (in °C) on the axis of an α-particle track with a heat source of the form

$$q = \frac{\omega}{2\pi r_0^2} \frac{dE}{dx} \exp\left(-\omega t - \frac{r^2}{r_0^2}\right)^*$$

E, Mev	$1/\omega \leqslant 10^{-13}$	$1/\omega = 10^{-12}$ sec	$1/\omega = 10^{-11}$ sec
5	2000	700	200
1,6	12200	2400	600

---

*On the assumption that $a = 3 \cdot 10^{-3}$ cm² sec⁻¹.

$E_\alpha < 6$ Mev the value of t_q for the range of ϑ' of interest virtually does not depend on r (Table 1); consequently,

$$\overline{B} = \eta' + (\eta_0 - \eta') \int_0^{E_0} \exp\left\{-\frac{\eta_0 t_q}{\eta' \tau_0}\right\} \frac{dE}{E_0}. \qquad (5')$$

The quenching in the main track may be regarded as complete if $\overline{B}/\eta_0 \leqslant D_{\alpha\beta}$, i.e., $\overline{B}/\eta_0 \leqslant 0.01$. It will be evident from Table 2 that complete quenching can be realized for stilbene at room temperature and higher ($\vartheta' < 100$). For dibenzil at room temperature ($\vartheta' = 40$) the quenching amounts to only 20%. The degree of quenching of the main track of α-particles will be even lower in polystyrene and polyvinyltoluene (see Fig. 1).

There may be raised the following objections. According to Eq. (2) most of the excited molecules are at a temperature appreciably exceeding ϑ' (Table 1); hence one may not be warranted in equating η' to the yield of the melt near the melting point. Moreover, it is possible that under conditions of deformation or the shock wave accompanying the "thermal spike" there may occur an additional decrease in the luminescence yield sufficient to bring about complete quenching of the main track.

Let us turn to the other aspect of the problem, namely, if the principal track of a 5 Mev α-particle is fully quenched, what yield can one expect for α-particles of lower energies? Let us consider, for example, the case of the track of an α-particle with $E_\alpha = 0.2$ Mev. It will be evident from Table 1 that for $r \leqslant R_m = 24$ Å there obtain more intense temperature conditions than for $E_\alpha = 5$ Mev. The maximum energy of secondary electrons produced by a 0.2 Mev α-particle is $T_m = 108$ ev. For this energy the transverse displacement of the electrons does not exceed 10 Å.* Consequently, the luminescence yield must be negligibly small. Experiment yields a value of ~0.06 the yield for fast electrons.[14] Similar calculations for an α-particle energy of 0.4 Mev lead to $R_m = 28$ Å, $T_m = 217$ ev, a mean displacement of secondary electrons not exceeding 20 Å, and a yield equal to 0.03 the yield for fast electrons.

Thus the hypothesis of complete quenching of the main track as yet cannot be reconciled with the experimental data. On the other hand, one cannot reject this hypothesis entirely (see above). The disagreement can be alleviated if we assume that temperature quenching (or, in more general form, quenching owing to "thermal spikes") does not play a decisive role in the scintillation process. This in turn is possible if the amplitude of the "spike" is not too great. If we assume, for example, that the conversion of electronic excitation energy to heat occurs not instantaneously (within 10^{-13} sec), but over a period of 10^{-11} sec, the amplitude of the "thermal spike" is reduced by a factor of 10 or more (see Table 3). This assumption is in qualitative agreement with the results of Birks & Cameron[15] who found that the efficiency of energy transfer depends on the height of the excitation level.

References

1. H.Kallmann & G.J.Brucker, Phys.Rev., 108, 1122 (1957).
w. M.D.Galanin & Z.A.Chizhikova, Optika i spektroskopiya, 4, 196 (1958).
3. I.M.Rozman, Ibid., 8, No.4 (1960). (Trans.Optics & Spectroscopy.)
4. M.D.Galanin, Ibid., 4, 758 (1958).
5. L.Herforth & H.Kallmann, Ann.phys., 4, 231 (1949).
6. A.F.Kulakova & I.M.Rozman, Optika i spektroskopiya, 8, 140 (1960). (Trans. Optics & Spectroscopy.)
7. Z.A.Chizhikova, Thesis, Phys.Inst. of the USSR Ac.of Sci., M., 1959.
8. I.M.Rozman, Optika i spektroskopiya, 2, 480 (1957).
9. I.M.Rozman, Thesis, Sukhumi (Georgian SSR), 1957.
10. D.C.Lorents & E.J.Zimmerman, Phys.Rev., 113, 1199 (1959).
11. E.J.Williams, Proc.Roy.Soc., A, 139, 163 (1933).
12. M.D.Galanin & A.P.Grishin, Zhur.eksp.i teor.fiz., 30, 33 (1956). (Trans. Soviet Physics - JETP.)
13. R.K.Swank & W.L.Buck, Rev.Scient.Instrum., 26, 15 (1956).
14. E.J.Zimmerman, Phys.Rev., 99, 1199 (1955).
15. J.B.Birks & A.J.W.Cameron, Proc.Phys.Soc., 72, 53 (1958).

---

*A description of the calculations and the detailed results thereof will be published elsewhere.

EFFECT OF TEMPERATURE ON THE ELECTRONIC SPECTRA OF COMPLEX MOLECULES IN SOLUTIONS

- L.G.Pikulik

As will be evident from examination of recent publications[1] and the transactions of previous conferences on luminescence[2,3] there have been very few joint investigations of the luminescence and absorption spectra of complex molecules at low temperatures. For example, in the work of Levshin & Tarasova[4] and Klockhov[5] the fluorescence and absorption spectra of solutions of a number of compounds were studied only to ~100°, i.e., only in the temperature range in which the medium does not undergo a change in state. In the work of Shpak[6] the luminescence and absorption spectra at liquid hydrogen temperature were obtained for only one compound.

The lack of sufficient experimental data makes it impossible to check a number of deductions that follow from the theory of the contour of spectrum bands of complex molecules, developed by Stepanov & Kazachenko[1,7]. According to this theory, the fluorescence and absorption spectra should be shifted with decreasing temperature in opposite directions, away from the frequency of the purely electronic transition: the absorption peak should be shifted to the side of higher frequencies; the emission peak to the side of lower frequencies. This shift of the spectra is presumably due to redistribution of the molecules over vibrational levels owing to the change in temperature. The probability for electronic-vibrational transitions is assumed to remain constant. In the case of change in the transition probability the fluorescence and absorption bands may shift towards the frequency of the electronic transition (the absorption peak - to the side of lower frequencies; the emission peak - the side of higher frequencies). In the case of the complex molecule model used in calculating the band contours, this is associated with decrease of the fundamental parameters, namely, the quasielastic constant k of the potential curves and the difference Δr between the equilibrium radii of the ground and excited electronic states.

In order to elucidate the reasons for the shift of the spectra of solutions with decrease in temperature we investigated the absorption and fluorescence spectra of a number of phthalimides as well as of a number of typical dyes at liquid nitrogen temperature.

We used the experimental procedure described earlier.[8] By way of solvents we employed both media retaining their transparency incident to freezing as well as a number of solvents that crack and fissure when frozen. Among the solvents that freeze without fissuring* we used ethyl, propyl and isobutyl alcohols. By way of media which become glass-like when frozen but do not fissure to any great extent we tried glycerol, glycol, benzyl alcohol and cyclohexanol. Displacement of the fluorescence spectra of phthalimides in these solvents with decrease of temperature was observed earlier.[9] In addition to the above, we prepared solid solutions based on gelatin, sugar and starch. We also found it convenient to work with transparent plastics (lucite) and nitrocellulose films colored with the investigated compounds.

The results of measurements of the fluorescence and absorption spectra of seven phthalimides** (4-aminophthalimide, 4-amino-N-methylphthalimide, 4-dimethylamino-N-methylphthalimide, 3-aminophthalimide, 3-amino-N-methylphthalimide, 3-monomethylaminophthalimide, and 3-monomethylamino-N-methylphthalimide) dissolved

---

*Fissuring is frequently inhibited by a small addition of petroleum ether which has no noticeable effect on the spectra.

**Some of the results were published earlier in Ref.8.

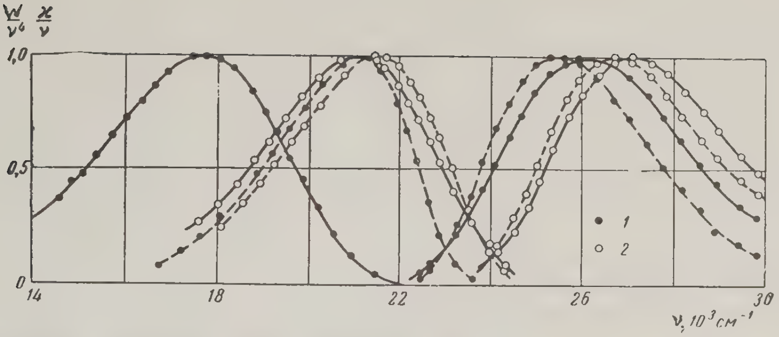

ig.1. Fluorescence and absorption spectra of 4-amino-N-methylphthalimide in ethyl alcohol (1) and lucite (2) at +20° (solid lines) and -196° (dashed lines).

n the above listed media* showed that the character of the spectrum shifts is the ame in all cases.

With decrease in the temperature of the medium the absorption and fluorescence eaks shift towards the frequency of the electronic transition and the effect does ot depend on the specific properties of the medium. For solid solutions the shift f both peaks is approximately the same and averages 200 cm^{-1}. For media which ndergo a change of state in the process of cooling, the shift of the fluorescence and is appreciably greater than the shift of the absorption band. By way of ilustration the spectra of 4-amino-N-methylphthalimide in ethyl alcohol and transarent plastic are reproduced in Fig.1.

Such displacement of the fluorescence and absorption bands towards the elecronic transition frequency is exhibited by substances of other types. We observed t, for example, in alcohol solutions of dyes: acridine yellow, auramine, chrysodine, coryphosphine, fluorescein, and aminochloromaleinimide (in the case of non-luorescent compounds one can, naturally, only speak of displacements of the long avelength absorption bands to the side of lower frequencies). Similar shifts have een reported for acridines by Levshin & Tarasova[4], for some simple polycyclic ydrocarbons by Shpak[6], for chlorophyll by Kravtsov[10], and for dyes adsorbed on ellophane by Ermolenko[11].

Thus in the case of all the compounds under consideration deep cooling results n shift of the fluorescence and absorption bands towards the frequency of the lectronic transition. It will be noted that this shift is contrary to that preicted by the theory if one takes into account only changes in the population of he molecular levels. At the same time, according to the theory, the observed efect can be explained by change in the probability for electronic-vibrational tranitions. Consequently, the shift of the peaks away from the frequency of the purey electronic transition, i.e., the shift due to redistribution of the molecules ver vibrational levels, is suppressed or counteracted by the reverse shift towards he purely electronic transition frequency, owing to change in the transition proability. In the case of absorption there is increase in the relative number of ransitions to lower-lying vibrational levels of the upper electronic state: the osorption band peak is shifted to the side of lower frequencies. Accordingly, in nission the number of transitions to lower-lying vibrational levels of the ground

---

*The spectra of each substance were measured mainly in some definite part of ne medium. Analysis of the results gives reason to assert that for all the inestigated substances in all the listed media the general character of the temperaure induced shift is the same.

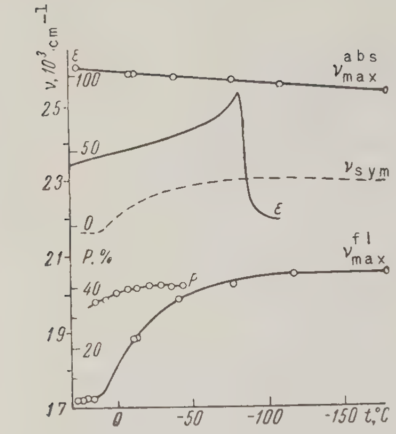

Fig.2. Temperature dependences of the frequency of the absorption and fluorescence peaks, the symmetry frequency and the polarization of fluorescence of 4-amino-N-methylphthalimide in glycerol. ϵ - variation of the dielectric constant of glycerol with temperature.

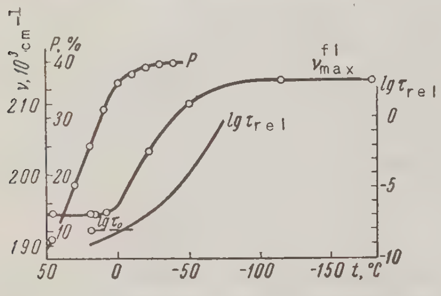

Fig.3. Temperature dependences of the frequency of the fluorescence peak of 3-aminophthalimide in glycerol, the relaxation time of glycerol and the polarization of luminescence; τ_0 - lifetime of the excited state of 3-aminophthalimide at +20°.

state is increased: the maximum of the fluorescence band is shifted to the side of higher frequencies. The decisive role in this effect must be attributed to the solvent, which with decrease in temperature exerts a stronger influence on the fluorescent molecules.[9,12]

From the standpoint of the complex molecule model this change in transition probability is connected with decrease of the quasielastic constant k of the potential curves or decrease of the difference Δr of the equilibrium radii of the ground and excited states. In an earlier paper[8] we hypothesized that in the investigated cases change of Δr is more probable. This possibly indicates that with decrease of temperature of the medium the fluorescent molecule finds itself under more "rigid" conditions and the relative increase of the molecule's configuration incident to excitation is reduced.

As already noted, freezing of liquid solutions of the investigated phthalimides is accompanied by an appreciable shift of the fluorescence spectra (Fig.1). The kinetics of this process* is presented in Figs.2 & 3.

In order to obtain additional information on the state of the fluorescent molecules, we measure the degree of polarization of the fluorescence under the same temperature conditions. The limiting polarization of phthalimides is known[13]; hence from the degree of polarization of the fluorescenc one can judge of the relative rotational freedom of the molecules in solutions. As will be evident from comparison of the polarization curve with the curve for the shift of the fluorescence spectrum (Figs.2 & 3), the change in degree of polarization is small** in the temperature interval corresponding to the principal shift of the fluorescence spectrum, and the polarization attains its limiting value.[13] This indicates that during the lifetime of the excited state rotation of the molecule is relatively small, i.e., the molecules are virually "fixed" in space. Hence it is obvious that the changes in the medium that lead to the appreciable spectrum shift begin after "fixation" of the fluorescent molecule in the medium.

Bakhshiev[14] relates the displacement of the luminescence and absorption spectra of phthalimides in different media with change in the static dielectric constant ϵ and the index of refraction of n of the solven If Bakhshiev's inference is correct increase of ϵ and n of the medium in the case of our phthalimide solutions should lead to shift of the symmetry frequency $\nu_{sym} = (\nu^{abs}_{max} - \nu^{fl}_{max})/2$ to the side of lower frequencies. Our experimental results (Fig. 2), however, are in conflict with this inference. It will be seen from the curves that increase of the dielectric constant* is accompanied by shift of ν_{sym} to the side of higher frequencies.

---

*Student F.Dreitser participated in this part of the work.

**Both 4-amino-N-methylphthalimide and 3-aminophthalimide in glycerol are characterized by an appreciable change in polarization with increasing temperature with virtually no change in the position of the fluorescence spectrum.

The appreciably greater shift of the fluorescence spectrum as compared with that of the absorption spectrum in the case of media undergoing a change in state is probably connected with orientational polarization of the solvent surrounding the solute molecules.[16] If during the lifetime of the excited state, owing to change of the dipole moment of the fluorescent molecule, there occurs a change in the polarization of the solvent molecules surrounding it, the height of the electronic level may be lowered. In case of freezing of the medium the possibility of change of the orientational polarization during the lifetime of the excited state is eliminated and hence the enhanced influence of the solvent on the position of the excited level is suppressed. Evidence in favor of this inference is furnished by comparison of the lifetime of the excited state of 3-aminophthalimide in glycerol ($\tau_0 = 13.6 \cdot 10^{-9}$ sec) with the temperature dependence of the relaxation time of glycerol[15]. It will be evident from Fig.3 that the shift of the fluorescence spectrum begins approximately from the instant of coincidence of these times. Comparison of the respective times for 4-amino-N-methylphthalimide leads to the same result. In 4-amino-N-methylphthalimide the lifetime of the excited state ($\tau_0 = 4.3 \cdot 10^{-9}$ sec) is shorter than in 3-aminophthalimide; consequently, the shift of the fluorescence spectrum should begin at higher temperatures, and this is in fact the case.

It must be emphasized that in all our experiments the shift of the fluorescence band with decrease in temperature occurred to the side of higher frequencies. Zelinskii & Kolobkov[12] report observing displacement of the fluorescence band of phthalimides incident to freezing of their solutions to the side of lower frequencies. This effect was observed in solvents which when cooled transform into an opaque snow-like mass. It may be assumed that in the case of such media there occurs crystallization of the phthalimide itself and hence the fluorescence spectrum is shifted to the position characteristic of the crystals. There are a number of facts and considerations that are in conflict with the inferences drawn by Zelinskii & Kolobkov. It must be noted that investigation of the absorption spectra under such conditions is very difficult, although it may yield additional information regarding the influence of temperature and the character of the medium on fluorescent molecules.

I am indebted to A.N.Sevchenko, B.I.Stepanov and V.V.Zelinskii for valuable discussions.

Institute of Physics,
Academy of Sciences of the Belorussian SSR

---

*The temperature dependence of ϵ was taken from Ref.15.

References

1. B.I.Stepanov, Lyuminestsentsiya sloznykh molekul (Luminescence of complex molecules), Pub.Belorussian SSR Ac. of Sci., 1956.

2. Transactions of the Sixth Conference on Luminescence, Izv.AN SSSR, Ser.fi 22, No.11, (1958) & 23, No.1 (1959). (Trans.Bulletin, 22, No.11 and 23, No.1.)

3. Transactions of the Eleventh All-Union Conference on Spectroscopy, Izv. AN SSSR, Ser.fiz., 22, Nos.6, 9 & 11 (1958). (Trans.Bulletin, 22, Nos.6,9 & 11.)

4. V.L.Levshin & T.M.Tarasova, Izv.AN SSSR, Ser.fiz., 15, 573 (1951).

5. V.P.Klochkov, Zhur.fiz.khim., (Jour.Phys.Chem.), 29, 1432 (1955).

6. M.T.Shpak, Ukr.fiz.zhur. (Ukrainian Physics Journal) 2, 347 (1957).

7. L.P.Kazachenko & B.I.Stepanov, Optika i spektroskopiya, 2, 339 (1957).

8. L.G.Pikulik & M.A.Solomakho, Inzh.-fiz.zhur. (Engin.Phys.Journ.) No.6 (1960).

9. L.G.Pikulik & M.A.Solomakho, Izv.AN SSSR, Ser.fiz., 22, 1391 (1958). (Trans. Bulletin, 22, 1381.)

10. L.A.Kravtsov, Ibid., 23, 78 (1959). (Trans.Bulletin, 23, 77.)

11. I.N.Ermolenko, Spektroskopiya v khimii okislennykh tsellyuloz (Spectroscopy in the chemistry of oxidized celluloses), Minsk, 1959.

12. V.V.Zelinskii & V.P.Kolobkov, Optika i spektroskopiya, 5, 423 (1958).

13. A.M.Sarzhevskii & A.N.Sevchenko, Izv.AN SSSR, Ser.fiz., 22, 1412 (1958). (Trans.Bulletin, 22, 1402.)

14. N.G.Bakhshiev, Optika i spektroskopiya, 7, 52 (1959). (Trans.Optics & Spectroscopy.)

15. P.P.Kobeko, E.V.Kuvshinskii & N.I.Shishkin, Zhur.tekh.fiz. (Jour.Tech. Phys.) 8, 715 (1938).

16. E.Lippert, Z.Electrochemie, 61, 962 (1957).

DISCUSSION

G.M.Kislyak: We also observed shift of the absorption spectra with decrease in temperature for some organic dyes in different solvents. Specifically, we investigated trypaflavine, fluorescein and rivanolacridine yellow in different alcohols (methyl, ethyl, butyl & isoamyl) and acids (formic, acetic & sulfuric). The experiments were carried out at room temperature and liquid oxygen temperature. The short wavelength section of the absorption spectra at liquid oxygen temperature was shifted some 8-12 mμ to the long wavelength side relative to the position at room temperature. It must be noted, however, that the long wavelengt part of the absorption spectra did not change and that the anti-Stokes region of the spectrum remained unaltered.

INFLUENCE OF SOME FLUORESCENCE QUENCHERS ON THE QUANTUM EFFICIENCY OF PHOTOCHEMICAL CONVERSION OF 9-METHYLANTHRACENE AND 9-METHYL-10-METHOXYMETHYLANTHRACENE

- T.M.Vember & A.S.Cherkasov

It has been shown[1,2] that photochemical conversion of anthracene derivatives can be described by the following kinetic scheme:

	Rate constants
$A + h\nu \rightarrow A^* \rightarrow {}^1A$	
${}^1A \rightarrow {}^3A$	t
${}^1A \rightarrow A + h\nu_f$	f
${}^1A + A \rightarrow A_2$	d
${}^1A + A \rightarrow {}^3A + A$	p
${}^1A + O_2 \rightarrow {}^3A + O_2$	q
${}^3A + S \rightarrow A + S$	k_1
${}^3A + O_2 \rightarrow AOO$	k_2
$AOO \rightarrow A + O_2$	k_3
$AOO + A \rightarrow AO_2 + A$	k_4

Here A, ${}^1A$ and ${}^3A$ are, respectively, anthracene molecules in the unexcited, the excited singlet and the excited triplet states, O_2 is an oxygen molecule, S is a solvent molecule, AOO is the intermediate photo-oxide, A_2 is a photodimer and AO_2 is the final photo-oxide.

We felt it would be of interest to determine whether the above kinetic scheme holds in cases when the photochemical reaction occurs in the presence of a known fluorescence quencher and to obtain some information on the mechanism of the effect of such quenchers on photochemical processes.

To this end we investigated the influence of n-toluidine, potassium iodide and hydroquinone on the quantum efficiencies of fluorescence and photochemical conversion of 9-methyl-10-methoxymethylanthracene, which forms only a photo-oxide, and 9-methylanthracene, which in oxygen free solutions forms only photodimers.*

The above listed quenchers do not absorb in the region of the long wavelength absorption of anthracene derivatives (including the exciting 365 mμ wavelength) and their presence has no effect on either the absorption or the fluorescence spectra of the investigated substances. Potassium iodide partially decomposes under the influence of radiation with the release of iodine, but the fraction of incident light absorbed by this liberated iodine even under the most unfavorable conditions does not exceed 5%, which lies within the limits of the experimental error. Nevertheless, the absorption of the iodine was taken into account in calculating the percent of reacted material.

Fig.1,a shows the variation of the fluorescence efficiency of the investigated anthracene derivatives with the concentration of potassium iodide and hydroquinone. For these quenchers, as for n-toluidine[4], there obtains a virtually linear dependence of the reciprocal of the quantum efficiency as a function of the quencher concentration, i.e., the concentration dependence is described by the Stern-Folmer formula.

The relative coefficient of fluorescence quenching by the investigated quenchers was calculated from the data on quenching in the range of low concentrations in air and in an oxygen-free medium. For calculating the absolute quenching rate coefficients (m) from the relative coefficients $\left(\frac{m}{f+t}\right)$, we used the known value for the sum of the coefficients $(f + t)$ (Ref.2), the value of which is $14.4 \cdot 10^7$ sec^{-1} for 9-methylanthracene and $7.4 \cdot 10^7$ sec^{-1} for 9-methyl-10-methoxymethylanthracene.

---

*The experimental procedure was similar to that employed in the work of Ref.3.

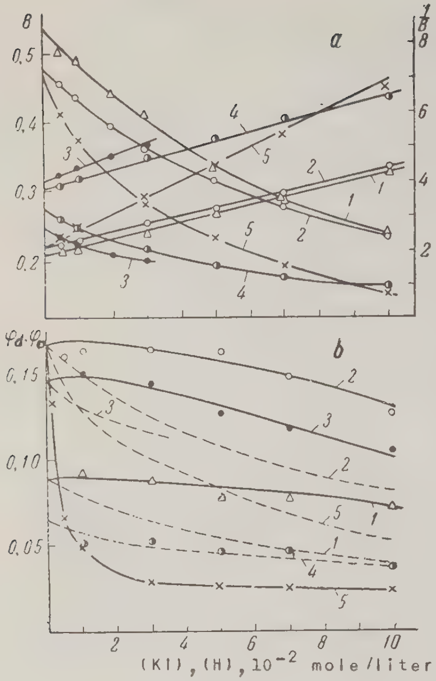

Fig.1. Variation of the quantum efficiencies of fluorescence B (a), photodimerization φ_d and photo-oxidation φ_o (b) of 9-methylanthracene (M) and 9-methyl-10-methoxymethylanthracene (MM) with the concentration of potassium iodide (KI) (1-4) and hydroquinone (H) (5): 1 - (MM) = $3\cdot10^{-3}$ mole/liter, $(O_2) = 1.3\cdot10^{-3}$ mole/liter; 2 - (MM) = $6\cdot10^{-3}$ mole/liter, $(O_2) = 1.3\cdot10^{-3}$ mole/liter; 3 - (MM) = $3\cdot10^{-3}$ mole/liter, $(O_2) = 6.4\cdot10^{-3}$ mole/liter; 4 - (M) = $6\cdot10^{-3}$ mole/liter, $(O_2) = 0$, 5 - (MM) = $6\cdot10^{-3}$ mole/liter, $(O_2) = 1.3\cdot10^{-3}$ mole/liter.

The values of the absolute quenching coefficients lie in the range from $2\cdot10^9$ to $5\cdot10^9$ liter/mole sec.

In view of the kinetic scheme given above one should expect the quantum efficiency of dimerization in the presence of a quencher to decrease in proportion to the decrease in the quantum efficiency for fluorescence. As will be evident from Fig.1,b, this was substantiated by the experimental results. The curves in this figure show the quencher concentration dependences of the quantum efficiency of dimerization calculated on the assumption that the efficiencies decrease in proportion to the fluorescence efficiency. The poin give the experimental values of the quantum efficiencies. It will be seen that the agreement is satisfactory.

The quantum efficiency of photo-oxidation in the presence of n-toluidine also decreases[4], but the efficiency values are considerably lower than if the decrease were proportional to the decrease in fluorescence efficiency. Thus the influence of the quencher on photoexcitation is more comple than on photodimerization, and in order to explain the experimental results one must assume that in addition to deactivation of the singlet-excited molecules there occur other processes also leading to reduction of the quantum efficiencies for the formation of photo-oxides. We hypothesize that there may also occur the following processes involving the quencher:

	Rate constants
1. $^1A + T \rightarrow A + T$	m'
2. $^1A + T \rightarrow {}^3A + T$	m
a. $^3A + T \rightarrow A + T$	m_1
b. $AOO + T \rightarrow A + TOO$	m_2

(T is a quencher molecule).

Adding these processes in different combinations to the initial reaction scheme, we obtain a number of new schemes and corresponding equations for the quantum efficiencies of fluorescence (B) and photoexcitation (φ_o). In order to choose among these possible schemes, we used the following experimental facts: the ratio of the quantum efficiency of fluorescence of 9-methyl-10-methoxymethylanthracene to the quantum efficiency of photo-oxidation (B/φ_o) in the presence of n-toluidine (at constant concentrations of the anthracene derivative and oxygen) is a linear function of the n-toluidine concentration (Fig.2). This linear dependence follows only from the equations corresponding to the schemes of Fig.1, i.e., to the cases when the singlet-excited molecules are quenched without transition to the triplet state and there is interaction of the quencher with the triplet molecules or with the intermediate photo-oxide. Comparing the experimental data with the quantities calculated by means of the equations corresponding to these schemes, we found tha

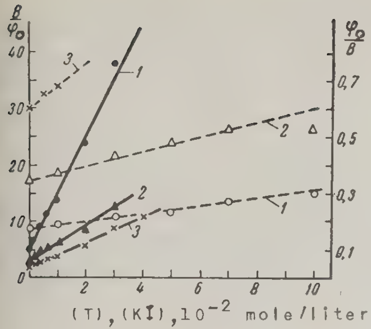

←Fig.2. Variation of the ratio of fluorescence efficiency B to the quantum efficiency of photoexcitation φ_o of 9-methyl-10-methoxymethylanthracene (MM) with the concentration of n-toluidine (T) (solid lines) and the variation of the ratio φ_o/B for 9-methyl-10-methoxymethylanthracene with the potassium iodide (KI) concentration (dashed lines): 1 - (MM) = = $3 \cdot 10^{-3}$ mole/liter, $(O_2) = 1.3 \cdot 10^{-3}$ mole/liter; 2 - (MM) = $6 \cdot 10^{-3}$ mole/liter, $(O_2) = 1.3 \cdot 10^{-3}$ mole/liter; 3 - (MM) = $3 \cdot 10^{-3}$ mole/liter, $(O_2) = 6.4 \cdot 10^{-3}$ mole/ /liter.

the mechanism 1,b is most consistent with the experimental dependence.[4] Thus investigation of the influence of n-toluidine on photoexcitation of 9-methyl-10-methoxymethylanthracene leads to the following deductions.

1. Toluidine quenches singlet-excited molecules without transition of the molecules to the triplet state.
2. Toluidine interacts with the intermediate photo-oxide, yielding the initial substance.
3. Toluidine does not deactivate triplet molecules.

Investigation of the influence of potassium iodide on the fluorescence and photochemical conversion of 9-methyl-10-methoxymethylanthracene (Fig.1) showed that in this case the fluorescence is suppressed appreciably more strongly than photoexcitation, although a small decrease in the quantum efficiency of photo-oxidation is observed with increase of the KI concentration. The variation of the quantum efficiency of photo-oxidation of 9-methyl-10-methoxymethylanthracene as a function of the KI concentration calculated on the assumption that this efficiency is proportional to the fluorescence efficiency is shown in Fig.1,b; the points in this figure give the corresponding experimental values. It was also found that the ratio of the experimental values of the photoexcitation efficiency to the fluorescence efficiency (φ_o/B) for constant concentrations of 9-methyl-10-methoxymethylanthracene and oxygen is a linear function of the potassium iodide concentration (Fig.2).

Assuming that in the case of potassium iodide there may occur the same processes as with n-toluidine and analyzing the equations following from the inferred reaction schemes, we found that the condition for linear variation for φ_o/B with KI concentration is satisfied by the equations for the quantum efficiencies of photo-oxidation and fluorescence following from the scheme obtained by adding only process 2, i.e., the process of transition of singlet-excited molecules to the triplet state:

$$B = \frac{\frac{f}{f+t}}{1 + \frac{p+d}{f+t}[A] + \frac{q}{f+t}[O_2] + \frac{m}{f+t}[T]};$$

$$\varphi_o = \frac{\frac{t}{f+t} + \frac{p+d}{f+t}[A] + \frac{q}{f+t}[O_2] + \frac{m}{f+t}[T]}{1 + \frac{p+d}{f+t}[A] + \frac{q}{f+t}[O_2] + \frac{m}{f+t}[T]} \cdot \frac{\frac{k_2}{k_1}[O_2]}{1 + \frac{k_2}{k_1}[O_2]} \cdot \frac{\frac{k_4}{k_3}[A]}{1 + \frac{k_4}{k_3}[A]}.$$

A second variant of the scheme yielding a linear dependence is the scheme including processes 1 and 2, i.e., the case when the transition of singlet-excited molecules to the triplet state under the influence of potassium iodide occurs with a probability smaller than unity (we denote this case by K2). The KI concentration dependences of the photo-oxidation efficiency for different 9-methyl-10-

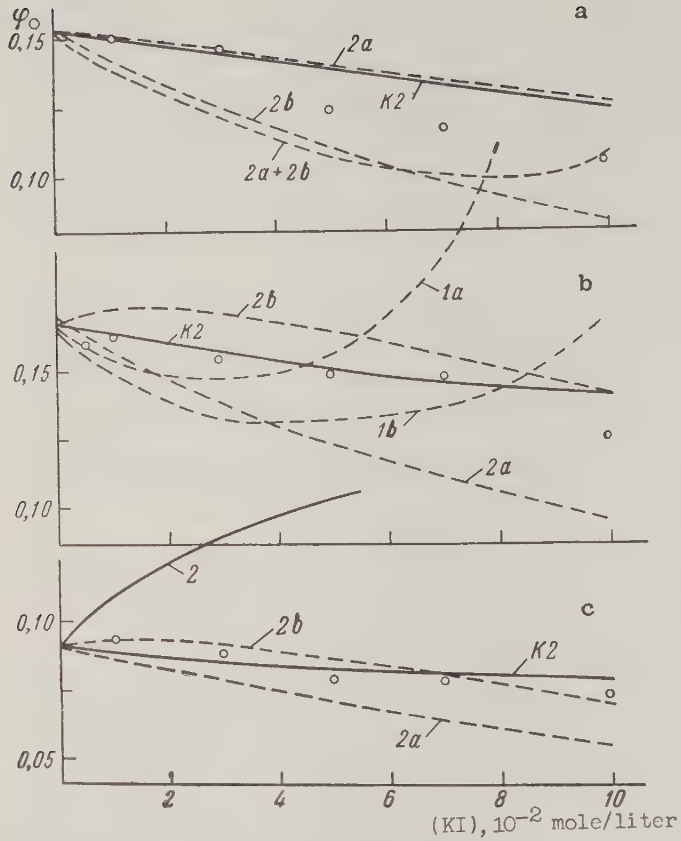

Fig.3. Experimental and theoretical dependences of the quantum efficiency of photo-oxidation of 9-methyl-10-methoxymethylanthracene (MM) on the potassium iodide concentration (KI): a - (MM) = $= 3 \cdot 10^{-3}$ mole/liter, $(O_2) = 6.4 \cdot 10^{-3}$ mole/liter; b - (MM) = $6 \cdot 10^{-3}$ mole/liter, $(O_2) = 1.3 \cdot 10^{-3}$ mole/liter; c - (MM) = $3 \cdot 10^{-3}$ mole/liter, $(O_2) =$ $= 1.3 \cdot 10^{-3}$ mole/liter. Lines - calculated curves (see text); points - experimental.

methoxymethylanthracene and oxygen concentrations calculated on the basis of different scheme are shown in Fig.3. The points in the figure give the experimental values of the quantum efficiency. The solid lines show the dependences calculated from the equations satisfying linear variation of φ_0/B with the KI concentration. The dashed lines give the dependences corresponding to some of the other equations. It will be evident that mechanism 2 is not consistent with the experimental data, i.e., there must exist some other processes further decreasing the quantum efficiency of photo-oxidation. The best, although far from satisfactory, agreement is secured by using the equations corresponding to process K2. Somewhat poorer agreement is obtained for mechanisms 2,a and 2,b, processes involving quenching of singlet-excited molecule with transition to the triplet state, and deactivation by potassium iodide of triplet molecules or reduction by the KI of the intermediate photo-oxide to the initial substance. Hence we draw the following conclusions.

1. Quenching of the fluorescence of the investigated anthracene derivatives in liqui solutions by potassium iodide is due to transition of the molecules from the singlet-excited state to the triplet state.

2. It is impossible to determine on the basis of the data now available whether the observed decrease in photo-oxidation efficiency is due primarily to quenching with transition of singlet-excited molecules to the ground state, quenching of triplet molecules by potassium iodide, or reduction of the intermediate photo-oxide; it is not impossible that all three processes contribute in some measure to the decrease in photo-oxidation efficiency.

It must be noted also that Zelinskii & Kolobkov[5] observed in solid solution of some aromatic compounds an increase of the ratio of the phosphorescence to fluorescence efficiency in the presence of potassium iodide; this change in relative efficiencies indicates transition of singlet-excited molecules to the triplet state.

Investigation of the quantum efficiencies of fluorescence and photo-oxidation of 9-methyl-10-methoxymethylanthracene in the presence of different concentrations of hydroquinone showed that in this case, as in the case of n-toluidine, the photo-oxidation efficiency is lower than would be the case if the quenching occurred only on the singlet level (Fig.1). However, we found that in this case hydroquinone itself reacts photochemically with the 9-methyl-10-methoxymethylanthracene.

Thus our investigation showed that the mechanism of interaction of different quenching agents with excited anthracene derivative molecules differs, but that in all cases one can in some measure explain the observed effects in the framework of the proposed reaction scheme. Obviously, in each case under consideration there may occur concurrently other processes, but apparently their role is minor.

References

1. E.J.Bowen & D.W.Tanner, Trans.Faraday Soc., 51, 475 (1955).
2. A.S.Cherkasov & T.M.Vember, Optika i spektroskopiya, 6, 503 (1959). (Trans.Optics & Spectroscopy.)
3. A.S.Cherkasov & T.M.Vember, Ibid., 4, 203 (1958).
4. A.S.Cherkasov & T.M.Vember, Ibid., 7, 321 (1959). (Trans.Optics & Spec.)
5. V.V.Zelinskii & V.P.Kolobkov, Ibid., 1, 560 (1956).

INFLUENCE OF TEMPERATURE ON THE LUMINESCENCE OF HALIDE SOLUTIONS OF HEAVY METALS

- M.U.Belyi & B.F.Rud'ko

Although the fact that aqueous solutions of salts of the heavy metals (Tl, Pb & Sn) luminesce has long been known, hitherto there have not been available sufficient experimental data to determine the precise mechanism of absorption and luminescence of such solutions. Investigation of the temperature behavior of the absorption and emission spectra should yield some indication of the nature of this mechanism; moreover, such studies can yield valuable information on the interaction of heavy metal ions with the surrounding medium in the process of luminescence.

To facilitate observation of the effects in question we chose for our investigation only water solutions of the heavy metal salts that transform readily a transparent glass-like mass upon cooling. The halide ions were introduced by dissolving LiHal salts or by the addition of HHal acids, which in the case of solutions is admissable inasmuch as introduction of the extraneous ions has no significant effect on the absorption and emission spectra.

The measurements were carried out by means of ISP-51 and ISP-28 spectrographs with a photoelectric attachment incorporating an EPP-09 recorder.[1] The source in all the experiments was a hydrogen discharge tube. The temperature of the solution in the thermostat cell was measured to within ±3°C by a thermocouple.

We investigated the luminescence and absorption spectra of chlorine and bromine solutions of thallium, lead and tin at different temperatures. Some of the experimental results are shown in Figs.1, 2 & 3. The first and most important point to be noted is that all the investigated heavy metal solutions behaved in a similar fashion: the absorption spectra are deformed relatively little with change in temperature (the absorption band is somewhat narrowed, the peak becomes higher and is shifted slightly to the short wavelength side); the luminescence spectra upon cooling are first shifted somewhat to the long wavelength side and then with further reduction of the temperature undergo a pronounced shift to the side of shorter wavelengths.

Decrease in temperature is accompanied by an appreciable increase of the quantum efficiency. Thus, for example, in the case of chlorine solutions of lead reduction of the temperature from room temperature to that of liquid oxygen results in a sevenfold increase of the luminescence yield. The increase in luminescence efficiency occurs mainly in the temperature interval corresponding to the initial long wavelength shift of the luminescence spectrum. Further reduction of the temperature, resulting in the short wavelength shift of the emission band, leads to only an insignificant further increase of the luminescence yield. For convenience in plotting, all the spectra in Figs.1, 2 & 3 were normalized to the same height.

It is known that the process of quenching depends on the persistence of luminescence and on the temperature. The luminescence of the investigated solutions has a fairly long persistence (for example, the decay time of Tl solutions is reported[2] to be of the order of 10^{-5}-10^{-6} sec). Hence one can expect a high probability for quenching. On the other hand, a factor favoring decrease of quenching is reduction of the temperature. Upon cooling the investigated solutions rapidly increase in viscosity. As a result, thermal motion of the ions in the solution is sharply reduced and conversion of the absorbed energy to heat decreases significantly. Inasmuch as at a certain temperature the viscous solution solidifies to a glass-like mass, the sharp increase in luminescence intensity is observed mainly above this vitrification temperature. Further lowering of the temperature is accompanied by only a slight increase in luminescence yield. By way of example of intense temperature quenching one can cite the case of bromine solutions

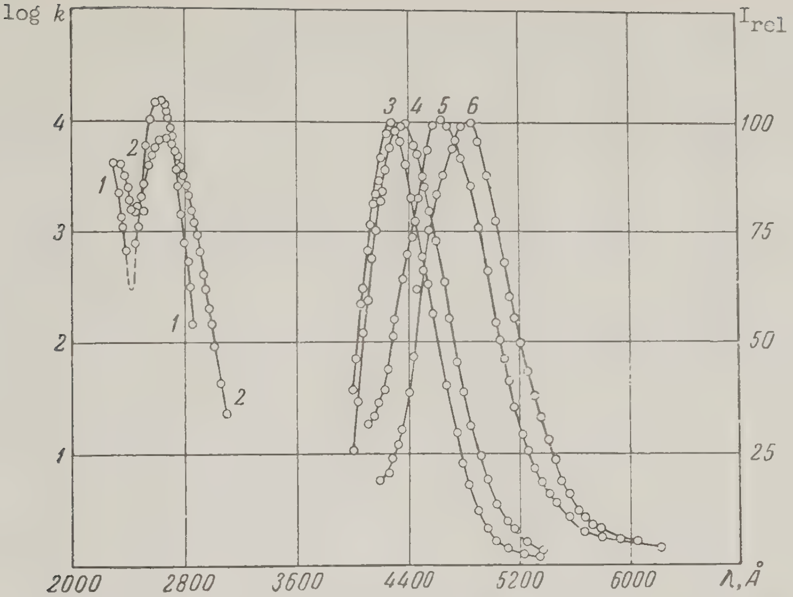

Fig.1. Absorption (1,2) and luminescence (3-6) spectra of solutions of TlBr in LiBr (12 mole/liter): 1) 115°K, 2) 290°K, 3) 115°K, 4) 153°K, 5) 290°K, 6) 210°K.

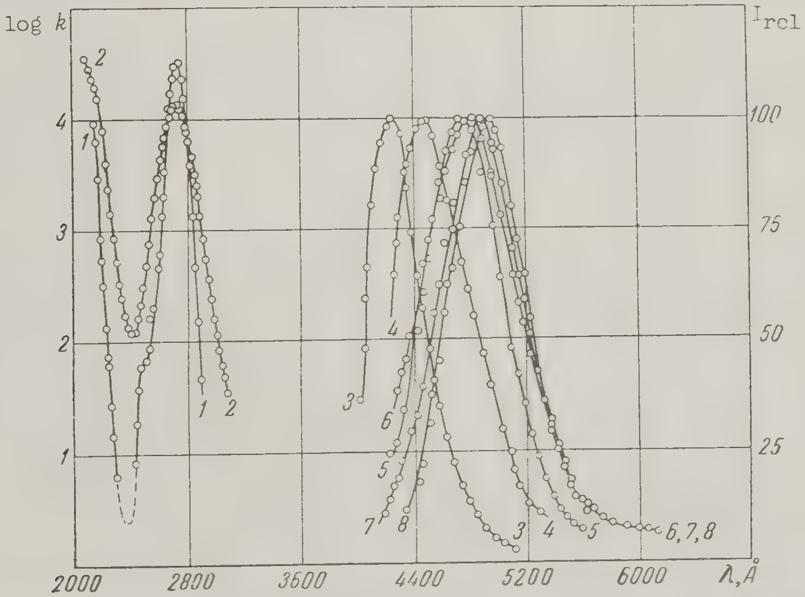

Fig.2. Absorption (1,2) and luminescence (3-8) spectra of solutions of $PbCl_2$ in HCl (7 mole/liter): 1) 115°K, 2) 290°K, 3) 115°K, 4) 140°K, 5) 153°K, 6) 290°K, 7) 218°K, 8) 200°K.

of tin and lead which at room temperature do not luminesce at all, while at low temperatures emit rather intense radiation in the 5750 and 4250 Å regions, respectively. Similar strong temperature quenching was observed by Sevchenko & Volod'ko[3] in solutions of uranyl salts.

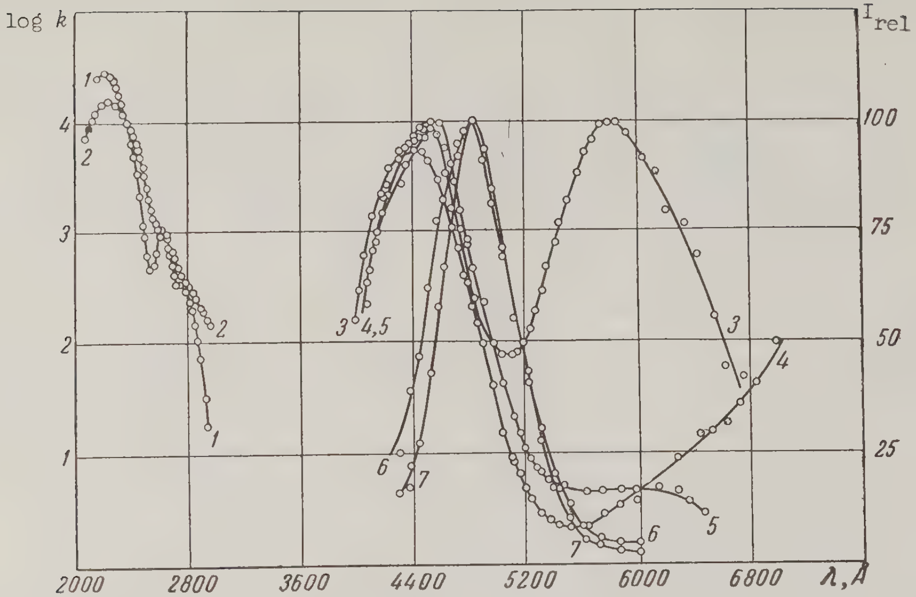

Fig.3. Absorption (1,2) and luminescence (3-7) spectra of solutions of $SnCl_2$ in HCl (8 mole/liter): 1) 115°K, 2) 290°K, 3) 115°K, 4) 140°K, 5) 153°K, 6) 290°K, 7) 218°K.

It is interesting to note that the optical properties of the investigated solutions have much in common with crystal phosphors of similar composition. In both cases there is observed an appreciable divergence between the peaks of the potential curves for the ground and excited states, as evinced by the Stokes losses. At low temperatures no vibrational structure is discernible in either the absorption or luminescence spectra. Consequently, here, as in similar crystal phosphors, there is appreciable liberation of heat.[4] Analogous behavior for comparable substances has been observed in investigating the absorption and luminescence spectra incident to reduction of temperature. Thus in both cases we have an insignificant shift to the short wavelength side and narrowing of the absorption band.[5] If we compare the behavior of our solutions in the vitreous state with the behavior of crystal phosphors of similar composition, we readily discern similarities as regards variation of the luminescence bands: with decrease of temperature the position of the luminescence peak shifts to the side of shorter wavelengths.[6] It must be emphasized that the observed displacements of the luminescence bands of the solutions are appreciably greater than the corresponding shifts of the bands of crystal phosphors. In the accompanying table we give some data on the positions of the luminescence peaks in the spectra of some of the investigated solutions as a function of the temperature.

In view of the similar behavior of the investigated solutions and crystal phosphors of like composition we are warranted in interpreting the origin of the absorption and luminescence bands of the solutions by analogy with the corresponding crystal phosphors. Consequently, we can assume that the long wavelength absorption bands of the solutions (which approximately coincide in the wavelength scale with the corresponding bands for crystal phosphors) are due to ${}^1S_0 \rightarrow {}^3P_1$ electron transitions, while the luminescence bands are associated with ${}^3P_1 \rightarrow {}^1S_0$ transitions.[4,7]

Substancc	290° K	218° K	210° K	200° K	153° K	140° K	115° K
Sn in HCl	4800	4820	—	—	4500	4500 & >7000	4400 & 5820
Pb in HCl	4820	4900	—	4940	4740	4490	4220
Tl in LiBr	4630	—	4830	—	4360	—	4290

On the basis of this assumption we can attempt to interpret the shift of the luminescence bands with variation in temperature. As was indicated above, with decrease of temperature from room temperature to that of vitrification there is observed a shift of the luminescence spectrum to the long wavelength side. Our observations show that in this temperature interval there occurs an appreciable volumetric compression (contraction) of the solution (there is little further reduction in volume with further cooling). According to the data of Kirs[8], the position of the luminescence spectrum of crystal phosphors varies with the degree of hydrostatic compression inasmuch as such compression alters the parameters of the crystal lattice. Kirs, however, found that with increase of pressure the luminescence bands of crystal phosphors shift to the short wavelength side, whereas we observed a shift to the long wavelength side with cooling (contraction). This contradiction can readily be explained if we assume that in the case of all the solutions we are dealing with simple luminescence bands and that the equilibrium ionic configuration of the excited state is realized for smaller values of the coordination coordinates than the corresponding configuration of the ground state. Precisely such arrangement of the potential curve is assumed for a number of crystal phosphors.[7] Admittedly, it is possible that there operates here a different mechanism, producing a shift of the luminescence spectrum to the long wavelength side. However, taking into account the appreciable change in volume with reduction of temperature in the indicated interval, the effect of compression should be regarded as the most important factor responsible for the long wavelength shift of the luminescence bands.

As for the short wavelength shift of the emission spectrum, observed with further lowering of the temperature, taking into account its appreciable magnitude and the fact that the position of the absorption peak remains virtually constant, this shift of the luminescence band can be interpreted as being due to the existence of a wide smeared out potential curve for the excited state of the heavy metal ion, in contrast to the potential curve for the ground state, which is characterized by a sharp potential energy minimum. If this is the case, a small increase in the equilibrium configuration coordinate of the excited state, due to change in interaction of the excited ion with the surrounding medium, should lead to an appreciable short wavelength shift of the luminescence spectrum with little change in the position of the absorption peak. As noted above, this is precisely what we observed in our experiment. The minor displacement of the absorption spectrum to the short wavelength side occurring in this case can be explained if we recall that some further minor contraction (compression) occurs with further decrease of temperature. It is interesting to note that in the case of chlorine solutions of tin at low temperatures there appears a new luminescence band in the red region; at 115°K this peaks at about 5820 Å. The intensity of this band differs substantially in LiCl as against HCl solutions of tin. The nature of this band has not yet been clarified.

"T.G. Shevchenko" Kiev State University

References

1. B.F.Rud'ko, Visnik KDU No.2 (News, Kiev State Univ. No.2) Chemical-physical Series, Issue 1, 75 (1959).

2. I.I.Kondilenko, Thesis, Kiev State University, 1949.

3. A.N.Sevchenko & L.V.Volod'ko, Izv.AN SSSR, Ser.fiz., 20, 464 (1956). (Trans. Bulletin, 20, 422.)

4. Ch.B.Lushchik, N.E.Lushchik & K.K.Shvarts, Trudy (Proceedings), Institute of Physics and Astonomy, Estonian SSR Ac. of Sci., 8, 3 (1958); 6,5 (1957).

5. H.Lorenz, Z.Phys., 46, 558 (1928).

6. D.A.Patterson & C.C.Klick, Phys.Rev., 105, 401 (1957).

7. N.N.Kristofel', Optika i spektroskopiya, 7, 78 (1959). (Trans.Optics & Spec.)

8. Ya.Ya.Kirs, Trudy (Proceedings), Physical Institute of Physics and Astronomy, Estonian SSR Ac. of Sci., 4, 108 (1956).

DIELECTRIC EFFECTS AND THE ELECTRONIC SPECTRA OF POLYATOMIC ORGANIC MOLECULES IN SOLUTIONS

- N.G.Bakhshiev

The influence of the solvent on the spectral characteristics of the molecules of the dissolved substance is fundamental in molecular spectroscopy, inasmuch as most investigations in this field are carried out with solutions or substances in the condensed state. The emitting or absorbing molecule in a solution is always under the influence of neighboring molecules of the medium, which can produce a substantial alteration of the optical properties of the molecule. Hence the experimental absorption and fluorescence spectra observed in this case will characterize not the properties of the investigated molecule per se but the properties of the system molecule + medium.

Despite the fact that since the middle of the last century there have been numerous investigations of this problem, it cannot be regarded as solved, inasmuch as until recently no one succeeded in describing the phenomenon in general form; moreover, the results of many investigations are contradictory. Only within the last few years has there been some progress in this field[1-8] and this has been due to an appreciable extent to utilization of the concepts regarding the structure of solutions borrowed from the theory of the molecular structure of liquids.

In accord with modern views[8], molecular interactions in solutions can be divided into two basic types: 1) universal interactions connected with the influence of the aggregate (collective) of the surrounding solvent molecules on the solute molecule, and 2) specific (individual) interactions between the solute molecule and one or more of the surrounding particles. This terminology is meaningful inasmuch as the indicated types of interaction are obviously not equivalent: one can imagine systems in which there are no specific interactions, whereas collective interactions obtain in all cases.

We believe that a complete description of an actual system can be realized only by considering both the collective (macroscopic description) and the individual (microscopic description) effect of the molecules of the surrounding medium on the spectrum of the solute molecule. In actual systems specific interactions are always present to some degree. We believe, therefore, that the molecule of the dissolved substance, linked by specific interactions with a molecule of the solvent or an extraneous particle, must be regarded as a new center of absorption or emission, subject, in turn, to the universal action of the aggregate of the surrounding particles, which are described by the internal field in the solution[8]. In view of this, the first stage in elucidating the influence of the solvent must consist in investigating the general, universal effects and clarifying their contribution to the phenomenon as a whole. We must emphasize the fact that taking into account this universal interaction is particularly important precisely from the standpoint of investigation of specific interactions, which always and inevitably are evinced against the "background" of the universal influence of the medium.

In view of the above, the question of the influence of molecular interactions on the spectra of solutions must be approached in the following manner. First, one must take into account the influence of universal interactions on the spectrum of the absorption or emission centers, and then, analyzing the spectrum of the centers, judge of the nature and strength of the specific interactions. Then the divergence between experiment and the theory describing the universal influence of solvents will be a measure of the specific interactions. It must be noted that in studies devoted to specific interactions (hydrogen bonds, complex formation, solvation, association and the like) generally no specific effort has been made to segregate or isolate the effects of universal character. In some cases this may be unimportant in view of the pronounced predominance of the specific interactions, but in other cases this approach may lead to erroneous interpretations and confusion.

The purpose of the present paper is to consider briefly the universal interactions, methods of investigating them and ways of isolating them from the total effect observed experimentally.

Theoretical consideration of the influence of collective actions, connected with the necessity of summing the actions of the surrounding particles on the molecule of the dissolved substance, is necessarily predicated (at least at present) on the introduction of a specific model representing the investigated system. The sole reliable criterion for the applicability of any given model is obviously agreement of the theory based on this model with more or less extensive experimental data.

In the work of Refs.2-8, devoted to investigations of the influence of the solvent on absorption spectra, the model commonly utilized to represent the system particle + medium is the Onsager model, in which the molecule is regarded as a dipole (sum of the premanent moment of the molecule and the moment induced by the light wave) located in a dielectric medium and exposed to the influence of the internal field of the solvent. The difference between the strengths of this dipole in the ground and excited states of the molecule determines the different changes in the position of the levels and, consequently, the shift in the spectra.

In earlier work[6,7] we deduced the following expression, based on the Onsager model, for the shift of the spectra of solutions relative to the spectra of vapor

$$\Delta\nu = \nu_{\mathrm{sol}} - \nu_{\mathrm{vap}} = \frac{1}{r^3}\left[C_1\frac{2\varepsilon-2}{2\varepsilon+1} + (C_2 + fC_3)\frac{2n^2-2}{2n^2+1}\right], \qquad (1)$$

here r is the effective Onsager radius, which is virtually equal to the radius of the molecule, ε is the dielectric constant, n is the index of refraction of the solvent, and f is the oscillator strength of the investigated electronic transition; the constants C_1 and C_2 represent functions of the permanent dipole moment of the molecule in the lower and upper electronic states, and the constant C_3 depends on the frequency of the purely electronic transition. Despite the simplicity of the model on which it is based, this equation describes the shift of the spectra for all possible combinations from the case of dipole molecules in a polar solvent to the case of dipoleless molecules in a nonpolar medium. In the latter case, although $C_1 = C_2 = 0$, the very existence of spectra $(f \neq 0)$ implies the possibility of some shift thereof.

The applicability of these model concepts is illustrated by the data of Figs. 1, 2 & 3, wherein we have plotted the shift of the spectra of solutions relative to the spectra of the respective vapors for anthracene (molecule without a permanent dipole) and two phthalimide derivatives and α-naphthol (dipole molecules) in a form corresponding to Eq.(1), i.e., in the form of variation of the shift as a function of ε and n. As will be evident from the figures, the linear variation predicted by (1) is on the whole closely adhered to, including the points pertaining to the vapors (origin). As might be expected for the dipoleless molecules of anthracene there is evinced a dependence only on the index of refraction of the solvent. In the case of dipole molecules (phthalimides and α-naphthol) there is evinced a dependence on both the index of refraction and the dielectric constant of the medium, the character of this dependence being determined by the ratio of the values of the permanent and induced dipole moments in the normal and excited states of the respective molecules.

From analysis of the experimental data we can draw a number of inferences regarding the properties of the molecules under consideration and, in particular, regarding the character of the changes in their permanent dipole moments incident

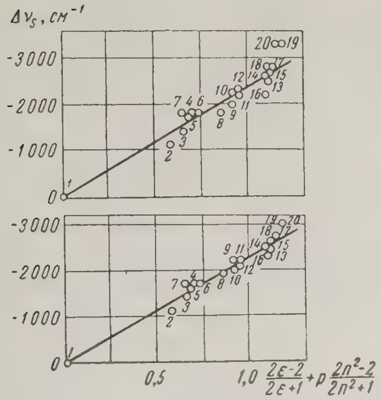

Fig.1

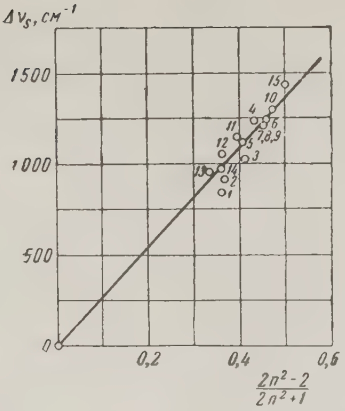

Fig.2

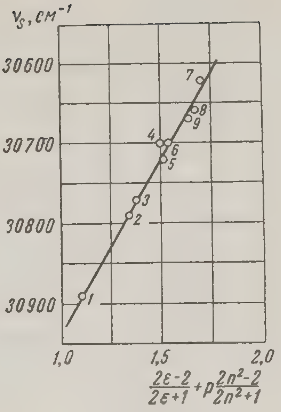

Fig.3

Fig.1. Variation in the shift of the symmetry frequency ν_s in the spectra of 3-monoethylaminophthalimide (a) and 3-dimethylaminophthalimide (b) with the dielectric constant ε and the index of refraction n of the solvent.[7] 1) Vapors; solvents: 2) n-heptane, 3) CCl_4, 4) benzene, 5) toluene, 6) xylene, 7) dioxane, 8) ethyl ether, 9) anisole, 10) butyl acetate, 11) chloroform, 12) ethyl acetate, 13) pyridine, 14) isoamyl alcohol, 15) isobutyl alcohol, 16) acetone, 17) ethyl alcohol, 18) methyl alcohol, 19) glycerol, 20) water.

Fig.2. Variation in the shift of the symmetry frequency ν_s in the spectra of anthracene as a function of the index of refraction of the solvent.[9-12] Solvents: 1) n-pentane, 2) n-hexane, 3) cyclohexane (110°), 4) CCl_4 (110°), 5) dioxane, 6) benzene, 7) toluene, 8) xylene, 9) mesitylene, 10) chlorobenzene, 11) amyl alcohol, 12 & 14) ethyl alcohol, 13) methyl alcohol, 15) naphthalene (90°).

Fig.3. Variation in the position of the frequency symmetry ν_s in the spectra of α-naphthol with the dielectric constant ε and the index of refraction n of the solvent.[3] Solvents: 1) n-hexane, 2) benzene, 3) toluene, 4) butyl acetate, 5) ethyl acetate, 6) methyl acetate, 7) butyl alcohol, 8) ethyl alcohol, 9) methyl alcohol.

to excitation; moreover, we can follow the influence on the position of the absorption spectra of specific interactions obtaining in some solutions.

The availability of a large amount of data (at present we have either investigated ourselves or extracted from the literature data on the spectra of the vapors and solutions of over 60 organic substances characterized by different types of electronic transitions) gives reason to assert that the proposed model concept and the theory in its relatively simple form correctly describe the universal interaction and can serve as the basis for systematic analysis of many experimental results.

In conclusion, we note that the expedience of dividing interactions of molecules in solutions into universal and specific interactions is to a certain degree a formal approach to describing the effects in question. In actual systems there is obviously a gamut of interactions ranging from pair interaction to the integral action of the collective of surrounding particles on the solute molecule. Undoubtedly, in some actual cases it may be difficult to classify a given form of interaction in one category or the other. Moreover, it is highly probable that the considered variant of the theory describes, if only formally, systems in which there are partially evinced specific interactions, not fully consistent with the model concept of a dissolved molecule in the form of a dipole subjected to the averaged effect of the medium. Obviously, the present version of the theory taking into account primarily universal interactions must and should be improved. Nevertheless, we believe that the proposed classification of interactions as universal or specific (macro- or microscopic) is at present not only warranted but a necessary and useful expedient.

References

1. N.Baylis & E.McRee, J.Phys.Chem., 58, 1002 (1954).
2. Y.Ooshika, J.Phys.Soc.Japan., 9, 594 (1954).
3. N.Mataga, Y.Kaifu & M.Koizumi, Bull.Chem.Soc.Japan, 28, 690 (1955); Ibid., 29, 465 (1956).
4. E.McRae, J.Phys.Chem., 61, 562 (1957).
5. E.Lippert, Z.Electrochemie, 61, 962 (1957).
6. N.G.Bakhshiev, Izv.AN SSSR, Ser.fiz., 22, 1387 (1958). (Trans.Bulletin, 22, 1377 (1958).
7. N.G.Bakhshiev, Optika i spektroskopiya, 7, 52 (1959). (Trans.Optics & Spectroscopy.)
8. B.S.Neporent & N.G.Bakhshiev, Ibid., 8, 777 (1960). (Trans.Ibid.)
9. S.Sambursky & G.Wolfsohn, Trans.Faraday Soc., 36, 427 (1940).
10. S.Sambursky & G.Wolfsohn, Phys.Rev., 62, 357 (1942).
11. A.S.Cherkasov, Zhur.fiz.khim. (Jour.Phys.Chem.), 29, 2209 (1955).
12. S.Veljković, Trans.Faraday Soc., 53, 1181 (1957).

INFLUENCE OF THE SOLVENT ON THE FLUORESCENCE SPECTRA OF ACETYLANTHRACENES

- A.S.Cherkasov

The wavelength of the fluorescence spectra of many organic compounds is strongly dependent on the solvent. This is true, for example, for various phthalimides derivatives[1-3], stilbene[4] and acridone[5]. A number of investigators have attempted to correlate the influence of the solvent on the absorption and emission spectra with the dielectric constant ϵ and the index of refraction n of the solvent. Experimental checks of the theoretically deduced dependences[3] showed that there is a definite relationship between these quantities, but the large number of experimental deviations from the results predicted by theory has impelled many authors to question the validity of correlating the influence of the solvent on the spectrum with its macroscopic characteristics. Thus, for example, Zelinskii et al[1] advanced the hypothesis that the influence of the solvent is due primarily to interaction of the solute molecules with charges concentrated on the individual atoms of the solvent molecules. In substantiation of this view they cite the fact that solvents having the same functional groups often exert a like influence on the spectra.

Thus there is no unanimity of views regarding the influence of the solvent on the spectra of organic substances; this is partially due to lack of sufficiently extensive and reliable experimental data.

In our experiments we found that the nature of the solvent is an important factor where the fluorescent spectra of 1- and 2-acetylanthracene are concerned. Thus, in going from hexane, the solvent in which the fluorescence spectra of the acetylanthracenes occupy the highest frequency position (22 450 cm^{-1} for 1-acetylanthracene and 23 450 cm^{-1} for 2-acetylanthracene) to water the fluorescence peaks shift as much as 4950 cm^{-1} (see table).

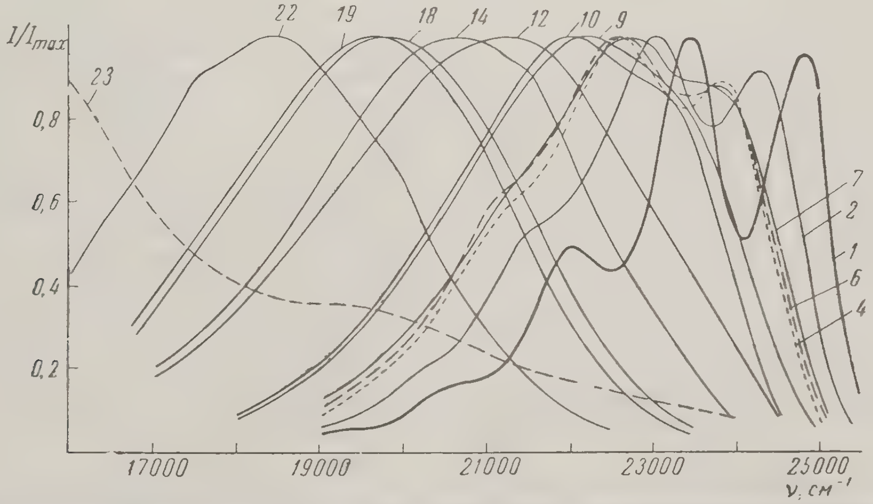

Fig.1. Fluorescence spectra of 2-acetylanthracene in different solvents. Concentration 2·10^{-5} mole/liter. The numbers at the curves identify the solvents as listed in the accompanying table.

At the same time there is observed a gradual smearing out of the vibrational structure (Fig.1), which in the case of the spectra of 2-acetylanthracene in hexane has a typical "anthracene" character (in the spectra of 1-acetylanthracene the structure is less clearly pronounced), while in alcohols and water it is almost completely effaced. It should be noted that the influence of the solvent on un-

Shift of the fluorescence peaks of 1-acetylanthracene ($\Delta\nu_1$) and 2-acetylanthracene ($\Delta\nu_2$) in different solvents relative to the position in *n*-hexane*

No.	Solvent	ε	n_D	$\Delta\nu_1$, cm⁻¹	$\Delta\nu_2$, cm⁻¹
1	*n*-Hexane	1,89	1,37	0	0
2	Ether	4,33	1,35	550	350
3	Carbon tetrachloride	2,23	1,46	650	550
4	Benzene	2,23	1,50	950	750
5	Toluene	2,29	1,50	950	—
6	Dioxane	2,21*	1,42	1000	700
7	Ethyl acetate	6,02*	1,37	1000	650
8	Chlorobenzene	5,62*	1,52	1150	1050
9	Acetone	21,45	1,36	1450	1200
10	Pyridine	12,5	1,51	1550	1400
11	Chloroform	4,8	1,44	1650	1500
12	Acetic anhydride	20,5	1,39	2300	2150
13	Cyclohexanol	15,0*	1,46**	2550	2700
14	*n*-Octyl alcohol	10,3	1,43	—	2750
15	*n*-Heptyl alcohol	12,1	1,42	—	2800
16	*n*-Hexyl alcohol	13,3*	1,42	—	2950
17	Ethyl alcohol	25,8	1,36	2950	—
18	Methyl alcohol	33,1	1,33	3550	3650
19	Benzyl alcohol	13,0	1,54	—	3750
20	Ethylene glycol	37,7*	1,43	3750	4100
21	Glycerol	42,5*	1,47*	4450	—
22	Water	80,4	1,33	4950	4950
23	Acetic acid	7,1	1,37	—	—
24	Glucose (20°)	6	—	—	2800
25	Glucose (80°)	23	—	—	4700

---

*Note: the figures with no asterisks pertain to values of ϵ and *n* at 20°; with one asterisk to values of 25°; with two asterisks to values of 30°.

excited acetylanthracene molecules is apparently minor, inasmuch as the position of the absorption spectra is virtually independent of the nature of the solvent, and there is evident only a certain smearing out of the structure of the long wavelength band in polar solvents.

Careful examination of the data listed in the accompanying table shows that in nonpolar solvents (hexane, CCl_4, benzene) the peak of the fluorescence spectrum consistently shifts to the long wavelength side with increase of the index of refraction (for the given solvents the variation is linear within the limits of the experimental error). In all the investigated polar solvents (except ether) the magnitude of the shift is greater than in nonpolar solvents, but there is no consistent correlation with the value of the dielectric constant. Thus, acetone and pyridine, for which the values of ϵ are 21.4 and 12.5 (n_D = 1.36 and 1.51) produce an appreciably smaller shift than octanol and benzyl alcohol, for which ϵ = 10.3 and 13 (n_D = 1.36 and 1.54) and even a smaller displacement than chloroform (ϵ = 4.8, n_D = 1.44).

For the purpose of clarifying the relation between ϵ and the magnitude of the spectrum shift one can utilize the fact that ϵ varies greatly with temperature in some solvents that undergo vitrification.

Fig.2 shows the results we obtained in investigating the influence of temperature on the fluorescence spectra of solutions of 2-acetylanthracene in glucose. As will be evident from the figure, change in temperature produces a simultaneous change in the position of the fluorescence peak and the value of the dielectric constant; the fluorescence peak wave number vs temperature curve virtually repeats the dielectric constant vs temperature curve. Shift of the fluorescence

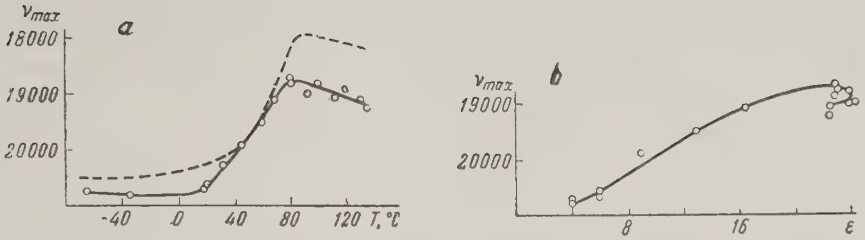

Fig.2. Variation in the frequency of the fluorescence peaks of 2-acetylanthracene dissolved in glucose as a function of the temperature (a) and the dielectric constant (b). Acetylanthracene concentration $2 \cdot 10^{-5}$ mole/liter. The dashed line represents the temperature variation of ϵ according to the data in the literature[8].

peak plotted against the dielectric constant yields nearly a straight line. It must be noted that glucose exerts a particularly strong influence on the position of the fluorescence spectra of acetylanthracenes. Even at low temperatures, when the value of ϵ is only 4-6, the peak of the fluorescence spectrum is shifted some 2500-2800 cm^{-1} relative to its position in a hexane solution.

The experimental results show that all solvents producing a strong shift of the spectrum contain hydroxyl groups, which gives reason to infer that these groups are capable of entering into some sort of specific interaction with the acetylanthracenes.

Investigation of the fluorescence spectra of acetylanthracenes in mixtures of hexane with other solvents[7] showed that if the second solvent is pyridine or acetone, with increase in the concentration of these substances the fluorescence spectrum is gradually smeared out and shifted to the side of lower frequencies; there is, however, no significant change in the spectra in the range of concentrations of the second component under 1% by volume. On the other hand, if alcohols are added to the hexane solution, even at concentrations of the order of 0.1-0.2%, there is an appreciable alteration in the appearance of the spectra: the vibrational structure is smeared out and they appear to consist of the surposition of at least two somewhat different spectra. Further increase in the concentration of alcohol leads to a sharp shift of the spectrum to the side of lower frequencies.* As will be evident from Fig.3, at a concentration of benzyl, methyl or octyl alcohol of 1 mole/liter (10, 4 and 17% by volume, respectively) the fluorescence peak is shifted 3000, 2400 and 1800 cm^{-1}, which amounts to 80, 66 and 65% of the total shift observed in going from hexane to the pure alcohol. In contrast, at a concentration of 1 mole/liter (7-8 volume %) of pyridine, acetone and dioxane the magnitude of the shift is only 20-25% of the total shift for the pure substances. Moreover, dilution of the hexane with pyridine and acetone, which have high values of the dielectric constant, has approximately the same effect as dilution with dioxane, the dielectric constant of which is only 2.2.

The strong effect on the fluorescence spectra of small admixtures of alcohols in neutral solvents in evidence of the distinctive character of the interaction of alcohols with excited acetylanthracene molecules; it is logical to assume that they form hydrogen bonds. Further evidence in favor of this assumption is the fact that the influence of alcohols is diminished when they are present in mixture not with neutral hexane but with solvents capable of forming hydrogen bonds with alcohols (pyridine, dioxane and acetone). This is evinced, in particular, in the flatter slop of the curve characterizing the magnitude of the fluorescence peak shift with the alcohol concentration in the above mentioned solvents (Fig.3).

---

*Changes in the position of the fluorescence peaks with variation in the concentration of the second component in mixed solvents is accompanied by a change in the quantum efficiency, which tends to increase with shift of the spectrum to the side of lower frequencies; for any given mixture of two solvents the variation is nearly linear. This effect will be described in greater detail in another paper.

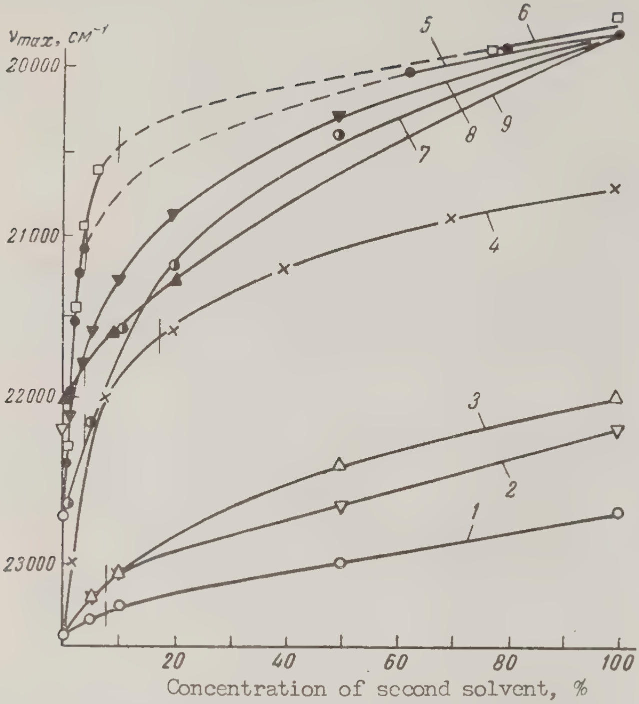

Fig.3. Variation in the position of the fluorescence peak of 2-acetylanthracene as a function of the second component concentration in mixed solvents: 1 - *n*-hexane (I) + dioxane (II), 2 - I + acetone (III), 3 - I + pyridine (IV), 4 - I + *n*-octyl alcohol, 5 - I + methyl alcohol (V), 6 - I + benzyl alcohol, 7 - V + II, 8 - V + III, 9 - V + IV. The vertical bars indicate the volume percentage of the second solvent corresponding to a concentration of 1 mole/liter. The dashed sections of the curves correspond to concentration ranges in which the given solvents are not miscible.

It is interesting to note that if to a solution of 2-acetylanthracene in hexane already containing a small amount of alcohol one adds a quantity of a solvent like pyridine, dioxane, ether or ethyl acetate, the fluorescence peak tends to approach its position in the spectrum for the solution without alcohol.[7] The spectrum shifts to the side of higher frequencies, and vibrational structure appears. The alterations in the spectrum are so pronounced and characteristic, that this effect could be utilized for detecting molecular interactions of alcohols with other solvents.

Analysis of the results of all the investigations of the fluorescence spectra of acetylanthracenes shows that the observed differences as regards the influence of polar solvents on the spectra cannot be consistently related with the values of ϵ and n of the solvent. A correlation is clearly observed only when one compares solvents with a similar structure (for example, aliphatic series alcohols) or when the dielectric properties of the same solvent are varied by changing the temperature (for example, solutions of acetylanthracene in glucose).

In general, a consistent relation between the position of the fluorescence peak and the dielectric properties can obtain because many of the properties of the solvent that determine the degree of its effect on the solute molecule also determine the value of its macroscopic characteristics such as the dielectric constant and index of refraction. However, there must also always be evinced in some degree the distinctive, individual character of the influence of these properties on the position of the fluorescence peak and the values of ϵ and n. Disregarding other factors, one can say that this distinctive influence should obtai if only because ϵ reflects the behavior of the molecules in a uniform field, whereas the field of the molecules of the dissolved substance with which the solvent interacts is not uniform. This in particular must lead to formation of a more or less appreciable oriented layer or "shell" of solvent molecules about each solute molecule, a circumstance which cannot be negligible in many cases. It may also be assumed that the presence in the solvent molecules of a quadrupole moment, which has no significant effect on the dielectric constant of the solvent, will exert an appreciable influence on the strength of the molecular interaction and hence on the magnitude of the spectrum shift. This probably explains why the influence of dioxane on the fluorescence spectrum of acetylanthracenes is greater than might be expected from the values of ϵ and n of this solvent.

References

1. V.V.Zelinskii, V.P.Kolobkov & I.I.Reznikova, Termodinamika i stroenie rastvorov (Thermodynamics and structure of solutions) (Conference transactions), p.262, Pub.Moscow State University, 1959; V.V.Zelinskii, V.P.Kolobkov & L.G. Pikulik, Optica i spektroskopiya, 2, 402 (1957).

2. V.P.Klochkov, Ibid., 1, 546 (1956); V.P.Klochkov, Zhur.fiz.khim., 29, 1432 (1955).

3. N.G.Bakhshiev, Optika i spektroskopiya, 7, 52 (1959) (Trans.Optics and Spectroscopy); N.G.Bakhshiev, Izv.AN SSSR, Ser.fiz., 22, 1387 (1958). (Trans. Bulletin, 22, 1377.)

4. E.Lippert & F.Moll, Z.Elektrochem., 58, 718 (1954); E.Lippert, J.phys.et radium, 15, 627 (1954).

5. H.Kokubun, Z.phys.Chem. (BRD), 17, 281 (1958); H.Kokubun, Z.Elektrochem., 62, 599 (1958).

6. E.McRae, J.Phys.Chem., 61, 562 (1957); N.Mataga, J.Kaifu & M.Koisumi, Bull. Chem.Soc., Japan, 29, 115, 465 (1956); J.Ooshika, J.Phys.Soc., Japan, 9, 594 (1954); W.Bailiss & E.McRae, J.Phys.Chem., 58, 1002 (1954).

7. A.S.Cherkasov, Doklady AN SSSR, 130, 1288 (1960). (Trans.Doklady.)

8. S.B.Thomas, J.Phys.Chem., 35, 2103 (1931); F.R.Cattoir & G.S.Parks, J. Phys.Chem., 33, 879 (1929).

PRESENT VIEWS REGARDING THE INFLUENCE OF THE SOLVENT ON THE SPECTRA OF COMPLEX ORGANIC MOLECULES

(Summary of report) - I.A.Zhmyreva, V.V.Zelinskii, V.P.Kolobkov, A.S.Kochemirovskii & I.I.Reznikova

Analysis of the data in the literature[1-5] indicates that it is feasible to construct a universal series or scale of solvents according to their effect on the electronic spectra of organic molecules. The intensity-of-effect scales given in Refs.6 and 7 coincide.

There are two essentially different ways of interpreting the action of solvents on the electronic spectra of organic compounds. Attempts at quantitative description of the influence of solvents by means of the macroscopic characteristics of the solvent (i.e., in terms of the dielectric constant and the index of refraction) lead in many cases to appreciable deviations of the experimental values from the calculated ones. Lippert[4] explains most of the deviations in terms of microinteraction of the solvent with the solute.

According to the viewpoint of Kosower[6] and the present authors, microinteraction in most cases exceeds the dipole-dipole interaction dependent on the macrocharacteristics. The ostensible agreement of some experimental data with the results of calculations based on macroproperties is explained in this case by the fact that the factors or quantities determining the value of the dielectric constant and index of refraction are essentially averaged microproperties: the permanent dipole moments and the polarizabilities of individual atoms and linkages in the molecules. The apparent agreement is also partially due to the presence of a large number of constants in the formulas, the values of which are necessarily determined from experiment.

Zelinskii, Kolobkov & Pikulik[8] pointed out that there may be another mechanism responsible for the difference in the variation of the absorption and fluorescence spectra. This mechanism may be described as follows. An absorption event, occurring in conformity to the Franck-Condon principle, raises the molecule to an excited level; there are, however, conserved the interatomic separations that are equilibrium separations for the ground state but nonequilibrium for the excited state. The nonequilibrium state in which the molecules find themselves after absorption have a higher energy than the energy corresponding to the equilibrium separation for the excited state. The following relaxation during the lifetime of the excited state leads to reduction of the electronic energy. This process is responsible for part of the Stokes shift. The other part of the Stokes shift is determined by the fact that in conformity with the Franck-Condon principle the de-excitation (emission) occurs from an equilibrium state of the excited level to a state that is not in equilibrium for the ground level, with an energy exceeding the energy of the equilibrium state for a ground level. Thus the excitation energy is the sum of the energy of the purely electronic transition and the Franck-Condon energy increment ΔE, while the energy of emission is equal to the difference between the energy of the purely electronic transition and ΔE.

In going from one solvent to another, the change in the equilibrium separations in the ground as compared with the excited states will in general be different. Obviously, greater changes in the difference between the equilibrium separations will correspond to greater shifts in the position of the absorption and fluorescence spectra. Consequently, if with increased polarity of the solvent the difference between the equilibrium separations increases, this will involve an increase of the Stokes shift. This explanation of the variation in the Stokes shi is, in principle, in agreement with the explanation suggested by Lippert. However, from this point of view, the change in the spectra under the influence of the solvent depends to an appreciably lesser degree on the rigidity of the medium.

To what extent any given mechanism is responsible for the observed changes in the spectra of organic substances can only be determined by further investigation.

References

1. A.I.Kipriyanov & V.E.Petrun'kin, Zhur.organ.khim. (Journ.Organic Chem.), 10, 613 (1940); A.I.Kipriyanov & E.S.Tinyushenko, Ibid., 17, 1468 (1948); Yubil. sbornik AN USSR (Jubilee volume of the Ukrainian SSR Ac.of Sci.), Kiev, 1950; A. I.Kipriyanov, Ukr.khim.zhur. (Ukrainian Chem.Jour.), 19, 339 (1952); A.I.Kipriyanov, Ibid., 14, 275 (1942).

2. L.G.S.Brooker, Revs.Mod.Phys., 14, 275 (1942); L.G.S.Brooker, Revs.Mod. Phys., 14, 281 (1942); L.G.S.Brooker, G.H.Keyes & D.W.Heseltine, J.Amer.Chem.Soc., 73, 5350 (1951); L.G.S.Brooker, Experimentia, Suppl., 11-IX; 229 (1945); L.G.S. Brooker, G.H.Keyes, R.H.Spraqul, R.H.Van Dyke, E.Van Lare, G.Van Zandt, F.L.White, H.W.J.Grossman & S.G.Dent, J.Amer.Chem.Soc., 73, 5332 (1951).

3. K.Dimroth, Angew.Chem., 60, 70 (1948); K.Dimroth, Ann.Chem., 604, 221 (1957).

4. E.Lippert, J.Phys.et radium, 15, 627 (1954); E.Lippert & F.Moll, Z.Electrochem., 58. 718 (1954); E.Lippert, Z.Electrochem., 61, 962 (1957).

5. V.V.Zelinskii, V.P.Kolobkov & L.G.Pikulik, Optika i spektroskopiya, 2, 402 (1957).

6. E.M.Kosower, J.Amer.Chem.Soc., 80, 3253 (1958).

7. V.V.Zelinskii, V.P.Kolobkov & I.I.Reznikova, Trudy soveshchaniya po termodinamike i stroeniyu rastvorov (Transactions of the Conference on Thermodynamics and Structure of Solutions), M., 1959; I.A.Zhmyreva, V.V.Zelinskii & V.P.Kolobkov, Doklady AN SSSR, 129, 1089 (1959). (Trans.Doklady.)

8. V.V.Zelinskii, V.P.Kolobkov & L.G.Pikulik, Optika i spektroskopiya, 2, 404 (1957).

DISCUSSION following the reports of N.G.Bakhshiev, A.S.Cherkasov and I.A.Zhymreva, V.V.Zelinskii, V.P.Kolobkov, A.S.Kochemirovskii & I.I.Reznikova

N.D.Sokolov: The question of the influence of the solvent on the properties of the dissolved substance is important in a number of fields of physics and chemistry. One need only mention the problem of solvation of ions, the role of solvation in elementary chemical processes, the influence of the solvent on infrared spectra, etc. The problem of the influence of the solvent on the electronic spectra is therefore not different in principle from the problem of its influence on various other properties of the solute.

One of the possible approximate ways of calculating the interaction energy of an ion or dipole molecule (A) with the surrounding medium is the following. In the immediate proximity of A the solvent, rigorously speaking, cannot be regarded as a continuous medium, the properties of which can be described simply by means of the dielectric constant and the index of refraction. However, the influence of remote parts of the solvent can be treated from this standpoint. Hence the procedure followed is to inscribe a sphere of effective radius r about the ion or molecule A; outside the sphere the interaction of A with the medium is considered phenomenologically, while inside it is treated from the standpoint of microtheory, taking into account the molecular structure of the solvent. This, however, is difficult to do in practice inasmuch as there is no adequate quantitative theory of molecular forces. In the final analysis one must make rough approximations and have recourse to semiempirical relationships.

The other approach consists in neglecting the microstructure of the solvent and simply setting the effective radius r equal to the radius of the molecule itself. In this approximation one obtains the theory described today by Bakhshiev. Its strong point is that it makes it possible to separate the substances for which the phenomenological theory is inadequate from the others, in considering which it is essential to take into account the molecular structure of the solvent. Such systems, apparently, include compounds of forming hydrogen bonds. Obviously, in such cases the influence of the immediate ambience of the ion or molecule may play a predominant role and then in the first approximation the problem must be treated by microtheory. It must be noted, however, that these two approaches are not contradictory or mutually exclusive; on the contrary, they must complement each other and any correct theory must be based on a synthesis of these two viewpoints.

It should be noted that the manner of taking into account the Franck-Condon principle set forth in the report of Bakhshiev is not quite accurate. The thing is that at the initial instant after transition of the electron to a new state, there is realized in the solvent a nonequilibrium polarization, inasmuch as the orientational polarization lags behind the electron motion. The free energy of the medium in such a case was calculated some years ago by Marcus (R.A.Marcus, J. Chem.Phys., 24, 966 (1954)). Marcus considered the specific case of transition of an electron from one particle to a neighboring one: the oxidation-reduction process. It is not impossible that application of the more precise formulas deduced by Marcus may reduce the divergence between the experimental data and the results of phenomenological theory.

In considering the influence of the solvent on the luminescence spectra of organic molecules one must bear in mind that this influence may consist not only in shift of the bands but in other effects, for instance, the appearance of new bands. An illustrative example was given by Lippert at the Fourth International Conference on Molecular Spectroscopy (Sept.1959). According to Lippert, it was found that in paracyanogen-dimethylaniline, which has two excited states ${}^1L_a$ and ${}^1L_b$, the first has a very large dipole moment (~26 D). In nonpolar solvents ${}^1L_b$ lies somewhat lower than ${}^1L_a$, and hence in such solvents there is observed only one fluorescence band corresponding to the ${}^1L_b \rightarrow {}^1A$ transition. In polar solvents there is a certain activation energy, necessary for reorientation of the solvent molecule in the strong field of the ${}^1L_a$ dipole state. Hence, although now ${}^1L_a$ lies lower than ${}^1L_b$, not all the molecules are able to go to the ${}^1L_a$ state during the lifetime of the excited state, as a result of which there appear two fluorescence bands.

V.V.Zelinskii: I cannot agree with the previous speaker that there is no difference of principle between the approaches to the question of the influence of the solvent proposed by Bakhshiev and by our group. There is a difference of principle and it consists in the fact that Bakhshiev considers it unnecessary to consider the influence of the interaction between the solute molecules and the solvent molecules in their immediate proximity. As we understood it, Bakhshiev considers that 1) in general such interactions are specific, i.e., peculiar to certain particular substance, 2) are negligibly weak, and 3) are somehow taken into account in the theory of Ooshika.

We, on the other hand, believe 1) that the approximate Ooshika theory does not take into account the interaction between the solute molecule and nearby solvent molecules, 2) that the interaction is universal in character, and 3) that the interaction of the solute molecule with nearby solvent molecules is predominant as regards the effects observed in the spectrum. We believe it is essential to check experimentally whether microaction can legitimately be neglected.

In the figures shown by Bakhshiev all the points fit the theoretical curves. As we have noted repeatedly, there exist other points which do not fit the plots. Bakhshiev appears to neglect them, classifying them as a result of specific, individual effects of the solvent. We feel that it is wrong to exclude from consideration all points that do not fit the theoretical curves, particularly when it is a question of checking the formulas.

The available experimental data do allow of deciding the question of what type of interaction is dominant: there are a number of cases when the macrocharacteristics of the solvent change with little variation in the microcharacteristics.

As was already noted, in going from one solvent to another changes in the spectra follow changes in the chemical nature of the solvent and prove to be insensitive to appreciable changes of the dielectric constant. This leads to deviation of many of the points from the calculated curves proposed by Bakhshiev. For example, deviation of the points for alcohols from the theoretical straight line plot is connected not with different positions of the spectra in different alcohols (the spectra in all alcohols coincide), but with the fact that the dielectric constants change and the spectra do not follow this variation but remain constant. In organic acids the situation is the same as in alcohols: the points deviate from the theoretical curves not because of some singular behavior of the spectra but because of the particular behavior of the dielectric constant, changes in which are not followed in the spectra. The dielectric constants of acids do not reflect the microfields of the hydroxyl groups, inasmuch as owing to association the elementary dipoles are directed opposite each other. Further, the substantial deviations of the case of dimethyoxymethane and dioxane are due not to peculiar behavior of the spectra in these solvents: the spectra in dioxane and dimethoxymethane are close to the spectra in ethers. Lippert explained the deviation of the points for dioxane precisely by the fact that in ethers and in dioxane, although the microfields are equal, the dielectric constants are different.

Particularly significant are the point deviating upward, i.e., the points for solvents in which the dielectric constant is high but the effect on the spectra is nevertheless weak, that is, where there is an apparent "effect-producing" factor, but no effect. In such cases one cannot attribute the deviation to the specific, individual influence of the medium.

In his report Bakhshiev does not mention the variation of the symmetry frequency shift with the volume of the molecule, a quantity which enters into the formulas. From the different variation of the symmetry frequency in the spectra of two different but related substances, the molecules of which differ little as regards volume, Bakhshiev calculates the difference in volumes and considers this fact to be an experimental substantiation of his theory. As we have indicated, however, in many cases even an appreciable change in the volume of the molecule in related compounds (a change by a factor of 2 or more) does not lead to any change in the dependence of the symmetry frequency on the solvent.

Thus the experimental data strongly indicate that microeffects, which are not taken into account in the theories proposed by Bakhshiev and others, exert a predominating influence.

Another question is to what extent can one describe the influence of microfields in terms of the macroproperties of the solvent? Obviously, in the simplest cases one can find a simple correlation inasmuch as often macroproperties are determined by the sum of the microproperties. We believe, however, that when the macroproperties depend in a complex manner on the microproperties such a description will not be satisfactory.

In conclusion, we want to note that the unity or similarity as regards microeffects of solvents on the spectra of organic substances offers an interesting possibility for the development of the pertinent theory inasmuch as it allows of considering from a single common standpoint the micropicture of interaction of the solute molecule with the solvent molecules without being diverted by a number of particular, extraneous details, which tend to obscure the situation.

N.G.Bakhshiev: The assertion that we do not consider the interaction between the solute molecule and its nearest neighbors is erroneous. In our theory we take into account the universal influence on the solute molecule of the entire aggregate of solvent molecules surrounding it, both those located close to it and those at a distance. By universal interactions we understand the interactions that occur in all cases when one molecule is surrounded by a conjunction of other molecules, regardless of the specific nature of the absorbing or emitting center, i.e., interactions of a dielectric character (dipole, polarization and the like). In this case, if between the solvent molecule and its nearest neighbors, in addition to the universal interactions, there also occur interactions of another type (for example, formation of hydrogen bonds, association), we consider these forms of interaction to be specific inasmuch as they are determined in each particular case by the individual properties of the solute and solvent molecules and in many systems may not occur at all.

The fact that we divide interactions into universal and specific does not mean that we consider the former to be strong and the latter weak. There are obviously many cases (strong hydrogen bonds, acid-base reactions) when the specific interactions can be very appreciable and result in deviation of the experimental points from the theoretical curves characterizing the universal influence of the medium. In fact, this is what allows us to distinguish specific interactions from universal ones and to investigate them separately. The instances, cited by Zelinskii, of deviations from theory correspond precisely to the cases when one might expect to observe a strong influence of specific attributes, i.e., the predominance of specific interactions (solutions in acid, and halogen derivatives).

The satisfactory quantitative agreement of our theory with extensive and diverse experimental data gives reason to assert that in many cases specific interactions between the solute molecule and the solvent molecules are either nonexistent or relatively weak as far as their influence on the spectrum is concerned, i.e., the effect of the solvent on the spectrum is determined in such cases primarily by its universal action as a physical dielectric medium.

In contradistinction to our view, Zelinskii treats as universal the individual microscopic interactions between the solute molecule and its nearest neighbors. I do not want to take time here to criticize the empirical concepts of Zelinskii in order to show that they are inconsistent and self-contradictory. I have done this in an article to be published in "optika i spektrokopiya" (Optics & Spectroscopy) where I have shown that all the experimental data obtained to date by Zelinskii and his co-workers can be interpreted and quantitatively explained precisely from the standpoint of our theory.

In conclusion, I want to note that hitherto in investigations of the influence of the solvent on the spectra of organic substances, no account was taken of effects of universal character: in some cases this may be relatively unimportant owing to the predominance of specific interactions (acid-base interactions, strong hydrogen bonds, etc.), but in other cases there may result misapprehensions connected with erroneous interpretation of predominating universal interactions as individual, specific interactions. This is, for example, true of the work of V.V.Zelinskii.

PRINCIPAL PROCESSES OF DEACTIVATION OF EXCITED STATES OF COMPLEX ORGANIC MOLECULES

- V.A.Borgman, I.A.Zhmyreva, V.V.Zelinskii & V.P.Kolobkov

In previous studies$^{1-3}$ it was shown that the fluorescence yield q_f of a number of organic compounds at room temperature is consistently related with the frequencies ν_f^{max} of the fluorescence peaks in their spectra. In general, the variation of q_f with ν_f^{max} is represented by a curve with two branches: an ascending branch and a descending branch.

It was hypothesized that deactivation, the probability for which increases with increase of ν_f^{max} is due primarily to increase in the probability r for transition to the metastable state. The subsequently observed$^{4-6}$ regular increase of the ratio of the phosphorescence and fluorescence yield q_{ph}/q_f with increase of ν_f^{max} seemed to be a confirmation of this hypothesis. It was found, however, that the ratio q_{ph}/q_f measured directly at -196° is appreciably lower than the ratio evaluated from the ν_f^{max} dependence of q_f at room temperature.^{6} To resolve this contradiction it was hypothesized that the transition responsible for deactivation of the labile state, with the short wavelength location of the spectrum, is not the transition to the metastable state but a transition to some intermediate level from which there may occur transitions to the metastable state and nonradiative transitions to the ground state, the ratio of the probabilities for these transitions being independent of the position of the spectrum.

Another possible explanation of the above mentioned contradiction was the hypothesis of increase of r with temperature (or decrease of the rigidity of the medium).

The present investigation of the spectral dependences of the absolute luminescence yield at -180° was undertaken with a view to clarifying the character of the deactivation process. The experimental procedure is described in Ref.7.

If the nonradiative deactivation is due to transitions of excited molecules to the metastable state, then at low temperatures the deficit in the fluorescence yield q_f will be made up by the phosphorescence appearing in this temperature range. On the other hand, investigation of deactivation is appreciably simplified at low temperatures inasmuch as temperature quenching of fluorescence is virtually nonexistent at -180°.^{3}

We investigated the spectral dependences of the luminescence yield at low temperature by comparing the values of q_f with the corresponding ν_f^{max} for related compounds with substituents of somewhat different character. Investigation of q_f at room temperature showed that in related compounds the effect of change of the substituent group on q_f is determined primarily by the corresponding resultant shift of the emission spectrum. It was natural to assume that a similar relationship would obtain at low temperature.

Comparison of the measured values of q_f with the corresponding ν_f^{max} in different series of related compounds is given in Figs.1 and 2. It will be evident from the figures that in the case of 3- and 3,6-derivatives of phthalimide q_f increases with increasing ν_f^{max} in the range of low ν_f^{max}. Then after attaining a certain maximum value, equal to unity in the case of the 3,6-derivatives, q_f with further increase of ν_f^{max} decreases. For the 3- and 3,6-derivatives of phthalimide and in the derivatives of naphtheurhodine the falling off of q_f is rather pronounced (the minimum values of q_f differ from the maximum values by a factor of 5 to 14). Thus it is found that q_f at low temperatures also related with the specific spectral characteristics of the emitting compounds, not only in the case of phthalimide derivatives but also in the case of derivatives of naphtheurhodine (according to our preliminary data, this is also true of the derivative of aminobenzoic acids and some other compounds). This gives reason to assume the regular variation of q_f with ν_f^{max} at low temperatures is a common phenomenon. It is found that the specific effect of change in the character of the substituent on q_f, if this change is not excessively great,

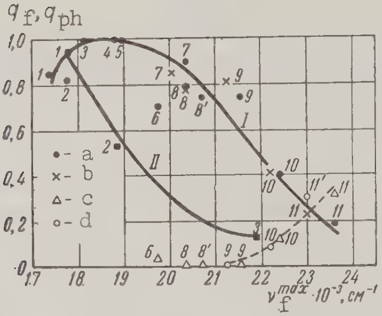

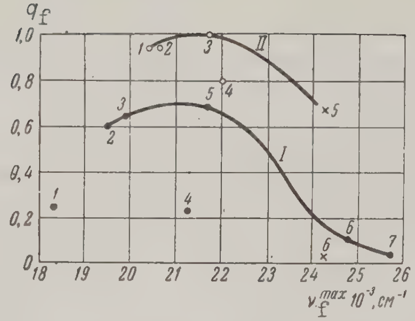

Fig.1. Variation of q_f (a,b) and q_{ph} (c,d) with ν_f^{max} at -180°: I - 3,6-derivatives of N-methylphthalimide in ethyl (a,c) and methyl (b,d) alcohols: 1) 3,6-tetramethyldiamino-, 2) 3-monomethylamino-6-amino-, 3) 3-dimethylamino-6-amino-, 4) 3,6-diamino-, 5) 3-dimethylamino-6-acetylamino-, 6) 3-dimethylamino-6-methylacetylamino-, 7) 3-methylacetylamino-6-methylacetylamino-, 8) 3-acetylamino-6-amino-, 9) 3-methylacetylamino-6-amino-, 10) 3,6-diacetylamino-, 11) 3-methylacetylamino-6-acetylamino-N-methylphthalimide (the primed numbers identify the corresponding methyl-less analogs); II - derivatives of naphtheurhodine in ethyl alcohol: 1) dimethylamino-, 2) amino-, 3) acetylaminonaphtheurhodine.

Fig.2. Variation of q_f with ν_f^{max} at -180°: I - 3-derivatives of N-methylphthalimide in ethyl alcohol: 1) 3-diphenylamino-, 2) 3-dimethylamino, 3) 3-monomethylamino-, 4) 3-hydroxy-, 5) 3-amino-, 6) 3-acetylamino-, 7) 3-methylacetylamino-N-methylphthalimide; II - 4-derivatives of N-methylphthalimide in ethyl (1-4) and methyl (5-6) alcohols: 1) 4-diphenylamino-, 2) 4-dimethylamino-, 3) 4-amino-, 4) 4-hydroxy-, 5) 4-acetylamino-N-methylphthalimide, 6) 4-acetylamino-N-phenylphthalimide.

is relegated to a secondary role, the primary role being played by the influence of the substituent on the position of the spectra, which determines the magnitude of q_f. It may be assumed that q_f is determined primarily by the shape and relative positions of the energy levels of the ground and excited electronic states.

In the case of substances the spectra of which are located in the short wavelength region and the fluorescence yield of which is already depressed relative to the maximum value, phosphorescence appears. However, the increase of q_{ph} is less than the decrease of q_f so that the total luminescence yield $q_{t.l}$ decreases.

We note that correlation between decrease of q_f and the appearance of phosphorescence is observed not only in the case of falling of q_f owing to increase of ν_f^{max}, but also in the case of decrease of q_f under the influence of certain substituents. It will be apparent from Fig.1 that in some compounds q_f proves to be lower than it should be with the given ν_f^{max} according to the general dependence. For all these compounds there is observed phosphorescence, whereas in the case of substances the points of which fall on the general curve, phosphorescence appears only at appreciably higher ν_f^{max}.

In the case of decrease of q_f under the influence of substituents having a specific effect, the decrease of q_f is also not compensated by the appearance of phosphorescence, so that the total luminescence yield is reduced.

The character of the ν_f^{max} dependence of q_f at -180° indicates that at low temperatures also the factors producing radiationless deactivation are different in the long wavelength and short wavelength regions of the spectrum. In the present paper we shall not discuss the process responsible for the increase of q_f with increase of ν_f^{max} with the spectrum in the long wavelength region.[3] The principal purpose of the present communication is to clarify the mechanism of the process responsible for the quenching of luminescence in the range of high ν_f^{max}. Decrease in the total luminescence yield cannot be attributed to radiationless deactivation of the metastable state T. Thus it was shown for some compounds that temperature quenching on the level T ceases at the boiling point of oxygen[8-13]. Evidence in favor of the absence of quenching on the metastable level at -180° is also furnished by the fact that in allied compounds the phosphorescence lifetimes τ_{ph} have as a rule close values, while q_{ph}/q_f and the deficit of $q_{t.1}$ vary in a very wide range. For example, in substances Nos.6, 10 & 11, among the 3,6-derivatives of N-methylphthalimide, τ_{ph} = 0.5-0.6 sec, while the deficits of $q_{t.1}$ are, respectively, 0.2 and 0.5. In the case of the 4-derivatives (Nos.5 & 6) τ_{ph} = 1.3 sec, while the deficits of $q_{t.1}$ are 0.25 and 0.94, respectively. In order to explain the observed difference between the deficits of $q_{t.1}$ one must assume that the natural lifetimes in very closely related compounds differ greatly.

Obviously, in addition to the process of temperature deactivation of the labile state and deactivation by transition to the metastable state, one must admit the existence of some other third process of deactivation of the excited state, a nonradiative transition of the molecule from the excited to the ground state, with a probability q_1^n that increases with the increase of ν_f^{max}. Admitting the existence of this process, we are faced with the following questions: 1) what is the mechanism of this process, 2) are the processes characterized by q_1^n and r independent (but with probabilities varying in parallel), or is there a relation between them and if so what is its nature, 3) what is the effect of increase of ν_f^{max} on the increase of r, and 4) how does the temperature (or rigidity of the medium) affect the probabilities of both processes?

According to Föster[14], nonradiative deactivation of the excited state at sufficiently high ν_f^{max} may occur as the result of predissociation. It is natural to assume that q_1^n characterizes the probability for predissociation.*

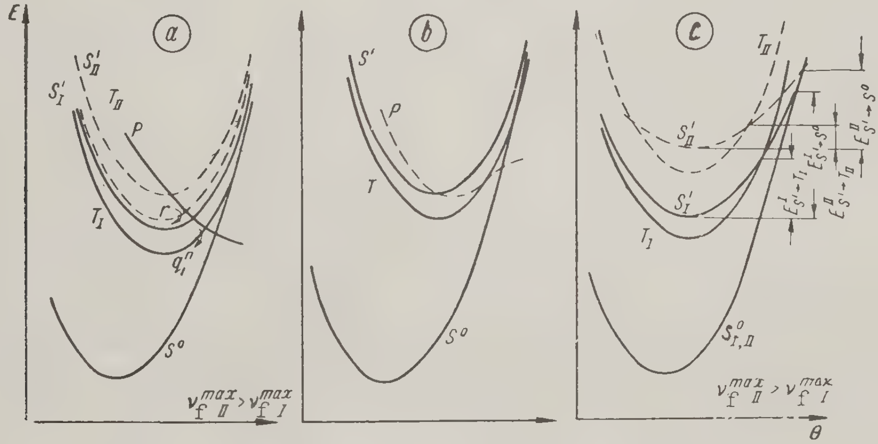

Fig.3. Potential curves of electronic states.

In the simplest scheme with three levels the increase of r with increase of ν_f^{max} cannot be explained without further assumptions regarding the special shape of the energy surfaces of the electronic states. Hence we must first consider the possibility of explaining the transition to the metastable state as one involving the participation of a fourth intermediate level (Fig.3,a).

---

*A number of objections may be raised against predissociation as the common cause of nonradiative deactivation of excited states of organic molecules. We do not, however, have space here to consider these objections in detail.

It is natural to assume that this fourth level P is the level that is introduced in considering predissociation. A molecule after transition from the labile level S' to the level P has a definite probability r for transition to the metastable state T and a probability q_1^n for nonradiative transition to the ground state S^o. This scheme explains the relation between the variation of luminescence quenching and the variation of q_{ph}. With increase of S' and the associated increase of ν_f^{max} with a more or less constant position of P, the point of intersection of S' with P is shifted to the region of populated vibrational levels of the excited state, which leads to increase of the transition frequency from S' to P and this in turn results in increase of the transition frequencies from P to S^o and from P to T.

Increase of the transition frequency from S' to P is explained in the framework of this scheme by the fact that change in the height of S' with a more or less constant position of P lowers the energy barrier which must be surmounted in order to attain the point of intersection of the energy curves S' and P (Fig.3,a). Evidence in favor of this interpretation of the role of the height of the excited level is the fact that the decrease of q_f with increase of ν_f^{max} is not abrupt. The transition frequency takes on high values only at rather high values of ν_f^{max}. The possibility of a high transition frequency is evidence of the greater probability for this transition in the case when the intersection of the curves S' and P occurs close to the minimum in the curve S'. According to the scheme with an intermediate level, the transition from the labile state to the metastable state is represented by a two-step process, consisting of a transition from S' to P and then from P to T. This representation of the transition from the labile level to the metastable state differs radically from the common concept regarding this process as a spontaneous transition from S' directly to T.

In view of the fact that intercombination is forbidden, the transition from P to T must occur more rarely than the transition to S^o. This is in accord with the fact that the deficit of $q_{t.l}$ as a rule is greater than q_{ph}. On the contrary, from this point of view the existence of a large q_{ph} in some cases appears anomalous (for example, in the case of Michler's ketone $q_{ph} = 0.65$).

The described scheme with a predissociation level as the intermediate level for the transition to the metastable state is in conflict with the data on quenching of fluorescence by halogens. As was shown in the work of Refs.1, 7 & 15, quenching by halogens consists in transition of the excited molecules to the metastable state. If, however, the transition to level P must be preceded by a transition to T, the frequency of the last process will determine the fluorescence quenching. The subsequent more or less probable transition to T under the influence of halogen cannot change the frequency of the preceding process. The introduction of the halogens can only alter the ratio between q_1^n and r. This conflict or inconsistency can be eliminated by introducing further assumptions regarding the shape of the predissociation curve or by replacing the predissociation level by some other type of level.*

In view of the fact that in our opinion the postulation of a predissociation level as the intermediate level for transitions to the metastable state is a serious step, not to be taken lightly, and the fact that the possible ensuing complications of the scheme are dubious, we propose yet another explanation of the observed experimental facts.

---

*According to the scheme shown in Fig.3,b, P has a shape and position relative to S' such that during the lifetime of the excited state there may occur repeated transitions between P and S' and back. As a result the halogens by increasing the probability for intercombinational transitions from P to T acquire the ability of influencing the frequency of transitions from S' to P.

We suggest that simultaneously with raising of the excited level S' there occurs an increasingly great deformation of the energy curve with respect to its shape in the ground state S^o: the energy curve becomes increasingly flatter. Then at a certain relation between the change in the height of S' and the deformation of the energy surface S' (Fig.3,c) increase of ν_f^{max} will lead to successive lowering of the energy barriers that must be overcome in order to obtain intersection of S' with T and S^o. In this case with increase of ν_f^{max} the transition frequency of excited molecules to T and S^o will also increase. The energy threshold for the transition to T will be lower, but in view of the inhibition of intercombination the probability of transition from S to T is lower than the probability for transition of the molecules that have attained the intersection of the corresponding energy curves to S^o. Under the influence of the halogens the probability of conversion increases and in view of the lesser height of the energy barrier the transitions to T will occur with a higher frequency than for the competing process of nonradiative deactivation ($q_1{}^n$). In order to explain by means of the proposed scheme the parallel variation of r and q_1^n as a result of introduction of certain substituents, it is sufficient to assume that these substituents affect the shape of the energy curves in the same way as increase of ν_f^{max}.

According to the proposed scheme, the transition to the metastable state is not a spontaneous process: a certain energy barrier must be surmounted for this transition to be realized.

In conclusion, we want to note that the considerations set forth above are not intended as an exhaustive interpretation of the observed regularities; they should be regarded only as a promising approach to explanation of the experimental results.

References

1. V.V.Zelinskii, N.P.Emets, V.P.Kolobkov & L.G.Pikulik, Izv.AN SSSR, Ser. fiz., 20, 507 (1956). (Trans.Bulletin, 20, 465.)
2. V.V.Zelinskii, V.P.Kolobkov & L.G.Pikulik, Optika i spektroskopiya, 1, 161 (1956).
3. V.V.Zelinskii, V.P.Kolobkov & N.D.Krasnitskaya, Ibid., 6, 417 (1959). (Trans.Optics & Spectroscopy.)
4. V.V.Zelinskii & V.P.Kolobkov, Doklady AN SSSR, 119, 922 (1958). (Trans. Doklady.)
5. L.E.Golikova, V.V.Zelinskii & V.P.Kolobkov, Optika i spektroskopiya, 5, 480 (1958).
6. V.V.Zelinskii, V.P.Kolobkov & I.I.Reznikova, Izv.AN SSSR, Ser.fiz., 23, 1269 (1959). (Trans.Bulletin, 23, 1259.)
7. V.V.Zelinskii & V.P.Kolobkov, Optika i spek., 1, 560 (1956).
8. V.V.Zelinskii & V.P.Kolobkov, Doklady AN SSSR, 106, 1042 (1956). (Trans. Doklady.)
9. B.A.Pyatnitskii & Vinokurova, Ibid., 62, 57 (1948); 68, 281 (1949); 68, 483 (1949).
10. V.V.Zelinskii & V.P.Kolobkov, Ibid., 101, 241 (1955).
11. B.Ya.Sveshnikov & Petrov, Ibid., 71, 461 (1950).
12. D.McClure, J.Chem.Phys., 17, 905 (1949).
13. Zinov'eva, Doklady AN SSSR, 68, 265 (1949).
14. T.Förster, Fluoreszenz organischer Verbindungen, Göttingen, 1951.
15. V.A.Borgman, I.A.Zhmyreva, V.V.Zelinskii & V.P.Kolobkov, Doklady AN SSSR, 131, No.4 (1960). (Trans.Doklady.)

INFLUENCE OF STRUCTURE ON THE LUMINESCENCE CHARACTERISTICS OF COMPLEX ORGANIC MOLECULES

- V.V.Zelinskii & I.I.Reznikova

In the preceding report[1] it was shown that the absolute fluorescence yield q_f at liquid oxygen temperature in the case of minor changes in the character of the substituent is determined by the change in the position of the fluorescence spectrum occurring in going from one substituent to another. However, some clearly identifiable changes in substituents lead to deviation of the compounds containing these substituents from the general variation of the absolute fluorescence yield q_f as a function of the fluorescence peak frequency ν_f^{max} at -180°. Among such substituents, for example, are the hydroxyl and nitro groups, phenyl and the halogens (I and Br). Let us examine the influence of these groups on the value of q_f at -180°.

It is evident from Fig.1 of the preceding article that as compared with 4-amino-N-methylphthalimide (the value of q_f for which is equal to 1 and fits the general q_f vs ν_f^{max} curve, and which exhibits no phosphorescence) in the case of 4-hydroxy-N-methylphthalimide at a value of ν_f^{max} close to that for the amino derivatives the value of q_f is appreciably lower. The decrease of q_f in case of replacement of the amino group by the hydroxy group is observed to an even more pronounced degree in the series of 3-derivatives of phthalimide. In both hydroxy derivatives, in contrast to the amino derivatives, together with decrease of q_f there is observed the appearance of phosphorescence, the yield of which does not compensate the decrease of q_f.

The total luminescence yield $q_{t.l}$ for compounds containing the hydroxyl group remains lower than for the corresponding amino derivatives. The deficit in $q_{t.l}$ is explained by anomalous increase in the probability q_1^n for nonradiative deactivation of the excited molecules under the influence of the hydroxyl group.

In an earlier publication[2] we noted that phenyl, when introduced into a molecule instead of an imide hydrogen, sharply increases the ratio of the absolute phosphorescence and fluorescence yield $\delta = q_{ph}/q_f$, which indicates increase of the probability r for transition to the metastable state.

It is clearly evident in the instance of 4-acetylamino-N-phenylphthalimide that phenyl in replacing the imide hydrogen also markedly increases the probability q_1^n. Whereas for 4-acetylamino-N-methylphthalimide $q_f = 0.68$ and $q_{t.l} = 0.75$, for the corresponding phenyl derivative $q_f = 0.03$ and $q_{t.l} = 0.06$, while both compounds are characterized by virtually the same frequency of the fluorescence peak.

Moreover, the same substituent but attached in different positions in the molecule may have a different effect on the probabilities r and q_1^n. For example, we reported earlier[2] that 3-derivatives of phthalimide are characterized by a higher probability r than 4-derivatives with the same values of ν_f^{max}. In the present report we want to emphasize that the effect of isomerism is evinced also in increase of the probability q_1^n. For this it is sufficient to compare the values of q_f for 3- and 4-hydroxy-N-methylphthalimides or 3- and 4-acetylamino-N-methylphthalimides. Thus in the case of the hydroxy substituted 4-derivative q_f is almost four times greater than in the corresponding 3-derivative, while the value of δ is ten times smaller. In the case of 4-acetylamino-N-methylphthalimide q_f is seven times greater than for the 3-derivative, while the value of δ is twenty times smaller. It will be evident from Fig.1 of the preceding paper that when the substituent is a monomethylacetyl grouping the influence of isomerism is evinced in a similar manner: 3-monomethylacetylamino-N-methylphthalimide is characterized by a higher probability r and higher probability q_1^n than the corresponding 4-derivative.

It is evident from the above that substituents that produce an increase of the probability r also induce an increase in the probability q_1^n.

It also follows from what has been said above that in going from 4-derivatives to 3-derivatives, the influence of the substituent on the probability q_1^n is sharply enhanced. Lowering of the curve characterizing the variation of q_f with ν_f^{max} at -180° for 3-derivatives with respect to the curve characterizing the variation for 4-derivatives can be explained by the fact that the probability r, like the probability q_1^n, regardless of the substituent group is higher in 3-derivatives than in 4-derivatives.

In the study of Ref.2 we noted the fact, observed for a number of nitro derivatives of N-methylphthalimides that r increases under the influence of the nitro group. However, merely the presence of the nitro group in the molecule is not sufficient in all cases to produce quenching. Lippert[3,4] reported in the case of a sufficiently long wavelength position of the fluorescence spectrum, phosphorescence is also exhibited by nitro-substituted compounds.

We want to note that in the case of a certain degree of complexity of the luminescent molecule, the quenching of fluorescence may not occur despite the fact that the position of the fluorescence peak is the same as for related compounds for which significant quenching of fluorescence is observed. In the case of meta- and para-nitroanilines the fluorescence is strongly quenched. Thus in the case of the meta-isomer for which ν_f^{max} = 18 300 cm^{-1}, $q_f = 0.135$, while for the para-isomer $q_f = 0.05$ with ν_f^{max} = 21 000 cm^{-1}. At the same time in compounds with a fairly complex structure of the substituent, such as, for example, 4-dimethylaminobenzal-4-nitroaniline (a para-nitroaniline) in which the amino group hydrogen is replaced by a dimethylaminobenzal grouping, the luminescence consists solely of fluorescence with a fairly high efficiency. The value of ν_f^{max} for this substance coincides with the value for meta-nitroaniline, while $q_f = 0.86$, whereas for meta-nitroaniline $q_f = 0.135$. Obviously, the lengthening of the conjugated bond chain in the molecule suppresses the quenching effect of the nitro group.

It has been reported by Ermolaev & Svitashov[5] and Gilmore et al[6] that the presence in a molecule of a heavy halogen sharply increases the probability r. The effect of iodine or bromine on q_f differs greatly from that of other substituents, in particular from the effect of such a strong fluorescence quencher as the nitro group. Iodine or bromine increase the probability r to such an extent that the yield of compounds containing these substituents sharply increases. Thus whereas for 3-acetylamino-N-methylphthalimide $q_{ph} = 0.3$ with $q_{t.1} = 0.4$, for 3-acetylamino-6-iodo-N-methylphthalimide the luminescence is represented solely by phosphorescence and $q_{ph} = 0.7$, i.e., increases by a factor of 2. In the case of 3-acetylamino-6-bromo-N-methylphthalimide $q_{ph} = 0.6$ with $q_{t.1} = 0.63$.

Thus the introduction of iodine or bromine by way of substituent into these molecules not only does not decrease $q_{t.1}$, which is observed in other cases, but on the contrary, leads to an appreciable increase of the total luminescence yield. The increase of q_{ph} and $q_{t.1}$ indicates that the probability r increases under the influence of these substituents much more than the probability q_1^n. In contrast to the effect of iodine, the nitro group produces a very appreciable increase in the probability for nonradiative deactivation of the excited molecules. Yet, measurements of the fluorescence yields at room temperature would not disclose any difference as regards the effects of the nitro group and iodine.

Thus the quenching by the nitro group or phenyl, on the one hand, and the halogens, on the other, occurs as a result of entirely different deactivation processes. Inasmuch as at room temperature the only effect of these processes is quenching of the fluorescence, inferences drawn on the basis of data on the fluorescence yield measured at room temperature may lead to entirely misleading conclusions.

References

1. V.A.Borgman, I.A.Zhmyreva, V.V.Zelinskii & V.P.Kolobkov, Present issue of the Bulletin, preceding article.

2. V.V.Zelinskii, V.P.Kolobkov & I.I.Reznikova, Doklady AN SSSR, 121, 315 (1958). (Trans.Doklady.)

3. E.Lippert, Z.phys.Chem., N.F., 2, 328 (1954).

4. E.Lippert, Z.Elektrochem., 61, 962 (1957).

5. V.L.Ermolaev & K.K.Svitashov, Optika i spektroskopiya, 7, 664 (1959). (Trans.Optics & Spectroscopy.)

6. E.H.Gilmore, G.E.Gibson & D.S.McClure, J.Chem.Phys., 20, 829 (1952).

OPTICAL PROPERTIES OF CHLOROPHYLL AND PHEOPHYTIN AT LOW TEMPERATURES

- L.A.Kravtsov

There are only fragmentary data in the literature on the luminescence of chlorophyll solutions at low temperatures. Zscheile & Harris[1] measured the variation in intensity of the principal luminescence peak of chlorophyll in the temperature range from +28° to -62°. Otherwise the luminescence spectra of chlorophyll at low temperatures have received scant attention[2]. The absorption spectra at low temperatures were investigated by Freed & Sancier[3,4] and Rabinowitch[5]. The results obtained by these investigators pertain to chlorophyll dissolved in mixtures of solvents.

In the present work we investigated the effect of temperature in the range from +20 to -100° on the luminescence spectra and relative efficiencies and on the red absorption band of solutions of chlorophyll a and pheophytin a. By way of solvents we used isobutyl alcohol and petroleum ether, which can be frozen and cooled to low temperatures without loss of transparency but which differ significantly as regards their physical properties.

The quartz cell containing the solutions was mounted at the upper end of a copper rod, the lower end of which was immersed in liquid air. The cell and the upper part of the rod were enclosed in a special airtight chamber with double walls and double quartz windows. Moisture in the air between the chamber walls and between the inner wall of the chamber and the rod and cell was absorbed by silica gel. The experimental arrangement allowed of monitoring the transparency of the solution and windows at all times. The outer quartz windows were heated by means of an electric heater consisting of a spiral of fine nichrome wire. The temperature was measured by a thermocouple immersed in the solution at the level of the light beam. The apparatus allowed of cooling the solutions down to -110°.

The luminescence spectra were measured by means of a UM-2 monochromator; the radiation detector was an FEU-22 photomultiplier coupled to a dc amplifier with a 2D2P electrometer tube. The luminescence was excited by an SVDSh-250 or SVD-120 ultraviolet tube through a UFS-4 light filter and a solution of copper sulfate. The SVD-120 tube was supplied from a ferroresonance regulator and its light output was monitored by an STsV-6 phototube mounted in the path of the light beam after the solution cell. In measuring the luminescence spectra the concentration of the chlorophyll and pheophytin in the solutions was chosen so that from 3 to 10% of the light energy at 365 mμ would be absorbed. The distortions due to reabsorption were minor owing to the low concentration and the fact that only a thin surface layer of the solution was excited.

In measuring the temperature dependence of the luminescence efficiency the concentrations of chlorophyll and pheophytin were some 5-10 times higher. In the investigated temperature range the contours of the luminescence bands of chlorophyll and pheophytin virtually did not change; hence the relative efficiency (yield) was determined from the variation in intensity of the principal absorption band. In these experiments the monochromator slit was widened to approximately the half-width of the band (200-250 cm^{-1}). The absorption in the 365 mμ region for chlorophyll a and pheophytin a in the temperature range from +25° to -100° remained virtually constant (within ±2-5%). The constancy of absorption was further checked by means of an SF-4 spectrophotometer at the same wavelength (365 mμ). The absorption spectra of chlorophyll and pheophytin at low temperatures were measured on an SF-4 spectrophotometer especially adapted for work at low temperatures.

The contours of the red absorption bands and principal luminescence bands of chlorophyll a and pheophytin a in isobutyl alcohol and petroleum ether are reproduced in Fig.1. With decrease of temperature both the absorption band and the luminescence band become narrower; and the two bands shift towards each other. In

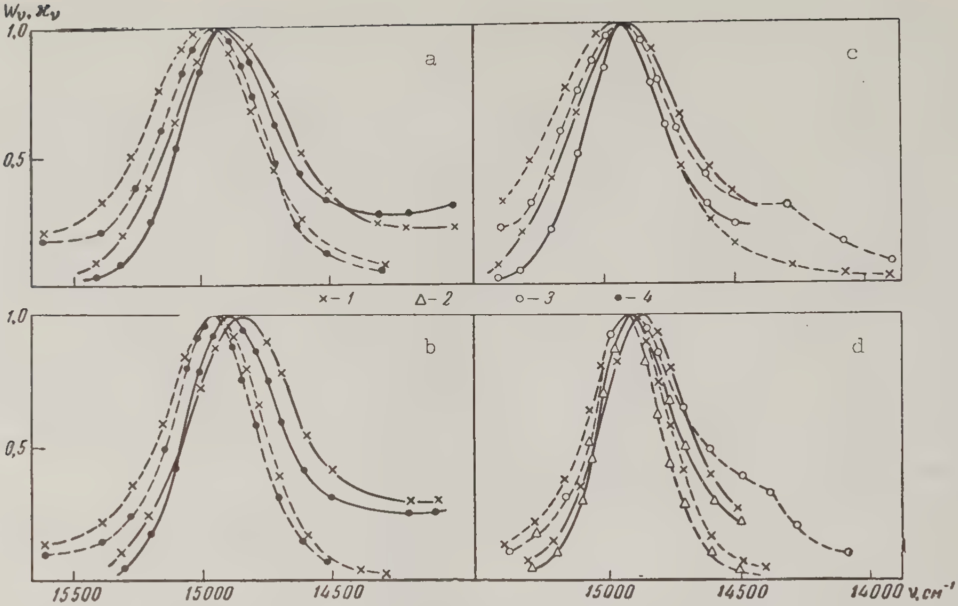

Fig.1. Absorption (dashed lines) and luminescence (solid lines) spectra of chlorophyll a (a,c) and pheophytin a (b,d) in isobutyl alcohol (a,b) and petroleum ethe (c,d) at 1) +25°, 2) -40°, 3) -70°, 4) -90°.

the case of chlorophyll a the shift of the absorption peak is more noticeable, while in the case of pheophytin a the greater shift is exhibited by the luminescence peaks. In the case of both chlorophyll and pheophytin in petroleum ether at temperatures below -60° there appears a noticeable hump on the long wavelength side of the absorption band at about 14 200-14 300 cm^{-1} (700 mμ). With decrease of the temperature the long wavelength side of the absorption band of pheophytin a in petroleum ether at first becomes steeper (in Fig.1,d only the curve for -40° is shown), and then at -70° there appears a sharp shoulder. No appreciable increase in steepness of the long wavelength side of the absorption band of chlorophyll a in petroleum ether is observed at -25° and -40°; a pronounced shoulder appears only at -70°.

The temperature induced shift of the absorption and luminescence bands of chlorophyll and pheophytin is similar to displacement of the spectral bands in the spectra of phthalimides reported by Pikulnik & Solomakho[6]. These authors explain the shift of the bands by change in the transition probability owing to change in the interaction of the luminescent molecules with the solvent. On the basis of the one dimensional harmonic oscillator model, which is usually used for calculating the band contours[7], the drawing together of the absorption and luminescence bands at low temperatures can be explained by decrease of the distance Δr between the positions of equilibrium in the excited and ground states.

Freed & Sancier[3] obtained the absorption spectra of chlorophylls a and b in a mixture of solvents at temperatures down to -193°. At low temperatures they observed displacement of the absorption bands, including the red band, into the long wavelength region. Initially these authors explained this by isomerization of chlorophyll, but later they hypothesize that with lowering of the temperature there occurs solvation of the chlorophyll[4,8,9] or formation of complexes with water[10].

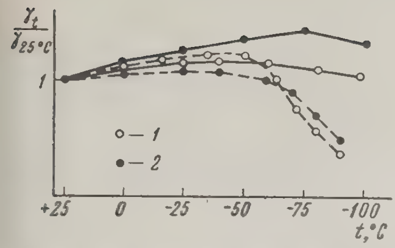

Fig.2. Variation of the relative luminescence efficiency of pheophytin a (1) and chlorophyll a (2) in isobutyl alcohol (solid lines) and petroleum ether (dashed lines) with decrease in temperature.

Strain[11] hypothesized that the effects observed by Freed & Sancier are due to formation of colloidal particles. In view of the fact that the observed effects are reversible, Rabinowitch[5] questions Strain's hypothesis on the ground that phase transitions are unlikely to be reversible.

It is known that any aggregation of chlorophyll molecules leads to almost complete disappearance of luminescence. In connection with this we measured the variation in the relative efficiency (yield) of chlorophyll a and pheophytin a in isobutyl alcohol and petroleum ether. The values of the relative efficiency are shown in Fig.2 (measurement accuracy 10-15%). With reduction of the temperature to -100° the relative efficiency of chlorophyll a increases in isobutyl alcohol, i.e., chlorophyll a behaves like most dyes. The relative efficiency of pheophytin a in isobutyl alcohol remains virtually constant with decrease in temperature. In petroleum ether the relative yield of both chlorophyll a and pheophytin a with reduction of the temperature to -50 to -60° increases slightly; further reduction of the temperature leads to a sharp decrease of the relative efficiency.

All the above described changes occurring with decrease of temperature in the absorption and luminescence spectra of chlorophyll a and pheophytin a in isobutyl alcohol and petroleum ether (including the variations in relative efficiency) are reversible.

The above described experimental results and specifically the decrease in relative efficiency of chlorophyll a and pheophytin a in petroleum ether at a temperature of -60° and the concurrent appearance of a hump on the long wavelength side of the red absorption band of these substances in the same solvent give reason to assert that in petroleum ether at these temperatures there form some sort of groupings or aggregates of chlorophyll and pheophytin molecules. The new formation is characterized by its own distinctive absorption spectrum and does not luminesce.

I desire to express my deep gratitude to B.I.Stepanov and L.G.Pikulik for valuable advice.

Institute of Physics,
Academy of Sciences of the Belorussian SSR

References

1. F.P.Zscheile & D.G.Harris, J.Phys.Chem., 47, 623 (1943).
2. L.A.Kravtsov, Izv.AN SSSR,Ser.fiz.,23, 78 (1959). (Trans.Bulletin,23,77.)
3. S.Freed & K.M.Sancier, Science, 114, 275 (1951).
4. S.Freed & K.M.Sancier, Ibid., 116, 175 (1952).
5. E.Rabinowitch, Photosynthesis. (Cited in Russian trans.)
6. L.G.Pikulik & M.A.Solomakho, Optika is epsktroskopiya, 8, 338 (1960). (Trans.Optics and Spectroscopy.)
7. B.I.Stepanov, Lyuminestsentsiya slozhnykh molekul (Luminescence of complex molecules), Belorussian SSR Ac. of Sci., 1955.
8. S.Freed & K.M.Sancier, Science, 117, 655 (1953).
9. S.Freed, Ibid., 125, 1248 (1957).
10. S.Freed & K.M.Sancier, J.Amer.Chem.Soc., 76, 198 (1954).
11. H.H.Strain, Science, 116, 174 (1952).

LUMINESCENCE EFFICIENCY OF CHLOROPHYLL IN DIFFERENT SOLVENTS

- N. P. Ivanov

Investigation of the luminescence efficiency of chlorophyll is fraught with difficulty due partly to the complexity of the measurement procedure in general and partly to the specific nature of this compound. Chlorophyll is unstable: it decomposes rapidly when exposed to light and enters into interaction with the surrounding medium. Appreciable errors may be introduced by reabsorption, which is particularly strong in chlorophyll. This may explain why until recently there have been no reliable data on the quantum efficiency of chlorophyll.

Prior to the 1950's it was generally held that the quantum efficiency of chlorophyll is not over 10%.[1] In 1952 there appeared the report of Förster & Livingston[2] who found that the maximum quantum efficiency attains 24-26% (in some solvents). Among recent studies of the luminescence of chlorophyll one can cite the work of Latimer, Bannister & Rabinowitch[3], who used a special integrating sphere and found that the quantum efficiency is some 40% higher than reported by Förster & Livingston. The error in the earlier result may be explained by inadequacy of the equipment. Subsequent calculations of the quantum efficiency from the results of measurements of the lifetime of the excited state of chlorophyll and the integral absorption[4] substantiated the above high value of the quantum efficiency.

In view of this we felt it would be of interest to determine the luminescence efficiency by means of a different technique and to see how the efficiency varied with changes in solvent. We investigated the efficiency under ordinary conditions the samples were held at room temperature in contact with air so that there were always present polar impurities in the solutions. The observations of Livingston[5] showed that solutions of chlorophyll in purified nonpolar solvents do not luminesc but the presence of even a trace of some polar impurity (water, alcohol) is sufficient for luminescence to appear.

To determine the quantum efficiency we measured the luminescence spectra of the samples and of a standard (3-aminophthalimide) with a known quantum efficiency under identical conditions of absorption of the exciting light. The quantum efficiency was determined from the areas of the luminescence bands.

The luminescence spectra were obtained on a UM-2 monochromator. The radiatio detector was an FEU-22 photomultiplier connected to a dc amplifier. The sensitivity of the set-up was sufficient for obtaining the spectra of both the standard and chlorophyll. The excitation sources were SVDSh-250 and SVD-120 mercury tubes. A solution of copper sulphate served as the heat filter and to cut off the red regio of the mercury spectrum. The luminescence was excited by the 365 mμ light through standard light filters. The sample cell holder with entrance and exit apertures was mounted in the position corresponding to minimum reabsorption of the luminescence entering the monochromator. In measuring quantum efficiencies by the comparison method it is essential that the luminescence standard and the sample absorb the same amount of radiation. A light filter similar to that in the excitation beam and STsV-6 phototube connected to a galvanometer were mounted behind the sample cell. The sensitivity of this phototube is virtually constant over the spectral range involved in the experiments. The filter in front of the phototube served to separate the luminescence and the exciting light passing through the cell with the luminescent solution or the pure solvent. The galvanometer recorded the amount of light absorbed and at the same time monitored the intensity and stability of the excitation source. The operation of the apparatus proved to be stable: virtually identical readings were obtained for the same solution of 3-aminophthalimide tested at 15-20 min intervals. Among the shortcomings of our procedure is the appreciable difference between the positions in the wavelength scale of the luminescence spectra of 3-aminophthalimide and chlorophyll, which naturally introduces an additional error in evaluating the efficiency.

By way of samples we used chlorophyll a separated by two-fold sugar chromatography. The chlorophyll was extracted with ethyl alcohol; the solution was evaporated at low temperature under vacuum. The dry chlorophyll was then dissolved in the chosen solvent. All the solvents were specially purified. The quantum efficiency of the solutions were measured for different concentrations of chlorophyll in the range from $1 \cdot 10^{-6}$ to $6 \cdot 10^{-6}$ mole/liter. The correction for reabsorption did not exceed 5%. As noted above, the standard was a solution of 3-aminophthalimide in ethyl alcohol, the quantum efficiency of which according to the measurements of Alentsev is 60%.

The luminescence spectra of chlorophyll and the 3-aminophthalimide standard were recorded under identical conditions; each complete recording required 5-6 min. The quantum efficiency with excitation by 365 mμ light agrees within 2-3% with the efficiency with excitation by the 405 mμ line.

It is known that under irradiation chlorophyll bleaches; however, the luminescence of solutions changes differently with time in different solvents. A special check of the rate of bleaching of chlorophyll solutions was necessary in order to obtain reliable results. We observed the changes in the luminescence and absorption spectra after irradiation of samples by non-filtered light from a GSVD-120 krypton-xenon tube. The test showed that chlorophyll bleaches most rapidly in carbon tetrachloride, methyl alcohol, octane and nonane, and at the slowest rate in ethyl ether, ethyl alcohol and petroleum ether. The results of these bleaching tests helped correct the inaccuracy in measurements of the quantum efficiencies of the rapidly deteriorating samples. In these tests by way of standard we used a solution of chlorophyll in ethyl alcohol; the luminescence was measured integrally over the spectrum (i.e., with a wide monochromator slit). Determination of the yield by this procedure required 1-2 min.

The luminescence efficiency of chlorophyll was measured in 23 solvents. According to approximate evaluation the accuracy of our measurements was 10-15%. The results are summarized in the accompanying table. Most of the values are averages for four series of experiments.

Luminescence Efficiency γ of Chlorophyll in Different Solvents

Substance	γ %
I. Saturated hydrocarbons and their derivatives	
Hexane	31
Octane	32
Nonane	32
Carbon tetrachloride	25
Petroleum ether	31
II. Alcohols	
Methyl	30
Ethyl	32
Propyl	32
Butyl	32
Isobutyl	31
Isoamyl	32
Diacetone	33
III. Ethers	
Ethyl	29
Acetoacetic	30
IV. Acids	
Acetic	27
V. Ketones	
Acetone	33
VI. Aromatic hydrocarbons and their derivatives	
Benzene	30
o-Xylene	32
m-Xylene	31
Toluene	31
Chlorobenzene	26
VII. Heterocyclic compounds	
Dioxane	31
Pyridine	31

It will be evident from the table that in most solvents the luminescence efficiency is of the order of 30-33%. This constancy of the efficiency is in conflict with the preliminary results of some authors[7-10]. True these authors measured not the quantum efficiency as such but the initial intensity of luminescence, which can only serve as an indirect measure of the relative quantum efficiency. Some authors[7-9] assert that there is an appreciable difference between the initial intensity values for different solvents. For example, according to Zscheile & Harris[7] the luminescence intensity of chlorophyll in ethyl alcohol is half the intensity in benzene and only one third the intensity in acetone. Such marked differences in the luminescence intensity were also observed for other solvents. These divergent results can be explained by the fact that the absorption of chlorophyll in different solvents differs. This becomes obvious from examination of the data on the absorption spectra of chlorophyll in different solvents. At the same chlorophyll concentration the absorption bands differ substantially, the greatest difference being observed in the tails of the bands, i.e., precisely in the region where most of the active absorption occurs.

Our data indicate that in the first approximation the character of the solvent does not effect the quantum efficiency, at least in the case of fresh solutions and in the range of low chlorophyll concentrations.

I desire to express my deep gratitude to B.I.Stepanov for guidance in the work and to P.A.Naumenkov for assistance carrying out some of the measurements.

Institute of Physics,
Academy of Sciences of the Belorussian SSR

References

1. J.A.Prins, Nature, 134, 457 (1934).
2. L.S.Förster & R.Livingston, J.Chem.Phys., 20, 1315 (1952).
3. P.Latimer, T.T.Bannister & E.Rabinowitch, Science, 124, No.3222, 585 (1956).
4. V.Brody & E.Rabinowitch, Science, 125, No.3247, 155 (1957).
5. R.Livingston, W.F.Watson & I.McArdle, J.Amer.Chem.Soc., 71, 1542 (1949).
6. S.Yu.Luk'yanov, Fotoelementy (Phototubes), M.-L., 1949.
7. F.P.Zscheile & D.G.Harris, J.Phys.Chem., 47, 623 (1943).
8. V.M.Albers & H.V.Knorr, Phys.Rev., 46, 336 (1934).
9. H.V.Knorr & V.M.Albers, Cold Spring Harbor Simposia Quant.Biol., 3, 98 (1935).
10. E.Rabinowitch, Photosynthesis, Vol.II.(Cited in Russian translation.)

AGGREGATION OF CHLOROPHYLL AND CHLOROPHYLLIDE MOLECULES

- R.V.Efremova

The question of the state of chlorophyll in leaves is obviously important in the study of photosynthesis. There are hypotheses that the chlorophyll is linked to proteins and also that chlorophyll is in the colloidal state in leaves. In this connection we felt it would be of interest to investigate the aggregation of chlorophyll molecules and those of its derivatives.

It is usually assumed that chlorophyll in organic solvents does not dimerize. Solutions of chlorophyll in the concentration range from 10^{-6} to 10^{-4} mole/liter do not show a deviation from Bouguer's (Lambert's) law.[1] Some authors[2-5] indicate, however, that chlorophyll does form dimers in nonpolar solutions in the absence of polar molecules. It is also known that chlorophyll is polymerized in colloidal suspensions and in the solid state.[6-8]

We investigated the absorption and luminescence spectra of chlorophyll and chlorophyllide for the purpose of determining the ability of these molecules to aggregate, i.e., to form dimers and higher polymers.

The absorption spectra were studied on an SF-5 spectrometer; the luminescence spectra, on an UM-2 monochromator with the radiation being detected by an FEU-22 photomultiplier. The spectra of chlorophyll and chlorophyllide solutions were investigated in a number of individual solvents and also in some binary solvent mixtures. The concentration was varied in the range from 10^{-7} to 10^{-3} mole/liter. In the course of the investigation we also checked the influence of temperature and the pH of the medium on the spectra.

The presence of water in an alcohol solution of chlorophyll favors aggregation of the pigment. A small amount of water leads to dimerization of the chlorophyll molecules; with increase in the percentage of water there form higher polymers. At the same time the absorption and luminescence of the solutions decrease.

The absorption and luminescence spectra for chlorophyll a in ethyl alcohol ($C = 5 \cdot 10^{-6}$ mole/liter) with different amounts of water are shown in Fig.1. The presence of 20% water leads to a shift of the absorption peak from 666 to 668 mμ. A further increase of the water content (to 55%) leads to a strong smearing out of the absorption band and shift of the peak to 672 mμ; the spectrum becomes characteristic of that for colloids. The spectral absorption curves characterizing solutions with up to 30% water have common points at 647 and 676 mμ. The presence of at least one such point of intersection indicates the presence of complexes of two types in the solutions. It

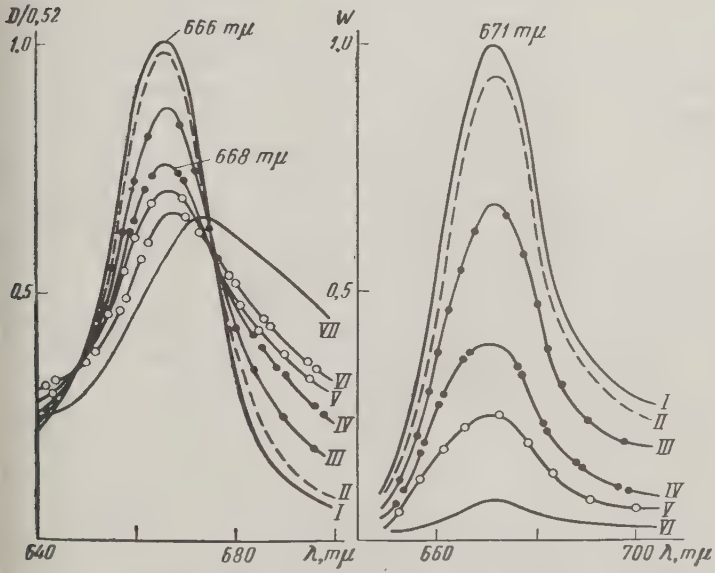

Fig.1. Absorption (D) and luminescence (W) spectra of chlorophyll a in ethyl alcohol-water solutions (chlorophyll concentration $5 \cdot 10^{-6}$ mole/liter): I - chlorophyll a in pure ethyl alcohol, II - 12% water, III - 16%, IV - 20%, V - 25%, VI - 30%, VII - 55%.

is natural to assume that these curves correspond to chlorophyll monomers and dimers. It will be evident from Fig.1 that the absorption maximum of the dimer lies at about 668 mμ. Only solutions the absorption spectra of which pass through a common point are capable of luminescing. The luminescence of these solutions decrease with increase of the water content. Although the luminescence peak decreases in height, its position remains constant at 671 mμ. The absence of a shift of the luminescence peak indicates that only the monomer form of chlorophyll luminesces.

Heating of the chlorophyll solution with the absorption peak at 668 mμ (20% water) to +40° results in a reverse shift of the peak to 666 mμ, which indicates that the dimers decompose into monomers. These inferences regarding the aggregation of chlorophyll are in agreement with the result of Eustigneev[5].

The process of aggregational chlorophyll in binary mixtures is influenced by the chlorophyll concentration. In more highly concentrated solutions the formation of complexes begins at a lower water content. At a concentration of $2\cdot10^{-5}$ mole/liter the presence of only 8% water in the alcohol-water solution is sufficient for the appearance of dimers.

The aggregation behavior of chlorophyll in the case of solutions in the binary system acetone-water is similar to that in the alcohol-water system.

On the other hand, we were not able to produce dimerization of chlorophyll by increasing the concentration in solutions of ethyl alcohol, isobutyl alcohol, acetone and ethyl ether. Solutions of chlorophyll in these solvents in the concentration range from 10^{-7} to 10^{-3} mole/liter show no deviation from Bouguer's law; the absorption band contour remains unchanged.

The process of aggregation of dye molecules in general depends substantially on the nature of the dye and the nature of the solvents. The chlorophyllide molecule is hydrophilic and differs from the chlorophyll molecule by replacement of the lipophilic radical $C_{20}H_{39}$ by a hydrogen. Water, the medium in which chlorophyllide is usually found, is most favorable for aggregation.

With a view to elucidating the state of chlorophyllide in solutions, we carried out a systematic investigation of the influence of its concentration on the absorption and luminescence spectra of water solutions (Fig.2). The concentration effect can be explained by aggregation of the chlorophyllide a molecules. The fact that there is a point of intersection of the absorption curves for solutions in the concentration range from $1.6\cdot10^{-6}$ to $6.4\cdot10^{-6}$ mole/liter indicates that two types of molecules are present in the solutions. The first peak (at about 630 mμ) can be attributed to the monomer form of chlorophyllide; the second peak (at 652 mμ) to the dimer form. The curves for solutions with a concentration of the order of 10^{-5} mole/liter bear evidence of a higher degree of aggregation. In contrast to chlorophyll, chlorophyllide luminesces in the associated form.

The concentration dependence of the spectra of chlorophyllide indicates that chlorophyllide is in the monomer form only in solutions with a concentration of the order of 10^{-6}-10^{-7} mole/liter. With increase in concentration there occurs dimerization and then further polymerization of the molecules on to formation of colloidal particles which do not have the ability to luminesce.

The variation of the spectra of chlorophyllide with changes in concentration cannot be attributed to influence of the acidity of the medium. In the above range of chlorophyllide concentrations the pH of the solutions varied from 7.2 to 11. To reduce the pH of concentrated chlorophyllide solutions we added an appropriate amount of acid; this produced no noticeable change in the shape of the spectra.

For chlorophyllide in binary water-ethyl alcohol solutions variation in the proportion of water to alcohol leads to changes similar to those observed in varying the chlorophillide concentration (Fig.3). The peak at 652 mμ corresponding

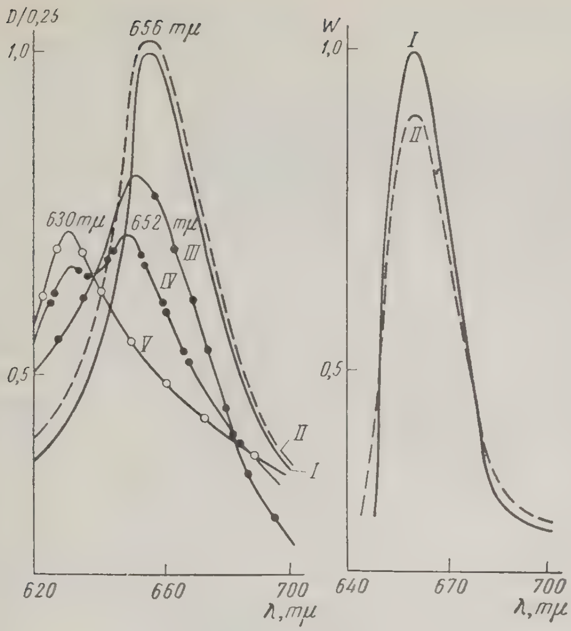

Fig.2

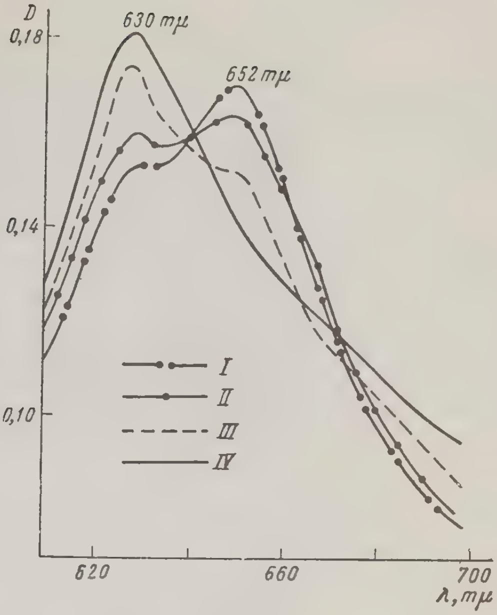

Fig.3

Fig.2. Absorption and luminescence spectra of chlorophyllide a in water at different concentrations (in mole/liter): I - $2.4 \cdot 10^{-5}$, II - $1.2 \cdot 10^{-5}$, III - $6.4 \cdot 10^{-6}$, IV - $3.2 \cdot 10^{-6}$, V - $1.6 \cdot 10^{-6}$.

Fig.3. Absorption spectra of chlorophyllide a in water-ethyl alcohol solutions (chlorophyllide concentration $3 \cdot 10^{-6}$ mole/liter): I - water, II - 4% ethyl alcohol, III - 10%, IV - 15%.

to dimers gradually decreases in height with increased ethyl alcohol concentration; at a 15% ethyl alcohol content there is evident only the peak at 630 mμ corresponding to monomers. Evidently the polar ethyl alcohol molecule hinders association of chlorophyllide and tends to break up any dimers present.

With increase in temperature at 50° the spectrum of concentrated chlorophyllide solutions becomes similar to the spectrum of low concentration solutions. Increase in temperature results in dissociation of the aggregated chlorophyllide molecules.

It should be noted that the shift of the chlorophyllide absorption peak in going from the monomer to the dimer form is 22 mμ, whereas the corresponding shift for chlorophyll is only 2 mμ. This may be indicative of differences in the nature of chlorophyll and chlorophyllide complexes.

I desire to express my gratitude to B.I.Stepanov for guidance in the work.

Institute of Physics,
Academy of Sciences of the Belorussian SSR

References

1. E.Rabinowitch, Photosynthesis. (Cited in Russian translation.)
2. R.Livingston, W.F.Watson & I.McArdle, J.Amer.Chem.Soc.,71,1542 (1949).
3. A.A.Krasnovskii & L.M.Kosobutskaya, Doklady AN SSSR, 85, 177 (1952).
4. A.A.Krasnovskii, L.M.Kosobutskaya & K.K.Voinovskaya, Doklady AN SSSR, 85, 389 (1952).
5. V.B.Evstigneev, Izv.AN SSSR, Ser.fiz.,23, 74 (1959).(Trans. Bulletin,23,74.)
6. D.I.Ivanovskii, Ber.Dtsch.bot.Ges., 25, 416 (1907).
7. B.Hubert, Rec.trav.notan.Neerland., 32, 323 (1935).
8. J.Wakkil, G.Proc.Acad.Sci. Amsterdam, 38, 1082 (1935).

ABSORPTION AND FLUORESCENCE SPECTRA OF PERYLENE AT LOW TEMPERATURES

- R.I.Personov

In this paper we give some of the results of investigation of the spectra of the five-ring aromatic hydrocarbon, perylene, in frozen solutions at 77°K. For obtaining the absorption and fluorescence spectra we use the method of frozen normal paraffin solutions developed by Shpolskii and his co-workers[1-6].

The quasi-line fluorescence spectrum of perylene in hexane at 77°K was first obtained by Bowen & Brocklehurst[7]. They observed 16 principal band peaks, but did not subject the spectrum to further analysis. Yet vibrational analysis of this sharp spectrum is of particular interest inasmuch as observation of the Raman spectrum of perylene is hampered by strong fluorescence in the visible region. Investigation of the spectra of perylene is also of interest from the practical standpoint. Perylene, in addition to other aromatic hydrocarbons, is encountered in the products of pyrolysis of organic substances (soot, tar, gums) and sometimes in natural or mineral products (for example, in petroleums[8] and bitumens[9]) and the spectroscopic data for it can be utilized for analytic purposes.

1. We studied the long wavelength region of the absorption spectra of frozen (77°K) solutions of perylene in ethyl alcohol and normal paraffins from hexane to nonane. The long wavelength absorption region of perylene solutions begins at about 4400 Å and extends some 700 Å to the side of shorter wavelengths. In the absorption spectrum of the alcohol solution there are clearly discernible groups of bands with a separation of approximately 1330 cm^{-1}. The relatively broad (100-150 cm^{-1}) absorption bands of perylene in alcohol (Fig.1,a) are resolved in hexane into groups of narrow bands with a width of ~10 cm^{-1} (Fig.1,b). In other normal paraffins the spectra repeat those of the hexane solution, i.e., consist of narrow bands, virtually lines, with approximately the same frequency intervals, but in going to heptane, octane and nonane the lines are smeared out somewhat and the entire spectrum is shifted 40, 75, 110 cm^{-1}, respectively, relative to the spectrum in hexane.

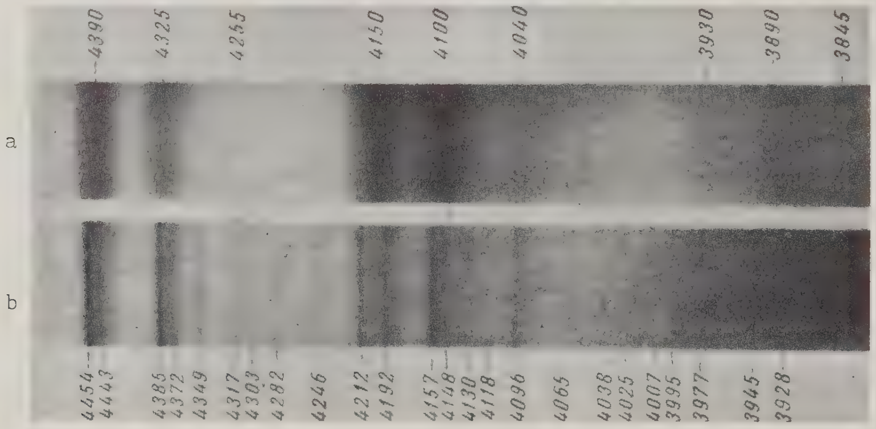

Fig.1. Absorption spectra of perylene at -77°K in a) ethyl alcohol and b) hexane. Fuss spectrograph; dispersion 42 Å/mm at 4500 A.

2. We investigated the fluorescence spectra of perylene at 77°K in the crystalline state, in ethyl alcohol and in normal paraffins from hexane to nonane. In the crystalline state perylene has a bright orange-red fluorescence lying beyond 6000 Å. This spectrum is diffused and strongly shifted to the side of longer wavelengths compared to the spectra of solutions (Fig.2,a). In solutions the

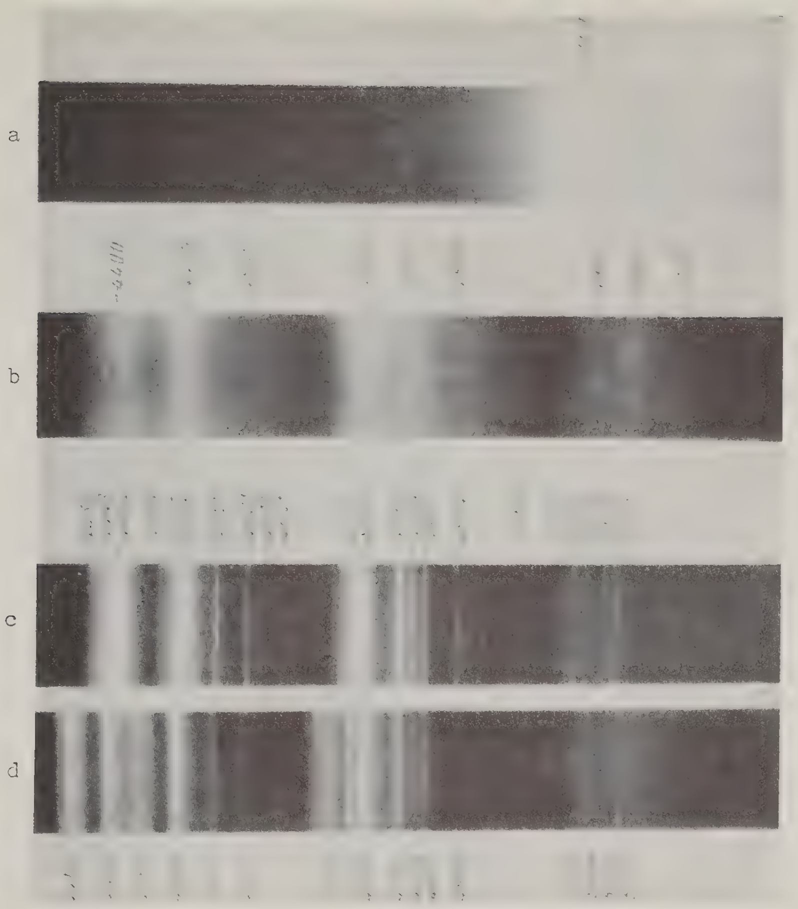

Fig.2. Fluorescence spectra of perylene at 77°K: a) in the crystalline state, b) in ethyl alcohol, c) in hexane, d) in heptane. Fuss spectrograph.

fluorescence becomes blue-azure. The fluorescence spectrum of the alcohol solution consist of four groups of bands. Each group consists of four bands some 100-150 cm^{-1} wide (Fig.2,b); as in the case of the absorption spectra, the separation between the band groups is approximately 1330 cm^{-1}.

A substantially different picture is obtained for paraffin solutions. The diffuse fluorescence bands observed for alcohol solutions, in hexane solutions are resolved into groups of lines 10-20 cm^{-1} wide (Fig.2,c). The fluorescence spectra in heptane, octane and nonane have the same quasi-line character and simulate the spectra of the hexane solution, but in going from hexane to higher paraffins the lines become increasingly diffused and the entire spectrum is shifted to the short wavelength side relative to the spectrum in hexane by approximately the same amount as the absorption spectra. There are, however, details distinguishing the spectra in different paraffins. Thus in the fluorescence spectrum of perylene in hexane the two first most intense lines at 4454 and 4526 Å are accompanied by satellites on the short wavelength side (Fig.2,c). These are not evident in the spectra of other paraffin solutions. In heptane, octane and nonane there appear three diffused lines (their wavelengths in heptane are 4410, 4480 and 4686 Å - Fig.2,d, which have no discernible analogs in the spectrum of the hexane solution. The last two lines are separated from the first by intervals of about 350 and 1335 cm^{-1}. These intervals are close to the principal frequency differences in the main spectrum of perylene.

3. Comparison of the sharp absorption and fluorescence spectra of perylene in hexane showed that the most intense short wavelength line in the fluorescence spectrum (4454 Å) coincides with the longest wavelength intense line in the absorption spectrum. Hence we attributed it to the $0 \rightarrow 0$ transition.

Analysis of the spectra shows that the frequency differences between the 0—0 line and almost all the other absorption lines (in all there are 38), with few exceptions (four lines), can be represented as combinations or harmonics of five frequencies, namely, 358, 548, 1290, 1402 and 1602 cm^{-1}. The most intense of the lines are associated with the 358 and 1402 cm^{-1} frequencies. Likewise almost all the intervals in the fluorescence spectra (there are over 40) reckoned from the 0—0 (4454 Å) line can be interpreted in terms of five frequencies: 358, 550, 1298, 1375 and 1578 cm^{-1}. The most intense of these are 358 and 1375 cm^{-1}. It will be evident that the frequencies observed in the excited state differ little from the frequencies for the ground state. Comparison of the absorption and fluorescence spectra of frozen perylene solutions therefore indicates the presence of nearly mirror symmetry.

It is of obvious interest to compare the vibrational frequencies of perylene and naphthalene molecules, inasmuch as there are a number of facts indicating that the perylene molecule may be regarded as a conjunction of two relatively weakly linked naphthalene groupings. Thus, for example, x-ray defraction determination of the length of the bonds in perylene[10] shows that the bonds linking the two naphthalene groupings are anomalously long (1.50 Å) compared with the other bonds (1.38 Å). Further evidence in favor of this structure of perylene is the fact that perylene is readily synthesized from naphthalene. These two molecules belong to the same point symmetry group (D_{2h}), for which according to the selection rules there should be evidenced in the electronic-vibrational and Raman spectra the same vibration frequencies, symmetrical relative to the center of inversion of the molecules (A_{1g}, B_{1g}, B_{2g}, B_{3g}). Comparison of the observed frequencies of perylene with the frequencies of naphthalene obtained from the Raman spectra[11] brings out the presence of two frequencies that coincide within the limits of the experimental error:

Naphthalene	Perylene
1379	1375
1576	1578

The frequencies 1379 and 1576 cm^{-1} belong to the intense frequencies in the Raman spectrum of naphthalene and pertain to fully symmetrical vibrations.

The reason for the appearance in the fluorescence spectra of certain detailed features characteristic of a given solvent (for example, the short wavelength satellites of the first intense lines of the spectrum in hexane, the three diffuse bands in other paraffins) so far remain unclear. Possibly the appearance of the two short wavelength satellites is connected with the presence of series repeating each other, as occurs, for example, in coronene[3], pyrene and 3,4-benzopyrene[6], but the first two series are very weak so that we observe only their first terms.

4. By way of illustration of the practical utilization of the above data we can refer to a number of analyses for the presence of perylene carried out by us in collaboration with A.A.Il'ina, with reference to the fluorescence spectra of frozen solutions. Fig.3 shows the fluorescence spectra of a hexane solution of an extract of natural bitumen. There are clearly discernible all the principal

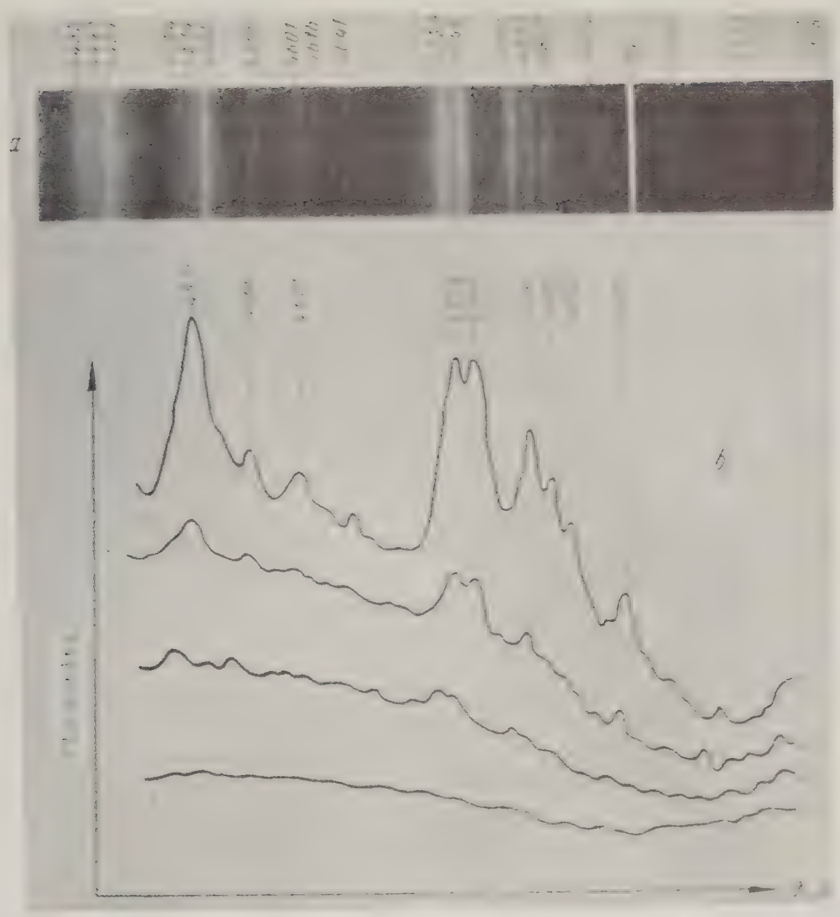

Fig.3. a - Fluorescence spectrum of bitumen in hexane at 77^{O}K, b - photometric traces of fluorescence spectra of solutions of mineral oils in hexane with the addition of perylene at 77^{O}K; perylene concentration: 1) 0.001%, 2) 0.0025%, 3) 0.005%, 4) 0.01%.

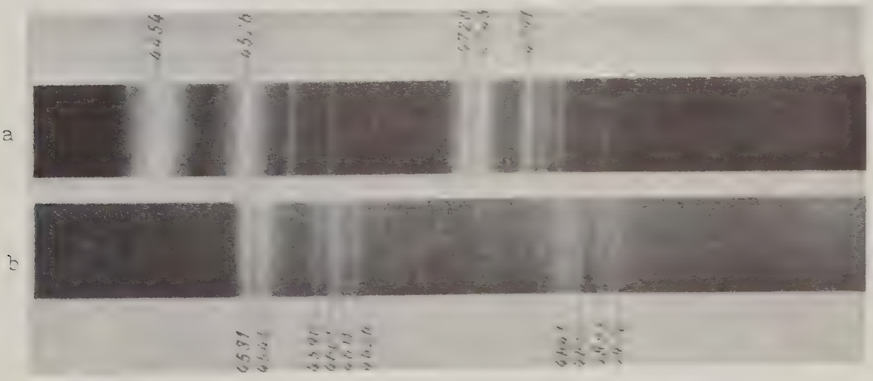

Fig.4. Fluorescence spectra of hexane solutions of perylene (a) and the products of photochemical reaction of perylene in chloroform (b) at 77^{O}K. ISP-67 spectrograph; f = 500 mm camera.

lines of perylene. Particularly characteristic are the bright lines of the 4728-4745 doublet and the 4791-4809-4827 triplet. Photographs of the fluorescence spectra of frozen hexane solutions of various petroleums and petroleum fractions showed that traces of perylene can be detected in the oil fractions of a number of petroleums.

For purposes of semiquantitative analysis we prepared standard samples of mineral oils with a known perylene concentration. It is evident from the photometric traces of the fluorescence spectra of frozen hexane solutions of these samples (Fig.3,b) that the presence of 0.001% perylene in the oil is virtually undetectable; at a concentration of 0.0025% perylene, however, there appear against the background of the continuous spectrum traces of the 4526, 4728, 4745 and 4791 Å lines of perylene. At a concentration of 0.005% almost all the principal lines are clearly discernible. Thus the 4526, 4728, 4745 and 4791 Å lines can be used as the analytic lines. (The first very intense fluorescence line at 4454Å (0—0) is frequently distorted by reabsorption; hence we do not include it among the analytic lines.)

5. Worthy of note is the high photochemical activity of perylene in chloroform: after 15 minutes illumination by standard daylight the solution loses its blue fluorescence and the emission becomes greenish. The spectrum of a frozen hexane solution of irradiated perylene after removal of the chloroform by distillation also consists of sharp lines but is shifted to the long wavelength side (Fig.4). We have not yet been able to establish the specific product responsible for this spectrum. Possibly this is the spectrum of one of the chlorine derivatives of perylene.

I desire to express my deep gratitude to E.V.Shpol'skii for his guidance and constant interest in the work.

"V.I.Lenin" State Pedagogical Institute

References

1. E.V.Shpol'skii, A.A.Il'ina & L.A.Klumova, Doklady AN SSSR, 87, 935 (1952).
2. E.V.Shpol'skii & L.A.Klimova, Izv.AN SSSR, Ser.fiz., 18, 673 (1954). (Trans.Bulletin, 18, 357.)
3. E.V.Shpol'skii & L.A.Klimova, Ibid., 20, 471 (1956). (Trans.Bulletin, 20, 428.)
4. E.V.Shpol'skii & L.A.Klimova, Doklady AN SSSR, 103, 1227 (1956).
5. E.V.Shpol'skii, E.A.Girdzhiyauskaite & L.A.Klimova, Transactions of the Tenth Conference on Spectroscopy, Vol.1, p.24, L'vov, 1957.
6. E.V.Shpol'skii & E.A.Girdzhiyauskaite, Optika i spektroskopiya, 4, 620 (1958).
7. E.J.Bowen & B.Brocklehurst, J.Chem.Soc., (L), 8, 4320 (1955).
8. R.Schnurmann, W.F.Maddams & M.C.Barlow, Analyt.Chem., 25, 1010 (1953).
9. A.A.Il'ina, Transactions of the Fourth Conference on Luminescence, p.41, Minsk, 1956.
10. J.M.Robertson, Organic Crystals and Molecules, Cornell 1953.
11. A.L.McClellan & G.C.Pimentel, J.Chem.Phys., 23, 245 (1955).

SPECTROSCOPY OF SOME PYRENE DERIVATIVES IN FROZEN SOLUTIONS

- A.Ya.Khesina

In the present paper we shall summarize the results of spectroscopic investigation of three complex aromatic hydrocarbons of the pyrene series. This investigation is one of a series of studies of the molecular spectra of aromatic hydrocarbons by the method of frozen alkane solutions, proposed by E.V.Shpol'skii and developed in his laboratory.

During the past few years Shpol'skii and his colleagues, as well as a number of spectroscopists abroad, carried out investigations of the fine structure of various polynuclear and simple aromatic hydrocarbons in frozen solutions.[1-8] The spectra of coronene, pyrene and 3,4-benzopyrene have been studied in most detail.

With a view to elucidating the influence of a substantial complication of the molecular structure and decrease in the degree of symmetry of the molecule on the quasi-line character of the spectra of frozen solutions, we chose for the present investigation the three derivatives of pyrene characterized by the structural formulas shown below:

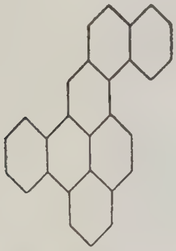

I - 3,4-naphtho-6,7-benzopyrene

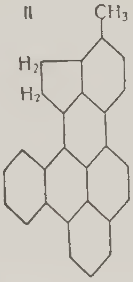

II - 3'-methyl-4',5-ethylene-3,4,6,7-dibenzopyrene

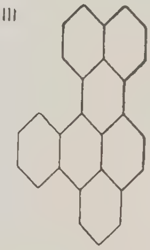

III - 3,4,5,6,7-tribenzopyrene

Spectroscopic investigation of these substances is also of interest because pyrene derivatives are carcinogenic; hence investigation of the molecular spectra of pyrene derivatives by the method of frozen alkane solutions may be helpful for identification of such carcinogenic substances.

1. Crystals of substances I-III emit bright green fluorescence, consisting of several diffuse bands (10 in the spectrum of substance I, 12 in the spectrum of II and 5 in the spectrum of III); the band width is of the order of 200 cm^{-1} in the spectra of I and II and 300-400 cm^{-1} in the spectrum of III. Cooling of the crystals down to 77°K has no significant effect on the spectra.

The fluorescence spectra of solutions of substances L-III are shifted some 2000-3000 cm^{-1} to the short wavelength side relative to the spectra of the crystals and hence lie in the blue-violet region. At room temperature the solution spectra consist of diffuse bands 200-250 cm^{-1} wide.

Decrease of the temperature has no significant effect on the spectra of oil and alcohol solutions of the three substances; if, however, one of the normal alkanes is used as the solvent, the wide bands narrow and split into "lines" that are sharp enouth to permit determining their positions to within 10 cm^{-1}.

In the course of experiments with solvents from hexane to decane it was found that the best resolution (line separation) for each substance obtains in one particular in each case, namely, for substance I in hexane and for substances II and III in octane. In going to other solvents, the spectra are smeared out to some extent.

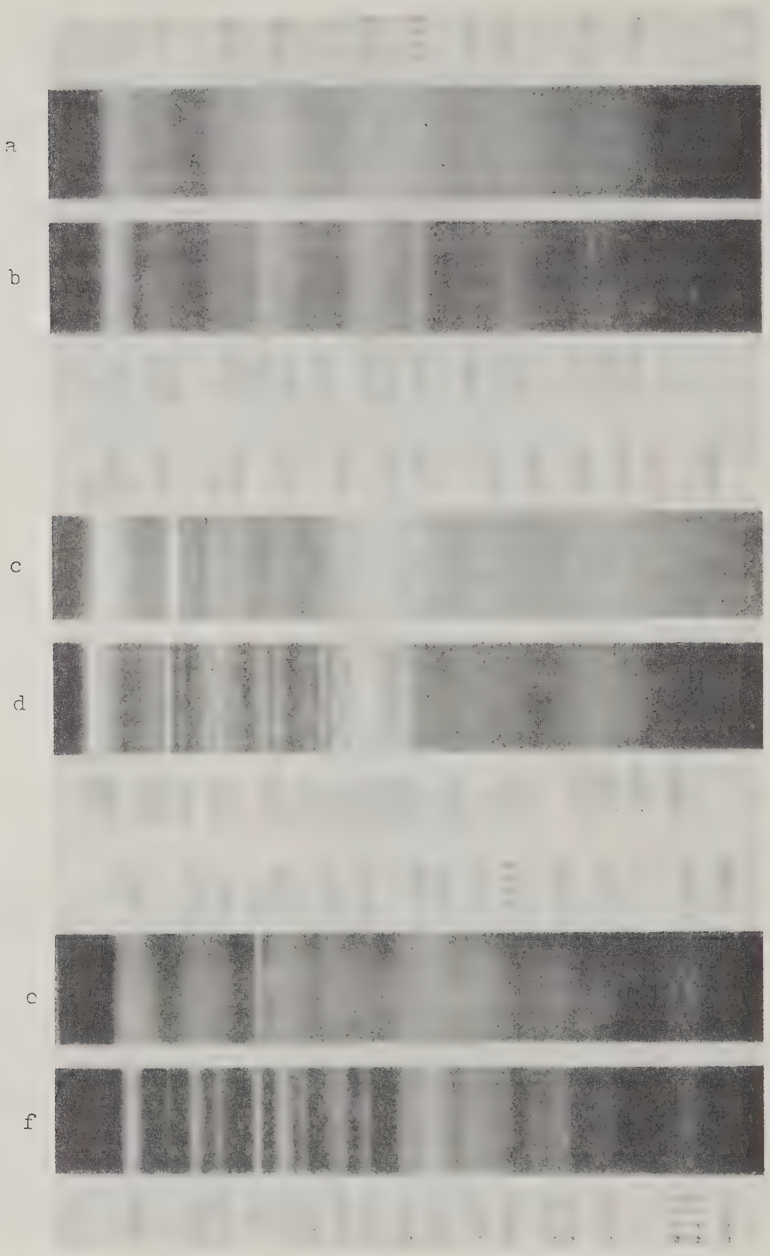

Fig.1. Fluorescence spectra of the pyrene derivatives in solutions at 77°K: a) I in ethyl alcohol, b) I in hexane, c) II in ethyl alcohol, d) II in octane, e) III in ethyl alcohol, f) III in octane.

Photographs of the fluorescence spectra of the investigated substances at liquid nitrogen temperature in ethyl alcohol and in the normal paraffin in which the spectrum of the given substance is best resolved are reproduced in Fig.1. In the figure we have indicated the wavelength of the most intense lines in the fluorescence spectra of substances I-III in the indicated solvent. In other solvents the spectra more or less repeat the spectra shown in Fig.1 with the same frequency interval referred to the 0—0 band.

Examination of the spectrograms shows that the spectra of alkane frozen solutions of substances I-III consist in a number of cases not of individual lines but of "multiplets" - groups of lines repeating over the spectrum. It will be evident from Fig.1 that the spectrum of substance I in hexane consists of doublet with a component separation of 35 cm^{-1}; the spectrum of III in octane also consists of doublets but with a component separation of 20 cm^{-1}, while the spectrum of II in octane consists of singlets.

Inasmuch as measurements show that the separation between the components of a multiplet remains constant over the entire spectrum and the relative intensity of the component also does not change, the spectrum consisting of multiplets can be represented as a superposition of n (the number of components in the multiplet) sequences identical as regards vibrational structure but shifted $\Delta\nu$, the distance between the multiplet components in cm^{-1}, in the frequency scale.

2. In order to identify the 0—0 band, in addition to the fluorescence spectra, we obtained the absorption spectra of solutions of substances I-III at 77°K. It was found that for all these substances the longest wavelength band in the absorption spectra coincides within the limits of the experimental error with the shortest wavelength band in the fluorescence spectra and is therefore the band associated with the 0→0 transition.

By way of illustration we give the results of the determination of the 0—0 band in the fluorescence and absorption spectra of the hexane solution of substance I at 77°K:

	Fluorescence	Absorption
1.	4169.3 (weak)	4169.8 (weak)
2.	4180.3 (int)	4181.1 (int)
3.	4185.9 (int)	4186.1 (int)
4.	4198.5 (weak)	4199.0 (weak)

The 0—0 multiplet in this case consists of four components; however, the first and fourth components are so weak that they are not discernible in the higher wave number multiplets. As a result, the spectrum of substance I in hexane consists of a superposition of two spectral sequences.

3. The quasi-line character of the spectra of alkane frozen solutions and the precise determination of the 0→0 transition enabled us to carry out a vibrational analysis of the fluorescence spectra. In cases when the spectrum consisted of multiplets, i.e., was the result of superposition of several shifted molecular spectra, the vibrational analysis was carried out separately for each of the identified sequences.

The analysis showed 1) that the vibrational structure is identical in all the spectral sequences evinced in a given solvent and 2) that the vibrational structure of the spectra is the same in all solvents.

In view of the above it may be asserted 1) that the spectra of frozen alkane solutions of the investigated substances consist of one or more superposed electronic-vibrational spectra of the emitting molecules, 2) that the vibrational structure of the investigated molecules does not depend on the solvent, 3) that the influence of the solvent reduces to alteration in the sharpness of the bands or lines and to insignificant change in the energy of the electronic transition, which does not exceed 70 cm^{-1} in the case of the investigated pyrene derivatives.

Vibrational analysis showed that all the frequencies evinced in the fluorescence spectra can be represented with an accuracy to within 10 cm^{-1} as linear combinations of a relatively small number of natural frequencies. In Table 1 we list the frequency of the normal vibrations of molecules I-III in the ground electronic state as deduced from analysis of the fluorescence spectra.

Table 1

Substance	Frequencies of the normal vibrations of molecules I-III in the ground state (cm^{-1})
I	205 (int), 280 (av), 315 (av), 560 (int), 635 (int),
	745 (int), 785 (int), 1340 (int), 1440 (int), 1624 (int),
II	251 (int), 312 (int), 410 (av), 445 (int), 602 (int),
	635 (int), 854 (int), 1236 (int), 1354 (int), 1415 (int),
	1633 (int),
III	286 (int), 387 (int), 415 (av), 500 (av), 655 (int),
	690 (int), 1267 (int), 1311 (int), 1419 (int), 1634 (int).

4. It was found that at 77°K solutions of substances I-III yield bright orange-red to red phosphorescence, which we could investigate only to 6500 Å owing to the limited sensity of our photographic plates.

The phosphorescence spectra of frozen crystalline solutions of substances I-III, like the fluorescence spectra, are quasi-line spectra. By way of illustration the phosphorescence spectra of substance I in a number of solvents and of substances II and III in heptane and nonane, respectively, are reproduced in Fig.2

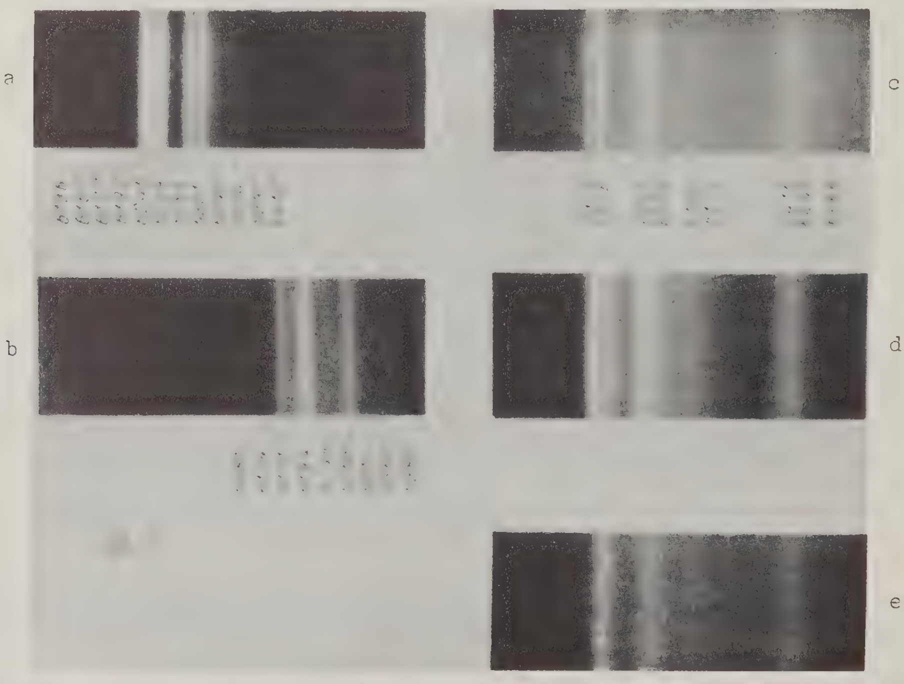

Fig.2. Phosphorescence spectra of the pyrene derivatives in alkane solutions at 77°K: a) substance III in nonane, b) II in heptane, c) I in hexane, d) I in heptane, e) I in octane.

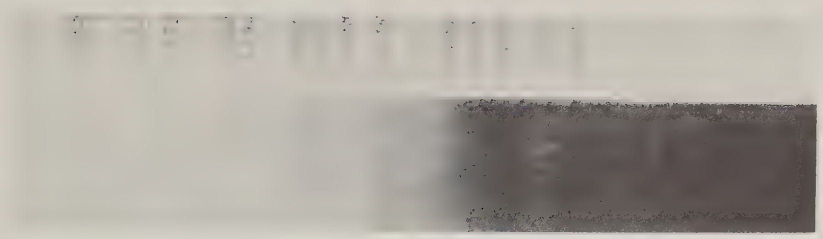

ig.3. Long wavelength section of the absorption spectrum of substance I in hexane at 77°K.

Vibrational analysis of the phosphorescence spectra showed that the frequency ifferences in the phosphorescence spectrum can within the limits of the experiental error be represented by linear combinations of the normal molecular vibraion frequencies obtained in analysis of the fluorescence spectra. For example, he phosphorescence spectrum of substance I can be characterized by the frequencies 80, 315, 560, 635, 1340 and 1624 cm^{-1}; these are the natural frequencies that erve for interpretation of the fluorescence spectrum of substance I (see Table 1).

These results are in agreement with the fact that both forms of luminescence re due to transitions from low-lying excited levels (singlet in the case of fluoescence and triplet in the case of phosphorescence) to different vibrational levls of the ground state.

5. The long wavelength parts of the absorption spectra of frozen alkane soluions of substances I-III are as clearly resolved into lines as the luminescence pectra. By way of illustration, a photograph of the long wavelength section of he absorption spectrum of substance I in hexane at 77°K is shown in Fig.3.

The multiplet splittings in the absorption spectra coincide with the splitings in the fluorescence spectra in the same solvent; this was shown for the case f the 0—0 band of the hexane solution of substance I.

Vibrational analysis showed that, as in the case of luminescence, the vibraional structure of the absorption spectra does not depend on the solvent.

In Table 2 we list the frequencies of the normal vibrations of molecules I-II in the excited state as found by vibrational analysis of the long wavelength art of the absorption spectra.

Table 2

ubstance	Frequencies of the normal vibrations of molecules I-III in the excited state as found by vibrational analysis of the long wavelength part of the absorption spectra (cm^{-1})			
I	190 (int),	313 (av),	471 (int),	540 (int),
	740 (int),	770 (int),	1370 (int),	1580 (int),
II	245 (av),	270 (int),	385 (int),	440 (int),
	600 (av),	635 (int),	850 (int),	1236 (av), 1415 (int),
III	283 (int),	385 (int),	411 (av),	620 (int), 645 (int).

Comparison of the normal vibrational frequencies of molecules I-III in the round (Table 1) and excited (Table 2) states showed that for all three of pyrene erivatives investigated there obtains approximate mirror symmetry of the fluoresence spectra with respect to the long wavelength part of the absorption spectra.

6. Our investigation of frozen crystalline solutions of the three pyrene erivatives enabled us 1) to establish the characteristic wavelengths in the lumi-

nescence and absorption spectra of these three complex aromatic compounds, i.e., to obtain data that can be utilized for precise identification of substances I, II and III, and 2) to establish the vibrational structure of the ground and first excited states and to determine the frequencies of the normal vibrations of the investigated molecules.

I desire to express my deep gratitude to E.V.Shpol'skii for assistance and interest in the work and to B.A.Arbuzov for making available to our laboratory the pyrene derivatives synthesized by him.

"V.I.Lenin" State Pedagogical Institute

References

1. E.V.Shpol'skii, A.A.Il'ina & L.A.Klimova, Doklady AN SSSR, 87, 935 (1952).
2. E.V.Shpol'skii & L.A.Klimova, Izv.AN SSSR, Ser.fiz., 18, 673 (1954). (Trans.Bulletin, 18, 357.)
3. E.V.Shpol'skii & L.A.Klimova, Ibid., 20, 471 (1956). (Trans.Bulletin, 20, 428.)
4. E.Bowen & B.Brocklehurst, J.Chem.Soc., London, November, 3875 (1954).
5. E.Bowen & B.Brocklehurst, J.Chem.Soc., London, December, 4320 (1955).
6. E.V.Shpol'skii & E.Z.Girdzhiyauskaite, Optika i spektroskopiya (Optics & spectroscopy), 4, 620 (1958).
7. E.V.Shpol'skii & L.A.Klimova, Izv.AN SSSR, Ser.fiz., 23, 23 (1959). (Trans.Bulletin, 23, 22.)
8. T.N.Bolotnikova, Ibid., 23, 29 (1959). (Trans.Bulletin, 23, 29.)

Bulletin of the USSR Academy of Sciences - Physical Series
Vol.24, No.5 - May, 1960
Transactions of the Eighth Conference on Luminescence
(To be concluded in Vol.24, No.6)

TABLE OF CONTENTS

	Page Orig.	Page Trans.
pening address - V.L.Levshin	488	495
nternal conversion from the fluorescence to the phosphorescence level in naphthalene derivatives - V.L.Ermolaev, I.P.Kotlyar & K.K.Svitashev	492	499
uminescence of matter with arbitrary absorption and emission bands in volumes of finite size - A.M.Samson	496	503
econdary light absorption and emission processes - B.I.Stepanov & A.M.Samson	502	509
robability method of calculating absorption and emission properties - P.A.Apanasevich	509	516
pectroscopic investigation of vibrational energy transfer in collisions of complex molecules (Summary of report) - S.O.Mirumyants & B.S.Neporent	514	521
nvestigation of the temperature dependence of the interaction between aromatic molecules in the vapor state - V.P.Klochkov	516	523
emperature dependence of the fluorescence efficiency of complex molecule vapors - N.A.Borisevich & V.A.Tolkachev	521	527
ngular distribution of resonance radiation from vapors - P.A. Apanasevich & G.S.Kruglik	525	531
n agreement between the classical and quantum theories of the interaction of light with harmonic oscillators - V.P.Gribkovskii & B.I.Stepanov	529	535
onlinear optical effects in a system of particles with three energy levels - B.I.Stepanov & V.P.Gribkovskii	534	540
alculation of the probability of electronic-vibrational transitions for an anharmonic oscillator - K.K.Rebane & O.I.Sil'd	539	545
lectronic spectra of anthraquinone vapors - N.A.Borisevich & V.V.Gruzinskii	545	551
uminescence of anthracene solid solutions - V.L.Broude & V.S. Medvedev	549	555
uminescence of crystalline naphthalene containing minor impurities - M.T.Shpak & E.F.Sheka	553	559
oncerning the luminescence and photoconductivity of anthracene crystals - A.N.Faidysh	556	562
ffect of β-radiation on the photoluminescence of molecular crystals - Sh.D.Khan-Magometova, N.D.Zhevandrov & V.I.Gribkov	561	567
n the possible role of temperature quenching in scintillation of organic substances - I.M.Rozman	567	573
ffect of temperature on the electronic spectra or complex molecules in solutions - L.G.Pikulik	572	578
nfluence of some fluorescence quenchers on the quantum efficiency of photochemical conversion of 9-methylanthracene and 9-methyl-10-methoxymethylanthracene - T.M.Vember & A.S.Cherkasov	577	583
nfluence of temperature on the luminescence of halide solutions of heavy metals - M.U.Belyi & B.F.Rud'ko	582	588

Dielectric effects and the electronic spectra of polyatomic organic molecules in solutions - N.G.Bakhshiev 587 593
Influence of the solvent on the fluorescence spectra of acetylanthracenes - A.S.Cherkasov 591 597
Present views regarding the influence of the solvent on the spectra of complex organic molecules (Abstract) - I.A.Zhmyreva, V.V.Zelinskii, V.P.Kolobkov, A.S.Kochemirovskii & I.I.Reznikova 596 602
Principal processes of deactivation of excited states of complex organic molecules - V.A.Borgman, I.A.Zhmyreva, V.V.Zelinskii & V.P.Kolobkov 601 607
Influence of structure on the luminescence characteristics of complex organic molecules - V.V.Zelinskii & I.I.Reznikova 607 612
Optical properties of chlorophyll and pheophytin at low temperatures - L.A.Kravtsov 610 615
Luminescence efficiency of chlorophyll in different solvents - N.P.Ivanov 613 618
Aggregation of chlorophyll and chlorophyllide molecules - R.V.Efremova 616 621
Absorption and fluorescence spectra of perylene at low temperatures - R.I.Personov 620 624
Spectroscopy of some pyrene derivatives in frozen solutions - A.Ya.Khesina 623 629

Translated in 1961 by
Columbia Technical Translations
5 Vermont Ave., White Plains, N.Y.

Transactions
# of the
Ninth All-Union Conference on Cathode Electronics
(Moscow, 21-28 October 1959)

Some of the reports presented at the Ninth All-Union Conference on Cathode Electronics are being published in Radiotekhnika i elektronika (Trans. Radio Engineering & Electronics) and Elektronika (Electronics.

INFLUENCE OF THE ELECTRIC FIELD ON THE TEMPERATURE THRESHOLD FOR THE APPEARANCE OF POSITIVE IONS IN SURFACE IONIZATION

- É.Ya.Zandberg

The most general treatment[1-3] of the temperature dependence of the surface ionization current is based on the assumption that the degree of covering of the surface by the adatoms (adsorbed atoms) of the ionized element is low at all temperatures under consideration. As a rule, this is valid for high surface temperatures.

In the range of relatively low surface temperatures decrease of the temperature with a constant flux of atoms leads to a continuous decrease in the degree of covering of the surface. Hence the law characterizing the variation of current in the region of low temperatures differs from that obtaining at high temperatures. It is known that in the case of ionization of alkali metals on tungsten, molbydenum and tantalum, increase in the degree of covering leads to a sharp fall off of the current and at a certain threshold temperature T_0 the surface ionization current virtually ceases.

Let us consider the conditions of ionization in the region of relatively low surface temperatures in the presence of electric fields drawing off the forming ions.

With a constant flux n_0 of atoms to the surface the threshold temperature T_0 is determined by the heat of evaporation l of the adatoms from the surface. The concentration N of adatoms on the surface at temperature T is related with the atomic flux n_0, and under steady state conditions is given by the formula

$$n_0 = N\left(C \exp\frac{-(l_+ - \psi_1)}{kT} + D \exp\frac{-(l_0 + \psi_2)}{kT}\right), \tag{1}$$

where C and D are coefficients weakly dependent on T; l_+ and l_0 are the isothermal heats of evaporation for the ions and atoms, respectively, and ψ_1 and ψ_2 are the corrections to these heats in the presence of an electric field E at the surface.

We assume the field strength not to exceed a few Mv/cm and consider only such metal-atom pairs for which the temperature threshold is clearly pronounced. Such pairs satisfy the condition

$$[V - (\varphi_{k\min} + \xi)] < 0, \tag{2}$$

where V is the ionization potential for the atoms under consideration, $\varphi_{k\min}$ is the minimum local work function for a nonuniform surface, and ξ is the correction to the work function due to the presence of a field at the surface. Condition (2) is fulfilled, for example, in the case of ionization of Cs, Rb and K atoms from a tungsten surface.

When condition (2) is fulfilled and the degree of covering θ of the surface is low, the adatoms are evaporated primarily in the ionic state, and Eq.(1) becomes

$$n_0 \approx NC \exp\frac{-(l_+ - \psi)}{kT}. \tag{3}$$

If the adatoms are distributed over the surface in patches, Eq.(3) can also be applied for high values of θ. In this case Eq.(3) describes the ionization from sections of nearly clean metal.

In strong electric fields drawing off the ions the heat of evaporation decreases owing to partial compensation of the Schottky forces of ionic attraction by the repulsive force of the external field (Fig.1). We determine ψ in (3) on the basis of the concepts of the statistical theory of surface ionization.

For $E = 0$, we have

$$l_+ = A + \int_{x_{cr}}^{\infty} \frac{\varepsilon^2}{4x^2}\,dx, \tag{4}$$

where x_{cr} is the critical distance for charging of an adatom at the surface, A is the work performed in removing an adatom from the metal surface the distance x_{cr}, and ε is the charge of an ion.

In the presence of a field E at the surface the heat of evaporation of an ion equals

$$(l_+)_E = A + \int_{x_{cr}}^{x_0} \left(\frac{\varepsilon^2}{4x^2} - \varepsilon E\right) dx, \tag{5}$$

where x_0 is the distance from the surface at which the mirror image force is compensated by the force of the field (it is assumed that the values of x_{cr} and A do not depend on E).

It follows from (4) and (5) that

$$\psi = l_+ - (l_+)_E = \frac{\varepsilon^2}{4x_0} + \varepsilon E x_0 - \varepsilon E x_{cr}. \tag{6}$$

The condition $\frac{\varepsilon^2}{4x_0^2} = \varepsilon E$ gives $x_0 = \frac{1}{2}\sqrt{\frac{\varepsilon}{E}}$, and Eq.(6) yields

$$\psi = \varepsilon\sqrt{\varepsilon E} - \varepsilon E x_{cr}, \tag{7}$$

which agrees with the usual Schottky expression for $x_{cr} \ll x_0$.

Thus Eq.(3) becomes

$$n_0 \approx NC \exp \frac{-(l_+ - \varepsilon\sqrt{\varepsilon E} + \varepsilon E x_{cr})}{kT}. \tag{8}$$

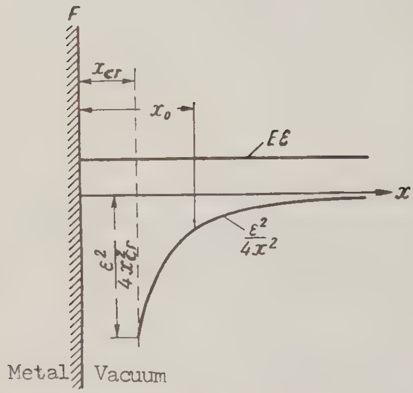
F
x_{cr}
x_0
$E\varepsilon$
x
$\frac{\varepsilon^2}{4x^2}$
$\frac{\varepsilon^2}{4x_{cr}^2}$
Metal
Vacuum

Fig.1. Variation of the forces acting on an ion as a function of the distance from the metal surface.

It follows from (8) that $N = f(n_0, l_+, E, T)$, and for maintaining the surface in a steady state as regards the concentration of adsorbed atoms with increase of n_0 with E=const one must increase the temperature, while with increase of E with n_0=const one must reduce the temperature. It is natural to assume that under conditions of such variation of E and T with n_0=const, under which the degree of covering of the surface remains constant (N=const), the surface ionization current will also remain constant. Consequently, with increase of the field strength with n_0=const the prethreshold sections of the temperature ionization curve must shift into the region of lower surface temperatures, which was observed both in earlier studies[4,5] and in the present investigation (Figs.2 & 3).

The law of displacement of the threshold with increase of the field must change at a field value E_0 at which there is attained the maximum possible decrease of the heat of evaporation, i.e., at $x_0 = x_{cr}$.

From (7), invoking the fact that $x_0 = 1/2\sqrt{\frac{\varepsilon}{E_0}}$, we can find the appropriate value of the correction to the heat of evaporation ψ_{max}.

$$\psi_{max} = {}^1/_2\, \varepsilon\sqrt{\varepsilon E_0}; \tag{9}$$

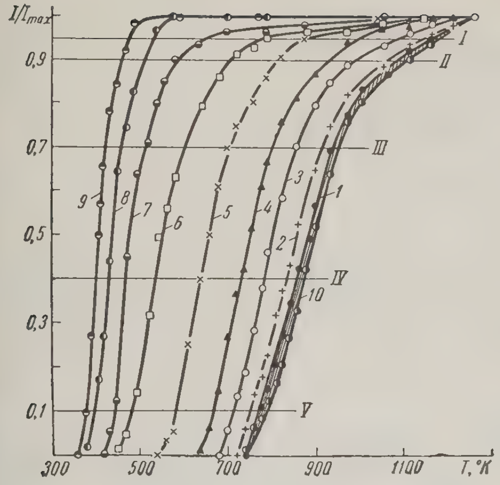

Fig.2. Temperature curves of ionization of CsCl for different fields E: 1) 35.2 kv/cm, 2) 105.6 kv/cm, 3) 352 kv/cm, 4) 704 kv/cm, 5) 1.76 Mv/cm, 6) 2.81 Mv/cm, 7) 4.22 Mv/cm, 8) 5.63 Mv/cm, 9) 0.74 Mv/cm, 10) 35.2 kv/cm (at the end of measurement).

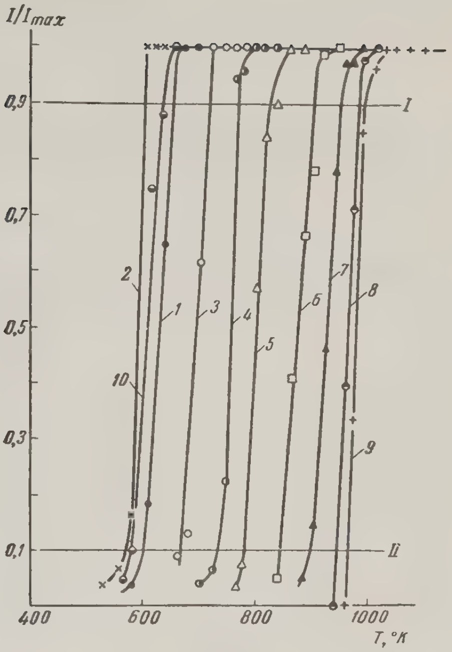

Fig.3. Temperature curves of ionization of K in different fields E: 1) 5.63 Mv/cm, 2) 6.35 Mv/cm, 3) 4.22 Mv/cm, 4) 2.81 Mv/cm, 5) 1.76 Mv/cm, 6) 7.04 kv/cm, 7) 352 kv/cm, 8) 105.6 kv/cm, 9) 35.2 kv/cm, 10) 5.63 Mv/cm (at the end of measurement).

hence we can also determine x_{cr}. From (6) we have

$$\psi_{\max} = \frac{\varepsilon^2}{4x_{cr}}, \qquad (10)$$

and from (9) and (10)

$$x_{cr} = {}^1/_2\sqrt{\frac{\varepsilon}{E_0}}. \qquad (11)$$

Equation (11) can also be deduced directly from the condition of equality of the forces at the critical distance: $\frac{\varepsilon^2}{4x_{cr}^2} = \varepsilon E_0$. If the maximum experimental field $E_{\max} < E_0$, one can evaluate only the upper bound for x_{cr}:

$$x_{cr} < {}^1/_2\sqrt{\frac{\varepsilon}{E_{\max}}}. \qquad (12)$$

However, the temperature shift of the prethreshold sections of the ionization curves with increase of E in the range to $E_{\max} < E_0$ can be utilized for closer evaluation of x_{cr} (for $n_0 = \text{const}$ and small θ). For equal currents there is fulfilled the condition following from Eq.(8):

$$\frac{l_+ - \varepsilon\sqrt{\varepsilon E} + \varepsilon E x_{cr}}{kT} = \text{const}, \qquad (13)$$

and from deviation of T = $f(\sqrt{E})$ from the linear dependence for a number of values of E one can evaluate $\varepsilon E x_{cr}$ and x_{cr} more accurately than by means of Eq.(12).

In the region of fields for which $\varepsilon E x_{cr} \ll \varepsilon\sqrt{\varepsilon E}$, i.e., where the function T = $f(\sqrt{E})$ is linear, Eq.(13) becomes

$$\frac{l_+ - \varepsilon\sqrt{\varepsilon E}}{kT} = \text{const}; \qquad (14)$$

hence one can readily determine the heat of evaporation of ions from the surface if we have the temperature ionization curves for two values of E:

$$l_+ = \varepsilon\sqrt{\varepsilon}\,\frac{T_2\sqrt{E_1} - T_1\sqrt{E_2}}{T_2 - T_1}\ . \qquad (15)$$

This gives a new method for determining the heat of evaporation of ions provided $V < \varphi$. All the quantities entering into Eq.(15) can be measured directly. If the surface is not uniform what is determined by this method, as by other procedures, is a value of l_+ averaged over the entire surface.

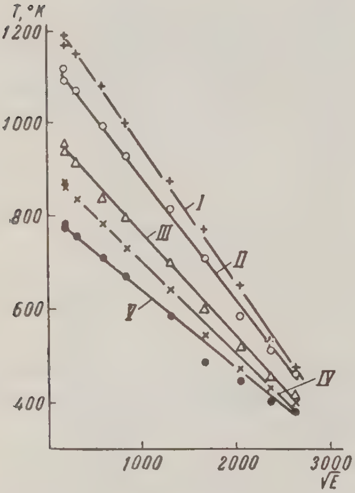

Fig.4. Variation of T with E for different θ in the case of ionization of CsCl: I) I/I$_{max}$ = 0.90, II) 0.9, III) 0.7, IV) 0.4, V) 0.1.

We undertook a series of experiments aimed at investigating the temperature dependence of the surface ionization current in electric fields up to 7 Mv/cm. We used the cylindrical capacitor procedure described in Ref.1; in order to obtain such fields, potentials up to 20 kv were applied between the 10 mm diameter cylinder and the 8 μ diameter tungsten filament. The specially designed suspension system insured a constant position of the filament inside the cylinder at all temperatures and fields. We studied the ionization of CsCl molecules and K atoms. The experimental procedure has been described in detail in Ref.6 so that here we give only the principal results. The experimental $I/I_{max} = f(T)$ curves for different E are reproduced in Figs.2 and 3. The lower the value of the ratio I/I_{max}, the higher the degree of covering of the surface, which is assumed to remain the same with a constant value of I/I_{max}.

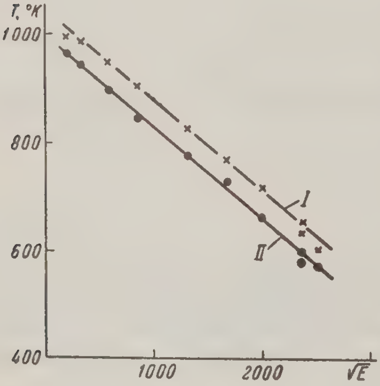

Fig.5. Same as Fig.4 but for K: I) I/I$_{max}$ = 0.9, II) 0.1.

Figs.4 and 5 give the T = $f(\sqrt{E})$ curves plotted for different values of I/I_{max} on the basis of the experimental curves given in Figs.2 and 3. Within the limits of the experimental error in measuring the temperature, which is apparently of the order of 20-25° in the 600 to 700°K interval, the T vs $\sqrt{E}$ curves are straight lines in the entire experimental range of variation of E.

Evaluation of x_{cr} by means of Eq.(12) yields $x_{cr} < 7$ Å. A more precise evaluation of x_{cr} was carried out on the basis of formula (13). In Fig. 6 we give the temperature dependences of $\sqrt{E}$ for K ions calculated by means of Eq.(13) for different x_{cr}. For the calculations we used the experimental values of E, T = 1000°K and l_+ = 2.2 ev - the mean value from our experiments, which is close to the value obtained earlier by other procedures. It will be evident that for x_{cr} = 2 Å the calculated curve can still be approximated by a straight line, but for x_{cr} = 4 Å the deviation from a straight line is appreci-

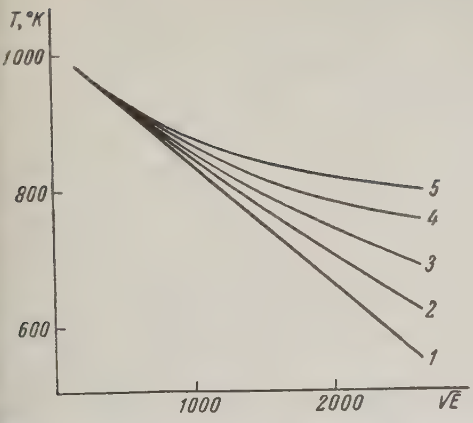

Fig.6. T = $f(\sqrt{E})$ curves calculated by means of Eq.(13): 1) x_{cr} = 0, 2) 2 Å, 3) 4 Å, 4) 6 Å, 5) 8 Å.

ably greater than the scatter of experimental points. Hence it must be assumed that $x_{cr} \lesssim 4$ Å and, consequently, is of the order of magnitude of atomic dimensions.

The heat of evaporation of potassium ions from the surface of polycrystalline tungsten (not free under our conditions from an adsorbed coating of residual gas ions) proved to be 2.2-2.3 ev (formula (15)). This value is close to the values obtained earlier by different methods[7-9] (in the experiments referred to the tungsten surface also was not atomically clean).

The developed procedure for determining the heat of evaporation of ions from metal surfaces allows of following qualitatively the character of the variation of the heat of evaporation of ions as a function of degree of covering θ of the metal surface by the adsorbed ionized atoms. It was found, for example, that in the case of ionization of potassium ions on tungsten the heat of evaporation l_+ remains constant in the range of variation of I/I_{max} from 0.9 to 0.1, i.e., over the range wherein one might expect a substantial variation of the degree of covering of the surface by the K adatoms. This fact indicates that the covering must be patchy. In the case of CsCl the value of l_+ proved to be dependent on I/I_{max} and, consequently, on θ. Possibly this dependence is due to the influence of adsorption of Cl atoms (Cl forms on the surface owing to dissociation of CsCl) on the adsorption of Cs atoms.

A number of further inferences may be drawn on the basis of the experimental data obtained.

Fig.2 shows, for example, that the saturation value of the current in the case of ionization of CsCl molecules in a 7 Mv/cm field is attained at only 500°K. Consequently, the CsCl molecules on the tungsten surface are completely dissociated at this temperature. The mechanism of this process is presumably catalytic in nature.

The observed linear relation between T and $\sqrt{E}$ for surface ionization can serve as experimental substantiation of the fact that the potential barrier at $x >$ Å from a metal surface is determined by polarization forces (mirror image forces). The shape of the potential barrier at the surface in the range of such small distances cannot be determined from experiments on the Schottky thermionic effect owing to the surposition of field emission in strong fields.

I am indebted to N.I.Ionov for interesting discussions.

Leningrad Physical-Technical Institute,
Academy of Sciences of the USSR

References

1. E.Ya.Zandberg, Zhur.tekh.fiz., 28, 2434 (1958). (Trans.Soviet Physics - Tehcnical Physics.)
2. É.Ya.Zandberg, Ibid., 28, 2444 (1958).(Trans.Ibid.)
3. É.Ya.Zandberg, Uspekhi fiz.nauk, 67, 581 (1959). (Trans.Soviet Physics - Uspekhi.)
4. N.I.Ionov, Zhur.tekh.fiz., 26, 2200 (1956). (Trans.Soviet Physics - Tech.Phys.)

5. É.Ya.Zandberg, Ibid., 27, 2583 (1957). (Trans.Ibid.)
6. É.Ya.Zandberg, Ibid., 30, 206 (1960). (Trans.Ibid.)
7. R.C.Evans, Proc.Roy.Soc., 139, 604 (1933).
8. U.Arifov & V.M.Lovtsov, Doklady AN SSSR, 75, 365 (1950).
9. S.V.Starodubtsev, Zhur.tekh.fiz., 19, 215 (1949).

* * * * * * *

ELECTRON EMISSION FROM A COLD BARIUM CATHODE, APPEARING AFTER A CURRENT PULSE IN THE AMBIENT GAS

- N.V.Tatarinova & P.N.Chistyakov

Recently one of us in collaboration with Sinel'nikov & Rybinskaya[1] reported observing post-discharge emission from Ba cathodes in argon-filled tubes and from Mg and Al cathodes in a hydrogen atmosphere. The emission occurs at room temperature, in complete darkness and in an electric field not exceeding 10^4 v/cm. The maximum emission current was recorded for a cathode consisting of a Ba coating on an Ni substrate.

The principal aim of the present work was investigation of the time variation of the emission from a barium cathode down to the level of currents commensurate with the background currents produced by cosmic radiation. In addition, we felt it would be of interest to determine the influence of the following factors: 1) the degree of cleanness of the cathode and purity of ambient gas, 2) the surface properties of the cathode and, 3) the amount of electricity involved in the exciting discharge.

1. Experimental Procedure

Current measurement

The currents were measured by the pulse breakdown technique which allows of detecting individual electrons.[3] In this procedure one employs square voltage pulses, the height of which appreciably exceeds the static discharge ignition voltage V_s. If the pulse voltage is equal to 2-3 times V_s, then under the conditions (pd) corresponding to the right-hand branch of Paschen's curve, the discharge formation time becomes much shorter than 1 μsec (Ref.4) and the probability for initiation of a pulse discharge by each initial electron emitted from the cathode equals 1. Under these conditions, the discharge formation lag time of 10 μsec or more is entirely the statistical time.

The mean statistical discharge time $\bar{t}_l$ is related to the electron current by the following expressions:[2,3]

$$I = 1/\bar{t}_l \tag{1}$$

or

$$I = 1/t \ln(N/n), \tag{2}$$

where N is the total number of tests, and n is the number of tests in which the lag exceeds t. Relations (1) and (2) give a simple method for determining very weak currents in a gas. In utilizing this method we assumed that the phenomenon of emission is reproduced in repeated pulses. This assumption was substantiated by determination of the emission current I as a function of the number of pulses N.

Table 1

Emission current, 10^{-15} amp

Number of pulses	No. of tube		
	4	5	6
25	2,00	2,9	2,2
50	1,93	2,8	2,6
100	1,83	2,4	2,4

Table 2

Emission current, 10^{-15} amp

No. of tube	Before tests	After 6 months
4	3,6	1,8
5	2	2,4
6	3,8	2,4

The results, calculated according to Eq.(1), are given in Table 1 (the emission current was determined 1 minute after cessation of the exciting pulse).

Fig.1. Block diagram of the experimental set-up for measuring emission: 1) 3G-10 oscillator, 2) OK-17M oscillograph, 3) discharge tube, 4) square pulse generator.

The variation of the emission current as a function of N for any given experimental tube proved to be small; such variation as exists is apparently connected with statistical determination of $\bar{t}_l$ and, accordingly, I with increase of N and not with any substantial variation of the emission effect with the number of tests.

This is indicated by the results - listed in Table 2 - of measurements of the emission current prior to the beginning of the regular tests of the tubes and six months later, after completion of all the tests. Despite the fact that in the interim thousands of current pulses passed through each tube, the emission current did not change by a factor exceeding 2 for any of the tubes. The data of Table 1 were obtained with the same tubes as the data of Table 2 at the end of the six month test period.

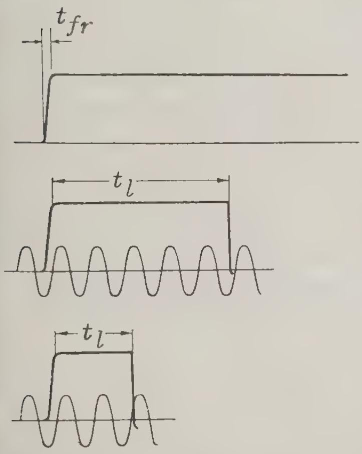

Fig.2. Determination of the statistical discharge lags.

A block diagram of the experimental set-up is shown in Fig.1. Square pulses of amplitude $V = 2.5\ V_s$ and duration from 10 μsec to 1 sec were produced by a single pulse generator. The measurements were carried out by means of a specially adapted OK-17M oscillograph.

Fig.2 shows oscillograms of an undistorted voltage pulse and pulses in the presence of breakdown, from which t_l was determined.

Experimental tubes

The design of the experimental tubes is shown in Fig.3. The circular electrodes 20 mm in diameter and 0.4 mm thick were prepared of nickel containing not over 0.01% impurities. To one of the electrodes there was welded a piece of Fe-Ba wire which contained pure Ba. In the process of evacuation the electrodes were heated by high frequency current at a pressure not lower than $5\cdot10^{-6}$ mm Hg; in the course of outgassing the temperature was gradually increased: for the plain electrode from 700 to 850°, for the electrode with Fe-Ba from 600 to 700°. The total electrode heating time was 6-10 hours. At the end of the process, in a vacuum of $\sim10^{-6}$ mm Hg, barium was slowly sputtered on the electrode heated to 750-800°; at the same time there was deposited on the glass of the tube a broad annular layer of barium (zone C in Fig.3). Evaporation of the barium was stopped when this layer became opaque. The tubes were then filled with argon to a pressure of 11 mm Hg and sealed off.

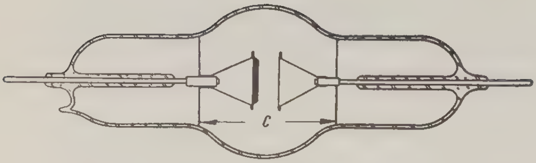

Fig.3. Design of experimental tubes.

2. Results and Discussion
Variation of the emission with time

The variation of the emission current with time for 10 tubes, similar in design and identical in preparation, is shown by the hatched band in Fig.4. Each plotted point was determined from 25 measurements of the statistical lag time t_l.

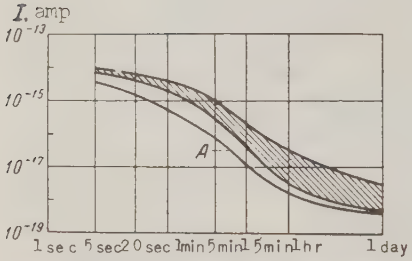

Fig.4. Variation of the emission with time for 10 experimental tubes (hatched region). Curve A was obtained for a tube prepared under "inferior" technological conditions.

The scatter of current values for different experimental tubes did not exceed one order of magnitude. It will be evident from the figure that the variation of I with time is characterized by a descending curve. Five seconds after cessation of the discharge, the emission is of the order of 10^{-14} amp, and falls off to 10^{-18} amp at the end of 24 hours. The character of the I vs t curves indicates that the factor responsible for the emission weakens with time; in particular, if this factor, as in the Malter effect[5], is the positive charge building up on the dielectric film, this charge is presumably neutralized with time by the electrons emerging from the metal.

The rate of decrease of the emission during the first minute is low, but then increases, and 5 min after the end of the exciting current pulse the time dependence becomes approximately exponential. Possibly the complex time dependence of the emission current is due to the fact that a number of different processes, rather than a single one, occur in the barium cathode.

Factors determining the emission

In preparing one of the tubes the cathode was not heated by high frequency current and the barium was evaporated in a vacuum of 10^{-2} mm Hg. The surface obtained in this manner emitted a weaker current (curve A in Fig.4). Also the shape of the I vs t curve for this tube was somewhat different. Thus it is apparent that the degree of cleanness of the cathode and purity of the gas affect the emission.

In another experiment we investigated the influence on the emission of gradual removal of the barium layer from the cathode by means of an anomalous glow discharge. This experiment was carried out using tubes prepared in the usual manner. We judged of the state of the cathode surface from the value of V_{cp} and from the shape of the current-voltage characteristic of the glow discharge. The emission current was measured 20 sec and 1 min after the end of the current pulse.

The variation of the emission current with V_{cp} is shown in Fig.5; the initial points A_1 and A_2 correspond to a relatively high value of V_{cp} (67.5 V) and weak emission. Treatment (cleaning) of the cathode by a dc glow discharge leads to reduction of V_{cp} to 61 V and increase of the emission by a factor of up to 1.5. This effect was observed with all the tubes used in the experiments. The glow discharge treatment apparently distributes the barium more uniformly over the

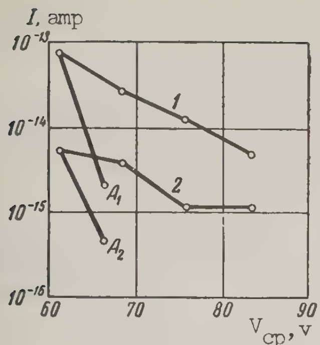

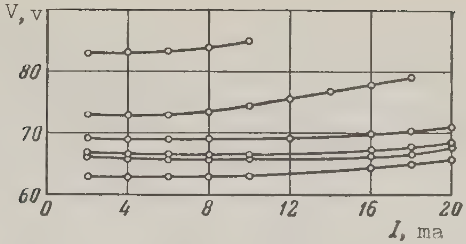

Fig.6. Current-voltage characteristics obtained in investigating $I = f(V_{cp})$.

←Fig.5. Variation of the emission with V_{cp}: 1) 20 sec and 2) 1 min after the end of the exciting pulse.

surface; it may also produce some sort of structural or chemical changes enhancing the emission.

The lowest value of V_{cp} obtained by the glow discharge treatment was 61 ± 2 v; possibly this value should be identified with the precise value of V_{cp} for the Ba-A pair. Subsequently, the cathode was methodically disintegrated by continuing the anomalous dc glow discharge, which led to increase of V_{cp} and a sharp drop in emission. It is interesting to note that the variation of ln I with V_{cp} is linear.

One can analyze the V_{cp} dependence of I and elucidate the nature of the post-discharge emission if the relation between V_{cp} and the work function φ_0 of the cathode surface is known. Güntherschulze[6] proposed the following empirical formula

$$V_{cp} = C\varphi_0, \qquad (3)$$

where C is a constant for the given gas. This formula is still in need of rigorous experimental verification on the basis of up-to-date data on V_{cp} and φ_0.

If, however, we assume that formula (3) is valid, the observed exponential variation of the emission with V_{cp}, and accordingly with φ_0, indicates that the nature of the emission is close to either thermionic or autoelectric (field). At present it appears more probable that the post-discharge emission in the presence of thin insulating films is a form or variant of the Malter effect, i.e., is essentially field emission.[2,3,7,8] Admittedly, however, the question is still open where barium cathodes are concerned; hence it would be highly desirable to obtain further experimental data on the relation between the emission current and the diverse properties of the cathode surface.

Fig.6 shows the current-voltage characteristics for glow discharges in our experimental tubes. It will be evident from the curves that the change in properties occurs simultaneously over the entire surface of the cathode since there is no significant change in the shape of the characteristics with increase of V_{cp}.

We carried out another experiment with a view to determining the influence on the emission of the magnitude of the charge passing through the gas during the exciting pulse. With variation of the charge in the range from 10^{-4} to 10^{-8} coul the emission remained virtually the same. This result can be explained from the standpoint of the Malter effect: the dielectric film retains a charge Q smaller than 10^{-8} coul and dependence of the emission on the charge passing through the gas can be evinced only for values of $Q < 10^{-8}$ coul. We plan to continue and extend these experiments in the future.

Moscow Engineering-Physical Institute

References

1. P.N.Chistyakov, M.V.Sinel'nikov & Zh.G.Rybinskaya, Radiotekhnika i elektronika, 4, 870 (1959). (Trans.Radio Engineering & Electronics).
2. E.Llewellyn-Jones & E.Perrelle, Proc.Roy.Soc., A216, 267 (1953).
3. H.Paetow, Z.Phys., 111, 770 (1939).
4. A. von Engel & M.Steenbeck, Elektrische Gasenladungen, ihre Physik und Tecknik, Vol.2, Berlin 1949. (Cited in Russian trans.)
5. L.Malter, Phys.Rev., 49, 478 (1936); Ibid., 50, 48.
6. A.Günthershulze, Z.Phys., 24, 52 (1924).
7. F.Llewellyn-Jones, Proc.Phys.Soc.B62, 366 (1949).
8. G.Morgan & D.Harcombe, Proc.Phys.Soc., 66, 665 (1953).

* * * * * * *

ELECTRON-OPTICAL CONTRAST IN OBSERVATION OF PATCH FIELDS ON EMITTERS

- G.V.Spivak, I.A.Pryamkova & N.N.Sedov

Introduction

Study of the factors determining the contrast of the image in electron mirror type devices with a reflecting electrode and in emission electron-optical systems is of interest because the contrast is connected with local distribution of the work function over the surface of the emitter. Important from the standpoint of cathode electronics are both the magnitude of the total current and the structure of the electron-optical image of the emitter. The distribution of the work function is intimately related with the distribution of contrast in the image of "patch fields" on complex emitters. In a number of cases there are superimposed on the picture effects produced by other surface microfields (pseudocontrast). Below we shall consider the question of contrast of the images obtained with both emission and quasiemission (mirror type) electron-optical systems.

Influence of the normal and tangential components of the field on the electron kinetics

The magnitude of the total current from a patchy surface is determined by the distribution of the normal component of the local resultant field $E_{z\ res}$, comprised of a) E_{zo} - the external uniform field, b) $E_{z\ ro}$ - the roughness field, i.e., the field associated with geometrical roughness of the surface, c) E_{zR} - the space charge field, d) E_{zs} - the field arising due to charging of the surface by the electron beam or owing to inadequate conductivity of the surface, and e) E_{zc} - the contact field of the "patch". If the collector surrounds the emitter, the local tangential field $E_{t\ res}$ determines only the point of incidence of the group of electrons emitted from the given section of the surface but does not affect the magnitude of the current. The combination of the accelerating field with the "patch" field E_{zc} gives rise to the anomalous Schottky effect.*

---

*Here we are disregarding other microfields, for example, the space charge field.

In the region of weak external fields the influence of the patch field, which always acts to return the electrons to the emitter, becomes noticeable. In order to overcome this effect and obtain the saturation current one must have a sufficiently strong external accelerating field. The patch fields therefore give rise to distortion (elongation) of the normal retarding potential curve and simulate the presence of "electrons with inadequate energies". Direct observation of the configuration of patch fields was described earlier in Ref.1.

The space charge field may give rise to a potential minimum. Then the magnitude of the total current is determined by the path length from the surface of the emitter to the coordinate of the potential minimum.

Whereas the normal component determines the magnitude of the current, the tangential component $E_{t\ res}$ characterizes the contrast and the resolution in the image. Usually in electron-optical systems E_{zo} is large compared with the other normal components and the normal velocity v_z at the screen may be regarded as constant. The position of the screen for receiving the given electrons is determined by the local value of $E_{t\ res}$. Consequently, the contrast and resolution are determined by the sum of the tangential components:

$$E_{t\ res} = E_{t\ ro} + E_{tR} + E_{ts} + E_{tc}.$$

The possibility of suppressing surface microfields by a strong external field was examined in the work of Ref.2. For a smooth surface and in the absence of space charge "microlenses" the normal component E_{zc} is greatly weakened or suppressed by the field E_{zo}, inasmuch as usually $E_{zo} \gg E_{zc}$. In the case of a smooth surface the accelerating field, lacking a tangential component, naturally, cannot influence the tangential component of the patch field.* In practice therefore the patch field can be fully suppressed only by a combination of strong normal components of the electric and magnetic fields. In this case E_{tc} is suppressed** by the magnetic field H_z (see Eqs.(7) and (8) in Ref.2).

Mechanism of formation of contrast

An electron mirror device with a reflecting electrode may be regarded as a quasiemission system. In order to understand the mechanism of formation of contrast in the picture observed in an emission system it is expedient to consider the patch field not in isolation but in conjunction with a uniform external accelerating electric field.

A patch field is formed by a contact difference of potentials: areas with a low work function become charged positively relative to areas with a high value of φ. This causes distortion of the equipotential planes. Contrast is produced only by the tangential component of the patch field.***

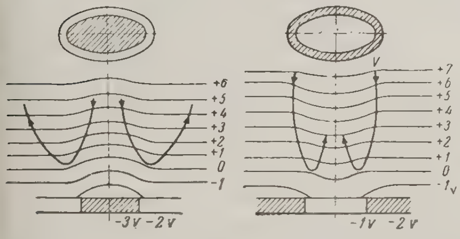

a b

Fig.1. Mechanism of formation of contrast in imaging a patch field. The periphery of the patch is charged positively (a) or negatively (b) relative to its central portion. The resultant contrast is shown in the upper part of the figure.

---

*Popov & Druzhinin[3] in asserting that the patch field is suppressed by the accelerating field, failed to take into account the presence of the field E_{tc}, forming the contrast.

**In the notation of Ref.2, $E_x = E_{tc}$.

***Inasmuch as $E_{zo} \gg E_{zc}$.

Depending on the polarity of E_{tc}, the equipotential surfaces over the given point of the emitter become convex (Fig.1,a) or concave (Fig.1,b).

The field E_{tc} gives rise in the planes parallel to the emitter surface to redistribution in the density of the incident homogeneous electron beam; accordingly the electrons are deflected either away from the normal (Fig.1,a) or towards it (Fig.1,b). The contrast in a patch is determined by the polarity and magnitude of the contact difference of potentials between the two neighboring regions. Owing to the fact that the electrons have a certain initial velocity (0.1--0.2 ev), the scattering of the beam occurs not in the zero equipotential plane but in a certain finite layer of thickness $s = 0.1/E_{zo}$. Thus the electron mirror yields information on the configuration of the field not at the very surface of the electrode but in a certain more or less contorted surface standing some distance away from the electrode. It is important to note that in the case of a quasiemission system the contrast must be higher than in the case of a conventional emission system inasmuch as in the quasiemission case the field acts twice. The contrast, of course, is not increased by a factor of two but by a somewhat smaller factor inasmuch as in approaching the mirror electrode an electron first undergoes the influence of weaker and then stronger deflecting fields. Hence where the formation of contrast is concerned the paths "to" and "from" the mirror are not fully equivalent.

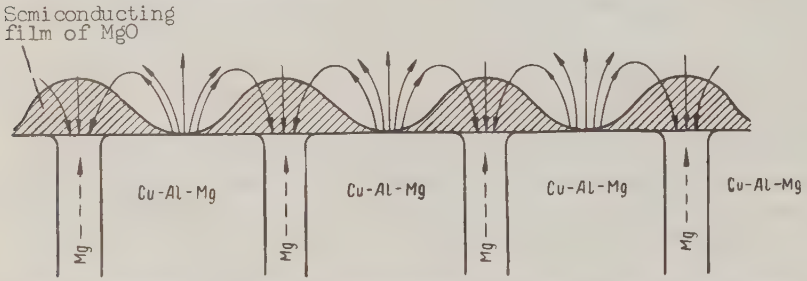

Fig.2. Model of the structure of the surface layer and the contact patch microfield on dynodes of Cu-Al-Mg alloy.

An important attribute of electron mirrors is that the microfield can be investigated at any temperature. The emission characteristics of a thermionic cathode can be utilized for monitoring its quality. We note that in the range of high temperatures the emission image of a thermionic cathode is essentially a surposition of the images produced by the roughness, local space charge and patch field microlenses.[4,5] There are obvious difficulties in separating or isolating these three images. In order to discriminate the patch image, it is expedient to use not an emission system but an electron mirror, owing to its higher contrast and the absence of the space charge effect (there is no need to take off the emission current). On the basis of the data of Fig.1 and the results of direct observations (see, for example, Fig.3,a in Ref.1) one can construct a model representing the structure of the surface layer and the patch fields for dynodes of Cu-Al-Mg alloy (Fig.2).

Influence of patch fields on the resolution of an immersion objective

Derivation of the formula for the resolution in an emission system is usually based on the concept[6] of independent, noninteracting "emission centers" on a smooth surface. In other words, the aperture of the broad incident beam is assumed to be defined by the angular scatter of the vectors of the initial velocity with average energy ε. This concept, however, does not correspond to the actual conditions obtaining for complex cathodes. In reality the emission centers must be surrounded by regions with an enhanced work function: there appears a patch field, the equipotential surfaces are distorted, and the tangential component of

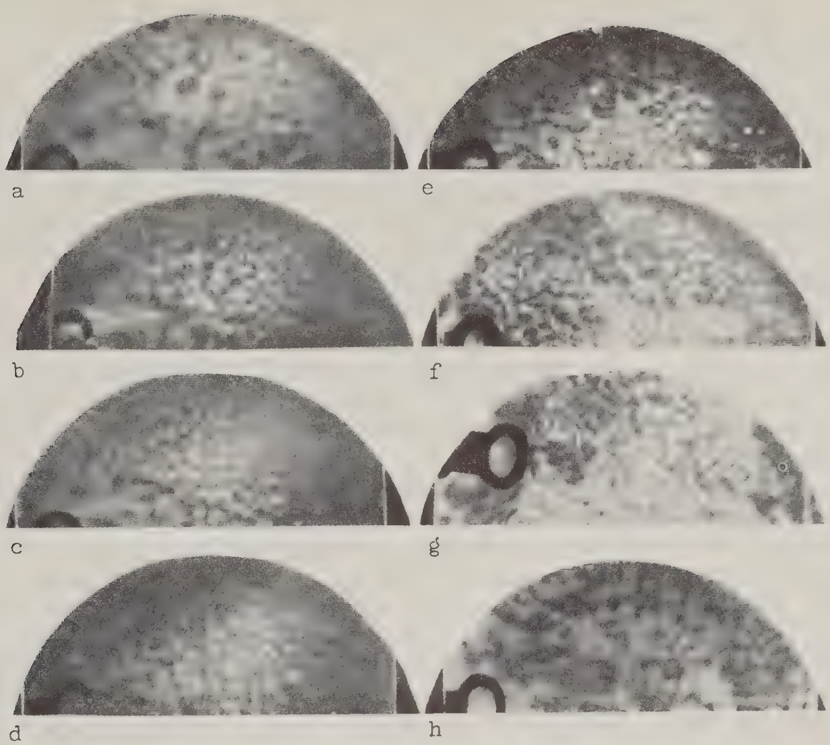

Fig.3. Mirror (a-e) and thermal emission (f-h) images of an oxide coated cathode (100 X); heater voltage V_h: a) 0, b) 1.5 v, c) 2 v, d) 2.5 v, e) 3 v, f) 3 v, g) 3.5 v, h) 5 v.

the patch field also modulates the width of the beam. If in the central portion of the patch the work function is higher than at the periphery (for example the grain of an L-cathode* surrounded by pores containing Ba), the patch field will tend to broaden the beam. Hence instead of $\delta \approx \varepsilon / E_{z0}$, the formula for the resolution should be

$$\delta \approx \frac{\varepsilon \pm \Delta_{xy}}{E_{zo}}.$$

The correction term Δ_{xy} depends on the contact difference of potentials of the central area relative to its surroundings. It may vary in magnitude from a fraction to several electronvolts. The resolution is therefore a local quantity and depends on the structure of the patch field. For thermionic cathodes, for which $\varepsilon \sim 0.1$-0.2 ev, the correction Δ_{xy} is very appreciable.

Local Microfields on Emitting Surfaces

Patch fields on dynodes and L-cathodes

We observed patch fields on polished, well-activated dynodes of Cu-Al-Mg alloy and on slightly rough L-cathodes.[1] The contrast corresponds to the distribution of the work function, as pictured in Fig.1,a. Decrease of the work function towards the edges of the patch, which appears light, is due to diffusion of alloy components with a reduced work function to the surface. It may be assumed that in the case of smooth surfaces the contrast is due solely to patch fields and correctly reproduces the work function distribution.

---

*L-cathode = porous metal film or "filled" type cathode.

Microfields on rough oxide-coated cathodes and comparison of mirror, thermionic and photoemission images

The formation of contrast in the image of a "emission center" is due to the action of a conjunction of microlenses: the microlenses of the patch field, the microgeometry, and the space charge. Comparison of the secondary and thermal emission images led us to the conclusion that in the case of secondary emission images the contrast is formed primarily owing to roughnesses of the surface, while in the case of thermal emission images it is formed owing to inhomogeneity of the work function, i.e., due to patch fields. However, the general distribution of "emission centers" repeats the surface "topography". It was shown also that the secondary emission image may lack in sharpness owing to charging of the surface of an inadequately activated cathode.[4,5]

With a view to elucidating the mechanism of formation of contrast in the image of oxide-coated cathodes, we compared the mirror and emission images for the same cathode. The roughnesses of the investigated cathode had dimensions of the order of 10-20 μ. The cathode was investigated under conditions under which the reflecting electrode had the potential of the Wehnelt cylinder. Owing to strong charging of the surface, we could not at first obtain a mirror image of the nonactivated cold cathode. However, after slight heating (to 200°) we observed a noticeable improvement of the mirror image and the appearance of new details. The temperature of the cathode was measured by a chromel-alumel thermocouple.

We obtained a number of mirror images of the oxide-coated cathode at different temperatures, set by the heater voltage V_h (Fig.3). In all cases the photographic plate was located directly under the beam. The soft, somewhat diffuse images shown in Figs.3,a & b are due to charging of the poorly conducting surface by the electron beam. With increase of the heater voltage and hence cathode temperature and conductivity, the "cloudiness" noticeably decreases (Fig.3,c-e). In all the mirror-image photographs there are discernible the same "centers" changing slightly in configuration with increasing temperature of the cathode. It is interesting to compare the photographs recorded at the same temperature but with different modes of operation, i.e., the mirror (e) and thermionic images (f). At a temperature of about 500° the intensity of the latter was weak and the "mirror" image predominated. Hence by heating the cathode we succeeded, first, in photographing the mirror image (exposure ~20 sec), and then, having cut off the electron beam, the thermionic image (exposure ~120 sec). It will be evident that the two images are very similar. Consequently, the contrast under these different emission conditions in the case of rough oxide-coated cathodes is formed by identical or at least similar processes.

Thermal emission images obtained at higher temperatures are reproduced in Fig.3,g & h (V_h = 3.5 v and 5 v). Here the character of the thermionic images already differs from that of the mirror image. In interpreting the nature of the contrast of the images we must take into account superposition of the microfields of all the above mentioned types.

We carried out a similar comparison by means of a special combination electron microscope which allowed of observing the same surface under conditions of photo and thermionic emission. The construction of this instrument differs somewhat from similar tubes described in the literature[7]. The microscope, which is diagramed in Fig.4, is a metal-glass assembly with two stages of magnification.

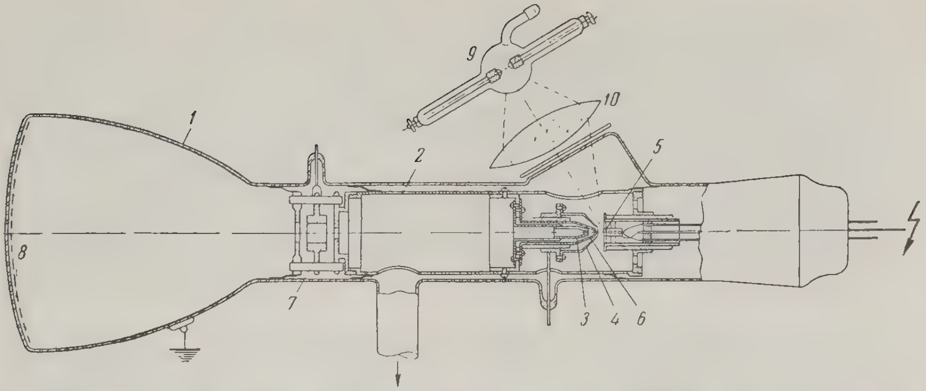

Fig.4. Microscope tube for combined investigation of photo and thermionic emission.

By virtue of the use of a glass envelope 1, a vacuum of 10^{-6} mm Hg can be maintained in the instrument. The glass envelope houses the premounted and preadjusted electron-optical system. The main structural component is the thin wall cylinder 2 of stainless steel to which all the electrodes are attached. The anode 3 and the focusing electrode 4 of the immersion objective are conical, a shape convenient for "illumination" of the cathode. The cathode 5 is mounted in a ceramic insulator and can be heated by a tungsten spiral.

The microscope has provision for installation of a defining aperture 6. All the electrodes can be adjusted axially by means of micrometric screws and a special microscope.

A separately mounted single lens 7 is screwed on the far end of the cylinder 2. The total magnification can be varied from 50 X to 500 X. The photoemission is excited by the ultraviolet source 9 consisting of an SVDSh-250 mercury discharge tube. The light is concentrated by the large quartz lens 10. The glass envelope has a uviol window under the lens to admit the ultraviolet. A UFS-1 light filter is employed to cut off the visible part of the spectrum.

This design allowed of combining the advantages of a glass system - simplicity and a high vacuum - with the advantages of a metallic system - ease of adjustment and two stages of magnification.*

We observed the surface of an impregnated oxide-coated cathode under conditions of photo and/or thermionic emission. The photoemission image of the cathode obtained at room temperature is shown in Fig.5,a. Then the temperature of the cathode was gradually increased. In the range of slight elevated temperatures, but before the beginning of any appreciable thermionic emission, the impregnated cathode, like ordinary oxide-coated cathodes, exhibited an appreciable increase of photoemission.[8]

With increase of the cathode temperature thermionic emission was added to the photoemission. Such a combined photo-thermionic image is shown in Fig.5,b. Then, after cutting off the illumination, we obtained the purely thermionic image of the cathode (Fig.5,e). Comparing the same areas of the cathode (identified by arrows) we note that the images are almost identical.

With further increase of the heater temperature, space charge begins to form at the cathode surface and the space charge microlenses cause defocusing of the

---

*We take this opportunity to thank N.V. Sigareva, who participated in the design of the instrument.

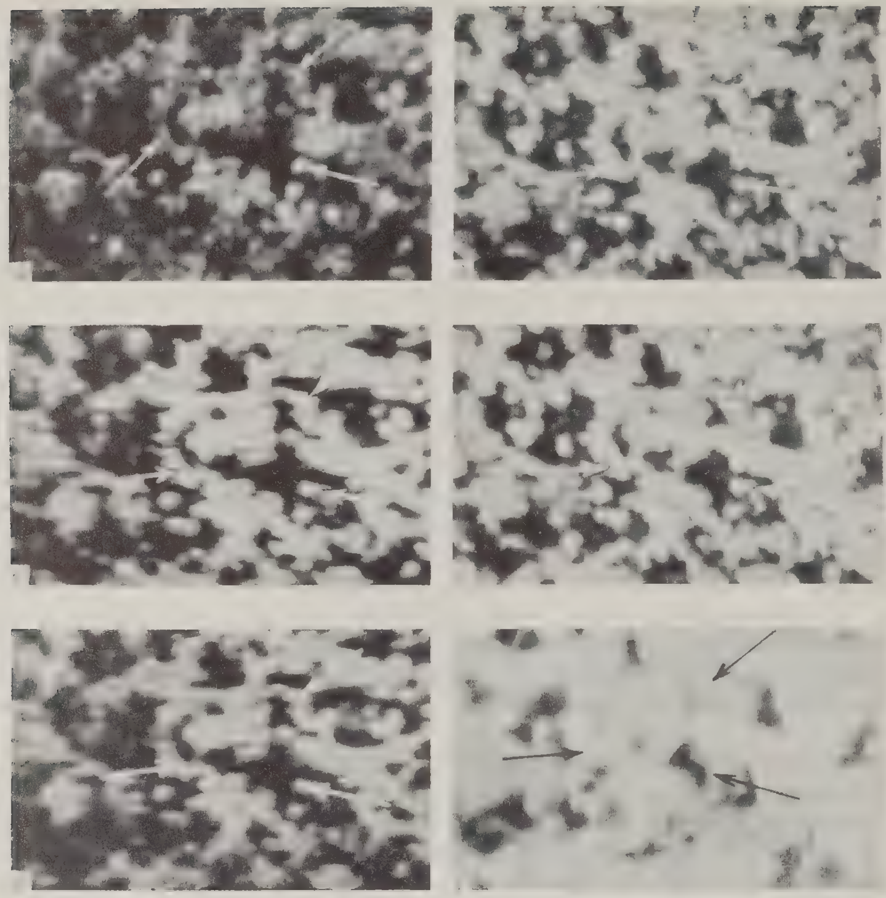

Fig.5. Emission images of an impregnated oxide-coated cathode (75 X): a) photoemission, t = 20°, b) same, t = 300°, c) same, t = 550°, d) photoemission and thermionic emission, t = 750°, e) thermionic emission without illumination, t = = 750°, f) thermionic emission without illumination, t = 820°.

image (Fig.5,f).

The similarity of the photo and thermionic emission images of the cathode indicates that in both cases the same factors are involved in the formation of the image. Such factors may be the geometric topography of the cathode, patch fields and electric fields of other origin. Since the impregnated cathode had a fairly smooth surface, it may be assumed that the decisive role in the formation of the image in both cases was played by the last two factors. At a sufficiently high heater voltage space charge microlenses may also contribute to the effect.[4,9]

Typical case of formation and reversal of contrast as a result of surposition of microfields

The cathode surface may be either smooth or rough, but in both cases, patch fields and space charges may be present. In both cases the configuration of the microfields may be affected by a) a strong external locally acting field (normal and anomalous Schottky effects), and b) poisoning and ionic bombardment of the cathode.

The simplest case is that obtaining in the presence of a good vacuum, a smooth surface, and patch fields. Such conditions are realized in the case of electron image observation of the patch fields on Cu-Al-Mg dynodes.[1] The case of a rough surface with patch fields is illustrated by the mirror images reproduced in Fig.3,b,d, & e; and that of a rough surface with patch fields and space charge microlenses is illustrated by the emission images shown in Fig.3,g & h.

The contrast is also affected by conditions (a) and (b) mentioned above.

With a view to clarifying the reasons for the similarity of the mirror and thermionic images pictured in Figs.3,e and f, let us consider in more detail the influence on the contrast of patch fields and microgeometry. In the case of an appreciable roughness, the contrast will be influenced by $E_{z\ ro}$ owing to a possible Schottky effect reducing the work function and modifying the patch field and by the field $E_{t\ ro}$ distorting the equipotential surfaces. Specifically, let us consider two extreme cases, A and B.

Case A. The roughness field does not affect the value of the work function but only modifies the local curvature of the equipotential surfaces. In this case four principal combinations of formation of contrast by the integral field are possible. The axis of a hillock (point) or depression may coincide with the geometric axis of a patch (a or b in Fig.1); then the contrasts will reinforce or counteract each other depending on how the roughness deforms the curvature of the equipotential surface caused by the patch, i.e., on whether the two effects are "in phase" or "in antiphase".

Case B. The roughness field is so strong that it itself forms areas with a reduced work function on the emitter. In this case the contrast produced by the "initial" patch field will be insignificant compared with the contrast produced by the new emission centers. If the strong field is produced by a hillock, the formation of contrast will in turn be determined by the effect of two opposed factors: in the vicinity of the hillock the equipotential surfaces will be convex which reduces the contrast, while the increase of the work function at this point leads to increase of the contrast. In cases when the strong field is produced by a double layer, there is no distortion of the equipotential surfaces, and the contrast is determined only by the effect of reduction of the work function by the external field and the possible onset of field emission.

In view of the above one can readily understand why the contrast in the image of a rough oxide-coated cathode is "modulated" by the microgeometry. In areas where the local roughness field is weak, the contrast produced primarily by a patch field is enhanced wherever a hillock is surrounded by a region of reduced work function or a depression is edged by a region of enhanced work function. In other words, the contrast is increased wherever a patch field is "in phase" with a roughness field.

It will be evident from a comparison of Figs.3,g & h that with increase of the emitter temperature the size of the light areas increases, which is apparently connected with the effect of space charge microlenses.

With increase of the distance of the image plane from the cathode there occurs reversal of the contrast (image) formed by the space charge[4,9] and roughness[10] microlenses. On the basis of the proposed patch field model, one may also expect to observe reversal inasmuch as in the case pictured in Fig.1,a the topography of the equipotential surfaces is similar to that of a geometric hillock and in the case of Fig.1,b to the geometry of a depression.

Obviously, lack of sharpness of the image cannot always be attributed to a local space charge inasmuch as the different microlenses may have different focal lengths and the image is the result of superposition of the images produced by all three types of microlenses.

Physics Faculty,
Moscow State University

References

1. G.V.Spivak, I.A.Pryamkova & V.N.Lepeshinskaya, Doklady AN SSSR, 130, 751 (1960). (Trans.Soviet Physics - Doklady.)

2. G.V.Spivak & V.I.Lyubchenko, Izv.AN SSSR, Ser.fiz., 23, 697 (1959). (Trans. Bulletin, 23, 691.)

3. B.N.Popov & A.V.Druzhinin, Radiotekhnika i elektronika, 3, 1084 (1958). (Trans.Radio Engineering & Electronics.)

4. G.V.Spivak, E.M.Dubinina, I.S.Sbitnikova, I.A.Pryamkova & D.P.Vinogradov, Ibid., 3, 1077 (1958). (Trans.Ibid.)

5. I.S.Sbitnikova, E.M.Dubinina, G.V.Spivak & D.V.Fetisov, PTE, No.5, 78, (1958). (Trans.Instruments & Exp.Techniques.)

6. Elektronnaya mikroskopiya (Electron Microscopy), Edited by A.A.Lebedev, Chapter VI, M., 1954.

7. L.N.Bykhovskaya & Yu.M.Kushnir, Zhur.tekh.fiz., 25, 2477 (1955); Ibid., 152, 1 (1958). (Trans.Soviet Physics - Technical Physics.)

8. S.V.Ptitsyn & N.N.Panteleev, Transactions of the (First) Conference on Cathode Electronics, P.25, Kiev, 1952.

9. D.P.Vinogradov, Izv.AN SSSR, Ser.fiz., 23, 722 (1959). (Trans.Bulletin, 23, 718.)

10. D.P.Vinogradov, Ibid., 20, 1120 (1956). (Trans.Bulletin, 20, 1011.)

KINETICS OF FORMATION AND SOME ATTRIBUTES OF OXYGEN FILMS ADSORBED ON TUNGSTEN

- N.D.Morgulis & A.G.Naumovets

Introduction

In connection with diverse important problems encountered in modern cathode and semiconductor electronics and the physics of high and ultrahigh vacuum, increasing attention has been paid in recent years to the intriguing complex of questions involved in the behavior of different gases at low pressures adsorbed on solid surfaces. Investigations in this field usually have as their purpose elucidation of one or more of the following three independent problems: 1) the kinetics of formation and removal of adsorbed gas films, 2) the nature of the chemical reactions occurring on the solid surface and 3) the alterations occurring in the electronic properties of the said surfaces under the influence of the adsorbed films.

The present work was devoted primarily to the first of these problems in the specific case of oxygen adsorbed on tungsten (the third problem is considered in Ref.1). The choice of this particular system was dictated by its importance from the standpoint of understanding the character of the chemical reaction of electronegative oxygen on the surface of tungsten in the range of low pressures; it may also be noted that tungsten is both convenient for such investigations and is an important material in electronic engineering. Frankly, we are not satisfied with the results of the investigations listed under Ref.2.

Accordingly, we planned an extensive research program. Our work was also stimulated by the at first glance strange data on the extremely low yield of the surface chemical reaction of the poisoning effect of oxygen on the thermionic emission of efficient oxide-coated and porous metal cathodes^3.

It is known that the rate of formation of an adsorbed film by condensation from the gaseous phase can be characterized by the formula

$$N = \frac{dn}{dt} = \nu\sigma = \frac{p}{\sqrt{2\pi MkT_0}}\gamma f(\theta) e^{-E/kT}, \qquad (1)$$

where p is the pressure and T_0 is the temperature of the gas, γ is the condensation coefficient, $f(\theta)$ is a function characterizing the variation of the condensation probability with the degree of covering θ of the substrate by the film (for $\theta = 0$, $f(\theta) = 1$), E is the activation energy for adsorption, and n is the surface concentration of the adsorbed atoms; the quantity

$$\sigma = \gamma f(\theta) e^{-E/kT} \qquad (2)$$

is called the condensation probability. By investigating the parameters comprised in Eq.(2) one can clarify some of the distinctive features of the kinetics and nature of adsorption of atoms on a solid surface.

Experimental Procedure

In the present work we employed the methods of contact potential and partial-ionization flashes.

The design of the experimental tubes used in our work is shown in Fig.1. The principal components were a long rolled tungsten ribbon 1, an electron gun 2 by means of which one could measure the contact potential W of the tungsten ribbon by the method of shift of the current-voltage characteristics of the electron current on its surface, an Alpert pressure gage 3 for measuring the pressure of the gas in the tube in the vacuum and high-vacuum range both in the process of adsorption and at the instant of target flash (the gage was also utilized for the final ionization pumping of the tube), and a nickel tube 4 filled with barium peroxide, which was heated to introduce a controlled amount of pure oxygen at the requisite pressure into the main tube. In addition, later versions of this tube contained a small ionic-sorbtion titanium pump and an omegatron system for monitoring the degree of purity of the oxygen in the tube in the course of the experiment.

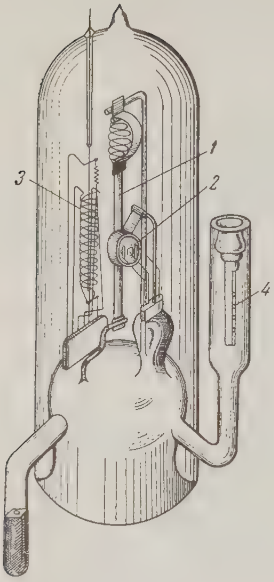

Fig.1. Experimental tube.

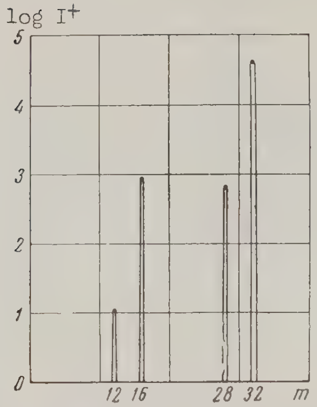

Fig.2. Mass spectrogram of the oxygen utilized in our experiments.

The conditions of preparation of pure oxygen from a source of our type were investigated beforehand by B.A.Chuikov by means of a high-vacuum mass spectrometer.[4] As will be evident from the mass spectrogram reproduced in Fig.2, in the region of oxygen pressures obtaining in our experiments ($\sim 5 \cdot 10^{-8}$ mm Hg), the gas contained virtually only one impurity, namely, a very minor amount of carbon monoxide. The presence of an appreciable admixture of CO, of course, constitutes a threat to the "purity" of such experiments: some CO could be formed[5] as a result of reaction of the oxygen with traces of carbon contained in the tungsten ribbon and in the filaments of the ion source and ionization gage. The high purity of our oxygen was also proved by the results of special experiments performed with the omegatron system in the tube directly in the process of measuring the contact potential (see below). (It is also substantiated by the indirect data of Ya.M. Kucherov, which will be reported upon elsewhere.) Incidentally, the effect of conversion of oxygen to CO is substantially reduced in the process of operation of the tungsten filament owing to gradual burning out of any impurity carbon present.

The Alpert gage, which was located in the immediate proximity of the tungsten filament, was calibrated taking into account the oxygen atmosphere with reference to an LM-2 pressure gage, which was in turn calibrated on the basis of the data of the supply plant laboratory. In the process of preparation and evacuation our experimental tubes were thoroughly aged in accordance with all the requirements of present-day ultravacuum technique. As a result, the pressure of the gas background in the tube was reduced to $\sim 10^{-9}$ mm Hg, i.e., to an appreciably lower level than the oxygen pressure (10^{-6}-10^{-8} mm Hg).

After every experiment the oxygen was withdrawn from the tube by pumping and the tungsten filament cleansed and repurified by short-term high temperature heating. Then new oxygen was introduced by heating the barium peroxide source, the operation being repeated for each succeeding experiment. All the tests were repeated a number of times with good reproducibility of the experimental data; this substantiated the stability of the surface structure (roughness) of our tungsten ribbon, which was also thoroughly and extensively aged in the process of preparing the tube.

Judging from the available data for Ba-W (V.K.Medvedov), the adsorptive properties (adsorption energy and its variation with θ) of tungsten ribbons of the type used in our experiments differ little from the properties of single crystal tungsten ribbons. Lastly, control experiments carried out by Yu.S.Vedula showed the virtual absence of any influence on the tungsten ribbon of any possible products of evaporation from the filaments of the ionization gage and electron gun.

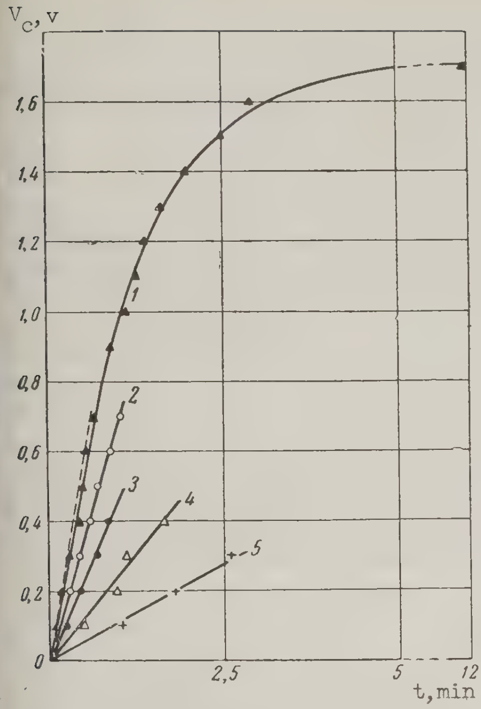

Fig.3. Variation of the contact potential V_C with the oxygen adsorption time at different oxygen pressures: 1) $3.6\cdot10^{-7}$, 2) $2.4\cdot10^{-7}$, 3) $1.8\cdot10^{-7}$, 4) $9\cdot10^{-8}$, 5) $6\cdot10^{-8}$ mm Hg.

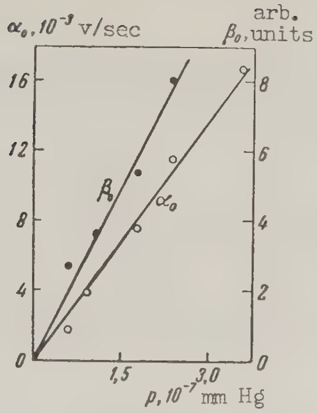

Fig.4. Variation of the slopes α_0 and β_0 with the oxygen pressure.

Kinetic of formation of adsorbed oxygen films on tungsten

As noted above, we relied primarily on the contact potential method. This method amounts to determining the variation of the contact potential V_C with the exposure time t of the previously cleaned tungsten ribbon in an atmosphere of pure oxygen at constant pressure. In cases when the tungsten ribbon was in the cold (300°K) state, we obtained curves identical with curve 1 in Fig.3.

It is important to note that over the initial portion of the curve the variation is linear; after a certain time, however, without any fluctuations, the curve bends over and approaches a saturation value equal to the well known one for the O-W system, namely, $V_{Cm} \approx 1.7$ v. In the same figure we give a family of the initial truly linear sections of the corresponding curves for other oxygen temperatures, the tungsten substrate temperature in every case being 300°K. The dashed curve in the figure represents the initial part of the "control" time variation of V_C determined at a pressure of $5\cdot10^{-7}$ mm Hg under conditions when it was shown by omegatron measurements that virtually only pure oxygen was contained in the tube; it will be evident that this straight line does not differ noticeably in character from the corresponding solid curves in Fig.3.

We determined the slopes of the initial sections

$$\alpha_0 = \left(\frac{dV_C}{dt}\right)_{t=0}$$

of the family of curves and plotted the resultant values against the oxygen pressure. It will be evident from Fig.4 that the plot is a straight line passing through the origin. It can be shown, knowing the slope of this straight line, that one can determine the condensation probability σ and the condensation coefficient γ of oxygen on tungsten. Thus

$$V_C = 4\pi\mu n, \tag{3}$$

where μ is the dipole moment of the adsorbed atoms or molecules, which in general may depend on their concentration n. Hence invoking Eq.(1), we can write

$$\alpha = \frac{dV_C}{dt} = 4\pi\mu\frac{dn}{dt} = 4\pi\mu\nu\sigma. \tag{4}$$

In our case, however, during the initial instants, i.e., during the period corresponding to the lower straight line part of the adsorption curve, there undoubtedly occurs spontaneous dissociation of the oxygen molecules into two atoms*, $f(\theta) = 1$, the adsorption activation energy $E = 0$ and $\mu = \mu_0$. Hence here $\sigma = \gamma$, and the slope of the straight line in Fig.4

$$\frac{d\alpha_0}{dp} = 4\mu_0\sqrt{\frac{2\pi}{MkT_0}}\,\gamma = A\gamma, \tag{6}$$

whence we can determine the value of γ. Unfortunately, in order to do this we must first know μ_0, which is not available in the literature and which, as we shall show below, it is impossible to measure (for example, by the flash technique). Hence we must make an approximate evaluation of this quantity on the basis of the relation

$$\mu_0 = \frac{V_{cm}}{4\pi n_1}\,\frac{t_1}{t_2} \approx 0.7\,D,$$

here the value $V_{cm} \approx 1.7$ v pertains to a monatomic coating; $n_1 \approx 1.0\cdot10^{15}$ at/cm; t_1 and t_2 are the times for attainment of V_{cm} according to curve 1 and its extrapolated rectilinear section, respectively. The value of n_1 assumed here corresponds to almost all recent evaluations[2] of this quantity for O-W, taking into account dissociation of the oxygen molecules adsorbed on the surface.

Inserting these data in (6) we arrive at the value of the condensation coefficient for oxygen on tungsten, namely, $\gamma \approx 0.05 \lesssim 0.1$. Even with the most pessimistic evaluation of the errors involved in evaluating n_1 and the oxygen pressure, it will be obvious that the condensation coefficient must be much smaller than unity and cannot even possibly approach this value. For comparison we note that on the basis of the data given by the authors listed under Ref.2, there is obtained the value $\gamma \approx 0.2$-0.6, i.e., a value appreciably greater than ours, although one can also find in the literature substantially lower values, that is, values approaching ours (for example, see Ref.6 for the value of the condensation coefficient for the oxygen-silicon system).

So low a value for the coefficient of condensation of O_2 on W is admittedly surprising. Thus it might be thought that in this case when the adsorption energy for the main film at $\theta = 0$ is rather high (of the order of 5-7 ev), while the molecules incident on the surface have a very low mean thermal energy, that there should obtain complete absorption with no reflection, i.e., that γ should be equal to or close to unity. Various hypotheses may be advanced to explain the result

*This is evident if only from consideration of the cyclic process consisting of adsorption of an O_2 molecule on the W surface, its subsequent dissociation into two atoms, desorption of these atoms and their final recombination to form an O_2 molecule. Hence the energy balance can be written in the form

$$Q_M - q' - 2Q_a + q = 0, \tag{5}$$

where $q = 5.1$ ev, $Q_a \approx 6.5$ ev, i.e., $q' < 0$.

obtained; however, we do not as yet have sufficient data to draw any definitive deductions. At the same time it must be noted that the value $\gamma<1$ is apparently not an exception but is consistent with the general regularity, inasmuch as similar low values obtain for other gases such as N_2, H_2 and CO on W.[7] On the other hand, theoretical interpretation of this phenomenon is not feasible owing to the lack of theoretical investigations of the subject.[8] Lastly, we note that the low value of the condensation coefficient serves to explain the low rate of chemical reaction of oxygen with efficient thermionic cathodes (see below). Here there is evident a certain parallelism between the rates of condensation and surface chemical reaction, requiring, obviously, intimate interaction between the reacting partners.

In view of the recent widespread use of the method of ionization flashes, which has been employed both for determining the condensation probability in different systems[7] and for determining the pressure of the condensed fraction of residual gases in the ultravacuum range[9], we decided to test it for our O-W system. In utilizing this method, however, one must bear in mind the following: the heat-up of the substrate, i.e., the "target flash", requires a certain brief but still finite time, during which there may also occur partial absorption of the gas desorbed from the walls of the envelope and the electrodes. This is particularly troublesome and annoying because the degree of absorption may vary during the said interval owing to gradual saturation and may be different in different tubes and for different gases. All this may have a complex and unpredictable effect on the time variation of the measured discontinuity - the flash pressure rise Δ_p - which makes the flash procedure somewhat ambiguous, so that one must be extremely careful in utilizing it, particularly in the case of the O-W system where, in addition, at the high temperature of the flash (~2400°K), there is a strong probability for the occurrence of diverse surface chemical reactions.

In our qualitative experiments on the application of this method we purely empirically took Δ_p to be its amplitude value, as determined by means of an oscillograph. Hence, simultaneously with the data of Fig.3, we also determined the variation of Δ_p with the time of preliminary adsorption of oxygen on the tungsten at T = 300°K and different oxygen pressures.

The family of curves obtained in this manner is shown in Fig.5. These curves, like the curves of Fig.3, are at first virtually linear and then bend over and approach a saturation value Δ_{pm}. As before, we determined the slopes

$$\beta_0=\left(\frac{d\Delta_p}{dt}\right)_{t=0}$$

of the initial sections of the curves and plotted them against pressure; as will be evident from Fig.4, the dependence is linear and the plot passes through the origin. It can be shown that in principle one can determine the coefficient of condensation γ from the slope of this straight line. Thus in the complete absence of absorption and chemical reaction of the desorbed gas

$$\Delta_p=\frac{nS}{V}kT\,, \tag{7}$$

where S is the surface of the tungsten ribbon, and V is the volume of the tube. Thus the slope of the initial sections of the curves in Fig.5, taking into account Eq.(1), is described by

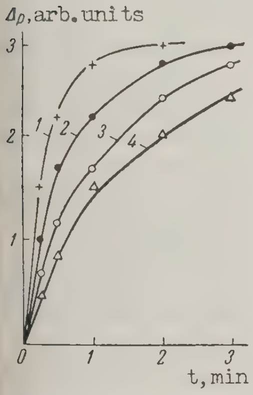

Fig.5. Variation of the flash pressure rise Δ_p with the time of adsorption of oxygen at different pressures: 1) $2.4\cdot10^{-7}$, 2) $1.8\cdot10^{-7}$, 3) $1.1\cdot10^{-7}$, 4) $5.4\cdot10^{-8}$ mm Hg.

$$\beta = \frac{d\Delta_p}{dt} = \frac{S}{V} kT \frac{dn}{dt} = \frac{S}{V} kT\nu\sigma. \tag{8}$$

Consequently, the slope of the straight line in Fig.4 equals

$$\frac{d\beta_0}{dp} = \frac{2ST}{V}\sqrt{\frac{k}{2\pi MT_0}}\,\gamma = \beta\gamma, \tag{9}$$

so that one can readily determine the condensation coefficient γ. In view of the reasons adduced above, however, we do not feel it justifiable at the present stage of the investigation, to utilize the data of Figs.4 and 5 for determining γ, and hence only note the important fact that the quantity β_0 is directly proportional to the pressure in the case of the O-W system as well.

Some attributes of oxygen films adsorbed on tungsten

Together with the family of $V_C = f(t)$ curves (Fig.3) at a constant substrate temperature and different oxygen pressures, we should consider the analogous family of curves obtained for a constant oxygen pressure of $3.6 \cdot 10^{-7}$ mm Hg but at different temperatures of the substrate ranging from 300 to 1500°K. At temperatures above 1500°K the tungsten ribbon begins to yield an appreciable thermionic emission distorting the measurements. The results obtained in these experiments are shown in Fig.6; analyzing them we note the following.

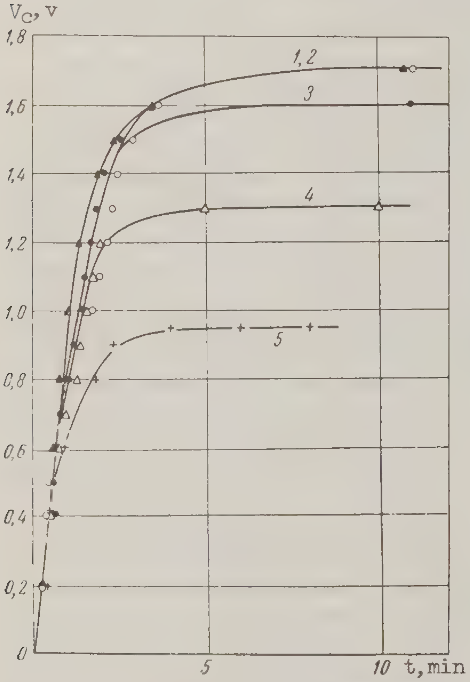

Fig.6. Variation of the contact potential with the oxygen adsorption time and the temperature of the tungsten substrate: 1) 300°K, 2) 1800°K, 3) 1220°K, 4) 1350°K, 5) 1470°K.

1. The slope $\alpha_0 = \left(\frac{dV_C}{dt}\right)_0$ of the initial section of the curves remains virtually the same in the entire, rather wide temperature interval. In view of relations (2) and (4) this means a) that the condensation coefficient remains constant, i.e., that γ is independent of the substrate temperature, b) that the activation energy E for adsorption of O_2 on W is virtually zero, and c) that there is no appreciable formation of surface films of tungsten oxide and carbon monoxide which, naturally, have entirely different electronic properties. It is important to emphasize that the fact that under our conditions (substrate temperatures under 1500°K) the oxygen does not react chemically with the tungsten follows also from the data reported by Dushman[10], while the fact that the oxygen does not react with the carbon in the tungsten is substantiated by the results of omegatron measurements carried out in our laboratory by Ya.M.Kucherov.

2. With increase of the substrate temperature the limiting value of the contact potential V_{cm} at first ($T \leqslant 1100$°K) remains constant and only later gradually falls off, apparently owing to appreciable desorption of oxygen. Each limiting contact potential corresponds to a certain state of dynamic

equilibrium between the adsorption of O_2 from the gaseous phase, on the one hand, and the temperature desorption, on the other hand. To illustrate the above in Fig.7 we have plotted (solid curves) the variation of V_{cm} with T for two values of p. It will be noted that the dependence is monotonic in the entire temperature range from 300 to 1500°K. On the other hand, the limiting values of the flash rise Δ_{pm}, as taken off Fig.5, vary with the temperature as shown in Fig.7 by the dashed curve; it will be seen that this curve is qualitatively analogous to the solid curves for V_{cm}. This, in our opinion, is not consistent with the deduction drawn by some authors[11] on the basis of observation of field emission that there may form an appreciable second adsorbed film of oxygen on tungsten with a lower ($Q \approx 2.3$-2.5 ev) adsorption energy and, accordingly, a reduced (~ 750°K) temperature region of desorption.

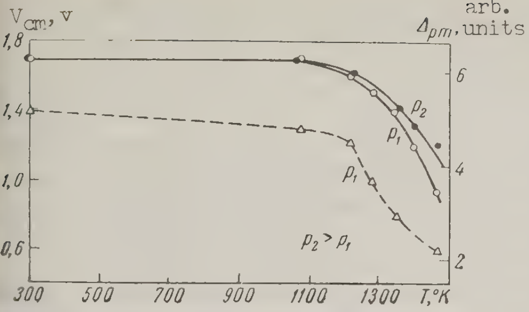

Fig.7. Variation of the limiting value of the contact potential (solid curves) and the flash rise (dashed curve) with the substrate temperature.

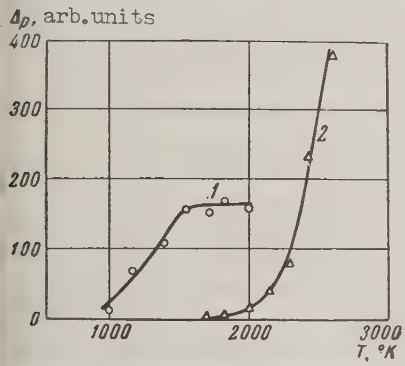

Fig.8. Variation of the pressure rise of the flash with its temperature for pure carbon monoxide (1) and pure oxygen (2).

Moreover, we could not detect any appreciable amount of this second low temperature adsorption phase (second molecular film) of O_2 on W even by the flash method up to $T \approx 1500$°K; to this end we used both the integral method employing the Alpert pressure gage and the differential method using the megatron adjusted for O_2. This is evident, for example, from Fig.8 (measurements of Ya.M.Kucherov) which shows the variation of a one second duration flash pressure rise as indicated by the Alpert gage with the flash temperature for the cases of specially converted pure CO at $2 \cdot 10^{-7}$ mm (curve 1) and pure O_2 at $6 \cdot 10^{-7}$ mm (curve 2) after their 4 minute exposure on cold tungsten. We see that the $T \approx 1500$°K region is a sort of boundary between two phases; in our case it is shifted somewhat to the right owing to the short flash time. In this temperature region desorption of CO is already completed (the presence of CO in tubes with O_2 owing to conversion of the oxygen has not generally been suspected hitherto) and there begins desorption of the O_2. In view of these results, we believe there is reason to doubt the existence of a low temperature phase of adsorbed oxygen on tungsten.

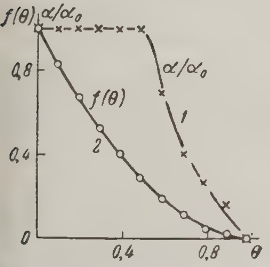

Fig.9. Variation of the factors α/α_0 and $f(\theta)$ on the degree of covering θ.

We note that from the form of the time variation of V_c one can draw an interesting inference regarding the function $f(\theta)$ in Eq.(2). Thus, let us assume that the degree of covering of the substrate by the film can be defined in terms of $\theta = V_c/V_{cm}$; this is valid to the extent that the value of μ from (3) can be regarded as constant and the state of the film inalterable. Then from (2) it is evident that the ratio of the slopes α/α_0 must give the value of $f(\theta)$. Applying this procedure to curve 1 in Fig.3, we obtain the functional dependence $\alpha/\alpha_0 = f(\theta)$ represented by curve 1 in Fig.9. While there might be some question regarding the true shape of the curve as far as its right-hand part is concerned, for the left hand part (for $\theta < 0.4$-0.5), where the entire family of curves in Fig.3 is rectilinear, the value of $f(\theta)$ is undoubtedly constant and equal to unity. For comparison, in the same figure, we also give the curve (curve 2) for the theoretical dependence[12]

$$f(\theta) = \frac{z(1-\theta)^2}{(z-\theta)} \approx (1-\theta)^2, \tag{10}$$

where z is the coordination number. It will be evident that this theoretical dependence differs appreciably from the experimental one. One can explain the character of the experimental curve on the assumption that the adsorbed oxygen film is mobile to the extent that it may creep over the tungsten surface from coated areas to the neighboring vacant areas even at room temperature of the substrate; this assumption is not in conflict with what other experimental data are now available.

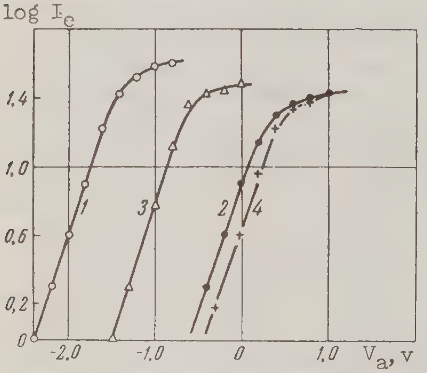

Fig.10. Retarding potential curves: 1) clean W, 2) W in pure O_2, 3) W in pure CO, 4) W in O_2 + CO mixture.

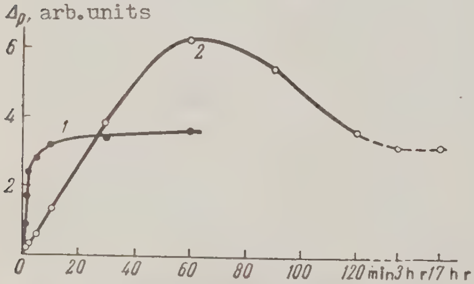

Fig.11. Variation of the flash with the adsorption time of oxygen at different pressures: 1) $4 \cdot 10^{-8}$, 2) $3 \cdot 10^{-9}$ mm Hg.

In the case of adsorption of oxygen on tungsten in the presence of an admixture of other gases the following interesting effect is sometimes observed. Thus, let us determine the total variation of the contact potential of the W ribbon V_{cm} for separate adsorption on the tungsten in the cold state of a) pure oxygen, b) pure carbon monoxide and c) a mixture of O_2 + CO in approximately equal proportions. All these gases were present in our tube and their composition in the process of measurements was monitored by means of the omegatron. The family of current-voltage characteristics obtained in this manner and plotted with reference to the characteristic for clean W (curve 1) is shown in Fig.10. It will be evident from the shift of the characteristics that 1) for the case of adsorption of pure O_2 there is obtained the characteristic 2, i.e., $V_{cm} \approx 1.8$ v, as reported above, 2) for the case of adsorption of pure CO there is obtained characteristic 3, i.e., $V_{cm} \approx 0.9$ v, which is in agreement with the data in the literature[7], and 3) for the case of adsorption of the 50-50 O_2 + CO mixture after an appropriate exposure there is unexpectedly obtained characteristic 4, i.e., $V_{cm} \approx 2.0$ v, that is, a characteristic very similar to that for the adsorption of pure O_2. Obviously, this interesting result may be interpreted as adsorptive displacement of CO molecules by O_2 molecules in the process of their joint adsorption on a tungsten surface.

With a residual gas pressure of $\lesssim 3 \cdot 10^{-9}$ mm Hg in the tube there was introduced oxygen at different pressures, following which we recorded the time variation of Δ_p. In cases when the oxygen pressure was $\geqslant 10^{-8}$ mm Hg the curves obtained had the normal appearance, as is illustrated, for example, by curve 1 in Fig.11, for $p = 4 \cdot 10^{-8}$ mm Hg. The rate of rise of all such curves in the initial section fell off with decrease of p, and all the curves monotonically approached the same saturation value Δ_{pm}. When, however, the pressure of the introduced oxygen was reduced to the level of the residual gases ($\sim 3 \cdot 10^{-9}$ mm Hg), there was obtained curve 2, i.e., a curve that first went through a pronounced maximum and then dropped off to the common saturation value Δ_{pm}. This result also indicates joint adsorption on a tungsten surface. We note that the components of the residual gases adsorbed on cold W are mainly H_2, CH_4 and $N_2 + CO$;[9] usually these gases are readily desorbed when the tungsten substrate is heated to ~1200°K.

This adsorptive displacement of some gases by oxygen is presumably connected with the appreciably greater adsorption energy characteristic of oxygen on W as compared with all other gases.

Thus our data on the kinetics of adsorption of O_2 on tungsten surfaces and on some of the attributes of such adsorbed films help give some insight into this extremely complex and important problem. As for conversion of O_2 to CO and other allied processes, we plan to discuss them in a future paper.

We desire to thank Yu.G.Ptushinskii for assistance in carrying out the present work.

Institute of Physics
Academy of Sciences of the Ukrainian SSR

References

1. Yu.Vedula, V.Gavrilyuk & N.Morgulis, Zhur.fiz.tverdogo tela, 1, 1717 (1959). (Trans.Soviet Physics - Solid State.)

2. J.Morrison & J.Roberts, Proc.Roy.Soc.A, 173, 1 (1939); R.Rosworth, J.Roy.Soc.N.S.W., 79, 53 (1945); R.Schlier, J.Appl.Phys., 29, 1162 (1958); J.Eisinger, J.Chem.Phys., 30, 412 (1959).

3. S.Wagener, Proc.Phys.Soc.B67, 369 (1954); A.Kulik & N.Nakhodkin, Izv.AN SSSR, Ser.fiz., 20, 1096 (1956) (Trans.Bulletin, 20, 989); Ya.Zingerman & V.Soltyk, Radiotekhnika i elektronika, 2, 1512 (1957) (Trans.Radio Engineering & Electronics).

4. G.Pikus, Izv.AN SSSR, Ser.fiz., 20, 1085 (1956) (Trans.Bulletin, 20,980); PTE (in press) (Trans.Instr. & Experimental Techniques).

5. J.Wagener & P.Marth, J.Appl.Phys., 28, 1027 (1957); R.Schlier, Ibid., 29, 1162 (1958).

6. J.Eisinger & J.Law, J.Chem.Phys., 30, 410 (1959); R.Schlier & H.Farnsworth, Ibid., 30, 917 (1959).

7. J.Becker & C.Hartman, Ibid., 57, 153 (1953); J.Eisinger, Ibid., 27, 1206 (1957); Ibid., 28, 165 (1958); Ibid., 29, 1154 (1958); R.Schlier, J.Appl.Phys., 29, 1162 (1958); T.Hirkmott & F.Hudda, J.Chem.Phys., 28, 506 (1958); T.Hickmott & G.Ehrlich, J.Phys.Chem.Solids, 5, 47 (1958).

8. Ya.Frenkel', Usp.fiz.nauk, 20, 117 (1938); H.S.T.Massey & E.H.S.Burhop, Electronic and Ionic Impact Phenomena, Oxford 1952. (Cited in Russian trans.); P.Kisliuk, J.Phys.Chem.Solids, 3, 95 (1957).

9. D.Hagstrum, Rev.Sci.Instr., 24, 1135 (1953); N.Morgulis, Zhur.tekh.fiz., 25, 1667 (1955); G.Ehrlich, J.Phys.Chem., 60, 1388 (1956); N.Morgulis, Yu.Ptushinskii & B.Chuikov, Doklady AN SSSR, 128, 930 (1959) (Trans.Sov.Phys. - Doklady.)

10. S.Dushman, Scientific Foundations of Vacuum Technique, N.Y., 1949 (Cited in Russian trans.); R.Schlier, J.Appl.Phys., 29, 1162 (1958).

11. J.Becker & R.Brandes, J.Chem.Phys., 23, 1323 (1955); R.Gomer & J.Hulm, Ibid., 27, 1363 (1957).

12. B.Trepnel, Chemosorption (Cited in Russian trans.).

VARIATION OF ION-ELECTRON EMISSION AS A FUNCTION OF CERTAIN PARAMETERS OF THE TARGET AND THE BOMBARDING IONS

- U.A. Arifov & R.R. Rakhimov

Introduction

When a metal target is bombarded with positive ions that satisfy the condition $V_i > 2\varphi$ (V_i is the ionization potential of the atom, and φ is the work function of the metal), in addition to kinetic knocking out of electrons, there may also occur potential ejection at the expense of the internal energy of the incident ions. There have been a number of experimental studies of potential ejection of electrons.[1-3] Despite the appreciable divergence between the results of these investigations, probably due to differences in the vacuum conditions, the results consistently indicate that potential ejection of electrons does occur.

Over the past few years Hagstrum[4] and his co-workers have carried out a series of experimental investigations of ejection of electrons from metals by noble gas ions. Through the use of a "drastic" evacuation procedure (vacuum $\lesssim 10^{-9}$ mm Hg) and special measures to insure thorough outgassing, Hagstrum was able to obtain almost atomically clean targets. He explains the results obtained under these conditions by an Auger-type process involving the internal energy of the incident ions. Thus Hagstrum's results are further substantiation of the existence of the effect of potential ejection of electrons.

A more recent investigation, however, carried out by Tel'kovskii[5] under equally good vacuum conditions led to results disagreeing with those of the studies referred to above. Tel'kovskii's data indicating linear variation of the coefficient γ of secondary emission as a function of the ion velocity with a clear electron ejection threshold and the fact that μ is independent of the ionization potential of the bombarding particles led this author to deny the possibility of potential emission of electrons. Thus Tel'kovskii's results put under question the very existence of the potential mechanism of electron ejection.

In our preceding work[6] with Mo bombarded by argon atoms, we showed that the absence of potential emission found by Tel'kovskii[5] was due to irreversible contamination of the target surface incident to heat treatment in the presence of oil vapor, i.e., is a consequence of formation of molybdenum carbide. In this work we also determined the vacuum conditions necessary for cleaning of the metal to the purely metallic state and therefore the conditions essential for observation of potential emission comparable to that reported by Hagstrum[4].

Now that the requisite conditions for potential emission are known it is of interest to investigate the potential and kinetic emission of electrons as a function of different parameters of the target and the bombarding ions. In the present report we give the results of our further experimental investigation of the variation of potential and kinetic ejection of electrons as a function of the temperature and work function of the target and the energy of the bombarding ions in the range to 10 kev.

Apparatus and Experimental Procedure

The experiments were carried out in the vacuum equipment diagramed in Fig.1. The figure also shows the electronic circuit for measurements by the double modulation oscillographic procedure.[7] The glass apparatus free of joints and valves consisted of an ion source and a detecting section separated by a vacuum "diaphragm" 3 in the form of a 10 mm long channel with a 1 mm diameter aperture.

In working with noble gas ions the ion beam was extracted from the discharge between the filament 1 and the anode 2, located in the magnetic field MF of the

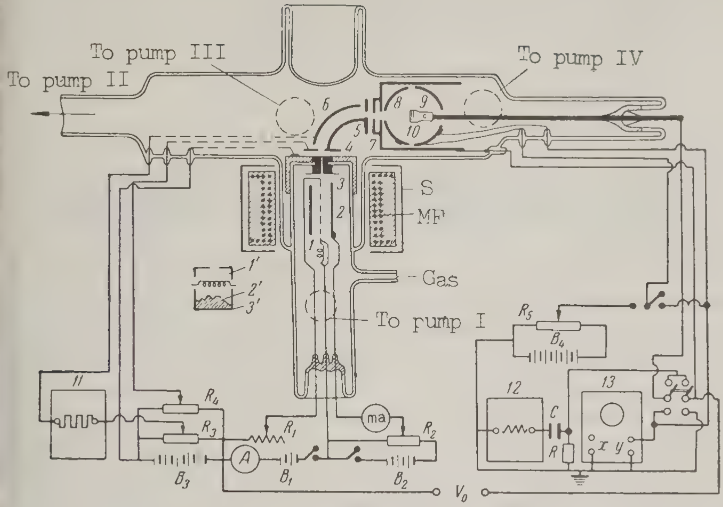

Fig.1. Apparatus and associated electric circuit.

solenoid which was surrounded by a thick iron shield S.[8] In work with alkali metal ions the source was a heated spiral 1' (see insert) located above the cup 3' containing the appropriate alkali halide salt 2'. This source was installed instead of the magnetic one after completion of the experiments with the noble gas ions.

The receiving-detecting part of the apparatus consisted of the shielding cylinder 7, the collector consisting of two hemispheres 8 and 9, and the target 10. The use of a two-part collector made it possible to carry out separate measurements of the secondary positive ion and electron currents with a relatively small potential difference between the collectors and the target, the desired potential difference being set and regulated by the battery B_4 and potentiometer R_5.[9]

The operation of the electric circuit when employing the double modulation technique may be described as follows. In the case of noble gas ions (or alkali metal ions) the ion beam was extracted by the field between the filament 1 (1') and the aperture 3, accelerated by the field between electrodes 3 and 4, and entered the field of the cylindrical capacitor 6.

In the cylindrical capacitor the ion beam was separated from neutral particles, focused and modulated in intensity by the square pulse generator 11 (first modulation) and directed onto the target 10. An accelerating potential V_0 of up to 10 kv was applied between the plates 5 and 7.

The secondary emission current was collected by collectors 8 and 9, the potential of which relative to the target was modulated by the sawtooth voltage oscillator 12 (second modulation). The current from the collectors was applied to the input of the vertical-plate amplifier of oscillograph 13, the horizontal sweep of which was synchronized with the output of the sawtooth voltage oscillator. The frequency of the sawtooth voltage was 50 cps. The frequency of the square pulses could be varied in the range from 500 to 1000 cps. By virtue of interruption of the primary beam by the square pulse generator and the presence of the sawtooth voltage between the target and the collector, the oscilloscope beam automatically traced the current-voltage characteristic of the secondary current with an appropriate zero line.

The secondary emission coefficient γ was determined by dividing the value of the electron saturation current, found from the voltage-current characteristic, by the intensity of the primary ion beam, as measured in the target-collector circuit. We evaluate the measurement error to be $<$2-3%.

The apparatus was evacuated by four three-stage glass pumps, which, after outgassing of the glass walls of the apparatus and electrodes, provided a vacuum of the order of $1 \cdot 10^{-7}$ mm Hg. The noble gas ion source operated at pressures of $\cdot 10^{-5}$ to 10^{-4} mm Hg. The use of differential pumping assured a pressure differential between the source and the receiving-detecting part of over two orders of magnitude. In the case of working with the alkali metal ions, after prolonged outgassing of the source with the alkali halide salt, the pressure of the residual gases in the receiving-detecting section was reduced to $\sim 1 \cdot 10^{-7}$ mm Hg. The inert gases were admitted into the source tube by means of a needle type metering valve.

Experimental Results

Variation of the coefficients of potential (γ_π) and kinetic (γ_k) electron emission as a function of the temperature and work function of the target

In investigating the temperature dependence of the emission coefficients γ_π and γ_k, we used a molybdenum target in the form of a 30 x 5 x 0.015 mm ribbon. The target was bombarded by A and K ions with kinetic energies of 200 and 5000 ev, respectively. In investigating the work function dependence of γ_π we also used Ne ions.

It is a known fact[10] that ion-electron emission strongly depends on contamination of the metal by foreign atoms, the quantity of which on the metal surface depends in turn on the temperature. Hence in measurements of the emission coefficient it is essential to attain as high a degree of cleanness of the target as possible, i.e., to eliminate both the particles absorbed by the metal earlier and to minimize contamination of the surface owing to adsorption of residual gas molecules during the time between outgassing and actual measurement. In our experiments the first requirement was satisfied by prolonged outgassing of the target at temperatures of 2300-2400°K; the second, by performing the measurements by the lag-free oscillographic procedure described above, which allowed of determining the secondary current at the given temperature immediately after flashing the target (short term heating to 2300°K). Moreover, the technique of modulating the intensity of the primary ion beam allowed of separate measurement of the secondary electron and thermal electron currents[11] even at very high temperatures; the experiments were carried out in the temperature range from 300 to 1600°K.

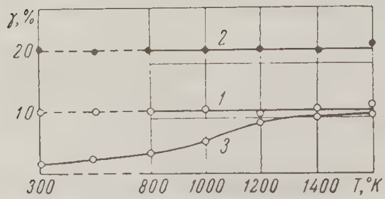

Fig.2. Variation of the emission coefficients γ_π (1) and γ_k (2) with the temperature of a molybdenum target; curve 3 was obtained for an Mo surface covered with a monolayer of adsorbed molecules.

Curves 1 and 2 in Fig.2 show the variation of γ_π and γ_k with the temperature of an Mo target. Curve 3 was obtained for argon bombardment of a molybdenum surface coated with a monomolecular layer formed by adsorption of residual gas molecules. It will be evident from curves 1 and 2 that in the temperature range from 300 to 1600°K the values of γ_π and γ_k for clean molybdenum remained virtually constant. In contrast, in the presence of surface contamination there is evinced a strong temperature dependence of γ_π and γ_k; this is due to variation of the coating density with temperature.[10]

In order to investigate the variation of γ with the work function of the bombarded metal we used targets of Pt, Ni W, Mo, Ta, Zr and Mg, for which the values of φ varied from 5.29 to 3.46 ev. All the targets, except the Mg target, were prepared in the form of foil ribbons: 30 x 5 x 0.15 mm strips in the case of Ni, W, Mo and Ta, and 30 x 5 x 0.03 mm strips in the case of Pt and Zr. The magnesium target was prepared by sputtering magnesium on a clean molybdenum backing from a special furnace at a rate much higher (20 monatomic layers per sec) than the rate of formation of an equilibrium coating owing to absorption of residual gas molecules on the surface (0.1 monatomic layer per sec).

The W, Ta and Mo targets were outgassed at 2800, 2600 and 2300°K, respectively, and the Pt, Ni and Zr targets at temperatures 100-150°K below the melting points for these metals, the heating time in all cases being 18-20 hours. After such "heat treatment" we assumed the work functions of the W, Mo, Ta, Ni and Zr ribbon targets to be equal to the work functions of equivalent filaments measured after identical heat treatment under the same vacuum conditions by the method of Richardson plots. For the work function of the Mg target we took the value from the literature[12].

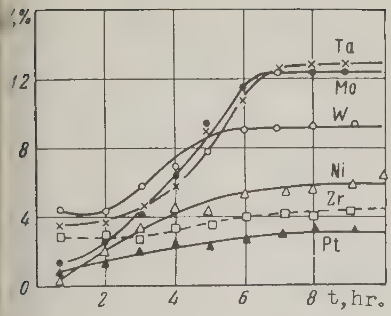

ig.3. Variation of γ with he time of the outgassing eat treatment for different targets.

The validity of utilizing for ribbon targets work function values determined for filaments was checked by investigating the character of adsorption and desorption of residual gas molecules on the surface of ribbon targets and filaments by the "flash" procedure. It was established that heating of Pt, Ni, W, Mo and Ta to the above indicated temperatures led to evaporation of the adsorbed molecules in amounts virtually proportional to the surface area of the target or filament. However, heating of Zr almost to the melting point and Ta to 2000°K was accompanied by impairment of the vacuum, which could be taken as indication of additional absorption of residual gas by these metals in the heated state. In the case of Ta at higher temperatures there begins evaporation of the adsorbed molecules of the equilibrium coating and at 2500-2600°K the amount of liberated gas is comparable with that observed for Mo at 2000°K.

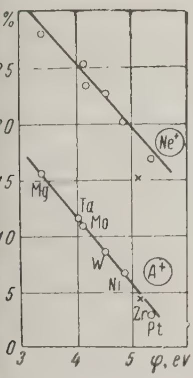

ig.4. Variation of with φ for A and e ions. The points re taken from the aturation section f curves similar to those shown in Fig.3.

In the course of the outgassing heat treatment of each of the metals we carried out measurements of γ_π with bombardment by A ions. It will be evident from the curves, shown in Fig.3, that in initial stages of heat treatment the value of γ_π for all metals is small and increases with further heating to a saturation value, i.e., a value that remains virtually constant with further heating up to the melting point. Fig.4 shows the variation of γ_π with φ for A and Ne ions; each point for these curves was taken from he region of saturation of the curves of Fig.3.

It will be evident from the curves of Fig.4 that γ_π depends greatly on the ork function: thus with increase of the work function from 3.46 to 5.29 ev, γ_π or A ions falls off from 16 to 2.5%, while γ_π for Ne ions decreases almost linerly from 28.5 to 17.5%.

Taking into account the above work function dependence of γ_π together with he virtual temperature independence of γ_π (Fig.2), one can explain the temperaure variation of the work function of metals reported by Dobretsov[13] which, hower, for Mo with variation of the temperature to 1600°K proves to be $(1-6)\cdot10^{-2}$ v. It must be noted that this change leads to a decrease of γ_π amounting to only 0.5%, which is less than our experimental error.

Variation of γ_π and γ_k with the ion energy E_o

The results of measurements of γ as a function of E_o in the range from 0.1 o 10 kev for noble gas and alkali metal ions bombarding W, Ta and Mo targets are

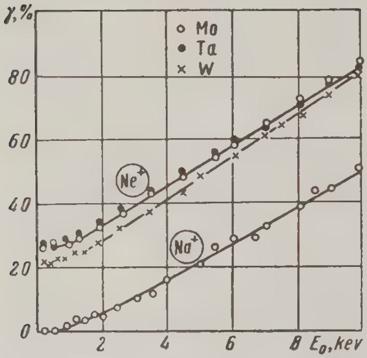

Fig.5.

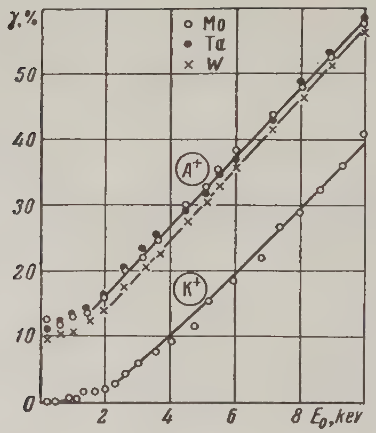

Fig.6.

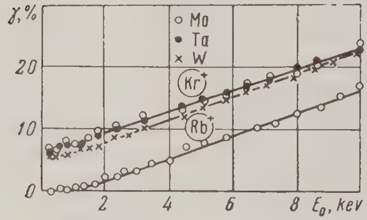

Fig.7.

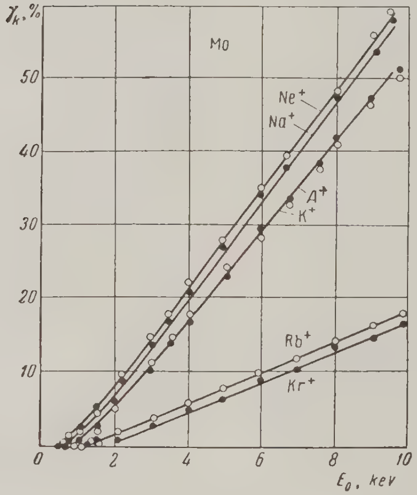

Fig.8.

Fig.5. $\gamma = f(E_0)$ curves obtained for bombardment of Mo, Ta and W targets by Ne ions and an Mo target by Ni ions.

Fig.6. $\gamma = f(E_0)$ curves for bombardment of Mo, Ta and W by A ions and Mo by K ions.

Fig.7. $\gamma = f(E_0)$ curves for bombardment of Mo, Ta and W by Kr ions and Mo by Rb ions.

Fig.8. $\gamma = f(E_0)$ curves for the ion pairs Ne & Na, A & K and Kr & Rb. The noble gas curves were obtained from the curves of Figs.5,6 & 7 by subtracting the part of the emission parallel to the E_0 axis, i.e., the inferred constant value of γ_{κ}.

shown in Figs.5,6 & 7. Prior to these measurements the targets were outgassed by prolonged heating at 2700°K for W, 2600°K for Ta and 2300°K for Mo. Each point for the γ vs E_0 curves was obtained at a temperature of 1400-1500°K immediately after flashing the target.

It will be evident from the curves for Ne, A and Kr ions that in the ion energy range from 0.1 to 1 kev for all targets and types of ions γ virtually does not depend on the kinetic energy of the incident ions. This fact together with the increase of γ observed in going from ions with a low ionization potential to ions with a high V_i (i.e., in going from Kr to Ne) is evidence of the potential character of the electron emission in the ion energy range below 1 kev.

Examination of the curves shows that with increase of the energy of noble gas ions from 1 to 10 kev there occurs a linear increase of γ. The beginning of the rise and the slope of the γ vs E_0 curves depend primarily on the type of ion and do not depend to any significant extent on the nature of the target.

In the case of alkali metal ions the value of γ is very small in the energy range under 1 kev and then increases linearly with increase of the ion energy to 10 kev. Our data on the variation of γ_k with E_0 for bombardment of targets by alkali metal ions with energies to 4 kev are in agreement with the results of Brunnee[9], Arifov et al[10], and Eremeev[14]. With further increase of E_0 to 10 kev the emission coefficient continues to increase linearly.

Our curves for γ vs E_0 obtained for M_0 and W targets bombarded with noble gas ions with energies to 1 kev agree with the data of Hagstrum[4]. This agreement of our results with the data of the above cited authors in the range of relatively low bombarding energies may be taken as proof that the degree of cleanness of the target surfaces achieved in our experiments was equal to that obtaining in the other investigations referred to.

On the basis of the experimental fact that the potential emission from metal surfaces does not vary with the energy of the primary ions in the range up to 1 kev, we infer that the potential emission does not depend on the ion energy in general, i.e., in the higher energy range as well. On the basis of this assumption we can compare the part of the secondary emission that does depend on the energy of noble gas ions with the γ vs E_0 curves for alkali ions for which there is only kinetic emission of electrons.

In Fig.8 we have plotted the E_0 dependences of γ for Ne, A and Kr ions after subtracting the value of the emission parallel to the E_0 axis, i.e., the part of the total emission contributed by the potential emission, together with the E_0 dependences of γ for Na, K and Rb ions bombarding an Mo target. It will be evident from the figure that the γ vs E_0 plots for the ion pairs Ne & Na, A & K and Kr & Rb nearly coincide. Inasmuch as the listed noble gas and alkali metal ion pairs have virtually the same masses and, hence, nearly equal velocities for each given kinetic energy, one may expect them to produce an equal kinetic emission, which is what the near coincidence of the plots in Fig.8 indicates.

Consequently, the increase in secondary emission beginning with a primary ion energy of ~1 kev in the case of bombardment of the various metals by noble gas ions is due to initiation of kinetic knocking out of electrons. Further, the near agreement of the γ vs E_0 curves for the above mentioned ion pairs substantiates our inference that the potential emission does not depend on the energy of the primary ions even in the range of higher energies.

The almost equal values of γ for different targets in the range of high energies (>8 kev) indicate, moreover, that the kinetic emission does not depend substantially on the work function of the target in the range of high primary ion energies.

Conclusions

1. The coefficients of potential (γ_π) and kinetic (γ_k) electron emission do not depend on the temperature of the bombarded metal.

2. The potential emission coefficient decreases linearly with increase of the work function.

3. The linear increase of the total emission coefficient with the ion energy in the case of both noble gas ions and of alkali metal ions is due to ejection of electrons by the kinetic energy of the bombarding ions.

4. The potential emission of electrons does not substantially depend on the kinetic energy of the incident ions in the energy range to 10 kev.

5. Whereas in the region of relatively low ion energies the kinetic emission is noticeably dependent on the type of metal, in the range of higher energies this influence becomes insignificant and at ion energies above 8 kev the emission

coefficient has almost the same value for Mo, Ta and W.

Institute of Nuclear Physics,
Academy of Sciences of the Uzbeck SSR

References

1. M.L.Oliphant, Proc.Roy.Soc.A, 127, 373 (1930).
2. F.Penning, Proc.Roy.Ac.Sci., 33, 841 (1931).
3. A.Rostagni, Z.Phys., 88, 55 (1934).
4. H.D.Hagstrum Phys.Rev., 89, 244 (1953); Phys.Rev., 96, 325 (1954); Phys. Rev., 104, 672 (1956).
5. V.G.Tel'kovskii, Doklady AN SSSR, 108, 444 (1956) (Trans.Soviet Physics - Doklady); Izv.AN SSSR, Ser.fiz., 20, 1179 (1956) (Trans.Bulletin, 20, 1070).
6. U.A.Arifov & R.R.Rakhimov, Izv.AN UzSSR, Ser.fiz.-mat.nauk (Bulletin, Uzbek SSR Ac.of Sci. Phys-Math. Sciences Series), No.5, 5 (1958).
7. U.A.Arifov, A.Kh.Ayukhanov & S.V.Starodubtsev, Zhur.eksp.i teor.fiz., 26, 714 (1954).
8. S.A.Slutskin, Zhur.tekhn.fiz., 5, 1362 (1935).
9. K.Brunnee, Z.Phys., 147, 161 (1957).
10. U.A.Arifov & A.Kh.Ayukhanov, Izv.AN SSSR, Ser.fiz., 20, 1165 (1956).(Trans Bulletin, 20, 1057.)
11. U.A.Arifov, A.Kh.Ayukhanov, S.V.Starodubtsev & Kh.Kh.Khadzhimukhamedov, Doklady AN SSSR, 124, 60 (1959). (Trans.Doklady.)
12. G.W.C.Kaye & T.H.Laby, Tables of Physical & Chemical Constants. (Cited in Russian trans., M., 1949.)
13. L.N.Dobretsov, Zhur.eksp.i teor.fiz., 18, 727 (1948).
14. M.A.Eremeev & V.V.Shestukhina, Zhur.tekh.fiz., 22, 1262 (1952).

SECONDARY ELECTRON EMISSION FROM SODIUM FILMS BOMBARDED WITH ARGON IONS

- U.A.Arifov & D.A.Tashkhanova

Introduction

There have been many studies devoted to investigation of secondary emission of metals under the influence of bombardment with positive ions. In many cases, however, there is disagreement between the results of different studies, presumably owing to differences in the state of the surface of the targets. In fact, even the results of some comparatively recent studies are in conflict: thus whereas Hagstrum[1] established the existence of electron emission at low ion energies and obtained a number of regularities indicating the potential character of the emission in the case when $V_i > 2\varphi$ (V_i is the ionization potential of the bombarding ions, and φ is the work function of the target), Tel'kovskii[2] on the basis of his experiments was led to deny the existence of potential emission.

In the work of Ref.3 it was shown that the reason for the absence of potential ejection of electrons under the conditions of Tel'kovskii's experiments is contamination of the target surface owing to the presence of oil vapors during the outgassing heat treatment. Further it was demonstrated[3] that potential emission can occur under the condition $V_i > 2\varphi$ provided the metal surface is clean.

Emission of electrons from high melting point metals under the influence of alkali metal ions was studied in the investigations listed under Refs.4-6. It was established that whereas in the primary ion energy E_0 range up to 1 kev the magnitude of the secondary emission coefficient γ is small, increase of E_0 to a few kev is accompanied by a linear increase of the yield. This proved the presence of only kinetic emission under conditions when $V_i < 2\varphi$. Ayukhanov[7] also established that the coefficient for kinetic emission of electrons is small in the case of bombardment of alkali metal (Na, K, Rb & Mg) targets by alkali metal ions.

We felt it would be of interest to investigate the secondary emission from the alkali metals under the influence of noble gas ions, inasmuch as the relatively low value of the work function φ in this case should make it possible to elucidate the role of this important physical parameter of the target in potential emission of electrons. Below we give the preliminary results of our experiments on secondary electron emission from sodium films under bombardment by argon ions.

Apparatus and Experimental Procedure

The experiments were carried out in the apparatus employed in our earlier work[3] and modified as described in Ref.8 (preceding article).

The sodium target was prepared by evaporative deposition of metallic sodium on a tantalum backing (30 x 7 x 0.015 mm); the backing was supported by heavy molybdenum leads, which served to conduct the current for heating the target to the requisite temperature.

The vaporizer unit consisted of a tantalum heater oriented towards the surface of the target at an angle of 45° to the normal. The atomic beam obtained by evaporation of the sodium charge in the heater was incident on the target surface through an aperture in the shielding cylinder and collector. The rate of evaporation and hence deposition was regulated by varying the heater temperature.

Use of the method of continuous deposition of the sodium coating imposed certain special requirements on the measurement procedure. As the procedure meeting these requirements we employed the method of double modulation proposed in Ref.9 (also see preceding article), which allows of obtaining the secondary current volt-ampere characteristics on the screen of an oscillograph for each state of the target surface. The rapidly varying oscillograph pattern was recorded by means of a motion picture camera at intervals of 0.5 sec with an exposure of 0.2 sec. Thus from the values taken off the consecutive oscillograms we could plot the variation of the secondary emission coefficient as a function of the coating density. In the range of high deposition rates the indicated exposures and intervals between photographs did not provide for obtaining a sufficient number of intermediate points. Hence the recording in the range of high layer guild-up rates was realized by simultaneous switching on the target heater and the motion picture camera, which somewhat extended the duration of the transition process and enabled us to observe the variation of the pattern in the process of cooling of the target.

Experimental Results

The current-voltage characteristics obtained by the method of double modulation in the case of A ion bombardment of Na films in the process of deposition on a Ta backing differ substantially from the corresponding characteristics obtained in the case of bombardment of alkali metal targets[10]. Fig.1 shows a typical current-voltage characteristic obtained in bombardment of an Na film on Ta by 900 ev A ions. It will be evident from the shape of the current-voltage characteristics that the secondary emission comprises two distinct groups of negative particles. One group has a relatively soft energy spectrum, while the other is characterized by a hard spectrum.

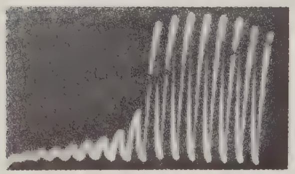

Fig.1. Typical current-voltage characteristic of the secondary negative emission obtained in bombardment of an Na film on Ta with 900 ev argon ions.

Fig.2 shows a series of oscillograms obtained in the process of build-up of the Na coating on the Ta backing with continuous bombardment by 720 ev argon ions; this series pertains to the highest possible rate of deposition (~20 monatomic layers per second) and with a getter operating in the apparatus.

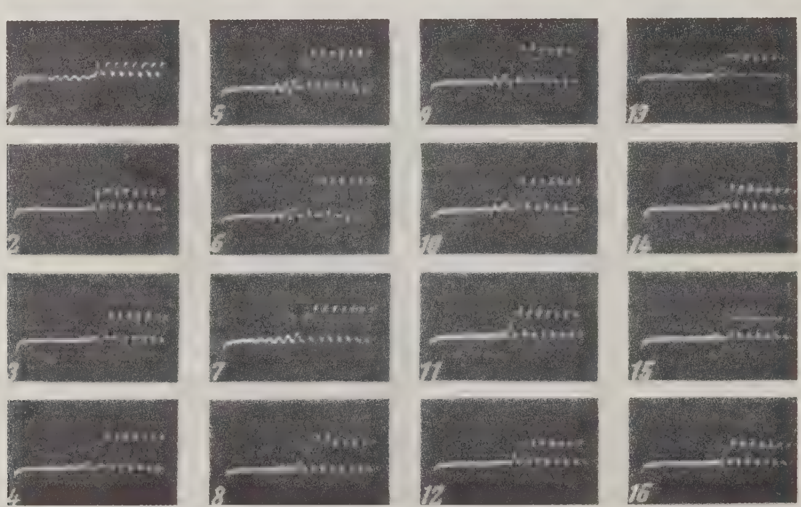

Fig.2. Series of current-voltage oscillgrams recorded at intervals of 0.5 sec with an exposure of 0.2 sec in the process of build-up of an Na coating on a Ta backing under bombardment with 720 ev A ions.

Fig.3 shows the variation with the Na coating density of the coefficients of secondary emission of the negative particles with the soft (a) and the hard (b) energy spectrum; these curves were obtained from a series of oscillograms similar

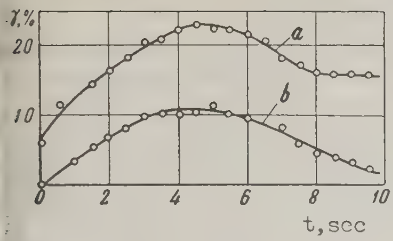

Fig.3. Variation of the coefficients of emission of particle groups with a soft (a) and hard (b) energy spectrum as a function of the thickness (deposition time) of the Na coating on the Ta backing. The curves are based on the series of oscillograms similar to those shown in Fig.2.

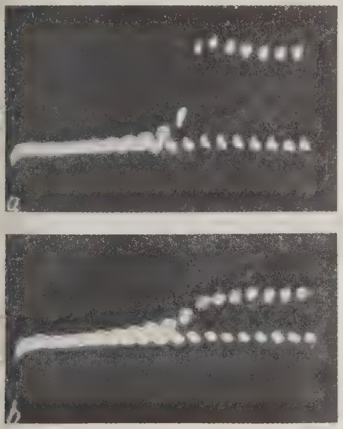

Fig.4. Current-voltage oscillograms obtained in bombarding an Na coating on Ta with 900 ev A ions in the absence (a) and in the presence (b) of a deflecting magnetic field.

to those shown in Fig.2. It will be evident from Fig.3 that emission of the "soft" particles obtains under all conditions of the bombarded surface. In contrast, emission of the "hard" particles is absent in the case of bombardment of a clean Ta surface, and appears and grows with increase in the density of the Na film; it attains a certain maximum value γ_{eff} and then falls off to a lower final value γ_{∞} with further increase in the coating density. This shape of the curves give reason to infer that the "hard" particle group (oscillograms 3-12 in Fig.2) is comprised of negative ions of the adsorbed gases[10].

When a tantalum target is bombarded by argon ions there occurs potential ejection of electrons,[1,11] inasmuch as $(V_i)_A > 2\varphi_{Ta}$. The existence of potential type emission from Ta is also evident from our oscillograms obtained prior to application of the Na film (oscillogram 1 in Fig.2). With deposition of the Na film on the Ta backing the relation between the ionization potential of the bombarding ions and the work function of the target surface can only change in the direction of increase of the above inequality. Consequently, potential ejection of electrons under the action of the incident A ions must obtain for all densities of the Na coating. Hence it may be concluded that the "soft" emission consists of emission of electrons owing to the potential energy of the incident ions.

This inference was checked by further experiments with the same equipment by separation of the electrons from the negative ions by means of a deflecting magnetic field. To this end we introduced an auxiliary collector consisting of two joined semicylinders, located symmetrically about the target; the axis of the collector was aligned with the direction of the primary beam. In the absence of a magnetic field part of the secondary particles is picked up by the main collector, while the other part is received by the auxiliary collector. Now if a magnetic field of 30-40 oersted is applied in the direction parallel to the line connecting the centers of the two semicylinders, the major portion of the secondary electrons will be deflected to the auxiliary collector. Hence in this case there is a noticeable decrease in the number of "soft" particles incident on the main collector.

Fig.4 shows two current-voltage characteristics obtained for the circuit of the main collector in the case of bombardment of Na coating having the density corresponding to oscillgrams 4-11 (Fig.2) with and without a deflecting magnetic field. From a comparison of these two oscillograms it will be evident that the group of secondary particles having the soft energy spectrum is actually removed by a magnetic field, whereas the particles with the hard energy spectrum are not deflected by a magnetic field of the indicated intensity, so that their flux remains virtually unchanged.

This experiment substantiates our inference and shows that it is feasible to separate the secondary electrons from the negative secondary ions.

Application of a magnetic field in the case of coating densities corresponding to oscillograms 1-3 and 14-16 (Fig.2) resulted in almost complete disappearance of all secondary particles. This is evidence of a high degree of cleanness of the Na surface in the deposition stages corresponding to oscillograms 14-16. Thus the value of the potential emission coefficients increases from 6% for clean Ta to 16-17% for Na, which clearly showed that the coefficient of potential emission of electrons depends on the work function of the target metal.

Institute of Nuclear Physics,
Academy of Sciences of the Uzbeck SSR

References

1. H.D.Hagstrum, Phys.Rev., 96, 325 (1954); Phys.Rev., 104, 672 (1956).
2. V.G.Tel'kovskii, Doklady AN SSSR, 108, 445 (1956) (Trans.Doklady); Izv. AN SSSR, Ser.fiz., 20, 1179 (1956). (Trans.Bulletin, 20, 1070.)
3. U.A.Arifov & R.Rakhimov, Izv.AN UzSSR, Ser.fiz.-mat.nauk, (Bulletin, Uzbek SSR Ac. of Sci., Phys.-Math.Science Series), No.5, 5 (1958).
4. U.A.Arifov & A.Kh.Ayukhanov, Doklady AN UzSSR (Doklady, Uzbek SSR Ac. of Sci.) 4, 12 (1951); Izv.AN SSSR, Ser.fiz., 20, 1165 (1956). (Trans.Bulletin, 20, 1057.)
5. M.A.Eremeev & V.V.Shestukhina, Zhur.tekh.fiz., 22, 1262 (1952).
6. C.Brunee, Z.Phys., 147, 161 (1957).
7. A.Kh.Ayukhanov, Thesis, Physical-Technical Institute, Uzbek SSR Ac. of Sci., Tashkent, 1956.
8. U.A.Arifov & R.R.Rakhimov, Present issue of the Bulletin, p.666.
9. U.A.Arifov, A.Kh.Ayukhanov & S.V.Starodubtsev, Zhur.eksp.i teor.fiz., 26, 714 (1954).
10. U.A.Arifov, A.Kh.Ayukhanov & S.N.Starodubtsev, Izv.AN UzSSR, Ser.fiz.-mat. nauk (Bulletin, Uzbek SSR Ac.of Sci., Phys.-Math.Science Series), No.2, 49 (1958).
11. U.A.Arifov & R.Rakhimov, Ibid., No.6, (1958).

ON THE PROBLEM OF MEASURING PROTON BEAM CURRENTS*

- P.Görlich, C.Keck, H.Krause, A.Krohs, H.-J.Pohl & F.Schlott

Introduction

In the course of investigating[1] selenium phototubes we arrived at the conclusion that in some cases for detecting radiation from radioactive isotopes and other sources it may be preferable to employ a photocell in conjunction with a scintillator instead of the usual scintillator + photomultiplier combination.

The data for comparison were obtained by investigating the suitability of different photoelectric devices for measuring proton fluxes. We worked both with and without scintillators, i.e., tested direct irradiation of the photocell by the proton flux. For some detector combinations we determined the relative value of the signal current and its variation with the proton current.

By way of scintillators we chose thallium activated CsI single crystals** since selenium photocells are particularly efficient in converting the green luminescence of such crystals to an electric signal.

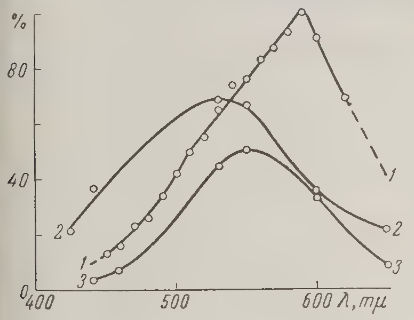

Fig.1. Spectral distribution of the scintillation of a CsI(Tl) single crystal (1) and the quantum efficiency of a selenium type F photocell (2); curve 3 is the product of curves 1 and 2.

Fig.1 shows the wavelength distribution of the response of a type F selenium photocell[1], and the product of the spectral distribution of the emission of a CsI(Tl) crystal by the quantum efficiency of the selenium photocell. It will be evident from the figure that this photocell converts 40-50% of the scintillation into an electric signal. Despite the obvious nonlinearity obtaining at high current values, this combination is entirely acceptable. We also note that it is feasible to fabricate such photocells with any desired shape and size of the sensitive element, and that one can also enhance their sensitivity as regards response in the low luminance range.

It might be assumed that the light output of inorganic single crystals in the high flux range may not be proportional to the proton current density. In order to check this we combined a CsI(Tl) scintillator with a linear response photocell. As is known, the maximum quantum efficiency of photocells does not exceed unity, inasmuch as the amplification mechanism (like the amplification mechanism of photoconductors) cannot be very efficient in such cells. In order to explore the possibility of increasing the sensitivity we also used photoconductors in the form of a CdS single crystal and a flat type CdSe cell. The spectral distribution curves of a CsI(Tl) scintillator in conjunction with both types of photocells are in fairly good agreement. In a separate series of experiments the photocells and photoconductors were subjected to direct proton bombardment.

Experimental Procedure and Results

The proton source utilized for the measurements was the Dresden cyclotron. The ratio of the current on and off times was constant and equal to 1:1 (sometimes

---

*Some of the results of this investigation were presented by H.-J.Pohl at the conference held in Dubna, 24-26 February 1960.

**The single crystals were obtained from the laboratory of the C.Zeiss National Enterprise.

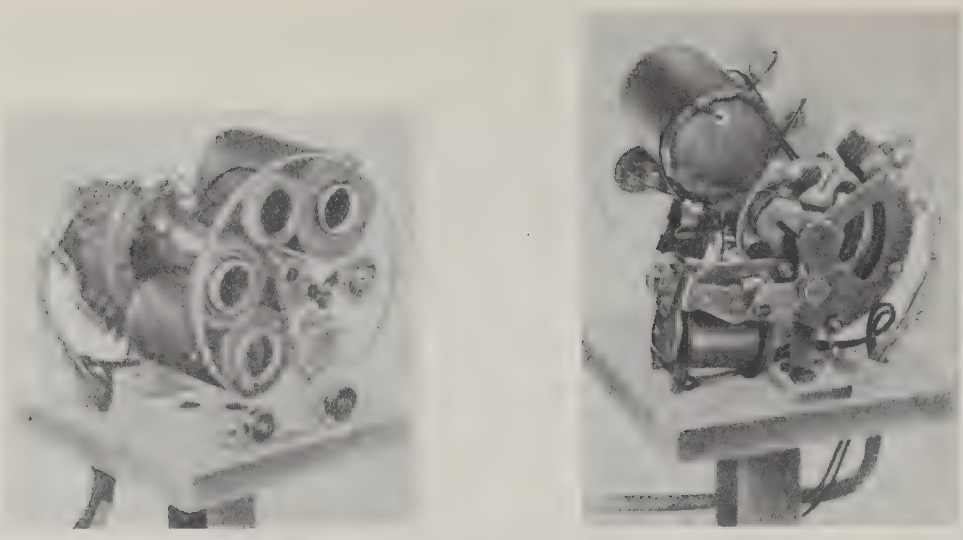

Fig.2. Front and rear views of the indexing device mounting six test detectors.

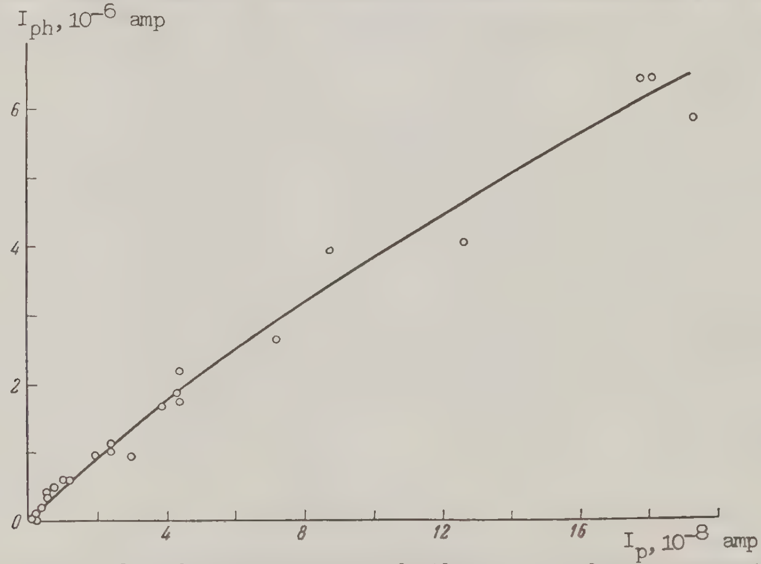

Fig.3. Variation of the photocurrent with the proton beam current for the photocell + CsI scintillator combination.

1:2) at a pulse frequency of 25 cps. The proton beam incident on the detectors was defined by a tungsten diaphragm with a 15 mm diameter aperture. The effective working area of all the photoelectric detectors was the same (except for the CdS single crystals which measured 0.15 x 5 mm). The magnitude of the proton current was varied in the range from $1 \cdot 10^{-8}$ to $2 \cdot 10^{-7}$ amp by defocusing the beam before it entered the reaction chamber. The proton energy was 6.7 Mev. The different detectors were mounted in the revolving disk of the indexing device shown in Fig.2. The interchangeable detectors comprised a) a CdS single crystal, b) a flat type CdSe photocell coupled to a CsI(Tl) scintillator, c) a photocell coupled to a CsI(Tl) scintillator, d) an F type* selenium photoelectric cell coupled to a

---

*F type cell = selenium photocell with a thin CdS film between the barrier layer and the transparent coating.

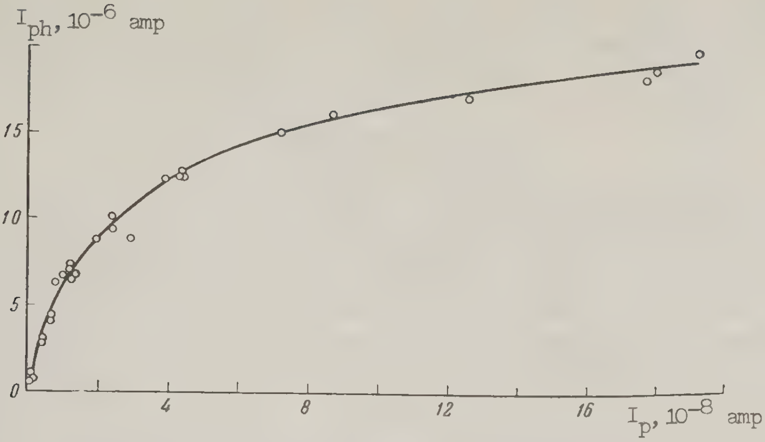

Fig.4. Variation of the photocurrent with the proton current for the type F selenium cell + scintillator combination.

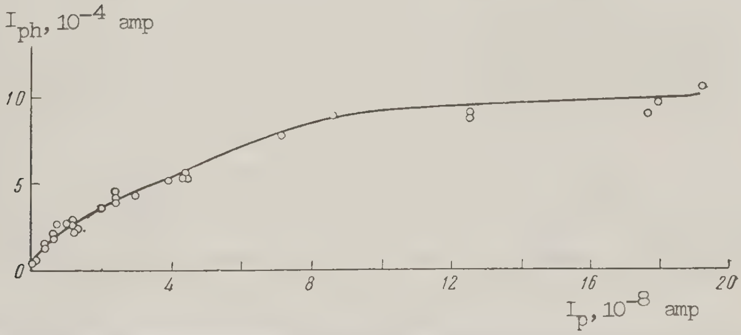

Fig.5. Variation of the photocurrent with the proton current for the flat CdSe cell + scintillator combination.

CsI(Tl) scintillator, e) an F type selenium photoelectric cell and f) a 50 mm long Faraday cylinder.

The experimental results obtained for the various detectors are shown in Figs. 3 through 7. It was impossible to maintain a rigorously constant proton beam current for a sufficiently long time to test all the detectors in sequence; consequently, the results are not as accurate as might be desired.

It will be evident from Fig.3 that in the range of high loads the scintillation output of the CsI single crystal is not fully proportional to the proton beam current.

Figs.4 & 5 show the results of experiments in which the light from the scintillator crystal was incident on a type F selenium photoelectric cell and on a flat type CdSe cell. The CdSe photoconductor grid covered approximately 50% of the surface turned to the light. With a better grid design one could expect a higher sensitivity. The operating voltage was 6 v. It should be possible to increase the amplification factor by increasing the voltage. Thus the CdSe photoconductor + CsI(Tl) scintillator combination assures a 100 times greater signal current than the selenium photoelectric cell + CsI(Tl) scintillator combination.

The results of direct bombardment of the barrier type selenium cell and a CdS single crystal photoconductor are shown in Figs.6 & 7. For both types of photocells there were obtained curves similar to those recorded with excitation of the respective cells by scintillations. On the basis of the data obtained so far one

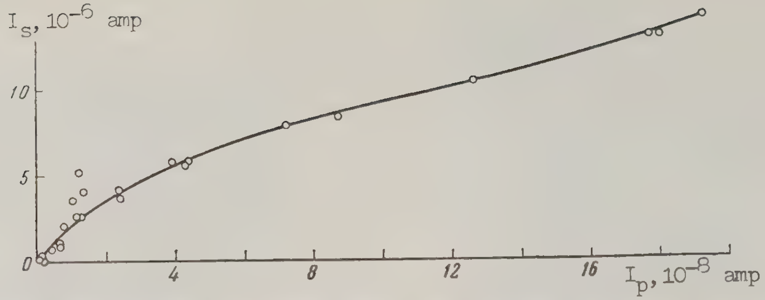

Fig.6. Variation of the signal current with the proton current in case of direct bombardment of the F type selenium photocell.

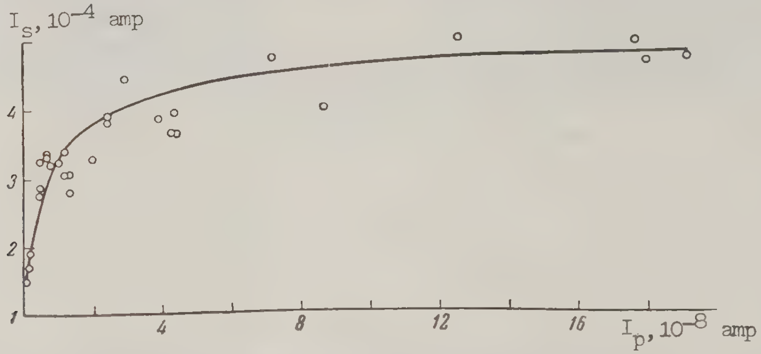

Fig.7. Variation of the signal current with the proton current in the case of direct bombardment of a CdS single crystal.

cannot say whether the mechanism of proton excitation is similar to the photoeffect mechanism; further and more thorough studies are necessary to answer this question.

We call the ratio of the signal current to the proton beam current the effective yield and denote it by A. For the scintillator + photocell combination we obtained A = 34 at a proton current of 0.2 μa, while for the scintillator + selenium cell combination we obtained A = 100. The higher value of A in the second case is explained by the higher quantum efficiency of the selenium cell in the region of the scintillator emission. Actually the emission of an NaI(Tl) scintillator would be more suitable for a Cs_3Sb type photocathode, but NaI scintillators have a number of undesirable properties (for example, they are highly hygroscopic). It is feasible to increase the yield and obtain a linear response for the scintillator + selenium photocell combination by reducing the operating resistance.

For the CsI(Tl) scintillator + CdSe photoconductor cell we obtained A ≈ 5000. Increase of the yield is possible by changing the ratio of the grid area to the receptor area, which in our case was 1:1, and by increasing the voltage applied to the cell, which in our case was 6 v.

In the case of direct incidence of the protons on the F type selenium photoelectric cell we obtained A = 70 for I_p = 0.2 μa and A = 180 for I_p = 0.02 μa. The readings in this case were characterized by exceptional stability. Direct proton bombardment of the photoconductor led to unexpectedly high values of the signal current. At a proton current of 0.2 μa, we obtained A = 860 000, while at a proton current of 0.02 μa, the yield A = 8 000 000.

With excitation by 6 Mev protons the quantum yield proves to be 100-1000 times greater than with excitation by green light. Thus the CdS photoconductive cell proves to be an extremely sensitive and compact detector for proton currents, although admittedly its stability is inferior to that of a selenium phototube.

Conclusions

The use of photoelectric devices (with and without scintillators) as radiation detectors* enabled us to investigate a number of hitherto unexplored effects. Thus, for example, we found it possible to measure directly proton currents in the range under 10^{-10} amp, i.e., proton fluxes amounting to 10^{10} protons/sec. In the case of proton fluxes $>10^{6}$ proton/sec, measurements by means of conventional scintillation equipment are difficult owing to the inadequate time resolution of the digital registers.

We note that for our integral measurements we utilized scintillators with a rather large working area (25 mm diameter) in conjunction with selenium photoelectric cells; on the other hand, the sensitivity and small size of the CdS photoconductive cells facilitated investigation of the spatial relationships of the radiation fields.

We believe the detectors tested by us would be convenient for measurements of low intensities in working with mass spectrometers. We plan to continue our investigations and hope to obtain information regarding the changes occurring in selenium phototubes and in cadmium sulfide and cadmium selenide photolayers under the influence of proton bombardment. Such data could serve for more precise determination of the operating stability of proton detectors.

We desire to express our gratitude to the Chief of the Cyclotron Section, Chief Engineer Hickman (Department of Nuclear Physics under Prof.Schintlmeister) for assistance in the measurements.

Central Institute for Nuclear Studies, Dresden &
C.Zeiss National Enterprise, Jena, German Democratic Republic

Reference

1. G.Dietzel, P.Görlich & A.Krohs, Arbeitstagung Festkörperphys. u. Phys. d. Leuchtstoffe in Erfurt, 110 (1958); Jenaer Jb., 1, 203 (1958).

INVESTIGATION OF COLLISION OF IONS WITH METAL SURFACES

- N.N.Petrov

Impact of ions on metal surfaces is accompanied by a number of different processes, investigation of which is of both practical and scientific interest. Investigation of ion-electron emission and the reflection of ions from a metal surface can yield important information on electronic transitions occurring incident to collision of the ions with the atoms of the target and can further our understanding of the nature of the collision mechanism.

Recently there have been notable advances in the investigation[1-4] of potential ejection of electrons, a process which does not necessarily require actual impact of the bombarding particles on the surface, a close approach being sufficient. In contrast, kinetic knocking out of electrons has not been as thoroughly studied, for there have been relatively few experimental investigations carried out with reproducible and well defined conditions of the target surface. It has been definitely established only that up to an ion energy of the order of 1 kev kinetic ejection of electrons both by alkali metal ions[5,6] and by noble gas ions[2,3] (for He^+ up to $E \approx 0.4$ kev) is virtually nil. As yet there are no reliable quantitative data on the variation of the emission coefficient γ as a function of the ion energy.

In order to elucidate the processes occurring incident to kinetic ejection of electrons and to establish the regularities involved in the effect, we undertook an investigation of the emission from targets of high melting point metals under ion bombardment; in designing the experiments we paid particular attention to the state of the target surface.

With a view to establishing the role of the structure of the electron shells of the bombarding ions in the process of kinetic ejection we decided to carry out comparative measurements of the secondary emission from targets bombarded with atoms of potassium and argon, elements that neighbor in the periodic table. The electron configuration of a potassium ion is similar to the configuration of an argon atom (the $3p$ shell is filled), while the configuration of the electron shell of an argon ion is similar to the configuration of a chlorine atom (one electron missing from the $3p$ shell).

The principal experimental difficulty in working with alkali metal ions is contamination of the target surface by the ion beam itself. It is important to note also that during the measurement of ion-electron emission from a heated target the current of particles undergoing positive surface ionization on the target is blocked, which greatly hampers cleaning of the target. Hence we developed a special technique which made it possible for the first time to measure an appreciable thermionic emission at high temperatures of the target.

The ion beam was modulated with a frequency of several hundred cycles.[7] The target-collector network comprised a resonance circuit tuned to this frequency. This circuit passed the dc component of the thermionic emission, but discriminated the first harmonic of the modulated secondary emission current, which was applied to a narrow band amplifier connected to an oscillograph and a vacuum tube voltmeter. Comparing the secondary and primary current oscillograms we could judge of the polarity of the secondary current, while the vacuum-tube voltmeter facilitated determining its absolute magnitude. We took the ratio of the amplitude of the secondary current, with the collector-to-target potential $V_c \gg 0$ high enough to obviate limiting of the current by space charge, to the amplitude of the primary ion current as the coefficient α, which in the absence of reflected ions with an energy exceeding ϵV_c becomes the secondary emission coefficient γ.

Measurements of the coefficients α and γ, carried out at target temperatures up to 2000°K, showed that these coefficients did not depend on the intensity of

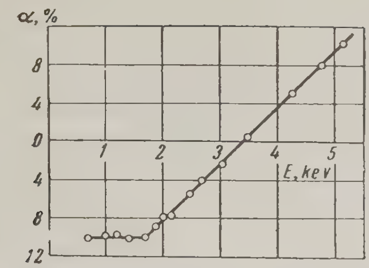

Fig.1. Variation of the coefficient α with the K ion energy for a tungsten target.

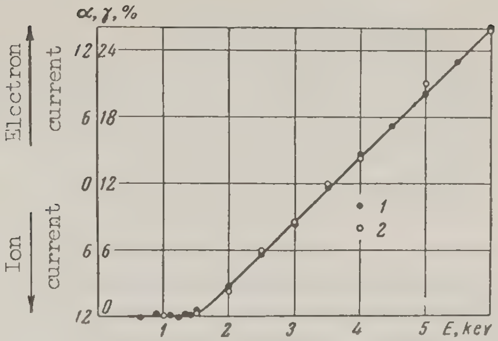

Fig.2. Variation of the kinetic electron ejection coefficient with the energy of bombarding potassium (1) and argon (2) ions.

the ion beam, which was taken as evidence that the target surface was truly clean. All measurements were made at pressures not exceeding $1 \cdot 10^{-6}$ mm Hg. The collector potential was lower than the target potential at all times except at the actual instants of measurement of α.

Fig.1 shows the variation of α with the energy E for potassium ions bombarding a tungsten target at $T = 1900^{\circ}K$. Up to $E \approx 1.6$ kev the coefficient α is negative and does not depend on the ion energy. At higher ion energies the coefficient begins to increase linearly, the increase continuing uniformly over the entire investigated energy interval. Variation of the target temperature had only a weak effect on the value of α in the range of low ion energies; the α plateau persisted and there was no change in the slope of the $\alpha = f(E)$ line relative to the energy axis in the region $E > 1.7$ kev. Similar data were obtained for a tantalum target; within the limits of the experimental error we obtained the same value of E corresponding to the break in the curve and the same slope of the straight line plot for $E > 1.5$-1.8 kev.

It will be evident from the experimental data that at energies $E < 1.6$ kev the collector receives a current of fast reflected ions: approximately 8-11% of the primary ions are reflected from the target, retaining energies exceeding ϵV_c (the data of Fig.1 were obtained with $V_c = + 300$ v). At the same time there is virtually no ejection of electrons from the target in this energy range; electron ejection begins only at $E > 1.5$-1.7 ev, and thereafter the coefficient γ varies linearly with the primary ion energy. This linear variation obtains if the fraction of fast ions reaching the collector does not depend on the energy of the primary ion beam.

The solid circle points in Fig.2 give the averaged values of γ for Ta and W targets obtained by setting $\gamma = 0$ for the emission level of the α plateau. It will be evident that the end-point energy E_{ep} equals approximately 1.5 kev, while the value of γ attains 26% for $E = 6$ kev.

Experiments[8] with argon ions were carried out in a different apparatus with a gas discharge type ion source and a sector type magnetic mass analyzer. In these experiments we used the static galvanometer measurement procedure inasmuch as noble gas ions cannot "contaminate" the target surface (at the experimental temperatures - 1400-$1500^{\circ}K$ - the probability for retention of noble gas atoms in the metal lattice is vanishingly small[9]). The preliminary treatment of the target, as in the work with K ions, consisted of prolonged heating at $> 2000^{\circ}K$. The pressure of the adsorbable residual gas components was lower than 10^{-6} mm Hg.

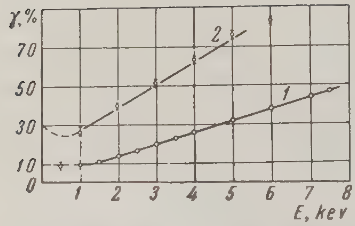

Fig.3. Variation of the coefficient γ with the energy of argon (1) and helium (2) ions bombarding a tantalum target.

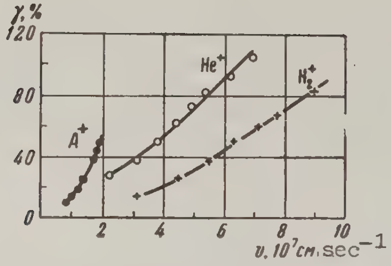

Fig.4. Variation of the coefficient γ with the velocity of H_2^+, He^+ and A^+ ions bombarding a tantalum target.

The data for A ions bombarding a heated tantalum target are shown in Fig.3 (curve 1). It will be seen that at ion energies > 1.5 kev there occurs linear increase of γ over the entire investigated energy interval (to 7.5 kev). In the range of low energies the emission coefficient is approximately 10% and does not depend on E, which indicates that in this interval the electron ejection is potential in character (cf. Hagstrum[2,3]). Assuming that the emission due to the potential ejection mechanism is 10%, and subtracting this value from the experimental data, we find the values of γ due solely to the kinetic energy of the incident ions, i.e., to kinetic ejection. Naturally, the data obtained in this manner will be valid only provided the potential ejection in the range $E > 1.5$ is also independent of the ion energy; however, this can hardly be doubted. The average results obtained in this manner have been plotted in Fig.2 (open circles), and show that there is complete agreement as regards kinetic ejection by potassium and argon ions.

Investigation of the secondary emission from a tantalum target bombarded with helium ions (curve 2 in Fig.3), as well as by molecular hydrogen ions[2], showed that the E dependence of γ is essentially linear in the energy range from 1 to 5 kev for He^+ and 1 to 4 kev for H_2^+, while in the ragne of higher ion energies there is observed a decrease in the rate of growth of γ with energy ($d^2\gamma/dE^2 < 0$).

Thus the energy dependence of the emission coefficient can be written in analytic form

$$\gamma = \gamma_{pot} + C(E - E_{ep}),$$

where γ_{pot} is the emission coefficient due to potential ejection of electrons (in the first approximation it is assumed to be independent of E), E_{ep} is the end-point ion energy, and $C = d\gamma/dE$. Obviously, for $E < E_{ep}$, the constant $C = 0$; for $E > E_{ep}$, C remains constant over some energy interval and then decreases and in fact at very high values of E may even become negative. Thus the parameters γ_{pot}, C and E_{ep} fully characterize the variation of the ion-electron emission as a function of the ion energy. The constant C depends on the type of ions and is usually of the order of a few percent per kiloelectronvolt.

In addition to the ion energy dependence of γ, it is of interest to consider the ion velocity dependence of this coefficient; the said dependence can readily be calculated from the γ vs E data (Fig.4). For He^+ and H_2^+ ions with energies above approximately 5 kev, there obtains a linear dependence of γ on v, i.e., a dependence analogous to that observed by Tel'kovskii[10] for a molybdenum target.

It should be noted, however, that extrapolation of the linear sections of the plots does not yield a physically meaningful "threshold" velocity, inasmuch as at ion energies close to E_{ep} the curves bend over and the linear dependence of γ on the velocity fails.

Our earlier experiments[8] on ion-electron emission from Mo and W targets under the influence of Cd^+ ions with energies from 0.3 to 1 kev and Zn^+ ions with energies up to 1.6 kev showed that in these cases also there is no kinetic ejection of electrons in these low energy intervals.

Thus on the basis of all the experimental data we arrive at the following deductions.

1. There is a certain ion end-point energy E_{ep} below which the ions do not knock out electrons through expenditure of their kinetic energy.

2. Above E_{ep} the energy dependence of the emission coefficient γ is linear in an energy interval that is the wider, the greater the mass of the bombarding particles.

3. With further increase of the ion energy there still obtains a linear dependence of γ on the ion velocity, but at still higher values of E the growth of γ with v also slows down.

4. K and A ions, despite a substantial difference between their electron shells, yield equal kinetic ejection of electrons, which in the 0.5 to 6 kev ion energy interval does not depend on the type of target (Ta or W).

Consideration[11] of the processes leading to ion-electron emission led us to the conclusion that kinetic ejection of electrons is due primarily to excitation by the incident ion of the bound electrons of the metal, to which, however, there can be transferred only an energy above a certain minimum value determined by the width of the forbidden gap and the filled part of the conduction band. Consequently, there must exist a certain end-point energy, below which kinetic ejection should not be observed. Inasmuch as presumably only a fraction of the total ion energy can be transferred to an electron, it must be assumed that the height of this "threshold" for kinetic ejection cannot be very low.

One may tentatively describe the process of collision of an ion with the surface of a metal as follows. Upon approaching the surface, the ion enters into intimate interaction with one or two ions of the lattice, as a result of which the potential energy of the system of colliding particles is increased at the expense of the kinetic energy of the ion.

For slow ions there may obtain inverse energy conversion, that is, all the potential energy is converted to kinetic energy of the colliding particles and there occurs repulsion, i.e., reflection of the primary particles and cathode sputtering. At ion energies $E \approx E_{ep}$ the potential energy of the system of particles at the instant of closest approach increases to the extent where one of the most weakly bound electrons can be excited above the Fermi level in the metal, which is sufficient for the appearance of ion-electron emission (in the case of filling of a hole in the main band, the energy liberated by an Auger type process may be transferred to another electron in the conduction zone, which can then emerge into the vacuum).

The mechanism of transfer and conversion of the potential energy of the system of interacting particles to kinetic energy of one of the electrons is admittedly still obscure. In order to clarify it, it is essential to carry out a quantum mechanical treatment of all the processes accompanying collision; these are presumably similar to those obtaining in collisions of ions with gaseous atoms. Close approach of the particles involves overlapping of their electron clouds, the extent of which will be the greater, the higher the kinetic energy of the ion, and to satisfy the Pauli principle, the electrons must occupy coordinates in phase space corresponding to maximum momentum values. In the case of sufficiently close approach of the particles ($E \approx E_{ep}$), it becomes possible for one of the electrons of the system of interacting particles to be excited into the unoccupied band of the metal.

Comparing the results of the various experimental investigations with what might be expected on the basis of the proposed hypothesis, we note satisfactory qualitative agreement. In particular, we can explain such hitherto puzzling matters as the absence of correlation between the ion-electron emission and the work function of the target, and the influence of contamination of the target on the electron yield. As is known, the presence of foreign particles on the target surface usually increases γ, which can be explained by hypothesizing the existence on such contaminated surfaces of localized electrons that are more weakly bound than the proper electrons of the metal. The proposed hypothesis also serves to explain the much greater kinetic ejection of electrons from dielectrics as compared with metals[12] (electrons in most dielectrics are more weakly bound than the electrons in the main band of metals, and there are no energy losses owing to interaction with conduction electrons).

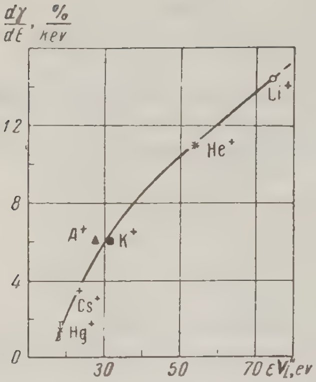

Fig.5. Variation of $d\gamma/dE$ with the second ionization potential of atoms of elements the ions of which bombard the target; energy range $E > E_{ep}$.

In analyzing the above data for K and A ions it is important to bear in mind another point. At first glance one might think that the principal reason for the equal kinetic ejection of electrons by these ions is the near identity of their masses. However, data for other types of ions[5,7,8] show that Li^+ more effectively knocks out electrons than lighter He^+, while Cs^+ is more effective than the heavier Hg^+, that is, there is no direct correlation between the efficiency as regards kinetic ejection and the mass of the bombarding ions. However, aside from having close mass values, potassium and argon atoms have very close values of the second ionization potential, which characterizes the energy of the outer electron in the ions of these elements. Hence we plotted the variation of $d\gamma/dE$ as a function of the second ionization potential of the atoms of elements, the ions of which were used for bombarding targets (Fig.5 - data from Refs.5,7 & 8). It will be seen that the experimental points fit a single curve, which can readily be extrapolated to the zero value of $d\gamma/dE$. Such extrapolation shows that kinetic ejection should be absent below values of $\varepsilon V_i'' \approx 17$ ev. At very low values of the second ionization potential V_i'', however, one can expect some stripping of electrons from the bombarding ions, i.e., one may still expect to observe ejection of electrons, but actually from the bombarding ions rather than the bombarded target.

The available experimental data are still inadequate to establish the precise variation of the slope of the $\gamma = f(E)$ lines with the second ionization potential of the atoms comprising the bombarding particles, but further investigation in this direction may yield valuable information for understanding the mechanism of kinetic ejection of electron by ions.

References

1. Sh.Sh.Shekhter, Zhur.eksp.i teor.fiz., 7, 750 (1937).
2. H.D.Hagstrum, Phys.Rev., 96, 325 (1954); Phys.Rev., 104, 317 (1956).
3. H.D.Hagstrum, Ibid., 104, 672 (1956).
4. H.D.Hagstrum, Ibid., 96, 336 (1954).
5. M.A.Eremeev, Thesis, Leningrad Polytechnic Institute, L., 1952.

6. U.A.Arifov, Thesis, Leningrad Physical-Technical Institute, USSR Ac. of Sci. & Phys.-Tech.Inst., Uzbek SSR Ac. of Sci., Leningrad-Tashkent, 1954.
7. N.N.Petrov, Zhur.fiz.tverdogo tela, 2, No.5 (1960). (Trans.Soviet Physics - Solid State.)
8. N.N.Petrov, Ibid., 2, No.5 (1960). (Trans.Ibid.)
9. S.Thulin, Arkiv.fys., 9, 107 (1955).
10. V.G.Tel'kovskii, Izv.AN SSSR, Ser.fiz., 20, 1179 (1956). (Trans.Bulletin, 20, 1070.)
11. N.N.Petrov, Zhur.fiz.tverdogo tela, 2, No.6 (1960). (Trans.Soviet Phys. - Solid State.)
12. G.M.Batanov & N.N.Petrov, Ibid., 1, 1856 (1959). (Trans.Ibid.)

* * * * * * * * *

ETCHING DISINTEGRATION OF SEMICONDUCTOR SURFACES BY ION BOMBARDMENT

- I.G.Sirotenko & G.V.Spivak

The present investigation was concerned with cathode sputtering of polycrystalline and single crystal semiconductors: germanium, silicon and ferrites. Our principal aims were the following.

1. To subject to ion-bombardment etching a large and extensive group of semiconductors, since hitherto such etching of only germanium and silicon has been studied and the published results are to some extent contradictory.
2. To conduct the experiments in the region of ion kinetic energies appreciably above the threshold value ($\geqslant 1$ kv) and thus determine the sputtering conditions for semiconductors, under which oriented formations develop on the surface within a reasonable time.
3. To investigate the microrelief appearing on semiconductors with a view to utilizing the surface projections for possible future investigation of field emission.
4. To identify the etching effects on semiconductor surfaces that might occur in thermionic tubes and similar devices, and impair their normal operation.

As a result of cathode sputtering in discharges in noble gases there form on the targets at the points of imperfections of their crystal lattice etch figures, the shape and orientation of which are generally characteristic of the given grain or face.[1-3] These oriented formations are similar to the figures developed by chemical etching of metals. Thus the figures produced by cathode sputtering can serve for determining the symmetry of single crystal faces and polycrystalline grains, and also for bringing out irregularities in the surface layers.

The ion bombardment etching technique allows of carrying on observations at high temperatures and insuring a high degree of cleanness of the surface, conditions which cannot be realized in chemical etching. Ionic disintegration of germanium and silicon has been investigated by a number of authors, particularly in connection with preparation of atomically clean surfaces. Honig[4] observed the appearance of pits and hillocks on the surfaces of germanium and silicon. Wolsky[5] reported on the etching of germanium and silicon as a result of bombardment with argon ions in a low pressure discharge. On the other hand, Dillon & Farnsworth[6] did not observe preferential etching of germanium surfaces under bombardment with argon ions. The above mentioned investigators worked in the ion energy region to 400 ev and with low current densities. Wehner[7] investigated the sputtering of germanium single crystals by normal incident Hg ions with energies close to the threshold value (50-100 ev), in a low pressure (~1 μ) plasma; he found that there appear on the germanium surface oriented depressions correlated with the orientation of the crystal. Meckel & Swalin[8] describe the appearance of truncated conical hillocks on the (111) and (110) faces of germanium as a result of bombardment with argon ions. Hence the investigation of surfaces subjected to controlled sputtering by ion bombardment can yield interesting information from the standpoint of crystallography and metallography.

Experimental Procedure and Results

Initially we investigated cathode sputtering of silicon, germanium and ferrites in a glow discharge in a two-electron tube in argon and krypton and in neon in the UIT-1 ionic etching unit. In these cases, however, cathode sputtering is a function of the geometry of the tube and gas pressure, and owing to appreciable energy straggling of the bombarding ions and variations in their angle of incidence on the target and also because of return of part of the sputtered material back to the target, interpretation of the results is difficult. Moreover, noticeable etching effects in such devices appear only after rather prolonged sputtering.

Clearer and more prompt results are obtained when the target is immersed in a low pressure plasma of high density.[9] In etching by this technique a relatively low gas pressure is utilized in the tube containing a heated cathode; return deposition of the sputtered material on the target can be reduced to a minimum, and the number of ion-atom collisions in the ion sheath is materially reduced. Moreover, high density of the ion current obviates contamination of the target surface, and the sputtering process is noticeably accelerated. If the target is large compared with the thickness of the ion sheath, the angle of incidence of the ions will be normal to the surface. In our experiments targets of germanium, silicon and ferrites were immersed in a krypton plasma, which was produced in a three-electrode tube between the anode and the tungsten cathode, which was heated to promote ionization of the discharge gap. In most cases the specimens were sputtered with a discharge current of 1.5 amp and a krypton pressure from 1 to 50 μ. To allow of rapid interchange of specimens, the tube was of the demountable type and was not outgassed. Prior to being immersed in the plasma, the specimens were polished mechanically with alumdum or chromic oxide, followed by washing in alcohol

Our experiments definitely showed that under the influence of ion bombardment there occurred etching disintegration of the semiconductor surfaces; on the low-index planes there frequently appeared oriented etch figures, reflecting the symmetry of the given face. Fig.1 shows a photograph of a (100) plane of a germanium single crystal after etching at a voltage of 1 kv, a current density of 8 ma/cm^2 and a pressure of 1 micron for 30 min. The surface consists of formations of fourfold symmetry with flat sections almost parallel to the face. It is interesting to note that in cases of sputtering of the same face but at other voltages and current densities and at a higher pressure, there was obtained a different relief consisting of etch pits but devoid of oriented figures.

In the case of sputtering of the (110) face of a germanium single crystal there appear figures of twofold symmetry (Fig.2). The illustrated figures were obtained as a result of 55 min sputtering at 1 kv with a current density of 5 ma/cm^2 and a pressure of 1 micron.

As a result of sputtering of the (111) face of a germanium single crystal for one hour at $V = 1$ kv, $i = 5$ ma/cm^2 and $p = 2 \cdot 10^{-2}$ mm Hg, there appeared on this surface rounded figures of threefold symmetry (Fig.3).

In another case we observed the formation of truncated conical etch pits on a germanium surface close to the (111) plane, etched for 45 min at a pressure of 1 micron.

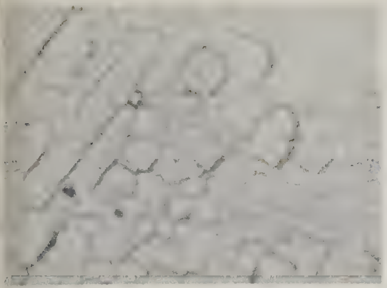

Fig.1. Micrograph of (100) plane of Ge. Sputtering conditions: V = 1 kv, i = 8 ma/cm^2, p = 10^{-3} mm Hg, t = = 30 min. 250 X.

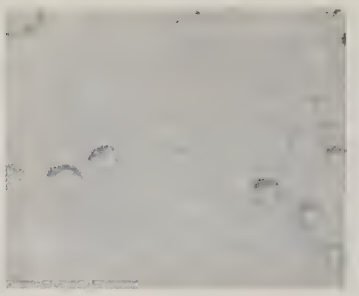

Fig.2. Micrograph of (110) plane of Ge. Sputtering conditions: V = 1 kv, i = 5 ma/cm^2, p = 10^{-3} mm Hg, t = = 55 min. 250 X.

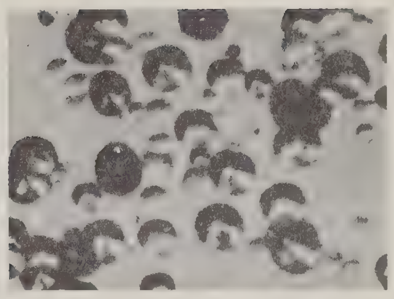

Fig.3. Micrograph of (111) plane of Ge. Sputtering conditions: V = 1 kv, i = 5 ma/cm^2, p = 2·10^{-2} mm Hg, t = = 1 hr. 250 X.

Fig.4. Germanium surface close to (111) plane. Sputtering conditions: V = 1 kv, i = 3 ma/cm^2, p = 10^{-3} mm Hg, t = 45 min. 600 X.

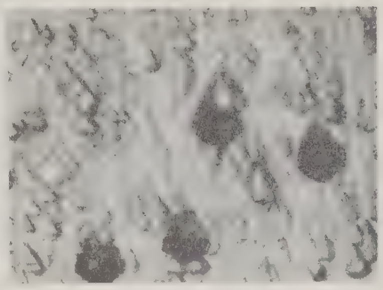

Fig.5. Cleavage plane of manganese ferrite. Sputtering conditions: V = = 1.4 kv, i = 12 ma/cm^2, p = 2·10^{-2} mm Hg, t = 2 hr. 600 X.

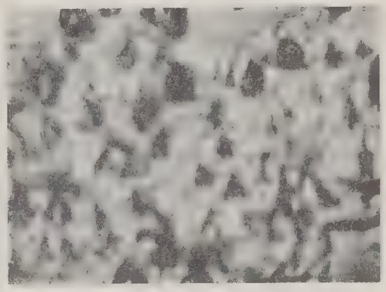

Fig.6. Micrograph of manganese ferrite surface (orientation not determined). Sputtered for 1 hour. 600 X.

Thus oriented figures appear on the crystallographic faces of germanium as a result of etching at voltages of the order of 1 kv and current densities from 3 to 8 ma/cm^2. On the surface of a manganese ferrite single crystal, close to the (100) cleavage plane there appeared after etching for 2 hours at V = 1.4 kv, i = 12 ma/cm^2 and p = 2·10^{-2} mm Hg tetrahedral pyramids, elongated somewhat in one direction (Fig.5).

As a result of one hour sputtering of one of the faces of a manganese ferrite single crystal (orientation not determined) there appeared the relief shown in the micrograph of Fig.6. In addition to single crystal ferrites, we also sputtered polycrystalline specimens. Sometimes the figures appearing on germanium and silicon surfaces consisted primarily of etch pits and are reminiscent of the pattern obtained by chemical etching (Fig.7). A typical surface pattern obtained after prolonged sputtering of the (111) face of germanium is shown in Fig.8.

Wolsky & Pattel[10] observed the formation of hillocks and pits as a result of sputtering with slow ions. In the case of the (100) plane of germanium and the (111) face of silicon there were obtained numerous spiral formations. The

Fig.7. Micrograph of (111) face of silicon. Sputtering conditions: $V = 1.2$ kv, $i = 3$ ma/cm^2, $p = 3\cdot10^{-2}$ mm Hg, $t = 1.6$ hr. 250 X.

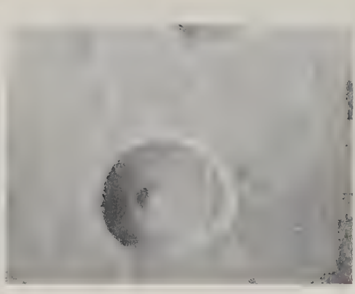
Fig.8. Micrograph of (111) germanium surface subjected to prolonged sputtering. 600 X.

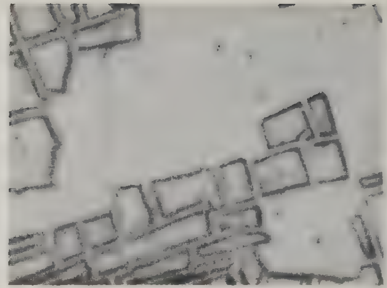
Fig.9. Micrograph of (111) face of silicon after sputtering in krypton with $i = 10$ ma/cm^2. 250 X.

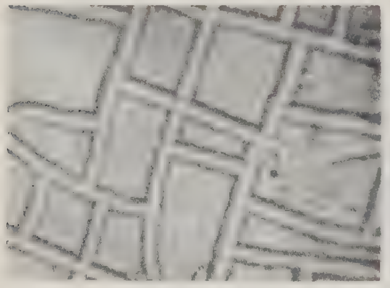
Fig.10. Enlarged section of the same face as in Fig.9. 600 X.

Fig.11. Protuberances on silicon sputtered for 1 hour at $V = 1.5$ kv, $i = 7$ ma/cm^2, $p = 10^{-3}$ mm Hg.

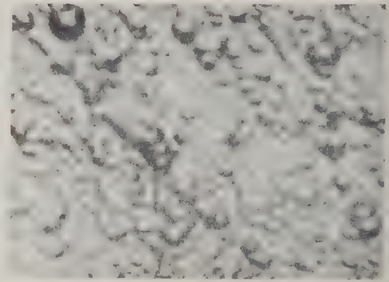
Fig.12. Hillocks and pits on Si surface. 250 X.

origin of these pits is still unclear, but it is doubtful whether they are necessarily associated with dislocations. The (111) face of a silicon crystal after sputtering in krypton at a current density of 10 ma/cm^2 is shown magnified 250 X and 600 X in Figs.9 and 10, respectively. As will be evident from the micrograph, parts of the surface become covered with a rectangular pattern. The formation of this relief is apparently connected with structures of the type observed in metal single crystals with impurities.

In our opinion investigation of the formation of oriented figures as a result of sputtering is of considerable interest. In connection with his study of controlled sputtering of germanium by low energy (close to the threshold) ions Wehner[3] showed that the atoms are ejected in the direction of closest packing. Thus, apparently, at low energies a significant role may be played by preferential sputtering of the material in certain crystallographic directions. In this case one can explain the appearance of oriented figures on the basis of momentum theory. Yurasova[11], however, showed that symmetrical figures in the case of a copper single crystal can also appear under bombardment with fast ions (to 6 kev). However, the figure contours in this case become less sharp.

Hence we felt it would be of interest to determine whether a regular relief appears at ion energies significantly above the threshold value in the case of semiconductor single crystals. Accordingly, we bombarded germanium, silicon and ferrite single crystals with high energy (>1 kev) ions. The oriented figures appearing on the surface of crystals in such cases are for the most part depressions, but in some cases[2-3] there has been observed the growth of oriented hillocks.

Wehner[3] advanced the hypothesis that the faceted hillocks appear in sputtering of faces with closest packing, inasmuch as in this case an appreciable fraction of the atoms is ejected along close packed directions, parallel to the face, and hence is trapped by projections rising above the surface.

However, Yurasova[12] showed that the formation of oriented hillocks is not connected solely with the packing density of the atoms on the sputtered face inasmuch as in sputtering the (0001) face of bismuth there appear on the very same faces depressions under some conditions and protuberances under others.

Hence it may be inferred that hillocks develop in the case of intense sputtering when the vapor of the sputtered material can condense on the surface, giving rise to growth of microcrystals (high current densities and pressures). Thus we come to the conclusion that the growth of elevated features is due either to crystal growth owing to condensation of the target material vapor or to trapping of ejected atoms by incipient projections on the surface. Symmetrical depressions develop owing to an enhanced rate of sputtering in certain crystallographic directions.

We observed the growth of hillocks on the faces of a silicon single crystal bombarded with krypton ions for one hour at $V = 1.5$ kv, $i = 7$ ma/cm^2 and $p = 1$ micron (Fig.11). Under the given conditions return of the sputtered material back to the target must be negligible, so that the growth of the hillocks must be attributed to surface migration, involving emergence of deeper lying atoms to the surface of the crystal. Simultaneously with development of hillocks on silicon crystal faces there occurs selective etching leading to the formation of etch pits (Fig.12).

Physics Faculty,
Moscow State University

References

1. G.V.Spivak, V.E.Yurasova, I.N.Prilezhaeva & E.N.Pravdina, Izv.AN SSSR, Ser.fiz., 20, 1189 (1956). (Trans.Bulletin 20, 1075.)
2. V.E.Yurasova, Kristallografiya, 2, 770 (1957). (Trans.Soviet Physics - Crystallography.)
3. G.K.Wehner, Phys.Rev., 102, 690 (1956).
4. R.E.Honig, Bull.Amer.Phys.Soc., 2, 34 (1957).
5. S.P.Wolsky, J.Electrochem.Soc., 104, 142 (1957).
6. J.A.Dillon & A.E.Farnsworth, J.Appl.Phys., 28, 174 (1957).
7. G.K.Wehner, Ibid., 29, 2, 217 (1958).
8. B.B.Meckel & R.A.Swalin, Ibid., 30, 1, 89 (1959).
9. G.V.Spivak, I.N.Prilezhaeva & O.I.Savochkina, Zhur.tekh.fiz., 23, 225 (1953).
10. S.P.Wolsky & J.R.Pattel, Nineteenth Ann.Conf.on Phys.Electronics, 1959.
11. V.E.Yurasova, Zhur.tekh.fiz., 28, 1968 (1958). (Trans.Soviet Physics - Tech.Phys.)
12. V.E.Yurasova, Thesis, Moscow State University, 1958.

CONTRIBUTION TO THE THEORY OF SCATTERING OF IONS FROM METAL SURFACES

- V.N.Vapnik, L.G.Gurvich & N.V.Zinov'ev

In general there have been very few theoretical investigations of ion-ion emission. In fact it was only recently that an attempt was made by Roos[1] to develop a theory of secondary ion-ion emission on the basis of certain specific assumptions. In his work Roos treats the process of secondary ion-ion emission as collision of a stream of ions (gas) with the "gas" of atoms comprising the solid. This model enables Roos to utilize for purposes of mathematical description of the emission process Boltzmann's kinetic equation and the method of solution of this equation developed in the theory of moderation of neutrons. It must be noted, however, that in contrast to the motion of neutrons in a solid, the motion of ions in a solid can be described from the gas-kinetic standpoint only with some approximation, inasmuch as in its motion through the solid an ion constantly interacts with atoms, while a neutron is involved only in individual collision with nuclei.

Another serious obstacle in the way of development of a theory of secondary ion-ion emission is the scarcity of experimental data on ion-atom scattering cross sections for the energy range from a few electron volts to several kiloelectron volts.

Finally, a consistent ion-ion emission theory must take into account also inelastic interaction processes, specifically, charge exchange and neutralization of ions, that occur simultaneously with scattering.

The double modulation procedure developed in the Academy of Sciences of the Uzbek SSR permits of simultaneous observation and recording of all secondary processes occurring incident to interaction of ions with the atoms of solids.[2] This procedure[3,4] makes it possible to distinguish between scattered, evaporated and diffusion ions, which enables one to judge of the relative proportions of these different ions in ion-ion emission.

Actually, all the proposed theories of ion-ion emission allow of calculating the scattered ion current. As Arifov et al[4] showed for the case of potassium ions bombarding tungsten, scattered ions are virtually the only component of the emission up to a target temperature of the order of 1000°K; only at higher temperatures do there begin to appear evaporated and diffusion ions. This temperature criterion is important and should be borne in mind in comparing the results of calculations with experimental data. Nevertheless, theoretical investigators are faced with the problem of simultaneously taking into account all the above-mentioned processes However, whereas the processes of diffusion and evaporation have been fairly adequately treated from the theoretical standpoint, at least where certain specific elastic cases are concerned, development of the theory for scattered ions encounter a number of so far insuperable difficulties. An illustration of this is the theory of Roos.

As noted, Roos utilized Boltzmann's kinetic equation, which is known to be inapplicable for ion energies of the order of the binding energy, although in the range of higher ion energies it should be applicable, albeit with a number of limitations and restrictions.

Furthermore, inadmissible in the theory of Roos is use of the Born approximation for calculation of the ion-atom interaction cross section in the energy range where this approximation is known to be inapplicable. Replacement of this incorrect cross section by another differing from it by two or three orders of magnitude in discarding the second and higher order terms of the series in which the Born cross section is expanded is even more erroneous. The results of calculation of the coefficient of ion-ion emission for rubidium, potassium and cesium ions bombarding molybdenum are 3-4 times greater than the experimental data obtained by Brunnee for an incident ion energy of 2000 ev. Thus Roos' calculations contain a number of inaccuracies, and owing to arbitrary cut-off of the series are not correlated with the earlier determined cross section for ion-atom interaction.

Hence we felt it would be of interest to carry out calculations of the coefficient of ion-ion emission on the basis of a definite ion-atom interaction cross section corresponding to a given energy. Comparison of the results obtained in this manner with the experimental data for scattered ions should provide a basis for judging of the character of the interaction of incident ions with the atoms in the solid target.

In a number of studies[6-7] devoted to the interaction of ions with atoms and atoms with each other it is inferred that for energies under 1000 ev the interaction cross section for scattering must be spherically symmetrical. Inasmuch as there are reliable experimental data for this energy region, we decided to carry out a calculation of the coefficient of ion-ion emission by means of the approximation utilizing the solution of Boltzmann's kinetic equation:

$$\frac{\partial N(\mathbf{r}, \mathbf{v}, \mathbf{t})}{\partial t} = -nQ(\mathbf{v})\,\mathbf{v}N(\mathbf{r}, \mathbf{v}, t) + n\int f(\mathbf{v}', \mathbf{v})\,\mathbf{v}'Q(\mathbf{v}')\,N(\mathbf{r}, \mathbf{v}', t)\,d\mathbf{v}', \tag{1}$$

in which n is the integral number of scattering centers per unit volume, and $f(\mathrm{v}',\mathrm{v})$ is the probability for change of the ion velocity from v' to v in a single collision. For solution of our problem one can utilize the steady state kinetic equation

$$\begin{gathered} K\cos\vartheta\,\frac{\partial}{\partial z}N(z, K, \vartheta) = -nQ(K)\,KN(z, K, \vartheta) + \\ + n\int f(K', K, \vartheta', \vartheta)\,Q_s(K')\,K'N(z, K', \vartheta')\,dK'd\Omega', \end{gathered} \tag{2}$$

where z is the distance from the surface of the solid, K' and K are the momenta of the ion before and after the collision, and ϑ' and ϑ are the angles between the z axis and the direction of motion of the ion before and after collision.

We used the mathematical methods developed by Weymouth[6] for solving Eq.(2), and assumed that the cross section is spherically symmetric in the center of mass system and is of the form

$$dQ = \frac{\sigma_0}{2}\sin\theta\left[\frac{2}{\mu}\cos\theta + \sqrt{1 - \frac{\sin^2\theta}{\mu^2}} + \frac{\cos^2\theta}{\mu^2\sqrt{1 - \frac{\sin^2\theta}{\mu^2}}}\right]d\theta, \tag{3}$$

where σ_0 is the total cross section, $\mu = \frac{m_1}{m_2}$ is the mass ratio of the atoms of the target and the bombarding atoms, and θ is the scattering angle, which is related with the momenta K' and K by

$$\cos\theta = \frac{1-\mu}{2}\frac{K'}{K} + \frac{1+\mu}{2}\frac{K}{K'}. \tag{4}$$

To facilitate solution, Eq.(3) was replaced by the approximate expression

$$dQ = -\frac{\sigma_0}{2}\left[\frac{2}{\mu}\cos\theta + (1 - 1/\mu^2 + \frac{2}{\mu^2}\cos^2\theta) \times (1 + 1/2\mu^2 - \frac{1}{2\mu^2}\cos^2\theta)\right]d\cos\theta, \tag{5}$$

which is used in solution of Eq.(2) for calculation of the ion-ion coefficient. For our solution we also used the method of subdivision into so-called impact intervals according to energies:

the first

$$E_0 \geqslant E \geqslant E_0\left(\frac{1-\mu}{1+\mu}\right)^2, \tag{6}$$

second

$$\left(\frac{1-\mu}{1+\mu}\right)^2 E_0 \geqslant E \geqslant \left(\frac{1-\mu}{1+\mu}\right)^4 E_0 \tag{7}$$

and so on.

The specific values of the first two impact intervals for some atom pairs are listed in the accompanying table. It will be evident that for cesium and rubidium incident on molybdenum one need consider only the first impact interval, while for cesium on tungsten use of only one impact interval will yield an underestimate for the coefficient of ion-ion emission.

Ion	Target	μ	$\left\lvert\frac{1-\mu}{1+\mu}\right\rvert$	$\left(\frac{1-\mu}{1+\mu}\right)^2$	$\left(\frac{1-\mu}{1+\mu}\right)^4$	$\left(\frac{1-\mu}{1+\mu}\right)^6$
Li^6	Mo^{96}	16	0,881	0,744	0,553	0,306
K^{39}	Mo^{96}	2,46	0,422	0,176	0,031	0,001
Rb^{87}	Mo^{96}	1,10	0,045	0,002	0,000	0,000
Cs^{133}	Mo^{96}	0,72	0,170	0,029	0,001	0,000
Rb^{87}	W^{184}	2,11	0,357	0,130	0,017	0,000
Cs^{133}	W^{184}	1,38	0,160	0,026	0,001	0,000

We found the coefficient of ion-ion emission for the first impact interval in the form of the following series:

$$\rho = \sum_{n=1} \int_{\left(\frac{1-\mu}{1+\mu}\right)^2}^{1} \frac{(-1)^{n-1} b_n(\mu)}{(n-1)!\,2^n} (\ln x)^{n-1} dx. \qquad (8)$$

The values of the ion-ion emission coefficient for groups of reflected ions with energies within the first impact interval are plotted for different μ in Fig.1. The dashed line in the figure indicates the probable shape of the curve obtained on the basis of qualitative analysis taking into account the second and subsequent impact intervals.

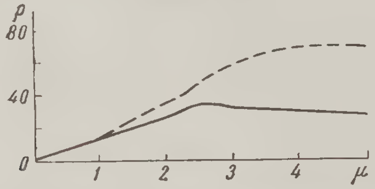

Fig.1

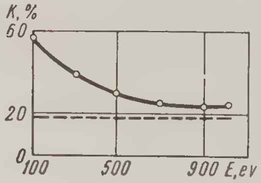

Fig.2

The solid curve in Fig.2 shows the energy dependence of the coefficient for cesium atoms scattered from tungsten according to the measurements of Arifov et al[4], while the dashed line gives the calculated coefficient for the first impact interval, which, as might be expected, is somewhat smaller than the measured coefficient; in the computations there were excluded reflected ions with energies less than 0.026 the energy of the incident ions. In view of the tentative nature of the calculations the agreement between the numerical values of the measured and calculated coefficients for reflection of cesium from tungsten in the incident ion range from 700 to 1000 ev may be regarded as satisfactory. However, it will be evident that the calculated and experimental curves do not coincide inasmuch as spherical symmetry of the cross section assumed by us leads to the cross section and, consequently, the calculated ion-ion emission coefficient being independent of the energy, whereas the experimental data indicate that the emission coefficient decreases with increasing energy.

This behavior of the ion-ion emission coefficient indicates that either the cross section is energy dependent, i.e., is not spherically symmetric, or that the model assuming ion motion in the solid as in a "gas" is inadmissible. For energies of the order of magnitude of the atomic binding energy in solids, the gas model is undoubtedly inapplicable, while for energies of the order of hundreds and thousands of electron-volts there must obviously be evinced some energy dependence of the scattering cross section. The experimentally observed increase of the ion-ion emission coefficient with decrease of energy can in general be represented as increase of the effective mass of the atoms of the solid because of binding with neighboring atoms or owing to triple coincidences. Obviously, this leads to increase of μ even for spherically symmetrical scattering (dashed curve in Fig.1) and growth of the coefficient of secondary ion-ion emission. Thus the available experimental data on ion-ion emission are inadequate for drawing definitive conclusions regarding the symmetry of the scattering or the energy dependence of the interaction cross section, which for energies of the order of hundreds of electron-volts according to Firsov[7] is supposed to be spherically symmetrical.

To solve this problem one must turn to experiments on single scattering of ions in the indicated energy region. Even now, however, there are grounds for regarding as doubtful the assumptions of spherical symmetry and energy independence of the scattering cross section for collision energies of the order of hundreds of electron volts and higher.

References

1. O.Roos, Z.Phys., 147, 184 (1957).
2. U.A.Arifov, A.Kh.Ayukhanov & S.V.Starodubtsev, Zhur.eksp.i teor.fiz., 26, 714 (1954).
3. U.A.Arifov, A.Kh.Ayukhanov, S.V.Starodubtsev & Kh.Kh.Khadzimukhamedov, Izv.AN UzSSR, Seriya fiz.-mat.nauk. (Bulletin, Uzbek SSR Ac.of Sci., Phys.-Math. Series), No.5, 15 (1958).
4. U.A.Arifov & Kh.Kh.Khadzhimukhamedov, Ibid., No.2, 47 (1959).
5. C.Brunnee, Z.Phys., 147, 161 (1957).
6. J.W.Weymouth, Phys.Rev., 84, 766 (1951).
7. O.B.Firsov, Zhur.eksp.i teor.fiz., 34, 448 (1958). (Trans.Soviet Physics -- JETP.)

INVESTIGATION OF THE INTERACTION OF FAST DEUTERIUM IONS WITH METALS

- V.M.Gusev, M.I.Guseva, V.P.Vlasenko & N.P.Elistratov

Investigation of the interaction of fast deuterons with metal surfaces is of particular interest at present in connection with the problem of obtaining hot deuterium plasmas in the discharge chambers of special purpose installations. Sputtering of the chamber walls under the influence of fast deuteron bombardment leads to contamination of the plasma by heavier atoms, as a result of which the radiative energy loss increases appreciably. The immanation of fast deuterium atoms into the chamber walls and their subsequent desorption may have an appreciable influence on the process of build up of fast ions in the hot plasma.[1]

In view of this we undertook measurements of the coefficient of sputtering of copper by deuterium ions with energies from 10 to 30 kev, as well as measurements of the amount of deuterium driven into copper, stainless steel and some other metals under bombardment with 25 kev deuterons. In addition, we investigated the desorption of the absorbed deuterium as a result of heating of the bombarded target.

Sputtering

All the measurements were carried out in the chamber of a small 180° focusing electromagnetic separator. For obtaining the deuteron beam we used an ion source (similar to that described in Ref.1) in which there was maintained an oscillating arc discharge in a strong uniform magnetic field. In the magnetic field of the separator the beam of atomic ions was focused on the target of the investigated metal, mounted normal to the ion beam at a distance of 20 cm from the source. The experimental arrangement is diagrammed in Fig.1.

The duration of the experiments for determining the sputtering coefficient was 4 to 6 hours. The number of sputtered atoms was determined from the weight loss of the target; our microbalance was accurate to within $2 \cdot 10^{-5}$ g. The number

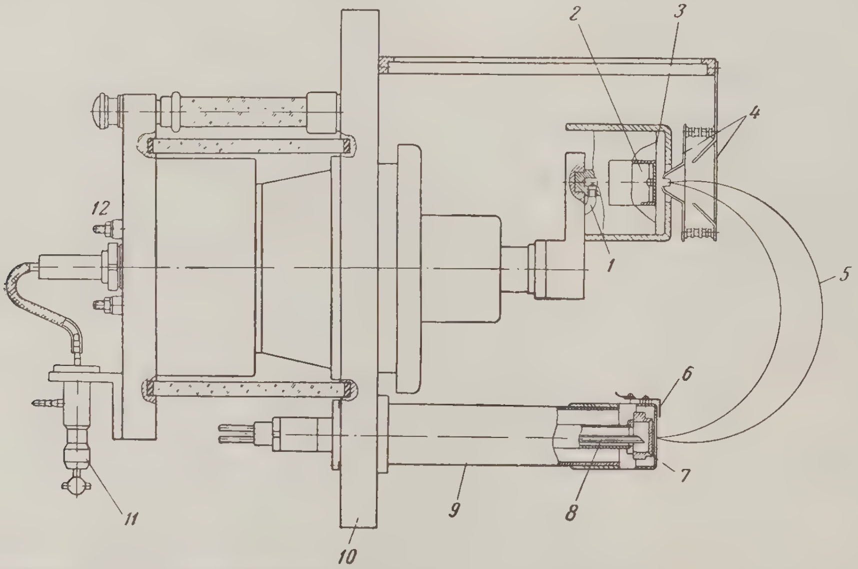

Fig.1. Arrangement of ion source and target: 1) gas supply, 2) gas discharge chamber, 3) discharge, 4) accelerating electrodes, 5) deuteron beam, 6) alignment guide, 7) target, 8) tube supplying water for cooling target, 9) screen, 10) source mounting flange, 11) needle type valve, 12) high voltage lead to source.

of ions incident on the target was measured by a current integrator. The influence of secondary electron emission on the measured current was excluded owing to the presence of the strong uniform magnetic field in the region of the target. Arrival of electrons, compensating the space charge of the beam, on the target and departure from the target of slow secondary electrons was prevented by applying a negative potential of ~500 v to the target. A vacuum of $(2\text{-}3) \cdot 10^{-5}$ mm Hg was maintained in the chamber. Oil vapor from the diffusion pump was frozen out by a freon trap installed between the pump and the chamber. During bombardment the target was heated to 300-400° by the liberated energy of the bombarding ions. Prior to bombardment the targets were cleaned by mechanical polishing and washed with alcohol. Special control experiments showed that the sputtering coefficient does not depend on the irradiation time or on the density of the ion current. This indicates that the target surfaces were adequately clean.

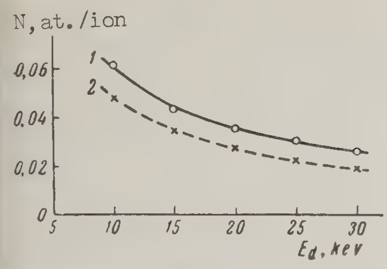

Fig.2. Experimental (1) and calculated (2) dependences of the coefficient of sputtering of copper by deuterium ions (i_d = = 1 ma/cm^2).

The results of measurements of the sputtering coefficient of copper in the deuterium ion energy range from 10 to 30 kev with a current density of 1 ma/cm^2 are given by curve 1 in Fig.2. It will be seen that with increase of the deuteron energy from 10 to 30 kev, the sputtering coefficient for copper decreases from 0.06 to 0.026 atoms per ion.

It must be noted that according to the data of our earlier measurements the coefficients of sputtering of copper by A, Kr, Xe and Cu ions increase with increase of the ion energy in the same energy interval.[3]

The observed deuteron energy dependence of the sputtering coefficient can be explained if we regard the primary collisions of the deuterons with the atoms of the target as Coulomb interactions of ionic charges with unscreened nuclei.[4]

Kinchin & Pease[5] showed that this assumption is valid for bombardment of materials with $Z < 30$ by deuterons with energies >10 kev. Inasmuch as the cross section for Coulomb interaction and, consequently, the number of primary collisions decreases with increase of energy, the sputtering coefficient must also decrease with increasing energy.

Curve 2 in Fig.2 shows the variation of the sputtering coefficient with the deuteron energy as calculated by the Kinchin-Pease formula. It will be evident from the figure that the experimental and theoretical curves are similar in shape, but that all the experimental points lie somewhat below the calculated curve. The divergence between the theoretical and experimental curves may be explained by the fact that in their calculations Kinchin & Pease assumed that in sputtering there are ejected half the atoms displaced in the first three atomic layers. Apparently, in reality, a somewhat larger fraction of displaced ions emerges from the target.

Immanation

When a metal target is bombarded with deuterium ions having energies of some tens of electron-volts, the deuterons penetrate into the metal to a depth of $\sim 10^{-5}$ cm and stick in the metal lattice. For investigating the processes of immanation of deuterons into different metals and reverse desorption of the knocked in atoms as a result of heating of the target we used the procedure based on measuring the neutron yield of the $D(d,n)He^3$ reaction, which takes place between the ejected deuterium atoms and the bombarding deuterons. The knocked out deuterium atoms

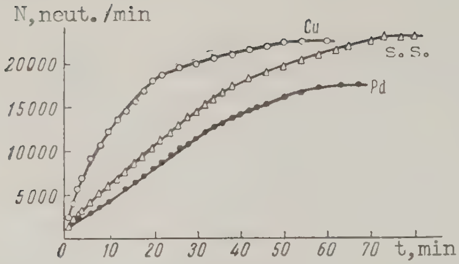

Fig.3

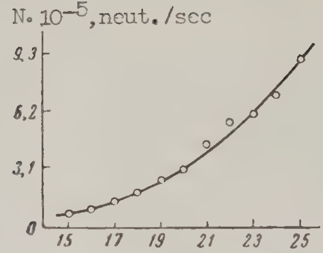

Fig.4

Fig.3. Variation of the neutron yield with the time of bombardment of copper, stainless steel and palladium targets with deuterium ions (E_d = 25 kev, i_d = 1.4 ma/cm^2). S.s = stainless steel.

Fig.4. Variation of the neutron yield from an aluminum target with the bombarding deuteron ion energy in the range from 15 to 25 kev (i_d = 1.4 ma/cm^2).

are essentially target nuclei for the subsequently arriving deuterons bombarding the metal.

By virtue of the large cross section for the d,d reaction and the use of intense deuteron beams, we obtained in our experiments a readily detectable neutron yield at a deuteron energy of 25 kev. For detecting the neutrons we used a boron counter, which was mounted at a distance of 300 mm from the target. The counter and associated circuits were calibrated by means of a Ra + Be source of known activity. Hence we were able to determine the absolute intensity of the neutron emission resulting from bombardment of the targets.

The targets used in the immanation experiments were circular metallic disks 30 mm in diameter and 1-1.5 mm thick. The mounting arrangement had provision for water cooling of the target.

It is known[6,7] that in the case of bombardment of metallic targets by fast noble gas ions only a limited number of gas atoms can be knocked into the target, i.e., there occurs saturation of the surface layer of the metal by the gas atoms.

By measuring the neutron yield as a function of the bombardment time one can readily establish whether saturation of the surface of the metal with D atoms does occur, what time is necessary for attainment of saturation, and how the saturation time and the limit concentration of knocked in atoms depends on the intensity and energy of the deuteron beam.

Fig.3 shows the time variation of the neutron yield for targets of copper, stainless steel and palladium bombarded with 25 kev deuterons. It will be evident that only a limited number of deuterium atoms can be knocked into the enumerated targets. The saturation amount of deuterium for copper and stainless steel is virtually the same, while for palladium it is approximately 1.3 times lower. The time to saturation is shortest for copper ($t_s \approx 40$ min), and longest for stainless steel ($t_s \approx 80$ min). In the course of the experiments it was established that interruption in bombardment has no effect on the progress of saturation. There were cases during the work when bombardment of the target had to be interrupted for several hours. Upon resumption of irradiation there was obtained the initial (pre-interruption) neutron yield, regardless of whether the target was in vacuum or in air.

It is interesting to note that the lowest limit concentration for knocked in deuterium atoms obtains for palladium, in which the rate of diffusion of hydrogen is appreciably higher than in copper and stainless steel.

Our experiments showed that with increase of the ion current to the target the limit deuterium concentration decreases somewhat. Thus, for example, in case of a fourfold increase of the current the neutron yield from stainless steel in the saturation region increases by a factor of only 2.5. This means that the limit concentration of the deuterium in the stainless steel target is decreased by a factor of 1.5. An analogous effect was obtained for the copper target. The decrease in limit concentration of the knocked in atoms with increase in the intensity of the deuteron beam can be explained by increase of the rate of diffusion of deuterium in the metal owing to rise of the effective temperature of the layer in which the deuterons are stopped.[8]

Fig.4 shows the variation of the neutron yield from an aluminum target in the deuteron ion energy range from 15 to 25 kev. It will be evident that with increase of the deuteron energy the intensity of the resultant neutron emission increases more rapidly than the cross section for the d,d-reaction. It may therefore be concluded that the limit concentration of knocked in deuterium atoms increases with increasing deuteron energy. Evaluations show that the limit deuteron concentration is approximately proportional to the energy of the bombarding deuterons. This result can be explained if we recall that the range of deuterons with an energy of a few tens of electron-volts in aluminum and, accordingly, the thickness of the layer penetrated by deuterium atoms, is approximately proportional to the deuteron energy.[9]

The total neutron yield per cm^2 in bombardment with 25 kev deuterons ($i = 1.4$ ma/cm^2) is $1.2 \cdot 10^6$ neutrons/sec for copper and stainless steel and $9 \cdot 10^5$ neutrons/sec for palladium. In terms of yield per incident deuteron, the corresponding values are $1.4 \cdot 10^{-10}$ neutrons for copper and stainless steel and $1 \cdot 10^{-10}$ neutrons for palladium, which is equal to 1/3 and 1/5, respectively, the intensity of the neutron yield from the d,d reaction on a heavy ice target.[10]

By comparing the absolute neutron yield from the investigated target with the yield from a heavy ice target one can evaluate the amount of deuterium effectively introduced into the metal, if one assumes that the knocked in atoms are uniformly distributed in the layer in which the deuterons are stopped. Such evaluation shows that the number of deuterium atoms that can be knocked into 1 cm^2 of copper and stainless steel under bombardment by 25 kev deuterons with an ion current density of 1.4 ma/cm^2 is $\sim 2 \cdot 10^{18}$ particles. Hence it follows that the number of deuterons knocked into targets of stainless steel or copper during the time necessary for attainment of saturation amounts to 5 to 10% of the total number of particles incident on the target during this period. It is noteworthy that the ratio of immanated to incident deuterons decreases with time: during the first minute of bombardment a copper target absorbs about 50% of the incident particles. It may safely be assumed that during the first seconds of irradiation an even higher percentage of the incident particles is knocked in.

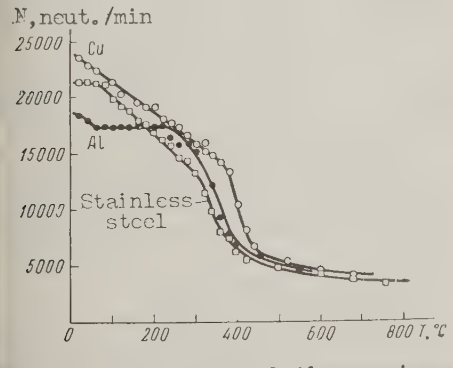

Fig.5. Variation of the neutron yield with the target temperature (E_d = 25 kev, i_d = 1.4 ma/cm^2).

With heating of the target the limit concentration of deuterium atoms decreases owing to increase in the rate of diffusion of deuterium in the metal. In our experiments the rate of desorption of the knocked in deuterium atoms as a result of heating of the target was determined by measuring the temperature dependence of the neutron yield from the investigated targets deuteron-saturated at E_d = 25 kev and i_d = 1.4 ma/cm^2 (Fig.5). In going from room temperature to 350-400° the amount of deuterium retained in the targets decreases by a factor of approximately 2. At 500° the neutron yield from all the tested targets was approximately the same and amounted to ~20% of the initial (room temperature) value.

We desire to express our gratitude to I.F.Kvartskhava and N.D.Morgulis for helpful discussion of a number of problems connected with the work and to members of the Electromagnetic Isotope Separation Group for assistance in carrying out the experiments.

References

1. I.V.Kurchatov, Atomnaya energiya, 5, 105 (1958). (Trans.Jour.of Atomic Energy).
2. P.M.Morozov & M.S.Ioffe, Ibid., 2, 272 (1957).
3. M.I.Guseva, Zhur.fiz.tverdogo tela, 1, 1540 (1959). (Trans.Soviet Physics Solid State).
4. D.Kraston et al, Report Presented at the Second International Conference on the Peaceful Uses of Atomic Energy, 1958.
5. G.Kinchin & R.Pease, Reports on Progress in Physics, 18, 1 (1955).
6. S.A.Kuchai & A.M.Rodin, Atomnaya energiya, 2, 202 (1958). (see Ref.1).
7. S.Thulin, Arkiv phys., 9, 107 (1954).
8. K.Fiebiger, Z.angew.Phys., 9, 213 (1957).
9. J.R.Joung, J.Appl.Phys., 27, 1 (1956).
10. V.A.Davidenko et al, Yadernye reaktsii na legkikh yadrakh (Nuclear reactions on light nuclei), M., 1957.

CONCERNING ANISOTROPY OF CATHODE SPUTTERING OF DIELECTRICS

- A.I.Krokhina & G.V.Spivak

Introduction

It has been firmly established that the disintegration of metal[1,2], dielectric[3] and semiconductor[4] surfaces by ion bombardment does not occur chaotically but is clearly correlated with the crystal structure. This has made it possible to develop procedures and construct ionic etching units[5] for bringing out the structure of solids (grain, dislocations, temperature induced effects, surface films and so on). A distinctive advantage of this etching technique is that it can be used under conditions when chemical or thermal etching is impossible. Clearly, the disintegration of crystal surfaces by ion bombardment is anisotropic. Our experiments with ion bombardment of glass showed that in this case also one can bring out some characteristics of the surface, for instance, the silica skeleton of glass.[3]

It may also be assumed that structural anisotropy will be evinced in variation of the number of atoms ejected by ion impact from a given point in different crystallographic directions. Thus in investigating the ejection of atoms from the (110) face of a silver single crystal by observing the deposit pattern on a glass cylinder, Wehner[6] established in the case of bombardment by slow ions that there occurs preferential sputtering in the direction of closest packing.

Yurasova[1,7] observed a similar effect in cathode sputtering of a copper single crystal by ions of appreciably higher energy (to 6 kev). This result is usually interpreted from the standpoint of the momentum theory of cathode sputtering.

Below we cite experimental data that show that there exists yet a third form of anisotropy in cathode sputtering, namely, anisotropy due to inhomogeneity of the bombarding ion beam itself. This leads to anisotropy in the density of the deposits collected on the screen and to the appearance of distinctive "etch" figures on the disintegrated surface.

Description of the Experiments and Interpretation

In earlier reports[3] we showed that in sputtering of dielectric single crystals there does obtain anisotropy actually bringing out the crystal structure; this was evinced by appearance of distinctive etch figures on different crystal cuts of the same single crystal. These experiments were carried out in discharges at a pressure of ~0.1 mm Hg. In some cases the cathode-specimen was an electrode containing metal in addition to the dielectric; in other cases the cathode was a dielectric which was heated to an appropriate temperature in order to enhance its conductivity. The anode was a tantalum or aluminum disk.

In such a two-electrode tube one cannot conveniently collect deposits of the sputtered material. Moreover, the presence of a metal grid over the dielectric would result in contamination of the deposits with sputtered grid metal.

A prime requisite for sputtering discharge tubes is the possibility of obtaining at a pressure of the order of 10^{-3} mm Hg a sufficiently high current density (10-15 ma/cm^2), preferably with provision for varying the current density on the target without changing the pressure in the tube. So low a pressure is necessary because the thickness of the ion sheath should be small compared with the ion free path. This precludes collisions in the sheath and insures normal incidence of the ions. On the other hand, the mean free path of the sputtered ions must be greater than the distance from the sputtered surface to the collecting screen, for otherwise the deposit pattern will not be representative. Wehner realized these conditions by immersing the target in a low pressure mercury plasma of high density.

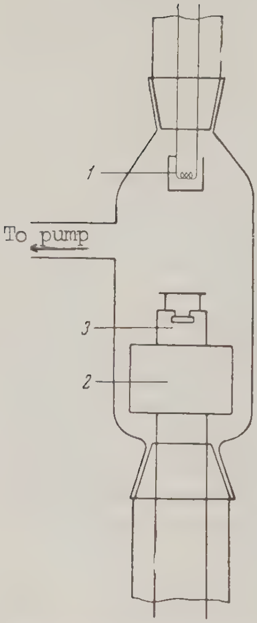

Fig.1. Experimental tube: 1) cathode, 2) anode, 3) target holder.

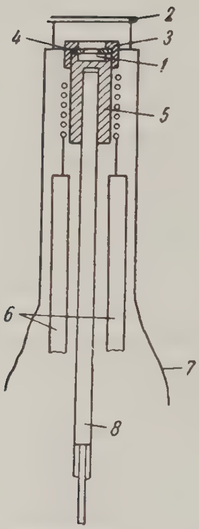

Fig.2. Target holder: 1) dielectric target, 2) collector, 3) porcelain insulator, 4) mica shield, 5) graphite specime holder, 6) leads to heater, 7) quartz insulators, 8) thermocouple.

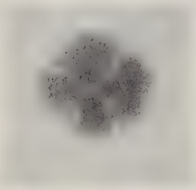

Fig.3. Deposits obtained in cathode sputtering of a (111) plane of NaCl at V = 1000 v, i = = 7 ma, and p - $7 \cdot 10^{-3}$ mm Hg; t = = 3 min; T = 320°; enlargement 1.5 X.

The tube used in the present experiments was a three-electrode tube containing an independently heated tungsten cathode (Figs.1 & 2). The discharge was realized in xenon, neon and residual air at pressures of $\sim 10^{-3}$ mm Hg. The bombarded target was essentially a large negative probe. We sputtered crystal disks of NaCl, KCl and KBr (5 mm diameter, 2-4 mm thick). The crystals were mounted in a special holder (Fig.2) with provision for heating them to assure the requisite conductivity. We worked with both annealed and nonannealed specimens. Polished and ground surfaces as well as cleavage faces were subjected to sputtering.

The experimental tube was not specially outgassed. However, the specimen and its holder were heated to 300° for 1-2 hours with continuous pumping of the tube. The cathode, anode and internal walls of the tube were subjected to outgassing in the process of preliminary discharge. Then the inert gas was introduced into the tube and the specimen sputtered. The current on the specimen was varied in the range from 1 to 10 ma with a potential of 500 to 10 000 v on the specimen relative to the tube cathode. The discharge was realized at a constant voltage and the current in the plasma could be varied in the range from 0.1 to 1.5 amp by controlling the emission of the tungsten cathode.

The sputtered particles were collected on a glass screen located at a distance of 5-7 mm from and parallel to the plane of the target. In cathode sputtering of the (100) planes of NaCl, KCl and KBr we observed deposits in the form of discrete spots. Generally, the deposit consisted of four spots located at the corners of the square. In some cases there appeared a central spot and a faint cross, i.e., light diagonal lines passing through the center of the square. This pattern could reflect the fourfold symmetry of the sputtered (100) plane. However, in sputtering the (111) plane of NaCl we obtained similar discrete spot deposits, which of course did not correspond to the symmetry of the (111) plane (Fig.3).

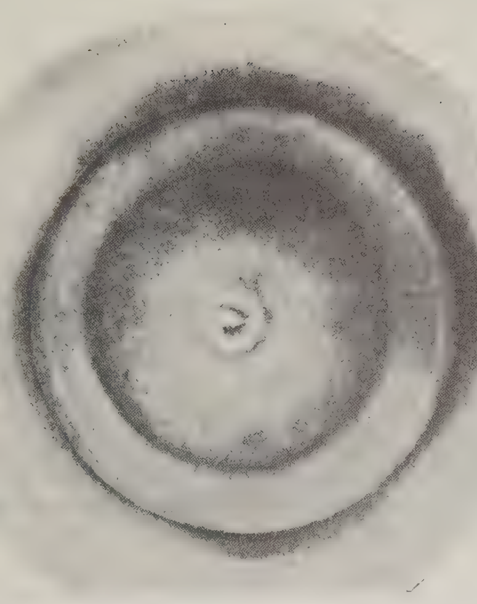

Fig.4. Distribution of deposit obtained in cathode sputtering of a (100) plane of KBr at V = 1200 v, i = 15 ma and p = $8 \cdot 10^{-3}$ mm Hg; t = 8 min; T = 400°; enlargement 4.5 X.

The process of formation of the deposit may be described as follows. During the first 3-4 minutes there appeared on the collector glass four spots, located at the corners of a 4 mm square. At approximately the same time there became evident on the sputtered surface areas of most intense sputtering, arranged at the corners of a 2 mm square (the specimen was covered with mica shield with a 2 mm diameter opening). Then there appeared the central spot and the faint cross between the initial four spots. A similar pattern was observed on the sputtered surface. Upon continued bombardment, the ion current was localized at the center of the specimen, where it etched a deep funnel. At this stage the sputtered material is deposited on the collecting glass in the form of rings of varying density (Fig.4).

Thus the results of our experiments show that in some cases the deposit pattern from a sputtered dielectric is not necessarily correlated with the symmetry of the crystal specimen but may be due to inhomogeneity of the ion flux incident on the specimen.

If the sputtering is continued for some time, the formation of a recess in the specimen leads to further concentration of the ion flux along its symmetry axis. It was shown in the work of Ref.8 that the sputtering from depressions and recesses must be more intense than from level smooth sections of the cathode. Thus we see that the configuration of the specimen or a defining shield placed over it may significantly affect the current density distribution. On the other hand, at low pressures there may form individual symmetrically located anode glow spots[9] which are the principal source of ions in a plasma; this in the final analysis leads to variations in the density of the bombarding ion flux. Moreover, an anode drop region may develop not at the anode but on or near the collector (screen).

In view of the fact that the collector is located at a short distance (5-7 mm) from the target and is necessarily bombarded by fast electrons from the target, at electron energies of a few hundred or a few thousand electron-volts a positive charge may build up on the collector owing to secondary emission. If this charge is nonuniform,[9] the anode emission from the anode aperture of the collector will also be nonuniform and this will give rise to an inhomogeneous but symmetrical disintegration of the target, a disintegration independent of its crystal structure.

We note that in the numerous cathode sputtering experiments described in the literature no attention was paid to the homogeneity of the ion flux. We believe that in any attempt to associate the anisotropy of deposits of the sputtered material with the crystallographic structure of the target (metal, semiconductor or dielectric) one should first make sure that there are not present any extraneous factors capable of giving rise to spurious anisotropic patterns.

Physics Faculty,
Moscow State University

References

1. V.E.Yurasova, G.V.Spivak & F.F.Kushnir, Izv.AN SSSR, Ser.fiz., 23, 744 (1959). (Trans.Bulletin, 23, 739.)

2. G.V.Spivak, V.E.Yurasova, A.I.Klenova & T.A.Vlasova, Fiz.metallov i metallovedenie, 7, 893 (1959). (Trans.Physics of Metals & Metallography.)

3. G.V.Spikva, A.I.Krokhina & L.V.Lazareva, Doklady AN SSSR, 104, 579 (1955); G.V.Spivak, A.I.Krokhina, T.K.Yavorskaya & Yu.A.Durasova, Ibid., 114, 1001 (1957) (Trans.Doklady); A.I.Krokhina & G.V.Spivak, Izv.AN SSSR, Ser.fiz., 23, 741 (1959) (Trans.Bulletin, 23, 736.)

4. I.G.Sirotenko & G.V.Spivak, Present issue of the Bulletin, p.687.

5. G.V.Spivak, V.E.Yurasova, F.F.Kushnir & I.N.Prilezhaeva, PTE (Instruments & Experimental Techniques), No.2, 106 (1957); I.I.Popenova & A.I.Frimer, Zavodsk. laboratoriya (Industrial Laboratory), 21, 423 (1955).

6. G.Wehner, Phys.Rev., 102, 690 (1956).

7. V.E.Yurasova, Zhur.tekh.fiz., 28, 1966 (1958). (Sov.Phys. - Tech.Physics.)

8. G.V.Spivak, V.E.Yurasova, I.N.Prilezhaeva & E.K.Pravdina, Izv.AN SSSR, Ser.fiz., 20, 1189 (1956). (Trans.Bulletin, 20, 1075.)

9. N.A.Neretina & B.N.Klyarfel'd, Radiotekhnika i elektronika, 4, 1301 (1959) (Trans.Radio Engineering & Electronics.)

EFFECT OF POLARIZATION OF THE INCIDENT LIGHT ON THE EMISSION OF COMPLEX PHOTOCATHODES*

- P.Görlich & H.Hora

Introduction

We felt it would be of interest to continue our earlier investigation[1] of the effect of polarization of the incident light on the external photoeffect in semiconductor type photocathodes. This effect in the case of semiconductor photocathodes is evinced much more weakly than in the case of metallic cathodes and cathodes with an adsorbed monomolecular coating. In view of the rough nature of the surface of semiconductor photocathodes, the results for such cathodes must be interpreted with caution. It is also important to take into account the effect of polarization. We note that the influence of polarization on the external photoeffect may be regarded as a characteristic attribute of the surface photoeffect and adsorbed monomolecular layers.

We investigated transparent complex semiconductor cathodes of Cs_3Sb (Ref.2) and Cs_2O (Ref.3), i.e., of the type frequently employed in phototubes and photomultipliers. There are theoretical indications that by means of polarization measurements one can obtain some data on the photoemission mechanism in semiconductors. This is particularly interesting in view of the fact that so far there have not been obtained for Cs_3Sb definite data on the energy levels in the band diagram[4] and difficulties are encountered in interpreting the behavior of this material in the framework of the general quantum mechanical theory of photoemission.

Even in our first experiments we obtained unexpected results. In cases when for a given cathode the emission current varies with the direction of polarization of the light incident at an angle, the photoemission proves to be more appreciable if the electric vector is oriented parallel to the plane of incidence.[3] A higher emission in the direction parallel to the electric vector is also observed in the case of excitation by photons in the x-ray region.[5] In contrast, in the case of transparent Cs_3Sb cathodes there is always observed a higher photoemission if the electric vector E is oriented perpendicular to the plane of incidence, i.e., parallel to the surface. Some polarization measurements for thin Cs_2O cathodes have been carried out earlier by Klüge.[6] In view of the nonreproducibility of the results obtained for Cs_2O type emitters, we undertook a series of similar measurements for Cs_3Sb for purposes of comparison.

Experimental Data

In our experimental arrangement we used a narrow monochromatic beam of linearly polarized light, which was incident at different angles on a transparent Cs_3Sb photocathode of a photomultiplier. We used commercial multiplier tubes.[7] In some cases (in investigating the quantum yield) we recorded the reflection and absorption of the photocathodes. The light from an incandescent bulb was refracted by a mirror monochromator, collected into a narrow beam, linearly polarized and allowed to fall on the photocathode of the multiplier, the response of which was recorded by means of an appropriate instrument.

Polaroid type sheets were used for linear polarization of the light in the visible and infrared regions. The direction of oscillation of the light waves was controlled making use of Brewster's law. The light from the mirror monochromator had elliptical polarization, dependent on the aperture of the beam entering the monochromator, the width of the slit and the wavelength. Hence the results obtained for different cases of polarization had to be normalized to the same intensity of the incident light. We used the ratio of the quantum efficiencies for the cases when the electric vector of the incident light was perpendicular and, respectively, parallel to the plane of incidence; we call this ratio the ratio of the polarization yields or simply the ratio K (not to be confused with the "vector ratio" commonly employed in investigating the photoeffect). First, we measured the efficiency for an angle of incidence of 45° at a certain point of the transparent photocathode in a specially prepared M-12 FS60 photomultiplier - see Fig.1. At point A there was a transparent window, so that in addition to the light reflected at point B, we could measure the transmitted light. Fig.2 shows the spectral dependence of the ratio K, using the quantum yields reduced to equal intensities of the incident light (1), the light entering the photomultiplier (2) and the absorbed light (3).

---

*We take this opportunity to thank Dr. Hora for permission to publish the report and for kindly checking the translation. Translation Editor.

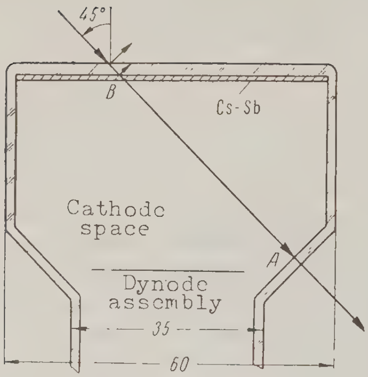

Fig.1. Cathode space of the M-12 FS60 type photomultiplier employed in the experiments.

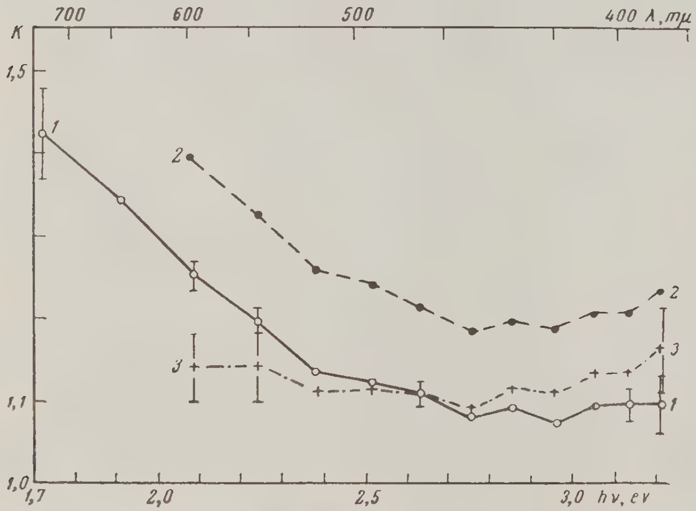

Fig.2. Spectral dependence of the polarization efficiency of photomultiplier tube No.260; angle of incidence - 45°.

Weak magnetic fields (of the order of the Earth's field) have no detectable effect on the efficiency. Under the influence of a stronger (one order of magnitude) homogeneous magnetic field, the anode current in the photomultiplier changed appreciably, but the value of the polarization efficiency still remained the same within the limits of the experimental error for all the investigated wavelengths. Measurements at different points of the cathode with different sensitivities showed that the scatter of the values of K for different wavelengths and different angles of incidence lies within the limits of the measurement error.

Fig.3 illustrates the photon energy dependence of K' (i.e., the ratio K with the quantum yield referred to equal light intensities (entering the photomultiplier for a Cs_3Sb cathode at different angles of incidence. The values of K measured for the same points of the cathode are shown in Fig.4. Similar results were obtained for all the other Cs_3Sb cathodes, i.e., increase of efficiency with increase of the angle of incidence and monotonic decrease of K and K' (from values greater than unity) with increase of the photon energy. The minor fluctuations shown in Figs.3 & 4, i.e., the deviations from the rough shape of the spectral dependence curve, are not susceptible of interpretation at present. However, these variations

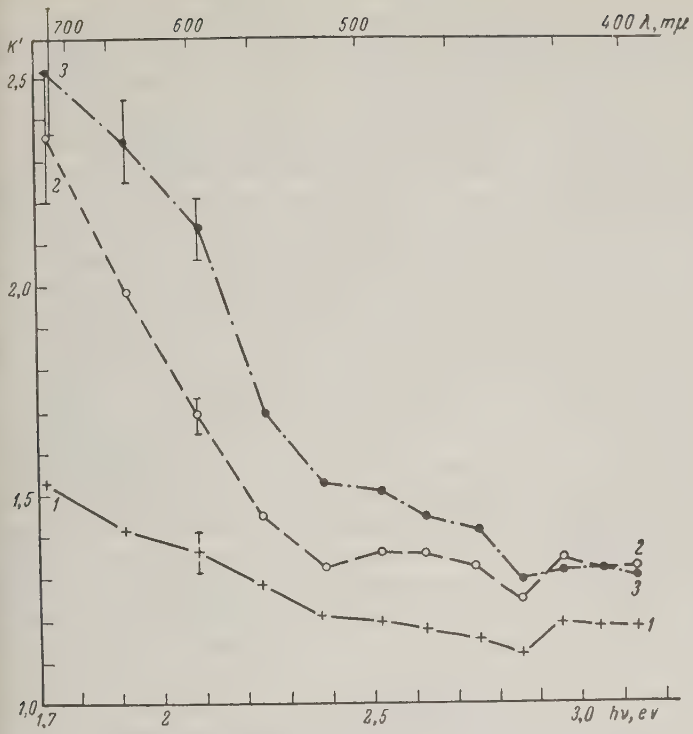

Fig.3. Spectral dependence of K' at different angles of incidence for an M-12 FS35 photomultiplier with a Cs_3Sb cathode (tube No.284). Angles of incidence: 1) 45°, 2) 60°, 3) 75°.

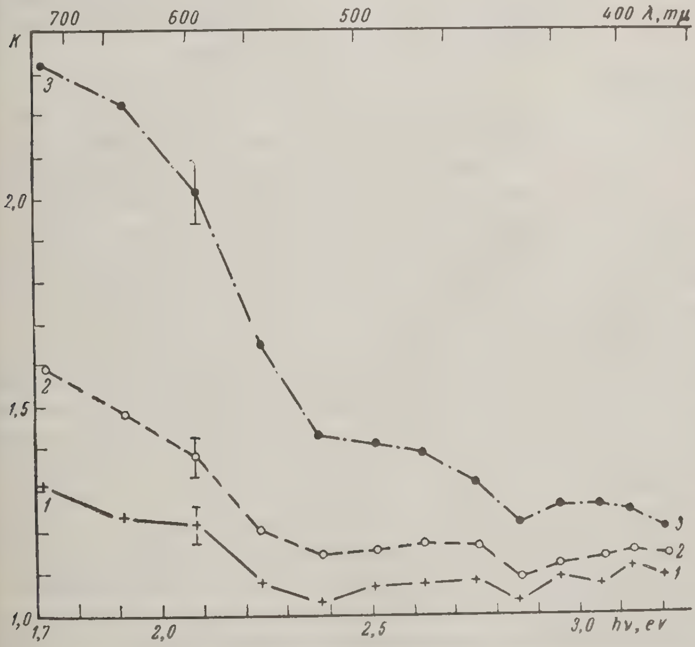

Fig.4. Same as Fig.3 but for K.

for a layer thickness of $3 \cdot 10^{-6}$ cm and an appreciable absorption cannot be explained by interference effects.

The spectral dependence of the efficiency of Cs_2O type cathodes is different. The values of K and K' for a Cs_2O cathode for a number of angles of incidence are shown in Figs.5 & 6. The long wavelength peak of this cathode lies at 827 mμ. For a number of obviously different transparent Cs_2O cathodes, the long wavelength peaks of which varied in the wavelength scale from 727 to 937 mμ, there were obtained similar ratios: in contrast to the results obtained for Cs_3Sb cathodes, the efficiencies for the Cs_2O cathodes fluctuate about unity in the indicated range with some slight tendency to decrease with increase of the angle of incidence.

Discussion

As noted above, with the electric vector parallel to the plane of incidence the efficiency is higher than in other cases of polarization. We obviously first had to determine whether this anomaly was not due to some special optical properties of transparent cathodes. The photoelectric properties of a transparent cathode can be evaluated on the basis of the reflection and absorption characteristics of the photomultiplier. The observed values of K', taking into account the experimental errors (see Fig. 3), show that the photoelectric process in the case of oscillation of the electric vector E perpendicular to the plane of incidence actually does depend on the polarization. At present we have not arrived at a definitive interpretation of this phenomenon.

The results of measurements

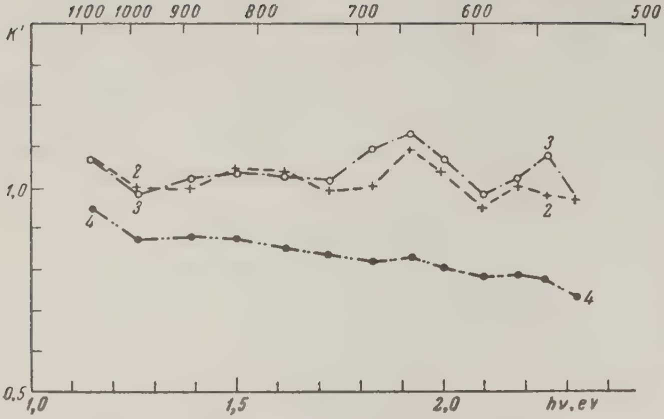

Fig.5. Spectral dependence of K' at different angles of incidence for an M-12 FS35 photomultiplier with a Cs_2O cathode (tube No.445). Angles of incidence: 1) 30°, 2) 45°, 3) 60°, 4) 75°.

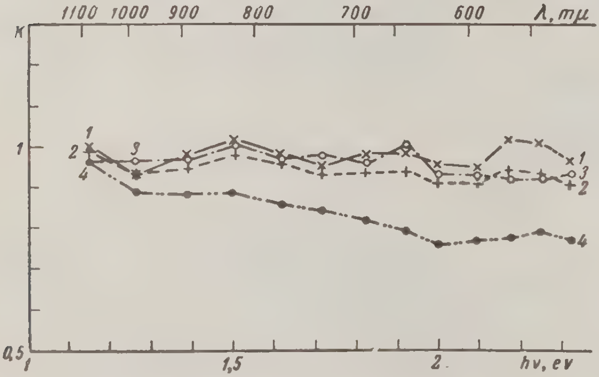

Fig.6. Same as Fig.5 but for K.

carried out by Thomas[8] and Mayer & Thomas[9] are in conflict with the earlier theory[10] of the surface photoeffect. At the same time, it must be noted that there is as yet no complete quantum mechanical theory for the volume photoeffect. Hence the results we have obtained are of great interest. They are significant for explaining the photoelectric processes of excitation in semiconductor cathodes. It may tentatively be concluded that there must exist a preferred direction for photoelectric excitation processes and that this direction is perpendicular to the electric vector. In contradiction to this it is known that for photoemission in the x-ray region, as theoretically described by the single electron model[5], there exists a preferred direction of emission and this direction is parallel to the electric vector. It is difficult to imagine that this difference can be explained by difference in the electron eigenfunctions employed in the calculations. Possibly the electrons in Cs_3Sb have a distinctive ground state, differing from the ground state of the electrons in a hydrogen atom.

We can show by an example how the lattice symmetry may affect the electron ground state. In the case of CdS single crystals for more precise measurement of the excitation behavior, which depends on exciton processes, there was utilized the fact of variation of the absorption with the direction of polarization of the incident light.[11] There remains the question of whether this influence of the lattice is sufficient to explain why the preferred direction for emission is the opposite of the preferred direction for the x-ray photoeffect. Apparently, it must be assumed that the process of electron excitation cannot be described in terms of simple interaction of the electron with the incident photon. This indicates that in photoemission there may be involved a "third impact partner"

We constructed a hypothetical model of the emission mechanism for the purpose of partial explanation of the increase in the ratio K with increase of the angle of incidence and the wavelength in the case of Cs_3Sb cathodes. Where the excitation process is concerned, first, there obtains the usual angular distribution characterized by the $\cos^2 \varphi$ law but with the maximum perpendicular to E, second, the interaction between the excited electrons and the lattice (as in the Hinteregger model[12]) is negligibly small, and third, there occurs simple reflection of the electrons at the potential discontinuity on the surface of the cathode. Hence one can deduce a definite analytic expression for the efficiency. Having chosen

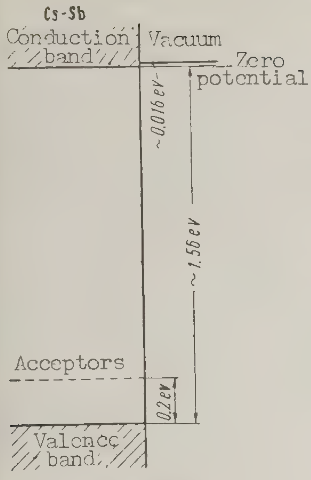

Fig.7. Band model for Cs_3Sb. The width of the forbidden band and the depth of the bottom of the conduction band below the vacuum level correspond to the model under consideration. The assumed height for the acceptor level was obtained from the limit frequency 1.35 ev observed for Cs_3Sb.[14]

two parameters in this expression, one can compare them with the measured values. From the very rough agreement between the calculated and experimental data as regards the spectral dependence and the dependence on the angle of incidence, it may be concluded that the given model is representative of some of the actual facts. The parameters chosen for comparison with experiment are energies of the order of the width of the forbidden band and the depth of the conduction band below the vacuum level. On the basis of this result and in agreement with the phenomenological theory[13] one can deduce a band model for Cs_3Sb cathodes (Fig.7). Our earlier measurements[1] for Rb_3Sb cathodes under certain conditions show a similar spectral variation of the efficiency and with the aid of the hypothetical model yield reasonable values for the energy levels.

As regards Cs_2O cathodes, one cannot on the basis of the polarization yield, which fluctuates weakly about unity, draw conclusions similar to those made for Cs_3Sb cathodes. In order to infer on the basis of the experimental data for Cs_2O cathodes that there exists a preferred direction or that owing to other properties of the material (for example, a rougher surface) this direction is diffused. Which of these two alternatives is more plausible is not clear at present. It is obvious even now, however, that there is a fundamental difference between these two types of cathodes as regards the emission mechanism. The difference in excitation processes could be explained on the assumption that the photoemission in the case of Cs_2O occurs from defects and in the case of Cs_3Sb from the valence band. The emission from Cs_3Sb is apparently connected with an exciton mechanism; hence it is interesting to compare our results with those obtained by Gross & Razbirin[11]. The smearing out of the preferred direction for the process of excitation in Cs_2O type cathodes may be explained by the submicroscopic roughness of their surface.

Thus we have shown that the results of polarization measurements leave open the question of the existence of definite structure or a structure of the type proposed by Borzyak et al[15]. It clearly follows, however, from the results of polarization measurements on Cs_3Sb type cathodes that such models are not valid for Cs_3Sb; the hypothesized

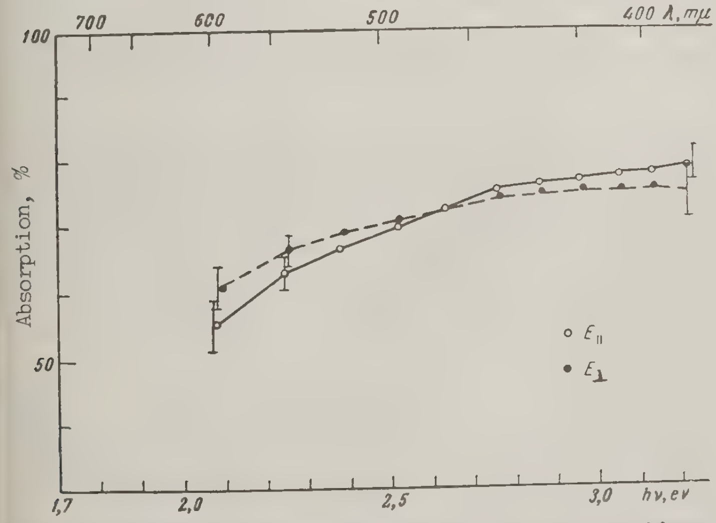

Fig.8. Wavelength dependences of the absorption of Cs_3Sb.

homogeneity of structure is substantiated for the case of Cs_3Sb.

Note added in proof.

In the light of the discussion following presentation of this report we would like to make some additional remarks. The optical data were obtained for photomultipliers of the type diagrammed in Fig.1. In addition to measuring the reflection and absorption for the assembled tube, we also determined the absorption by a layer of Cs_3Sb. It will be evident from Fig.8 that at an angle of incidence of 45^o the absorption is virtually independent of the polarization. This is substantiated by the fact that according to Fig.2 the values of K and K_{abs} are almost equal. The thickness of the cathode was $2.83 \cdot 10^{-5}$ cm; the spectral curve obtained for the absorption coefficients is reminiscent of the curve obtained by Burton[16]

There arises the question regarding the regimes of absorption in complex cathodes mainly in connection with the fact that the vectorial effect is explained purely optically, namely, by the absorption spectrum[17] or by standing waves in thin layers of metals[18]. For monatomic alkali metal films[9] there was also observed a correlation between the polarization dependences of the photoemission and absorption, on the basis of which it could be concluded in the framework of the theory of the surface photoeffect that absorption belongs among effects connected with photoemission. In contrast to the observed effects in metals, we could proceed in our discussion on the assumption that the absorption does not depend on the polarization and that owing to this the polarization dependence of the photoemission observed for Cs_3Sb type cathodes is photoelectric in nature. We did not, however, draw this rigorous conclusion, but gave, as was briefly indicated in our report, a precise evaluation in which, first, we took into account the light passing through the frontal cathode and hence capable of producing a photoeffect at other points of the cathode volume. In addition, as regards the region important for photoemission, we raised the question of the maximum and minimum light intensities that may obtain under any optical regimes (the reflection was varied from 0 to 1). If it is assumed that the photoelectric process of excitation does not depend on polarization, then in the case of variation of the optical regimes, the maximum emission currents should differ at most by a factor of two. On the basis of the data of Fig.3, which show that the ratio of the polarization efficiencies is greater than two, it may be asserted that there does exist a polarization dependence of the photoelectric process of excitation with a preferred direction perpendicular to the electric vector.

Our inferences (beginning with the words, "We constructed a hypothetical model...") should not be regarded as generally applicable: they are made on the assumption that equal effective light intensities in both cases are important where the value of K is concerned. This hypothesis is consistent with the experimental results and theoretical evaluations, but we do not consider it to be fully validated as yet. The physical utility of this hypothesis follows from the results pertaining, for example, to the energy diagram of Fig.7 and obtained by means of the proposed model.

C.Zeiss National Enterprise, Jena, German Democratic Republic

References

1. P.Görlich, Z.techn.Phys., 18, 460 (1937), Phil.Mag., 25, 256 (1938).
2. P.Görlich, Z.Phys., 101, 335 (1936).
3. P.Görlich, Die lichtelektrischen Zellen, Geest und Portig., Leipzig, 1951.
4. P.Görlich, Advances in Electronics and Electron Physics, 11 (1959).
5. F.Kirchner, Phys.Z., 27, 385 (1926); G.Wentzel, Ibid., 40, 574 (1926).

6. W.Kluge, Ibid., 34, 465 (1933).
7. P.Görlich, A.Krohs, H.-J.Pohl, R.Reichel & L.Schmidt, Z.angew.Phys., 10, 303 (1958).
8. H.Thomas, Z.Phys., 147, 395 (1957).
9. H.Mayer & H.Thomas, Ibid., 147, 419 (1957).
10. S.W.Wonsowski, A.W.Sokolow & W.I.Wexler, Fortsch.Phys., 4, 115 (1956).
11. E.F.Gross & B.S.Razbirin, Zhur.tekhn.fiz., 27, 1398 (1957). (Trans.Soviet Physics - Tech.Physics.)
12. H.D.Hinteregger, Phys.Rev., 96, 538 (1954).
13. P.Görlich, H.Hora & W.Macke, Jenaer Jb., 91 (1957); Exp.Tech.Phys., 5, 217 (1957); P.Görlich & H.Hora, Optik, 15, 116 (1958).
14. L.Apker, E.Taft & J.Dickey, J.Opt.Soc.Amer., 43, 115 (1953).
15. P.G.Borzyak, V.F.Bibik & G.S.Kramarenko, Izv.AN SSSR, Ser.fiz., 20, 1039 (1956). (Trans.Bulletin, 20, 939.)
16. I.A.Burton, Phys.Rev., 72, 531 (1947).
17. B.Gudden & R.W.Pohl, Z.Phys., 34, 245 (1925).
18. H.E.Ives, Phys.Rev., 38, 1209 (1931).

* * * * * * *

CONCERNING NEUTRALIZATION OF FAST POSITIVE IONS ON METAL SURFACES

- U.A.Arifov & Kh.Kh.Khadzhimukhamedov

Bombardment of a metal surface by positive ions gives rise to a number of complex phenomena: secondary emission of electrons and ions, diffusion and evaporation of ions, sputtering of the target and any adsorbed atoms, and neutralization of the primary atoms on the metal surface.

Of all the above listed phenomena, neutralization has been least studied. This is explained by the extreme difficulty of recording the number of neutral particles involved in the process. Hitherto there has not been available an experimental technique suitable for investigation of the neutralization of primary atoms as a function of the parameters and conditions of interaction of the colliding particles. The fact that there have been published only a few studies on neutralization of ions is further evidence of the difficulty of investigating this process.

Below we propose a procedure for determining the integral coefficient of neutralization of positive ions bombarding a target; this procedure is based on the double modulation method developed in our laboratory.[5,6] We also give the results of a study of neutralization of Na^+, K^+, Rb^+ and Cs^+ ions on targets of W, Mo and Ta as a function of the target temperature and ion energy.

Procedure for Determination of Coefficient of Neutralization

We used the double modulation method described in Ref.4 for measuring the primary and secondary ion currents at high target temperatures. Using this method we obtained oscillograms similar to those reproduced in Fig.1. This figure shows three oscillograms recorded in succession with a filamentary tungsten target at 1800°K, bombarded with 840 ev K ions.

Assume that the target temperature has been chosen close to the threshold for thermal electronic emission (1500°K), that a sawtoothed voltage is applied between the target and the collector, and that the primary beam has been cut off. In this case there will appear on the oscilloscope screen a horizontal trace, i.e., the zero or base line. In the presence of thermionic emission (i.e., at 1800°K), with a positive potential on the collector there will occur a vertical deflection of the trace corresponding to the value of the nonmodulated thermoelectronic current I_{te} (trace 2 in Fig.1). If at this instant the intensity-modulated primary beam is directed onto the target, there will appear on the screen a current-voltage characteristic (1 in Fig.1), comprising three components of the secondary ion current plus the thermoelectronic current.

The values of the individual components are given by the expressions

$$I_e = I_{e+s} - I_s \text{ and } I = I_d' - I_{te}. \quad (1)$$

The coefficients

$$K_s = I_s/I_p,\ K_e = I_e/I_p \text{ and } K_d = I_d/I_p \quad (2)$$

characterize the magnitude of each component of the secondary ion emission with respect to the primary ion current I_p (3 in Fig.1). These are, respectively, the coefficients of scattering, of evaporation and of ion diffusion. The sum

$$K_s + K_e + K_d = K_\Sigma \quad (3)$$

gives the coefficient of secondary ion emission under the given experimental conditions. Obviously, the secondary ion emission is the sum of three components.

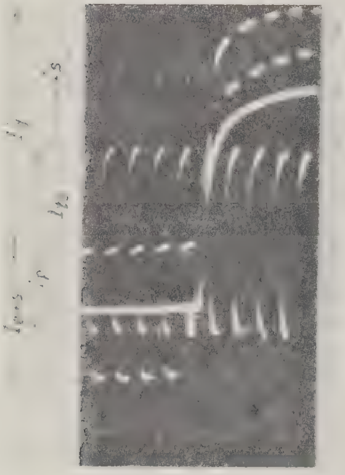

Fig.1. Oscillograms of the current-voltage characteristics for the primary ion current (I_p), and the currents of the scattered (I_d), evaporated (I_e) and diffused (I_d) ions, and the thermoelectronic current (I_{te}) obtained during bombardment of a tungsten target at 1800°K by 840 ev K^+ ions. Here $I_d' = I_{te} + I_d$.

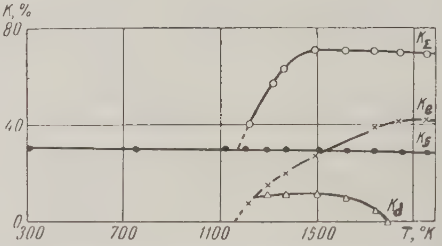

Fig.2. Temperature dependences of the coefficients K_d, K_s, K_e and K_Σ for 560 ev K^+ ions on W (φ = 4.57 ev).

In order to investigate the neutralization of positive ions on the target surface as a function of target temperature, we recorded similar oscillograms at different target temperatures with a constant known primary ion energy. Fig.2 gives the temperature dependences of K_s, K_e, K_d and K_Σ obtained on the basis of such oscillograms for a tungsten target bombarded with 560 ev K^+ ions.

It will be evident from Fig.2 that K_s does not depend on the target temperature in the investigated range and has a mean value of ~30%. Owing to the absence of noticeable evaporation at temperatures below 1200°K I_e and I_d are virtually zero in this temperature range. Above this temperature, the coefficients K_e and K_d differ from zero and increase with temperature. In the temperature interval from 1300 to 1600° the value of K_d is almost constant, while above 1600°K this coefficient decreases, dropping to zero at 1800°K.

We note that the temperature at which K_d drops coincides with the temperature of saturation of K_e. Thus the evaporation and diffusion ion currents supplement each other. This conjunction of the ion diffusion current with the current of evaporated ions at high target temperatures may be explained by the fact that the lifetime of the diffusion ions, which decreases with rising temperature, becomes comparable with the lifetime of the evaporated ions.

The K curve in Fig.2 gives the temperature variation of the total coefficient $K_s + K_e + K_d$. Such curves are typical for the case when the ionization potential V_i is lower than the work function φ of the target (for example, for K^+, Rb^+, and Cs^+ on W). When $V_i > \varphi$ (Li^+ and Na^+ on W), the currents I_e and I_d virtually vanish.

The law of conservation of matter requires that the sum of the coefficient of secondary ion emission K and the integral coefficient of neutralization K_o be equal to 100% for each point of the K_Σ vs T curve (Fig.2), i.e.,

$$K_\Sigma + K_o = 100\%. \qquad (4)$$

Hence the region above the K_Σ vs T curve can be attributed to the neutralized fraction of the primary ions. It will be evident from Fig.2 and Eq.(4) that the ratio of the coefficients K_Σ and K_o will vary, depending on the physical parameters and conditions of interaction of the colliding particles.

Experimental Part

The apparatus and vacuum equipment used in the present experiments were identical with those described in Ref.8. With liquid nitrogen in the trap, a residual gas pressure of $\sim 10^{-7}$ mm Hg was attained in the experimental tube. In order to drive off possible contaminants, the target was heated to a high temperature (to 3000°K for W) for 10 to 15 hours. Use of filamentary targets made it possible to carry out investigations in the presence of appreciable thermoelectronic emission and to monitor the state of the surface by measuring the work function φ. The target temperature was determined from the filament current. The work function of the target was determined by the method of Richardson plots, an appropriate correction for the Schottky effect being introduced.

The integral value of the coefficient of neutralization K_o for different experimental conditions was determined from the temperature and energy dependences of K_Σ by means of Eq.(4).

Experimental Results

Temperature dependence of the neutralization coefficient

We investigated the neutralization of 560 ev Cs^+ ions incident on a tungsten target at temperatures in the range from 300 to 1700°K.

Fig.3 shows the temperature dependences of K_s, K_Σ and K_o obtained in bombarding the tungsten target with 560 ev Cs^+ ions. As will be evident from the figure, the coefficient K_s at a constant ion energy, as in the case of K^+ on W (Fig.2), is independent of the target temperature. The value of K_Σ below 1200°K is equal to the value of K_s owing to the fact that K_e and K_d are zero ($I_e = I_d = 0$), while above 1300°K K_Σ attains 100%.

This shows that all the ions incident on the target at $T > 1300$°K leave it in the form of scattered, evaporated and diffused ions, and that there are no neutral atoms in the emission. On the basis of this balance of primary and secondary particles, the region above the K_Σ vs T curve can be designated as the region of neutralization.

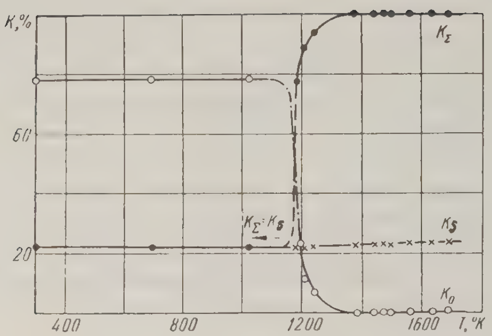

Fig.3. Variation of the coefficients K_o, K_Σ and K_s with the target temperature for Cs$^+$ on W (φ = 4.51 ev, E_p = = 560 ev).

It will be evident from the K_o vs T curve that in the 300 to 1200°K interval the neutralization coefficient is constant and equal to ~77%; then in the temperature interval from 1100 to 1300°K the coefficient falls off abruptly to zero owing to the onset of thermal ionization effects at these temperatures. The difference between the coefficients K_Σ and K_s in Fig.3 characterizes the surface ionization current.

Similar results were obtained with Rb$^+$ ions on W (the curves are not reproduced here). In this case, in contrast to the preceding one, in the target temperature range above 1200°K the coefficient K_o differs from zero and equals ~20%. The reason for this is the difference between the ionization potentials V_i of rubidium and cesium.

Energy dependence of the neutralization coefficient

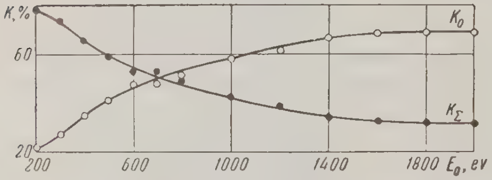

Fig.4. Variation of the coefficients K_o and K_Σ with the energy of K ions bombarding an Mo target at 1500°K.

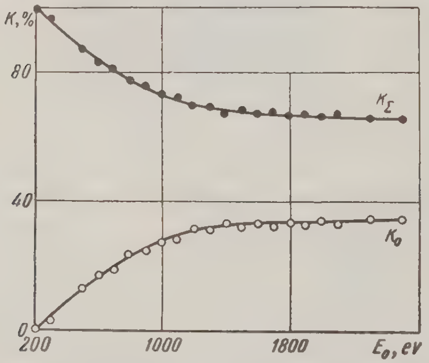

Fig.5. Variation of the coefficients K_o and K_Σ with the energy of Rb ions bombarding a Ta target at 1500°K.

We investigated the energy dependence of K_Σ and K_o for K$^+$ and Rb$^+$ on Mo, Rb$^+$ on Ta and Na$^+$ on W at a target temperature of ~1500°K and the primary ion energy range from 200 to 2500 ev.

Figs.4 and 5 show the ion energy dependences of K_Σ and K_o for K$^+$ on Mo and Rb$^+$ on Ta. As will be evident from the figures, K_Σ decreases, while K_o increases, with increase of the primary energy, and the values of both coefficients tend to saturation at high ion energies.

Similar energy dependences for K_Σ and K_o were obtained for Rb$^+$ on Mo and Na$^+$ on W. The curves obtained in these cases were similar to those reproduced in Figs.4 and 5, differing only as regards the magnitude of the coefficients.

Below we give the experimental data for K_o as a function of the values of $V_i - \varphi$ corresponding to different target materials and types of ions for E_p = 1200 ev and T $\approx$ 1500°K:

Ion	Metal	$V_i - \varphi$, ev	K_o,%
Na$^+$	W	0.57	76
K$^+$	Mo	0.17	62
Rb$^+$	Mo	0	35
Rb$^+$	Ta	-0.05	30
Cs$^+$	W	-0.63	0

It will be apparent that the coefficient K_o increases with increase of $V_i - \varphi$. This serves to explain the almost total neutralization of inert gas ions on targets of the same materials[9,10], when the magnitude of $V_i - \varphi$ exceeds 10 ev.

Thus the experimental results show that the value of the integral neutralization coefficient, as determined by our procedure, is a complex function of the parameters of the colliding particles, specifically, the temperature and work function of the target, and the energy and ionization potential of the primary ions.

Institute of Nuclear Physics,
Academy of Sciences of the Uzbek SSR

References

1. N.D.Morgulis & M.P.Bernadiner, Zhur.eksp.i teor.fiz., 9, 998 (1939).
2. V.I.Veksler, Izv.AN Uzbek SSR, Ser.fiz.-mat.nauk (Bulletin, Uzbek SSR Ac. of Sci., Phys.-Math.Science Series), 4, 34 (1959).
3. L.N.Dobretsov, V.N.Lepeshinskaya & I.E.Bronshtein, Zhur.tekh.fiz., 22, 961 (1952).
4. M.L.E.Oliphant, Proc.Roy.Soc. A124, 228 (1929).
5. U.A.Arifov, A.Kh.Ayukhanov & S.V.Starodubtsev, Zhur.eksp.i teor.fiz., 26, 714 (1954).
6. U.A.Arifov, Thesis, Leningrad Physical-Technical Institute of the USSR Ac.of Sci. & Physical-Technical Institute of the Uzbek SSR Ac. of Sci., Leningrad-Tashkent, 1954.
7. U.A.Arifov & A.Kh.Ayukhanov, Izv.AN SSSR, Ser.fiz., 20, 1165 (1956). (Trans.Bulletin, 20, 1057.)
8. U.A.Arifov, A.Kh.Ayukhanov, S.V.Starodubtsev & Kh.Kh.Khadzhimukhamedov, Doklady AN SSSR, 124, 60 (1959) (Trans.Soviet Physics - Doklady); Izv.AN Uzbek SSR, Ser.fiz.-mat.nauk (see Ref.2), No.5, 15 (1958).
9. H.D.Hagstrum, Phys.Rev., 104, 672 (1956).
10. U.A.Arifov & R.R.Rakhimov, Izv.AN Uzbek SSR, Ser.fiz.-mat.nauk (see Ref. 2), No.6, 29 (1958).

ON SCATTERING OF SLOW ALKALI METAL IONS FROM METAL SURFACES

- U.A.Arifov, A.Kh.Ayukhanov & D.D.Gruich

On the basis of earlier studies[1-4] of the interaction of 150 to 3000 ev alkali metal ions (Li, Na, K, Rb and Cs) with cold and hot clean Ta, W, Mo and Sn targets, it was established that the secondary ions have a continuous energy spectrum and that the maximum secondary ion energy agrees within the limits of the experimental error with the values calculated by means of the familiar equation for elastic collision of ions with individual target atoms. On the basis of these results we concluded that secondary ions with maximum energies appear as the result of single scattering of primary ions from free atoms at the target surface. Secondary ions of intermediate energy are assumed to originate due to multiple scattering from individual free atoms of the target, located at different depths.

Subsequent investigations[4-6] showed that the secondary ion emission comprises, in addition to ions scattered and evaporated from the surface, ions that have diffused from the depth of the target. These diffusion ions appear only at sufficiently high primary ion energies ($E_p >$ 200-250 ev), at high target temperatures ($T > 1000^oK$), and on condition that the ionization potential V_i of the incident particles is smaller than the work function φ of the target. It was also shown that these diffusion ions are mainly primary ions that penetrated deep into the target.

In the work of Ref.5 we investigated the variation of the secondary ion emission as a function of the relative masses of the target atoms (m_1) and the bombarding ions (m_2). It was found that in case of bombardment of a hot (1300°K) nickel target with 400 ev Cs ions ($m_1 < m_2$ and $V_i < \varphi$) the diffusion ions account for about 14% of the emission, while those evaporated from the surface amount to 86%. With the given conditions, there are no scattered ions. The absence of scattered ions when $m_1 < m_2$ substantiated our earlier inference[1-4] that the secondary ions with maximum energies appear as the result of single scattering of primary ions from free atoms in the target; this gives reason to assert that ions with intermediate energies appear as the result of multiple scattering from free atoms of the target.

Brunnee[7] investigated ion scattering from a clean Mo surface under bombardment with alkali metal ions in the energy range from 200 to 4000 ev. Brunnee notes that the great increase of the scattering coefficient K_s in the range of low energies is connected with manifestation of the atomic bonding energy of the target atoms. Increase of K_s is evinced first in bombarding metal surfaces with successively heavier ions - Cs, Pb, K, Na and Li - because already at a primary energy of 1000 ev for Cs and Rb ions their energy after a central collision is close to the atomic bonding energy (35 ev). At higher primary energies, K_s is virtually constant, so that apparently the influence of the bonding energy on K_s can be neglected.

It may be assumed that at primary ion energies commensurate with the bonding energy of the atoms in the target, the interaction of elementary particles with clean metals will differ radically from the type of interaction observed at medium and high energies.

Apparatus and Procedure

In the present experiments we used the equipment employed in our earlier studies[4,5,8] with some minor modifications, necessary for working with slow ions.

In order to reduce the energy spread of the primary beam we used an equipotential anode of tungsten (indirect heating). The ion beam was focused onto the target by means of a three-aperture electrostatic lens located at the entrance to the receiving-detecting section. This electrostatic system also slowed down the ions to the requisite energy. The distance from the target to the retardation section was made minimal: 5-5.5 mm. Over this short path in the indicated energy range and with the given current strength (10^{-7} amp) there could be no appreciable divergence of the beam due to space charge effects.

For measuring the secondary currents we employed the oscillographic procedure developed earlier[4-6,8]. The instantaneous response assured by this procedure made it possible to carry out measurements of the secondary currents prior to any appreciable contamination of the surface, i.e., immediately after flashing the target.

Experimental Results

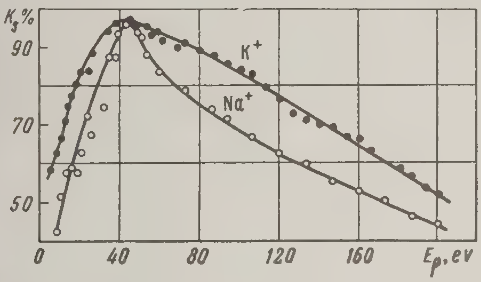

Fig.1. Variation of the scattering coefficient K_s with the energy of Na and K ions bombarding a clean tungsten surface.

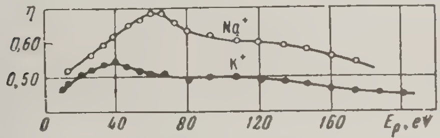

Fig.3. Variation of η with the energy of Na and K ions bombarding a clean tungsten surface ($\eta = E/E_p$ is the ratio of the maximum energy of the scattered ions to the energy of the primary ions).

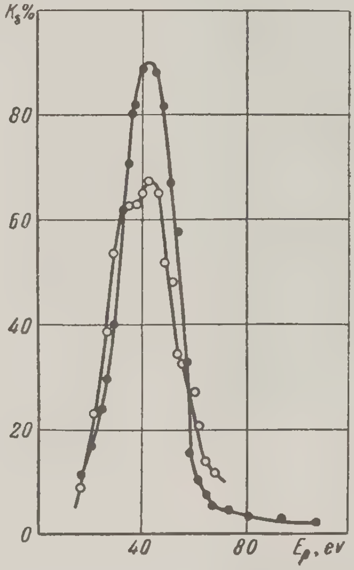

Fig.2. Variation of the scattering coefficient K_s with the energy of Cs ions bombarding a thoroughly cleaned Ni surface (solid points) and a surface less thoroughly cleaned (open circle points).

Fig.1 shows the variation of the scattering coefficient K_s for Na and K ions from a clean tungsten target as a function of the primary ion energy E_p. It will be evident from the curves that with decrease of the Na ion energy from 200 to 44 ev the coefficient gradually increases to a maximum (95%) at 44 ev. With further decrease of the energy the scattering coefficient falls off and becomes 42% at 8 ev.

For K ions the variation of the scattering coefficient with energy is approximately the same as for Na ions, but the curve lies somewhat higher. In this case the curve goes through a flatter maximum ($K_s = 96\%$) at ~43 ev.

Fig.2 shows the variation of K_s with E_p for Cs ions bombarding a clean nickel target. At a primary energy of 200 ev (not shown in the figure) $K_s \approx 0$. An abrupt increase of K_s (curve 1) begins only at $E_p = 68$ ev, where $K_s = 6\%$. With further decrease of the primary ion energy K_s rises sharply. At $E_p = 42$ ev, K_s attains a maximum value of 90%. With further decrease of the ion energy the coefficient falls off and equals 10% at $E_p \approx 17$ ev. Curve 2 in Fig.2 shows the variation of K_s with E_p for a less thoroughly cleaned target. This curve is less smooth and there is a dip in the region of the maximum ($E_p = 32$-44 ev).

Fig.3 shows the variation of η with E_p (η is the ratio of the maximum energy E of the scattered ions to the primary ion energy E_p). It will be evident from the curve for Na ions that η increases with decrease of E_p, goes through a maximum ($\eta = 0.68$) at 63 ev and then decreases. The curve for K ions has approximately the same shape but lies below the curve for Na. The maximum in this case is located at $E_p = 40$ ev, where $\eta = 0.54$.

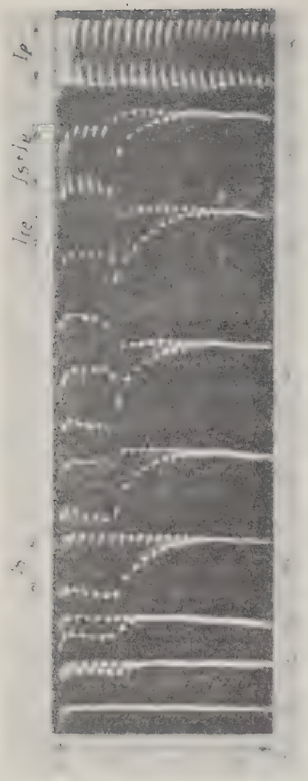

Fig.4. Oscillograms obtained in bombarding a tungsten target with 43 ev K ions. I_p - primary ion current on target, I_s - current of ions scattered from the target, I_e - current of ions evaporated from the target, I_{te} - thermoelectronic emission current from the target.

Fig.4 shows a series of oscillograms (current-voltage characteristics of the secondary ions emission) obtained in bombardment of a tungsten target with 43 ev K ions with different conditions of the target surface. Oscillogram 1 characterizes the modulated primary ion beam. The right-hand part, i.e., the current-voltage characteristics above the zero voltage base line, in each case (2 through 9) represents the current of scattered ions; the left-hand part, where there occurs saturation of the ion current to the collector, represents all the secondary ions.

Oscillogram 2 was recorded at a target temperature of 1300°K after the target had been kept in the cold state for several minutes. It will be seen that in the left-hand side of this oscillogram there is evinced an abrupt alteration of the square pulses to exponential ones, which indicates the presence of ions due to surface ionization. Oscillograms 3 through 6 were obtained in the process of cooling the target after flashing it to 2500°K. The character of these oscillograms indicates the absence of evaporated ions. Oscillograms 7 through 9 were recorded successively at longer intervals after the target had cooled to room temperature. As a film forms on the target surface due to absorption of residual gas molecules, the number of scattered ions decreases to the vanishing point.

The oscillograms reproduced in Fig.5 were obtained from bombardment of a clean nickel target by 42 ev Cs ions. Oscillogram 1 characterizes the modulated primary current. Oscillogram 2 represents the distribution in energy of scattered ions. The beginning of the oscillogram corresponds to zero potential on the collector. It will be evident from these oscillograms that all the ions are scattered with energies greater than 3 ev (the maximum ion energy is 8 ev). Oscillogram 3 represents the current-voltage characteristic recorded at a lower primary beam intensity. In order to display the voltage base line, the target was heated to a temperature somewhat above the threshold for thermionic emission. It is

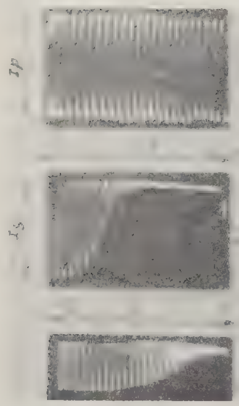

Fig.5. Oscillograms obtained in the range of bombarding ion energies corresponding to the maximum of scattered ions, i.e., bombardment of a clean Ni target with 42 ev Cs ions.

evident that the break in the characteristic for scattered ions begins in the region of a higher retarding potential on the collector.

Discussion

In view of the results obtained by Brunnee[7], we could expect to observe appreciable values of the scattering coefficient K_s at primary ion energies commensurate with the bonding energy of the target atoms.

It follows from the curves reproduced in Fig.1 that in the case of bombardment of clean tungsten with Na atoms K_s actually does increase with decrease of the primary ion energy and attains a maximum value (95%) at $E_p \approx 45$ ev. In the case of K^+ on clean W the coefficient attains 96% at $E_p \approx 43$ ev.

In the case of Cs^+ on Ni (Fig.2) K_s attains 90% at $E_p = 42$ ev. Thus we see that the expected high values of K_s are realized.

In our earlier investigations[1-3,5] it was established that the maximum energies of the scattered ions agree within the limits of the experimental error with the values calculated by means of the equation for elastic collision of ions with individual atoms of the target. It is known that in such elastic interaction the ratio η of the maximum scattered ion energy to the energy of the primary ions should not vary with the primary ion energy, i.e., η should remain constant.

Actually, however, the η vs E_p curves obtained for Na and K ions bombarding a clean tungsten target (Fig.3) show a definite increase of η with decrease of the primary energy; for Na ions η attains a maximum value of 0.68 at ~60 ev. For K ions the curve lies somewhat lower, and η attains a maximum value of 0.54 at $E_p = 40$ ev. With further decrease of the primary ion energy the values of the ratio decrease.

It must be emphasized that the values shown in Fig.3 are probably underestimates. Lower-than-true values for the maximum scattered ion energy could result from deviation of the target-collector system from spherical shape and owing to systematic errors in scaling off the maximum energy values from the current-voltage characteristics.

The fact that η varies with the primary ion energy indicates that the character of the interaction is influenced by the bonding energy of the target atoms. At such low primary ion energies the ion interaction occurs not with individual atoms of the target, but with some sort of collective entity with an effective mass greater than the mass of an individual target atom.

This inference is substantiated by the results given in Fig.2, which shows that in the case of Cs ions bombarding a nickel target ($m_1 < m_2$) there obtains a large number of scattered ions (K_s = 90% at $E_p = 42$ ev). Further substantiation of the influence of the atomic bonding energy on K_s is the fact that at primary ion energies corresponding to the maximum value of η there are observed only scattered ions, most of which have high energies.

References

1. U.A.Arifov & A.Kh.Ayukhanov, Doklady AN Uzbek SSR Ac.of Sci., No.4, 12 (1951).
2. M.A.Eremeev, Doklady AN SSSR, 79, 775 (1951).
3. U.A.Arifov & A.Kh.Ayukhanov, Zhur.eksp.i teor.fiz., 1(7), 87 (1954).
4. U.A.Arifov & A.Kh.Ayukhanov, Izv.AN SSSR, Ser.fiz., 20, 1165 (1956). (Trans.Bulletin, 20, 1057.)
5. U.A.Arifov, A.Kh.Ayukhanov & S.V.Starodubtsev, Zhur.eksp.i teor.fiz., 4, 845 (1957). (Trans.Soviet Physics - JETP.)

6. U.A.Arifov, A.Kh.Ayukhanov, S.V.Starodubtsev & Kh.Kh.Khadzhimukhamedov, Doklady AN SSSR, 1, 60 (1959). (Trans.Soviet Physics - Doklady.)

7. C.Brunnee, Z.Phys., 147, 161 (1957).

8. U.A.Arifov & A.Kh.Ayukhanov, Doklady AN Uzbek SSR, No.1, 13 (1953); S.V. Starodubtsev, Zhur.eksp.i teor.fiz., 6, 714 (1954).

* * * * * * *

USE OF A DYNAMIC TYPE MASS SPECTROMETER FOR INVESTIGATION OF SECONDARY PROCESSES

- A.Kh.Ayukhanov & G.I.Iskhakov

It is commonly known that positive ion bombardment of solids is accompanied by a number of complex effects.[1-4] Thus, in the primary energy range from 100 to 6000 ev there occurs elastic scattering of the primary ions from individual atoms of the bombarded surface, adsorption and immanation of these ions into the depth of the target, cathode sputtering of the target material and any adsorbed film, kinetic and potential ejection of electrons, and neutralization of the primary ions. Usually these effects are studied by measuring the integral emission of positive and negative particles and their distributions in energy, etc., during bombardment of the surfaces assumed - with more or less justification - to be atomically clean.

It must be noted, however, that methods based on measuring the integral emission are applicable only for investigation of the effects occurring on truly clean surfaces. These conventional methods are not adequate for investigation of effects occurring in bombardment of only quasiclean surfaces. In an earlier contribution[5] we noted the necessity of discriminating between the electronic and ionic components of secondary emission of negative particles, for it was found that with reduction of the work function of the bombarded surface by deposition of electropositive films, the extraneous atoms, possessing an appreciable electron affinity, adsorbed on the surface are preferentially sputtered in the form of negative ions. Thus in the case of ion bombardment of quasiclean surfaces there occurs emission not only of electrons but also of negative ions in appreciable numbers; consequently, by measuring the integral emission of negative particles one cannot determine the nature and abundance of each of these types of emission separately.

Clearly, in the case of quasiclean surfaces a similar situation will obtain for secondary positive ions, i.e., the secondary positive ions will not consist entirely of scattered or evaporated primary ions. Part of the secondary positive ions may be ions of the target material or ions of an adsorbed film forming as a result of complex processes involving dissociation, evaporation and cathode sputtering.

We therefore came to the conclusion that for investigation of secondary emission from complex and quasiclean surfaces it was essential to develop a new procedure, a procedure that would provide for separate investigation of the electron and negative ion components, i.e., would allow of complete mass spectrometric analysis of the positive and negative particles emitted under different conditions from the bombarded surface.

However, investigation of the above mentioned effect by means of conventional mass spectrometers is virtually impossible owing to the delay characteristics of these instruments. Conventional mass spectrometers can be used only for studying steady secondary processes, which means that one must be able to provide a known and reproducible state of the bombarded surface. Owing to the lack of suitble procedures for monitoring and continuous ion bombardment of metal surfaces, t is at present virtually impossible to provide such constant and reproducible tates of the bombarded surface. In view of this it is more expedient to investiate the dynamics of secondary processes during changes in the state of the bomarded surface, but this is possible only by means of a lagfree mass spectrometer. ence, to investigate secondary emission during bombardment of a surface underoing rapid changes we had recourse to a magnetic mass spectrometer with modulaion of the ion energy in conjunction with an electron multiplier for detecting he ions.

Experimental Equipment and Procedure

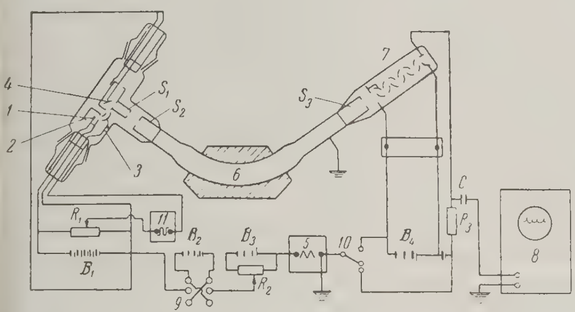

ig.1. Mass spectrometer and associated lectronic equipment.

Mass spectrometers with energy modulation have been described in the literature[6], hence we will not dwell here on their general attributes. The experimental arrangement used in our experiments is diagrammed in Fig.1.

The beam of positive ions, obtained by surface ionization of an appropriate alkali halide salt on heater spiral 1, is extracted by the electric field (produced by battery B_1) applied between the spiral and the source housing 2. The ions passing through the slit in the source housing, enter the cylinder 3, where hey are separated from the neutral atoms and molecules, and impinge on the surace of the target 4. The secondary particles from the target, after passing hrough slit S_1, are accelerated by the electric field, produced by the battery $_2$ and the sawtooth pulse generator 5, and directed into the analyzer 6.

The analyzer is a wedge shaped magnet providing a uniform magnetic field with deflecting angle of 78°. The selected particles emerging from slit S_3 fall on he first dynode of the electron multiplier[7], which is coupled to the input of the scillograph 8, the horizontal sweep of which is synchronized with generator 5. t a given value of the magnetic field, there appears on the oscillograph screen mass spectrogram, the width of which depends on the depth of modulation of the on energy by generator 5. The described equipment can be employed for analysis f positive or negative ions (the direction of the magnet current is reversed by hrowing switches 9, 10 and another switch not shown in the figure). In case of etection of positive ions, before entering the electron multiplier, these are iven an added acceleration equal in magnitude to the voltage applied to the multilier. To insure obtaining a clear mass spectrometer zero line the circuit comrises a square-pulse generator 11, which modulates the primary ion beam. To perit measuring the depth of modulation of the ions entering the analyzer and measureent of the energy width of the peaks, the electronic circuit has provision for mooth variation of the dc component of the accelerating voltage (battery B_3 and otentiometer R_2).

During the experiments a pressure of between $3 \cdot 10^{-6}$ and $7 \cdot 10^{-6}$ mm Hg was mainained in all sections of the apparatus by a TsVL-100 vacuum pump.

As noted above, the principal purpose of the present work was investigation f secondary effects in the process of variation in the state of the bombarded urface. This variation was realized by deposition on a metallic backing of diferent films from a special vaporizer with a variable rate of evaporation. This method of varying the state of the bombarded surface was extremely convenient in that it allowed of investigating under the same vacuum conditions the secondary emission characteristics of the backing-target, the dynamics of the secondary effects during transition states of the target surface, and the secondary emission of thick films, assumed to be identical with the properties of the bulk material. The use of a high melting point metal, tantalum in most cases, enabled us to repeat the experiments, successively removing the deposited films by heating and then redepositing them on the cooled target.

By way of films we tested both alkali metals and alkali halide salts. In the case of the former we were dealing essentially with transition from one metal (tantalum) to a different metal (the alkali metal); in the second case, with a transition from a metal to a dielectric.

The usual experimental procedure was the following: after attainment of the requisite vacuum and outgassing of the target, we switched on the ion source and evaporator, which were first outgassed for an appreciable period at low heat. After re-establishment of the requisite vacuum, we switched on the recording part of the instrument (mass spectrometer) and slowly increased the temperature of the source spiral and evaporator. Then, after attainment of the working vacuum, depending on the rate of change in the abundance of the particles passing through the analyzer, we established the necessary rate of deposition. Investigation of the composition of the secondary positive and negative ions during bombardment of the clean backing was carried out at a high temperature of the target both with the vaporizer turned on and off. The composition of the secondary ion emission in the case of thick films was investigated using the highest possible rate of deposition of the film consistent with a constant intensity of the secondary emissio For intermediate states of the bombarded surface we recorded the dynamics of the process, i.e., the variation in intensity of different ions, by photographing the oscillograph screen with a motion picture camera. The relative abundances of the different types of ions were determined without taking into account the difference of their secondary emission coefficients from the surface of the first dynode of the multiplier.

Results

The composition of the secondary positive ion emission from a clean (no film) metal target is not complicated. The secondary emission observed in bombardment of such cold metal surfaces with alkali metal ions consists of primary ions scattered from individual atoms of the target.

Fig.2 shows the peaks of positive secondary Na ions photographed on the scree of the oscillograph during bombardment of a clean tantalum target with Na ions having energies from 135 to 480 ev. These traces represent the distribution of secondary ions in energy in differential form as a function of the primary ion energy. Clearly evident is the broad nature of the secondary ion spectrum with a sharply pronounced limit energy, dependent linearly on the energy of the primary ions. These limit or maximum energies are consistent with the values for scattered ions obtained by calculations using the equation for elastic collision of the bombarding ions with individual atoms of the tantalum target.

In the case of thick alkali metal films, secondary emission of positive ions is virtually nil both in the case of equality of the masses of the film atoms and bombarding ions and in the case when the mass of the bombarding ions is smaller than the mass of the film atoms. Consequently, in the case of clean alkali metal surfaces there is virtually no noticeable cathode sputtering or scattering of the ions from individual atoms of the target.

For intermediate states of the bombarded surface, when the density of the surface coating on the backing is relatively low, there is observed both scattering of primary ions from the atoms of the target and cathode sputtering in the form of positive ions. With increase of the thickness of the film there occurs gradual decrease of the scattering simultaneously with increase of cathode sputtering.

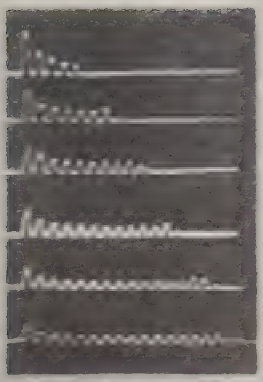

Fig.2. Oscillograms characterizing the distribution of secondary (scattered) positive Na ions in bombardment of a tantalum target with positive Na ions.

In investigation of secondary emission from ion-bombarded complex surfaces the emission of negative ions is particularly important. Hitherto, in most cases, the entire secondary emission of negative particles was lumped as ion-electron emission. Careful analysis showed, however, that this secondary electron-ion emission in the case of bombardment of complex surfaces comprises an appreciable fraction of different negative ions. Hence we felt it would be of interest to elucidate the composition of the negative ion emission.

In the case of ion bombardment of a clean tantalum surface there is virtually no emission of negative ions of any type. When, however, there are even traces of an alkali metal coating on the tantalum backing there begin to appear different negative ions, the abundances of which increase to a certain saturation value with increasing density of the alkali coating.

Fig.3 shows the observed variation in the abundance of negative O, O_2, H, OH, Cl^{35} and Cl^{37} ions observed in bombardment of an Na coating on the Ta target with Na^+ ions as a function of the film density. It will be evident that the functional dependence differs for each type of ion.

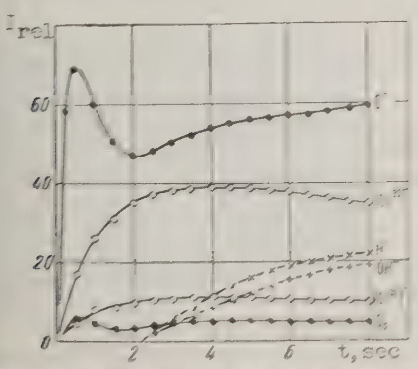

ig.3. Variation of the abundances of O, O_2, H, OH, Cl^{35} and Cl^{37} ions with the density of the Na film on Ta bombarded with 600 ev Na^+ ions.

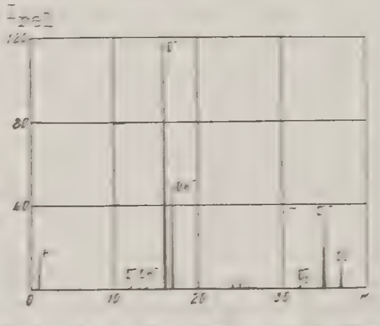

Fig.4. Relative abundances of the different negative ions appearing in bombardment of an Na film on Ta with 600 ev Na^+ ions in the process of slow deposition of the Na film.

Moreover, the composition of the negative ions and the film thickness dependence of the variation in their abundance depend strongly on the composition of the residual gases in the tube and on the rate of deposition of the film. For example, in the case of low rates of deposition of Na on Ta (of the order of an atomic layer per second) and bombardment with 600 ev Na^+ ions, we observed the following ions in the negative ion emission: H, C, CH, N, O, OH, O_2, Cl and ions with A = 24,

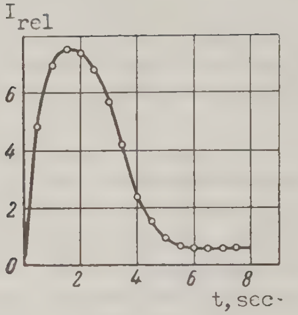

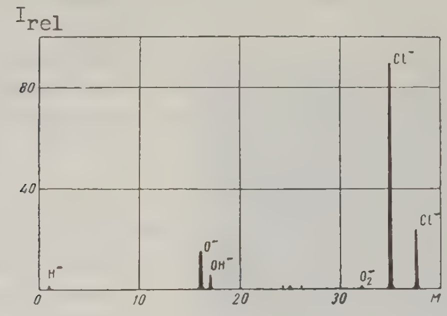

Fig.5

Fig.6

Fig.5. Variation in the abundance of negative oxygen ions ejected by 600 ev K^+ ions as a function of the thickness of an Na film deposited at a high rate on the tantalum target.

Fig.6. Relative abundances of different negative ions emitted in bombardment with Na^+ ions of a KCl film deposited at a high rate on the tantalum target.

25, 26 and 42. The relative abundances of the listed negative ions in one particular experiment are shown in Fig.4. It must be emphasized, however, that this composition of the negative ion emission is not constant and that the relative abundances are entirely different under different experimental conditions. For example, at high rates of deposition (over 10 atomic layers per second) and with appearance of an Na deposit on the walls of the apparatus all the above enumerated negative ions except O and O_2 virtually disappear.

Fig.5 shows the dynamics of the variation in abundance of negative oxygen ion ejected by 600 ev K^+ ions in the process of deposition on the Ta backing of an Na film at high rates of deposition and in the presence of an Na deposit on the walls of the apparatus. As will be evident from the figure, the abundance of oxygen ions for intermediate states of the bombarded surface goes through a maximum, but for thick films under the indicated conditions it is also very low.

Thus in the case of slow deposition of an alkali metal coating, when the rate of the competing adsorption of residual gases is comparable with the rate of deposition of the coating, the composition of the secondary negative ion emission includes a large number of different negative ions. In the case of rapid deposition, owing to change in the ratio between the rate of deposition of the film and the competing adsorption of residual gases (with resultant decrease in the relative quantity of gases occluded in the film), emission of negative ion virtually ceases. The appearance of a maximum abundance of negative oxygen ions at low deposition rates and the continuing emission of oxygen ions at the maximum deposition rates may be explained by the fact that despite all the measures taken in our experiments to outgas the tantalum target, it was still not entirely free of oxygen; with only a thin alkali metal coating on the target the oxygen occluded in the tantalum is ejected with high efficiency in the form of negative ions. Consequently, the composition of the secondary negative ion emission during slow deposi tion of an alkali metal coating yields information on the composition of the residual gases in the apparatus, while in the case of rapid deposition there is still evinced the presence of gases adsorbed on the surface of the target-backing.

Similar results were obtained in experiments involving deposition of alkali halide salts on a tantalum backing. Where positive ion emission is concerned here again we observe transition from scattering of the primary ions from individual toms of the target to sputtering of positive ions of the alkali metal from the lkali halide salt film forming on the surface, as well as sputtering of the pri-ary ions knocked into the film; the intensity of the positive emission depends n the rate of deposition of the film and on the intensity and energy of the pri-ary ions.

The composition of the secondary negative ion emission in the case of slow eposition of an alkali halide salt film is essentially the same as in the case f slow deposition of an alkali metal coating. Fig.6 shows the relative abundances f different negative ions recorded in the case of Na^+ bombardment of a KCl film eposited at a high rate on the tantalum target. As will be evident from the fig-re, in this case the highest peak is that of Cl. In the case of rapid deposition f the KCl film, the abundance of all the negative ions (except Cl) is greatly re-uced and almost the entire negative ion emission consists of negative chlorine ons.

Energy Distribution of the Secondary Ions

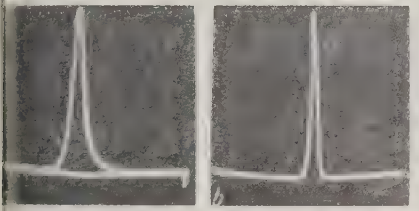

ig.7. Peaks obtained for Na ons ejected by Na ion bombard-ent from an Na film on tanta-um (a) and by surface ioniza-ion of the Na film on the Ta urface (b).

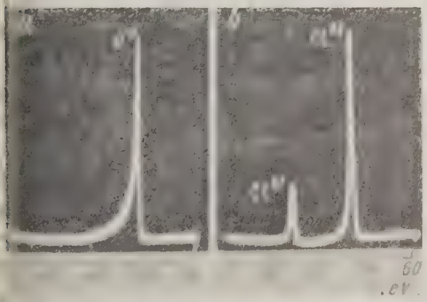

ig.8. Peaks recorded for egative O^{16} (a) and Cl^{35} nd Cl^{37} (b) ions under rdinary conditions.

As was noted above, the energy distribution of the secondary ions can be deduced from the shape and height of the corresponding peaks in the mass spectrograms. Fig.7,a shows the peak for Na^+ ions ejected from an Na film on Ta under bombardment with Na ions. Fig.7,b shows the peak of Na ions emitted by the tantalum target at high temperature as a result of surface ionization of the Na ions. Comparison of the spectrograms shows that the ions ejected by bombardment have a "harder" energy spectrum than those obtained by surface ionization.

The secondary negative ions also exhibit a broad energy spectrum, similar to the energy spectrum of ejected Na^+ ions; from this one might conclude that identical mechanisms are involved in the ejection of both positive and negative ions.

More careful examination, however, discloses certain differences between the energy spectra of different ions. Fig.8 shows the peaks recorded for negative O and Cl ions under nearly the same conditions. It will be evident that the O ions have an appreciably wider energy spectrum than the Cl^{35} ions. Moreover, in a number of experiments we obtained indications that the energy distribution of the secondary ions depends in a complex manner on the energy of the primary ions and the thickness of the film; the results of these experiments give reason to hypothesize that there occurs direct energy transfer from the bombarding ions to the secondary positive and negative ions.

Discussion

The principal advantage of the developed experimental technique is that it llows of making rapid measurements and thereby following the variation in the oundance of different components of the secondary ion emission as a function of apid variation in the state of the bombarded surface. The experimental results obtained so far show that in the process of deposition of alkali metal films on a Ta target the ionic component of the secondary emission undergoes great variations. Of particular interest is the appearance of negative ions. Thus, in the case of a tantalum surface free of alkali metal film, despite the obvious presence of adsorbed gases on the Ta surface, the emission of negative ions is virtually nil. In contrast, the presence of even a thin deposit of alkali metal ions on the Ta surface leads to a very intense sputtering of the adsorbed gases in the form of negative ions.

Emission of negative ions is also observed in bombardment of thick alkali metal film contaminated with adsorbed residual gases and also from thick films of alkali halide salts. In all these cases we note the common factor that the sputtering of the atoms, having an appreciable electron affinity, in the form of negative ions occurs only when conditions are favorable for the formation of chemical compounds on the bombarded surface; hence the process is presumably accompanied by dissociation of molecules.

The negative ion emission obtained under these conditions may have practical significance, inasmuch as the coefficients of secondary ion emission for some of the negative ions attain high values. Employing the described procedure, we were not able to determine the values of the secondary emission coefficients for individual negative ions owing to the difference in the values of the coefficients of secondary ion-electron emission from the surface of the first dynode of the multiplier. But it is known from experiments involving separate measurements of the electron and negative ion components of the secondary emission that in some cases the coefficient of secondary negative ion emission of, for example, oxygen, may be as high as 100%.

Institute of Nuclear Physics,
Academy of Sciences of the Uzbeck SSR

References

1. U.A.Arifov, A.Kh.Ayukhanov & S.V.Starodubtsev, Zhur.eksp.i teor.fiz., 26, 714 (1954).

2. U.A.Arifov & A.Kh.Ayukhanov, Izv.AN SSSR, Ser.fiz., 20, 1165 (1956). (Tran Bulletin, 20, 1057.)

3. M.A.Eremeev, Doklady AN SSSR, 79, 775 (1951).

4. C.Brunnee, Z.Phys., 147, 161 (1957).

5. U.A.Arifov, A.Kh.Ayukhanov & S.V.Starodubtsev, Izv.AN UzSSR, Ser.fiz.-mat, nauk (Bulletin, Uzbeck SSR Ac.of Sci., Phys.-Math. Sciences Series), 2, 107 (1958)

6. W.Siri, Rev.Sci.Instr., 18, 540 (1947).

Transactions
# of the
Eighth Conference on Luminescence

(Molecular luminescence and luminescence analysis)

(Minsk, 19-24 October 1959)

(Concluded from Vol. 24, No. 5)

ULTIMATE LINES OF 3,4-BENZOPYRENE DISSOLVED IN NORMAL HYDROCARBONS AT DIFFERENT TEMPERATURES

- S.G.Bogomolov, F.D.Pemova & L.P.Kolosova

Shpol'skii et al[1] found that the luminescence spectra of some aromatic hydrocarbons dissolved in normal paraffins when recorded at liquid nitrogen temperature represent a sequence of lines. They found that the luminescence spectra of some complex organic molecules are reminiscent of the atomic spectra of elements. It has proved feasible to utilize such observations for clarifying the structure of complex molecules, for experimental determination of the normal vibration frequencies of molecules and also for analytic purposes. Thus, for example, Dikun[2] utilized the line emission spectrum of 3,4-benzopyrene to prove that this compound is present in a number of chemical products. He made qualitative determinations of the 3,4-benzopyrene content using a semiquantitative technique based on recording the absorption spectra by means of a specially equipped SF-4 spectrophotometer.[3]

We undertook to develop a semiquantitative procedure for determination of 3,4-benzopyrene in samples by means of a conventional spectrograph with glass optics. Such a procedure would allow of determining 3,4-benzopyrene in any laboratory possessing a spectrograph.

The basic ideas on which the developed procedure is based are the following. Emission spectrum analysis is based on the fact that the atomic spectrum of each element consists of a large number of lines differing in intensity. With decrease in the concentration of the element in the sample the intensity of the lines decreases and consequently so does the number of lines discernible on the photographic plate. For each element one can identify certain lines which disappear last with decrease in concentration. As is known, such lines are called ultimate lines or raies ultimes. Investigation of these lines in atomic spectra showed that the ultimate lines are in most cases atomic resonance lines.

Inasmuch as the fluorescence spectrum of 3,4-benzopyrene in hexane solution at liquid nitrogen temperature consists of narrow lines reminiscent of the lines in atomic spectra, it could be expected that with decrease of the 3,4-benzopyrene concentration in the sample the number of lines in its spectrum will decrease. Thus we reasoned that one can find a number of ultimate lines not only for an atomic emission spectrum but also for the fluorescence spectrum of 3,4-benzopyrene in frozen solutions in normal paraffins. To check this we photographed the luminescence spectra of solutions of 3,4-benzopyrene in hexane in the range of concentrations from 16^{-4} to 10^{-8} g/ml. In general, the intensity of lines in a spectrogram depends on the radiation source, the sensitivity of the photographic plate, the conditions of development, the aperture of the spectrograph and a number of other factors. It follows therefore that the ultimate lines will be determined not only by the concentration of the element (or in our case 3,4-benzopyrene) in the sample but also by the analytic conditions. For the data obtained in one laboratory can be used in other laboratories, the work must be carried out under standard conditions.

We photographed the luminescence spectra on an ISP-51 spectrograph. We used both a camera with a focal length of 270 mm (plate factor in the 4000 Å region 19 Å/mm) and a UF-84 camera (plate factor in the same region 6.5 Å/mm). The spectra were photographed on Type II spectroscopic plates (speed 16 GOST units) and also on aerial film (speed 350 GOST units). The luminescence spectra were excited by a universal OU-1 source with a PRK-2 mercury tube and a filter transmitting 3650 Å radiation. The cell containing the 3,4-benzopyrene solution in hexane was contained in a Dewar with liquid nitrogen.

As we expected, our tests showed that with reduction of the 3,4-benzopyrene concentration the number of lines in the fluorescence spectrum decreased (see tabl

Variation in the number of lines in the luminescence spectrum of 3,4-benzopyrene dissolved in hexane at liquid nitrogen temperature with variations in the benzopyrene concentration (wavelengths in Å)

Line No.	10^{-4} g/ml	10^{-5} g/ml	10^{-6} g/ml	10^{-7} g/ml	10^{-8} g/ml	Line No.	10^{-4} g/ml	10^{-5} g/ml	10^{-6} g/ml	10^{-7} g/ml	10^{-8} g/ml
1	4015	4015	4015	4015	—	12	4165	4165	4165	—	—
2	4020	4020	4020	4020	4020	13	4205	4205	—	—	—
3	4025	4025	4025	4025	4025	14	4208	4208	—	—	—
4	4068	4068	4068	—	—	15	4212	4212	—	—	—
5	4075	4075	4075	4075	—	16	4215	4215	—	—	
6	4078	4078	4078	4078	—	17	4220	4220	4220	4220	—
7	4125	4125	—	—	—	18	4225	4225	4225	—	—
8	4132	4132	—	—	—	19	4250	4250	4250	4250	4250
9	4137	—	—	—	—	20	4255	4255	4255	4255	4255
10	4155	—	—	—	—	21	4260	4260	4260	4260	—
11	4160	4160	4160	—	—						

Thus in the 4000 to 4260 A region there are 21 lines of 3,4-benzopyrene present in the frozen solution spectrum when the benzopyrene content in the sample is 10^{-4} g/ml. As a concentration of 10^{-6} g/ml there are 13 lines; at 10^{-7} g/ml 9 lines, and at 10^{-8} g/ml only 4 lines, namely, 4020, 4025, 4350 and 4255 Å. These are presumably the ultimate lines in this part of the spectrum. Under our analytic conditions the appearance of these four lines indicates that 3,4-benzopyrene is present in the sample in the concentration of 10^{-8} g/ml. It will be evident from the microphotometric traces of the spectrum of 3,4-benzopyrene dissolved in hexane at liquid nitrogen temperature (see accompanying figure) that the ultimate lines are as a rule the most intense lines in the spectrum.

For purposes of practical utilization of the ultimate lines it is important to note that these same lines at a 3,4-benzopyrene concentration of 10^{-8} g/ml in

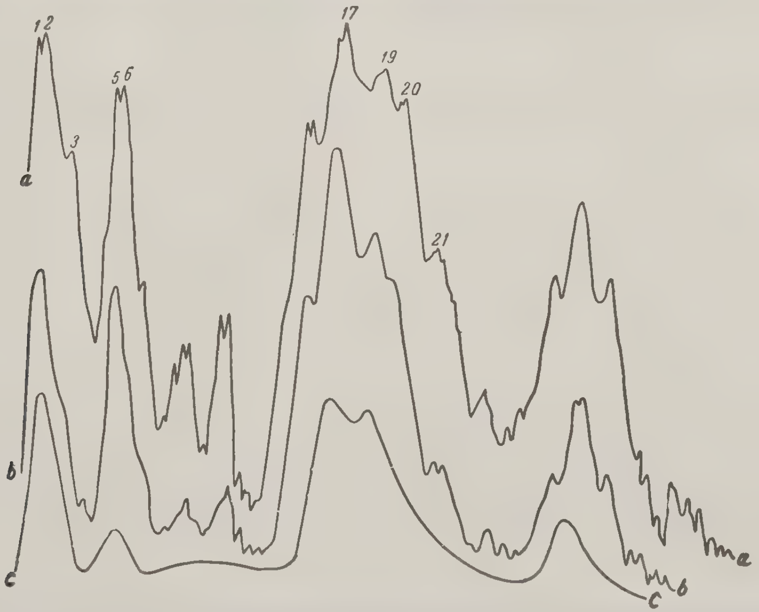

Photometric traces of the luminescence spectrum of 3,4-benzopyrene in hexane solution: a) at -196°, b) at -120°, c) at +18°.

the sample were discerned in the spectrum when this was recorded by the camera with f = 270 mm instead of the UF-84 camera. In this case the exposure time was reduced by a factor of 9 (naturally at higher concentration of 3,4-benzopyrene in the sample one can record a much larger number of lines by means of the UF-84 camera).

We obtained similar results in using n-octane as a solvent. On the other hand, no discreet spectrum was obtained in tests with isooctane.

We tested the developed ultimate line procedure by determining the 3,4-benzopyrene content in a number of industrial samples. The results were compared with the data obtained by photometric measurements and the agreement proved to be satisfactory.

In order to determine the influence of temperature in the luminescence spectrum of 3,4-benzopyrene we recorded the spectra at room temperature and at a number of intermediate temperatures between the freezing point of the solvent and liquid nitrogen temperature.

The character of the changes occuring will be evident from an examination of the photometric traces reproduced in the accompanying figure. The spectrum of 3,4-benzopyrene at room temperature consists of a few diffused bands. With decrease of the temperature these bands increase in intensity. At about -150° the bands begin to separate into broad, often overlapping lines. With further decrease of the temperature the lines become narrower and increase in number. The number of ultimate lines differs at different temperatures.

Sverdlovsk Medical Institute

References

1. E.V.Shpol'skii, Uspekhi fiz.nauk, 68, 51 (1959). (Trans.Soviet Physics - Uspekhi.)
2. P.P.Dikun, Report presented at the Sixth Conference on Luminescence, Leningrad, 1958.
3. P.P.Dikun, Voprosy onkologii (Problems of Oncology), No.4, 34; No.5, 24 (1955).

LUMINESCENCE OF SOLUTIONS OF THIOINDIGO AND ITS DI-DERIVATIVES AT 77°K

- R.N.Nurmukhametov, D.N.Shigorin & N.S.Dokunikhin

We extended the procedure for obtaining the luminescence spectra and the ong wavelength absorption band with clear structure, developed by E.V.Shpol'skii nd his co-workers[1] for aromatic hydrocarbons, to compounds containing heterotoms. In such compounds there occur two types of transitions: $n \rightarrow \pi^*$ and $\pi \rightarrow \pi^*$. I.Kasha[2], who analyzed the experimental material available in 1950, noted that one f the distinctive features of these substances is that the spectrum associated ith the $n \rightarrow \pi^*$ electronic transition is more diffused and smeared out than the pectrum associated with the $\pi \rightarrow \pi$ transition.

On the other hand, our earlier investigations[3] of the luminescence spectra of olutions of anthraquinone and some of its derivatives at 77°K, associated with he $n \rightarrow \pi^*$ transition, yielded a distinct quasi-line structure, which indicates hat the distinction remarked on by Kasha does not always obtain. In the present eport we give data obtained in investigating the spectra of thioindigo, 5,5'-imethylthioindigo and 6,6'-diethoxythioindigo, all of which exhibit a certain olubility in normal hydrocarbons.

Frozen solutions of these compounds at 77°K yielded spectra with a clearly iscernible vibrational structure, which gradually smeared out in going from hexne to nonane as the solvent. We also obtained an absorption spectrum with strucure for tioindigo in hexane. The relative simplicity of the spectrum allows of nterpreting it by means of three frequencies: 220, 480 and 1540 cm^{-1} in the case f the luminescence spectrum and 200, 480 and 1500 cm^{-1} in the case of the absorpion spectrum.

The most characteristic frequency in the spectrum is 1540 cm^{-1}, which is close o the frequency of the $>C = C<$ group (1535 cm^{-1}) evinced in the emission spectra f stilbene.[4] The frequency of the CO group in the thioindigo molecule which acording to infrared spectroscopic data[5] equals 1650 cm^{-1}, is not evinced in the lectronic spectrum. The observed spectrum must be attributed to transition of π electron in the $>C = C<$ group. Thus, although the thioindigo molecule contains our hetero-atoms, the long wavelength absorption band and the long wavelength emision band must be associated with the $\pi \rightarrow \pi^*$ transition and not with the $n \rightarrow \pi^*$ ransition as is usually the case[6].

Rogers et al[7] investigated the spectra of benzene solutions of thioindigo and ts derivatives. In their work they detected photoisomerization of the thioindigo olecule:

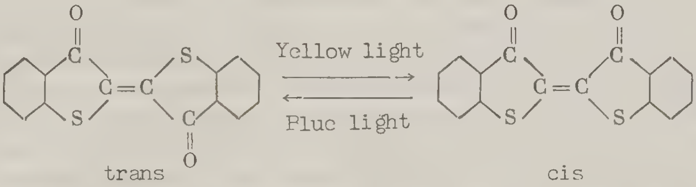

The structured spectra help understand the nature of the trans-cis photoisoerization process. The excitation energy is localized in the $>C = C<$ group, which eads not only to loosening of the second bond of this group but also to a higher robability for transfer of excitation energy to torsional vibrations favoring hotoisomerization. Ried[6] reported that thioindigo does not luminesce in alcohol olutions and cellophane films; he explained the quenching by the presence of interolecular H bridges.

We found that an alcohol solution, which virtually does not luminesce at room emperature, when frozen to 77°K yields an emission spectrum which, although somewhat smeared out, agrees as regards position with the spectra of normal hydrocarbon solutions of thioindigo.

The similarity in the behavior of alcohol and neutral solutions indicates that the deactivation of the thioindigo molecules in alcohol is not determined only by the formation of hydrogen bonds. In cellophane films thioindigo exhibits a weak luminescence even at room temperature, a luminescence which does not increase upon cooling. The spectrum in cellophane is shifted to the long wavelength side relative to the spectra of solutions. Investigation of the different influence of media with possible intermolecular hydrogen bonds is of independent interest. A more detailed description and analysis of the spectra will be found in Ref.8.

"L.Ya.Karpov" Physical-Chemical Institute

References

1. E.V.Shpol'skii, Usp.fiz.nauk, 68, 51 (1959) (Trans.Sov.Physics - Uspekhi); E.V.Shpol'skii, A.A.Il'ina & A.A.Klimova, Doklady AN SSSR, 87, 935 (1952).
2. M.Kasha, Disc. of the Faraday Soc., Sept.14, 1950.
3. D.N.Shigorin, N.A.Shcheglova, R.N.Nurmukhametov & N.S.Dokunikhin, Doklady AN SSSR, 120, 1242 (1958). (Trans.Soviet Physics - Doklady.)
4. K.W.Hausser, R.Kuhn & E.Kuhn, Z.phys.Chem.B, 29, 417 (1935).
5. D.N.Shigorin, N.S.Dokunikhin & A.E.Gribova, Zhur.fiz.khimii (Journal of Phys.Chem.), 29, 867 (1955).
6. Reid, J.Chem.Phys., 21, 1906 (1953).
7. D.A.Rogers, J.D.Margere & G.M.Wyman, J.Amer.Chem.Soc., 79, 2464 (1957).
8. R.N.Nurmukhametov, D.N.Shigorin & N.S.Dokunikhin, Zh.fiz.khimii (Journ. Phys.Chem.), 34 (1960).

* * * * * * *

TEMPERATURE DEPENDENCE OF THE FLUORESCENCE EFFICIENCY OF SOME PHTHALIMIDES IN DIFFERENT SOLVENTS

- L.G.Pikulik & A.N.Sevchenko

Increase in the temperature of the medium or solvent usually leads to decrease of the fluorescence yield. This is connected with increase in the probability for nonradiative transitions, dependent on the vibrational energy of the molecule. Nonradiative deactivation of the excited state may also occur for other reasons. Zelinskii et al[1,2] showed that for some phthalimides the quantum efficiency in different solvents at 20° is consistently correlated with the position of the fluorescence spectrum. In such cases the decisive role in the quenching of fluorescence is played by the relative position of the ground and excited states.

The curve characterizing the variation of the quantum efficiency with the frequency of the luminescence peak may have two branches: an ascending section and then a descending section corresponding to further increase in the frequency of the peak (Fig.1). In the case of substances obeying this regularity, change of the solvent results, together with a shift of the fluorescence spectrum, in a corresponding change in the quantum efficiency. Shift of the fluorescence peak is also observed as a result of change in the temperature of the solution.[3-5] In these cases one may also expect a change in the probability for nonradiative transitions connected with the position of the spectrum.

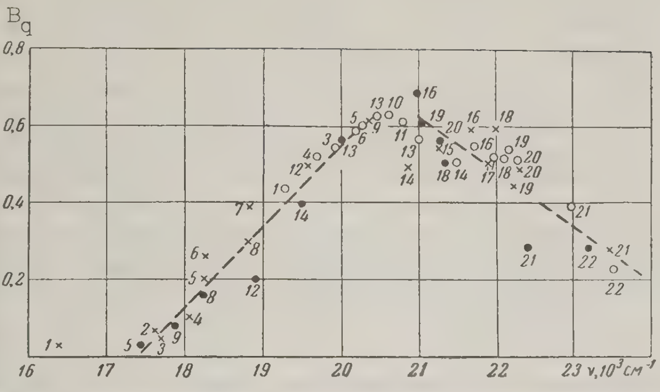

Fig.1. Variation of the fluorescence efficiency of phthalimide with the frequency of the fluorescence peak in different solvents at 20°C: 1) water, 2) glycerol, 3) acetic acid, 4) butyric acid, 5) methyl alcohol, 6) ethyl alcohol, 7) cyclohexanol, 8) nonylic acid, 9) butyl alcohol, 10) isobutyl alcohol, 11) isopropyl alcohol, 12) ethyl acetate, 13) pyridine, 14) acetone, 15) chloroform, 16) dioxane, 17) anisole, 18) diethyl ether, 19) chlorobenzene, 20) benzene, 21) carbon tetrachloride, 22) n-hexane. x - 4-amino-N-methylphthalimide; ● - 4-methylamino-4-methylphthalimide; O - 3-amino-N-methylphthalimide.

The shift of the spectra incident to heating of the solution occurs to the short wavelength side,[3,5] i.e., the frequency of the fluorescence peak increases. Hence for substances with the indicated ν^f_{max} dependence of the fluorescence yield B_q one can predict the character of the variation in efficiency accompanying the temperature shift of the spectra. As will be evident from Fig.1, a higher value of efficiency corresponds to higher values of the peak frequency in the 16 500 to 20 200 cm^{-1} region (region of the ascending branch of the curve); at the same time in the 20 200 to 24 000 cm^{-1} region (descending branch) the efficiency either remains constant or decreases with increase of ν^f_{max}. Consequently, for solvents in which the peak of the fluorescence band of phthalimides at 20° lies in the region of the ascending branch of the curve, a temperature induced shift of the spectra to the short wavelength side should lead to increase in efficiency. For solvents in which the fluorescence peak lies in the region of the descending branch, a like short wavelength shift of the fluorescence spectrum may in some cases be accompanied by no change in efficiency but in most cases will lead to decrease in the efficiency.

It should be emphasized that the above inferences regarding the change in efficiency accompanying temperature induced shifts in the spectra do not take into account conventional temperature quenching of fluorescence. Such quenching in general may more or less completely suppress the increase in efficiency due to shift of the fluorescence peak with increasing temperature.

In the present investigation we determined the temperature dependences of the fluorescence efficiency of a number of phthalimides in high boiling point solvents.* In these solvents there was observed an appreciable shift of the luminescence bands with increasing temperature.[5]

The fluorescence spectra and the temperature dependences of the relative quantum efficiency were investigated on a photoelectric set-up assembled about a UM-2 monochromator. The absorption of the solutions was measured by means of an SF-4 spectrophotometer.

The fluorescence spectra of 4-dimethylamino-N-methylphthalimide in different solvents at different temperatures are shown in Fig.2. In each case the area under the fluorescence curve characterizes the relative number of photons emitted. It will be evident from the figure that for solutions in benzyl alcohol and cyclohexanol the number of photons emitted increases substantially with increase in

---

*Student L.Volod'ko participated in the measurements.

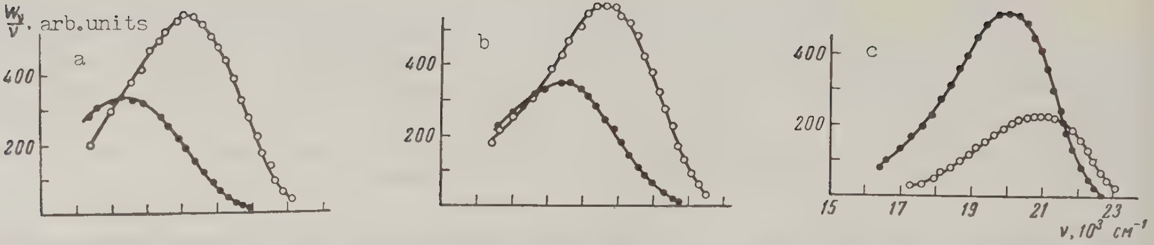

Fig.2. Variation of the fluorescence spectrum of 4-dimethylamino-N-methylphthalimide with the temperature in different solvents: a) benzyl alcohol, b) cyclohexanol, c) dimethylphthalate; ● - t = 20°, O - t = 160°, 150° and 170° for a, b and c, respectively.

temperature. In view of the fact that in the indicated temperature interval the absorption of the solutions increases by only 10-15%, the observed increase in intensity indicates a marked increase in quantum efficiency. On the other hand, for the solution of this phthalimide in dimethylphthalate increase in temperature leads to decrease of the quantum efficiency. It should be noted that in this case the fluorescence spectrum at 20° is shifted to the short wavelength side compared with the spectra in benzyl alcohol and cyclohexanol.

Fig.3,a shows the temperature dependences of the quantum efficiency of 4-amino-N-methylphthalimide. As will be evident from the figure, in benzyl alcohol, glycol and cyclohexanol solutions the efficiency increases with rise in temperature. On the other hand, in the dimethylphthalate solution there occurs temperature quenching of the fluorescence. Temperature quenching was also observed in vaseline oil, ethyl acetoacetate, and ethyl benzoate, i.e., in the solvents in which the peak of the fluorescence band lies in the 22 000 to 24 000 cm⁻¹ region. Analogous temperature behavior of the quantum efficiency in the enumerated solvents was also observed for 4-aminophthalimide.

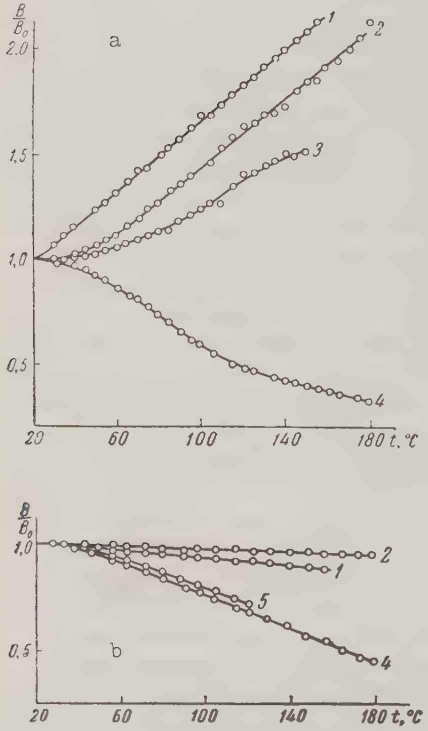

Fig.3. Variation of the relative quantum efficiency of 4-amino-N-methylphthalimide (a) and 3-aminophthalimide (b) with temperature in different solvents: 1) benzyl alcohol, 2) glycol, 3) cyclohexanol, 4) dimethylphthalate, 5) pinene.

Levshin[6] describes cases of increase of the quantum efficiency with increase in temperature. This effect was observed for concentrated dye solutions and is presumably connected with break up of non-luminescing complexes. In our case variation of the concentration of 4-amino-N-methylphthalimide in cyclohexanol solution in the range from 10^{-5} to 10^{-3} mole/liter did not result in any noticeable change in the temperature dependence of the efficiency, which gives reason to infer that in the indicated concentration range concentration quenching is negligible. In addition, one might assume that increase in the quantum efficiency of the phthalimide is evinced in certain specific solvents and is connected with some specific properties of the solvent, properties that stimuate the fluorescence with increase in temperature. This hypothesis is disproved, however, by the temperature dependence of the efficiency of 3,6-diacetoamino-N-methylphthalimide in benzyl alcohol. For this substance the quantum efficiency does not vary with ν^{f}_{max} in the manner characterized by the curve of Fig.1; hence there should be no increase in efficiency with increase of temperature; and experiments show that this is in fact the case.

The described temperature variations in quantum efficiency can readily be explained on the basis of the ν^{f}_{max} dependence of B_q. Increase in efficiency with rising temperature is accompanied by an appreciable shift of the spectra. Accordingly, a higher efficiency B_q should correspond to a higher value of ν^{f}_{max} for solvents in which the fluorescence peak lies within the range of the ascending branch of the curve. In the case of 4-amino-N-methylphthalimide in cyclohexanol at 20° ν^{f}_{max} = 18 800 cm^{-1}, and the efficiency is approximately 40%. According to the curve of Fig.1, with the fluorescence peak at 20 200 cm^{-1}, the efficiency should be about 60%. With increase of the temperature of the cyclohexanol solvent to 150° the fluorescence peak is shifted approximately 1400 cm^{-1} (ν^{f}_{max} = 20 200 cm^{-1}), and the efficiency, as will be evident from Fig.3,a, increases by a factor of about 1.5, i.e., actually does rise to 60%. Thus the correlation between the efficiency and the position of the fluorescence peak is also evinced in cases when the shift of the spectrum is produced not by change of the solvent but by variation of the temperature. The effect is evident because in the given case ordinary temperature quenching is virtually nil.

It should also be noted that the rate of increase in efficiency with increase in temperature decreases as the frequency of the fluorescence peak at 20° is displaced to the side of higher frequencies (4-amino-N-methylphthalimide in benzyl alcohol ν^{f}_{max} = 18 200 cm^{-1}; in glycol - 18 500 cm^{-1}; in cyclohexanol - 18 800 cm^{-1}; in dimethylphthalate - 21 400 cm^{-1}).

The ν^{f}_{max} dependences of B_q for 3-amino-N-methylphthalimide and 4-amino-N-methylphthalimide are somewhat different (Fig.1). In the case of the former the increase in efficiency with shift of ν^{f}_{max} to the side of higher frequencies is relatively small, and the shift of the spectrum with increase in temperature is weaker than for 4-derivatives[5]; hence increase in the efficiency is less probable. The temperature dependences of the efficiency of 3-aminophthalimide is shown in Fig.3,b.* As will be seen from the figure, there is no increase in fluorescence efficiency with increase in temperature for this substance. It will readily be evident, however, that the character of the temperature quenching varied consistently with the shift of ν^{f}_{max} to the short wavelength region. The fluorescence peaks of 3-aminophthalimide in benzyl alcohol, glycol and cyclohexanol at 20° are located in the 20 000 to 20 400 cm^{-1} region. Thus in these solvents there is observed little or no change in efficiency with increase in temperature. For solutions of 3-aminophthalimide in dimethylphthalate and pinene in which ν^{f}_{max} = 21 100 cm^{-1} and 22 000 cm^{-1}, respectively, the fluorescence quenching is appreciably stronger.

In order to obtain additional information on the character of the temperature quenching of the fluorescence of phthalimide solutions we measured the lifetimes of the excited state at room temperature and at higher temperatures. The resultant data are summarized in the accompanying table, where they are juxtaposed with the relative efficiencies under the same conditions.

As will be evident from the table, change in the relative efficiency B/B_o is accompanied by a corresponding change in the relative lifetime τ/τ_o of the excited state. Thus it may be asserted that the investigated quenching processes as well as the fluorescence stimulation processes are not connected with changes in inactive

---

*Under equal condition the efficiencies of 3-aminophthalimide and 3-amino-N-methylphthalimide agree within the limits of the experimental error.

Solvent	4-amino-N-methylphthalimide		3-aminophthalimide	
	B/B_0	τ/τ_0	B/B_0	τ/τ_0
Benzyl alcohol	2,15	1,9	0,88	0,88
Glycol	1,98	1,67	0,9	0,99
Cyclohexanol	1,5	1,7	0,95	0,95
Dimethylphthalimide	0,35	0,36	0,45	0,54

absorption. According to the classification of Vavilov[7,8], we are dealing here with quenching of the second order. This is further substantiation of existence of consistent correlation between the efficiency and the position of fluorescence spectra, or more accurately speaking, between the efficiency and the relative positions of the potential curves for the ground and excited states.

We desire to express our sincere gratitude to V.V.Zelinskii for valuable observations and to A.M.Bonch-Bruevich and G.A.Tishchenko for permission to carry out the fluorometric measurements.

Institute of Physics,
Academy of Sciences of the Belorussian SSR

References

1. V.V.Zelinskii, N.P.Emets, V.P.Kolobkov & L.G.Pikulik, Izv.AN SSSR, Ser. fiz., 20, 507 (1956). (Trans.Bulletin, 20, 465 (1956).)
2. V.V.Zelinskii, V.P.Kolobkov & L.G.Pikulik, Optika i spektroskopiya, 1, 161 (1956).
3. L.G.Pikulik, Ibid., 2, 676 (1957).
4. V.V.Zelinskii, V.P.Kolobkov & N.D.Krasnitskaya, Ibid., 6, 417 (1959).
5. L.G.Pikulik & M.A.Solomakha, Izv.AN SSSR, Ser.fiz., 22, 1391 (1958). (Trans.Bulletin, 22, 1381 (1958).)
6. V.L.Levshin, Fotolyuminestsentsiya zhidkikh i tverdykh veshchestv (Photoluminescence of solids and liquids) M.-L., 1951.
7. S.I.Vavilov, Doklady AN SSSR, 3, 271 (1936).
8. S.I.Vavilov & A.N.Sevchenko, Ibid., 3, 277 (1936).

CONCERNING THE RELATION BETWEEN THE ABSORPTION AND LUMINESCENCE SPECTRA OF COMPLEX MOLECULES

- M.N.Alentsev & L.A.Pakhomycheva

One of the most characteristic features of complex molecules in solution is the invariability of their luminescence spectra, i.e., the fact that the frequency distribution of the energy in their luminescence virtually does not depend on the method of excitation. In view of this it may be asserted that in such substances there must be established by the instant of emission a "standard" distribution of the molecules over the vibrational levels of the excited electronic state.

On the assumption that this distribution is an equilibrium distribution dependent on the temperature of the medium, Stepanov[1] in 1957 deduced the following relation between the absorption and luminescence spectra of complex molecules:

$$\frac{E_\nu}{\varkappa_\nu} = D\nu^3 e^{-\frac{h\nu}{kT}}. \tag{1}$$

Since its publication this relation has been subjected to repeated experimental checks.[2-4] The experimental data on the absorption and luminescence spectra have been processed in the following manner.[2] Taking the logarithm of both sides of Eq.(1) and discarding the terms not dependent on ν, we readily obtain

$$3 \ln \nu - \ln \frac{E_\nu}{\varkappa_\nu} = \frac{h}{kT}\nu. \tag{2}$$

The expression on the left, which we shall designate by F_ν, in case Eq.(1) is fulfilled, must be a linear function of ν, and from the slope of the straight line plot representing this function one can readily evaluate the temperature.

It was found, however, that the temperature T_1 calculated in this manner in many cases proved to be higher than the experimental temperature R even in the case of substances in the condensed phase (liquid solutions). The hypothessis that excited molecules in solution do not have time to attain thermal equilibrium with the medium appears highly doubtful.

Hence we decided to analyze the experimental conditions for some specific luminescent substance in order to clarify the actual degree of divergence between T_1 and T. For our investigation we chose aqueous solutions of erythrosine. This choice was dictated by the fact that according to old data[2] erythrosine was characterized by the largest discrepancy between T_1 and T. In addition, the low luminescence yield of aqueous solutions of erythrosine made it possible to disregard secondary luminescence in taking into account reabsorption. We used solutions of low concentration ($\sim 10^{-6}$ mole/liter) in order to avoid complications due to association.

Our preliminary experiments showed that it is very difficult to obtain reproducible results with erythrosine. Different results were obtained depending on the method of preparation of the solution (direct solution or dilution of a concentrated solution), the age of the solution and the extent of exposure to light in the interval between preparation and measurement; in all cases, however, T_1 was always larger than T.

Particularly inconvenient was the rapid bleaching of the solutions under illumination. In view of the low luminescence yield of water solutions of erythrosine, the luminescence spectra were measured in a set-up with a Wood's elliptical illuminator (of the type employed in photographing Raman spectra). Under these conditions the illumination was so strong that the absorption fell off by an appreciable factor even within one hour. Hence all further measurements were made using fresh solutions, i.e., the solutions were replaced every few minutes.

It was noted that with the passage of time there appeared in the absorption spectra of the solutions a minor supplementary absorption that greatly distorted the absorption spectra in the region of low absorption. This of course could be the reason for the divergence between T_1 and T. It was found, however, that even in the case of freshly prepared aqueous solutions this divergence persisted (Fig.1,a): T_1 = 380°K, T = 293°K.

This led us to hypothesize that the molecular composition of the aqueous solution is not homogeneous. Further evidence in favor of this hypothesis is the fact that the absorption and luminescence bands of the water solutions have an appreciable width.

Narrower spectra were obtained for solutions of erythrosine in acetone (Fig.1,b). In this case calculation of the temperature by means of Eq.(2) yielded T_1 = 305°K, which is almost in agreement with the experimental temperature T = 293°K.

These results suggest that in cases when there is obtained a divergence between T_1 and T we are dealing not with a uniform solution but with a mixture or assortment of molecules differing somewhat as regards their optical properties.

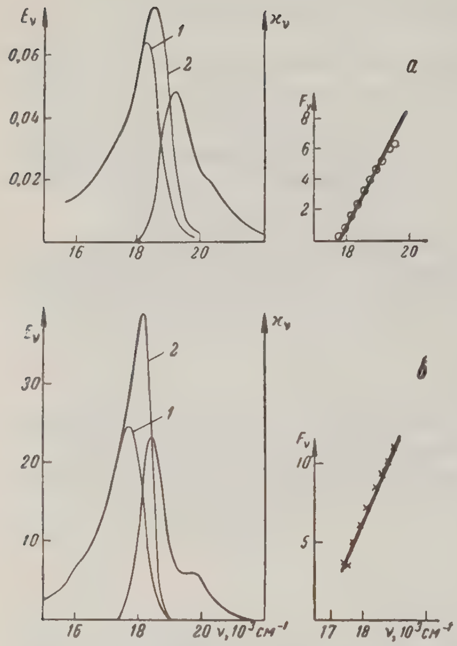

Fig.1. Absorption and luminescence spectra of erythrosine solutions: a) in water (T = = 293°K, T_1 = 380°K), b) in acetone (T = 293°K, T_1 = 305°K); 1 - neglecting reabsorption, 2 - taking reabsorption into account.

It can readily be seen that this could lead to an apparent increase of T_1. In Fig.2 the absorption and luminescence spectra are represented by gaussian curves (I), the parameters of which and the separation between the peaks of which are chosen so that the temperature calculated by means of Eq.(2) would be ~300°K. The presence of additional active absorption or additional luminescence (spectra II in Fig.2,a & b, respectively) leads to distortion of the observed spectra (dashed curves III), so that the slope of the F_ν vs ν plot is reduced (straight line plots 2 and 1 in the upper part of Fig.2), and the value of T_1 obtained from Eq.(2), i.e., the slope of the plot, proves to be higher than T.

The role of inhomogeneous composition was particularly clearly evinced in supplementary experiments with fluorescein solutions. It is known[5] that in alkaline media fluorescein molecules have the form

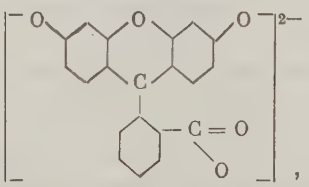

while in acid media they are characterized by the structural formula

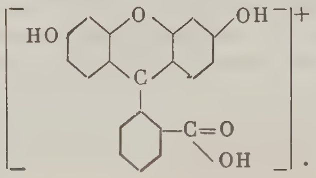

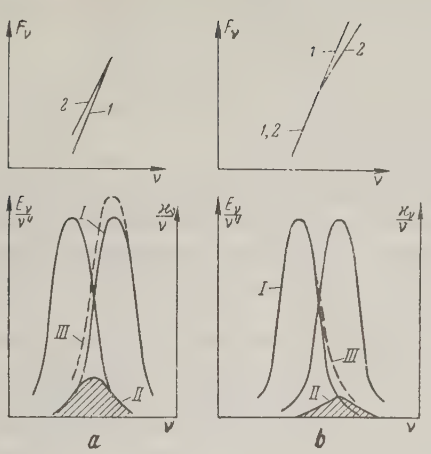

Fig.2. Influence of additional inactive absorption (a) and additional luminescence (b) on the slope of the F_ν vs ν plots.

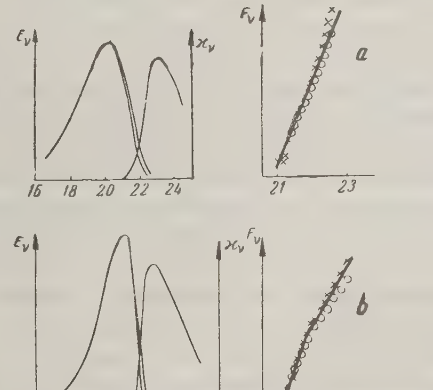

Fig.3. Absorption and luminescence spectra of fluorescein solutions: a - in sulfuric acid ($T = 293^\circ K$, $T_1 = 308^\circ K$); b - in water ($T = 293^\circ K$, $T_1 = 293^\circ K$, $T_1' = 400^\circ K$); c - in 1% aqueous NaOH solution ($T = 293^\circ K$, $T_1 = 305^\circ K$).

In nearly neutral media one can expect the appearance of intermediate molecules with gradual loss of the H atoms as the pH is increased.

Measurements of the absorption and luminescence spectra of fluorescein solutions of different pH yielded the results shown in Fig.3.

It will be evident that in the extreme cases when there should be present molecules of only one type, T_1 proves to be equal to T. In the intermediate region, however, where one may assume an inhomogeneous molecular composition there is an appreciable divergence between T_1 and T.

This gives reason to infer that in all other cases of luminescent substances in the condensed phase when the temperature T_1 calculated by means of Eq.(2) proves to be higher than the experimental temperature T, we are dealing with an inhomogeneous assortment of luminescent molecules. There is no reason to doubt that the equilibrium distribution of excited molecules over vibrational levels, corresponding to the temperature of the medium, is always attained.

Viewing the results from a different standpoint one can assert that deviation of T_1 from T may be taken as a sure indication of inhomogeneous composition of the investigated luminescent substance.

"P.N.Lebedev" Physical Institute,
Academy of Sciences of the USSR

References

1. B.I.Stepanov, Doklady AN SSSR, 112, 839 (1957). (Trans.Doklady.)
2. M.N.Alentsev, Optika i spektroskopiya, 6, 690 (1959). (Trans.Optics & Spec.)
3. B.I.Stepanov, Izv.AN SSSR, Ser. fiz., 22, 1367 (1958). (Trans.Bulletin, 22, 1357.)
4. M.N.Alentsev & L.A.Pakhomycheva, Ibid., 22, 1377 (1958). (Trans.Bulletin, 22, 1367.)
5. A.N.Terenin, Fotokhimiya krasitelei (Photochemistry of Dyes), p.24, M.-L., 1947.

INFLUENCE OF SECONDARY IMPURITIES ON THE ABSORPTION AND LUMINESCENCE SPECTRA OF THE PRIMARY IMPURITY IN MOLECULAR CRYSTALS

- A.V.Solov'ev

It has been found that different types of deformation of molecular crystals lead to alteration of the spectra of such crystals.[1,2]

Impurity molecules upon being incorporated into a crystal distort its lattice owing to the fact that the impurity molecules differ in size from the host molecules. Hence one can expect different impurity molecules introduced into the same crystal to distort the structure of the lattice to different degrees; moreover, with increase in the impurity concentration, the distortions must increase, which should be evinced in the spectrum.

In order to check these inferences we investigated the luminescence spectra of naphthacene impurity in dibenzil crystals at 20°K as a result of introduction of a second impurity, namely, diphenyl acetylene. The naphthacene concentration in the dibenzil crystals was kept constant. The diphenyl acetylene concentration was increased in steps for each specimen. It will be recalled that the absorption bands of naphthacene and diphenyl acetylene lie in different regions of the spectrum.[3,4]

The changes observed in the appearance of the spectra are illustrated in Figs.1 and 2. At a certain diphenyl acetylene concentration the bands in the naphthacene spectra are smeared out and the low intensity lines are effaced; with further increase in the diphenyl acetylene concentration there form entirely new bands, the polarization of which is similar to that of the bands in the spectrum of naphthacene in diphenyl acetylene crystals; they are, however, highly diffused and shifted some 60 cm^{-1} to the high frequency side.

Similar changes in the spectra of naphthacene in dibenzil are observed if stilbene is introduced into the crystal as an additional impurity. In such cases one can simultaneously observe the two types of bands in the absorption spectrum, while in the luminescence spectrum there appear bands at nearly the same frequencies.[5]

The luminescence spectra in all cases repeat the changes occurring in the absorption spectra (Fig.2). In the range of low stilbene concentrations there is a noticeable increase in the absorption in the region of the last band in the naphthacene spectrum; with further increase in the stilbene concentration this band is weakened. At the same time there is evident an appreciable weakening of a whole series of bands located at vibrational intervals characteristic of naphthacene molecules from this end band.[5]

If one hypothesizes that the described changes in the spectrum of naphthacene as a result of introduction of a minor amount of diphenyl acetylene are connected with interaction between the two impurities, one should expect to observe in the spectra of naphthacene in diphenyl acetylene upon the introduction of dibenzil impurities a more sharp structure of the bands in this spectrum, similar to that observed in the spectrum of naphthacene in dibenzil; this, however, is not the case (Fig.1,f & g).

It may be inferred that the clear sharp bands in the spectrum of naphthacene impurity in dibenzil crystals are connected with the crystal structure of the host, and that the alterations observed in the spectrum in the range of low concentrations of the additional impurity are connected with distortion of the host crystal lattice. If this is the case one should expect a similar change in the character of the spectrum regardless of the nature of the second impurity introduced. And, experiments actually do show that the introduction of paraditolyl instead of diphenyl acetylene and stilbene into dibenzil crystals leads to similar changes in the spectrum (Fig.2,h). Moreover, these changes are similar to those observed in

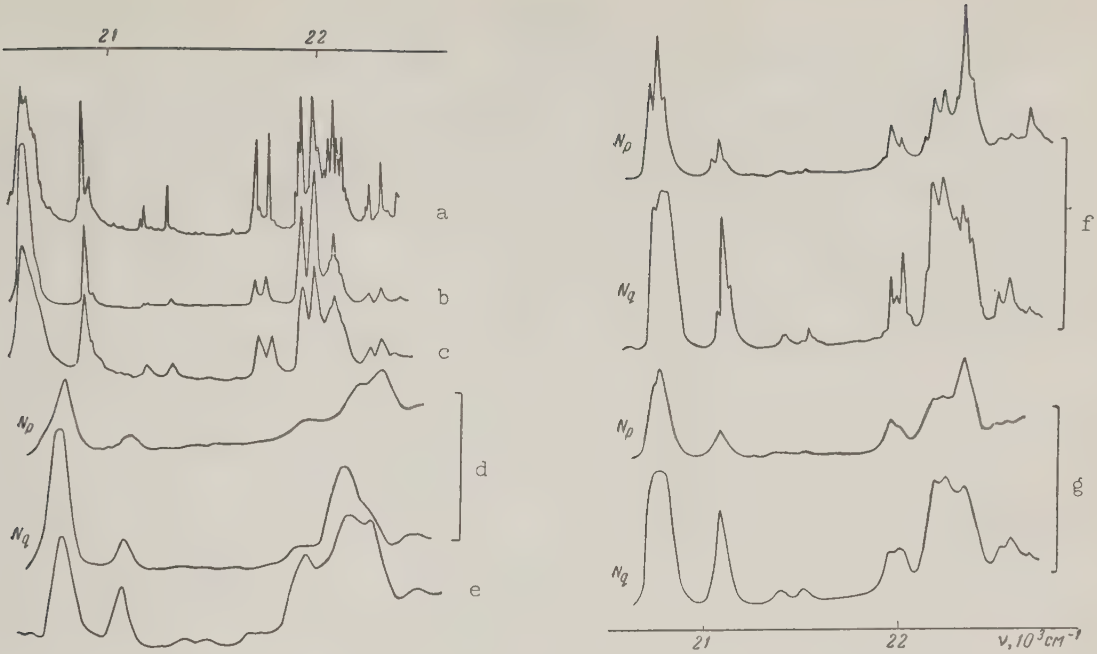

Fig.1. Photometric traces of absorption spectra: a) naphthacene in dibenzil crystal, b-e) same with additional diphenyl acetylene impurity (naphthacene concentration constant; diphenyl acetylene concentration increases from b to e); f) naphthacene in diphenyl acetylene crystal; g) same with additional dibenzil impurity. The spectra were obtained with light polarized along the N_p and N_q axes of the dibenzil and diphenyl acetylene crystals at 20°K. In cases a,b & e, the blackening curves for the two polarization components have the same shape, hence only the curve for one component is given in the figure; in cases d,f & g, the shape of the two components differs, hence both are given.

the spectra of molecular crystal subjected to mechanical deformation: the bands become broader and more diffuse.[1,2]

The new bands appearing at high concentrations of the second impurity are obviously connected with the direct interaction between the impurity molecules. The changes observed in the spectra of impurities in the range of their high concentrations are also apparently connected with such interaction (compare, for example, the spectra of stilbene in diphenyl acetylene crystals at high concentrations[4], naphthacene in stilbene crystals[6], and anthracene in diphenyl crystals[7]). A significant role may be played in such cases by the fact that the impurity molecules are not distributed uniformly through the crystal but are clustered in groups. X-ray diffraction studies[8] show, for example, that this is the case for stilbene in dibenzil crystals.

Institute of Physics,
Academy of Sciences of the Ukrainian SSR

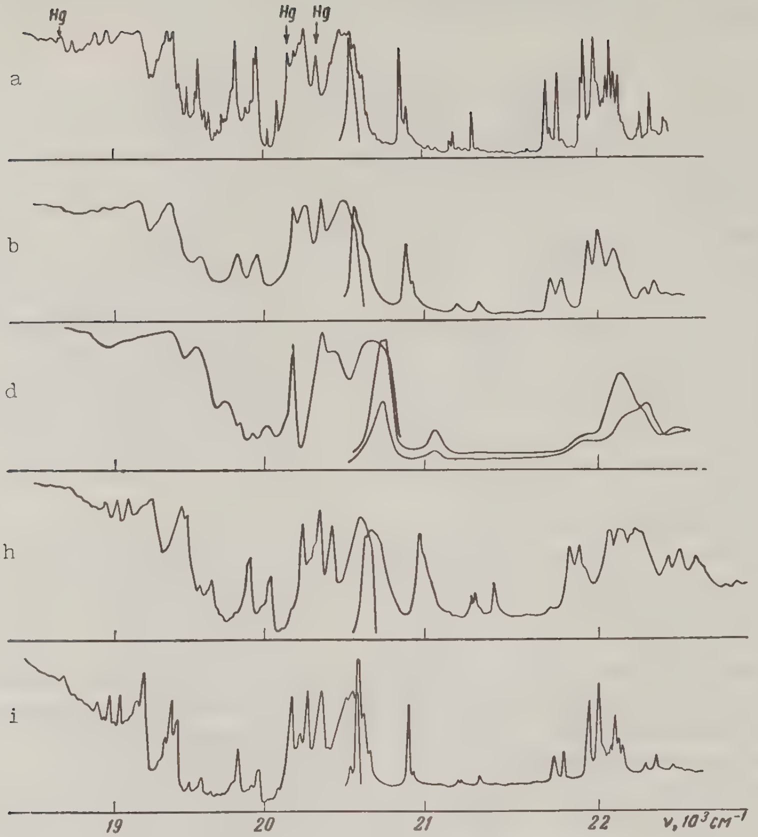

Fig.2. Luminescence and absorption spectra: a,b & d) see Fig.1; i) naphthacene in dibenzil crystal; h) same with additional paraditolyl impurity. The coinciding bands in the absorption and luminescence spectra have been matched. The luminescence was excited by light from an SVDSh-1000 tube (the excitation lines are identified by Hg).

References

1. V.L.Broude, O.S.Pakhomova & A.F.Prikhot'ko, Optika i spektroskopiya, 2, 323 (1957).
2. V.L.Broude, V.V.Eremenko, V.S.Medvedev, O.S.Pakhomova & A.F.Prikhot'ko, Ukr.fiz.zhur. (Ukrainian Physics Journal), 3, 232 (1958).
3. A.F.Prikhot'ko & A.V.Solov'ev, Ibid., 4, 92 (1959).
4. A.F.Prikhot'ko & M.T.Shpak, Optika i spektroskopiya, 4, 17, 30 (1958).
5. A.V.Solov'ev, Ibid., 4, 258 (1959). (Trans.Optics & Spectroscopy).
6. A.F.Prikhot'ko & A.V.Solov'ev, Ukr.fiz.zhur., 4, 229 (1959).
7. A.V.Solov'ev, Ibid., Vol.5 (1960).
8. A.I.Kitaigorodskii, Kristallografiya, 2, 456 (1957). (Trans.Soviet Physics - Crystallography.)

POLARIZATION OF THE LUMINESCENCE OF MOLECULAR CRYSTALS IN DIFFERENT REGIONS OF THE SPECTRUM

- V.I.Gribkov, N.D.Zhevandrov & Sh.D.Khan-Magometova

The present work was a continuation of our earlier investigation[1,2] by polarization methods of the role of free and trapped excitons in the luminescence of molecular crystals. We reported[2] observing a marked change in the degree of polarization at the short wavelength edge of the luminescence spectrum of a stilbene crystal with observation perpendicular to the *ab* plane of the crystal. This abrupt change in polarization was interpreted as being due to the emission of free excitons polarized along the *b* axis and accounting for less than 10% of the total luminescence intensity. We felt that this result was interesting and significant. In view of this we undertook a further detailed investigation of the effect, taking into account the various factors that might complicate it.

For the study we used the spectropolarimetric photoelectric recording set-up incorporating a UM-2 monochromator and a birefringent prism with a large angle of divergence, described in Ref.2. First we measured the wavelength dependence of the polarization of luminescence with excitation by 365 mμ light for stilbene crystals cut along different crystallographic planes. The results are shown in Fig.1. The polarization in the long wavelength region of the spectrum is approximately constant in all cases and corresponds to the emission of trapped excitons[1,2]. The marked changes in polarization at the short wavelength edge of the spectra correspond, as will be clear from comparison of the results for different orientations of the crystals, to emission polarized along the *b* axis, i.e., to luminescence due to free excitons.

As noted in our earlier report[2], there is, however, the possibility that the observed effect may be partially due to (or distorted by) dichroism of the crystals.

Moreover, there might have been an admixture of exciting light in the short wavelength part of the luminescence spectrum. Control experiments showed that the exciting light could not directly enter the monochromator slit, but there was the possibility of the entry of some light scattered from the surface of the crystal. Excitation was realized by natural light, but this could be partially polarized owing to dichroism of the crystal.

We measured the dichroism spectra of the investigated stilbene plates. These are reproduced in Fig.2. The absorption in the region corresponding to the short wavelength part of the luminescence spectrum is approximately the same for light polarized along the *a* and *c′* axes and weaker for light polarized along the *b* axis. Hence it is obvious that dichroism must be taken into account.

In order to elucidate how an admixture of exciting light might influence the results we carried out the following experiments: First, we carried out measurements of crystals of different thickness (in a 1 to 10 range); it was found that the thickness of the crystal has no effect on the wavelength dependence of the polarization of luminescence. Second, we carried out a series of experiments in which we realized excitation by light linearly polarized in the direction perpendicular to the *b* axis of the crystal, i.e., the component of the excited light that might preferentially pass through the crystal was extinguished by a polaroid; the wavelength dependence of the polarization did not change (see Fig.1,c, curve 2). These experiments showed that the observed effect cannot be due to an admixture of exciting light. In order to double check this we carried out experiments employing short wavelength (302 and 254 mμ) excitation; through control experiments with a nonfluorescent frosted quartz plate we made sure of the complete absence of any admixture of exciting light in the region of the luminescence spectrum. These measurements proved to be rather difficult owing to the low excitation intensity,

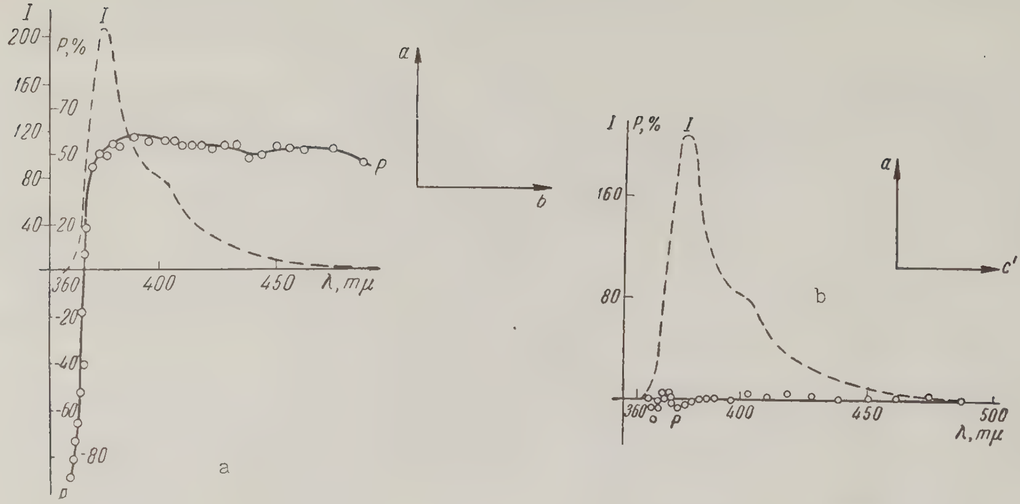

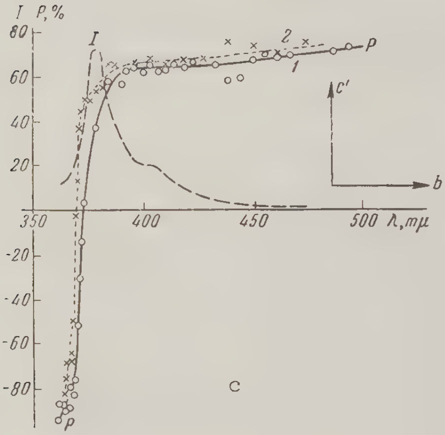

Fig.1. Wavelength dependence of the polarization of luminescence of stilbene single crystals (λ = 365 mμ excitation): a - *ab* cut; b - *ac'* cut; c - *bc'* cut (1 - excitation with natural light; 2 - excitation with vertically polarized light). The arrows indicate the directions of the crystallographic axes.

but we were able to carry them out, thanks to the high sensitivity of our set-up. Some of the results obtained for excitation with 302 mμ light and the *bc'* plane of the crystal are shown in Fig.3. It will be evident that in general the result is similar to that with excitation by 365 mμ light. Thus it is reasonable to assume that the marked change in polarization at the short wavelength edge of the spectrum is not connected with admixture (leakage) of exciting light.

Further, as noted, it was necessary to take into account dichroism in the reabsorption of luminescence. In order to introduce the necessary corrections for the change in the true polarization of the luminescence owing to dichroism of reabsorption one can make use of the familiar formulas for the correction for reabsorption introduced by Förster[3] and applied in his work to molecular single crystals by Choudhury[4]:

$$\rho = \frac{K_b}{K_{c'}} \rho' ;$$

here $\rho' = \frac{I_b}{I_{c'}}$ is the measured polarization ratio $\left(P' = \frac{1-\rho'}{1+\rho'}\right)$, ρ is the true polarization ratio $\left(P = \frac{1-\rho}{1+\rho}\right)$, P is the degree of polarization, and

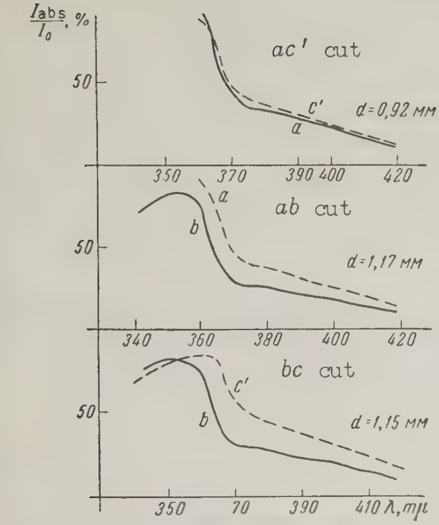

Fig.2. Dichroism spectra of stilbene crystals.

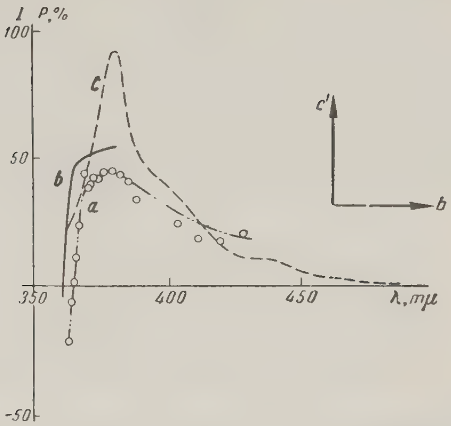

Fig.3. Wavelength dependence of the polarization of the luminescence of a stilbene crystal (*bc*′cut; excitation λ = 302 mμ): a - measured, b - with corrections for dichroism, c - luminescence spectrum.

$$K_b = \frac{1 - e^{-\mu_{1b}d}}{e^{-\mu_{2b}d} - e^{-\mu_{1b}d}} \cdot \frac{\mu_{1b} - \mu_{2b}}{\mu_{1b}},$$

where d is the thickness of the crystal, μ_{1b} is the coefficient of absorption of the exciting light (302 mμ) polarized along the b axis, and μ_{2b} is the coefficient of absorption of the luminescence light at the given point in the spectrum polarized along b (the expression for $K_{c'}$ is analogous). These formulas pertain to the case when the luminescence is excited "from behind". Using these formulas we computed the corrections in the region of reabsorption. The value of the λ = 302 mμ absorption coefficient for stilbene was taken from Brodin[5].

The wavelength dependence of the polarization at the edge of the luminescence spectrum taking into account these corrections is shown by curve b in Fig.3. It will be apparent from the curve that the pronounced change in polarization at the edge of the spectrum persists even after the introduction of all the above mentioned corrections and elimination of all the complicating factors. This clearly indicates that the luminescence of stilbene comprises emission due to free excitons.

In view of the above results we felt it would be of interest to investigate the polarization of luminescence with other types of excitation. Hence, we compared the polarization of luminescence of stilbene with photo- and β-excitation (Sr^{90} source). So far measurements have been made only of the integral luminescence spectrum. For the same crystal in the same orientation, the change in the degree of polarization with photoexcitation by natural light (365 mμ) and with β-excitation proved to be virtually the same (32.7% and 33.1%, respectively). This result shows that the luminescence mechanism does not depend on the type of excitation and that the polarization of the luminescence is determined primarily by the structure and properties of the crystal itself.

We also investigated the wavelength dependence of the polarization of anthracene crystals doped with naphthacene. The results for one naphthacene concentration are shown in Fig.4. The change in polarization in the region of the anthracene spectrum is the same as for pure anthracene. The abrupt change at the short wavelength edge of the spectrum was investigated earlier and interpreted as being associated with the emission of free excitons.[2] There are no marked changes in

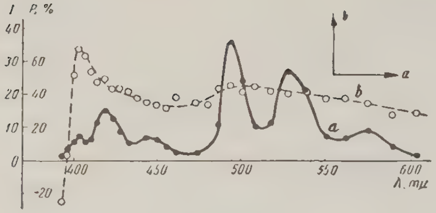

Fig.4

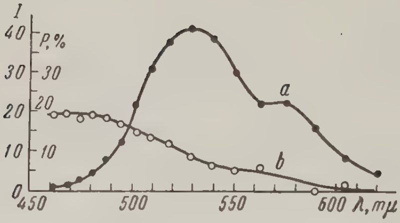

Fig.5

Fig.4. Luminescence spectrum (a) and wavelength dependence of the polarization (b) of an anthracene single crystal doped with naphthacene (10^{-3} g/g).
Fig.5. Luminescence spectrum (a) and wavelength dependence of the polarization (b) of a benzil single crystal (along the optical axis).

polarization in the region of the naphthacene spectrum; this is as might be expected inasmuch as no free excitons can exist in the "interstitial" naphthacene lattice. The degree of polarization in the naphthacene spectrum is somewhat higher than in the long wavelength region of the anthracene spectrum. From this it may be inferred that the naphthacene molecules are oriented somewhat differently in the lattice than the anthracene molecules. The difference in orientation, however, is minor.

Of particular interest is investigation of the polarization of luminescence of benzil crystals. Benzil crystals are hexagonal. The unit cell contains three molecules arranged along a spiral. Owing to this structure, benzil crystals exhibit optical activity, which was investigated by Chandrasekhar.[6] The optical activity of benzil is characterized by strong dispersion; the rotatory power increases appreciably in the short wavelength part of the spectrum. Benzil emits bright green luminescence. In the case of optically active substances one can expect elliptically polarized luminescence inasmuch as the emitting molecule must be represented not as a linear oscillator but as two separate but coupled mutually perpendicular oscillators. Neunhoeffer & Ulrich[7] report observing elliptical polarization of the luminescence of one optically active substance both in the crystalline state and in solutions. Earlier attempts to detect elliptical polarization were apparently unsuccessful primarily because the experimenters studied the luminescence of planar molecules not possessing optical activity.

For our work benzil single crystals were grown in tubes from the melt by the technique described by Chandrasekhar[6] and also by crystallization from a supersaturated solution. In the latter case, there were obtained small needle-like crystals which could be investigated only on a polarimeter equipped with a microscope.[8] Crystals of macroscopic size grown by the Chandrasekhar technique could be investigated on our spectropolarimetric set-up. The degree of polarization of the integral luminescence proved to be 20% in the direction perpendicular to the optical axis and 5% in the direction parallel to the optical axis. The wavelength dependence of the polarization (in the direction parallel to the optical axis) at room temperature is shown in Fig.5. The polarization increases towards the short wavelength edge of the spectrum and attains 20% at the very edge.

Analysis of the polarization with a view to establishing the presence or absence of ellipticity was carried out by the conventional procedure by means of λ/4 plates inserted between the luminescent crystal and the analyzer nicol.[9] In order to eliminate the effects of anisotropy of the photocathode the photomultiplier was rotated together with the nicol analyzer.

Our analysis showed that neither the integral luminescence of benzil crystals nor the luminescence in different parts of the spectrum (including the short wavelength edge where the rotary power is appreciable) is elliptically polarized either at room temperature or at liquid nitrogen temperature. Within the limits of the experimental error (±2°) the polarization is entirely partial. We obtained the same results in analyzing the polarization of the integral luminescence of glycerol solutions of optically active substances, namely, tryptophan (luminescence is the near ultraviolet peaking at 330-340 mμ) and riboflavin (visible luminescence peaking at 550 mμ). Thus the case of elliptical polarization of the luminescence of an optically active substance reported by Neunhoeffer & Ulrich[7] appears to be unique so far.

"P.N.Lebedev" Physical Institute
Academy of Sciences of the USSR

References

1. N.D.Zhevandrov, Izv.AN SSSR, Ser.fiz., 22, 1332 (1958). (Trans.Bulletin, 22, 1323.)
2. N.D.Zhevandrov, V.I.Gribkov & V.N.Varfolomeeva, Ibid., 23, 57 (1959). (Trans.Bulletin, 23, 59.)
3. T.Förster, Fluor.org.Verbindungen, S.35, Göttingen, 1951.
4. N.K.Choudhury, Z.Phys., 151, 93 (1958).
5. M.S.Brodin, Optika i spektroskopiya, 1, 876 (1958).
6. S.Chandrasekhar, Proc.Ind.Acad., A 39, 243 (1954).
7. O.Neunhoeffer & H.Ulrich, Z.Electrochem., 59, 122 (1955).
8. N.D.Zhevandrov, Doklady AN SSSR, 83, 677 (1952).
9. F.Weigert, Optical Methods in Chemistry. (Cited in Russian trans.)

* * * * * * *

MIXED ORGANIC SINGLE CRYSTALS, THEIR LUMINESCENCE AND SCINTILLATION PROPERTIES

- Yu.V.Naboikin, V.K.Dobrokhotova & V.V.Uglanova

In connection with widespread investigation of energy transfer in mixed organic systems there are now grounds for preparing new scintillation crystals of readily available substances, the luminescence properties of which vary substantially as a result of deliberately introduced impurities.

Impurities in molecular crystals may be regarded as a unique sort of lattice defects. The question of the role of defects in the luminescence of crystals was first raised in the work of Prikhot'ko and his colleagues[1]. On the basis of investigation of the electronic spectra at low temperatures they advanced the hypothesis that in molecular crystals impurities form different types of lattice defects. There are, however, no definite data in the literature on the structure of impurity defects, hence investigation of this problem is of particular interest. Growth of a large number of different organic single crystals and determination of the solubility of impurities in the solid phase made it possible to establish some of the general conditions necessary for the formation of solid solutions. These conditions are in agreement with Kitaigorodskii's[2] theory of close packing of molecules in organic crystals, and enable us in some cases to judge of the specific structure of impurity luminescence centers.

It must be noted, however, that the structure of impurity defects is determined not only by the nature of the impurity molecule itself but also by distortion of the host lattice about this molecule. Hence in investigating mixed organic systems one must always take into account the conditions of formation, namely, the rate of growth of the crystals, the temperature gradient, the solubility of the impurity in the solid phase, etc. Unfortunately, these factors were not taken into account in a number of studies on excitation energy transfer in such systems. For example, in the work of Bowen et al[3] the mixtures were prepared simply by fusing the chosen substances, no account being taken of the solubility or lack of solubility of the impurity in the solid phase.

In the present work we made an attempt to evaluate the influence of some of the above mentioned factors on excitation energy transfer and consequently on the scintillation properties of doped organic single crystals.

All our experiments were carried out with single crystals grows by the Stockbarger technique. The host materials were thoroughly purified naphthalene and bephenyl. The naphthalene was purified by the zone procedure[4,5]; the biphenyl by chromatography and sublimation. The degree of purity was evaluated from the luminescence spectra of the crystals. The impurities to be introduced were chosen from a series of aromatic hydrocarbons and their derivatives. For investigating the scintillation properties, the single crystals were packed in aluminum containers of the conventional type. The size of the single crystals was the same in all cases. The scintillation yield was evaluated by means of an FEU-29 photomultiplier with reference to a standard stilbene crystal. The luminescence spectra were measured on an SF-4 spectrophotometer equipped with a special attachment incorporating an FEU-18 photomultiplier.[6] The solubility of the impurities in the solid phase was determined by dissolving single crystals in heptane and measuring the absorption in the characteristic bands of the impurity. To some extent one could also judge of the solubility of the impurities from the luminescence spectra of the single crystals.

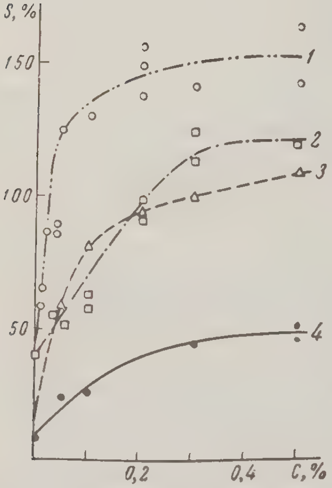

Fig.1. Variation of the scintillation yield of mixed single crystals with the concentration of the impurity added to the melt: 1) naphthalene with phenylbiphenylylethylene, 2) naphthalene with α,α'-dinaphthylethylene, 3) biphenyl with dibiphenylylethylene, 4) biphenyl with phenanthrene.

As a result of testing a large number of different impurities there were obtained a number of new scintillators based on naphthalene and biphenyl. Fig.1 shows the variation of the relative scintillation yield as a function of the impurity concentration in the melt for a number of the more interesting scintillator crystals. It will be evident from the figure that the scintillation yield tends to a saturation value, i.e., at first increases fairly rapidly with increasing impurity concentration and then levels off.

The impurity concentration dependence of the relative photoluminescence efficiency of the mixed single crystals is approximately the same as the concentration dependence of the scintillation yield. By way of illustration in Fig.2 we give the variation of the luminescence efficiency of naphthalene and phenylbiphenylylethylene dissolved in it with the concentration of the impurity. The luminescence in this case was excited by mercury lines in the region below 320 mμ. Thus there was excited only the host material; direct excitation of the impurity was negligible. In order to obtain the relative quantum efficiencies we compared the areas under the curves in the luminescence spectra of the host and impurity. Examples of the spectral curves

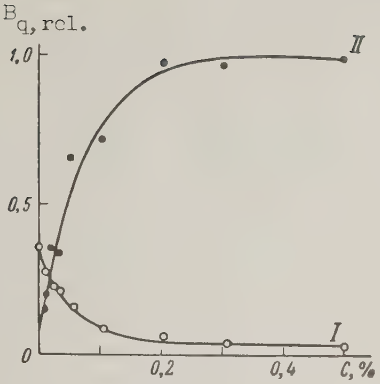

Fig.2

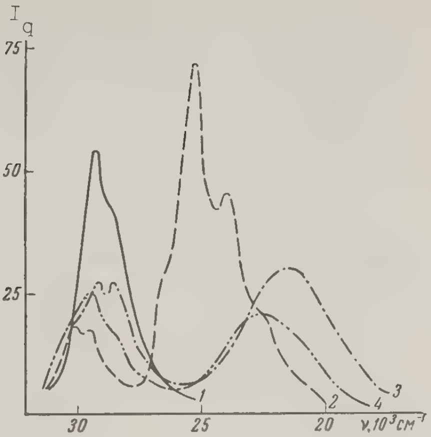

Fig.3

Fig.2. Variation of the relative photoluminescence efficiency of naphthalene (I) and phenylbiphenylylethylene (II) with the concentration of the impurity added to the melt before growing the crystals.

Fig.3. Fluorescence spectra of single crystals with excitation and observation from the same side: 1) naphthalene, 2) naphthalene with phenylbiphenylylethylene, 3) naphthalene with salicylamide, 4) naphthalene with α,α'-dinaphthylethylene.

for naphthalene single crystals doped with different impurities are shown in Fig.3.

Noteworthy is the fact that the luminescence efficiency of pure naphthalene single crystals is almost three times lower than the luminescence efficiency of crystals doped with phenylbiphenylylethylene. This clearly indicates that in naphthalene crystals there occurs intensive nonradiative energy transfer. If as a result of absorption of light by naphthalene, there form in a unit volume per unit time N excitons, while N_r excitons break up with the emission of radiation, obviously $N - N_r$ excitons, as a result of scattering from phonons and possibly lattice defects, do not yield luminescence. This difference is decreased as a result of introduction of the impurity inasmuch as trapping of excitons at impurity defects leads to radiative transitions. The impurity thus favors more complete conversion of excitation energy to luminescence.

If we take the luminescence efficiency of phenylbiphenylylethylene dissolved in naphthalene to be 0.9, we see from the data given in Fig.2 that the luminescence efficiency of pure naphthalene is 0.3. The above value for the luminescence efficiency of phenylbiphenylylethylene is reasonable inasmuch as the scintillation yield of naphthalene with this impurity is close to the scintillation efficiency of anthracene.

As will be evident from the accompanying table and Fig.1, both the naphthalene and biphenyl base single crystals are characterized by relatively high values of the scintillation yield; at the same time the two types of crystals differ as regards solubility of the impurities in the solid phase. In order to evaluate the influence of impurities on the scintillation properties of single crystals and, consequently, on the efficiency of energy transfer it is not sufficient to compare merely the luminescence efficiencies, it is essential also to take into account the true concentration of the impurities dissolved in the solid phase. In the accompanying table, in addition to the data on the solubility of the impurities and the scintillation yield, we give the values of S/S_0C, which characterizes the change in the scintillation yield of pure single crystals as a result of intro-

Scintillation yields of organic single crystals and values of the distribution coefficient K

Host material and its light yield S_0, %	Impurity	Scintillation yield S, %	$\frac{S}{S_0}$	Concentration in the solid phase, 10^{-4} mole/mole	Change in yield per unit concentration, $(S/S_0C) \times 10^4$	Distribution coefficient K
(35,0) 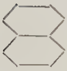	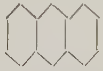 Anthracene	60,0	1,7	0,01	170,0	$1{,}5\cdot10^{-3}$
	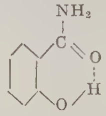 Salicylamide	75,0	2,1	4,0	0,5	0,1
	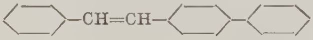 Phenylbiphenylylethylene	155,0	4,5	0,48	9,3	$2{,}0\cdot10^{-2}$
	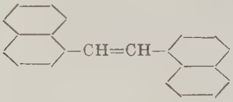 α,α'-Dinaphthylethylene	105,0	3,0	0,07	43,0	$6{,}0\cdot10^{-3}$
(10,0) 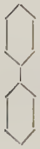	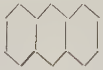 Anthracene	50,0	5,0	33,0	0,15	1,3
	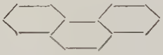 Phenanthrene	50,0	5,0	145,0	0,03	4,4
	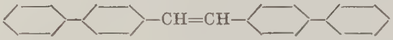 Dibiphenylylethylene	95,0	9,5	8,4	1,1	1,1
	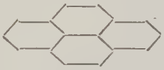 Pyrene	18,0	1,8	0,3	6,0	0,01

duction of a unit amount of impurity per unit volume of the host substance. Even if we disregard the intrinsic luminescence yield of the impurities in the solvent lattice, which for different impurities varies in the relatively narrow range from 0.5 to 0.9, we readily note how great in most cases is the influence of the impurities on the luminescence of naphthalene as compared with biphenyl. It should be noted that the greater the value of S/S_0C, the lower the coefficient K of distribution of the impurity between the solid and liquid phases. Hence one can reasonably explain the observed effects as follows.

If the distribution coefficient K is appreciably smaller than unity, then in growing the single crystals there will generally be reached a point where the impurity concentration in the solid phase levels off: the impurity concentrates increasingly in the melt and under certain conditions no further growth of the crystal will occur. In such cases each molecule of the impurity will deform the host lattice to the extent that until and unless the effect is healed in the process of growth the new impurity molecule will not be dissolved in the solid phase. Thus, the crystallization boundary will be sensitive to the state of the lattice for several lattice constants. Consequently, there will form an appreciable imperfection region about each impurity molecule which, naturally, leads to sharp decrease in the cross section for exciton trapping by the impurity luminescence centers. The lattice defects produced by the impurity facilitate trapping of excitons, and a favorable location of the impurity levels with respect to the lowest exciton band in the crystal leads to luminescence of the impurity molecules.

On the other hand, when the solubility of the impurity is high ($K > 1$), the deformation about an impurity molecule is limited to a few lattice constants; hence the probability for exciton trapping by the impurity centers is reduced and only in the case of high impurity concentrations are there obtained single crystals with a high scintillation yield. The good solubility of impurities in biphenyl is, apparently, connected with the structural characteristics of this compound. Whereas in the case of naphthalene the formation of a solid solution occurs only through deformation of the lattice, inasmuch as the molecules have a rigid structure, in the case of biphenyl there may occur deformation of individual molecules which naturally severely limits the effective size of the impurity defects.

The data listed in the table are only approximate and intended primarily for purposes of evaluation; this is due not only to the relatively low experimental accuracy, but also to the fact that a number of factors were neglected (overlapping of the absorption spectrum of the impurity and the luminescence spectrum of the host, the intrinsic luminescence yield of impurity molecules incorporated in a foreign lattice, etc.). Taking these factors into account, however, presumably will not substantially alter the results inasmuch as in some cases the values of S/S_0C differ by several orders of magnitude.

In considering the solubility of impurities in the solid phase, one must clearly distinguish between different causes leading to saturation of the luminescence yield with increase in concentration. On the one hand, this effect may be connected simply with the solubility limit for the given impurity ($K \ll 1$); on the other hand, there may obtain resonance interaction of the molecules leading to concentration quenching of the luminescence. Further investigations in this direction should be of interest and we plan to continue our research.

We desire to express our gratitude to L.Ya.Malkes for making available some of the substances used in the present study and to A.M.Ratner and I.O.Kulik for valuable discussions.

References

1. V.L.Broud, A.F.Prikhot'ko & E.I.Rashba, Usp.fiz.nauk, 67, 99 (1959). (Trans.Soviet Physics - Uspekhi.)
2. A.I.Kitaigorodskii, Organicheskaya kristallokhimiya (Organic Crystallochemistry), M., 1955.
3. E.J.Bowen, E.Mikiewicz & F.W.Smith, Proc.Phys.Soc., A62, 26 (1949).
4. M.T.Shpak & A.F.Prikhot'ko, Optika i spektroskopiya, 6, 119 (1959). (Trans.Optics & Spectroscopy.)
5. N.N.Spendiarov, V.K.Dogrokhotova, E.N.Pavlova, Yu.V.Naboikin & B.S. Aledsandrov, Trudy VNII khimicheskikh reaktivov (Proceedings of the All-Union Scientific Research Institute for Chemical Reagents), No.23, p.4, M., 1959.
6. A.P.Kilimov, L.L.Nagornaya & B.A.Zadorozhnyi, PTE, No.3, 105 (1959). (Tans.Instruments & Experimental Techniques.)

CORRESPONDENCE BETWEEN THE ABSORPTION AND LUMINESCENCE SPECTRA OF URANYL SALT SOLUTIONS

- L.V.Volod'ko, A.N.Sevchenko & D.S.Umreiko

The luminescence and absorption spectra of solutions of uranyl salts at room temperature do not exhibit mirror symmetry, although a certain degree of mirror similarity was reported for these spectra as far back as 1937 by Levshin[1]. The maximum intensity in the fluorescence spectrum occurs in the second band, reckoning from the band associated with the purely electronic transition; the maximum absorption lies in the fifth band, reckoning in the same manner.

Yet for the electronic spectra of uranyl compounds there are fulfilled all the conditions necessary for the appearance of mirror symmetry. The vibrations of the uranyl ion in the normal and excited electronic states are virtually harmonic in the investigated spectral ranges. The "fine structure" of the spectral bands does not show any dependence (within the limits of the experimental error) on the energy of vibration of the uranyl ion.[2] Hence the systems of sublevels of each energy level of the fully symmetric valence vibrations of the uranyl ion are identical. Thus the system of energy levels of the upper electronic state is similar to within a constant factor (due to the lower value of the vibration frequency of the UO_2^{++} ion in the excited state) to the level system of the lowest electronic state.

Moerman & Kraak[3] analyzed the absorption and luminescence spectra of uranyl salts from the standpoint of the Franck-Condon principle and came to the conclusion that the probability for transition from the zero energy levels of the fully symmetrical valence vibrations of the uranyl ion in the ground electronic state to the level with one energy quantum of these vibrations in the excited electronic state is equal to the probability for the reverse (symmetrical with the first) electronic transition with emission of light. The spectral bands associated with these transitions must be the most intense. The probability for a pure electronic transition with absorption and the equal probability for the reverse transition without change in the zero energy of vibration of the uranyl ion are low.

The existence of symmetry of the absorption and luminescence spectra close to the purely electronic transition with equality of the transition probabilities for the symmetrical frequencies indicates equality of the energy distribution functions in the ground and excited electronic states. This also follows from the constancy of the fluorescence spectra of uranyl salts at different stages of decay and the fact that the fluorescence spectrum and the quantum efficiency are independent of the wavelength of the exciting light.[4] The harmonicity of the vibrations of the uranyl ion in both states with a relatively small frequency difference gives reason to infer that proportionality obtains as regards the probabilities for the symmetrical direct and reverse electronic-vibrational transitions for all energy levels of these vibrations usually observed in the fluorescence spectra.

Fulfillment of the conditions necessary for the appearance of mirror symmetrical absorption and luminescence spectra makes it possible to evaluate the degree of deviation from mirror symmetry in the spectra of solutions of uranyl salts and to determine the reason for this deviation. Difference between the vibration frequencies of the uranyl ion in the ground and excited electronic states leads to compression of the absorption spectrum as compared with the luminescence spectrum. Hence one can expect only quasisymmetry of the spectra. The contour of the absorption spectra, quasisymmetrical with respect to the fluorescence spectrum, is described by the formula:[5]

$$\frac{W_{\nu_e - \Delta\nu}}{(\nu_e - \Delta\nu)^4} = \mu \frac{\varkappa_{\nu_e + \alpha\Delta\nu}}{\nu_e + \alpha\Delta\nu},$$

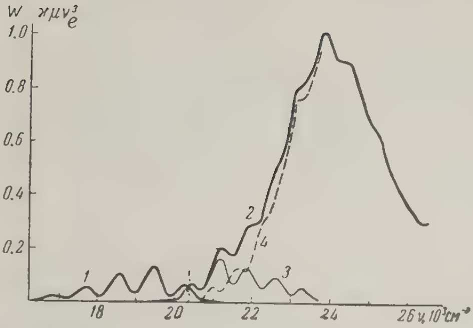

Fig.1. Luminescence and absorption spectra of aqueous solution of uranyl sulfate: 1) fluorescence spectrum, 2) absorption spectrum obtained experimentally, 3) absorption spectrum calculated from the fluorescence spectrum, 4) difference between spectra 2 and 3.

where $W_{\nu_e - \Delta\nu}$ is the luminescence power of frequency $\nu_{\text{lum}} = \nu_e - \Delta\nu$; $\varkappa_{\nu_e + \alpha\Delta\nu}$ is the absorption coefficient for the frequency $\nu_{\text{abs}} = \nu_e + \alpha\Delta\nu$; ν_e is the frequency of the purely electronic transition; $\Delta\nu = |\nu_e - \nu_{\text{ob}}|$ is the difference between the frequency of the purely electronic transition and the frequency observed in the spectrum; μ is a proportionality factor. The factor $\alpha = \nu_c^*/\nu_c$ taking into account the frequency difference between the fully symmetrical valence vibrations of the uranyl ion in the excited (ν_c^*) and ground (ν_c) electronic states, is introduced in order to reconcile the calculated absorption spectrum with the experimentally observed spectrum.

The calculations were carried out for the absorption and luminescence spectra of a 0.1 M solution of uranyl sulfate in water at room temperature. The frequency of the purely electronic transition was determined by comparing the luminescence spectrum of this solution with the spectra of crystalline uranyl sulfate at -185° and -269°, wherein the frequency of the purely electronic transition has been determined with a high degree of precision. In the solution the frequency of the purely electronic transition is 20 380 cm^{-1}, i.e., is shifted 50 cm^{-1} to the side of shorter wavelengths relative to the position in the crystal spectrum. The frequencies of the fully symmetrical valence vibrations of the uranyl ion were determined from the frequency difference of the anti-Stokes band and the first Stokes bands in the luminescence spectrum of the solution. In the excited electronic state they are equal to ~700 cm^{-1}; in the unexcited state to ~850 cm^{-1}.

Fig.1 shows the luminescence spectrum of the water solution of uranyl sulfate (curve 1), the experimental absorption spectrum for this solution (curve 2), the calculated absorption spectrum, quasisymmetrical with respect to the fluorescence spectrum (curve 3), and the difference between the last two spectra (curve 4). The vertical scale for the luminescence spectrum is laid off in terms of the luminescence power W; that for the absorption spectra in terms of $\varkappa\mu\nu_e^3$.

It will be evident from the figure that the actual absorption spectrum of the aqueous solution of uranyl sulfate is considerably more complex than the absorption spectrum calculated on the basis of the fluorescence spectrum. The contours of the calculated and experimental spectra agree only within the range of half the first band. Over the rest of the spectrum the fraction of absorbed energy in the calculated spectrum rapidly falls off with increasing frequency.

The disparity between the experimental and calculated absorption spectra may be due to the presence of a number of excited electronic states in uranyl. The number of lines in the absorption spectrum of uranyl salt crystals at low temperatures appreciably exceeds the number of lines in the fluorescence spectrum. The relatively high line density begins in the second band of the absorption spectrum, whereas the first absorption band has the same structure as the bands of the luminescence spectrum. A number of lines located on the short wavelength side of the second absorption band split into two components in a magnetic field parallel to the optical axis of the crystal. No Zeeman splitting is observed for either the lines in the first band of the absorption spectrum or any of the lines of the fluorescence spectrum. Uranyl salts are not paramagnetic at low temperatures. Consequently the ground electronic state is a Σ state. The lines of the absorption

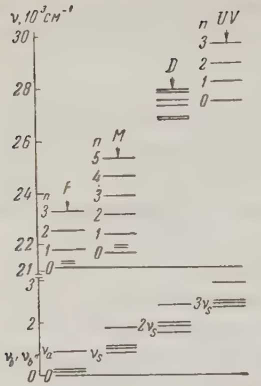

← Fig.2. Diagram of the electronic-vibrational series in the absorption spectra of uranyl compounds (after Dieke & Duncan[6]): F - "fluorescent" series, M - "magnetic" series, D - "sharp" series, UV - "ultraviolet" series; ν_s - frequency of the symmetrical valence vibrations of the UO_2^{++} ion; ν_a - frequency of the antisymmetrical valence vibrations of the UO_2^{++} ion; $\nu_{b'}$ and $\nu_{b''}$ - doubly degenerate frequency of deformational vibrations of the UO_2^{++} ion.

spectrum not exhibiting the Zeeman effect are associated with $\Sigma \rightarrow \Sigma$ transitions, while the lines that split in a magnetic field should be attributed to $\Sigma \rightarrow \Pi$ transitions.[6]

As a result of experimental investigation of the Zeeman effect and measurement of the polarization of the lines in the absorption spectra of a large number of different crystalline uranyl salts Dieke & Duncan[6] grouped the detected lines into four series: a "fluorescent" series F, a "magnetic" series M, a "sharp" series D, and an "ultraviolet" series UV. The different behavior of the lines of the different series in a magnetic field and their different polarization indicate that these line groups are associated with transitions to different electronic states of the uranyl ion. The arrangement of the different series in the absorption spectra is shown in Fig.2.

Application of the principle of mirror symmetry to uranyl compounds makes it possible to discriminate one of the above indicated electronic states (the so-called "fluorescent" state). The absorption associated with the quasisymmetrical ("fluorescent") electronic state amounts to only 10% of the total absorption in the visible region. Consequently the main absorption of solutions of uranyl salts at room temperature in this region occurs owing to $\Sigma \rightarrow \Pi$ transitions, which are responsible for the "magnetic" series.

"V.I.Lenin" Belorussian State University

References

1. V.L.Levshin, Izv.AN SSSR, Ser.fiz., 2, 185 (1937).
2. B.I.Stepanov & A.N.Sevchenko, Trudy GOI, Sessiya, posvyashchennaya pamyati akad.S.I.Vavilova (Proceedings of the State Optical Institute. Session dedicated to the memory of Academician S.I.Vavilov), Oborongiz, 1953.
3. N.F.Moerman & H.H.Kraak, Des Travaux Chimiques des Pays-Bas, 58, 34 (1939).
4. V.L.Levshin & G.D.Sheremet'ev, Zhur.eksp.i teor.fiz., 17, 204 (1947); A.N. Sevchenko, Izv.AN SSSR, Ser.fiz., 13, 188 (1949); S.S.Solomin, Doklady AN SSSR, 31, 741 (1941); M.N.Alentsev, Trudy, (Proceedings), Physics Institute of the USSR Ac.of Sci., 5, 499 (1950).
5. B.I.Stepanov, Lyuminestsentsiya slozhnykh molekul (Luminescence of Complex Molecules), Part I, Minsk, 1955.
6. G.H.Dieke & A.B.Duncan, Spectroscopic Properties of Uranium Compounds, N.Y., 1949.

INFLUENCE OF THE ADSORBENT SURFACE ON THE LUMINESCENCE OF URANYL IONS

- G.I.Kobyshev

In recent years the structure and the nature of the bonds in complex compounds of uranyl have attracted the attention of investigators.[1-3] It should be noted, however, that investigation of the photochemical and, particularly, the photocatalytic activity of uarnyl ions is of independent interest. As Terenin[4] noted, in order to clarify some of the problems involved in the activation of molecules adsorbed on solid surfaces it is worth while studying the behavior of uranyl atoms which exhibit a high degree of sensitivity of the luminescence spectra to the nature of the addend.[5]

In the present work we utilized the luminescence spectra with vibrational structure of the coordinated uranyl ion as a sort of spectral indicator of the changes undergone by the ion under conditions of adsorption and the influence on it of extraneous molecules. By way of adsorbents we utilized Grebenshchikov's[6] quartzoid microporous glass, silica gel, alumogel, alumosilica gel, magnesium oxide gel, etc.

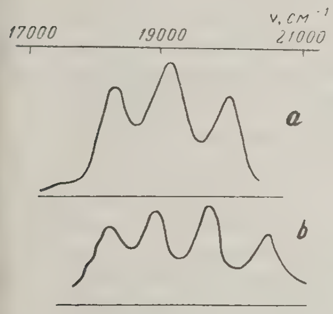

Fig.1. Luminescence spectra of the hydrated uranyl ion under conditions of adsorption at $77^{\circ}K$: a) on microporous glass, b) on magnesium oxide.

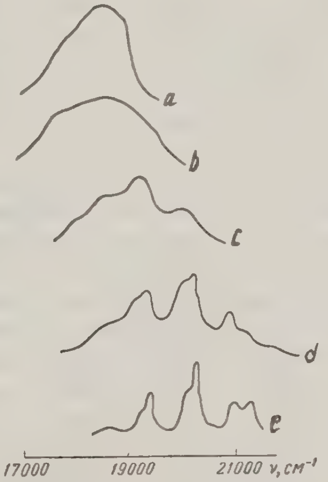

Fig.2. Luminescence spectra at $77^{\circ}K$: a) dehydrated uranyl ion adsorbed on microporous glass, b) UN = $UO_2(NO_3)_2$, c) after admission of water vapor to the dehydrated ion, d) after admission of gaseous NO_2 to the dehydrated ion, e) UN·$2NO_2$.

Photometric traces of the luminescence spectra at $77^{\circ}K$ of hydrated uranyl ions in the state of adsorption on microporous glass and magnesium oxide are reproduced in Figs.1 & 2. As will be evident from the figures, the spectrum depends on the type of adsorbent. Even at $77^{\circ}K$ there is no clear line structure such as that characteristic of the crystalline state. The schematic representation of the spectra given in Fig.3 serves to compare the positions of the peaks in the luminescence spectra of the crystal hydrates, the hydroxide and uranyl glass (UN = abbreviation for $UO_2(NO_3)_2$.

The spectrum of the adsorbate differs from the spectrum of the crystal hydrates[7], water solutions of uranyl nitrate[8], and also from the spectra of uranyl glass[9] and uranyl hydroxide[10]. In the adsorbed state even at room temperature there occurs an appreciable (~50-fold) increase in the luminescence intensity of the adsorbate as compared with the solutions; this is apparently explained by increase in the absorption coefficient. There is also a change in the position and number of the most intense bands; the frequency of the symmetrical valence vibrations is reduced some 30-50 cm^{-1} as compared with the crystal and solution. There is also a change in the lifetime of the excited state of the uranyl ion. Aside from the above mentioned changes in the luminescence spectrum, the fact that the uranyl ion is in the state of adsorption is indicated by a number of other factors, in particular by the fact that the uranyl ion may be replaced by a different ion. On the basis of ion exchange reactions carried out by us, it may be inferred that the bonds between the

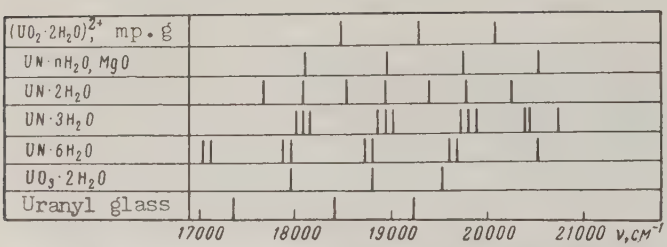

Fig.3. Schematic representation of the principal peaks in the absorption spectrum at 77°K. UN = $= UO_2(NO_3)_2$; mp.g = microporous glass.

surface and the uranyl ion are ionic in character to an appreciable degree, as in the case of adsorption of other cations (Refs.11 & 12). No substantial changes are observed either in the position of the peaks in the luminescence spectra of the uranyl ion under conditions of adsorption on different hydroxyl-containing adsorbents or in the spectral distribution of the luminescence. This indicates that the action of the surface of these adsorbents is monotypic, presumably involving the replacement of a proton of the surface hydroxyl by a uranyl ion. The observed variations in the intensity of the luminescence are due to differences in the nature of the adsorbents.

Thus the distinctive features of the luminescence spectrum of the hydrated uranyl ion on the surface of a solid and the difference of this spectrum, as noted above, from the spectra of solutions, crystals, uranyl glass and uranyl hydroxide, in conjunction with the cited experimental results, give reason to conclude that the uranyl ion is actually in an adsorbed state on the solid substrate, i.e., that we are not dealing simply with a case of adhesion or deposition of crystallites of the salt.

The arrangement of the bands in the 90°K luminescence spectrum of the adsorbed ion having coordination bound water $(UO_2 \cdot nH_2O)^{2+}$ differs from the position of the luminescence bands in the spectra of solutions wherein the hexahydrate is present and is in best agreement with one of the series of bands in the spectrum of uranyl nitrate dihydrate[8]. Thus it is natural to attribute the observed luminescence to an ion having two water molecules in its coordination sphere.

Further experiments were carried out under vacuum with adsorbates from which there was gradually removed the capillary, the adsorbed and finally the coordination bound water. In the case of samples held in vacuum for 2-5 hours at 150-200°, at low temperature there is observed a decrease in the intensity of luminescence over the entire spectrum with a more appreciable change in the intensity of the short wavelength band. At the same time all the spectral bands are strongly smeared out. Further dehydration for 15 hours or more results in a substantial decrease in intensity and complete effacement of structure; at the same time the intensity maximum is shifted to the long wavelength side (to 18 300 cm^{-1}). The spectrum in this case has the appearance of a wide asymmetrical band. Prolonged (6-15 days) pumping without heating (i.e., at room temperature) leads to a similar change in the spectrum as in the case of heating. Consequently, the transformation of the structured luminescence spectrum to a structureless one is due to a change in the degree of hydration of the uranyl ion. The above described changes in the spectrum are reversible: structure reappears within a few hours of admission of water vapor to the uranyl-microporous glass system. The luminescence spectrum of the uranyl ion devoid of coordination bound water is shown in Fig.2,a. Under the influence of water vapor on the dehydrated uranyl ion, the spectrum from a wide asymmetrical band transforms into the spectrum with three clearly pronounced peaks characteristic of the hydrated ion. The effect of gaseous NO_2 is similar as regards alteration of the structureless spectrum, but in this case there is observed a different distribution of the luminescence intensities and a different position of the luminescence bands. For comparison in Fig.2 we give the luminescence spec-

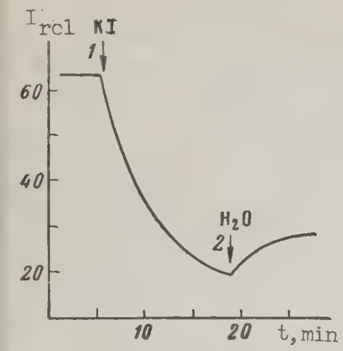

Fig.4. Photometric trace of the variation in intensity of luminescence as a result of introduction of quenching anions (1) and decrease in their concentration (2).

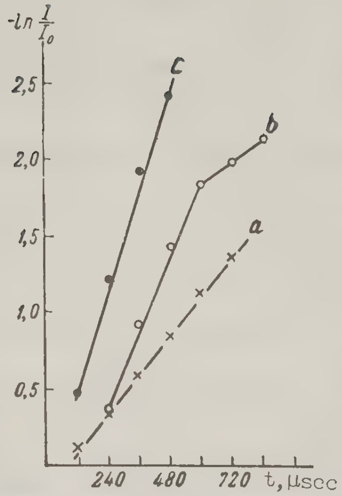

Fig.5. Decay in the luminescence intensity at 290°K: a - $UN \cdot 6H_2O$, b - $(UO_2 \cdot 2H_2O)^{2+}$ - microporous glass, c - same + KI.

tra of the complex compound $UN \cdot 2NO_2$ and anhydrous uranyl nitrate. Thus it may be concluded that the structured luminescence spectrum appears as a result of coordination of addends by the uranyl ion, as indicated earlier[5], with formation of a complex surface compound.

The uranyl ion is bound to the surface of the adsorbent by substantial forces and even prolonged washing with water does not result in removal of the adsorbed ion. This circumstance was utilized for investigating the process of quenching of luminescence in the adsorbed state by I and NO_2 ions. No changes in the spectral distribution of the luminescence as a result of quenching were observed. It was found that the process is fully reversible, i.e., with decrease in the concentration of the quencher the luminescence intensity increases and upon complete elimination of the quenching anion the initial luminescence intensity is restored (Fig.4). The quenching process is described in a wide range of quencher concentrations by the linear Stern-Folmer formula. Simultaneously with decrease in the luminescence intensity there is observed a decrease in the lifetime of the excited state of the uranyl ion (Fig.5). Under conditions of adsorption the decay becomes more complex in character. We detected the presence of two excited states with lifetimes of $\tau_1 = 9 \cdot 10^{-4}$ sec and $\tau_2 = 10^{-4}$ sec, which were measured by two photoelectric procedures (taumeter and pulse excitation).

Conclusions

1. The uranyl ion exists on solid surfaces in the adsorbed state; crystallites of the uranyl salt are not formed.
2. The surface of the adsorbents under vacuum dehydrates the adsorbed uranyl ions. As a result of dehydration the luminescence intensity is sharply reduced. A structured luminescence spectrum appears in case of coordination of the ion with H_2O and NO_2 molecules with the formation of a complex compound on the surface.
3. In the adsorbed state the uranyl ion is not coordinated with atoms of the surface. Adsorption occurs as a result of replacement of a proton of the surface hydroxyl group by a uranyl ion.
4. The process of quenching by I^- and NO_2^- ions is fully reversible and is described by the linear Stern-Folmer formula.

Laboratory of Photosynthesis,
Scientific Research Physical Institute,
"A.A.Zhdanov" Leningrad State University

References

1. L.V.Volod'ko & A.N.Sevchenko, Optika i spektroskopiya, 4, 40 (1958).
2. V.M.Vdovenko, M.G.Juzina & A.A.Lipovskii, Zhur.neorgan.khim. (Journal of Inorganic Chemistry), 2, 970 (1957).
3. B.M.Gatehouse & A.E.Comyns, J.Chem.Soc., 3965 (1958).
4. A.N.Terenin, Vestnik (Bulletin), Leningrad State University, No.1, 13 (1946); No.11, 143 (1953).
5. G.I.Kobyshev & D.N.Suglobov, Doklady AN SSSR, 120, 330 (1958). (Trans. Doklady.)
6. O.S.Molchanova & I.V.Grebenshchikov, Zhur.obshch.khim (Journ.Gen.Chem.), 12, 537 (1942).
7. A.N.Sevchenko, V.M.Vdovenko & T.V.Kovaleva, Zhur.eksp.i teor.fiz., 21, 204 (1951).
8. B.E.Gordon, Ukr.khim.zh. (Ukrainian Chem.Jour.), 17, 688 (1951); Izv. AN SSSR, Ser.fiz., 15, 625 (1951).
9. F.A.Kröger, J.M.Sterels & P.G.Botden, Philips Res.Rep., 3, 46 (1951).
10. D.F.Vier & M.Z.Schultz, JOSA, 38, 811 (1948).
11. M.T.Roger & R.Van der Vennen, JACS, 75, 1751 (1953).
12. C.M.French & J.P.Howard, Trans.Faraday Soc., 52, 102 (1956).

* * * * * * *

VITRIFICATION OF POLYMERS AND PHOSPHORESCENCE

- E.V.Anufrieva & A.D.Zaitseva

Vitrification of polymers involves immobilization of the macromolecules (or individual parts thereof). In the temperature range below T_g (the vitrifying point), the equilibrium structure obtaining at higher temperatures is frozen. When a polymer is cooled below T_g, its viscosity becomes so high and the relaxation time of the macromolecules increases to such an extent that no significant rearrangement of the structure during the time of a normal experiment can be realized.[1-3]

The mobility of macromolecules in polymers can be investigated by the method of dielectric losses, nuclear magnetic resonance, luminescence[4] and other procedures. Certain typical attributes may serve as indications of freezing of the structure at T_g. These include the density, the index of refraction, the intensity of the infrared spectra, and the optical activity.

Zhurkov & Levin[5], in investigating the infrared spectra of vitrifying systems with hydrogen bonds, succeeded in showing that the hydrogen bonds are frozen in the process of vitrification. Reduction of the temperature in the $T > T_g$ range is accompanied by growth in the number of bound hydroxyl groups; in the range $T < T_g$ this increase stops. There is established a certain equilibrium between the free and bound hydroxyl groups.

The influence of vitrification on the optical activity (or the molecular gyration constant) is particularly strong in systems with hydrogen bonds.[6]

In the present work we investigated the influence of vitrification of polymers on the phosphorescence* of the luminophor introduced into the polymer or on the specific interaction of the luminophor with the medium, i.e., the interaction responsible for the appearance of phosphorescence. It has been established that

---

*We refer here to the persistent emission coinciding in the spectrum with the fluorescence.

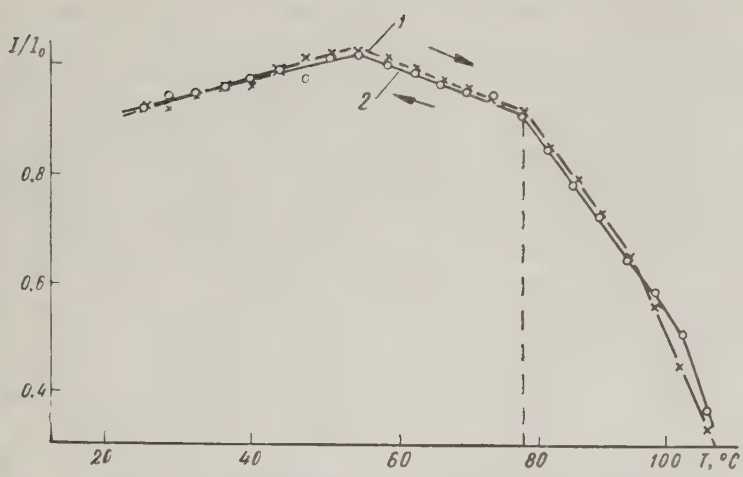

Fig.1. Temperature dependence of the phosphorescence intensity of rhoduline orange in polyvinyl alcohol: 1 - heating, 2 - cooling.

phosphorescence appears in "rigid" media in the presence of bonding between the luminophor and medium stronger than the coupling due to van der Waals' forces.[7] All media and systems exhibiting phosphorescence are substances capable of association by means of hydrogen bonds. Thus, among the polymers investigated by us the strongest phosphorescence was yielded by polyvinyl alcohol and polyacrylamide.

We investigated the temperature dependences of the phosphorescence intensity of 1) rhoduline orange, 2) rhodamine B, 3) 3,6-diaminophthalimide, and 4) 1-dimethylaminonaphthalene-5-sulfonylchloride in polyvinyl alcohol in the range from 20° to 100°, i.e., in the range encompassing the vitrification point T_g of polyvinyl alcohol.

The phosphorescence vs temperature curves for all the systems have a characteristic break at T_g for the polymer. In the $T > T_g$ range the phosphorescence intensity decreases sharply with increasing temperature. This variation is reversible. A break in the I vs T curves at T_g is observed both in cooling and heating the polymer. By way of illustration, in Fig.1 we reproduce the temperature vs phosphorescence intensity curves for rhoduline orange in polyvinyl alcohol. We did not observe any decrease in phosphorescence intensity for the same luminophors in polyacrylamide at $T = 80°$; polyacrylamide vitrifies at a higher temperature. Consequently, the observed break in the I vs T curves at T_g for polyvinyl alcohol is due to changes that occur in the polymer itself, i.e., is due to vitrification of the polyvinyl alcohol, not to changes of the luminophors per se.

The alteration in the phosphorescence intensity incident to vitrification of the polymer can be explained on the assumption that the decisive role in the appearance of phosphorescence is played by hydrogen bonds linking the luminophor and medium.[7] The phosphorescence intensity of the luminophor-polyvinyl alcohol system in the investigated range of temperatures both above and below T_g varies in the same way as the concentration of the bound hydroxyl groups. Even a minor increase in phosphorescence intensity incident to cooling in the vitrified state may be correlated with a corresponding increase in the number of bound hydroxyl groups in polyvinyl alcohol down to 55°.[5]

The intensity of the fluorescence (or the integral luminescence) of the investigated systems either does not change in going through T_g or diminishes only slightly in heating above T_g (Fig.2). Thus vitrification of the polymer substantially alters the conditions determining the appearance of phosphorescence.

As noted above, vitrification of polymers involves virtually complete immobilization of the macromolecules or individual parts thereof. As part of our work we explored the possibility of investigating the mobility of macromolecules in polymers by the method of polarized luminescence. The probability that the polarization of the luminescence of the luminophor introduced into the polymer will be

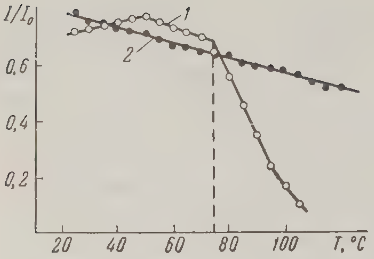

Fig.2. Temperature dependences of the phosphorescence (1) and fluorescence (2) intensities of 1-dimethylaminonaphthalene-5-sulfonylchloride in polyvinyl alcohol.

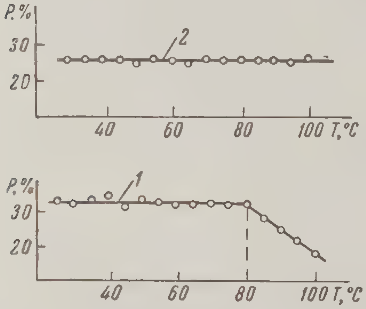

Fig.3. Temperature dependence of the polarization of phosphorescence (1) and fluorescence (2) of rhoduline orange in polyvinyl alcohol.

affected by the mobility of the macromolecules (or the luminescent molecules) will be the higher, the greater the persistence of luminescence. Hence we investigated the temperature dependence of the polarization P of the phosphorescence of rhoduline orange in polyvinyl alcohol. The measurements were carried out at temperatures both below and above T_g. It will be evident from the P vs T curve shown in Fig.3 that the degree of polarization gradually decreases with cooling of the sample to T_g, and that there is no further change as a result of cooling below T_g. The $P = f(T)$ curve has a characteristic break at T_g for the polymer. In contrast, the polarization of fluorescence of rhoduline orange in polyvinyl alcohol remains constant at all temperatures, both below and above T_g (curve 2 in Fig.3).

Comparison of the temperature dependences of the polarization of phosphorescence and fluorescence shows that changes in the relative orientation or position of the macromolecules of polyvinyl alcohol in the temperature range just above T_g are realized within a time equal to the persistence of phosphorescence, but do not have time to occur within a time equal to the persistence of fluorescence ($\sim 10^{-8}$ sec). Thus we have obtained significant information on the relaxation time of macromolecules in polymers at temperatures close to the vitrification point.

Institute of High Molecular Compounds,
Academy of Sciences of the USSR

References

1. P.P.Kobeko, Amorfnye veshchestva (Amorphous Substances), M., 1952.
2. G.O.Jones, Glass, London, 1956.
3. M.V.Vol'kenshtein & O.B.Ptitsyn, Zhur.tekhn.fiz., 26, 2204 (1956). (Trans. Soviet Physics - Tech.Physics.)
4. E.V.Anufrieva, M.V.Vol'kenshtein & T.V.Razgovorova, Optika i spektroskopiya 4, 414 (1958); Ibid., 7, 505 (1959). (Trans.Optics & Spectroscopy).
5. S.N.Zhurkov & B.Ya.Levin, Doklady AN SSSR, 67, 89 (1949); Ibid., 72, 269 (1950).
6. I.A.Bolotina, N.M.Bazhenov, M.V.Vol'kenshtein & Zh.S.Sogomonyants, Zhur. fiz.tverdogo tela, 1, 489 (1959). (Trans.Soviet Physics - Solid State.)
7. A.N.Terenin, Zhur.fiz.khim., 18, 1 (1944); Izv.AN SSSR, Ser.fiz., 8, 305 (1945).

LUMINESCENCE OF SYSTEMS WITH HYDROGEN BONDS

- B.A. Zadorozhnyi & Yu.V. Naboikin

1. Despite the fact that there have been relatively few studies devoted specifically to the luminescent manifestations of the hydrogen bond, it can safely be asserted that the hydrogen bond is evinced in the luminescence of substances in a manner similar to its manifestation in absorption spectra. Virtually the only theoretical treatment of this question published so far is that of Pimentel[1]. Pimentel's work helped clarify the matter of the direction and magnitude of the spectral shifts incident to formation of hydrogen bonds. Pimentel deduced the following relationships:

$$\Delta\nu_a = W_0 - W_1 + \omega_1, \tag{1}$$

$$\Delta\nu_l = W_0 - W_1 - \omega_0, \tag{2}$$

$$\Delta\nu_{0-0} = W_0 - W_1, \tag{3}$$

where $\Delta\nu_a$ is the shift of the absorption band peak due to formation of a hydrogen bond, $\Delta\nu_l$ is the corresponding shift of the luminescence peak, $\Delta\nu_{0-0}$ is the shift in the frequency of the purely electronic transition, W_0 is the energy of the hydrogen bond in the ground electronic state of the system, W_1 is the energy of the hydrogen bond in the excited state of the system, ω_0 is the stimulation (perturbation) of the vibrations of the atoms linked by the hydrogen bridge in the ground electronic state (inferred on the basis of the Franck-Condon principle), and ω_1 is the corresponding quantity for the excited state of the system.

Pimentel's results have been substantiated by a number of experimental studies, for example, those of Mataga et al[2,3], Brealy & Kasha[4] and others.

2. Further consideration of the question of the influence of hydrogen bonds on the electronic spectra of substances leads to rather interesting results. Thus from the diagram of Fig.1 one can readily deduce the following relationship (we consider shifts to the short wavelength side to be positive +; to the long wavelength side to be negative -):

$$\Delta\nu^{\mathrm{H}} = \Delta\nu + (\Delta\nu_a - \Delta\nu_l), \tag{4}$$

where $\Delta\nu$ is the magnitude of the Stokes shift in the absence of a hydrogen bond, and $\Delta\nu^{\mathrm{H}}$ is the shift after formation of a hydrogen bond. Taking the values of $\Delta\nu_l$ and $\Delta\nu_a$ from Pimentel's formulas, we obtain

$$\Delta\nu^{\mathrm{H}} = \Delta\nu + (\omega_0 + \omega_1). \tag{5}$$

In the case of Stokes excitation ω_0 and ω_1 are always positive. Hence from Eq.(5) we conclude that as a result of formation of a hydrogen bond the Stokes shift always increases; the magnitude of this increase varies, depending on the specific values of ω_0 and ω_1. Consequently, the increase of the Stokes shift can serve as an indication that a hydrogen bond has formed in the system. Experimental confirmation of this can be found in our experimental work[5-8] as well as in the results of other authors. Typical examples are shown in the accompanying table.

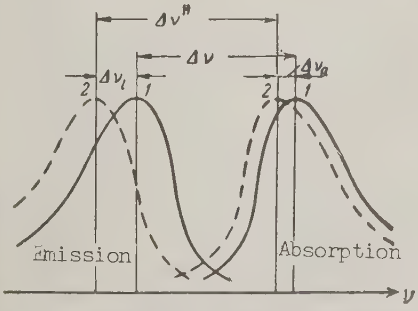

Fig.1. Change in the electronic spectra as a result of formation of a hydrogen bond: 1 - no hydrogen bond, 2 - hydrogen bond formed.

Positions of the absorption and luminescence peaks in the spectra of different substances in the absence and presence of hydrogen bonds

Type H bond	Substance	Solvent	No hydrogen bond			With hydrogen bond		
			ν_a, cm^{-1}	ν_l, cm^{-1}	$\Delta\nu$, cm^{-1}	ν_a^H, cm^{-1}	ν_l^H, cm^{-1}	$\Delta\nu^H$, cm^{-1}
Inter-molecular	1-naphthol*	Hexane	31100	29300	1800	—	—	
		Hexane + butyl acetate	—	—	—	31000	29000	2000
	2-naphthol*	Hexane	30500	28700	1800	—	—	—
		Hexane + butyl acetate	—	—	—	30200	28200	2000
	1,4-hydroxynaphthoic acid	Toluene	31900	27000	4900	—	—	—
		Methanol	—	—	—	31900	26000	5900
	Methyl 1,4-hydroxynaphthoic ester	Toluene	32200	27800	4400	—	—	—
		Methanol	—	—	—	31600	25300	6300
	Methyl 2,3-methoxynaphthoic ester	Heptane	29400	26000	3400	—	—	—
		Methanol	—	—	—	29100	24000	5100
Intra-molecular	Methyl 1,4-hydroxynaphthoic ester	Toluene	32200	27800	4400	—	—	—
	Methyl 2,3-hydroxynaphthoic ester	Benzene	—	—	—	27200	15400	11800
	Methyl 2,3-methoxynaphthoic ester	Methanol	29100	24000	5100	—	—	—
	2,3-Methoxynaphthoic acid	Methanol + HCl	—	—	—	29400	19300	10100

*According to Mataga et al[3].

From the formal standpoint, relation (5) simply reflects the experimentally observed dependence. Its physical meaning is the following: as the result of formation of a hydrogen bond there appear new vibrations in the system; naturally, in this case, incident to electronic transitions, there will be expended a larger amount of energy for inducing vibrations of the system than in the absence of hydrogen bridges, i.e., there will be an increase of the "Stokes losses" and the magnitude of the Stokes shift will increase. We note that here there is no difference between intra- and intermolecular hydrogen bonds.

3. Examination of the available experimental data shows that among the different substances capable of forming intramolecular hydrogen bonds there are frequently encountered compounds with an anomalously great Stokes shift. We have explained this interesting effect in an earlier contribution[6]; here we shall attempt to give a clearer description of the processes involved. As will be evident from Fig.2, the hydrogen bond is evinced in the electronic spectra only when its strength (energy) in the excited state differs from the strength of the hydrogen bond in the ground state; when $W_1 = W_0$ no changes are apparent. It will be evident that the perturbation or stimulation of the vibrations of the atoms linked by the hydrogen bond increases with increase of the difference between W_1 and W_0. Whereas, for example, in case b the values of ω_0 and ω_1 are small, when $W_1 \ll W_0$ (case c), these values are much greater: ω_0 almost attains the value of W_0, while ω_1 greatly exceeds W_1, i.e., the hydrogen bond is ruptured in the process of absorption. Thus in case of an appropriate relation between the energies of the hydrogen bond in the ground (W_0) and excited (W_1) states there can occur rupture

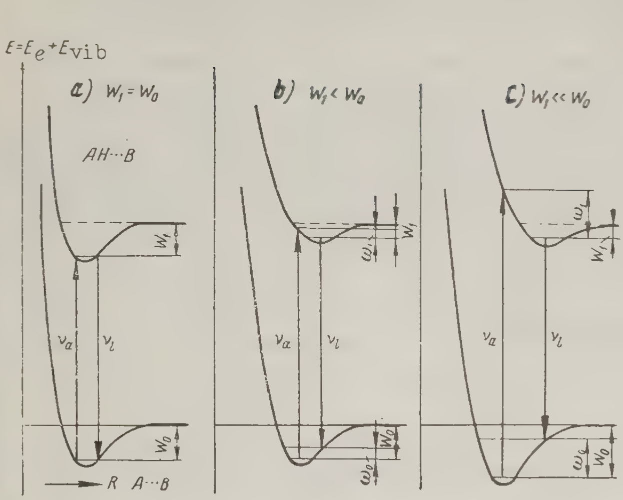

Fig.2. Potential curves of systems with hydrogen bonds.

of the hydrogen bond either in the event of absorption or in that of emission or even incident to both transitions; the necessary condition for this is only that there be a substantial difference between the bond energies W_0 and W_1. A direct consequence of such bond ruptures incident to absorption or emission events is sharp increase of ω_0 and ω_1, the sum of which quantities determines the increment of the Stokes shift incident to the formation of the hydrogen bonds (relation (5)).

4. Two bands are observed in the luminescence spectra of some substances with intramolecular hydrogen bonds. Whereas, in view of the above said, the long wavelength band may be associated with fluorescence of molecules with hydrogen bonds, the short wavelength emission must be attributed to molecules without such bonds. The results of our experiments[7,8] show that these bands may be located at different distances from each other; for example, in the spectrum of the methyl ester of 2,3-hydroxynaphthoic acid, they are located at 430 mμ and 650 mμ, i.e., are well separated; in the spectrum of phenyl salicylate they are so close that they almost merge.

The relative intensity of these two bands depends in the final analysis on the equilibrium constant K^* of the process of formation of the hydrogen bond in the excited state:

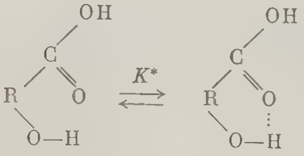

I II

or, what is essentially the same thing on the relative probabilities for emission by form I and form II. In view of this, although in principle there should always be two bands in the luminescence spectra of substances with hydrogen bonds, actually there are frequently encountered cases when one of the bands is very weak[9] or even invisible[6].

5. In experimental investigation of the luminescence of systems with hydrogen bridges one must always bear in mind the possibility that the relatively weak manifestations of the hydrogen bonds may be masked by stronger effects associated with other factors, for example, ionization. Thus the above mentioned two luminescence bands of the methyl ester of 2,3-hydroxynaphthoic acid are clearly discernible both in benzene and in methanol solutions. In the case of 2,3-hydroxynaphthoic acid itself, however, observation of the respective bands (located at 420 mμ and ~650 mμ) is feasible only in inert solvents, inasmuch as in methanol this compound is ionized to an appreciable degree and there appears in its luminescence spectrum only one very intense band at 515 mμ, due to the emission of fully ionized molecules.[8]

6. As was shown above, hydrogen bonds produce substantial changes in the electronic spectra only when the strength of the bonds in the excited state differs substantially from the strength of the hydrogen bonds in the ground state. Obviously, in such cases the potential curves of the electronic states will be characterized by different degrees of anharmonicity and, consequently, by a different structure of the energy levels. Hence Levshin's mirror symmetry rule will not be fulfilled for the spectra of systems with hydrogen bonds. And, actually, mirror symmetry of the absorption and luminescence spectra was not observed for the substances with hydrogen bonds investigated by us; we plan to investigate the question of symmetry in greater detail in the future.

Conclusions

1. The formation of hydrogen bonds - intermolecular or intramolecular - leads to increase of the Stokes shift.

2. The hydrogen bonds may be ruptured incident to electronic transitions (absorption or emission); this leads to the appearance of fluorescence bands strongly displaced to the long wavelength side.

3. In many cases there may be simultaneously present two luminescence bands in the spectra of substances with hydrogen bonds.

References

1. G.C.Pimentel, J.Amer.Chem.Soc., 79, 3323 (1957).
2. N.Mataga and others, Nature, 175, 731 (1955).
3. N.Mataga and others, Bull.Chem.Soc.Japan, 29, 115 (1956).
4. G.G.Brealy & M.Kasha, J.Amer.Chem.Soc., 77, 4462 (1955).
5. Yu.V.Naboikin, B.A.Zadorozhnyi & E.N.Pavlova, Izv.AN SSSR, Ser.fiz., 23, 9 (1959). (Trans.Bulletin, 23, 9.)
6. Yu.V.Naboikin, E.N.Pavlova & B.A.Zadorozhnyi, Optika i spektroskopiya, 6, 366 (1959). (Trans.Optics & Spectroscopy.)
7. Yu.V.Naboikin, B.A.Zadorozhnyi & E.N.Pavlova, Ibid., 6, 492 (1959).
8. Yu.V.Naboikin, B.A.Zadorozhnyi & E.N.Pavlova, Ibid., 8, 505 (1960).
9. A.Weller, Z.Elektrochem., 60, 1140 (1956).

REASONS FOR ELIMINATION OF INTERNAL NONRADIATIVE TRANSITIONS IN ORGANIC MOLECULES INCIDENT TO FORMATION OF INTRACOMPLEX COMPOUNDS WITH CATIONS

- E.A.Bozhevol'nov

The most sensitive luminescence analysis reagents for determination of cations are compounds in which intramolecular nonradiative transitions are suppressed or eliminated as a result of formation of an intracomplex compound with cations.* An illustration of a reaction of this type is furnished by the formation of an intracomplex compound by salicylal-o-aminophenol with aluminum.[1,2]

It will be evident from Fig.1 that the fluorescence spectrum of this intracomplex compound exhibits mirror symmetry with its absorption spectrum, while the original reagent (salicylal-o-aminophenol) has only an absorption spectrum and exhibits no fluorescence.

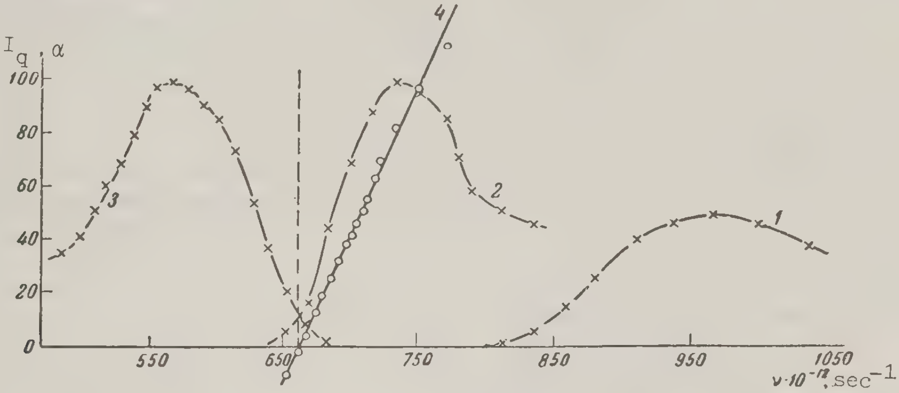

Fig.1. Absorption spectrum of solutions of salicylal-o-aminophenol (1) and its complex with aluminum (2) and the fluorescence spectrum of this intracomplex compound (3). The straight line 4 illustrates the symmetry of curves 2 & 3.[3]

The question of what characteristics or attributes of organic molecules are responsible for their ability to luminesce is one of the fundamental questions in the field of luminescence.[4] Extant concepts and theoretical considerations[5,6] do not allow of predicting the luminescence behavior of organic molecules with a nonrigid structure; yet precisely among such molecules we encounter a number of luminescent reagents, lumogens and microbiological stains.

In an earlier contribution[7] we suggested that in constructing the molecular model according to extant rules[8,9] particular attention should be paid not only to the molecular skeleton but also to the range of action and the zone of overlapping of the constituent molecules. This allows of judging of the complanarity of the molecules and of the presence or absence of conformational isomers, factors which are directly related with the luminescent properties of organic molecules.

On the basis of comparison of the fluorescent properties of solutions of organic substances with the respective molecular models, we found that molecules with a nonrigid structure absorbing light in the near ultraviolet or in the short wavelength region of the visible spectrum and not having in their composition fluorescent quenching substituents (for example, $-NO_2$) are fluorescent provided their

---

*Another, second type of luminescent reaction is accompanied by shift of both the absorption and fluorescence spectra. For example, as a result of formation of an intracomplex compound of alizarin red with boron the absorption peak is shifted from 485 to 505 mμ, the fluorescence peak from 600 to 620 mμ.

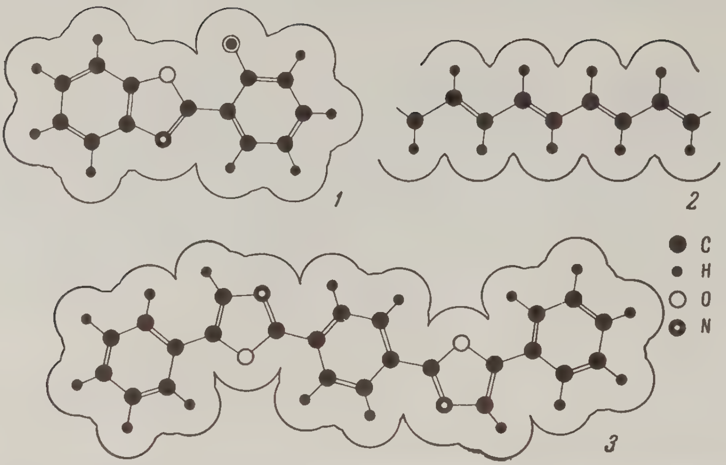

Fig.2. Examples of molecular models of organic compounds fluorescing in solutions: 1 - 2-(o-hydroxyphenyl)-benzoxypyrole, 2 - polyene chain, 3 - POPOP.

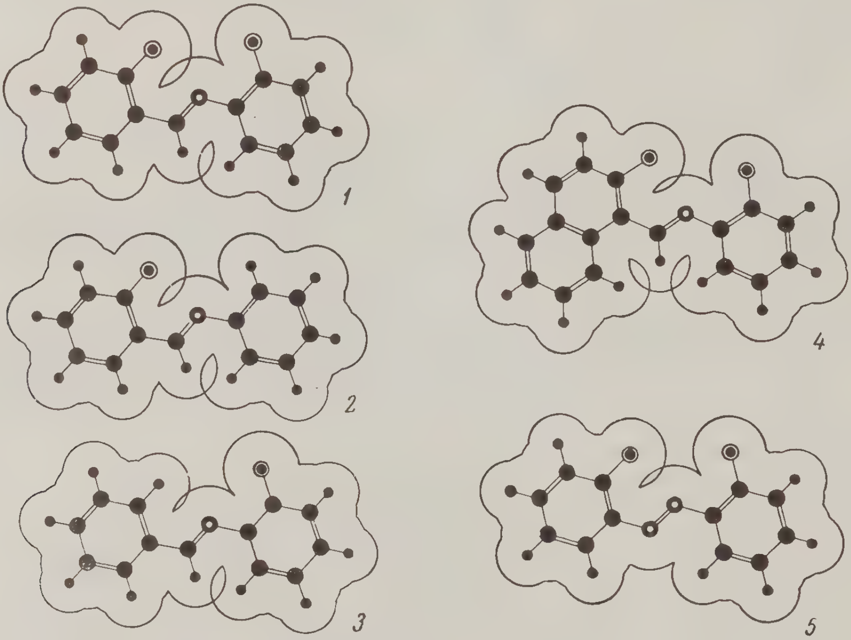

Fig.3. Examples of organic compounds not fluorescing in solutions: 1 - salicylal-o-aminophenol, 2 - salicylal-aniline, 3 - benzal-o-aminophenol, 4 - 2-hydroxynaphthal-o-aminophenol, 5 - o,o'-dihydroxyazobenzene.

model does not comprise overlap zones, and vice versa. This is illustrated in Figs.2 and 3.

The absence of fluorescence is characteristic for noncomplanar molecules possessing conformational isomers; hence we infer that internal nonradiative transitions in this case are associated with an expenditure of the excitation energy by the molecule for transition from one conformational isomer to another.

It is of obvious interest to evaluate the height of the potential barrier that must be overcome for transition from one conformational isomer to another. It is known[10] that the potential barrier energy for such a simple molecule as that of ethane is 3 kcal/mole, while for different biphenyl derivatives[11] the corresponding values range from 20 (for 2-nitro-6-carboxy-6'-ethoxybiphenyl to 46 kcal/mole (for 2,2'-diamino-6,6'-dimethylbiphenyl). In view of the existence in complex molecules of several conformational isomers and the high rate of isomerization[12] (10^{10} sec^{-1}) the possibility of dissipation of excitation energy by this process appears highly likely.

Consequently, molecules with a nonrigid structure the models of which have overlap zones may be fluorescent in the presence of intramolecular forces hindering the formation of conformational isomers. Such forces may be the bonding forces with metallic cations, appearing as a result of formation of intramolecular compounds and generally bringing the molecule to a complanar state, as well as the forces of intramolecular hydrogen bonds. Hence among the compounds listed in Fig. 3 one can expect the appearance of fluorescence in the presence of aluminum not only in the case of salicylal-o-aminophenol, but also for 2-hydroxynaphthol-o-aminophenol and o,o'-dihydroxyazobenzene. For the same reason one cannot expect the appearance of fluorescence in the case in intracomplex compounds of salicylal-aniline and benzal-o-aminophenol with aluminum inasmuch as the formation of these intramolecular compounds does not preclude the existence of conformational isomers.

Experimental observation of the fluorescence of the enumerated compounds and their complexes with aluminum fully substantiated our inferences. We found no exceptions to the above rules in investigating over 60 azomethin and azoxy compounds* and some chromesalt dyes described in the literature; we were able to predict correctly the luminescent properties of a number of compounds.

The rules and concepts developed herein may be useful for establishing the structure of organic molecules. An example demonstrating this is the error we found in the structural formula for chromesalt black given by Ladenbauer et al[13]. If this dye had the structural formula (1) given by these authors, it could not form a fluorescent intramolecular compound with gallium. In connection with the fact that Ladenbauer et al report observing fluorescence of this dye in the presence of gallium one must question formula (1). Actually, it is known[14] that chromesalt black consists of a mixture of two products one of which is that described by Ladenbauer et al, while the other (the principal component) has the structure given by formula (2).

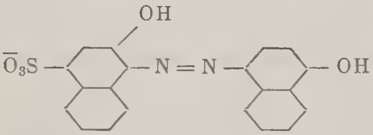

(1)

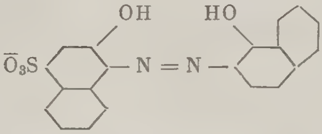

(2)

Accordingly, we propose that to discover new luminescent reagents one should search for molecules with a nonrigid structure, a noncomplanar model and functional-analytic groupings leading in the case of metallic complexes to the elimination of the possibility of formation of conformational isomers; another approach would be to seek lumogens, the molecules of which do not have a rigid structure and the atoms of which do not have overlapping zones in the molecular model.

---

*Synthesized by A.M.Lukin.

Among the practical results of the present research is the discovery of new luminescent reagents for determining gallium[15,16], magnesium[17,18] and a number of other metals[19,20].

All-Union Scientific Research Institute for Chemical Reagents

References

1. Z.Holzbecher, Chem.Listy, 47, 680 (1953).

2. E.A.Bozhevol'nov, Trudy IREA (Proceedings of the Inst.of Chem.Reagents) No.22, p.70, Goskhimizdat, 1958; E.A.Bozhevol'nov & V.M.Yanishevskaya, Lyuminestsentnyi analiz (Luminescence analysis - collection of reports presented at the Eighth Conference on Luminescence), Minsk, 1960.

3. V.L.Levshin, Fotolyuminestsentsiya zhidkikh i tverdykh veshchestv (Photoluminescence of liquids and solids), M., 1951.

4. B.I.Stepanov, Lyuminestsentsiya slozhnykh molekul (Luminescence of complex molecules), Minsk, 1955.

5. P.P.Feofilov, Doklady AN SSSR, 45, 387 (1944).

6. M.D.Galanin, Trudy (Proceedings), Inst.of Physics, USSR Ac.of Sci., 5, 339 (1950).

7. E.A.Bozhevol'nov, Trudy IREA, No.23, p.147, Goskhimizdat, 1959 (See Ref.1).

8. A.I.Kitaigorodskii, Organicheskaya kristoallokhimiya (Organic Crystallochemistry), M., 1955.

9. J.Czekalla, Chem.Labor.und Betrieb, 11, 467 (1956).

10. J.D.Kemp & K.S.Pitzer, J.Chem.Phys., 4, 748 (1936).

11. F.Cagle & Wm.H.Eyring, J.Amer.Chem.Soc., 73, 5628 (1951).

12. S.S.Urazovskii, Molekulyarnyi polimorfizm (Molecular polymorphism), p.211, Kiev, 1956.

13. I.M.Ladenbauer, F.Korkisch & F.Hecht, Mikrochimica Acta, 5-6, 1076 (1955).

14. Color Index, Ed.R.M.Rowe, Bradford, 1924.

15. E.A.Bozhevol'nov, A.M.Lukin & M.N.Gradinarskaya, Inventor's Certificate No.116838, May 13, 1958.

16. A.M.Lukin & E.A.Bozhevol'nov, Zhur.analit.khim., 15, 43 (1960). (Trans. Jour.Analytical Chemistry).

17. G.V.Serebryakova, A.M.Lukin & E.A.Bozhevol'nov, Inventor's Certificate No.129273, September 7, 1959.

18. E.A.Bozhevol'nov & G.V.Serebryakova, Lyuminestsentnyi analiz (Luminescence analysis - collection of reports presented at the Eighth Conference on Luminescence) Minsk, 1960.

19. E.A.Bozhevol'nov & A.M.Lukin, Inventor's Certificate No.111859, July 1, 1957.

20. E.A.Bozhevol'nov, A.A.Pryanishnikov & B.S.Pal'chits, Inventor's Certificate No.114463, January 11, 1958.

PHOSPHORESCENCE OF CERTAIN SOLVENTS AND THEIR EFFECT ON THE ABSORPTION SPECTRA OF ORGANIC PHOSPHORS

- G.M.Kislyak

In our investigation of the phosphorescence of organic dyes we employed primarily formic and acetic acids, which belong in the group of carboxylic acids. The use of these acids as solvents helps gain a deeper understanding of the influence of acid media on the phosphorescence of organic dyes at low temperature.

Earlier we reported[1] that the addition of formic acid to water solutions of trypaflavine results in appreciable deformation of the absorption spectrum and alteration of the phosphorescence decay law.

In the present work we observed a similar influence of formic acid on the luminescence characteristics of other acridine dyes, namely, acridine yellow and riboflavin.

As will be evident from Fig.1 the absorption spectra of acridine yellow and riboflavin in 85% formic acid solution are shifted to the short wavelength side. There remains, as in the case of trypaflavine, a diffuse secondary peak at 450 mμ. Acetic acid does not deform the absorption spectra of acridine yellow and trypaflavine but, like 85% formic acid, it does deform the absorption spectrum of riboflavin. The influence of acetic and formic acids on the absorption spectrum of riboflavin is of the same nature, inasmuch as both absorption curves (see Fig.1) virtually coincide in the short wavelength part of the spectrum and diverge only slightly in the long wavelength part.

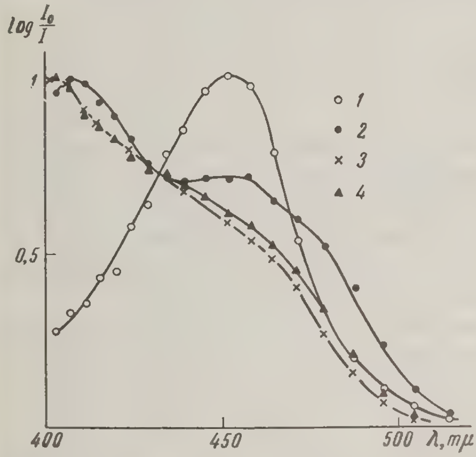

Fig.1. Absorption spectra: 1) acridine yellow in acetic acid, 2) acridine yellow in 85% formic acid, 3) riboflavin in acetic acid, 4) riboflavin in 85% formic acid. $C = 10^{-4}$ g/cm^3.

In view of the fact that this influence of formic acid (and partially acetic acid) is observed only for acridine dyes, we undertook a series of experiments with a view to determining the reason for this effect. First, we recorded the absorption spectrum of a water solution of trypaflavine. Then we prepared water solutions of trypaflavine with different concentrations of formic acid (85, 25, 5 and 1%); these solutions were then evaporated to dryness, the trypaflavine residue was dissolved in water and the absorption spectra again recorded. The results of these experiments are shown in Fig.2, from which it will be evident that decrease in the formic acid concentration gradually brings the absorption spectra of trypaflavine to the form characteristic of the initial solution of trypaflavine in pure water. It was found that only formic acid has this effect on the absorption of trypaflavine; this will be evident from Fig. 3 which shows the results of similar experiments with trypaflavine dissolved in water and isoamyl alcohol (analogous results were obtained for solutions of acetic acid).

One of the main reasons for the apparent influence of formic acid on the phosphorescence decay law of trypaflavine at low temperature may be the superposition of the intrinsic strong afterglow of the solvent on the phosphorescence of the dye, which should obviously result in a "complex" decay law.

The fact that formic acid at low temperature emits strong phosphorescence after excitation with ultraviolet has been known since 1905.[2] The phosphorescence

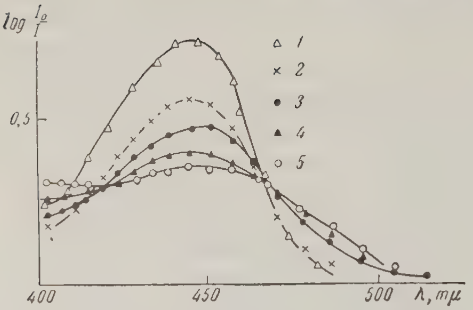

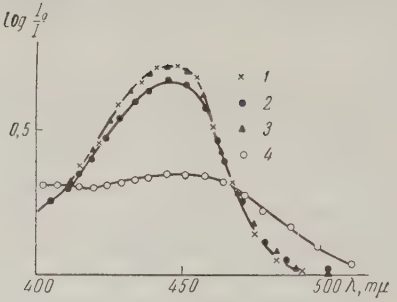

Fig.2. Absorption spectra of trypaflavine: 1) in water, 2) redissolved in water after evaporation of a 1% formic acid solution, 3) in water after evaporation of 5% formic acid, 4) in water after evaporation of 25% formic acid, 5) in water after evaporation of 85% formic acid. $C = 10^{-5}$ g/cm^3.

Fig.3. Absorption spectra of trypaflavine: 1) in water, 2) redissolved in water after evaporation of a water solution, 3) in water after evaporation of isoamyl alcohol, 4) in water after evaporation of 85% formic acid. $C = 10^{-5}$ g/cm^3.

of acetic acid was partially investigated in the work of Osada[3], who used acetic acid as a solvent for sodium and potassium acetates; Osada investigated the variation in the phosphorescence of the solutions with changes in temperature from -30 to -60°. He observed two phosphorescence bands - a green and a blue band, the origin of which Osada attributes to Na and K ions incorporated as impurities in the lattice of solid acetic acid and interacting with the lattice ions.

We investigated the persistence of phosphorescence of formic and acetic acids and the influence of the wavelength of the exciting light on this persistence. The experiments were carried out at liquid oxygen temperature. The frozen acid solutions were excited by light from a PRK-2 mercury tube passing through a UFS-1 filter and by monochromatic light in the visible region selected by an MS-3 monochromator. The decay curves were recorded on photographic film by means of the oscillographic set-up described in Ref.4.

It was found that in the case of monochromatic excitation by wavelengths in the visible region from $\lambda_{ex} = 400$ mμ to $\lambda_{ex} = 500$ mμ, no significant afterglow is observed. Hence the deformation of the τ vs λ_{ex} curve for trypaflavine in 85% formic acid cannot be explained by the phosphorescence of the solvent. In the case of excitation with ultraviolet light passing through the USF-1 filter, however, there is observed an appreciable afterglow for both formic and acetic acid.

The phosphorescence decay of these acids follows a complex law; the decay curve can be approximated by two exponential curves. In the beginning (up to 0.1-0.15 sec), the decay curve deviates from an exponential one, and the primary short term luminescence is evinced only during the first second.

We assume that the principal reason for the afterglow of these acids is the presence of the carboxyl group COOH, which, as is known, is responsible for the strong phosphorescence of other carboxylic and, particularly, dibasic acids.*

---

*In discussing the present report A.N.Terenin suggested another reason for the afterglow of the investigated acids at low temperature, namely, the presence of organic impurities; that such impurities were present is highly probable inasmuch as the acids employed in the experiments were not chemically purified.

The reason for the influence of formic acid on the absorption spectra of acridine dyes in our opinion is the following. As is known, formic acid is the strongest carboxylic acid and has the highest ionization constant - 12 times greater than acetic acid[5]. In our experiments we used only 85% formic acid, hence it is logical to assume that some of the acid molecules decomposed into H^+ and $R—COO^-$ ions. Consequently, some of the trypaflavine molecules could link up to a hydrogen ion, as a result of which the absorption peak is shifted 48-50 mμ to the short wavelength side, in accord with the data of Terenin[6]. Moreover, at 450 mμ there persists an auxiliary peak, which corresponds to the maximum in the absorption spectrum of pure trypaflavine in water. This also serves to explain the deformation of the τ vs λ_{ex} curve for trypaflavine in 85% formic acid with excitation in the Stokes region.

Thus we have shown that formic and acetic acids at low temperature have a significant intrinsic phosphorescence. Moreover, formic acid (and to some extent acetic acid) deforms the absorption spectra of acridine dyes and also significantly alters the decay of their phorphorescence. These factors should not be neglected in investigating the phosphorescence of acridine dyes.

References

1. G.M.Kislyak, Optika i spektroskopiya, 6, 226 (1959). (Trans.Optics and Spectroscopy.)
2. P.Borisov, ZhRFKhO (Journal of the Russian Physical & Chemical Society) Physics Section, 37, 249 (1905).
3. K.Osada, J.Phys.Soc.Japan, 12, 1420 (1957).
4. G.M.Kislyak, Izvestiya (Bulletin), Crimean Pedagogical Institute, 29, 358 (1958).
5. E.S.Khotinskii, Kurs organicheskoi khimii (Course in organic chemistry) Khar'kov, 1952.
6. A.N.Terenin, Fotokhimiya krasitelei (Photochemistry of dyes), M.-L., 1947.

* * * * * * *

CORRELATION BETWEEN THE ABSORPTION AND LUMINESCENCE SPECTRA OF SOME ORGANIC COMPOUNDS

- E.F.Ryazanova, M.S.Fadeeva & T.S.Pavlina

It is of obvious interest to test experimentally some of the inferences arrived at in the recent theoretical investigations of Stepanov[1,2], Alentsev & Pakhomycheva[3], and Neporent[4] devoted to the relation between the luminescence and absorption spectra of complex molecules.

Stepanov deduced the following universal relationship between the luminescence and absorption spectra of complex molecules:

$$\frac{W_\nu^{\text{lum}}}{\varkappa_\nu} = d(T)\,\nu^3 e^{-\frac{h\nu}{kT}}, \tag{1}$$

The temperature computed by means of this equation from the experimental data can then be compared with the actual temperature of the medium surrounding the luminescing molecules.

Experimental checks[1,3,5] of relation (1) showed that the calculated temperature T* is generally of the order of magnitude of the experimental temperature T, but in some cases appreciably exceeds T.

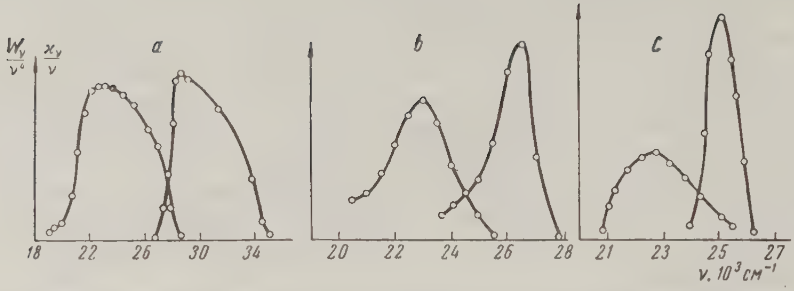

Fig.1. Absorption and luminescence spectra at room temperature: a) m-phenylenediamine, b) brassylic acid c) adipic acid.

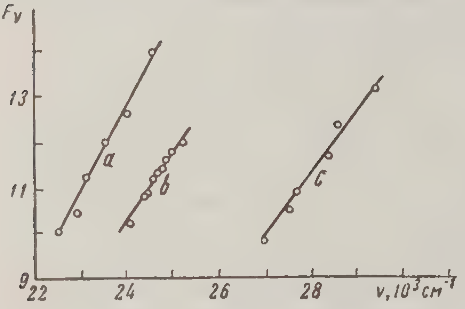

Fig.2

←Fig.2. Frequency dependences of F_ν: a) brassylic acid (T* = 345°K), b) adipic acid (T* = 366°K), c) m-phenylenediamine (T* = 388°K).

The fact that T* is greater than T was explained by Stepanov[1] by the absence of complete equilibrium between the degrees of freedom of the excited molecule and the solvent molecules.

We investigated the luminescence and absorption spectra at room temperatures of the following organic compounds: m-phenylenediamine $C_6H_4(NH_2)_2$, brassylic acid $H_{41}C_{21}COOH$ and adipic acid $HOOC(CH_2)_4COOH$. The substances were investigated in the crystalline state: either a thin layer of the compound was deposited on a quartz plate by sublimation or a thin layer of the crystalline powder was compressed between two quartz plates.

The luminescence spectra were recorded on an ISP-51 spectrometer and the photographic plates were scanned on an MF-2 microphotometer; the absorption spectra in the visible and ultraviolet regions were recorded on an SF-4 quartz spectrophotometer. The luminescence was excited by 313 mμ and 405 mμ light.

The luminescence and absorption spectra of the investigated compounds are shown in Fig.1 (all curves have been normalized with respect to area - see Refs. 4,6 & 7). It will be evident from the figure that the luminescence and absorption spectra of all the substances overlap to some extent. As plotted in the frequency scale all the spectra are asymmetrical.

Check of relation (1) shows that the quantity

$$F_\nu = 3 \ln \nu - \ln \frac{W_\nu}{x_\nu}$$

is a linear function of the frequency and that the experimental points for all the investigated compounds fall on a straight line (Fig.2). The values of the temperature T* calculated from the slope of these straight line plots are consistently higher than the experimental temperature T.

The appreciable divergence between T* and T for the investigated compounds cannot be explained by the influence of the solvent molecules on the excited molecules of the luminescent substance during the brief process of redistribution of energy over vibrational degrees of freedom.

Inasmuch as the divergence between T* and T in the crystalline state is approximately the same as for a number of solutions investigated earlier[1,3,5], it may be assumed that the decisive role here is played not by the nature of the solvent but by the specific characteristics of the excited state of the luminescent molecules, a factor that requires further experimental and theoretical study.

We call attention to the following interesting fact concerning the absorption spectrum in the visible region and the phosphorescence spectrum of m-phenylenediamine. In addition to the short wavelength absorption band, in the spectrum of this substance there appears a second clearly pronounced absorption band that lies in the visible region of the spectrum. The phosphorescence spectrum is shifted relative to the second absorption band to the side of longer wavelengths (Fig. 3) and the two spectra overlap somewhat in the wavelength scale, i.e., the relation between the phosphorescence spectrum (excited by the integral radiation from a PRK-4 mercury discharge tube) and the second absorption band is the same as between the fluorescence spectrum and the first absorption band. This fact can be explained if we hypothesize the existence of a second metastable level as suggested earlier on the basis of our investigation of the phosphorescence spectra of this substance at different temperatures and the temperature quenching of its phosphorescence.

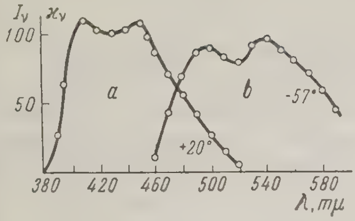

Fig.3. Spectra of m-phenylenediamine: a) absorption (second band), b) phosphorescence.

We desire to express our sincere gratitude to N.K.Rudnevskii and N.N.Vyshinskii for making possible the spectral photometric measurements.

"M.Gor'kii" Gorkii State Pedagogical Institute

References

1. B.I.Stepanov, Izv.AN SSSR, Ser.fiz., 22, 1367 (1958). (Trans.Bulletin, 22, 1357.)
2. B.I.Stepanov & L.P.Kozachenko, Optika i spektroskopiya, 2, 339 (1957).
3. M.N.Alentsev & L.A.Pakhomycheva, Izv.AN SSSR, Ser.fiz., 22, 1377 (1958). (Trans.Bulletin, 22, 1367.)
4. B.S.Neporent, Ibid., 22, 1372 (1958). (Trans.Bulletin, 22, 1362.)
5. L.A.Kravtsov, Ibid., 23, 78 (1959). (Trans.Bulletin, 23, 77.)
6. B.S.Neporent, Doklady AN SSSR, 20, 30 (1958). (Trans.Soviet Physics - Doklady.)
7. B.S.Neporent & N.G.Bakhshiev, Optika i spektroskopiya, 5, 634 (1958).
8. M.S.Fadeeva, Izv.AN SSSR, Ser.fiz., 23, 147 (1959) (Trans.Bulletin, 23, 139); B.A.Pyatnitskii & M.S.Fadeev, Ibid., 20, 524 (1956) (Trans.Bulletin, 20, 479.)

---

[*] As was indicated in the report of Alentsev & Pakhomycheva presented at the present conference, there is an appreciable divergence between T* and T in the case of water solutions of erythrosine (T* = 380°K; T = 293°K), while in the case of acetone solutions of erythrosine the values of T* and T are close (T* = 304°K; T = 293°K).

INVESTIGATION OF THE LUMINESCENCE OF IONIC FORMS OF URANIN AND FLUORESCEIN

- E.V.Grigoryan, L.T.Kantardzhyan & S.S.Chirkinyan

Usually the luminescence of fluorescein is attributed either to the doubly charged anion in basic solutions or to the cation in acid solutions.[1-3] However, earlier one of us[4] showed that in a rather wide pH range the luminescence of fluorescein and uranin (sodium fluorescein) solutions is due to the simultaneous presence of both anions and cations. Recently Zanker & Peter[5] through analysis of the absorption spectra demonstrated the existence of a new ionic form of fluorescein, namely, the singly charged anion.

We investigated the luminescence spectra of uranin and fluorescein solutions in a wide range of pH values for the purpose of clarifying the influence of the singly charged anion on the spectral curve. We also made an attempt to establish the relation between the variation in the luminescence spectrum and changes in the proportions of different ionic forms.

Medium	pH	I_{515}/I_{530}
48% diaxane + 52% water	7	0.92
39% dioxane + 61% water	7.2	0.97
19% dioxane + 81% water	7.2	1.02
5% dioxane + 95% water	7.8	1.08
100% water	8	1.15
10% dioxane + 90% ammonia (0.3 N water solution)	11.2	
100% ammonia (0.3 N water solution)	11.2	
60% dioxane + 30% water - 10% NaOH	>12*	
35% dioxane + 65% 0.1 N H_2SO_4	1.6	
5% dioxane + 95% 0.1 N H_2SO_4	1.2	
99% water + 1% 12 N HNO_3	1.6	
90% water + 10% 12 N HNO_3	1.0	
80% water + 20% 12 N HNO_3	<1*	
60% water + 40% 12 N HNO_3	<1*	

---

*Our pH-meter allowed of measuring the pH values only in the range from 1 to 12.

The luminescence spectra were measured on a photoelectric set-up similar to that described in Ref.6. The luminescence was excited by the 365 mμ line isolated by a UG-1 filter from the radiation of a PRK-4 mercury discharge tube. Reabsorption was reduced to a minimum by appropriate choice of the dye concentrations and thickness of the solution cell. In all the experiments with uranin, the uranin concentration was the same, namely, $5 \cdot 10^{-5}$ g/ml.

The luminescence spectra of uranin and fluorescein solutions were investigated in mixtures of dioxane + water, dioxane + sulfuric acid, dioxane + ammonia (water solutions) and also in solutions of caustic soda and nitric acid.

Inasmuch as the luminescence spectra of fluorescein and uranin in both basic and acid solutions proved to be identical, we do not reproduce the spectra of fluorescein here.

Fig.1 gives the luminescence spectra of uranin in solutions of dioxane + water. It will be evident from the figure that the spectrum comprises three bands peaking at 515, 530 and 550 mμ. The integral intensity increases with increase of the relative amount of water in the mixture, which increase is accompanied by increase in the pH of the solution (see accompanying table).

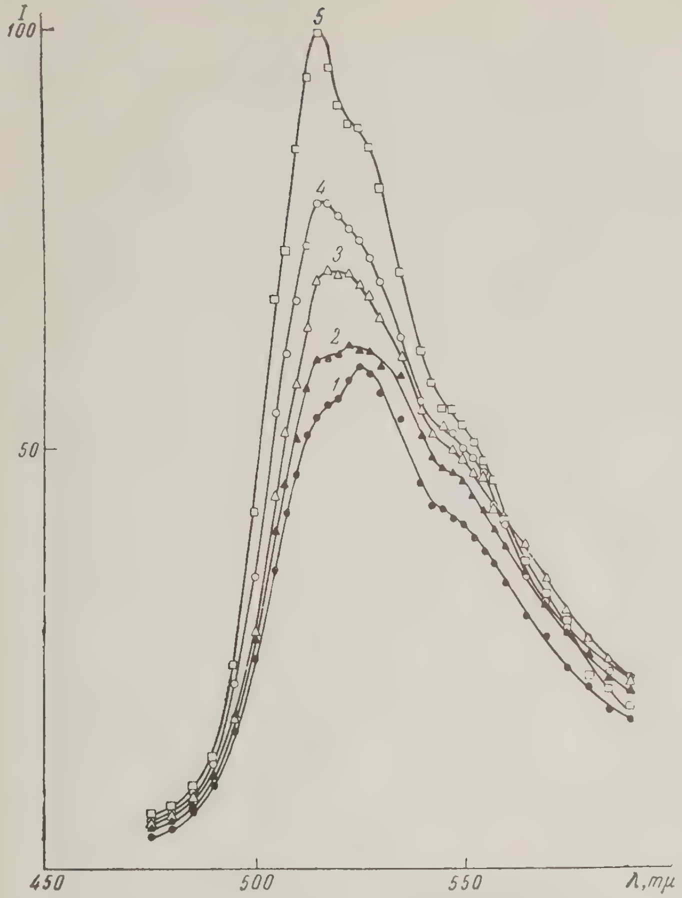

Fig.1. Luminescence spectra of uranin solutions in mixtures of dioxane + water: 1) 48% dioxane + + 52% water, 2) 39% dioxane + 61% water, 3) 19% dioxane + 81% water, 4) 5% dioxane + 95% water, 5) 100% water.

In strong basic solutions (pH > 11) no peak at 530 mμ is observed in the spectrum (Fig. 2). Increase in the pH of the solution in this case also results in increase of the integral luminescence intensity. Fig.3 shows the spectrum of strongly acid solutions of uranin. In this case increase in the general luminescence intensity is observed with decrease of pH. It will be evident from the figures that the luminescence spectra of uranin in sulfuric acid (Fig.3, 1 & 2) differ from the spectra of uranin in alkaline solutions (Fig.2).

Moreover, the spectra of uranin in nitric acid differ from the above. They are characterized by the presence of a new diffused band in the 470-475 mμ region, the intensity of which increases with increase of the HNO_3 concentration (Fig. 3,3-6). Owing to the increase in intensity of this band the spectrum as a whole is shifted to the short wavelength side.

On the basis of the experimental results, in agreement with Zanker & Peter[5], we assume that there exist three forms of ions in uranin solutions. The observed variations in the spectra of basic uranin solutions (Figs.2 & 3) can apparently be explained by variation in the relative concentrations of singly and doubly charged ions with change in the pH of the solution. Inasmuch as in strongly alkaline solutions only one peak - that at 515 mμ - is clearly evident, it is natural to assume that the peak at 530 mμ is associated with the singly charged anions. Identification of the peak associated with the cations is more difficult inasmuch as in sulfuric acid solutions the peak at 550 mμ is very strong, while in nitric acid solutions the most predominant peak is that at 475 mμ (Fig.3). The existence of the 475 mμ peak in nitric acid solutions of uranin was first noted by Kantardzhyan (see Fig.1, curve 1 in Ref.4).

Thus our investigation of the ionic forms of uranin through analysis of the luminescence spectra showed that the problem of associating specific luminescence bands with the different ionic forms of the dye is complicated by the appreciable influence of the solvent on the optical properties of the different ions.

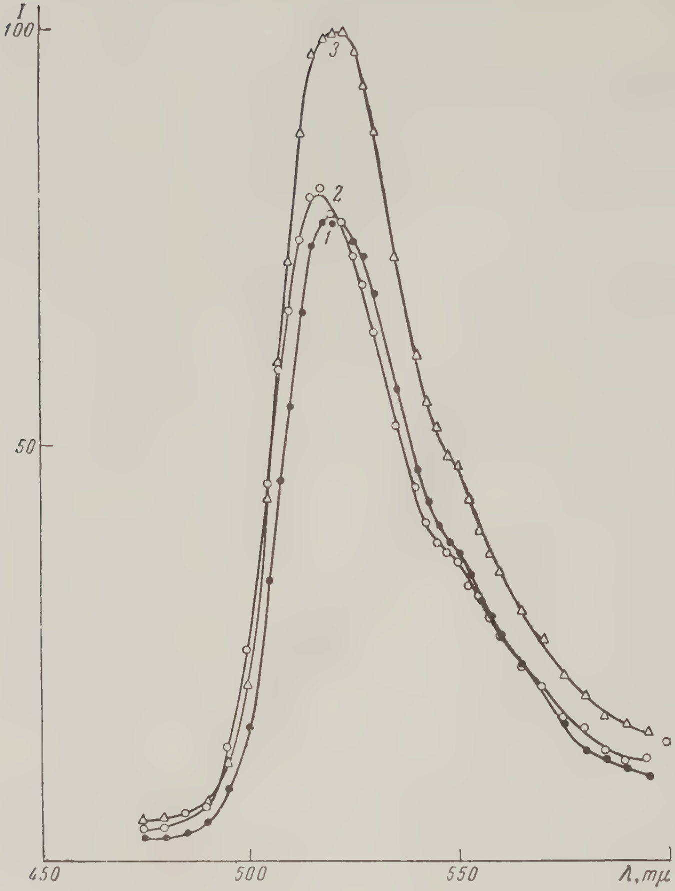

Fig.2. 1) Luminescence spectrum of uranin solution in 10% dioxane + 90% ammonia (0.3 N water solution) by volume; 2) same in 100% ammonia (0.3 N water solution); 3) luminescence spectrum of uranin solution in 60% dioxane + 30% water + 10% caustic soda by weight.

We desire to express our gratitude to A.T.Vartanyan for valuable comments in discussing the experimental results and to M.A.Khumaryan and E.V.Simonyan for assistance in the work.

Institute of Electrical Engineering,
Academy of Sciences of the Armenian SSR

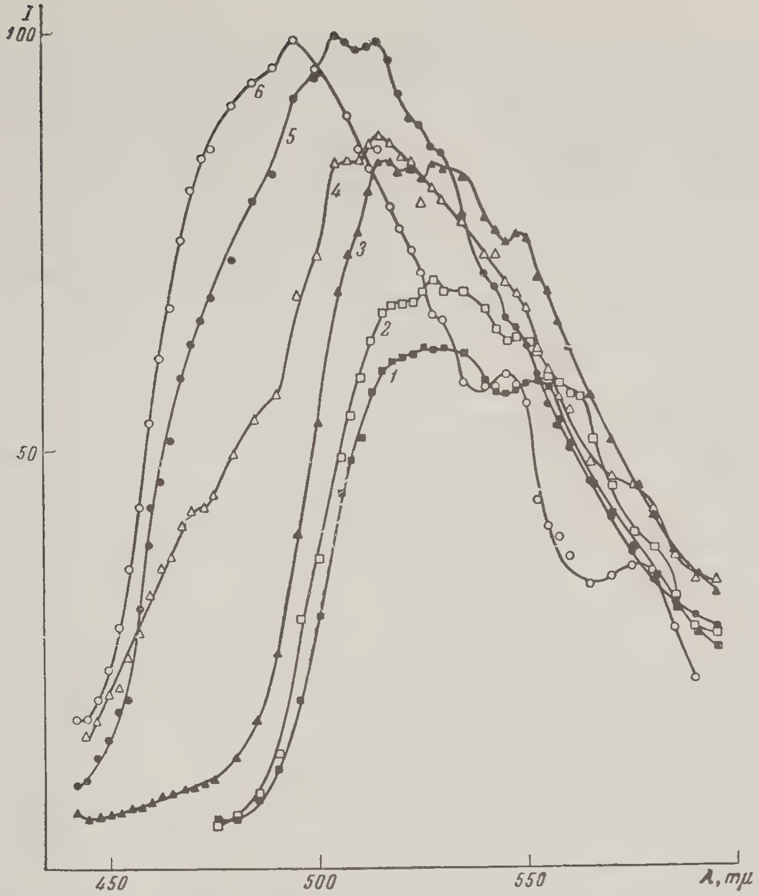

Fig.3. 1-2) Luminescence spectra of uranin solutions in dioxane + 0.1 sulfuric acid: 1 - 35% dioxane + 65% H_2SO_4, 2 - 5% dioxane + 95% H_2SO_4; 3-6) luminescence spectra of uranin in water + 13 N nitric acid: 3 - 99% water + 1% HNO_3, 4 - 90% water + 10% HNO_3, 5 - 80% water + 20% HNO_3, 6 - 60% water + 40% HNO_3.

References

1. B.Batscha, Chem.Ber., 59, 311 (1926).
2. V.L.Levshin, Fotolyuminestsentsiya zhidkikh i tverdykh veshchestv (Photoluminescence of liquids and solids), M.-L., 1955.
3. P.Pringsheim, Fluorescence and Phosphorescence, N.Y., 1949.(Cited in Russiam trans.)
4. L.T.Kantardzhyan, Izv.AN SSSR, Ser.fiz., 23, 131 (1959). (Trans.Bulletin, 23, 125.)
5. V.Zanker & W.Peter, Chem.Ber., 1, 572 (1958).
6. L.T.Kantardzhyan, Optika i spektroskopiya, 2, 378 (1957).

CONCERNING THE ELECTRONIC SPECTRA OF COMPLEX MOLECULES

- S. I. Kubarev

In general the adiabatic approximation may be regarded as applicable to the long wavelength electronic absorption of complex molecules.[1] The relatively high luminescence efficiencies associated with this absorption may also be taken as evidence in favor of the applicability of the adiabatic approximation.

If the adiabatic approximation is justified, i.e., if one can speak of the existence of a vibrational subsystem for a number of the low-lying electronic levels, the problem of absorption and emission of light by complex molecules may be treated from a unified and rather general standpoint. In this case the spectral density of absorption and emission can be represented, using the method of Lax[2], in compact form convenient for investigation:

$$I(\nu) = \int \exp(-2\pi i\nu t)\, I(t)\, dt,$$

where the Fourier transforms of the spectral densities of absorption and emission are, respectively,

$$\left.\begin{aligned} \underset{(a\to b)}{I_{\text{abs}}}(t) &= \frac{\operatorname{Sp}\left(M^{*} e^{\frac{it}{\hbar}\hat{H}_b} M e^{-\frac{it}{\hbar}\hat{H}_a} e^{-\beta\hat{H}_a}\right)}{\operatorname{Sp}\left(e^{-\beta\hat{H}_a}\right)}, \\ \underset{(b\to a)}{I_{\text{em}}}(t) &= \frac{\operatorname{Sp}\left(M e^{-\frac{it}{\hbar}\hat{H}_a} M^{*} e^{\frac{it}{\hbar}\hat{H}_b} \rho\right)}{\operatorname{Sp}(\rho)}. \end{aligned}\right\} \qquad (1)$$

Here ρ is the distribution function for the vibrational states in the excited state, $\hat{H}_a$ and $\hat{H}_b$ are the vibrational Hamiltonians for the electronic states a and b, and M is the moment of the transition.

Our specific problem is to show that for most complex molecules the fundamental spectroscopic effects (origin of the continuous bands, the shape of the bands, their temperature dependence, etc.) can be considered on the basis of equations (1).

1. One of the possible explanations of the origin of continuous bands is that in the case of absorption or emission of light in a "fast" subsystem part of the vibrational degrees of freedom may be regarded as semiclassical. Physically this means that the final state of such oscillators corresponds to large quantum numbers, and in accordance with the principle of correspondence they can be treated classically. We note that in a number of cases the semiclassical approximation can be utilized formally since the interaction with different bonds broadens the levels of the excited state. Further, it is possible that the approximation $M = \text{const}$, usually utilized for simplifying the calculations, is inadequate particularly for low frequencies (see, for example, Lax[2]).

There is another possible explanation which may be more natural for complex molecules, particularly for molecules where one cannot assume the existence of strong coupling between the optically active electrons and the nuclei. Optically active electrons in complex molecules (for example, the π-electrons) are always bound with only part of the molecular skeleton. Stepanov[3], for example, proposed subdividing the molecule into two parts, one of which is associated with absorption, and the other plays the role of a heat reservoir. The significant fact is that in this case there is no necessity to postulate strong anharmonicity for describing the coupling between these parts. Thus if we designate by x the conjunction of normal coordinates of the active part and by y the conjunction of normal coordinates for the reservoir, the vibrational Hamiltonians in the harmonic approximation can be written in the form

$$\left.\begin{aligned}\hat{H}_a &= \hat{H}_a(x) + H(y) + \Sigma A_{jk}x_k y_j + \ldots,\\ \hat{H}_b &= \hat{H}_b(x) + H(y) + \Sigma B_{jk}x_k y_j + \ldots.\end{aligned}\right\} \tag{2}$$

It will be evident that strong coupling between the two parts of the molecule can be assured even in the linear approximation in y. This is important for justifying the oscillator approximation for complex molecules.

If the number of normal vibrations, corresponding to the concomitance of coordinates y, is large, then the semiclassical approximation is applicable, at least formally. In this case

$$I(t) = Av\left\{\left(\exp\frac{it}{\hbar}\Sigma B_{jk}x_k y_j\right)M^*\exp\left(\frac{it}{\hbar}\hat{H}_b(x)\right)M \times \exp\left(-\frac{it}{\hbar}\hat{H}_a(x)\right)\exp\left(-\frac{it}{\hbar}\Sigma A_{jk}x_k y_j\right)\right\}. \tag{3}$$

Each line of the electron-vibrational spectrum, corresponding to an electron transition $a \to b$ will be broadened. It will be evident from (3) that this broadening is due to averaging over y. The magnitude of the broadening depends on the difference $B_{jk} - A_{jk}$.

2. Back in 1922 Vavilov[4] advanced the hypothesis of universality of the long wavelength absorption bands of complex molecules. Numerous measurements made since then showed that the universality is only relative in character. The question of the shape of the bands is solved in principle by calculation of $I(t)$, however, the traces of (1) can be calculated only in some particular cases. It is found that for complex molecules there is no great need for calculating the traces of (1), inasmuch as a number of deductions pertaining to the shape of the bands, the degree of universality, etc. can be arrived at on the basis of the central limit theorem.[5] Its content in this case is that the distribution of the normalized quantity $q = \frac{\nu - \bar{\nu}}{\sigma}$ tends to a normal function in the limit as $n \to \infty$. Here $\bar{\nu}$ is the position of the maximum, σ^2 is the second moment, and under n we understand the effective total number of vibrational quanta in the molecule.

In comparatively complex molecules n is large and the distribution may be represented by an asymptotic expansion. One such expansion, proposed back in 1905 by Edgeworth[5], is of the form (also see Ref.2):

$$\begin{aligned}I(q) = \varphi(q) - \frac{1}{3!}\frac{\mu_3}{\sigma^3}\varphi^{(3)}(q) + \frac{1}{4!}\left(\frac{\mu_4}{\sigma_4} - 3\right)\varphi^{(4)}(q) + \frac{10}{6!}\left(\frac{\mu_3}{\sigma^3}\right)^2\varphi^{(6)}(q) - \frac{1}{5!}\left(\frac{\mu_5}{\sigma^5} - 10\,\frac{\mu_3}{\sigma^3}\right)\varphi^{(5)}(q) + \\ + \frac{35}{7!}\frac{\mu_3}{\sigma^3}\left(\frac{\mu_4}{\sigma^4} - 3\right)\varphi^{(7)}(q) - \frac{280}{9!}\left(\frac{\mu_3}{\sigma^3}\right)^3\varphi^{(9)}(q) + \ldots.\end{aligned} \tag{4}$$

Here $\varphi(q) = \frac{1}{\sqrt{2\pi}}\exp\left(-\frac{q^2}{2}\right)$, $\varphi^{(i)}(q)$ is the i-th derivative of $\varphi(q)$, the μ_i are the central moments, and $\mu_2 \equiv \sigma^2$. This series gives the expansion of $I(q)$ in powers of $1/\sqrt{n}$ with a remainder of the order of the first discarded term.[5] For finite n the deviations from the gaussian shape may be appreciable, however, for large n one can restrict the expansion to terms of order $1/n$, i.e., to the first three terms in (4). Thus, we note that for a large class of complex molecules the spectral density of both the absorption and the emission are represented by the same expression. The individual peculiarities of the molecule are comprised in the moments μ_i, which are calculated from (1). Thus one can speak of universality only in the limited sense. For high temperatures or very complex molecules the distribution tends to the gaussian shape.

However, the question of the band shape can be approached directly. For simplicity, we set $M = \text{const}$; then

$$I_{\text{abs}}(t) = Av\, \exp_{[-]} \left[\frac{i}{\hbar} \int\limits_0^t U\, \Delta\, EU^{-1}(s)\, ds \right]; \tag{5}$$

$$\Delta E = \hat{H}_b - \hat{H}_a; \quad U(s) = \exp \frac{is}{\hbar}\, \hat{H}_a .$$

If we formally apply the semiclassical approximation, we will in any case obtain the approximate envelope of the spectrum. The semiclassical approximation corresponds to the case of taking into account only the first term in the expansion

$$U\Delta EU^{-1} = \Delta E + \frac{is}{\hbar}[\hat{H}_a\Delta E] + \frac{1}{2!}\left(\frac{is}{\hbar}\right)^2[\hat{H}_a[H_a\Delta E]] + \ldots \tag{6}$$

Taking into account higher terms improves the approximation for the envelope; in particular, there is automatically taken into account any deviation from the Franck-Condon principle.

3. The mirror relationship between the absorption and emission spectra is, of course, not absolute in character, but if we agree to treat the experimental data in a certain way, i.e., plot $\frac{\varkappa_\nu}{\nu}$ in the absorption spectrum and $\frac{W_\nu}{\nu^4}$ in the luminescence spectrum, in this case mirror correspondence of the spectra will involve symmetry of the matrix elements and its analysis may lead to certain relationships between $\hat{H}_a$, $\hat{H}_b$ and M. Moreover, we believe it is important not just to identify the conditions for mirror symmetry, but to evaluate the possibility of treating mirror correspondence of the first and second types from a unified standpoint, which was previously questioned[6]. Analysis of the conditions for mirror symmetry leads to the inference that both types of mirror correspondence are exceptions rather than the rule. The conditions for mirror correspondence in the wavelength scale lead, in particular, to the following formula for λ_s line symmetry:

$$\lambda_s = \frac{hc}{h\nu_0 - \frac{\hbar}{2}\, \Sigma\, \Gamma_j \operatorname{cth} \frac{\beta\omega_j\hbar}{2}}, \tag{7}$$

$$\Gamma_j = \omega_j(a) - \omega_j(b).$$

Inasmuch as usually $\Gamma_j > 0$, we obtain from (7) that the frequency of the purely electronic transition is shifted to the side of the absorption peak, which is in agreement with experiment[7]. The physical meaning of this shift is that the zero energy changes incident to a transition in a "fast" subsystem.

In conclusion, we note that in the framework of the given method there may be drawn qualitative and, in certain cases, semiquantitative deductions regarding certain factors and dependences, for example, regarding the temperature dependence of spectral bands, the temperature dependence of the luminescence efficiency, the influence of the solvent on molecular spectra, and so on.

Institute of Chemical Physics
Academy of Sciences of the USSR

References

1. M.A.El'yashevich, Usp.fiz.nauk, 71, 156 (1960). (Trans.Soviet Physics - Uspekhi).
2. M.Lax, J.Chem.Phys., 20, 1752 (1952).

3. B.I.Stepanov, Izv. (Bulletin), Belorussian SSR Ac.of Sci.), No.5, 65 (1954).

4. S.I.Vavilov, Collected works, Vol.1 Article 8, M., 1954.

5. H.Cramer, Mathematical Methods of Statistics, Princeton, 1946. (Cited in Russian trans.)

6. B.S.Neporent, Doklady AN SSSR, 119, 682 (1958). (Trans.Doklady.)

7. N.A.Borisevich, Ibid., 99, 695 (1954).

* * * * * * *

LUMINESCENCE SPECTRA OF HALOGEN DERIVATIVES OF ANTHRAQUINONE IN FROZEN SOLUTIONS

- D.N.Shigorin, N.A.Shcheglova & N.S.Dokunikhin

The present work was devoted to investigation of the structure and the mutual influence of the atoms and radicals in excited molecules by observation of their luminescence spectra.

Earlier[1] we showed that for the purpose of such investigations one can successfully use the method of frozen solution developed by Shpol'skii[2], a procedure that allows of obtaining electronic spectra with fine vibrational structure.

Specifically, in the present work we studied the luminescence spectra of α and β halogen derivatives of anthraquinone in normal paraffin solutions at 77°K ($c = 10^{-4}$-10^{-5} mole/liter; excitation by the 313 mμ line of Hg). In view of the peculiarities of the structure of α and β halogen derivatives of anthraquinone, one may reasonably expect substantial differences between their spectra. Replacement of the hydrogen atom in the α position by a halogen atom results in nonequivalence of the two carbonyl groups in the anthraquinone ring, since one of the C═O groups may exert a mutual influence on the C—Hal group through π-electron interaction, inasmuch as the two groups simultaneously interact with the same carbon atom. This does not occur in β derivatives because in them the carbonyl groups are virtually equivalent. One must also take into account the nature of the halogen atom on the spectra of the α and β derivatives of anthraquinone. It is known that the electronegativity decreases in going from fluorine ($E = 4$) to iodine ($E = 2.4$). The values of the electronegativity of iodine and carbon ($E = 2.5$) are close. In view of this the probability of participation of the unshared electron pairs of the halogens in the π-electron interaction will increase in going from fluorine to iodine, which is in accord with the amount of energy expended on their excitation.

Thus the F atom is characterized by a strong inductive effect that can lead to a certain deformation of the π-electron density at the neighboring carbon atoms, which is equivalent to some shortening of the conjugated chain. Hence introduction of fluorine should lead to shift of the bands to the short wavelength side. Characteristic of Cl, Br and particularly I atoms is participation of the unshared electron pairs in the π-electron interaction of the molecules, which can lead to lengthening of the conjugated chain and, consequently, to shift of the bands to the side of longer wavelengths. These differences in the behavior of halogen atoms should be evinced particularly strongly in the excited state of the molecules.

The substantial difference between the size of the halogen atoms can also result in differences in their effect on the luminescence spectra of α halogen derivatives of anthraquinone. Whereas in view of its small size ($R_B = 1.35$ Å) the F atom cannot have a steric deforming influence on the C═O group, Cl and, particularly, Br and I ($R_B = 2.15$ Å) should have a steric deforming effect. Repulsive forces arise between the halogen atoms with large radii (Cl, Br and, particularly,

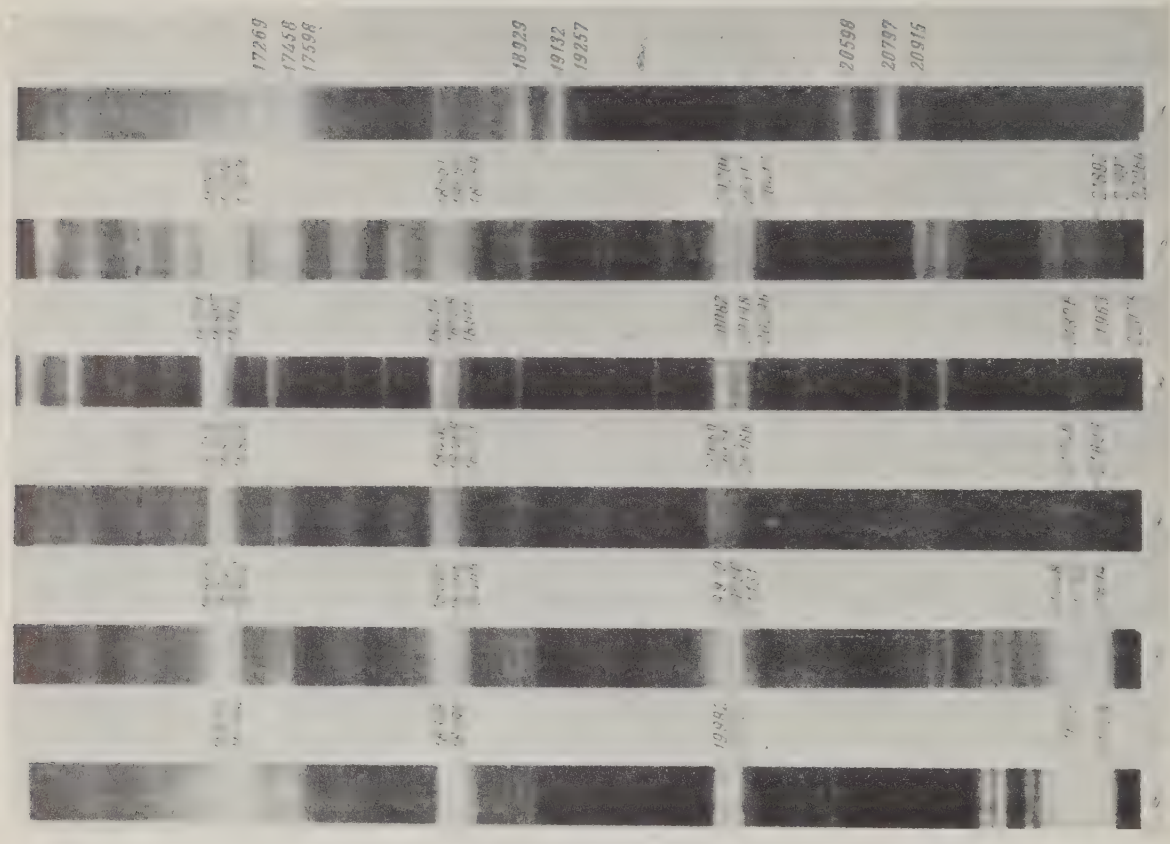

Luminescence spectra of anthraquinone and its halogen derivatives in heptane at 77°K (excitation by the 313 mμ line of Hg; ISP-67 spectrograph): 1) α-fluoroanthraquinone, 2) β-fluoroanthraquinone, 3) anthraquinone, 4) β-chloroanthraquinone, 5) β-bromoanthraquinone, 6) β-iodoanthraquinone.

I) and the oxygen atom of the C=0 group; these repulsive forces lead to distortion of valence angles of the >C=0 and >C—Hal bonds and to some alteration of the electronic state of the groups. It is known that this effect does obtain in similar molecules. One can also expect the nature and position of the halogen atoms in the anthraquinone ring to exert a definite influence on the intensity and character of changes in the electronic-vibrational spectra of the molecules.

The results of our experimental investigation of the luminescence spectra of the halogen derivatives of anthraquinone largely substantiated the above inferences. Spectra with fine vibrational structure were obtained for all the α and β monohalogen derivatives.

The corresponding components of the electronic-vibrational bands (as in the spectra of other anthraquinone derivatives exhibiting a fine vibrational structure) are separated by an average distance of 1665 cm^{-1}, which characterizes the frequency of the valence vibrations of the C=0 group in the ground electronic state. However, the spectra of α-chloro-, α-bromo- and α-iodianthraquinone are poorer in lines and have a continuous background in the long wavelength part of the spectrum (see accompanying table and figure). The spectra of these α halogen

Positions (cm^{-1}) of the components of the principal peaks in the spectra of monohalogen derivatives of anthraquinone in heptane at 77°K

Peak No.	Component Number	α-fluoroanthraquinone	β-fluoroanthraquinone	anthraquinone	β-chloroanthraquinone	β-bromoanthraquinone	β-iodoanthraquinone
Initial band	1	—	22064 w.	22075 w.	—	21804 v.w.	21730 v.in.
	2	—	21991 m.	21963 w.	21809 v.w.	21732 v.w.	21659 v.in.
	3	—	21893 w.	21826 w.	21746 w.	21648 m.	—
1	1	20915 m.	20413 v.w.	20296 w.	20188 m.	20131 in.	20053 in.
	2	20797 in.	20317 in.	20198 in.	20131 in.	20050 in.	19982 in.
	3	20598 m.	20206 in.	20082 in.	20059 in.	19970 w.	—
2	1	19257 w.	18759 v.w.	18611 w.	18523 m.	18466 m.	18390 in.
	2	19132 in.	18667 in.	18538 in.	18469 m.	18396 m.	18318 in.
	3	18929 in.	18561 in.	18419 in.	18402 m.	18305 w.	—
3	1	17598 w.	17076 v.w.	16962 w.	16886 m.	16822 m.	16744 m.
	2	17458 in.	17010 m.	16887 in.	16823 m.	16747 m.	16670 m.
	3	17269 in.	16912 m.	16771 v.in.	16752 m.	16663 w.	—

Note: w = weak, v.w = very weak, m = medium, in = intense, v.in = very intense.

derivatives are similar and in many respects are reminiscent of the spectra of anthraquinone itself.

The spectrum of α-fluoroanthraquinone differs markedly from the spectra of the other α halogen derivatives. The spectral bands become decreasingly diffuse in going from octane to hexane, whereas the opposite situation obtains for the other α halogen derivatives and anthraquinone. In octane solution there is observed doublet splitting of the most intense components of the principal peaks. In contrast to the case of other α-monohalogen derivatives, in the spectrum of α-fluoroanthraquinone there is observed an appreciable shift of the principal peaks to the short wavelength side relative to the position of the principal peaks in the spectrum of anthraquinone ($\Delta\nu$ = 480 to 630 cm^{-1}).

In the spectrum of α-fluoroanthraquinone, in addition to the intense principal peaks (shifted to the short wavelength side relative to the principal peaks of anthraquinone), we also observed less intense bands agreeing as regards structure and position with the principal bands of anthraquinone.

It was found, however, that the weak peaks characteristic of anthraquinone do not appear in the spectrum of 1,5-difluoroanthraquinone.

On the other hand, no fine structure is observed in the spectra of 1,5-dichloro-, 1,5-dibromo-, and 1,5-diiodoanthraquinone. The spectra of these compounds become similar to the diffuse region of the spectra of α-chloro-, α-bromo- and α-iodoanthraquinone. This behavior of the spectra can be explained on the assumption that there exists two $n \rightarrow \pi^*$ electronic transitions for α-monohalogen derivatives of anthraquinone, connected with the presence in these compounds of two nonequivalent carbonyl groups. The probability for these $n \rightarrow \pi^*$ transitions depends strongly on the state of the C=O group. In the case of α-chloro-, α-bromo- and α-iodoanthraquinone, the spectrum with fine vibrational structure, similar to the spectrum of anthraquinone, is apparently due to transitions of the free C=O group, while the transitions associated with the other C=O group have a low probability and are evinced in the form of a continuous spectrum; this is apparently connected with the strong deformation of the C=O bond as a result of the influence of the steric factor and with participation of the unshared electron pair of the halogen atom, mentioned above. From this standpoint one can also explain the absence of fine vibrational structure in the spectra of dichloro-, dibromo- and di iodoanthraquinones.

Both of the electronic transitions are evinced in the spectrum of α-fluoroanthraquinone, the $n \rightarrow \pi^*$ transition of the "unfree" C═O group being manifested with appreciably higher probability. This, apparently, is explained by the fact that the fluorine atom, which has a relatively small radius, does not exert any appreciable deforming steric effect on the carbonyl group (in the α-position) and, in accord with its nature, acts as an electronegative atom (inductive effect), and its unshared electron pairs do not participate in the π-electron interaction in the system. This favors increase of the electron charge on the oxygen atom of the C═O group, which, apparently, leads to increase in the probability for the $n \rightarrow \pi^*$ transition in this group.

The luminescence spectra of the β-halogen derivatives of anthraquinone exhibit fine vibrational structure (see table and figure). The influence of the solvent is evinced in the different multiplicity of the principal electronic-vibrational bands and in variation of the relative intensity of their components.

The influence of the nature of the halogen atom located in the β-position is evinced in the luminescence spectra in that in going from fluorine to chlorine, bromine and iodine, all the components of the principal peaks are regularly shifted to the long wavelength side ($\Delta\nu$ = 100-150 cm^{-1}). Anthraquinone occupies an intermediate position between β-fluoroanthraquinone and β-chloroanthraquinone (see table), which is fully consistent with the arguments adduced above. The participation of the unshared electron pairs of the I and Br atoms in the π-electron interaction of the system at the instant of emission by the molecule leads to an intensity distribution differing from that obtaining in the spectra of anthraquinone and its α and β derivatives that yield spectra with fine vibrational structure. Whereas in the latter cases in going from the violet to the red region the intensity of the bands at first increases and then after attaining a certain maximum falls off, in the spectra of β-bromo-, and particularly, β-iodoanthraquinones there is observed a gradual monotonic decrease in the intensity of the bands (see figure).

The most intense in the spectra of β-bromo- and β-iodoanthraquinone are the shortest wavelength bands; this is explained, in agreement with the Franck-Condon principle, by the small change in the internuclear equilibrium separation for the excited electronic level. Hence in the case of the β-bromo and β-iodo derivatives the $0''$—$0'$ transition is allowed by the Franck-Condon principle. For precise determination of the $0'' \rightarrow 0'$ frequency one must have the absorption spectra of these compounds under the same conditions (so far we have been unable to obtain these). If, however, we identify the most intense short wavelength bands in the spectra of the β-bromo and β-iodo derivatives with the $0''$—$0'$ transition, the values of the frequencies corresponding to the purely electronic transitions are found to be 21 730 cm^{-1} (β-iodo) and 21 804 cm^{-1} (β-bromo).

Thus in the excited molecules of β-bromo and particularly β-iodo derivatives of anthraquinone, by virtue of the effect of participation of the unshared electron pairs of the halogen atoms in the π-electron interaction (owing to possible $n - \pi^*$ transitions) there occur no substantial changes in the distribution of electron density in the C═O groups, in contrast to the case in anthraquinone and its other derivatives. This presumably explains the increased relative luminescence efficiency of β-bromo- and β-iodoanthraquinones. Most of the monohalogen derivatives of anthraquinone exhibit phosphorescence (persistence 2 to 10 sec); this matter, however, requires separate investigation.

References

1. D.N.Shigorin, N.A.Shcheglova, R.N.Nurmukhametov & N.S.Dokunikhin, Doklady AN SSSR, 120, 1242 (1958) (Trans.Doklady); Izv.AN SSSR, Ser.fiz., 23, 37 (1959) (Trans.Bulletin, 23, 39.)

2. E.V.Shpol'skii, E.Z.Girdzhiyauskaite & L.A.Klimova, Transactions of the Tenth All-Union Conference on Spectroscopy, p.24, L'vov, 1957.

Bulletin of the Academy of Sciences of the USSR - Physical Series
Vol. 24, No. 6 - June 1960

Transactions of the Ninth All-Union Conference on Cathode Electronics

TABLE OF CONTENTS

	Page Orig.	Page Trans.
Influence of the electric field on the temperature threshold for the appearance of positive ions in surface ionization - É.Ya.Zandberg	629	639
Electron emission from a cold barium cathode, appearing after a current pulse in the ambient gas - N.V.Tatarinova & P.N. Chistyakov	635	644
Electron-optical contrast in observation of patch fields on emitters - G.V.Spivak, I.A.Pryamkova & N.N.Sedov	640	648
Kinetics of formation and some attributes of oxygen films adsorbed on tungsten - N.D.Morgulis & A.G.Naumovets	647	657
Variation of ion-electron emission as a function of certain parameters of the target and the bombarding ions - U.A. Arifov & R.R.Rakhimov	657	666
Secondary electron emission from sodium films bombarded with argon ions - U.A.Arifov & D.A.Tashkhanova	664	673
On the problem of measuring proton beam currents - P.Görlich, C.Keck, H.Krause, A.Krohs, H.-J.Pohl & F.Schlott	668	677
Investigation of collision of ions with metal surfaces - N.N.Petrov	673	682
Etching disintegration of semiconductor surfaces by ion bombardment - I.G.Sirotenko & G.V.Spivak	679	687
Contribution to the theory of scattering of ions from metal surfaces - V.N.Vapnik, L.G.Gurvich & N.V.Zinov'ev	685	692
Investigation of the interaction of fast deuterium ions with metals - V.M.Gusev, M.I.Guseva, V.P.Vlasenko & N.P.Elistratov	689	696
Concerning anisotropy of cathode sputtering of dielectrics - A.I.Krokhina & G.V.Spivak	694	701
Effect of polarization of the incident light on the emission of complex photocathodes - P.Görlich & H.Hora	698	705
Concerning neutralization of fast positive ions on metal surfaces - U.A.Arifov & Kh.Kh.Khadzhimukhamedov	705	711
On scattering of slow alkali metal ions from metal surfaces - U.A.Arifov, A.Kh.Ayukhanov & D.D.Gruich	710	716
Use of a dynamic type mass spectrometer for investigation of secondary processes - A.Kh.Ayukhanov & G.I.Iskhakov	715	720

Transactions of the Eighth Conference on Luminescence (Concluded from Vol.24,No.5)

	Page Orig.	Page Trans.
Ultimate lines of 3,4-benzopyrene dissolved in normal hydrocarbons at different temperatures - S.G.Bogomolov, F.D.Pemova & L.P.Kolosova	725	728
Luminescence of solutions of thioindigo and its di-derivatives at 77°K - R.N.Nurmukhametov, D.N.Shigorin & N.S.Dokunikhin	728	731
Temperature dependence of the fluorescence efficiency of some phthalimides in different solvents - L.G.Pikulik & A.N.Sevchenko	729	732
Concerning the relation between the absorption and luminescence spectra of complex molecules - M.N.Alentsev & L.A.Pakhomycheva	734	737

Influence of secondary impurities on the absorption and luminescence spectra of the primary impurity in molecular crystals - A.V.Solov'ev 737 740
Polarization of the luminescence of molecular crystals in different regions of the spectrum - V.I.Gribkov, N.D.Zhevandrov & Sh.D. Khan-Magometova 740 743
Mixed organic single crystals, their luminescence and scintillation properties - Yu.V.Naboikin, V.K.Dobrokhotova & V.V.Uglanova 744 747
Correspondence between the absorption and luminescence spectra of uranyl salt solutions - L.V.Volod'ko, A.N.Sevchenko & D.S.Umreiko 749 752
Influence of the adsorbent surface on the luminescence of uranyl ions - G.I.Kobyshev 752 755
Vitrification of polymers and phosphorescence - E.V.Anufrieva & A.D.Zaitseva 755 758
Luminescence of systems with hydrogen bonds - B.A.Zadorozhnyi & Yu.V.Naboikin 758 761
Reasons for elimination of internal nonradiative transitions in organic molecules incident to formation of intracomplex compounds with cations - E.A.Bozhevol'nov 762 765
Phosphorescence of certain solvents and their effect on the absorption spectra of organic phosphors - G.M.Kislyak 766 769
Correlation between the absorption and luminescence spectra of some organic compounds - E.F.Ryazanova, M.S.Fadeeva & T.S.Pavlina 769 771
Investigation of the luminescence of ionic forms of uranin and fluorescein - É.V.Grigoryan, L.T.Kantardzhyan & S.S.Chirkinyan 771 774
Concerning the electronic spectra of complex molecules - S.I.Kubarev 775 778
Luminescence spectra of halogen derivatives of anthraquinone in frozen solutions - D.N.Shigorin, N.A.Shcheglova & N.S.Dokunikhin 778 781

Translated in 1961 by
Columbia Technical Translations
5 Vermont Ave., White Plains, N.Y.